Experimental Cell Research

Volume 235, 1997

Academic Press

http://www.apnet.com

Copyright © 1997 by Academic Press
All Rights Reserved

No part of this publication may be reproduced or transmitted in any form or by any means, electronic or mechanical, including photocopy, recording, or any information storage and retrieval system, without permission in writing from the Publisher. *Exceptions:* It is the policy of Academic Press that authors need not obtain permission in the following cases only: (1) to use their original figures or tables in their future works; (2) to make copies of their papers for use in their classroom teaching; and (3) to include their papers as part of their dissertations.

The appearance of the code at the bottom of the first page of an article in this journal indicates the Publisher's consent that copies of the article may be made for personal or internal use, or for the personal or internal use of specific clients. This consent is given on the condition, however, that the copier pay the stated per copy fee through the Copyright Clearance Center, Inc. (222 Rosewood Drive, Danvers, Massachusetts 01923), for copying beyond that permitted by Sections 107 or 108 of the U.S. Copyright Law. This consent does not extend to other kinds of copying, such as copying for general distribution, for advertising or promotional purposes, for creating new collective works, or for resale. Copy fees for pre-1997 articles are as shown on the article title page; if no fee code appears on the title page, the copy fee is the same as for current articles.

0014-4827/97 $25.00

MADE IN THE UNITED STATES OF AMERICA

This journal is printed on acid-free paper.
∞

Contents of Volume 235

Number 1, August 25, 1997

Editorial

URBAN LENDAHL 1

Regular Articles

MADELINE LI, BARBARA CHOO, ZEU-MING WONG, JORGE FILMUS, AND RONALD N. BUICK. Expression of OCI-5/Glypican 3 during Intestinal Morphogenesis: Regulation by Cell Shape in Intestinal Epithelial Cells 3

HELEN E. GRUBER, E. CARL FISHER, JR., BHALOO DESAI, AUDREY A. STASKY, GRETCHEN HOELSCHER, AND EDWARD N. HANLEY, JR. Human Intervertebral Disc Cells from the Annulus: Three-Dimensional Culture in Agarose or Alginate and Responsiveness to TGF-β1 13

OLIVER LANGHOLZ, DAGMAR ROECKEL, DIRK PETERSOHN, EVA BROERMANN, BEATE ECKES, AND THOMAS KRIEG. Cell–Matrix Interactions Induce Tyrosine Phosphorylation of MAP Kinases ERK1 and ERK2 and PLCγ-1 in Two-Dimensional and Three-Dimensional Cultures of Human Fibroblasts 22

ALEJANDRO ABALLAY, NORA G. ARENAS, ANDREW F. G. QUEST, AND LUIS S. MAYORGA. A Factor with a Zinc- and Phorbol Ester-Binding Domain Is Necessary for Endosome Fusion 28

SYLVETTE AYALA-TORRES, PETER C. MOLLER, BETTY H. JOHNSON, AND E. BRAD THOMPSON. Characteristics of 25-Hydroxycholesterol-Induced Apoptosis in the Human Leukemic Cell Line CEM 35

M. ISABELLA PÖRN-ARES, SEK C. CHOW, J. PETER SLOTTE, AND STEN ORRENIUS. Induction of Apoptosis and Potentiation of TNF- and Fas-Mediated Apoptosis in U937 Cells by the Xanthogenate Compound D609 48

GERRY MELINO, MURIEL DRAOUI, LORENZA BELLINCAMPI, FRANCESCA BERNASSOLA, SERGIO BERNARDINI, MAURO PIACENTINI, UWE REICHERT, AND PAUL COHEN. Retinoic Acid Receptors α and γ Mediate the Induction of “Tissue” Transglutaminase Activity and Apoptosis in Human Neuroblastoma Cells 55

LI ZHANG, MARIA LUISA MARTELLI, CATERINA BATTAGLIA, FRANCESCO TRAPASSO, DONATELLA TRAMONTANO, GIUSEPPE VIGLIETTO, ANTONIO PORCELLINI, MASSIMO SANTORO, AND ALFREDO FUSCO. Thyroid Cell Transformation Inhibits the Expression of a Novel Rat Protein Tyrosine Phosphatase 62

MICHINORI KITAGAWA, HIDEYUKI MUKAI, AND YOSHITAKA ONO. Molecular Cloning and Characterization of a Novel Mitochondrial Phosphoprotein, MIPP65, from Rat Liver 71

ESPEN STANG AND ODDMUND BAKKE. MHC Class II-Associated Invariant Chain-Induced Enlarged Endosomal Structures: A Morphological Study 79

KAZUTO NAKADA, JUN-ICHI MIYAZAKI, RIE SABA, AND TAMIO HIRABAYASHI. Natural Occurrence of Fast- and Fast/Slow-Muscle Chimeric Fibers in the Expression of Troponin T Isoforms 93

SYLVIANE HENNEBICQ-REIG, DANIEL TETAERT, BENOIT SOUDAN, ISABELLE KIM, GUILLEMETTE HUET, GILBERT BRIAND, COLETTE RICHET, DOMINIQUE DEMEYER, AND PIERRE DEGAND. O-Glycosylation and Cellular Differentiation in a Subpopulation of Mucin-Secreting HT-29 Cell Line 100

SONYA J. KAMDAR, JANE A. FULLER, SHIN-ICHI NISHIKAWA, AND ROBERT EVANS. Priming of Mouse Macrophages with the Macrophage Colony-Stimulating Factor (CSF-1) Induces a Variety of Pathways That Regulate Expression of the Interleukin 6 (*Il6*) and Granulocyte–Macrophage Colony-Stimulating Factor (*Csfgm*) Genes 108

EMMAPAOLA STURANI, ADELE ABBONDIO, PAOLA BRANDUARDI, CRISTINA FERRARI, RENATA ZIPPEL, ENZO MARTEGANI, MARCO VANONI, AND SUZANNE DENIS-DONINI. The Ras Guanine Nucleotide Exchange Factor CDC25Mm Is Present at the Synaptic Junction 117

ANDRÉ LOCHTER AND MELITTA SCHACHNER. Inhibitors of Protein Kinases Abolish ECM-Mediated Promotion of Neuronal Polarity 124

V. T. SOLOV'YAN, I. O. ANDREEV, T. YU. KOLOTOVA, P. V. POGRIBNIY, D. T. TARNAVSKY, AND V. A. KUNAKH. The Cleavage of Nuclear DNA into High Molecular Weight DNA Fragments Occurs Not Only during Apoptosis but Also Accompanies Changes in Functional Activity of the Nonapoptotic Cells 130

MASARU KUBOTA, IKUYA USAMI, KEN-ICHIRO WATANABE, MACHIKO SAWADA, AKIHIRO KATAOKA, SEIJI KOISHI, YING-WEI LIN, YUICHI AKIYAMA, AND KENSHI FURUSHO. Apoptosis-Resistant Phenotype Selected by Alternating Exposure to Camptothecin and Etoposide 138

RAJALA V. S. RAJU, TERENCE N. MOYANA, AND RAJENDRA K. SHARMA. *N*-Myristoyltransferase Overexpression in Human Colorectal Adenocarcinomas 145

KAORU J. TAKANO, TAKAKO TAKANO, YASUKO YAMANOUCHI, AND TAKAAKI SATOU. Pressure-Induced Apoptosis in Human Lymphoblasts 155

ASIT B. MUKHERJEE AND SAMUEL THOMAS. A Longitudinal Study of Human Age-Related Chromosomal Analysis in Skin Fibroblasts 161

ROSER PAGAN, ISABEL MARTÍN, MIQUEL LLOBERA, AND SENÉN VILARÓ. Growth and Differentiation Factors Inhibit the Migratory Phenotype of Cultured Neonatal Rat Hepatocytes Induced by HGF/SF 170

SARI ATULA, REIDAR GRENMAN, AND STINA SYRJÄNEN. Fibroblasts Can Modulate the Phenotype of Malignant Epithelial Cells *in Vitro* 180

LEDA RAPTIS, HEATHER L. BROWNELL, YING LU, THOMAS PRESTON, RADHA P. NARSIMHAN, STEPHEN ANDERSON, ERIK SCHAEFER, AND TINA HALIOTIS. v-Ras and v-Raf Block Differentiation of Transformable C3H10T1/2-Derived Preadipocytes at Lower Levels Than Required for Neoplastic Transformation 188

KRZYSZTOF REISS, WEI CHENG, PIOTR PIERZCHALSKI, SATISH KODALI, BAOSHENG LI, SHENGLUN WANG, YU LIU, AND PIERO ANVERSA. Insulin-like Growth Factor-1 Receptor and Its Ligand Regulate the Reentry of Adult Ventricular Myocytes into the Cell Cycle 198

XUENING WANG AND GEORGE P. STUDZINSKI. Antiapoptotic Action of 1,25-Dihydroxyvitamin D_3 Is Associated with Increased Mitochondrial MCL-1 and RAF-1 Proteins and Reduced Release of Cytochrome c 210

HIDETOSHI YAMASHITA, AKIRA SHIMIZU, MITSUYASU KATO, HIDEKI NISHITOH, HIDENORI ICHIJO, AKI HANYU, IKUO MORITA, MICHIO KIMURA, FUSAO MAKISHIMA, AND KOHEI MIYAZONO. Growth/Differentiation Factor-5 Induces Angiogenesis *in Vivo* 218

JACQUES ROBERT, DEBORAH M. BROWN, LOUIS DU PASQUIER, AND NICHOLAS COHEN. Antibody Cross-Linking of the Thymocyte-Specific Cell Surface Molecule CTX Causes Abnormal Mitosis and Multinucleation of Tumor Cells 227

SHU MING LIU AND TOMMY SUNDQVIST. Nitric Oxide and cGMP Regulate Endothelial Permeability and F-Actin Distribution in Hydrogen Peroxide-Treated Endothelial Cells 238

Jill D. Coursen, William P. Bennett, Lauren Gollahon, Jerry W. Shay, and Curtis C. Harris. Genomic Instability and Telomerase Activity in Human Bronchial Epithelial Cells during Immortalization by Human Papillomavirus-16 E6 and E7 Genes 245

Michael A. Burg, Akiko Nishiyama, and William B. Stallcup. A Central Segment of the NG2 Proteoglycan Is Critical for the Ability of Glioma Cells to Bind and Migrate toward Type VI Collagen 254

Jacqueline M. T. Klein Gunnewiek, Yvonne van Aarssen, Annemiete van der Kemp, Rob Nelissen, Ger J. M. Pruijn, and Walther J. van Venrooij. Nuclear Accumulation of the U1 snRNP-Specific Protein C Is Due to Diffusion and Retention in the Nucleus 265

Suzanne Crawley, Eleanor M. Farrell, Weigwang Wang, Maojian Gu, Hui-Yu Huang, Vu Huynh, Bradley L. Hodges, Douglas N. W. Cooper, and Stephen J. Kaufman. The $\alpha7\beta1$ Integrin Mediates Adhesion and Migration of Skeletal Myoblasts on Laminin 274

Shin Nakamura, Hiroshi Watanabe, Masahiko Miura, and Takehito Sasaki. Effect of the Insulin-like Growth Factor I Receptor on Ionizing Radiation-Induced Cell Death in Mouse Embryo Fibroblasts 287

Short Notes

Eunkyung Lee, Eric A. Shelden, and David A. Knecht. Changes in Actin Filament Organization during Pseudopod Formation 295

Maria Grazia Romanelli, Florian Weighardt, Giuseppe Biamonti, Silvano Riva, and Carlo Morandi. Sequence Determinants for hnRNP I Protein Nuclear Localization 300

Number 2, September 15, 1997

Milan Mrksich, Laura E. Dike, Joe Tien, Donald E. Ingber, and George M. Whitesides. Using Microcontact Printing to Pattern the Attachment of Mammalian Cells to Self-Assembled Monolayers of Alkanethiolates on Transparent Films of Gold and Silver 305

Robert V. Skibbens and E. D. Salmon. Micromanipulation of Chromosomes in Mitotic Vertebrate Tissue Cells: Tension Controls the State of Kinetochore Movement 314

J. L. Jones, J. E. Royall, D. R. Critchley, and R. A. Walker. Modulation of Myoepithelial-Associated $\alpha6\beta4$ Integrin in a Breast Cancer Cell Line Alters Invasive Potential 325

Debendranath Banerjee, Marilis Rodriguez, and Ayyappan K. Rajasekaran. Rapid Movement of Newly Synthesized Chicken Apolipoprotein AI to Trans-Golgi Network and Its Secretion in Madin–Darby Canine Kidney Cells 334

K. Nakabayashi, T. Ogata, M. Fujii, H. Tahara, T. Ide, R. Wadhwa, S. C. Kaul, Y. Mitsui, and D. Ayusawa. Decrease in Amplified Telomeric Sequences and Induction of Senescence Markers by Introduction of Human Chromosome 7 or Its Segments in SUSM-1 345

G. C. Gobé, J. Halliday, I. S. Dunn, B. V. Harmon, E. Schoch, S. M. Khan, and D. J. Allan. Expression and Localization of the Retinoblastoma Gene during Radiation-Induced Apoptosis in Neonatal Rat Kidney 354

Shuichi Akiyama, Takenobu Katagiri, Mana Namiki, Noboru Yamaji, Naoya Yamamoto, Katsuyoshi Miyama, Hiroshi Shibuya, Naoto Ueno, John M. Wozney, and Tatsuo Suda. Constitutively Active BMP Type I Receptors Transduce BMP-2 Signals without the Ligand in C2C12 Myoblasts 362

Chunlin Yang, Shi-Wu Li, Heikki J. Helminen, Jaspal S. Khillan, Yunhua Bao, and Darwin J. Prockop. Apoptosis of Chondrocytes in Transgenic Mice Lacking Collagen II 370

Junken Aoki, Satoshi Koike, Hiroaki Asou, Iku Ise, Hiroshi Suwa, Toshiyuki Tanaka, Masayuki Miyasaka, and Akio Nomoto. Mouse Homolog of Poliovirus Receptor-Related Gene 2 Product, mPRR2, Mediates Homophilic Cell Aggregation 374

Nathalie Dourdin, Jean-Jacques Brustis, Denis Balcerzak, Najat Elamrani, Sylvie Poussard, Patrick Cottin, and André Ducastaing. Myoblast Fusion Requires Fibronectin Degradation by Exteriorized m-Calpain 385

Eric M. J. Bindels, Marcel Vermey, Johanna M. J. Rebel, Ellen C. Zwarthoff, and Theodorus H. Van Der Kwast. *In Vitro* Modulation of Implantation and Intraepithelial Expansion of Bladder Tumor Cells by Epidermal Growth Factor 395

Xiaohua Qian, Thomas N. Wang, Vicki L. Rothman, Roberto F. Nicosia, and George P. Tuszynski. Thrombospondin-1 Modulates Angiogenesis *in Vitro* by Up-Regulation of Matrix Metalloproteinase-9 in Endothelial Cells 403

Laszlo Perlaky, Benigno C. Valdez, and Harris Busch. Effects of Cytotoxic Drugs on Translocation of Nucleolar RNA Helicase RH-II/Gu 413

Manon van Engeland, Helma J. H. Kuijpers, Frans C. S. Ramaekers, Chris P. M. Reutelingsperger, and Bert Schutte. Plasma Membrane Alterations and Cytoskeletal Changes in Apoptosis 421

Short Note

J. E. Cartwright, G. St. J. Whitley, and A. P. Johnstone. Endothelial Cell Adhesion Molecule Expression and Lymphocyte Adhesion to Endothelial Cells: Effect of Nitric Oxide 431

Author Index for Volume 235 435

NOTICE

The Subject Index for Volume 235 will appear in the December 15, 1997, issue as part of a cumulative index for the year 1997.

ISSN 0014-4827
Volume 235, Number 1, August 25, 1997

Experimental Cell Research

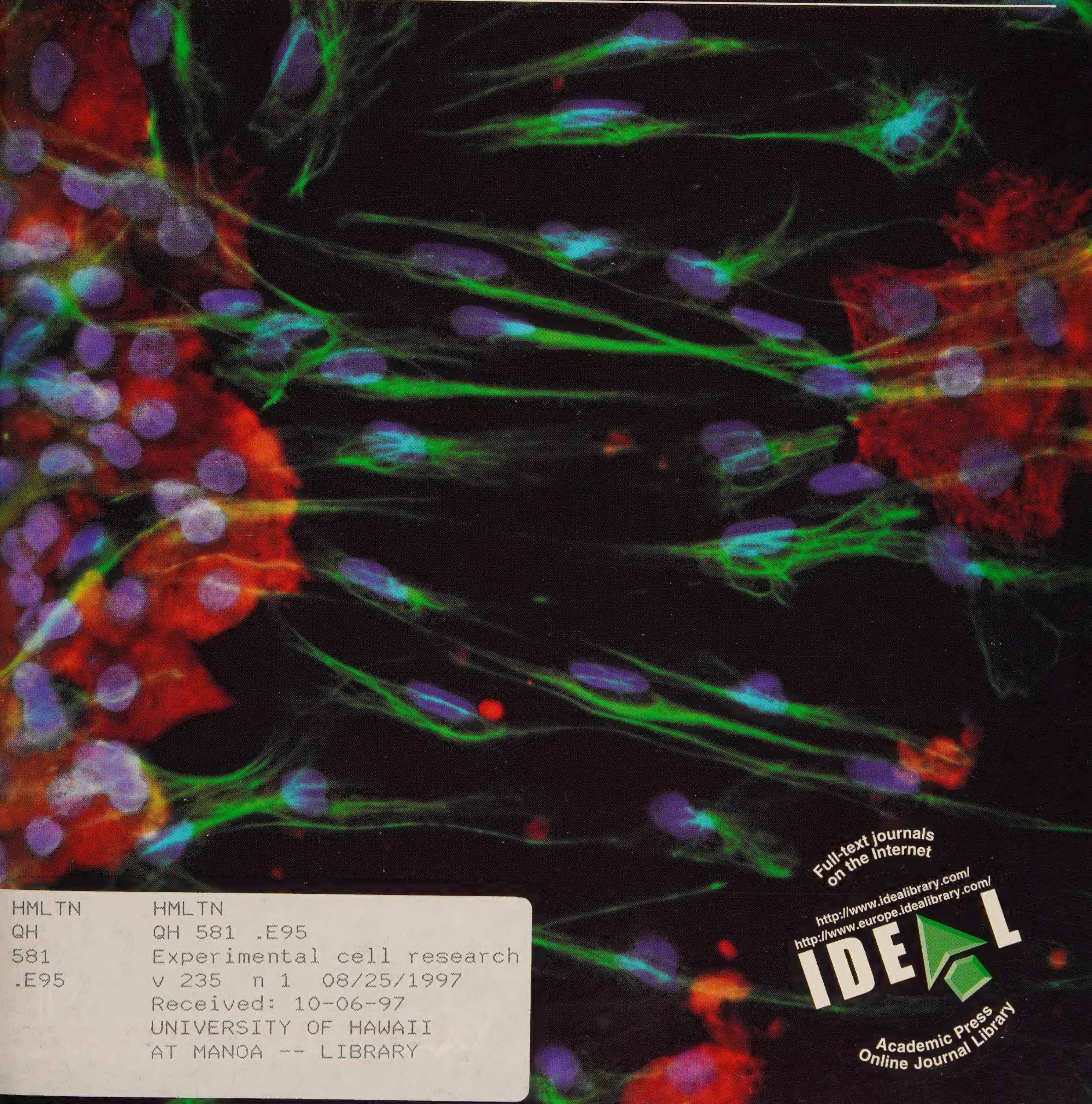

HMLTN QH 581 .E95
HMLTN
QH 581 .E95
Experimental cell research
v 235 n 1 08/25/1997
Received: 10-06-97
UNIVERSITY OF HAWAII
AT MANOA -- LIBRARY

Full-text journals on the Internet
http://www.idealibrary.com/
http://www.europe.idealibrary.com/
IDEAL
Academic Press Online Journal Library

EXPERIMENTAL CELL RESEARCH

Editor-in-Chief
Urban Lendahl
Department of Cell and Molecular Biology, Medical Nobel Institute
Doktorsringen 2 D, Karolinska Institute, S-171 77 Stockholm, Sweden

Associate Editor for North America
Renato Baserga
Kimmel Cancer Center, Thomas Jefferson University
624 Bluemle Life Sciences Bldg., 233 S. 10th Street
Philadelphia, PA 19107-5541, U.S.A.

Assistant Editor
Christer Höög
Department of Cell and Molecular Biology, Medical Nobel Institute
Doktorsringen 2 A, Karolinska Institute,
S-171 77 Stockholm, Sweden

Editors

Denise P. Barlow
Amsterdam, THE NETHERLANDS

Helen M. Blau
Stanford, CA 94305-5332

Eduardo Boncinelli
Milan, ITALY

Rodrigo Bravo
Princeton, NJ 08543-4000

Bruno Calabretta
Philadelphia, PA 19107-6799

Judith Campisi
Berkeley, CA 94720

Graham Carpenter
Nashville, TN 37232-0146

Francesco Clementi
Milan, ITALY

Paolo Comoglio
Torino, ITALY

Vincent J. Cristofalo
Philadelphia, PA 19129

Zbigniew Darzynkiewicz
Elmsford, NY 10523

Siegfried W. de Laat
Utrecht, THE NETHERLANDS

David T. Denhardt
Piscataway, NJ 08855-1059

Gideon Dreyfuss
Philadelphia, PA 19104-6148

William C. Earnshaw
Edinburgh, UK

Stanislav Fakan
Lausanne, SWITZERLAND

Norbert E. Fusenig
Heidelberg, GERMANY

Giulio Gabbiani
Geneve, SWITZERLAND

Frederick Grinnell
Dallas, TX 75235-9039

Joyce L. Hamlin
Charlottesville, VA 22908

Jan H. J. Hoeijmakers
Rotterdam, THE NETHERLANDS

Lester F. Lau
Chicago, IL 60612-7309

Benjamin L. Margolis
Ann Arbor, MI 48109-0650

Michael McBurney
Ottawa, CANADA

Wouter H. Moolenaar
Amsterdam, THE NETHERLANDS

Peter K. Müller
Lübeck, GERMANY

Pierluigi Nicotera
Konstanz, GERMANY

Tuneko Okazaki
Nagoya, JAPAN

Charles P. Ordahl
San Francisco, CA 94143-0452

Moshe Oren
Rehovot, ISRAEL

Sten Orrenius
Stockholm, SWEDEN

Mary Osborn
Göttingen, GERMANY

Harvey L. Ozer
Newark, NJ 07103-2714

Denise Paulin
Paris, FRANCE

Kristofer Rubin
Uppsala, SWEDEN

Gary S. Stein
Worcester, MA 01655

George Studzinski
Newark, NJ 07103-2484

Kazuhiko Umesono
Nara, JAPAN

Klaus von der Mark
Erlangen, GERMANY

Erwin F. Wagner
Vienna, AUSTRIA

Bengt Westermark
Uppsala, SWEDEN

Founding Editors: T. Caspersson and J. Runnström
Editor Emeritus: N. Ringertz

Editorial Offices:
Karolinska Institutet, CMB, Doktorsringen 2 D, 17177
Stockholm, Sweden Tel. Nat.: 08-34 04 53; Int.: +46 8-34 04 53;
Telefax: +46 8-34 54 29; E-mail: ecr@cmb.ki.se

Dr. Renato Baserga, Associate Editor for North America,
Experimental Cell Research, U.S. Editorial Office, 525 B Street, Suite
1900, San Diego, California 92101-4495

Cover photo. Hepatocyte growth factor-induced migratory phenotype in cultured neonatal rat hepatocytes. Neonatal hepatocytes were treated with HGF/SF and double-immunostained with monoclonal antibodies against vimentin (green) and cytokeratin (red). Nuclei were stained with Hoechst 33342 (blue). The photograph was obtained by triple exposure. (Pagan *et al.*, 1997, *Exp. Cell Res.* **235,** 170–179).

EXPERIMENTAL CELL RESEARCH

Volume 235, Number 1, August 25, 1997

http://www.apnet.com

Copyright © 1997 by Academic Press
All Rights Reserved

No part of this publication may be reproduced or transmitted in any form or by any means, electronic or mechanical, including photocopy, recording, or any information storage and retrieval system, without permission in writing from the Publisher. *Exceptions:* It is the policy of Academic Press that authors need not obtain permission in the following cases only: (1) to use their original figures or tables in their future works; (2) to make copies of their papers for use in their classroom teaching; and (3) to include their papers as part of their dissertations.

The appearance of the code at the bottom of the first page of an article in this journal indicates the Publisher's consent that copies of the article may be made for personal or internal use, or for the personal or internal use of specific clients. This consent is given on the condition, however, that the copier pay the stated per copy fee through the Copyright Clearance Center, Inc. (222 Rosewood Drive, Danvers, Massachusetts 01923), for copying beyond that permitted by Sections 107 or 108 of the U.S. Copyright Law. This consent does not extend to other kinds of copying, such as copying for general distribution, for advertising or promotional purposes, for creating new collective works, or for resale. Copy fees for pre-1997 articles are as shown on the article title page; if no fee code appears on the title page, the copy fee is the same as for current articles.

0014-4827/97 $25.00

MADE IN THE UNITED STATES OF AMERICA

This journal is printed on acid-free paper.
∞

EXPERIMENTAL CELL RESEARCH

(ISSN 0014-4827)

Published monthly (except semimonthly in February, May, August, and November) by Academic Press,
6277 Sea Harbor Drive, Orlando, FL 32887-4900

1997: Volumes 230–237. Price: $2125.00 U.S.A. and Canada; $2125.00 all other countries
All prices include postage and handling.

All correspondence and subscription orders should be addressed to the office of the Publishers at 6277 Sea Harbor Drive, Orlando, FL 32887-4900. Send notices of change of address to the office of the Publishers at least 6 to 8 weeks in advance. Please include both old and new addresses. POSTMASTER: Send changes of address to *Experimental Cell Research,* 6277 Sea Harbor Drive, Orlando, FL 32887-4900.

Periodicals postage paid at Orlando, FL, and at additional mailing offices.

Copyright © 1997 by Academic Press

Digitized by the Internet Archive
in 2026

https://archive.org/details/experimental-cell-research_1997_235_contents

THE ACADEMIC PRESS ONLINE LIBRARY

GET HANDS ON ACCESS TO THE IDEAL SOLUTION

IDEAL, the Academic Press Online Library, addresses the difficult issues facing scholarly communication today, bringing full-text research journals directly to the end-user's desktop. This IDEAL system provides all the information from the printed journals, enhanced with efficient electronic access to the primary information.

Reducing administrative costs while providing the ability for instant targeted searches across a large archive, IDEAL significantly increases the value of your consortium, library, and institution. Authorized users can browse, search, view, and print tables of contents, abstracts, and complete articles without restriction for personal use, course packs, or internal company business purposes. Based on non-proprietary modular architecture, IDEAL's mirrored sites ensure efficient access from all points on the globe 24 hours a day, 365 days a year.

Technology holds the potential to advance scientific enterprise, yet **Academic Press** recognizes that librarians, users, publishers, and information services must work together to realize change. When you invest in the IDEAL solution, you enter into a partnership with Academic Press. From this practical philosophy, IDEAL was conceived and continues to grow. We invite you to join us.

ACCESS ➤

QUALITY ➤

INTERACTIVITY ➤

RELIABILITY ➤

FLEXIBILITY ➤

AP

FOR MORE INFORMATION, PLEASE CONTACT:

Academic Press Marketing Department
525 B Street, Suite 1900, San Diego, CA 92101-4495

Academic Press Limited
24-28 Oval Road, London NW1 7DX, U.K.

1-800-894-3434 or 1-619-699-6742
E-MAIL: apsubs@acad.com

http://www.idealibrary.com/
http://www.europe.idealibrary.com/

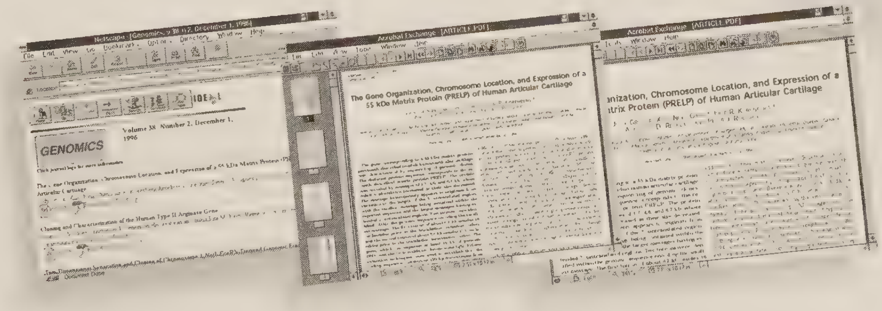
GENOMICS
Volume 38 Number 2, December 1, 1996
The Gene Organization, Chromosome Location, and Expression of a 55 kDa Matrix Protein (PRELP) of Human Articular Cartilage

EXPERIMENTAL CELL RESEARCH **235,** 1–2 (1997)
ARTICLE NO. EX973722

EDITORIAL

On July 1, I succeeded Nils Ringertz as Editor-in-Chief for *Experimental Cell Research* (*ECR*). My scientific career started with thesis work concerning the evolution of gene families, but as a postdoctoral fellow at MIT in Ron McKay's laboratory (1987 to 1989) I switched to neurobiology and developmental biology and have stayed in this field since my return to the Karolinska Institute in 1989. My research interests are centered on the role and function of cytoskeletal proteins in the developing CNS, with a particular focus on the intermediate filament nestin. In addition, my research group carries out work on the Notch signaling pathway in mammals.

I am honored to have been entrusted with the responsibility of becoming the new Editor-in-Chief for *ECR,* and I would like to thank my predecessor, Nils Ringertz, for patiently sharing his vast scientific and editorial expertise with me during my 6 years as Assistant Editor. In addition to his significant contributions in many areas of cell biology, ranging from the techniques of cell fusion to the detailed architecture of the nucleus of the cell, Nils Ringertz has been associated with *ECR* in various capacities for more than three decades, including 10 years as Editor-in-Chief. He has developed *ECR* into a leading journal in cell and molecular biology and has orchestrated a number of important and vitalizing changes to the journal. In addition, he has organized a very effective editorial office in Stockholm, for which I am very grateful. Nils Ringertz' unique blend of a renaissance type of scientific knowledge, organizational talent, and computer wit has been crucial to *ECR,* and I am convinced that the same qualities will prove useful in his new challenging project, "building" the Electronic Nobel Museum. I wish Nils Ringertz the best of luck in this new capacity.

I would also like to thank Renato Baserga, the North American Editor, for doing an outstanding job for *ECR.* Renato Baserga not only established the North American Editorial Office in 1987, but also has made it grow and prosper. The success of this operation is obvious, as manifested by the steadily increasing number of submissions to the North American Editorial Office. On this occasion, I would also like to express my gratitude to all the Editors of *ECR* for first-class work on soliciting and handling manuscripts, for promotion of *ECR,* and for providing us with many valuable comments over the years. Furthermore, I wish to welcome Christer Höög as my successor as Assistant Editor. His expertise in cell cycle research, gene regulation, and the biology of meiosis and mitosis will prove a very valuable asset to *ECR.* Finally, my heartfelt thanks to the editorial secretaries at the Stockholm Editorial Office, Nina Sunden and Lorenette Gozzo, for running the office so smoothly and professionally, which allows Christer Höög and I to concentrate on the scientific aspects of *ECR.*

ECR has a long tradition of publishing work in cell and molecular biology and is in fact one of the oldest journals in this field; *ECR* will celebrate its 50th anniversary at the turn of the century. During these years, *ECR* has remained one of the important journals in the field, and we will certainly do our best to keep things this way. *ECR* has a strong reputation in many areas, but as certain aspects of cell and molecular biology develop very rapidly, it is natural for *ECR* to broaden its scope and to put particular interest and emphasis on new and expanding areas. Examples of such dynamic branches of research are the cell cycle, gene regulation, cell signaling, signal transduction,

0014-4827/97 $25.00
Copyright © 1997 by Academic Press
All rights of reproduction in any form reserved.

intracellular trafficking, programmed cell death, and research on the dynamics and function of the cytoskeleton, cell membrane, and extracellular matrix. As noted in an earlier Editorial, work in cancer research is also given priority, in particular when addressing fundamental aspects of cell and molecular biology. To further emphasize the interest of *ECR* in the areas described above, the Notice to Authors has been modified accordingly, starting with this issue.

In addition to original papers, *ECR* also plans to increase the number of review articles, particularly in the Minireview format. The aim is, after some time, to present at least one review per issue on current topics of particular interest, and it is our hope that these reviews will be informative and stimulating to the readership of *ECR.* While many of the reviews will be solicited, we also welcome suggestions as to possible topics for review articles, and anyone interested in contributing review articles is encouraged to discuss this with the European or American Editorial Offices, as is noted in the modified Notice to Authors.

ECR is published by Academic Press, and we are very grateful for the support and commitment of the Publisher in their efforts to maintain *ECR* as one of the leading journals in cell and molecular biology. This has been demonstrated by the large number of recently introduced, and planned, changes in the layout of the journal, for example, introducing a new cover layout and new masthead, allowing one high-quality color plate per article free of charge, increasing the number of issues from 12 to 16 per year, and including full titles in the reference list. Academic Press has also been very active and helpful in implementing electronic publishing of *ECR,* via the IDEAL system. The presence of *ECR* on the Internet will allow our readers to have increased access to the journal.

We are committed to keeping *ECR* one of the leading journals in cell and molecular biology, and we hope that the journal will continue to improve. At the same time, we are fully aware that this does not happen simply by writing Editorials, but that a large part is dependent upon your support, in the form of submission of interesting manuscripts, reviewing manuscripts, and providing us with valuable comments and criticisms about the journal. We thank you in advance for your continued commitment to *ECR,* and we look forward to transforming this commitment into an extension of *ECR*'s long tradition of publishing dynamic and leading work in cell and molecular biology.

Urban Lendahl
Editor-in-Chief

EXPERIMENTAL CELL RESEARCH **235,** 3–12 (1997)
ARTICLE NO. EX973629

Expression of OCI-5/Glypican 3 during Intestinal Morphogenesis: Regulation by Cell Shape in Intestinal Epithelial Cells

Madeline Li,*,‡,[1] Barbara Choo,* Zeu-Ming Wong,*,‡ Jorge Filmus,‡,§ and Ronald N. Buick†

**Ontario Cancer Institute/Princess Margaret Hospital, Toronto, Ontario, Canada; ‡Department of Medical Biophysics, University of Toronto, Toronto, Ontario, Canada; and §Division of Cancer Research, Sunnybrook Health Science Centre, Toronto, Ontario, Canada*

OCI-5, the rat homologue of human glypican 3 (GPC3), is believed to be involved in morphogenesis and growth control during development. The finding that GPC3 is mutated in patients with the Simpson–Golabi–Behmel overgrowth syndrome is consistent with this idea. In this report, using RNA *in situ* hybridization, expression of OCI-5 in the developing intestine is detected in both endoderm- and mesenchyme-derived cells in a phased manner related to age and proximal/distal position. To investigate the mechanism of its regulation during intestinal development, OCI-5 expression was studied in the primitive rat intestinal epithelial cell line IEC-18. The expression of the OCI-5 transcript is increased in IEC-18 cells at confluence, in low calcium media, and during spheroid culture, all conditions which result in the cells acquiring a more rounded cell shape. In contrast, cytoskeletal disruption with colchicine causes cells to flatten and spread and abolishes both the confluence- and the low calcium-dependent induction of OCI-5. Treatment with vanadate, a phosphatase inhibitor, causes cells to acquire a spindle-shaped morphology and prevents OCI-5 induction in all situations. Nuclear run-on analysis demonstrates that the rate of OCI-5 transcription is increased at confluence, in low calcium media, and during spheroid culture of IEC-18, and decreased by treatment of cells with colchicine. Together, these data suggest that OCI-5 expression is regulated in IEC-18 by cell shape. The pattern of expression of OCI-5 in the developing intestine is consistent with it playing a role in epithelial–mesenchymal interactions during intestinal morphogenesis, when cell shape changes are likely to occur. © 1997 Academic Press

INTRODUCTION

Morphogenesis of the intestinal epithelium is a rapid and late event during rodent development, occurring during the last 5 days of the 22-day gestation period [4, 5]. Development from a pseudostratified to a simple columnar epithelium occurs as a cephalocaudal wave of cytodifferentiation, being essentially completed in the proximal duodenum by Day 20 of gestation, while only just beginning in the distal ileum. The early rat duodenum (Day 15) is composed of a two- to three-cell layer of undifferentiated stratified epithelium separated from mesenchymal cells by a well-defined basal lamina. Over the next few days, rapid cell proliferation results in an enlarged lumen and a four- to eight-cell-layer-thick epithelium. At Day 17 focal areas of epithelial vacuolization appear, forming secondary lumina while the tunica propria migrates into the epithelium. Direct contact between the epithelium and mesenchyme is established by numerous epithelial cytoplasmic processes which project through gaps in the basal lamina into the lamina propria. By Day 19, the secondary lumina have coalesced with the main lumen and the epithelium has reorganized through a combination of cell death and cell migration to cover nascent villi. Cellular differentiation initiates coincident with formation of the villi, and development of the crypts of Lieberkuhn follows shortly thereafter. Morphogenesis is completed in the third postnatal week, when a monolayered epithelium lines the crypts and villi, which represent continuously regenerating proliferative and differentiated cellular compartments, respectively.

Mechanisms which control gene expression during the period of developmental differentiation and morphogenesis of the intestinal mucosa are currently unknown. Such knowledge would be of interest since genes which function in lineage determination or have roles in tumorigenesis might be expected to be expressed in fetal intestinal cells. Indeed, many of the same surface membrane antigens are expressed by fetal intestinal cells, intestinal crypt cells, and colon tumor cell lines [6–8]. A candidate gene in which to study mechanisms of gene regulation during intestinal development is OCI-5, a member of the glypican family [1, 2], which was originally isolated as a cDNA clone from

---

[1] To whom correspondence and reprint requests should be addressed at Ontario Cancer Institute/Princess Margaret Hospital Toronto, 8-105, 610 University Avenue, Toronto, Ontario, Canada M5G 2M9. Fax: (416) 946-2086.

† Deceased July 20, 1996.

0014-4827/97 $25.00
Copyright © 1997 by Academic Press
All rights of reproduction in any form reserved.

the primitive rat intestinal epithelial cell line IEC-18 [9]. Glypicans are heparan sulfate proteoglycans which are associated with the cell surface through a glycosyl–phosphatidylinositol anchor. They are highly conserved across species and each have developmental and tissue-specific patterns of expression [10]. Proteoglycans are thought to play a role in growth and differentiation through regulating cell–cell/cell–matrix contacts, cell migration, or modulation of growth factor action [11–14].

Recently, glypican 3 (GPC3), the human homologue of OCI-5, was identified as the defective gene in the Simpson–Golabi–Behmel overgrowth syndrome (SGBS) [3]. SGBS is an X-linked disorder characterized by pre- and postnatal overgrowth, developmental malformations in multiple organs and tissues, and an increased risk of embryonal tumors such as Wilms' tumor and neuroblastoma during early childhood [15]. An understanding of the role of GPC3 in growth control and morphogenesis may contribute to elucidating the pathogenesis of SGBS. In this respect it is interesting to note that several gastrointestinal abnormalities have been described in this syndrome [16, 17]

The OCI-5 transcript is maximally expressed in the embryonic intestine at Day 16 of development and gradually decreases from Day 19, becoming undetectable by Day 24 postparturition. In IEC-18 cells expression of the OCI-5 transcript is abrogated by oncogenic transformation [1] and is highly induced with confluence [18]. Here, analysis of OCI-5 transcript in the developing intestine is extended to reveal a complex pattern of expression in endodermal and mesenchymal cells, following temporal and spatial gradients which move with the wave of intestinal morphogenesis. Expression of OCI-5 in IEC-18 cells is demonstrated to be regulated by changes in cell shape, being increased when cells attain a more rounded morphology, such as might occur during intestinal morphogenesis.

MATERIALS AND METHODS

Materials. Sprague–Dawley rats were obtained from Charles River Ltd. (Wilmington, MA). Bovine pancreatic RNase A was obtained from Boehringer–Mannheim (Mannheim, Germany); placental ribonuclease inhibitor (RNasin) and SP6 polymerase were obtained from Promega Biotech. Colchicine, cytochalasin D, sodium orthovanadate, and poly(2-hydroxyethyl methacrylate) (poly (HEMA)) were purchased from Sigma Chemical Co. (St. Louis, MO).

In situ hybridization. Riboprobes were prepared by inserting a 218-bp *Hin*dIII fragment (530–748) from the open reading frame of OCI-5 into the pGEM3Z transcription vector in both sense (negative control) and antisense (positive probe) orientations. *In vitro* transcription was performed in the presence of ^{35}S-UTP (410 Ci/mmol). The size of the radiolabeled RNA probes was analyzed by agarose gel electrophoresis and specificity for the OCI-5 transcript was confirmed by probing Northern blots prepared from IEC-18 (positive control) and IEC-14 (negative control) cell lines (not shown). Tissue preparation and *in situ* hybridization were performed according to Davis *et al.* [18a]. Sections of small intestine and colon were isolated from fetal rats after 15–20 days of gestation and embedded in OCT freezing medium. Cryosections 7 μm thick were prepared using a cryostat microtome at −17°C and collected on poly-L-lysine-coated, acid-washed glass slides. Sections were fixed in 4% paraformaldehyde and acetylated in 25 m*M* acetic acid in 100 m*M* triethanolamine, pH 7.5, before hybridization of consecutive serial sections with sense and antisense riboprobes. Hybridization was performed with 30 MBq probe/ml of hybridization mix containing 50% formamide, 10 m*M* Tris–HCl, pH 7.5, 1 m*M* EDTA, 1× Denhardt's solution, 10% dextran sulfate, 0.3 *M* sodium chloride, 100 m*M* dithiothreitol, 200 μg/ml sheared salmon sperm DNA, and 400 μg/ml each of tRNA, yeast RNA, and poly(A), under mineral oil at 53°C overnight. Nonspecifically bound probe was removed by digestion with 20 μg/ml RNase A for 30 min at 37°C and washing at 0.1× SSC, 10 m*M* β-mercaptoethanol for 60 min at 65°C. Sections were dehydrated in a graded ethanol series supplemented with 0.3 *M* ammonium acetate, air-dried, and dipped in Kodak NTB-2 emulsion, diluted with an equal volume of 0.6 *M* ammonium acetate at 45°C. Slides were developed and fixed according to the manufacturer's instructions. Light and dark field photomicrographs were obtained using a Wild Photomakroskop M400. As negative controls, sections were treated with RNase before hybridization (not shown).

Cell culture. IEC-18 (9) rat intestinal epithelial cells were maintained in DMEM supplemented with 20 m*M* glucose, 2 m*M* glutamine, 0.27 units/ml insulin, and 5% fetal bovine serum. For experiments performed in low Ca^{2+} conditions, cells were first acclimatized by a single passage in the same medium except that the $CaCl_2$ concentration was reduced to 50 μ*M*. All experiments were performed with cells between passage 20 and passage 30. Confluence, defined as the density at which cells cease to proliferate, was determined to be approximately 6 × 10^6 cells/100-mm dish. Tissue culture plastic was coated with poly(HEMA) at a concentration that completely prevented cell attachment. A 2.8-ml volume of 2.4% poly(HEMA) in 95% ethanol was added to a 60-mm dish and allowed to evaporate under sterile conditions. To form spheroidal aggregates, a single-cell suspension of 10^6 IEC-18 cells was added to the poly(HEMA)-coated dish in 5 ml complete medium and incubated at 37°C for 24 h.

Northern blot analysis. For Northern blot analysis, total RNA was isolated from IEC-18 cells with Trizol reagent (Gibco, BRL, Gaithersburg, MD), according to manufacturer's specifications. RNA (10 μg) was separated by electrophoresis on 0.75% agarose–formaldehyde gels in phosphate buffer and transferred to Zetaprobe membranes (Bio-Rad Laboratories, Richmond, CA) in 10× SSC. Filters were prehybridized at 42°C in 45% formamide, 5× Denhardt's, 2% SDS, 5× SSPE, and 100 μg/ml each of salmon sperm DNA and poly(A)$^+$. Hybridization was performed under the same conditions using random-primed, ^{32}P-labeled cDNA probes. For OCI-5 probing, the 2.3-kb *Eco*RI insert cDNA was used [1]. Probes used to verify loading included tubulin [19], GAPDH [20], and ribosomal protein L32 [21]. Filters were washed in 2× SSC, 0.2% SDS for 30 min at 42°C, followed by a 30-min wash in 1× SSC and 0.1% SDS at 65°C before exposure to a PhosphorImager screen and quantification using ImageQuant software (Molecular Dynamics).

Nuclear run-on analysis. To prepare nuclei, 10^7 cells were washed in PBS, lysed in 10 m*M* Tris, pH 7.4, 10 m*M* NaCl, 3 m*M* $MgCl_2$, 0.5% NP-40 at 4°C, and flash frozen with liquid nitrogen in 100 μl of glycerol buffer (50 m*M* Tris, pH 8.3, 5 m*M* $MgCl_2$, 0.1 m*M* EDTA, 40% glycerol). Frozen nuclei were stored at −70°C until required. To radiolabel newly synthesized RNA, an equal volume of reaction buffer (10 m*M* Tris, pH 8.0, 5 m*M* $MgCl_2$, 300 m*M* KCl, 0.5 m*M* each of ATP, CTP, and GTP, and 0.1 mCi [^{32}P]UTP (800 Ci/mmol) was added to the nuclei and incubated at 30°C for 30 min. RNA was isolated using the Trizol reagent and unincorporated nucleotides

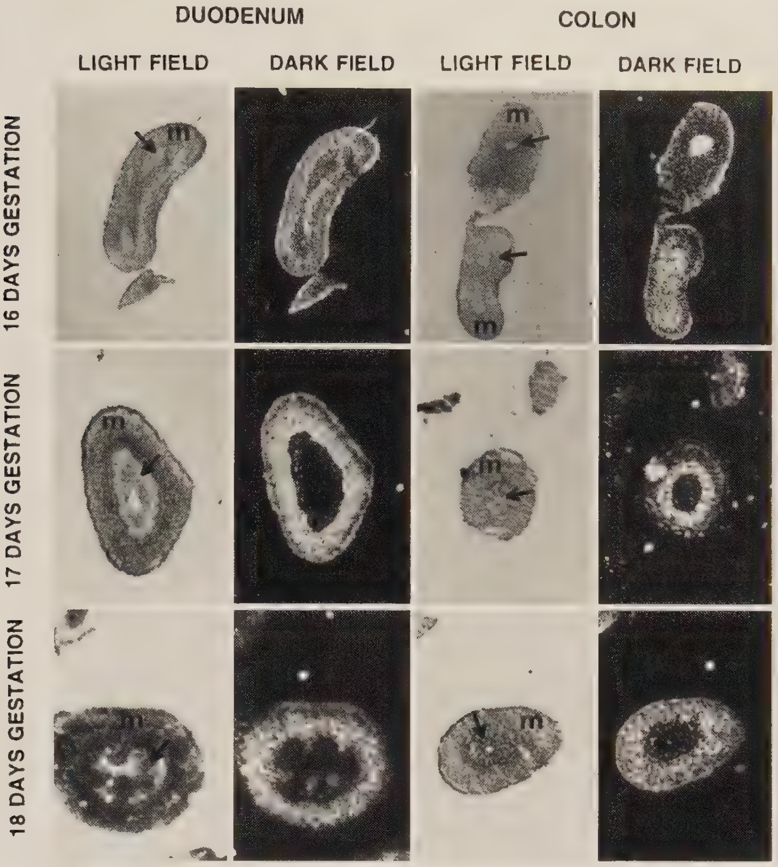

FIG. 1. Expression of OCI-5 transcripts in the developing rat intestine. Light field micrograph sections of duodenum and colon from 16-, 17-, and 18-day-old embryos were hybridized to an antisense OCI-5 riboprobe (dark field). Mesodermal (m) and endodermal (arrows) components are indicated in the light field sections.

were removed by ammonium acetate/ethanol precipitation. Radiolabeled RNA (3×10^6 cpm) was hybridized to dot blots containing 0.5 μg of gel-purified OCI-5 insert, PUC18 plasmid, and GAPDH insert on Hybond-N membranes (Amersham) in 50% formamide, 5% SSPE, 5× Denhardt's reagent, 0.5% SDS, and 20 μg/ml denatured salmon sperm DNA at 42°C for 48 h. Filters were washed in 2× SSC, 0.1% SDS 30 min at 42°C followed by a 30-min wash at 42°C in 0.1× SSC, 0.1% SDS, and exposure to a PhosphorImager screen.

RESULTS

OCI-5 Expression Pattern in the Developing Intestine

Figure 1 shows the results of *in situ* hybridization of intestinal sections from Day 16 to Day 18 of gestation with the antisense OCI-5 probe. High levels of the transcript were observed in all sections with the pattern of expression changing dramatically over that time period. In the 16-day colon very high levels of expression were restricted to the endoderm, while in the more developed duodenum, expression was high in both endoderm and mesenchyme. At 17 days of gestation, the duodenum expressed the OCI-5 transcript at high levels in a ring encompassing three-quarters of the thickness of the mesenchyme, while expression in the endoderm decreased rapidly to barely detectable levels. In the colon, high levels of expression were concentrated in a ring of cells adjacent to the endoderm, less than half the thickness of the mesenchyme. The initially high levels of expression in mesenchymal cells decrease and become more diffuse throughout the tissue by 18 days of gestation. The OCI-5 transcript is thereafter downregulated, with continued decreases until Postnatal Day 11, after which no expression is detectable in the intestine either by Northern blot analysis [1] or by *in situ* hybridization (data not shown).

In addition to the dramatic switch in expression from the endoderm to the mesenchyme, the amount of OCI-5 transcript diminishes earlier in the duodenum than in more distal regions of the intestine, reflecting the differences in the time course of development along the proximal/distal axis of the intestine. This pattern is consistent with OCI-5 playing an important role in intestine morphogenesis.

Expression of OCI-5 Is Induced by Cellular Confluence and Low Ca^{2+} Culture

To analyze what mechanisms may be regulating OCI-5 expression during intestinal development its confluence-dependent induction in the primitive intestinal epithelial cell line IEC-18 was characterized. The OCI-5 transcript is dramatically induced in multiple cell lines at confluence [18]. In IEC-18, the magnitude of induction decreases with serial passage of the cells, but in very early passages it has been observed to be up to 30-fold [18]. Four experiments were performed in an attempt to understand, on a cellular level, what mechanism underlies the effect that confluence has upon OCI-5 expression.

Studies were performed to determine whether confluence-induced upregulation was an indirect consequence of confluence-induced quiescence. Subconfluent cultures either were allowed to grow to confluence, brought to quiescence by serum starvation for 72 h, or had serum reintroduced after quiescence and were allowed to grow to confluence. The levels of OCI-5 transcript were analyzed and found to be the same in quiescent and subconfluent cells, while they increased in cells allowed to grow to confluence or when serum was reintroduced (data not shown). To determine whether the basement membrane of confluent or growing cells could alter the expression of OCI-5, cells were seeded at low density on basement membrane prepared by removing confluent or growing IEC-18 cells with 0.1% NH_4OH (22). RNA was harvested for 4 consecutive days as the cells approached confluence. Northern probing revealed a similar increase in OCI-5 expression as cells grown on plastic, confluent or subconfluent basement membrane approached confluency (data not shown). Similarly, the inductive signal was shown not to be a factor elaborated into the conditioned medium of the cells. Confluent and subconfluent cells cocultured using permeable Transwell membrane inserts (Costar) showed the same levels of OCI-5 transcript as cells grown alone (not shown). It appears, therefore, that OCI-5 expression is not mediated by the quiescent state of confluent cells, basement membrane, or a factor present in conditioned medium.

As a culture approaches confluence, cells begin to crowd and cell–cell contacts are increased. To address whether cell–cell contacts were critical to the induction of OCI-5, cells were grown in low Ca^{2+} medium. Figure 2A compares the confluence-dependent induction of OCI-5 in full medium (2 mM Ca^{2+}) to low Ca^{2+} medium (50 μM Ca^{2+}). In full medium, a 3.4-fold induction of OCI-5 is observed in 100% confluent cells relative to 25% confluence. Cells grown in low Ca^{2+} medium show a surprising increase in OCI-5 expression at 25% confluence (2.4-fold) and a superinduction at 100% confluence (10.8-fold). Examination of these cultures under light microscopy reveals that under conditions of low Ca^{2+} cells acquire a more rounded morphology, most likely as a result of decreased cell–cell and cell–substratum contacts (Fig. 2B). Although not apparent from the perspective of these photographs, low Ca^{2+} cultured cells are also elevated from the plane of the tissue culture plate in a rounded fashion, compared to their counterparts grown in full medium. This elevation change is readily demonstrated by a difference in their plane of focus under light microscopy. Thus, low Ca^{2+} culture appears to exacerbate the normal change from a flattened, elongated cytoplasm of subconfluent cells to a more rounded cell shape as cells crowd and compact at confluence. These findings suggest that cell–cell contacts are not required and that it is a change in cell shape, resulting from the highly compacted cellular architecture, which mediates the effect of confluence on OCI-5 expression.

Spheroid Culture of IEC-18 Upregulates OCI-5

To test the possibility that OCI-5 is regulated by changes in cell shape, IEC-18 cells were cultured as three-dimensional, multicellular aggregates or "spheroids." Cells were plated as a single-cell suspension onto a tissue culture dish coated with a concentration of poly(HEMA) which was empirically determined to completely inhibit cell attachment. Cells quickly organized into multicellular aggregates and within 24 h, OCI-5 expression was induced roughly four- to fivefold relative either to the cells immediately before plating or to the cells plated onto tissue culture plastic at low density (Fig. 3). Increased expression is detectable up to 48 h, after which the aggregates dissolved and cell death ensued as evidenced by permeability to eosin staining and poor clonogenic ability in colony-forming assays (data not shown).

OCI-5 Is Downregulated by Cytoskeletal Changes Which Elongate Cells

The role of the cytoskeleton in regulating cell shape and its effect on OCI-5 expression were investigated using the cytoskeletal poison colchicine, an inhibitor of tubulin polymerization, and cytochalasin D, which prevents polymerization of actin filaments. On exposure to 2 μM colchicine IEC-18 cells irregularly spread and flattened out within 24 h (Fig. 4B). Concurrent with this change in morphology, a downregulation of OCI-5 in response to colchicine is observed (Fig. 5A). As shown in Fig. 5B, this is a dose-dependent response. Eosin exclusion confirmed that the cell shape change and OCI-5 downregulation occurred at nontoxic doses of colchicine.

Similar treatment of IEC-18 cells with cytochalasin D

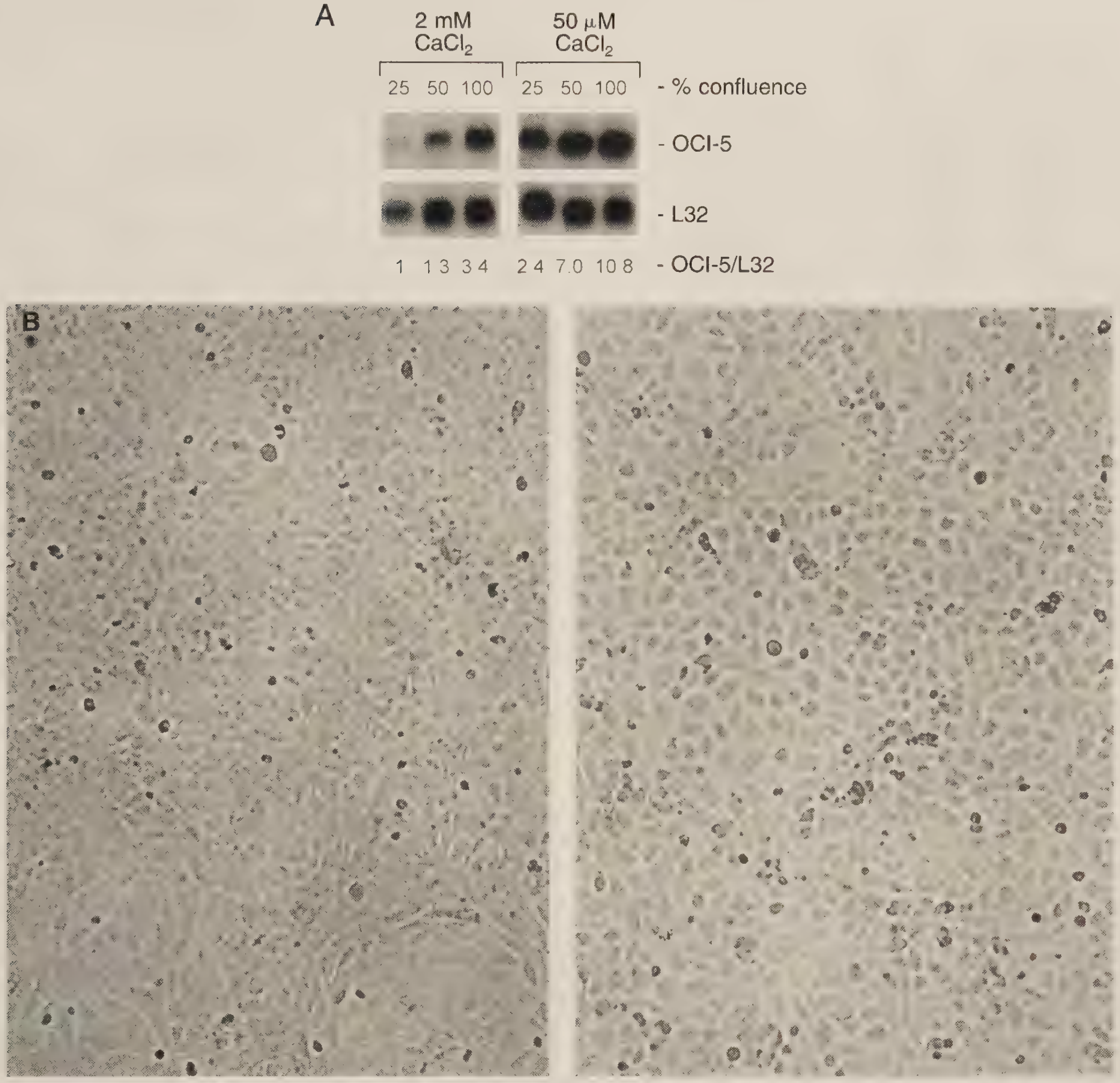
A
2 mM CaCl2
50 μM CaCl2
25 50 100 25 50 100 - % confluence
- OCI-5
- L32
1 1 3 3 4 2 4 7.0 10 8 - OCI-5/L32
B

FIG. 2. Analysis of IEC-18 in full and low Ca^{2+} medium. (A) Northern blot analysis of OCI-5 expression in full medium (2 m*M* $CaCl_2$) and low Ca^{2+} medium (50 *μM* $CaCl_2$) as cells grow to confluence. Levels of OCI-5 transcript are expressed as ratios generated from scanning densitometric data, normalized to ribosomal L32 as a loading control. The OCI-5 level at 25% confluence in full medium is arbitrarily set as 1, with other lanes expressed relative to it. (B) Photomicrographs of IEC-18 cells. Left, confluent cells in medium containing 2 m*M* $CaCl_2$. Right, confluent cells in low Ca^{2+} medium (50 *μM* $CaCl_2$). Original magnification 32×.

has no significant effect on OCI-5 expression relative to untreated controls (Fig. 5A). Consistent with this finding, there is no demonstrable alteration in the morphology of the cells in response to cytochalasin D (Figs. 4A and 4C). Thus, regulation of OCI-5 expression in IEC-18 is not a general effect of cytoskeletal poisons, but appears to be a function of the alteration in cell morphology.

Colchicine Inhibits both Confluence- and Low Ca^{2+}-Dependent Induction of OCI-5

To investigate whether confluence-, low Ca^{2+}-, and spheroid-induced upregulation of OCI-5 are all dependent on cytoskeletal tubulin polymerization, colchicine treatment was applied to each experimental situation. The effects of colchicine on OCI-5 expression in IEC-18 spheroids could not be assessed. Without an intact cytoskeleton, cells failed to form spheroids and quickly degraded such that no RNA could be recovered from the cells. Colchicine treatment of confluent IEC-18 is depicted in Fig. 5A where a 3.3-fold reduction in OCI-5 expression relative to untreated controls is observed. Similar results are seen when treating subconfluent cells with colchicine except that OCI-5 levels decrease

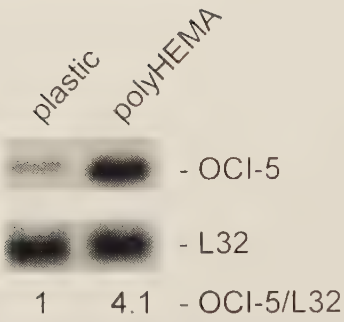

FIG. 3. Northern blot analysis of OCI-5 in IEC-18 cultured over poly(HEMA). Subconfluent cells were plated either onto tissue culture plastic at low cell density or onto a dish coated with 0.4 mg/cm^2 poly(HEMA). RNA harvested 24 h later was analyzed for OCI-5 expression, normalized to ribosomal L32. Ratios of OCI-5/L32 are expressed relative to cells on plastic.

beyond the limits of detection by Northern probing (not shown).

The ability of colchicine to inhibit the induction of OCI-5 in IEC-18 cultured under conditions of low Ca^{2+} is seen in Fig. 6. The level of OCI-5 expressed by subconfluent cells in full medium is designated 1. Colchicine treatment abrogates the low Ca^{2+}-dependent induction of OCI-5 in subconfluent cells (2.9- to 1.6-fold) and the superinduction seen in confluent cells (7.1- to 1.7-fold). In both cases, the levels of OCI-5 expression are reduced to approximately that of subconfluent cells grown in full medium, suggesting that colchicine, at least at a concentration of 2 μM, does not completely abolish the effects of low Ca^{2+} culture.

Vanadate Can Abolish OCI-5 Induction

One of the hallmarks of confluence is the phenomenon of contact inhibition, the precise underlying mechanism of which remains to be ascertained. However, protein–tyrosine phosphatases (PTPs) have been directly linked to density-dependent growth arrest (23) and the PTP inhibitor sodium orthovanadate (vanadate) has been used to permit cells to overcome contact inhibition and stimulate anchorage-independent proliferation [24, 25]. Thus, vanadate treatment confers malignant-like properties to cells. The induction of OCI-5 with confluence and its complete downregulation during *ras*-induced oncogenic transformation suggested that vanadate might affect OCI-5 expression. To address this hypothesis, IEC-18 cells were allowed to grow to confluence in the presence of vanadate and under these conditions, a dose-dependent inhibition of OCI-5 induction was observed (Fig. 7). Similar to what was observed when IEC-18 cells were oncogenically transformed (26), vanadate additionally had the effect of forcing the cells to adopt a more spindly configuration.

When vanadate was added to low Ca^{2+} or spheroid cultures of IEC-18, a reduction in the expression of OCI-5 was observed in both cases (Fig. 8). The magni-

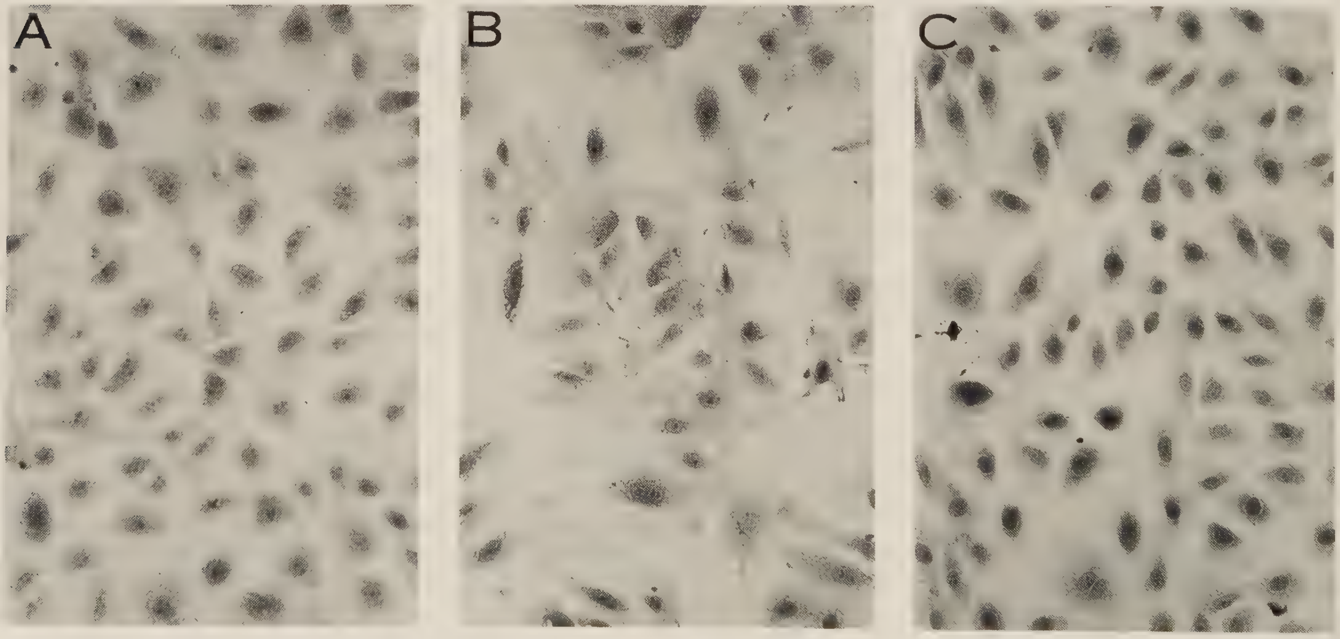

FIG. 4. Photomicrographs of IEC-18 cells treated with cytoskeletal poisons. IEC-18 cells were plated for 24 h in (A) the absence of cytoskeletal poison, (B) in the presence of 2 μM colchicine, and (C) in the presence of 2 μM cytochalasin D. Original magnification, 64×, MG/G stain.

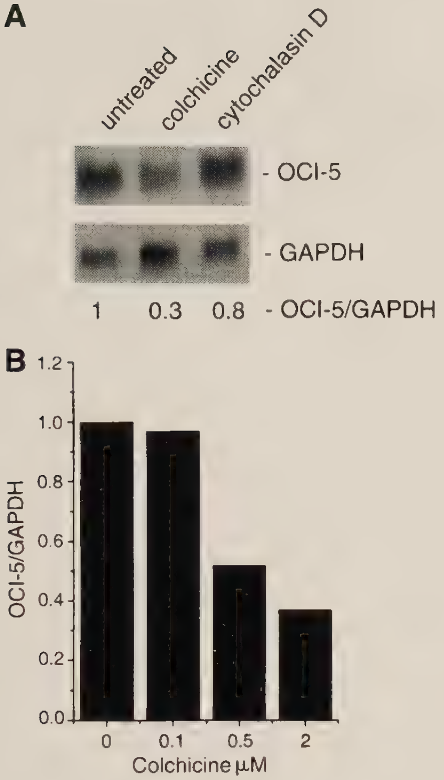

FIG. 5. Northern blot analysis of IEC-18 cells treated with cytoskeletal poisons. (A) Confluent IEC-18 cells were treated for 24 h with 2 μM colchicine or cytochalasin D. Ratios generated from scanning densitometric data are normalized to GAPDH as a loading control and expressed relative to untreated cells. (B) Dose-dependent downregulation of OCI-5 by colchicine. Bars represent scanning densitometric data from Northern blots. Levels of OCI-5, normalized to GAPDH, are expressed relative to untreated cells. Similar results are obtained when OCI-5 levels are normalized to ribosomal L32.

tude of the reductions caused by vanadate treatment in low Ca^{2+} or spheroid cultures are roughly consistent with the levels of induction by these same treatments seen previously, i.e., approximately two- and fivefold, respectively. Thus, it appears that confluence, low Ca^{2+}, and spheroid induction of OCI-5 expression are all mediated through a signaling pathway which involves PTPs.

Induction of OCI-5 Expression Is Regulated at the Level of Transcription

The induction of OCI-5 in IEC-18 cells with confluence and its downregulation upon *ras* transformation are regulated at the transcriptional level (unpublished observations). To determine whether the same mechanism applies to the induction of OCI-5 by changes in cell shape, nuclear run-on analysis was performed. Figure 9A shows the relative effects on the transcription rate of OCI-5 of confluence and low Ca^{2+} culture. These observations are consistent with what is seen on a Northern blot with these cells. Confluence increases OCI-5 transcription by 3.3-fold (relative to the subcon-

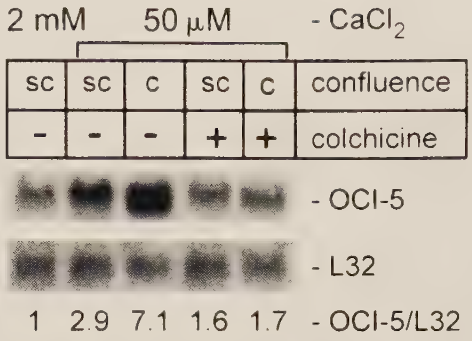

FIG. 6. Northern blot analysis of the effects of colchicine on low Ca^{2+} culture. IEC-18 cells were cultured in low Ca^{2+} medium (50 μM $CaCl_2$) at subconfluence (sc) and confluence (c) in the presence or absence of 2 μM colchicine for 24 h before RNA was harvested. OCI-5 levels, normalized to ribosomal L32, are expressed relative to the level of OCI-5 in subconfluent cells grown in full medium (2 mM $CaCl_2$).

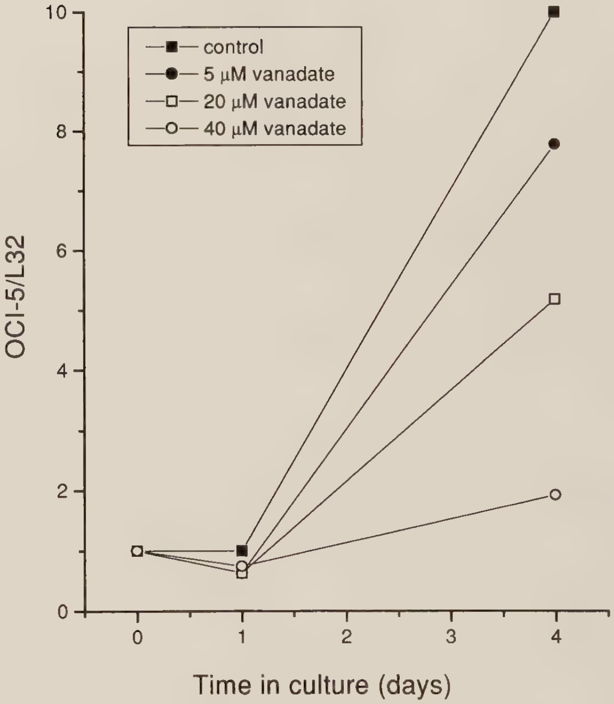

FIG. 7. Treatment of IEC-18 with sodium orthovanadate. RNA was harvested on the days indicated from cells allowed to grow to confluence in the presence of 0–40 μM vanadate. Data were generated from scanning densitometric analysis of Northern blots with OCI-5 levels normalized to L32. Similar results were obtained in three separate trials and when normalized to GAPDH.

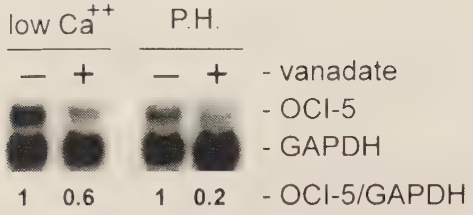

FIG. 8. Northern blots demonstrating effects of vanadate on culture of IEC-18 in low Ca^{2+} and poly(HEMA). Cells grown in either low Ca^{2+} or polyHEMA (P.H.) were treated with 20 μM vanadate for 24 h before RNA was isolated. OCI-5 transcript levels are expressed relative to untreated parallel cultures in each case.

fluent cells in full medium) and low Ca^{2+} culture by 5-fold. The superinduction of OCI-5 expression in low Ca^{2+} medium at confluence is also observed when the rate of OCI-5 transcription is compared (12-fold).

Similarly, Fig. 9B depicts the transcriptional downregulation of OCI-5 after treatment of cells with colchicine. The fourfold reduction in transcription is roughly consistent with the magnitude of the reduction seen on a Northern blot. Nuclear run-on analysis of spheroid cells could not be performed due to technical difficulties in dissociating the spheroids and maintaining intact nuclei.

DISCUSSION

Heparin sulfate proteoglycans are often abundant and developmentally regulated at sites of active morphogenesis. To investigate the expression of the OCI-5 transcript in the developing intestine, different regions of the fetal intestine were analyzed over Days 16 to 18 of gestation in the rat. During this time period the intestinal endoderm undergoes rapid proliferation and morphogenesis from a stratified epithelium to the simple epithelium lining the crypts and villi characteristic of the adult tissue. Initially, the OCI-5 transcript is detected at high levels in the stratified endoderm but not in the surrounding mesoderm. As the endodermal cells proliferate and differentiate, they rapidly lose their expression of OCI-5. The decrease in expression in the endoderm is correlated with a dramatic increase in expression in a ring of the mesenchyme adjacent to the endoderm. As the intestine develops, expression of OCI-5 in the mesenchyme radiates toward the outer perimeters of the intestine away from the lumen, becoming more diffuse as the mesenchyme undergoes morphological changes to form the mature crypt–villus structure.

Similar patterns of transient and reciprocal endodermal/mesenchymal expression during development have also been reported for neuregulin [12], CdxA [13], and syndecan-1 [15]. These molecules are believed to be involved in the condensation and differentiation of mesenchymal cells in epithelial–mesenchymal interactions during morphogenesis. Critical interactions between the endoderm and the surrounding mesenchyme during morphogenesis may be modulated by proteoglycans present at the cell surface. The pattern of expression of OCI-5 is consistent with such a function. In addition, *in situ* hybridization can detect OCI-5 expression in other tissues undergoing significant epithelial–mesenchymal interactions such as the kidney, tooth, trachea, and lungs as well as in developing bone and liver (Z. M. Wong, unpublished observations), all tissues which are known to be affected in SGBS.

To address the paucity of information concerning mechanisms of gene regulation during intestinal morphogenesis, the confluence-dependent induction of OCI-5 in the primitive intestinal epithelial cell line IEC-18 was characterized. Attempts to elucidate which aspect of cellular confluence mediates the induction of OCI-5 reveals no role for cellular quiescence, signals in the basement membrane, or factors secreted into the conditioned medium. Using IEC-18 cells, it is demonstrated that manipulations which result in the cells acquiring a more rounded or spherical morphology result in an upregulation of OCI-5 expression. These manipulations include (1) cellular compaction at confluence, (2) culture in low Ca^{2+} medium, and (3) organization into multicellular spheroids. Conversely, conditions which result in the cells taking on a more spread, flattened, elongated, or spindle shape, including (1) subconfluence, (2) *ras* transformation, (3) cytoskeletal disruption with colchicine, and (4) treatment with vanadate, bring about a downregulation of OCI-5 expres-

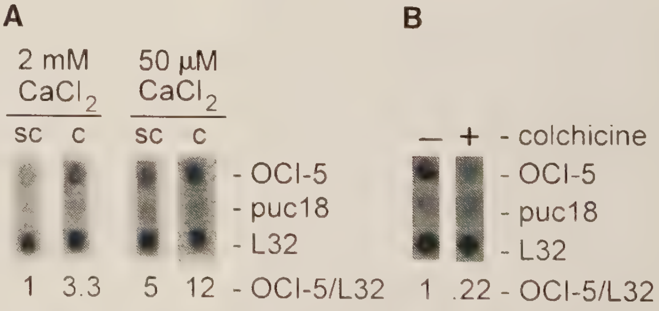

FIG. 9. Nuclear run-on analysis of OCI-5 transcription in high and low Ca^{2+} concentration and in the presence and absence of colcicine. (A) The rate of OCI-5 transcription in subconfluent (sc) and confluent (c) IEC-18 in full medium (2 mM CaCl$_2$) and low Ca^{2+} medium (50 μM CaCl$_2$). Relative rates of OCI-5 transcription are expressed with respect to that seen in subconfluent IEC-18 cells cultured in full medium. (B) Transcription rate of OCI-5 after treatment of IEC-18 with 2 μM colchicine for 24 h expressed relative to untreated parallel cultures. For quantitation, the densitometric counts from the negative control, puc18, were subtracted within each sample before OCI-5 levels were normalized to that of L32.

sion. Taken together, these data suggest that OCI-5 is regulated in IEC-18 cells by cell shape.

The OCI-5 transcript is also upregulated in confluent, differentiating CaCo-2, a human colon carcinoma cell line. At high cell density, these cells begin to form dome-like structures, and differentiation over many weeks is paralleled by a steady increase in OCI-5 expression (J. Hamid, unpublished observations). Differentiation of IEC-18 cells at confluence, on plastic, was not observed and, to our knowledge, has never been reported. It is therefore unlikely that differentiation induces the expression of OCI-5 at confluence.

That confluence and low Ca^{2+} culture operate through the same mechanism is suggested by the finding that their induction of OCI-5 is sensitive to the cytoskeletal poison colchicine. Nuclear run-on analysis also demonstrates that confluence, low Ca^{2+}, and colchicine all affect OCI-5 transcription rates. In addition to transcriptional initiation, confluence-dependent induction of OCI-5 has been shown to be regulated by the release of a block to elongation [18]. It remains to be determined whether the cell shape-associated changes in OCI-5 transcription rate also include a contribution from elongation control.

A common molecular pathway for cell shape-regulated expression of OCI-5 is further supported by abrogation of its confluence-, low Ca^{2+}-, and spheroid-mediated induction by treatment of cells with vanadate. Downregulation by a tyrosine phosphatase inhibitor implies a role for PTPs in the expression of OCI-5: the increased PTP activity associated with cellular confluence may mediate the induction of OCI-5.

That cell shape can regulate gene expression and cell growth is a long-standing concept [27] which has recently taken on new interest in the areas of tissue-specific and developmental biology [28, 29]. Genes which are known to be regulated by changes in cell shape include Wnt5a [29a], lactoferrin [30], and 92-kDa gelatinase B [31], in addition to many of the cytoskeletal proteins [32]. A novel approach to the field of cell shape and gene regulation has recently been described in the elegant studies of Ingber and colleagues. Their mechanochemical model for signal transduction [33, 34] states that mechanical stresses within the cytoskeleton can be transduced into signals which alter a cell's gene expression and behavior. Either by plating cells on substrata having various abilities to resist cytoskeletal tensions, or through the use of ligand-coated magnetic beads and external magnetic fields, their model has been validated in multiple cell types [35–37]. Whether mechanotransduction is involved in the regulation of OCI-5 remains an intriguing question.

RNA *in situ* hybridization has revealed patterns of OCI-5 expression which support a role for this proteoglycan in morphogenesis of the intestinal epithelium. Cell-surface proteoglycans such as OCI-5 may act as coordinators of cell growth and migration through interactions with other cells, matrix components, or growth factors, processes which are critical during tissue rearrangement and morphogenesis. The density-dependent induction of OCI-5 in IEC-18 cells has been shown to be a function of the change in cell shape associated with cell confluence. Conditions where the cell acquires a more rounded or spherical shape lead to an increase in OCI-5 gene transcription. Cells are likely to assume such a morphology during intestinal morphogenesis, when cells must initially compact and then break cell–cell and cell–matrix contacts to facilitate cellular migration and reordering. Once morphogenesis is complete, downregulation of OCI-5 is correlated with enterocytes acquiring the cuboidal shape characteristic of this columnar epithelium. Cell shape regulation of gene expression may be a convenient mechanism whereby a developing tissue can control the expression of critical genes precisely at the time when their functions are required.

We thank Dr. Danielle Cano-Gauci for critically reading the manuscript and Rose Pullano for excellent technical assistance. This work was supported by a Terry Fox Program Project to R.N.B.

REFERENCES

1. Filmus, J., Church, J. G., and Buick, R. N. (1988) *Mol. Cell. Biol.* **8**(10), 4243–4249.
2. Filmus, J., Shi, W., Wong, Z. M., and Wong, M. J. (1995) *Biochem. J.* **311**(Part 2), 561–565.
3. Pilia, G., Hughes-Benzie, R. M., MacKenzie, A., Baybayan, P., Chen, E. Y., Huber, R., Neri, G., Cao, A., Forabosco, A., and Schlessinger, D. (1996) *Nature Genet.* **12**(3), 241–247.
4. Trier, J. S., and Moxey, P. C. (1979). *Ciba Found. Symp.* **70,** 3–29.
5. Deren, J. J. (1987) *in* "Handbook of Physiology. Vol. III. Intestinal Absorption," chap. 62, Am. Physiol. Soc., Washington, DC.
6. Quaroni, A. (1986) *Proc. Natl. Acad. Sci. USA* **83**(6), 1723–1727.
7. Quaroni, A. (1986) *J. Natl. Cancer Inst.* **76**(4), 571–585.
8. Benchimol, S., Fuks, A., Jothy, S., Beauchemin, N., Shirota, K., and Stanners, C. P. (1989) *Cell* **57**(2), 327–334.
9. Quaroni, A., and Isselbacher, K. J. (1981) *J. Natl. Cancer Inst.* **67**(6), 1353–1362.
10. Watanabe, K., Yamada, H., and Yamaguchi, Y. (1995) *J. Cell Biol.* **130**(5), 1207–1218.
11. David, G. (1993) *FASEB J.* **7**(11), 1023–1030.
12. Kato, M., Saunders, S., Nguyen, H., and Bernfield, M. (1995) *Mol. Biol. Cell* **6**(5), 559–576.
13. Salmivirta, M., and Jalkanen, M. (1995) *Experientia* **51**(9–10), 863–872.
14. Steinfeld, R., Van Den Berghe, H., and David, G. (1996) *J. Cell Biol.* **133**(2), 405–416.
15. Hughes-Benzie, R. M., Hunter, A. G., Allanson, J. E., and Mackenzie, A. E. (1992) *Am. J. Med. Genet.* **43**(1–2), 428–435.

16. Golabi, M., and Rosen, L. (1984) *Am. J. Med. Genet.* **17,** 345–358.

17. Terespolsky, D., Farrell, S. A., Siegel-Bartelt, J., and Weksberg, R. (1995) *Am. J. Med. Genet.* **59,** 329–333.

18. Li, M., Pullano, R., Li, H. L., Filmus, J., and Buick, R. N. (1997) *Oncogene,* in press.

18a. Davis, C. A., Noble-Topham, S. E., Rossant, J., and Joyner, A. L. (1988) *Genes Dev.* **2**(3), 361–371.

19. Elliott, E. M., Sarangi, F., Henderson, G., and Ling, V. (1985) *Can. J. Biochem. Cell. Biol.* **63**(6), 511–518.

20. Fort, P., Marty, L., Piechaczyk, M., el Sabrouty, S., Dani, C., Jeanteur, P., and Blanchard, J. M. (1985) *Nucleic Acids Res.* **13**(5), 1431–1442.

21. Rajchel, A., Chan, Y. L., and Wool, I. G. (1988) *Nucleic Acids Res.* **16**(5), 2347.

22. Gospodarowicz, D., Lepine, J., Massoglia, S., and Wood, I. (1984) *J. Cell Biol.* **99**(3), 947–961.

23. Pallen, C. J., and Tong, P. H. (1991) *Proc. Natl. Acad. Sci. USA* **88**(16), 6996–7000.

24. Klarlund, J. K. (1985) *Cell* **41**(3), 707–717.

25. Rijksen, G., Voller, M. C., and Van Zoelen, E. J. (1993) *J. Cell. Physiol.* **154**(2), 393–401.

26. Buick, R. N., Filmus, J., and Quaroni, A. (1987) *Exp. Cell Res.* **170**(2), 300–309.

27. Folkman, J., and Moscona, A. (1978) *Nature* **273**(5661), 345–349.

28. Ingber, D. E., and Folkman, J. (1989) *Cell* **58**(5), 803–805.

29. Ingber, D. E., Dike, L., Hansen, L., Karp, S., Liley, H., Maniotis, A., McNamee, H., Mooney, D., Plopper, G., Sims, J., *et al.* (1994) *Int. Rev. Cytol.* **150,** 173–224. (a) Huguet *et al.* (1995).

29a. Huguet, E. L., Smith, K., Bicknell, R., and Harris, A. L. (1995) *J. Biol. Chem.* **270**(21), 12851–12856.

30. Howlett, A. R., Close, M. J., Roskelley, C. D., Desprez, P. Y., Bailey, N., Teng, C. T., Stampfer, M. R., Bissell, M. J., and Yaswen, P. (1995) 86th Annual Meeting of the American Association for Cancer Research, Toronto, Canada.

31. MacDougall, J. R., and Kerbel, R. S. (1995) *Exp. Cell. Res.* **218**(2), 508–515.

32. Ben-Ze'ev, A. (1991) *BioEssays* **13**(5), 207–212.

33. Plopper, G. E., McNamee, H. P., Dike, L. E., Bojanowski, K., and Ingber, D. E. (1995) *Mol. Biol. Cell* **6**(10), 1349–1365.

34. Wang, N., Butler, J. P., and Ingber, D. E. (1993) *Science* **260**(5111), 1124–1127.

35. McNamee, H. P., Liley, H. G., and Ingber, D. E. (1996) *Exp. Cell Res.* **224**(1), 116–122.

36. Hansen, L. K., Mooney, D. J., Vacanti, J. P., and Ingber, D. E. (1994) *Mol. Biol. Cell* **5**(9), 967–975.

37. Ingber, D. E., Prusty, D., Sun, Z., Betensky, H., and Wang, N. (1995) *J. Biomech.* **28**(12), 1471–1484.

Received November 21, 1996
Revised version received April 8, 1997

EXPERIMENTAL CELL RESEARCH **235,** 13–21 (1997)
ARTICLE NO. EX973647

Human Intervertebral Disc Cells from the Annulus: Three-Dimensional Culture in Agarose or Alginate and Responsiveness to TGF-β1

Helen E. Gruber,[1] E. Carl Fisher, Jr., Bhaloo Desai, Audrey A. Stasky,
Gretchen Hoelscher, and Edward N. Hanley, Jr.

Department of Orthopaedic Surgery, Carolinas Medical Center, P.O. Box 32861, Charlotte, North Carolina 28232

Cell culture procedures were developed for use with surgical and normal control specimens of the annulus of the human intervertebral disc. Cells were established in monolayer explant culture and seeded into three-dimensional growth environments of alginate or agarose; under these growth conditions cells assumed a rounded phenotype and formed colonies. A novel method of layering suspensions of cells onto cell well inserts proved technically much easier than the microbead culture method. Immunohistochemistry was utilized to demonstrate *in vitro* production of the following extracellular matrix components: types I, II, III, and VI collagen, 4-*S*-chondroitin sulfate, and keratan sulfate. Young and old age- and gender-matched cells grown in the presence of TGF-β1 showed significant enhancement of proliferation after 4 days of exposure to TGF-β with a lessened mitogenic response present after 10 days. Molecular studies of proteoglycan gene expression showed that at 4 days young normal cells had increased biglycan, but not decorin, message levels. Decorin expression was unchanged at Day 4 and decreased or shut off by Day 10. Results support the use of three-dimensional culture systems for *in vitro* evaluation of human disc cell function and expand our understanding of the *in vitro* behavior of these cells.

© 1997 Academic Press

INTRODUCTION

In spite of the large health care costs associated with degenerative disc disease [1], the cell biology of the human intervertebral disc cell has been neglected compared to the knowledge available on chondrocytes or bone cell populations. Chelberg *et al.* have studied human disc cells cultured in alginate beads and have provided evidence that more than one distinctive cell population resides in the disc [2]. Maldonado and Oegema have used the alginate bead technique to study canine disc cells in culture [3], and cells from the rat disc have been grown in monolayer culture by Ichimura *et al.* [4].

The present study focuses upon development of cell culture techniques that are applicable to culture of human cells from small portions of disc removed during surgical procedures. Because of the limited amount of tissue available from surgery, and because of the low cell numbers present in the adult disc, we have found that collagenase digestion techniques often could not yield a sufficient number of cells for experimental study. The present report describes an explant methodology for establishment of primary cultures which can then be cryopreserved, further passaged in monolayer culture, or seeded into alginate or agarose three-dimensional microenvironments. Three-dimensional cell culture is a preferred culture method for chondrocytes, a cell type similar to at least some members of the disc cell population, and is known to dedifferentiate in monolayer culture and reexpress a characteristic type II collagen extracellular matrix production when placed in agarose culture [5–7]. Since the alginate bead technique is tedious, the novel application described here of seeding cells into alginate or agarose and then layering the cell suspension onto culture plate well inserts is a useful technical approach which lends itself well to cell proliferation assays, proteoglycan synthesis analysis, light and electron microscopic morphologic studies, and molecular methods for determination of gene expression. Using these methodologies, evidence is presented which shows that cells from the human annulus of both old and young individuals can respond to the mitogenic stimulus of TGF-β1. These data help advance our understanding of cell populations derived from the human disc and their behavior in three-dimensional culture.

MATERIALS AND METHODS

Surgical and normal donor specimens. Experimental study of disc surgical specimens was approved by our institutional Research Review Committee and human subjects Institutional Review Board. Patient specimens were taken from surgical disc procedures performed on individuals with idiopathic scoliosis, herniated disc, degenerative disc disease, recurrent disc herniation, or spinal stenosis.

---

[1] To whom reprint requests and correspondence should be addressed. Fax: (704) 355-2845. E-mail: hgruber@carolinas.org.

0014-4827/97 $25.00
Copyright © 1997 by Academic Press
All rights of reproduction in any form reserved.

Specimens were transported to the laboratory (less than 30 min after surgical removal) in sterile modified minimal essential medium with Earle's salts (MEM, Gibco, Grand Island, NY) with 1% (v/v) L-glutamine (Irvine Scientific, Santa Ana, CA), 1% (v/v) nonessential amino acids (Irvine Scientific), and 1% (v/v) penicillin–streptomycin (Irvine Scientific), but without added serum. Control specimens, obtained via the NCI Cooperative Human Tissue Network, were shipped overnight to the laboratory in MEM with penicillin–streptomycin. Specimens were incubated in three 15-min rinses of MEM with 1% Fungizone (Irvine Scientific) as a precaution against contamination during specimen removal at participating donor centers.

Data are reported here for results of studies with cells derived from the annulus. Cultures from the nucleus have been obtained using the protocol described here. Since surgical specimens consist of tissue from the annulus, however, experimental results reported here focus on cells derived from the annulus only.

For both normal and patient specimens, data were recorded on age and gender, cause of death (for normal specimens), medications, and other medical conditions if information was available.

Disc cell culture. All cultures were grown at 37°C under conditions of 95% relative humidity and 5% CO_2. Agarose and alginate studies described below used cells seeded at a concentration of 50,000 cells per insert (1.0×10^6 cells/ml).

Primary disc cell cultures. Using sterile reagents and aseptic techniques under a laminar flow hood, surgical specimens were rinsed with phosphate-buffered saline (PBS, pH 7.4) and regions of annulus or nucleus visually identified. Representative pieces were designated for subsequent use in morphology or cell culture. Portions designated for culture were further examined and any cartilaginous or vascular regions carefully removed. Tissue was rinsed twice in MEM to remove residual debris, minced with a scalpel into small portions (1–2 mm^2), plated into T25 tissue culture flasks (Costar, Cambridge, MA), and anchored by placement of a sterile nylon mesh (Spectra Mesh, Spectra Laboratory Products) over explant fragments. Cells were grown in MEM as described above with the addition of 20% (v/v) fetal bovine serum (Gibco) and fed every 2 days.

Subsequent disc cell passages. Cells were observed and photographed at feedings. When primary cultures showed a confluent outgrowth of cells from the nylon mesh, cell cultures were trypsinized (1:250, trypsin (0.5 g/liter), EDTA (0.2 g/liter)) (Irvine Scientific) and a split ratio of 1:4 was used for subculturing. Cell viability, determined by trypan blue exclusion, averaged 96% on monolayer culture.

Alginate preparation and culture of disc cells in alginate. Alginate was prepared as a modification of methods of Maldonado *et al.* [3] and Guo *et al.* [8]. A 1.2% solution of Keltone LV alginate (Kelco, San Diego, CA) was prepared in 0.9% physiological saline with stirring for 1 h. The alginate solution was sterilized by filtering through a 0.2-μm bottle-top filter fitted onto a sterile bottle. Trypsinized cell cultures were assayed for cell viability, the required volume of cell suspension was centrifuged at 500 rpm for 5 min in an IEC MP4R centrifuge, and the medium was subsequently aspirated off. An appropriate volume of sterile 1.2% Keltone LV alginate solution was added to attain the desired cell/alginate suspension. Cells were mixed in the alginate by gentle thorough pipetting.

Costar Transwell Clear Inserts (Costar) were placed in multiwell plates, and the desired amount of alginate/cell suspension was carefully added to the bottom of the insert well without formation of air bubbles. If the alginate did not completely cover the bottom of the well, the plate was gently tapped on the work surface of the hood to move the alginate to the bottom. A correctly prepared insert showed a fully covered filter with a meniscus formed in the insert. For a 24-well plate, 50 μl of alginate/cell suspension was added to each insert. After the alginate/cell suspension was in place, each insert was carefully lifted with sterile forceps and the desired volume of 102 m*M* $CaCl_2$ polymerizing solution was added to the well. This volume covered the bottom of the filter, but was not enough to allow the $CaCl_2$ solution to enter into the insert. For a 24-well plate, 1 ml of 102 m*M* $CaCl_2$ polymerizing solution was added per well. The inserts were incubated in $CaCl_2$ polymerizing solution for 4 min, which was then aspirated out by carefully lifting the filter insert to introduce a pipette. Wells were rinsed with MEM with 20% FBS (2.5 ml/well for 24-well plates). The rinsing volume filled both well and insert, was allowed to stand for 1 min, and was aspirated off, and wells were filled with MEM plus serum (as described above), 1.0 mg/well for 24-well plates.

Depolymerization of alginate/cell suspensions. To remove cells from the alginate, wells were rinsed twice with 0.15 *M* $NaCl_2$ (2.5 ml/well for 24-well plates) by lifting the insert and pipetting into the well. The rinse solution was incubated for 1 min and was aspirated off via the solution under the insert (the solution within the insert was not aspirated off). After the second rinse, the remaining liquid from the insert was wicked off by gently touching a twisted sterile gauze square to the side of the tipped well. Three times the volume of the alginate in dissolving buffer (55 m*M* sodium citrate and 0.15 *M* $NaCl_2$) was added to the inside of the insert and plates were incubated at 37°C for 10 min with shaking. The contents of the insert were gently pipetted to ensure complete dissolution of the alginate. From this point, cells were either passaged for further study or assayed with additional methods described below.

Cell culture in agarose. Cells were also studied in low-gelling-temperature agarose (SeaPlaque or SeaPrep, FMC Bioproducts, Rockland, ME) using the insert methodologies described above for alginate, adapting the methods of Aydelotte *et al.* [9, 10]. Both types of agarose were dissolved with heat at a concentration of 1.25% in PBS (Biofluids, Rockville, MD). SeaPlaque agarose was filter sterilized with a 0.45-μm syringe filter (Nalgene, Rochester, NY); SeaPrep agarose was autoclaved.

Proteoglycan synthesis. Total proteoglycan synthesis was determined using modifications of the methods of Guo *et al.* [8] and Bayliss *et al.* [11]. When used with alginate cell suspensions, the alginate was first depolymerized (see above). Cells were incubated in the presence of 10 μCi/ml [^{35}S]sulfate for the desired period and were extracted with 4 *M* guanidine hydrochloride, 0.05 *M* sodium acetate, in the presence of the protease inhibitors 0.01 *M* EDTA, 0.1 *M* 6-aminohexanoic acid, and 0.005 *M* benzamidine hydrochloride for 48 h at 4°C. Dialysis was performed using an Amicon Stirred Cell unit with a YM-2 filter under nitrogen. Dialyzed extracts were eluted through a Sephadex G-50 column with guanidinium hydrochloride, 25 0.5-ml fractions were collected, and radioactivity was determined with liquid scintillation spectrometry.

Tritiated thymidine incorporation assay. DNA synthesis was measured by pulse labeling the cultures with 2 μCi/ml of [^{3}H]-thymidine (Amersham) during the last 24 h of culture. Aliquots were taken and analyzed to determine total DNA content using a fluorometric procedure [12]. NaOH (5 *N*, 25 μl) was added to additional aliquots and the tubes were incubated overnight in a shaking (150 rpm) water bath at 58°C. The next day, 100 μl of a 10 mg/ml bovine serum albumin (Fluka Biochemical, Switzerland) solution was added to each test tube. DNA was precipitated at 4°C for 1 h with the addition of 900 μl of 10% trichloroacetic acid (Sigma) solution. The DNA precipitate was collected on 2.5-cm glass microfiber filters (Whatman, Maidstone, England) and radioactivity was determined using a Beckman LS-6000 scintillation counter (Beckman Instruments, Fullerton, CA). Results were expressed as cpm [^{3}H]thymidine uptake/μg DNA. Each point is the mean of three to six replicate samples.

Experimental design for TGF-β experiments. Studies of the effects of TGF-β and IGF-I on disc cells utilized a design testing age- and gender-matched patient and normal cells. Cells from both young and old normals and patients were tested. Growth factors were solubilized in PBS at a concentration of 10 μg/ml and stored in aliquots at −80°C to minimize freeze/thaw alterations.

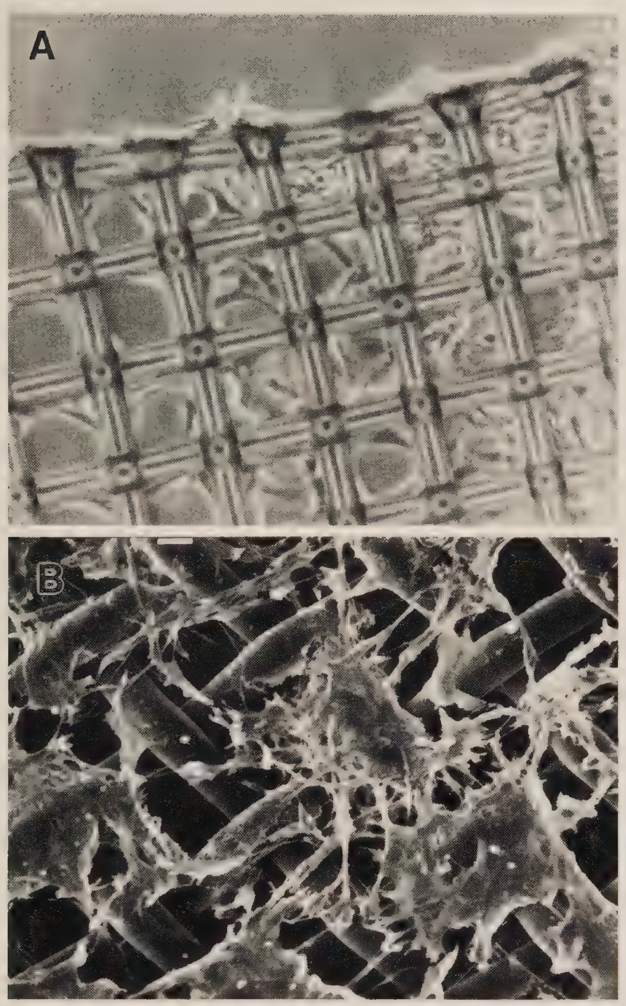

FIG. 1. Explant culture. (A) Phase-contrast photomicrograph of cells growing out from a disc explant fragment onto the nylon mesh (×130). (B) Scanning electron micrograph of cells spreading and extending processes onto the mesh (bar at upper left, 10 μm).

The dose–response study of the effect of TGF-β1 on cell proliferation utilized cells suspended in 1.25% LV Keltone alginate (Kelco) at a concentration of 1.0×10^6 cells/ml. Cell suspensions were plated into 24-well inserts and polymerized by the addition of 1.0 ml of 102 m*M* $CaCl_2$ for 4 min. Four inserts were set up for each concentration at each time point (Days 6, 8, and 10). Each well was fed with MEM supplemented with TGF-β1 (Sigma) at the following doses: control (no TGF-β1), 0.25, 0.50, 1.0, 2.5, and 5.0 ng/ml. Cell proliferation data, expressed as total [^{3}H]thymidine uptake/μg DNA, were obtained on Days 6, 8, and 10.

Experimental design for in vitro cell characterization of cells. Cells established in monolayer primary culture were seeded either into alginate or agarose layers on inserts (see above) (P1 cultures) or continued as monolayer P1 cultures which were subsequently split and used as the cell source for sequential P2, P3, or P4 passages seeded into alginate. Several cryopreserved cultures were thawed and expanded as P1 passages on monolayer with subsequent P2 and later passages seeded into alginate. Three-dimensional cultures were grown for 10 days with feeding three times per week. At the end of 10 days, medium was withdrawn and cultures were fixed with 1% neutral buffered formalin for 5 min. The insert was carefully cut from the plastic holder, wrapped gently in lens paper, placed in a tissue cassette in 70% ethanol, and processed using the short-cycle run on a paraffin processor (Shandon Lipshaw Hypercenter XP, Pittsburgh, PA). Adjacent sections cut *en face* were collected and utilized for immunohistochemical localization of rabbit anti-human collagen type I (1:100 dilution) or rabbit anti-human collagen type II (1:150 dilution) (Biodesign International, Kennebunk, ME), monoclonal anti-proteoglycan delta DI-4S (ICN, Costa Mesa, CA), monoclonal anti-keratan sulfate (Seikagaku Corp., Tokyo, Japan) using previously described techniques [13], monoclonal anti-human type III collagen (1:200 dilution) (Biodesign International), and monoclonal anti-human type VI collagen (1:400 dilution) (Seikagaku Corp.). Negative controls were processed minus primary antibodies. Localization utilized DAB colorimetric visualization of extracellular matrix constituents on serial sections of inserts.

Molecular methodologies. For these experiments, 500,000 cells/well were layered into alginate and placed on inserts and treated as described above. Paired replicate design utilized probing of RNA from control or TGF-β-treated cells for a housekeeping gene (GAPDH) and subsequently for either decorin or biglycan. With this design, the same RNA was probed and densitometric data could be expressed relative to GAPDH expression; this was important because of variable RNA loading/lane. Total RNA was isolated at Days 4 and 10 using the Clontech microisolation kit. Yields varied from 2 to 15 μg of total RNA. RNA was separated on a 1% agarose gel containing 3% formaldehyde. Gels were then transferred onto Boehringer nylon membranes overnight by standard capillary transfer. Membranes were cross-linked using a UV Stratalinker, after which blots were hybridized with the housekeeping probe GAPDH (Clontech) or with probes to aggrecan (GAP$_1$, bases 1816–2705; 889 bp), decorin (DEC, full length; 1600 bp), or biglycan (BIG, full length; 1685 bp) (probes courtesy of Dr. Peter Roughley with permission of Dr. Larry Fisher). Probes were labeled with [α-^{32}P]dCTP (Amersham) using the random-prime labeling method (Boehringer). Nylon blots were prehybridized using the Amersham rapid hybridization buffer for 5 h at 65°C using a Hybaid hybridization oven. Hybridization was performed using the same solution containing the denatured (100°C for 5 h) labeled probe for 18 h at 65°C. Excess probe label was removed with washes starting at 2× SSC (standard saline citrate)/0.1% SDS for 20 min at 65°C and ending with a wash in 0.1× SSC/0.1% SDS for 10 min.

Hybridized blots were exposed to X-ray film for 18 h at −80°C or to a Fujifilm Bio-imaging Analyzer BAS-1500 PhosphorImager screen for 18 h at room temperature, and the image was captured via an IP-MacBAS version 2 software package with subsequent quantitative densitometric analysis of the expressed bands. Values were first standardized to GAPDH gene expression and then results were expressed as percentages of control.

Morphologic studies. In vitro cell documentation utilized a phase-contrast microscope with Hoffman modulation contrast optics. For routine light microscopic study, alginate preparations were fixed in 10% neutral buffered formalin, embedded in paraffin or glycol methacrylate, sectioned, and stained with hematoxylin and eosin or Goldner's stain. For scanning microscopy, primary explants on nylon mesh were fixed in Karnovsky's fixative, dehydrated, critical point dried, and viewed with a JEOL 35C scanning electron microscope (10 kV). Transmission electron microscopy studies utilized preparations fixed in Karnovsky's fixative, postfixed in osmium tetroxide supplemented with 0.1% ruthenium red to enhance proteoglycan visualization [14], embedded in Spurr resin, thin-sectioned with an LKB ultramicrotome, grid stained, and viewed in a Phillips CM10 electron microscope.

Statistical analysis. Data are presented as mean ±SEM. SAS (version 6.11, SAS Institute, Inc., Cary, NC) and InStat (version 2.0, GraphPad Software, San Diego, CA) software were utilized for data analysis. One-way analysis of variance was conducted to examine

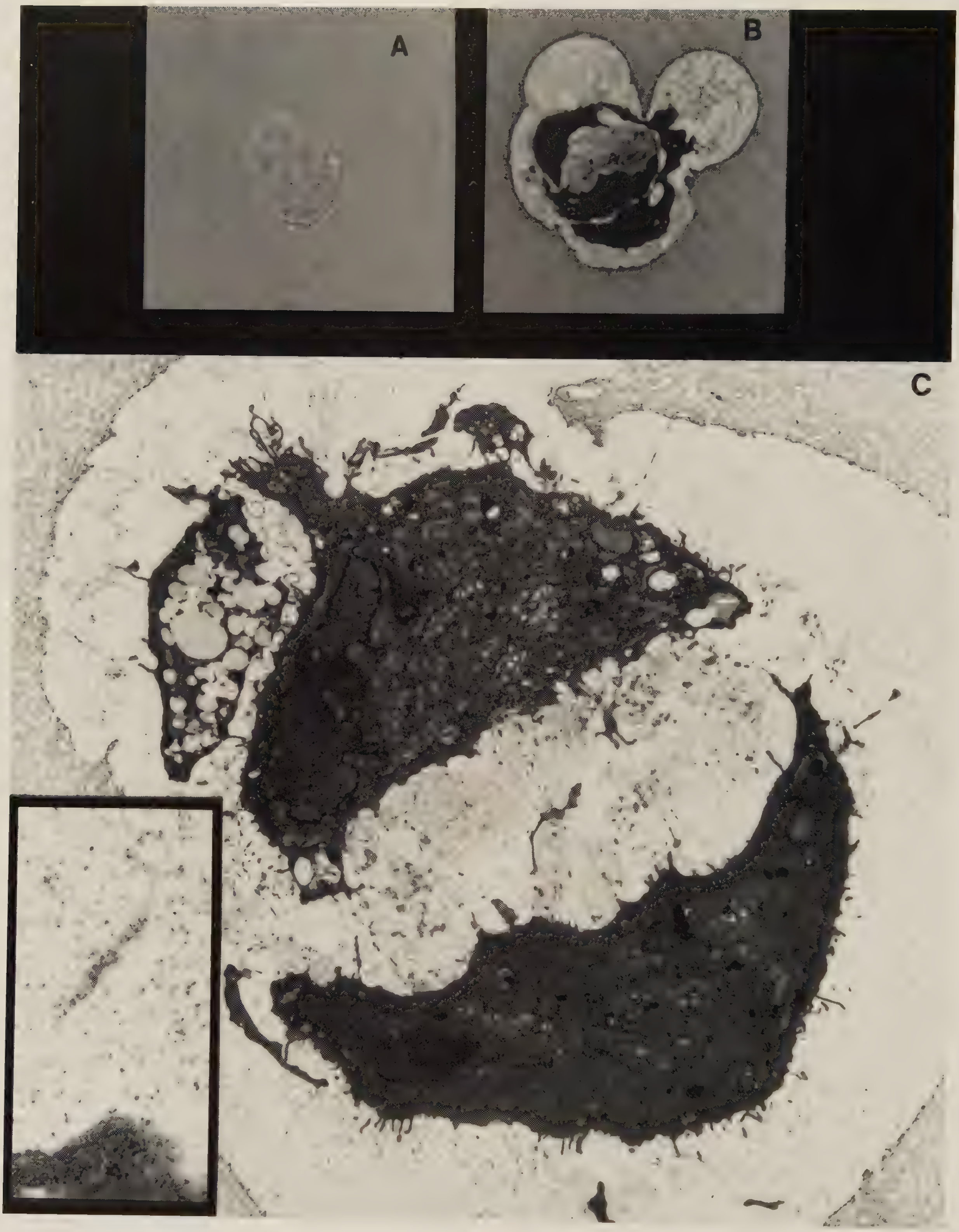

FIG. 2. Cells from the annulus of a 37-year-old female patient, first passage, growing in alginate. (A) Phase-contrast photomicrograph showing two small colonies which have formed after 11 days of culture (×30); (B) light micrograph of a colony from the culture in A embedded in glycol methacrylate and stained with Goldner's stain. Note the presence of matrix in the central region of the colony (×1900); (C) transmission electron micrograph of the same culture fixed in the presence of ruthenium red to enhance proteoglycans; inset shows banded collagen fibers in the extracellular matrix (×4200; insert, ×37,800).

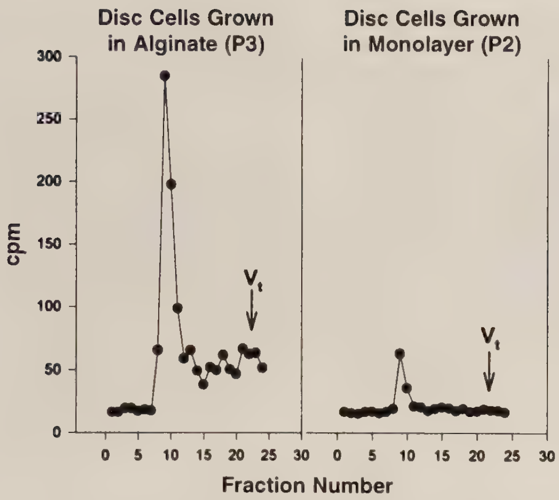

FIG. 3. Third-passage cells from a 44-year-old female patient show greatly increased ^{35}S incorporation in proteoglycans when cultured in alginate as compared to second passage cells from the same patient cultured in monolayer. (V_t is the inorganic K^+ peak, determined by atomic absorption spectroscopy, which is coincident with the inorganic salt peak and which marks the end of the eluted sample.)

the effects of growth factor dosage at specific time points for each individual cell culture. To determine significance between the doses in a single group, a Tukey–Kramer posttest was performed. Statistical significance was determined based upon P values $\leqslant 0.05$. Comparison of group means between different cell cultures was determined using Student's *t* test.

RESULTS

Establishment of Cultures in Monolayer and Alginate or Agarose

Use of the nylon mesh anchoring technique not only simplifies the feeding of cultures by anchoring fragments and thus preventing loss of fragments during cell feeding, but also provides a substrate for cell outgrowth (Fig. 1). Disc cells from both the annulus and the nucleus grew well on the mesh lattice and could easily be trypsinized. Early experiments tested various types of media (data not shown). α-MEM, which provides a greater calcium concentration, was not superior to MEM with 20% FBS. Neither ascorbic acid supplementation (50 μg/ml) nor use of Fetal Clone III medium or Nu-Serum offered any advantage. Nu-Serum plus ascorbic acid, in fact, appeared to significantly depress cell growth compared to MEM with either 10 or 20% FBS.

Even in the presence of high (20%) FBS, cells from the disc grew slowly; in some cases, cells required up to a month from initiation of explants until P1 cultures could be established. Doubling time in the presence of 10% FBS was 6.2 days, in 20% FBS was 3.4 days, and in 25% FBS was 3.5 days. Experience showed that cells completely deprived of serum for use as controls in growth factor experiments were not well maintained; for this reason control cells in the present studies were grown in the presence of 1% FBS, a technique which

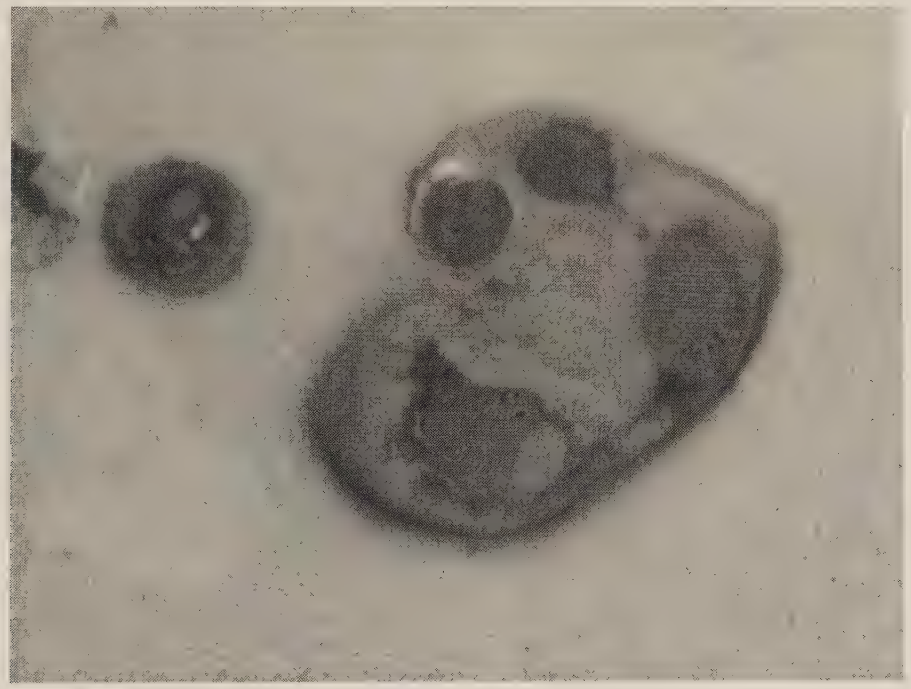

FIG. 4. Light photomicrograph of disc cells grown in agarose and stained with toluidine blue (Spurr embedment). Extracellular matrix is prominent between cells which were P4 and derived from the annulus of a 70-year-old normal donor (×980).

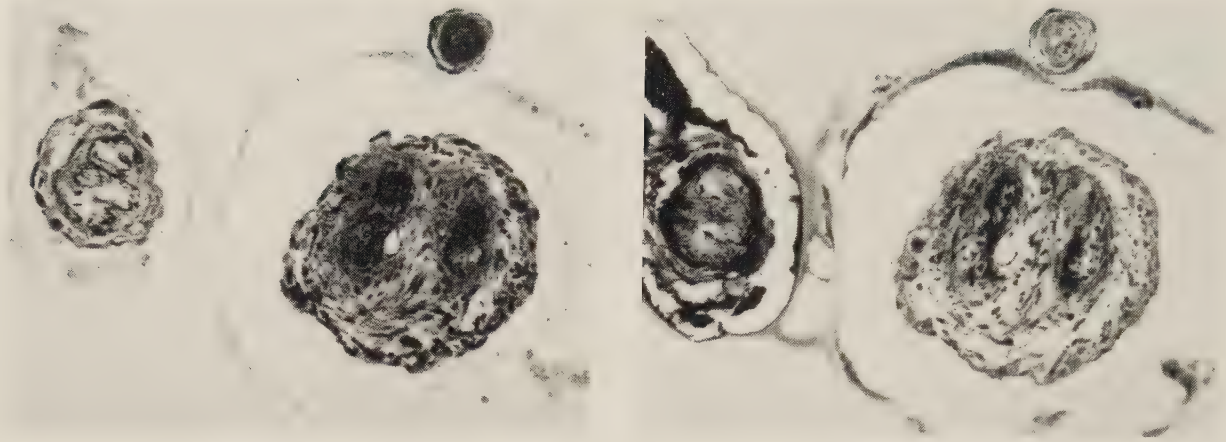

Type I Collagen Type II Collagen

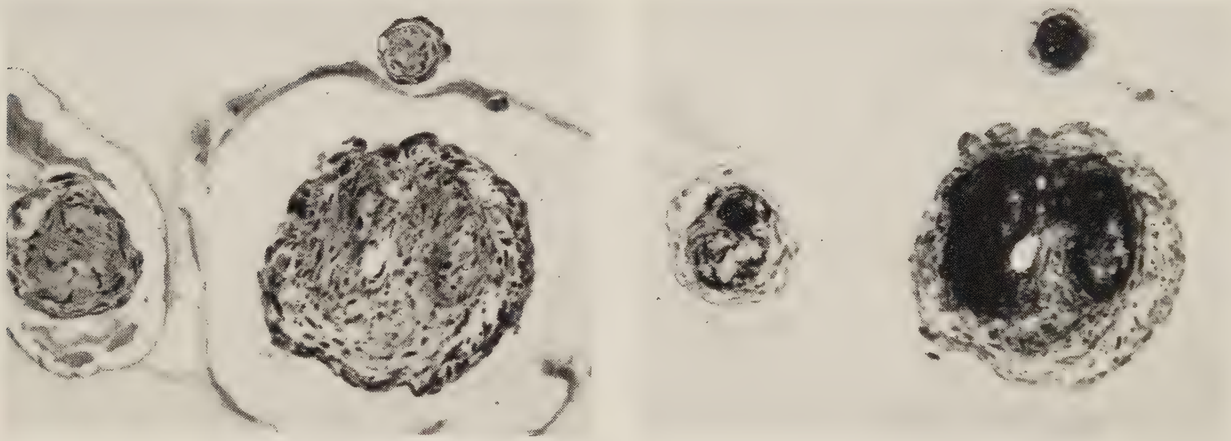

Type III Collagen Type VI Collagen

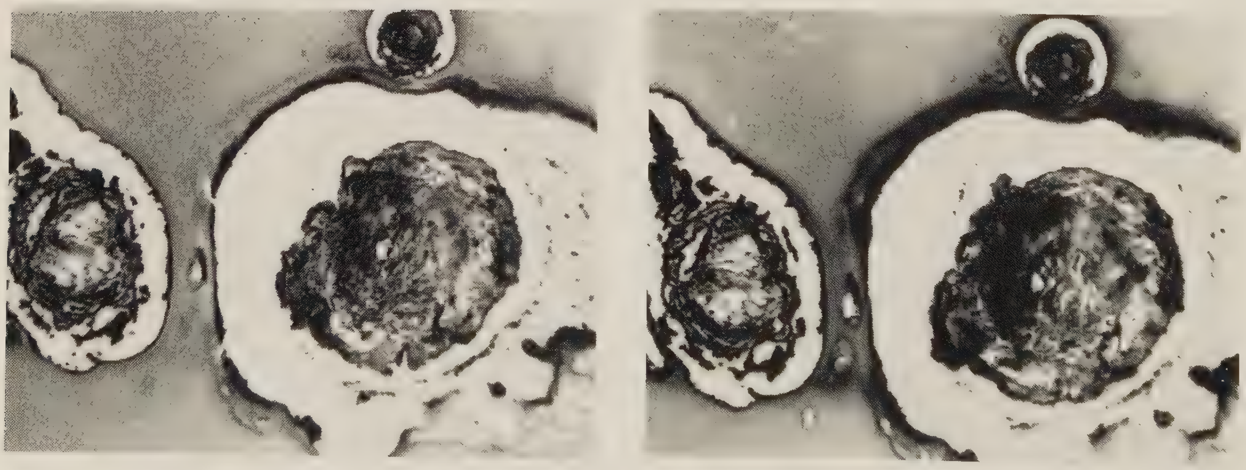

4-S-Chondroitin Sulfate Keratan Sulfate

FIG. 5. Photomicrographs of immunohistochemical localization of extracellular matrix products around first-passage cells grown in agarose from a 24-year-old normal subject. Micrographs show sequential serial sections with localizations of types I, II, III, and VI collagen, 4-*S*-chondroitin sulfate, and keratan sulfate; positive immunoreactivity is shown by dark staining DAB reaction product (×100).

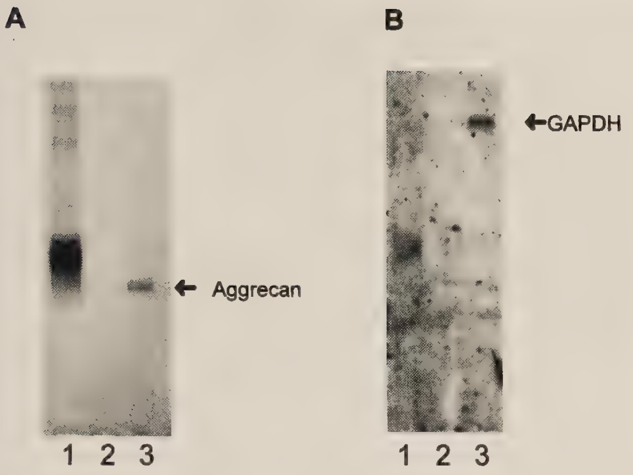

FIG. 6. Northern blot hybridization for aggrecan (A) and GAPDH (B). 12 µg of total RNA was isolated from human disc cells from a 49-year-old control subject; gels were transferred to a nylon membrane and hybridized with a ^{32}P-labeled probe specific for human aggrecan. The blot was exposed to X-ray film for 7 days. The same blot was then hybridized with the GAPDH probe and exposed to X-ray film for 18 h (GAPDH is utilized as a "housekeeping" gene).

has also been found to be useful in similar studies with human chondrocytes [15].

Disc cells attached to the mesh or growing on plastic in monolayer culture exhibited a fibroblast-like phenotype; when seeded into alginate or agarose suspension culture, disc cells assumed a rounded morphology and formed multicelled colonies with successive cell divisions (Fig. 2A). Morphologic studies of cells grown in these three-dimensional microenvironments show that the cells lie in a lacunar space and that matrix is deposited between and around the disc cells (Fig. 2B). With ultrastructural examination, matrix material was seen to consist of proteoglycans and banded and nonbanded collagen (Fig. 2C). Production of extracellular matrix was much greater in the alginate or agarose microenvironment than in cells grown in monolayer culture.

Extracellular Matrix Produced by Cells in Vitro

Morphologic studies of embedded alginate inserts showed the presence of extracellular matrix material between and around cell colonies. ^{35}S incorporation was utilized to assess total proteoglycan synthesis. As shown in Fig. 3, cultures from a surgical specimen from a 44-year-old female patient showed markedly greater ^{35}S incorporation from alginate culture conditions than from the same cells grown in monolayer (Fig. 3).

Routine staining with toluidine blue showed matrix well demarcated in both paraffin- and plastic-embedded three-dimensional cultures sampled for histologic examination (Fig. 4). Extracellular matrix components were further examined using immunohistochemical localization of selected matrix components. Immunohistochemical evaluation of extracellular matrix produced by cells grown in agarose from the annulus of a 24-year-old normal male donor showed the presence of type I, II, III, and VI collagen, 4-*S*-chondroitin sulfate, and keratan sulfate (Fig. 5).

As shown in Fig. 6, cells grown in the three-dimensional microenvironment also express aggrecan as documented by Northern blot techniques.

Responsiveness of Alginate-Grown Disc Cells to TGF-β1

Preliminary studies showed a mitogenic effect of TGF-β1 over doses of 0.25, 0.5, 1.0, 2.5, or 5.0 ng/ml for 6, 8, or 10 days (data not shown). Presented here are results of exposure of cells from male donors age 41 and 62 years and patients age 42 and 60 to either 1% FBS (control) or 1 ng/ml TGF-β1 for 4 or 10 days. As shown in Fig. 7, at Day 4, cells from the older normal subject showed the most marked elevation in proliferation compared to controls (603%); by 10 days, the proliferative response had returned to control levels whereas the older patient continued to show a 279% increase.

Relative basal and TGF-β1-induced levels of gene expression for biglycan and decorin are shown graphically in Fig. 8. Basal levels of expression for these extracellular matrix products remained relatively steady. TGF-β1 exposure for 4 days resulted in increased biglycan expression in the young normal cells, but no change in decorin relative expression. At Day 10, only the young patient cells showed increased biglycan expres-

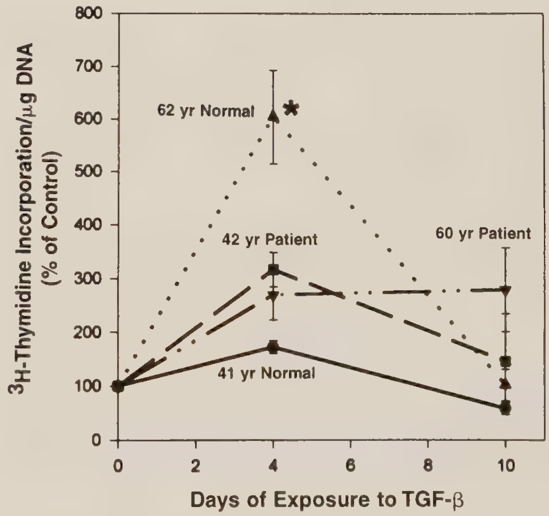

FIG. 7. Mitogenic response of age- and gender-matched normal and patient cells exposed for 4 or 10 days to 1 ng/ml TGF-β1. The asterisk marks significant mitogenic response at 4 days for cells from the 62-year-old normal subject compared to the control levels. Data are means ± SEM expressed as percentages of relevant control.

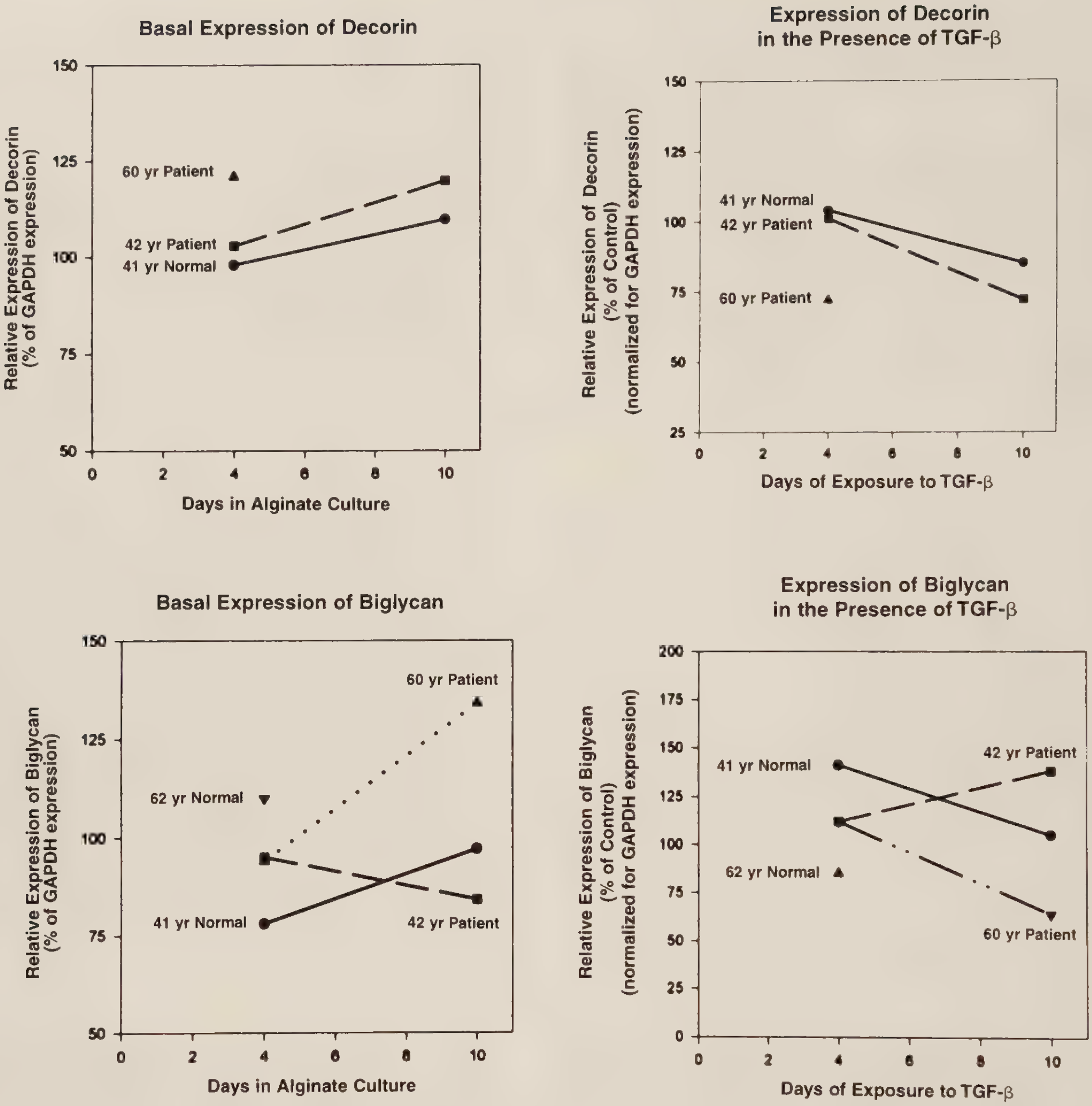

FIG. 8. Relative levels of decorin (top) and biglycan (bottom) in cells from the experiment shown in Fig. 7. Shown are both basal levels of expression (left) and relative expressions (right) following 4 or 10 days of exposure to 1 ng/ml TGF-β1.

sion, while other cells showed basal or nondetectable levels.

DISCUSSION

The tissue culture techniques presented here were developed to provide methods which can be applied to our objective of defining normal disc cell function based upon *in vitro* cell characterization. Unlike osteoblasts, with a characteristic type I collagen gene product, and cartilage, with characteristic types II and X collagen gene products, the human disc produces a wide variety of matrix products whose synthesis and turnover have been shown to alter with age and degeneration *in vivo* [16–19]. The studies presented here utilized cell proliferation and production of extracellular matrix, which are two major criteria of cell function. Three-dimensional culture produced a rounded cell phenotype with formation of cell colonies with progressive cell divisions. Morphologic studies demonstrated deposition of collagenous and proteoglycan-rich matrix in the lacunar spaces and between cells in colonies. Immunohistochemistry of serial sections showed a variety of collagenous, sulfate-rich, and less-sulfated matrix products which were secreted by these cells.

Cell suspensions in alginate or agarose layered onto cell well inserts represent a technical advance which is easier to use in large experimental designs. Cells grown in inserts were easy to feed and to harvest for traditional proliferation, [^{35}S]sulfate incorporation, and light and ultrastructural morphology studies; in addition, use of larger inserts with more cells yields sufficient RNA for Northern analysis as demonstrated with the present studies of decorin and biglycan message levels.

Growth factors function in a variety of cell responses, including differentiation, metabolism, growth, immune regulation, inflammation, tissue repair, and transformation. The role of growth factors in disc health and disease and receptors for growth factors present in disc cells are new areas of important research. TGF-β1 has widespread regulatory effects on multiple cell processes, including a frequent mitogenic action. In a study using explant slices of canine disc, Thompson *et al.* showed a fivefold mitogenic stimulation of cells in the nucleus and the transition zone, but no response in the annulus of the explants [20]. Weinstein *et al.* have identified cytokine mRNA levels in 8 of 10 disc surgical specimens; IL6, phospholipase A_2, and fibroblast growth factor were also found to be produced by disc cells [21]. In the present study, we report a prominent mitogenic effect in cells from the annulus and provide evidence for modulation of proteoglycan expression by TGF-β1. Modulation of extracellular matrix components by TGF-β *in vitro* has previously been reported in myocardial fibroblasts [22], kidney fibroblasts and myoblasts [23], neural crest-derived neuroblastoma cells [24], and human chondrocytes [15].

Results presented here show that TGF-β can induce changes in proliferative and extracellular matrix cellular activities in cells which were obtained from surgical or normal specimens and grown in three-dimensional culture. Our broad objectives are to achieve a greater insight into the regulation of gene expression of the disc cell *in vitro,* increase understanding of the interaction between the disc cell and its local microenvironment, and identify growth factors/bioactive agents which can appropriately enhance disc cell proliferation and function. Cell technologies associated with the explosion of interest in tissue bioengineering over the past few years have opened new therapeutic possibilities in the use of autologous cells in a variety of clinical orthopedic applications. We hope that one day autologous disc cell therapy may also be an available therapeutic option.

The authors thank Donna Crawford, Terry A. Loeb, and Steven Anderson for expert technical assistance and Dr. Peter Roughley for kindly providing molecular probes. This work was supported in part by grants from the Charlotte-Mecklenburg Health Services Foundation.

REFERENCES

1. Hanley, E. N. J. (1992) *in* The Diagnosis and Treatment of Low Back Pain (Weinstein, J. N., Ed.), pp. 125–133, Raven Press, New York.
2. Chelberg, M. K., Banks, G. M., Geiger, D. F., and Oegema, T. R., Jr. (1995) *J. Anat.* **186,** 43–53.
3. Maldonado, B. A., and Oegema, T. R. J. (1992) *J. Orthop. Res.* **10,** 677–690.
4. Ichimura, K., Tsuji, H., Matsui, H., and Makiyama, N. (1991) *J. Spinal Disord.* **4,** 428–436.
5. Benya, P. D., and Shaffer, J. D. (1982) *Cell* **30,** 215–224.
6. Kolettas, E., Buluwela, L., Bayliss, M. T., and Muir, H. I. (1995) *J. Cell Sci.* **108,** 1991–1999.
7. Bonaventure, J., Kadhom, N., Cohen-Solal, L., Ng, K. H., Bourguignon, J., Lasselin, C., and Freisinger, P. (1994) *Exp. Cell Res.* **212,** 97–104.
8. Guo, J., Jourdian, G. W., and MacCallum, D. K. (1989) *Connect. Tissue Res.* **19,** 277–297.
9. Aydellote, M. B., and Kuettner, K. E. (1988) *Connect. Tissue Res.* **18,** 205–222.
10. Aydellote, M. B., Greenhill, R. R., and Kuettner, K. E. (1988) *Connect. Tissue Res.* **18,** 223–234.
11. Bayliss, M. T., Urban, J. P. G., Johnstone, B., and Holm, S. (1986) *J. Orthop. Res.* **4,** 10–17.
12. Ramp, W. K., Dillaman, R. M., Lenz, L. G., Gay, D. M., Roer, R. D., and Ballard, T. A. (1991) *Bone Mineral* **15,** 1–17.
13. Schwob, J. E., Szumowski, K. E. M., and Stasky, A. A. (1992) *J. Neurosci.* **12,** 3896–3919.
14. Aulthouse, A. L., Becker, K., and Beck, M. (1994) *Microsc. Res. Tech.* **28,** 520–526.
15. Roughley, P. J., Melching, L. I., and Recklies, A. D. (1994) *Matrix Biol.* **14,** 51–59.
16. Antoniou, J., Steffen, T., Nelson, F., Winterbottom, N., Hollander, A. P., Poole, R. A., Aebi, M., and Alini, M. (1996) *J. Clin. Invest.* **98,** 996–1003.
17. Eyre, D. R. (1988) *in* The Biology of the Intervertebral Disc (Ghosh, P., Ed.), Vol. I, pp. 171–188, CRC Press, Boca Raton, FL.
18. Wu, J.-J., Eyre, D. R., and Slayter, H. S. (1987) *Biochem. J.* **248,** 373–381.
19. Eyre, D. R. (1979) *Int. Rev. Connect. Tissue Res.* **8,** 227–291.
20. Thompson, J. P., Oegema, T. R. J., and Bradford, D. S. (1991) *Spine* **16,** 253–260.
21. Weinstein, M. A., Ivashiv, L. B., Boskey, A. L., Cammisa, F. P., and O'Leary, P. F. (1996) *Trans. 42nd Annu. Meet. Orthop. Res. Soc.* **21,** 675. [Abstract]
22. Heimer, R., Bashey, R. I., Kyle, J., and Jimenez, S. A. (1995) *J. Mol. Cell. Cardiol.* **27,** 2191–2198.
23. Bassols, A., and Massague, J. (1988) *J. Biol. Chem.* **263,** 3039–3045.
24. Rogers, S. L., Cutts, J. L., Gegick, P. J., McGuire, P. G., Rosenberger, C., and Krisinski, S. (1994) *Exp. Cell Res.* **211,** 252–262.

Received December 31, 1996
Revised version received May 8, 1997

EXPERIMENTAL CELL RESEARCH **235,** 22–27 (1997)
ARTICLE NO. EX973640

Cell–Matrix Interactions Induce Tyrosine Phosphorylation of MAP Kinases ERK1 and ERK2 and PLCγ-1 in Two-Dimensional and Three-Dimensional Cultures of Human Fibroblasts

Oliver Langholz,[1] Dagmar Roeckel,[1] Dirk Petersohn, Eva Broermann, Beate Eckes, and Thomas Krieg[2]

Department of Dermatology, University of Cologne, Cologne, Germany

Using immunoprecipitation and phosphotyrosine detection by Western blotting, intracellular signaling intermediates were analyzed in human primary dermal fibroblasts, either seeded as monolayers on collagen I coats (2D) or seeded within three-dimensional collagen I lattices (3D). Previous results demonstrated that integrin activation in these systems resulted in a cascade of protein tyrosine phosphorylation, including focal adhesion kinase (D. Roeckel and T. Krieg, 1994, *Exp. Cell Res.* 211, 42–48). Further downstream signaling events are now shown to include coordinate activation of ERK1 and ERK2 at 2 h after cell–collagen contact, irrespective of 2D or 3D culture conditions. Applying U-73122, an inhibitor of PLC, inhibits collagen lattice contraction in a dose-dependent fashion. Immunoprecipitation identified the isoform PLCγ-1 as playing a role as signaling intermediate in fibroblast–collagen interactions. PLCγ-1 becomes phosphorylated within 10 min after culture initiation and declines after 2 h. So far, no qualitative differences in signaling intermediates between 2D and 3D cultures have been identified. © 1997 Academic Press

INTRODUCTION

The interaction of cells with their extracellular matrix environment is important in mediating tissue remodeling during physiological and pathophysiological processes, e.g., embryonic development, wound healing, and fibrosis [1]. These interactions can be studied either by performing adhesion experiments on defined substrata or by cultivating cells within a three-dimensional environment reconstituted from purified matrix components. For example, type I collagen lattices which are populated by fibroblasts have been widely used; this system provides a suitable *in vitro* model to examine cell–matrix interactions during connective tissue reorganization [2]. Fibroblasts and other cell types [reviewed in 3] are able to reorganize and contract the three-dimensional gel structure. During this process, a dramatic reprogramming of phenotype and metabolism takes place in fibroblasts with the downregulation of collagen I and the induction of interstitial collagenase (MMP-1) being the most striking features. Using this system, it could be shown that induction of MMP-1 is controlled at the transcriptional level, whereas regulation of collagen is more complex and involves transcriptional as well as posttranscriptional control mechanisms [4–7].

In addition to providing a structural link between the extracellular matrix (ECM) and the cytoskeleton during cell adhesion and migration, the integrins, a family of heterodimeric integral plasma membrane proteins, have been well established as cell surface receptors with signal transducing capacities [for review see 8, 9]. In our laboratory it was demonstrated that in human skin fibroblasts, $\alpha_1\beta_1$ and $\alpha_2\beta_1$ integrins are the major receptors mediating the interaction with a collagenous environment and subsequent remodeling: $\alpha_1\beta_1$ mediates the signals inducing downregulation of collagen gene expression, whereas $\alpha_2\beta_1$ mediates induction of collagenase (MMP-1) [10]. In the collagen lattice system, the integrin $\alpha_2\beta_1$ was demonstrated to be the receptor responsible for mediating reorganization of collagen fibrils and contraction of the matrix by fibroblasts [11, 12].

Studying this system, several groups began to elucidate the signaling pathways involved in the three main events displayed by the system, i.e., lattice contraction, downregulation of collagen I synthesis, and MMP-1 induction. Evidence presented so far suggests that cell–ECM interactions via integrins in general involve protein kinase C (PKC), that, however, the choice of a specific transduction pathway seems to depend upon the ECM glycoprotein and/or the integrin receptor involved in the interaction [13]. Lattice contraction in

---

[1] These authors contributed equally to this study.

[2] To whom reprint requests should be addressed at Department of Dermatology, University of Cologne, Joseph Stelzmann Strasse 9, D-50924 Köln, Germany. Fax: ++49-221-478-4538.

0014-4827/97 $25.00
Copyright © 1997 by Academic Press
All rights of reproduction in any form reserved.

particular appears to depend upon PKC activity [10, 14], possibly including the atypical PKCζ isoform [15], and protein tyrosine phosphorylation [10, 16]. Tyrosine kinase activity seems also required for MMP-1 induction, although reports on chemical inhibition diverge [10, 16]. In contrast, collagen regulation in the 3D system which involves the $\alpha_1\beta_1$ receptor, apparently engages different signaling cascades, since none of the applied inhibitors interfered with this process.

Thus, the exact way by which signals are transduced via integrins is still unknown, but during the past few years it became evident that the activation of tyrosine kinases and of the Ras/mitogen-activated protein (Ras/MAP) kinase pathway seems required [for review see 8, 9]. Particularly central to integrin signaling is the focal adhesion kinase (FAK), which appears to bind directly to integrins, becomes activated by autophosphorylation on tyrosine, and transmits the signal to its substrates through tyrosine phosphorylation [17, 18]. We demonstrated that contact between fibroblasts and 2D collagen coats or 3D collagen networks triggered FAK phosphorylation and that this was independent of contraction, as FAK phosphorylation was also observed in cells incapable of matrix contraction due to lack of the α_2 integrin subunit [19]. The link between integrin and FAK is provided by the cytoplasmic domain of β_1, which can efficiently bind to the amino terminal domain of FAK [17]. Further downstream signaling events include Grb2, which was shown to be an important substrate of FAK and which may link FAK to the Ras/MAP kinase pathway [20]. This pathway in turn relays signals from the cell surface to regulate transcriptional events in the nucleus. Indeed, activation of MAP kinases has been demonstrated to result from integrin-mediated cell adhesion to ECM [20–23].

In addition, during integrin-mediated signaling, other second messenger systems are activated, such as those resulting from stimulation of phospholipases, in particular phospholipase C [24, 25]. Another isoform, phospholipase D, was found activated upon stress relaxation in fibroblasts that were cultured in attached collagen lattices and then released, thereby resulting in stress dissipation and contraction [26].

In a previous report, we showed that culture of primary human dermal fibroblasts either as monolayers on type I collagen or in three-dimensional lattices resulted in an increase of phosphotyrosine-containing proteins, one of which, appearing at 2 to 6 h after seeding, was identified as FAK [19]. The other prominent protein, pp42, has further been characterized, and we show here that it represents MAP kinase. A third protein, PLCγ-1, becomes activated by tyrosine phosphorylation upon 2D or 3D contact of fibroblasts with a collagenous environment.

MATERIALS AND METHODS

Cell culture and adhesion to substrates. Cultures of primary human fibroblasts were established by outgrowth from skin biopsies of healthy volunteers. Cells were maintained in Dulbecco's modified Eagle's medium, supplemented with 10% fetal calf serum, 0.05 mg/ml sodium ascorbate, 0.3 mg/ml glutamine, 100 U/ml penicillin, 100 U/ml streptomycin, and grown in the moist atmosphere of a CO_2 incubator (5% CO_2) at 37°C. Cells were passaged by trypsinization (0.1% trypsin, 0.02% EDTA in PBS; Boehringer Mannheim) and were used at a confluent stage in passages 5–9.

For adhesion studies, petri dishes were coated with purified type I collagen (see Preparation of Collagen Lattices) at 0.03 mg/ml by incubation at room temperature for several hours. The coated dishes were allowed to dry overnight and rinsed with PBS before use.

Preparation of collagen lattices. Native porcine collagen (I) was purchased from Deutsche Gelatine Fabriken Stoess AG (Eberbach, Germany), purified by dialysis against 0.01 *M* phosphate buffer, pH 7.2, and redissolved at 3 mg/ml in sterile 0.1% acetic acid. Three-dimensional collagen lattices were prepared as described [7], containing 10^7 cells/lattice (150 mm diameter, 30 ml volume) and a 1 mg/ml concentration of type I collagen. Rates of lattice contraction were monitored by determining the remaining surface area.

For inhibition studies, U-73122, an inhibitor of PLC (BIOMOL, Germany) (27), was added in varying concentrations to the collagen lattice mix as the last component. In three independent experiments using cells from different donors, supernatants were tested for the presence of lactate dehydrogenase, indicating cytotoxic concentrations of the inhibitor. The effective concentration showed no cytotoxic effects.

SDS–PAGE and Western blot analysis. For preparing total protein extracts cells were scraped with a rubber policeman into cold PBS containing 0.1 m*M* sodium orthovanadate, washed twice, and lysed in 0.1 ml RIPA buffer (0.01 *M* sodium phosphate, pH 7.62, 0.15 *M* NaCl, 1% sodium deoxycholate, 1% NP-40, 0.1% SDS, 1 m*M* DTT, 50 μ*M* leupeptin, and 0.2 m*M* sodium orthovanadate) per 150-mm plate. Cells were released from collagen lattices by several washes in PBS containing 0.1 m*M* orthovanadate and lysed as described above. Lysates were clarified by centrifugation for 10 min at 4°C in a microfuge at 14,000 rpm and mixed with an equivalent volume of 2× reducing Laemmli sample buffer [28]. Samples containing equal amounts of total protein were electrophoresed on either 7.5% or 10% SDS–polyacrylamide gels under reducing conditions [28] and blotted onto nitrocellulose [29]. The nitrocellulose was blocked with 5% dried milk powder in TBS-T (20 m*M* Tris–HCl, pH 7.6, 137 m*M* NaCl, 0.2% Tween 20) and incubated with specific antibodies for 1 h. The following antibodies were used: monoclonal anti-phosphotyrosine antibodies 4G10 (UBI, Inc.) or PY20 (Paesel + Lorei, Hanau, Germany), polyclonal anti-MAP kinase antibodies R2 (ERK1-CT; UBI, Inc.), polyclonal anti-tyrosine-phosphorylated MAP kinase (New England Biolabs, Inc.), and monoclonal anti-PLCγ-1 antibodies (UBI, Inc.). Concentrations were applied according to the manufacturer's instructions. For detection, the ECL detection system was used (Amersham International plc, UK). Protein molecular weight standards were purchased from Boehringer Mannheim.

Immunoprecipitation. Total protein extracts were prepared as described above. Monoclonal anti-PLCγ-1 antibodies (UBI, Inc.), polyclonal anti-MAP kinase (ERK1-CT, UBI, Inc.), or polyclonal anti-phospho-MAP kinase (NEB, Inc) was added to the clarified extracts (5 μg for 600 μg of cell protein) and incubated for 2 h on ice. For the PLCγ-1 immunoprecipitation, affinity-purified rabbit anti-mouse antibodies (Jackson ImmunoResearch Laboratories, Inc.) were added for 1 h. Immunocomplexes were sedimented by protein A–Sepharose CL-4B (Pharmacia), washed three times in RIPA buffer, and then released for SDS–PAGE and blot analysis by boiling in 2× reducing Laemmli sample buffer for 5 min. The protein concentrations in the cell extracts were determined using a Bio-Rad protein assay (Richmond, CA).

RESULTS

Two- and Three-Dimensional Collagen I Culture Systems Induce Activation of MAP Kinases

It has been reported that activation of members of downstream signaling cascades, including components of the MAP kinase cascade, is directly due to the adhesion of cells to the ECM or antibody-mediated clustering of surface integrins [20–23]. Activation of the MAP kinase family is achieved by phosphorylation on tyrosine (and threonine) at specific sites, best characterized for the two main members ERK1 and ERK2 (extracellular signal related kinase 1 and 2) with molecular masses of 44 and 42 kDa, respectively [30]. In order to determine the nature of pp42, a band that we described earlier [19] which becomes phosphorylated in cells grown on collagen, but not polylysine, and which is not dephosphorylated upon trypsin treatment, we investigated fibroblasts seeded onto collagen-coated dishes and grown for 10 min, 2 h, and 6 h. Total protein extracts were analyzed by Western blotting, using a set of three different antibodies: a monoclonal anti-phosphotyrosine antibody, a polyclonal anti-MAP kinase antibody, and a polyclonal anti-tyrosine-phosphorylated MAP kinase antibody (described under Materials and Methods). As shown in Fig. 1A, enhanced tyrosine phosphorylation of a M_r 42,000 protein, previously described as pp42 [19], was detected after 2 to 6 h culture time. An initial period of 10 min was not sufficient for visible phosphorylation. When reprobing the exact same filter with antibodies specific for MAP kinase, it became evident that during the adhesion process MAP kinase became activated. The anti-P-MAP kinase antibody exclusively recognized the phosphorylated, hence activated, forms of ERK1 and ERK2 (Fig. 1D). After 2 h the two isoforms could be detected with a much stronger signal for ERK2 than ERK1. Whereas ERK1 was not seen in the extract of the suspended cell culture (time point 0′) and of the adhesion culture after 10 min, low levels of ERK2 were visible in small amounts in both cases. ERK2 corresponded to pp42 of Fig. 1A in its molecular weight and its time course of appearance. The typical "upward gel shift" due to phosphorylation [31] was observed in Fig. 1C with an antibody recognizing both activated and inactive forms of ERK1 and ERK2 with the degree of shifting reaching a maximum 2 h after the cells were plated on collagen. Identification of the indicated bands as ERK1 and ERK2 was verified by immunoprecipitation, using both anti-MAP kinase antibodies in protein extracts from cells cultured for 6 h on collagen-coated dishes (Fig. 1B).

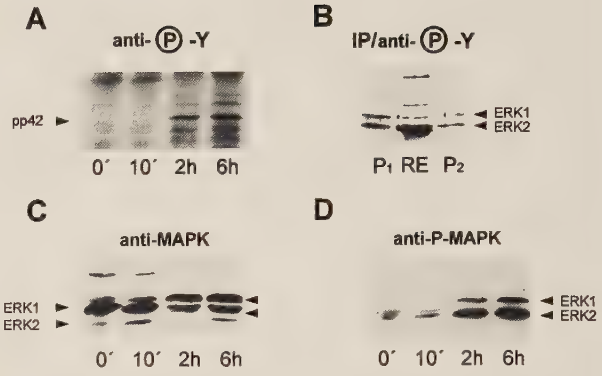

FIG. 1. Activation of ERK1 and ERK2 by 2D fibroblast–collagen contact. Primary human dermal fibroblasts were cultured on collagen I coated plastic for the times indicated. Lane 0′ represents the lysate from cells suspended by trypsinization just before plating. (A) Western blot staining was performed with 4G10, detecting phosphotyrosine; (B) Immunoprecipitation was carried out using either anti-P-MAPK which detects the activated (phosphorylated) forms of ERK1 and ERK2 (lane P1) or ERK1-CT, detecting the unphosphorylated as well as tyrosine- and threonine-phosphorylated ERK forms (P2). The precipitates and an aliquot of the cell extract (RE) were subjected to Western blot analysis using the phosphotyrosine-specific antibody PY20. Western blot staining using antibody ERK1-CT (C), detecting the unphosphorylated as well as tyrosine- and threonine-phosphorylated ERK forms; note the "upward mobility shift" of activated forms or anti-P-MAPK (D), which detects the activated (phosphorylated) forms of ERK1 and ERK2.

When cells were not cultivated as monolayers but in three-dimensional collagen I lattices, the exact same pattern of MAP kinase activation was observed in a corresponding time course (data not shown), indicating that adhesive contact is sufficient for MAP kinase activation and that three-dimensional contact is not required.

Contact of Fibroblasts with Collagen Results in Tyrosine Phosphorylation of PLCγ-1

There is evidence that integrin signaling involves tyrosine phosphorylation and hence activation of PLCγ. Thus, PLCγ-1 was activated by cross-linking β_2 integrin in T cells and by adhesion of epithelial cells to collagen [24, 25]. In order to evaluate the importance of PLCγ for signal transduction we applied U-73122, an inhibitor of PLC [27], in our collagen lattice system. Culturing human dermal fibroblasts in 3D collagen lattices in the presence of this inhibitor resulted in significant inhibition of lattice contraction at 10 μM, lasting for 24 h (Fig. 2). This concentration of U-73122 did not cause cytotoxic effects as shown by two lines of evidence: First, no LDH activity differing from controls was detected in culture supernatants. Second, RNA was extracted from inhibitor-treated and control cultures which showed comparable levels of α_1 (I) procollagen and GAPDH transcripts (not shown).

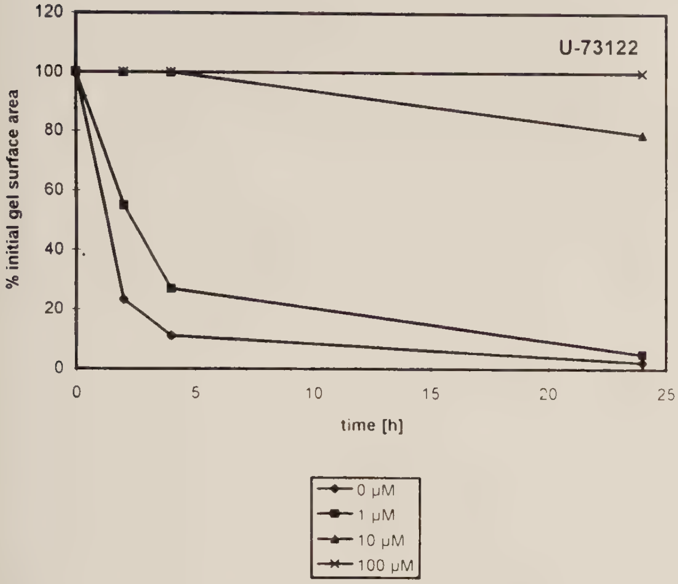

FIG. 2. Effect of PLC inhibitor on fibroblast-mediated contraction of 3D collagen lattices. Primary human dermal fibroblasts were cultured in collagen I lattices for 24 h in the absence or in the presence of the indicated concentrations of U-73122, an inhibitor of PLC. Contraction of lattices is shown as a percentage of initial gel surface area (mean of triplicate values).

For monitoring expression and possible activation of PLCγ-1 total protein extracts from fibroblasts cultured as monolayers on collagen I or within 3D collagen lattices for 10 min, 2 h, and 6 h were prepared. Western blot staining with anti-PLCγ-1 antibodies of total protein extracts indicated that the amount of PLCγ-1 protein decreased during the time course analyzed in both culture systems (Fig. 3A). To further investigate a possible role of PLCγ-1 tyrosine phosphorylation and hence activation upon contact to type I collagen, immunoprecipitation experiments of PLCγ-1 were performed. Therefore, protein extracts of monolayer and collagen lattice cultures were prepared following a time course, immunoprecipitated, and analyzed by Western blotting. In Fig. 3B, staining with anti-phosphotyrosine antibodies is shown. In monolayers and lattices an approximately fivefold increase in tyrosine phosphorylation of PLCγ-1 was observed right after 10 min in culture with a following decline to the starting point after 6 h. To verify that equal amounts of immunoprecipitates were loaded, the same blot was counterstained with anti-PLCγ-1 antibodies (Fig. 3C).

These results indicate that, while the amount of PLCγ-1 protein decreases throughout the experiment, activation of PLCγ-1 is reached equally in both 2D and 3D culture systems within 10 min and declines after 2 h.

DISCUSSION

Tyrosine phosphorylation of cellular proteins is an important mechanism of signal transduction by integrins which mediate cell–matrix interactions. In this study, we showed that in addition to FAK two major downstream signaling components, namely MAP kinase and PLCγ, become phosphorylated on tyrosine and hence become activated after two- and three-dimensional contact of primary human fibroblasts with collagen I.

The MAP kinase family, with ERK1 and ERK2 being its best studied members, is a family of protein–serine/threonine kinases that are activated and tyrosine phosphorylated in response to growth factor binding [for review see 32]. Since MAP kinase is believed to regulate the activity of certain transcription factors, e.g., c-*myc*, activation of this enzyme represents an important link between extracellular events and gene expression. Over the past few years it has become evident that the MAP kinase family is not only activated by growth factors and their corresponding (tyrosine kinase) receptors, but also by adhesion of cells to the ECM such as fibronectin, laminin, type IV collagen, and vitronectin, or by antibody-mediated clustering of integrins [20–23]. Our data further support this concept and extend

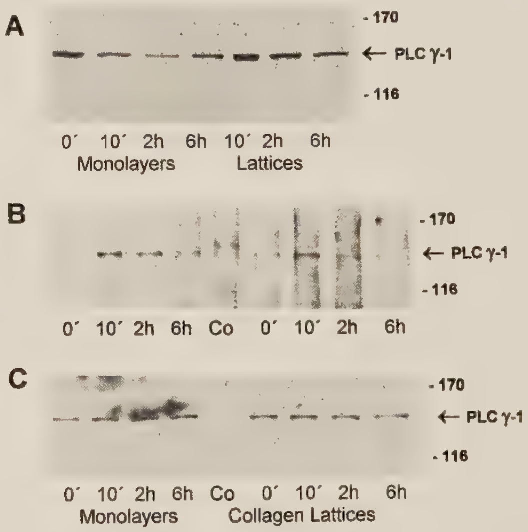

FIG. 3. Protein amount and activation of PLCγ-1 during 2D and 3D fibroblast–collagen contact. Primary human dermal fibroblasts were cultured on dishes coated with type I collagen or in collagen I lattices for various times as indicated. Lane 0′ represents the cell lysate from cells suspended by trypsinization just before plating. (A) Western blot of total protein extracts, stained with anti-PLCγ-1 antibodies. (B) Western blot of anti-PLCγ-1 immunoprecipitates, stained with anti-phosphotyrosine antibodies or (C) with anti-PLCγ-1 antibodies. Co represents negative control (immunoprecipitation without first antibody). Positions of molecular weight markers (in kDa) are indicated.

the findings to type I collagen and the three-dimensional culture system (collagen lattices). Whereas some authors [21–23] observed a rapid activation within minutes, followed by a decrease of activity, in our experiments MAP kinase was active only after 2 h of culture time and stayed active over the measured time period. This result confirms data by Zhu and Assoian [23], who reported a gradual and persistent stimulation of MAP kinase activity by fibronectin associated with cell spreading rather than cell attachment. Interestingly, this parallels the observation we made with FAK activation and phosphorylation in response to collagen I (19) and implies MAP kinase activation as a downstream event of FAK signaling. Indeed, Schlaepfer and co-workers [20] provided direct evidence that integrin-mediated signal transduction activated the Ras/MAP kinase pathway by binding of the adapter protein Grb2 to the FAK.

The γ-1 isoform of phospholipase C is activated by tyrosine phosphorylation and represents the key enzyme responsible for inositol triphosphate and diacylglycerol generation in the phosphatidylinositol signaling pathway [33, 34]. Regarding integrin signaling, there is evidence that integrins can be directly linked to a tyrosine kinase pathway that stimulates signaling by PLCγ-1: Kanner *et al.* [25] demonstrated that by cross-linking β_2 integrin, PLCγ-1 was activated in T cells. Collagen-stimulated phospholipase activation through adhesion was observed in rat glomerular epithelial cells and could be partially inhibited by anti-β_1 integrin Fab fragments (24). Anti-β_1 integrin antibodies have been shown to interfere with lattice contraction, a process that is mediated by $\alpha_2\beta_1$ integrin [11, 12]. In this study, we showed that by using a PLCγ inhibitor that did not affect cell viability or synthesis of extracellular matrix, contraction was inhibited for 24 h and gave further support to the importance of PLCγ in β_1 integrin signaling. In addition, activation of this enzyme was shown by tyrosine phosphorylation to be optimal after 10 min of culture time with a subsequent decline. Apparently, downstream events seem to be necessary for continuing contraction which is triggered by an initial activation of PLCγ. By generating diacylglycerol, PLCγ is a direct supplier for the stimulation of PKC which in turn was shown to be involved in lattice contraction [10, 14]. So far, the exact link between PLCγ and integrin is not known and there is no evidence that PLCγ could be a substrate of FAK. In contrast, in our hands activation of FAK was shown after 2 h of culture time [19] when PLCγ was already down to a background level.

Our report gives further evidence that activation of MAP kinase and PLCγ is an integral part of signal transduction triggered by cell–matrix interactions. Alternative routes might be taken to lead to individual responses which are initiated by different integrins, as is suggested by the differential regulation of collagen I and MMP-1 via $\alpha_1\beta_1$ and $\alpha_2\beta_1$, respectively. Three-dimensional culture systems might still involve signaling components not needed in monolayer or 2D cultures.

We thank Dr. Barry D. Sudbeck for stimulating discussion and Gabi Hüppe for excellent technical assistance. This study was supported by a grant from the Deutsche Forschungsgemeinschaft (Kr 558/6).

REFERENCES

1. Grinnell, F. (1994) *J. Cell Biol.* **124,** 401–404.
2. Bell, E., Ivarsson, B., and Merrill, C. (1979) *Proc. Natl. Acad. Sci. USA* **76,** 1274–1278.
3. Eckes, B., Krieg, T., Nusgens, B. V., and Lapiere, Ch. M. (1995) *Wound Rep. Reg.* **3,** 248–257.
4. Eckes, B., Mauch, C., Hüppe, G., and Krieg, T. (1993) *FEBS Lett.* **318,** 129–133.
5. Lambert, C. A., Soudant, E. P., Nusgens, B. V., and Lapiere, C. M. (1992) *Lab. Invest.* **66,** 444–451.
6. Mauch, C., Hatamochi, A., Scharffetter, K., and Krieg, T. (1988) *Exp. Cell Res.* **178,** 493–503.
7. Mauch, C., Adelmann-Grill, B., Hatamochi, A., and Krieg, T. (1989) *FEBS Lett.* **250,** 301–305.
8. Dedhar, S., and Hannigan, G. E. (1996) *Curr. Opin. Cell Biol.* **8,** 657–669.
9. Schwartz, M. A., Schaller, M. D., and Ginsberg, M. H. (1995) *Annu. Rev. Cell Biol. Dev. Biol.* **11,** 549–600.
10. Langholz, O., Roeckel, D., Mauch, C., Kozlowska, E., Bank, I., Krieg, T., and Eckes, B. (1995) *J. Cell Biol.* **131,** 1903–1915.
11. Klein, C. E., Dressel, D., Steinmayer, T., Mauch, C., Eckes, B., Krieg, T., Bankert, R. B., and Weber, L. (1991) *J. Cell Biol.* **115,** 1427–1436.
12. Schiro, J. A., Chan, B. M. C., Roswit, W. T., Kassner, P. D., Pentland, A. P., Hemler, M. E., Eisen, A. Z., and Kupper, T. S. (1991) *Cell* **67,** 403–410.
13. Gimond, C., and Aumailley, M. (1992) *Exp. Cell Res.* **203,** 365–373.
14. Guidry, C. (1993) *J. Cell Physiol.* **155,** 358–367.
15. Xu, J., Zutter, M. M., Santoro, S. A., and Clark, R. A. F. (1996) *J. Cell Biol.* **134,** 1301–1311.
16. Broberg, A., and Heino, J. (1996) *Exp. Cell Res.* **228,** 29–35.
17. Schaller, M. D., Otey, C. A., Hildebrand, J. D., and Parsons, T. J. (1995) *J. Cell. Biol.* **130,** 1181–1187.
18. Calalb, M. B., Polte, R. R., and Hanks, S. K. (1995) *Mol. Cell. Biol.* **15,** 954–963.
19. Roeckel, D., and Krieg, T. (1994) *Exp. Cell Res.* **211,** 42–48.
20. Schlaepfer, D. D., Hanks, S. K., Hunter, T., and van der Geer, P. (1994) *Nature (London)* **372,** 786–791.
21. Chen, Q., Kinch, M. S., Lin, T. H., Burridge, K., and Juliano, R. L. (1994) *J. Biol. Chem.* **269,** 26602–26605.
22. Morino, N., Mimura, T., Hamasaki, K., Tobe, K., Ueki, K., Kikuchi, K., Takehara, K., Kadowaki, T., Yazaki, Y., and Nojima, Y. (1995) *J. Biol. Chem.* **270,** 269–273.
23. Zhu, X., and Assoian, R. K. (1995) *Mol. Biol. Cell* **6,** 273–282.

24. Cybulsky, A. V., Carbonetto, S., Cyr, M.-D., McTavish, A. J., and Huang, Q. (1993) *Am. J. Physiol.* **264,** C323–C332.

25. Kanner, S. B., Grosmaire, L. S., Ledbetter, J. A., and Damle, N. K. (1993) *Proc. Natl. Acad. Sci. USA* **90,** 7099–7103.

26. He, Y., and Grinnell, F. (1995) *J. Cell Biol.* **130,** 1197–1205.

27. Thompson, A. K., *et al.* (1991) *J. Biol. Chem.* **266,** 23856.

28. Laemmli, U. K. (1970) *Nature (London)* **227,** 680–685.

29. Towbin, H., Staehelin, T., and Gordon, J. (1979) *Proc. Natl. Acad. Sci. USA* **76,** 4350–4354.

30. Ahn, N. G., and Krebs, E. G. (1992) *Curr. Opin. Cell Biol.* **4,** 992–999.

31. Cohen, P., and Marshall, C. J. (1992) *Cell* **71,** 335–342.

32. Blumer, K. J., and Johnson, G. L. (1994) *Trends Biochem. Sci.* **19,** 236–240.

33. Nishibe, S., Wahl, M. I., Hernandez-Sotomayor, S. M., Tonks, N. K., Rhee, S. G., and Carpenter, G. (1990) *Science* **250,** 1253–1256.

34. Rhee, S. G., and Choi, K. D. (1992) *J. Biol. Chem.* **267,** 12393–12396.

Received January 10, 1997
Revised version received May 12, 1997

EXPERIMENTAL CELL RESEARCH **235,** 28–34 (1997)
ARTICLE NO. EX973643

A Factor with a Zinc- and Phorbol Ester-Binding Domain Is Necessary for Endosome Fusion

Alejandro Aballay,* Nora G. Arenas,* Andrew F. G. Quest,† and Luis S. Mayorga*[,1]

*Instituto de Histología y Embriología, Facultad de Ciencias Médicas, Universidad Nacional de Cuyo–CONICET, 5500 Mendoza, Argentina; and †Institute of Biochemistry, University of Lausanne, CH-1066 Epalinges, Switzerland

An inhibitory effect of several zinc chelators on endosome fusion reconstituted in an *in vitro* system has been recently reported (A. Aballay *et al.*, 1995, *Biochem. J.* 312, 919–923). The factor that requires zinc for its activity is still unknown. Since the regulatory domain of protein kinase C (PKC) contains cysteine-rich motifs which coordinate zinc, we suspected that PKC or a PKC-like protein might be that factor. To test this hypothesis, we studied the effect of calphostin C, a specific inhibitor of PKC that interacts with the cysteine-rich motif, and PMA (phorbol 12-myristate 13-acetate), an activator of several PKC isoforms that bind to the same region, on endosome fusion. Calphostin C inhibited endosome fusion in a zinc-regulated manner, whereas PMA enhanced endosome fusion. Moreover, fusion was strongly stimulated when both PMA and zinc were added together to zinc-depleted fusion reactions. Inhibitors of the catalytic domain of PKC had no effect on the assay suggesting that the kinase activity is not required. In contrast, a glutathione *S*-transferase fusion protein containing a cysteine-rich region of the regulatory domain of PKCγ inhibited endosome fusion in a PMA-dependent manner. Western blot analysis demonstrated the presence of proteins containing PKC-like cysteine-rich regions that are released from endosomal fractions by zinc chelators. These results indicate that the previously proposed zinc-dependent factor required for endosome fusion could be either a PKC isoform or a protein containing the phorbol ester-binding domain of PKC. © 1997 Academic Press

INTRODUCTION

Intracellular trafficking of macromolecules among organelles is a complex and highly regulated process that requires several membrane fusion steps. Reconstitution studies of different intracellular transport processes in cell-free systems and the analysis of transport defective yeast mutants have shown that the fusion machinery shares several components in most of the transport events analyzed [1–3]. In cell-free systems, fusion among early endosomes requires *N*-ethylmaleimide-sensitive factors, including NSF [4, 5]. Additionally, endosome fusion is regulated by several GTP-binding proteins of the ARF [6], rab [7–9], and heterotrimeric [10, 11] families. In a recent report we showed that endosome fusion is blocked by the metal chelators TPEN[2] and BAPTA, suggesting that the process requires a metal ion [12]. Several experiments in that report indicate that the ion essential for endosome fusion is zinc. Now, more than 300 proteins that bind zinc have been described [13]. Among the zinc-binding proteins, PKC is a family of proteins with a well-defined zinc-binding domain that plays an important role in intracellular signal transduction in eukaryotic cells. In addition, PKC may have a role in several steps of vesicular transport. Requirements for PKC in regulated exocytosis [14–16], the regulation of cell surface receptor trafficking through the endocytic pathway [17], the transport of proteins through the Golgi apparatus [18], and the export of proteins from this organelle [19] have been reported.

Within the regulatory domain of all PKCs, highly conserved cysteine-rich regions $HX_{11/12}CX_2CX_nCX_2CX_4HX_2CX_{6/7}C$ (where X is any amino acid and n varies between 12 and 14) which coordinate zinc are present (for review, see [20]). Moreover, the use of deletion mutants of different PKC isoenzymes revealed that the cysteine-rich region is necessary for zinc and phorbol ester binding [21–25].

In this study, we have examined the importance of a PKC-like molecule in endosome fusion. The membrane-

---

[1] To whom reprint requests should be addressed at Instituto de Histología y Embriología, Casilla de correo 56, 5500 Mendoza, Argentina. Fax: (54) (61) 494117 or 380232 or 380150. E-mail: lmayorga@fmed2.uncu.edu.ar.

[2] Abbreviations used: BAPTA, 1,2-bis(*o*-aminophenoxy)ethane-*N,N,N′,N′*-tetraacetic acid; CPC, calphostin C; DAG, diacylglycerol; DNP, dinitrophenol; DTT, dithiothreitol; GST–Cys2, COOH-terminal fusion protein of glutathione *S*-transferase with the second PKCγ cysteine-rich region (amino acids 92–173); PMA, phorbol 12-myristate 13-acetate; TPEN, *N,N,N′,N′*-tetrakis-(2-pyridylmethyl)ethylenediamine.

0014-4827/97 $25.00
Copyright © 1997 by Academic Press
All rights of reproduction in any form reserved.

permeant inhibitor of PKC calphostin C (CPC) and the diacylglycerol (DAG) analog phorbol 12-myristate 13-acetate (PMA) were found to have inhibitory or stimulatory effects, respectively, in an *in vitro* assay that reconstitutes fusion among endosomes. Moreover, a glutathione *S*-transferase fusion protein containing the Cys2 region of the regulatory domain of PKCγ (GST–Cys2 protein) inhibited endosome fusion in a PMA-dependent manner. Proteins containing Cys2-like regions were released from endosomal fractions by zinc chelators. We conclude that a protein with a Cys2-like domain of PKCγ that interacts with phorbol ester is required for endosome fusion and it is probably the zinc-binding factor previously described.

MATERIALS AND METHODS

Reagents. TPEN was purchased from Molecular Probes (Eugene, OR). All other reagents were obtained from Sigma Chemical Company (St. Louis, MO).

In vitro endosome fusion assay. Early endosomes were prepared by loading J774 E-clone macrophages with aggregated monoclonal anti-dinitrophenol (DNP) mouse IgG (via the Fc receptor) or with DNP–β-glucuronidase (via the macrophage mannose receptor) as previously described [26]. After uptake, cells were washed and homogenized in 250 m*M* sucrose, 20 m*M* Hepes–KOH, 0.5 m*M* EGTA (homogenization buffer). Postnuclear supernatants were stored in liquid nitrogen. To obtain endosome-enriched fractions, the postnuclear fractions were diluted 15-fold in homogenization buffer and centrifuged sequentially at 35,000*g* for 1 min and at 50,000*g* for 5 min. The second pellet was used for fusion reactions [27]. Fusion between two populations of endosomes containing either the antibody or the enzyme was performed as previously described [26]. The fusion buffer (250 m*M* sucrose, 0.5 m*M* EGTA, 20 m*M* Hepes–KOH, pH 7.0, 1 m*M* dithiothreitol (DTT), 1.5 m*M* $MgCl_2$, 50 m*M* KCl, 1 m*M* ATP, 8 m*M* creatine phosphate, 31 U/ml creatine phosphokinase, and 0.25 mg/ml DNP–BSA) was supplemented with gel-filtered cytosol, GST–Cys2 protein, CPC, PMA, $ZnCl_2$, $CdCl_2$, $NiCl_2$, $CoCl_2$, or $FeCl_2$, as required. Samples were incubated at 37°C for 45 min and the reaction was stopped by cooling on ice. Fusion was measured as previously described [26].

Expression and purification of GST–Cys2 protein. The expression plasmid pGEX2T containing the DNA-encoding segment of the Cys2 (amino acids 92–173) region of PKCγ was obtained as described [25]. XL1B *Escherichia coli* were transformed with the mentioned plasmid. The GST–Cys2 fusion protein was expressed in *E. coli* and isolated from cell lysates by affinity chromatography on a glutathione–agarose matrix as described [24].

Zn^{2+} measurement. Free zinc concentrations were measured using Fura II fluorescent ratio (340/380 nm excitation, 510 nm emission) [12, 28]. To calculate free ion concentrations, a 3 n*M* dissociation constant from zinc–Fura II complex was used (Molecular Probes catalog) [28].

Western blot analysis. Early endosomes, prepared as described above, were washed three times with homogenization buffer containing 50 m*M* NaCl, 1 μg/ml leupeptin, 50 μg/ml PMSF, 1 μg/ml pepstatin, and 50 μg/ml trypsin inhibitor. The samples were then resuspended in the same buffer and incubated for 15 min at 25°C in the presence of increasing concentrations of TPEN. The membranes were pelleted at 50,000*g* for 5 min and the supernatants were resolved on 10% SDS–polyacrylamide gels and transferred to nitrocellulose membranes. Blots were probed with polyclonal antisera raised against the pseudosubstrate peptide of PKCα/β and two different peptide sequences present in the Cys2 region of PKCγ (peptides 3 and 4) [24]. Detection was accomplished using the ECL detection system (Amersham). These antibodies recognize PKCγ and PKCα but present weak or non-cross-reactivity with PKCζ, PKCϵ, and PKCδ (A. Quest, unpublished observations). To estimate the amount of protein present, films were scanned and bands intensities were quantitated using the NIH Image I program.

RESULTS

Calphostin C Inhibits Fusion between Endosomes in a Zinc-Dependent Fashion

It has been reported that PKC is required in several events in intracellular trafficking. We have shown that zinc is necessary for endosome fusion [12]. Since PKCs contain a well-defined zinc-binding domain, we wondered whether the factor that requires zinc to promote fusion in the endocytic pathway might be PKC or a PKC-related protein. To test this hypothesis, the effect of divalent cations and CPC, a membrane-permeant inhibitor of PKC, was tested in the fusion assay. CPC inhibits PKC by irreversibly oxidizing the phorbol ester binding site in a light-dependent manner [29]. In the endosome fusion assay, 2 μ*M* CPC alone had no effect. However, addition of $ZnCl_2$ to the fusion buffer caused a dramatic inhibition of endosome fusion by CPC. Maximum inhibition was observed in the presence of 70 n*M* free zinc. This effect was specific for zinc, since other metal ions tested at different concentrations, had no effect (Fig. 1a). These results were not anticipated since a zinc requirement for CPC inhibition had not been described. Therefore, we wondered whether the *in vitro* fusion mixture contained some components that could protect the putative PKC-like factor from inhibition caused by CPC. To identify such a component, samples were preincubated at 25°C in the presence of CPC and in fusion buffer lacking DTT, ATP, KCl, or $MgCl_2$. Fusion was then assessed in the presence of the missing component at 37°C. When DTT was excluded during preincubation, inhibition of fusion was observed with low concentrations of CPC (Fig. 1b), suggesting that DTT prevents inhibition caused by CPC. As expected, the protective effect was abolished by the presence of zinc (Fig. 1b). The absence of ATP, KCl, or $MgCl_2$ during the preincubation did not promote CPC inhibition (data not shown). Previously, CPC has been shown to interact preferentially with activated PKC since inhibition is promoted by phorbol esters [29]. Similarly, inhibition of endosome fusion by CPC was also enhanced in the presence of PMA (Fig. 1c).

Pretreatment of membranes with CPC prior to endosome isolation had a more dramatic effect than cytosol treatment (Figs. 2a and 2b). These observations suggest that a large proportion of the CPC-sensitive factor is membrane associated. Interestingly, control but not CPC-treated cytosol supported fusion among endosomes

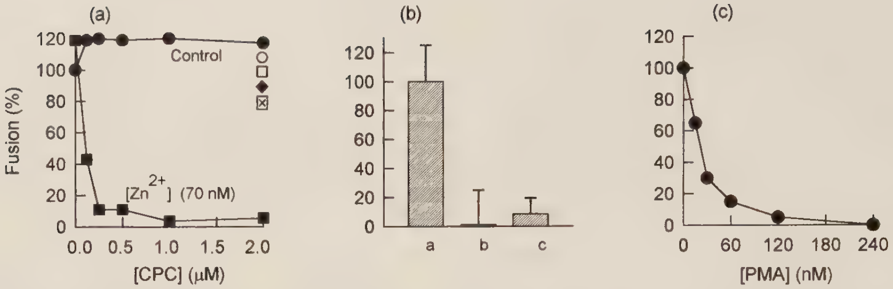

FIG. 1. Inhibition of endosome fusion by calphostin C is modulated by zinc and PMA. (a) Endosome fusion was assessed in the presence of 1 mg of cytosolic protein/ml and increasing concentrations of calphostin C in the presence (■) or absence (●) of 70 n*M* free zinc (0.4 m*M* $ZnCl_2$ added to the fusion buffer). Other metal ions tested were (□) Co^{2+}, (♦) Cd^{2+}, (○) Fe^{2+}, and (⊠) Ni^{2+} at different concentrations with very little effect. Fusion in the presence of 0.4 m*M* metal ion is shown. Free concentration was not determined for these ions. Values are expressed as a percentage of control fusion without any addition. The data are representative of at least five independent experiments. (b) Endosome fusion was assessed in the presence of 1 mg of cytosolic protein/ml. Vesicles were incubated for 15 min at 25°C, in the presence of 1 μ*M* CPC in complete fusion buffer (column a), in fusion buffer without DTT (column b), and in complete fusion buffer plus 70 n*M* free zinc (column c). DTT was added to condition b and samples were incubated for 45 min at 37°C. Fusion was assessed as described under Materials and Methods. Values are expressed as a percentage of control fusion without any addition. The data represent the mean ± SD for three independent experiments. (c) Effect of increasing concentrations of PMA in the presence of 1 mg of cytosolic protein/ml and 0.5 μ*M* CPC is shown. The fusion was expressed as a percentage of the value without PMA. The data are representative of at least three independent experiments.

washed with TPEN, a zinc chelator with low affinity for calcium and magnesium (Fig. 2c). This observation suggests that a membrane-associated factor is released by zinc chelation and that this factor is present in control cytosol but absent (or inactivated) in CPC-treated cytosol.

As CPC must be activated by light to be effective as a PKC inhibitor, we tested whether the CPC-dependent inhibition of fusion was light dependent. As expected for a PKC-like factor, the inhibitory effect was not observed when vesicles were incubated with CPC in darkness (data not shown).

Taken together, these results suggest that a factor with a PMA- and zinc-binding domain necessary for fusion is irreversibly inhibited by CPC.

PMA Stimulates Endosome Fusion, but PKC Kinase Activity Is Not Required

The role of PKC in various biological processes has been frequently investigated by using phorbol esters, such as PMA [30], that are potent activators of the enzyme. To test the hypothesis that the zinc-binding factor required for endosome fusion is a PMA-binding protein, we investigated the effect of PMA on endosome fusion in the presence or absence of TPEN. A slightly stimulatory effect of PMA in endosome fusion was observed under control conditions (Table 1). The PMA stimulatory effect became more pronounced when endosome fusion was inhibited with TPEN (Table 1). Fusion was stimulated even further when both PMA and zinc were added together to zinc-depleted fusion reactions (Table 1). These results are consistent with previous reports showing enhanced phorbol ester binding to PKC in the presence of zinc [31, 32]. These results suggest that the active conformation of the factor necessary for fusion is induced by zinc and PMA.

Inhibitors of the catalytic domain of PKC were used to investigate whether kinase activity of PKC was required

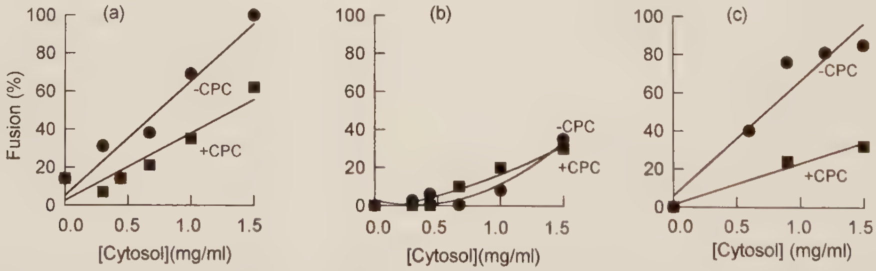

FIG. 2. Effect of CPC-treated endosomal membranes or cytosol on endosome fusion. Postnuclear fractions were incubated for 15 min at 25°C with no additions, with 1 μ*M* CPC, or with 4 m*M* TPEN. After incubation, the samples were diluted with homogenization buffer and endosomal fractions were isolated as described under Material and Methods. Cytosol was treated in homogenization buffer for 15 min at 25°C with or without 1 μ*M* CPC and gel filtered through Sephadex G-25 columns to remove excess reagent. (a) Endosome fusion between control vesicles was assessed in the presence of increasing concentration of CPC-treated cytosol (■) and control cytosol (●). (b) Endosome fusion between CPC-treated vesicles in the presence of increasing concentration of CPC-treated cytosol (■) and control cytosol (●). (c) Endosome fusion between TPEN-washed vesicles in the presence of increasing concentration of CPC-treated cytosol (■) and control cytosol (●). Values are expressed as a percentage of control fusion without any addition. The data are representative of at least three independent experiments.

TABLE 1

Effect of PMA on TPEN-Inhibited Endosome Fusion

Experimental conditions	Percentage of endosome fusion	SD
No addition	100	±12
PMA	123	±7
TPEN	9	±7
TPEN + PMA	39	±9
TPEN + Zn^{2+}	43	±6
TPEN + Zn^{2+} + PMA	87	±15

Note. Endosome fusion (1 mg of cytosolic proteins/ml) was tested with no addition or in the presence of 50 n*M* PMA, 1.7 m*M* TPEN, 1.7 m*M* TPEN plus 50 n*M* PMA, 1.7 m*M* TPEN plus 2 n*M* free zinc, or 1.7 m*M* TPEN plus 2 n*M* free zinc plus 50 n*M* PMA. Values are expressed as a percentage of control fusion without any addition. The data represent the mean ± SD of at least four independent experiments. TPEN, *N,N,N′,N′*-tetrakis-(2-pyridylmethyl) ethylenediamine; PMA, phorbol 12-myristate 13-acetate.

TABLE 2

Inhibitors of the Catalytic Domain of PKC Do Not Inhibit Fusion between Endosomes

Experimental conditions	Percentage of endosome fusion	SD
No addition	100	±15
PS peptide	98	±17
PMA + PS peptide	108	±6
Chelerythrine	94	±6
Staurosporine	94	±14

Note. Endosome fusion (1 mg of cytosolic proteins/ml) was assessed with no additions or in the presence of 30 *μM* pseudosubstrate, 100 n*M* PMA plus 30 *μM* pseudosubstrate, 10 *μM* chelerythrine, or 10 *μM* staurosporine. Values are expressed as a percentage of control fusion without any addition. The data represent the mean ± SD of at least three independent experiments. PS peptide, pseudosubstrate peptide; PMA, phorbol 12-myristate 13-acetate.

for fusion. A pseudosubstrate peptide has been reported to inhibit kinase activity of PKC activity *in vitro* [33–35]. This peptide was tested in the assay and did not inhibit endosome fusion at a concentration of 30 *μM* (Table 2). Lower concentrations have been reported to inhibit kinase activity in other systems [33–35]. The pseudosubstrate inhibitor competes more efficiently for activated forms of PKC [33]; therefore, we tested the effect of the peptide in the presence of stimulatory concentrations of PMA (100 n*M*). We did not observe inhibition under this condition either (Table 2). Since the pseudosubstrate peptide does not inhibit equally well all isoforms of PKC, other inhibitors were used. Cheleritrine, a potent and selective inhibitor of PKC (IC_{50} = 660 n*M*), which acts on the catalytic domain and which is a competitive inhibitor with respect to the phosphate acceptor and a noncompetitive inhibitor with respect to ATP [36], did not inhibit the fusion (Table 2). Staurosporine, a broad spectrum inhibitor of protein kinases, which inhibits CaM kinase (IC_{50} = 20 n*M*), myosin light chain kinase (IC_{50} = 1.3 n*M*), protein kinase A (IC_{50} = 7 n*M*), protein kinase C (IC_{50} = 8 n*M*), and protein kinase G (IC_{50} = 8.5 n*M*) [37, 38], neither inhibited the endosome fusion (Table 2). These results suggest that PKC kinase activity is not required for fusion among endosomes.

Proteins Containing a PKC-Like Cysteine-Rich Domain Are Associated to Endosomes in a Zinc-Dependent Manner

The observation that CPC-treated cytosol cannot support fusion among TPEN-washed endosomes suggests that a phorbol ester-binding protein is released by zinc depletion. Coomassie blue-stained gels revealed that several proteins are released from endosomal fraction by zinc chelators (data not shown). To assess whether some of these proteins contain a cysteine-rich region, they were blotted to nitrocellulose and analyzed using polyclonal anti-peptide antibodies raised against two different peptide sequences present in the Cys2 region of PKCγ. Only a double band of proteins of about 50 kDa was recognized by the two antibodies. Figure 3

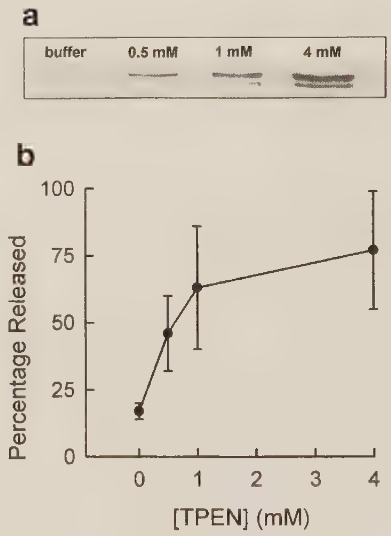

FIG. 3. Proteins containing a PKC-like cysteine-rich region are released from endosomal fractions by incubation with TPEN, a zinc chelator. Endosomal fractions were incubated with different concentrations of TPEN at 25°C for 15 min, the membranes were separated by centrifugation, and the supernatants were resolved on 10% SDS–polyacrylamide gel electrophoresis, transferred to nitrocellulose membranes, and probed with two polyclonal antibodies that recognize peptides of the Cys2 region of PKCγ. The result with anti-peptide 3 is shown in (a). The films of four experiments were scanned and the amount of both proteins released by different concentrations of TPEN was quantitated and expressed as a percentage of the amount released by 20 m*M* TPEN plus 0.5 *M* KCl (b).

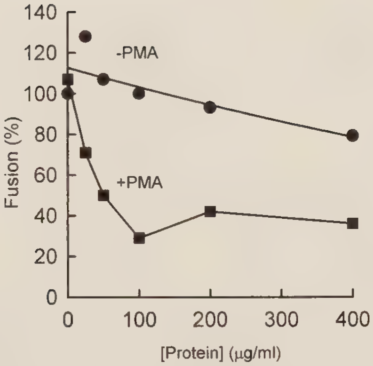

FIG. 4. The Cys2 region of PKCγ inhibits endosome fusion in a PMA-dependent manner. Endosomal fractions were washed with 30 m*M* EGTA for 10 min at 25°C and the endosome fusion was assessed in the presence of 0.5 mg of cytosolic protein/ml and increasing concentration of GST–Cys2 protein in the presence (■) or absence (●) of 500 n*M* PMA. Values are expressed as a percentage of control fusion without any addition. The data are representative of at least three independent experiments.

shows the release of the 50-kDa proteins by increasing concentrations of TPEN detected by anti-peptide 3 antibody. The efficiency of different chelators to release these proteins was TPEN > BAPTA > EGTA (data not shown). This order is consistent with the affinity of the chelators for zinc [12]. No reactivity was observed with an anti-pseudosubstrate peptide antibody (data not shown). These results indicate that a protein(s) with a cysteine-rich region similar to the Cys2 region of PKCγ is present in endosomal fractions and that zinc is required for its association to the membrane.

A GST Fusion Protein Containing the Cys2 Region of PKCγ Inhibits Endosome Fusion in a PMA-Dependent Manner

All the previous evidence suggests that the zinc- and PMA-binding site of the factor is important for its role in membrane fusion. We then tested a GST fusion protein containing the Cys2 region of PKCγ in the *in vitro* assay. Endosomes were washed with 30 m*M* EGTA prior to the assay to release factors attached to membranes. Under the conditions assessed, the GST–Cys2 protein was strongly inhibitory. Interestingly, inhibition was only observed in the presence of PMA (Fig. 4). This result suggests that the PMA-bound conformation of the Cys2 region of PKCγ can compete with the phorbol ester-binding factor for a target molecule.

DISCUSSION

Macromolecular trafficking among organelles requires a complex machinery that forms transport vesicles in donor compartments, moves the vesicles through the cytoplasm, and then fuses them with the membrane of the acceptor compartment. Several components of this machinery have been identified. However, the process is still not completely characterized. In addition to the set of factors that fit in the present model for budding, transport, docking, and fusion of vesicles [2, 3], other proteins have been implicated in the intravesicular transport process or in its regulation (e.g., protein phosphatases, phospholipase A2, protein kinase C, annexins, calmodulin). The function of these factors is mostly unknown. By using a cell-free assay, we have described a zinc requirement for endosome fusion [12]. Several factors implicated in the intracellular transport, such as rabphilin [39], ARF1 GTPase-activating protein [40], Mss4 [41], and PKC [14–19], contain putative zinc-binding domains. In the case of PKC, the cysteine-rich regions bind the physiological activator diacylglycerol as well as phorbol ester pharmacophores and represent thoroughly well-characterized zinc-coordinating motifs. Additionally, the same regions are irreversibly altered by CPC. In this report we present several lines of evidence showing that a zinc- and phorbol ester-binding protein, sensitive to CPC, is necessary for endosome fusion. First, both zinc and PMA promote CPC-dependent inhibition of endosome fusion; second, both zinc and PMA restore endosome fusion in the presence of a zinc chelator; third, CPC inactivates a factor necessary for fusion released from membranes by zinc chelation; and fourth, a protein containing the Cys2 region of PKCγ inhibits fusion in a PMA-dependent manner. Thus, we conclude that a zinc- and phorbol ester-binding protein is necessary for endosome fusion.

PMA and zinc are two factors that regulate membrane association of PKC. Likely these two factors promote endosome fusion—at least in part—by favoring the membrane association of the phorbol ester-binding factor. In contrast, zinc chelation by TPEN may inhibit fusion by promoting the release of the factor from endosomal membranes. Consistent with this hypothesis, proteins recognized by anti-Cys2 region antibodies were released from membrane fractions by zinc chelators. The observation that addition of cytosol restores fusion among TPEN-washed endosomes indicates that the factor can partition between cytosol and membranes. In addition, PMA and zinc may potentiate CPC inhibition of endosome fusion by bringing the phorbol ester-binding factor to the membranes, where it would be inactivated by the liposoluble inhibitor.

The protective effect of DTT against CPC inhibition in endosome fusion may be related to the reducing properties of this reagent that may quench oxidation by CPC. However, it can also be connected to a zinc requirement. It has been shown that DTT can protect PKC from inhibition by mercury, lead, and methyl mercury [42] suggesting that the dithiol reagent can regulate the interaction between PKC and metal ions. In addition, DTT can complex zinc and decrease free concentrations of the ion in the fusion buffer (Aballay and Mayorga, unpublished data obtained by using the APTRA–BTC fluorescent reagent; Molecular Probes).

Both zinc and PMA restored fusion under zinc-depletion conditions. Zinc and PMA bind to the cysteine-rich region of PKC. However, the elements of a cysteine-rich region required to bind zinc and phorbol esters do not completely overlap [25]. Deletion analysis indicates that the second cysteine-rich region of PKCγ can still bind PMA when only one of the two coordinated zincs is present [25]. A synthetic peptide of the same region binds phorbol ester without detectable coordinated zinc, albeit with significantly reduced affinity [43]. Therefore, it is possible that PMA and free zinc independently contribute to stabilize the factor in an active conformation. When both molecules are present, the factor is held in the active conformation and endosome fusion is maximized.

The best characterized phorbol ester-binding proteins belong to the PKC family. For these proteins, the cysteine-rich domains are crucial regulatory domain elements involved in modulating kinase activity. However, according to our results, PKC kinase activity is not required for endosome fusion. Similar conclusions have been reported by other authors analyzing the role of PKC in intracellular trafficking [44, 45]. Zinc-finger domains that bind phorbol esters are not exclusive for PKC. Several other proteins present similar domains that may be important for specific interaction with membranes [46–50].

What could the role of a phorbol ester-binding protein be in the fusion mechanism? Two functions for phorbol ester-binding proteins that may be important for vesicular transport and do not involve protein phosphorylation have been characterized, the activation of PLD by PKC [51] and the rac–GTPase-activating property of *N*-chimaerin [49]. Activation of PLD produces phosphatidic acid that has been implicated in a cascade of events leading to the formation of a membrane microdomain enriched in acidic phospholipids that can promote membrane destabilization and fusion [52]. On the other hand, several GTPases are involved in vesicle formation and membrane fusion; therefore, a phorbol ester-binding protein with GAP activity may have an important role in the regulation of these proteins. In addition, PLD activation and GTP-binding protein regulation may be interconnected since PKCα and small GTPases, such as rho and ARF, work synergically to activate PLD.

The possibility that the phosphorylating activity of some PKC isoenzymes might play a role in vesicular transport cannot be ruled out. Some steps of the complex mechanism of vesicle formation, transport, and fusion are regulated by protein phosphorylation. Indeed, some of the effects of PKC on intracellular transport reported by other authors are dependent on protein phosphorylation [14, 16, 53].

In conclusion, our results indicate that a protein with a phorbol ester-binding domain, analogous to the cysteine-rich domain of PKCγ, is required for endosome fusion. This region of PKCγ coordinates two atoms of zinc; therefore, the inhibitory effect of zinc depletion on endosome fusion [12] is probably due to inactivation of the phorbol ester-binding factor. However, the possibility that zinc chelation can affect additional proteins cannot be ruled out.

We thank Cheryl Adles and Alejandra Challa for excellent technical assistance. This work was partly supported by an International Research Scholar of the Howard Hughes Medical Institute and by grants of the National Science Foundation–CONICET International Program, CONICET, CIUNC, and Fundación Antorchas. A.A. is supported by a CONICET fellowship. L.S.M. is a fellow of the Rockefeller Foundation Biotechnology Career. A.F.G.Q. is supported by the Swiss National Science Foundation (SNF 3100-040477) and The Swiss Cancer League (FOR 645).

REFERENCES

1. Pryer, N. K., Wuestehube, L. J., and Schekman, R. (1992) *Annu. Rev. Biochem.* **61,** 471–516.
2. Rothman, J. E. (1994) *Nature* **372,** 55–63.
3. Rothman, J. E., and Wieland, F. T. (1996) *Science* **272,** 227–234.
4. Diaz, R., Mayorga, L. S., Weidman, P. J., Rothman, J. E., and Stahl, P. D. (1989) *Nature* **339,** 398–400.
5. Rodriguez, L., Stirling, C. J., and Woodman, P. G. (1994) *Mol. Biol. Cell* **5,** 773–783.
6. Lenhard, J. M., Kahn, R. A., and Stahl, P. D. (1992) *J. Biol. Chem.* **267,** 13047–13052.
7. Gorvel, J. P., Chavrier, P., Zerial, M., and Gruenberg, J. (1991) *Cell* **64,** 915–925.
8. Barbieri, M. A., Li, G. P., Colombo, M. I., and Stahl, P. D. (1994) *J. Biol. Chem.* **269,** 18720–18722.
9. Stenmark, H., Vitale, G., Ullrich, O., and Zerial, M. (1995) *Cell* **83,** 423–432.
10. Colombo, M. I., Mayorga, L. S., Casey, P. J., and Stahl, P. D. (1992) *Science* **255,** 1695–1697.
11. Colombo, M. I., Inglese, J., D'Souza-Schorey, C., Beron, W., and Stahl, P. D. (1995) *J. Biol. Chem.* **270,** 24564–24571.
12. Aballay, A., Sarrouf, M. N., Colombo, M. I., Stahl, P. D., and Mayorga, L. S. (1995) *Biochem. J.* **312,** 919–923.
13. Coleman, J. E. (1992) *Annu. Rev. Biochem.* **61,** 897–946.
14. Ozawa, K., Szallasi, Z., Kazaniets, M. G., Blumberg, P. M., Mischak, H., Mushinski, J. F., and Baeven, M. A. (1993) *J. Biol. Chem.* **268,** 1749–1756.
15. Buccione, R., Di Tullio, G., Caretta, M., Marinetti, M. R., Bizzarri, C., Francavilla, S., Luini, A., and De Matteis, M. A. (1994) *Biochem. J.* **298,** 149–156.
16. Akita, Y., Ohno, S., Yajima, Y., Konno, Y., Saido, T. C., Mizuno, K., Chida, K., Osada, S., Kuroki, T., Kawashima, S., and Suzuki, K. (1994) *J. Biol. Chem.* **269,** 4653–4660.
17. Cardone, M. H., Smith, B. L., Song, W., Mochly-Rosen, D., and Mostov, K. E. (1994) *J. Cell Biol.* **124,** 717–727.
18. De Matteis, M. A., Santini, G., Kahn, R. A., Di Tullio, G., and Luini, A. (1993) *Nature* **364,** 818–821.

19. Simon, J.-P., Ivanov, I. E., Shopsin, B., Hersh, D., Adesnik, M., and Sabatini, D. D. (1996) *J. Biol. Chem.* **271,** 16952–16961.
20. Gschwendt, M., Kittstein, W., and Marks, F. (1991) *Trends Biochem. Sci.* **16,** 167–169.
21. Muramatsu, M. A., Kaibuchi, K., and Arai, K. I. (1989) *Mol. Cell. Biol.* **9,** 831–836.
22. Kaibuchi, K., Miyajima, A., Arai, K., and Matsumoto, K. (1989) *Proc. Natl. Acad. Sci. USA* **83,** 8172–8176.
23. Bell, R. M., and Burns, D. J. (1991) *J. Biol. Chem.* **266,** 4661–4664.
24. Quest, A. F. G., Bardes, E. S. G., and Bell, R. M. (1994) *J. Biol. Chem.* **269,** 2953–2960.
25. Quest, A. F. G., Bardes, E. S. G., and Bell, R. M. (1994) *J. Biol. Chem.* **269,** 2961–2970.
26. Diaz, R., Mayorga, L., and Stahl, P. (1988) *J. Biol. Chem.* **263,** 6093–6100.
27. Diaz, R., Mayorga, L. S., Mayorga, L. E., and Stahl, P. D. (1989) *J. Biol. Chem.* **264,** 13171–13180.
28. Atar, D., Backx, P. H., Appel, M. M., Gao, W. D., and Marban, E. (1995) *J. Biol. Chem.* **270,** 2473–2477.
29. Rotenberg, S. A., Huang, M. H., Zhu, J., Su, L., and Riedel, H. (1995) *Mol. Carcinogen.* **12,** 42–49.
30. Nishizuka, Y. (1992) *Science* **258,** 607–614.
31. Forbes, I. J., Zalewski, P. D., Giannakis, C., Petkoff, H. S., and Cowled, P. A. (1990) *Biochim. Biophys. Acta* **1053,** 113–117.
32. Hubbard, S. R., Bishop, W. R., Kirschmeier, P., George, S. J., Cramer, S. P., and Hendrickson, W. A. (1991) *Science* **254,** 1776–1779.
33. House, C., and Kemp, B. E. (1987) *Science* **238,** 1726–1728.
34. Kazanietz, M. G., Bustelo, X. R., Barbacid, M., Kolch, W., Mischak, H., Goodnight, H., Mushinski, J. F., and Blumberg, P. M. (1993) *Mol. Pharmacol.* **44,** 298–307.
35. Kochs, G., Hummel, R., Meyer, D., Hug, H., Marme, D., and Sarre, T. F. (1993) *Eur. J. Biochem.* **216,** 597–606.
36. Barg, J., Belcheva, M. M., and Coscia, C. J. (1992) *J. Neurochem.* **59,** 1145–1152.
37. Tischler, A. S., Ruzicka, L. A., and Perlman, R. L. (1990) *J. Neurochem.* **55,** 1159–1165.
38. Yanagihara, N., Tachikawa, E., Izumi, F., Yasugawa, S., Yamamoto, H., and Miyamoto, E. (1991) *J. Neurochem.* **56,** 294–298.
39. Shirataki, H., Kaibuchi, K., Sakoda, T., Kishida, S., Yamaguchi, T., Wada, K., Miyazaki, M., and Takai, Y. (1993) *Mol. Cell. Biol.* **13,** 2061–2068.
40. Cukierman, E., Huber, I., Rotman, M., and Cassel, D. (1995) *Science* **270,** 1999–2002.
41. Yu, H., and Schreiber, S. L. (1995) *Biochemistry* **34,** 9103–9110.
42. Rajanna, B., Chetty, C. S., Rajanna, S., Hall, E., Fail, S., and Rotenberg, S. A., Huang, M. H., Zhu, J., Su, L., and Riedel, H. (1995) *Mol. Carcinogen.* **12,** 42–49.
43. Wender, P. A., Irie, K., and Miller, B. L. (1995) *Proc. Natl. Acad. Sci. USA* **92,** 239–243.
44. Fabbri, M., Bannykh, S., and Balch, W. E. (1994) *J. Biol. Chem.* **269,** 26848–2685.
45. Simon, J. P., Ivanov, I. E., Adesnik, M., and Sabatini, D. D. (1996) *J. Cell Biol.* **135,** 355–370.
46. Li, P., Wood, K., Mamon, H., Haser, W., and Roberts, T. (1991) *Cell* **64,** 479–482.
47. Coppola, J., Bryant, S., Koda, T., Conway, D., and Barbacid, M. (1991) *Cell Growth Differ.* **2,** 95–105.
48. Ahmed, S., Kozma, R., Lee, J., Monfries, C., Harden, N., and Lim, L. (1991) *Biochem. J.* **280,** 233–241.
49. Ahmed, S., Lee, J., Kozma, R., Best, A., Monfries, C., and Lim, L. (1993) *J. Biol. Chem.* **268,** 10709–10712.
50. Kazanietz, M. G., Lewin, N. E., Bruns, J. D., and Blumberg, P. M. (1995) *J. Biol. Chem.* **270,** 10777–10783.
51. Conricode, K. M., Brewer, K. A., and Exton, J. H. (1992) *J. Biol. Chem.* **267,** 7199–7202.
52. Liscovitch, M., and Cantley, L. C. (1995) *Cell* **81,** 659–662.
53. Buccione, R., Bannykh, S., Santone, I., Baldassarre, M., Facchiano, F., Bozzi, Y., Di Tullio, G., Mironov, A., Luini, A., and De Matteis, M. A. (1996) *J. Biol. Chem.* **271,** 3523–3533.

Received January 10, 1997
Revised version received May 12, 1997

EXPERIMENTAL CELL RESEARCH **235,** 35–47 (1997)
ARTICLE NO. EX973630

Characteristics of 25-Hydroxycholesterol-Induced Apoptosis in the Human Leukemic Cell Line CEM

Sylvette Ayala-Torres, Peter C. Moller, Betty H. Johnson, and E. Brad Thompson[1]

Department of Human Biological Chemistry and Genetics, The University of Texas Medical Branch, Galveston, Texas 77555-0645

Cholesterol and related compounds can give rise to oxygenated sterol molecules (oxysterols) which are potent regulators of lymphoid cell growth. Oxysterols added exogenously cause cell death of several lines of cultured cells, and on the basis of limited criteria, it has been suggested that this death is apoptosis. In the present study, we show definitive evidence that 25-hydroxycholesterol (25OHC) kills cells of the clone CEM-C7 by apoptosis and establish the temporal sequence of related cellular and biochemical events. Cell shrinkage was evident as early as 12 h, while cell death was not evident until after 24 h. It mounted rapidly after that, and by 72 h, virtually all cells were dead. Electron microscopic analysis shows that by 24 h after treatment and before the onset of cell death, early ultrastructural features typical of apoptosis were present. DNA breaks were detected by TUNEL assay prior to the onset of cell death. Two types of specific DNA pieces often associated with apoptosis were found as increasing numbers of cells died. DNA fragments of 300 and 50 kbp were not appreciable until 42 h, and internucleosomal cleavage was observed by 48 h after oxysterol addition. None of these effects were seen in an oxysterol-resistant CEM subclone, establishing the specificity for apoptosis of the biochemical and morphological events. z-VAD.FMK, a peptide inhibitor of ICE-related proteases delayed but did not prevent the apoptosis of CEM-C7 cells induced by 25OHC. The addition of mevalonate partially protected CEM-C7 cells from apoptosis but did not restore cell growth. © 1997 Academic Press

INTRODUCTION

Through autooxidation or enzymatic reactions, cholesterol and related compounds give rise to a number of sterols containing additional oxygens (oxysterols). Oxysterols have been identified in cholesterol-containing food, in tissues, in cells, and in blood, where they are associated with serum lipoproteins and specifically with albumin [55, 52]. Oxysterols are potent regulatory molecules which can prevent lymphoid cell growth, arresting the cells in the G1 phase of the cell cycle [10, 18, 34]. They cause death of several lines of cultured cells [55, 25]. Based on the differential sensitivity of malignant and normal cells to oxysterols *in vitro,* it has been suggested that oxysterols could be useful therapeutic agents [26, 38, 41, 43, 61].

Little is known about the mechanism(s) involved in oxysterol-induced cell death. Some reports on a few cell lines have correlated internucleosomal DNA fragmentation and apoptosis induced by oxysterols [2, 5, 13, 42]. Some of these reports combined the detection of DNA ladders with the analysis of cellular DNA content by using flow cytometric analysis [2, 13]. It is the consensus that before concluding that apoptosis is the mechanism behind a given example of death, both ultrastructural and biochemical criteria should be met. In only one case has this been done carefully for oxysterols in bovine aortic endothelial cells [36]. We present an analysis of leukemic lymphoid cell death evoked by oxysterols that clearly shows this to be an apoptotic process. Apoptosis is defined fundamentally by morphology, with dying cells showing loss of cell junctions and microvilli, cell shrinkage, membrane budding, a distinctive pattern of chromatin margination, nuclear breakdown, and cell breakage into discrete membrane-bound apoptotic bodies [28, 29, 16]. Oncosis, a term proposed as synonym of nonapoptotic or accidental cell death, is morphologically characterized by cellular swelling, an irregular pattern of chromatin organization, and membrane disintegration [37].

Human leukemic CEM cells are killed by oxysterols [4]. The critical morphological criteria that define the process of apoptosis in oxysterol-induced death have yet to be fulfilled in lymphoid cells; specifically, these criteria have never been studied in human lymphoblastic leukemia cells. We therefore have performed a comprehensive study of the effects of 25-hydroxycholesterol (25OHC),[2] a potent oxysterol, on the cellular morphology of cell clones derived from the human lymphoblastic leukemia line CEM. We further compare the timing

---

[1] To whom correspondence and reprint requests should be addressed at Department of Human Biological Chemistry and Genetics, The University of Texas Medical Branch, 301 University Boulevard, 605 Basic Science Building, Galveston, TX 77555. Fax: (409) 772-5159. E-mail: bthompso@msp01.med.utmb.edu.

[2] Abbreviation used: 25OHC, 25-hydroxycholesterol.

0014-4827/97 $25.00
Copyright © 1997 by Academic Press
All rights of reproduction in any form reserved.

and sequence of these changes with the appearance of several classes of DNA fragments that evidence nucleolysis, a classic biochemical correlate of apoptosis. Recently it has been suggested that activation of the ICE family of cysteine proteases (caspases) play a core role in the execution of apoptosis [19]. Therefore, we have also investigated the possible involvement of an ICE-related protease(s) in 25OHC-induced apoptosis of CEM cells.

Oxysterols are potent regulatory molecules known to suppress cholesterol biosynthesis. Oxysterols inhibit several critical enzymes involved in the cholesterol pathway, in particular the rate-limiting enzyme 3-hydroxy-3-methylglutaryl coenzyme A reductase (HMG-CoAR) [11, 58]. Because CEM cells are killed by oxysterols and these oxygenated steroids are potent supressors of HMGCoAR in CEM-C7 cells [59], we also tested the ability of added mevalonic acid, the immediate product of HMGCoAR, to prevent cell death induced by 25OHC.

MATERIALS AND METHODS

Materials. The 25OHC (5-cholestene3β,25-diol), mevalonolactone, bovine serum albumin (BSA), and Dulbecco's phosphate-buffered saline (PBS) were purchased from Sigma Chemical Co. (St. Louis, MO). The culture medium RPMI 1640 was obtained from Mediatech, Inc., and fetal bovine serum (FBS) was obtained from Atlanta Biologicals (Norcross, GA). SeaKem LE agarose was purchased from FMC Products (Rockland, ME). The high-molecular-weight DNA markers were obtained from Gibco, BRL (Grand Island, NY) and the λ DNA and DNase I were obtained from Promega (Madison, WI). The TUNEL detection kit was purchased from Boehringer-Mannheim (Mannheim, Germany) and ribonuclease A was obtained from Worthington Biochemical Corp. (Freehold, NJ). Both Ac–Tyr–Val–Ala–Asp–CHO (y-VAD-CHO, inhibitor of interleukin-1β-converting enzyme) and *z*-Val–Ala–DL–Asp–fluoromethylketone (z-VAD.FMK, inhibitor of CPP32) were purchased from Alexis Biochemicals (San Diego, CA).

Cell culture and oxysterol treatment.. CEM-C7 cells were selected by cloning the original CEM line of acute lymphoblastic leukemia cells [45]. M10 cells were selected from CEM-C7 for growth in agarose in the presence of a high concentration of 25OHC. M10R5 cells were subcloned from M10 cells on soft agarose and further selected in high doses of 25OHC [3]. Cells were cultured in RPMI 1640 medium, pH 7.4, containing 5% heat-inactivated whole serum, at 37°C under humidified conditions of 95% air and 5% CO_2, until logarithmic conditions of growth were attained. Cells (2×10^5 cells/ml) were then shifted to RPMI 1640 medium with 2.5% delipidated serum for 24 h prior to the addition of vehicle only (<1% ethanol) in 1% BSA-containing PBS or an ethanolic solution of 25OHC in 1% BSA, to give a final concentration of 300 n*M* 25OHC. For the studies involving the addition of mevalonate, the biologically active compound was obtained by hydrolyzing the mevalonolactone with equimolar base (10 *N* NaOH). For the growth studies involving ICE-related enzymes, the protease inhibitors were added to the cells 1 h prior to the addition of 25OHC. Delipidated serum [51] was used to avoid additional effects from sterols that are present in whole serum. After treatment, cells were harvested at the various times indicated and processed for the assays. The number of viable cells was determined by using the trypan blue exclusion method [49]. With no further treatment cells were fully viable in this medium containing delipidated serum.

Light microscopy. Analysis of cell morphology by light microscopy was carried out on cells in tissue culture flasks using a Leitz microscope and 320× magnification. At chosen times, cells were photographed using Kodak Tmax film (400 ASA).

Transmission electron microscopy. CEM-C7 cells were fixed in 2% glutaraldehyde in PBS, pH 7.4, for 90 min, rinsed in PBS, and postfixed in 1% OsO_4 for an additional 90 min. The samples were then stained *en bloc* with uranyl acetate (0.3%/50% ethanol) for 60 min, dehydrated in a graded series of ethanol, and embedded in Spurr low-viscosity embedding medium [57]. Prior to the electron microscopic evaluation, thin sections were stained with uranyl acetate (3%/H_2O, pH 5) and lead citrate. Three early ultrastructural features of apoptosis were evaluated as follows: 400 consecutive, unselected cells were evaluated, using all evaluable cells in each field. Cells showing $\geqslant$50% decrease in the number of microvilli, partial chromatin packing and aggregation toward the nuclear periphery, and/or aggregates of cytoplasmic vacuoles localized to a particular area were counted as early apoptotic. The frequency of these changes in control cells was evaluated for comparison, using random fields.

Cell volume analysis. An aliquot of live cells was placed in a hemocytometer and viewed under a Leitz Laborlux D light microscope. A live image of cells was obtained on the screen of an IBM PC computer monitor by using the BioQuant Meg IV-Vista system as the measurement software (R&M Biometrics). The area of individual cells was determined by scanning 100 consecutive cells at 12, 24, and 48 h after treatment. Lines were drawn around the perimeter of each cell using a Summa Sketch II board and mouse. Area values were obtained from the measurement program and converted to volumetric units for these nearly spherical cells, using the equations for area and volume of a sphere.

Field inversion gel electrophoresis (FIGE). The detection of and discrimination between high-molecular-weight DNA fragments was done according to a modified method of Anand and Southern [1]. Electrophoresis was carried out to separate DNA fragments either in the 50- to 300-kbp size range (112 V [6 volts/cm gel], reverse time 0.1–10 s, forward time 0.3–30 s, 20 h, and 14 min, 10°C) or in the 10- to 50-kbp size range (141 V [7.5 v/cm gel], reverse time 0.01–0.59 s, forward time 0.025–1.475 s, 14 h, and 49 min, 14°C) using a horizontal gel system from Bio-Rad Laboratories (Hercules, CA). After the gels were stained with ethidium bromide (0.5 μg/ml), they were visualized in a 254-nm UV transilluminator and photographed using Polaroid film type 55. The relative amounts of DNA were determined by image analysis of the picture negatives using an image analyzer (Biological Visions Inc., San Mateo, CA).

Conventional gel electrophoresis. Detection of small DNA fragments was done according to the method of Duke and Cohen with some modifications [21]. Cells (2×10^6) were washed with PBS and lysed using Nonidet-P40. The cells were vortexed for 10 s and centrifuged at 13,000*g* for 15 min at 4°C to remove intact chromatin and debris. The fragmented nucleic acids in the supernatant were precipitated overnight at −20°C by adding 5 *M* NaCl and 2 vol of ice-cold isopropanol. The supernatant was centrifuged for 30 min at 13,000*g*, the precipitated nucleic acids were washed with 70% ethanol, and the pellet was dissolved in 20 μl of TE buffer (10 m*M* Tris–HCl, 1 m*M* EDTA) after air drying. After the addition of 0.1 vol of 10× sample loading buffer the samples were heated at 65°C, loaded in a 1.2% agarose gel, and subjected to electrophoresis for 2 h (50 V) using TBE (0.09 *M* Tris–borate, 2 m*M* EDTA) as the running buffer. The gel was stained with ethidium bromide (0.5 μg/ml), visualized in a 302-nm UV transilluminator, and photographed using Polaroid film type 55.

Terminal deoxynucleotidyl transferase-mediated dUTP nick end labeling (TUNEL) assay. The TUNEL assay was performed according to the specifications provided by the manufacturer (Boehringer-Mannheim) of the kit employed with some modifications. Prior to fixation, 6×10^6 cells were centrifuged at 1000 rpm for 10 min using a Beckman 12 microfuge (Palo Alto, CA) and the pelleted cells were washed twice with 1% BSA-containing PBS, pH 7.4. The washed cells were resuspended in 1% BSA-containing PBS and divided equally in duplicate tubes, fixed in 4% paraformaldehyde, buffered to pH 7.4 with 1 N NaOH, washed with 1% BSA-containing PBS, centrifuged, and stored at 4°C until all the time points were harvested. The labeling was done by resuspending the cells in the TUNEL reaction mixture for 60 min in a 37°C water bath. For each assay that was performed, both negative and positive controls were included. The negative controls did not receive the deoxynucleotidyl transferase, whereas cells used for the positive controls were incubated in the presence of DNase I (1 μg/ml) for 10 min at 37°C after being permeabilized. Cells were stained with propidium iodide according to the method herein described.

Propidium iodide staining. DNA staining with propidium iodide was performed according to a method similar to that described by Van Houten and Budd [60]. Aliquots of 100 μl containing cells from the TUNEL reaction were spun down and resuspended in 250 μl of low-salt propidium iodide stain solution (3% polyethylene glycol 8000, 50 μg/ml propidium iodide, 180 units/ml RNase A, 0.1% Triton X-100 in PBS/1% sodium azide, 4 mM sodium citrate) and incubated in a 37°C water bath for 20 min with gentle mixing. The same cells were incubated in 250 μl of high salt stain solution (3% polyethylene glycol 8000, 50 μg/ml propidium iodide, 0.1% Triton X-100, 400 mM sodium chloride) and stored overnight at 4°C. Samples (20,000 cells each) were analyzed for DNA content and DNA breaks by flow cytometry using a FACScan (Becton–Dickinson). For the TUNEL analysis, the Cell Quest 1.2 (Becton–Dickinson) software was used. Analysis was done using an argon-ion laser with excitation at 488 nm. Doublets and cell aggregates were gated out and only the singlet cell population was analyzed. Red (propidium iodide) and green (fluorescein–dUTP) fluorescences were detected using 530- and 584-nm filters, respectively.

RESULTS

CEM-C7 Cells Treated with Oxysterol Show Typical Morphological Changes of Apoptosis

We have reported that 25OHC kills the clonal line of CEM human lymphoid cells, CEM-C7, while a subline, M10, showed significant but not absolute resistance [3]. In the present study, we compared the effects of 25OHC on CEM-C7 cells with those on M10R5, a more highly oxysterol-resistant subclone of M10 cells. Figure 1A shows that under the conditions used herein, the oxysterol-sensitive cells grow normally for about 18 h, leveling off after about 24 h. A significant reduction in viable CEM-C7 cells is seen by 42 h after the addition of 300 nM 25OHC, a concentration 9–10× the LD_{50} for these cells when cultured for 4 days in 5% delipidated serum [45]. Here, by 72 h, virtually all 25OHC-treated CEM-C7 cells are dead, whereas M10R5 cells were not killed or growth inhibited (Fig. 1B). The morphology of both of these cell clones was studied after 25OHC addition. Under light microscopy (Fig. 2) it can be seen that 48 h after the addition of the steroid, there is obvious shrinkage of many CEM-C7 cells, one of the hallmark morphological changes of apoptotic cell death. In addition, some entire cells have become apoptotic or have fragmented into dense bodies. Cell swelling (oncosis) was not seen. Unlike the sensitive CEM-C7 cells, the M10R5 cells do not show any signs of shrinkage, have obviously continued to divide, and appear quite healthy (Fig. 2D).

Electron microscopic analysis of CEM-C7 cells treated with 25OHC (Fig. 3) shows that control CEM-C7 cells (Fig. 3a) contain large nuclei with diffuse heterochromatin and one or more nucleoli. The cytoplasm shows normal ultrastructural features and the plasma membrane shows the presence of numerous microvilli. Beginning 24 h after treatment (Figs. 3b and 3c), and before the onset of obvious cell death, early ultrastructural features typical of apoptosis are observed in both the nucleus and the cytoplasm. Of 400 consecutive, unselected cells that were examined as described under Materials and Methods, 19% showed early signs of chromatin condensation toward the nuclear periphery; 26% showed reduction or complete loss of microvilli; and 7% exhibited increased vacuolization (Figs. 3b and 3c). Only 4.5, 7.5, and 1.5% of control cells showed the respective apoptotic changes. Also, a substantial reduction in the size of the cell and the nucleus was obvious in most of the cells that were evaluated after 24 h in the presence of the oxysterol. By 48 h after the addition of 25OHC (Fig. 3d) the reduction in cell volume was much more striking, and both the nucleus and the cytoplasm were highly condensed. The heterochromatin became highly electron dense and packed against one inner side of the nuclear membrane in an even distribution, unlike the irregular chromatin aggregates seen in some examples of necrosis [30, 31]. The plasma membrane of cells treated for 24 h with the steroid showed normal features except for loss of microvilli; however, after 48 h in the presence of the oxysterol the cell membrane in some cells looked partially disrupted as is the case with the cell shown in Fig. 3d. Thus, we show that the ultrastructural features induced by 25OHC treatment of CEM-C7 cells are those of classical apoptosis, e.g., equivalent to those observed in the apoptosis induced in human lymphoblastoid cells by glucocorticoids [50].

25OHC Induces Cell Shrinkage of CEM-C7 Cells

The apparent reduction in cell volume induced by 25OHC treatment was quantified using image analysis. As early as 12 h after the addition of the steroid, a significant reduction in cell volume of the oxysterol-sensitive clone was observed (Fig. 4A). The resistant M10R5 cells showed random changes in size, with no significant trend (Fig. 4B). Only at 48 h was the average size of 25OHC-treated M10R5 cells statistically less than its time-matched control, but the treated cell average for all the time points studied was not significantly different from that of the control cells at 0 h or the average of all control values. CEM-C7 cells, on the other hand, clearly underwent a progressive decrease in average volume of 19, 40, and 53% at 12, 24, and 48 h after treatment, respectively, compared to time-matched controls (Fig. 4A). Further data analysis suggested a rapid transition to a smaller cell size, perhaps as a result of most of the cell population undergoing shrinkage suddenly in the absence of G0/G1 arrest, since the percentage of CEM-C7 cells at G1 did

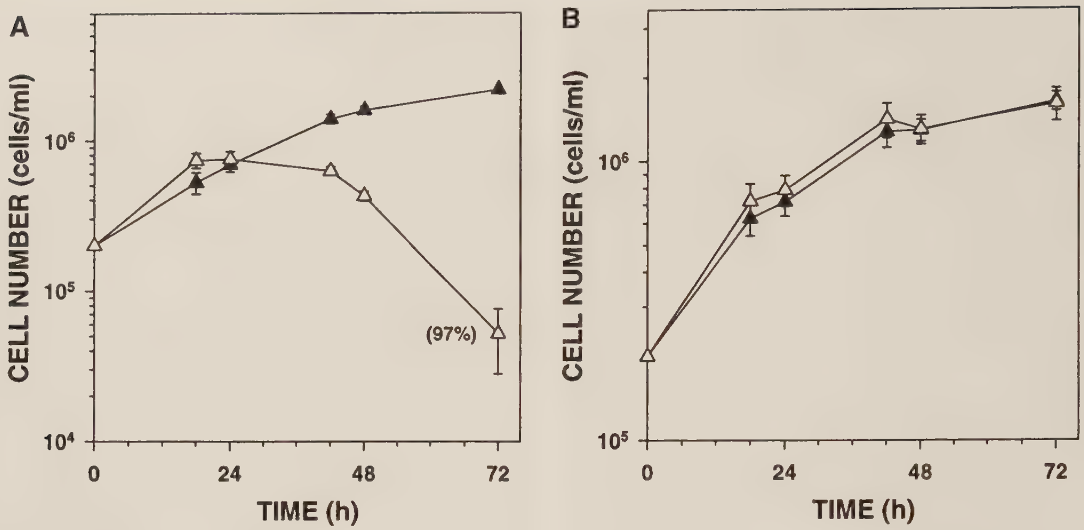

FIG. 1. Effects of 300 n*M* 25OHC treatment on CEM-C7 (A) and M10R5 (B) cell growth and viability. Oxysterol-sensitive CEM-C7 cells and oxysterol-resistant M10R5 cells were grown in the presence of 300 n*M* 25OHC or vehicle only. The quantity of viable cells (cells/ml) was determined by hemacytometer counts using the trypan blue dye exclusion method. Each point represents the mean ± 1 SD from four independent experiments. The deficit in viable cells at the 72-h time point in the 25OHC-treated CEM-C7 cells compared with control is shown as a percentage in parentheses in A. Closed symbols, cells treated with $<1\%$ ethanol carrier only; open symbols, 25OHC-treated cells.

not increase after 24 h of steroid treatment (data not shown). Histograms of distribution of cell size per cell for oxysterol sensitive CEM cells showed a minimal shift to a smaller size after 12 h of steroid treatment (data not shown), whereas the majority of the cell population moved to the left after 24 h, indicating that the further significant reduction in cell size observed at this time occurred relatively quickly (Fig. 4D). It is possible that these cells represent a preapoptotic population, since the average cell volume has decreased by 50% after 24 h in 25OHC; yet growth suppression of the overall culture has just begun, and removal of the steroid or rescue by the addition of mevalonate allows continued growth [4]. Note that all cells used for volumetric measurements completely excluded the vital dye trypan blue at the times that we studied, although at the final 48-h time point many intermingled cells in the culture were already dead (dye positive). Thus, these data show that 25OHC causes a significant reduction in cell volume early in the processes it initiates, prior to outright cell death. This is an effect of 25OHC treatment linked to ultimate cell death, because the resistant M10R5 cells do not suffer any consistent change in size in medium containing the same steroid (Fig. 4B).

25OHC Induces Formation of Specific Large and Internucleosomal DNA Fragments in CEM-C7 Cells

Fragmentation of DNA into two general size classes may occur during apoptosis, resulting in internucleosomal multiples of 180 bp and large, 10- to 300-kbp fragments [47]. It has been suggested that the large fragments are more pathognomonic and that they may be precursors to the internucleosomal pieces [47, 32]. Because the ladder of internucleosomal units sometimes is not seen [62, 46, 53], one of the most useful biochemical criteria to identify apoptosis may be the cleavage of DNA to large fragments of 300 and/or 50 kbp. We find that during the time that CEM-C7 cells undergo cell death caused by 25OHC, large DNA fragments are produced. Figure 5A shows an example of the time course of formation from 25OHC-treated CEM-C7 cells of DNA fragments in the size range 50- to 300-kbp. Low levels of fragments that resolved as discrete bands of 300 and 50 kbp in length are seen at equal levels in both treated and untreated cell DNA only at time points tested earlier than 42 h (Figs. 5A and 5B). We believe that the initially higher levels of DNA fragmentation that are observed in the control DNA are the result of acutely shifting the cells to medium containing delipidated serum, since DNA from cells in whole serum (0 h) do not show DNA fragmentation (data not shown). DNA after 1, 4, 8, and 12 h also shows equal levels of cleavage in control and treated cells (data not shown). However, an increase in the 300- and 50-kbp fragments in the DNA from 25OHC-treated, sensitive cells is first detected with certainty at 42 h after treatment (Figs. 5A, lane 6). These fragments increase in intensity as more cells die, becoming very striking after 72 h, when there are many apoptotic cells in the culture. Further analysis using conditions that better resolve 10- to 50-kbp DNA revealed the presence of a DNA doublet around 50 kbp and a smear of many sized DNA fragments in the 10- to 40-kbp size range (Fig.

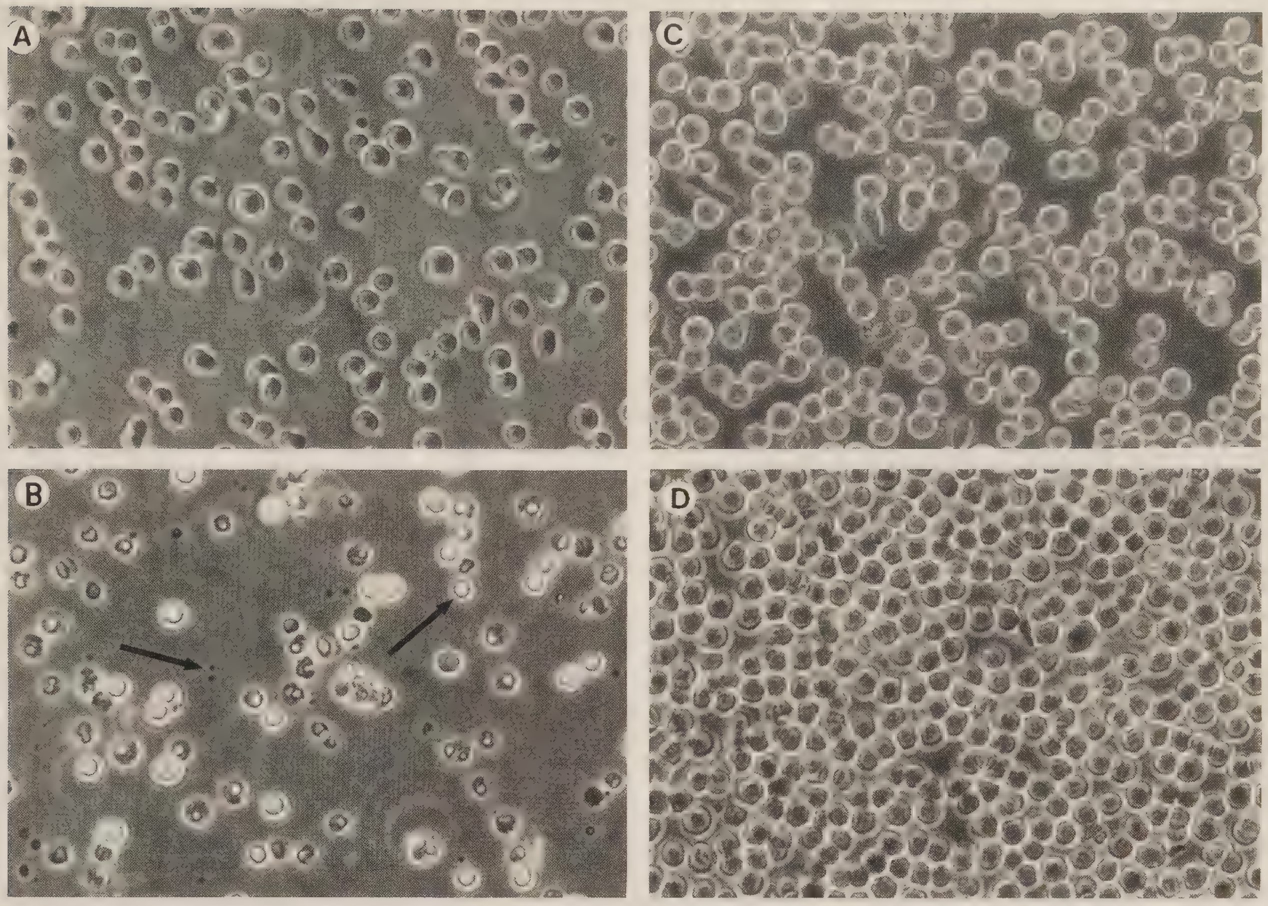

FIG. 2. CEM-C7 but not M10R5 cells show apoptotic morphology after treatment with 25OHC. The photomicrographs were made under light microscopy directly from the tissue culture flasks in which the cells were grown, 48 h after initiation of treatment. (A and B) Control and 300 n*M* 25OHC-treated CEM-C7 cells, respectively. (C and D) M10R5 cells, control and 300 n*M* 25OHC, respectively. Original magnification, 320×. Arrows in (B) indicate examples of shrunken cells and apoptotic bodies.

5B). Both the DNA doublet and the smear significantly increase in the 25OHC-treated, sensitive cells, following the same time course. However, the timing of the appearance of large fragments may be somewhat dose dependent since we have observed by FIGE, fragments in the range 36- to 42-h when a somewhat higher concentration of the steroid was used [27]. DNA from the 25OHC-resistant cells, M10R5, does not show any significant fragmentation under the same conditions at any of the times tested. Only the data from the 72-h treatment are shown (Figs. 5A and 5B, lanes 11 and 12). When the changes in the relative amounts of the three major classes of large DNA fragments from both CEM-C7 and M10R5 cells are plotted against time (Fig. 5C) it can be seen that the 300-, 50-, and <50-kbp fragments that appeared at 42 h may have gradually accumulated up to 48 h, but increased rapidly thereafter, as the number of apoptotic cells escalated. None of the fragments appeared transiently, but with time, the 50-kbp fragment became relatively more abundant than the 300-kbp fragment. In order to determine if internucleosomal DNA fragmentation was induced by 25OHC in CEM-C7 cells and whether the large DNA fragments were acting as precursors to the smaller internucleosomal fragments, we analyzed cellular DNA for 180-bp ladders using conventional gel electrophoresis. Twenty-four hours after addition of 25OHC to the cultures there is no change in internucleosomal fragmentation from controls. Because changes in only a few cells might be missed due to the insensitivity of the assay, we analyzed up to 3× the usual number of cells at the 24-h time point, without detecting this type of fragmentation (data not shown), but a typical 180-bp apoptotic ladder can be demonstrated after a 48-h incubation period only in cells of the sensitive CEM-C7 clone and not in the oxysterol-resistant M10R5 cells (Fig. 6). At the time points evaluated our results suggest that 25OHC treatment of oxysterol-sensitive lymphoid cells induces cleavage of DNA into high- and low-molecular-weight fragments concomitant with cell death.

25OHC Causes DNA Breaks before Irreversible Apoptotic Events

To determine whether DNA breaks not detected by electrophoretic analysis were occurring in the treated

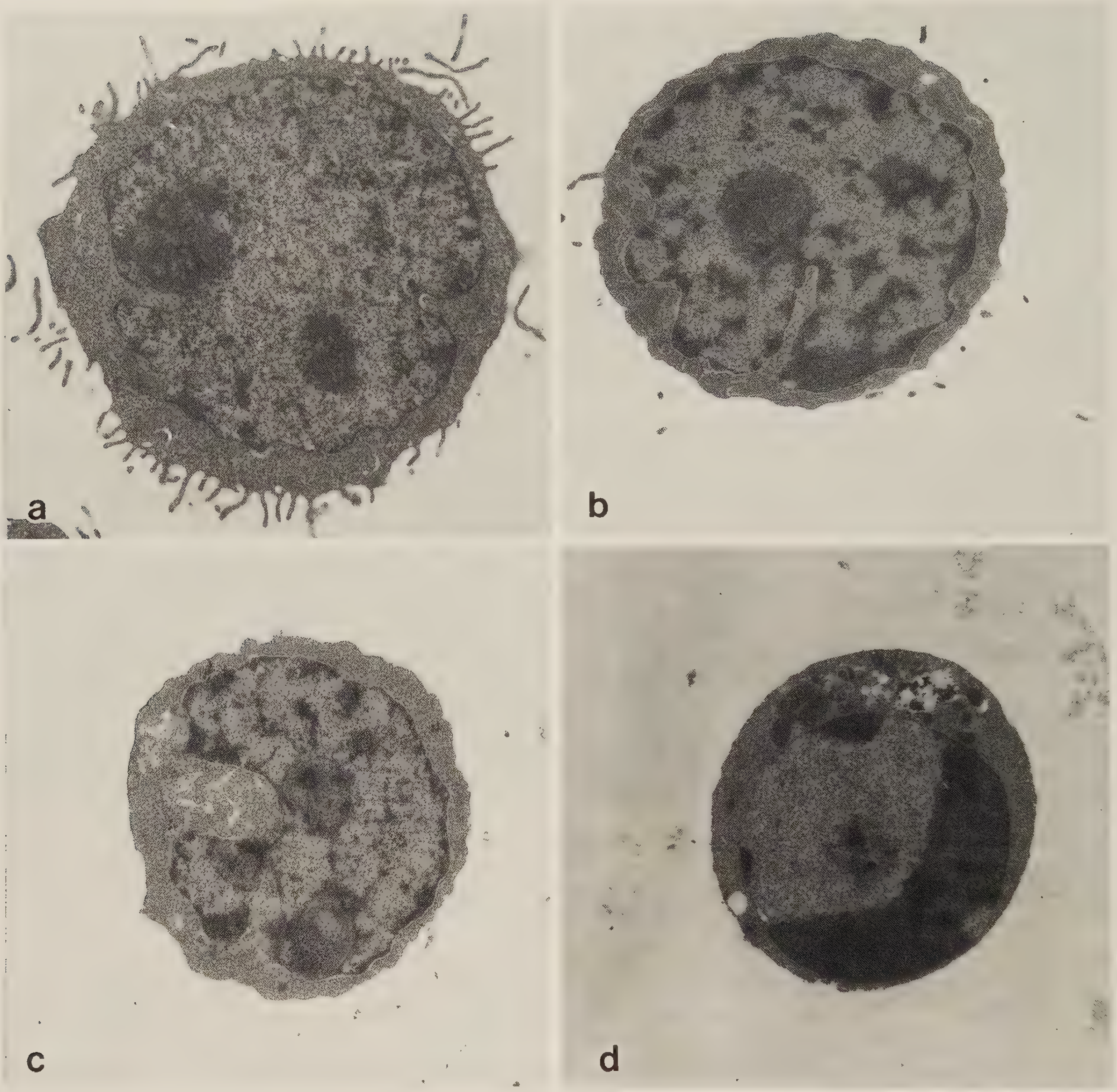

FIG. 3. Treatment with 300 n*M* 25OHC induces ultrastructural features of apoptosis in CEM-C7 cells. (a) Control CEM-C7 cell after 24 h in culture. (b and c) CEM-C7 cells treated with 300 n*M* 25OHC and examined 24 h after treatment showing shrinkage, early heterochromatin changes, and loss of microvilli. (d) Fully apoptotic CEM-C7 cell 48 h after the addition of 25OHC. Magnification, 8200×.

cells prior to cell death, we used TUNEL, a more sensitive assay which follows the incorporation of fluoresceinated dUTP into the 3′OH sites in nicked DNA. The data in Fig. 7 are from a typical experiment. Figure 7A shows that as early as 24 h after addition of 25OHC to CEM-C7 cells, a time when no difference in the number of viable cells in treated vs control cultures can be demonstrated, and a time when removal of the steroid allows unimpeded growth, there is a significant increase in the number of CEM-C7 cells that contain DNA breaks. The level of DNA breaks increases further in the sensitive cells with time. Only a low level of strand breaks is detected in the oxysterol-resistant M10R5 cells (Fig. 7A). By 48 h, the quantity of cells with breaks in the control cultures has increased, probably concomitant with the culture approaching the stationary phase. But the 25OHC-treated culture shows a dramatic increase in TUNEL-positive cells. In order to obtain a correlation between 25OHC-induced DNA strand breaks and cell cycle phase distribution, we counterstained the cells with propidium iodide and carried out two-color FACS analysis. Figure 7B shows a representative two-dimensional plot of incorporated fluorescein–dUTP versus the propidium iodide (DNA content) fluorescence for control

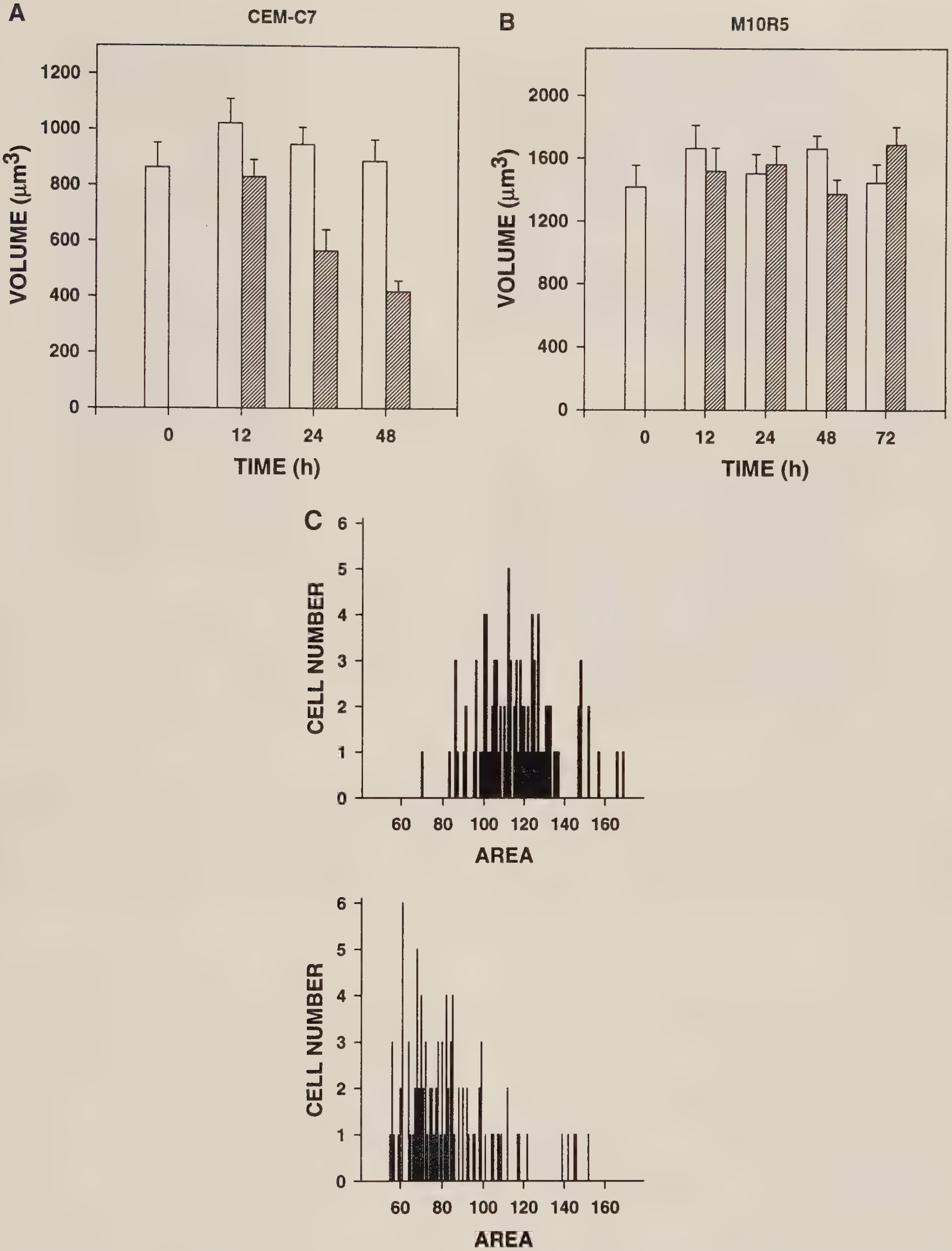

FIG. 4. 25OHC treatment significantly reduces cell volume in oxysterol-sensitive CEM-C7 cells but has no effect in the oxysterol-resistant M10R5 cells. Aliquots of CEM-C7 cells (A) and M10R5 cells (B) treated with either 300 n*M* ethanolic 25OHC or ethanol only were placed in a hemocytometer, and the area of 100 cells was determined by image analysis under a Leitz microscope as described under Materials and Methods. Error bars represent the mean ± 1 SD of the average cell sizes from two experiments in each of which 50 consecutive viable cells were evaluated for each time point. Values for control and treated CEM-C7 cells at 12, 24, and 48 h are statistically different at the $P \leqslant 0.001$ level, compared by a paired Student's *t* test. (C) Area distribution of CEM-C7 cells 24 h after the addition of ethanol (top) or 25OHC (bottom).

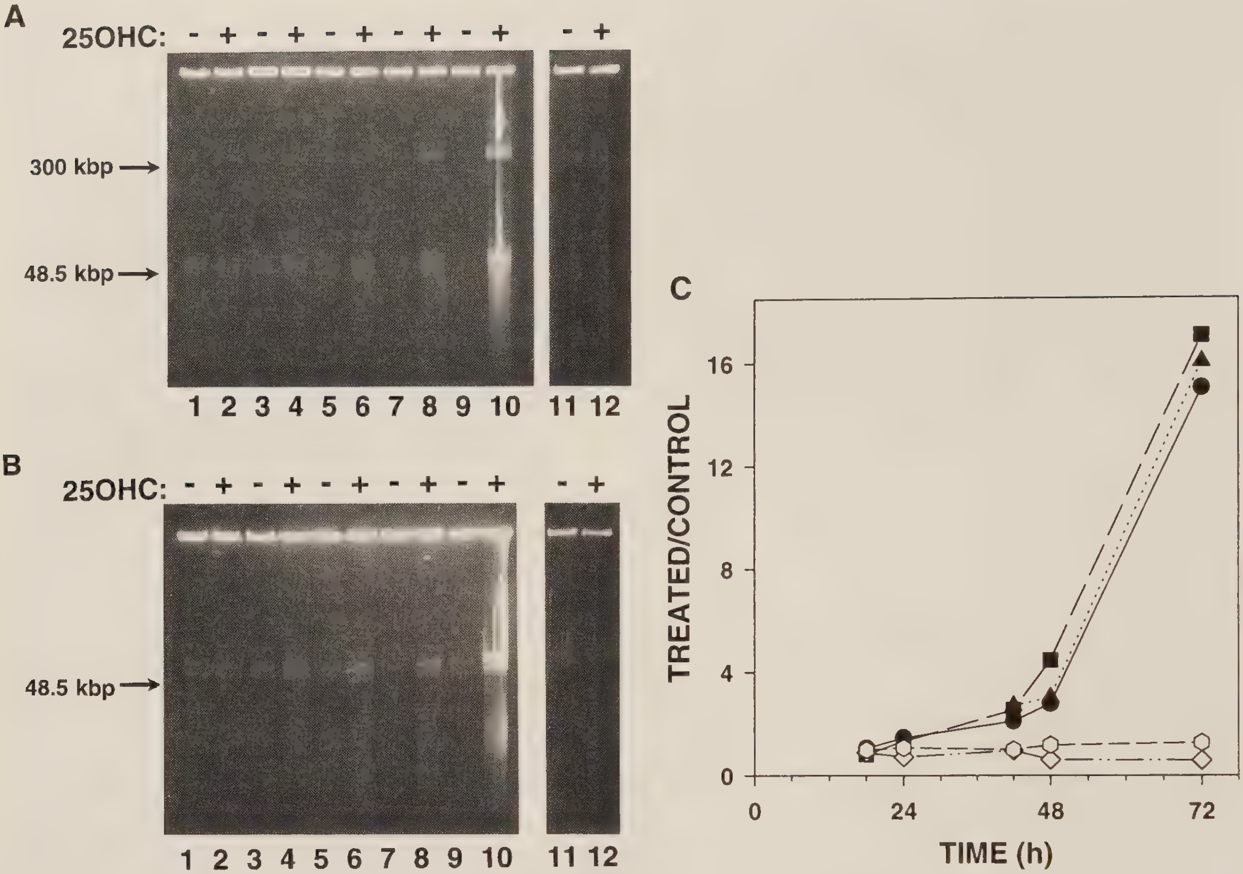

FIG. 5. Induction of large DNA fragments in CEM-C7 but not in M10R5 cells after 300 n*M* 25OHC treatment. For the detection of high-molecular-weight DNA fragments, FIGE was performed under conditions that separate DNA fragments either in the 50- to 300-kbp size range (A) or in the 10- to 50-kbp size range (B). Lanes 1–10, CEM-C7 cells at 18, 24, 42, 48, and 72 h in the absence (−) and presence (+) of 300 n*M* 25OHC, respectively; lanes 11 and 12, M10R5 cells 72 h after the addition of ethanol (−) or 25OHC (+). Note the increase in the 300- and 50-kbp fragments and a smear of DNA fragments of <50 kbp by 42 h in CEM-C7 cells and only basal levels of fragmentation in the oxysterol-resistant M10R5 cells. (C) Densitometric analysis of the relative amounts of fragmented DNA from the above experiment; Closed symbols, DNA fragments of CEM-C7 cells; ■, 50 kbp; ▲, <50 kbp; ●, 300 kbp. Open symbols, 50- and 300-kbp fragments in M10R5 cells; no <50-kbp fragments were seen. Results are representative of two individual experiments.

and treated CEM-C7 cells at 48 h after treatment. Most of the TUNEL-positive CEM-C7 cells are in the G0/G1 and early S phases of the cell cycle. The small number of CEM-C7 cells that show fluorescence incorporation in the absence of treatment is considered to reflect normal DNA damage and repair. The data showing an increase in strand breaks after 24 h of 25OHC treatment indicate that before the onset of cell death a significant number of DNA breaks are present in completely viable cells. The data show that most of the cells with DNA breaks are G0/G1 interphase cells and that 25OHC-induced DNA breaks in lymphoid CEM-C7 cells precede the large DNA fragmentation detectable by FIGE or conventional gel electrophoresis.

z-VAD.FMK Delays but Does Not Prevent 25OHC-Induced Apoptosis of CEM-C7 Cells

In order to determine if ICE-related protease activity plays a role in 25OHC-induced apoptosis of CEM-C7 cells, we cultured the cells in the presence of the caspase inhibitors z-VAD.FMK and y-VAD.CHO. Each of these inhibits a different subclass of caspases. In preliminary experiments, the toxic concentration of each inhibitor was determined; a somewhat lower concentration was then employed to test for the effect on 25OHC-evoked apoptosis. Figure 8 shows that when 100 μM z-VAD.FMK was added for 1 h prior to the addition of 300 n*M* 25OHC, CEM-C7 cells are not protected from 25OHC-induced apoptosis but rather, cell apoptosis has been postponed for about 1–2 days. In 25OHC plus z-VAD.FMK, CEM-C7 cells did not die up to 48 h; however, the number of apoptotic cells significantly increased thereafter. z-VAD.FMK alone at this concentration does not kill or inhibit the growth of CEM-C7 cells. The ICE inhibitor y-VAD.CHO did not protect at all. When CEM-C7 cells were cultured in the presence of 25OHC and 50 μM y-VAD.CHO, cells suffered apoptosis with identical kinetics as shown by

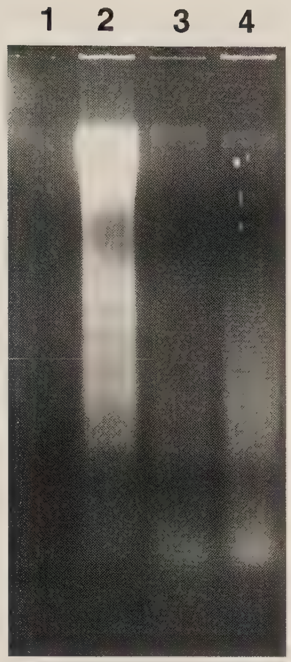

FIG. 6. Treatment with 300 n*M* 25OHC causes internucleosomal DNA fragmentation in CEM-C7 cells but not in M10R5 cells. Cells were treated for 48 h and their DNA was analyzed by conventional gel electrophoresis as described under Materials and Methods. Lanes 1 and 2, control and 25OHC-treated CEM-C7 cells, respectively. Lanes 3 and 4, control and 25OHC-treated M10R5 cells, respectively.

the cells cultured in 25OHC only (data not shown). y-VAD.CHO alone at a higher concentration (100 μM) induced apoptosis (data not shown). These data suggest that inhibition of the CPP32 class of proteases is not sufficient to prevent apoptosis of CEM-C7 cells induced by 25OHC.

Mevalonic Acid Partially Prevents 25OHC-Induced Apoptosis of CEM-C7 Cells

We have previously shown that the addition of mevalonate or cholesterol reversed 25OHC-induced cytotoxicity of CEM cells cultured in serum-free medium, though addition of 25OHC overcame the protection afforded by cholesterol [4]. To determine whether 25OHC-evoked apoptosis of CEM-C7 cells grown in delipidated serum medium is mediated through the supression of the cholesterol pathway, we tested whether the addition of mevalonic acid could prevent apoptosis. By performing dose–response studies (not shown), we determined that 4 m*M* mevalonic acid gave the maximal protection, although it was not absolute. We then held mevalonate constant at that concentration and tested the effect of increasing 25OHC (Fig. 9). At 300 n*M* 25OHC, the mevalonate delays the onset of cell loss for 24 h and greatly lessens the subsequent rate of death. At 1 μM 25OHC, there is no delay in the onset of cell loss, but the effect of lower rate of cell death is still apparent. Under microscopic examination, in contrast to cells in z-VAD.FMK plus 25OHC, most cells in 1 μM 25OHC and mevalonate appeared healthy (not shown). These data suggest that depletion of mevalonate may contribute to 25OHC-induced apoptosis of CEM-C7 cells, but it is not the only mechanism that is involved.

DISCUSSION

Oxysterols exhibit a diverse array of biological effects, including inhibition of cholesterol synthesis, prevention of cell growth, and induction of cell death [52, 20]. It has been suggested that oxysterols kill by initiating apoptosis [2, 5, 13, 42]. Here we report proof of the induction of apoptosis by 25OHC in the CEM line of human acute lymphoblastic leukemia cells by documenting an ordered array of morphological and biochemical events. Our work is the first we are aware of to report definitive morphological data of 25OHC-induced apoptosis and a time sequence of cellular and biochemical events in a human lymphoblastic leukemia cell line. We compared oxysterol-sensitive and -resistant cloned cells to differentiate the oxysterol effects from nonspecific processes. The morphologic and biochemical changes described are observed only in the oxysterol-sensitive cells, indicating that the effects are specific to the processes that lead to cell apoptosis.

We show that a relatively low concentration of 25OHC (300 n*M*) induced significant cell death 42 h after the addition of the steroid (Fig. 1). Light microscopic analysis revealed the presence of shrunken cells, and by using image analysis, we show that an early morphological change induced by 25OHC in the sensitive CEM-C7 cells was a decrease in cell volume (Fig. 4), statistically detectable as an average decrease in cell volume 12 h after steroid treatment. A significant proportion of the cells suffered a loss in cell volume after 24 h of incubation, a time when CEM-C7 cells can be rescued by removal of the steroid [4]. Thus at least a significant degree of cell shrinkage is reversible. Between 12 and 24 h the percentage of significantly small cells dramatically increased (Fig. 4C), suggesting that at least two possible processes contribute to the 25OHC-induced overall cell shrinkage: an overall shrinkage of the cell population progressing through the cell cycle and more abrupt shrinkage of cells that have been arrested at a specific stage of the cell cycle. It has been shown that many 25OHC-treated cells arrest at the G1 phase of the cell cycle. Since the sensitive CEM-C7 cells do not undergo accumulation at G1 after steroid treatment, our data suggest that CEM-C7 cells are suffering the sharp reduction in cell volume at various stages of the cell cycle. Little is known about the mechanisms involved in the reduction of cytoplasmic volume during apoptosis, but concomitant loss of intracellular osmolytes and water content have been sug-

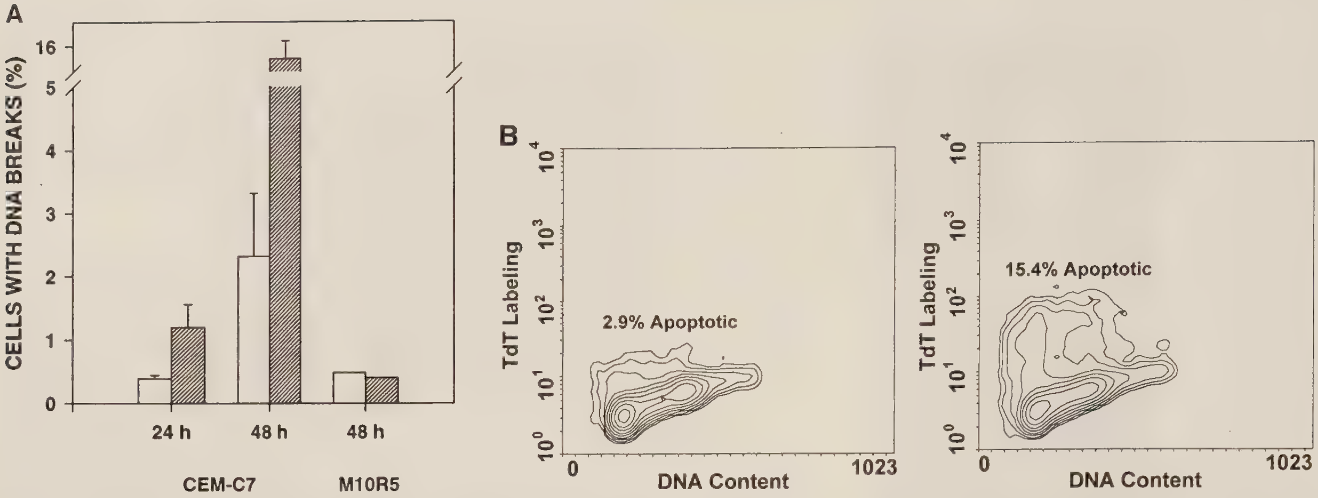

FIG. 7. TUNEL assay indicates that DNA breaks are induced by exposure to 300 n*M* 25OHC prior to cell death in CEM-C7 but not in M10R5 cells. The percentage of TUNEL-positive cells was determined by flow cytometry after counterstaining with propidium iodide for DNA content. (A) Percentage of CEM-C7 (at 24 and 48 h) and M10R5 (at 48 h) cells that were positive for the TUNEL assay. Open bars, control cells; closed bars, cells treated with 300 n*M* 25OHC. Error bars indicate the mean ± 1 SE of four experiments performed in duplicate for the 24-h point and of three experiments for the 48-h time point. Values for the control and treated cells were significantly different at the $P \leq 0.004$ and the $P \leq 0.02$ levels at 24 and 48 h, respectively, as determined by a paired Student's *t* test. (B) Contour graphs of fluorescein–dUTP incorporation in CEM-C7 cells after 48 h of 25OHC (right) or ethanol (left) treatment only.

gested to be associated with the process [8, 33]. How oxysterols regulate cell volume is still quite unknown. In high concentrations oxysterols have been shown to affect the physicochemical properties of the plasma membrane, including the activity of the Na^+/K^+ ATPase and Ca^{2+} flux [48, 44], but it seems unlikely that the free 25OHC levels in our experiments could cause such direct effects. In general, cells respond to hypertonicity by increasing the intracellular concentration of KCl and by regulating the transcription of osmolyte transporters [33]. It has been shown that in mouse L-cells oxysterols decrease the intracellular concentration of potassium [12]. A recent study has shown that the loss in CEM-C7A cell volume during dexamethasone-induced apoptosis is associated with a net loss of potassium [7]. In our experiments, 25OHC could be triggering cellular shrinkage by altering the intracellular concentration of electrolytes such as potassium by either a direct effect on membrane osmolyte transporters or through regulation of their expression.

The normal ultrastructure of CEM cells is characterized by a high nucleus to cytoplasm ratio, as might be expected for leukemic blasts. Electron microscopic analysis of 25OHC-treated CEM-C7 cells showed that several initial morphological changes of death by apoptosis were evident at a time of complete cell viability and were observed simultaneously in the cytoplasm, nucleus, and plasma membrane (Figs. 4B and 4C). These results are consistent with the fundamental hypothesis of apoptosis that the ultrastructural changes occur prior to the loss of cell viability. The only observed change in the structure of the plasma membrane up to 24 h after treatment of CEM-C7 cells was the disappearance of microvilli. The loss of microvilli after 25OHC treatment has been documented in mouse L-cells [35]. The overall integrity of the membrane was kept, however, as evidenced by the absence of swelling. We did not see the budding described as one characteristic of apoptosis. Loss of integrity of the cytoplasm and membrane was observed in some cells only after 48 h of 25OHC treatment (Fig. 4D). However, organelles such as mitochondria were intact in the apoptotic cells. The reduction in cell volume occurs prior to the condensation of chromatin, suggesting that perhaps the loss of the cellular volume could be contributing to the induction of changes in the nuclear architecture. Moreover, at the time when there has been a 50% reduction in cell volume (24 h), there has been no net loss of nuclear DNA as determined by the absence of a sub G0/G1 peak when cells were analyzed for DNA content (data not shown). The early nuclear changes induced by 25OHC precede the production of large DNA fragments and could be contributing to the initiation of DNA cleavage by physically exposing areas of the DNA that in turn can become targets for an endonuclease. The production of large DNA fragments and chromatin condensation in rat thymocytes after dexamethasone or etoposide treatment has been shown to occur concomitantly [15].

Oxysterol-induced cleavage of DNA to large fragments of 300 and 50 kbp showed a similarity to that previously observed in some human tumor cells after serum withdrawal or the addition of etoposide and in rat thymocytes after treatment with dexamethasone

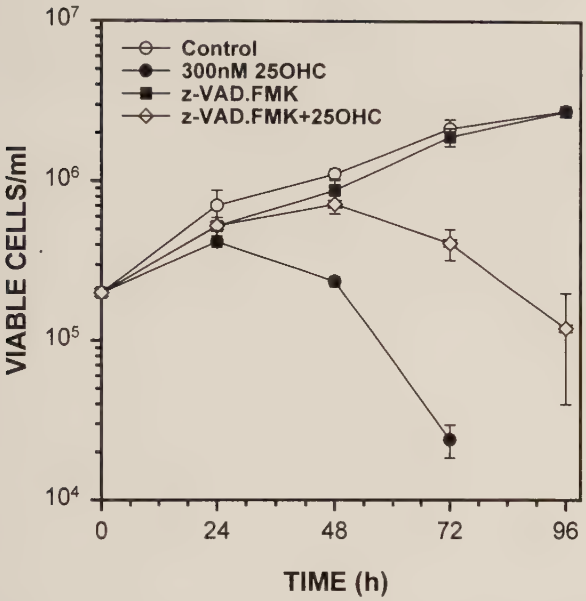

FIG. 8. Treatment with z-VAD.FMK results in a delayed induction of CEM-C7 apoptosis by 25OHC. Oxysterol-sensitive CEM-C7 cells were treated with 100 μM z-VAD.FMK for 1 h prior to the addition of 300 nM 25OHC. The quantity of viable cells (cells/ml) was determined as described in the legend to Fig. 1. Each point represents the mean ± two independent experiments performed in triplicate. Open circles, cells treated with ethanol carrier only; closed circles, cells treated with 300 nM 25OHC; closed squares, z-VAD.FMK alone; open triangles, cells treated with 100 μM z-VAD.FMK and 300 nM 25OHC together.

or topoisomerase II inhibitors [9, 47, 63]. These large fragments have been suggested to represent cleavage of high-order chromatin structure [24], though there is little direct evidence for this as yet. There is no general consensus as to the temporal occurrence of DNA fragmentation and apoptosis. Studies in rat thymocytes after glucocorticoid treatment and in some human epithelial cells after induction of apoptosis by different treatments support the hypothesis that large fragments precede the formation of internucleosomal fragments [9, 47]. The production of internucleosomal DNA has been reported to occur in various time frames and moreover to be completely absent during apoptosis of various systems [6, 14, 17, 40, 46, 56, 65]. Within the limits imposed by the sensitivity of the assays that we employed, we found that in CEM-C7 cells 25OHC-induced outright DNA fragmentation does not occur prior to the occurrence of cell death but rather concomitantly with apoptosis (Fig. 5). By the time DNA fragments are detected by either FIGE or conventional electrophoresis, the oxysterol-sensitive cells have begun to die outright. Although DNA fragmentation is an important part of 25OHC-induced apoptosis in CEM-C7 cells, it does not seem to be a prerequirement for apoptosis and perhaps results from the process itself. Furthermore, our data are equally consistent with DNA fragmentation into large pieces shortly preceding or occurring concomitantly with fragmentation into 180-bp multimers.

DNA breaks short of outright fragmentation, however, are present at significant levels prior to cell death in preapoptotic cells (Fig. 7). Our data suggest that the initial DNA breaks represent early stages of apoptosis in our cell system, and that these breaks might be associated to the changes in the nuclear morphology, since both events are evident 24 h after steroid addition. Our data also suggest that the DNA breaks during early apoptosis are not sufficient to cause apoptosis since up to this point cell death is reversible [4].

Several lines of evidence have revealed a correlation between apoptosis and the cell cycle [22]. We observed that although cells with DNA breaks are detected at all stages of the cell cycle, most of the cells with DNA breaks featured a DNA content of G0/G1, with the next most prominent group of cells in S phase (Fig. 7B). It has been shown that in rat thymocytes both dexamethasone and etoposide can induce apoptotic cell death from different stages of the cell cycle [23].

Activation of caspases seems to be a critical step in many though not all cases of apoptosis. The transient inhibition of apoptosis by z-VAD.FMK does not allow the conclusion that ICE-related proteases such as CPP32 are essential mediators of 25OHC-induced apoptosis in CEM-C7 cells. However, we cannot exclude the possibility that there are still other functional proteases that

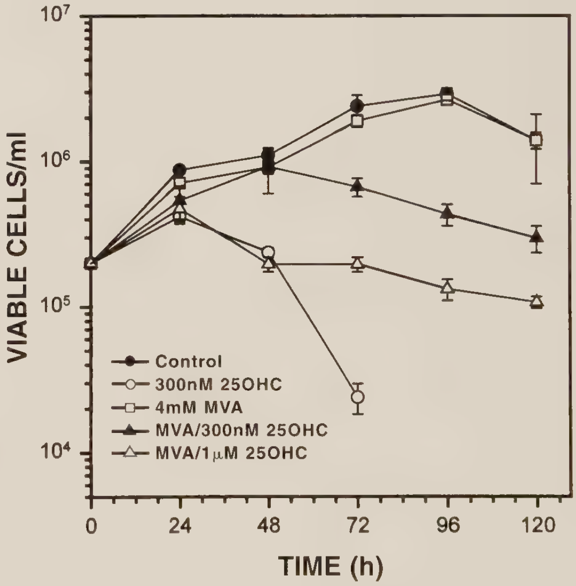

FIG. 9. Partial prevention of apoptosis of CEM-C7 cells by constant mevalonic acid in the presence of increasing concentrations of 25OHC. Cells were simultaneously treated with 300 nM 25OHC (closed triangles) or 1 μM 25OHC (open triangles) and 4 mM mevalonic acid for several days and the number of viable cells was determined as described in the legend to Fig. 1. Points represent the mean ± two independent experiments performed in duplicate.

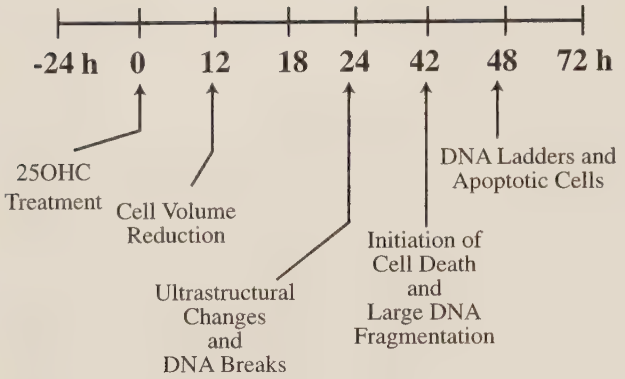
-24 h
0
12
18
24
42
48
72 h
25OHC Treatment
Cell Volume Reduction
Ultrastructural Changes and DNA Breaks
Initiation of Cell Death and Large DNA Fragmentation
DNA Ladders and Apoptotic Cells

FIG. 10. Temporal sequence of certain morphological and biochemical events during 25OHC-induced apoptosis of CEM-C7 cells. By 12 h after the addition of 25OHC there is a significant reduction in cell volume. By 24 h, early ultrastructural features of apoptosis are observed as well as the onset of DNA breaks. These events occur prior to CEM-C7 cell death. By 48 h and concomitant with cell death we observed the induction of large DNA fragments. Internucleosomal fragments occur at or near 48 h and apoptotic cells are observed at and after 48 h of 25OHC treatment.

were not inhibited by z-VAD.FMK and thus were responsible for the eventual apoptosis of CEM-C7 cells induced by 25OHC. However, our data are also consistent with the possibility that the ICE family of proteases is activated to mediate apoptotic CEM-C7 cell death induced by 25OHC but that other dominant, slower mechanisms may be involved as well. Our results also suggest that the suppression of the cholesterol synthesis pathway by 25OHC may be contributing at least in part to apoptosis of CEM-C7 cells. It is well known that the products that result from the cholesterol side pathways may affect cell viability [20, 39, 54], but the failure of mevalonate to completely block the effects of 25OHC suggests the involvement of other mechanisms during 25OHC-induced apoptosis of these lymphoid cells.

In summary, 25OHC seems to be targeting the plasma membrane, the nucleus, and the cytoplasm before the onset of cell death, as evidence by the dramatic loss in cell volume, the apoptotic ultrastructural changes, and the DNA breaks. Though relatively slow in overall time, the morphologic and DNA damage fit classic patterns for apoptosis (Fig. 10). The time sequence is consistent with 25OHC provoking changes in gene regulation that cause or contribute to the eventual apoptosis. We conclude that apoptosis is induced in the human lymphoblastic leukemia cell line CEM-C7 at a low pharmacological concentration of 25OHC. The fact that 25OHC can induce apoptosis of human leukemia cells raises the possibility of a chemotherapeutic application.

This work was supported by NIH NCl Grant 2RO1 CA41407 (E.B.T.), NIEHS training grant predoctoral fellowship ESO 7254 (S.A.T.), and a Meadows Foundation Equipment Award (S.A.T.). The authors thank Dr. Gwendolyn Childs for the helpful advice and assistance with the cell volume analysis.

REFERENCES

1. Anand. R., and Southern, E. M. (1990) *in* Gel Electrophoresis of Nucleic Acids: A Practical Approach (Rickwood, D., and Hames, B. D., Eds.), pp. 101–123, IRL Press, Oxford.
2. Aupeix, K., Weltin, D., Mejia, J. E., Christ, M., Marchal, J., Freyssinet, J.-M., and Bischoff, P. (1995) *Immunobiology* **194,** 415–428.
3. Ayala-Torres, S., Johnson, B. J., and Thompson, E. B. (1994) *J. Steroid Biochem. Mol. Biol.* **48,** 307–315.
4. Bakos, J. T., Johnson, B. J., and Thompson, E. B. (1993) *J. Steroid. Biochem. Mol. Biol.* **46,** 415–426.
5. Bansal, N., Houle, A., and Melnykovych, G. (1991) *FASEB J.* **5,** 211–216.
6. Barry, M. A., Behnke, C. A., and Eastman, A. (1990) *Biochem. Pharmacol.* **40,** 2353–2362.
7. Benson, R. S. P., Heer, S., Dive, C., and Watson, J. M. (1996) *Am. J. Physiol.* **270,** (*Cell Physiol.* **39**) C1190–C1203.
8. Bortner, C. D., and Cidlowski, J. A. (1996) *in* Program Cell Death (Scott, D. D., Shi, Y. B., Shi, Y., and Yu, X., Eds.), Plenum Publishing [in press].
9. Brown, D. G., Sun, X.-M., and Cohen, G. M. (1993) *J. Biol. Chem.* **268,** 3037–3039.
10. Chen, H. W., Heiniger, H. J., and Kandutsch, A. A. (1977) *Exp. Cell Res.* **109,** 253–262.
11. Chen, H. W., Kandutsch, A. A., and Waymouth, C. (1974) *Nature* **251,** 419–421.
12. Chen, H. W., Heiniger, H.-J., and Kandutsch, A. A. (1978) *J. Biol. Chem.* **253,** 3180–3185.
13. Christ, M., Mejia, J. E., Moosbrugger, I., and Bischoff, P. (1993) *Immunology* **78,** 455–460.
14. Cohen, G. M., Sun, X.-M., Snowden, R. T., Dinsdale, D., and Skilleter, D. N. (1992) *Biochem. J.* **286,** 331–334.
15. Cohen, G. M., Sun, X.-M., Fearnhead, H., MacFarlane, M., Brown, D. G., Snowden, R. T., and Dinsdale, D. (1994) *J. Immunol.* **153,** 507–516.
16. Cohen, G. M., and Duke, R. C. (1992) *Annu. Rev. Immunol.* **10,** 267–293.
17. Compton, M. M., and Cidlowski, J. A. (1986) *Endocrinology* **118,** 38–45.
18. Cuthbert, J. A., and Lipsky, P. E. (1981) *J. Immunol.* **126,** 2093–2099.
19. Dixit, V. M. (1996) *Adv. Exp. Med. Biol.* **406,** 113–117.
20. Doyle, J. W., and Kandutsch, A. A. (1991) *in* Advances in Cholesterol Research (Esfahani, M., and Swaney, J. B., Eds.), p. 89, Telford Press. West Caldwell, NJ.
21. Duke, R. C., and Cohen, J. J. (1992) *in* Current Protocols in Immunology (Coligan, J. E., Kruisbeek, A. M., Margulies, D. H., Shevach, E. M., and Strober, W., Eds.), pp. 3.17.1–3.17.16, Green and Wiley–Interscience, New York.
22. Evan, G. I., Brown, L., Whyte, M., and Harrington, E. (1995) *Curr. Opin. Cell Biol.* **7,** 825–834.
23. Fearnhead, H. O., Chwalinski, M., Snowden, R. T., Ormerod, M. G., and Cohen, G. M. (1994) *Biochem. Pharmacol.* **48,** 1073–1079.
24. Filipski, J., Leblanc, J., Youdale, T., Sikorska, M., and Walker, P. R. (1990) *EMBO J.* **9,** 1319–1327.
25. Guardiola, F., Codony, R., Addis, P. B., Rafecas, M., and Boatella, J. (1996) *Biol. Food Chem. Toxicol.* **34,** 193–211.
26. Hietter, H., Bischoff, P., Beck, J. P., Ourisson, G., and Luu, B. (1986) *Cancer Biochem. Biophys.* **9,** 75–83.
27. Johnson, B. H., Ayala-Torres, S., Chan, L.-N. L., El-Naghy, M., and Thompson, E. B. (1997) *J. Steroid Biochem. Mol. Biol.* **61.**

28. Kerr, J. F. R. (1971) *J. Pathol.* **105,** 13–20.
29. Kerr, J. F. R., Wyllie, A. H., and Currie, A. R. (1972) *Br. J. Cancer* **26,** 239–257.
30. Kerr, J. F. R., Winterford, C. M., and Harmon, B. V. (1993) *Cancer* **73,** 2013–2026.
31. Kerr, J. F. R., Gobé, G. C., Winterford, C. M., and Harmon, B. V. (1995) *Methods Cell Biol.* **46,** 1–26–28.
32. Kokileva, L. (1994) *Int. Arch. Allergy Immunol.* **105,** 339–343.
33. Kwon, H. M., and Handler, J. S. (1995) *Curr. Opin. Cell Biol.* **7,** 465–471.
34. Larsson, O., and Zetterberg, A. (1995) *Cell Prolif.* **28,** 33–43.
35. Lin, P.-S., and Chen, H. W. (1979) *Cell Biol. Int. Rep.* **3,** 51–59.
36. Lizard, G., Deckert, V., Dubrez, L., Moisant, M., Gambert, P., and Lagrost, L. (1996) *Am. J. Pathol.* **148,** 1625–1638.
37. Majno, G., and Joris, I. (1995) *Am. J. Pathol.* **146,** 3–15.
38. Maltese, W., Reitz, B., and Volpe, J. J. (1981) *Cancer Res.* **41,** 3448–3452.
39. Maltese, W. A. (1990) *FASEB J.* **4,** 3319.
40. Martin, S. J., Bonham, A. M., and Cotter, T. G. (1990) *Biochem. Soc. Trans.* **18,** 634–636.
41. Moog, C., Frank, N., Luu, B., and Bertram, B. (1993) *Anticancer Res.* **4,** 953–958.
42. Nishio, E., Arimura, S., and Watanabe, Y. (1996) *Biochem. Biophys. Res. Commun.* **22,** 413–418.
43. Nordman, P., Diez-Ibáñez, M., Chessebeuf-Padieu, M., Luu, B., Mack, G., and Mersel, M. (1989) *Cell Biol. Toxic.* **5,** 261–270.
44. Neyses, L., Stimpel, M., Locker, R., Kueffer, B., and Vetter, W. (1985) *J. Hypertension* **2** (Suppl. 3), 489–492.
45. Norman, M. R., and Thompson, E. B. (1977) *Cancer Res.* **37,** 3785–3791.
46. Oberhammer, F., Bursch, W., Parzefall, W., Breit, P., Erber, E., Stadler, M., and Schulte-Hermann, R. (1991) *Cancer Res.* **51,** 2478–2485.
47. Oberhammer, F., Wilson, J. W., Dive, C., Morris, I. D., Hickman, J. A., Wakeling, A. E., Walker, P. R., and Sikorska, M. (1993) *EMBO J.* **12,** 3679–3684.
48. Peng, S. K., Morin, R. J., and Sentovich, S. (1985) *J. Am. Oil Chem. Soc.* **62,** 634–635.
49. Philips, H. J. (1973) *in* Tissue Culture: Methods and Applications (Kruse, M. K., Jr., and Patterson, P. F., Jr., Eds.), pp. 406–408, Academic Press, New York.
50. Robertson, A. M. G., Bird, C. C., Waddell, A. W., and Currie, A. R. (1973) *J. Pathol.* **126,** 181–187.
51. Rothletat, G. H., Arbogast, L. Y., Owelette, L., and Howard, B. V. (1976) *In Vitro* **12,** 554–557.
52. Saucier, S. E., Kandutsch, A. A., Gayen, A. K., Swahn, D. K., and Spencer, T. A. (1989) *J. Biol. Chem.* **264,** 6863–6869.
53. Schwartz, L. M., Smith, S. W., Jones, M. E. E., and Osborne, B. A. (1993) *Proc. Natl. Acad. Sci. USA* **90,** 980–984.
54. Sinensky, M., and Lutz, R. J. (1992) *Bioassays* **14,** 25.
55. Smith, L. L., and Johnson, B. H. (1989) *Free Radical Biol. Med.* **7,** 285–332.
56. Sun, X.-M., Snowden, R. T., Dinsdale, D., Ormerod, M. G., and Cohen, G. M. (1994) *Biochem. Pharmacol.* **47,** 187–195.
57. Spurr, A. (1969) *J. Ultrastruct. Res.* **26,** 31–43.
58. Taylor, F. R., Saucier, E. S., Shown, E. P., Parish, E. J., and Kandutsch, A. A. (1984) *J. Biol. Chem.* **259,** 12382–12387.
59. Thompson, E. B., and Ayala-Torres, S. (1997) *in* Biochemistry and Function of Sterols (Parish, E. J., and Ness, W. D., Eds.), pp. 65–72, CRC Press, Boca Raton, FL.
60. Van Houten, N., and Budd, R. C. (1992) *J. Immunol.* **149,** 2513–2517.
61. Werthle, M., Bochelen, D., Adamczyk, M., Kupferberg, A., Poulet, P., Chambon, J., Lutz, P., Privat, A., and Mersel, M. (1994) *Cancer Res.* **54,** 998–1003.
62. Ucker, D. S., Obermiller, P. S., Eckhart, W., Apgar, J. R., Berger, N. A., and Meyers, J. (1992) *Mol. Cell. Biol.* **12,** 3060–3069.
63. Walker, P. R., Smith, C., Youdale, T., LeBlanc, J., Whitfield, J. F., and Sikorska, M. (1991) *Cancer Res.* **51,** 1078–1085.
64. Walker, P. R., Kokileva, L., LeBlanc, J., and Sikorska, M. (1993) *BioTechniques* **15,** 1032–1040.
65. Zakeri, Z., Quaglino, D., Latham, T., and Lockshin, R. A. (1993) *FASEB J.* **7,** 470–478.

Received January 16, 1997
Revised version received May 5, 1997

EXPERIMENTAL CELL RESEARCH **235,** 48–54 (1997)
ARTICLE NO. EX973641

Induction of Apoptosis and Potentiation of TNF- and Fas-Mediated Apoptosis in U937 Cells by the Xanthogenate Compound D609

M. Isabella Pörn-Ares,*[1] Sek C. Chow,*[2] J. Peter Slotte,† and Sten Orrenius*

**Institute of Environmental Medicine, Division of Toxicology, Karolinska Institutet, 17177 Stockholm, Sweden; and †Department of Biochemistry and Pharmacy, Åbo Akademi University, 20521 Turku, Finland*

Apoptosis induced by ligation of either the tumor necrosis factor (TNF) p55 receptor or the Fas/APO-1/CD95 receptor has been suggested to require ceramide as a signaling molecule. Ceramide is formed as a result of sphingomyelinase (SMase) activation in the sphingomyelin cycle, and ligation of TNF and Fas receptors has been reported to stimulate SMase activity. We have studied the effects of D609, a xanthogenate compound with antitumoral properties, on TNF- or Fas-induced apoptosis of monocytic U937 cells. First, the effects of D609 on SMase activity were assessed using *in vitro* assays for neutral and acidic SMase, and the results suggested that D609 caused a modest stimulation of the activity of both SMases in U937 cells. Exposure of U937 cells for 6 h to TNF or anti-Fas mAb induced apoptosis in 40–45% of the cells, as measured by fluorescent staining of nuclear chromatin. Cotreatment with D609 potentiated TNF- as well as Fas-mediated apoptosis up to 70 and 90%, respectively. Furthermore, in incubations with D609 alone, 60% of the cells became apoptotic within 16 h. Since D609 has been reported to inhibit protein kinase C (PKC) activity, the effect of phorbol 12-myristate 13-acetate (PMA) on D609-induced apoptosis was investigated. PMA was found to inhibit D609-induced apoptosis in U937 cells as well as cell death induced by TNF and anti-Fas mAb. Thus, PKC inactivation may play an important role in the regulation of apoptosis in U937 cells. In summary, the present results show that D609 stimulates SMase activity, potentiates TNF- and Fas-induced apoptosis, and induces apoptosis on its own in U937 cells. © 1997 Academic Press

INTRODUCTION

The p55 receptor for tumor necrosis factor (TNF)[3] and the Fas (APO-1, CD95) receptor belong to the same receptor family and are known to trigger apoptosis in a number of different cell types upon ligand binding [1–4]. Both receptors contain an approximately 70-amino-acid domain in the cytoplasmic region known as the death domain, which is required for the cytotoxic effects [5, 6]. Binding of TNF to its receptor is known to stimulate sphingomyelin degradation with the subsequent formation of ceramide [7–10], and cell-permeable ceramide analogs, as well as natural ceramide, have been shown to induce apoptosis in leukemia cells [11–13]. Furthermore, treatment of cells with exogenous bacterial sphingomyelinase (SMase) was reported to induce apoptosis in leukemic and fibrosarcoma cells [14]. Ceramide is therefore likely to be an important signaling molecule in the TNF-induced apoptotic pathway [15]. A role for ceramide in Fas-mediated apoptosis has also been suggested by several laboratories [16–18], although the typical, early, and transient peak of SMase activity usually observed upon TNF stimulation has not been reproducibly observed in the Fas system [18].

Three distinct types of intracellular SMase have been demonstrated: (i) a "neutral" SMase, which is membrane bound and requires Mg^{2+} and pH 7.4 for optimal activity [19, 20]; (ii) an "acidic" SMase located in the endosomal/lysosomal compartments with a pH optimum of 5.0 [21]; and (iii) a Mg^{2+}-independent cytosolic SMase with a neutral pH optimum [22]. TNF has been shown to activate both the acidic and the neutral SMase [23, 24], and it is presently unclear which of the SMases mediate TNF-induced cytotoxicity. The acidic SMase is thought to be stimulated by diacylglycerol [25]. Schütze and co-workers [23] have suggested that TNF-induced acidic SMase stimulation is mediated through phosphatidylcholine-specific phospholipase C (PC-PLC) activity, which can be inhibited by treatment

---

[1] To whom reprint requests should be addressed at Institute of Environmental Medicine, Division of Toxicology, Karolinska Institutet, Box 210, S-17177 Stockholm, Sweden. Fax: +46-8-329 041. E-mail: Isabella.Ares@imm.ki.se.

[2] Present address: Centre for Mechanisms of Human Toxicity, University of Leicester, Leicester LE1 9HN, UK.

[3] Abbreviations used: anti-Fas mAb, anti-human Fas monoclonal antibody; C_2, acetyl; D609, tricyclodec-9-yl dithiocarbonate; FCS, fetal calf serum; HMW, high molecular weight; PC-PLC, phosphatidylcholine-specific phospholipase C; PKC, protein kinase C; PMA, phorbol 12-myristate 13-acetate; SDS, sodium dodecyl sulfate; SMase, sphingomyelinase; TNF, tumor necrosis factor-α.

0014-4827/97 $25.00
Copyright © 1997 by Academic Press
All rights of reproduction in any form reserved.

with D609 (tricyclodecan-9-yl-xanthogenate). Pretreatment of cells with D609 has been used for investigation of the role of PC-PLC and acidic SMase in TNF/Fas-mediated signal transduction [23, 24, 26, 27], but the direct effects of the drug have not been characterized in detail.

In the present study, we show that D609 stimulated SMase activity and caused apoptosis and potentiated TNF- and Fas-mediated apoptosis in U937 cells.

MATERIAL AND METHODS

Chemicals. Human recombinant TNF was a generous gift from Dr. Grace Wong, (Genentech, Inc., San Francisco, CA). Anti-human Fas monoclonal antibody (IgM, clone CH-11) was purchased from Medical and Biological Laboratories Co., Ltd., Nagoya, Japan. Calphostin C came from Calbiochem (La Jolla, CA). *H*-7-Dihydrochloride (*H*-7), arachidonic acid, and C_2-ceramide were obtained from Biomol, Hamburg, Germany. Sphingomyelinase (EC 3.1.4.12., *Staphylococcus aureus*), phorbol 12-myristate 13-acetate (PMA), Hoechst 33342, proteinase K, RNase, and D609 (tricyclodec-9-yl dithiocarbonate) were purchased from Sigma. Ultrapure agarose came from Life Technologies, Paisley, Scotland.

Cell culture. U937 cells (human monocytic leukemia cell line) were grown in RPMI 1640 medium supplemented with 10% heat-inactivated fetal calf serum, 100 U/ml penicillin, and 100 μg/ml streptomycin in a humidified atmosphere of 5% CO_2 in air at 37°C.

Analysis of oligonucleosomal and HMW DNA fragments. After appropriate incubations, 10^6 cells were transferred to Eppendorf tubes, and the cells were centrifuged at 2000*g* for 5 min. For analysis of DNA fragments of <50 kb, the method of Sorenson and co-workers was used [28]. Briefly, cells were treated with RNase (10 mg/ml) for 20 min, after which loading buffer (5 μl) was added to the sample. The samples were then loaded into a 1.8% agarose gel, with a piece of digestion gel (0.8% Ultrapure agarose, 2% SDS, and 0.6 mg/ml proteinase K) at the upper end. The gel was run at 20 V overnight and stained with ethidium bromide after which the DNA fragments were visualized using uv illumination. For analysis of HMW DNA fragments, cell pellets were resuspended in 50 μl PBS and mixed with 50 μl low-melting-point agarose (1%) before being pipetted into the wells of a plug mold. The agarose plugs were digested for 48 h with Pronase (1 mg/ml) at 50°C. For field inversion gel electrophoresis, one-quarter of each plug was inserted into a well containing a 1% agarose gel, and DNA fragments were electrophoresed as previously described [29], stained with ethidium bromide, and visualized using uv illumination.

Assessment of apoptotic nuclei. At appropriate times during incubation, 3×10^5 cells were collected and spun down at 2000*g* for 5 min. The pellets were resuspended in paraformaldehyde (4% in PBS) and spread on a poly-L-lysine-treated glass microscope slide and left to dry. The fixed cells were then rehydrated in H_2O and stained with Hoechst 33342 (10 μg/ml in PBS) in the dark for 10 min. Slides were rinsed five times with water, dried in the dark, and mounted with glycerol/PBS (1/1 v/v) using a coverslip. The fluorescent nuclei were viewed with a Leitz Diaplan fluorescence microscope, and 150–200 nuclei were analyzed per sample.

Analysis of sphingomyelinase activity. The activity of acidic and neutral SMases was measured according to the method of Quintern and Sandhoff with some modifications [24, 30, 31]. U937 cells were resuspended at a density of 4×10^6/ml in serum-free RPMI culture medium containing 2% fatty-acid-free albumin and were left to equilibrate for 2 h. Cells were then treated in triplicates with 100 ng/ml of TNF and/or 100 μg/ml of D609 (dissolved in sterile PBS at the day of experiment). At appropriate times, drug treatment was stopped by immersing the vials in a methanol–dry ice bath. Cells were spun for 5 min at 4°C and washed with ice-cold PBS. To measure neutral SMase, pellets were dissolved in a buffer containing 20 m*M* Hepes (pH 7.4), 10 m*M* $MgCl_2$, 2 m*M* EDTA, 5 m*M* DTT, 0.1 m*M* Na_3VO_4, 0.1 m*M* Na_2MoO_4, 30 m*M* *p*-nitrophenylphosphate, 10 m*M* β-glycerophosphate, 750 μM ATP, 1 m*M* PMSF, 10 μM leupeptin, 10 μM pepstatin, and 0.2% Triton X-100. After incubation for 5 min at 4°C, the cells were homogenized by repeated squeezing through an 18-gauge needle. Nuclei and cell debris were then removed by centrifugation at 800*g*. Next, 30–50 μg of cell protein was incubated for 60 min at 37°C in a buffer (50 μl final volume) containing 20 m*M* Hepes, 10 m*M* $MgCl_2$, 250 μM ATP, and 0.4 μCi/ml of [*N-methyl*-^{14}C]-sphingomyelin (sp act 47–56 mCi/mmol; Amersham, Buckinghamshire, UK). The reaction rate was linear within this time frame, and the amount of hydrolyzed [^{14}C]sphingomyelin did not exceed 10% of the total amount added. Phosphorylcholine was extracted with 800 μl of chloroform/methanol (2/1 v/v) and 250 μl of 0.1% phosphorylcholine in water. Radioactive phosphorylcholine produced from [^{14}C]-sphingomyelin was routinely determined in the aqueous phase by scintillation counting. Phosphorylcholine was also identified by thin-layer chromatography. For measurement of acidic SMase, cells treated with TNF or D609 were washed, and the pellets were resuspended in 100 μl of 0.2% Triton X-100 and incubated for 15 min at 4°C. Cells were then homogenized and spun at 14,000 rpm in a microcentrifuge. From the supernatants 30–50 μg of protein was incubated for 30 min at 37°C in a buffer (total volume 50 μl) containing 250 m*M* sodium acetate, 1 m*M* EDTA (pH 5.0), and 0.4 μCi/ml of [*N-methyl*-^{14}C]sphingomyelin. The amount of radioactive phosphorylcholine produced was determined as described above.

RESULTS

Effects of D609 on SMase Activity

Because D609 has been used as a tool to block SMase activity [24, 26], we examined the effects of D609 on the activity of the two different SMases in U937 cells under acidic (pH 5.0) and neutral (pH 7.4) conditions *in vitro*. As shown in Fig. 1A, TNF induced a transient increase in neutral SMase activity reaching a maximum at 1.5 min, which is in good agreement with previous reports [18, 24]. Exposure of cells to D609 also resulted in an increase in neutral SMase activity which, however, was sustained for several minutes (Fig. 1A). In the presence of both TNF and D609, a sustained increase in neutral SMase activity was observed. TNF treatment alone had no effect on the activity of SMase under acidic conditions, whereas a slight, but significant, increase in sphingomyelin degradation was observed after 5 min of treatment with D609 (Fig. 1B). D609 did not decrease the basal activity of acidic SMase in U937 cells during a 60-min incubation (data not shown).

Effects of D609 on TNF- and Anti-Fas mAb-Induced Apoptosis

TNF and anti-Fas mAb are well-known inducers of apoptosis in the monocytic cell line U937. Ceramide has been implicated as a mediator of apoptosis caused

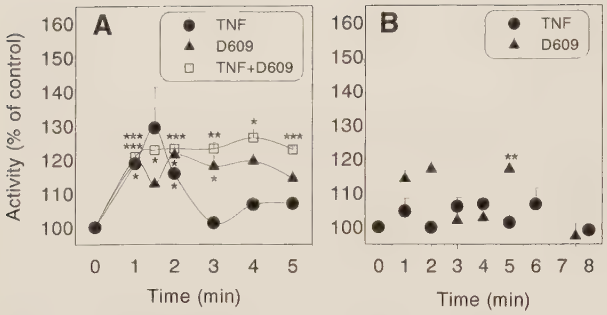

FIG. 1. Effects of TNF and D609 on SMase activity in U937 cells. Serum-starved U937 cells at a density of 4 × 10^6/ml were exposed to TNF (100 ng/ml), D609 (100 μg/ml), or both compounds together for the indicated times. The reaction was stopped by immersion of tubes into a dry ice/methanol bath for 10 s. Samples were then processed and analyzed for neutral SMase activity (A) or acidic SMase activity (B) as described under Materials and Methods. Data are expressed as a percentage of control values, which were ~3000 and ~6600 dpm of water-soluble [^{14}C]choline per sample for neutral and acidic SMase, respectively. Results are the mean ± SEM from four separate experiments. Statistical significance was determined using unpaired Student's *t* test. *$P < 0.05$, **$P < 0.005$, and ***$P < 0.0005$ for treated samples compared to control level.

by ligation of the TNF receptor [11], which seems to be coupled to two different SMase pathways with different pH optimi [24]. Ligation of Fas receptor has also been suggested to induce an early ceramide signal for induction of apoptosis [17], although contradictory findings have been presented [18]. TNF and anti-Fas treatment induced chromatin fragmentation typical of apoptosis in ~40% of the U937 cells within 6 h (Fig. 2). D609 (100 μg/ml) initially appeared to have some protective effects on TNF-induced apoptosis at early time points. However, after 6 h both TNF- and Fas-induced apoptosis were potentiated by D609, with up to ~70 and 90%, respectively, of the cells exhibiting apoptotic nuclei (Fig. 2). A similar effect was observed when D609 was added to cultures 30 min prior to TNF or anti-Fas mAb (data not shown). D609 alone did not have any effects on cell viability within 6 h, as shown in Fig. 2.

D609 Induces Chromatin Cleavage and Internucleosomal DNA Fragmentation in Long-Term Experiments

Since D609 caused a stimulation of SMase activity, the effect of D609 on U937 cell viability was further examined in long-term experiments. When cells were incubated with D609 alone for 16 h, 50–100 μg/ml D609 was found to induce chromatin condensation and fragmentation typical of apoptosis. The dose-dependent increase in chromatin fragmentation is shown in Fig. 3A. Exposure of U937 cells to 100 μg/ml D609 induced chromatin fragmentation in 60% of the cells within 16 h, and 50–100 μg/ml D609 induced the characteristic DNA laddering pattern observed in apoptosis (Fig. 3B).

Apoptosis in U937 cells has been shown to involve the formation of HMW DNA fragments of 50–300 kb, which precedes the formation of oligonucleosomal DNA fragments [32, 33]. When U937 cells were treated with 100 μg/ml D609, the formation of HMW DNA fragments was observed as early as 6 h after the addition of D609 to the cells, and the largest amount of fragments was detected after 8 h (Fig. 3C). After 16 h of D609 treatment, few HMW DNA fragments were detected, although a significant number of cells still had intact chromatin (Fig. 3C), suggesting that the susceptibility of U937 cells to D609-induced apoptosis may be cell cycle dependent. When the time courses for the formation of HMW and oligonucleosomal DNA fragments were compared, they clearly indicated that the HMW fragments preceded and most likely were precursors of the oligonucleosomal fragments. The largest amount of oligonucleosomal fragments was observed after 16 h of treatment with 100 μg/ml D609, when HMW DNA fragments were no longer visible (Fig. 3D).

Involvement of PKC during Apoptosis in U937 Cells

Since D609 has previously been reported to inhibit PKC activity [34, 35], the effects of PKC activation on D609-induced apoptosis were examined. As illustrated in Fig. 4, D609-induced internucleosomal DNA degradation was inhibited by cotreatment with the phorbol ester PMA (50 n*M*), suggesting that PKC may play a key role in modulating D609-induced apoptosis. Furthermore, the PKC inhibitors *H*-7 (50 μ*M*) and calphos-

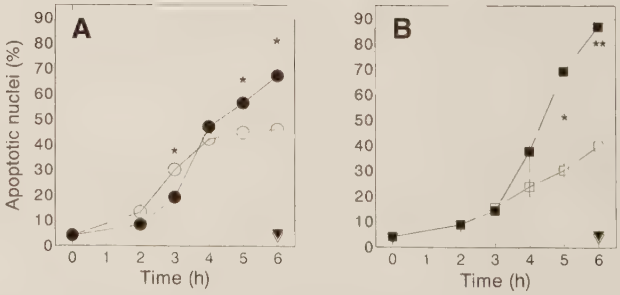

FIG. 2. Effects of D609 on TNF- and Fas-mediated apoptosis in U937 cells. Cells were resuspended in RPMI 1640 medium at a density of 10^6/ml and exposed to (A) 20 ng/ml TNF (○), TNF + 100 μg/ml D609 (●), (B) 150 ng/ml anti-Fas mAb (□), or anti-Fas mAb + D609 (■). Control cells were left untreated (▽) or received D609 alone (▼). After indicated incubation times, cells were collected and analyzed for apoptotic nuclei using Hoechst 33342 dye, as described under Material and Methods. Results are the mean ± SD from three separate experiments. Statistical significance was determined for differences between samples treated with TNF and TNF + D609. *$P < 0.05$, **$P < 0.0005$.

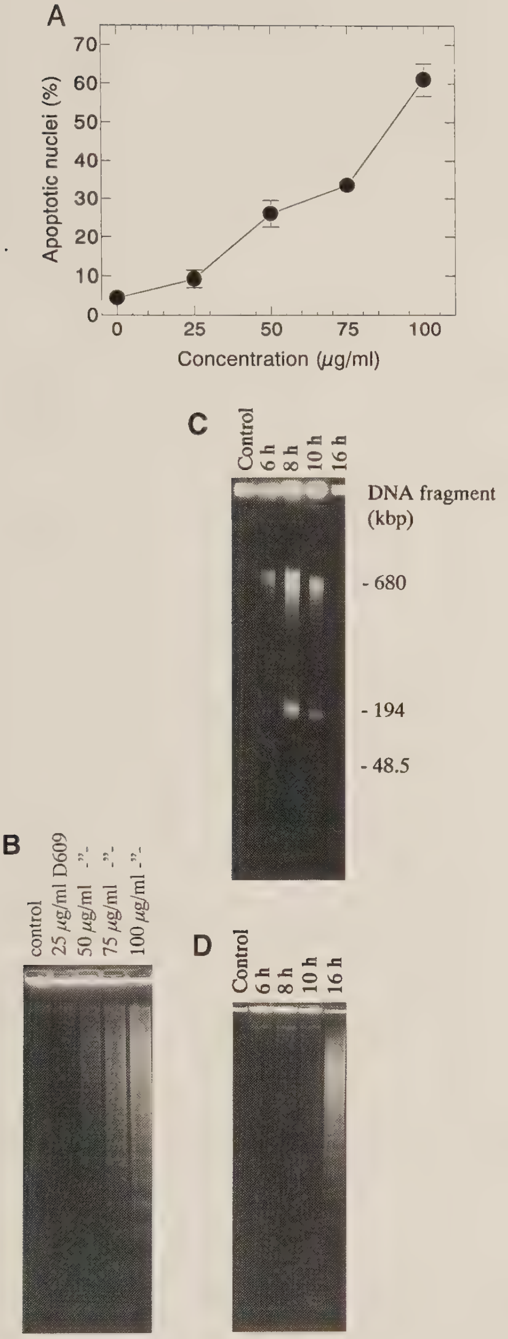

FIG. 3. D609-induced chromatin cleavage and DNA fragmentation in U937 cells. Cells were resuspended at a density of 10^6 cells/ml and exposed to various concentrations of D609 as indicated for 16 h. (A) Apoptotic nuclei were determined using fluorescence microscopy after staining with the Hoechst 33342 dye. Results are the mean ± SD from three separate experiments. (B) Internucleosomal DNA fragmentation induced by D609 was analyzed by conventional gel electrophoresis. Time course for D609-induced DNA fragmentation. U937 cells were exposed to 100 μg/ml D609 for the time indicated and cellular DNA was analyzed using field inversion gel electrophoresis for HMW fragments (C) or with conventional gel electrophoresis for internucleosomal fragmentation (D).

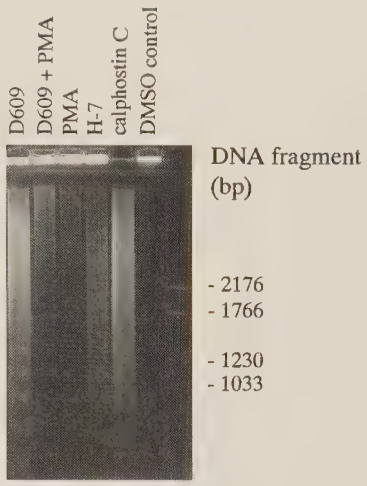

FIG. 4. Induction of DNA fragmentation by PKC inhibitors. U937 cells were resuspended at a density of 10^6 cells/ml and exposed to D609 (100 μg/ml), PMA (50 n*M*), *H*-7 (50 μ*M*), calphostin C (100 n*M*), or carrier solvent (DMSO, 0.1%) as a control. After incubation at 37°C for 16 h, cells were centrifuged at 2000*g* and DNA fragments from the cell pellet were separated using agarose gel electrophoresis as described under Material and Methods.

tin C (100 n*M*) also induced apoptosis in U937 cells (Fig. 4). Because D609-induced apoptosis was inhibited by PMA, we also examined the effects of PMA on TNF- and Fas-induced apoptosis. As illustrated in Fig. 5, 50

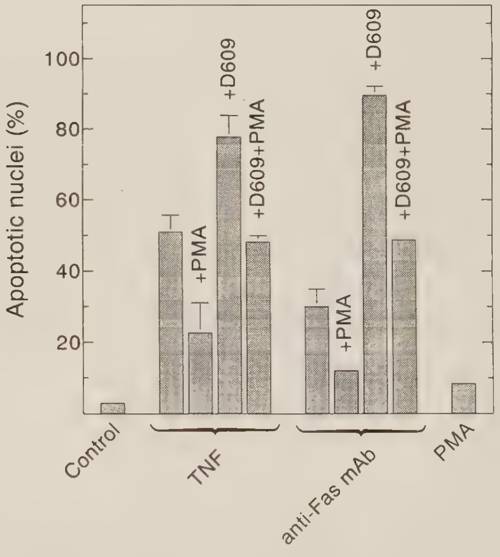

FIG. 5. Effects of PMA on TNF- and Fas-induced apoptosis. U937 cells were exposed to TNF (20 ng/ml), anti-Fas mAb (150 ng/ml), or PMA (50 n*M*) for 6 h. Appropriate dishes of cells were cotreated with 50 n*M* PMA (added 30 min before TNF or anti-Fas mAb), 100 μg/ml D609, or PMA and D609 together. The percentage of cells with apoptotic nuclei was determined by staining with Hoechst 33342 dye, as outlined under Material and Methods. Results are the mean ± SD from three separate experiments.

TABLE 1

Apoptosis Induced by Lipid Mediators in U937 Cells

Treatment	Apoptotic nuclei (%)
Control (10% FCS)	6.4 ± 0.7
SMase	26.3 ± 4.2
C_2-ceramide	22.3 ± 5.3
Arachidonic acid	26.0 ± 6.0
Control (5% FCS)	6.2 ± 2.2

Note. U937 cells resuspended at a cell density of 10^6 cells/ml in RPMI medium containing 10% FCS were exposed to C_2-ceramide (40 μM) or SMase (0.05 U/ml) for 24 h. In order to decrease the binding of arachidonic acid to serum components, arachidonic acid (150 μM) treatments were performed in medium containing only 5% FCS. After 24 h, cells were collected and the number of apoptotic cells was determined using Hoechst 33342 staining, as described under Materials and Methods. Results are means ± SD from three separate experiments.

n*M* PMA was found to inhibit TNF- and Fas-induced chromatin fragmentation in U937 cells by ~60%. PMA was also able to reduce the potentiation of TNF- and Fas-induced apoptosis by D609. These results suggest that PKC inhibition may be an important step in the activation of cell death in U937 cells by TNF, anti-Fas mAb, and D609.

Induction of Apoptosis in U937 Cells by Lipid Mediators

To verify that the U937 cells used in this study were susceptible to being killed by short-chained ceramide and exogenously added SMase, we incubated the cells for 24 h in the presence of C_2-ceramide or bacterial SMase, and the formation of apoptotic nuclei was determined. As shown in Table 1, both C_2-ceramide and SMase treatment clearly induced apoptosis in U937 cells. Arachidonic acid, which has been implicated as a mediator of neutral SMase activation and TNF-induced apoptosis [36, 37], also caused apoptosis in 26% of the U937 cells within 24 h (Table 1), compared to 6% apoptosis in the untreated control cells.

DISCUSSION

Recent studies have demonstrated that apoptosis induced by TNF and anti-Fas mAb appears to involve ceramide as a signaling molecule, and an increased rate of sphingomyelin degradation has been reported to occur in several different apoptotic systems [15]. It is, however, unclear whether the increased SMase activity detected during apoptosis is of the acidic or the neutral type (or both). Our present findings demonstrate that the exposure of U937 cells to D609 results in a stimulation of neutral SMase activity, which precedes apoptosis. TNF failed to induce an increased activity of acidic SMase, which is contrary to some previous observations [24, 27], but in good agreement with a recent report [38] where TNF treatment stimulated only the neutral—not the acidic—SMase activity in leukemia cells. Since the results of the present study suggest that the effects of D609 on cellular SMases may be stimulatory rather than inhibitory, the use of D609 as an inhibitor to study SMase activity in cells must be exercised with great caution.

Krönke and co-workers [24] have shown that deletion of the TNF p55 receptor region, which is responsible for the activation of PC-PLC and acidic SMase, confers resistance to TNF toxicity, suggesting that stimulation of acidic SMase would be important for the triggering of cell death. In addition, apoptotic cell death caused by Fas receptor ligation has also been suggested to involve acidic SMase [16]. Results from studies involving the use of monensin, however, argue against the importance of acidic enzymes in TNF- and Fas-mediated signaling [18]. Data obtained from patients with Niemann–Pick disease (acidic SMase deficiency) indicate that acidic SMase plays an important role in the bulk processing of lipids entering the endosomal/lysosomal pathway [39]. Kolesnick and co-workers [40] have recently reported that lymphoblasts from Niemann–Pick patients fail to respond to ionizing radiation with ceramide generation and apoptosis. When acidic SMase activity was restored in these cells by retroviral transfer of human acidic SMase cDNA, the cells responded normally and underwent apoptosis upon irradiation. Thus, at least in some cell types, acidic SMase activity may be required for apoptosis. However, the fact that apoptosis can be triggered by treatment with bacterial SMase [14, this study], which acts at the plasma membrane at a neutral pH, suggests that neutral SMase may in some instances be sufficient to cause apoptosis. In the present study, apoptosis in U937 cells was increased after exposure to arachidonic acid, which has been reported to stimulate only the neutral SMase [36]. The type of enzyme responsible for ceramide generation may not be as important as the actual cellular location of the product, since ceramide presumably needs to interact with protein phosphatases and/or kinases in order to induce the apoptotic response.

The present findings, that D609 induced apoptosis by itself and potentiated TNF-induced apoptosis in U937 leukemia cells, may provide an explanation for the recent observations, that D609 in combination with TNF caused partial regression of human tumor transplants in athymic mice [41] and complete regression of equine sarcoid [42]. D609 potentiated both the SMase activation and the apoptosis induced by TNF in U937 cells, suggesting that ceramide may act as a modulator of TNF-induced responses. Treatment of U937 cells with sphingomyelinase or short-chained ceramide only caused a low level of apoptosis within 24 h, implying that the accumulation of intracellular ceramide alone is not sufficient for rapid induction of apoptosis in these cells.

The inhibition of D609-, TNF-, and Fas-induced apoptosis by PMA suggests that PKC activity may play a critical role in the regulation of apoptosis in U937 cells [11, 18, 43, and present findings]. Furthermore, C_2-ceramide-induced apoptosis is inhibited by phorbol ester treatment [11]. It has also been shown that diacylglycerol, which activates PKC, inhibits apoptosis in leukemia cells [44]. Because diacylglycerol has been reported to activate acidic SMase [25], the protective effect of diacylglycerol may involve the stimulation of acidic SMase, suggesting that stimulation of this enzyme does not always result in apoptosis. It is well known that inhibitors of PKC induce apoptosis in a number of different cell types [45, 46]. Our results clearly show that inhibitors of PKC, like calphostin C and *H*-7 readily induced apoptosis in U937 cells (cf. Fig. 4). By inhibiting PC-PLC, and thereby the formation of diacylglycerol, D609 may down-regulate PKC as reported previously [34, 35]. Furthermore, PKC inhibitors like calphostin C and chelerythrine induce apoptosis and ceramide production in WEHI-231 cells through the activation of neutral SMase [47], which is in good agreement with our present findings. Ceramide is known to inactivate cellular PKC-α [48], and other downstream targets include a ceramide-activated protein kinase [49] and a ceramide-activated protein phosphatase [50]. Their possible role in the regulation of apoptosis remains to be elucidated.

This study was supported by grants from the Academy of Finland, the Swedish Medical Research Council (Grant 13X-02471-29B), and the Wenner–Gren Foundation.

REFERENCES

1. Elias, E., Moore, P. B., and Rose, S. M. (1988) *Biochem. Biophys. Res. Commun.* **157,** 963–969.
2. Itoh, N., Yonehara, S., Ishii, A., Yonehara, M., Mizushima, S., Sameshima, M., Hase, A., Seto, Y., and Nagata, S. (1991) *Cell* **66,** 233–243.
3. Wright, S. C., Kumar, P., Tam, A. W., Shen, N., Varma, M., and Larrick, J. W. (1992) *J. Cell. Biochem.* **48,** 344–355.
4. Oehm, A., Behrmann, I., Falk, W., Pawlita, M., Maier, G., Klas, C., Li-Weber, M., Richards, S., Dhein, J., Trauth, B. C., Ponsting, H., and Krammer, P. H. (1992) *J. Biol. Chem.* **267,** 10709–10715.
5. Itoh, N., and Nagata, S. (1993) *J. Biol. Chem.* **268,** 10932–10937.
6. Tartaglia, L. A., Ayres, T. M., Wong, G. H. W., and Goeddel, D. V. (1993) *Cell* **74,** 845–853.
7. Kim, M.-Y., Linardic, C., Obeid, L., and Hannun, Y. (1991) *J. Biol. Chem.* **266,** 484–489.
8. Dressler, K. A., Mathias, S., and Kolesnick, R. N. (1992) *Science* **255,** 1715–1718.
9. Wiegmann, K., Schütze, S., Kampen, E., Himmler, A., Machleidt, T., and Krönke, M. (1992) *J. Biol. Chem.* **267,** 17997–18001.
10. Yanaga, F., and Watson, S. P. (1992) *FEBS Lett.* **314,** 297–300.
11. Obeid, L. M., Linardic, C. M., Karolak, L. A., and Hannun, Y. A. (1993) *Science* **259,** 1769–1771.
12. Dbaibo, G. S., Obeid, L. M., and Hannun, Y. A. (1993) *J. Biol. Chem.* **268,** 17762–17766.
13. Ji, L., Zhang, G., Uematsu, S., Akahori, Y., and Hirabayashi, Y. (1995) *FEBS Lett.* **358,** 211–214.
14. Jarvis, W. D., Kolesnick, R. N., Fornari, F. A., Traylor, R. S., Gewirtz, D. A., and Grant, S. (1994) *Proc. Natl. Acad. Sci. USA* **91,** 73–77.
15. Pushkareva, M., Obeid, L. M., and Hannun, Y. A. (1995) *Immunol. Today* **16,** 294–297.
16. Cifone, M. G., De Maria, R., Roncaioli, P., Rippo, M. R., Azuma, M., Lanier, L. L., Santoni, A., and Testi, R. (1994) *J. Exp. Med.* **177,** 1547–1552.
17. Gulbins, E., Bissonnette, R., Mahboubi, A., Martin, S., Nishioka, W., Brunner, T., Baier, G., Baier-Bitterlich, G., Byrd, C., Lang, F., Kolesnick, R., Altman, A., and Green, D. (1995) *Immunity* **2,** 341–351.
18. Tepper, C. G., Jayadev, S., Liu, B., Bielawska, A., Wolff, R., Yonehara, S., Hannun, Y. A., and Seldin, M. F. (1995) *Proc. Natl. Acad. Sci. USA* **92,** 8443–8447.
19. Gatt, S. (1976) *Biochem. Biophys. Res. Commun.* **68,** 235–241.
20. Rao, B. G., and Spence, M. W. (1976) *J. Lipid Res.* **17,** 506–515.
21. Schneider, P. B., and Kennedy, E. P. (1967) *J. Lipid Res.* **8,** 202–209.
22. Okazaki, T., Bielawska, A., Domae, N., Bell, R. M., and Hannun, Y. A. (1994) *J. Biol. Chem.* **269,** 4070–4077.
23. Schütze, S., Potthoff, K., Machleidt, T., Berkovic, D., Wiegmann, K., and Krönke, M. (1992) *Cell* **71,** 765–776.
24. Wiegmann, K., Schütze, S., Machleidt, T., Witte, D., and Krönke, M. (1994) *Cell* **78,** 1005–1015.
25. Kolesnick, R. N. (1987) *J. Biol. Chem.* **262,** 16759–16762.
26. Schulze-Osthoff, K., Krammer, P. H., and Dröge, W. (1994) *EMBO J.* **13,** 4587–4596.
27. Cifone, M. G., Roncaioli, P., De Maria, R., Camarda, G., Santoni, A., Ruberti, G., and Testi, R. (1995) *EMBO J.* **14,** 5859–5868.
28. Sorenson, C. M., Barry, M. A., and Eastman, A. J. (1990) *J. Natl. Cancer Inst.* **82,** 749–755.
29. Brown, D. G., Sun, X.-M., and Cohen, G. M. (1993) *J. Biol. Chem.* **268,** 3037–3039.
30. Quintern, L. E., and Sandhoff, K. (1991) *Methods Enzymol.* **197,** 536–540.
31. Boucher, L.-M., Wiegmann, K., Fütterer, A., Pfeffer, K., Machleidt, T., Schütze, S., Mak, T. W., and Krönke, M. (1995) *J. Exp. Med.* **181,** 2059–2068.
32. Bicknell, G. R., Snowden, R. T., and Cohen, G. M. (1994) *J. Cell Sci.* **107,** 2483–2489.
33. Vanags, D. M., Pörn-Ares, M. I., Coppola, S., Burgess, D. H., and Orrenius, S. (1996) *J. Biol. Chem.* **271,** 31075–31085.
34. Müller-Decker, K., Doppler, C., Amtmann, E., and Sauer, G. (1988) *Exp. Cell Res.* **177,** 295–302.

35. Müller-Decker, K. (1989) *Biochem. Biophys. Res. Commun.* **162,** 198–205.
36. Jayadev, S., Linardic, C. M., and Hannun, Y. A. (1994) *J. Biol. Chem.* **269,** 5757–5763.
37. Müller, G., Ayoub, M., Storz, P., Rennecke, J., Fabbro, D., and Pfizenmaier, K. (1995) *EMBO J.* **14,** 1961–1969.
38. Higuchi, M., Singh, S., Jaffrezou, J.-P., and Aggarwal, B. B. (1996) *J. Immunol.* **156,** 297–304.
39. Spence, M. W., and Callahan, J. W. (1989) *in* The Metabolic Basis of Inherited Disease (Schriver, C. R., Beaudet, A. C., Sly, W. J., and Valle, D., Eds.), pp. 1655–1676, McGraw–Hill, New York.
40. Santana, P., Pena, L. A., Haimovitz-Friedman, A., Martin, S., Green, D., McLoughlin, M., Cordon-Cardo, C., Schuchman, E. H., Fuks, Z., and Kolesnick, R. N. (1996) *Cell* **86,** 189–199.
41. Amtmann, E., and Sauer, G. (1990) *Int. J. Cancer* **45,** 1113–1118.
42. Otten, N., Marti, E., Söderström, C., Amtmann, E., Burger, D., Gerber, H., and Lazary, S. (1994) *J. Vet. Med. A* **41,** 757–765.
43. Copeland, K. F. T., Haaksma, A. G. M., Goudsmit, J., Krammer, P. H., and Heeney, J. L. (1994) *AIDS Res. Hum. Retroviruses* **10,** 1259–1268.
44. Jarvis, W. D., Fornari, F. A., Jr., Browning, J. L., Gewirtz, D. A., Kolesnick, R. N., and Grant, S. (1994) *J. Biol. Chem.* **269,** 31685–31692.
45. Bertrand, R., Solary, E., O'Connor, P., Kohn, K. W., and Pommier, Y. (1994) *Exp. Cell Res.* **211,** 314–321.
46. Jarvis, W. D., Turner, A. J., Povirk, L. F., Traylor, R. S., and Grant, S. (1994) *Cancer Res.* **54,** 1707–1714.
47. Chmura, S. J., Nodzenski, E., Weichselbaum, R. R., and Quintans, J. (1996) *Cancer Res.* **56,** 2711–2714.
48. Lee, J. Y., Hannun, Y. A., and Obeid, L. M. (1996) *J. Biol. Chem.* **271,** 13169–13174.
49. Mathias, S., Dressler, K. A., and Kolesnick, R. N. (1991) *Proc. Natl. Acad. Sci. USA* **88,** 10009–10013.
50. Dobrowsky, R. T., and Hannun, Y. A. (1992) *J. Biol. Chem.* **267,** 5048–5051.

Received January 24, 1997
Revised version received May 2, 1997

EXPERIMENTAL CELL RESEARCH **235,** 55–61 (1997)
ARTICLE NO. EX973656

Retinoic Acid Receptors α and γ Mediate the Induction of "Tissue" Transglutaminase Activity and Apoptosis in Human Neuroblastoma Cells

Gerry Melino,* Muriel Draoui,† Lorenza Bellincampi,* Francesca Bernassola,* Sergio Bernardini,‡ Mauro Piacentini,§ Uwe Reichert,‖ and Paul Cohen†[1]

**Biochemistry Laboratory, Istituto Dermopatico dell'Immacolata (IDI-IRCCS), c/o Department of Experimental Medicine, University of Rome, Tor Vergata, Rome, Italy: and Department of Biology, University L'Aquila, L'Aquila, Italy; †Laboratoire de Biochimie des Signaux Régulateurs Moléculaires et Cellulaires, Université Pierre et Marie Curie, URA 1682 CNRS, 96 Boulevard Raspail, Paris 75006, France; ‡Post Graduate School in Biochemistry and Clinical Chemistry, University of Camerino c/o Bambino Gesù Hospital-IRCCS, Rome, Italy; §Department of Biology, University of Rome Tor Vergata, Rome, Italy; and ‖Centre International de Recherches Dermatologiques-GALDERMA, BP87, 06902 Sophia-Antipolis, France*

All-*trans* retinoic acid (RA) reduces human neuroblastoma growth by inducing either differentiation or apoptosis. The apoptotic program in these cells is regulated by RA and is paralleled by the transcriptional induction of "tissue" transglutaminase (tTG). tTG is a protein cross-linking enzyme, which specifically accumulates in cells undergoing apoptosis in various *in vivo* and *in vitro* systems. In neuroblastoma cells, tTG is detected exclusively in the cells expressing the S-type phenotype and showing an increased apoptosis. The present study was undertaken to identify the retinoid receptors which are involved in the regulation of tTG and apoptosis as well as in the *in vitro* neuronal differentiation of the human SK-N-BE(2) neuroblastoma cell line. We have previously characterized the retinoid acid receptors expressed in this cell line. In the present study, by using synthetic retinoids selectively activating RAR/RXR isoforms, we have identified the RAR/RXR receptors involved in the induction of either apoptosis or differentiation. We have also studied the effect of the selective RA analogs on tTG activity. We observed that while RARα- and RARγ-selective retinoids alone were able to induce tTG activity, only the combined stimulation of both RARα and RARγ induced apoptosis. Conversely, several combinations of RAR/RXR closely mimicked the differentiation effects observed with all-*trans* retinoic acid. These results indicate that, at variance with differentiation, the induction of apoptosis in human SK-N-BE(2) neuroblastoma cells is under the specific control of RARα and RARγ. These data seem relevant for the reported ability of RARγ to suppress the clinically malignant tumor phenotype in patients. © 1997 Academic Press

INTRODUCTION

The transglutaminase family includes intracellular and extracellular enzymes that catalyze Ca^{2+}-dependent reactions in which γ-carboxamide groups of peptide-bound glutamine residues serve as acyl donors and in which primary amino groups of several compounds function as acceptor substrates [1, 2]. The reaction results in posttranslational modifications, establishing ϵ(γ-glutamyl)lysine cross-linkages and/or covalent incorporation of biogenic amines (di- and polyamines and histamine) into proteins. Diamines and polyamines also participate in cross-linking reactions through the formation of *N,N*-bis(γ-glutamyl)polyamine cross-bridges [1, 3, 4]. The transglutaminase-dependent formation of stable cross-linkages leads to protein polymerization, which confers high resistance to mechanical breakage and chemical attack to the polypeptides involved in the linkage [5, 6]; in fact, these polymers can be destroyed only by proteolytic degradation of protein chains [6].

In mammals, increased "tissue" transglutaminase (tTG)[2] gene expression is observed in cells undergoing apoptosis or programmed cell death [3, 4, 7–10]. The GTP- and Ca^{2+}-dependent activation of the enzyme leads to the formation of a detergent-insoluble cross-linked protein scaffold in cells undergoing programmed cell death [3, 4, 7, 8]. This insoluble protein scaffold could stabilize the integrity of the dying cells before their clearance by phagocytosis, thus preventing the release of harmful intracellular components (i.e., lysosomal enzymes, nucleic acids, etc.) and consequently inflammatory responses and scar formation in neighboring tissues [8, 11]. Indeed, a key feature of apoptosis

---

[1] To whom correspondence and reprint requests should be addressed. Fax: (33)1-42221398.

[2] Abbreviations used: RA, all-*trans* retinoic acid; RAR, retinoic acid receptor; RXR, retinoid X receptor; RARE, retinoic acid-responsive element; tTG, tissue transglutaminase; PBS, phosphate-buffered saline; FBS, fetal bovine serum; MEM, minimal essential medium.

0014-4827/97 $25.00
Copyright © 1997 by Academic Press
All rights of reproduction in any form reserved.

is the targeting of singly scattered cells and the absence of inflammation [12]. In some models, the dependence on RNA and protein synthesis indicates that the expression of specific genes is needed for the completion of the apoptotic program [11]. However, the detailed biochemical events leading to the morphological features characterizing cells undergoing apoptosis are still largely unknown [10–12]. We have previously shown that transfection of a tTG cDNA, in sense or antisense orientation, into human neuroblastoma SK-N-BE(2) cells led, respectively, to a marked enhancement or reduction of apoptosis [13]. These data in human neuroblastoma cells support the idea that tTG could be an effector of apoptosis.

Human neuroblastoma cell lines established in culture [14–17] show two morphologically and biochemically distinct phenotypes (i.e., neural "N-type" and flat substrate-adherent "S-type") which undergo bidirectional phenotypic interconversion [15–17]. In several studies aimed at investigating the regulation of tTG gene expression by retinoic acid (RA) in human neuroblastoma cell lines, we demonstrated that these cells show differential phenotype-specific regulation of tTG expression [13, 18]. In fact, the RA-dependent increase of tTG expression was paralleled by an enhanced apoptotic index only in the S variant, whereas N-cells expressed a very low tTG protein level and were less sensitive to RA-induced apoptosis [13]. Some cell lines are composed of both phenotypes. These phenotypes are observed in the SK-N-BE(2) cell line used in this study.

The biological activity of retinoids is exerted through binding to specific nuclear receptors which belong to the steroid/thyroid hormone family. Two major classes of retinoid receptors, the RARs and RXRs, have been identified; each of these two classes comprises three distinct receptor subtypes, namely, α, β, and γ. Ligand-activated RARs and RXRs may form either homodimers or heterodimers and function as *trans*-acting nuclear transcription factors which bind to their respective retinoic acid response elements (RAREs) [19–22]. Galderma Co. (Sophia-Antipolis, France) has synthesized and provided various retinoid compounds that stimulate selectively a specific RAR isoform or all three RXR isoforms [23, 24]. The selectivity of various retinoids was measured by the binding affinity of various compounds to RARα, RARβ, RARγ, or RXR receptors. Upon binding of these synthetic retinoid analogs to their respective receptors, transactivation of their established promoters is observed. These synthetic retinoid analogs thus act as selective RAR or RXR receptor agonists. Recently, we have identified the retinoid receptors expressed in neuroblastoma cells; however, their presence or absence could not be correlated to the induction of cell death [23]. The pattern of RA receptors present in the SK-N-BE(2) cell line was previously measured by RT–PCR and Northern blot. In this cell line, the RARα, RARγ, and RXRα receptors were upregulated by RA. RARβ mRNA expression was only present after RA exposure [23]. Therefore, it was suggested that the relative amounts of the various receptor subtypes could influence the homodimer and heterodimer formation altering gene expression. As RARE elements have been identified on the mouse tTG promoter, the present study was undertaken to identify the retinoid receptors which could be involved in the regulation of tTG activity, apoptosis, and the *in vitro* neuronal differentiation of the human SK-N-BE(2) neuroblastoma cell line.

METHODS

Reagents. Tissue culture plastics and reagents were obtained from Flow Laboratories Ltd. (Herts, UK). Protein concentration was assayed using bicinchoninic acid from Pierce (Rockford IL). The synthetic RA analogs were supplied by CIRD Galderma Co.. We used CD14 (all-*trans* RA), CD336 (Am 580), which selectively binds to RARα, CD666, an agonist for RARγ, CD2314, an agonist for RARβ, CD2624, an RXR-selective agonist. All retinoids were dissolved in DMSO under low light and stored at −20°C. The specificity and assays for RAR/RXR binding and transactivation activity were described previously [23, 24].

Cell culture and cell differentiation. The SK-N-BE(2) cell line (104th–107th passage) was provided by Dr. June Biedler (Memorial Sloane-Kettering Cancer Hospital, New York). Cells were grown in monolayer cultures in a 1:1 mixture of MEM and Ham's F-12 media supplemented with 15% heat-inactivated FBS, sodium bicarbonate (1.2 mg ml^{-1}), Hepes buffer (15 m*M*), L-glutamine (2 m*M*), and nonessential amino acids (1% v/v). Cells were treated with either 1 μM RA (5 m*M* stock solution in 70% ethanol) or 1 μM synthetic retinoid analogs (5 m*M* stock solution in DMSO); 0.07% ethanol or DMSO was added to the control cultures. The growth curve was performed either as previously described [13] or by the standard hexosaminidase method. The Neurite Outgrowth Index [14] was evaluated as the percentage of differentiated cells per number of neurites/cell per length of neurites in micrometers. In order to obtain more quantitative data, three independent observers scored 500 cells each and the results were pooled together. The data reported in Fig. 2 are the average of two separate experiments ± SEM (3000 cells were counted for each point).

Quantification of DNA fragmentation and tissue transglutaminase assay. DNA fragmentation of dead cells was evaluated by flow cytometry following staining with propidium iodide (50 mg/ml) [13, 18] on a FACScan flow cytometer (Becton–Dickinson, CA); 10,000 events were triggered by the forward side scatter (FSC) signal and gated for FSC-H/FSC-A/SSC (where H is height, A is area, and SSC is side scatter) to avoid aggregates.

For the tTG assay, cells were mechanically removed from flasks, washed with phosphate-buffered saline (PBS without Ca^{2+} and Mg^{2+}), and sonicated at 4°C for 20 s. tTG activity was measured by detecting the incorporation of [^{3}H]putrescine into *N,N′*-dimethylcasein; data were normalized per milligram of protein, as previously reported [13, 18].

RESULTS

Effect of Synthetic Retinoid Agonists on the Differentiation of Human Neuroblastoma Cells

Galderma Co. has synthesized various retinoid-selective compounds; CD14 binds equally to all three RAR

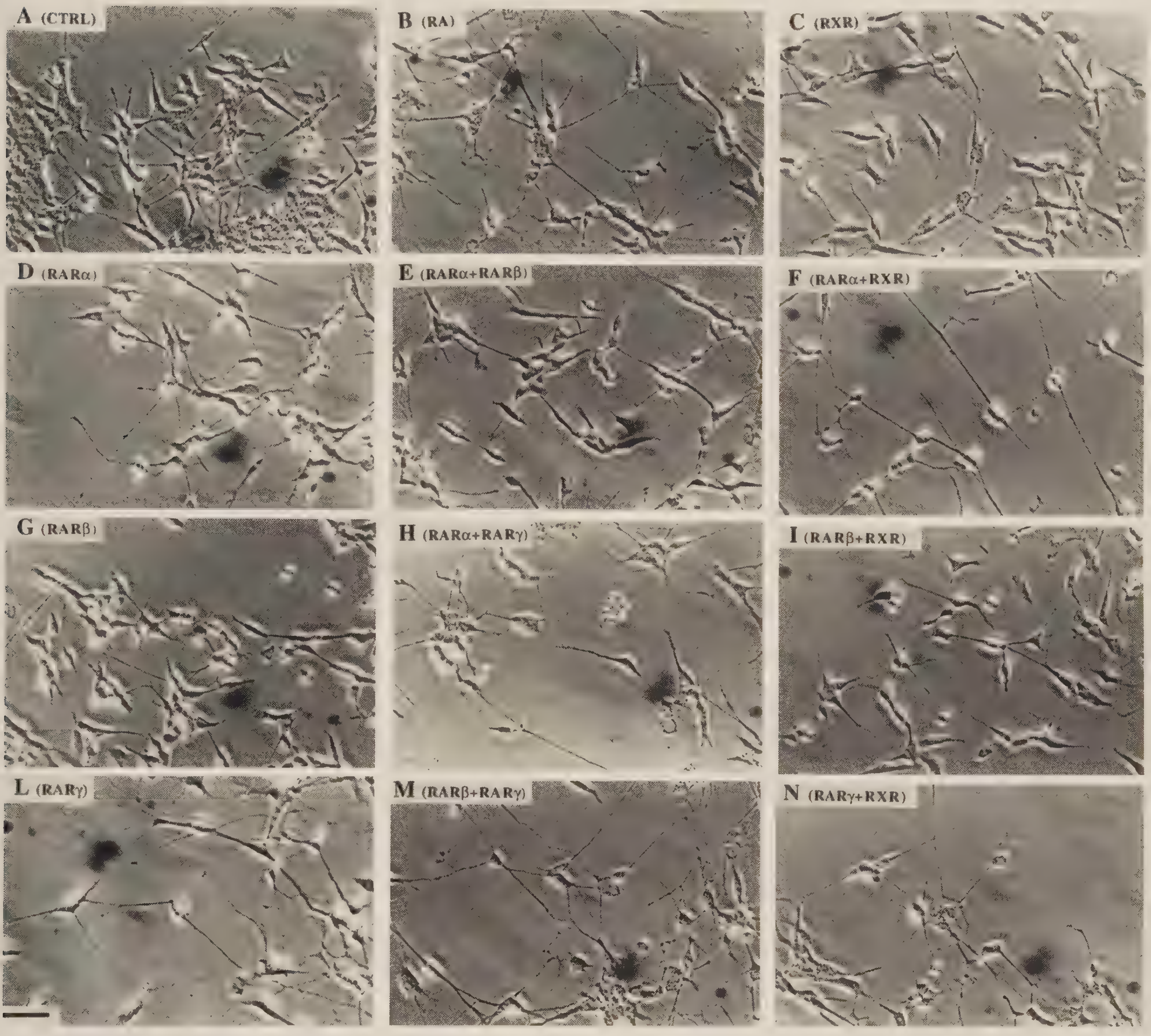

FIG. 1. Effects of synthetic retinoid agonists on neuroblastoma cell differentiation. SK-N-BE(2) cells were treated for 7 days with 1 μM RA, 1 μM RAR/RXR synthetic retinoids, or the indicated combination of those compounds. The selectivity of the ligand used is indicated in brackets in each panel (A–N). Bar, 15 μm.

receptor isoforms, whereas CD336 binds preferentially to RARα, CD 666 to RARγ, and CD 2314 to RARβ. CD2624 exhibits the highest affinity for the RXR receptors. By taking advantage of these selective retinoids, we analyzed various combinations of RARs/RXRs for their ability to induce differentiation. The effect of selective RAR/RXR ligands on the stimulation and induction of neuronal differentiation in the SK-N-BE(2) neuroblastoma cell line was evaluated over a 7-day period (Fig. 1). The SK-N-BE(2) cell line did not respond to the RXR-selective agonist but significantly responded to RARα- and RARγ-inducing agonists. Several combination of RAR/RXR mimicked the effect observed with RA, except for the heterodimer RXR–RARβ. Although RARβ seems to have inhibitory effects, at least with respect to neurite outgrowth, we do not feel that the experimental settings could allow such a strong conclusion. In order to measure the neuronal differentiation induced by RA or its synthetic analogs, we evaluated the Neurite Outgrowth Index [14] (percentage of differentiated cells × number of neurites/cell × length of neurites in micrometers) (Fig. 2A). The Neurite Outgrowth Index was determined by three independent observers on 500 cells for each experimental point; the average of

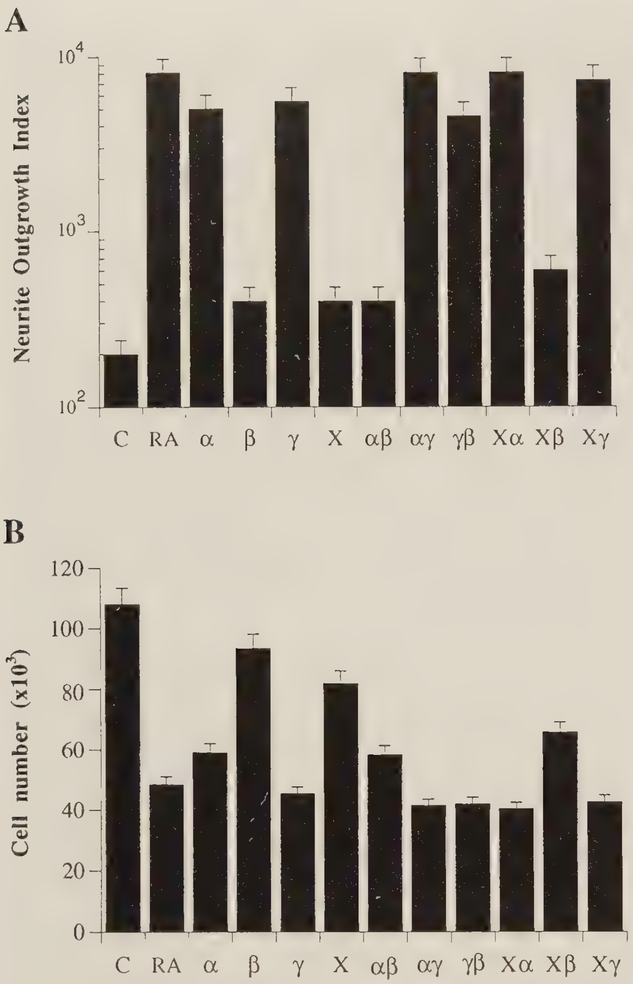

FIG. 2. Comparison of Neurite Outgrowth Index and cell number of SK-N-BE(2) cells upon exposure to retinoic acid and retinoid agonists. (A) Neurite Outgrowth Index (expressed as percentage of differentiated cells × number of neurites per cell × length of neurites in micrometers). Three independent observers scored 500 cells each; the average of two separate experiments ± SEM is reported in the figure. (B) Cell growth after 7 days exposure to RA and synthetic retinoid agonists used either individually or in combination. The control (C) represents cells treated with 0.07% ethanol. The selective receptor stimulated by the synthetic retinoids is indicated as α, β, γ (for RARs), and X (for pan-RXRs). Results are expressed as the mean ± SEM of three different experiments, each carried out in duplicate.

the measurements is reported in the figure. Similarly, we analyzed the growth pattern of the SK-N-BE(2) cell line, exposed to RA and to synthetic agonists either individually or in combination (Fig. 2B). The number of cells counted after 7 days of culture correlates inversely with the Neurite Outgrowth Index, measured to quantify the degree of differentiation (Fig. 2).

Effect of Synthetic Retinoid Agonists on Tissue Transglutaminase Activity and Apoptosis

The retinoid receptors involved in the modulation of tTG activity in the SK-N-BE(2) cell line were analyzed. Stimulation of RARβ, RXR, or their combination showed no changes in transglutaminase activity when compared to the control (Fig. 3). However, the other synthetic RARs agonists (RARα, RARγ), used individually, stimulated transglutaminase activity, mimicking RA. When used in combination with RXR, the effect of the RARα and RARγ agonists on transglutaminase activity was even greater. Interestingly, the greatest effects were observed by the combined stimulation of the RARα/RXR or RARγ/RXR receptors.

The percentage of apoptotic bodies was measured by FACS analysis of the SK-N-BE(2) cells treated for 3 days with 1 μM RA, 1 μM synthetic retinoids, or a combination of synthetic retinoids (Fig. 4). Using RARα- and RARγ-selective agonists no increase in the percentage of apoptotic bodies was observed; however, a significant increase (evaluated by the Kolmogorov–Smirnoff analysis, program Lysis II, Becton–Dickinson) in apoptosis was triggered using RARα- and RARγ-selective agonists simultaneously. RAR/RXR-selective agonists used either independently or in combination (other than the ones just mentioned) had no effect on apoptosis. The fact that only the simultaneous stimulation of RARα/RARγ induces apoptosis in the SK-N-BE(2) neuroblastoma cell line implies that more complex events than the induction of tTG are required for the triggering of cell death.

DISCUSSION

RA reduces human neuroblastoma growth by inducing differentiation, death by apoptosis, or both [13, 14,

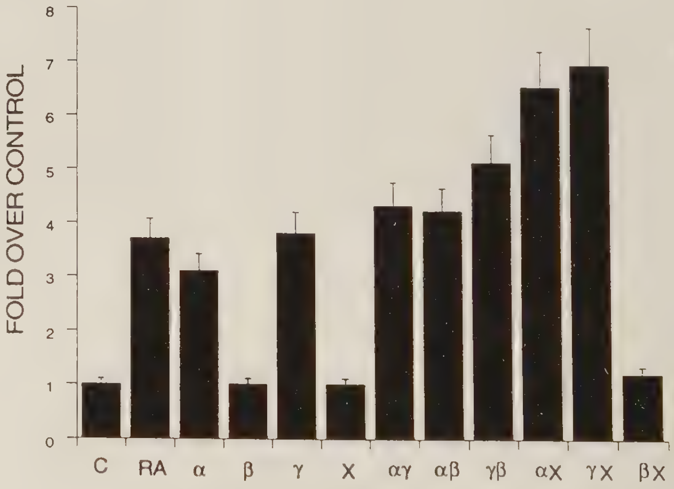

FIG. 3. Modulation of transglutaminase activity by synthetic retinoid agonists. SK-N-BE(2) cells were treated for 3 days with either 1 μM RA or 1 μM synthetic retinoids, as indicated. The control (C) represents cells treated with 0.07% ethanol (or DMSO). The selective receptor stimulated by synthetic retinoids is indicated as α, β, γ (for RARs), and X (for pan-RXRs). Transglutaminase activity was evaluated as described under Methods; activity has been measured as pmol/h/mg protein and it is reported as a percentage of control values. Results are the mean ± SEM of three different determinations, each performed in triplicate.

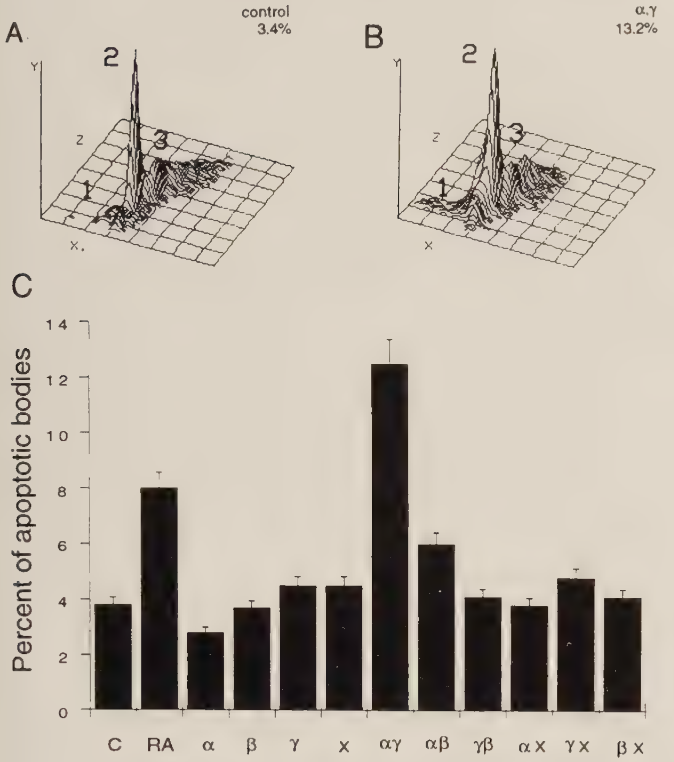

FIG. 4. Effects of RA and synthetic retinoids on the percentage of apoptotic body formation in the SK-N-BE(2) neuroblastoma cell line. (A) control; (B) cells treated with RARα+RARγ agonists (1 μM). The axes represent forward scatter (z), number of events (y), fluorescence intensity at 580 nm (x) of propidium iodide (DNA content). The peaks represents cycling G_2/M cells (3), noncycling G_0/G_1 cells (2), or hypodiploid events (1) with fragmented DNA (apoptotic bodies). (C) Effect of all synthetic retinoids on SK-N-BE(2) cells stimulated with selective RARs agonists (α, β, or γ) or with a pan-RXR agonist (X). SK-N-BE(2) neuroblastoma cells were incubated for 3 days with 0.07% ethanol (C), 1 μM RA, 1 μM RAR/RXR synthetic retinoid agonists, or a combination, as indicated. The measurement of apoptotic body formation was performed by flow cytometry as described under Methods; 10,000 events were evaluated for each sample. The values are the average ± SEM of two separate experiments performed in duplicate.

18]. We have previously shown that the apoptotic program in these cells of neuroectodermal origin is strictly regulated by RA and is paralleled by transcriptional induction and enzymatic activation of tTG [18]. The enzyme was detectable exclusively in the cells expressing the S-type phenotype and was paralleled by an increase in the apoptotic index [4].

In the present study, we demonstrate that the molecular mechanisms by which retinoids induce tTG and apoptosis in SK-N-BE(2) human neuroblastoma cells can be activated by specific RAR/RXR ligands and their related transduction pathways. We did not report the protein levels of tTG, nor its mRNA steady-state level, because the enzyme is finally regulated at the posttranscriptional level by local concentrations of Ca^{2+}, GTP, putrescine, and redox potential. Therefore, a possible correlation has to be found with enzyme activity. The specificity of the synthetic retinoid agonist has proven informative in identifying precisely the receptors modulating tTG expression. The data clearly showed that stimulation of RARα and RARγ was sufficient to individually transactivate tTG expression. However, only the simultaneous stimulation of RARα/RARγ was able to fully induce apoptosis, whereas RAR/RXR heterodimer activation failed to accelerate cell death. Therefore, although tTG may act as an effector of apoptosis in human neuroblastoma cells, its expression is not sufficient per se to lead to apoptosis. In fact, a comparison of the effects of various synthetic retinoids on tTG levels with those obtained by morphological parameters clearly suggested that other factors may be necessary to trigger apoptosis in this particular cell line. In contrast to the cell death program, the regulation of neuronal differentiation is widely modulated by several receptor ligands or their combination.

Recent works provided evidence for an RA-dependent induction of tTG and apoptosis in several cellular models, such as epithelial cell lines [25], T-cell hybridomas [26], and in leukemia cells [27]. Although the direct transcriptional activation of the gene encoding tTG by RA and retinoids has not been fully elucidated, there is now evidence indicating that the promoter region of the mouse tTG gene contains RA-sensitive responsive elements [28] which were not detectable in the first 1.74-kb flanking DNA sequence characterized [29] in the human tTG gene. Indeed, a novel retinoid responsive element with three repeats, rather than two, has been found on the mouse tTG promoter, suggesting that the expression of tTG requires the binding of three receptors, one of which is RXR [28]. The tTG promoter is therefore quite unusual, being induced by ligand-dependent stimulation operated by both RAR-specific and RXR-specific retinoids through a tripartite RARE [28]. This feature might explain why tTG expression always occurs in parallel to the onset of apoptosis irrespective of the cell type (e.g., HL60 versus human neuroblastoma) and the diverse RAR/RXR dimers which are stimulated. In keeping with these findings, tTG was found to be regulated at multiple complex levels from its mRNA expression to its posttranslational regulation by Ca^{2+}, GTP [30] and intracellular polyamines [31].

In the present work, we have investigated the retinoid receptors which may regulate tTG and apoptosis in human neuroblastoma cells. However, the interpretation of these data is complicated by the intricacy of the cellular situation in which multiple differentiation potential as well as transdifferentiation between the S, N, I phenotypes may compete. Our data indicate that the simplistic idea of different receptors responsible for different cellular responses, apoptosis or differentiation, is complicated by the fact that, in broad terms, the same synthetic retinoids able to stimulate N-type differentiation also induce tTG. This complication may be due to different intracellular settings, such as retinoid coactivators or corepressors or other modulators of transcription, which may or may not be related to the N, S, I phenotypes. Further work is therefore needed to test a possible correlation with the cell phenotype or with transcriptional regulators of retinoids. We have shown that both tTG expression and apoptosis are linked to the S phenotype [13, 18]. This indicates that other factors may be involved to either differentiate these cells or to drive them to apoptosis. The recently identified thyroid–retinoic acid-associated corepressors (TRAC), the 168-kDa SMRT [32], and the 270-kDa N-CoR [33] might be responsible for the fine regulation of RARα action in neuroblastoma cells. TRAC proteins function as silencing factors of the thyroid hormone and retinoic acid receptors. These protein complexes are also sensitive to the polarity of the responsive elements. RAR/RXR heterodimers activate transcription in DR+5 elements in response to RAR-specific ligands (RA), whereas DR+1 repeats are repressed in some cases by RXR [34]. This intricate regulation thus depends upon the different ligands, DR repeats, cofactors, and retinoic acid receptors which are present.

Furthermore, other pathways could be involved in the regulation of apoptosis by retinoids, as pointed out by the recent discovery of a relationship between retinoic acid, 3-hydroxymethylglutaryl coenzyme A (HMG-CoA) reductase [35] and apoptosis [36]. The fact that RARα or RARγ alone is sufficient to mediate tTG activity, but their combination is needed for the induction of apoptosis, suggests strongly a very complex tripartite RARE, as indicated by recent data obtained in the mouse system [28, 32], a fine posttranslational regulation of tTG *in vivo,* or the involvement of yet to be clarified additional events.

The induction of apoptosis by RARα and RARγ stimulation might have obvious clinical consequences, since those two receptors are well expressed in tumor biopsies. While 9-*cis* RA enhances the differentiation of neuroblastoma cells more effectively than all-*trans* RA [37, 38], increased RARγ expression seems to reduce the malignant phenotype of children affected by neuroblastomas [39].

We are grateful to CIRD-Galderma (Sophia-Antipolis, France) for providing the retinoid synthetic analogs. We also thank Margherita Annicchiarico-Petruzzelli, Lucia Piredda, and Giorgia Santilli for their scientific support. M.D. was successively supported by a postdoctoral fellowship from the Association pour la Recherche sur le Cancer (ARC) and from the Associazione Italiana per la Ricerca contro il Cancro (AIRC). This work was supported in part by funds from the CNRS (URA 1682), from the Ministère de la Recherche et de l'Enseignement Supérieur to Université Paris VI, from the ARC (6358); AIRC to (M.P.); from the Ministero della Sanità to IDI-IRCCS (G.M.), CNR pr. ACRO subpr 8 (G.M.), Associazione Neuroblastoma (G.M.), and Telethon (1996, E413 to G.M.).

REFERENCES

1. Folk, J. E. (1980) *Annu. Rev. Biochem.* **49,** 517–531.
2. Greenberg, C. S., Birckbichler, P. J., and Rice, R. H. (1992) *FASEB J.* **5,** 3071–3077.
3. Piacentini, M., Autuori, F., Dini, L., Farrace, M. G., Ghibelli, L., Piredda, L., and Fesus, L. (1991) *Cell Tissue Res.* **263,** 227–235.
4. Piacentini, M., Fesus, L., Farrace, M. G., Ghibelli, L., Piredda, L.. and Melino, G. (1991) *Eur. J. Cell Biol.* **54,** 246–254.
5. Green. H. (1977) *Cell* **11,** 405–416.
6. Folk, J. E., and Finlayson, S. (1977) *Adv. Protein Chem.* **31,** 1–133.
7. Fésüs, L., Thomázy, V., and Falus, A. (1987) *FEBS Lett.* **224,** 104–108.
8. Fésüs, L., Thomázy, V., Autuori, F., Cerù-Argento, M. P., Tarcsa, E., and Piacentini, M. (1989) *FEBS Lett.* **245,** 150–154.
9. Knight, C. R. L., Rees, R, C., and Griffin, M. (1991) *Biochim. Biophys. Acta* **1096,** 312–320.
10. Strange, R. L. F., Saurerm S., Burkhard, A., and Friis, R. R. (1992) *Development* **115,** 49–58.
11. Fésüs, L., Davies, P. J. A., and Piacentini, M. (1991) *Eur. J. Cell Biol.* **56,** 170–177.
12. Wyllie, A. H., Kerr, J. F. R., and Currie, A. R. (1980) *Int. Rev. Cytol.* **68,** 251–306.
13. Melino, G., Annicchiarico-Petruzzelli, M., Piredda, L., Candi, E., Gentile, V., Davies, P. A. J., and Piacentini, M. (1994) *Mol. Cell Biol.* **14**(10), 6584–6596.
14. Melino, G., Stephanou, A., Annicchiarico-Petruzzelli, M., Knight, R. A., Finazzi-Agro, A., and Lightman, S. L. (1993) *Neurosci. Lett.* **151,** 187–191.
15. Biedler, J. L., Spengler, B. A., Chang, T. D., and Ross, R. A. (1988) *Prog. Clin. Biol. Res.* **271,** 265–276.
16. Ciccarone, V., Spengler, B. A., Meyers, M. B., Biedler, J. L., and Ross, R. A. (1989) *Cancer Res.* **49,** 219–225.
17. Ross, R. A., Spengler, B. A., and Biedler, J. L. (1983) *J. Natl. Cancer Inst.* **71,** 741–747.
18. Piacentini, M., Annicchiarico-Petruzzelli, M., Oliverio, S., Piredda, L., Biedler, J. L., and Melino, G. (1992) *Int. J. Cancer* **52,** 271–278.
19. Chambon, P., Zelent, A., Petkovich, M., Mendelsohn, C., Leroy, P., Krust, A., Kastner, P., and Brand, N. (1991) *in* Retinoids: 10 Years in Basel (Saurat, J. H., Ed.), pp. 10–27, Karger, Basel.
20. Petkovich, M., Brand, N. J., Krust, A., and Chambon, P. (1987) *Nature* **330,** 444–450.
21. Brand, N. J., Petkovich, M., Krust, A., Chambon, P., De The, H., Marchio, A., Tiollais, P., and Dejean, A. (1988) *Nature* **332,** 850–853.
22. Delescluse, C., Cavey, M. T., Martin, B., Reichert, U., Maignan, J., Darmon, M., and Shroot, B. (1990) *Mol. Pharmacol.* **40,** 556–562.
23. Melino, G., Draoui, M., Bernardini, S., Bellincampi, L., Reichert, U., and Cohen, P. (1996) *Cell Growth Differ.* **7,** 787–796.
24. Martin, B., Bernardon, J. M., Cavey, M. T., Bernard, B., Carlavan, I., Charpentier, B., Pilgrim, W. R., Shroot, B., and Reichert, U. (1992) *Skin Pharmacol.* **5,** 57–65.
25. Zhang, L., Mills, K. J., Dawson, M. I., Collins, S. J., and Jetten, A. M. (1995) *J. Biol. Chem.* **270**(11), 6022–6029.
26. Bissonnette, R. P., Brunner, T., Lazarchik, S. B., Yoo, N. J., Boehm, M. F., Green, D. R., and Heyman, R. A. (1995) *Mol. Cell Biol.* **15**(10), 5576–5585.

27. Nagy, L., Thomázy, V. A., Shipley, G. L., Fésüs, L., Lamph, W., Heyman, R. A., Roshantha, A. S., Chandraratna, A. S., and Davies, P. J. A. (1995) *Mol. Cell Biol.* **15**(7), 3540–3551.
28. Nagy, L., Saydak, M., Shipley, N., Lu, S., Basilion, J. P., Yan, Y. H., Syka, P., Chandraratna, R. A. S., Stein, J. P., Heyman, R. A., and Davies, P. J. A. (1996) *J. Biol. Chem.* **271**(8), 4355–4365.
29. Lu, S., Saydak, V., Gentile, V., Stein, J. P., and Davies, P. J. A. (1995) *J. Biol. Chem.* **270**(17), 9748–9756.
30. Achyuthan, K. E., and Greenberg, G. S. (1987) *J. Biol. Chem.* **262,** 1901–1906.
31. Melino, G., Farrace, M. G., Cerù, M. P., and Piacentini, M. (1988) *Exp. Cell Res.* **179,** 429–445.
32. Chen, D., and Evans, R. M. (1995) *Nature* **377,** 454–457.
33. Hörlein, A. J., Näär, A. M., Heizel, T., Torchia, J., Gloss, B., Kurokawa, R., Ryan, R., Karnei, Y., Söderström, M., Glass, C. K., and Rosenfeld, M. G. (1995) *Nature* **377,** 397–404.
34. Kurokawa, R., Söderström, M., Hörlein, A. J., Halachmi, S., Brown, M., Glass, C. K., and Rosenfeld, M. G. (1995) *Nature* **377,** 451–454.
35. Dimitroulakos, J., and Yeger, H. (1996) *Nature Med.* **2,** 326–333.
36. Han, Z., and Wyche, J. H. (1996) *Cell Death Differ.* **3,** 223–228.
37. Han, G., Chang, B., Connor, M. J., and Sidell, N. (1995) *Differentiation* **59,** 61–64.
38. Redfern, C. P. F., Lovat, P. E., Malcolm, A. J., and Pearson, A. D. J. (1995) *Eur. J. Cancer* **31A**(4), 486–94.
39. Marshall, G. M., Cheung, B., Stacey, K. P., Camacho, M, L., Simpson, A. M., Kwan, E., Smith, S., Haber, M., and Norris, M. D. (1995) *Oncogene* **11,** 485–491.

Received January 27, 1997
Revised version received April 27, 1997

EXPERIMENTAL CELL RESEARCH **235,** 62–70 (1997)
ARTICLE NO. EX973659

Thyroid Cell Transformation Inhibits the Expression of a Novel Rat Protein Tyrosine Phosphatase

Li Zhang,* Maria Luisa Martelli,* Caterina Battaglia,* Francesco Trapasso,* Donatella Tramontano,* Giuseppe Viglietto,† Antonio Porcellini,* Massimo Santoro,‡ and Alfredo Fusco*[,1]

**Dipartimento di Medicina Sperimentale e Clinica, Facoltà di Medicina e Chirurgia di Catanzaro, Università degli Studi di Reggio Calabria, via Tommaso Campanella 5, 88100 Catanzaro, Italy; †Instituto dei Tumori di Napoli, via Mariano Semmola, 80131 Naples, Italy; and ‡Centro di Endocrinologia ed Oncologia Sperimentale del C.N.R., c/o Dipartimento di Biologia e Patologia Cellulare e Molecolare, Facoltà di Medicina e Chirurgia, Università di Napoli "Federico II," via S. Pansini, 5, 80131 Naples, Italy*

We have isolated a rat thyroid cDNA encoding a novel rat receptor-type tyrosine phosphatase protein. This gene, on the basis of its homology to another tyrosine phosphatase, the recently isolated human DEP-1/HPTPη, has been named r-PTPη. In rat thyroid cells the r-PTPη gene acts as a differentiation marker. Indeed, the block of thyroid cell differentiation induced by viral and cellular oncogenes is associated with the inhibition or marked reduction of the expression of this gene, and its expression is positively regulated by thyrotropin, the physiological stimulator of thyroid cell growth. © 1997 Academic Press

INTRODUCTION

The phosphorylation of protein tyrosine residues is a crucial event in the regulation of normal cellular processes such as proliferation and differentiation; it is also involved in the malignant transformation of cells [1–3]. The phosphorylation state of tyrosine residues in a target substrate is governed by the coordinated action of protein–tyrosine kinases (PTKs) and protein–tyrosine phosphatases (PTPases) [1–10]. The PTK and PTPase families include soluble, cytosolic, and receptor-like transmembrane members that contain a wide variety of structural and regulatory domains in association with the catalytic domains [3, 10–19]. Each PTPase contains at least one conserved domain of 240 amino acids that is characterized by the signature motif (I/V)HCXAGXGR(S/T)G. The structural diversity within the PTPase family arises primarily from the variety of putative regulatory sequences linked to the catalytic domains [15–17].

Among the cytosolic PTPases, PTPH1 [20] and MEG [21] show homology to several cytoskeletal-associated proteins, which suggests that they play a role in controlling cytoskeletal integrity. SHP-1 contains two copies of src homology (SH2) domain, which suggests direct linkage of PTPs to the growth factor receptor machinery [22].

The structure of receptor-like PTPases can generally be described in terms of an intracellular segment containing one or two phosphatase domains: a single transmembrane domain and a variable extracellular segment, which might represent binding sites for putative ligands [12, 16–18]. Receptor-like protein tyrosine phosphatases (RPTPases) are divided into groups according to the diverse structural characteristics of their extracellular domains, which presumably reflect an equivalent diversity in the variety of ligands to which they may respond. Some of them, like PTPμ and PTPκ, promote cell–cell aggregation through homophilic binding interactions [23–25]. RPTPases also play a role in the control of nervous system differentiation and development [26–28]. In fact, PTPδ and receptor-type PTPβ (RPTPβ/PTPζ) are highly expressed in cells of neural origin [29–31]; the carbonic anydrase domain of RPTPβ/PTPζ is a ligand for the axonal recognition molecule contactin [30]; and three transmembrane tyrosine phosphatases, DLAR, DPT69D, and DPT99A, play a role in motor axon guidance in *Drosophila melanogaster* [32, 33].

The role of PTPases and RPTPases in the differentiation process of cells of nonneural origin has not yet been investigated. The rat thyroid cell system is a good model for the study of epithelial cell growth and differentiation because the cell lines retain all the markers of thyroid differentiation *in vitro*, i.e., thyroglobulin (TG) synthesis and secretion, the capability of trapping iodide from the culture medium, and dependence on thyroid stimulating hormone (TSH) for growth [34, 35], and because the oncogene-transformed cell lines show different degrees of malignancy and differentiation [34–38]. To date little is known about the role of PTPases in thyroid cell proliferation and differentiation. We recently demonstrated that somatostatin in-

---

[1] To whom correspondence and reprint requests should be addressed. Fax: 39 81 7463037. E-mail: afusco@synapsis.it.

0014-4827/97 $25.00
Copyright © 1997 by Academic Press
All rights of reproduction in any form reserved.

hibits PC Cl 3 thyroid cell proliferation through modulation of phosphotyrosine phosphatase activity and that the stable expression of the adenovirus E1A gene in these cells completely abolishes this antiproliferative effect [39]. The aim of the present study was to identify thyroid-specific PTPases by PCR amplification using degenerate primers.

We isolated a gene that may be considered the rat homologue of the recently identified human PTPase DEP-1/HPTPη [40, 41]. This gene, which we designated r-PTPη, is expressed ubiquitously, but is found mainly in the brain, liver, and spleen. The expression of the r-PTPη gene is induced by TSH in normal thyroid cells and correlates with the differentiation state of thyroid cells.

MATERIALS AND METHODS

Isolation and characterization of r-PTPη. PCR amplification of cDNA was performed to clone portions of potential PTPases with PCR degenerate primers corresponding to conserved sequences of known PTPases, i.e., amino acid sequences 5′ DYINA 3′ and 3′ VHCSAG 5′. Total RNA was extracted from rat PC Cl 3 cells by the acid–guanidine phenol–chloroform method [42]. Poly(A)$^+$ RNA was enriched by three passages through an oligo(dT) column. Complementary DNA (cDNA) was then synthesized starting from 1 μg of poly(A)$^+$ RNA using the Gene Amp RNA kit (Perkin–Elmer Cetus) following standard protocols [43]. The reaction occurred at 42°C for 30 min. After reverse transcriptase inactivation at 99°C for 5 min, primers at a final concentration of 0.75 μM, a mixture containing 10 m*M* Tris–HCl, pH 8.3, 50 m*M* KCl, 2.5 m*M* MgCl$_2$, 0.01% gelatin, all four dNTPs (each at 0.2 m*M*), and 2.5 units of *Taq* polymerase were added. The PCR amplification was performed for 30 cycles, with each cycle including denaturation at 94°C for 1.5 min, annealing at 37°C for 3 min, and primer extension at 72°C for 3 min [44]. The sense and antisense primers used were: 5′ ATGGATCCGGAT(C) TAT (C) ATNAAT(C) GC 3′ and 3′ CAG (C) GTG (A)ACG (A)TCG(A)G-CNCCC GAATTCGC-5′, respectively. The primers contained flanking *Bam*HI and *Eco*RI sites (underlined), respectively, to facilitate subsequent cloning. The PCR products were analyzed on a 1% agarose gel. DNA fragments of 450 basepairs were obtained, which were eluted from the gel and digested with *Bam*HI and *Eco*RI. The DNA was then electrophoresed on a 1.5% agarose gel, recovered, and subcloned into *Bam*HI/*Eco*RI-digested pGem 3Z vector. Subsequently, the subclones were sequenced by dideoxy termination methods [45] using the Pharmacia kit. Among the 10 clones sequenced, one novel cDNA encoding a PTPase domain was isolated (Phos-C1). This fragment was used to screen a cDNA library from rat brain in λgT 10 (Stratagene). Gene walking was then performed.

Northern blot analysis. Northern blot and hybridization procedures were performed according to standard procedures [43]. A GAPDH probe was used to ascertain equal RNA loading [46].

Cell cultures. The PC Cl 3 cell line is a thyroid epithelial cell line derived from 18-month-old Fischer rats [34]. The oncogene-transfected PC cells lines are described elsewhere [35–38]. The normal and infected rat cell lines were cultured in modified F12 medium, supplemented with 5% calf serum (Flow Laboratories) and six growth factors (thyrotropin, hydrocortisone, insulin, transferrin, somatostatin, and glycil-histidyl-lysine; Sigma Chemical Corp.).

RESULTS

Isolation and Sequencing of a Novel Tyrosine Phosphatase

To isolate novel tyrosine phosphatases from thyroid cells, poly(A)$^+$ RNA extracted from the rat thyroid PC Cl 3 cells was amplified with PCR, as described under Materials and Methods. PCR products were cloned and 10 subclones were isolated and sequenced. Nine of them were identical to other PTPases. One clone, named Phos-C1, showed homology, but not identity, with the tyrosine phosphatase catalytic domain of several PTPases. This DNA fragment was used for Northern blot analysis using RNA extracted from PC Cl 3 and rat brain. A band of approximately 7.8 kb was detected in both samples, even though the expression was at least fivefold higher in brain (data not shown). A weak band of approximately 5.5 kb was also detected. Subsequently, a cDNA library prepared from rat brain was screened with the same cDNA fragment, and a phage, named 21 B, was isolated. Other cycles of library screening led to the isolation of three other phages, named 23B, 32B, and BB, that cover all of the coding sequence of this PTPase cDNA (Fig. 1). The inserts of these phages were sequenced, and a 3984-bp-long open reading frame was found.

The primary structure of the cDNA and its predicted translation product is shown in Fig. 2. The first methionine found in this open reading frame is at position 36 and poorly matches the Kozak consensus [47, 48] for a translation initiation site. In contrast, the two methionine residues, located at positions 216 and 372, respectively, match the Kozak consensus. The methionine at position 216 is followed by 52 hydrophilic amino acids, while the one at position 372 is followed by 25 highly hydrophobic amino acids. Since this stretch of hydrophobic amino acids may represent a signal peptide, we presume that the real translation initiation codon is at position 372. The predicted mature protein is composed of an extracellular domain of 849 amino acids, a transmembrane domain of 25 amino acids, and a cytoplasmic region of 341 amino acids.

The cytoplasmic region of the predicted protein sequence contains the conserved sequence motifs found in all PTPases isolated so far [7, 8]. Thus, our protein contains a single PTPase domain in its cytoplasmic domain, as do DEP1/HPTPη [40, 41], SAP-1 [49], HPTPβ, and DPTP 10 D, a *Drosophila* homologue of HPTP β [18, 50]. Moreover, the Phos-C1 sequence contains eight fibronectin type III (FN-III)-like repeats and no immunoglobulin (Ig)-like domains in the extracellular region.

The comparison of the amino acid and nucleotide sequences of Phos-C1 with those of known PTPs showed a remarkable homology with DEP1/HPTPη (Fig. 3); in some regions the homology, at the level of amino acids, is more than 90%. However, in the extracellular region there is a large amino-terminal region with a homology of only 65% and a stretch of 17 amino acid residues in Phos-C1 (amino acids 71–87) which does not have any homology in the corresponding region of DEP-1/HPTPη (amino acids 152–173). Moreover, the 79 amino acids

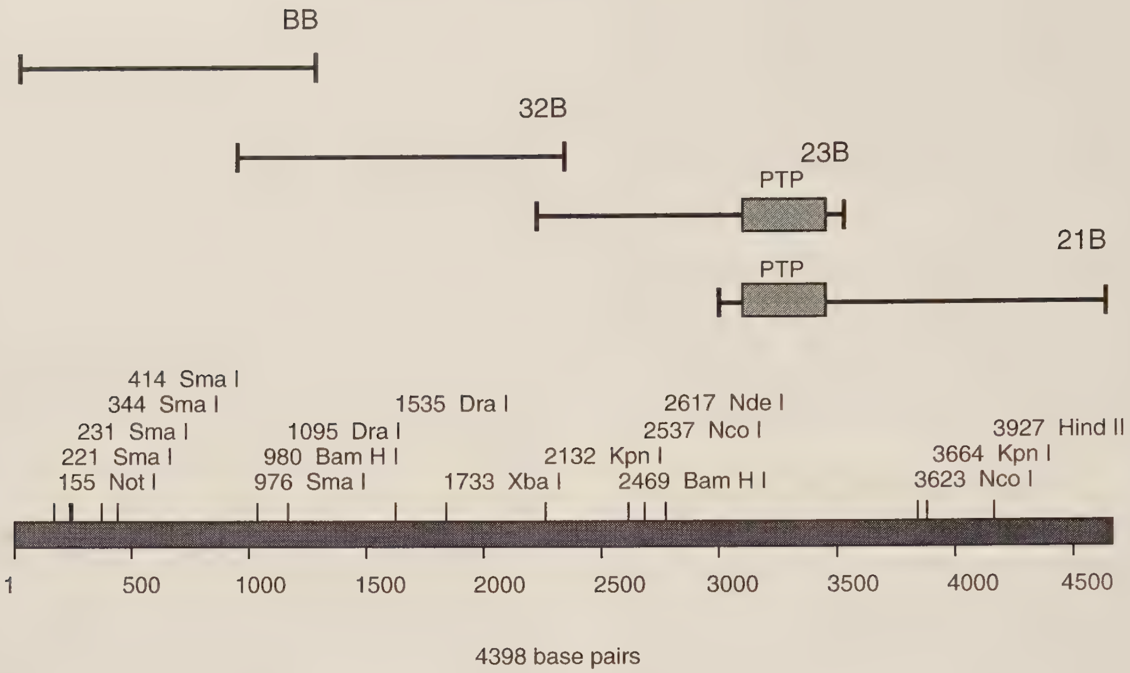

FIG. 1. Restriction mapping and cDNA clones obtained for r-PTPη. Overlapping r-PTPη cDNA clones (top) and restriction map of the complete cDNA (bottom). Shaded boxes represent the tyrosine–phosphatase domain (PTP).

between residues 239 and 318 of DEP-1/HPTPη are replaced in Phos-C1 by 44 completely different amino acids (amino acids 154–197). The differences between rat and human species may account for an imperfect identity between the two sequences. Alternative splicing may account for the completely different stretches. Byp, a murine receptor-type tyrosine phosphatase similar to human DEP-1/HPTPη, was cloned while our work was in progress [51]. In most regions, the homology of Byp and Phos-C1 is higher than 95%. The main difference between Byp and Phos-C1 consists of a 24-amino-acid sequence in Byp (from amino acid 197 to aa 220), which is not present in the Phos-C1 clone. In the amino-terminal region from amino acids 50 to 200 the homology between these two genes is only 65%. In the remaining extracellular region the homology between these two genes is close to 90%.

Even though we cannot exclude that Phos-C1 and DEP1/HPTPη may be two members of the same family, the similarity of the mRNA messenger size, together with a very high homology in a large part of the genes, suggests that Phos-C1 is the rat homologue of DEP1/HPTP. We have therefore named this novel gene rat PTPη (r-PTPη).

Tissue Distribution and Expression

A Northern blot of poly(A)$^+$ RNA from adult rat tissues was hybridized with the radiolabeled 462-bp *Sma*I–*Sma*I cDNA fragment (from nucleotides 414 to 976) of the r-PTPη gene. This gene is ubiquitous, but its expression is greater in liver, brain, and spleen (Fig. 4) than in testis and skeletal muscle. Ubiquitous expression of the r-PTPη gene was confirmed in mouse tissues (data not shown).

Expression of the r-PTPη Gene in PC Cl 3 Cells Transformed by Several Viral Oncogenes

Two rat thyroid epithelial cell lines (PC Cl 3 and FRTL-5 Cl 2), expressing thyroid differentiation markers (TG synthesis and secretion, uptake of iodide, and dependence on TSH for growth) were previously infected with several murine retroviruses carrying different oncogenes. The introduction of viral and cellular oncogenes into thyroid cells generated cell lines showing different patterns of differentiation. The characteristics of these cell lines are summarized in Table 1. Some cell lines (e.g., PC MPSV, PC E1A + v-raf, PC E1A + v-abl, PC v-abl, PC v-raf, FRTL-5 Cl 2 KiMSV, and FRTL5 Cl 2 MPSV cells) lost the expression of all the differentiated thyroid phenotypic markers. Other cell lines (PC E1A, PC HE4, and PC KiMSV cells) expressed only some parameters of thyroid differentiation, e.g., a partial TSH dependency for growth and a reduced capability to synthesize TG. Finally, the PC c-myc cell line retained all the thyroid differentiation markers [34–38].

The foregoing cell lines were analyzed for the expression of the r-PTPη gene. The RNAs were extracted from

```
   1                              GGCCGAGCGCTCCGGCTCCCTGCAGCCGGAGCCGCATGACGCGCGGAGGAG
  52 GCAGAGGGAGCAGCCGGGGCCGCGGGAGCCCGGAGCTGGACGCCACGCGCGGGGGGTGGGCGCCGCTTGCTCCGCCCCGC
 132 GAAGCCCCTGCGTGTCTAGGGCCGCGGCCGCTCCGCGTTAGGAGCGCTAGGCTCCGCCGTGTGGCCGCCGCCGCCGCGC
 212 TGCCATGTCCCCGGGGAAGCCCGGGGCGGGCGGAGCGGGGACTAGGCGGACCGGCTGGCGGAGAAGGAGGCGGAGGCGTC
 292 GGCTGGAGGCGGAGACCAGGGCGCCCGGCTTCGGGCACACGGCGGGGCGCGTCCCGGGCACGTTCCAGGGCGCGCAGGGC

 372 ATG AAG CCC GCG GCG CGG GAG ACG CGG ACA CCC CCG CGC TCG CCC GGG CTC CGC TGG GCG
   1 Met lys pro ala ala arg glu thr arg thr pro pro arg ser pro gly leu arg trp ala

 432 CTG CTG CCG CTG CTG CTG TTG CTA CGC CAG GGC CAG GTT GTG TGC GCA GGT GCG GCG CCC
  21 leu leu pro leu leu leu leu leu arg gln gly gln val val cys ala gly ala ala pro

 492 AGT CCT GTA TTT GAC GTT GAA GCT GTC ACC AGC CCT ACC AGT GTG GTA TTA ACG TGG AAA
  41 ser pro val phe asp val glu ala val thr ser pro thr ser val val leu thr trp lys

 552 CAC AAT GAT TCA GCC ACT TCA GAA TAT AAG ATA AAT GAG GGA AAC ACG CTG CGG TAT ACT
  61 his asn asp ser ala thr ser glu tyr lys ile asn glu gly asn thr leu arg tyr thr

 612 GTT AAA AAC CAG ACA TCA TTT AAC ATC ACA GGC TTA AGC CCA GCT ACT TCC TAC AAA TTC
  81 val lys asn gln thr ser phe asn ile thr gly leu ser pro ala thr ser tyr lys phe

 672 TCC ATC ACC TTG GGA ACA GTC AAT GAG ACC TCA GGA AAG CCC ACA TAC AAA AAT ATC ACA
 101 ser ile thr leu gly thr val asn glu thr ser gly lys pro thr tyr lys asn ile thr

 732 ACA GAG CCC TGG CCA GTG TCG GAT CTC CAA GTC GCC TAC ATC GGT GTG ACA CAG GCT CTT
 121 thr glu pro trp pro val ser asp leu gln val ala tyr ile gly val thr gln ala leu

 792 CTC GCC TGG AGC AAT GCA AAC GGC ACC GCT TCT TAC CGG ATG CAG ATT GTA GAG CTG ACC
 141 leu ala trp ser asn ala asn gly thr ala ser tyr arg met gln ile val glu leu thr

 852 ACA AAT TCA TCA GGT GGT ATT TCA GAT CTG AAG CCG GGG ACC CAT AAG AGC TTG GCT GTC
 161 thr asn ser ser gly gly ile ser asp leu lys pro gly thr his lys ser leu ala val

 912 CAA GGA TCG AAT GAG ACC CAG CAT GAC TTA TGG GTC ACA GAA GGC GTC TCG GAC CCA CCC
 181 gln gly ser asn glu thr gln his asp leu trp val thr glu gly val ser asp pro pro

 972 TCT GCC CGG GAT CCC TCC CTC ACA GAG GTC TTG CTC ACT GAG CTA AAG CCT GAT ACT CAG
 201 ser ala arg asp pro ser leu thr glu val leu leu thr glu leu lys pro asp thr gln

1032 TAC AAA GTC ACC ATT TAT TCT CAA GCA GCA GAT GGC ACA GAA GGA CAG CCT GGG AAC AAA
 221 tyr lys val thr ile tyr ser gln ala ala asp gly thr glu gly gln pro gly asn lys

1092 GTG TTT AAA ACA AAT CCC ATC CAA GTT TCT GAC ATC CGA GCT GTG AAC ATC AGT GAC TCG
 241 val phe lys thr asn pro ile gln val ser asp ile arg ala val asn ile ser asp ser

1152 AAC ATG ACC CTG ACC TGG AAA AGC AAC AAT AAT GAG TCC CAT GCT TCA TTT ACC TAC AAA
 261 asn met thr leu thr trp lys ser asn asn asn glu ser his ala ser phe thr tyr lys

1212 ATA TAC GTG GCT GGG GGT TCC GAC TCC ATC AAC GAA ACT GTC AAT GAG ACT CAG GCC GTC
 281 ile tyr val ala gly gly ser asp ser ile asn glu thr val asn glu thr gln ala val

1272 ATC CGT GGA CTC AGC TCC AGT ACC TTG TAC AAC ATC ACA GTG CTT CCT TTC CTG GGT CAG
 301 ile arg gly leu ser ser ser thr leu tyr asn ile thr val leu pro phe leu gly gln

1332 ACC GCG GGT ATA CCA GGC TTC CTC CAA GTG TAC ACT TCC CCC CGT CCT GTT TCT GAC TTC
 321 thr ala gly ile pro gly phe leu gln val tyr thr ser pro arg pro val ser asp phe

1392 CGA GTG ACA AAT GTC AGC CTG AGG GAA ATC GGT TTG GCT TGG AGA AGC AAT GAC TCG GAG
 341 arg val thr asn val ser leu arg glu ile gly leu ala trp arg ser asn asp ser glu

1452 TCA TTC GAG ATT TTC ATC ACG CAG GAG GGA AGT GAG AAA CGT TGG AAT GCT TCG ACG GGA
 361 ser phe glu ile phe ile thr gln glu gly ser glu lys arg trp asn ala ser thr gly

1512 GAC CTG AGC TAT ATC GTT GAA AAT TTA AAG CCT GGG ACC AGT TAC CAA TTT GAA ATA TTC
 381 asp leu ser tyr ile val glu asn leu lys pro gly thr ser tyr gln phe glu ile phe

1572 CCA CGA GGA CCA AAT GGG ACT GAA GGG CCA TCC CAG ACA GTT GTT GGT AGA ACT GAC TGC
 401 pro arg gly pro asn gly thr glu gly pro ser gln thr val val gly arg thr asp cys

1632 AGT GCT GTG ACT GAC ATC CGC GTG GTC AGC GTT AGC ACC ACT GAA ATA CAG CTG GAG TGG
 421 ser ala val thr asp ile arg val val ser val ser thr thr glu ile gln leu glu trp

1692 CAG AAT ACA GAC AGT GCT TCT GGA TAC ACT TAC CAT TTA GTT CTA GAG TCT GAG AAT GGC
 441 gln asn thr asp ser ala ser gly tyr thr tyr his leu val leu glu ser glu asn gly

1752 TCC ATC AAG ACC AAC AGT TCT CAG AAA TGG ATC ACA GTG GGG GGC CTT ACC CCA GGC ACC
 461 ser ile lys thr asn ser ser gln lys trp ile thr val gly gly leu thr pro gly thr

1812 TTA TAC AAT GTT ACA ATC TTT CCA GAA GTG GAC CAG ATG GAG GGC AAC TCC AGC TCT ATT
 481 leu tyr asn val thr ile phe pro glu val asp gln met glu gly asn ser ser ser ile

1872 ACC CAG TAC ACA AGG CCC AGC AAT GTG TCC TAC ATT GAA GTA AAC ACC AAC ACC ACC GTG
 501 thr gln tyr thr arg pro ser asn val ser tyr ile glu val asn thr asn thr thr val

1932 GCA GCC ATC CAG TGG AAG AAC CTG GAC GCA GCC TCT GCT TCC TAC TCC TAC TCC GTT CTT
 521 ala ala ile gln trp lys asn leu asp ala ala ser ala ser tyr ser tyr ser val leu

1992 ATC TTG AAG GCT GGA GAT GGC AGC AAT GTA ACC AGC AGG GTC AGA GAC ATC CCT TCT GTC
 541 ile leu lys ala gly asp gly ser asn val thr ser arg val arg asp ile pro ser val

2052 ACC ATC CCT GGG CTA ATC CCC GGC GTC TCT TAC GAA GTG AAG ATC TTT ACA AAG ATT AGG
 561 thr ile pro gly leu ile pro gly val ser tyr glu val lys ile phe thr lys ile arg

2112 AAT ACA GAG GTT GGG AAT GAG GTA CCT GGT CAG AAG CTG TTC TGT ATG GAA CCT GCA CAA
 581 asn thr glu val gly asn glu val pro gly gln lys leu phe cys met glu pro ala gln

2172 GTG GAT TCC TTA CAC TGT GAA GTG GTC CCG AAG GAG CCA GCG CTG GTT CTG AAG TGG GCC
 601 val asp ser leu his cys glu val val pro lys glu pro ala leu val leu lys trp ala

2232 TGC CCC CCT GGC ATG AAC TCA GGC TTT GAA CTG GGG GTC AGG AGT GAT GCT TGG GAC AAT
 621 cys pro pro gly met asn ser gly phe glu leu gly val arg ser asp ala trp asp asn

2292 ATG ACA CAC TTG GAG AAC TGC ACT TTG GAC AAT GAC ACA GAG TGC AGG ACA GAA GTC ACC
 641 met thr his leu glu asn cys thr leu asp asn asp thr glu cys arg thr glu val thr

2352 TAT TTG AAT TTT TCT ACC TCG TAC AAC ATC AGC ATT GCC ACC TTG TCA TGT GGA AAG ATG
 661 tyr leu asn phe ser thr ser tyr asn ile ser ile ala thr leu ser cys gly lys met

2412 GCA TTG CCC ACC CAG AGC ACC TGC ACC ACT GGC ATC ACA GAC CCA CCT CCT CCA GAT GGA
 681 ala leu pro thr gln ser thr cys thr thr gly ile thr asp pro pro pro pro asp gly

2472 TCC CCT AAT ATT ACA TCG GTC AGT CAC AAT TCA GTA AAG GTG AAG TTC AGT GGT TTT GAA
 701 ser pro asn ile thr ser val ser his asn ser val lys val lys phe ser gly phe glu

2532 GCC AGC CAT GGA CCT ATC AAA GCC TAT GCT GTC CTT CTC ACC ACA GGG GAA GCT GGC CAA
 721 ala ser his gly pro ile lys ala tyr ala val leu leu thr thr gly glu ala gly gln

2592 CCC TCC ACA GAT GTT TTG AAG TAC ACA TAT GAA GAT TTC AAA AAG GGA GCC TCC GAT ACT
 741 pro ser thr asp val leu lys tyr thr tyr glu asp phe lys lys gly ala ser asp thr

2652 TAT GTG ACA TAC CTC ATA AGG ATA GAA GAG AAG GGA CAG TCT CAG GGC TTG TCT GAA GCA
 761 tyr val thr tyr leu ile arg ile glu glu lys gly gln ser gln gly leu ser glu ala

2712 TTG AAC TAT GAG ATT GAT GTG GGG AAC CAA TCC ACT ACC CTC GGC TAC TAC AAC GGG AGG
 781 leu asn tyr glu ile asp val gly asn gln ser thr thr leu gly tyr tyr asn gly arg

2772 CTA GAG CCT CTG GGC TCC TAC CGG GCT TGC GTT GCT GGC TTT ACC AAT ATT ACC TAC AAC
 801 leu glu pro leu gly ser tyr arg ala cys val ala gly phe thr asn ile thr tyr asn

2832 CTT CAG AAC GAT GGC CTT ATT AAT GGG GAT GAG AGC TAT GTA TCT TTC AGT CCG TAT TCA
 821 leu gln asn asp gly leu ile asn gly asp glu ser tyr val ser phe ser pro tyr ser

2892 GAG GCC GTG TCC TTG CCT CAA GAT CCA GGT GTC ATC TGC GGA GCG GTG TTC GGA TGT ATC
 841 glu ala val ser leu pro gln asp pro gly val ile cys gly ala val phe gly cys ile

2952 TTT GGT GCC CTG GCC ATT GTG GCT GTG GGA GGC TTC ATC TTC TGG AGA AAG AAA AGG AAA
 861 phe gly ala leu ala ile val ala val gly gly phe ile phe trp arg lys lys arg lys

3012 GAT GCC AAG AAT AAT GAA GTG TCC TTT TCT CAA ATT AAA CCT AAA AAA TCC AAG TTA ATC
 881 asp ala lys asn asn glu val ser phe ser gln ile lys pro lys lys ser lys leu ile

3072 CGA GTG GAG AAT TTT GAG GCC TAC TTT AAG AAA CAG CAA GCC GAC TCC AAC TGT GGG TTT
 901 arg val glu asn phe glu ala tyr phe lys lys gln gln ala asp ser asn cys gly phe

3132 GCA GAG GAA TAT GAG GAT CTG AAG CTG ATT GGA ATA AGT TTA CCT AAA TAT GCA GCG GAA
 921 ala glu glu tyr glu asp leu lys leu ile gly ile ser leu pro lys tyr ala ala glu

3192 ATA GCT GAA AAC AGG GGG AAG AAC CGC TAC AAC AAC GTC CTG CCC TAT GAT ATT TCT CGA
 941 ile ala glu asn arg gly lys asn arg tyr asn asn val leu pro tyr asp ile ser arg

3252 GTC AAA CTT TCA GTC CAG ACC CAT TCG ACA GAC GAC TAC ATC AAT GCC AAC TAT ATG CCT
 961 val lys leu ser val gln thr his ser thr asp asp tyr ile asn ala asn tyr met pro

3312 GGC TAC CAT TCC AAG AAA GAT TTC ATT GCC ACA CAA GGA CCT TTA CCC AAC ACT TTG AAA
 981 gly tyr his ser lys lys asp phe ile ala thr gln gly pro leu pro asn thr leu lys

3372 GAT TTT TGG CGT ATG GTT TGG GAG AAA AAC GTA TAT GCC ATT GTT ATG CTG ACC AAA TGT
1001 asp phe trp arg met val trp glu lys asn val tyr ala ile val met leu thr lys cys

3432 GTG GAG CAG GGA AGG ACC AAA TGT GAA GAG TAC TGG CCT TCC AAG CAG GCT CAG GAC TAC
1021 val glu gln gly arg thr lys cys glu glu tyr trp pro ser lys gln ala gln asp tyr

3492 GGG GAC ATA ACT GTG GCA ATG ACA TCA GAA GTT GTT CTT CCG GAA TGG ACC ATC AGA GAT
1041 gly asp ile thr val ala met thr ser glu val val leu pro glu trp thr ile arg asp

3552 TTT GTG GTG AAA AAT ATG CAG AGT AGT GAG AGT CAT CCT CTG CGG CAG TTC CAT TTC ACC
1061 phe val val lys asn met gln ser ser glu ser his pro leu arg gln phe his phe thr

3612 TCC TGG CCT GAC CAT GGT GTT CCT GAC ACC ACC GAC CTG CTC ATC AAC TTT CGG TAC CTG
1081 ser trp pro asp his gly val pro asp thr thr asp leu leu ile asn phe arg tyr leu

3672 GTC CGG GAT TAC ATG AAG CAG ATC CCC CCT GAG TCA CCA ATC CTG GTG CAT TGC AGT GCT
1101 val arg asp tyr met lys gln ile pro pro glu ser pro ile leu val his cys ser ala

3732 GGG GTT GGA AGG ACG GGC ACT TTC ATT GCT ATT GAT CGC CTG ATC TAT CAG ATA GAG AAC
1121 gly val gly arg thr gly thr phe ile ala ile asp arg leu ile tyr gln ile glu asn

3792 GAG AAC ACC GTG GAT GTG TAT GGC ATT GTC TAC GAT CTT CGG ATG CAC AGG CCT CTG ATG
1141 glu asn thr val asp val tyr gly ile val tyr asp leu arg met his arg pro leu met

3852 GAT CAG ACA GAG GAC CAG TAT GTT TTC CTC AAT CAG TGT GTG TTG GAT ATT ATC AGA GCC
1161 asp gln thr glu asp gln tyr val phe leu asn gln cys val leu asp ile ile arg ala

3912 CAG AAA GAC TCA AAA GTT GAC CTC ATC TAT CAG AAC ACA ACC GCA ATG ACA ATC TAT GAA
1181 gln lys asp ser lys val asp leu ile tyr gln asn thr thr ala met thr ile tyr glu

3972 AAC CTC GAG CCA GTG AGC ATG TTT GGA AAG ACT AAT GGT TAC ATC GCC TAG TTC CAA AGC
1201 asn leu glu pro val ser met phe gly lys thr asn gly tyr ile ala  •

4032 AAACCCTTCTGAAGCTAACCAGACCGTCACACCCACAGTGAAGGAGAACGCCCTGACGGGGACATGTTTTATGTGTCTCA
4112 TTTCTCAATTCTTTGTTCTGTTCTGTTAGAACTACTTGGAGGGCATGGGGCTGTGCATGTAAAACATGGCAGATAGGCAG
4192 TTGGGGCTCTCAGGGGCTGTGGGCAGGTGGTGTGTAAATCAGCTGCATTCCTGATTACCAATGGGATGGGTTCGCTTTCT
4272 GTTTTTCTTTCCTTGAGAATTGTGAACCAGGAAAAGTGAGCTATGTTTTTGTTTTCCAAGCAGGTTTGTTCTCCTCTCTT
4352 TCTATTCCTCCCCCTTCTCTCTCTCCCTCCCCTGCCTCTCTCT
```

FIG. 2. Nucleotide sequence (uppercase) and predicted amino acid sequence (lowercase) of r-PTPη. Multiple putative initiation codons were found (single underlining); the ATG at position 372 is presumed to be the translation initiation codon because in this region the homology with H-PTPη is 90%. The putative signal peptide and the transmembrane region are double underlined; the phosphatase domains are single underlined.

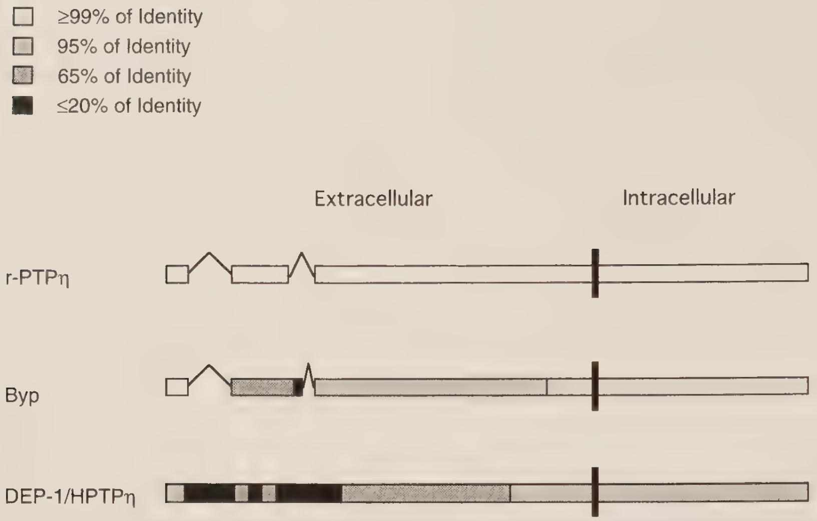

FIG. 3. Comparison of the predicted r-PTPη protein with Byp and HPTPη. Shaded boxes indicate the percentage of amino acid identity between r-PTPη and other RPTPases. Gaps are indicated by the thin lines.

normal and transformed cells at a confluent stage. Figure 5 shows that r-PTPη is expressed in PC Cl 3, FRTL-5 Cl 2, PC c-myc cells, and rat thyroid gland, showing all the parameters of thyroid differentiation (Figs. 5A, lanes 1, 2 and 7, and 5B, lane 2, respectively). A weak expression was observed in PC E1A, PC KiMSV (lanes 3 and 8), and PC HE4 cells (lane 11), which are PC Cl 3 cells transfected with a variant of the adenovirus E1A gene deriving from Adenovirus 2. Conversely, no expression at all was detected in FRTL-5 KiMSV, PC MPSV, PC E1A + v-raf, and PC E1A + v-abl cells, which show a very malignant phenotype that results in the complete loss of any thyroid marker (lanes 6, 9, 10, and 12, respectively). The R-PTPη gene was not expressed in PC v-raf and PC v-abl cells (lanes 4 and 5). The PC v-erbA cells, which are characterized by a reduced ability to trap iodide as the only alteration of the differentiation pattern [38], and PC PyMLV cells, which retain the ability to synthesize thyroglobulin and to trap iodide [36], showed r-PTPη gene expression comparable to that of PC Cl 3 (Table 1). PC HaMSV, PC PTC, FRTL-5 Cl 2 MRSV, FRTL-5 MPSV, and FRTL-5 v-raf, which are negative for thyroid marker expression, did not express the r-PTPη gene (Table 1). Similarly, there was no r-PTPη expression in the FRT-FIBRO cells, fibroblasts of thyroid origin [34], which did not show any marker of thyroid differentiation (Fig. 5B, lane 1). The levels of expression of the r-PTPη gene in rat thyroid tissue were similar to those of the rat thyroid cells PC Cl 3 and FRTL-5 Cl 2 (Fig. 5B, lane 2).

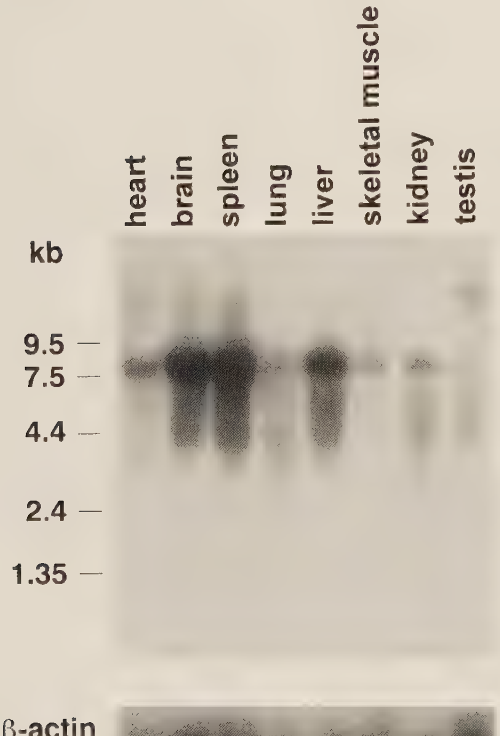

FIG. 4. Expression pattern of the r-PTPη mRNA. Poly(A)$^+$ RNA from rat adult tissues was loaded as indicated. The lanes of the blots contain 2 μg of pure poly(A)$^-$ RNA from specific tissues. β-actin was used as an internal control for uniform RNA loading.

To confirm the loss of r-PTPη gene expression in highly malignant cells, we used RT-PCR associated with two couples of r-PTPη-specific primers to determine r-PTPη expression in the PC E1A + v-raf, PC E1A + v-abl cell lines: no expression of the gene was

TABLE 1

Characteristics of Normal and Transformed Rat Thyroid Cells

Cell lines	Oncogene	TSH dependency	TG expression[a]	Tumorigenicity[b]	R-PTPη expression[c]
PC Cl 3	—	+	+++	−	+++
PC myc	c-myc	+	+++	−	+++
PC v-erbA	v-erbA	+/−	+++	−	+++
PC E1A	Adenovirus 5 E1A	+/−	−	−	+−−[d]
PC HE4	Adenovirus 2 E1A	+/−	−	−	+−−
PC PyMLV	Middle T	+/−	++−[e]	+	++−[f]
PC trk	trk	+/−	+++	−	++−
PC PTC	RET/PTC	+/−	−−−	−	−
PC KiMSV	v-ras-Ki	−	+−−	−	+−−
PC v-abl	v-abl	−	−	−−	−
PC v-raf	v-raf	−	−	−	−
PC E1A + v-raf	Ad5 E1A + v-raf	−	−	+	−
PC E1A + v-abl	Ad5 E1A + v-abl	−	−	+	−
PC MPSV	v-mos	−	−	+	−
FRTL-5 Cl 2	—	+	+++	−	+++
FRTL KiMSV	v-ras Ki	−	−	+	−
FRTL HaMSV	v-ras-Ha	−	−	+	−
FRTL v-raf	v-raf	−	−	−	−
FRTL-MPSV	v-mos	−	−	+	−
FRTL-MRSV	v-src	−	−	+	−
FRT-FIBRO	—	−	−	−	−
FRT-KiMSV	v-ras-Ki	−	−	+	−

[a] Assayed by Northern blot.
[b] Tumorigenicity was assayed by injecting 2×10^6 cells into nude mice.
[c] Assayed by Northern blot.
[d] Less than 20% versus the normal cells.
[e] More than 50% versus the normal cells.
[f] More than 50% versus the normal cells.

detected even with this very sensitive technique (data not shown).

Induction of r-PTPη Gene Expression by TSH in Rat Thyroid Cells

Thyroid stimulating hormone is the thyroid cell growth physiological stimulator and acts through the TSH-receptor, which is specifically expressed in thyroid cells. Therefore, to understand better the role of the r-PTPη gene in thyroid cell physiology, we analyzed its expression after stimulation of the rat thyroid PC Cl 3 cells with TSH. The PC Cl 3 cells were cultured for 5 days in a medium containing only 0.5% calf serum. Subsequently, TSH was added to the medium and the RNA was extracted from the TSH-treated cells at various times (1, 2, 4, 8, 12, 24, and 48 h) and analyzed by Northern blot with a probe covering the 5′-region of the r-PTPη gene. The expression of the r-PTPη gene was negligible in TSH-deprived thyroid cells (Fig. 6). The r-PTPη mRNA level increased as early as 60 min after the addition of TSH to the culture medium, the peak of stimulation occurring at 8 h after TSH addition (lane 5). At 48 h, r-PTPη gene expression was still higher than that observed in TSH-deprived cells.

The Induction of r-PTPη Gene Expression Is Dependent on RNA but Not on Protein Synthesis

To further investigate the molecular mechanism whereby TSH regulates r-PTPη gene expression in thyroid cells, we studied the effects of the RNA polymerase inhibitor 5-6,Dichloro-1β-ribofuranosylbenzimidazole (DRB) at the dose of 25 μg/ml on the induction of r-PTPη exerted by TSH (Fig. 7B). In the presence of DRB, the TSH-induced increase in the level of r-PTPη mRNA was strongly reduced, indicating that TSH stimulation of r-PTPη may occur at the transcriptional level. To further characterize the mechanism for TSH-induced upregulation of r-PTPη, we examined the effects of the protein synthesis inhibitor cycloheximide (CHX) on TSH-dependent r-PTPη expression. In PC Cl 3 cells, the TSH-induced increase in the r-PTPη transcript level was not modified by simultaneous treatment with CHX (Fig. 7A), indicating that protein synthesis is not necessary for TSH regulation of r-PTPη gene expression. These results indicate that *de novo* RNA synthesis is necessary for TSH regulation of the r-PTPη gene; however, expression of the r-PTPη gene in the thyroid cell does not require protein synthesis.

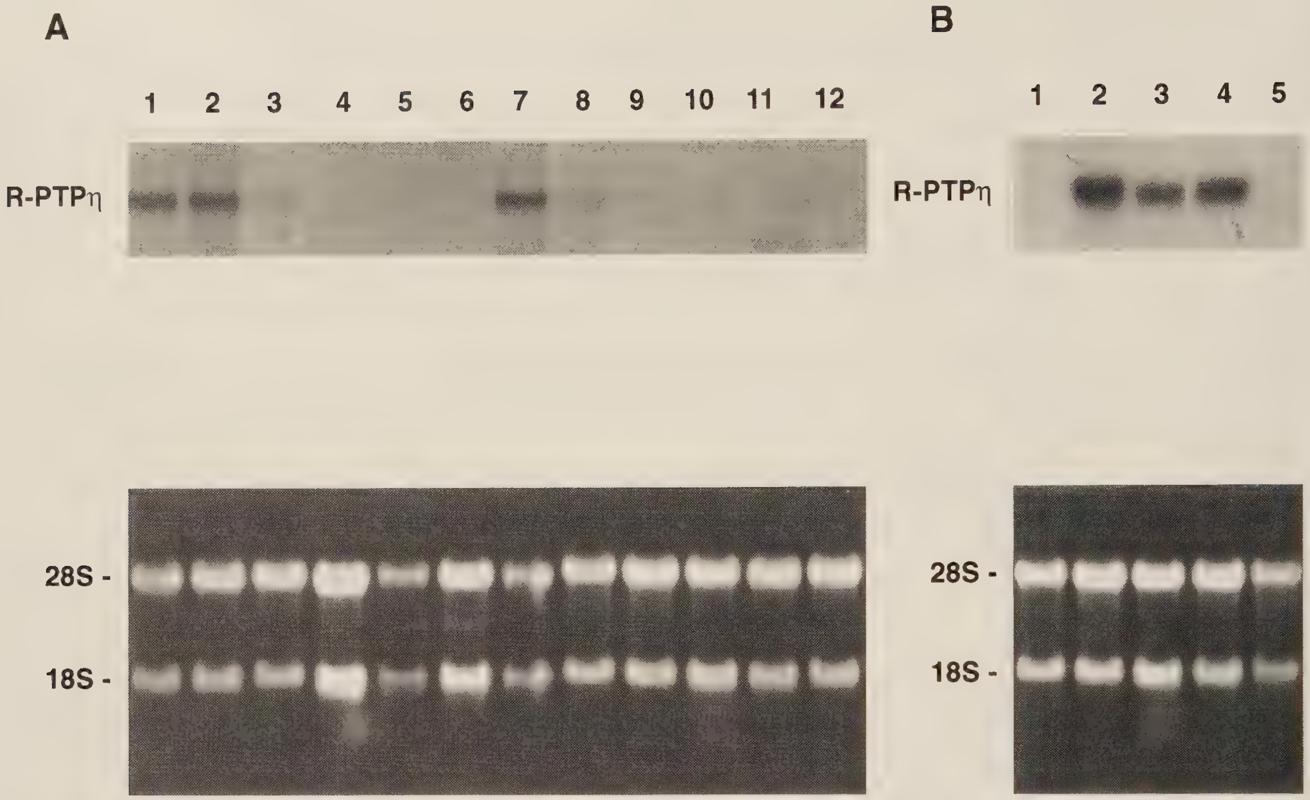

FIG. 5. Expression of the r-PTPη gene in PC Cl 3 cells transformed with several oncogenes. Ten micrograms of total RNA for each cell line was size-fractionated on a 1.2% denaturing formaldehyde–agarose gel, blotted onto hybond-N nylon filters (Amersham), and probed with r-PTPη. Sources of RNA: (A) Lane 1, PC Cl 3 cells; lane 2, FRTL5 Cl 2 cells; lane 3, PC E1A cells; lane 4, PC v-*raf* cells; lane 5, PC v-*abl* cells; lane 6, FRTL5 KiMSV cells; lane 7, PC myc cells; lane 8, PC KiMSV cells; lane 9, PC E1A plus v-*raf* cells; lane 10, PC E1A plus v-*abl* cells; lane 11, PC HE4 cells; lane 12, PC MPSV cells. (B) Lane 1, FRT-FIBRO cells; lane 2, Fischer rat thyroid gland; lane 3, PC Cl 3 cells; lane 4, FRTL-5 Cl 2; lane 5, PC MPSV cells. Ethidium bromide-stained gels are shown in the bottom part.

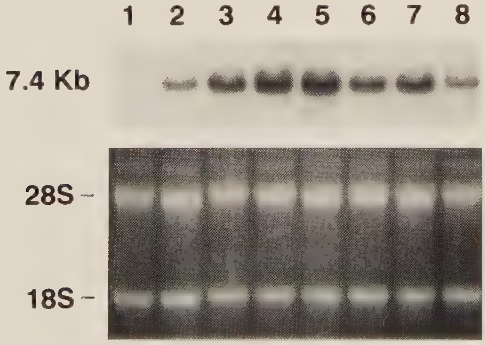

FIG. 6. Time course analysis of TSH regulation of r-PTPη gene expression in PC Cl 3 cells. Ten micrograms of total RNA for each sample was size-fractionated on a 1.2% denaturing formaldehyde–agarose gel, blotted onto hybond-N nylon filters (Amersham), and probed with r-PTPη. The PC Cl 3 cells were deprived of TSH for 5 days, then stimulated with TSH for different lengths of time. The RNAs were extracted from PC Cl 3 cells stimulated with TSH as follows: lane 1, unstimulated PC Cl 3 cells (Time 0); lane 2, 60 min; lane 3, 2 h; lane 4, 4 h; lane 5, 8 h; lane 6, 12 h; lane 7, 24 h, and lane 8, 48 h. An ethidium bromide-stained gel is shown in the bottom part.

DISCUSSION

Here we report the isolation of a novel rat receptor-type tyrosine phosphatase gene that contains a single PTP domain in the cytoplasmic region and eight FN-III domains in the extracellular region. This gene has a strong homology with two other genes coding for tyrosine phosphatase proteins: Byp and DEP-1/HPTPη. The protein sequences of these three genes show a very high homology (more than 90%) in the cytoplasmic and transmembrane regions and in some parts of the extracellular region. The homology is much lower in other parts of the extracellular region, because of some completely divergent amino acid stretches. These divergences could be due to alternative splicings. Moreover, the extracellular domains of some receptor-like proteins vary significantly among species [52]. The HPTPη gene is located in the p11.2 region of human chromosome 11 [40]. This region corresponds to the E1-2 region of mouse chromosome 2, where the Byp gene was located. Taken together, these data strongly suggest that this novel receptor-type tyrosine phosphatase gene is the rat homologue of the human DEP-1/HPTPη

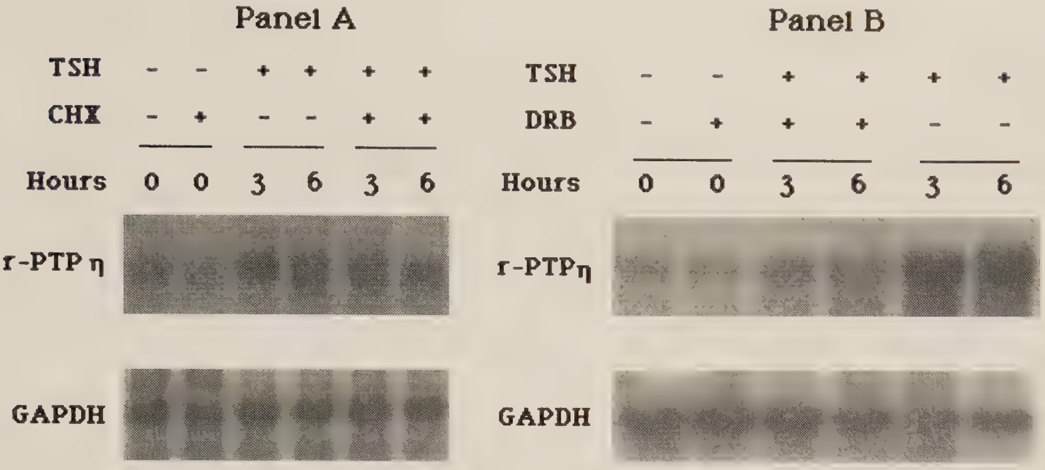

FIG. 7. The TSH r-PTPη gene upregulation induction does not require protein synthesis. (A) The effect of cycloheximide on TSH induction of r-PTP expression in PC Cl 3 cells. PC Cl 3 cells were treated with 10 mU/ml of TSH for 0, 3, and 6 h in the presence or not of cycloheximide (CHX) (5 μg/ml); Sources of RNAs: lane 1, untreated PC Cl 3 cells; lane 2, PC Cl 3 cells treated with CHX; lanes 3 and 4, TSH treatment for the indicated time in the absence of CHX; lanes 5 and 6, TSH treatment for the indicated time in the presence of CHX. (B) The effect of DRB on TSH induction of r-PTP gene expression in PC Cl 3 cells. PC Cl 3 cells were treated with 10 mU/ml of TSH for 3 and 6 h in the presence or not of DRB (25 μg/ml). Total RNA (20 μg/lane) was subjected to Northern blot analysis using the r-PTPη gene probe. Sources of the RNAs: lane 1, untreated PC Cl 3 cells; lane 2, PC Cl 3 cells treated with DRB; lanes 3 and 4, TSH treatment for the indicated time in the presence of DRB; lanes 5 and 6, TSH treatment for the indicated time in the absence of DRB. GAPDH was used as control for uniform RNA loading.

and the mouse Byp gene, and consequently we named it r-PTPη. However, we cannot exclude that these three genes are different members of the same family.

The r-PTPη gene is expressed in many rat and mouse tissues and is very well conserved during evolution. PTPη-related genes are present in *D. melanogaster* and yeast (data not shown), implying that its expression may be involved in the function of many normal organs.

Interestingly, we found that the r-PTPη gene is downregulated during the process of thyroid cell transformation induced by several viral oncogenes. Indeed, in several transformed thyroid cell lines, r-PTPη gene expression was correlated with the expression of thyroid differentiation markers. In fact, transformed thyroid cell lines fell into three groups: (1) completely dedifferentiated cells with reduced r-PTPη expression; (2) partially differentiated cells with low levels of r-PTPη-specific mRNA; and (3) cells that retain most of the thyroid markers and that maintain a level of r-PTPη gene expression comparable to the wild-type thyroid cells. Interestingly, a tyrosine phosphatase activity modulated by somatostatin and associated with an antiproliferative effect, present in PC Cl 3, was abolished in the PC E1A and PC E1A PyMLV cells [39].

r-PTPη gene expression is induced by TSH, which is itself a differentiating stimulus because it induces the appearance of thyroglobulin and thyroperoxidase genes. It is noteworthy that while in other systems the induction of PTPase activity by hormones such as the luteinizing hormone-releasing hormone and dopamine correlates with growth arrest [54, 55], in the case of thyroid cells the induction of r-PTPη by TSH is associated with a cell proliferation stimulus. Therefore, r-PTPη may plausibly play a role in the differentiation of rat thyroid cells. The induction of DEP1/HPTPη gene expression in HL60 [53] and in neuroblastoma cell lines (Battaglia *et al.,* manuscript in preparation) induced to differentiate by DMSO and retinoic acid, respectively, confirm the association of this gene with the differentiated phenotype in other cell systems.

We thank Dr. David Dankort of McMaster University, Hamilton, Canada for his suggestions regarding the PCR degenerate primers. We are grateful to Jean Gilder for editing the text. This work was supported by grants from AIRC (Progetto Speciale Oncosoppressori), Progetto Finalizzato "ACRO," and the Progetto Finalizzato "Biotecnologie e Biostrumentazione" of the CNR. M. L. Martelli and F. Trapasso were recipients of a fellowship from the Associazione Italiana Ricerche Oncologiche.

REFERENCES

1. Ullrich, A., and Schlessinger, J. (1990) *Cell* **61,** 203–212.
2. Cantley, L. C., Auger, K. R., Carpenter, C., Duckworth, B., Graziani, A., Capeller, R., and Soltoff, L. (1991) *Cell* **64,** 281–302.
3. Hunter, T. (1991) *Cell* **64,** 249–270.
4. Collet, M. S., and Erikson, R. L. (1978) *Proc. Natl. Acad. Sci. USA* **75,** 2021–2024.
5. Hunter, T., and Cooper, J. A. (1980) *Proc. Natl. Acad. Sci. USA* **77,** 1311–1315.
6. Witte, O. N., Dusgupta, A., and Baltimore, D. (1980) *Nature* **283,** 826–831.
7. Bishop, J. M. (1991) *Cell* **64,** 235–244.

8. Downward, J., Yarden, Y., Mayes, E., Scrace, G., Totty, N., Stockwell, P., Ullrich, A., Schlessinger, J., and Waterfield, M. (1984) *Nature* **30,** 521–527.
9. Sherr, C. J., Rettenmier, C. W., Sacca, R., Roussel, M. F., Look, A. T., and Stanley, E. R. (1985) *Cell* **41,** 665–676.
10. Yarden, Y., and Ullrich, A. (1988) *Annu. Rev. Biochem.* **57,** 443–478.
11. Tonks, N. K., Diltz, C. D., and Fisher, E. H. (1988) *J. Biol. Chem.* **263,** 6722–6730.
12. Charbonneau, H., Tonks, N. K., Kumar, S., Diltz, C. D., Harrylick, M., Cool, D. E., Trebs, E. G., Fisher, E. H., and Walsh, K. A. (1989) *Proc. Natl. Acad. Sci. USA* **86,** 5252–5256.
13. Hunter, T. (1989) *Cell* **58,** 1013–1016.
14. Streuli, M., Krueger, N. X., Tsai, A. Y. M., and Saito, H. (1989) *Proc. Natl. Acad. Sci. USA* **86,** 8698–8702.
15. Thomas, M. L. (1989) *Annu. Rev. Immunol.* **7,** 339–369.
16. Krueger, N. X., Streuli, M., and Saito, H. (1990) *EMBO J.* **9,** 3241–3252.
17. Fischer, E. H., Charbonneau, H., and Tonks, N. K. (1991) *Science* **253,** 401–406.
18. Saito, H. (1993) *Semin. Cell Biol.* **4,** 379–387.
19. Mourey, R. J., and Dixon, J. E. (1994) *Curr. Opin. Genet. Dev.* **4,** 31–39.
20. Yang, Q., and Tonks, N. K. (1991) *Proc. Natl. Acad. Sci. USA* **88,** 5949–5953.
21. Gu, M., York, J. D., Warshawsky, I., and Majerus, P. (1991) *Proc. Natl. Acad. Sci. USA* **88,** 5867–5871.
22. Shen, S. H., Bastien, L., Posner, B. I., and Chretien, P. (1991) *Nature* **352,** 736–739.
23. Brady Kalnay, S. M., Flint, A. J., and Tonks, N. K. (1993) *J. Cell Biol.* **122,** 961–972.
24. Jang, Y. P., Wang, H., D'Eustachio, P., Musacchio, J. M., Schlessinger, J., and Sap, J. (1993) *Mol. Cell. Biol.* **13,** 2942–2951.
25. Sap, J., Jiang, Y. P., Friedlander, D., Grumet, M., and Schlessinger, J. (1994) *Mol. Cell. Biol.* **270,** 1–9.
26. Grumet, M. (1991) *Curr. Opin. Neurobiol.* **1,** 370–376.
27. Yang, X., Seow, K. T., Bahri, S. M., Oon, S. H., and Chia, W. (1991) *Cell* **67,** 661–673.
28. Shock, L. P., Bare, D. J., Klinz, S. G., and Maness, P. F. (1995) *Mol. Brain Res.* **28,** 110–116.
29. Krueger, N. X., and Saito, H. (1989) *Proc. Natl. Acad. Sci. USA* **89,** 7417–7421.
30. Peles, E., Nativ, M., Campbell, P. L., Sakurai, T., Martinez, R., Lev, S., Clary, D. O., Schilling, J., Barnea, G., Plowman, G. D., Grumet, M., and Schlessinger, J. (1995) *Cell* **82,** 251–260.
31. Pulido, R., Krueger, N. X., Serra-Pages, C., Saito, H., and Streuli, M. (1995) *J. Biol. Chem.* **270,** 6722–6728.
32. Krueger, N. X., Van Vactor, D., Wan, H. I., Gelbart, W. M., Goodman, C. S., and Saito, H. (1996) *Cell* **84,** 611–622.
33. Desai, C. J., Gindhart, J. G., Jr., Goldstein, L. S. B., and Zinn, K. (1996) *Cell* **84,** 599–609.
34. Fusco, A., Berlingieri, M. T., Portella, G., Di Fiore, P. P., Grieco, M., and Vecchio, G. (1987) *Mol. Cell. Biol.* **7,** 3365–3370.
35. Berlingieri, M. T., Portella, G., Grieco, M., Santoro, M., and Fusco, A. (1988) *Mol. Cell. Biol.* **8,** 226–230.
36. Berlingieri, M. T., Santoro, M., Battaglia, C., Grieco, M., and Fusco, A. (1993) *Oncogene* **8,** 249–255.
37. Santoro, M., Melillo, R. M., Berlingieri, M. T., Grieco, M., Vecchio, G., and Fusco, A. (1993) *Cell Growth Differ.* **4,** 77–84.
38. Trapasso, F., Martelli, M. L., Battaglia, C., Angotti, E., Mele, E., Stella, A., Samarut, J., Avvedimento, V. E., and Fusco, A. (1996) *Oncogene* **12,** 1879–1888.
39. Florio, T., Scorziello, A., Fattore, M., D'Alto, V., Salzano, S., Rossi, G., Berlingieri, M. T., Fusco, A., and Schettini, G. (1996) *J. Biol. Chem.* **271,** 6129–6136.
40. Honda, H., Inazawa, J., Nishida, J., Yazaki, Y., and Hirai, H. (1994) *Blood* **84,** 4186–4194.
41. Ostman, A., Yang, Q., and Tonks, K. (1994) *Proc. Natl. Acad. Sci. USA* **91,** 9680–9684.
42. Chomoczynski, P., and Sacchi, N. (1987) *Anal. Biochem.* **162,** 156–159.
43. Sambrook, J., Fritsch, E. F., and Maniatis, T. (1989) Molecular Cloning: A Laboratory Manual, Cold Spring Harbor Laboratory, Cold Spring Harbor, NY.
44. Innis, M. A., Gelfand, D. H., Sninsky, J. J., and White, T. J. (1990) PCR Protocols. A Guide to Methods and Application, Academic Press, San Diego.
45. Sanger, F., Nicklen, S., and Coulson, A. R. (1977) *Proc. Natl. Acad. Sci. USA* **74,** 5463–5467.
46. Tokunaga, K., Taniguchi, H., Yoda, K., Shimizu, M., and Sakyama, S. (1986) *Nucleic Acids Res.* **14,** 2829–2836.
47. Kozak, M. (1986) *Cell* **44,** 283–292.
48. Kozak, M. (1987) *J. Mol. Biol.* **196,** 947–950.
49. Matozaki, T., Suzuki, T., Uchida, T., Inazawa, J., Ariyama, T., Matsuda, K., Horita, K., Noguchi, H., Mizuno, H., Sakamoto, C., and Kasuga, M. (1994) *J. Biol. Chem.* **269,** 2075–2081.
50. Kuramochi, S., Matsuda, S., Matsuda, Y., Saitoh, T., Ohsugi, M., and Yamamoto, T. (1996) *FEBS Lett.* **378,** 7–14.
51. Tian, S. S., Tsoulfas, P., and Zinn, K. (1991) *Cell* **67,** 675–685.
52. Yamamoto, T., Ikawa, S., Akiyama, T., Semba, K., Nomura, N., Miyajima, N., Saito, T., and Toyoshima, K. (1987) *Nature* **319,** 230–234.
53. Honda, H., Shibuya, M., Chiba, S., Yazaki, Y., and Hirai, H. (1993) *Leukemia* **7,** 742–746.
54. Florio, T., Pan, M. G., Newman, B., Hershberger, R. E., Civelli, O., and Stork, P. J. S. (1992) *J. Biol. Chem.* **267,** 24169–24172.
55. Lee, M. T., Liebow, C., Kamer, A. R., and Schally, A. V. (1991) *Proc. Natl. Acad. Sci. USA* **88,** 1656–1660.

Received January 28, 1997
Revised version received April 28, 1997

EXPERIMENTAL CELL RESEARCH **235,** 71–78 (1997)
ARTICLE NO. EX973658

Molecular Cloning and Characterization of a Novel Mitochondrial Phosphoprotein, MIPP65, from Rat Liver

Michinori Kitagawa,* Hideyuki Mukai,† and Yoshitaka Ono*,‡,[1]

*Graduate School of Science and Technology, †Radioisotope Research Center, and ‡Department of Biology,
Faculty of Science, Kobe University, Kobe, 657, Japan

A novel 65-kDa protein (designated MIPP65), which was phosphorylated by PKN *in vitro* in a manner highly dependent on arachidonic acid, was partially purified from the heat-stable proteins extracted from a 30,000*g* precipitate of rat liver. The cDNA clones were obtained by polymerase chain reaction using oligonucleotides based on partial amino acid sequences. The complete amino acid sequence deduced from the cDNAs contained two homologous regions with the mitochondrial NADH-ubiquinone oxidoreductase 9-kDa subunit precursor at the amino- and carboxyl-termini, whereas the central region was not related to any known proteins and contained a serine cluster. Northern blotting and immunoblotting analyses indicated that MIPP65 was expressed ubiquitously in rat tissues. Immunofluorescence analysis of the endogenous MIPP65 using polyclonal antiserum against MIPP65 showed a predominantly mitochondrial localization in C6 glioma cells. The recombinant MIPP65 expressed in COS7 cells showed a similar pattern of localization to that in C6 glioma cells. On the other hand, deletion of the amino-terminal region of MIPP65 abrogated such localization, indicating that the amino-terminal region contained a mitochondrial-targeting signal. From [^{32}P]orthophosphate-labeled C6 glioma cells, the endogenous MIPP65 could be immunoprecipitated as a phosphoprotein with antiserum against MIPP65. These results suggest that MIPP65 is a novel mitochondrial phosphoprotein that is a candidate substrate for PKN. © 1997 Academic Press

---

INTRODUCTION

Many protein kinases and kinase-catalyzed reactions play major roles in the regulation of a great variety of cellular processes. Several well-studied protein kinases such as protein kinase C (PKC), cAMP-dependent protein kinase (PKA), Ca^{2+}/CaM-dependent protein kinases, casein kinases, MAP kinases, and ligand receptor-associated tyrosine kinases mediate the responses of eukaryotic cells to external stimuli by phosphorylating specific protein substrates [1, 2]. However, there are only limited methods available for identification of the specific protein substrates relevant to these kinases. Recently, the yeast two-hybrid system, a genetic method for detecting protein interactions *in vivo,* has been used to identify protein substrates for several protein kinases [3–5]. We previously reported a serine/threonine protein kinase PKN with a catalytic domain homologous to the PKC family and a regulatory domain with a unique structure [6, 7] and have identified neurofilament proteins as candidate substrates for PKN using the two-hybrid system [8]. In the case of the second messenger-dependent protein kinases, the target substrates for the various kinases have been identified as proteins which can be phosphorylated in an activator-dependent manner [9–12]. PKN is activated by the small GTP-binding protein Rho in a GTP-dependent manner [13–15] and is also activated by several unsaturated fatty acids, such as arachidonic acid, at relatively low concentrations [7, 16], suggesting that these modifiers are *in vivo* modulators of PKN acting as messengers. To identify additional candidate substrates for PKN, we screened for proteins from fractions extracted from rat liver with the extent of phosphorylation by PKN *in vitro* as an indicator. We have partially purified a 65-kDa protein which was effectively phosphorylated by PKN *in vitro* in a manner highly dependent on arachidonic acid. In this report, we will discuss: (i) the cDNA cloning of this protein, designated MIPP65 (65-kDa mitochondrial phosphoprotein); (ii) the expression of MIPP65 in various tissues and cultured cells; (iii) the intracellular localization of MIPP65 in cultured cells; and (iv) the phosphorylation of MIPP65 in the cells.

MATERIALS AND METHODS

Materials. PVDF (polyvinylidene difluoride) membrane (Immobilon) and an ECL (Enhanced Chemiluminescence) immunoblotting

---

[1] To whom correspondence and reprint requests should be addressed. Telephone: (81-78)-803-1245. Fax: (81-78)-803-0322. E-mail: yonodayo@kobe-u.ac.jp.

0014-4827/97 $25.00
Copyright © 1997 by Academic Press
All rights of reproduction in any form reserved.

detection kit were purchased from Millipore and Amersham, respectively. Blue Sepharose, Protein A–Sepharose, and Sephasil C18 SC 2.1/10 were purchased from Pharmacia LKB Biotechnology Inc. MitoTracker Red CMXRos was purchased from Molecular Probes, Inc. Other chemicals were obtained from commercial sources.

Cell lines and cell culture. C6, COS7, NG108-15, and Rat1 cells were grown in Dulbecco's modified Eagle's medium (DMEM) containing 10% fetal calf serum. PC12 cells were grown in DMEM containing 10% fetal calf serum and 5% horse serum. Each cell line was cultured as described [17].

Isolation and peptide sequence of MIPP65 from rat liver. All procedures were carried out at 0–4°C. Rat liver (80 g wet wt) was added to 240 ml of buffer A (50 m*M* Tris–HCl, pH 7.5, 1 m*M* EDTA, 1 m*M* EGTA, 1 m*M* DTT, 1 μg/ml leupeptin, and 1 m*M* PMSF (phenylmethylsulfonyl fluoride)) and homogenized for 5 min with Polytron (KINEMATICA). The resulting crude homogenate was then centrifuged at 30,000*g* for 20 min. The precipitate was rehomogenized with 160 ml of buffer A and centrifuged at 30,000*g* for 20 min. This step was repeated eight times, and the final precipitate was homogenized with 120 ml of buffer A and subjected to heat treatment at 100°C for 15 min. The heated protein solution was kept in ice until the temperature dropped to 4° C and the suspension was then centrifuged at 30,000*g* for 20 min. The supernatant was loaded onto a 1/50 vol of a Blue Sepharose column equilibrated in buffer A. The column was then washed with a 10 column volume of buffer A and eluted with 2 column volumes of buffer A containing 1 *M* NaCl. The eluate was combined with 7/100 vol of 100% (w/v) trichloroacetic acid and 1/100 vol of 1.5% (w/v) sodium deoxycholate, and after standing at 4°C for 10 min, the resultant suspension was centrifuged at 30,000*g* for 20 min. The precipitate was suspended in 160 μl of SDS–polyacrylamide gel electrophoresis (PAGE) buffer and subjected to 8% SDS–PAGE. The 65-kDa polypeptide was cut from the gel and digested with endoproteinase Lys-C as described [18], and the peptides were partially purified by chromatography on a Sephasil C18 SC 2.1/10 reverse-phase column of the SMART system (Pharmacia LKB Biotechnology Inc.) The peptide sequences were determined using a gas-phase protein sequencer with an on-line PTH amino acid analyzer (Applied Biosystems Model 490).

Kinase assays. The phosphorylation of the heat-stable proteins extracted from the 30,000*g* precipitate of rat liver or the 1 *M* NaCl fraction of Blue Sepharose was carried out at 30°C in an assay mixture containing 20 m*M* Tris–HCl at pH 7.5, 8 m*M* $MgCl_2$, 100 μ*M* ATP, 185 kBq of $[\gamma\text{-}^{32}P]ATP$, phosphate acceptors, 20 ng/ml of PKN purified from rat testis [16], and with or without 40 μ*M* arachidonic acid as indicated in each experiment. After incubation for 5 min, the reaction was terminated by the addition of an equal volume of Laemmli's sample buffer and separated on SDS–polyacrylamide gels. The gels were dried under vacuum and the phosphorylation was visualized with an imaging analyzer (Fuji BAS1000).

Isolation and sequencing of cDNA clones for MIPP65. cDNAs for MIPP65 were amplified from rat brain cDNA by PCR using a pair of synthetic oligonucleotides based on the amino acid sequence of the isolated protein. The forward primer, 5′-AA(CT) CAN TT(CT) GGN GA(AG) (CA)GN GC-3′ (where N is A/C/G/T), corresponding to the sequence of NTFGERA (amino acid residues 370–376), and the reverse primer, 5′-GG (CT)TC (CT)TG NGT (AG)TC NCC NGG-3′, corresponding to the sequence of PGDTQEP (amino acid residues 403–409), were used to produce a cDNA of the expected length of 120 bp from rat brain cDNA. The PCR product was directly cloned into the pT7Blue (Novagen) vector and the nucleotide sequence was determined. cDNAs encoding the 5′- or 3′-coding region for MIPP65 were generated by the rapid amplification of cDNA end method (RACE) [19] using a Marathon-Ready cDNA kit from Clontech Laboratories. For the 5′-RACE, a first round of PCR was performed using AP1 primer (supplied with the kit) and an antisense MIPP65-specific primer; 5′ GGCTTCGCCGGCTGGCGCCTGGAACGT (residues 1165–1191). A second round of PCR used AP2 primer (supplied with the kit) and an antisense primer; 5′ TTTCGTCACTTTCTGGACATGCCGCCGA (residues 408–435). For the 3′-RACE, a first round of PCR was performed using AP1 primer and a sense primer; 5′ GGGAGATATTCGAAGACAGTTCCTGTTG (residues 1090–1117). A second round of PCR used AP2 primer and a sense primer; 5′ TTTGGAGAGAGAGCTGGACCACAACTGG (residues 1132–1159). The secondary PCR products were directly cloned into pT7Blue vector and sequenced.

Northern blot analysis. A rat multiple tissue Northern blot of poly(A)$^+$ RNA was purchased from Clontech Laboratories. The membrane was hybridized with a ^{32}P-labeled *Sph*I/*Nar*I-digested 0.8-kb cDNA fragment (nucleotides 381–1178 in Fig. 3) as a probe.

Preparation of antiserum against MIPP65. Antiserum against MIPP65 was obtained by immunizing rabbits with the bacterial synthesized fragment of amino acids 1–140 of rat MIPP65.

Preparation of crude homogenates of rat tissues and various cultured cells. The crude homogenates of rat tissues were prepared as described [16]. The crude homogenates of various cultured cells were prepared by homogenizing the cells in 10 vol of 50 m*M* Tris–HCl at pH 7.5 containing 1 m*M* EDTA, 1 m*M* EGTA, 0.5 m*M* DTT, 10 μg/ml leupeptin, 1 m*M* PMSF, 150 m*M* NaCl, 1% NP-40, with 30 strokes of a Dounce homogenizer. These samples were subjected to SDS–PAGE and immunoblotting.

Immunoblotting. Samples were separated by SDS–PAGE, and the proteins were transferred to a PVDF membrane. The membrane was incubated with antiserum, and the immunoreactive bands were visualized with an Enhanced Chemiluminescence immunoblotting detection kit (Amersham).

Construction of expression plasmids. A vector for the expression of rat MIPP65 in COS7 cells was constructed as follows: The fragment containing the entire coding region for rat MIPP65 was obtained by PCR from a cDNA library of rat brain using the specific primer set for MIPP65. The resulting PCR product was directly cloned into the pT7Blue vector (pT7-MIPP). After the confirmation of the nucleotide sequence of the insert, the 1.4-kb *Nco*I/*Bam*HI-digested fragment was inserted into the *Eco*RI site of pTB701 [20] by addition of *Eco*RI linker (pTB-MIPP). A vector for the expression of amino-terminal-deleted MIPP65 was constructed as follows: The 1.3-kb *Xho*I/*Bam*HI-digested fragment of pT7-MIPP was ligated with *Nco*I linker and digested with *Nco*I. Then, the fragment was blunted and inserted into the blunted *Eco*RI site of pTB701 (pTB-MIPP-ΔN). A vector for the expression of carboxyl-terminal-deleted MIPP65 was constructed by inserting the 0.4-kb *Nco*I/*Sph*I-digested fragment of pT7-MIPP into the *Eco*RI site of pTB701 by addition of *Eco*RI linker (pTB-MIPP-ΔC). These constructs were transfected into COS7 cells (2×10^5 cells/35-mm dish) with 2 μg of each DNA by electroporation.

Immunofluorescence. For immunofluorescence localization of MIPP65, C6 and COS7 cells grown in 35-mm plastic tissue culture dishes were washed twice with phosphate-buffered saline (PBS), fixed for 1 h at 4°C in 4% paraformaldehyde, rinsed with PBS, and then blocked for 1 h in PBS-T (PBS containing 0.05% Triton X-100) containing 5% normal goat serum. After washing with PBS, cells were incubated overnight at 4°C with each antiserum diluted with PBS-T at ~10 μg/ml. Coverslips were rinsed with PBS-T and incubated with fluorescein isothiocyanate (FITC)-conjugated goat anti-rabbit IgG (Medical and Biological Laboratories, Co. Ltd.) for 60 min. Coverslips were rinsed with PBS-T followed by PBS, mounted with glycerol-containing 0.1% 1,4-diazabicyclo(2,2,2)octane (DABCO), and viewed on a Zeiss laser scan microscope. For the staining of mitochondria, the medium was replaced with fresh medium containing 25 n*M* MitoTracker (Molecular Probes, Inc.) prior to the fixation. After 30 min, the cells were washed with PBS and then fixed. Nonspecific fluorescence, determined by incubation without primary antiserum, was negligible.

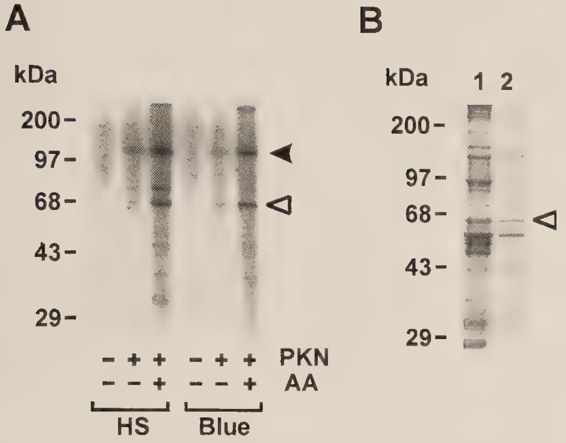

FIG. 1. Phosphorylation of partially purified MIPP65 by PKN. The position of MIPP65 is indicated by a white arrowhead. Molecular mass markers are indicated at left. (A) Autoradiographs of partially purified MIPP65 phosphorylated by PKN. The heat-stable proteins extracted from the 30,000*g* precipitate of rat liver (indicated by HS) and 1 *M* NaCl fraction of Blue Sepharose (indicated by Blue) were incubated with purified rat PKN (indicated by PKN) for 5 min at 30°C with or without 40 μM arachidonic acid (indicated by AA). The position of autophosphorylation of PKN is indicated by a black arrowhead. (B) Coomassie brilliant blue staining of heat-stable proteins extracted from the 30,000*g* precipitate of rat liver (lane 1) and 1 *M* NaCl fraction of Blue Sepharose (lane 2).

Phosphorylation of MIPP65 in vivo. Phosphorylation of MIPP65 *in vivo* was examined using C6 cells incubated in [^{32}P]-orthophosphate. C6 cells were grown in DMEM medium containing 10% fetal calf serum in 100-mm dishes. After reaching ~70% confluence, cells were washed three times with phosphate-free DMEM medium and incubated with 37 MBq carrier-free [^{32}P]orthophosphate in 2 ml of the same medium. After 3 h of incubation, cells were washed three times with PBS and suspended in 500 μl of 20 m*M* Tris–HCl, pH 7.5, containing 1 m*M* EDTA, 1 m*M* EGTA, 150 m*M* NaCl, 1 m*M* DTT, 50 μM sodium vanadate, 5 m*M* NaF, 1 μg/ml leupeptin, and 1 m*M* PMSF. The suspension was subjected to heat treatment at 100°C for 5 min in an Eppendorf tube. The heated solution was kept on ice until the temperature dropped to 4°C and the suspension was then centrifuged at 15,000*g* for 10 min. Then, antiserum (3 μl) raised against MIPP65 was added to the supernatant and rotated at 4°C for 1 h. Protein A–Sepharose (20 μl) was added to the mixture and rotation was continued at 4°C for 30 min. The beads were washed four times with cell lysis buffer and then heated with 20 μl of SDS–PAGE sample buffer at 98°C for 5 min. The supernatant was subjected to SDS–PAGE.

RESULTS AND DISCUSSION

Isolation of Rat Liver MIPP65

To identify potential substrates of PKN, we prepared heat-stable proteins to eliminate the endogenous protein kinase activity. It was previously reported that PKN was abundantly expressed in rat liver [16]. We first utilized rat liver extract as a substrate source, roughly separated by centrifugation at 30,000*g*. The protein band, which was significantly phosphorylated by PKN, was not observed in the heat-stable supernatant, whereas the heat-stable proteins extracted from the precipitate contained several proteins phosphorylated by PKN. As shown in Fig. 1A, a major band with an apparent molecular mass of 65 kDa was effectively phosphorylated in the presence of arachidonic acid. The 65-kDa protein was further separated by Blue Sepharose column chromatography and SDS–PAGE (Fig. 1B). The polypeptide band was excised from SDS–polyacrylamide gels and subjected to *in situ* digestion with endoproteinase Lys-C. The resultant peptides were separated by reverse-phase column chromatography, and their partial amino acid sequences were determined (Fig. 2).

Isolation and Characterization of cDNA Encoding MIPP65

As the peptide sequences of MIPP65 did not correspond to any known protein sequences in the protein sequence databank, cDNA cloning was carried out to deduce the complete protein sequence. First, we prepared a 120-bp cDNA fragment encoding a sequenced peptide from rat brain cDNA. The deduced amino acid sequence of the 120-bp fragment matched the determined sequence of the peptide. To determine the entire

1 S S P P P S S Y P S V E N T G G A V A
2 G P E L E W K
3 N T F G E R A G P Q L E G T F Q A P A G E A P P T D A G P P Q E A P G D T Q E P T L V
4 T E S V F K
5 L L D T H T A A A L S K
6 E S T E L F E A E G I L P G H R K

FIG. 2. Amino acid sequence of peptides derived from the endoproteinase Lys-C treated MIPP65. Protease-treated sample was applied to reverse-phase chromatography and separated peptides were sequenced from the amino-terminus by a gas-phase sequencer.

```
                  20                  40                  60                  80                 100
CGCCCGGGCAGGTGTACCATGGCGGTCTCTCTCCTGCTGCGGGGAGGACGAATCCGGGCGCTGAAGGCTGCCCTTCTCGAGGCAAAGGTGTTCCGAGGAG
                   M  A  V  S  L  L  L  R  G  G  R  I  R  A  L  K  A  A  L  L  E  A  K  V  F  R  G
                 120                 140                 160                 180                 200
AACTGGCTTCTACAGTGCCCCTGTCTACAGAGTCCGAGAATAATAAAAAGGCGGCAGGACCAACTAGCAAGACGGAAAGTGTGTTCAAAGATGTGGTGGG
E  L  A  S  T  V  P  L  S  T  E  S  E  N  N  K  K  A  A  G  P  T  S  K  T  E  S  V  F  K  D  V  V  G
                 220                 240                 260                 280                 300
AGCAGAGGAGAGGGCCAAGCTCCTAGACACTCACACAGCAGCGGCACTGTCCAAAAGCTCCCCTCCACCCAGTTCTTACCCATCAGTGGAGAACACAGGT
  A  E  E  R  A  K  L  L  D  T  H  T  A  A  A  L  S  K  S  S  P  P  P  S  S  Y  P  S  V  E  N  T  G
                 320                 340                 360                 380                 400
GGGGCTGTCGCAGGCCTGCCGCTCACAGACTTGTCAAGAAAGACTTTGGTAGCGTTTCCTCAGAAAGTTACGCCTCCACCGCATGCCTGGGCTTCTGACT
 G  A  V  A  G  L  P  L  T  D  L  S  R  K  T  L  V  A  F  P  Q  K  V  T  P  P  P  H  A  W  A  S  D
                 420                 440                 460                 480                 500
CGGAGGCTCGGCGGCATGTCCAGAAAGTGACGAAAGATTCATCTTCATCTTCCTCATCCAGCTCCTCAGATTCAGACTCTGATGGGGAGGAACATGGCTC
S  E  A  R  R  H  V  Q  K  V  T  K  D  S  S  S  S  S  S  S  S  S  S  D  S  D  S  D  G  E  E  H  G  S
                 520                 540                 560                 580                 600
CGACATTGGTCCCCGAGTGGCAAGCAAAAGCAAGGCAGGGTTTTCCAAACCTGAGGCTTCTCGTCCCTCGAAGAACGGAGCCCCTAAGATCACAGTTTTT
  D  I  G  P  R  V  A  S  K  S  K  A  G  F  S  K  P  E  A  S  R  P  S  K  N  G  A  P  K  I  T  V  F
                 620                 640                 660                 680                 700
GCAAAAGAGAAGGCCAAGGTGCAGAAGCCACACACAGATGTCACCTACCCAGAGAAGCCCCTGCAGCCTAAGAAGAAAGGGACTTTCACCAAGCCTGTAG
 A  K  E  K  A  K  V  Q  K  P  H  T  D  V  T  Y  P  E  K  P  L  Q  P  K  K  K  G  T  F  T  K  P  V
                 720                 740                 760                 780                 800
AAGATAGTAAAGAAATCAGGTCCAAGCTCATGACATCCAAGCCACAGTCCAGTGAGGTTTTGGAGCAAAAAATGAAGGAAAAACAGCACCAGGGAAAACG
E  D  S  K  E  I  R  S  K  L  M  T  S  K  P  Q  S  S  E  V  L  E  Q  K  M  K  E  K  Q  H  Q  G  K  R
                 820                 840                 860                 880                 900
GAGACCAGACAAGACAGGAAAGGAAAGCACAGAGCTGTTTGAAGCTGAAGGAATTTTACCCGGCCACAGGAAAGCCAGAGTTTCCACACAGCCCACAACC
  R  P  D  K  T  G  K  E  S  T  E  L  F  E  A  E  G  I  L  P  G  H  R  K  A  R  V  S  T  Q  P  T  T
                 920                 940                 960                 980                1000
GGAACACAAGAGGCCAGCGCAGAACTCCGGCCAGCCGCTGCCCCCGAGTCGGGAGCTAGACAGGAAGCCAAAGGGCCAGAGCTCGAATGGAAGACCGCTT
 G  T  Q  E  A  S  A  E  L  R  P  A  A  A  P  E  S  G  A  R  Q  E  A  K  G  P  E  L  E  W  K  T  A
                1020                1040                1060                1080                1100
CTCCCCTGGTCAGAAAAGAAAGCCTGGAGAAGCAGGTGCCAGAAGGGAGCTTCCAGGCGGAGGAGGAGACCTCAGGAGATCAGACACTAGGGAGATATTC
S  P  L  V  R  K  E  S  L  E  K  Q  V  P  E  G  S  F  Q  A  E  E  E  T  S  G  D  Q  T  L  G  R  Y  S
                1120                1140                1160                1180                1200
GAAGACAGTTCCTGTTGAGGAGAAAAATACCTTTGGAGAGAGAGCTGGACCACAACTGGAGGGGACGTTCCAGGCGCCAGCCGGCGAAGCCCCGCCCACT
  K  T  V  P  V  E  E  K  N  T  F  G  E  R  A  G  P  Q  L  E  G  T  F  Q  A  P  A  G  E  A  P  P  T
                1220                1240                1260                1280                1300
GATGCAGGCCCACCCCAGGAAGCCCCAGGCGACACACAGGAGCCCACACTGGTTCCCGAGTCGAGTGACACCACCACCTACAAGAACCTGCAGCATCATG
 D  A  G  P  P  Q  E  A  P  G  D  T  Q  E  P  T  L  V  P  E  S  S  D  T  T  T  Y  K  N  L  Q  H  H
                1320                1340                1360                1380                1400
AGTACAACGCATTCACCTTCCTAGACCTGAACCTGGACCTCTCCAAGTTCAGGCTGCCACAGCCGTCTTCGGGACGAGAGTCGCCCCGGCACTGAACTCA
E  Y  N  A  F  T  F  L  D  L  N  L  D  L  S  K  F  R  L  P  Q  P  S  S  G  R  E  S  P  R  H
                1420                1440                1460                1480                1500
ACTCAGGGTAGACCCCCGTGTGGTCCCTTGAATTCTTGCCTGTGAGAATAAAAGTCAGAGGCACAAATAAAAAAAAAAAAAAAAAAAAAAAAAAAAAA
```

FIG. 3. Nucleotide and deduced amino acid sequence of the MIPP65. The deduced amino acid sequence of an open reading frame is given in single-letter code below the nucleotide sequence. Amino acid sequences derived from purified peptides are underlined. The initiation and termination codons are in boldface. The poly(A) addition signal sequence is double-underlined. DDBJ, EMBL, and GenBank Accession No. AB000098.

sequence of MIPP65 cDNA, 5′ and 3′ RACE methods were employed. As shown in Fig. 3, the combined cDNA clone has approximately 1.5 kb, with a 5′ noncoding region of 18 bp, a 3′ noncoding region of 105 bp, and a coding region of 1377 bp, encoding a polypeptide of 458 amino acids. The deduced amino acid sequence of the cDNA contained all of the sequenced peptides. To verify that the cDNA encoded MIPP65 from rat liver, antiserum was raised against the bacterially expressed amino-terminal region of the cDNA. The antiserum specifically reacted with the partially purified rat liver MIPP65 (data not shown). Analysis of the amino acid sequence revealed that the amino- and carboxyl-terminal regions of MIPP65 were highly homologous to the 9-kDa subunit of NADH-ubiquinone oxidoreductase (Complex I) [21]. The amino acid alignment of the homologous regions of MIPP65 with the 9-kDa subunit showed 65% sequence identity and 89% homology (Fig.

```
MIPP    1  MAVSLLLRGGRIRALKAALLEAKVFRGELASTVPLSTESENNKKAAGPTSKTESVFKDVVGAE  63
           **·***** **  ***··**** **** ·*··*·**·**··*·*·  *··*··*  *· *·*
NUO9    1  MAASLLLRQGRAGALKTVLLEAGVFRG-VAPAVSLSAESGKNEKGLPPNPKKQSPPKKPVSAA  62


MIPP  412  VPESSDTTTYKNLQHHEYNAFTFLDLNLDLSKFRLPQPSSGRESPRH  458
            ·*· *·*********·*···*************·************
NUO9   63  PTEPFDNTTYKNLQHHDYSTYTFLDLNLDLSKFRMPQPSSGRESPRH  109
```

FIG. 4. Amino acid sequence comparison of the MIPP65 versus NADH-ubiquinone oxidoreductase 9-kDa subunit precursor. Sequence alignment was done using GENETYX (Software Development Co., Ltd., Tokyo, Japan). The deduced amino acid sequences are shown in one-letter code. The amino acid sequence of the NADH-ubiquinone oxidoreductase 9-kDa subunit precursor is from the report by Skehel *et al.* [21]. The matched residues are connected by asterisks. Conservative substitutions are indicated by dots. A gap introduced to maximize homology is indicated by a dash. MIPP, MIPP65; NUO9, NADH-ubiquinone oxidoreductase 9-kDa subunit precursor.

4). A sequence analysis program (PSORT, GenomeNet WWW server, Japan) predicted that the amino-terminal region of MIPP65 contained a mitochondrial targeting signal. Mitochondrial targeting signal sequences do not show extensive amino acid sequence homology but are rich in basic, hydroxylated, and hydrophobic amino acids [22]. This characteristic feature was observed in the amino-terminal region of MIPP65. Outside the homologous regions (amino acid residues 64–411), the MIPP65 sequence showed no significant similarity to other known proteins. Interestingly, the nonsimilar region contained a serine cluster (residues 141–154) found in several proteins such as Nopp140, a shuttle protein between the nucleus and the cytoplasm [23], or phosvitin, a constituent protein of oocytes of several species [24], although the function of the cluster is still unclear. The predicted molecular weight of the MIPP65 protein encoded by the cDNA was 49,299, which is considerably less than that of the MIPP65 protein partially purified from rat liver. To confirm whether the cDNA contained the entire coding region for the MIPP65 protein, COS7 cells were transfected with an MIPP65 expression vector. As expected, immunoblotting analysis with polyclonal antiserum raised against the bacterially expressed amino-terminal region of MIPP65 showed that the recombinant protein migrated as a 65-kDa band on SDS–PAGE, indicating that the cloned cDNA encoded the full-length MIPP65 protein (Fig. 6B, lane 6). The difference between calculated and observed molecular masses of MIPP65 might be due to

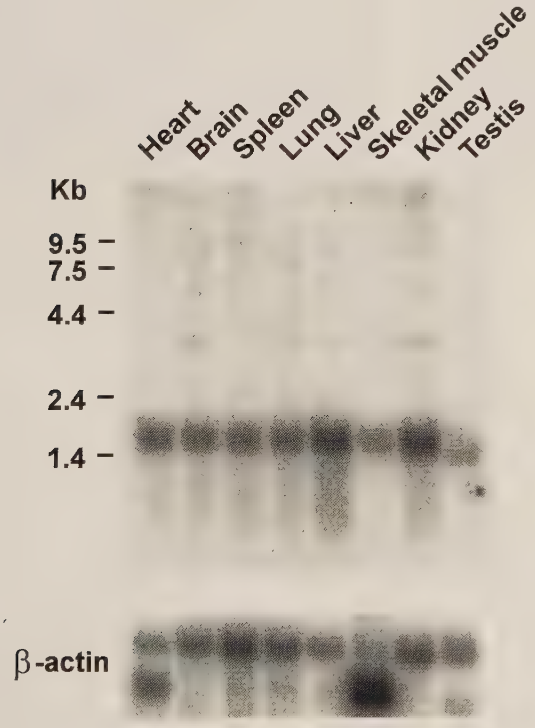

FIG. 5. Northern blot analysis of MIPP65 RNA in rat tissues. β-Actin expression is shown at the bottom as the internal control.

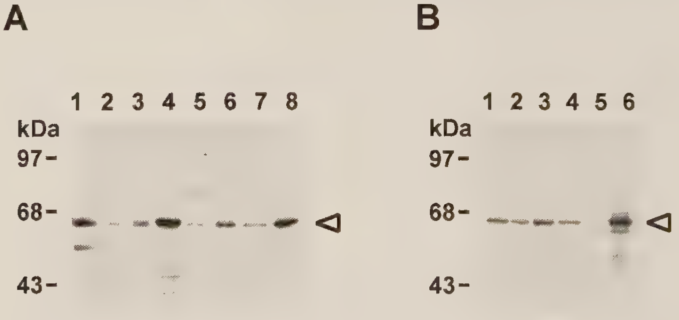

FIG. 6. Immunoblot analysis of MIPP65 in various rat tissues and cultured cells. For each lane, 10 μg of protein of crude lysate was loaded and the proteins were resolved by 10% SDS–PAGE. The position of MIPP65 is indicated by a white arrowhead. Molecular mass markers are indicated at left. (A) Immunoblot analysis of various rat tissues. Lanes: 1, brain; 2, heart; 3, kidney; 4, liver; 5, lung; 6, spleen; 7, testis; 8, thymus. (B) Immunoblot analysis of various cultured cells. Lanes: 1, rat C6 glioma cells; 2, NG108-15 hybridoma cells; 3, rat pheochromocytoma PC12 cells; 4, Rat1 rat embryo fibroblast cells; 5, monkey kidney COS7 cells; 6, COS7 cells transfected with pTB-MIPP.

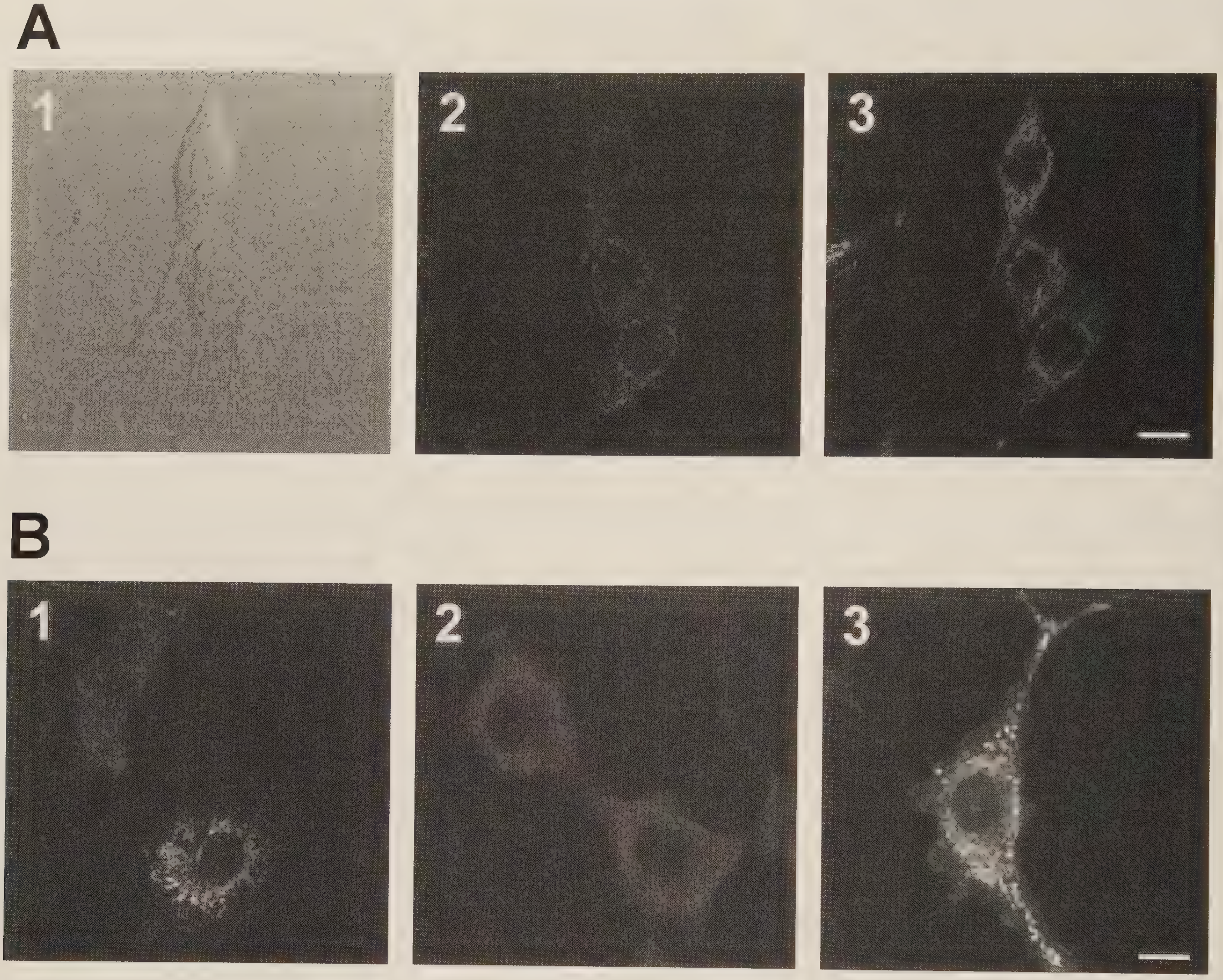

FIG. 7. Immunofluorescence localization of MIPP65 in cultured cells. Bars, 10 μm. (A) Double-labeling with the antiserum against MIPP65 and a mitochondrial fluorescent dye in C6 cells. C6 cells incubated with MitoTracker dye were fixed and incubated sequentially with the antiserum and fluorescein-conjugated goat anti-rabbit IgG and then viewed by phase-contrast microscopy (1) or by fluorescence microscopy with FITC (2), or a rhodamine B isothiocyanate (3) filter. (B) Immunofluorescence localization of various recombinant MIPP65 in COS7 cells. COS7 cells were transiently transfected with pTB-MIPP (1), pTB-MIPP-ΔN (2), or pTB-MIPP-ΔC (3) plasmid DNA, incubated with antiserum against MIPP65, and then viewed by fluorescence microscopy with an FITC filter.

posttranslational modification. Northern blotting analysis using an ~800-bp cDNA probe corresponding to the unique midportion of MIPP65 revealed that ~1.5-kb MIPP65 mRNA was expressed ubiquitously in various rat tissues (Fig. 5); it was abundant in liver and kidney and was expressed at moderate levels in other tissues.

Immunoblotting Analysis of MIPP65

Antisera raised against recombinant amino-terminal or carboxyl-terminal regions of MIPP65 reacted consistently with a major 65-kDa protein in various rat tissues (Fig. 6A). MIPP65 was relatively abundant in brain, liver, and thymus. The antisera also reacted with faint minor bands that varied between tissues and that were possibly due to the nonspecific cross-reaction. Moreover, C6, NG108-15, PC12, and Rat1 cells, which are all derived from rat tissues, showed MIPP65 immunoreactivity as a single band of 65 kDa, suggesting that MIPP65 is ubiquitously expressed in glial, neuronal, and fibroblastic cells (Fig. 6B). COS7 cells, derived from monkey tissues, showed no detectable levels of MIPP65 immunoreactivity, which suggests that the antiserum scarcely cross-reacts with the monkey homolog of MIPP65 or that the native expression of monkey homolog of MIPP65 is low in COS7 cells.

Immunolocalization of MIPP65 in Mammalian Cells

We examined the subcellular localization of the endogenous MIPP65 in C6 cells by using antisera against MIPP65. No detectable immunofluorescence was obtained using nonimmune serum or immune serum preabsorbed with the antigen (data not shown). As shown in Fig. 7A-2, most of the MIPP65 immunofluorescence was associated with structures that appeared to be mitochondria on the basis of their cytoplasmic localization and shape. Double-labeling with antiserum against MIPP65 and a rhodamine-like dye which is specifically imported into mitochondria (MitoTracker) confirmed that a large portion of MIPP65 was associated with mitochondria (Fig. 7A-3). Biochemical subcellular fractionation of rat brain revealed that MIPP65 immunoreactivity was abundant in the P2D fraction, supporting the mitochondrial localization of MIPP65 (data not shown). Moreover, the fluorescence pattern of COS7 cells transfected with the expression vector encoding the full length of MIPP65 (Fig. 7B-1) was similar to that seen in C6 cells. To determine the region of MIPP65 responsible for mitochondrial localization, deletion mutants of the protein were constructed and expressed in COS7 cells. Cells transfected with an expression vector encoding a mutant MIPP65 lacking part of the putative mitochondrial targeting signal (amino acid residues 1–20) showed diffuse staining in the cytosol (Fig. 7B-2). On the other hand, deletion of the carboxyl-terminal region of MIPP65 (lacking amino acid residues 123–458) resulted in a staining pattern similar to that seen with the full-length MIPP65 (Fig. 7B-3). These results suggest that the amino-terminal region of MIPP65 functions as a mitochondrial targeting signal.

Phosphorylation of MIPP65 in Vivo

Phosphorylation of MIPP65 *in vivo* was investigated using C6 cells incubated in [^{32}P]orthophosphate. Labeled cells were lysed and the endogenous MIPP65 was immunoprecipitated from the supernatant with the antiserum. Then, the immunoprecipitant was subjected to SDS–PAGE and autoradiography. As shown in Fig. 8, the major band of radioactivity occurred at a position corresponding to approximately 65 kDa. Some weak bands of radioactivity were present at a high-molecular-weight position and were possibly due to contamination. Further evidence to support the endogenous presence of the MIPP65 as a phosphoprotein was obtained by analysis of the electrophoretic mobility of MIPP65. Dephosphorylation of the partially purified MIPP65 from rat liver resulted in an apparent increase in mobility (~1 kDa) on SDS–PAGE (data not shown). These results suggest that the protein was metabolically phosphorylated as a posttranslational modification in the cells and that some protein kinase was involved in this phosphorylation of MIPP65 *in vivo*. From the results of *in vitro* phosphorylation experiments, PKN is a likely candidate for the protein kinase responsible. However, further investigations at the cellular level are required to confirm the role of MIPP65 in the PKN signaling pathway.

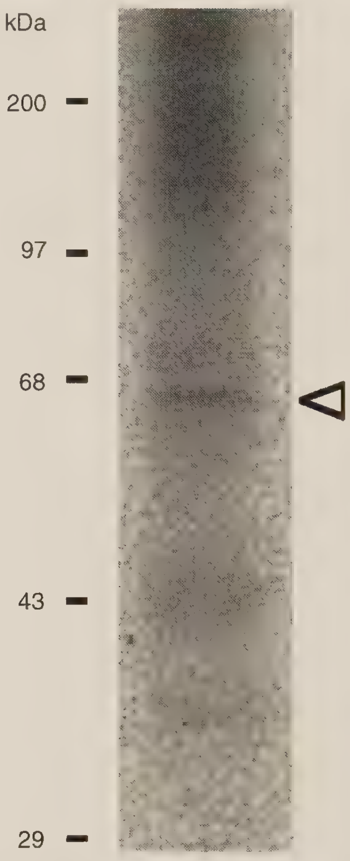

FIG. 8. SDS–PAGE and autoradiography of MIPP65 phosphorylated *in vivo*. C6 cells were incubated for 2 h in [^{32}P]orthophosphate. Proteins were extracted and MIPP65 was immunoprecipitated with antiserum against MIPP65. Molecular mass markers are indicated to the left. The arrowhead indicates the band of radioactivity at a position corresponding to 65 kDa.

The function of MIPP65 is not known at present. Since the N-terminal and the C-terminal regions of MIPP65 were highly similar to the 9-kDa subunit of Complex I, MIPP65 may be a rat isoform of the 9-kDa subunit separated by insertion of an ~340-amino-acid unique sequence. Masui *et al.* indicated by structural analysis that the 9-kDa subunit is a constituent of only the mammalian Complex I [25], the major entry point for electrons into the respiratory chain. However, this

9-kDa subunit does not contain FMN or iron–sulfur centers which are involved in electron transfer between NADH and ferricyanide, and thus the function of this subunit is not yet clear. Consensus phosphorylation sites for casein kinase and PKC were found in the primary sequence of the 9-kDa subunit. However, phosphorylation of this subunit has not yet been reported. In our *in vitro* phosphorylation experiments using various deletion mutants of MIPP65 as substrates, PKN efficiently phosphorylated the unique midportion of MIPP65 (data not shown). MIPP65 thus might be a new subunit of oxidoreductase that was acquired during evolution and that confers regulation via phosphorylation.

We thank Dr. Y. Nishizuka for encouragement. We thank Dr. S. Kuroda for the determination of peptide sequences. This work was supported in part by research grants from the Ministry of Education, Science, Sports, and Culture, Japan, research fellowships of the Japan Society for the Promotion of Science for Young Scientists, "Research for the Future" program, The Japan Society for the promotion of Science, the Senri Life Science Foundation, the Japan Foundation for Applied Enzymology, the Sankyo Foundation of Life Science,and Kirin Brewery Co., Ltd.

REFERENCES

1. Edelman, A. M., Blumenthal, D. K., and Krebs, E. G. (1987) *Annu. Rev. Biochem.* **56,** 567–613.
2. Yarden, Y., and Ullrich, A. (1988) *Annu. Rev. Biochem.* **57,** 443–478.
3. Yang, X., Hubbard, E. J., and Carlson, M. (1992) *Science* **257,** 680–682.
4. Municio, M. M., Lozano, J., Sanchez, P., Moscat, J., and Diaz-Meco, M. T. (1995) *J. Biol. Chem.* **270,** 15884–15891.
5. Colwill, K., Pawson, T., Andrews, B., Prasad, J., Manley, J. L., Bell, J. C., and Duncan, P. I. (1996) *EMBO J.* **15,** 265–275.
6. Mukai, H., Kitagawa, M., Shibata, H., Takanaga, H., Mori, K., Shimakawa, M., Miyahara, M., Hirao, K., and Ono, Y. (1994) *Biochem. Biophys. Res. Commun.* **204,** 348–356.
7. Mukai, H., and Ono, Y. (1994) *Biochem. Biophys. Res. Commun.* **199,** 897–904.
8. Mukai, H., Toshimori, M., Shibata, H., Kitagawa, M., Shimakawa, M., Miyahara, M., Sunakawa, H., and Ono, Y. (1996) *J. Biol. Chem.* **271,** 9816–9822.
9. Stumpo, D. J., Graff, J. M., Albert, K. A., Greengard, P., and Blackshear, P. J. (1989) *Nucleic Acids Res.* **17,** 3987–3988.
10. Kosik, K. S., Orecchio, L. D., Bruns, G. A., Benowitz, L. I., MacDonald, G. P., Cox, D. R., and Neve, R. L. (1988) *Neuron* **1,** 127–132.
11. Doye, V., Soubrier, F., Bauw, G., Boutterin, M. C., Beretta, L., Koppel, J., Vandekerckhove, J., and Sobel, A. (1989) *J. Biol. Chem.* **264,** 12134–12137.
12. Hoeffler, J. P., Meyer, T. E., Yun, Y., Jameson, J. L., and Habener, J. F. (1988) *Science* **242,** 1430–1433.
13. Watanabe, G., Saito, Y., Madaule, P., Ishizaki, T., Morii, N., Mukai, H., Ono, Y., Kakizuka, A., and Narumiya, S. (1996) *Science* **271,** 645–648.
14. Amano, M., Mukai, H., Ono, Y., Chihara, K., Matsui, T., Okawa, K., Iwamatsu, A., and Kaibuchi, K. (1996) *Science* **271,** 648–650.
15. Shibata, H., Mukai, H., Inagaki, Y., Homma, Y., Kimura, K., Kaibuchi, K., Narumiya, S., and Ono, Y. (1996) *FEBS Lett.* **385,** 221–224.
16. Kitagawa, M., Mukai, H., Shibata, H., and Ono, Y. (1995) *Biochem. J.* **310,** 657–664.
17. Mukai, H., Miyahara, M., Sunakawa, H., Shibata, H., Toshimori, M., Kitagawa, M., Shimakawa, M., Takanaga, H., and Ono, Y. (1996) *Proc. Natl. Acad. Sci. USA* **93,** 10195–10199.
18. Matsudaira, P. (1993) A Practical Guide to Protein and Peptide Purification for Microsequencing, Academic Press, San Diego.
19. Borson, N. D., Sato, W. L., and Drewes, L. R. (1992) *PCR Methods Appl.* **2,** 144–148.
20. Ono, Y., Fujii, T., Ogita, K., Kikkawa, U., Igarashi, K., and Nishizuka, Y. (1988) *J. Biol. Chem.* **263,** 6927–6932.
21. Skehel, J. M., Pilkington, S. J., Runswick, M. J., Fearnley, I. M., and Walker, J. E. (1991) *FEBS Lett.* **282,** 135–138.
22. Hurt, E. C., and van Loon, A. P. G. M. (1986) *Trends Biochem. Sci.* **11,** 204–207.
23. Meier, U. T., and Blobel, G. (1992) *Cell* **70,** 127–138.
24. Byrne, B. M., de Jong, H., Fouchier, R. A., Williams, D. L., Gruber, M., and Ab, G. (1989) *Biochemistry* **28,** 2572–2577.
25. Masui, R., Wakabayashi, S., Matsubara, H., and Hatefi, Y. J. Bioche. (1991) *J. Biochem.* **110,** 575–582.

Received February 10, 1997
Revised version received April 28, 1997

EXPERIMENTAL CELL RESEARCH **235,** 79–92 (1997)
ARTICLE NO. EX973617

MHC Class II-Associated Invariant Chain-Induced Enlarged Endosomal Structures: A Morphological Study

Espen Stang and Oddmund Bakke[1]

Department of Biology, Division of Molecular Cell Biology, University of Oslo, Oslo, Norway

The major histocompatibility complex class II-associated invariant chain is believed to direct newly synthesized class II to endocytic compartments. Invariant chain synthesized at high levels in transiently transfected cells induces formation of large vesicular structures. We have examined the effect of stable expression of invariant chain in human fibroblasts by light and electron microscopy. Invariant chain expression dramatically modified endocytic compartments and induced the formation of greatly enlarged structures. These modifications were not lethal. Ultrastructurally, at least three morphologically distinct enlarged compartments could be discerned in the cells. These three compartments may represent early and late endosomes and lysosomes. Internalization of anti-invariant chain antibodies shows that invariant chain may reach the large endosomes via rapid internalization from the plasma membrane. Internalized protein remained in the enlarged vesicles for 4–6 h, indicating an invariant chain-induced delay in the pathway to lysosomes. Although the large invariant chain-induced vesicles have not yet been seen in professional antigen-presenting cells, the invariant chain-induced effects may play a role in regulating the endocytic pathway, creating a special environment for MHC class II to bind antigen. © 1997 Academic Press

INTRODUCTION

The major histocompatibility complex class II molecules are expressed on the cell surface of antigen-presenting cells. The function of class II is to present foreign antigen to T-helper cells. The antigen is generally formed after endocytosis and processing in the antigen-presenting cell. In endosomes processed antigen binds to the class II molecules and together these are transported to the cell surface for presentation (see [1] for review). Class II consists of two nonidentical glycoproteins, the α- and β-chains, which immediately associate with the invariant chain (Ii)[2] after synthesis in the endoplasmic reticulum (ER) [2, 3]. Ii is thought to have at least two important functions in antigen presentation. Association of Ii with class II prevents binding of antigen created in the ER or Golgi [4], and the cytosolic tail of Ii contains signals which direct class II molecules to endosomes [5–8]. In endosomes Ii is degraded and the class II molecules may bind antigen.

There is no consensus as to where the Ii/class II complex is found. Immunocytochemical studies by Pieters *et al.* [9] localized Ii and class II to early endosomes, endosomal carrier vesicles (multivesicular bodies), and late endosomes/prelysosomes, while Peters *et al.* [10] judged the compartments to represent lysosomes or a special class II compartment. How the complex reaches its endosomal/lysosomal destination is also not settled. Some reports suggest that newly synthesized class II molecules reach the endosomes directly from the trans Golgi network [10, 11], whereas we have previously found that a major fraction of both Ii and class II/Ii may be routed to endosomes via the plasma membrane [12, 13].

In transiently transfected cells Ii has been reported to induce the formation of enlarged early endocytic compartments (macrosomes) based on light microscopic analysis [14, 15]. The formation of macrosomes was also found to cause a delay in transport from endosomes to lysosomes [15]. A delayed endosomal transport may play a role in processing and loading of antigen.

To characterize these morphological changes in more detail we have stably transfected Ii alone or Ii together with the class II molecules into human fibroblast cells. Ii expression induces formation of enlarged endocytic compartments which have characteristics of early as well as late endosomes and lysosomes. A major route

---

[1] To whom reprint requests should be addressed at MCB, Biological Institute, University of Oslo, P.O. Box 1050 Blindern, 0316 Oslo, Norway Fax: 47 22854605.

[2] Abbreviations used: BSA, bovine serum albumin; Ii, invariant chain; 3MA, 3 methyl adenine; MHC, major histocompatibility complex; LAMP, lysosome-associated membrane protein; MPR, mannose 6-phosphate receptor; PFA, paraformaldehyde; PAG, protein A-coated colloidal gold.

0014-4827/97 $25.00
Copyright © 1997 by Academic Press
All rights of reproduction in any form reserved.

of Ii to both normal and enlarged endosomes is found to be via the cell surface and internalization.

MATERIALS AND METHODS

Cells

The transfected human fibroblast cell lines (M1DRIi) were a kind gift of Drs. Dave Carp and Eric Long (NIH, Rockville, MD). The generation of these cell lines has been described earlier [7]. In brief, the major form of the human c-DNA Ii (33 kDa) in a vector with CMV transcriptional factors was transfected in the human fibroblast cell line M1 that was already transfected with the HLA-DRA and HLA-DRB cDNAs under the SV40 early promoter. Cells expressing Ii were enriched with magnetic beads coupled with goat anti-mouse Ig (Dynal, Oslo, Norway), after binding the mouse IgM anti-POP.I4.3. A variable fraction of the cells displayed large vesicles after enrichment and a batch where about 30% of the cells contained these structures was used in these studies. After the enrichment, the cells were not maintained in culture for more than 10 passages.

In a few experiments we also used M1 cells transfected with Ii alone (M1Ii).

Antibodies

BU45 (IgG) and BU43 (IgM) (The Binding Site, Birmingham, UK) are monoclonals directed toward the luminal end of Ii. Vic Y1 [16], a monoclonal IgG recognizing the cytosolic tail of Ii, was a gift of Dr. W. Knapp (Vienna, Austria). The polyclonal anti-Ii antibodies HC20 (against the luminal end) and HC12 (against the cytosolic tail) were a gift of Dr. B. Dobberstein (Heidelberg, Germany). Polyclonal rabbit anti HLA-DR [11] was a gift of Dr. J. Neefjes (Amsterdam, the Netherlands). FITC- and Texas red-conjugated secondary antibodies specific for the primary antibodies were obtained from Dianova (Hamburg, Germany) and Southern (Birmingham, AL).

Polyclonal antibodies to the chicken cation-independent mannose 6-phosphate receptor (MPR) were made available by Dr. G. Griffiths (EMBL, Heidelberg) and antibodies against the lysosomal glycoproteins LAMP 1 and LAMP 2 [17] were a gift of Dr. Carlsson (Umeå, Sweden). Transferrin and the transferrin receptor were localized using anti-human transferrin FITC (Becton Dickinson) and anti-transferrin receptor FITC (Serotec).

To detect and enhance the labeling intensity of the thawed cryosections we used rabbit anti-mouse IgM (Nordic Immunology) as secondary antibodies for the BU43.

Light Microscopy

Fixation and immunofluorescence labeling. For light microscopy cells were grown on coverslips until 75% confluence. For fluorescence studies the cells were fixed with either methanol for 5 min at −20°C or for 30 min with 3% paraformaldehyde (PFA) at room temperature using 0.1% Triton X-100 for 10 min to permeabilize the cells as described [5]. The cells were labeled with the appropriate antibodies for 30 min at room temperature and the secondary fluorochrome-tagged antibodies for another 30 min before mounting in Mowiol. The cells were observed in a Nikon microscope equipped with a 20X and a 60X objective with filters for Texas red and FITC. Unfixed cells were observed using the 40X objectives with phase-contrast or Nomarski contrast equipment.

Uptake of endocytic markers. To identify endocytic compartments, the cells were allowed to endocytose FITC- or Texas red-conjugated BSA (1 mg/ml medium) (Molecular Probes, Eugene, OR) for various lengths of time followed by extensive washing. The cells were fixed and labeled as described above immediately or after a chase in normal growth medium. Early endosomes were also identified by endocytosis of holo-transferrin and labeled for transferrin or the transferrin receptor. The transferrin (20 μg/ml) (Sigma) was dissolved in medium and cells were incubated for 60 min before washing in transferrin-free medium. The cells were either fixed immediately or fixed after a 5-min chase and labeled as described above.

Antibody uptake and exposure to leupeptin, chloroquine, and Brefeldin A. To follow internalization of surface Ii, the cells were incubated with BU43 (IgM) for 30 min on ice. After an extensive wash in cold medium the cells were chased in normal prewarmed medium and fixed in PFA and permeabilized as described above. Total Ii was labeled with VicY1 (IgG) and the two antibodies were visualized using specific FITC- and Texas red-conjugated secondary antibodies. As a control the antibodies were reversed; BU45 was internalized and BU43 labeled total antigen and this gave in every case very similar results.

To see if drugs had an effect on the internalization of Ii the cells were preincubated with either 150 μM chloroquine (Sigma) or 0.3 mg/ml leupeptin (Sigma) for 1 to 6 h at 37°C. Following preincubation the cells were incubated for 30 min either on ice or at 37°C with anti-Ii antibodies dissolved in drug-containing medium and then washed and chased in anti-Ii-free, drug-containing medium for 15 min at 37°C, PFA fixed, and labeled as described above. The effect of Brefeldin A on internalization of Ii was studied as described for chloroquine and leupeptin using a concentration of 5 μg/ml Brefeldin A (Epicentre Techn., Madison, WI) and chasing in Brefeldin A-containing medium for 30 to 180 min.

Identification of acidic intracellular compartments. To identify acidic intracellular compartments, cells at 37°C on a coverslip were placed in a miniature incubation chamber mounted on the fluorescence light microscope. Medium containing 5 ng/ml acridine orange (Sigma) was added to the cells and emitted red fluorescence observed in the microscope.

Treatment of cells with autophagy inhibitor. The influence of autophagy on the localization of invariant chain was studied using the autophagy inhibitor 3-methyl adenine (3MA) (Sigma). Cells were starved in Seglens suspension buffer with and without 10 mM 3MA [18, 19] for 4 h before fixation and labeling for Ii. Control cells were grown in normal medium with and without 10 mM 3MA for the same time period.

Electron Microscopy

For conventional transmission electron microscopy endocytic compartments were identified by incubating the cells with BSA-coated colloidal gold (Zymed) [20]. After coating, the gold was pelleted by centrifugation and resuspended in medium at about 15 times the original concentration. The cells were first incubated with 5-nm BSA–gold for 3 h. At end of pulse the cells were extensively washed and reincubated in fresh gold-free medium overnight. The last hour prior to fixation the cells were continuously incubated with 20-nm BSA–gold. The cells were detached by proteinase K (50 μg/ml) (Merck) on ice [21] and pelleted in Eppendorf tubes containing 1 ml cell suspension together with 0.5 ml 2% glutaraldehyde in 0.18 M cacodylate buffer. After the supernatant was removed, 1% glutaraldehyde in 0.18 M cacodylate buffer was added and following an additional centrifugation the pellets were left overnight at 4°C. Postfixation was performed using 2% OsO_4 and 1.5% potassium ferrocyanide in distilled H_2O for 30 min followed by 1.5% uranylacetat in water overnight [22]. The cells were dehydrated in an ethanol series followed by propylene oxide before embedding in Epon and polymerization. Sections were stained using Pb–citrate.

For immunocytochemical labeling cells were detached as described above but fixed in 8% PFA in Soerensen phosphate buffer. Following fixation cells were infused with 2.3 M sucrose, mounted on silver pins, frozen, and stored in liquid N_2 [23]. Endocytic compartments were identified in the same way as described for conven-

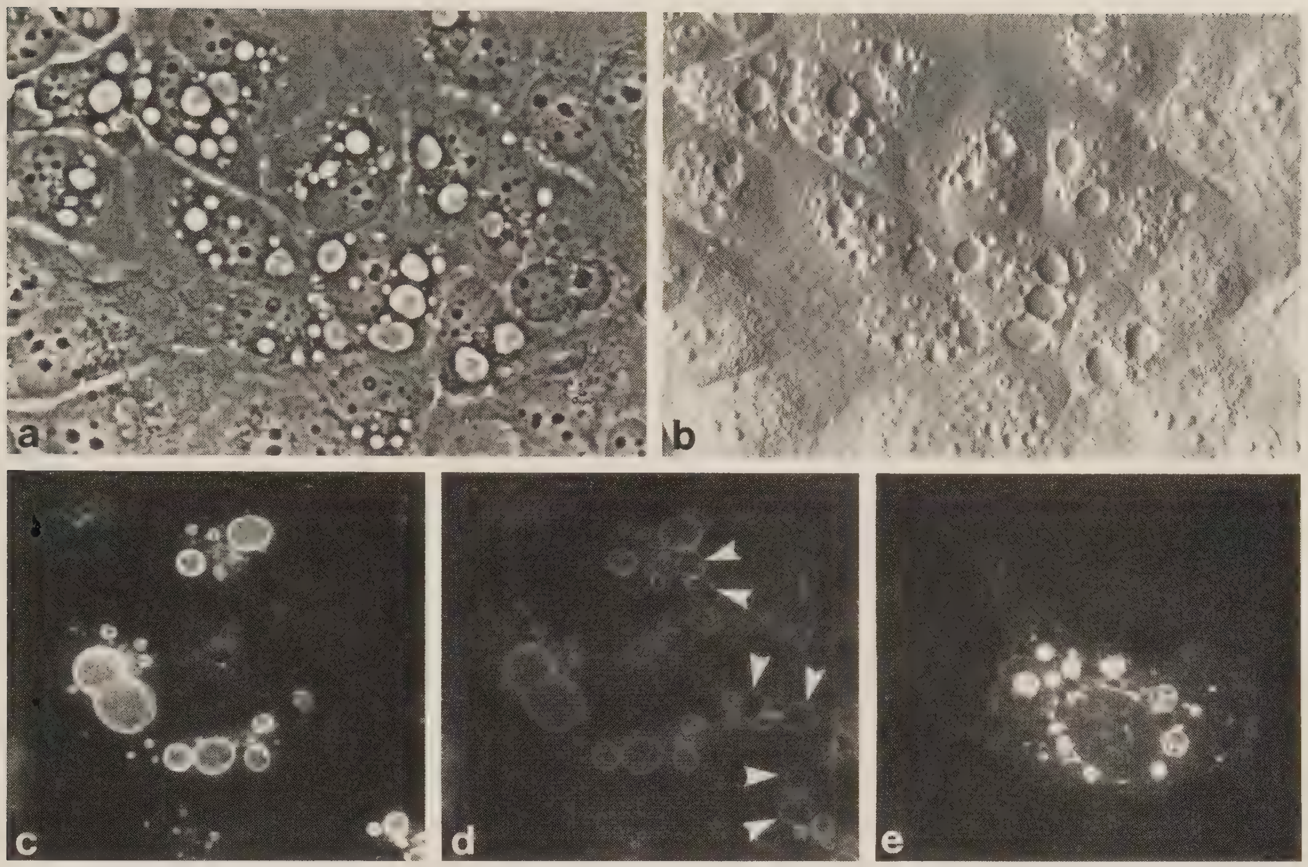

FIG. 1. Visualization of enlarged compartments in Ii-transfected human fibroblasts. (a, b) Micrographs of the same area of living M1DRIi cells viewed in phase (a) and Nomarski contrast (b). (c, d) The same type of transfectants are fixed and labeled for Ii (c) and class II (d); note the existence of some compartments that only label for class II (arrowheads). (e) Similar compartments in a cell transfected with Ii only (M1Ii cell).

tional electron microscopy using BSA–gold of varying size and various length of pulse and chase. Sections were cut at −95°C on a Sorval MT 5000 ultramicrotome using tungsten-coated glass knives [24, 25]. Thawed cryosections were labeled mainly as described by Griffiths *et al.* [23], and double labeling was performed according to Geuze *et al.* [26]. The bound antibodies were visualized using protein A-coated colloidal gold (PAG) of varying size (purchased from J. Slot, Utrecht, Netherlands). The sections were observed in a Jeol 100CX electron microscope.

RESULTS

Light Microscopy

Ii-induced enlarged endosomal compartments in stably transfected M1 cells. The human fibroblast cell line M1 was transfected with Ii together with class II (HLA-DR) as described earlier [7]. As Ii was expressed using the strong CMV promoter and class II using the early SV40 promoter, Ii was produced in excess over class II [7]. In the M1DRIi cells having a high level of Ii expression, phase-contrast and Nomarski contrast microscopy revealed that a large percentage of the cells contained large vacuolar compartments as shown in Figs. 1a and 1b. A large fraction of these compartments label with the BU45 antibody, which is directed toward the luminal end of Ii. Double labeling generally shows colocalization of Ii and class II although some large vesicles are positive for class II and negative for BU45 (Figs. 1c and 1d). In culture, cells with large endosomes divide into daughter cells with the same characteristics. Even though the relative number of cells with large endosomes decreases with time, the phenotype was maintained after months in culture, indicating that large endosomes are not lethal to the cells. Large compartments similar to those found in the Ii class II-transfected cells were also observed in M1 cells transfected with Ii alone (M1Ii) (Fig. 1e). In untransfected M1 cells or cells transfected with class II alone or Ii lacking the 11 first N-terminal amino acids we could not observe the large compartments (data not shown), indicating that the induction of vacuoles is dependent on an Ii with a full-length tail. Expression of a lysosomal glycoprotein (LIMP II) also did not induce large

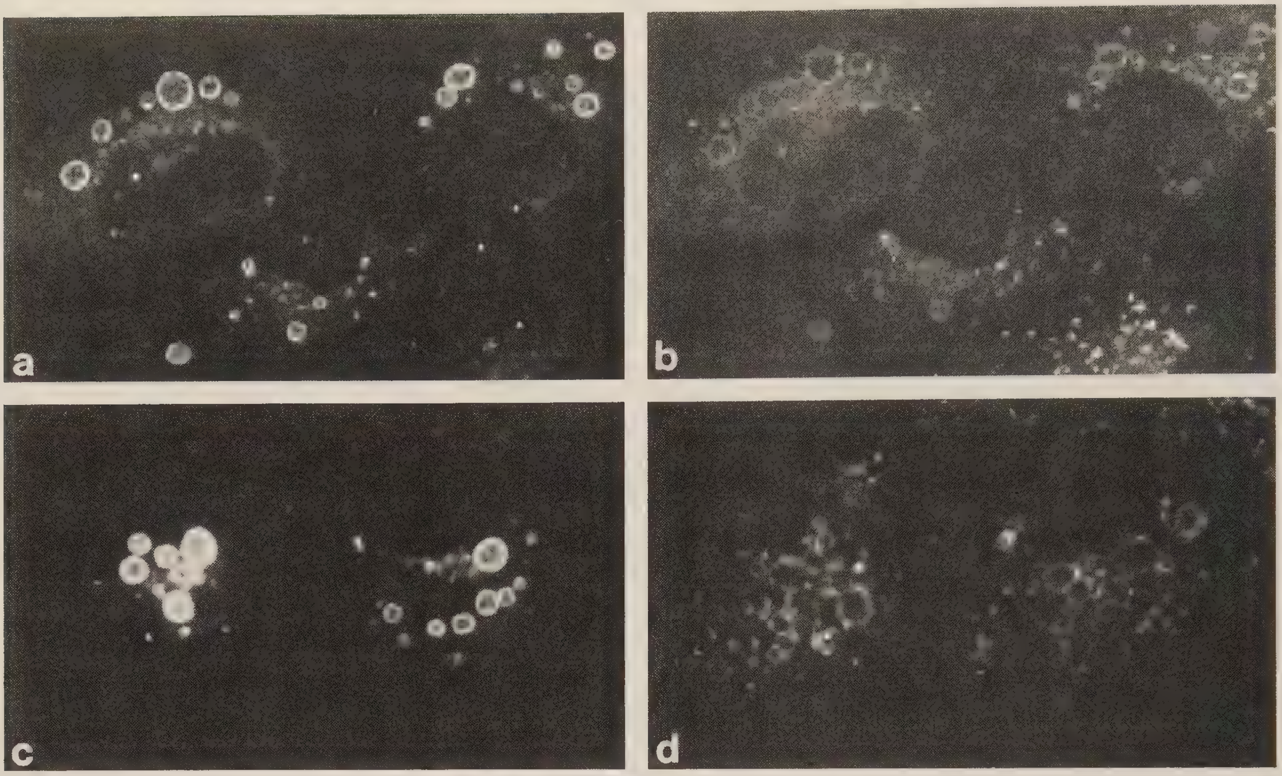

FIG. 2. Double labeling for Ii and proteins associated with endosomal compartments. M1DRIi cells double labeled for Ii (a) and MPR (b) or Ii (c) and LAMP (d). In the vacuolar compartments Ii (BU45) colocalize with MPR but not with LAMP which localize to enlarged BU45 negative compartments.

vesicles (results not shown). This is in line with studies from transient expression systems where the induction of similar large vacuoles depends on Ii with an intact cytosolic tail [14, 15].

Most of the large BU45-positive compartments also label for the cation-independent mannose 6-phosphate receptor (MPR), a protein known to be localized to the endocytic pathway (Figs. 2a and 2b). In addition a few BU45-positive and several BU45-negative large compartments label with antibodies toward the lysosomal membrane protein LAMP 1 (Figs. 2c and 2d). Ii is degraded from the luminal end, and using Vic Y1, an antibody toward the cytosolic tail of Ii, one would expect that the more protease-rich vesicles should also be labeled. Using Vic Y1 as label, the number of vesicles that colocalize with LAMP 1 was in fact increased although several of the large LAMP 1-positive compartments were still Ii negative (data not shown). Labeling the cells with antibodies against MPR and LAMP 2 revealed that the large compartments were of three kinds, (MPR^+ and $LAMP^-$), (MPR^+ and $LAMP^+$), and (MPR^- and $LAMP^+$), strengthening the observation that the large vesicles are not homogeneous.

Both the morphology and the labeling pattern suggest that the enlarged compartments are modified endocytic structures. To identify endosomes we incubated the cells with BSA–FITC as shown in Fig. 3. As soon as after 10 min (5-min pulse, 5-min chase) the endocytic marker was found in Ii-positive large compartments. Most of these compartments also labeled for the MPR, but were LAMP 1 negative. After 40 min (25-min pulse, 15-min chase) BSA–FITC started to appear in the LAMP 1-positive compartments and after longer chase periods most of the BSA-containing compartments were LAMP positive. The endocytosed marker remained in large compartments for up to 5–7 h, whereas the marker disappeared after 1–2 h in cells without the large organelles. This may reflect a low proteolytic activity in the large vesicles and/or a reduced transfer of internalized marker to lysosomes.

The rapid internalization of BSA to enlarged endosomes indicated that at least some of these represent early endosomes. To examine this, the cells were incubated with holotransferrin for 1 h at 37°C and either fixed immediately or fixed after a short chase (5 min). Transferrin is known to be recycled to the cell surface after delivering iron to early endosomes and is therefore used to identify this compartment. Labeling with anti-transferrin or anti-transferrin receptor antibodies showed that most of the large compartments were neg-

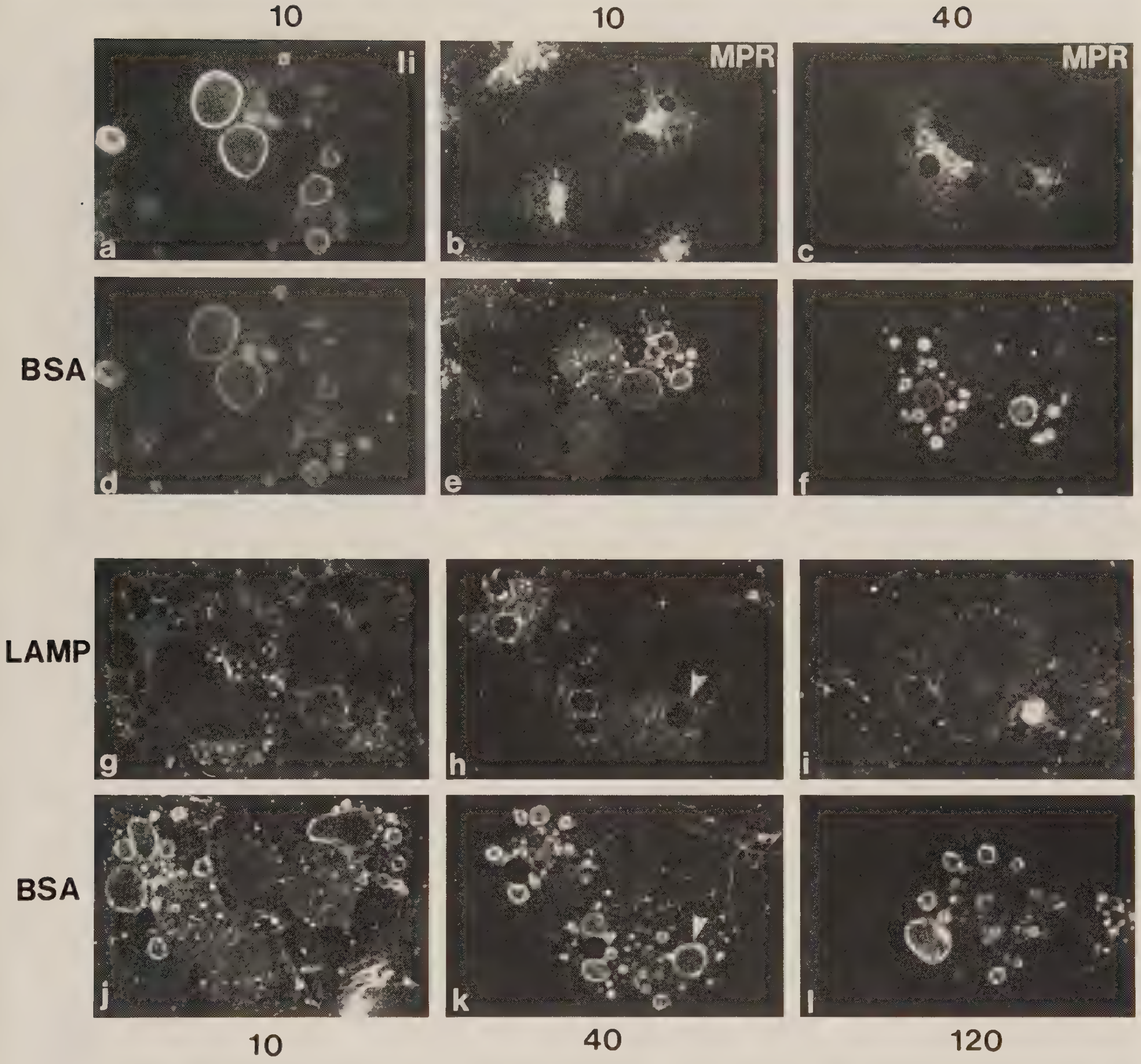

FIG. 3. Localization of endocytosed material to enlarged endosomes with different characteristics. To characterize the endosomal nature of the enlarged compartments BSA–FITC (d–f and j and l) was internalized for various length of time. Total length of incubations (in min) is shown above (a–f) or below (g–l) the corresponding pair of micrographs. Following fixation the cells were labeled for Ii (a), MPR (b, c), or LAMP (g–i). After a short internalization period (5-min pulse, 5-min chase) BSA–FITC (d, e, j) was found in vacuolar compartments. These compartments are clearly positive for Ii (a); they also seem to label for MPR (b) but are negative for LAMP (g). After longer chase periods (15-min pulse, 25-min chase) BSA–FITC (f, k) is found in compartments which are all clearly MPR positive (c) while it has just started to appear in the LAMP positive compartment (h, arrow head). Further incubation (60-min pulse, 60-min chase), however, results in BSA-containing compartments (l) which all are LAMP positive (i).

ative for both markers whereas a few large endosomes were positive as shown in Fig. 4. From this we conclude that only a subpopulation of the large compartments is made up of typical transferrin/transferrin receptor positive early endosomes. In addition Fig. 4 shows a patchy localization of transferrin and the transferrin receptor, indicating that only limited regions of the membrane contain this marker.

Antibodies to invariant chain are rapidly internalized to enlarged endosomes. As we have recently

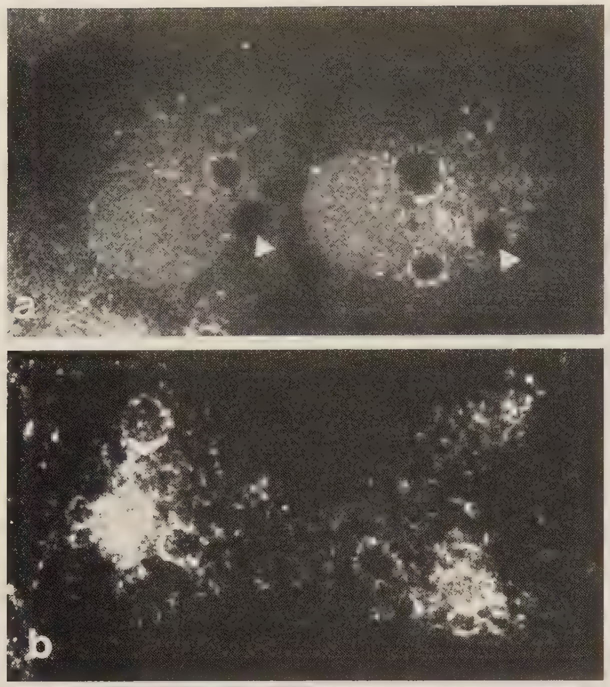

FIG. 4. Internalized transferrin and the transferrin receptor localize in enlarged endosomal compartments. Transferrin internalized by M1DRIi cells (a) appear in some but not all enlarged endosomal compartments. Arrowheads indicate transferrin-negative enlarged compartments. Labeling for the transferrin receptor (b) reveals that this also localizes to enlarged compartments.

shown, both biochemically and by immunofluorescence, an important pathway for transport of Ii to endosomes is via the plasma membrane [13]. For those experiments cells were labeled with BU45 or BU43 on ice and the antibodies were rapidly internalized into small, "normal" sized endosomes at 37°C. Using the M1DRIi cells displaying large endosomes, the anti-Ii antibodies were internalized into these compartments after 5 min at 37°C (Figs. 5c and 5d). Longer chase periods increased the labeling intensity in the enlarged endosomes (Figs. 5e and 5f) and while anti-Ii internalized in small endosomes seems to be almost totally degraded after a 2-h chase [13], the large compartments still show a clear labeling (Figs. 5g and 5h) which was maintained for up to 5–7 h (data not shown). Thus, together with the delayed disappearance of BSA–FITC described above, this further indicates that the degradation process in cells with large vacuoles is retarded compared to the degradation in cells with small endosomes.

Brefeldin A but not chloroquine or leupeptin inhibits Ii from reaching the plasma membrane. Our earlier work with M1 cells transfected with DR and Ii [7, 13] indicated that the Ii/class II complex internalized from the cell surface may represent newly synthesized proteins. To study endosomal processing and transport of Ii from the plasma membrane to large vesicles we applied drugs that are known to affect transport processes. Incubation with Brefeldin A, a drug that affects transport of newly synthesized proteins and retains these in the ER–Golgi regions of the cells, clearly reduced surface staining and internalization of Ii (Figs. 6a–6f). In untreated cells antibodies to Ii were internalized in all Ii-positive cells, whereas after a 30-min preexposure to Brefeldin A the number of cells internalizing anti-Ii was strongly reduced. Prolonged drug exposure increased this effect and after 2 h almost no Ii internalization was observed. Staining for total cellular Ii showed labeling of enlarged endosomes even after 2 h of Brefeldin A but at the same time ER staining had increased. As Brefeldin A inhibits transport of newly synthesized Ii, the staining for Ii in endosomal compartments must be due to a slow turnover of Ii. Drugs that affect processing and possibly recycling of endocytosed material had, however, no effect on internalization of Ii as treatment with leupeptin or chloroquine did not prevent internalization. In cells treated with leupeptin for up to 6 h both "normal" and enlarged endosomes showed labeling for internalized Ii (Fig. 6g). The same was true after treating the cells with chloroquine (Fig. 6h). However, in these cells it was difficult to distinguish the enlarged endosomes from normal endosomes as chloroquine induces a general swelling of endosomal compartments [8]. Since Brefeldin A, which blocks transport of newly synthesized proteins to the plasma membrane but does not block endocytosis [27], prevents internalization of anti-Ii, we conclude that newly synthesized Ii is transported to the enlarged endosomes.

The enlarged endosomes are acidic compartments. Acridine orange added to cells *in vitro* at pH 7.4 has been reported to traverse the plasma membrane and accumulate in the lumen of acidic organelles as a protonated, fluorescent molecule [28]. When acridine orange was added to the M1DRIi cells it quickly accumulated in and gave a red fluorescence to both the en-

FIG. 5. Anti-Ii antibodies are rapidly internalized to enlarged endosomal compartments. M1DRIi cells were incubated with BU43 on ice for 30 min before washing and chasing at 37°C in BU43-free medium for 0 (a), 5 (c), 60 (e), and 120 min (g) prior to fixation with PFA and staining with secondary antibodies. (b, d, f, h) The same cells stained with VicY1 for total Ii. BU43 is seen at the plasma membrane before the chase (a) and after heating to 37°C it rapidly appeared in the enlarged compartments (c). Longer chase periods increased the staining intensity for internalized BU43 and even after 120 min the anti-Ii was not degraded.

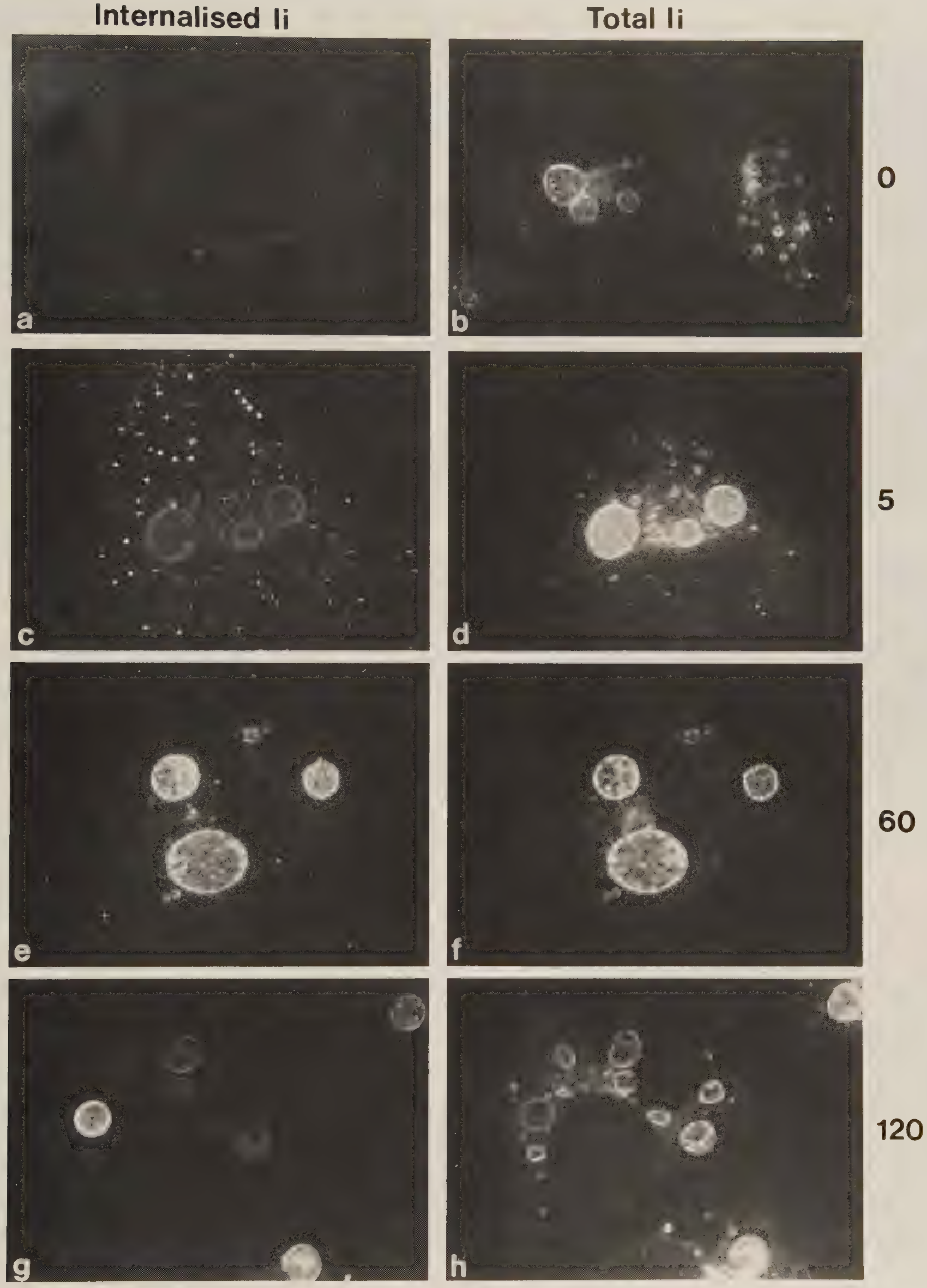
Internalised Ii
Total Ii
a
b
0
c
d
5
e
f
60
g
h
120

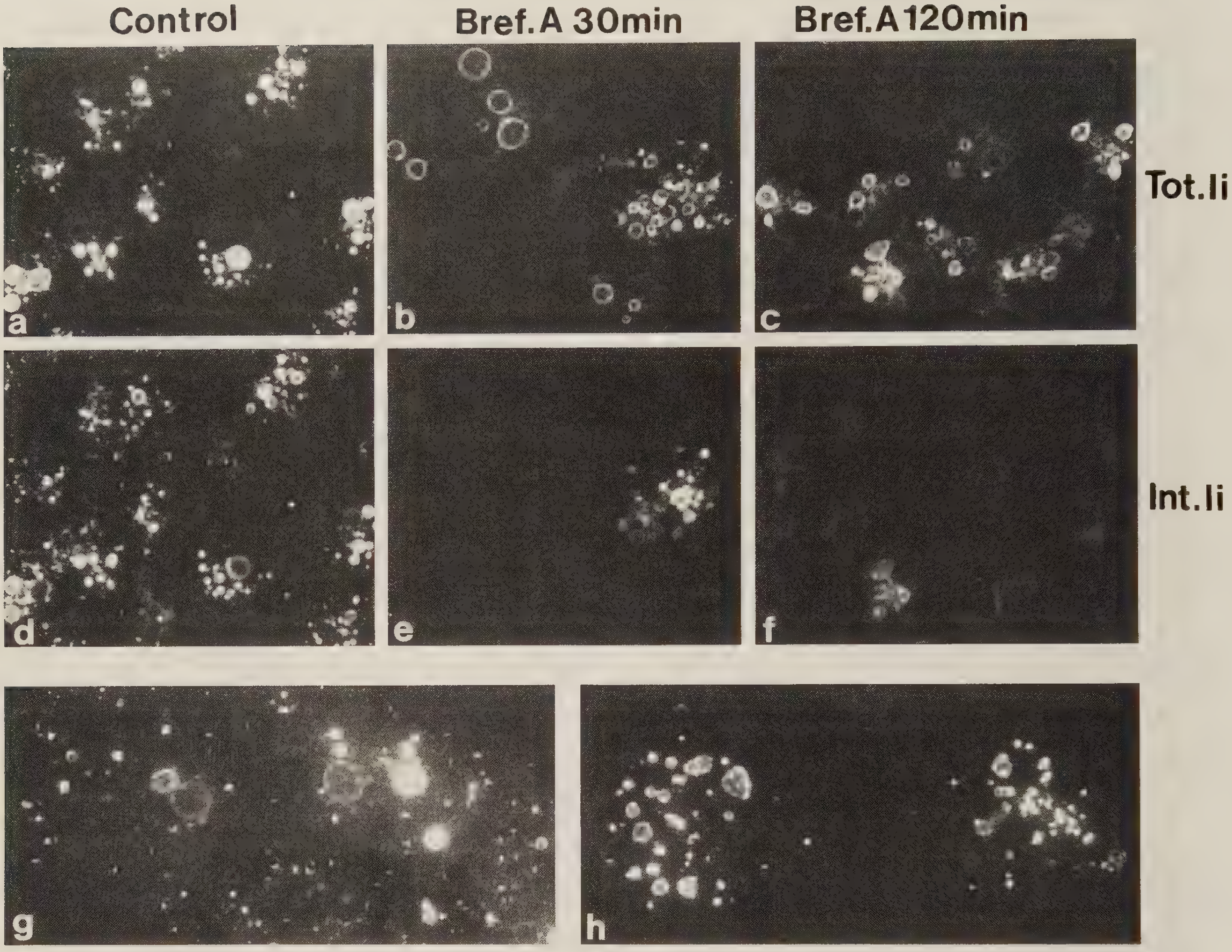

FIG. 6. Effects of drug treatments on internalization of anti-Ii antibodies. In the control all Ii-positive MiDRIi cells (a) internalized BU43 (d). After a 30-min preincubation with Brefeldin A, however, only a few of the cells showed internalization (e) and after 2 h only small amounts of internalized BU43 was observed (f). Labeling for total Ii (a–c) started to show a clear ER pattern with prolonged incubation with the drug (c). Incubation with leupeptin (g) and chloroquine (h) had no effect on internalization of Ii but chloroquine induced a general swelling of endosomal compartments.

larged vesicular compartments and many smaller vesicles (data not shown). The intensity of the fluorescence varied somewhat between the different enlarged compartments, possibly reflecting variable acidic pH.

The autophagy inhibitor 3MA has no effect on enlarged endosomes. Ultrastructurally some of the enlarged endosomes showed similarities to autophagic vacuoles (see Fig. 8) and it has also been suggested that vesicles seen after Ii transfection in fact are of autophagic origin [6]. Autophagy may be inhibited by 3-methyl adenine (3MA) [19]. To determine whether 3MA had any effect on the formation of the large vesicles M1DRIi cells were cultivated in normal medium or under nutritional step-down conditions (medium without serum and amino acids) in the absence or in the presence of the autophagy inhibitor 3MA. Cells grown with 3MA in normal medium, as well as cells starved with or without 3MA, all express the large compartments labeling for Ii, and no treatment influenced expression of Ii in vacuoles or the general morphology of the large compartments (Fig. 7).

Electron Microscopy

Ultrastructural studies reveal three different enlarged endosomal compartments. To investigate the enlarged endosomes at high resolution in the electron microscope, M1DRIi cells which had endocytosed BSA–gold were embedded in conventional resin. Typically, three different large endocytic compartments could be identified. The 20-nm gold endocytosed for 1 h was found in large

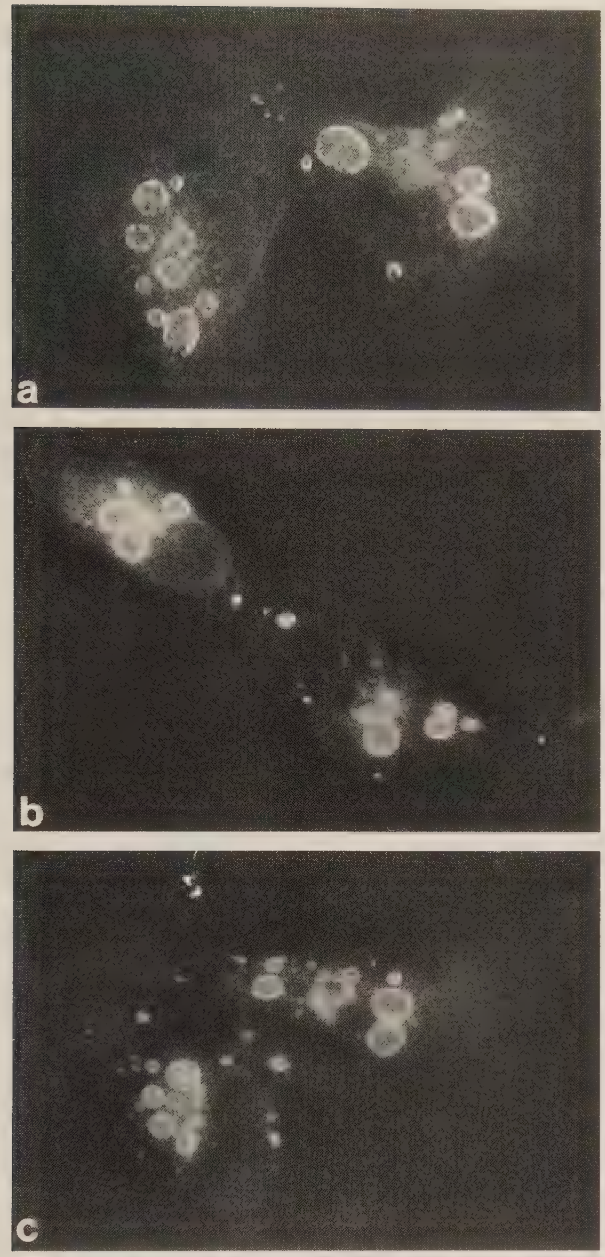

FIG. 7. Starvation or autophagy inhibition has no effect on the enlarged compartments. Labeling for Ii (BU45) shows that starvation (a) or 3MA (b, c) has no effect on the enlarged compartments. M1DRIi cells starved for 4 h (a) did not show any morphological changes or increased expression of the enlarged compartments; neither did cells kept in normal medium containing 3MA (b) or cells starved in the presence of 3MA (c).

seemingly empty vacuoles (Figs. 8a and 8b), while BSA–gold chased overnight was found in two different kinds of large compartments. One of these was filled with membrane structures forming sheets or tubules (Figs. 8c and 8e) while the other was very electron dense (Figs. 8c and 8d). The electron-dense compartment contained, in addition to membrane structures arranged in tubules and sheets, granular electron-dense matter.

The enlarged endosomes contain Ii and class II. As specific molecules cannot be localized in sections of Epon embedded material, immunocytochemical labeling was performed on thawed cryosections. Labeling of the cryosections with anti-Ii antibodies revealed that the large compartments characterized by conventional EM also displayed various labeling characteristics. Both the large empty vacuoles which take up BSA–gold at early time points and the large membrane-filled compartments which contain gold at later time points label for both the luminal and the cytosolic part of Ii (Figs. 9 and 10) as well as for class II (data not shown). The structure of the empty vacuoles was slightly different in cryosections compared to sections prepared for conventional EM (Fig. 8). In Epon sections the compartments seemed surrounded by a single membrane, while in cryosections several membranes were visible with endocytosed gold in the intermembrane space, but not in the seemingly empty lumen. It should be noted that cells expressing enlarged endosomal compartments also contained normal size early endosomes. The large membrane-filled compartments showed labeling for Ii as well as class II, MPR, and LAMP 1 (Fig. 10). The structure of these compartments was often less well preserved in the cryosections and the internal membrane system was often not found or seemed to be dislocated. This is probably a combined effect of the mild fixation used to maintain the antigenicity of the thawed cryosections and the lack of supporting material around the structures. The large electron-dense compartments containing gold chased overnight showed almost no labeling for Ii, class II, and MPR, while they labeled for LAMP 1, indicating that these are of lysosomal origin (Fig. 10). Except for endosomes, no other intracellular compartments showed altered morphology. The Golgi apparatus was normal although this compartment showed high content of Ii (data not shown).

DISCUSSION

When the MHC class II-associated invariant chain is expressed transiently at a relatively high level in CV1 or COS cells, large endosomal structures are induced [14, 15]. The induction of these large vacuolar structures is specific to Ii as Ii with a full-length tail but not a truncated mutant lacking the 11 amino-terminal residues induces these large vacuolar structures [14, 15]. Similarly expression of endosome proteins had no effect. We now show that this phenotype is also independent of the expression system; Ii stably transfected into human M1 cells (this report) or canine MDCK cells (Simonsen and Bakke, unpublished) displayed similar characteristics to previous transient expression experi-

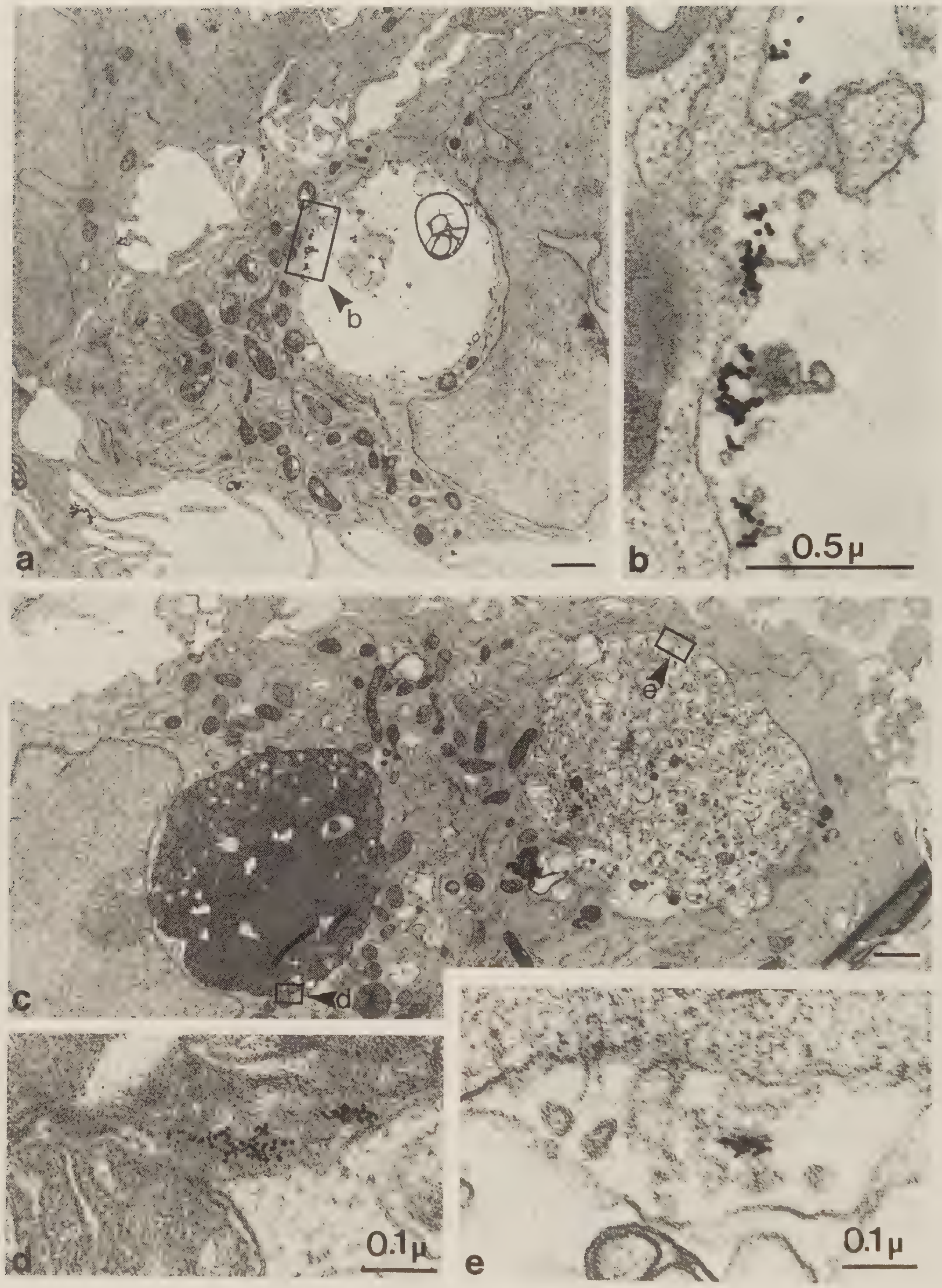

FIG. 8. Three ultrastructurally different enlarged endocytic compartments can be visualized in sections of Epon-embedded M1DRIi cells. Cells were incubated with BSA-gold (5 nm) for 3 h, chased overnight, and further incubated with 20 nm BSA-gold for 1 h before fixation and preparation for conventional EM. (a) A cell with a seemingly almost empty large vacuolar compartment. The endocytic nature of this compartment is shown in b (high magnification of the framed area in a); the compartment contains BSA-gold endocytosed for 1 h. The cell in c contains two ultrastructurally different enlarged endocytic compartments, one filled with membrane structures and the other filled with more dense material. As shown in d and e (higher magnifications of the framed areas in c) both compartments contain endocytosed gold chased overnight. Unless otherwise indicated, bars represent 1 μm.

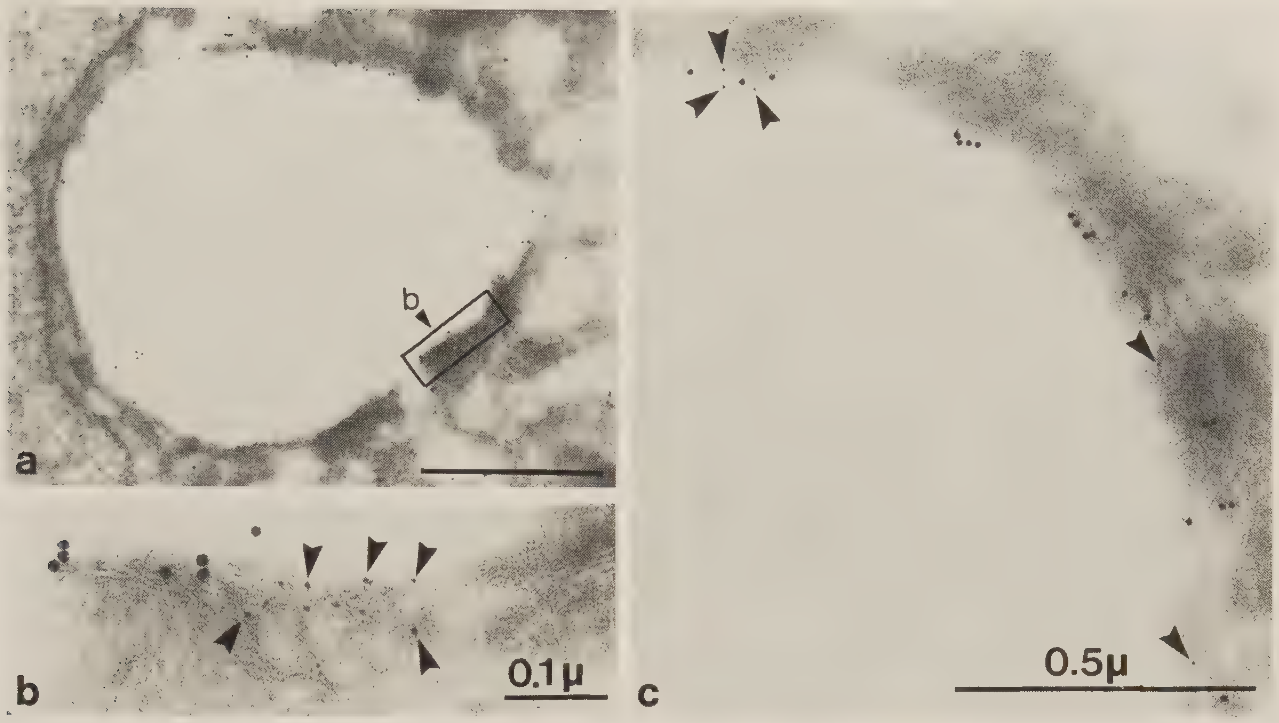

FIG. 9. Immunocytochemical localization of Ii to enlarged endosomes in M1DRIi cells. (a) An overview of an Ii-positive enlarged endosome; the endocytic nature of the compartment is shown in b (enlargement of the framed area in a). The large gold particles show labeling for Ii (BU43) while the small gold particles (arrowheads) are BSA-gold endocytosed by the cell (1-h pulse, 3-h chase). Note that the endocytosed gold is localized to the membrane network surrounding the compartment and not to the seemingly empty lumen. (c) Part of a similar compartment as shown in a double labeled for the C- (small gold particles, arrowheads) and N-terminal ends (large gold particles) of Ii. Unless otherwise indicated, bars represent 1 μm.

ments. The enlarged endocytic compartments are induced by Ii and we find these compartments in cells expressing Ii alone and in cells expressing high levels of Ii together with class II, although in the latter the expression of enlarged endosomes is slightly lower than in cells expressing Ii only at the same level.

For COS cells it was argued that the Ii-induced "macrosomes" are mainly early endosomes [15], while our observations in the M1DRIi cells show that Ii can also induce large vesicles having characteristics of late endosomes/prelysosomes and possibly lysosomes. Our ultrastructural studies show at least three different enlarged compartments and only one of these may be characterized as an early endosome.

The empty compartments contain endocytic markers after short internalization periods and thus represent early endosomes. In the Epon-embedded cells these compartments appear as large vacuoles with endocytosed material in the lumen, while in cryosections at least two membranes seem to surround the compartment and endocytosed gold localizes in the space between these membranes. Such differences in ultrastructural preservation have also been reported for normal early endosomes. In resin-embedded sections they usually appear as vesicles and in cryosections as cisternae enclosing a seemingly empty space with endocytosed material between the cisternal membranes [29]. In cryosections we find that the membranes enclosing these large empty compartments label strongly with antibodies toward both the luminal and the cytosolic domains of Ii. In addition the same membranes label for class II molecules and to some extent MPR. It should be noted that the labeling for MPR gave some unexpected results, the majority of the Ii-positive compartments shows colocalization with MPR while colabeling with LAMP showed that several MPR-positive (+) compartments were LAMP negative (−). This was unexpected since in general MPR is assumed to localize to late LAMP+ endosomes. Geuze *et al.* [30] have, however, described a MPR+ LAMP− intermediate along the endocytic pathway and Ludwig *et al.* [31] found that early endosomes may label for MPR. That most of the large Ii-positive compartments are LAMP negative, however, is in agreement with transient expression studies in CV1 cells (Bakke, unpublished) and COS cells [15].

The membrane-filled endosomes, which label for both Ii and class II as well as MPR and LAMP, represent most likely a late endosomal/prelysosomal compartment. Except for their size these show similarities to normal late endosomes/prelysosomes which often are

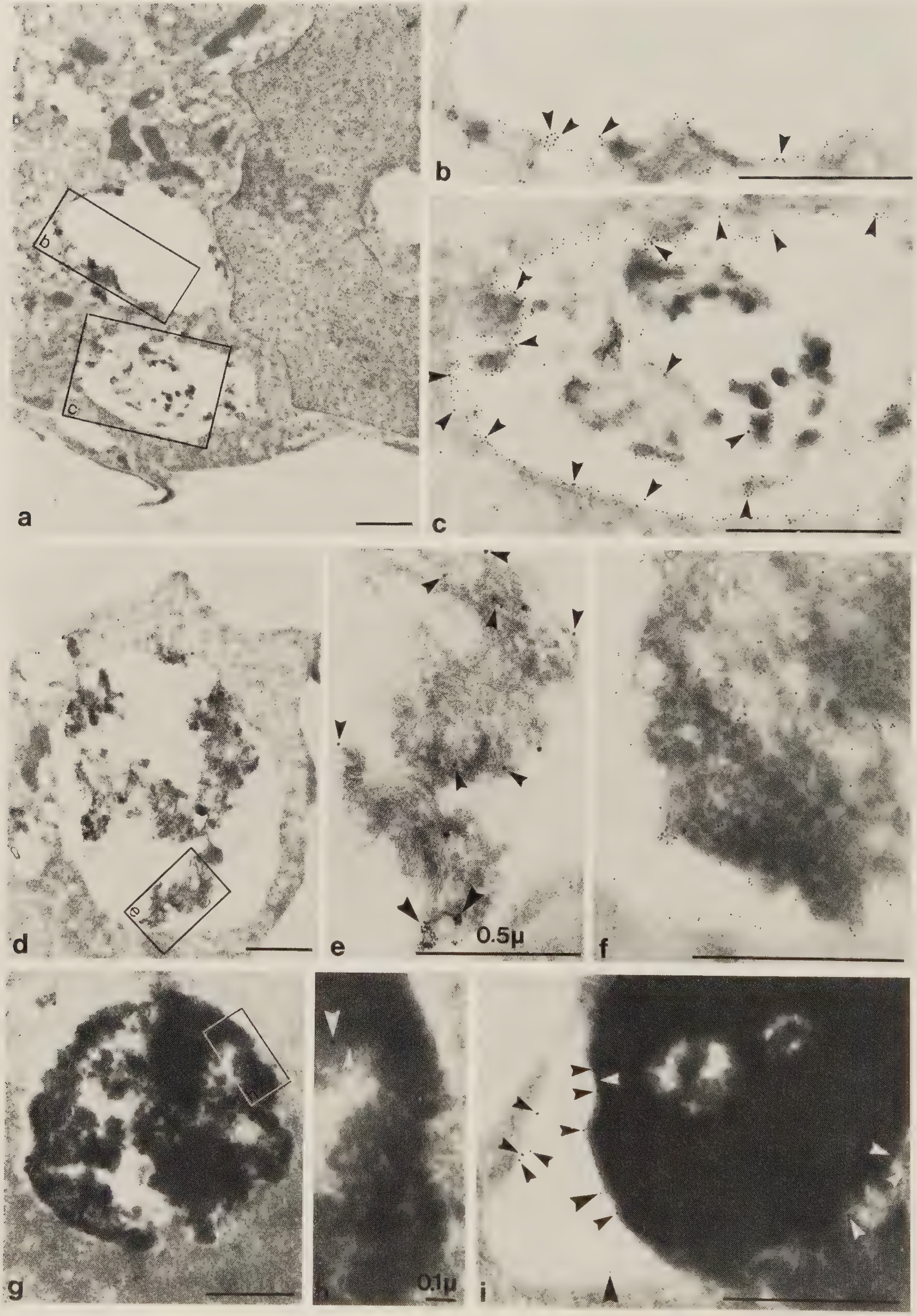
b
c
a
b
c
d
e
e
0.5μ
f
h
g
h
0.1μ
i

found as membrane-filled compartments labeling for MPR and lysosomal glycoproteins [32]. Although the membrane-filled compartments also show many ultrastructural similarities with autophagic compartments, we could not find any evidence for this. Neither 3MA, an inhibitor of the formation of autophagic vacuoles [19], nor starvation, which is known to induce autophagy, altered the frequency or the morphology of the large compartments.

The dense Ii, class II, and MPR negative- but LAMP 1-positive, compartment may represent lysosomes as they show the same labeling pattern and also morphological similarities (except for size) to lysosomes found in other cells. The assumption that the dense enlarged compartments represent lysosomes is further strengthened by the observation that they contain endocytosed gold only after a very long incubation period. The enlarged compartments were also found to be acidic and the variable red fluorescence after addition of acridine orange may reflect differences in pH between the compartments as would be expected if these represent different compartments within the lysosomal pathway.

Routing of the Ii/class II complex to endosomal compartments has been studied extensively, but it is still a matter of discussion. It is known that the cytosolic tail of Ii contains a signal sequence(s) that directs the complex to endocytic compartments [5, 6, 8, 12], but the transport route is not clear. The class II/Ii complex has been reported to be found at various stages of the endosomal/lysosomal pathway (for review see [33]). Our observations are compatible with localization of Ii in both early and late endosomes.

We show that transport of Ii to large endosomes may occur via rapid internalization from the plasma membrane. This is in agreement with sorting of Ii to normal endosomes [13]. Transport of Ii/class II to the cell surface followed by internalization may be advantageous for antigen binding as it ensures that class II is present all along the endocytic pathway.

Loss and Sant [34] reported that drugs such as chloroquine and leupeptin retain class II in intracellular compartments and argue that the Ii/class II complex is transported directly to endosomes and retained there until Ii is degraded. Our results after treating the cells with different drugs strongly suggest that Ii is first present at the plasma membrane before it is internalized to endosomes, a route which is not excluded by the above study. Brefeldin A quickly inhibited internalization of anti-Ii antibodies, suggesting that Ii localized on the cell surface is newly synthesized and not recycled from an endocytic compartment. If newly synthesized Ii first enters endosomes, it would be expected that chloroquine and leupeptin treatment would retain Ii intracellularly and prevent Ii from reaching the plasma membrane. Neither of these treatments, however, had any effect on internalization of anti-Ii antibodies and although we cannot conclude that transport via the plasma membrane is the only way newly synthesized Ii can reach endosomes, our results strongly support such a pathway.

The staining for Ii in enlarged compartments even after a 2-h treatment with Brefeldin A shows that turnover of Ii is slow in these compartments. That a general delay in processing occurs in the enlarged compartments is also supported by other observations. Results from COS cells [15] indicate that transport to lysosomes is delayed in cells expressing the enlarged compartments. Our results show that endocytosed BSA appeared quickly in MPR-positive enlarged endosomes and much later in LAMP-positive enlarged compartments. Endocytosed BSA remained in large compartments for several hours, whereas it disappeared relatively quickly in cells without these structures. Likewise internalized anti-Ii antibodies were very slowly degraded in the large vesicles. In cells expressing normal endosomes internalized anti-Ii was not detected after 120 min [13], whereas in the large endosomes we still found an intense labeling at this time point. One reason for such a delay could be that these large endosomes were not normally acidified. However, experiments with acridine orange clearly showed that these compartments are acidic. The delay can be explained by both the models (maturation and vesicle shuttling) that exist for endocytosis [35, 36]. Due to their large size such endosomes need more time than small endosomes do to exchange their membrane abilities (mature) or transfer their content to other endosomes (vesicle shuttling).

In the M1DRIi cells used in this study, overexpression of Ii leads to large vesicular structures but the cellular mechanisms behind this phenomena are not clear. It

FIG. 10. Immunocytochemical labeling of enlarged late endosomes and lysosomes. (a) An overview of two Ii, MPR-positive enlarged compartments. The labeling is shown in b and c which are high magnifications of the framed areas in a. Both compartments show intense labeling for Ii (small gold particles) and varying labeling intensity for MPR (large gold particles, arrowheads). The endocytic nature of the membrane-filled compartments is shown in d and e. The cell had endocytosed 5 nm BSA-gold for 1 h followed by chase overnight (large arrowheads in e) and was double labeled for Ii (middle sized gold particles, small arrowheads) and MPR (large gold particles). (f) Part of a membrane-filled enlarged compartment which labeled intensively for LAMP. (g–i) Electron dense enlarged compartments double labeled for Ii and MPR (g, h) and Ii and LAMP (i). The compartments label clearly for LAMP (small arrowheads in i) but show only minor labeling for Ii (large arrowheads in h and i) and MPR (small arrowhead in h). The compartment shown in i shows some compression, probably due to differences in density between the compartment and the surrounding cytoplasm. Unless otherwise indicated, bars represent 1 μm.

can be due to either an increased fusion or a decreased ability to undergo fission events. Though needed for the formation of these compartments, intact Ii does not seem necessary for their maintenance. This is clear from the immunofluorescence studies where several of the late compartments were found to be negative when labeling with the BU45 and BU43 antibodies which are directed toward the luminal parts of Ii. Labeling with Vic Y1 directed toward the cytosolic tail of Ii also reveals enlarged compartments without the cytosolic domain of Ii. It seems that the endosomal enlargement is Ii specific as overexpression of other proteins localized to the lysosomal pathway has not been reported to induce such structures. High expression of class II or the lysosomal glycoprotein LIMP II alone in M1 cells also does not induce enlarged endosomal structures (Madsen and Bakke, unpublished). Cells with endogenous levels of Ii and class II are not reported to display the large endosomal vesicles. The formation of the enlarged vesicles is presumably due to an imbalance of Ii compared to endogenous proteins specific to these cells. Such a view is supported by studies in CV 1 cells where expression of high levels of HLA DR suppress the formation of Ii-induced large vesicles (Bakke, unpublished). Although the biological phenomena described in this article have been observed only in transfected cells, this does not preclude a biological relevance and a similar less pronounced effect of Ii in antigen-presenting cells. More refined experiments may possibly show a similar principle for endogenous proteins as well.

E. Stang was a recipient of a Norwegian Cancer Society fellowship. These studies were also supported by grants from the Research Council of Norway, The Novo Nordisk Foundation, and the Anders Jahres Foundation. The electron microscopical studies were performed at the Electronmicroscopical Unit for Biological Sciences, University of Oslo, and the authors thank the laboratory staff for the use of their facilities. We also thank K. Prydz, R. Parton, and T. Berg for critically reading the manuscript and we are grateful for the skilled technical assistance of H. Hardersen.

REFERENCES

1. Germain, R. N., and Margulies, D. H. (1993) *Annu. Rev. Immunol.* **11,** 403–450.
2. Kvist, S., Wiman, K., Claesson, L., Peterson, P. A., and Dobberstein, B. (1982) *Cell* **29,** 61–69.
3. Sung, E., and Jones, P. P. (1981) *J. Mol. Immunol.* **18,** 899–913.
4. Roche, P. A., and Cresswell, P. (1990) *Nature* **345,** 615–618.
5. Bakke, O., and Dobberstein, B. (1990) *Cell* **63,** 707–716.
6. Lotteau, V., Teyton, L., Peleraux, A., Nilsson, T., Karlsson, L., Schmied, S. L., Quaranta, V., and Peterson, P. A. (1990) *Nature* **348,** 600–605.
7. Roche, P. A., Teletski, C. L., Karp, D. R., Pinet, V., Bakke, O., and Long, E. O. (1992) *EMBO J.* **11,** 2841–2847.
8. Simonsen, A., Momburg, F., Drexler, J., Hammeling, G. J., and Bakke, O. (1993) *Int. Immunol.* **5,** 903–917.
9. Pieters, J., Horstmann, H., Bakke, O., Griffiths, G., and Lipp, J. (1991) *J. Cell Biol.* **115,** 1213–1223.
10. Peters, J. P., Neefjes, J. J., Oorschot, V., Ploegh, H. L., and Geuze, H. J. (1991) *Nature* **349,** 669–676.
11. Neefjes, J. J., Stollorz, V., Peters, P. J., Geuze, H. J., and Ploegh, H. (1990) *Cell* **61,** 171–183.
12. Bremnes, B., Madsen, T., Gedde-Dahl, M., and Bakke, O. (1994) *J. Cell Sci.* **107,** 2021–2032.
13. Roche, P. A., Teletski, C. L., Stang, E., Bakke, O., and Long, E. O. (1993) *Proc. Natl. Acad. Sci. USA* **90,** 8581–8585.
14. Pieters, J., Bakke, O., and Dobberstein, B. (1993) *J. Cell Sci.* **106,** 831–846.
15. Romagnoli, P., Layet, C., Yewdell, J., Bakke, O., and Germain, R. N. (1993) *J. Exp. Med.* **177,** 583–596.
16. Quaranta, V., Madjic, O., Stingl, G., Lidzaka, K., Honingsmann, H., and Knapp, W. (1984) *J. Immunol.* **132,** 1900–1905.
17. Carlsson, S. R., Roth, J., Piller, F., and Fukuda, M. (1988) *Biol. Chem.* **263,** 18911–18919.
18. Seglen, P. O. (1976) *in* Methods of Cell Biology (Prescott, D. M., Ed.), Vol. 13, pp. 29–83, Academic Press, New York.
19. Seglen, P. O., and Gordon, P. B. (1982) *Proc. Natl. Acad. Sci. USA* **79,** 1889–1892.
20. Roth, J. (1983) *in* Techniques in Immunocytochemistry 2 (Bullock, G. R., and Petrusz, Eds.), pp. 217–284, Academic Press, London.
21. Green, J., Griffiths, G., Louvard, D., Quinn, P., and Warren, G. (1981) *J. Mol. Biol.* **152,** 663–689.
22. Parton, R. G., Prydz, K., Bomsel, M., Simons, K., and Griffiths, G. (1989) *J. Cell Biol.* **109,** 3259–3272.
23. Griffiths, G., Simons, K., Warren, G., and Tokuyasu, K. T. (1983) *Methods Enzymol.* **96,** 466–485.
24. Stang, E. (1988) *J. Microsc.* **149,** 77–79.
25. Stang, E., and Johansen, B. V. (1988) *J. Ultrastruct. Mol. Struct. Res.* **98,** 328. [Abstract]
26. Geuze, H. J., Slot, J. W., Strous, G. J. A. M., Lodish, H. F., and Schwartz, A. L. (1983) *Cell* **32,** 277–287.
27. Miller, S. G., Carnell, L., and Moore, H. H. (1992) *J. Cell Biol.* **118,** 267–283.
28. Matteoni, R., and Kreis, T. E. (1987) *J. Cell Biol.* **105,** 1253–1265.
29. McDowall, A., Gruenberg, J., Rîmisch, K., and Griffiths, G. (1989) *Eur. J. Cell Biol.* **49,** 281–294.
30. Geuze, H. J., Stoorvogel, W., Strous, G. J., Slot, J. W., Bleekemolen, J. E., and Mellman, I. (1988) *J. Cell Biol.* **107,** 2491–2501.
31. Ludwig, T., Griffiths, G., and Hoflack, B. (1991) *J. Cell Biol.* **115,** 1561–1572.
32. Griffiths, G. (1989) *J. Cell Sci.* Suppl. **11,** 139–147.
33. Neefjes, J. J., and Momburg, F. (1993) *Curr. Opin. Immunol.* **5,** 27–34.
34. Loss, G. E., and Sant, A. J. (1993) *J. Immunol.* **150,** 3187–3197.
35. Griffiths, G., and Gruenberg, J. (1991) *Trends Cell Biol.* **1,** 5–9.
36. Murphy, R. F. (1991) *Trends Cell Biol.* **1,** 78–82.

Received February 14, 1997
Revised version received April 25, 1997

EXPERIMENTAL CELL RESEARCH **235,** 93–99 (1997)
ARTICLE NO. EX973654

Natural Occurrence of Fast- and Fast/Slow-Muscle Chimeric Fibers in the Expression of Troponin T Isoforms

Kazuto Nakada, Jun-Ichi Miyazaki, Rie Saba, and Tamio Hirabayashi[1]

Institute of Biological Sciences, University of Tsukuba, Tsukuba, Ibaraki 305, Japan

---

Rhomboideus, one of the back muscle tissues, and its single fibers were studied in chickens by immunostaining with antisera against fast- and slow-muscle-type troponin T isoforms. Nonuniform distribution of slow-muscle-type isoforms was for the first time detected in single fibers isolated from the muscle, although fast-muscle-type troponin T isoforms were distributed over the whole length of the fiber. Based on these observations, we conclude that fast- and fast/slow-muscle chimeric fibers exist in normal skeletal muscle tissue and that the existence of chimeric fibers is direct evidence showing that myonuclei subjected to different determination in troponin T isoform expression can together form a single muscle fiber. © 1997 Academic Press

---

INTRODUCTION

One of the unique characteristics of skeletal muscle is its diversity in morphological and biochemical characters. This diversity can be attributed to the heterogenous characters of the individual fibers and the mosaic composition of different fiber types [1]. It is generally accepted that no two skeletal muscle tissues of an animal are completely identical in composition of fiber type. Muscle fibers are roughly classified into two distinct fiber types on the basis of their histochemical appearance, fast-muscle type and slow-muscle type [2, 3]. The fast and slow fibers are also characterized by distinct myofibrillar proteins [4–7]. One of them is troponin T (TnT), which is the tropomyosin-binding subunit of troponin complex [8–11]. TnT has three kinds of isoforms specific for different fiber types of striated muscle, slow-, fast-, and cardiac-muscle types [12–17].

Each muscle protein is generally assumed to be uniformly distributed along the length of normal vertebrate muscle fibers. However, nonuniform distributions of myosin isoforms and ATPase activity have been demonstrated in regenerating fibers [18], chronically stimulated fibers [19], and cultured fibers [20–22]. Although two distinct isoforms in these examples seem to occupy different areas of one muscle fiber, the changing from the area of one isoform to that of the other is obviously gradual, without clear boundaries. In our previous study [23], however, the coexistence of fast-muscle-type (F-type) and slow-muscle-type (S-type) TnT isoforms in chicken single fibers was demonstrated in the regenerated muscle obtained by slow-muscle (anterior latissimus dorsi, ALD) transplantation into fast muscle (pectoralis major). The boundaries of fast and slow areas in these fibers were clear-cut, with no gradual transition. These chimeric fibers were supposed to be formed by the fusion of fast and slow myogenic cells during regeneration after muscle transplantation. Although these chimeric fibers were produced under experimental conditions, there is no reason for the absence of such chimeric fibers in natural muscle tissues. Since the existence of chimeric fibers is direct evidence for the different determination of myonuclei in isoform expression, detection of such chimeric fibers in normal skeletal muscle tissue is worth pursuing from the viewpoint of the gene expression mechanism.

To find the natural chimeric fiber, chicken rhomboideus and its single fibers were examined by immunostaining with antisera against fast-muscle-type and slow-muscle-type TnT isoforms. After many trials, we succeeded in detecting several types of natural chimeric fibers, some of which have a clear boundary between the areas stained with anti-F-type and anti-S-type TnT sera.

MATERIALS AND METHODS

Materials. White leghorn chickens (*Gallus domesticus* (L)) were obtained from commercial sources.

Histological techniques. Rhomboideus and ALD of 60-day-old (H60) chickens were fixed in Bouin's solution for 1 day and transferred to 70% ethyl alcohol. After dehydration, they were impregnated with graded butyl alcohol solutions, embedded in Paraplast (Oxford Labware), and sectioned serially at 7 μm in thickness. Most sections were used for immunostaining and some were stained with Mayer's hematoxylin and eosin for 30 and 6 min, respectively.

Preparation of single fibers. According to methods reported so far for single fiber preparation, we tried to separate single fibers from fresh or glycerinated muscle tissues with needles or by shaking in macerating solutions. In these trials, we could get single fibers, most of which, however, were either wound or rather short, and the number of fibers was too small to examine and to detect chimeric fibers

---

[1] To whom correspondence and reprint requests should be addressed. Fax: 81-298-53-6649.

0014-4827/97 $25.00
Copyright © 1997 by Academic Press
All rights of reproduction in any form reserved.

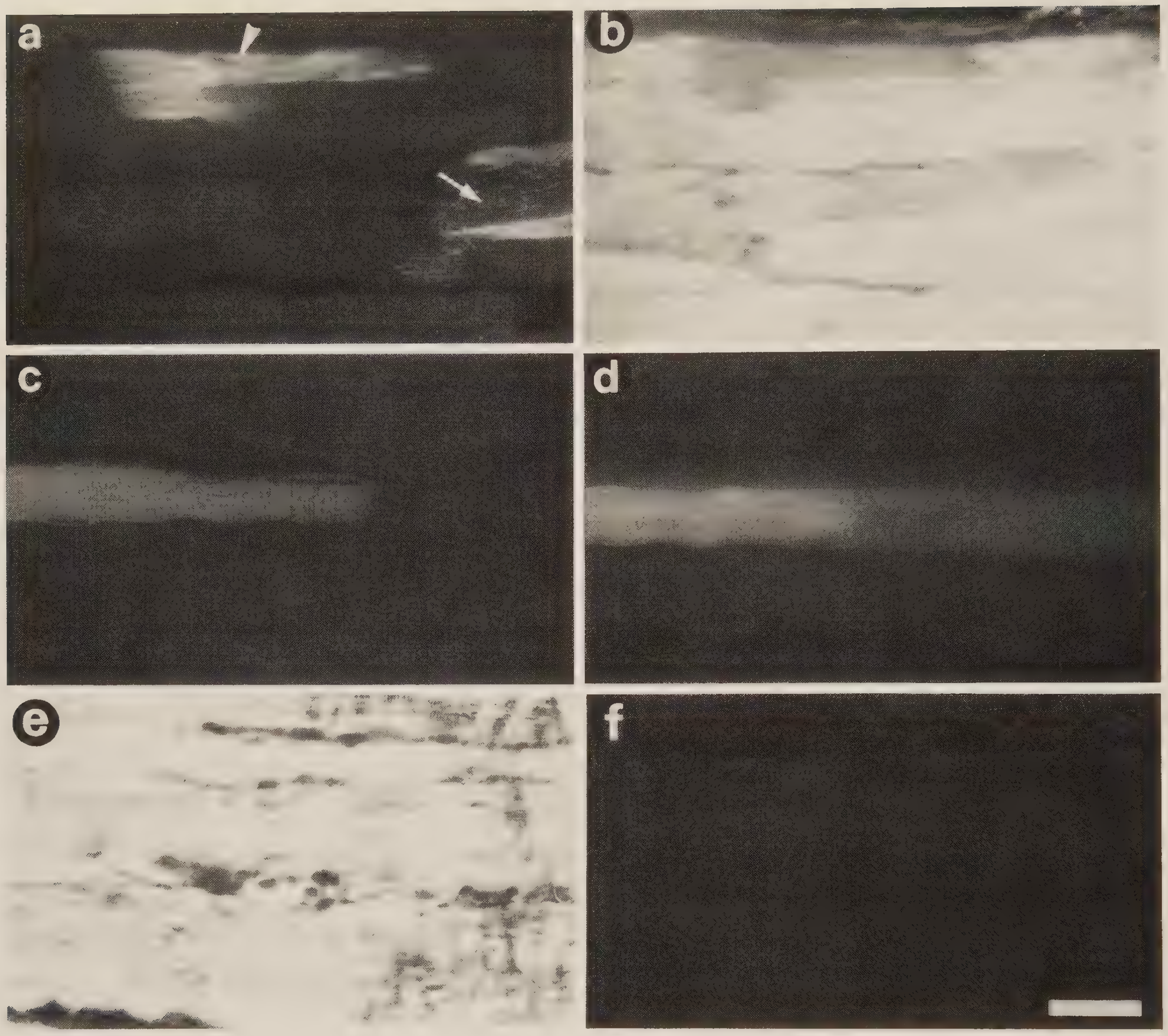

FIG. 1. Expression of troponin T isoforms in rhomboideus and anterior latissimus dorsi of 60-day-old chickens. Longitudinal serial sections of rhomboideus were stained with the anti-slow-muscle-type (a) and anti-fast-muscle-type (b) troponin T sera, respectively. (c and d) Longitudinal sections stained with anti-slow-muscle-type troponin T serum. Arrowhead and arrow indicate smeared stain and dotted stain with the anti-slow-muscle-type troponin T serum, respectively. As controls, longitudinal serial sections of anterior latissimus dorsi, which is a typical slow muscle tissue in the chicken, were stained with the anti-slow-muscle-type (e) and anti-fast-muscle-type troponin T (f) sera. Scale bar, 30 μm.

among fibers on slide glasses. After these trials, we combined the mechanical method with chemical ones used for epithelial cell separation and established the following technique by which many long and straight fibers could be separated from various kinds of muscle samples of young or aged chickens.

Rhomboideus muscles of 1-day-old (H1) chicks and H60 chickens fixed in Bouin's solution were used for single fiber preparation. The fixed tissues were washed in 70% ethyl alcohol for several days. The tissues were dissociated into single fibers by constant shaking in 30–40% potassium hydroxide solutions for 1–2 h, and the single fibers were collected by centrifugation at 500*g* for 10–15 min. The collected fibers were suspended in phosphate-buffered saline (PBS) and centrifugated again at 500*g* for 10–15 min. The suspending and centrifuging were repeated at least three times until the pH of the suspension became the same as that of PBS (pH 7.4). The single fibers were mounted on slide glasses coated with poly-L-lysine (0.1% poly-L-lysine solution, Sigma) and stained with hematoxylin–eosin or antisera.

Immunostaining. Serial sections and single fibers of rhomboideus were subjected to indirect immunostaining with anti-F-type and anti-S-type TnT (rabbit sera) as the first antibodies. Rhodamine (TRITC)-conjugated goat anti-rabbit IgG (H + L) was used as the second antibody. The anti-F-type TnT and anti-S-type TnT specifically recognized respective antigens, as previously reported [23, 24]. ALD excised from H60 chicken was used as a sample of slow muscle by the procedures mentioned above. Pictures were taken with a combination of a Nikon Optiphoto microscope and a Nikon FX-35WA camera.

RESULTS

Expression of Fast-Muscle-Type and Slow-Muscle-Type Troponin T Isoforms in Adult Chicken Rhomboideus

Longitudinal serial sections of H60 chicken rhomboideus were stained with anti-S-type TnT (Fig. 1a) and anti-F-type TnT (Fig. 1b). Two types of fiber staining were observed with the anti-S-type TnT, a smeared stain (Fig. 1a, arrowhead) and a dotted stain (Fig. 1a, arrow). The former is suggestive of orderly distribution of S-type TnT isoforms, while the latter is not. The former also suggests to us that the S-type TnT isoforms are expressed in only part of a long fiber (Fig. 1a).

When two serial sections stained with anti-S-type TnT (Fig. 1a) and anti-F-type TnT (Fig. 1b) are compared, one can recognize that the area of smeared stain with anti-S-type TnT corresponds with the area stained weakly with anti-F-type TnT. Although the stain with anti-F-type TnT is weak (Fig. 1b) we judge this stain positive by comparing it with the area of ALD stained with anti-F-type TnT (Figs. 1e and 1f) in the same experiment. ALD was completely negative in anti-F-type TnT staining. Therefore, in the area of the smeared stain with anti-S-type, S-type and F-type isoforms are colocalized, so that this area will be referred to as the F/S-positive area hereafter. Other examples of such staining were often found with varied morphologies in rhomboideus, as presented in Figs. 1c and 1d. As for the area of dotted stain (arrow in Fig. 1a), the correspondence with the brightness or dimness of the anti-F-type TnT staining was not clear, probably due to the small (dotted) area among the large areas stained brightly with anti-F-type TnT. The area including the dotted stain (arrow in Fig. 1a) was stained evenly with anti-F-type TnT (Fig. 1b). Whether the dotted stain is really on the fibers or not is also not clear. In order to confirm this, we performed the immunostaining with serial cross sections (7 μm) of the rhomboideus and found two types of staining (Fig. 2a) with anti-S-type TnT, corresponding to those in the longitudinal sections (Fig. 1a). In the serial cross sections, which cover a 42-μm distance, the gradual appearance of the dotted stain was observed in the arrowed fiber (Figs. 2b–2e). Therefore, we may conclude that the dotted stain is also distributed on a part of a long fiber.

Nonuniform Distribution of Fast-Muscle-Type and Slow-Muscle-Type Troponin T Isoforms in Single Fibers

Myofibrils in Figs. 1a–1d looked continuous from the F/S-positive area to the area stained only with the anti-F-type TnT (F-positive area). But still such histological observations are not definite evidence for concluding that the fibers are chimeric in TnT isoform distribution since

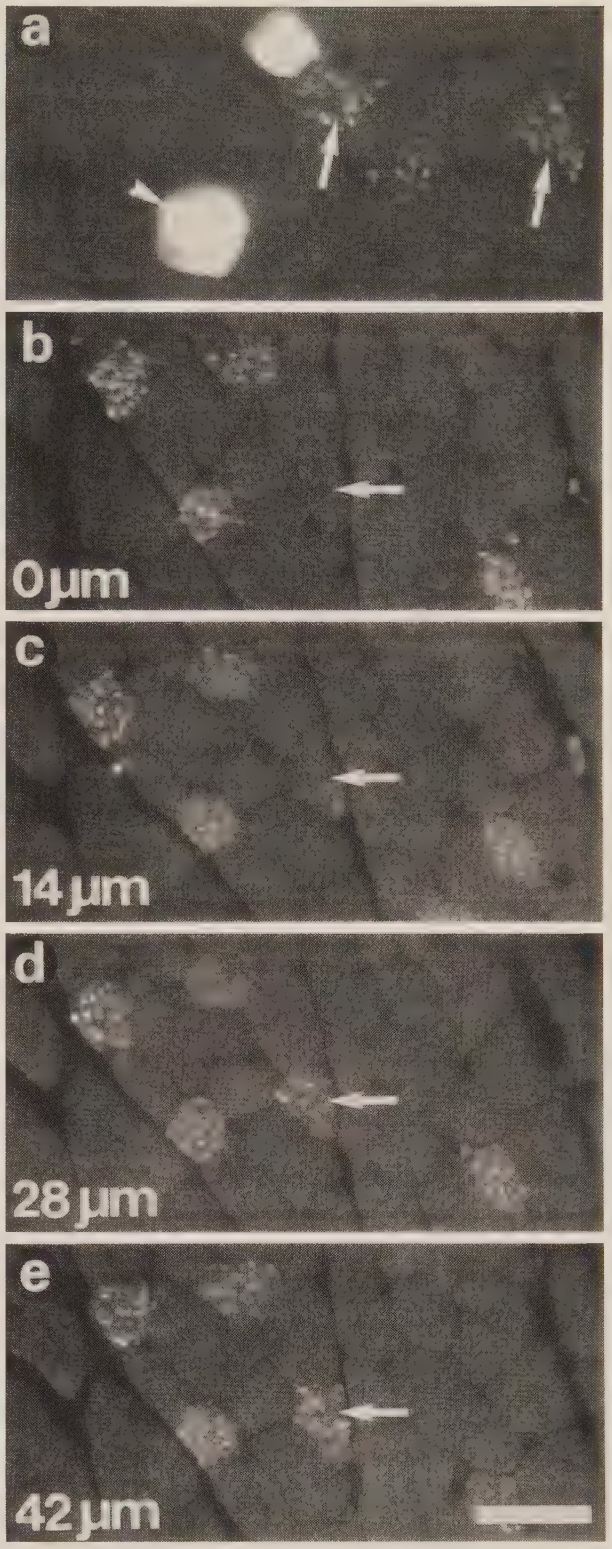

FIG. 2. Dotted stain in cross sections of rhomboideus. Two staining types, smeared stain (arrowhead) and dotted stain (arrows), were observed with the anti-slow-muscle-type troponin T serum in a. (b–e) Serial taken at 14 μm. The fiber arrowed in b was not stained with the serum, but dotted stain appeared in c–e. Scale bar, 30 μm.

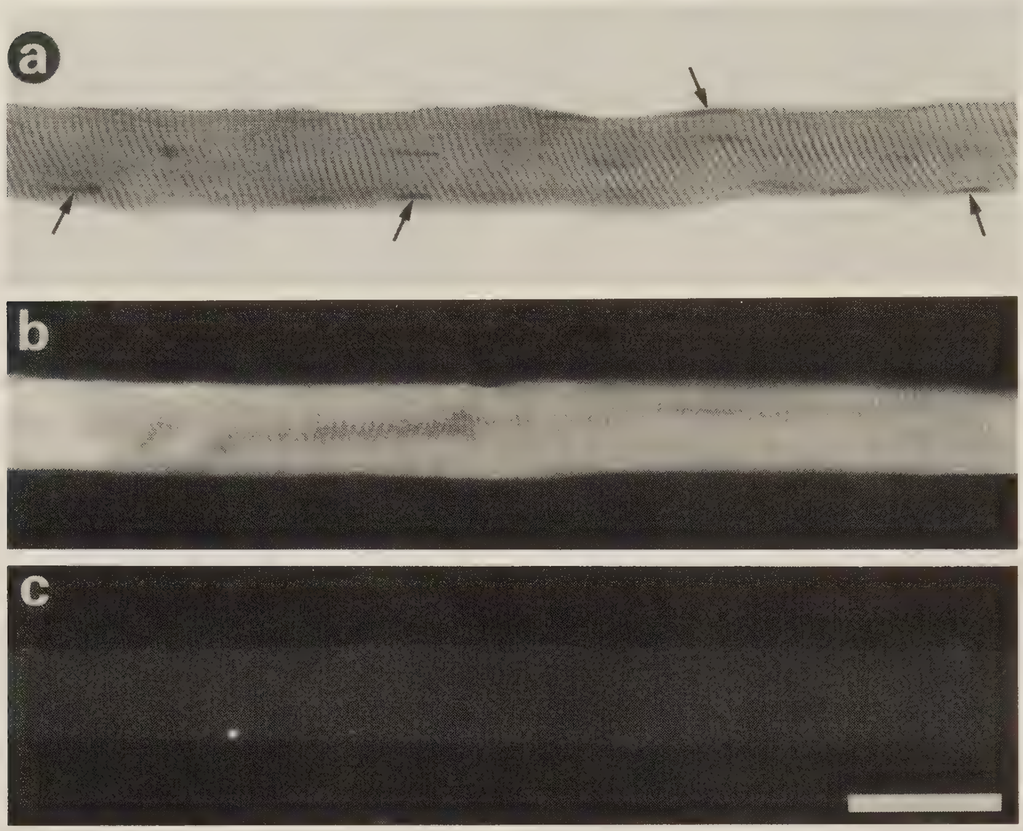

FIG. 3. Troponin T isoform expression in single fibers isolated from rhomboideus of 60-day-old chickens. Single fibers were stained with hematoxylin and eosin (a). Myonuclei of the fibers became visible, since the nuclei were stained with hematoxylin (arrows). Single fibers stained with the anti-fast-muscle-type and anti-slow-muscle-type troponin T sera are presented in b and c, respectively. All fibers were stained with anti-fast-muscle-type troponin T serum (b), while most fibers were not stained with anti-slow-muscle-type troponin T serum (c). Scale bar, 30 μm.

the fibers are too close to discern continuous myofibers. Therefore, we tried to separate the fibers mechanically or chemically for immunostaining and found it too difficult to separate single fibers mechanically from H60 rhomboideus. However, the mechanical method combined with chemical ones (see Materials and Methods) allowed us to separate single fibers (Fig. 3) from the muscle tissue. A single fiber stained with hematoxylin and eosin possessed myonuclei (arrows in Fig. 3a) and striations with histologically normal appearance. Myonuclei in 30 single fibers were counted and their lengths were measured. The fiber possessed 2.6 ± 0.38 myonuclei per 30 μm length, which is the bar length in all the figures in this paper.

When the single fibers were stained with anti-F-type TnT, all fibers were stained smoothly and brightly over the whole length (Fig. 3b). In contrast with this result, most fibers were not stained with anti-S-type TnT, as shown in Fig. 3c. However, parts of some fibers were stained with anti-S-type TnT in several ways (Fig. 4). Only a part of the fiber area was stained (Figs. 4a, 4c, 4e, and 4f), and the phase-contrast microscope gave no doubt of the single fiber construction (Figs. 4b and 4d). In Fig. 4a, the border of the anti-S-type TnT-stained area is vague and disappears into the unstained area, while the border is clear-cut, forming a boundary between stained and unstained areas in Fig. 4c. In other examples (Figs. 4e and 4f), the boundary was between the two extremes described above, with the stained area disappearing in a rather dispersed manner into the negative area. Formation of striations in the boundary area of the two areas seems to be quite normal since each striation in this area looks sound and continuous in phase-contrast micrographs (Figs. 4b and 4d).

These observations indicate that the expression of S-type TnT isoforms is limited to a part of the fibers of H60 rhomboideus, where F-type TnT isoforms are also expressed, that is, these are chimeric fibers of F- and F/S-positive areas, in which the expression of isoforms is fixed in the nucleus of each cell lineage [24, 25].

Expression of Slow-Muscle-Type Troponin T Isoforms in Single Fibers of 1-Day-Old Chick Rhomboideus

To examine the expression of S-type-TnT isoforms in rhomboideus of young chicks, we performed isolation

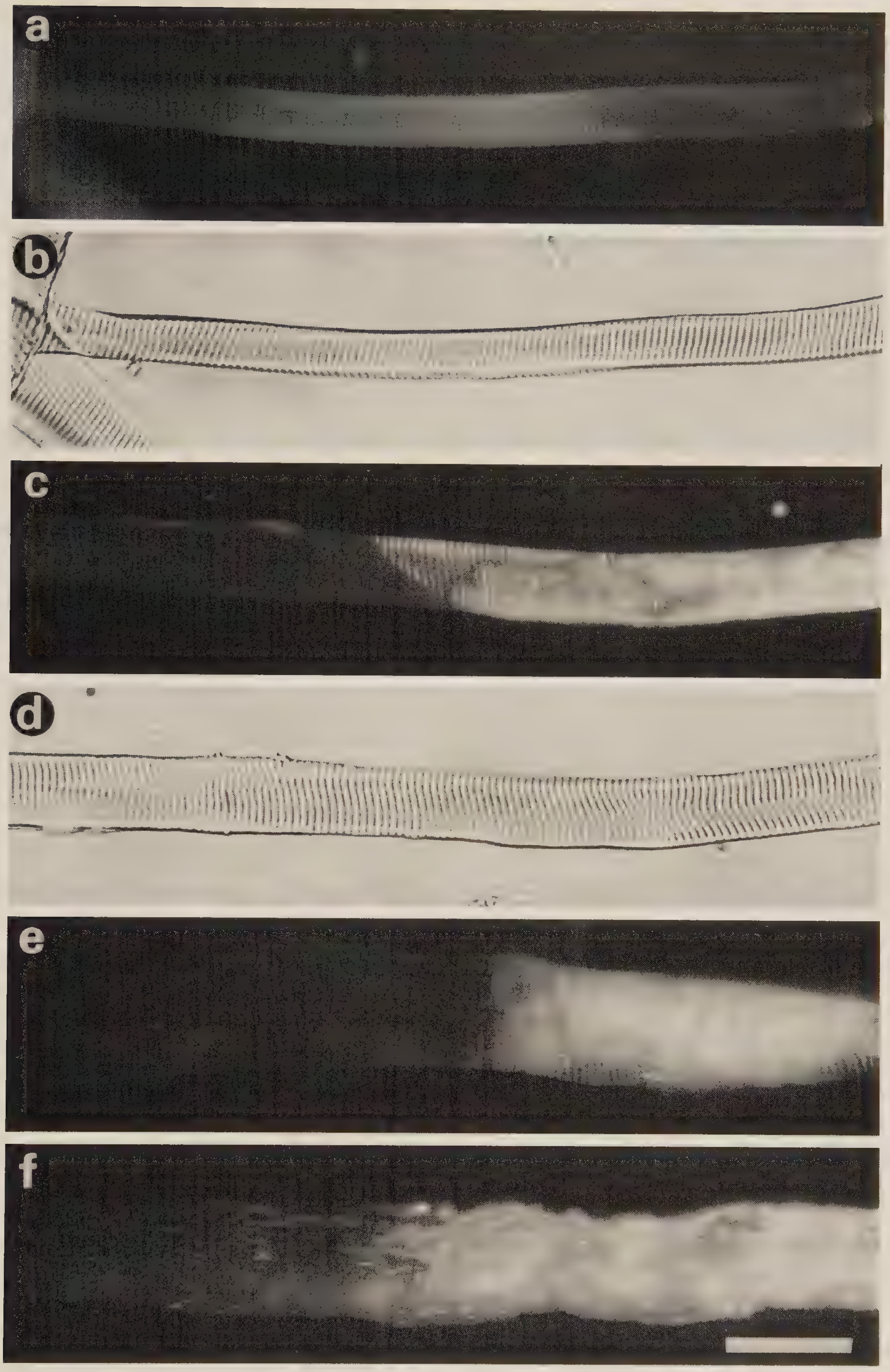

FIG. 4. Nonuniform distribution of slow-muscle-type troponin T isoforms in single fibers. Single fibers isolated from the rhomboideus of 60-day-old chickens were stained with the anti-slow-muscle-type troponin T serum. Nonuniform distribution of slow-muscle-type troponin T isoforms was observed (a, c, e, and f). Phase-contrast micrographs of the fibers in a and c are shown in b and d, respectively. Scale bar, 30 μm.

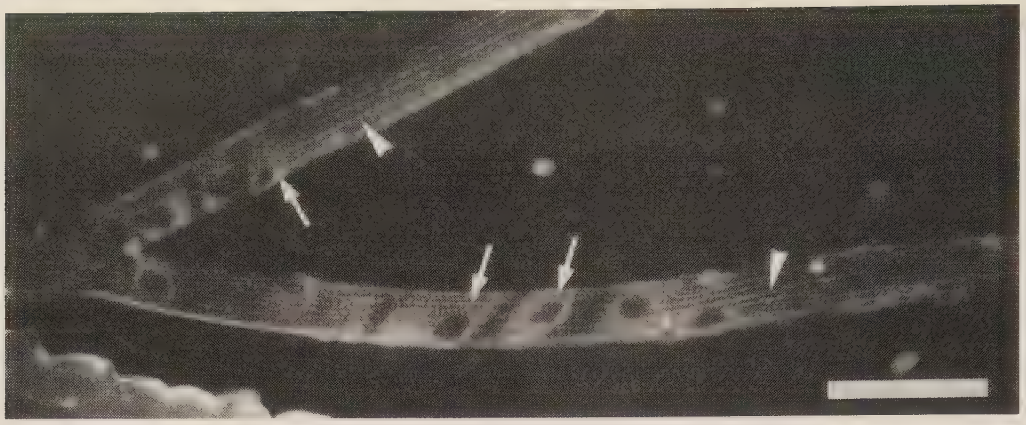

FIG. 5. Expression of slow-muscle-type troponin T in rhomboideus of 1-day-old chicks. Single fibers isolated from rhomboideus of 1-day-old chicks were stained with anti-slow-muscle-type troponin T serum. The cytoplasm around myonuclei was stained in a patchy way with the serum (arrows) and a bead-like distribution of the slow-muscle-type troponin T was observed along the fiber (arrowheads). Scale bar, 30 μm.

and immunostaining of single fibers from H1 rhomboideus. Most fibers were stained uniformly with anti-F-type TnT and only a few fibers stained with anti-S-type TnT. Some fibers were stained in a patchy way around the myonuclei (arrows in Fig. 5) and some were stained in a bead-like way along the fibers with the latter antiserum (arrowheads in Fig. 5). The patchy stain is suggestive of the compartmentalization with nascent isoforms and the bead-like stain of their quick incorporation into the primitive myofibrils.

DISCUSSION

The localization of muscle-specific proteins is generally accepted to be uniform along the entire length of muscle fibers. However, the present study confirmed that S-type TnT isoforms were distributed in only a part of some muscle fibers (Figs. 1, 2, and 4), although F-type isoforms are localized along the entire fiber length (Fig. 3). The fibers found in this experiment are natural chimeric ones expressing partly F-type and partly F/S-type TnT isoforms (F-F/S chimeric fiber). Diversity of skeletal muscle tissue is considered to be created by the mosaic composition of individual fibers which have a distinct fiber type [1–3] and probably increased with such chimeric fibers.

The chimeric fiber is important in elucidating the intrinsic heterogeneity of protein expression of the myonuclei in multinucleated fibers. The occurrence of such a fiber suggests that myogenic cells of different cell lineages in protein expression can fuse to form a myotube, although selective protein transportation cannot be ruled out completely. There are two possibilities for understanding the nuclear population in the F-F/S chimeric fiber. One is that the fiber has F-type and S-type nuclei expressing respective isoforms only. The other is that the fiber has F-type and F/S-type nuclei expressing only F-type and both F- and S-type isoforms, respectively.

In our previous work, only two types of myogenic cell populations, F type and F/S type in the expression of TnT isoforms [26], were isolated by cell culture from three chicken skeletal muscles, pectoralis major, ALD, and gastrocnemius of various ages, and no myogenic cell population expressing only S-type TnT isoforms was found *in vitro*. In contrast to this result, chicken ALD (slow muscle) transplanted into pectoralis major (fast muscle) could regenerate S-type muscle fibers [26], suggesting the existence of an S-type myogenic population *in vivo*. Why there is no S-type myogenic cell population *in vitro* and whether an F/S-type cell population exists *in vivo* are questions that remain to be studied.

Nonuniform distributions of myosin isoforms and ATPase activity were reported, but their boundaries were vague and gradual over distances of several hundred micrometers [19]. However, in some F-F/S chimeric fibers found in this work, the boundary of F- and F/S-positive areas was clear-cut, although dotted stain with anti-S-type TnT was gradual and extended several tens of micrometers at the longest. The expression of S-type TnT isoforms was restricted, probably due to the cluster formation of a prospective S-type or F/S-type cell population. A similar boundary of the areas was observed in artificial chimeric fibers of F-type and S-type TnT isoforms induced by muscle transplantation [23]. These observations suggest that TnT isoforms are concentrated near nuclei and cannot disperse so far. Actually, the expression of the S-type TnT isoform in single fibers isolated from H1 rhomboideus was detected in cytoplasm nearby the myonuclei (Fig. 5). The restricted distribution of the S-type TnT isoform seems to reflect the fact that each type of isoform is synthesized under the control of an individual nucleus which shares the cytoplasm with other nuclei.

Two general types of developmental strategy in myogenesis have been known in vertebrates. In one type, the differentiated state of a myogenic cell is controlled by its extrinsic factors, such as nerve, hormone, and exercising, stretch and force generation [27–30]. In the other, it is controlled by intrinsic factors of the muscle cell lineage [24, 31, 32]. Natural chimeric fiber is considered to be direct evidence of the latter. The example of the former is the incomplete transformation from fast to slow fibers, induced by chronic stimulation [19]. This fiber-type transformation might occur to adapt fibers to physiological conditions, because muscle tissue is an effector to trigger animal behavior. The F/S-positive area of natural chimeric fibers may have the plasticity to be transformed into an either F- or S-positive form.

In conclusion, we found natural F-F/S chimeric fibers in troponin T isoform expression. Existence of the natural chimeric fibers proved the heterogeneity of myonuclei in the program of TnT isoform expression in a single fiber and the stability of gene expression determined in the differentiation process of the cell lineage.

REFERENCES

1. Pette, D., and Staron, R. S. (1990) *Rev. Physiol. Pharmacol.* **116,** 1–76.
2. Gauthier, G. F. (1986) *in* Myology (Engel, A. G., and Banker, B. Q., Eds.), pp. 255–283, McGraw–Hill, New York.
3. Romanul, F. C. A. (1964) *Arch. Neurol.* **11,** 355–368.
4. Brooke, M. H., and Kaiser, K. K. (1970) *Arch. Neurol.* **23,** 369–379.
5. Staron, R. S., and Pette, D. (1987) *Biochem. J.* **243,** 687–693.
6. Staron, R. S., and Pette, D. (1987) *Biochem. J.* **243,** 695–699.
7. Schmitt, T., and Pette, D. (1988) *FEBS Lett.* **234,** 83–85.
8. Ebashi, S., Wakabayashi, T., and Ebashi, F. (1967) *J. Biochem. (Tokyo)* **62,** 137–138.
9. Flicker, P. F., Phillips, G. N., and Cohen, C. (1982) *J. Mol. Biol.* **162,** 495–501.
10. Hill, L. E., Mehegan, J. P., Butter, C. A., and Tobacman, L. S. *J. Biol. Chem.* **267,** 16106–16113.
11. Dhoot, G. K., and Perry, S. V. (1979) *Nature* **278,** 714–718.
12. Mikawa, T., Takada, S., Shimizu, T., and Kitaura, T. (1981) *J. Biochem. (Tokyo)* **89,** 1951–1962.
13. Toyota, N., and Shimada, Y. (1981) *J. Cell Biol.* **91,** 497–504.
14. Dhoot, G. K., Frearson, N., and Perry, S. V. (1979) *Exp. Cell Res.* **122,** 339–350.
15. Sabry, M. A., and Dhoot, G. K. (1991) *J. Muscle Res. Cell Motil.* **12,** 262–270.
16. Sabry, M. A., and Dhoot, G. K. (1991) *J. Muscle Res. Cell Motil.* **12,** 447–454.
17. Shiraishi, F., Nakamura, Y., and Ohtsuki, I. (1993) *Biomed. Res.* **14,** 93–97.
18. Kelly, A. M., and Rubinstein, N. A. (1980) *in* Plasticity of Muscle (Pette, D., Ed.), pp. 161–175, de Gruyter, New York.
19. Staron, R. S., and Pette, D. (1987) *Pflügers Arch.* **409,** 67–37.
20. Gauthier, G. F. (1990) *J. Cell Biol.* **110,** 693–701.
21. Cerny, L. C., and Bandman, E. (1986) *J. Cell Biol.* **103,** 2153–2161.
22. Düsterhöft, S., and Pette, D. (1993) *Differentiation* **53,** 25–33.
23. Yao, Y., Miyazaki, J.-I., and Hirabayashi, T. (1994) *Exp. Cell Res.* **214,** 400–407.
24. Yao, Y., Nakamura, M., Miyazaki, J.-I., Kirinoki, M., and Hirabayashi, T. (1989) *Dev. Biol.* **151,** 531–540.
25. Yao, Y., Kirinoki, M., and Hirabayashi, T. (1994) *J. Muscle Res. Cell Motil.* **15,** 21–28.
26. Mashima, J., Nakada, K., Yao, Y., Miyazaki, J.-I., and Hirabayashi, T. (1996) *Zool. Sci.* **13,** 571–576.
27. Snoj-Cvetko, E., Sketelj, J., Dolenc, I., Obreza, S., Janmot, C., d'Albis, A., and Eržen, I. (1996) *Histochem. Cell Biol.* **106,** 473–479.
28. Donovan, C. M., and Faulkner, J. A. (1987) *J. Appl. Phisiol.* **62,** 2507–2511.
29. Goldspink, G., Scutt, A., Loughna, P. T., Wells, D. J., Jaenicke, T., and Gerlach, G. F. (1992) *Am. J. Phisiol.* **262,** R356–R363.
30. Izumo, S., Nadal-Ginard, B., and Mahdavi, V. (1986) *Science* **231,** 597–600.
31. Stockdale, F. E., and Miller, J. B. (1987) *Dev. Biol.* **123,** 1–9.
32. Miller, J. B., and Stockdale, F. E. (1986) *J. Cell Biol.* **103,** 2197–2208.

Received February 26, 1997
Revised version received May 16, 1997

EXPERIMENTAL CELL RESEARCH **235**, 100–107 (1997)
ARTICLE NO. EX973638

O-Glycosylation and Cellular Differentiation in a Subpopulation of Mucin-Secreting HT-29 Cell Line

Sylviane Hennebicq-Reig,*,† Daniel Tetaert,*,[1] Benoit Soudan,* Isabelle Kim,† Guillemette Huet,*,†
Gilbert Briand,†,‡ Colette Richet,* Dominique Demeyer,* and Pierre Degand*,†

**Biologie et physiopathologie des cellules mucipares, INSERM Unité No. 377, Bâtiment G Biserte, place de Verdun, 59045 Lille Cedex, France; †Laboratoire de biochimie, Hôpital C Huriez, place de Verdun, Lille, France; and ‡Service Commun de Spectrométrie de Masse, Faculté de médecine, Université de Lille II, Place de Verdun, Lille, France*

Malignant transformation of epithelial cells is associated with abnormal glycosylation of mucins. The aim of this work was to evaluate the changes in the O-glycosylation processes during differentiation of tumor cells by performing *in vitro* reactions using crude microsomal preparations obtained from a subpopulation of HT-29 cells capable of differentiating into mucin-secreting cells (HT-29 MTX cells). The reactions of O-glycosylation were carried out at different times of culture: before confluence (Day 5), when cells are still undifferentiated, and after confluence (Day 21), when cells display a mucin-secreting phenotype. As acceptor for the UDP-*N*-acetylgalactosamine:polypeptide *N*-acetylgalactosaminyltransferase (GalNAc transferase), the peptide motif TTSAPTTS (tandem repeat deduced from MUC5AC human gastric gene, expressed in HT-29 MTX cells) was used. A higher rate of enzyme activity was observed in preconfluent cells, and analysis by capillary electrophoresis and electrospray mass spectrometry showed a different pattern of galactosaminylation in pre- and postconfluent cells. Core 1 UDP-galactose:*N*-acetyl-α-galactosaminyl-R 3-β-galactosyltransferase (3-β-galactosyltransferase) activity also decreased with the differentiation, whereas CMP-neuraminic acid:galactose–β-1, 3-*N*-acetyl-α-galactosaminyl-R 3-α-sialyltransferase activity increased. In comparison, the evolving process of mucin biosynthesis was tested by the analysis of purified mucins of HT-29 MTX cells, in amino acid and carbohydrate composition, and immunoreactivity assays using several antibodies and lectins. The results suggested that (i) no mucins were detected at Day 5, while the GalNAc transferase and 3-β-galactosyltransferase activities were already at high rates; (ii) the mucins purified from postconfluent cells showed a high content of sialic acid in an α-2,3-linkage to galactose residues; and (iii) cellular differentiation seemed to be accompanied by more regulated processes of glycosylation. This study of the O-glycosylation in HT-29 MTX cells is thus an interesting approach to analyzing the regulation of mucin biosynthesis during cellular differentiation.

© 1997 Academic Press

INTRODUCTION

Mucins are O-glycosylated high-molecular-weight glycoproteins, constitutive of the mucus secreted by the epithelial cells. The antigenicity and carbohydrate structure of the mucins differ according to the type of mucosa (i.e., gastric, colonic, or respiratory tracts). Moreover, malignant transformation of the cells is associated with an abnormal glycosylation pattern [1, 2]. In colon cancer, in particular, these changes include an increase in sialomucin, a decrease in O-acetylated sialic acid and sulfomucin, alterations in the expression of blood group antigens, and an increased expression of Tn and sialylTn antigens (GalNAc[2]–α-*O*-Thr/Ser and NeuAc–α2,6GalNAc–α-*O*-Thr/Ser) [1, 2]. The mucins produced in colon cancer cells are characterized by fewer and shorter oligosaccharide chains compared to normal colonic mucins [3]. Carbohydrate changes have also been found in mucin-secreting colon carcinoma cells in culture. In particular, investigations of the oligosaccharide structures of the mucins secreted by the C1 16-E clonal derivative of the HT-29 cell line have shown that elongation of carbohydrate chains is truncated by premature sialylation [4]. Mucin-secreting HT-29 cells are therefore a suitable model for studying abnormal O-glycosylation in colon cancer cells. HT-29 MTX cells obtained by stepwise adaptation of HT-29 cells to 10^{-5} *M* methotrexate (MTX) [5] constitute a subpopulation which also synthesizes sialylated mu-

---

[1] To whom correspondence and reprint requests should be addressed. Fax: (33) 03 20 53 85 62. E-mail: tetaert@biserte.lille.inserm.fr.

[2] Abbreviations used: GalNAc, *N*-acetylgalactosamine; GlcNAc, *N*-acetylglucosamine; GalNAc transferase, UDP-*N*-acetylgalactosamine:polypeptide *N*-acetylgalactosaminyltransferase; Gal, galactose; 3-β-galtransferase, core 1 UDP-galactose:*N*-acetyl-α-galactosaminyl-R 3-β-galactosyltransferase; ST3Gal I, CMP–neuraminic acid:galactose β1, 3-*N*-acetyl-α-galactosaminyl-R 3-α-sialyltransferase; HPLC, high-performance liquid chromatography; MTX, methotrexate; PBS, phosphate-buffered saline.

0014-4827/97 $25.00

Copyright © 1997 by Academic Press
All rights of reproduction in any form reserved.

cins [6]. The secretion of mucin is a growth-related phenomenon, starting after the cells reach confluence (Day 7) and increasing thereafter [7, 8]. The mucus gel becomes visible on the surface of the cell layer after 14 days of culture. In this way, cultured HT-29 MTX cells are a useful tool for studying O-glycosylation during cellular differentiation.

The heterogeneity of the peptide backbone is also important in mucin biosynthesis and, to date, the complete and partial primary structures of at least eight mucin genes (MUC1 to MUC7) have been reported. Each apomucin contains tandem repeat units of different sizes (8 to 169 residues) and different amino acid compositions depending on the organ and/or species considered. In the intestinal tract, different mucin genes are expressed: MUC2 and MUC3 for small intestine and colon [9, 10], in the gastric tract, MUC5AC or MUC6 is expressed [11–13]. Thus, MUC3 and MUC5AC are two different mucin genes normally found in colonic and gastric mucosa, respectively. These genes are also mainly encoded in the HT-29 MTX cell line and, as described by Lesuffleur *et al.* [8], their expression increases with cellular differentiation, particularly for MUC5AC. Moreover, the synthesis of specific apomucins, followed by the posttranslational O-glycosylation reaction, depends largely on the age of the culture, and this synthesis leads to the secretion of mucins of gastric type in the HT-29 MTX cells [8]. MUC5AC seemed thus to be of greater interest than MUC3 in our study.

In this work, the HT-29 MTX cell line was used at different stages of cellular differentiation (preconfluent undifferentiated cells at Day 5 and postconfluent, highly differentiated cells at Day 21) for different purposes. To analyze the control of the first step of O-glycosylation involving UDP-*N*-acetylgalactosamine: polypeptide *N*-acetylgalactosaminyltransferase (EC 2.4.1.41), microsomal preparations were assayed for the peptide substrate TTSAPTTS (motif deduced from the tandem repeat sequence of MUC5AC, which is preferentially expressed in human stomach and in the HT-29 cell lines). To appreciate later events occurring in O-glycosylation of the mucins, the activities of core 1 UDP-galactose:*N*-acetyl-α-galactosaminyl-R 3-β-galactosyltransferase (3-β-galactosyltransferase, EC 2.4.1.122) and CMP-neuraminic acid:galactose–β-1, 3-*N*-acetyl-α-galactosaminyl-R 3-α-sialyltransferase (ST3Gal I, EC 2.4.99.4) were also analyzed and the final products synthesized by these cells examined for their amino acid and carbohydrate composition and for their reactivity toward antibodies and lectins. The aim of the present contribution was to evaluate whether the glycosylation pattern of epithelial mucus-secreting cells may be changed during cellular differentiation.

MATERIALS AND METHODS

Cell Culture

Mucus-secreting HT-29 cells selected by adaptation to 10^{-5} *M* methotrexate and reversed to drug-free medium (HT-29 MTX) were obtained from Dr. T. Lesuffleur (Unité INSERM No. 178, Villejuif, France). Cells were grown in Dulbecco's modified Eagle's minimum essential medium (Eurobio, Paris, France) supplemented with 10% heat-inactivated (56°C, 30 min) fetal bovine serum (Boehringer Mannheim, Germany), at 37°C in a 10% CO_2/90% air atmosphere. For experimental purposes all cells were seeded at 1.5×10^6 cells in 75-cm^2 flasks (Corning Glassworks, Corning, NY). The medium was changed daily. At Days 5 and 21, after rinsing twice with PBS, the cells were scraped in PBS with a rubber policeman and gently centrifuged, and the cell pellet was stored at −80°C in a 0.2 *M* NaCl/0.25 *M* sucrose solution until further use.

Enzyme Preparation

GalNAc transferase and Galtransferase assays. Microsomal suspensions were prepared by sonication on ice of the cell pellet (10^6 to 2×10^8), followed by a centrifugation of 10 min at 16,000*g*. The supernatant was then ultracentrifuged for 20 min at 140,000*g*. The microsomal pellet was resuspended in an ice-cold 0.2 *M* NaCl/0.25 *M* sucrose solution. The protein concentration was determined according to the method of Peterson [14]. The solution was stored at −80°C until used for GalNAc transferase and 3-β-galactosyltransferase assays.

Sialyltransferase assays. For the ST3Gal I assays, cell homogenates were prepared using the protocol described by Delannoy *et al.* [15]. HT-29 MTX subconfluent and postconfluent cells were lysed on ice with 10 m*M* sodium cacodylate buffer, pH 6.5, containing 20% glycerol, 0.5 m*M* dithiothreitol, 1% Triton X-100, and 5 m*M* $MnCl_2$. Cell homogenates were then centrifuged at 10,000*g* for 15 min and the supernatants were used for enzymatic assays. Protein concentration was determined according to the method described by Peterson [14], using bovine serum albumin as standard.

Reactions of in Vitro O-Glycosylation

GalNAc transferase assays. The synthetic peptide substrate NH_2–TTSAPTTS–COOH was from Neosystem (Strasbourg, France). The purity of the peptide was checked by amino acid sequence determination, high-performance liquid chromatography analysis, and electrospray mass spectrometry. The incubation was performed under the conditions previously described [16] using the peptide TTSAPTTS (5 m*M*) as exogenous substrate, UDP-[^{3}H]-GalNAc (Amersham, France, 430 dpm/nmol, in 1 m*M* cold UDP-GalNAc; Sigma, St. Louis, MO), and the different microsomal preparations. After the addition of the enzyme, the samples were incubated for 3 h at 37°C and the reaction was stopped by the addition of 8 vol of 20 m*M* sodium borate–1 m*M* ethylenediaminetetraacetic acid (Sigma, pH 9.1). The products were separated on an AG1-X8 anion-exchange resin column (Bio-Rad, Vitry sur Seine, France) by elution with water and [^{3}H]GalNAc incorporation was counted. Before capillary electrophoresis or mass spectrometry, the samples were desalted on Sep-PaK C18 reversed-phase cartridges (Millipore, Waters Chromatography, Milford, MA), which were activated by passage of 10 ml methanol followed by 10 ml deionized water containing the counterion trifluoroacetic acid (TFA, 0.1%). Aqueous eluates from the exchanger AG1-X8 were applied and polar materials were washed through with 10 ml water/TFA, whereas the glycopeptidic fractions were obtained by elution with 10 ml acetonitrile 25% in water/TFA [17].

3-β-Galactosyltransferase assays. The assays were performed following a modified procedure of Brockhausen *et al.* [18]. The microsomal preparations were incubated for 3 h at 37°C at a final volume of 42 μl in the Mes buffer, pH 7.1, previously described [19], containing benzyl-α-GalNAc (2 m*M*), γ-galactonolactone (5 m*M*), UDP-[^{14}C]-galactose (Amersham, 890 dpm/nmol, in 1 m*M* cold UDP-Gal, Sigma). The reaction was stopped by the addition of 8 vol of 20 m*M* sodium borate–1 m*M* ethylenediaminetetraacetic acid (Sigma, pH 9.1). Products were separated on an AG1-X8 anion-exchange resin column, eluted with water, and then counted for [^{14}C]galactose incorporation.

ST3Gal I assays. Incubations were performed under the conditions described by Delannoy *et al.* [15] at a final volume of 120 μl, using 40 μl of cell extracts (140–200 μg of protein), Gal-β1, 3-GalNAc-α-paranitrophenol (1 m*M*) as exogenous acceptor, CMP-[^{14}C]-Neu5Ac (34,740 dpm/nmol, 53 μ*M*) as substrate, and 0.1 *M* sodium cacodylate buffer, pH 6.5, containing 0.2 m*M* galactose, 1 m*M* 2,3-dehydro-2-deoxy-Neu5Ac, and 1% Triton X-100. After 1 h at 37°C, the reaction was stopped by the addition of 1 vol ethanol, the samples were centrifuged for 5 min at 3000*g*, and the supernatants were directly processed for descending paper chromatography in ethyl acetate/pyridine/water (10/4/3, v/v) before ^{14}C counting [15]. All the glycosyltransferase assays were performed as duplicates, on at least two different passages.

Capillary Electrophoresis

The capillary electrophoresis was performed on a P/ACE Model 5000 system (Beckman, Fullerton, CA) controlled by the System Gold software V 810 (Beckman). UV absorbance was monitored by a fixed-wavelength detector at 200 nm. The fused silica capillary was 57 cm long × 75 μm i.d. and fitted in a cartridge with a modified mandrel to improve cooling. Migrations were run at 23°C using a 2 *N* formic acid buffer and the voltage across the capillary was maintained at 20 kV. The injections were carried out by pressure (duration 6 s, approximately 10–20 pmol) and after each separation the capillary was flushed with the appropriate buffer for 2 min [17].

Mass Spectrometry

The conditions of analysis by electrospray mass spectrometry using a mass spectrometer (Perkin–Elmer SCIEX, Toronto, Canada) have been previously reported [19].

Mucin Purification

After 5 or 21 days of culture, the cells were rinsed twice with PBS, scraped, and directly lysed by ultrasonication in PBS. Mucins were then prepared as described by Huet *et al.* [6], by centrifugation for 5 min at 1000*g* at 4°C, followed by an ultracentrifugation in cesium bromide for 72 h at 200,000*g* [20]. To further separate mucins from proteoglycans, anion-exchange HPLC was performed according to the method of Huet *et al.* [6].

Amino Acid Analysis

The samples were hydrolyzed in sealed tubes for 24 h in 5.6 *M* HCl at 105°C under vacuum. The hydrolysates were then applied through a Beckman 7300 amino acid analyzer (Palo Alto, CA) equipped with a high-performance sodium column (Beckman) to determine amino acid compositions.

Carbohydrate Composition

The carbohydrate composition was determined by gas chromatography after methanolysis (0.5 *M* hydrochloric acid–methanol for 24 h at 80°C), N-reacetylation, and trisilylation according to the method of Kamerling *et al.* [21], modified by Montreuil *et al.* [22].

Enzyme-Linked Immunosorbent Assay (ELISA)

The assays were performed in duplicate, as described in Emery *et al.* [23]. Monoclonal anti-T antibody BM22-19 [24] and monoclonal anti-Tn antibody Tn-5 [25] were kindly provided by Dr. Delannoy (Unité CNRS No. 111, Villeneuve d'Ascq, France) and biotinylated *Maackia amurensis* lectin was from Sigma. Mucins were plated overnight at 22°C on 96-well Maxisorb immunoplates and unbound sites were blocked with 4% bovine serum albumin (Sigma) in PBS. The plates were then washed six times with PBS–Tween 20 and antibodies or biotinylated lectins were added and left for 2 h at 37°C. After washing (×6) in the same buffer, mucins treated with antibodies were incubated with peroxidase-conjugated goat anti-mouse antibody (Jakson, Baltimore, MD) for 1 h at 37°C, while peroxidase-conjugated steptavidin (Pierce, Rockford, IL) was applied to the mucins treated with lectins. Plates were finally washed and the reaction was revealed using *O*-phenylenediamine (Sigma) at 1 mg/ml in 0.1 *M* phosphate–citrate buffer, pH 5.5, with 0.03% hydrogen peroxide. The reaction was stopped with 1 *N* HCl and the absorbance was measured at 492 nm. For neuraminidase treatment, after blocking reaction, the plates were incubated overnight with sialidase from 50 mU/ml *Clostridium perfringens* (Sigma) in 50 m*M* citrate buffer, pH 6.0, 0.9% NaCl, 0.1% $CaCl_2$ at 37°C prior to ELISA.

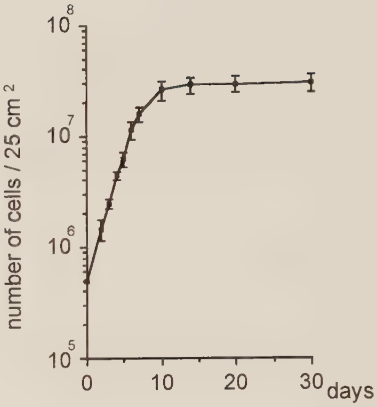

FIG. 1. Growth curve of HT-29 MTX cells. The values correspond to the mean of five different passages.

RESULTS

Glycosyltransferase Activities

Glycosyltransferase activities were comparatively analyzed in preconfluent HT-29 MTX cells (5 days after seeding) and postconfluent mucin-secreting cells (21 days after seeding). Five-day-cultured cells are undifferentiated, exponentially growing cells, as shown in Fig. 1. Cellular differentiation (mucus secretion, cell polarization, and cell to cell junction) starts after the cells have reached confluence (Day 7) and is optimum at Day 21 [7, 8].

Measurement of UDP-GalNAc:polypeptide N-acetylgalactosaminyltransferase activity. For the first step of the O-glycosylation reaction, the UDP-GalNAc:polypeptide *N*-acetylgalactosaminyltransferase activities (GalNAc transferase) from crude microsomal homogenates of cultured HT-29 MTX cells at two different stages of cellular differentiation (Days 5 and 21 after seeding) were assayed toward the peptide substrate TTSAPTTS. After elimination of the excess of UDP-GalNAc using anion-exchange chromatography, the GalNAc transferase activity was measured by the transfer of radiolabeled [^{3}H]GalNAc to the peptide substrate. The peptide motif TTSAPTTS containing six potential sites of O-glycosylation, in two clusters of hydroxyamino acids, was a good acceptor. Incorporation rates of 99.3 ± 1.2 nmol GalNAc/h/mg protein at Day

TABLE 1

In Vitro O-Glycosylation Assays

	Day 5	Day 21
UDPGalNAc:polypeptide *N*-acetylgalactosaminyltransferase (substrate TTSAPTTS)	99.3 ± 1.2	66.3 ± 1.3
3-β-galactosyltransferase (substrate benzyl-α-GalNAc)	57.5 ± 5.1	25 ± 0.5
ST3Gal I (substrate Galβ1-3GalNAc–α-paranitrophenol)	6.1 ± 0.5	14.6 ± 5.4

Note. Activities are expressed in nmol/h/mg protein.

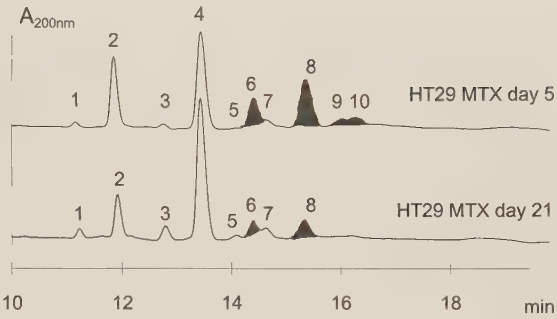

FIG. 2. Capillary electrophoresis profiles of *in vitro* O-glycosylated products. Peaks 6, 8, 9, and 10 correspond to the different forms of glycosylated peptide TTSAPTTS.

5 and 66.3 ± 1.3 nmol GalNAc/h/mg protein at Day 21 were obtained (Table 1). These times corresponded to stages at which no (Day 5) or extensive (Day 21) mucus was secreted by the cell layer. The incorporation activity in the peptide acceptor at Day 5 was thus 1.5-fold higher than that at Day 21.

To visualize the differences in O-glycosylation of the peptide by the different microsomal preparations, the samples were analyzed using electrophoretic techniques. Capillary electrophoresis, with the potential to give rapid separations with high resolution and good quantification [26], is a very powerful method with which to study the O-glycosylated products [17]. These products of O-glycosylation using microsomal HT-29 MTX preparations at Day 5 and Day 21 migrated between times of 10 and 16 min at 20 kV running voltage (Fig. 2). Under acidic conditions, electrophoresis gave very reproducible profiles, allowing us to compare the electrophoretic profiles obtained under different conditions (microsomal preparations incubated with or without UDP-GalNAc). The parent peptide was identified at 13.5 min (peak 4); the peaks 1–3, 5, and 7 were products resulting from the reaction between peptide and microsomes (mainly peptide proteolysis), whereas after addition of the second substrate UDP-GalNAc, extra fractions were found in peaks 6, 8, 9, and 10 corresponding to the glycopeptides (Fig. 2). The comparison of products obtained at Day 5 and Day 21 revealed the existence of two peaks of glycopeptides at Day 21 (peaks 6 and 8) and four peaks at Day 5 (peaks 6, 8, 9, and 10).

The analysis by electrospray mass spectrometry of the O-glycosylated products formed by the two microsomal preparations using the TTSAPTTS peptide (m/z = 765.4) showed the presence of one or two GalNAc O-linked to the peptide at Day 5 and only one GalNAc O-linked to the peptide at Day 21. The analysis by mass spectrometry of the products also revealed the addition of 2-threonine on the peptide backbone. The characterization of this dipeptidylaminotransferase activity is currently in progress. As shown in Fig. 3, different products have thus been identified as the unreacted TTSAPTTS peptide (m/z = 765.4), the 1-GalNAc O-linked peptides G1 (m/z = 968.5 TTSAPTTS-GalNAc and m/z = 1170.5 TTTTSAPTTS-GalNAc), and the 2-GalNAc O-linked peptide G2 (m/z = 1171.6 TTSAPTTS-2GalNAc). The ratio between the unreacted peptide and the glycosylated peptides was 5.1 at Day 5 and 18.4 at Day 21.

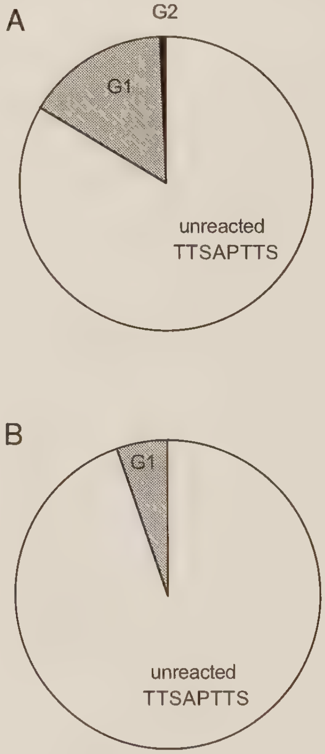

FIG. 3. Analysis by electrospray mass spectrometry of the relative proportion of the O-glycosylated products obtained with microsomal preparations of HT-29 MTX cells at Day 5 (A) and Day 21 (B). G1 corresponds to the glycopeptides TTSAPTTS–GalNAc m/z = 968.5 and TTTTSAPTTS–GalNAc m/z = 1170.5, while G2 is composed of the glycopeptide TTSAPTTS–2GalNAc m/z = 1171.5. The pies represent the relative proportion of the glycopeptides and the m/z = 765.5 unreacted TTSAPTTS peptide (deduced from values of cumulative signals obtained by the quadrupole detector).

Measurement of 3-β-galactosyltransferase. To analyze the subsequent steps of O-glycosylation reaction, core 1 UDP-Gal:GalNAc-R 3-β-galactosyltransferase (3-β-galactosyltransferase) activity issued from crude microsomal homogenates of cultured HT-29 MTX cells at Day 5 and Day 21 after seeding was assayed toward benzyl-α-GalNAc as exogenous substrate. After elimination of the excess of UDP-galactose using anion-exchange chromatography, the 3-β-galactosyltransferase activity was measured by the transfer of radiolabeled [^{14}C]galactose to the benzyl-α-GalNAc substrate. The incorporation activity was 2.3 times higher at Day 5 (57.5 ± 5.1 nmol/h/mg protein) than at Day 21 (25 ± 0.5 nmol/h/mg protein) (Table 1).

Measurement of the ST3Gal I. As the HT-29 MTX cells are known to synthesize highly sialylated mucins, the ST3Gal I activity was also tested using subconfluent (Day 5) and postconfluent (Day 21) cell homogenates. The use of Galβ1-3GalNAc–α-paranitrophenol allowed us to determine specifically the activity of the ST3Gal I [27]. The incorporation rates of [^{14}C]Neu5Ac on the substrate increased by 2.4-fold after late confluence (6.1 ± 0.5 nmol/h/mg protein at Day 5 and 14.6 ± 5.4 nmol/h/mg protein at Day 21) (Table 1).

Mucin Analysis

Mucin purification. We applied the procedure of mucin isolation to subconfluent and postconfluent cells, using ultracentrifugation and HPLC under the conditions previously described [6]. Eluates were collected in fractions which were analyzed for absorbance at 280 nm; orcinol reactivity was used to detect carbohydrate and dimethylmethylene blue (DMB) to detect glycosaminoglycans (Fig. 4). Mucins of HT-29 MTX postconfluent cells (at Day 21) were mainly eluted as a major peak with a retention time of 29 min, whereas proteoglycans eluted at later retention times (32–36 min) (Fig. 4B). A preparative HPLC was carried out for the postconfluent cells and the mucin fraction A (25–30 min) was collected. For HT-29 MTX cells at Day 5, no mucus could be detected at the surface of the cells. Indeed, while a high DMB reactivity was observed at retention times of 31–39 min (applying the same HPLC procedure to these subconfluent cells), only a very low orcinol reactivity was detected at the retention time of 24 min, indicating the absence of detectable mucins (Fig. 4A).

Amino acid analysis and carbohydrate composition of the mucins purified from the HT-29 MTX postconfluent cells. The preparative HPLC fraction A of HT-29 MTX cells at Day 21 was analyzed for amino acid content (Table 2). The hydroxy amino acid percentage and the Thr/Ser ratio were, respectively, 40.7% and 1.6 for fraction A, and a high proline content was observed (12.4%). High levels of sialic acid and galactose were found in the HPLC-purified fraction A from postconfluent cells and no mannose was detected (Table 3). These results are in total accordance with previously published amino acid analyses and carbohydrate composition of HPLC-purified HT-29 MTX mucins [6].

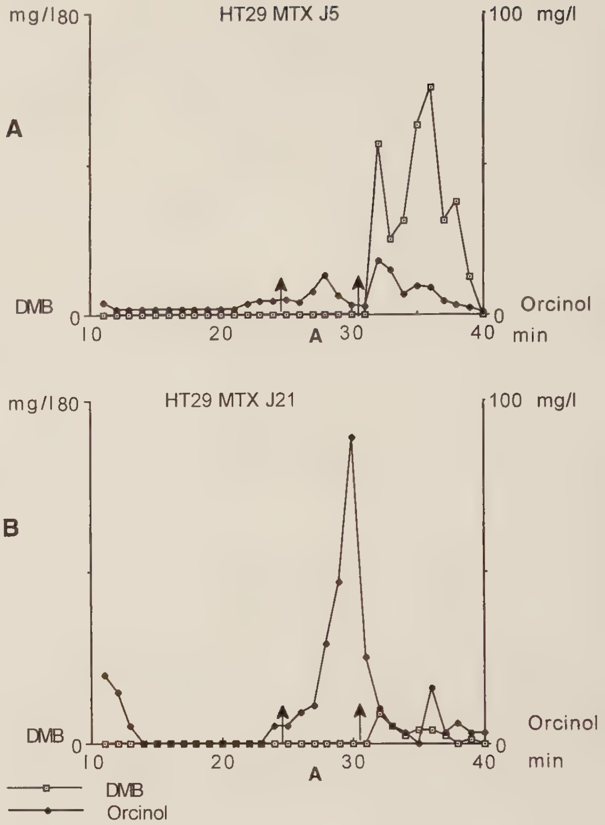

FIG. 4. HPLC profiles of ultracentrifuged preparation from HT-29 MTX cells. (A) Preconfluent HT-29 MTX cells at Day 5. (B) Postconfluent HT-29 MTX cells at Day 21.

Enzyme-linked immunosorbent assays. To further characterize the mucins synthesized by the cells at Day 21, the sensitive ELISA method was performed for fraction A obtained by preparative scale HPLC from postconfluent cells. The linkage of GalNAc or galactose was analyzed using antibodies directed to Tn (GalNAc–α-*O*-Thr/Ser) and T (Galβ1-3GalNAc–α-*O*-Thr/Ser) antigens, while *M. amurensis* lectin was used to detect sialic acid in an α-2,3 linkage. A slight immunoreactivity to the anti-Tn antibody was found (Fig. 5A) and the mucins were not immunoreactive to the T antibody (Fig. 5B). By contrast, mucins were highly reactive to *M. amurensis* lectin (Fig. 5C). After neuraminidase treatment, *M.* lectin reactivity disappeared (Fig. 5C), while an anti-T immunoreactivity appeared (Fig. 5B) and a slight increase in the anti-Tn immunoreactivity was observed (Fig. 5A).

DISCUSSION

Little is known concerning the O-glycosylation processes during cellular differentiation. The HT-29 MTX

TABLE 2

Amino Acid Analysis of HT-29 MTX HPLC Fraction A at Day 21 (%)

	A
Asx	4.28
Thr	25.02
Ser	15.73
Glx	6.20
Pro	12.33
Gly	6.49
Ala	6.97
Cys	0.67
Val	4.59
Met	0.74
Ile	2.66
Leu	3.10
Tyr	1.39
Phe	1.36
His	2.03
Lys	2.66
Arg	3.22

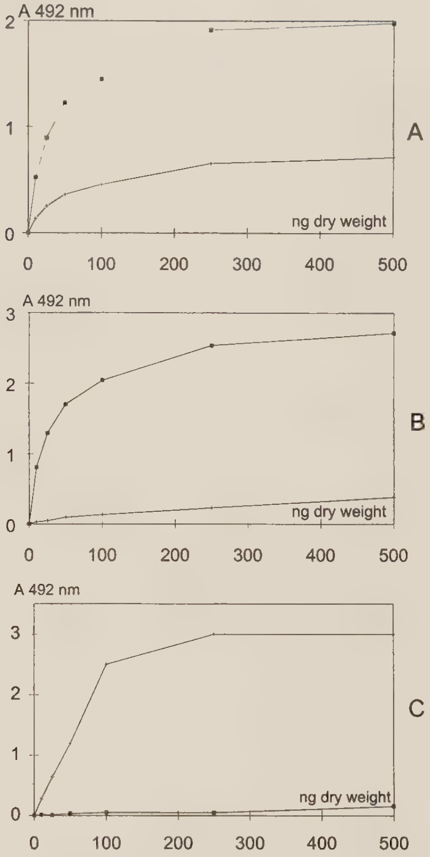

FIG. 5. Immunoassays with HT-29 MTX mucins purified by ultracentrifugation (■, with neuraminidase; +, without neuraminidase). (A) Immunoreactivity with the anti-Tn (Tn-5) antibody. (B) Immunoreactivity with the anti-T (BM-22.19) antibody. (C) Assays using the lectin from *M. amurensis* (MAA).

cell line is an excellent model for performing such a study, because these cells display a mucin-secreting phenotype with a growth-related cellular differentiation, starting after the cells have reached confluence [7, 8]. The mucus secretion is optimum after 21 days of culture. According to our results of mucin purification by ultracentrifugation and HPLC, a large amount of mucin can be collected from the cells at Day 21. Indeed, a high orcinol reactivity is detected in the HPLC-purified fraction A. This fraction A isolated from postconfluent HT-29 MTX cells is characterized by a high hydroxy amino acid content (40%), a Thr/Ser ratio of 1.6, a high proline content (12.4%), and a high sialic acid content, all structural features of mucins. For the preconfluent cells at Day 5, it is possible to collect a small amount of glycosylated product in the cells, by ultracentrifugation, but no mucin can be further purified by HPLC, as no orcinol reactivity is observed in preconfluent cells in fraction A, which normally contains the mucins. This lack of mucin synthesis is in accordance with morphological results showing a negative Alcian blue staining or no immunoreactivity of the cell layer to an anti-mucin antibody, 7 days after seeding [8]. Immunofluorescence techniques performed on frozen sections of postconfluent cells have demonstrated the reactivity of the mucus gel to *M. amurensis* lectin [8]. Using ELISA techniques, the high reactivity of the mucins from postconfluent cells (purified by ultracentrifugation and HPLC) to *M. amurensis* lectin was shown. This lectin specifically recognizes sialic acid in an α2-3 linkage to penultimate galactose residues [28]. Furthermore, as a T immunoreactivity is revealed after neuraminidase treatment of HT-29 MTX mucins, it can be assumed that these mucins mainly contain sialyl-α3-T antigen. These results can be related to the high level of activity at Day 21 of the ST3Gal I which transfers sialic acid in an α-2,3 linkage to Galβ1-3GalNAc [29] and is the major sialyltransferase expressed in HT-29 cells [30, 31]. Another important point concerning sialylation in HT-29 MTX cells is the increase of ST3Gal I activity during growth and cellular differentiation. These results are in accordance with a previous study of sialylation in HT-29 cells [30].

TABLE 3

Carbohydrate Composition of HT-29 MTX HPLC Fraction A at Day 21

	A
Gal	1.2
Man	ND
GalNAc	1
GlcNAc	0.6
Neu Ac	1.5

Note. ND, not detectable.

The pattern of activity is different concerning the evolution of 3-β-galactosyltransferase and GalNAc transferase during cellular differentiation. Concerning 3-β-galactosyltransferase, the incorporation rates of [^{14}C]galactose are much higher at Day 5 than at Day 21. The HT-29 MTX cells are known to have a high galactosyltransferase activity when the cells reach confluence, at Day 7 [32], but this enzyme activity seems to be already important even before confluence, at Day 5, when the cells do not yet synthesize mucins. In differentiated cells, in contrast, the enzyme activity is greatly decreased. Such a decrease in the activity of the 3-β-galactosyltransferase has already been described for the colonic cell line Caco-2 [18]. Although these cells express MUC genes and synthesize small amounts of mucin precursor [33], they display an enterocytic phenotype and mainly synthesize polylactosaminoglycans which contain some O-linked oligosaccharides [34]. 3-β-Galactosyltransferase is known to synthesize core 1 and core 2 mucins but is also involved in the synthesis of other membrane glycoproteins [35]. The high level of activity of this enzyme in preconfluent cells could thus be explained by an involvement of the enzyme in the synthesis of glycoproteins other than mucins in still undifferentiated cells.

For GalNAc transferase, the activity is 1.5 times higher in preconfluent cells than in postconfluent cells. Moreover, according to the mass spectrometry results, only one GalNAc is O-linked to the peptide in postconfluent differentiated cells, while the substitution by two GalNAc on the peptide acceptor is observed for subconfluent cells. The difference in the number of GalNAc linked to the peptide acceptor might be due to the higher GalNAc transferase activity in subconfluent cells than in postconfluent cells. But no change in the number of GalNAcs linked to the peptide acceptor has been observed when the microsomal preparations are incubated for a longer time (data not shown). This difference in the number of O-linked *N*-acetylgalactosamines could be due to the involvement of several GalNAc transferases in HT-29 MTX cells. Indeed, several GalNAc transferases have been described. GalNAc-T1 was purified from bovine colostrum and GalNAc-T2 was purified from human placenta. These transferases are encoded by two different genes, and the GalNAc-T1 gene is highly conserved and is also expressed in human tissues [36]. Furthermore, two other genes, coding for GalNAc-T3 and GalNAc-T4, have been cloned and sequenced [37]. The existence of a GalNAc transferase family is demonstrated and different GalNAc transferases could thus be expressed in the HT-29 MTX cells according to cellular growth and differentiation.

In conclusion, the glycosyltransferases display an evolving activity pathway in the growth and cellular differentiation of HT-29 MTX cells. The evolution differs according to the type of enzyme. ST3Gal I is highly efficient in postconfluent differentiated cells which produce mature mucins and its activity toward the mucins mainly results in sialyl-3-α-T antigen-type oligosaccharides, as shown by ELISA techniques. For initiation enzymes such as GalNAc transferases, the rate of activity decreases and the galactosaminylation of the peptide also tends to be more specific in postconfluent differentiated cells, suggesting that cellular growth and differentiation are accompanied by more regulated processes of glycosylation. Therefore, O-glycosylation processes can be influenced by both the growing state of the cells and the stage of differentiation.

We are very grateful to Dr. A. Zweibaum, who allowed us to publish the growth curves of HT-29 MTX cells. We also thank Mrs. B. Hemon and O. Moreau, who performed the cell cultures, and Mr. R. Groult and R. Just for technical assistance in capillary electrophoresis.

REFERENCES

1. Lesuffleur, T., Zweibaum, A., and Real, F. X. (1994) Mucins in normal and neoplastic human gastrointestinal tissues. *Crit. Rev. Oncol. Hematol.* **17,** 153–180.
2. Kim, Y. S., Gum, J., Jr., and Brockhausen, I. (1996) Mucin glycoproteins in neoplasia. *Glycoconjugate J.* **13,** 693–707.
3. Boland, C. R., and Deshmuckh, G. D. (1990) The carbohydrate composition of mucin in colonic cancer. *Gastroenterology* **98,** 1170–1177.
4. Capon, C., Laboisse, C., Wieruszeski, J. M., Maoret, J. J., Augeron, C., and Fovet, B. (1992) Oligosaccharide structures of mucins secreted by the human colonic cell line CL.16E. *J. Biol. Chem.* **267,** 19248–19257.
5. Lesuffleur, T., Barbat, A., Dussaulx, E., and Zweibaum, A. (1990) Growth adaptation to methotrexate of human colon carcinoma cells is associated with their ability to differentiate into columnar absorptive and mucus-secreting cells. *Cancer Res.* **50,** 6334–6343.
6. Huet, G., Kim, I., De Bolos, C., Lo-Guidice, J. M., Moreau, O., Hemon, B., Richet, C., Delannoy, P., Real, F. X., and Degand, P. (1995) Characterization of mucins and proteoglycans synthesized by a mucin-secreting HT-29 cell subpopulation. *J. Cell Sci.* **108,** 1275–1285.
7. Lesuffleur, T., Barbat, A., Luccioni, C., Beaumatin, J., Clair, M., Kornowski, A., Dussaulx, E., Dutrillaux, B., and Zweibaum, A. (1991) Dihydrofolate reductase gene amplification-associated shift of differentiation in methotrexate-adapted HT-29 cells. *J. Cell Biol.* **115,** 1409–1418.
8. Lesuffleur, T., Porchet, N., Aubert, J. P., Swallow, D., Gum, J. R., Kim, Y. S., Real, F. X., and Zweibaum, A. (1993) Differential expression of the human mucin genes MUC1 to MUC5 in relation to growth and differentiation of different mucus-secreting HT-29 cell subpopulations. *J. Cell Sci.* **106,** 771–783.
9. Gum, J. R., Byrd, J. C., Hicks, J. W., Toribara, N. W., Lamport, D. T. A., and Kim, Y. S. (1989) Molecular cloning of human intestinal mucin cDNAs. *J. Biol. Chem.* **264,** 6480–6487.
10. Gum, J. R., Hicks, J. W., Swallow, D., Lagace, R. L., Byrd, J. C., Lamport, D. T. A., Siddiki, B., and Kim, Y. S. (1990) Molecular cloning of cDNAs derived from a novel human intestinal mucin gene. *Biochem. Biophys. Res. Commun.* **171,** 407–415.
11. Audié, J. P., Janin, A., Porchet, N., Copin, M. C., Gosselin, B., and Aubert, J. P. (1993) Expression of human mucin genes in respiratory, digestive and reproductive tracts ascertained by in situ hybridization. *J. Histochem. Cytochem.* **41,** 1479–1485.
12. Guyonnet-Duperat, V., Audié, J. P., Debailleul, V., Laine, A.,

Buisine, M. P., Galiegue-Zouitina, S., Pigny, P., Degand, P., Aubert, J. P., and Porchet, N. (1995) Characterization of the human mucin gene MUC5AC: A consensus cysteine-rich domain for 11p15 mucin gene? *Biochem. J.* **305,** 211–219.

13. Toribara, N. W., Roberton, A. M., Ho, S. B., Kuo, W. L., Gum, E., Hicks, J. W., Gum, J. R., Byrd, J. C., Siddiki, B., and Kim, Y. S. (1993) Human gastric mucin. Identification of a unique species by expression cloning. *J. Biol. Chem.* **268,** 5879–5885.
14. Peterson, G. L. (1977) A simplification of the protein assay method of Lowry *et al.* which is more generally applicable. *Anal. Biochem.* **83,** 346–356.
15. Delannoy, P., Pelczar, H., Vandamme, V., and Verbert, A. (1993) Sialyltransferase activity in FR3T3 cells transformed with ras oncogen: Decreased CMP-NeuAc:Galβ1-3 GalNAc-α-2,3-sialyltransferase. *Glycoconjugate J.* **10,** 91–98.
16. Tetaert, D., Soudan, B., Lo-Guidice, J. M., Richet, C., Degand, P., Boussard, G., Mariller, C., and Spik, G. (1994) Combination of high-performance anion-exchange chromatography and electrospray mass spectrometry for analysis of the in vitro O-glycosylated mucin motif peptide. *J. Chromatogr. B* **658,** 31–38.
17. Hennebicq-Reig, S., Soudan, B., Tetaert, D., Briand, G., Richet, C., Demeyer, D., and Degand, P. (1996) Capillary electrophoresis separation of mucin motif MUC5AC glycopeptides from in vitro O-glycosylation reactions. *Carbohydr. Res.* **280,** 121–126.
18. Brockhausen, I., Romero, P. A., and Herscovics, A. (1991) Glycosyltransferase changes upon differentiation of Caco-2 human colonic adenocarcinoma cells. *Cancer Res.* **51,** 3136–3142.
19. Tetaert, D., Briand, G., Soudan, B., Richet, C., Demeyer, D., Boersma, A., and Degand, P. (1994) Analysis by electrospray mass spectrometry of glycopeptides from in vitro O-glycosylation reaction using human mucin motif peptide. *Anal. Biochem.* **222,** 409–416.
20. Houdret, N., Perini, J. M., Galabert, C., Scharfman, A., Humbert, P., Lamblin, G., and Roussel, P. (1986) The high lipid content of respiratory mucins in cystic fibrosis is related to infection. *Biochem. Biophys. Acta* **880,** 54–61.
21. Kamerling, J. P., Gerwig, G. J., Vliegenthart, J. F. G., and Clamp, J. R. (1975) Characterization by gas–liquid chromatography–mass spectrometry and proton magnetic-resonance spectroscopy of pertrimethylsilyl methyl glycosides obtained in the methanolysis of glycoproteins and glycopeptides. *Biochem. J.* **151,** 491–495.
22. Montreuil, J., Bouquelet, S., Debray, H., Fourquet, B., Spik, G., and Strecker, G. (1986) *in* Carbohydrate Analysis, a Practical Approach (Chaplin, M. F., and Kennedy, J. F., Eds.), pp. 143–204, IRL Press, Oxford.
23. Emery, N., Palfai, S. B., Place, G., Oriol, R., Hall, R. L., Roussel, P., and Lhermitte, M. (1995) A new monoclonal antibody (3D3) generated with human respiratory mucins and directed against Lewis determinants. *Glycobiology* **5,** 563–570.
24. Steuden, I., Duk, M., Czerwinski, M., Radzikowski, C., and Lisowska, E. (1985) The monoclonal antibody anti-asialoglycophorin from human erythrocytes specific for β-D-Gal-1, 3-α-D-GalNAc chains (Thomsen–Friedenreich receptors). *Glycoconjugate J.* **2,** 303–314.
25. Duk, M., Steuden, I., Dus, D., Radzikowski, C., and Lisowska, E. (1992) Application of chemically desialylated and degalactosylated human glycophorin for induction and characterization of anti-Tn monoclonal antibodies. *Glycoconjugate J.* **9,** 148–153.
26. Karger, B. L., and Foret, F. (1993) *in* "Capillary Electrophoresis Technology" (Guzman, N. A., and Dekker, M., Eds.), pp. 3–64, Dekker, New York.
27. Klohs, W. D., Matha, K. L., Bralow, J. J., and Bernaki, R. J. (1981) Phenyl 2 acetamido-2-deoxy-3-O-β-D-galactopyranosyl-α-D-galactopyranoside, a substrate for sialyltransferase. *Carbohydr. Res.* **89,** 350–354.
28. Wang, W. C., and Cummings, R. D. (1988) The immobolized leukoagglutinin from the seeds of Maackia amurensis binds with high affinity to complex-type Asn-linked oligosaccharides containing terminal sialic acid-linked α-2,3 to penultimate galactose residues. *J. Biol. Chem.* **263,** 4576–4585.
29. Harduin-Lepers, A., Recchi, M. A., and Delannoy, P. (1995) 1994, the year of sialyltransferases. *Glycobiology* **5,** 741–758.
30. Dall'Olio, F., Malagolini, N., Guerrini, S., and Serafini-Cessi, F. (1993) Resistance to methotrexate is associated with selective changes of α2,6-sialyltransferase activities toward *N*-acetyllactosaminic sequences in human colon cancer cell line HT-29. *Biochem. Biophys. Res. Commun.* **196,** 714–720.
31. Delannoy, P., Kim, I., Emery, N., De Bolos, C., Verbert, A., Degand, P., and Huet, G. (1996) Benzyl-*N*-acetyl-α-galactosaminide inhibits the sialylation and the secretion of mucins by a mucin secreting HT-29 cell subpopulation. *Glycoconjugate J.* **13,** 717–726.
32. Dahiya, R., Lesuffleur, T., Kwak, K. S., Byrd, J. C., Barbat, A., Zweibaum, A., and Kim, Y. S. (1992) Expression and characterization of mucins associated with the resistance to methotrexate of human colonic adenocarcinoma cell line HT-29. *Cancer Res.* **52,** 4655–4662.
33. Van Klinken, B. J. W., Oussoren, E., Weenik, J. J., Strous, G. J., Buller, H. A., Dekker, J., and Einerhand, A. W. C. (1996) The human intestinal cell lines Caco-2 and LS174T as models to study cell-type specific mucin expression. *Glycoconjugate J.* **13,** 757–768.
34. Youakim, A., and Herscovics, A. (1987) Differentiation-associated decrease in the proportion of fucosylated polylactosaminoglycans of Caco-2 human colonic adenocarcinoma cells. *Biochem. J.* **247,** 299–306.
35. Schachter, H., and Brockhausen, I. (1992) *in* Glycoconjugates, Composition, Structure and Function (Allen, H. J., and Kisailus, E. C., Eds.), pp. 263–332, Dekker, New York.
36. Clausen, H., and Bennett, E. P. (1996) A family of UDP-GalNAc:polypeptide *N*-acetylgalactosaminyl transferases control the initiation of mucin-type O-linked glycosylation. *Glycobiology* **6,** 635–646.
37. Bennett, E. P., Hassan, H., and Clausen, H. (1996) cDNA cloning and expression of a novel human UDP-*N*-acetyl-α-D-galactosamine polypeptide *N*-acetylgalactosaminyltransferase, GalNAc-T3. *J. Biol. Chem.* **271,** 17006–17012.

Received March 12, 1997
Revised version received May 12, 1997

EXPERIMENTAL CELL RESEARCH **235,** 108–116 (1997)
ARTICLE NO. EX973632

Priming of Mouse Macrophages with the Macrophage Colony-Stimulating Factor (CSF-1) Induces a Variety of Pathways That Regulate Expression of the Interleukin 6 (*Il6*) and Granulocyte–Macrophage Colony-Stimulating Factor (*Csfgm*) Genes

Sonya J. Kamdar, Jane A. Fuller, Shin-Ichi Nishikawa,* and Robert Evans[1]

*The Jackson Laboratory, Bar Harbor, Maine 04609; and *Department of Immunology, School of Life Science, Faculty of Medicine, Tottori University, Tottori, Japan*

Recent data have indicated that resident mouse peritoneal macrophages (PMø) transcribed the interleukin 6 (*Il6*) and granulocyte–macrophage colony-stimulating factor (*Csfgm*) genes in response to stimulation with the monocyte–macrophage colony-stimulating factor (CSF-1) but only *Il6* mRNA was translated into secreted protein. In this paper, we extend these observations. It is shown that resident PMø incubated with protein kinase (PK)C inhibitors, staurosporine (SP) and its derivative GF109203-X, showed a several fold increase in the levels of *Il6* mRNA in control and CSF-1-primed PMø and a parallel release of large amounts of protein. In contrast, SP was shown to have no effect on the release of GM-CSF from control or CSF-1-primed PMø, although it increased by approximately twofold the amount of *Csfgm* mRNA in CSF-1-primed Mø. When SP was added 4 h after CSF-1 priming to block CSF-1-induced protein kinase pathways, an increased amount of IL-6 release was again seen but without any increase in *Il6* mRNA levels. Under these conditions, *Csfgm* gene expression was relatively unaffected. Activation of PKC by phorbol myristate acetate (PMA) also resulted in increased *Il6* gene expression by control and CSF-1-primed PMø. PMA had no apparent effect on *Csfgm* transcription but appeared to influence translation at a low level, as measured by the release of small amounts of GM-CSF protein. The addition of lipopolysaccharide (LPS) to CSF-1-primed PMø resulted in a synergistic increase in the expression of both genes at the levels of transcription and protein release. The addition of SP to CSF-1-primed Mø before LPS, however, further enhanced IL-6 release but not GM-CSF release from the cells. The data indicate that CSF-1-priming drives a number of pathways involved in the regulation of expression of both genes and renders PMø highly susceptible to appropriate secondary stimulatory agents that transform the PMø into secretory inflammatory cells. © 1997 Academic Press

INTRODUCTION

It is well established that CSF-1 reacts with cells of the mononuclear phagocyte (MNP) lineage. Signaling is induced by the rapid phosphorylation of several proteins through protein tyrosine kinases associated with the CSF-1 receptor [1, 2]. How initial signaling events are linked to subsequent signal transduction pathways [3], particularly the activation of inflammatory cytokine genes, is not well understood. Although CSF-1 shows a high degree of specificity for MNP (as opposed to other cells types), it is evident that MNP subpopulations do not respond identically to CSF-1. For example, it was reported that resident murine peritoneal macrophages (PMø) responded to CSF-1 by transcribing the genes encoding the inflammatory proteins interleukin (IL)-6 [4], IL-1α, IL-1β, and granulocyte–macrophage colony-stimulating factor (GM-CSF), but not TNFα [5], while blood monocytes and thioglycollate-elicited PMø did not respond to CSF-1 in this way [4]. As shown by others, these last two subpopulations proliferate better than resident PMø in response to CSF-1 [6]. Indeed, blood monocytes and elicited PMø share several properties that clearly distinguish them from resident PMø [7–9]. Thus, it is evident that generalizations concerning the responsiveness of MNP subpopulations to CSF-1 in terms of their role in inflammatory responses cannot be made. In the present work, we use resident PMø as a heterogeneous population of Mø that are highly reactive to CSF-1 in terms of transcribing defined cytokine genes and are considered as proinflammatory MNP that have passed through a biological barrier to

---

[1] To whom reprint requests should be addressed at The Jackson Laboratory, 600 Maine Street, Bar Harbor, ME 04609. Fax: (207) 288-6079. E-mail: revans@jax.org.

0014-4827/97 $25.00
Copyright © 1997 by Academic Press
All rights of reproduction in any form reserved.

enter the peritoneal cavity but have not been exposed to inflammatory signals.

In terms of the role of second messengers following CSF-1-induced transduction, several lines of evidence suggest that CSF-1, protein kinase C (PKC) activity, and *Il6* gene expression may be linked. For example, CSF-1 treatment of human monocytes [10] or rat Kupffer cells [11] has been reported to activate the transcription factor NF-κB, which binds to the promoter of the *Il6* and *Csfgm* genes. This transcription factor, in turn, may be regulated by PKC-dependent and -independent mechanisms [12, 13]. Increased PKC activity has been reported following the interaction of CSF-1 with a variety of human and murine MNP subpopulations [10, 14, 15]. It has been reported that adherent human monocytes responded to CSF-1 by releasing IL-6 [16] and that constitutive IL-6 release was enhanced after incubating a mouse macrophage line with PKC inhibitors [17]. In the context of CSF-1-primed PMø, there is no information as far as we are aware on the pathways likely to be involved in regulating cytokine gene expression. We recently showed that *Il6* gene expression by resident PMø was regulated by PKC-dependent and -independent pathways [18].

The present work is based on the observation that CSF-1-priming of resident PMø results in increased transcription of the *Il6* and *Csfgm* genes with translation only of the *Il6* gene. This suggested activation of a common pathway up to the transcription stage but the involvement of different regulatory pathways subsequent to transcription. The questions addressed in this present paper are to what extent the expression of the *Il6* and *Csfgm* genes are regulated differently and whether the genes were activated to the same extent when the CSF-1-primed PMø were exposed to secondary stimulation by phorbol myristate acetate (PMA) or lipopolysaccharide (LPS). The data suggest that CSF-1 activates a number of pathways involved in the regulation of expression of both genes and renders PMø highly susceptible to appropriate secondary stimulatory agents that transform the PMø into secretory inflammatory cells.

MATERIALS AND METHODS

Mice. C57BL/6J (B6) male mice, 10–12 weeks of age, were obtained from The Jackson Laboratory Production Unit. NOD/LtSz mice homozygous for the severe combined immunodeficiency (*scid*) mutation of the same age were generously provided by Dr. David Serreze.

Culture medium and reagents. RPMI 1640 medium was supplemented with 2-mercaptoethanol (5×10^{-5} *M*) and gentamicin (50 μg/ml, Sigma Chemical Co., St. Louis, MO) and used either without the addition of serum or with 10% heat-inactivated fetal bovine serum (FBS, Atlanta Biologicals, Norcross, GA). Recombinant human CSF-1 (CSF-1 with an activity of 7×10^7 units/mg, generously provided by Chiron Corp., Emeryville, CA) was used in most experiments at a concentration of 0.143 μg/ml (=10^4 Chiron units), the optimal dose for the induction of cytokine gene expression by resident PMø established previously [5]. A rat monoclonal antibody to the murine CSF-1 receptor (c-fms) was prepared as reported recently [19]. Staurosporine (SP), bisindolylmaleimide X (GF-109203X), an analog of SP reported to have an improved selectivity for PKC isotypes over several tyrosine kinases compared with SP [20], and phorbol 12-myristate 13-acetate (all from LC Labs., Woburn, MA) were solubilized in DMSO, ethanol, and DMSO, respectively, as recommended by the manufacturer and used as described in the text. Neither solvent was toxic to macrophages at the concentrations cited in the text. All reagents including medium, serum, and CSF-1 were routinely checked for endotoxin contamination and found to contain no detectable activity at the concentrations used, as measured in the Limulus assay (Sigma).

Resident peritoneal macrophages. These were prepared by washing out the cavity with RPMI without prior stimulation, as fully described recently [4]. Peritoneal cells were used in suspension in polypropylene tubes to minimize adhesion and to aid in the extraction of RNA for mRNA analysis by the reverse transcriptase–polymerase chain reaction (RT-PCR, see below). Previous data indicated that peritoneal T and B cells did not contribute to the constitutive, CSF-1-induced, or LPS-induced IL-6 release [4, 5]. Because of this, together with the fact that the binding of CSF-1 is relatively specific for mononuclear phagocytes, the suspension cultures are referred to operationally as resident PMø.

Flow cytometry. Resident peritoneal cells were isolated and incubated with 10% FBS, CSF-1, or graded doses of PMA, as described in the text. After 1 h, the cells were fixed in cold 2% paraformaldehyde for 15 min at room temperature. The fixed cells were then processed for flow cytometric analysis using a Becton–Dickinson FACscan, as described previously [5]. In brief, the fixed cells were washed in Dulbecco's PBS and stained with FITC-labeled monoclonal antibody to F4/80 and biotinylated antibody to c-fms in the presence of phycoerythrin–streptavidin.

RNA extraction and RT-PCR. Total cellular RNA was extracted by a modified procedure described by Ogretmen and Safa [21] and analyzed for *Il6, Csfgm,* and β-actin (*act-b*) mRNA levels by RT-PCR using gene-specific primers. For signal detection, [^{32}P]dCTP (Amersham Corp., Arlington Heights, CT) was incorporated into the PCR mixture. Samples were electrophoresed on a 5% polyacrylamide gel and then exposed to a Fuji Imaging plate. Signals were analyzed using a Fuji bioimaging analyzer and normalized relative to the *act-b* signal. Data are expressed as relative mRNA levels.

Assays. Supernatant IL-6 and GM-CSF proteins were assayed using enzyme-linked immunoabsorbent assays (ELISAs) developed in this laboratory. For the IL-6 ELISA, two monoclonal antibodies derived from hybridoma clones MP5-20F3 and MP5-32C11 (ATCC by arrangement with DNAX, Palo Alto, CA) were used. The assay had a lower sensitivity of $\leq$35 pg/ml. Data are expressed as nanograms of IL-6 protein per milliliter. For the GM-CSF ELISA, the monoclonal antibodies (clones MPI-22E9 and MP1-31G6, ATCC by arrangement with DNAX) were used. This had a lower sensitivity of $\approx$15 pg/ml. Data are expressed as picograms of protein per milliliter.

Statistics. All data were analyzed by using Student's *t* test (StatView, Abacus Concepts, Inc., Berkeley, CA), whereby a value of $P < 0.05$ was used to denote that the value of the test sample was significantly different from that of the control.

RESULTS

Protein Kinase Inhibitors Influence Expression of the Il6 and Csfgm Genes

Recent data indicated that the optimal effects on *Il6* gene expression in resident PMø were induced by 6 n*M*

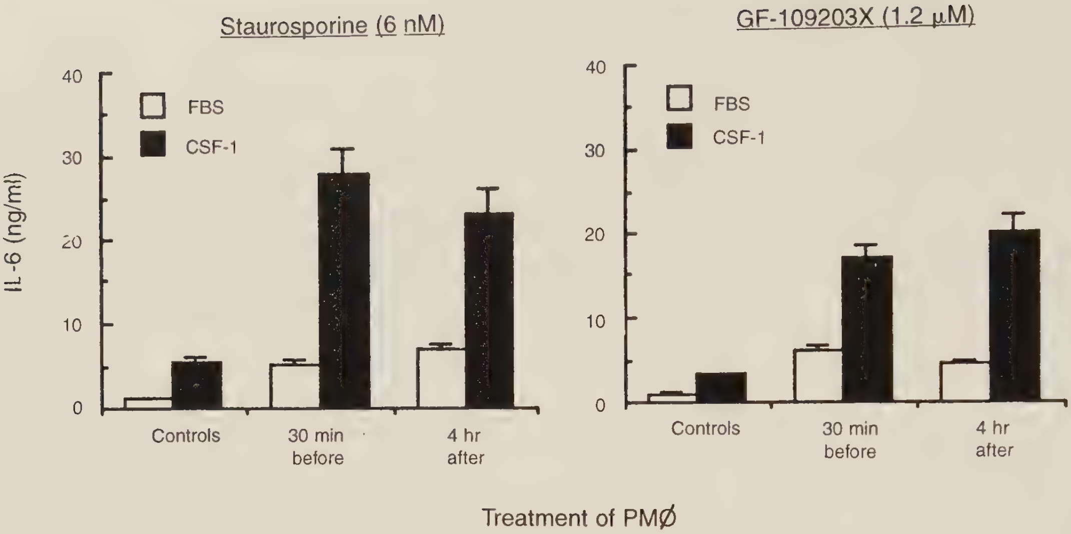

FIG. 1. The second signal inhibitors staurosporine (SP) and GF-109203X enhance IL-6 release from control FBS and CSF-1-primed PMø. SP (6 n*M*) or GF-109203X (1.2 μ*M*) was added to PMø either 30 min before or 4 h after CSF-1. IL-6 release was assayed 4 h after the addition of the inhibitors. SEM are also shown.

SP and 1.2 μ*M* GF-109203X [18]. The inhibitors were added to PMø at two different time points: (i) 30 min before the addition of CSF-1 to determine whether gene transcription resulting from CSF-1 priming might be negatively or positively regulated by undefined protein kinases; and (ii) 4 h after CSF-1 to determine whether PKs influenced ongoing gene expression. As reported previously, maximal *Il6* and *Csfgm* gene transcription occurred by about 4 h after the addition of CSF-1 [5]. Culture supernatants were assayed for IL-6 and GM-CSF 4 h after adding the inhibitors. RNA was also extracted (after SP treatment only) and amplified by RT-PCR using gene-specific primers. The data in Fig. 1 show that IL-6 release from control and CSF-1-treated PMø was considerably enhanced whether the inhibitors were added before or after CSF-1. However, neither inhibitor induced GM-CSF protein release above the low or undetectable constitutive levels (≤15 pg/ml) (data not shown). Analysis of mRNA levels indicated that when SP was added before CSF-1 (Fig. 2a), constitutive and CSF-1-induced expression of the *Il6* gene was elevated (3 to 4-fold) but in the case of *Csfgm* mRNA, SP significantly increased mRNA levels (*P* value 0.0006), inducing a 1.8- to 2.3-fold increase in different experiments. In addition, as shown in Fig. 2b, when SP was added 4 h after CSF-1, the inhibitor had no effect on *Il6* mRNA levels but appeared to slow the rate of reduction of *Csfgm* mRNA in the primed Mø. At the time of RNA extraction (8 h after CSF-1 priming), mRNA levels have been reported to be very low or undetectable by Northern analysis [5].

The enhancing effects of SP and GF109203-X on *Il6* gene expression were shown to be directed primarily toward PMø and not contaminating peritoneal T or B cells. This was shown by preincubating NOD-*scid* peritoneal cells containing ≈90% macrophages and <1% T or B cells [5] with either inhibitor followed by the addition of CSF-1. IL-6 release was assayed after overnight incubation. The data indicated the following: control NOD-*scid* PMø released 1.03 ng IL-6/ml compared with 5.67 or 2.1 ng after SP or GF109203-X treatment, respectively, and CSF-1-primed PMø released 9.6 ng/ml compared with 49.6 or 37.4 ng/ml after SP or GF109203-X treatment, respectively. In addition, we have shown that purified peritoneal B and T cells, as well as B6 mouse spleen cell populations (containing ≈60% B cells and 25% T cells), do not respond to CSF-1 ± SP in terms of IL-6 or GM-CSF release (unpublished data).

PKC Activation Enhances IL-6 and GM-CSF Release

To determine whether the action of the inhibitors was likely to be directed mainly toward PKC, we tested the hypothesis that activation of PKC by PMA should inhibit *Il6* gene expression seen in control and CSF-1-primed PMø as well as *Csfgm* gene expression in primed Mø. Thus, PMø were preincubated with CSF-1 for 4 h to induce maximal transcription, at which time graded doses of PMA were added to activate PKC. After an additional 4-h incubation, protein release and mRNA levels were assessed. The data in Fig. 3a show that PMA enhanced IL-6 release from control FBS and CSF-1-primed PMø in a dose-dependent manner, with the levels at 0.16 and 1.6 μ*M* being significantly higher compared with those at 0.016 μ*M*

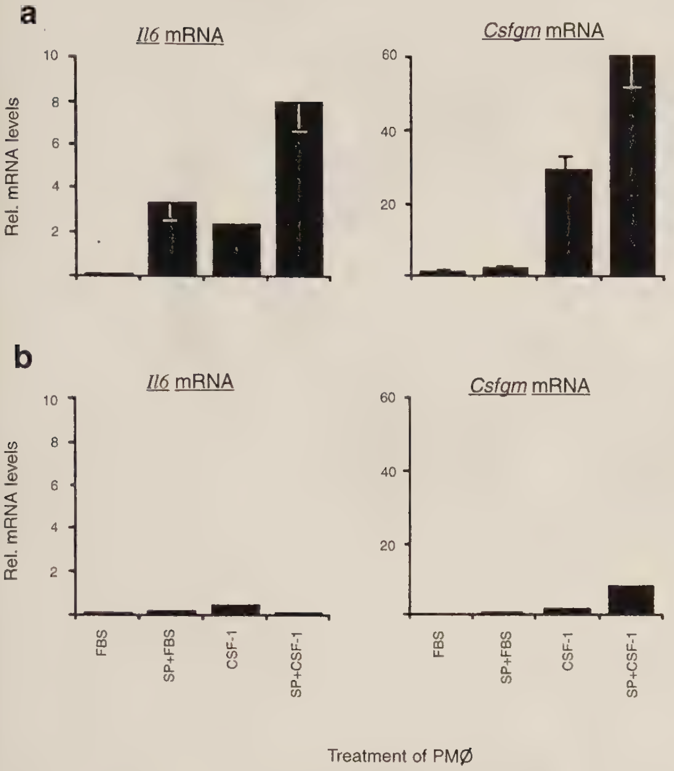

FIG. 2. The effect of SP on *Il6* gene transcription in control and CSF-1-primed PMø. SP (6 n*M*) was added to PMø (a) 30 min before or (b) 4 h after CSF-1. RNA was extracted 4 h after the addition of SP and amplified by RT-PCR.

or in untreated cultures ($P < 0.05$). PMA also induced a small but significant increase in constitutive GM-CSF release but had no additional effect in CSF-1-primed cultures. Figure 3b shows the relative mRNA levels. By 8 h of incubation (4 h after adding PMA to the cultures), *Il6* mRNA levels were barely amplifiable in control cultures and were at a low level in the CSF-1-primed PMø (no PMA, assigned a value of 1). In the presence of PMA, both control and CSF-1-primed Mø showed an increase only at the highest concentration. The levels of *Csfgm* mRNA by 8 h (no PMA) were also very low and it was also apparent that PMA induced little change in mRNA levels.

In all experiments involving PMA, activation of PKC was detected indirectly by its ability to down-regulate the expression of the *c-fms* gene product (the CSF-1 receptor). This was determined by two-color flow cytometric analysis of Mø expressing c-fms and F4/80. PMø were incubated in 10% FBS, CSF-1, or graded concentrations of PMA for 1 h, fixed with paraformaldehyde and stained as described under Materials and Methods. Cells were also fixed immediately on isolation from the peritoneal cavity (t = 0 h) to show any changes that might have occurred after 1 h of incubation. The data in Fig. 4 show that PMø incubated in CSF-1 or graded amounts of PMA for 1 h showed almost total down-regulation of c-fms expression, compared with cells incubated in FBS or fixed immediately on isolation. This down-regulation was seen to abrogate the typical IL-6 response to CSF-1 priming, while the PMA-induced enhancement of the constitutive IL-6 release, as described in Fig. 3a, was unchanged (data not shown).

LPS Superinduces IL6 and Csfgm Gene Expression in CSF-1-Primed PMø

Previous data indicated that when LPS was added to CSF-1-primed Mø, a synergistic IL-6 response was seen in that the large amounts of IL-6 released were greater than the sum of the amounts released after the individual treatments [4]. To determine whether LPS induced translation of *Csfgm* mRNA induced by CSF-1 priming, PMø were incubated for 4 h with CSF-1 to induce maximum levels of mRNA, at which time graded doses of LPS were added. Supernatants were assayed after a 20-h incubation for IL-6 and GM-CSF release and RNA was extracted at intervals. The data in Fig. 5 show that in control FBS cultures, a minimum of 0.25 ng LPS/ml was required to elicit an IL-6 response, while a minimum of 1.25 ng/ml was required to induce a significant GM-CSF response compared with release in the control FBS cultures ($P < 0.05$). Over the course of several experiments, the minimum amount required to induce release of either protein ranged from 0.1–0.25 ng/ml for IL-6 to 0.5–1.0 ng/ml for GM-CSF. However, when LPS was added to CSF-1-primed PMø, at least fivefold less LPS was required to elicit expression of both genes and the amount of protein released was clearly the result of synergy between the action of CSF-1 and LPS. Figure 6 show the transcriptional response to a single dose of LPS (1 ng/ml) in the presence and absence of CSF-1 over the initial 8 h of culture. It is seen that CSF priming resulted in peak *Il6* and *Csfgm* mRNA by 4–6 h, while LPS induced peak levels by 2 h. When both CSF-1 and LPS were present, gene transcription was amplified at all time points.

Despite the finding that LPS induced full activation of both genes, the addition of SP before LPS activation indicated that different regulatory pathways were involved. This was shown by priming PMø with CSF-1 for 4 h, followed by the addition of SP (6 n*M*) 5 min before LPS (1 ng/ml). The data in Fig. 7 show that SP enhanced the amount of IL-6 released in response to LPS, while GM-CSF release was unaffected by the presence of SP. The numbers in parentheses refer to the *P* values (see legend to Fig. 7).

DISCUSSION

Although SP and GF-109203X were used as established PKC-inhibiting agents, it is clear that they may

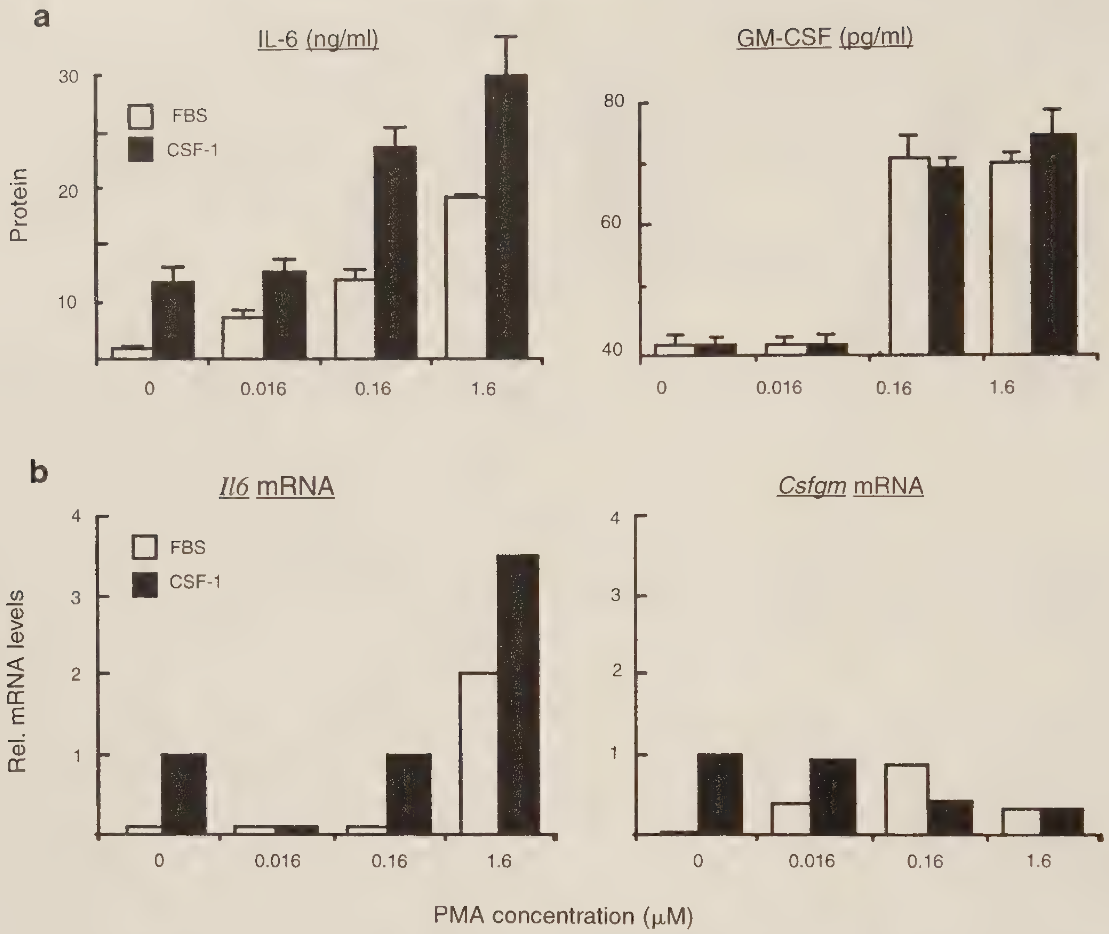

FIG. 3. The effect of activation of PKC by PMA on *Il6* and *Csfgm* gene expression. PMø were incubated for 4 h with CSF-1 followed by the addition of graded doses of PMA. (a) IL-6 and GM-CSF protein and (b) mRNA levels were assayed 4 h after the addition of PMA.

inhibit other PKs [20, 22, 23]. Thus, although it is likely that PKC was inhibited at the concentrations used, other PKs were also likely to be affected. In view of this, we tentatively conclude that the ability of the inhibitors to up-regulate *Il6* gene expression in both control and CSF-1-primed PMø indicates the presence of an inhibitable endogenous PK-dependent pathway that serves to down-regulate or repress *Il6* gene expression. The data also suggest two possible roles for CSF-1 when it activates *Il6* gene transcription. First, CSF-1 may enhance the extant constitutive pathway regulating *Il6* transcription in a direct manner, for example, by activating NF-κB [10]. Second, CSF-1 may mimic SP and GF109203X by activating a pathway that itself may down-regulate a similar repressor pathway modulating constitutive *Il6* gene expression. Interestingly, it was recently reported that to enhance constitutive *Il6* gene expression by the inhibitors, higher concentrations were required than needed to enhance gene expression in CSF-1-primed PMø [18]. This would support the notion that, in primed PMø, the inhibitors were effective at lower concentrations because CSF-1 complemented their inhibitory action. Since *Csfgm* gene transcription was also activated by CSF-1 and enhanced by SP, it seems likely that the same or similar pathways were involved in the transcriptional regulation of this gene. However, the lack of detectable GM-CSF secretion in CSF-1-primed PMø (with or without the inhibitors) clearly indicated that the *Csfgm* gene uses different posttranscriptional pathways from those used by the *Il6* gene. At this time, it is not clear whether the increased levels of mRNA seen when SP was added to PMø before CSF-1 signified increased transcription rates or stabilization of mRNA, either of which would explain the higher levels of IL-6 protein release. The fact that SP induced a further increase in IL-6 release when it was added 4 h after CSF-1 but did not augment mRNA levels (at least as measured 4 h later) might suggest that SP induced stability of transcribed mRNA. If this were so, then the data would imply that SP inhibited PKs that were involved in the destabilization/degradation of both *Il6* and *Csfgm* mRNA. The latter

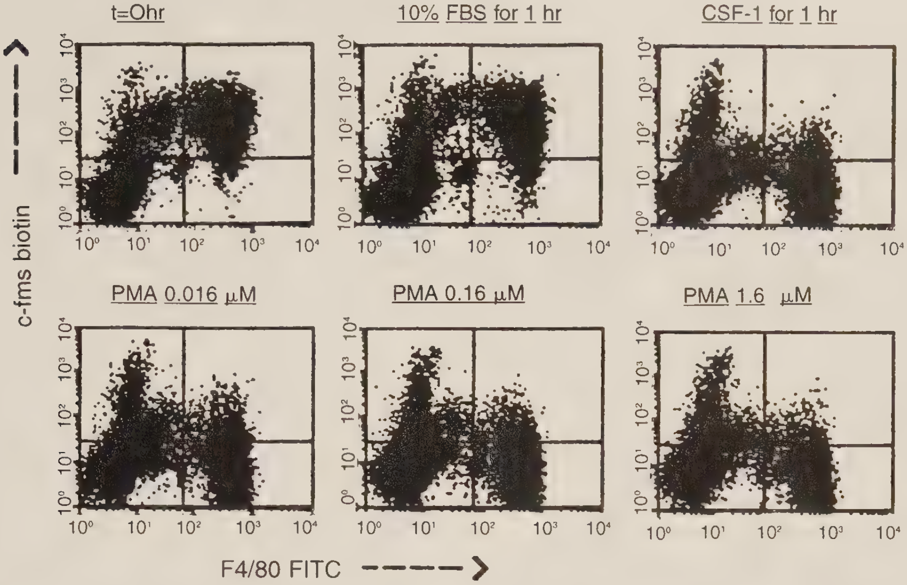

FIG. 4. PMA down-regulates expression of CSF-1 receptors (c-fms). PMø were incubated with graded doses of PMA, with CSF-1, or with 10% FBS for 1 h. The cells were then fixed in 2% paraformaldehyde and analyzed for expression of F4/80 and c-fms. Cells were also fixed immediately on isolation from the peritoneal cavity.

mRNA has been reported to be relatively unstable in diploid cell types and to require a secondary stimulus to induce stabilization for subsequent translation and protein release [24–28]. However, if SP treatment resulted in stabilization of mRNA, it is evident that under these conditions its inhibitory activities did not influence pathways regulating *Csfgm* translation or secretion of the gene product.

On the assumption that undefined endogenous PKs were involved in the modulation of *Il6* and *Csfgm* gene expression, an issue raised was to what extent, if any, PKC was involved. The use of the PKC activator PMA indicated that PKC was not likely to be involved in the proposed endogenous down-regulatory pathways. It was seen that the activation of PKC, rather than down-regulating *Il6* gene expression, augmented mRNA levels in and protein release from control and CSF-1-primed PMø. It was seen that by 4 h after adding graded doses of PMA to control or CSF-1-primed Mø, the levels of *Il6* mRNA were relatively low at 0.016 and

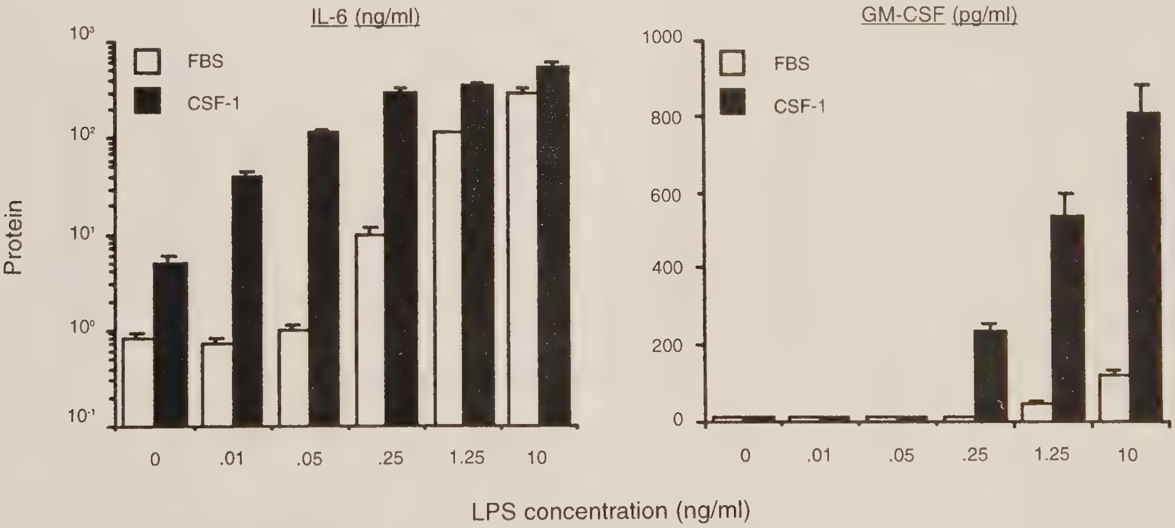

FIG. 5. LPS induces a synergistic release of IL-6 and GM-CSF from CSF-1-primed PMø. Cells were incubated for 4 h with CSF-1 followed by graded doses of LPS. Supernatants were assayed 20 h later.

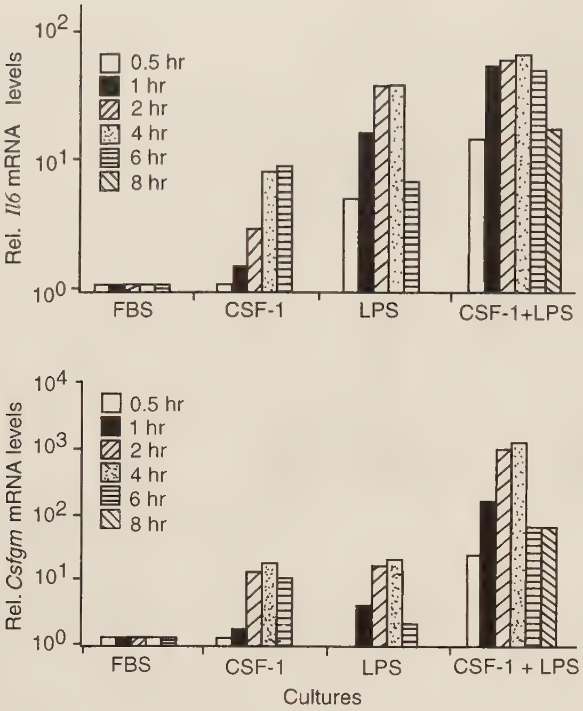

FIG. 6. LPS augments *Il6* and *Csfgm* mRNA levels in CSF-1-primed PMø. Cells were incubated for 4 h with CSF-1 at which time a single dose of LPS (1 ng/ml) was added. RNA was extracted at intervals over the initial 8 h of culture.

0.16 μM. Since by 4 h the levels of protein secretion were increased in parallel to the amount of PMA added, these data suggested that activation of PKC facilitated translation, thereby accounting for the decline in mRNA in the presence of these concentrations of PMA. However, the relatively high levels of *Il6* mRNA levels seen in the presence of 1.6 μM PMA also suggested that PKC augmented transcription. Overall, these data, together with the assumption that SP and GF109203-X inhibited PKC, would suggest that in resident PMø both PKC-dependent and PKC-independent pathways may regulate *Il6* gene expression. They also confirm a recent report showing that PMA enhanced *Il6* gene expression in PMø [18]. As suggested above, one candidate pathway for the PMA-enhanced *Il6* gene expression in control and CSF-1-primed PMø might involve activated NF-κB, which promotes *Il6* gene transcription. Both PMA and CSF-1 are reported to induce translocation of this transcription factor in MNP subpopulations [10, 11, 29].

In the context of *Csfgm* gene expression, activation of PKC was associated with the release of relatively small amounts of GM-CSF over a 4-h period (approximately twofold above background) regardless of whether the PMø had been primed. This low level of release, together with the observations that the PMA treatment did not induce high levels of *Csfgm* mRNA, suggested that PKC activation did not result in enhanced transcription but may have facilitated translation of the small amount of mRNA found in control PMø. The finding that the inhibition of PKC by SP was associated with increased *Csfgm* mRNA levels in primed Mø would support the view that PKC was not a requirement for gene transcription in resident PMø. However, if PKC was involved in posttranscriptional

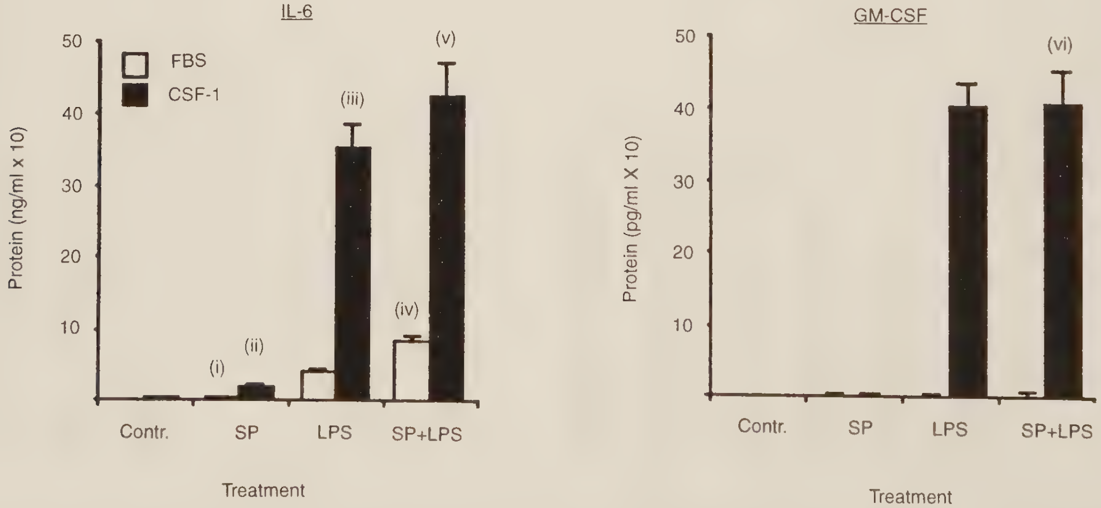

FIG. 7. SP enhances IL-6 release in PMø incubated with both CSF-1 and LPS but exerts no effect on GM-CSF release. PMø were incubated with CSF-1 for 4 h followed by the addition of SP (6 n*M*). LPS (1 ng/ml) was added 5 min later. Supernatants were assayed 20 h later. The *P* values are shown in parentheses: (i) FBS + SP vs FBS control ($P = 0.011$); (ii) CSF-1 + SP vs CSF-1 control ($P = 0.001$); (iii) LPS + CSF-1 vs LPS control in FBS ($P < 0.001$); (iv) SP + LPS vs LPS control ($P < 0.001$); (v) CSF-1 + SP + LPS vs CSF-1 + LPS ($P = 0.041$); (vi) CSF-1 + SP + LPS vs LPS control ($P = 0.982$).

events, the question arises why activation of PKC had no influence on translation of the relatively high levels of *Csfgm* mRNA present in CSF-1-primed Mø at the time PMA was added to the cells [5]. A simplistic explanation might be that PKC plays only a minor role in *Csfgm* gene expression (perhaps at the beginning or the end of a cascade of reactions) and, unless further signaling occurs, it can evoke only minimal translation of mRNA. Thus, when comparing the expression of the *Il6* and *Csfgm* genes, it is evident that PKC activation has a potent activation potential for the former but not for the latter gene.

It was evident that LPS provided the necessary signaling to transform the Mø into inflammatory cells based on increased constitutive mRNA levels and the relatively large quantities of IL-6 and GM-CSF released. Of note was the ability of LPS to synergize with CSF-1, thereby confirming a previous observation that such a synergistic response resulted in high *Il6* gene expression [4] and extending it by showing that synergy was also manifested by a *Csfgm* gene response. The pathways involved during the synergistic responses have yet to be determined. LPS-induced signal transduction in macrophages results in an extremely complex network of pathways [30, 31], as exemplified by reports that LPS and CSF-1 (as well as phorbol esters) activate an initial common pathway involving protein tyrosine kinases, ras and ref proteins, and mitogen-activated protein kinases [30–32]. While one may also speculate that enhanced transcription occurs via activation of NF-κB, cooperative effects among other transcription factors (AP-1, NF-AT, or NF-IL-6) are also a possibility [30, 31, 33]. In addition, the finding that LPS activation of PMø increased the stability of *Csfgm* mRNA via posttranscriptional events [34] suggests how large amounts of mRNA may accumulate. The finding that SP added to CSF-1-primed PMø before LPS significantly enhanced IL-6 protein release, but did not augment LPS-induced GM-CSF release, would appear to confirm the data summarized in Fig. 2b when only IL-6 protein release was affected by SP treatment.

In conclusion, it is evident that while CSF-1-priming appears to activate a common pathway that regulates the transcription of the *Il6* and *Csfgm* genes, it also appears to activate pathways that preferentially influence the expression of the *Il6* gene rather than the *Csfgm* gene. Clearly, CSF-1 is able to provide the full activating sequence of signals for *Il6* gene expression resulting in the secretion of copious amounts of IL-6 protein. However, the identity of these signals remains to be determined. Whether CSF-1 activates gene expression in a direct manner by intracellular signaling or induces secondary effects, such as the rapid release of biological mediators that act in an autocrine manner also remains to be determined. However, it is evident that these signals appear to be modulated by one or more inhibitable repressor pathways and that PKC is not involved in this negative regulation of gene expression. Indeed, PKC activation was shown to up-regulate *Il6* gene expression, but not *Csfgm* expression, in its own right. The use of LPS, a potent activator of MNP, appeared to show no discrimination in terms of the successful activation of both genes but the use of SP again suggested that inhibitable PKs preferentially regulated *Il6* gene expression. Overall, these data indicate that resident PMø, as a subpopulation of MNP, have immense inflammatory potential and, depending on the inflammatory cytokine gene, require appropriate secondary stimulation. It seems likely that the regulation of gene expression safeguards against the indiscriminate release of cytokines in the circulation or at noninflammatory sites where excessive quantities of cytokines may be harmful.

This publication was supported by PHS Grants CA27523 and CA34196 awarded by the National Cancer Institute. The authors express their appreciation to Drs. Len Shultz and David Serreze for their insightful comments. The Jackson Laboratory is fully accredited by the American Association for the Accreditation for Laboratory Animal Care.

REFERENCES

1. Sengupta, A., Liu, W.-K., Yeung, Y. G., Yeung, D. C. Y., Frackelton, A. R., Jr., and Stanley, E. R. (1988) *Proc. Natl. Acad. Sci. USA* **85,** 8062–8066.
2. Roussel, M. F. (1994) *J. Cell. Sci. Suppl.* **18,** 105–108.
3. Haiyan, E. C., Chang, S., Trub, T., and Neel, B. G. (1996) *Mol. Cell. Biol.* **16,** 3685–3697.
4. Kamdar, S. J., Chapoval, A. I., Phelps, J., Fuller, J. A., and Evans, R. (1996) *Cell. Immunol.* **174,** 165–172.
5. Evans, R., Kamdar, S. J., Fuller, J. A., and Krupke, D. M. (1995) *J. Leukocyte Biol.* **58,** 99–107.
6. Stanley, E. R., Chen, D.-M., and Lin, H.-S. (1978) *Nature* **274,** 168–170.
7. Weiel, J. E., Adams, D. O., and Hamilton, T. A. (1984) *Cell. Immunol.* **88,** 343–349.
8. Bursuker, I., and Goldman, R. (1983) *J. Reticuloendothel. Soc.* **33,** 207–220.
9. Iwama, A., Wang, M.-H., Yamaguchi, N., Ohno, N., Okano, K., Sudo, K., Takeya, M., Gervais, F., Morissette, C., Leonard, E. J., and Suda, T. (1995) *Blood* **86,** 3394–3403.
10. Brach, M. A., Henschler, R., Mertelsmann, R. H., and Herrmann, F. (1991) *Pathobiology* **59,** 284–288.
11. Tran-Thi, T. A., Decker, K., and Baeuerle, P. A. (1995) *Hepatology* **22,** 613–619.
12. Gross, V., Zhang, B., Geng, Y., Villiger, P. M., and Lotz, M. (1993) *J. Clin. Immunol.* **13,** 310–320.
13. Geng, Y., Zhang, B., and Lotz, M. (1993) *J. Immunol.* **151,** 6692–6700.
14. Datta, R., Imamura, K., Goldman, S. J., Dianoux, A. C., Kufe, D. W., and Sherman, M. L. (1992) *Blood* **79,** 904–912.
15. Serrez, D. V., Gaedeke, J. W., and Leiter, E. H. (1993) *Proc. Natl. Acad. Sci.* **90,** 9625–9629.
16. Navarro, S., Debili, N., Bernaudin, J.-F., Vainchenker, W., and Doly, J. (1989) *J. Immunol.* **142,** 4339–4345.

17. Tremblay, P., Houde, M., Arbour, N., Rochefort, D., Masure, S., Mandeville, R., Opdenakker, G., and Oth, D. (1995) *Cytokine* **7,** 130–136.

18. Kamdar, S. J., Fuller, J. A., and Evans, R. (1997) *Exp. Cell Res.* **232,** 439–442.

19. Sudo, T., Nishikawa, S., Ogawa, M., Kataoka, H., Ohnoi, N., Izawa, A., Hayashi, S., and Nishikawa, S. (1995) *Oncogene* **11,** 2469–2476.

20. Toullec, D., Pianetti, P., Coste, H., Bellevergue, P., Grand-Perret, T., Ajakane, M., Baudet, V., Boissin, P., Boursier, E., Loriolle, F., Duhame, L., Charon, D., and J. K. (1991) *J. Biol. Chem.* **266,** 15771–15781.

21. Ogretmen, B., and Safa, A. (1995) *BioTechniques* **19,** 374–376.

22. Tamaoki, T. (1991) *Methods Enzymol.* **201,** 340–347.

23. L. C. Laboratories. (1995) Catalog and Handbook, p. 71, Woburn, MA.

24. Hahn, S., and Moroni, C. (1994) *Lymphokine-Cytokine Res.* **13,** 247–252.

25. Akashi, M., Saito, M., and Koeffler, H. P. (1989) *Blood* **74,** 2383–2390.

26. Bickel, M., Cohen, R. B., and Pluznik, D. H. (1990) *J. Immunol.* **145,** 840–845.

27. Naora, H., and Young, I. G. (1994) *Blood* **83,** 3620–3628.

28. Ross, H. J., Sato, N., Uemama, Y., and Koeffler, H. P. (1991) *Blood* **77,** 1787–1795.

29. Beauparlant, P., and Hiscott, J. (1996) *Cytokine Growth Rev.* **7,** 175–190.

30. Sweet, M. J., and Hume, D. A. (1996) *J. Leukocyte Biol.* **60,** 8–26.

31. Sanghera, J. S., Weinstein, S. L., Aluwalia, M., Girn, J., and Pelech, S. L. (1996) *J. Immunol.* **156,** 4457–4465.

32. Baccarini, M., Sabatini, D. M., App, H., Rapp, U. R., and Stanley, E. R. (1990) *EMBO J.* **9,** 3649–3657.

33. Tsuboi, A., Maramatsu, M., Tsutsumi, A., Arai, K., and Arai, N. (1994) *Biochem. Biophys. Res. Commun.* **199,** 1064–1072.

34. Thorens, B., Mermod, J.-J., and Vassalli, P. (1987) *Cell* **48,** 671–679.

Received March 24, 1997
Revised version received May 5, 1997

EXPERIMENTAL CELL RESEARCH **235,** 117–123 (1997)
ARTICLE NO. EX973660

The Ras Guanine Nucleotide Exchange Factor CDC25Mm Is Present at the Synaptic Junction

Emmapaola Sturani,*[,1] Adele Abbondio,* Paola Branduardi,† Cristina Ferrari,* Renata Zippel,* Enzo Martegani,* Marco Vanoni,* and Suzanne Denis-Donini†[,2]

*Department of General Physiology and Biochemistry and †Department of Biology, University of Milan,
Via Celoria 26, 20133 Milano, Italia*

CDC25Mm, a mouse Ras-Guanine nucleotide Exchange Factor, is specifically expressed as a product of 140 kDa (p140) in the postnatal and adult brain. Immunohistochemical analysis indicates that it is present throughout the brain particularly concentrated in discrete punctate structures. Subcellular fractionation of the mouse brain shows that p140 is present in synaptosomes but not in highly purified synaptic vesicles. Moreover, isolated postsynaptic densities (PSDs) are largely enriched in CDC25Mm. This protein can be phosphorylated by calcium/calmodulin kinase II, the most abundant protein in PSDs. Altogether these results suggest that CDC25Mm is present at synaptic junctions and that it may be involved in synaptic signal transduction leading to Ras activation. © 1997 Academic Press

INTRODUCTION

Ras proteins play a central role in the control of cell proliferation and are involved in the differentiation of several cell types [1]. They are ubiquitously expressed, in particular in the brain, where they may play a role also in neuronal survival and synaptic activity [2].

The p21 Ras proteins are members of a superfamily of small GTPases that act as molecular switches by cycling between active GTP-bound and inactive GDP-bound states [3, 4]. The fraction of Ras in the active state depends on the activity of GTPase activating proteins [5] and of Guanine nucleotide Exchange Factors (GEFs) that, by promoting the release of bound GDP, allow the entrance of GTP and the attainment of the active state [6].

In mammals two families of Ras-specific GEFs have been identified: the Sos proteins, homologue of *Drosophila* Son of Sevenless [7, 8, 9] and the CDC25Mm/Ras-GRF (Guanine nucleotide Releasing Factor) 140-kDa protein, whose encoding cDNAs have been isolated from mouse [10, 11], rat [12], and human [13, 14].

CDC25Mm presents a C terminal catalytic domain that acts in an *in vitro* system as a Ras-specific exchange factor [15, 16]. In addition the full-length product contains two plextrin (PH) and one Dbl homology domain (DH) and a calmodulin binding IQ motif [17].

While the role of Sos proteins in Ras activation has been deeply analyzed and is well understood, less is known on the signalling pathway(s) in which CDC25Mm/Ras-GRF is involved. Recent evidence indicates that it is not coupled to tyrosine kinase receptors, but rather to pathways involving trimeric G proteins [18, 19]. Moreover, through its calmodulin-binding IQ motif it appears to mediate the calcium-induced Ras activation [17] and the ensuing downstream cascade leading to transcriptional activation.

In contrast to Sos which is ubiquitously expressed, the 140-kDa CDC25Mm/Ras-GRF protein product is present only in neuronal cells of the central nervous system [20], although it has been reported that the human homolog is present, at a reduced level, also in other tissues [21]. Moreover, in rodents p140 is developmentally regulated: it is not expressed in the embryo and can be detected in brain extracts only after birth [20, 22].

In the present paper we investigated by immunohistochemistry the cellular localization of CDC25Mm in the mouse brain and studied its subcellular distribution by tissue fractionation. The pattern of staining of brain sections suggests that CDC25Mm may be localized at synaptic junctions and this indication is sustained by the finding that the protein is present in synaptosomes and is largely enriched in postsynaptic density preparations. Such a localization favors the hypothesis that Ras-GRF/CDC25Mm and Ras may be involved in postsynaptic signal transduction, even though it does not exclude other localizations and roles.

MATERIALS AND METHODS

Antibodies. Ras-GRF polyclonal IgG (against the rat Ras-GRF) from Santa Cruz (C-20) and affinity-purified antibodies directed to the catalytic domain of CDC25 Mm [22] were used. The latter will be referred to as CDC25-Abs. Antiserum to synapsin I from bovine

---

[1] To whom correspondence and reprint requests should be addressed. Fax: 00 39 2 70632811.

[2] Permanent address: CNR Center of Cytopharmacology, Via Vanvitelli 32,20129, Milano, Italia.

0014-4827/97 $25.00
Copyright © 1997 by Academic Press
All rights of reproduction in any form reserved.

brain was a kind gift from F. Valtorta (Milan). Monoclonal antibodies to calcium/calmodulin-dependent protein kinase type II (CaM-Kinase II) are from Boehringer-Mannheim.

Immunohistochemistry of brain sections. Adult mice were deeply anesthetized with pentobarbital and a transcardial perfusion was made with 4% phosphate-buffered paraformaldehyde. After perfusion the brains were quickly removed, placed in fresh fixative overnight, washed extensively in PBS, dehydrated in graded ethanol, cleared in xylene, and embedded in paraffin. Nonserial sections (5 μm) were cut and mounted on gelatin-coated glass slides. The sections were deparaffinized, rehydrated, and processed for immunostaining [23]. They were incubated overnight at 4°C in antibodies to Ras-GRF (Santa Cruz) or to synapsin I diluted in PBS containing 2% BSA and 0.1% Triton X-100. Bound antibodies were visualized by a conventional avidin-biotin-peroxidase protocol (ABC) using the elite ABC-kit (Vectastain). Control sections were incubated in secondary antibody alone.

Synaptosomes and synaptic vesicles. A synaptosomal fraction (P3) was prepared from brain according to Huttner *et al.* [24]. Mice were killed by cervical dislocation followed by decapitation. The brains were quickly removed, placed into ice-cold buffer A (320 m*M* sucrose, 5 m*M* Hepes, pH 7.4), and homogenized in the same buffer (4 ml/brain) containing protease inhibitors (1 μg/ml apoprotinin, 1 μg/ml leupeptin, and 1 m*M* PMSF) in a glass-teflon homogenizer using 10 up and down strokes at 900 rpm. The homogenate was centrifuged for 10 min at 2,500 rpm in a Sorvall SS-34 rotor and the supernatant (S1) was centrifuged 15 min at 8,750 rpm yielding a supernatant S2 and a pellet P2. P2 was washed by resuspending in buffer A (3 ml/brain) and centrifuged for 15 min at 9,250 rpm yielding a supernatant (S3) and a pellet (P3). The latter is referred to as washed synaptosomal fraction.

Crude synaptic vesicles were obtained by hypoosmotic lysis of P3 in 9 vol of ice-cold 5 m*M* Hepes, pH 7.4, containing protease inhibitors. The suspension was homogenized with five up and down strokes in a Teflon/glass homogenizer driven at 1,500 rpm and kept on ice for 30 min. After centrifugation for 20 min at 14,500 rpm, a lysate pellet (LP1) and a lysate supernatant (LS1) were obtained. The supernatant (LS1) was centrifuged for 2 h at 100,000*g* yielding a supernatant LS2 and a pellet (LP2) of crude synaptic vesicles. Highly purified synaptic vesicles (provided by F. Valtorta) were obtained from the rat cerebral cortex [24, 25] and are referred to as CPG-V (controlled pore glass beads chromatography purified vesicles).

The protein concentration of the various subcellular fractions was determined by a Coomassie blue-based assay.

Extraction of p140 from synaptosomes. Aliquots of synaptosomes (100 μg protein) were incubated in phosphate buffer (50 m*M* Na_2HPO_4, 1 m*M* β-mercaptoethanol, pH 7.5) for 30 min at 0°C in a final volume of 200 μl in the presence or absence of 150 m*M* NaCl and 1% Triton X-100 (20 μl/mg protein), 1% sodium deoxycholate (NaDOC), or both. Aliquots were also incubated in a final volume of 5 ml (20 μg protein/ml) in the presence of various salts (1 *M* NaCl, 0.6 *M* KI, 1 *M* KSCN). Extraction with hydroxylamine was performed as described by Gross *et al.* [26]. The samples were then centrifuged for 1 h at 100,000*g* at 4°C and the pellets were resuspended directly in SDS-sample buffer and subjected to Western blotting.

Preparation of postsynaptic densities. Postsynaptic density fractions were prepared according to Carlin *et al.* [27]. Briefly, 20 mouse brains were homogenized in isotonic sucrose and centrifuged at low speed (1,400*g*). The supernatant (S1) was centrifuged at 710*g* and then at 13,800*g* to obtain P3, a mixed synaptosome/mitochondria-enriched fraction. Resuspended P3 was fractionated on a discontinuous sucrose density gradient. The synaptosomal fraction recovered at the 1.0–1.2 *M* sucrose interphase was adjusted to 0.5% Triton X-100, 6 m*M* Tris, pH 8.1, and the insoluble material was pelleted by centrifugation (PSD I). The PSD I fraction was then resuspended and centrifuged through a second discontinuous sucrose gradient. The material at the 1.5–2.0 *M* sucrose interphase, which is enriched in PSDs, was resuspended in 75 m*M* KCl containing 0.5% Triton X-100 and then pelleted by centrifugation. The final pellet containing purified PSDs (PSD II) was resuspended in 40 m*M* Tris, pH 8.0.

The protein concentration of all fractions denatured in Laemmli buffer was determined by a bicinchroninic acid protein assay using the BCA reagent from Pierce. Bovine serum albumine was used as a standard.

Western blotting. The various fractions (from 10 to 100 μg protein depending on the experiment) were separated by SDS–PAGE using a regular LKB electrophoresis chamber with 1.5-mm-thick gels and transferred to nitrocellulose. Immunoblot analysis was carried out with CDC25-Abs at a 1:250 dilution. Anti-synapsin I antiserum was used at a 1:2000 dilution; anti-calcium/Calmodulin-dependent protein kinase type II antibodies were used at a 1:800 dilution. Bound antibodies were detected with the ECL detection system (Amersham).

In vitro phosphorylation assays. Endogenous phosphorylation in PSDs was performed: PSDs were maintained in ice with 0.1 *M* dithiothreitol for 2 h prior to phosphorylation. Phosphorylation medium [28] contained 20 m*M* Hepes, pH 7.4, 10 m*M* $MgCl_2$, 10 μ*M* [γ-^{32}P]ATP (sp act 10 mCi/μmol), 0.4 μ*M* microcistin, and either 1 m*M* EGTA or 1 m*M* $CaCl_2$ and 40 μg/ml calmodulin as specified in the text. PSDs were incubated in the phosphorylation medium at a final concentration of 0.5 mg/ml for 20 min at 30°C. The reaction was then stopped with Laemmli buffer, heated, and analyzed by SDS–PAGE and autoradiography.

Recombinant CDC25Mm was also subjected to phosphorylation: p140 was immunoprecipitated from the NIHRG7 clone overexpressing the protein as previously described [18, 22]. It was then incubated for 20 min at 30°C in a phosphorylation medium containing 25 m*M* Hepes, pH 7.4, 10 m*M* $MgCl_2$, 0.5 m*M* DTT, 20 μ*M* [γ-^{32}P]ATP (sp act 80 mCi/μmol), 0.4 μ*M* microcistin, and, as specified in the text, either 1 m*M* EGTA or 1 m*M* $CaCl_2$ and 40 μg/ml calmodulin, together with 10 μg of the rat brain LS2 fraction (a crude vesicle high speed supernatant) enriched in CaM Kinase II (provided by Dr. M. Popoli, Milan). The beads were washed, resuspended in Laemmli buffer, heated, and analyzed by SDS–PAGE and autoradiography.

RESULTS

Immunohistochemistry

The spatial distribution of CDC25Mm was determined in frontal sections of adult mouse brain labeled with Ras-GRF antibodies (from Santa Cruz). Immunoreactivity was observed throughout the brain gray matter and no staining was present with nonimmune serum. The overall pattern of staining appears as discrete dots, superimposed in some nuclei with stained cell bodies and dendrites. In the cerebral cortex (Fig. 1A) a punctate pattern is evident. Pyramidal cell bodies are decorated by labeled dots and one can observe a fine striation due to the negative images of the pyramidal cell dendrites which run in parallel toward layer I. Such pattern visualized with the Ras-GRF antibodies is comparable to the one obtained with antibodies against synapsin I (Fig. 1D and Ref. 25).

In the hippocampus (Fig. 1B), after staining with Ras-GRF antibodies, the contour of pyramidal cell bodies appears underlined by labeled puncta. This is particularly evident in the CA3, CA1, and dentate girus regions. In other nuclei, such as caudate nucleus, reticular nuclei of the thalamus, medial habenula, basolateral amygdala, and in the endopyriform cortex, one can observe labeled cell bodies and dendrites. At high mag-

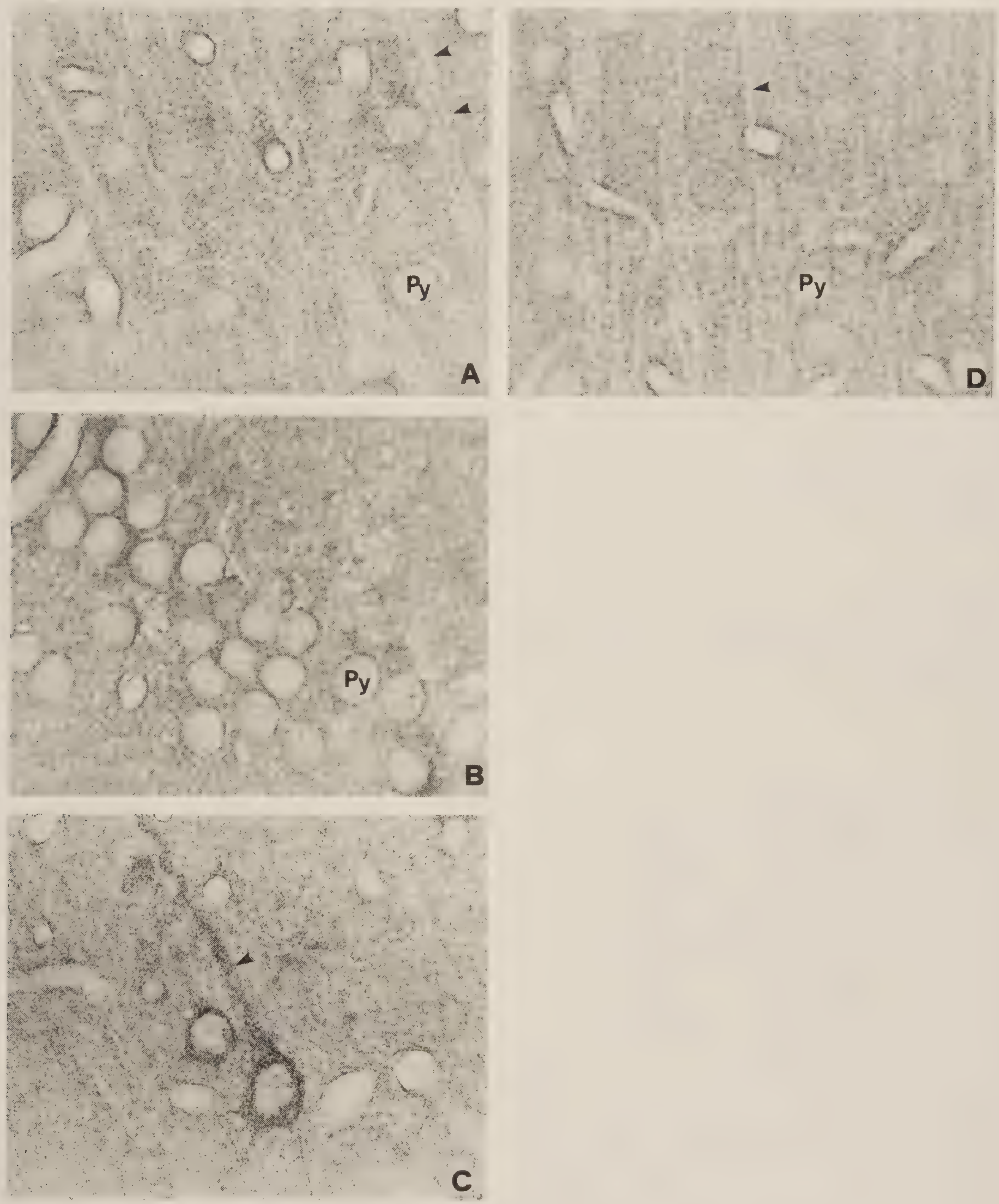

FIG. 1. Immunohistochemistry with Ras-GRF and synapsin I antibodies of frontal sections of the mouse brain. (A, B, and C) Immunohistochemistry with Ras-GRF antibodies. (D) Immunohistochemistry with synapsin I antibodies. In the cerebral cortex (A and D), with both antibodies pyramidal cell bodies (Py) are outlined by labeled dots. Their apical dendrites appear as negative images giving rise to a fine longitudinal striation (arrowheads). The similarity of the pattern obtained with both antibodies is evident. In the hippocampus (B), pyramidal cell layer of the area CA1; cell soma are delineated by labeled puncta. In the entorhinal cortex (C), pyramidal cells exhibit a cytoplasmic staining that at high magnification appears as labeled puncta that decorate both the soma and dendrite (arrowhead). Magnification, 550×.

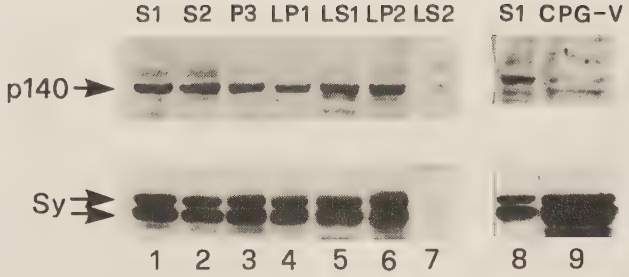

FIG. 2. Immunoblots of mouse brain subcellular fractions with antibodies directed to CDC25 Mm and synapsin I. Lanes 1–7, Subcellular fractions were obtained from mouse brain and designated as reported under Materials and Methods. S1, first supernatant; S2, supernatant of crude synaptosomes; P3, crude synaptosomal fraction (washed synaptosomes); LP1, hypoosmotic lysate pellet; LS1, hypoosmotic lysate supernatant; LP2, crude synaptic vesicles; LS2, lysate supernatant. Equal amounts of protein (100 μg) were analyzed on 8% gels, blotted on nitrocellulose, and immunodecorated with purified antibodies directed toward the catalytic domain of CDC25 Mm and with anti-synapsin I antiserum. Lanes 8 and 9, the rat brain cortex was fractionated with the same procedure as the mouse brain; highly purified synaptic vesicles were prepared from synaptosomes according to Huttner *et al.* [24]. 50 μg of S1 and controlled-pore glass vesicles (CPG-V) were analyzed. The positions of p140 and synapsin I are indicated by arrows.

nification the staining pattern can be resolved in labeled dots. As an example, in Fig. 1C a stained pyramidal cell and apical dendrite from the endopyriform cortex is shown.

Subcellular Distribution of p140 in the Brain of Adult Mouse

Our immunohistochemistry results prompted us to analyze the subcellular distribution of p140 by tissue fractionation. A washed synaptosomal fraction (P3), a hypoosmotic lysate pellet impoverished in synaptic vesicles and containing larger organelles and membranes (LP1), a fraction of crude synaptic vesicles (LP2), and a soluble supernatant (LS2) (see Methods) were analyzed by SDS–PAGE and Western blotting with CDC25-Abs as well as with antibodies to synapsin I (Fig. 2, lanes 1–7).

As shown in Fig. 2 both p140 and synapsin-I are distributed in a parallel manner in the various subcellular fractions: both of them are present in washed synaptosomes (P3), in the low-speed precipitate (LP1), and in the crude synaptic vesicle fraction (LP2) but absent in the crude vesicle high-speed supernatant (LS2).

The residual p140 in the supernatant of the crude synaptosomal fraction (S2) could be recovered in the pellet following high speed centrifugation (result not shown). Altogether these results suggest that p140 is entirely particulate.

In order to investigate whether p140 was specifically associated with synaptic vesicles or only cosedimented in the crude vesicle fraction we analyzed highly purified synaptic vesicles obtained from rat cerebral cortex by chromatography on controlled pore glass beads (CPG-V) [24]. As shown in Fig. 2 (lane 9), this fraction is highly enriched in synapsin I but does not contain p140. This negative result on rat synaptic vesicles cannot be attributed to the lack of recognition of the rat antigen by our antibodies since p140 is recognized in the rat S1 fraction (lane 8).

To determine the nature of the association of p140 with the synaptosomal fraction, a series of extraction experiments were carried out on synaptosomes. As shown in Fig. 3 (lane 3) the combined action of 150 m*M* NaCl and 1% Triton X-100 that largely solubilized synapsin I, was without effect on p140. Sodium deoxycholate also (lane 4) had no effect on p140, but a combination of Triton X-100 and NaDOC (lane 5) partially solubilized it. NaCl 1 *M* (lane 9) and chaotropic agents such as 0.6 *M* KI or 1 *M* KSCN (lanes 7 and 8, respectively) that released synapsin I had practically no effect on p140 that was always retained in the particulate fraction. The protein was entirely solubilized only by SDS and sodium lauryl sarcosinate.

To determine whether p140 was bound to membranes by a fatty acid modification, synaptosomes were incubated in 1 *M* hydroxylamine (pH 8.1), a treatment that cleaves thiol and oxygen esters [31]. Also in this condition p140 was not released from synaptosomes (Fig. 3, lane 2). Thus p140 is tightly bound to membrane–cytoskeletal structures.

Postsynaptic Densities Are Highly Enriched in p140

The resistance to Triton extraction of synaptosome-associated p140 suggested that it may be a component

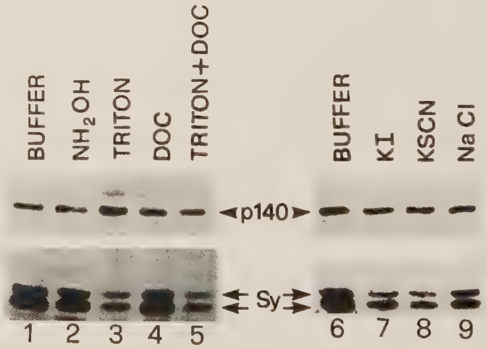

FIG. 3. Extraction of p140 and synapsin I from a washed synaptosomal fraction. Equal amounts (100 μg protein) of washed synaptosomes (P3) were incubated in the absence or presence of various reagents, incubated on ice for 30 min, and centrifuged (1 h at 100,000*g*, 4°C). The pelleted material was separated by SDS–PAGE and immunodecorated as described in the legend of Fig. 2. Lanes 1 and 6, 50 m*M* Na_2HPO_4, 1 m*M* β-mercaptoethanol (pH 7.5). Lane 2, 1 *M* NH_2OH, pH 8.1. Lane 3, 1% Triton X-100 (20 μl Triton/mg prot) and 150 m*M* NaCl. Lane 4, 1% NaDeoxycholate and 150 m*M* NaCl. Lane 5, 1% Triton X-100, 1% NaDeoxycholate, 150 m*M* NaCl. Lane 7, 0.6 *M* KI. Lane 8, 1 *M* KSCN. Lane 9, 1 *M* NaCl. The protein concentration was 20 μg/ml. The positions of p140 and synapsin I are indicated by arrows.

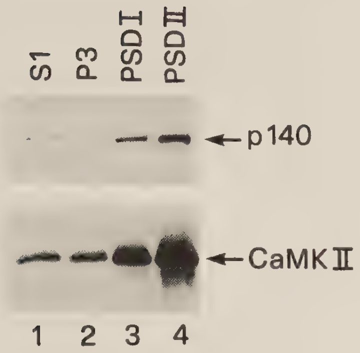

FIG. 4. p140 is highly enriched in purified PSDs. PSDs were purified from mouse brain according to Carlin *et al.* [8]. Fractions obtained at different steps were analyzed by Western blot with antibodies to CDC25^{Mm} and to CaMkinase II. S1, first supernatant; P3, synaptosomal pellet; PSD I, pellet obtained by the first Triton X-100 extraction of synaptosomes purified by sucrose gradient; PSD II, final purified PSD fraction. The amount of protein analyzed was 10 μg in all lanes.

of the postsynaptic density fraction (PSD) that is obtained from synaptosomes by subsequent Triton extractions and separations on sucrose gradients. Mouse brain PSDs were prepared following the protocol of Carlin *et al.* [27]. Equal amounts of protein (10 μg) from the fractions obtained at different steps of purification (the S1 supernatant, the P3 pellet containing synaptosomes and mitochondria, the PSD I fraction obtained after the first Triton extraction, and the final purified PSD II fraction) were analyzed by SDS–PAGE and Western blotting with CDC25Abs. Figure 4 shows that p140 is present in all fractions and is largely enriched in PSDs and in particular in the final PSD II fraction. The amount of p140 was quantified by densitometric scanning of the autoradiograms and was found to be 10.2-fold higher in the PSD II than in the S1 fraction.

CaM kinase II is the major protein in PSDs [28, 29, 32] and, although it is also present in other fractions, it can be considered a PSD marker. Therefore we probed our blots with antibodies to this kinase (Fig. 4). As expected, CaM kinase II was clearly enriched in the PSD II fraction and when quantified by densitometry scanning its content resulted to be 9.7-fold higher in the PSD II than in the S1 fraction. A 10-fold enrichment of both p140 and CaM kinase II on a protein basis was confirmed by analyzing different amounts of the various fractions (not shown).

CDC25Mm/Ras-GRF ectopically expressed in fibroblasts has been shown to be phosphorylated both under basal conditions and following stimulation with serum [33 and our unpublished results]. The presence of p140 in PSDs raised the possibility that it might be a substrate for CaM kinase II.

To investigate this point PSDs were incubated with [γ-^{32}P]ATP in the presence of either EGTA or calcium and calmodulin (Fig. 5A, lanes 1 and 2) and then fractionated by SDS–PAGE. The autoradiography of the gel shows that calcium and calmodulin (Fig. 5A, lane 2) elicit the appearance of a major phosphorylated band with an apparent molecular mass of 54 kDa, which corresponds to that of phosphorylated CaM kinase II. In effect autophosphorylation of this kinase has been reported to take place in isolated PSDs in response to calcium and calmodulin [28]. A phosphorylated band of 140 kDa is also present, whose intensity is highly enhanced in the presence of calcium and calmodulin (lane 2). Due to difficulties in performing immunoprecipitation from PSDs it was impossible to assess the identity of the 140-kDa phosphorylated band. However, we obtained evidence that CDC25Mm/Ras-GRF is a substrate for CaM Kinase II. Using CDC25 Abs, p140 was immunoprecipitated from the NIHRG7 cell line where it is ectopically expressed [18, 22], and a preimmune serum was used as control. The immunoprecipitates were then incubated with a crude vesicle-high speed supernatant (the LS2 fraction, see Materials and Methods), which is a good source of CaM Kinase II [34], in the presence of [γ-^{32}P]ATP and either EGTA or calcium and calmodulin. Figure 5B shows that when the immunoprecipitate was incubated with calcium and calmodulin, a 140-kDa protein became phosphorylated (lane 4). This band was absent when incubation was performed in the presence of EGTA (lane 3) or when a preimmune serum was used (lanes 1 and 2). The 54-kDa phosphorylated form of CaM Kinase II was also evident (lanes 2 and 4) when the incubation was

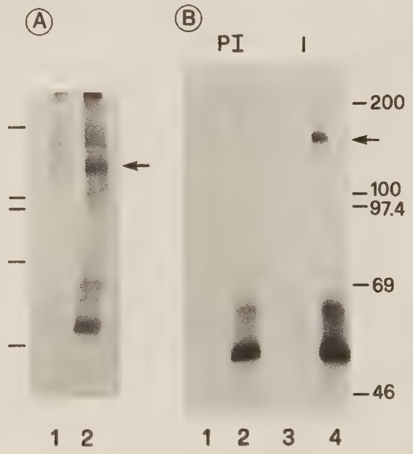

FIG. 5. *In vitro* phosphorylation of p140. (A) The PSD II preparation was incubated in phosphorylation medium and [γ-^{32}P]ATP with either 1 m*M* EGTA (lane 1) or calcium and calmodulin (lane 2) for 20 min at 37°C and analyzed by SDS–PAGE. (B) CDC25Mm was immunoprecipitated with CDC25-Abs (lanes 3 and 4) or preimmune serum (lanes 1 and 2) from NIHRG7 fibroblasts that ectopically express it [18]. The immunoprecipitates were then incubated in phosphorylation medium with the rat LS2 fraction and either EGTA (lanes 1 and 3) or calcium and calmodulin (lanes 2 and 4), and fractionated by SDS–PAGE. Autoradiography is shown. Molecular weight markers (myosin, phosphorylase b, bovine serum albumin, ovalbumin) are indicated.

performed with calcium and calmodulin. These data demonstrate that CDC25Mm can be phosphorylated by CaM Kinase II.

DISCUSSION

We have shown previously that the Ras-GRF/CDC25Mm encoded by the GRF1 gene [35] is exclusively expressed in neuronal cells of the central nervous system [20]. In order to define its localization, immunohistochemical experiments were performed on mouse brain sections. The results show that the protein is present throughout the brain, in accordance with *in situ* hybridization data [36, 20] and that it is mostly concentrated in discrete punctate structures. In the cerebral cortex, puncta delineate cell bodies and dendrites which appear as negative images. Such a pattern is strongly reminiscent of the one obtained with synapsin I antibodies and suggests that p140 is concentrated at synaptic sites. In the hippocampus also, pyramidal cell bodies are surrounded by labeled puncta. In some nuclei, such as the reticular formation of the thalamus, caudate nucleus, amygdala, and endopyriform cortex, some neurons also exhibit a cytoplasmic staining. Occasionally, dendrites are also stained; this is particularly evident in the endopyriform cortex (Fig. 1C). Such pattern of staining resembles the one observed after staining with antibodies to PSD-95 and SAP102 [30, 37], suggesting that at least in some neuronal populations, p140 might have a postsynaptic localization. This synaptic localization is in agreement with previous results, demonstrating that the expression of CDC25Mm starts within days after birth, when synapses become functional [20, 22].

In an attempt to better characterize the subcompartmentation of p140, brain subcellular fractionations were performed. The results show that p140 is present in the synaptosomal fraction. When synaptosomes are disrupted by hypoosmotic lysis, p140 is found in the fraction of synaptic junction components containing membranes and elements of the elaborate submembranous cytoskeleton and is not associated with highly purified synaptic vesicles. A similar subcellular localization has been reported for p21ras [38] and various SAPs [30]. The lack of effect of Triton on p140 solubilization and the tight association with membrane cytoskeletal structures is similar to the behavior of the CDC25 gene product of *S. cerevisiae* [26, 39]. In our synaptosomal preparations, the resistance to Triton suggested that p140 could be tightly associated to elements of postsynaptic densities. In fact, p140 was found to be far more enriched in PSD preparations than in synaptosomes, although this does not exclude that, like for instance CaMKinase II [34], it may be present in other localizations also. Electron microscopy studies either on brain sections or on isolated synaptosomal preparations [37] will help in definitely clarifying this point.

One of the most abundant proteins in PSDs is the α subunit of CaM kinase II [34, 28]. Autophosphorylation of this protein has been demonstrated to take place in isolated PSDs in the presence of calcium and calmodulin [28]. We have shown that in PSDs, under conditions allowing activity and autophosphorylation of this kinase, the phosphorylation of a 140-kDa protein is stimulated, and we were able to demonstrate that CDC25Mm can be phosphorylated by CaM kinase II.

Ras is largely expressed in fully differentiated neuronal cells [36, 38] and it has been recently shown that in neurons Ras and the Ras pathway are activated by increases in intracellular calcium such as those induced by several neurotransmitters [17, 40, 41]. The fact that CDC25Mm/Ras-GRF is present at postsynaptic sites, that in the presence of calcium, through its IQ motif, it can bind calmodulin [17, 20], and that it is a possible substrate of CaM kinase II, strongly suggests that it participates in this pathway, even though its mechanism of activation is still controversial [43]. In effect the expression of Ras-GRF in 293T cells has been shown to cause an increase in the Ras.GTP level and in MAP kinase activity in response to calcium entry [17]. In addition ectopic expression of Ras-GRF/CDC25Mm has been found to potentiate the Ras pathway in response to agonists acting through G protein-coupled receptors [22, 19].

In conclusion the finding that CDC25Mm is enriched in PSDs, where several proteins involved in signal transduction are clustered (CaM kinase II, G protein subunits, PSD-95, and neurotransmitter receptors [28, 29, 32, 42]), supports the view of an involvement of CDC25Mm and the Ras pathway in postsynaptic signal transduction mechanisms activated by calcium and G protein-coupled receptors.

We thank Dr. F. Valtorta, DIBIT, S. Raffaele Institut, Milan, for thoughtful suggestions and kindly providing highly purified rat synaptosomal vesicles and antibodies to synapsin I, and Dr. M. Popoli (University of Milan) for providing us the rat brain LS2 fraction. We also thank Dr. J. Meldolesi, DIBIT, S. Raffaele Institut for helpful discussion. This work was partially supported by AIRC (Italian association for Cancer Research), CEE, Contract BIO2CT-930005 and CNR, Progetto Finalizzato Ageing. A. Abbondio has been a recipient of a fellowship from FIRC.

REFERENCES

1. Barbacid, M. (1987) *Ann. Rev. Biochem.* **56,** 779–827.
2. Finkbeiner, S., and Greenberg, M. E. (1996) *Neuron* **16,** 233–236.
3. Bourne, H. R., Sanders, D. A., and McCormick, F. (1990) *Nature* **348,** 125–131.
4. Bourne, H. R., Sanders, D. A., and McCormick, F. (1991) *Nature* **349,** 117–127.
5. Bollag, G., and McCormick, F. (1991) *Ann. Rev. Cell Biol.* **7,** 601–632.
6. Downward, J. (1992) *Bioessays* **14,** 174–184.

7. Bowtell, D. D. L., Fu, P., Simon, M. A., and Senior, P. (1992) *Proc. Natl. Acad. Sci. USA* **89,** 6511–6515.
8. Chardin, P., Camonis, J. H., Gale, N. W., Van Aelst, L., Schlessinger, J., Wigler, M. H., and Bar-Sagi, D. (1993) *Science* **260,** 1338–1343.
9. Simon, M. A., Bowtell, D. D. L., Dodson, G. S., Laverty, T. R., and Rubin, G. M. (1991) *Cell* **67,** 701–716.
10. Martegani, E., Vanoni, M., Zippel, R., Coccetti, P., Brambilla, R., Ferrari, C., Sturani, E., and Alberghina, L. (1992) *EMBO J.* **11,** 2151–2157.
11. Cen, H., Papageorge, A. G., Zippel, R., Lowy, D. R., and Zhang, K. (1992) *EMBO J.* **11,** 4007–4015.
12. Shou, C., Farnsworth, C. L., Neel, B. G., and Feig, L. A. (1992) *Nature* **358,** 351–354.
13. Schweighoffer, F., Faure, M., Fath, I., Chevallier-Moulton, M. C., Apiou, F., Dutrillaux, B., Sturani, E., Jacquet, M., and Toque, B. (1993) *Oncogene* **8,** 1477–1485.
14. Wei, W., Schreiber, S. S., Baudry, M., Tocco, G., and Broek, D. (1993). *Mol. Brain Res.* **19,** 339–344.
15. Jacquet, E., Vanoni, M., Ferrari, C., Alberghina, L., Martegani, E., and Parmeggiani, A. (1992) *J. Biol. Chem.* **267,** 24181–24183.
16. Coccetti, P., Mauri, I., Alberghina, L., Martegani, E., and Parmeggiani, A. (1995) *Biochem. Biophys. Res. Comm.* **206,** 253–259.
17. Farnsworth, C. L., Freshney, N. H., Rosen, L. B., Ghosh, A., Greenberg, M. E., and Feig, L. A. (1995) *Nature* **376,** 524–530.
18. Zippel, R., Orecchia, S., Sturani, E., and Martegani, E. (1996) *Oncogene* **12,** 2697–2703.
19. Mattingly, R. R., and Macara, I. G. (1996) *Nature* **382,** 268–272.
20. Zippel, R., Gnesutta, N., Matus-Leibovitch, N., Mancinelli, E., Saya, D., Vogel, Z., and Sturani, E. (1997) *Mol. Brain Res.* in press.
21. Guerrero, C., Rojas, J. M., Chedid, M., Esteban, L. M., Zimonjic, D., Popescu, N. C., Font de Mora, J., and Santos, E. (1996) *Oncogene* **12,** 1097–1107.
22. Ferrari, C., Zippel, R., Martegani, E., Gnesutta, N., Carrera, V., and Sturani, E. (1994) *Exp. Cell Res.* **210,** 353–357.
23. Denis-Donini, S., and Estenoz, M. (1988) *Dev. Biol.* **130,** 237–249.
24. Huttner, W. B., Schiebler, W., Greengard, P., and De Camilli, P. (1983) *J. Cell Biol.* **96,** 1374–1388.
25. De Camilli, Cameron, R., and Greengard, P. (1983) *J. Cell Biol.* **96,** 1337–1354.
26. Gross, E., Marbach, I., Engelberg, D., Segal, M., Simchem, G., and Levitzki, A. (1992) *Mol. Cell. Biol.* **12,** 2653–2661.
27. Carlin, R. K., Grab, D. J., Cohen, R. S., and Siekewitz, P. (1980) *J. Cell Biol.* **86,** 831–843.
28. Dosemeci, A., Gollop, N., and Jaffe, H. (1994) *J. Biol. Chem.* **269,** 31330–31333.
29. Kennedy, M. B. (1993) *Curr. Opinion Neurobiol.* **3,** 732–737.
30. Muller, B. L., Kistner, U., Kindler, S., Chung, W. J., Kuhlendahl, S., Fenster, S. D., Lau, L. F., Veh, R. W., Huganir, R. L., Gundelfingert, E. D., and Garner, C. C. (1966) *Neuron* **17,** 255–265.
31. Bolanowski, M. A., Earles, B. J., and Lennarz, W. J. (1984) *J. Biol. Chem.* **259,** 4934–4940.
32. Cho, K. O., Hunt, C. A., and Kennedy, M. B. (1992) *Neuron* **9,** 929–942.
33. Shou, C., Wurmser, A., Ling, K., Barbacid, M., and Feig, L. A. (1995) *Oncogene* **10,** 1887–1893.
34. Braun, A. P., and Schulman, H. (1995) *Ann. Rev. Physiol.* **57,** 417–445.
35. Gariboldi, M., Sturani, E., Canzian, F., De Gregorio, L., Manenti, G., Dragani, T., and Pierotti, M. (1994) *Genomics* **21,** 451–453.
36. Wei, W., Schreiber, S. S., Baudry, M., Tocco, G., and Broek, D. (1993) *Mol. Brain Res.* **19,** 339–344.
37. Hunt, C. A., Schenker, L. J., and Kennedy, M. (1996) *J. Neurosci.* **15,** 1380–1388.
38. Mizogushi, A., and Takai, Y. (1989) *Mol. Brain Res.* **5,** 31–44.
39. Vanoni, M., Vavassori, M., Frascotti, G., Martegani, E., and Alberghina, L. (1990) *Biochem. Biophys. Res. Comm.* **172,** 61–69.
40. Ghosh, A., and Greenberg, M. E. (1995) *Science* **268,** 239–247.
41. Rosen, L. R., Ginnty, D. G., Weber, M. J., and Greenberg, M. E. (1994) *Neuron* **12,** 1207–1221.
42. Wu, K., Nigam, S. K., LeDoux, M., Huang, Y., Aoki, C., and Siekewitz, P. (1992) *Proc. Natl. Acad. Sci. USA* **89,** 8686–8690.
43. Baouz, S., Jaquet, E., Bernardi, A., and Parmeggiani, A. (1997) *J. Biol. Chem.* **272,** 6671–6676.

Received April 16, 1997
Revised version received May 16, 1997

EXPERIMENTAL CELL RESEARCH **235**, 124–129 (1997)
ARTICLE NO. EX973655

Inhibitors of Protein Kinases Abolish ECM-Mediated Promotion of Neuronal Polarity

André Lochter[1] and Melitta Schachner[2]

Zentrum für Molekulare Neurobiologie, Universität Hamburg, Martinistrasse 52, D-20246 Hamburg, Germany

Different extracellular matrix (ECM) molecules, when presented to hippocampal neurons in culture in a substrate-bound form, exert strikingly similar effects on the establishment of neuronal polarity, i.e., the growth of axon-like major neurites is favored, whereas extension of dendrite-like minor neurites is inhibited. To gain insight into the underlying signal transduction processes, we have investigated the effects of modulators of protein kinase activity on the morphology of neurons cultured on tenascin-R, tenascin-C, and laminin-entactin substrates. We found differential effects of broad-spectrum protein kinase inhibitors: H-7 promoted the growth of minor neurites, whereas H-8 reduced the growth of major neurites on ECM but not control substrates. In contrast, chelerythrine, a specific inhibitor of protein kinase C, selectively affected growth of both minor and major neurites on control, but not on ECM substrates. Finally, reagents which elevate intracellular cAMP levels facilitated growth of minor neurites and inhibited growth of major neurites and thus interfered with the establishment of a polarized phenotype on both ECM and control substrates. Our results suggest that protein kinases mediate the effects of ECM molecules on neuronal polarity and that different kinases control extension of axons and dendrites. © 1997 Academic Press

INTRODUCTION

The differentiation of axons and dendrites and the establishment of neuronal polarity are important features of nervous system development. Neuronal polarity *in vitro* and *in vivo* can be defined by morphological, functional, and molecular criteria [1, 2]. A critical property of neuronal polarity is the preferential sorting of cytoskeletal components, enzymes, and cell–cell and cell–substrate adhesion molecules into either the axonal or the somatodendritic compartment [1, 2]. Molecules enriched in axons include tau, microtubule-associated protein (MAP) $\frac{3}{4}$, the phosphorylated form of MAP1b (MAP5), the highly phosphorylated forms of neurofilament proteins, GAP-43, the 180-kDa isoform of N-CAM, L1, TAG-1, and the $\alpha8$ integrin subunit [1, 2]. Molecules largely restricted to the somatodendritic compartment include MAP2, neurotransmitter and transferrin receptors, and neurogranin [1, 2].

Although the mode and mechanism by which neuronal polarity is established during nervous system development is not known, it has been well documented in cell culture that neuron–glia communication conveys preferential development of either axons or dendrites depending on whether these interactions are hetero- or homotypic interactions, i.e., whether neurons and glial cells are derived from a different or the same brain region [3–6]. Neuronal polarity can also be affected by soluble factors such as neurotransmitters [7–9], neurotrophins [10], and osteogenic protein-1 [11, 12]. In addition, molecules of the extracellular matrix (ECM) are potent modulators of neuronal polarity [1, 2]. With the exception of dermatan sulfate, which promotes dendritic growth [13], elongation of axons is accelerated, whereas growth of dendrites is either not affected or retarded in the presence of ECM molecules [12–17]. The fact that neurons in culture can develop distinct axonal and dendritic compartments on "nonspecific" adhesive substrates, such as polyornithine or polylysine, raises the possibility that ECM molecules establish neuronal polarity by affecting the strength of neuron-to-substrate adhesion, as has been suggested previously [2, 18]. However, when hippocampal neurons were plated on substrates of varying adhesivity in the presence of constant amounts of substrate-bound ECM glycoproteins, elongation of axon-like major neurites was accelerated in an instructive manner independent of adhesive strength [19]. In contrast, growth of dendrites was susceptible to changes in the degree of substrate adhesivity [19]. Taken together these results strongly suggest that the signal transduction mechanisms leading to extension of axons and dendrites are divergent.

In a first step to study the intracellular signal transduction mechanisms involved in ECM-mediated promotion of neuronal polarity, we investigated the effects

---

[1] Present address: Life Sciences Division, Bldg. 83, Lawrence Berkeley Laboratory, 1 Cyclotron Rd., Berkeley, CA 94720.

[2] To whom correspondence and reprint requests should be addressed. Fax: +49-40-4717 6248.

0014-4827/97 $25.00

Copyright © 1997 by Academic Press
All rights of reproduction in any form reserved.

of several modulators of protein kinase activity on neuritogenesis of hippocampal neurons grown on polyornithine substrates coated with the ECM glycoproteins tenascin-R (previously designated janusin in the mouse [20] and restrictin in the chicken [21]), tenascin-C (previously designated tenascin [22]) or laminin-entactin. We show here that H-7, H-8, chelerythrine, and cAMP analogs display substrate- and/or compartment-specific activities which modulate neuronal morphology.

MATERIALS AND METHODS

ECM molecules. Tenascin-R was immunoaffinity purified from urea extracts of adult mouse brains [20]. In this study, only the 180-kDa, but not the 160-kDa, isoform of tenascin-R was investigated. Tenascin-C was immunoaffinity purified from brains of 1- to 15-day-old embryonic mice [22]. Laminin-entactin was purchased from Sigma (L 2020). Since this product, sold under the marketing name "laminin," contains significant amounts of entactin, we refer to it as laminin-entactin.

Preparation of substrates. Preparation of substrates was performed as described [16]. In brief, 96-well multiwell plates (Nunc) were coated with 1.5 μg/ml poly-DL-ornithine (Sigma), washed with water, and air-dried. Tenascin-R, tenascin-C, and laminin-entactin were then coated at a concentration of 25 μg/ml in Ca^{2+}- and Mg^{2+}-free Hanks' balanced salt solution (CMF-HBSS). For control, poly-DL-ornithine-coated wells were incubated with CMF-HBSS.

Cell culture. Hippocampal neurons were prepared from brains of 18- to 19-day-old embryonic SIV rats as described [16]. Dissected hippocampi were trypsinized, triturated, washed, pelleted by centrifugation, and resuspended in chemically defined medium consisting of Hepes-buffered DMEM/F12 supplemented with pyruvate, putrescin, selenium, insulin, transferrin, and progesterone. Cells were plated in 50 μl of medium per well at a density of 10,000 cells/cm^2. For morphometric analysis, neurons were fixed with glutaraldehyde and stained with toluidine blue after 21 h of culture [16]. Plating efficiencies and survival of neurons were determined as described [16] and found to be similar for all culture conditions (not shown).

Modulators of intracellular signaling systems. Modulators were added to the culture medium within 30 min after cell plating. The concentration of all modulators applied was titrated to give the highest effective but subtoxic concentration. H-7, H-8, H-89, chelerythrine, dibutyrylyl cAMP (db-cAMP), dibutyrylyl cGMP (db-cGMP), dibutyrate, and othovanadate were dissolved in water (100, 100, 2, 10, 200, 200, 200, and 100 m*M* stock solutions, respectively) and used at final concentrations of 100, 100, 20, 1.5 μM, 2, 2, and 2 m*M*, and 7.5 μM respectively. Forskolin was dissolved at a concentration of 90 m*M* in ethanol and used at a final concentration of 90 μM. Isobutylmethylxanthine (IBMX), staurosporine, ML-9, genistein, and okadaic acid were dissolved in dimethyl sulfoxide (100, 1, 50, 75, and 50 m*M* stock solutions, respectively) and used at final concentrations of 100 μM, 5 n*M*, 50 μM, 15 μM, and 1 n*M*, respectively. A 1:1000 dilution of ethanol or dimethyl sulfoxide in the culture medium did not affect neuronal morphologies after 21 h of culture (not shown). All modulators were purchased from Sigma, except chelerythrine, H-89, ML-9, genistein, and okadaic acid which were obtained from LC Laboratories.

Morphometry and statistical evaluation. Morphometric analysis was performed with an IBAS image analysis system (Kontron). Neuronal polarity was defined as the ratio of lengths of the longest neurite per cell (major neurite) to all other neurites of the same cell (minor neurites) [16]. Three independent experiments were performed for each experimental condition with 25 cells in each of two wells being analyzed per experiment. The proportion of cells with neurites was between 50 and 60% of all neurons for all culture conditions (not shown, but see [16]). The significance of differences between experimental and control values was analyzed by the same statistical methods as described [16].

RESULTS

Hippocampal neurons maintained for 21 h in culture on polyornithine substrates (control substrates) develop a polarized phenotype with one long axon-like major neurite and, on average, about four dendrite-like minor neurites [16, 23]. Major neurites were defined previously as immature axons on the basis of specific immunoreactivity for tau, while all other neurites were defined as minor neurites or immature dendrites [16, 17]. When plated on a polyornithine substrate coated with tenascin-R (tenascin-R substrate), the growth of major neurites was accelerated and both the number and the length of minor neurites were strongly reduced when compared to polyornithine alone (Fig. 1) [17]. The growth of hippocampal neurites on the control substrate was unaffected by the presence of the protein kinase inhibitor H-7 (Fig. 1a) [24, 25]. However, H-7 increased both the length and the number of minor neurites to control levels when added to cultures grown on the tenascin-R substrate (Fig. 1a). Under these conditions, the length of major neurites was not affected. In contrast, the protein kinase inhibitor H-8 reduced the elongation of major neurites on tenascin-R substrates to control levels without affecting the growth of minor neurites (Fig. 1b). As was the case for H-7, H-8 did not affect neuritogenesis on control substrates (Fig. 1b). Thus, H-8 selectively inhibited the growth promoting effect of tenascin-R on major neurites, whereas H-7 blocked the inhibitory action of tenascin-R on the growth of minor neurites.

Whereas H-7 and H-8 influenced extension on neurites only on tenascin-R, but not on control substrates, the protein kinase C inhibitor chelerythrine [25] showed an opposite substrate specificity. Neuritogenesis was only affected on control, but not on tenascin-R substrates (Fig. 1c). Chelerythrine mainly inhibited extension of minor neurites on control substrates, but major neurites were also slightly affected. These results suggest that protein kinase C is not required for establishment of neuronal polarity on tenascin-R substrates, but aids neurite elongation on control substrates.

To investigate whether cAMP might play a role in the establishment of neuronal polarity, we tested the cAMP analog db-cAMP and a combination of the adenylyl cyclase activator forskolin and the phosphodiesterase inhibitor IBMX [26, 27]. Both treatments yielded similar results in that growth of minor neurites was facilitated and growth of major neurites inhibited on both control and tenascin-R substrates (Figs. 2a and

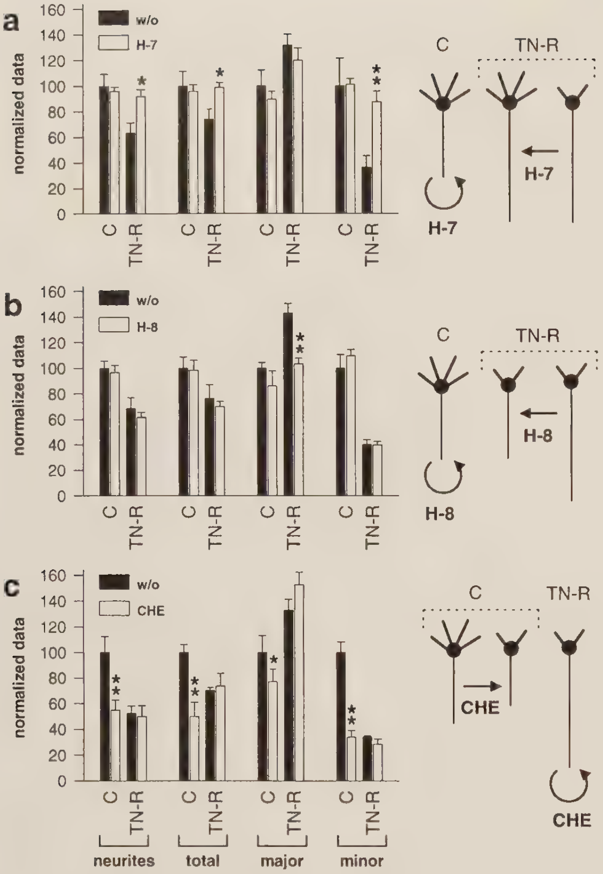

FIG. 1. Effects of H-7, H-8, and chelerythrine on neuronal polarity. Cells were cultured for 21 h on control (C) or tenascin-R (TN-R) substrates in the absence (filled bars, w/o) or the presence (open bars) of H-7 (a), H-8 (b), or chelerythrine (CHE, c) and the average number of neurites per cell (number), the average total neurite length per cell (total), the average length of major neurites per cell (major), and the average length of all minor neurites per cell (minor) were determined. Results were normalized with control values set to 100. Mean values ± standard deviations are shown. Significant differences between morphological parameters in the absence or the presence of the inhibitor are indicated by asterisks, $^{**}P \leqslant 0.001$, $^{*}0.01 \leqslant P \leqslant 0.05$. A schematic representation of results is shown on the right side of each panel. Axons are depicted as a thin line extending downward from the cell body (filled circle). Remaining processes represent minor neurites (thick lines).

2b). Neither the cGMP analog db-cGMP nor dibutyrate influenced neuritogenesis (Fig. 2c and not shown).

Since several ECM glycoproteins have similar effects on the neuritogenesis of hippocampal neurons [16, 17, 19], we examined the effect of modulators of second messenger cascades on cells maintained on tenascin-C and laminin-entactin substrates. As shown in Table 1, H-7 increased growth of minor neurites and H-8 reduced the elongation of major neurites on tenascin-C and laminin-entactin substrates to control levels. Chelerythrine did not influence neuritogenesis on tenascin-C or laminin-entactin and a combination of forskolin and IBMX decreased neuronal polarity on these substrates (Table 1). Thus, the effects of modulators of second messenger pathways were similar for all three ECM substrates examined.

We also tested the broad-spectrum protein kinase inhibitor staurosporine [24, 25, 28, 29], the protein kinase A inhibitor H-89 [30], the myosin light chain kinase inhibitor ML-9 [31], the broad-spectrum protein tyrosine kinase inhibitor genistein [32], the serine/threonine phosphatase inhibitor okadaic acid [33], and the protein tyrosine phosphatase inhibitor orthovanadate [34]. None of them had either substrate-specific

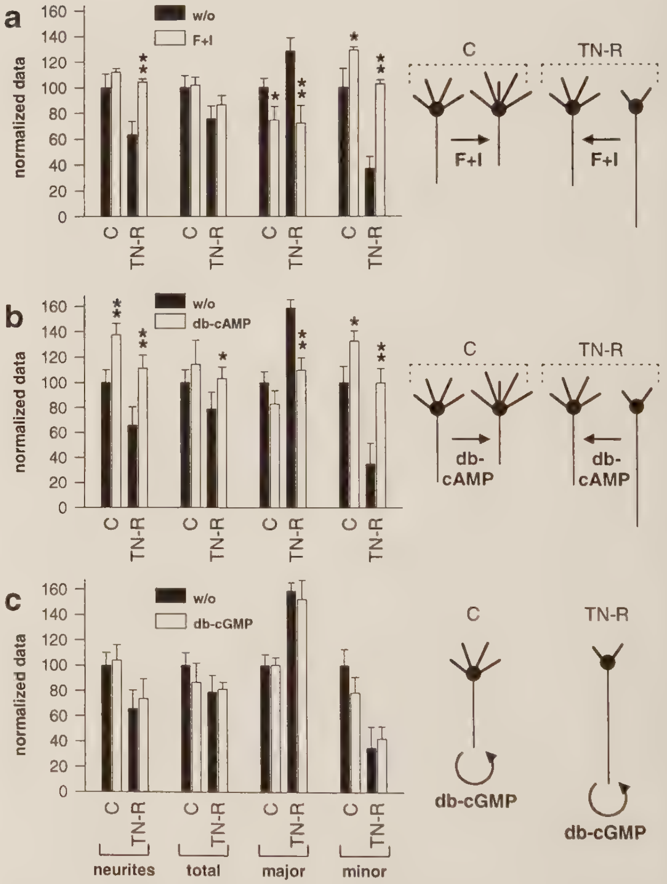

FIG. 2. Effects of forskolin/IBMX, db-cAMP, and db-cGMP on neuronal polarity. Cells were cultured for 21 h on control (C) or tenascin-R (TN-R) substrates in the absence (filled bars, w/o) or the presence (open bars) of forskolin + IBMX (F + I), db-cAMP, or db-cGMP and the average number of neurites per cell (number), the average total neurite length per cell (total), the average length of major neurites per cell (major), and the average length of all minor neurites per cell (minor) were determined. Results were normalized with control values set to 100. Mean values ± standard deviations are shown. Significant differences between morphological parameters in the absence or the presence of the modulator are indicated by asterisks, $^{**}P \leqslant 0.001$, $^{*}0.01 \leqslant P \leqslant 0.05$. A schematic representation of results is shown on the right side of each panel. Axons are depicted as a thin line extending downward from the cell body (filled circle). Remaining processes represent minor neurites (thick lines).

TABLE 1

Effects of Modulators on Neuronal Polarity on Tenascin-C and Laminin-Entactin Substrates

		Number of neurites		Length of major neurites		Length of minor neurites	
		w/o mod.	with mod.	w/o mod.	with mod.	w/o mod.	with mod.
H-7	Control	100.0 ± 8.38	93.8 ± 6.27	100.0 ± 12.07	95.8 ± 6.34	100.0 ± 21.26	82.5 ± 4.56
	TN-C	49.0 ± 9.81	$\boxed{91.5 \pm 14.78}$	145.7 ± 8.66	142.5 ± 9.51	27.8 ± 8.95	$\boxed{73.6 \pm 9.37}$
H-8	Control	100.0 ± 4.56	93.5 ± 12.05	100.0 ± 8.92	85.3 ± 14.47	100.0 ± 11.10	89.2 ± 9.2
	TN-C	37.4 ± 2.09	40.5 ± 8.36	140.1 ± 10.17	$\boxed{112.9 \pm 7.90}$	35.1 ± 2.96	43.5 ± 3.87
CHE	Control	100.0 ± 8.36	$\boxed{48.2 \pm 2.58}$	100.0 ± 12.07	94.5 ± 9.77	100.0 ± 21.26	$\boxed{33.1 \pm 5.19}$
	TN-C	49.0 ± 9.81	42.9 ± 7.14	145.7 ± 8.86	150.0 ± 8.15	27.8 ± 8.95	23.3 ± 3.96
F + I	Control	100.0 ± 16.14	112.5 ± 11.46	100.0 ± 12.10	$\boxed{74.8 \pm 1.04}$	100.0 ± 7.10	$\boxed{123.1 \pm 2.66}$
	TN-C	60.2 ± 5.85	$\boxed{96.4 \pm 8.37}$	131.5 ± 7.36	$\boxed{82.5 \pm 13.38}$	32.2 ± 9.09	$\boxed{93.0 \pm 3.39}$
H-7	Control	100.0 ± 6.34	105.9 ± 13.81	100.0 ± 18.33	109.4 ± 7.06	100.0 ± 15.69	92.3 ± 14.52
	LN-ENT	32.7 ± 6.91	$\boxed{76.6 \pm 6.89}$	154.7 ± 15.40	143.4 ± 14.99	29.4 ± 2.83	$\boxed{112.5 \pm 11.72}$
H-8	Control	100.0 ± 6.19	90.4 ± 13.55	100.0 ± 16.38	93.8 ± 8.26	100.0 ± 14.97	88.5 ± 16.67
	LN-ENT	41.4 ± 5.37	48.8 ± 7.25	161.0 ± 18.79	$\boxed{98.2 \pm 9.57}$	27.9 ± 6.49	36.1 ± 4.92
CHE	Control	100.0 ± 6.37	$\boxed{58.2 \pm 2.47}$	100.0 ± 8.87	97.1 ± 11.59	100.0 ± 14.79	$\boxed{34.0 \pm 10.29}$
	LN-ENT	42.8 ± 3.04	49.1 ± 4.66	178.9 ± 29.19	187.3 ± 16.69	50.1 ± 9.26	40.4 ± 6.73
F + I	Control	100.0 ± 12.81	$\boxed{136.5 \pm 11.17}$	100.0 ± 2.73	$\boxed{80.6 \pm 9.02}$	100.0 ± 13.20	$\boxed{140.6 \pm 7.38}$
	LN-ENT	40.9 ± 4.65	$\boxed{67.4 \pm 7.16}$	158.3 ± 15.64	$\boxed{100.8 \pm 9.68}$	29.5 ± 4.60	$\boxed{81.1 \pm 8.50}$

Cells were cultured for 21 h on control, tenascin-C (TN-C), or laminin-entactin (LN-ENT) substrates in the absence (w/o mod.) or the presence (with mod.) of H-7, H-8, chelerythrine (CHE), or forskolin + IBMX (F + I). The number of neurites per cell, the average length of major neurites per cell, and the average length of all minor neurites per cell were determined. Results were normalized with control values set to 100. Mean values ± standard deviations are shown. Values representing significant differences between morphological parameters in the absence and the presence of the modulator are boxed, $P \leq 0.05$.

(control versus tenascin-R, tenascin-C, or laminin-entactin) or compartment-specific (major versus minor neurites) effects, but interfered with neurite extension in general (not shown).

DISCUSSION

In this study we show that manipulation of protein kinase activity can block the neuronal polarity promoting activity of substrate-bound ECM molecules in a compartment-specific manner, that is, affecting either axon-like major neurites or dendrite-like minor neurites. Thus, H-8 impeded the growth of major neurites and H-7 promoted the growth of minor neurites on ECM substrates, resulting in lengths of neurites similar to those on the polyornithine control substrate. In addition to being compartment-specific, H-7 and H-8 were also substrate-specific because neurite growth was not modulated on control substrates. Although H-7 and H-8 inhibit a number of similar protein kinases comprising both serine/threonine and tyrosine kinases, the K_i values for H-7 and H-8 are different [24, 25]. Thus, a certain set of kinases, those which are inhibited by H-7, might be regulated by ECM substrates leading to decreased dendritic growth and other kinases, those inhibited by H-8, might convey the ECM signal resulting in accelerated growth of major neurites.

It should be stressed that ECM-specific effects of H-7 and H-8 were observed on tenascin-R, tenascin-C, and laminin-entactin substrates, suggesting that ECM molecules establish neuronal polarity [1, 2, 16] by similar signal transduction mechanisms. On the other hand, protein kinase C or other, yet unidentified, kinases which might be inhibited by chelerythrine appear to mediate growth of minor neurites on polyornithine substrates only in the absence of ECM molecules. In contrast to these substrate-dependent events are substrate-independent mechanisms involved in neurite outgrowth: We infer this from the observation that elevation of intracellular cAMP levels resulted in increased growth of minor and decreased growth of major neurites, hence resulting in decreased polarity on any of the substrates used in this study. Since the major enzymatic target of cAMP is protein kinase A, high activity of this enzyme might hinder the establishment of a polar phenotype, while basal activity of protein kinase A appears to be essential for proper neurite growth since inhibition of protein kinase A by H-89 impeded growth of all neurites on ECM and polyornithine substrates. Thus, as for the role of calcium in neurite growth [35], the exact concentration of cAMP is likely to be a key regulator of neuritogenesis. Several other protein kinase inhibitors, namely, staurosporine, ML-9, and genistein and the protein phosphatase inhibitors okadaic acid and orthovanadate, showed neither substrate nor compartment specificity, thus possibly interfering with neuritogenesis in general. These observations support the notion that the effects seen with H-7, H-8, chelerythrine, and the cAMP elevating agents are specific and might thus be indicators of physiological events *in vivo.*

During development, neurons are in contact with a temporally and spatially changing microenvironment. Neurons appear to adapt to these changes by altering their response to exogenous cues which promote neurite growth. For example, retinal neurons in culture respond to laminin with increased neurite outgrowth only at times where laminin is expressed *in vivo* along the paths of axonal growth [36, 37]. In the hippocampus, an age-dependent change in the responsiveness of neurons to the cell adhesion molecules N-CAM and N-cadherin has been reported [38]: Whereas hippocampal neurons from 17-day-old embryos extended much longer neurites on fibroblasts transfected with N-CAM, than on parental, nontransfected fibroblasts, they responded only poorly to fibroblasts transfected with N-cadherin. When hippocampal neurons from 4-day-old animals were used, they responded only weakly to N-CAM, but strongly to N-cadherin. Furthermore, each neuronal cell preparation contains a variety of both morphologically and functionally distinct phenotypes [39, 40]. It appears likely that such divergence is also manifested in differences in the signal transduction machinery which governs extension of axons and dendrites. We have used hippocampal neurons from 18- to 19-day-old rats, an age most commonly used in studying polarity development in these cells because their maturation in culture strikingly parallels their *in vivo* development [1, 39]. In light of the aforementioned observations on neuronal diversity, it remains to be seen whether and how the effects we observed with modulators of protein kinase activity on neuronal polarity on ECM substrates can be generalized to neuronal populations from different origin and/or developmental stage. Indeed, heterogeneity with regard to the outgrowth response of dendrites to neurotrophins has recently been demonstrated for different layers of the visual cortex [10]. Despite the fact that neurons in cortical layers 4, 5, and 6 responded to nerve growth factor, brain-derived growth factor, neurotrophin-3, and neurotrophin-4 with increased dendritic growth, a different neurotrophin was able to elicit maximal response for each layer.

The major class of ECM receptors is composed of integrins [41]. The fact that certain integrins can be selectively targeted to axons [42], and perhaps also to the somatodendritic compartment, makes them good candidates for conveying effects of ECM on neuronal polarity. Integrin signals are often transduced by tyrosine kinases, of which focal adhesion kinase is the best characterized [43]. However, in our assays, the broad-spectrum protein tyrosine kinase inhibitor genistein and the tyrosine phosphatase inhibitor vanadate interfered with neurite outgrowth on both polyornithine and ECM substrates. This might be expected since these inhibitors would also impair signal transduction through a variety of pathways unrelated to ECM, including cell–cell adhesion molecules and growth factor receptor signaling. However, both H-7 and H-8 might affect protein tyrosine kinases that could be directly or indirectly linked to integrins. The recent cloning of the $\beta 1$ and $\beta 3$ integrin-linked kinase ILK [44] indicates that serine/threonine kinases may play a previously underestimated role in signaling through integrin receptors. A target of phosphorylation by ILK is mitogen-activated protein kinase (MAP kinase) which relays signals from both the ECM and growth factor receptors [45, 46]. Activity of MAP kinase requires phosphorylation on both serine/threonine and tyrosine [47]. Thus, it is quite possible that the effects we observed with serine/threonine kinase inhibitors are mediated by one or several kinases which are linked to ECM-activated signaling pathways either by direct physical association [44, 46] or indirectly by triggering other intracellular events [48].

In a recent review [2], Prochiantz suggested that growth factors could influence neuronal polarity by modulation of transcription factors of the homeogene family which in turn could trigger changes in cell surface expression of cell–cell and cell–substrate adhesion molecules. Such an hypothesis also appears appealing in light of the cooperation of growth factor and integrin signaling pathways and is further supported by the recent identification of the POU domain protein Brn-3a as a neurite outgrowth promoting transcription factor [49, 50]. Thus, in addition to interfering directly with ECM-mediated intracellular signaling, our treatments could modulate expression or accessibility of ECM receptors and thereby alter the response of hippocampal neurons to ECM. That ECM substrates influence expression of matrix receptors and/or expression of growth factors and their receptors which might in turn modify neurite growth in an autocrine manner is an additional possibility.

REFERENCES

1. Craig, A. M., and Banker, G. (1994) *Annu. Rev. Neurosci.* **17,** 267–310.
2. Prochiantz, A. (1995) *Neuron* **15,** 743–746.
3. Tropea, M., Johnson, M. I., and Higgins, D. (1988) *Glia* **1,** 380–392.
4. Rousselet, A., Fetler, L., Chamak, B., and Prochiantz, A. (1988) *Dev. Biol.* **129,** 495–504.
5. Qian, J. A., Bull, M. S., and Levitt, P. (1992) *Dev. Biol.* **149,** 278–294.
6. di Porzio, U., Daguet, M. C., Glowinski, J., and Prochiantz, A. (1980) *Nature* **288,** 370–373.
7. Mattson, M. P., Dou, P., and Kater, S. B. (1988) *J. Neurosci.* **8,** 2087–2100.

8. McCobb, D. P., Haydon, P. G., and Kater, S. B. (1988) *J. Neurosci. Res.* **19,** 19–26.
9. McCobb, D. P., Cohan, C. S., Connor, J. A., and Kater, S. B. (1988) *Neuron* **1,** 377–385.
10. McAllister, A. K., Lo, D. C., and Katz, L. C. (1995) *Neuron* **15,** 791–803.
11. Lein, P., Johnson, M., Guo, X., Rueger, D., and Higgins, D. (1995) *Neuron* **15,** 597–605.
12. Lein, P., Guo, X., Hedges, A. M., Rueger, D., Johnson, M., and Higgins, D. (1996) *Int. J. Dev. Neurosci.* **14,** 203–215.
13. Lafont, F., Prochiantz, A., Valenza, C., Petitou, M., Pascal, M., Rouget, M., and Rousselet, A. (1994) *Dev. Biol.* **165,** 453–468.
14. Chamak, B., Prochiantz, A., Lein, P. J., and Higgins, D. (1989) *Development* **106,** 483–491.
15. Lein, P. J., and Higgins, D. (1989) *Dev. Biol.* **136,** 330–345.
16. Lochter, A., and Schachner, M. (1993) *J. Neurosci.* **13,** 3986–4000.
17. Lochter, A., Taylor, J., Fuss, B., and Schachner, M. (1994) *Eur. J. Neurosci.* **6,** 597–606.
18. Lafont, F., and Prochiantz, A. (1994) *Perspect. Dev. Neurobiol.* **2,** 259–268.
19. Lochter, A., Taylor, J., Braunewell, K. H., Holm, J., and Schachner, M. (1995) *J. Neurosci. Res.* **42,** 145–158.
20. Pesheva, P., Spiess, E., and Schachner, M. (1989) *J. Cell Biol.* **109,** 1765–1778.
21. Rathjen, F. G., Wolff, J. M., Chiquet-Ehrismann, R., Faissner, A., and Kruse, J. (1991) *Development* **113,** 151–164.
22. Faissner, A., and Kruse, J. (1990) *Neuron* **5,** 627–637.
23. Lochter, A., Vaughan, L., Kaplony, A., Prochiantz, A., Schachner, M., and Faissner, A. (1991) *J. Cell Biol.* **113,** 1159–1171.
24. Hidaka, H., Inagaki, M., Kawamoto, S., and Sasaki, Y. (1984) *Biochemistry* **23,** 5036–5041.
25. Herbert, J. M., Augereau, J. M., Gleye, J., and Maffrand, J. P. (1990) *Biochem. Biophys. Res.Commun.* **172,** 993–999.
26. Seamon, K. B., and Daly, J. W. (1983) *Trends Pharmacol. Sci.* **4,** 120–123.
27. Morgan, L., Jessen, K. R., and Mirsky, R. (1991) *J. Cell Biol.* **112,** 457–467.
28. Nakano, H., Kobayashi, E., Takahashi, I., Tamaoki, T., Kuzuu, Y., and Iba, H. (1987) *J. Antibiot.* **40,** 706–708.
29. Tamaoki, T., Nomoto, H., Takahashi, I., Kato, Y., Morimoto, M., and Tomita, F. (1986) *Biochem. Biophys. Res. Commun.* **135,** 397–402.
30. Chijiwa, T., Mishima, A., Hagiwara, M., Sano, M., Hayashi, K., Inoue, T., Naito, K., Toshioka, T., and Hidaka, H. (1990) *J. Biol. Chem.* **265,** 5267–5272.
31. Nagatsu, T., Suzuki, H., Kiuchi, K., Saitoh, M., and Hidaka, H. (1987) *Biochem. Biophys. Res. Commun.* **143,** 1045–1048.
32. Akiyama, T., Ishida, J., Nakagawa, S., Ogawara, H., Watanabe, S., Itoh, N., Shibuya, M., and Fukami, Y. (1987) *J. Biol. Chem.* **262,** 5592–5595.
33. Cohen, P., Holmes, F. B., and Tsukitani, Y. (1990) *Trends Biochem. Sci.* **15,** 98–192.
34. Nechay, B. R., Nanninga, L. B., Nechay, P. S. E., Post, R. L., Grantham, J. J., Macara, I. G., Kubena, L. F., Phillips, T. D., and Nielsen, F. H. (1986) *Fed. Proc.* **45,** 123–132.
35. Mills, L. R., and Kater, S. B. (1989) *In* The Assembly of the Nervous System, pp. 65–80, A. R. Liss, New York.
36. Cohen, J., Burne, J. F., McKinlay, C., and Winter, J. (1987) *Dev. Biol.* **122,** 407–418.
37. Cohen, J., Burne, J. F., Winter, J., and Bartlett, P. (1986) *Nature* **322,** 465–467.
38. Doherty, P., Skaper, S. D., Moore, S. E., Leon, A., and Walsh, F. S. (1992) *Development* **115,** 885–892.
39. Banker, G., and Cowan, W. M. (1977) *Brain Res.* **126,** 397–425.
40. Benson, D. L., Watkins, F. H., Steward, O., and Banker, G. (1994) *J. Neurocytol.* **23,** 279–295.
41. Hynes, R. O. (1992) *Cell* **69,** 11–25.
42. Bossy, B., Bossy-Wetzel, E., and Reichardt, L. F. (1991) *EMBO J.* **10,** 2375–2385.
43. Hanks, S. K., Calalb, M. B., Harper, M. C., and Patel, S. K. (1992) *Proc. Natl. Acad. Sci. USA* **89,** 8487–8491.
44. Hannigan, G. E., Leung-Hagesteijn, C., Fitz-Gibbon, L., Coppolino, M. G., Radeva, G., Filmus, J., Bell, J. C., and Dedhar, S. (1996) *Nature* **379,** 91–96.
45. Gotoh, Y., Nishida, E., Yamashita, T., Hoshi, M., Kawakami, M., and Sakai, H. (1990) *Eur. J. Biochem.* **193,** 661–669.
46. Chen, Q., Kinch, M. S., Lin, T. H., Burridge, K., and Juliano, R. L. (1994) *J. Biol. Chem.* **269,** 26602–26605.
47. Anderson, N. G., Maller, J. L., Tonks, N. K., and Sturgill, T. W. (1990) *Nature* **343,** 651–653.
48. Adams, J. C., and Watt, F. M. (1993) *Development* **117,** 1183–1198.
49. Lakin, N. D., Morris, P. J., Theil, T., Sato, T. N., Moroy, T., Wilson, M. C., and Latchman, D. S. (1995) *J. Biol. Chem.* **270,** 15858–15863.
50. Smith, M. D., Dawson, S. J., and Latchman, D. S. (1997) *Mol. Cell Biol.* **17,** 345–354.

Received May 5, 1997

EXPERIMENTAL CELL RESEARCH **235**, 130–137 (1997)
ARTICLE NO. EX973651

The Cleavage of Nuclear DNA into High Molecular Weight DNA Fragments Occurs Not Only during Apoptosis but Also Accompanies Changes in Functional Activity of the Nonapoptotic Cells

V. T. Solov'yan,[1] I. O. Andreev, T. Yu. Kolotova, P. V. Pogribniy,* D. T. Tarnavsky,* and V. A. Kunakh

*Institute of Molecular Biology and Genetics, National Academy of Science of Ukraine, Kyiv 252627, Ukraine; and *R. E. Kavetsky Institute of Experimental Pathology, Oncology and Radiobiology, National Academy of Science of Ukraine, Kyiv 252022, Ukraine*

In this paper we demonstrate that apoptosis in primary culture of murine thymocytes and in continuously growing human cells is associated with the progressive disintegration of nuclear DNA into high molecular weight (HMW)–DNA fragments of about 50–150 kb. We also show that the formation of similarly sized HMW–DNA fragments takes place in the same cells in the absence of apoptotic inducers. Unlike an apoptotic fragmentation of nuclear DNA, the formation of HMW–DNA fragments in nonapoptotic cells is rapidly induced, has no correlation with the cell death, and is not associated with the development of oligonucleosomal "ladder" or apoptotic changes in nuclear morphology. The disintegration of DNA into HMW-fragments is also observed in nuclei isolated from healthy, nonapoptosizing tissues of various eukaryotes. We show that the formation of HMW–DNA fragments in the absence of apoptotic inducers is strongly dependent on the ionic detergents, is responsive to the topoisomerase II-specific poison, teniposide, and is completely reversible under conditions that favor topoisomerase II-dependent rejoining reaction. Also, we demonstrate that the formation of HMW–DNA fragments in continuously growing cell lines caused either by serum deprivation or monolayer establishment is of a transient nature and rapidly reverses to the control level following serum addition or dilution of monolayer. The results suggest that the cleavage of nuclear DNA into HMW–DNA fragments is associated not only with apoptosis but also accompanies changes in functional activity of nonapoptotic cells. © 1997 Academic Press

INTRODUCTION

Genomic DNA within the eukaryotic cell nucleus appears to be organized into loop domains which are fixed to a protein backbone structure referred to as the nuclear matrix or chromosome scaffold [1–11]. Topoisomerase II has been shown to be a major component of the nuclear matrix and plays an important role in chromosome structure, chromosome condensation, and genome expression [12–14]. Several lines of evidence suggest that topoisomerase II is concentrated in a number of discrete anchoring complexes which probably form the bases of the chromatin loop domains [11, 12, 15, 16].

The organization of nuclear DNA into loop domains provides reasons to believe that each structural domain may correspond to individual functional genome units, which are compartmentalized relative to regulatory elements by DNA sequences that are bound to the nuclear matrix [17, 18]; for review see [19–22]. Several investigators have reported that changes in DNase I sensitivity, which can extend over tens of kilobases, accompany changes in expression of specific genes [11, 23, 24], with the boundaries of transcriptionally active nuclease-sensitive domains generally coinciding with matrix attachment regions [25–28]. In a number of studies, both replicating DNA and transcriptionally active sequences were shown to exhibit an altered interaction with nuclear matrix [6, 29–32]; reviewed in [33–36]. These data indicate that some functionally significant structural rearrangements of chromatin may accompany various cellular programs associated with the induction of cell proliferation or changes in transcription.

Recently, it was demonstrated that DNA loop domains in animal cells may be excised by topoisomerase II-mediated DNA cleavage at scaffold attachment sites when either intact cells or nucleoids (high-salt-extracted nuclei) were treated with inhibitors of topoisomerase II [37, 38]. The average size of cleaved DNA loop domains estimated by this approach ranged from 40 to 75 kb [37]. The fragmentation of nuclear DNA into similarly sized DNA fragments was observed in apoptotic cells [39–43], which led to the conclusion that the release of DNA loops from the nuclear scaffold is a crucial intracellular event in apoptotic cells (see review [44]).

---

[1] To whom correspondence and reprint requests should be addressed. Fax: +380-44-2660759. E-mail: kunakh@imbig.kiev.ua.

0014-4827/97 $25.00
Copyright © 1997 by Academic Press
All rights of reproduction in any form reserved.

In the present investigation we show that changes in the integrity of nuclear DNA, recognizable as an altered pattern of nuclear DNA cleavage into HMW–DNA fragments, take place not only in apoptotic cells but also accompany changes in functional activity of the nonapoptotic cells.

MATERIAL AND METHODS

Cell lines and culture conditions. Human lymphoblastoma-cultured cells (line CEM), HeLa, and primary cell culture of murine thymocytes obtained from the thymus of 4- to 5-weeks-old mouse (line BALB/C) were used for the analysis of DNA integrity. Human cultured cells were routinely incubated in RPMI 1640 medium supplemented with 10% fetal calf serum (FCS) in an atmosphere of 95% air, 5% CO_2 to give a final suspension of 5×10^6 cells/ml. Thymocyte primary cultures were prepared from intact thymocytes to give a final suspension of 1×10^7 cells/ml in RPMI 1640/10% FCS and incubated under conditions indicated above for at least 6 h either with or without apoptotic inducers. Apoptosis was induced by incubation of cells either with 1 μM dexamethasone or 7.5 μM teniposide (VM26). The cell survival fraction was estimated by Trypan blue exclusion and by calculation of Hoechst-positive cells.

DNA analysis in cellular preparations. Suspension (200 μl) of thymocytes or CEM cells containing approximately $1–2 \times 10^6$ cells were placed into the well of cell culture plate followed by addition of an equal volume of preheated (37°C) 1% low-melting point agarose prepared with TEN-buffer (10 mM Tris–HCl, pH 7.5, 1 mM EDTA, 150 mM NaCl). HeLa cells were washed with cultural medium to remove the dead cells, treated with tripsin to detach the cells, and embedded into agarose as described for thymocytes and CEM cells. After gelation an equal volume of lysis buffer (TEN + 1% SDS) was layered on the agarose-embedded cells, which were further incubated for 1 h at 37°C. Agarose plugs containing the DNA of lysed cells were analyzed by agarose gel electrophoresis.

Morphological examination of cells. Cells were harvested by centrifugation and resuspended in 100 ml of phosphate-buffered normal saline (PBS) at $\sim 10^7$ cells/ml and stained with 1 μg/ml of Hoechst 33342 for 30 min at 37°C. After washing cells were resuspended in 30 μl of PBS and fixed with 30 μl of 4% paraformaldehyde. For inspection of chromatin 10-μl aliquots were laid on glass slides coated with 3-aminopropyl-triethoxysilane. Microscopy was performed under conditions of normal illumination and fluorescent light using phase contrast optics. Apoptotic nuclei were easily distinguished from normal nuclei (pale euchromatic staining) as they were condensed, homogeneously labeled, brightly fluorescent, and often fragmented.

DNA cleavage assay in nuclei and nucleoids. Nuclei from various animal and plant tissues were isolated essentially according to the procedure described by Smith and Berezney [45]. The pellet of nuclei was obtained by homogenization of tissues in an ice-cold isolation buffer (50 mM Tris–HCl, pH 8.0; 0.1 mM EDTA; 0.3 M mannitol; 0.1% BSA (pental fraction); 4 mM 2-mercaptoethanol; 5 mM Mg^{2+}; 0.5% Triton X-100). Following filtration and centrifugation (1,000g for 15 min) the pellet was resuspended in the same buffer and layered onto a pad of 2.2 M sucrose prepared in isolation buffer. After centrifugation (80,000g for 2 h), the pellet of purified nuclei was washed with isolation buffer and then an equal volume of 1% (w/v) low-melting point agarose was added. The nuclei suspension was placed in inserts of 2-mm thickness and cooled to gelation.

Nucleoids (histone-depleted nuclei) were prepared by extraction of agarose-embedded nuclei with 2 M NaCl. Agarose-embedded nuclei were incubated with 10-fold excess of the extraction buffer (10 mM Tris–HCl, pH 8.0; 1 mM EDTA; 0.2 mM PMSF; 1 mM $CuSO_4$; 2 M NaCl) for 2 h at 4°C. After extraction nucleoids were washed with the cleavage buffer (25 mM Tris–HCl, pH 8.0; 0.1 mM EDTA; 5 mM $MgCl_2$) three times for 30 min at 4°C. Agarose-embedded nuclei and nucleoids were incubated for 20 min at 37°C in the cleavage buffer and then treated with the stop buffer (10 mM Tris–HCl, pH 8.0; 0.1 M EDTA; 1% SDS) for 1 h at 55°C. Agarose plugs containing the DNA of nuclei or nucleoids were analyzed by field inversion gel electrophoresis (FIGE). Noncleaved DNA was extracted from the agarose plugs left on the start by standard procedure that consisted in the melting of agarose at 65°C, treatment with 1% SDS and proteinase K (200 μg/ml), followed by gel-electrophoresis analysis.

Agarose gel electrophoresis. Cellular, nuclear, and nucleoid preparations were fractionated either by conventional or field inversion gel electrophoresis (FIGE) to analyze the integrity of nuclear DNA. Conventional gel electrophoresis was carried out in 1.4% agarose at 50 V for 4–5 h using 0.5× TBE buffer (0.089 M Tris, 0.089 M boric acid, 0.002 M EDTA, pH 8.5). FIGE was performed in 1% agarose at 85 V for 18 h in 0.5× TBE buffer under constant pulses of electric field (24 sec "forward" and 8 sec "backward") allowing resolution of DNA molecules sized up to 500 kb [51]. In some cases FIGE was carried out for 5–6 h allowing resolution of both low- and high-molecular weight DNA. After electrophoresis, the gel was stained with 1 μg/ml ethidium bromide for 10 min, viewed using a UV transilluminator, and photographed using Micrat 300 film.

RESULTS

Data presented in Fig. 1 show that apoptosis in continuously growing human lymphoblastoma cells (line CEM), induced either with dexamethasone or teniposide, is associated with the progressive DNA cleavage into HMW–DNA fragments of about 50 and 300 kb (300-kb DNA band represents the compression zone under FIGE employed), with the intensity of fragmentation being correlated with the cell death. At the same time in control cells the HMW–DNA cleavage is also observed (Fig. 1). The formation of HMW–DNA fragments in cells not induced to undergo apoptosis is gradually increased during the cell passage, and despite the comparable efficiency in the HMW–DNA cleavage occurring both in dexamethasone-treated and control cells, the formation of HMW–DNA fragments in control cells is not associated with changes in cell viability (Fig. 1B).

Like in human CEM cells, the dexamethasone-induced apoptosis in primary culture of thymocytes is associated with an extensive cleavage of nuclear DNA into HMW–DNA fragments (Fig. 2). An increased formation of HMW–DNA fragments takes place at the early stage of apoptosis and is associated with the internucleosomal DNA fragmentation and changes in nuclear morphology, both of which represent a hallmark of apoptosis in these cells (Fig. 2A). At the same time the formation of HMW–DNA fragments proceeds rapidly in freshly prepared thymocyte culture in the absence of apoptotic inducers (Fig. 2). In contrast to the apoptotic thymocytes, however, there is no progressive accumulation of HMW–DNA fragments and concomitant formation of oligonucleosomal "ladder", as well as apoptotic changes in nuclear morphology (Figs. 2B and

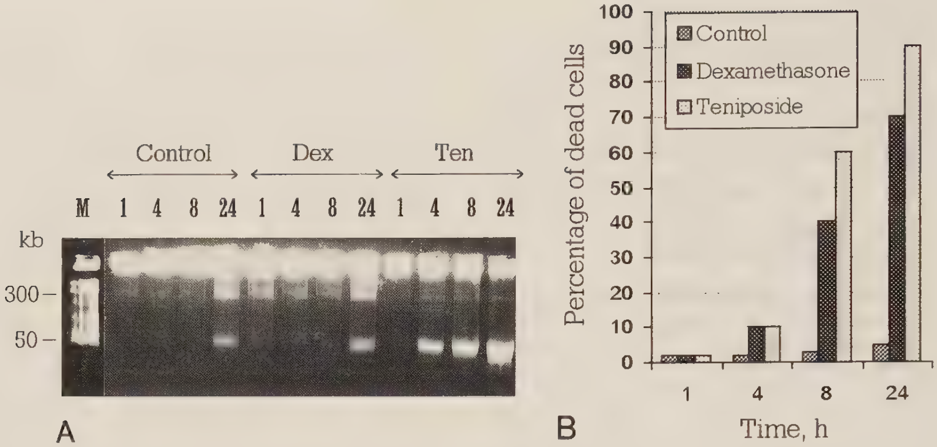

FIG. 1. The pattern of nuclear DNA cleavage during apoptosis in cultured CEM cells. Cells were incubated for 1–24 h without apoptotic inducers (Control) or in the presence of 1 μM dexamethasone (Dex) or 7.5 μM teniposide (Ten). After incubation, cells were embedded into agarose as described under Materials and Methods, treated with SDS and fractionated by FIGE. M, molecular weight standard, lambda-DNA oligomers. A demonstrates the HMW-DNA fragments separated by FIGE (ethidium bromide staining). B shows the time course of cell viability estimated by Trypan blue exclusion.

2C). In addition, *in vitro* incubation of freshly prepared thymocytes without apoptotic inducers is not associated with the progressive cell death as estimated by Hoechst-33342 staining (Fig. 2D).

The data obtained allow us to suggest that the formation of HMW–DNA fragments may occur both in apoptotic and nonapoptotic conditions. To further investigate the possibility of nonapoptotic formation of HMW–

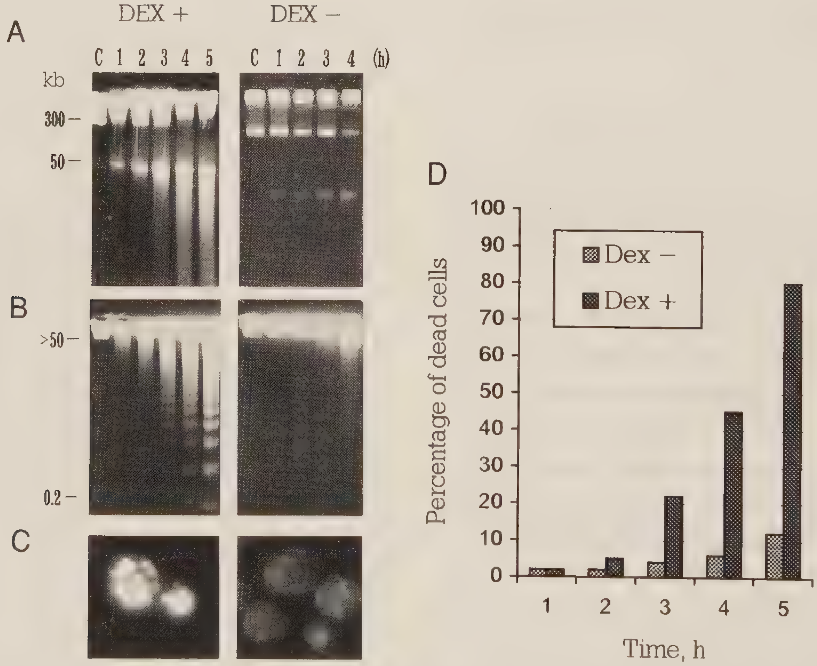

FIG. 2. The pattern of nuclear DNA cleavage in apoptotic and nonapoptotic thymocytes. Intact murine thymocytes were resuspended in RPMI medium supplemented with 10% FCS and allowed to incubate for 0–5 h either without (right panels) or in the presence of 1 μM dexamethasone (left panels). After incubation, an equal volume of preheated (37°C) TEN-buffer containing 1% low-melting point agarose was added to the cell suspension and cooled to gelation at room temperature. After gelation agarose-embedded cells were treated with 1% SDS for 1 h at 37°C and fractionated either by FIGE (A) or by conventional gel electrophoresis (B). C shows the typical morphological features of chromatin in Hoechst 33342-stained thymocytes after 5 h of *in vitro* incubation. D shows the time course of cell viability estimated by DNA-binding fluorochrome Hoechst 33342.

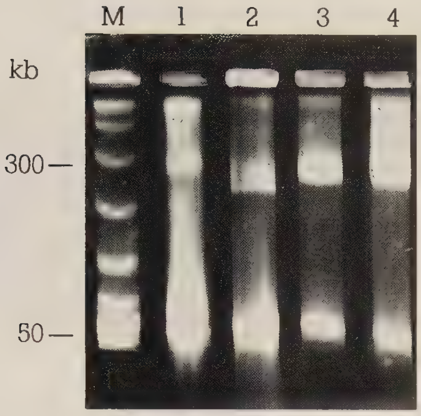

FIG. 3. The pattern of HMW–DNA cleavage in nuclei isolated from nonapoptosizing tissues of various eukaryotes. Agarose-embedded nuclei were incubated in the cleavage buffer (see Material and Methods) for 30 min at 37°C followed by treatment with 1% SDS and fractionation by FIGE. 1, rat liver; 2, human lymphocytes; 3, *Drosofila melanogaster;* 4, *Nicotiana tabacum;* M, molecular weight standards, lambda DNA oligomers.

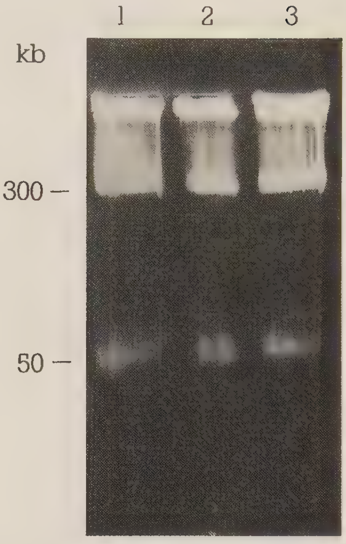

FIG. 4. The pattern of HMW–DNA fragmentation in intact cells (line 1), nuclei (line 2), and nucleoids (high-salt-extracted nuclei, lines 3). Human lymphocytes were collected by centrifugation, resuspended in PBS-buffer (see Material and Methods), and embedded in low-melting point agarose prepared in the TEN-buffer (see Material and Methods), containing 10 m*M* EDTA. After gelation, samples were treated with 1% SDS followed by FIGE fractionation. For preparation of nuclei, cells were resuspended in buffer containing 10 m*M* Tris–HCl, pH 8.0; 5 m*M* $MgCl_2$, 1% Triton X-100, 0.32 *M* sucrose. After centrifugation, nuclear pellet was resuspended in the same buffer without triton followed by addition of equal volume of 1% agarose prepared in TEN-buffer, containing 10 m*M* EDTA. Nucleoids were prepared as described under Material and Methods and washed three times with TEN-buffer, containing 10 m*M* EDTA. Agarose-embedded cells, nuclei, and nucleoids were treated with 1% SDS and fractionated by FIGE.

DNA fragments we examined the integrity of DNA in nuclei prepared from healthy, nonapoptosizing tissues of various eukaryotes.

Data presented in Fig. 3 show that different eukaryotes share the same pattern of HMW–DNA cleavage in the absence of apoptotic conditions. The formation of HMW–DNA fragments in nuclei of various eukaryotes seems to be not due to the apoptotic DNA fragmentation during the procedure of nuclear isolation since the comparable HMW–DNA cleavage takes place both in healthy human lymphocytes and in nuclei or nucleoids (high-salt-extracted nuclei) prepared from the same cells (Fig. 4).

In our experiments 20 to 70% of total DNA is usually released into the gel from cellular or nuclear preparations in the absence of apoptotic inducers. In order to elucidate the reason for such an unusual DNA disintegration we have investigated the properties of HMW–DNA cleavage in nonapoptosizing cellular/nuclear preparations. Data presented in Fig. 5 demonstrate that treatment of nuclear preparations with strong denaturing agents (SDS) represents the decisive prerequisite for HMW–DNA cleavage. No DNA fragments are released into the gel unless either intact nuclei or nucleoids were treated with SDS, even if they were incubated in the presence of Mg^{2+} ions (i.e., conditions that could provoke DNA cleavage). At the same time both HMW–DNA fragments and oligonucleosomal DNA ladder can be detected in high-salt-extracted apoptotic cells (Solovyan and Andreev, unpublished). The absence of HMW–DNA fragments in SDS-nontreated nucleoids clearly indicates that there are no preexisting ds DNA breaks in nuclei/nucleoids prepared from the nonapoptosizing cells, while the HMW–

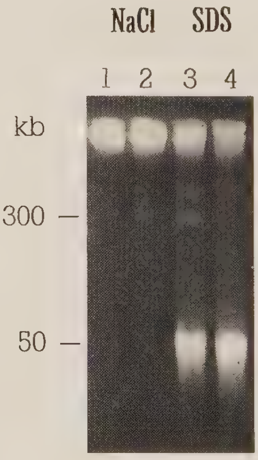

FIG. 5. SDS-dependent formation of HMW–DNA fragments in the absence of apoptosis. Agarose-embedded nuclei (lines 1, 3) and nucleoids (high-salt-extracted nuclei, lines 2, 4), prepared from the human lymphocytes, were incubated for 20 min at 37°C in the cleavage buffer (see Material and Methods). After incubation nuclei and nucleoids were treated with the stop buffer (see Material and Methods) without SDS (lines 1, 2) or with the same buffer, containing SDS (lines 3, 4), followed by FIGE fractionation.

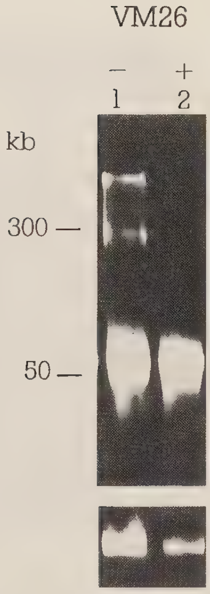

FIG. 6. The effect of teniposide (VM26) on the pattern of HMW–DNA cleavage in nucleoids (high-salt-extracted nuclei). Nuclei prepared from the human lymphocytes were embedded into agarose and extracted with sodium chloride as described under Material and Methods. Resultant nucleoids were incubated for 20 min at 37°C in the cleavage buffer containing 50 μ*M* teniposide (see Material and Methods), followed by SDS treatment and fractionation by FIGE. Top panel, DNA recovered into gel; bottom panel, noncleaved DNA left on the start.

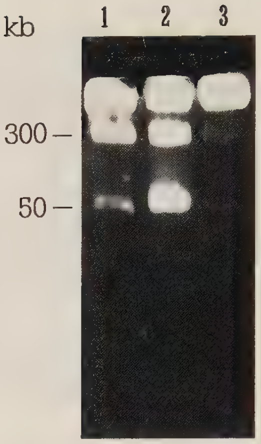

FIG. 7. The reversibility of HMW–DNA cleavage. Cell suspension of murine thymocytes was incubated at 37°C for 20 min without (line 1) or in the presence of 7.5 μ*M* teniposide (line 2). Following incubation with teniposide, the cells were incubated at 55°C for 10 min (conditions commonly used to induce the topoisomerase II-mediated reverse reaction, line 3). After incubation, an equal volume of preheated (37°C) TEN-buffer containing 1% low-melting point agarose, was added to the cell suspension and cooled to gelation at room temperature. After gelation agarose-embedded cells were treated with 1% SDS and fractionated by FIGE.

DNA cleavage is either induced or revealed by addition of detergent. SDS-dependent formation of HMW–DNA fragments makes the phenomenon observed strikingly analogous with the topoisomerase II-dependent DNA cleavage. This is further confirmed by the observation that the pattern of HMW–DNA cleavage occurring both in nucleoids (Fig. 6) and in intact cells (Fig. 7) is sensitive to the topoisomerase II-specific poison teniposide (VM26). Moreover, the conditions that favor topo II-dependent reunion reaction result in complete rejoining of HMW–DNA fragments into noncleaved DNA (Fig. 7).

As is evidenced from the data presented in Fig. 8, the formation of HMW–DNA fragments is of a transient nature. Thus, the incubation of both CEM suspension culture and attached HeLa cells in serum-deficient medium is accompanied by an increased HMW–DNA cleavage, which rapidly declines following serum addition and disappears after 24 h incubation with the fresh serum (Fig. 8).

Data presented in Fig. 9 show that the transient formation of HMW–DNA fragments takes place in HeLa cells in the absence of apoptotic inducers and accompanies changes in functional activity of the cells during the cell passage. Thus, an increased formation of HMW–DNA fragments can be observed in density-arrested cells. The dilution of monolayered cells with the medium is accompanied by the rapid changes in the pattern of HMW–DNA cleavage: an increased formation of ~50-kb DNA fragments takes place in cells after dilution, then the HMW–DNA cleavage is progressively decreased in growing cells followed by its rever-

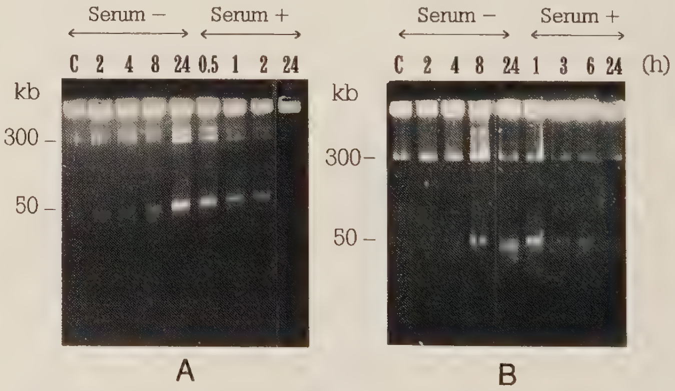

FIG. 8. The transient HMW–DNA cleavage in serum-deprived cells. Cells were incubated in serum-free medium (Serum−) for 0–24 h. Following incubation, serum was added to the cultural medium and cells were further incubated in serum-containing medium (Serum+) for 1.5–24 h. At different time-points the suspension of cells (for preparation of suspension of HeLa cells see Material and Methods) was embedded in agarose as described under Material and Methods, treated with SDS, and fractionated by FIGE. A shows the pattern of HMW–DNA cleavage in CEM suspension culture. B shows the pattern of HMW–DNA cleavage in attached HeLa cells. C, control cells before serum deprivation.

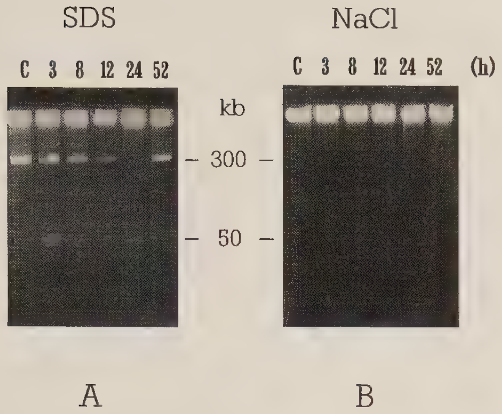

FIG. 9. The transient HMW–DNA cleavage in nonapoptosizing cells during the cell passage. Monolayered HeLa cells were additionally incubated for 24 h, washed with the cultural medium to remove debris, and treated with tripsin to detach the cells. The tripsinized cells were resuspended and diluted 1:4 with the fresh cultural medium (RPMI/10% FCS), aliquoted into wells of 24-well cell culture plate, and allowed to incubate for further 3–52 h. At different time points cells were washed with cultural medium, resuspended in tripsin solution (0.1%), followed by embedding into low-melting point agarose as described under Material and Methods. After gelation agarose-embedded cells were either treated with 1% SDS for 1 h at 37°C (A) or extracted with sodium chloride as described under Material and Methods for preparation of nucleoids (B). SDS-treated cells and SDS-non-treated nucleoids were fractionated by FIGE as described under Material and Methods. C, control (monolayered) cells. Note that there is no HMW–DNA fragmentation in nucleoids while the formation of both ~300-kb and ~50-kb DNA fragments in SDS-treated cells is increased immediately after attachment of the cells, which represent approximately 25% of the original cell population, and then is progressively decreased in growing cells despite the progressive increase of the cell number.

sal to the control level after the new monolayer has been established (Fig. 9A). At the same time there are no detectable HMW–DNA fragments in nucleoids prepared from the same cells (Fig. 9B), as well as changes in the morphology of Hoechst-stained nuclei during the cell passage (results not shown).

The data obtained indicate that the HMW–DNA cleavage occurs not only during apoptosis but also accompanies changes in functional activity of the nonapoptotic cells.

DISCUSSION

Our results as well as data obtained by others [39–42] show that an extensive fragmentation of nuclear DNA into HMW fragments takes place in cells induced to undergo apoptosis. At the same time our data indicate that the HMW–DNA cleavage occurs in the absence of apoptotic inducers. Thus, the formation of HMW–DNA fragments can be observed in continuously growing human lymphoblastoma- and HeLa cells (Figs. 1 and 9) and in freshly prepared murine thymocytes not induced to undergo apoptosis (Fig. 2). Unlike DNA degradation in apoptotic cells, the formation of HMW–DNA fragments in cells not induced to undergo apoptosis does not correlate with the cell death (Figs. 1 and 2). Furthermore, HMW–DNA cleavage occurring in murine thymocytes in the absence of apoptotic inducers is not associated with the development of characteristic oligonucleosomal DNA ladder or apoptotic changes in nuclear morphology (Fig. 2). These data suggest that the formation of HMW–DNA fragments proceeds not only during apoptosis but occurs in nonapoptotic cells. This is further confirmed by the observation that an extensive formation of HMW–DNA fragments can be observed in nuclei prepared from nonapoptosizing tissues of various eukaryotes (Fig. 3) as well as in nuclei isolated from various continuously growing cell lines [46].

Our data indicate that HMW–DNA cleavage which occurs in the absence of apoptosis possesses some intrinsic properties that have no common features with the genuine DNA degradation. Indeed, the extraction of nonapoptotic nuclei with high concentration of sodium chloride does not reveal the HMW–DNA fragmentation, while the treatment of high-salt-extracted nuclei with SDS results in extensive HMW–DNA cleavage (Fig. 5). These results indicate that the formation HMW–DNA fragments in the absence of apoptosis is not due to the preexisting ds DNA breaks. SDS-dependent formation of HMW–DNA fragments adds essential credence to the idea that topoisomerase II is involved in the cleavage of nuclear DNA into HMW fragments. This is further confirmed by the observation that teniposide, a topoisomerase II-specific poison, enhances the formation of HMW–DNA fragments both in nucleoids (Fig. 6) and in intact cells (Fig. 7), while conditions that favor topoisomerase II-dependent reunion reaction result in complete rejoining of HMW–DNA fragments into noncleaved DNA (Fig. 7).

Based on studies with purified topo II enzymes and DNA, a two-stage model for topoisomerase II-mediated cleavage/religation reactions has been proposed [49, 50]. According to this model, an enzyme/DNA cleavable complex is the key covalent intermediate in the topoisomerase II-mediated DNA turnover which is in rapid equilibrium with the noncleavable complex [49, 50]. The exposure of the cleavable complex to protein denaturants such as SDS or alkali results in a cleaved DNA product involving the covalent linking of topoisomerase II subunits to the 5′-ends of broken DNA [49, 50]. Proceeding from the properties of HMW–DNA cleavage it seems appropriate to interpret the formation of HMW–DNA fragments in nonapoptosizing cells as a topoII-mediated transition of DNA from “noncleavable” to “cleavable” state. This transition appears to have no common features with the genuine and irreversible DNA degradation usually occurring in apoptotic cells, that is in agreement with recently obtained results which do not support the involvement of topoisomerase II in apoptotic DNA degradation [47, 48].

Our data show that the formation of HMW–DNA fragments is of a transient nature. Thus, an increased HMW–DNA cleavage occurs in serum-deprived CEM cells, followed by the rapid decrease after serum addition (Fig. 8A). The transient formation of HMW–DNA fragments in CEM suspension culture is not due to the elimination of apoptotic cells during the serum deprivation because the similar pattern of HMW–DNA cleavage takes place also in attached serum-deprived HeLa cells (Fig. 8B). The data obtained suggest that the pattern of HMW–DNA cleavage reflects changes in functional activity of the alive cells. This is further confirmed by the observation that altered pattern of HMW–DNA cleavage takes place in continuously growing HeLa cells at different stages of cell passage (Fig. 9A). The transient formation of HMW–DNA fragments, which occurs during the cell passage in HeLa cells, is not associated with apoptotic changes in nuclear morphology (results not shown) and, more important, is strongly SDS-dependent (Fig. 9B), thus indicating the role of topoisomerase II in transient HMW–DNA cleavage.

Because any changes in functional activity of the cells may be interpreted as a putative signal to trigger the apoptotic machinery, it is conceivable to consider the formation of HMW–DNA fragments as a genomic reaction of "preapoptotic" cells or cells "predisposed" to undergo apoptosis. One could assume that the arrest of cell proliferation may underlie the SDS-dependent formation of HMW–DNA fragments. This is confirmed by the observation that the formation of HMW–DNA fragments is progressively decreased in actively growing HeLa cells or after stimulation of cell proliferation by serum addition, while an increased HMW–DNA cleavage occurs in serum-deprived or confluent cells (Figs. 8 and 9).

To summarize, it can be concluded that changes in the integrity of nuclear DNA, recognizable as an altered pattern of nuclear DNA cleavage into HMW–DNA fragments, represent a physiologically valuable genome reaction accompanying changes in functional activity of the cells. This reaction may be associated with changes in proliferative status of the cells and may be interpreted as a transition of topoisomerase II/DNA complex between "cleavable" and "noncleavable" states.

This work was supported by the Committee for Fundamental Research at the National Academy of Sciences, Ukraine. We thank Dr. Micholap Svetlana for help in performing the morphological examination of cell nuclei.

REFERENCES

1. Paulson, J. R., and Laemmli, U. K. (1977) *Cell* **12,** 817–828.
2. Adolph, K. W., Cheng, S. M., and Laemmli, U. K. (1977) *Cell* **12,** 805–816.
3. Benyajati, C., and Worcel, A. (1976) *Cell* **9,** 393–407.
4. Cook, P. R., and Brazell, I. A. (1976) *J. Cell. Sci.* **22,** 287–302.
5. Pardoll, D. M., Vogelstein, B., and Coffey, D. S. (1980) *Cell* **19,** 527–537.
6. Vogelstein, B., Pardoll, D. M., and Coffey, D. S. (1980) *Cell* **22,** 79–85.
7. Adolph, K. W. (1980) *Chromosoma* **76,** 23–33.
8. Lebkowski, J. S., and Laemmli, U. K. (1982) *J. Mol. Biol.* **156,** 309–324.
9. Mirkovitch, J., Mirault, M.-E., and Laemmli, U. K. (1984) *Cell* **39,** 223–232.
10. Ward, W. S., Partin, A. W., and Coffey, D. S. (1989) *Chromosoma* **98,** 153–159.
11. Gasser, S. M., and Laemmli, U. K. (1987) *Trends Genet.* **3,** 16–22.
12. Earnshaw, W. C., and Heck, M. M. S. (1985) *J. Cell. Biol.* **100,** 1716–1725.
13. Berrios, M., Osheroff, N., and Fisher, P. A. (1985) *Proc. Natl. Acad. Sci. USA* **82,** 4142–4146.
14. Cockerill, P. N., and Garrard, W. T. (1986) *Cell* **44,** 273–283.
15. Sperry, A. O., Blasquez, V. C., and Garrard, W. T. (1989) *Proc. Natl. Acad. Sci. USA* **86,** 5497–5501.
16. Adachi, Y., Kas, E., and Laemmli, U. K. (1989) *EMBO J.* **8,** 3997–4006.
17. Sippel, A. E., Stief, A., Hecht, A., Muller, A., Theisen, M., Borgmeyer, U., Rupp, R. A. W., Grewal, Th., and Grussenmeyer, Th. (1989) *in* Nucleic Acids and Molecular Biology (Eckstein, F., and Lilley, D. M. J., Eds.), Vol. 3, pp. 133–147, Springer-Verlag, Berlin/Heidelberg.
18. Marilley, M., and Gassend-Bonnet, G. (1989) *Exp. Cell. Res.* **180,** 475–389.
19. Cook, P. R. (1989) *Eur. J. Biochem.* **185,** 487–501.
20. Garrard, W. T. (1990) *in* Nucleic Acids and Molecular Biology (Eckstein, F., and Lilley, D. M. J., Eds.), Vol. 4, pp. 163–175, Springer-Verlag, Berlin/Heidelberg.
21. Georgiev, G. P., Vassetsky, Y. S., Luchnik, A. N., Chernokhvostov, V. V., and Razin, S. V. (1991) *Eur. J. Biochem.* **200,** 613–624.
22. Roberge, M., and Gasser, S. M. (1992) *Mol. Microbiol.* **6,** 419–423.
23. Weintraub, H., and Groudine, M. (1976) *Science* **193,** 848–856.
24. Weisbrod, S. (1982) *Nature* **297,** 289–295.
25. Phi-Van, L., and Stratling, W. H. (1988) *EMBO J.* **7,** 655–664.
26. Bodes, J., and Maass, K. (1989) *Biochemistry* **27,** 4706–4711.
27. Jarman, A. P., and Higgs, D. R. (1988) *EMBO J.* **7,** 3337–3344.
28. Levy-Wilson, B., and Fortier, C. (1990) *J. Biol. Chem.* **264,** 21196–21204.
29. Berezney, R., and Coffey, D. S. (1975) *Sciences* **189,** 291–293.
30. McCready, S. J., Godwin, J., Mason, D. W., Brazell, I. A., and Cook, P. R. (1980) *J. Cell Sci.* **46,** 365–386.
31. Robinson, S. I., Small, D., Idzerda, R., McKnight, G. S., and Vogelstein, B. (1983) *Nucleic Acids Res.* **11,** 5113–5130.
32. Ciejek, E. M., Tsai, M.-J., and O'Malley, B. W. (1983) *Nature* **306,** 607–609.
33. Berezney, R. (1991) *J. Cell. Biochem.* **47,** 109–123.

34. Cook, P. R. (1991) *Cell* **66,** 627–635.
35. Zlatanova, J. S., and van Holde, K. E. (1992) *Crit. Rev. Gene Expr.* **2,** 211–224.
36. Bodnar, J. W. (1988) *J. Theor. Biol.* **132,** 479–507.
37. Razin, S. V., Hancock, R., Iarovaia, O., Westergaard, O., Gromova, I., and Georgiev, G. P. (1993) *Cold Spring Harbor Symp. Quant. Biol.* **58,** 25–35.
38. Gromova, I. I., Thomsen, B., and Razin, S. V. (1995) *Proc. Natl. Acad. Sci. USA* **92,** 102–106.
39. Walker, P. R., Kokileva, L., LeBlanc, J., and Sikorska, M. (1993) *BioTechniques* **15,** 1032–1040.
40. Oberhammer, F., Wilson, J. W., Dive, C., Morris, I. D., Hickman, A., Wakeling, A. E., Walker, P. R., and Sikorska, M. (1993) *EMBO J.* **12,** 3679–3684.
41. Brown, D. G., Sun, X.-M., and Cohen, G. M. (1993) *J. Biol. Chem.* **268,** 3037–3039.
42. Cohen, G. M., Sun, X.-M., Fearnhead, H., MacFarlane, M., Brown, D. G., Snowden, R. T., and Dinsdale, D. (1994) *J. Immunol.* **153,** 507–516.
43. Beere, H. M., Chresta, C. M., Alejoherberg, A., Scladanowski, A., Dive, C., Larcen, A. K., and Hickman, J. A. (1995) *Mol. Pharmacol.* **47,** 986–996.
44. Alison, M. R., and Sarraf, C. E. (1995) *Toxicology* **14,** 234–247.
45. Smith, H. S., and Berezney, R. (1982) *Biochemistry* **21,** 6752–6761.
46. Szabo, G., Jr. (1995) *Exp. Cell Res.* **221,** 320–325.
47. Beere, H. M., Chresta, C. M., and Hickman, J. A. (1996) *Mol. Pharmacol.* **49,** 842–851.
48. Tanimoto, C., Hirakawa, S., Kawasaki, H., Hayakawa, N., and Ota, Z. (1995) *Acta Med. Okayama* **49,** 281–286.
49. Liu, L. F. (1989) *Annu. Rev. Biochem.* **58,** 351–375.
50. Osheroff, N. (1989) *Pharmacol. Ther.* **41,** 223–241.
51. Heller, Ch., and Pohl, F. M. (1989) *Nucleic Acids Res.* **17,** 5989–6003.

Received January 28, 1997
Revised version received April 28, 1997

EXPERIMENTAL CELL RESEARCH **235**, 138–144 (1997)
ARTICLE NO. EX973634

Apoptosis-Resistant Phenotype Selected by Alternating Exposure to Camptothecin and Etoposide

Masaru Kubota,[1] Ikuya Usami, Ken-ichiro Watanabe, Machiko Sawada, Akihiro Kataoka, Seiji Koishi, Ying-Wei Lin, Yuichi Akiyama, and Kenshi Furusho

Department of Pediatrics, Faculty of Medicine, Kyoto University, Kyoto, Japan

We selected an apoptosis-resistant subline (VC-33) in a human promyelocytic leukemia cell line, HL-60, by alternating exposure to camptothecin (CPT) and etoposide (VP-16). When wild-type (WT) and VC-33 cells were incubated with various concentrations of either CPT or VP-16 for 4 h, VC-33 showed several-fold resistance to apoptosis induced by these agents in comparison with WT cells. VC-33 cells also exhibited cross-resistance to apoptosis induced by 1-β-D-arabinofuranosylcytosine, hydroxyurea, a calcium ionophore (A23187), cycloheximide, or UV irradiation. The levels of protein–DNA cross-linking induced by CPT or VP-16, and the amounts of ara–CTP generation, tended to be smaller in VC-33 cells, but the difference was not sufficient to explain the difference in the sensitivity to apoptosis. The initial rise of intracellular calcium ions with A23187 and the expression of P-glycoprotein, Bcl-2, and Bcl-XL were comparable between WT and VC-33 cells. This mutant may represent a new phenotype of resistance to apoptosis induced by a variety of agents, and may thus be useful in the study of the mechanisms of apoptosis. © 1997 Academic Press

INTRODUCTION

Anti-cancer drugs can induce apoptosis in a variety of cell types [1]. Camptothecin (CPT), an inhibitor of topoisomerase I (Topo I), is known to cause apoptotic cell death in thymocytes [2], leukemia cells [3], and cortical neurons [4]. Apoptosis can also occur in leukemia cell lines [5, 6] or HeLa cells [7] treated with an inhibitor of topoisomerase II (Topo II), etoposide (VP-16). The stabilization of cleavable complex between Topo I or Topo II and DNA seems to be the initial cytotoxic lesion induced by these drugs [8, 9]. However, subsequent intracellular events leading to apoptosis after formation of protein–DNA cross-links are largely unknown at present.

In cultured cell lines, CPT- or VP-16-resistant cells have been established to elucidate the mechanism(s) of the cytotoxicity caused by these drugs. Irrespective of the selected drug, common mechanisms of resistance have been identified. These include (a) decreased drug accumulation; (b) reduced Topo I or II activity; and (c) generation of a mutated form of Topo I or II [10–12]. Such changes generally result in decreased formation of either Topo I–DNA or Topo II–DNA adducts. These mutants, however, are not useful for elucidating the mechanism of apoptosis after generation of protein–DNA cross-links. Recent investigations have presented the possibility of a common pathway to apoptosis, since protease inhibitors [13], anti-oxidants [14], or Bcl-2 oncoprotein [15] can prevent apoptosis induced by different stimuli.

In the present study, we have isolated a mutant resistant to both CPT and VP-16 by alternating exposure to these drugs. This unique method can efficiently eliminate a mutant which has its mutation in either Topo I or Topo II. Eventually, this mutant has the phenotype resistant to apoptosis induced by a variety of agents other than CPT and VP-16. Therefore, this mutant is considered useful for the study of the mechanisms of apoptosis.

MATERIALS AND METHODS

Cell line and mutant selection. A human promyelocytic leukemia cell line, HL-60, was grown in RPMI 1640 medium supplemented with 10% fetal bovine serum, L-glutamine (2 mM), penicillin (100 U/ml), and streptomycin (100 μg/ml). The culture was maintained at 37°C in a humidified atmosphere of 5% CO_2/95% air. For the selection of the mutant, wild-type (WT) cells were first exposed to CPT (0.5 μM) for 4 h. After being washed and resuspended in fresh medium, the cells were grown for 10–14 days. Surviving cells were then exposed to VP-16 (2 μM) for 1 h. The cells were again cultured for 10–14 days. These cycles were repeated several times with gradually increasing concentrations of CPT and VP-16. The final concentration used for mutant selection was 10 μM for each drug. The drug-resistant cell population was cloned twice by limiting dilution (0.5 cells/well). Several clones showing different degrees of resistance to apoptosis induced by CPT and VP-16 were obtained. Among them,

---

[1] To whom correspondence and reprint requests should be addressed at the Department of Pediatrics, Kyoto University, 54 Kawahara-cho, Shogoin, Sakyo-ku, Kyoto 606, Japan. Fax: +81 75 752 2361.

0014-4827/97 $25.00
Copyright © 1997 by Academic Press
All rights of reproduction in any form reserved.

one representative clone (VC-33) that was most resistant was chosen for further analysis.

Determination of apoptotic cells and cell growth following drug exposure. Cells at a density of 1 × 10^5/ml in their logarithmic growth phase were incubated with various agents. For the apoptotic cell studies, after 4 h of treatment, 100 μl of the cells was placed in a cytospin centrifuge and centrifuged on a glass microscope slide at 800 rpm for 2 min. The number of apoptotic cells, defined as cells with condensed and fragmented nuclei, was evaluated on May–Grünwald–Giemsa-stained preparations and expressed as a percentage of the total number of cells in drug-untreated cultures [16]. To determine the level of cell growth, VC-33 cells were exposed to either VP-16 or 1-β-D-arabinofuranosylcytosine (ara-C) for various intervals. Then, the viable cells which excluded trypan blue dye were counted at the indicated times. Cell growth was defined as the percentage of viable cells in the drug-treated cultures relative to viable cells in the drug-untreated control cultures.

Assay for internucleosomal DNA fragmentation. Cell pellets (3 × 10^6 cells) with or without treatment by various drugs were incubated in lysis buffer consisting of 150 m*M* NaCl, 25 m*M* ethylenediaminetetraacetic acid (EDTA), 100 μg/ml proteinase K, and 0.2% sodium dodecyl sulfate at 60°C overnight. The DNA was extracted twice with phenol/chloroform and once with chloroform. DNA was precipitated with 66% ethanol in the presence of 0.1 *M* CH_3COONa, rinsed with 70% ethanol, and dried. The DNA was dissolved in 10 m*M* Tris–HCl (pH 8) containing 1 m*M* EDTA and then treated with 50 μg/ml RNase A for 1 h at 37°C. The extraction and precipitation of DNA were repeated as described above. Approximately 10 μg DNA was placed on a 1.8% agarose gel containing 0.5 μg/ml ethidium bromide. Electrophoresis was carried out at 3 V/cm^2 for 10 h and photographs were taken under UV light [17].

Measurement of protein–DNA covalent links. Formation of covalent protein (Topo I or Topo II)–DNA in either CPT- or VP-16-treated cells was evaluated by the method of Rowe *et al.* [18]. Briefly, WT and VC-33 cells were labeled with [^{3}H]thymidine and treated with various concentrations of either CPT or VP-16 for 1 h. The cells were then harvested and lysed with prewarmed (65°C) lysis solution consisting of 1.25% SDS, 5 m*M* EDTA (pH 8.0), and 0.4 μg/ml of salmon sperm DNA. Aliquots of lysates were mixed vigorously with 325 m*M* KCL, cooled on ice for 10 min, and centrifuged for 10 min at 4°C. The radioactivity in the pellets was measured after two washings. The values are expressed as the percentage of radioactivity in precipitated total DNA.

Measurement of ara–CTP generation. Cells were incubated with various concentrations of ara-C for 1 h. After drug exposure and two washings with cold phosphate-buffered saline (PBS), the cells were extracted with 0.4 *N* perchloric acid and then neutralized with 2 *M* KOH. Ara–CTP was separated and quantified by high-performance liquid chromatography (HPLC) on a Partisil 10-SAX anion-exchange column eluted with 0.5 *M* KCl/0.25 *M* KH_2PO_4, pH 3.0, at a flow rate of 1.5 ml/min [19].

Measurement of $[Ca^{2+}]_i$. $[Ca^{2+}]_i$ was determined with a fluorescent Ca^{2+} indicator, indo-1 AM. Cells at a density of 2 × 10^7/ml were suspended in Hepes buffer consisting of 145 m*M* NaCl, 5 m*M* KCl, 1 m*M* Na_2HPO_4, 1 m*M* $CaCl_2$, 0.5 m*M* $MgSO_4$, 5 m*M* glucose, and 10 m*M* Na Hepes, pH 7.4. After the addition of indo-1 AM (1 mg/ml), the cells were kept at 37°C for 30 min. They were then washed twice with PBS and resuspended at 2 × 10^6/ml in ice-cold Hepes buffer. Various concentrations of A23187 were added to a sample of 2 × 10^6 cells in a cuvett, and 5 min later fluorescence was measured with a spectrofluorophotometer (Shimazu RF-510, Shimazu Co., Kyoto, Japan). The excitation and emission wavelengths were 331 and 410 nm, respectively. Calibrations were performed with the addition of 0.02% Triton X-100, 5 m*M* Tris, and 40 m*M* ethylene glycol bis(β-aminoethyl ether)-*N,N'*-tetraacetic acid according to the procedure described by Grynkiewicz *et al.* [20].

Flow cytometry. The cell cycle distribution was determined by flow cytometry using a propidium iodide staining method [21]. Approximately 1 × 10^6 cells in their logarithmic growth phase were fixed with 50% ethanol and stored overnight at −20°C. The cells were washed with PBS, followed by incubation with RNase (1 mg/ml) for 30 min at 37°C. After centrifugation, they were resuspended in staining solution containing 50 μg/ml of propidium iodide and incubated for 30 min at 25°C. DNA histograms were obtained by analyzing 10^4 cells in Ortho Cytron. The percentages of cells in G_1, S, and G_2 plus M of the cell cycle were evaluated by the computer analysis of Ortho Cytron. The expression of P-glycoprotein or Bcl-2 was assessed by using mouse monoclonal antibody against P-glycoprotein (Kyowa, Tokyo, Japan) or Bcl-2 (DAKO A/S, Denmark). After fixation by the method of Pollice *et al.* [22], the cells were incubated with the primary antibody for 1 h. Cells were washed twice with PBS and incubated with the appropriate FITC-conjugated secondary antibody for 20 min. Finally, the cells were subjected to analysis by flow cytometry.

Western blotting. WT or VC-33 cells (4 × 10^6) were collected by centrifugation, washed in ice-cold PBS, and lysed in 400 μl of a lysis buffer (10 m*M* Tris HCl (pH 7.4), 5 m*M* EDTA, 0.15 *N* NaCl, 0.1% SDS, 1% Triton X-100, 0.5% Nonidet P-40, 1 m*M* orthovanadate, 1% sodium deoxycholate, 1 m*M* phenylmethylsulfonyl fluoride, 0.23 units/ml aprotinin, 10 μ*M* leupeptin) at 4°C with sonication. The concentration of protein was measured by the Bio-Rad protein assay kit (Bio-Rad, Hercules, CA). SDS sample buffer (65 m*M* Tris–HCl (pH 6.7), 3.3% SDS, 10% glycerol, 5% 2-mercaptoethanol, and 0.2% bromophenol blue) was then added to each 40 μg of postlysate protein, which was boiled for 3 min and electrophoresed on a 12% SDS–polyacrylamide gel. The proteins were electrophoretically transferred from the gel onto an Immobilon-P, polyvinylidene difluoride membrane (Millipore, Bedford, MA). After blocking with 1% bovine serum albumin in TBST (10 m*M* Tris, 150 m*M* NaCl, 0.07% Tween 20), they were immunoblotted using mouse anti-Bcl-2 monoclonal antibody or rabbit anti-Bcl-X polyclonal antibody (Oncogene Research Products, Cambridge, MA) at a 1:500 dilution [23]. The primary antibody was detected using goat anti-mouse or goat anti-rabbit horseradish peroxidase-conjugated IgG (Santa Cruz, CA) at a 1:500 dilution and the ECL chemiluminescent detection system (Amersham, Arlington Heights, IL).

Statistical analysis and chemicals. Statistical differences were determined by Student's *t* test. A two-tailed *P* value of less than 0.01 was considered statistically significant. All chemicals were purchased from Sigma (St. Louis, MO) unless otherwise indicated.

RESULTS

Sensitivity to apoptosis induced by CPT or VP-16 in WT HL-60 and VC-33 cells. When WT cells were treated with VP-16 for 4 h, morphological changes typical of apoptosis were first detected at 1.25 μ*M* (Fig. 1). The number of apoptotic cells increased with increasing concentrations of VP-16 and reached a plateau level at approximately 30%. In contrast, VC-33 cells showed less than 5% apoptosis at 20 μ*M*, the highest concentration tested in this study. Resistance to apoptosis in VC-33 cells compared with that in WT cells was also observed against CPT (Fig. 1).

Sensitivity to apoptosis induced by agents other than the selection drugs. The sensitivity of VC-33 cells to apoptosis induced by agents other than the original selection drugs of the mutant was examined. As you can see from Table 1, ara-C, hydroxyurea, A23187, cycloheximide, or UV irradiation can induce apoptosis

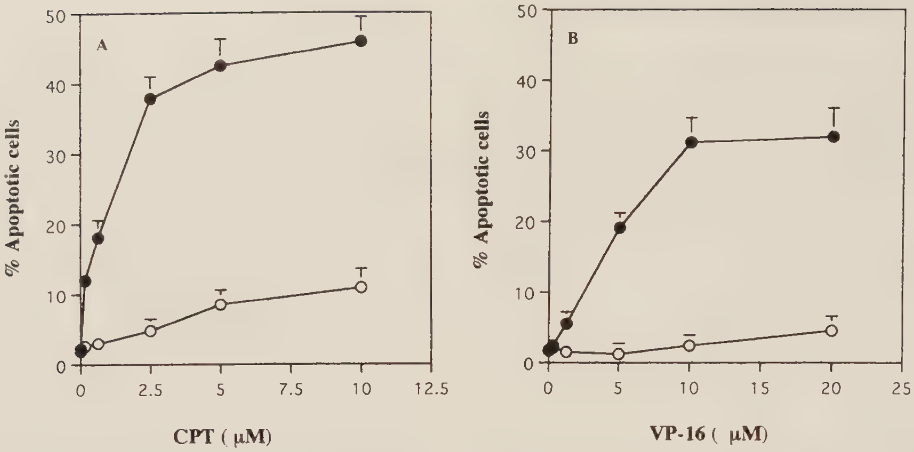

FIG. 1. Morphological apoptosis induced by CPT (A) or VP-16 (B) in WT HL-60 (●) and VC-33 cells (○). Cells were incubated with various concentrations of the drug for 4 h, and apoptotic cells were determined by May–Grünwald–Giemsa staining. Data represent the means ± SD of four experiments. The differences between WT and VC-33 cells are significant at all concentrations of both drugs.

in WT cells in a dose-dependent manner over 4–6 h of incubation. However, VC-33 cells exhibited marginal levels of apoptosis even at the highest dose of each inducer.

Long-term effects of VP-16 or ara-C on morphological apoptosis and cell growth. Next, we tried to answer the question of whether VC-33 cells still retained resistance to apoptosis when cells were incubated with the drug for longer intervals. Figure 2 demonstrates that the number of apoptotic cells gradually increased with time following treatment with a 5 *μM* concentration of either VP-16 or ara-C. They reached approximately 20% following 48 h of incubation. It is noteworthy that these values are equivalent to those induced by the same concentration of the drugs for 4 h in WT cells. On the other hand, cell growth had started to decrease following 12 h of incubation. At 48 h, cell growth in VP-16- or ara-C-treated cells revealed 16.8 or 50.1%, respectively, of that of drug-untreated control cultures.

TABLE 1

Morphological Apoptosis Induced by Various Agents

Agents	Concentrations	Cell type	
		WT	VC-33
Ara-C	1.25 *μM*	10.5 ± 1.2[a]	1.6 ± 0.3
	20	20.3 ± 4.8	2.1 ± 1.4
Hydroxyurea	0.5 m*M*	7.9 ± 1.9	1.9 ± 1.1
	2.0	23.3 ± 0.8	4.6 ± 1.7
A23187	1.0 *μM*	9.1 ± 0.5	1.7 ± 0.2
	4.0	20.4 ± 3.5	2.6 ± 1.2
Cycloheximide	50 *μM*	7.3 ± 0.1	2.0 ± 0.1
	200	20.7 ± 2.5	3.7 ± 0.8
UV irradiation	10 J/m^2	16.1 ± 3.0	1.6 ± 0.7
	20	27.1 ± 0.8	6.0 ± 0.1
No treatment		1.6 ± 0.2	1.3 ± 0.1

[a] Cells were incubated with various concentrations of the drugs for 4 h (except for cycloheximide; 6 h). For UV irradiation, cells were exposed to either 10 or 20 J/m^2 and further incubated for 4 h. Then, apoptotic cells were evaluated morphologically. Values indicate the mean ± SD of three experiments. The differences between WT and VC-33 cells are all statistically significant except for "No treatment."

Internucleosomal DNA fragmentation caused by VP-16 or ara-C. Figure 3 shows internucleosomal DNA fragmentation, one of the biochemical hallmarks of apoptosis, following treatment with VP-16 or ara-C. WT cells started to show detectable amounts of internucleosomal DNA fragmentation with 2 *μM* VP-16 or 0.5 *μM* ara-C at 4 h. On the other hand, internucleosomal DNA fragmentation could not be detected in VC-33 cells at 20 *μM* concentrations of each drug, which is consistent with the morphological study.

Growth characteristics of WT and VC-33 cells. It has been reported that the susceptibility to apoptosis induced by various antitumor agents is a function of the changes in cell cycle distribution [24, 25]. We therefore carried out the cell cycle study using the flow cytometric method. As Table 2 shows, we observed no significant difference between the cell cycle distributions of the two cell types. Moreover, these cells had almost similar doubling times and cloning efficiency, as determined by limiting dilution assay (data not shown).

Protein–DNA cross-links after incubation with CPT or VP-16. In order to examine the possibility that resistance to apoptosis is due to the reduction in initial DNA damage, we investigated protein–DNA cross-links after incubation with CPT or VP-16. As shown in Fig. 4, the accumulation of protein–DNA cross-links was slightly higher in WT cells for both drugs. However, it should be pointed out that the difference is not

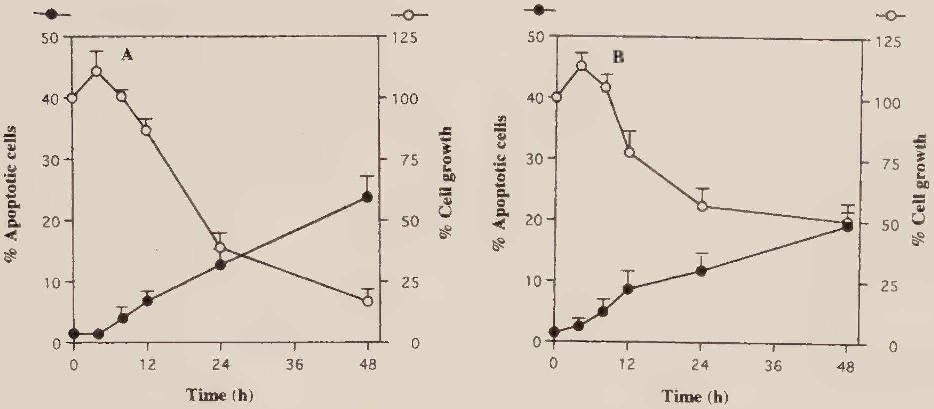

FIG. 2. Long-term effects of VP-16 or ara-C on morphological apoptosis and cell growth. VC-33 cells were incubated with either 5 μM VP-16 (A) or 5 μM ara-C (B) for various intervals up to 48 h. Cells were taken at the indicated times and apoptotic cells were determined morphologically by May–Grünwald–Giemsa staining. At the same time, the viable cells which excluded the dye trypan blue were enumerated at the indicated times. Cell growth was defined as the percentage of viable cells in the drug-treated cultures relative to those in the drug-untreated control cultures. Data represent the mean ± SD of three experiments. Apoptotic cells (●); cell growth (○).

sufficient to explain apoptosis resistance. For example, the levels of protein–DNA cross-links generated by VP-16 were comparable in WT cells at 5 μM and VC-33 cells at 10 μM, but the appearance of apoptotic cells was more than 15-fold higher in WT cells. This comparison holds true for CPT as well, when what is compared are the amounts of protein–DNA cross-linking with apoptosis at 1.25 μM in WT cells and at 2.5 μM in VC-33 cells.

Ara–CTP generation or $[Ca^{2+}]_i$ *after incubation with ara-C or A23187.* Ara–CTP synthesis is essential for ara-C to exert its toxicity [19]. The levels of ara–CTP in VC-33 cells were almost 80% of those of WT cells at every concentration of ara-C (Fig. 5A). Again, the slightly diminished formation of ara–CTP is not the main cause of apoptosis resistance to ara-C. Namely, VC-33 cells incubated with 20 μM ara-C generated more ara–CTP than did WT cells at 1.25 μM, but VC-33 cells did not undergo any apoptosis. The initial increase of $[Ca^{2+}]_i$ following incubation with various concentrations of A23187 was similar between the two cell types (Fig. 5B).

Expression of P-glycoprotein, Bcl-2, and Bcl-XL. Since VC-33 cells showed slightly decreased formation of both protein–DNA cross-links and ara–CTP, we assessed the expression of P-glycoprotein by flow cytometric analysis. As indicated in Fig. 6A, there was no significant difference in relative expression between WT and VC-33 cells. Next, we examined the possibility that VC-33 cells had elevated levels of Bcl-2 or Bcl-XL that rendered the cells resistant to apoptosis. The expression of Bcl-2 as determined by flow cytometry was, however, comparable between the two cell types

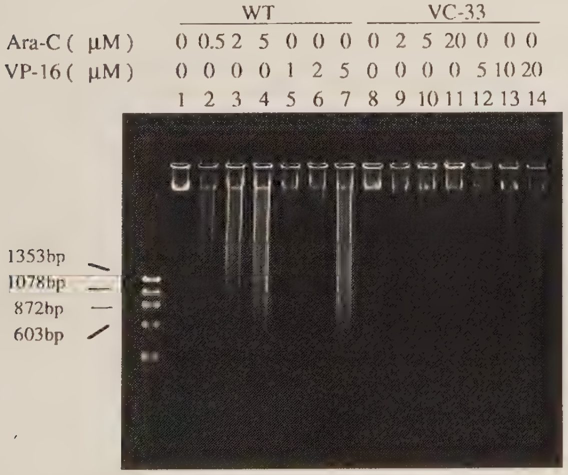
WT
VC-33
Ara-C (μM) 0 0.5 2 5 0 0 0 0 2 5 20 0 0 0
VP-16 (μM) 0 0 0 0 1 2 5 0 0 0 0 5 10 20
1 2 3 4 5 6 7 8 9 10 11 12 13 14
1353bp
1078bp
872bp
603bp

FIG. 3. Internucleosomal DNA fragmentation induced by VP-16 or ara-C in WT and VC-33 cells. Cells were incubated with various concentrations of the drug for 4 h. DNA was extracted by the method described under Materials and Methods and subjected to agarose gel electrophoresis. The ordinate shows sizes of OX174/*Hae*III-digested fragments in base pairs.

TABLE 2

Growth Characteristics of WT and VC-33 Cells

	WT	VC-33
Doubling time (h)	22.8 ± 0.5[a]	22.2 ± 0.3
Cell cycle (%)		
G_1	56.2 ± 2.5	56.8 ± 2.9
S	20.3 ± 1.7	21.2 ± 1.8
G_2 + M	23.5 ± 1.6	22.0 ± 1.9

[a] Data indicate the mean ± SD of three experiments. In all cases, the differences between WT and VC-33 cells are not statistically significant.

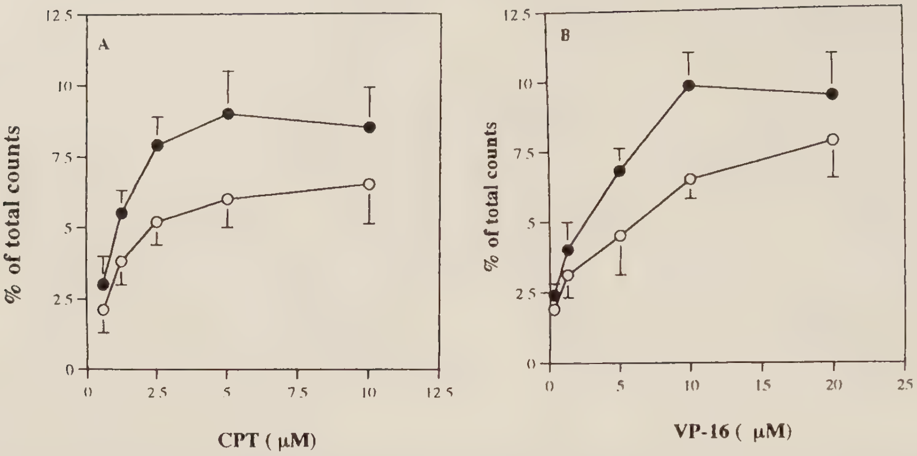

FIG. 4. Protein–DNA cross-links induced by CPT or VP-16 in WT (●) and VC-33 cells (○). Cells were labeled with [^{3}H]thymidine and incubated with various concentrations of either CPT (A) or VP-16 (B) for 1 h. DNA–protein cross-links were measured by SDS precipitation assay. Data represent the mean ± SD of three experiments. The differences between WT and VC-33 cells are significant only at 2.5 *μM* CPT and 10 *μM* VP-16.

(Fig. 6B). Furthermore, Western blot analysis revealed that the expression levels of Bcl-2 and Bcl-XL were similar between WT and VC-33 cells (Fig. 7).

DISCUSSION

Drug resistance is one of the major problems in cancer chemotherapy. In order to elucidate the mechanism(s) of drug resistance, it is considered useful to select and analyze mutants resistant to particular chemotherapeutic agents. These mutants are isolated by a single agent and usually have a phenotype which either decreases drug accumulation or alters the enzyme essential for the toxicity of a given drug [26]. Such mutants are not, however, suitable for investigating the cell death pathway subsequent to the initial drug–intracellular target interaction. To overcome this limitation, we exposed parent cells alternatively to CPT or VP-16 and, as a result, obtained a mutant that is resistant to apoptosis induced by CPT and VP-16. Because apoptotic cells were observed as the incubation time increased, it appears that apoptosis is only delayed in VC-33 cells rather than completely blocked. The mutant obtained for this study has two major characteristics: (i) it has cross-apoptosis resistance against a wide variety of agents, including ara-C, hydroxyurea, A23187, cycloheximide, and UV irradiation and (ii) the levels of protein–DNA cross-links caused by CPT or

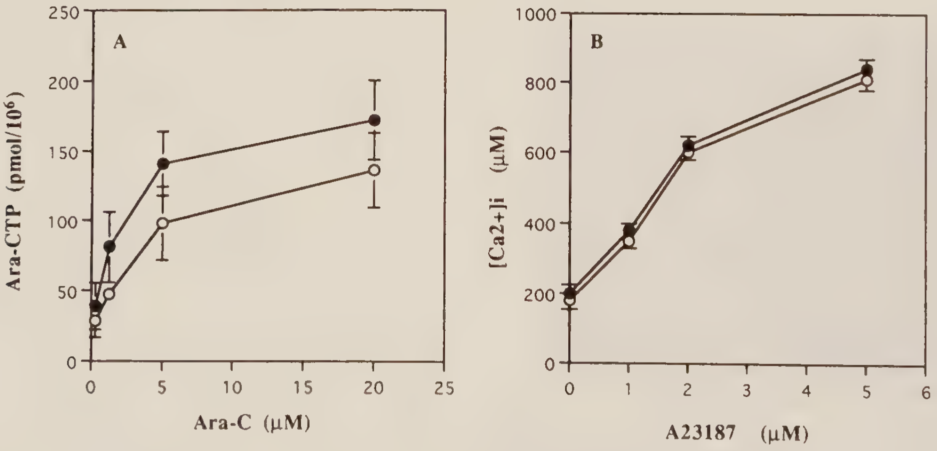

FIG. 5. Ara–CTP generation (A) and [Ca^{2+}]$_i$ after incubation with A23187 (B) in WT (●) and VC-33 cells (○). Cells were incubated with various concentrations of ara-C for 1 h. After extraction, ara–CTP was measured by HPLC. For [Ca^{2+}]$_i$ assay, cells were incubated with A23187 for 5 min. [Ca^{2+}]$_i$ was determined with a fluorescence indicator, indo-1 AM. Data represent the mean ± SD of three experiments. In all cases, the values of WT and VC-33 cells are not significantly different.

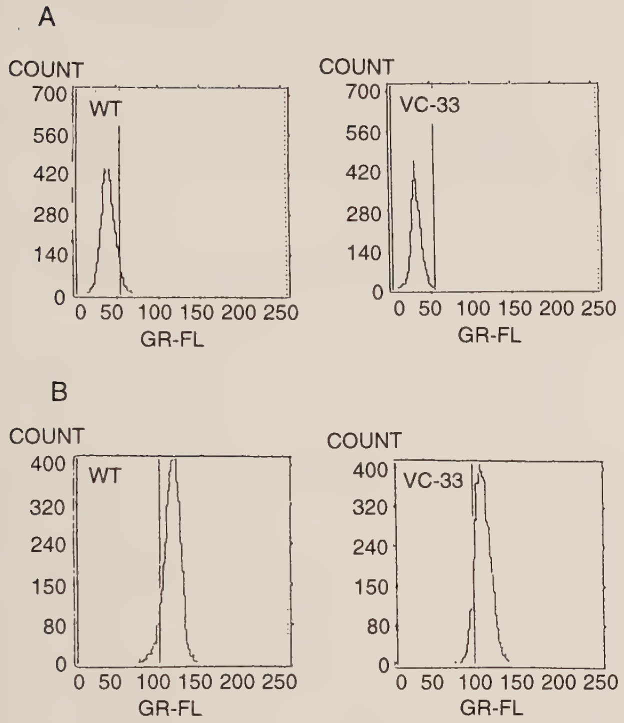

FIG. 6. P-glycoprotein (A) and Bcl-2 (B) expression in WT and VC-33 cells. The expression of P-glycoprotein or Bcl-2 was evaluated by flow cytometry. Histogram shows the representative experiment of three identical results.

VP-16 and the ara–CTP generation tend to be smaller in VC-33 cells, but the degree of difference is not sufficient to explain the difference in sensitivity to apoptosis. Furthermore, the initial rise of $[Ca^{2+}]_i$ with A23187 is comparable between WT and VC-33 cells. Therefore, it is quite possible that the mutation may be located somewhere along a common apoptotic pathway.

Several investigators have reported apoptosis-resistant cells selected by a single chemotherapeutic agent. It is noteworthy that these cells have exhibited cross-resistance to apoptosis induced by a drug(s) other than the original drug for the selection. For example, an L1210 murine leukemia cell line resistant to cisplatin did not undergo apoptosis with 5-azacytidine [27]. It has been speculated that the lack of a nuclear endonuclease in the mutant may be responsible for apoptosis resistance. Han *et al.* have described a variant of the HL-60 promyelocytic leukemia cell resistant to 8-chloroadenosine-3′,5′-cyclic monophosphate [28]. This subline was completely refractory to the apoptotic action of cycloheximide and staurosporine. The authors have discussed the possibility that a switch from expression of Bcl-2 to expression of Bcl-XL played a role in this resistance. A mutant resistant to apoptosis induced by VP-16 has been isolated in a human monocytic leukemia cell line, U937 [29]. This mutant has also proven to be resistant to apoptosis induced by a variety of antitumor agents, including ara-C, adriamycin, mitomycin C, camptothecin, and cycloheximide. These authors have not, however, postulated the mechanism(s) for this resistance.

Analysis of the characteristics of our mutant has revealed that: (i) WT HL-60 cells have already been shown to lack a nuclear constitutive endonuclease [30], (ii) the expression of Bcl-2, Bcl-XL, and Bax (data not shown) is comparable between WT and VC-33 cells, and (iii) the levels of protein–DNA cross-links induced by CPT or VP-16 tend to be smaller in VC-33 cells. Furthermore, VC-33 cells exhibit cross-resistance to apoptosis induced by agents that elevate $[Ca^{2+}]_i$, such as A23187 or thapsigargin (data not shown). This phenotype has not been described in any other apoptosis-resistant mutants described previously. In addition, our mutant was selected by a unique method, i.e., alternating exposure to CPT and VP-16. Taking these facts together, it is highly possible that VC-33 cells represent a new phenotype of apoptosis resistance. However, the site of mutation for the VC-33 cells has not yet been identified. Recently, multiple signaling pathways, including p53 [31], ceramide [32], protein kinase C [33], and tyrosine kinase [34] etc., have been postulated to be involved in apoptosis. Among them, we can now only rule out the possibility that mutation of p53 is the cause of this resistance in our mutant, since WT HL-60 cells are known to be deficient in p53 [35]. Because we have used a stepwise increase in drug concentration for selecting the mutant, it is also possible that more than one mechanism might be involved in the resistance. As an approach to clarifying the site of mutation in the VC-33 cells, a differential display experiment has been chosen and is currently under way in our laboratory.

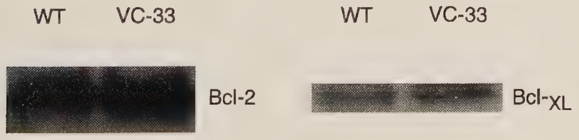

FIG. 7. Western blot analysis of Bcl-2 and Bcl-XL proteins in WT and VC-33 cells.

REFERENCES

1. Sen, S., and D'Incalci, M. (1992) *FEBS Lett.* **307,** 122–127.
2. Lee, E., Miura, M., Yoshinari, M., Iwai, H., and Kariya, K. (1994) *Biochem. Biophys. Res. Commun.* **202,** 128–134.
3. Thomas, A., El-Rouby, S., Reed, J. C., Krajewski, S., Silber, R., Potmesil, M., and Newcomb, E. W. (1996) *Oncogene* **12,** 1055–1062.
4. Morris, E. J., and Geller, H. M. (1996) *J. Cell Biol.* **134,** 757–770.
5. Kaufmann, S. H. (1989) *Cancer Res.* **49,** 5870–5878.

6. Shimizu, T., Kubota, M., Tanizawa, A., Sano, H., Kasai, Y., Hashimoto, H., Akiyama, Y., and Mikawa, H. (1990) *Biochem. Biophys. Res. Commun.* **169,** 1172–1177.
7. Lock, R. B., and Stribinskiene, L. (1996) *Cancer Res.* **56,** 4006–4012.
8. Hsiang, Y. H., Hertzberg, R., Hecht, S., and Liu, L. F. (1985) *J. Biol. Chem.* **260,** 14873–14878.
9. Ross, W., Rowe, T., Glisson, B., Yalowich, J., and Liu, L. (1984) *Cancer Res.* **44,** 5857–5860.
10. Withoff, S., De-Jong, S., De-Vries, E. G., and Mulder, N. H. (1996) *Anticancer Res.* **16,** 1867–1880.
11. Slichenmyer, W. J., Rowinsky, E. K., Donehower, R. C., and Kaufmann, S. H. (1993) *J. Natl. Cancer Inst.* **85,** 271–291.
12. Ferguson, P. J., Fisher, M. H., Stephenson, J., Li, D. H., Zhou, B. S., and Cheng, Y. C. (1988) *Cancer Res.* **48,** 5956–5964.
13. Patel, T., Gores, G. J., and Kaufmann, S. H. (1996) *FASEB J.* **10,** 587–597.
14. Bessho, R., Matsubara, K., Kubota, M., Kuwakado, K., Hirota, H., Wakazono, Y., Lin, Y. W., Okuda, A., Kawai, M., Nishikomori, R., and Heike, T. (1994) *Biochem. Pharmacol.* **48,** 1883–1889.
15. Reed, J. C. (1995) *Curr. Opin. Oncol.* **7,** 541–546.
16. Matsubara, K., Kubota, M., Adachi, S., Kuwakado, K., Hirota, H., Wakazono, Y., Akiyama, Y., and Mikawa, H. (1994) *Eur. J. Hematol.* **52,** 47–52.
17. Kataoka, A., Kubota, M., Wakazono, Y., Okuda, A., Bessho, R., Lin, Y. W., Usami, I., Akiyama, Y., and Furusho, K. (1995) *FEBS Lett.* **364,** 264–267.
18. Rowe, T. C., Chen, G. L., Hsiang, Y. H., and Liu, L. F. (1986) *Cancer Res.* **46,** 2021–2026.
19. Kubota, M., Takimoto, T., Tanizawa, A., Akiyama, Y., and Mikawa, H. (1988) *Biochem. Pharmacol.* **37,** 1745–1749.
20. Grynkiewicz, G., Poenie, M., and Tsien, R. Y. (1985) *J. Biol. Chem.* **260,** 3440–3450.
21. Krishan, A. (1975) *J. Cell Biol.* **66,** 188–193.
22. Pollice, A. A., McCoy, J. P., Shackney, S. E., Smith, C. A., Agarwal, J., Burholt, D. R., Janocko, L. E., Hornicek, F. J., Singh, S. G., and Hartsock, R. J. (1992) *Cytometry* **13,** 432–444.
23. Renart, J., Reiser, J., and Stark, G. R. (1979) *Proc. Natl. Acad. Sci. USA* **76,** 3116–3120.
24. Murakami, T., Li, X., Gong, J., Bhatia, U., Traganos, F., and Darzynkiewicz, Z. (1995) *Cancer Res.* **55,** 3093–3098.
25. Shih, S. C., and Stutman, O. (1996) *Cancer Res.* **56,** 1591–1598.
26. Fox, M., Boyle, J. M., and Kinsella, A. R. (1991) *Br. J. Cancer* **64,** 428–436.
27. Segal-Bendirdjian, E., and Jacquemin-Sablon, A. (1995) *Exp. Cell Res.* **218,** 201–212.
28. Han, Z., Chatterjee, D., Early, J., Pantazis, P., Hendrickson, E. A., and Wyche, J. H. (1996) *Cancer Res.* **56,** 1621–1628.
29. Kataoka, S., Naito, M., Tomida, A., and Tsuruo, T. (1994) *Exp. Cell Res.* **215,** 199–205.
30. Matsubara, K., Kubota, M., Adachi, S., Kuwakado, K., Hirota, H., Wakazono, Y., Akiyama, Y., and Mikawa, H. (1994) *Exp Cell Res.* **210,** 19–25.
31. Lotem, J., and Sachs, L. (1993) *Cell Growth Differ.* **4,** 41–47.
32. Kolesnick, R., and Fuks, Z. (1995) *J. Exp. Med.* **181,** 1949–1952.
33. Mizumoto, K., Rothman, R. J., and Farber, J. L. (1994) *Mol. Pharmacol.* **46,** 890–895.
34. Uckun, F. M., Tuel-Ahlgren, L., Song, C. W., Waddick, K., Myers, D. E., Kirihara, J., Ledbetter, J. A., and Schieven, G. L. (1992) *Proc. Natl. Acad. Sci. USA* **89,** 9005–9009.
35. Danova, M., Giordano, M., Mazzini, G., and Riccardi, A. (1990) *Leukemia Res.* **14,** 417–422.

Received January 16, 1997
Revised version received May 12, 1997

EXPERIMENTAL CELL RESEARCH **235**, 145–154 (1997)
ARTICLE NO. EX973679

N-Myristoyltransferase Overexpression in Human Colorectal Adenocarcinomas

Rajala V. S. Raju, Terence N. Moyana, and Rajendra K. Sharma[1]

Department of Pathology and Saskatoon Cancer Centre, College of Medicine,
University of Saskatchewan, Saskatoon, Saskatchewan S7N 4H4, Canada

Modification of proteins by myristoylation has been proposed as a chemotherapeutic target against colon cancer because it is important in the function of various signal transduction proteins. Recently we reported that the enzyme that catalyzes this modification, *N*-myristoyltransferase (NMT), is elevated in colorectal adenocarcinomas [Magnuson, B. A., Raju, R. V. S., Moyana, T. N., and Sharma, R. K. (1995) *J. Natl. Cancer. Inst.* 87, 1630–1635]. The purpose of the present study was to investigate whether the elevated activity of NMT in colorectal adenocarcinomas is due to an increase in the production of NMT or a change in the structure of the preexisting enzyme. The expression of NMT in normal colonic mucosa and adenocarcinomas from human colorectal surgical specimens was studied by immunoblotting, and its localization was confirmed by immunohistochemistry. The molecular weight of NMT was determined by fast protein liquid chromatography. In both normal mucosa and colorectal adenocarcinomas, NMT with a molecular mass of 48.5 kDa was identified with anti-human NMT and anti-peptide antibody. However, the expression of NMT was found to be higher in the colorectal tumors. This finding was further confirmed by immunohistochemical studies which showed stronger cytoplasmic staining in the tumors. These findings represent the first description of NMT overexpression in colorectal adenocarcinomas. This has implications with regard to (i) the design of chemotherapeutic drugs and (ii) prognosis, for instance, in monitoring colorectal cancer recurrence or metastases. © 1997 Academic Press

INTRODUCTION

Colorectal adenocarcinoma is one of the leading causes of death from cancer in North America. Protein modification by myristoylation has been proposed as a target for the design of chemotherapeutic drugs against colon cancer because it is important in the function of various viral proteins, cellular proteins, and oncoproteins [1]. N-Myristoylation is a cotranslational modification of proteins in which myristate is covalently attached to the N-terminal glycine residue of various viral proteins, cellular proteins, and oncoproteins [see reviews in 2, 3].

Several myristoylated proteins have been identified in intestinal cells. Normal intestinal epithelial cells express high levels of myristoylated pp60$^{c\text{-}src}$ and pp60$^{c\text{-}yes}$ [4, 5]. Intestinal-specific annexin is a myristoylated 35-kDa protein localized in the membrane of HT-29 cells derived from a human colon carcinoma [6]. Although the specific role of this protein is not known, other annexins have been implicated in signal transduction and cell growth regulation [7]. A gene called the cell adhesion regulator (CAR), cloned from a colonic cell line, encodes a protein which has an N-terminal myristoylation site and has been implicated in suppression of tumor invasion [8]. The N-terminus of enteropeptidase, a protease in the intestinal brush border membrane, has the known sequence requirements for protein myristoylation [9].

The importance of myristoylation of proteins in tumorigenesis was first suggested by studies demonstrating that myristoylation of the viral oncogene product pp60$^{v\text{-}src}$ is required for membrane association and cell transformation [10–12]. Blockage of the myristoylation of pp60$^{c\text{-}src}$ in colonic cell lines depressed colony formation, cell proliferation, and localization of pp60$^{c\text{-}src}$ to the plasma membrane [13]. The function and subcellular localization of other proteins involved in signal transduction are variously altered by mutations resulting in loss of myristoylation [3, 14, 15]. Therefore, there is evidence to support the hypothesis that myristoylation of proteins may be involved in the pathogenesis of the cancer. The tyrosine kinase activities of N-myristoylated pp60$^{c\text{-}src}$ and pp62$^{c\text{-}yes}$ protein kinases are also significantly elevated in primary colorectal adenocarcinoma as well as in their corresponding cell lines relative to those of normal cells [5, 16, 17]. It would appear that the high level of pp60$^{c\text{-}src}$ activity in colon cancer correlates with both an increase in enzyme synthesis and an association of the activated kinase with

---

[1] To whom correspondence and reprint requests should be addressed. Fax: (306) 655-2910.

0014-4827/97 $25.00
Copyright © 1997 by Academic Press
All rights of reproduction in any form reserved.

the cytoskeleton. Since a relationship has previously been established among pp60^{src} activity, cellular transformation, and an N-myristoylation-dependent association of both cellular and viral pp60^{src} with the cytoskeleton [11, 18], it is possible that the increased synthesis of pp60$^{c\text{-}src}$ in colon cancer requires increased levels of N-myristoylation in order to facilitate the *N*-myristoyl-dependent targeting of newly synthesized pp60$^{c\text{-}src}$ to the cytoskeleton.

Most recently, we reported for the first time that the enzyme that catalyzed this modification, *N*-myristoyltransferase (NMT), is more active in colonic epithelial neoplasms than in normal-appearing colonic tissue and that the increase in NMT activity appeared at an early stage in colonic carcinogenesis [19]. However, it is not yet clear whether there is an absolute increase in the production of NMT or whether the increased activity is due to a conformational change in the preexisting enzyme. This is a very important question because the overexpression of NMT in colorectal cancer has implications with regard to the development of chemotherapeutic agents. Previously, we were hampered in our efforts to ascertain the cause of the overexpression of NMT in colorectal cancer because of the lack of a specific antibody to this enzyme. However, in the present study, with the advent of antibody and anti-peptide antibodies directed against human NMT, we sought to address this issue.

MATERIALS AND METHODS

Human colorectal specimens. Surgical pathology specimens from eight patients who had undergone resection for colorectal adenocarcinoma were collected directly from the surgical operating room in the fresh state, i.e., before being immersed in tissue fixative. Following gross inspection, samples of tumors were dissected and immediately frozen at −80°C. Normal-appearing colonic mucosa far removed from the cancer was similarly dissected and frozen. Most of the remaining tissue was fixed in neutral buffered formaldehyde and processed for histological and immunohistochemical evaluation.

Preparation of tissue. All procedures were carried out at 4°C, unless otherwise stated. Tissues were homogenized in 100 m*M* Tris–HCl, pH 7.4, containing 1 m*M* EGTA, 1 m*M* EDTA, 10 m*M* 2-mercaptoethanol, 1 m*M* benzamidine, 0.2 m*M* phenylmethylsulfonyl fluoride, and 0.5 μg/ml leupeptin. The crude homogenate was centrifuged for 30 min at 10,000*g* and the supernatant was filtered through glass wool.

Construction of human NMT, Escherichia coli expression vector, and purification of NMT. The entire coding sequence of the human NMT (hNMT) gene [20] which was cloned as an *Nde*I/*Eco*RI fragment was inserted into the corresponding site of the *E. coli* expression vector pT7-7; the derived recombinant plasmid was designated pT7-hNMT. The resultant plasmid was maintained in *E. coli* BL21 (DE3) and the protein was expressed by induction with isopropyl-β-D-thiogalactoside. The expressed protein was purified 22-fold to a specific activity of 220 nmol/min/mg protein with the pp60^{src}-derived peptide substrate [21]. The yield of hNMT in *E. coli* is usually 5 mg per liter or higher [21].

Production of polyclonal antibodies. New Zealand white rabbits were immunized by subcutaneous injection of 100 μg of *E. coli*-expressed T7-hNMT and the antisera were purified according to the method described previously [21]. The antisera were then tested for NMT titer by enzyme immunoassay (EIA), performed in 96-well, flat-bottom plates according to the method described elsewhere [22].

Production of anti-peptide antibodies. The peptide NENYVEDDDNMFRFD, corresponding to the amino-terminal region from amino acids 97–112 of hNMT [20, 23], was synthesized (Applied Biosystems Model 430 A peptide synthesizer, Alberta Peptide Institute, Canada) utilizing t-Boc Nα protection and benzyl-type side chain protection. The peptide was coupled to two carrier proteins, bovine serum albumin (peptide to protein ratio 14:1) and keyhole lympet hemocyanin (KLH, peptide to protein ratio 10:1).

Solubilization of KLH peptide. Two milligrams of KLH–peptide conjugate was dissolved in 1 ml of 8 *M* urea in a 1.5-ml Eppendorf tube with occasional vortexing over a period of 4 h and centrifuged for 5 min, and the supernatant was decanted into a 6800 molecular weight cut-off dialysis bag. If a pellet was observed, 50 μl of glacial acetic acid was added with further occasional vortexing over a period of 30 min. Five hundred microliters of 8 *M* urea was added to the mixture and vortexed. The KLH conjugate was dialyzed against 0.9% NaCl overnight.

Anti-peptide antibody production. Antigen (500 μg) was mixed with 0.5 ml Freund's complete adjuvant and injected into rabbits [0.25 ml under each shoulder blade and 0.5 ml in one hip muscle (subscapular and gluteal injections)]. Two weeks later, 500 μg of antigen was mixed with Freund's incomplete adjuvant and injected. Blood was collected as described for NMT antibody production. The BSA–peptide conjugate was used to screen for anti-peptide antibody by EIA [22].

Preparation of BSA–peptide affinity column. BSA–peptide (10 mg) was dissolved in 10 ml of 0.1 *M* $NaHCO_3$, pH 9.6, and 2 g of activated CH Sepharose 4B (Pharmacia) prepared according to the manufacturer's instructions was added. The resultant slurry was mixed by rotation for 16 h at 4°C. The Sepharose 4B was pelleted by centrifugation (1000*g* for 5 min) and the extent of BSA–peptide coupling was determined by measuring the protein concentration of

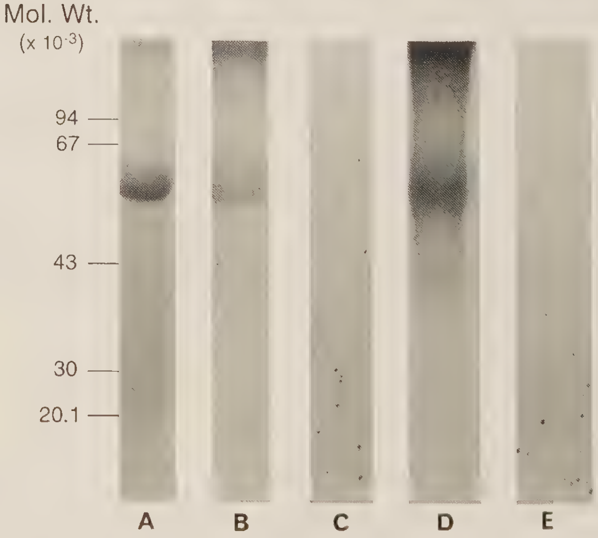

FIG. 1. Immunoblotting of purified hNMT expressed in *E. coli*. Samples of purified hNMT (5.0 μg) were immunoblotted using either affinity-purified anti-hNMT (B) or anti-peptide antibody (D). Lane A is Coomassie blue-stained hNMT. Lanes C and E were blotted with the antibodies plus antigen (50.0 μg), hNMT (C), or peptide BSA–conjugate (E).

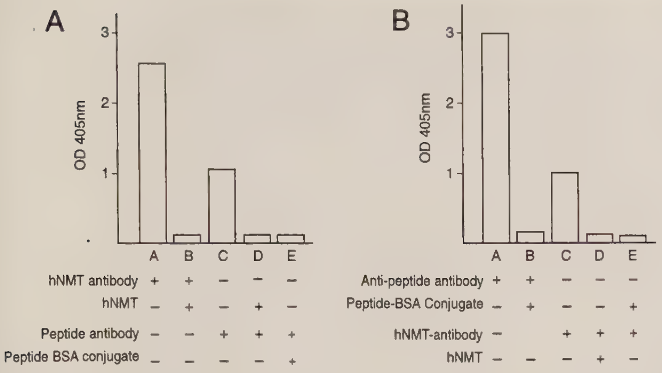

FIG. 2. Enzyme immunoassay of purified hNMT (100 ng; A) and peptide BSA–conjugate (1.0 μg; B) using either anti-hNMT or anti-peptide antibody. Lanes C, D, and E were derived from incubations in which the antibodies were co-incubated with either hNMT (1.0 μg) or peptide BSA–conjugate (10.0 μg); EIA was carried out as depicted. The results represent the mean of three determinations.

the peptide conjugate in the supernatant. More than 90% of the conjugate was coupled to Sepharose 4B. The BSA–peptide–Sepharose 4B was washed with 0.1 *M* $NaHCO_3$, pH 9.6, in a Buchner flask, and any remaining reactive groups were blocked by incubating the gel with 0.1 *M* Tris–HCl, pH 7.4, for 2 h at room temperature. The BSA–peptide–Sepharose 4B was washed alternately with low pH (0.1 *M* acetate buffer, pH 4.0) and high pH (0.1 *M* Tris–HCl, pH 8.0) buffers containing 0.5 *M* NaCl.

The anti-peptide antibodies were affinity-purified by adsorption to a 5-ml BSA–peptide–Sepharose 4B (10 × 1.5 cm) column. After adsorption, the column was washed with 0.1 *M* Tris–HCl, pH 8.0, containing 0.5 *M* NaCl. The anti-peptide antibodies were eluted using 100 m*M* glycine, pH 2.5. The eluted fractions were collected in tubes containing 3.5 ml of 1 *M* Tris–HCl at pH 8.0 and mixed immediately. The purified anti-peptide antibodies were concentrated by dialysis against 30% polyethylene glycol, suspended in 20 m*M* Tris–HCl, pH 7.0, 50% glycerol, and 0.02% NaN_3, and then stored at −70°C at a protein concentration of 0.9 mg/ml.

Immunohistochemical method. The study material consisted of eight cases of human colorectal adenocarcinoma specimens. Two tissue blocks were selected from each case, one from the tumor and the other from normal-appearing mucosa far removed from the cancer. Approximately 5-μm-thick sections were cut and subjected to the avidin–biotin complex (ABC) method as previously described [24] with the anti-peptide NMT antibody being used as the primary antibody at a concentration of 14 μg/ml. The negative controls included the substitution of a peptide–BSA conjugate or preimmune homologous serum for the anti-peptide antibody. A polyclonal antibody to carcinoembryonic antigen (CEA) (Dimension, Mississauga, Ontario, Canada) was used as a positive control. The extent of staining was graded on a 5-point scale from 0 to 4 as previously described [24], and the intensity of staining was noted as mild, moderate, or marked.

Molecular weight determination of colorectal NMT. The colorectal adenocarcinoma homogenate was applied to a Superose 12 (HR 10/30) gel filtration fast protein liquid chromatography (FPLC) column preequilibrated with phosphate buffer [50 m*M* potassium phosphate, pH 7.0, containing 0.1 m*M* EGTA, 10 m*M* 2-mercaptoethanol, 0.15 *M* NaCl, and 5% (w/v) sucrose]. Fractions were collected at a flow rate of 0.5 ml/min. An EIA was carried out to identify the elution of colonic NMT employing anti-peptide antibody [22].

Other methods. Immunoblotting was carried out essentially according to the method of Towbin *et al.* [25]. Polyacrylamide gel electrophoresis in the presence of sodium dodecyl sulfate was carried out according to the procedure of Laemmli [26] employing 10% gels. Protein concentration was determined by the method of Bradford [27] using bovine serum albumin as a standard.

RESULTS

The anti-hNMT and anti-peptide antibodies reacted strongly with the purified *E. coli* expressed hNMT in immunoblots (Fig. 1, lanes B and D). Detection of the enzyme on the immunoblot was prevented by co-incubating the affinity-purified anti-hNMT and anti-pep-

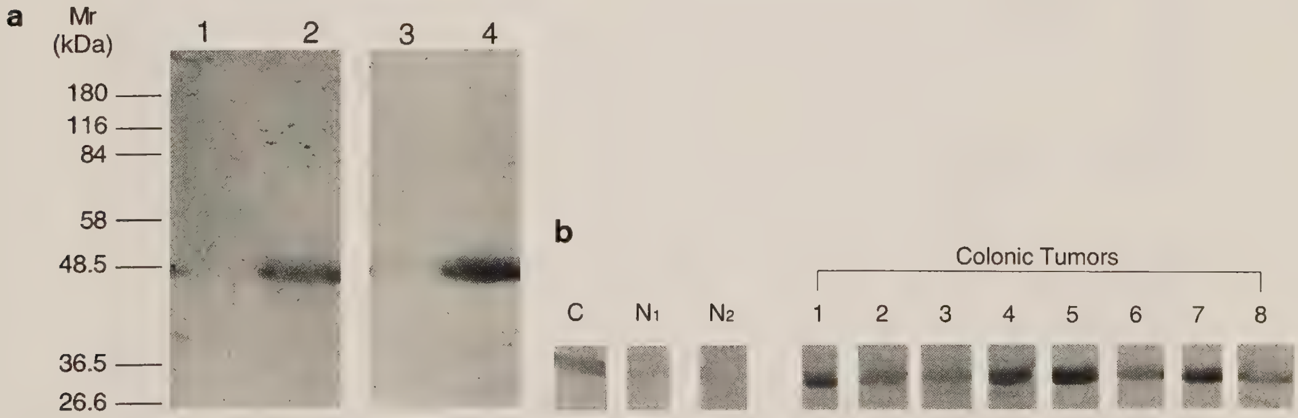

FIG. 3. (a) Immunoblot of normal mucosa (lanes 1 and 3) and colorectal tumor tissue (lanes 2 and 4) extracts with anti-hNMT (lanes 1 and 2) and anti-peptide NMT (lanes 3 and 4) antibodies. Fifteen micrograms of protein was loaded onto each lane of an SDS–polyacrylamide gel and immunoblotted with affinity-purified antibodies as described under Materials and Methods. Molecular weight markers used in this study were α_2-macroglobulin (180 kDa), β-galactosidase (116 kDa), fructose-6-phosphate kinase (84 kDa), pyruvate kinase (58 kDa), fumarase (48.5 kDa), lactate dehydrogenase (36.5 kDa), and triosephosphate isomerase (26.6 kDa). (b) Immunoblot of control NMT, normal mucosa, and colorectal tumor tissue extracts with anti-peptide NMT antibodies. Fifteen micrograms of protein was loaded onto each lane of an SDS–polyacrylamide gel and immunoblotted with affinity-purified antipeptide antibodies. C, control recombinant hNMT; N1 and N2, normal mucosa; colonic tumors (1–8).

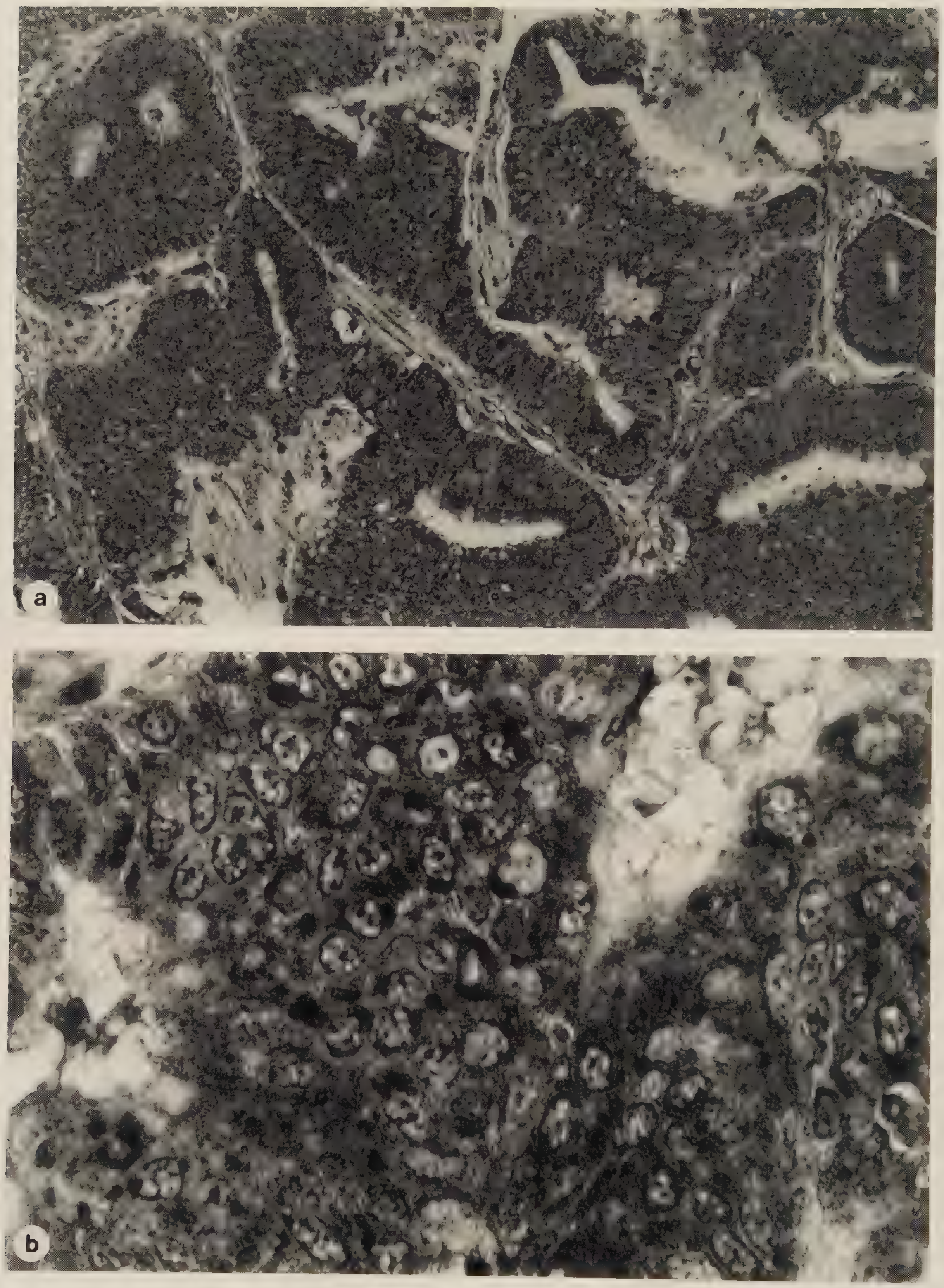

FIG. 4. (a) Section from colorectal adenocarcinoma showing a marked degree of antibody reactivity in most of the tumor cells (immunoperoxidase; original magnification, ×120). (b) High-power view depicting the cytoplasmic staining of the tumor cells. The nuclei appeared as ovoid spaces delimited by a nuclear membrane (immunoperoxidase; original magnification, ×600). (c) Negative control of colorectal adenocarcinoma showing no staining at all. This negative control was achieved by simply omitting the NMT peptide antibody from the staining procedure (immunoperoxidase; original magnification, ×300).

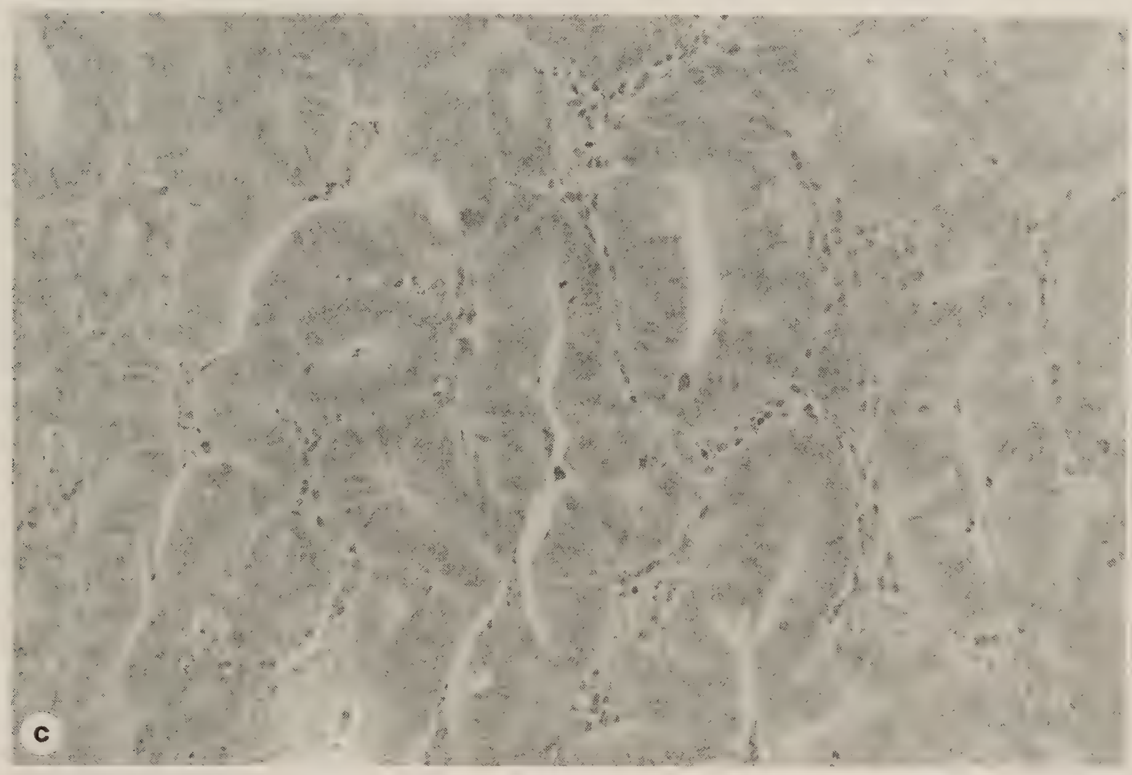

FIG. 4—*Continued*

tide antibodies with either hNMT or peptide conjugate (Fig. 1, lanes C and E); similar results were obtained when either the purified *E. coli* expressed hNMT or the peptide conjugate were adsorbed onto an EIA plate (Figs. 2A and B).

Equivalent amounts of protein from normal human colorectal mucosal tissue and adenocarcinomas were subjected to the immunoblotting method and probed with either anti-hNMT (Fig. 3a, lanes 1 and 2) or anti-peptide antibody to NMT (Fig. 3a, lanes 3 and 4). This resulted in a prominent overexpressed immunoreactive band with an apparent molecular mass of 48.5 kDa in colorectal tumors (Fig. 3a, lanes 2 and 4). However, the same 48.5-kDa band was poorly expressed in samples from normal mucosa (Fig. 3, lanes 1 and 3). The immunoblots were run separately for each of the eight patients (Fig. 3b). Immunohistochemical studies showed increased staining for NMT in colorectal tumors compared to normal mucosa. All eight cases of colorectal adenocarcinoma stained with the anti-peptide NMT antibody, with more than 50% of the cancer cells being positive in each case (Fig. 4a). The staining appeared to be cytoplasmic rather than nuclear (Fig.4b). The negative control (tumor tissue) without anti-NMT staining is given in Fig. 4c. There was some variation in the degree of immunoreactivity but most of the cases had areas depicting a moderate to marked degree of staining. In contrast, the mucosal sections taken distant from the tumor showed only mild reactivity (Fig. 5a). The transitional mucosa in the vicinity of the cancers did, however, stain more than normal mucosa albeit not to the same degree as the tumors (Fig. 5b). Similar staining results were also observed with the hNMT antibody (data not shown). The positive (CEA, Fig. 6a) and negative controls (peptide–BSA conjugate, Fig. 6b) which were run in parallel with tumor tissues further attested to the specificity and sensitivity of the immune reactions.

Under native conditions, colorectal NMT exhibited an apparent molecular mass of 48 kDa as determined on a calibrated gel filtration FPLC column (Fig. 7). SDS–polyacrylamide gel electrophoresis followed by immunoblotting showed a single immunoreactive band with an apparent molecular mass of 48.5 kDa (Fig. 3). These results suggest that colorectal NMT is a monomeric enzyme. Normal mucosal NMT also exhibits a molecular mass of 48 kDa similar to colonic tumor NMT (data not shown).

DISCUSSION

Our previous studies on colon cancer showed elevated levels of NMT activity in rat and human colonic tumors when compared to normal or normal-appearing mucosa [19]. However, it was not clear whether the increased activity of NMT was due simply to increased

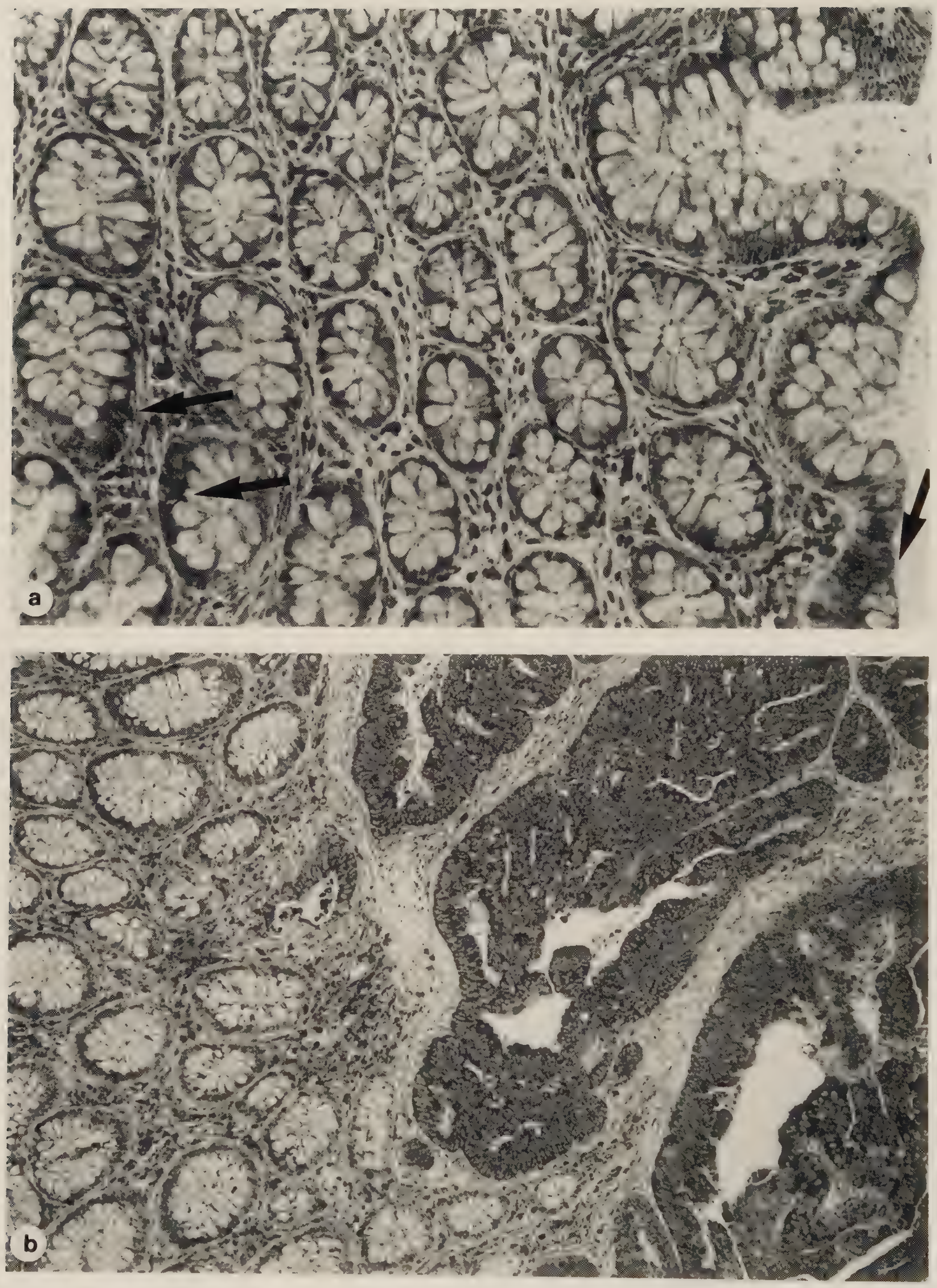

FIG. 5. (a) Section of normal mucosa far removed from tumor showing a mild degree of focal staining (see arrows) (immunoperoxidase; original magnification, ×120). (b) Section with transitional mucosa (on the left) showing a mild to moderate degree of diffuse reactivity compared to the strong tumor reactivity on the right (immunoperoxidase; original magnification, ×120).

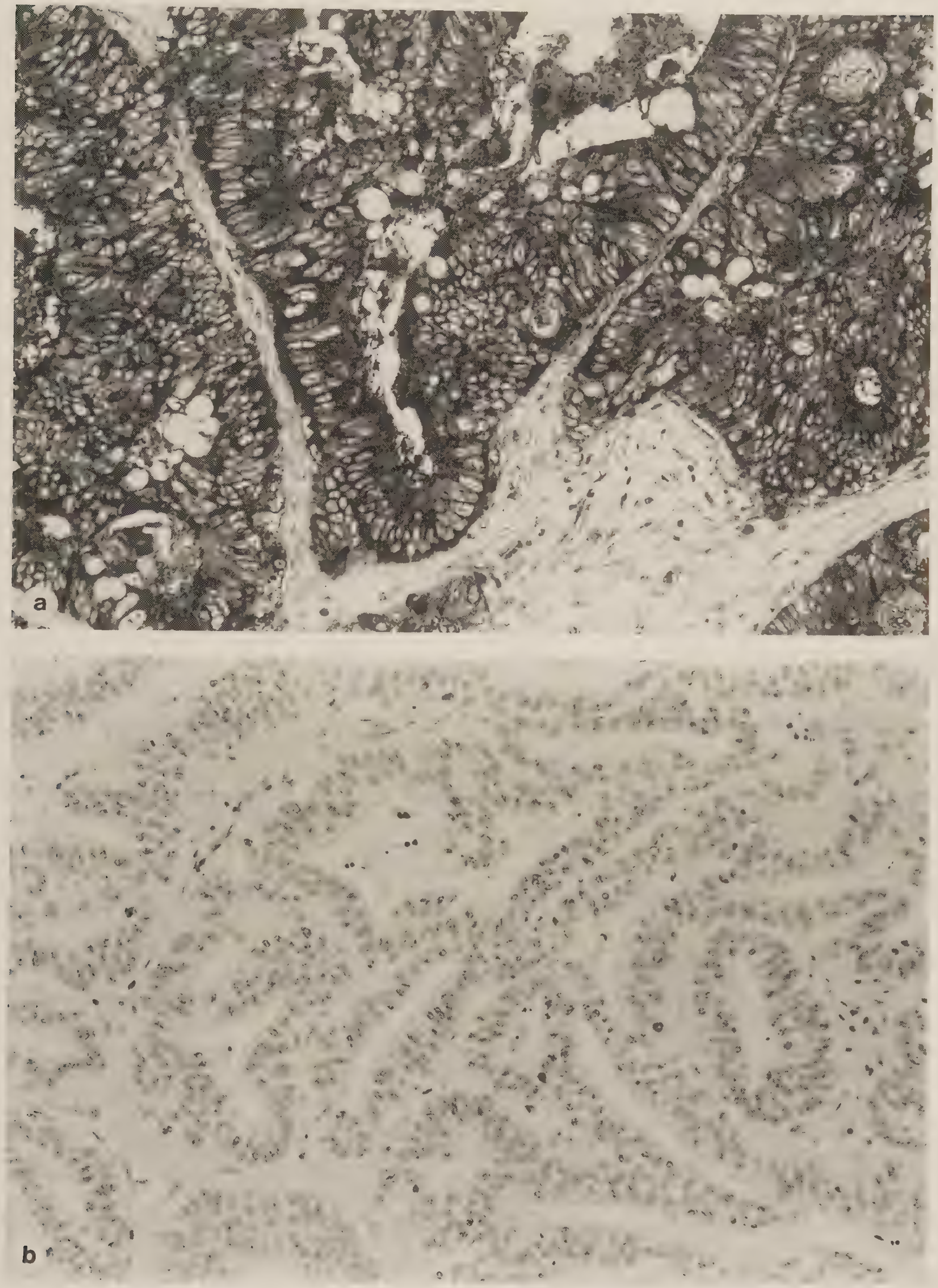

FIG. 6. (a) Marked degree of staining of colorectal carcinoma using anti-CEA antibody (immunoperoxidase; original magnification, ×240). (b) Negative control using the peptide–BSA conjugate. Colonic tumor tissue sections were co-incubated with anti-peptide antibody plus peptide BSA–conjugate (50.0 μg) and immunohistochemistry was carried out as described under Materials and Methods. Note the absence of any immunostaining (immunoperoxidase, original magnification, ×120).

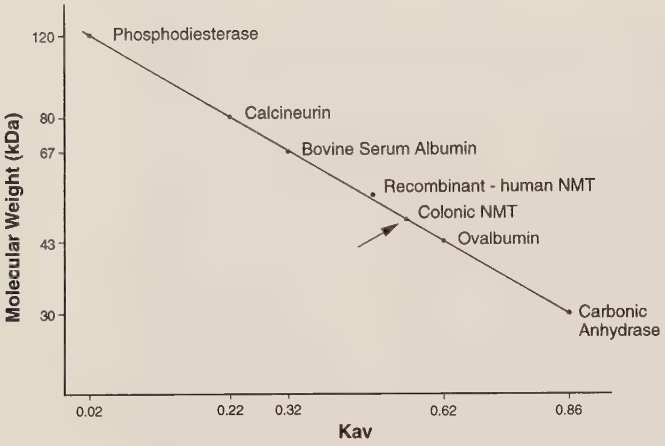

FIG. 7. Molecular weight determination of colorectal adenocarcinoma NMT by Superose 12 fast protein liquid chromatography. Colorectal mucosal homogenate (1.0 mg) was applied to a Superose 12 FPLC column. Partition coefficients (Kav) of known molecular weight proteins were calculated as described previously [41]. Molecular weight markers used in this study were calmodulin-dependent phosphodiesterase (120 kDa), calcineurin (80 kDa), bovine serum albumin (67 kDa), recombinant hNMT (50 kDa), ovalbumin (43 kDa), and carbonic anhydrase (30 kDa). Colonic mucosa NMT (indicated by arrow) was eluted with a Kav of 0.56 (48 kDa).

production of the enzyme or to a change in the conformation of the preexisting enzyme. The results from the current study suggest that elevated levels of NMT in colon cancer are not due to an alteration in the conformation of the enzyme resulting in higher intrinsic activity but are instead due to increased production of the enzyme. The possibility that the overexpression of NMT in colorectal adenocarcinomas could be due to increased stability of the NMT protein cannot be ruled out. Gene expression of NMT in normal mucosa and colorectal adenocarcinomas by reverse transcription-polymerase chain reaction revealed an increased expression of NMT mRNA in colorectal adenocarcinomas compared to that in normal mucosa (R. V. S. Raju, R. S. S. Datla, and R. K. Sharma, unpublished observation). These results suggest that NMT overexpression in colorectal adenocarcinomas is not due to increased stability of protein. NMT from the murine leukemia cell line L1210 [28] and NMT from bovine brain [2, 29] were reported to exist as multiple isoforms. However, our data suggest that colorectal tumor NMT is a single-isoform, monomeric protein. Monomeric 50-kDa human erythroleukemia cell line NMT [30], 50-kDa bovine spleen NMT [31], and 63-kDa HeLa cell NMT [32] have also been reported.

Our immunohistochemical studies showed increased staining for NMT in the colorectal tumors compared to normal mucosa, and the staining appeared to be localized in the cytoplasm. Data from different laboratories on NMT from various tissues also indicated cytosolic localization, e.g., in yeast [33], bovine brain [34], and spleen [35] as well as in the murine leukemia cell line L1210 [28] and human cell line HeLa [32]. The predominant expression of colorectal carcinoma NMT in the cytosol is consistent with myristoylation being a cotranslational process [36], since protein synthesis takes place in the cytoplasm.

Our results show that the anti-peptide NMT antibody gave a much stronger signal in differentiating the expression of NMT between colorectal carcinoma and normal mucosa than did the antibody derived from native hNMT. This could be due to the fact that the linear nature of the peptide permits better antigenic presentation to the immune system of the rabbit than the three-dimensional conformation of the native protein. Both the native hNMT antibody and the anti-peptide antibody, respectively, were also found to cross-react with NMTs from other tissues including bovine spleen, brain, and liver (data not shown). These results suggest that the 12-amino-acid peptide could be a common epitope or that it is highly conserved among various NMT species.

It appears that overexpression of NMT may be required during colon carcinogenesis because of the increased expression of various proteins that require myristoylation. The levels of tyrosine kinases pp60$^{c\text{-}src}$ and pp60$^{c\text{-}yes}$ are several-fold higher in colonic preneoplastic lesions and neoplasms compared with normal colon [16, 17, 37]. There may also be other myristoylated proteins involved in colon carcinogenesis that are yet to be identified. Higher levels of NMT activity due to overexpression might result in aberrant myristoylation of proteins, resulting in modification of signal transduction pathways.

Myristoylation has been identified as a possible target for the development of chemotherapeutic agents [1]. Tissue-specific inhibitors of this enzyme will facilitate further study of its role in the development of colorectal cancer. An endogenous inhibitor of NMT purified from bovine brain [38] inhibited NMT activity in the rat colonic cancer [19], bovine spleen [31], bovine brain [38], and hNMT [39] *in vitro*. Recently we also demonstrated for the first time the inhibition of HepG2 hepatocarcinoma cell line NMT expressed in *E. coli* [39] by human serum albumin [40].

In conclusion, we have demonstrated the overexpression of NMT in colorectal cancer tissues employing immunological approaches. This overexpression appears to be due to increased production of NMT rather than to a conformational change in the enzyme. These immunological studies indicated that antibodies to hNMT have potential utility as a diagnostic marker for the detection of colorectal cancer.

Dr. R. V. S. Raju is a recipient of a Research Fellowship from the Health Services Utilization and Research Commission of Saskatchewan. This work was partially supported by the Heart and Stroke Foundation of Saskatchewan. We thank Dr. Michael P.Walsh, Department of Medical Biochemistry, University of Calgary for his helpful suggestions and discussions regarding this paper.

REFERENCES

1. Felsted, R. L., Glover, C. J., and Hartmen, K. (1995) Protein myristoylation as a chemotherapeutic target for cancer. *J. Natl. Cancer. Inst.* **87,** 1571–1573.
2. Raju, R. V. S., Magnuson, B. A., and Sharma, R. K. (1995) Mammalian myristoyl CoA:protein *N*-myristoyltransferase. *Mol. Cell. Biochem.* **149/150,** 191–202.
3. Johnson, D. R., Bhatnagar, R. S., Knoll, L. J., and Gordon, J. I. (1994) Genetic and biochemical studies of protein N-myristoylation. *Annu. Rev. Biochem.* **63,** 869–914.
4. Zhao, Y. H., Krueger, J. G., and Sudol, M. (1990) Expression of cellular-yes protein in mammalian tissues. *Oncogene* **5,** 1629–1635.
5. Cartwright, C. A., Mamajiwalla, S., Skolnick, S. A., Eckhart, W., and Burgess, D. R. (1993) Intestinal crypt cells contain higher levels of cytoskeletal-associated pp60$^{c\text{-}src}$ protein tyrosine kinase activity than do differentiated enterocytes. *Oncogene* **8,** 1033–1039.
6. Wice, B. M., and Gordon, J. I. (1992) A strategy for isolation of cDNAs encoding proteins affecting human intestinal epithelial cell growth and differentiation: Characterization of a novel gut specific N-myristoylated annexin. *J. Cell. Biol.* **116,** 405–422.
7. Bandorowicz, J., and Pikula, S. (1993) Annexins-multifunctional, calcium-dependent, phospholipid binding proteins. *Acta Biochim. Pol.* **40,** 281–289.
8. Pullman, W. E., and Bodmer, W. F. (1992) Cloning and characterization of a gene that regulates cell adhesion. *Nature* **356,** 529–532.
9. Kitamato, Y., Yuan, X., Wu, Q., McCourt, D. W., and Sadler, J. E. (1994) Enterokinase, the initiator of intestinal digestion, is a mosaic protease composed of a distinctive assortment of domains. *Proc. Natl. Acad. Sci. USA* **91,** 7588–7592.
10. Krueger, J. G., Garber, A. E., Goldberg, A. R., and Hanafusa, H. A. (1982) Changes in amino-terminal sequences of pp60^{src} lead to decreased membrane association and decreased *in vivo* tumorigenicity. *Cell* **28,** 889–896.
11. Cross, F. R., Garber, E. A., Pellman, D., and Hanafusa, H. A. (1984) A short sequence in the p60^{src} N-terminus is required for p60^{src} myristoylation and membrane association and for cell transformation. *Mol. Cell. Biol.* **4,** 1834–1842.
12. Kamps, M. P., Buss, J. E., and Sefton, B. M. (1986) Rous sarcoma virus transforming protein lacking myristic acid phosphorylates known polypeptides substrates without inducing transformation. *Cell* **45,** 105–112.
13. Shoji, S., Kurosawa, T., Inoue, H., Funakoshi, T., and Kubato, Y. (1990) Human cellular src gene product: Identification of the myristoylated pp60^{src} and blockage of its myristoyl acylation with *N*-fatty acyl compounds resulted in the suppression of colony formation. *Biochem. Biophys. Res. Commun.* **173,** 894–901.
14. Blenis, J., and Resh, M. D. (1993) Subcellular localization specified by protein acylation and phosphorylation. *Curr. Opin. Cell Biol.* **5,** 984–989.
15. Wedegaertner, P. B., Wilson, P. T., and Bourne, H. R. (1995) Lipid modifications of trimeric G proteins. *J. Biol. Chem.* **270,** 503–506.
16. Bolen, J. B., Veillett, A., Schwartz, A. M., DeSeau, V., and Rosen, N. (1987) Activation of pp60$^{c\text{-}src}$ protein kinase activity in human colon carcinoma. *Proc. Natl. Acad. Sci. USA* **84,** 2251–2255.
17. Park, J., Meisler, A. I., and Cartwright, C. A. (1993) c-Yes tyrosine kinase activity in human colon carcinoma. *Oncogene* **8,** 2627–2635.
18. Hamaguchi, M., and Hanafusa H. (1987) Association of p60^{src} with Triton S-100 resistant cellular structure correlates with morphological transformations. *Proc. Natl. Acad. Sci. USA* **84,** 2312–2316.
19. Magnuson, B. A., Raju, R. V. S., Moyana, T. N., and Sharma, R. K. (1995) Increased *N*-myristoyltransferase activity observed in rat and human colonic tumors. *J. Natl. Cancer. Inst.* **87,** 1630–1635.
20. Duronio, R. J., Reed, S. I., and Gordon, J. I. (1992) Mutations of human myristoyl-CoA:protein *N*-myristoyltransferase cause temperature-sensitive myristic acid auxotrophy in *Saccharomyces cerevisiae. Proc. Natl. Acad. Sci. USA* **89,** 4129–4133.
21. Raju, R. V. S., Datla, R. S. S., and Sharma, R. K. (1996) Overexpression of human N-myristoyltransferase utilizing a T7 polymerase gene expression system. *Protein Expression. Purif.* **7,** 431–437.
22. Voller, A., Bartlett, A., and Bidwell, D. E. (1978) Enzyme immuno assays with special reference to ELISA techniques. *J. Clin. Pathol.* **31,** 507–520.
23. Mcilhinney, R. A. J., Patel, P. B., and McGlone, K. (1994) Characterization of a polyhistidine-tagged form of human myristoyl-CoA:protein *N*-myristoyltransferase produced in *Escherichia coli. Eur. J. Biochem.* **222,** 137–146.
24. Moyana, T. N., and Xiang, J. (1995) Expression of tumor-associated polymorphic epithelial mucin and carcinoembryonic antigen in gastrointestinal carcinoid tumors. *Cancer* **75,** 2836–2843.
25. Towbin, H., Staehelin, T., and Gordon, J. (1979) Electrophoretic transfer of proteins from polyacrylamide gels to nitrocellulose sheets: Procedure and some applications. *Proc. Natl. Acad. Sci. USA* **76,** 4350–4354.
26. Laemmli, U. K. (1970) Cleavage of structural proteins during the assembly of the head of bacteriophage T4. *Nature* **227,** 680–685.
27. Bradford, M. M. (1978) A rapid and sensitive method for the quantitation of microgram quantities of protein utilizing the principle of protein-dye binding. *Anal. Bicohem.* **72,** 248–254.
28. Boutin, J. A, Ferry, G., Ernould, A. P., Maes, P., Remond, G., and Vincent, M. (1993) Myristoyl-CoA: protein *N*-myristoyltransferase activity in cancer cells. Purification and characterization of a cytosolic isoform from the murine leukaemia cell line L1210. *Eur. J. Biochem.* **214,** 853–867.
29. Glover, C. J., Felsted, R. L. (1995) Identification and characterization of multiple forms of bovine brain *N*-myristoyltransferase. *J. Biol. Chem.* **270,** 23226–23233.
30. Kishore, N. S., Wood, D. C., Mehta, P. P., Wade, A. C., Lu, T., Gokel, G. W., and Gordon, J. I. (1993) Comparison of the acyl chain specificities of human myristoyl CoA synthetase and human myristoyl CoA:protein *N*-myristoyltransferase. *J. Biol. Chem.* **268,** 4889–4902.
31. Raju, R. V. S., Kalra, J., and Sharma, R. K. (1994) Purification and properties of bovine spleen *N*-myristoyl CoA protein: *N*-myristoyltransferase. *J. Biol. Chem.* **269,** 12080–12083.
32. McIlhinney, R. A. J., and McGlone, K. (1996) Immunocytochemical characterization and subcellular localization of human *N*-myristoyl-CoA:protein *N*-myristoyltransferase in HeLa cells. *Exp. Cell. Res.* **223,** 348–356.
33. Towler, D. A., Adams, S. P., Eubanks, S. R., Towery, D. S., Jackson-Machelski, E., Glaser, L., and Gordon, J. I. (1987) Purifica-

tion and characterization of myristoyl-CoA:protein *N*-myristoyltransferase. *Proc. Natl. Acad. Sci. USA* **84,** 2708–2712.

34. McIlhinney, R. A. J., McGlone, K., and Willis, A. C. (1993) Purification and partial sequencing of myristoyl CoA protein *N*-myristoyltransferase from bovine brain. *Biochem. J.* **290,** 405–410.
35. Raju, R. V. S., and Sharma, R. K. (1995) Myristoyl CoA:protein *N*-myristoyltransferase: Subcellular localization, activation and kinetic behaviour in the presence of organic solvents. *Biochem. Biophys. Res. Commun.* **208,** 617–623.
36. Wilcox, W., Hu, J. S., and Olson, E. N. (1987) Acylation of proteins with myristic acid occurs cotranslationally. *Science* **238,** 1275–1278.
37. Pena, S. V., Melhem, M. F., Meisler, A. I., and Cartwright, C. A. (1995) Elevated c-yes tyrosine kinase activity in premalignant lesions of the colon. *Gastroenterology* **108,** 117–124.
38. King, M. J., and Sharma, R. K. (1993) Identification, purification and characterization of a membrane-associated *N*-myristoyltransferase inhibitor protein from bovine brain. *Biochem. J.* **291,** 635–639.
39. Raju, R. V. S., Datla, R. S. S., and Sharma, R. K. (1996) Expression of human *N*-myristoyltransferase in *Escherichia coli.* Comparison with *N*-myristoyltransferases expressed in different tissues. *Mol. Cell. Biochem.* **155,** 69–76.
40. Raju, R. V. S., Datla, R. S. S., and Sharma, R. K. (1996) Reduction of oncoprotein transformation *in vitro* by albumin. *J. Natl. Cancer Inst.* **88,** 556–557.
41. Porath, J., and Flodin, P. (1959) Gel filtration: A method for desalting, and group seperation. *Nature* **183,** 1657–1659.

Received March 3, 1997
Revised version received June 3, 1997

EXPERIMENTAL CELL RESEARCH **235,** 155–160 (1997)
ARTICLE NO: EX973666

Pressure-Induced Apoptosis in Human Lymphoblasts

Kaoru J. Takano,*[,1] Takako Takano,† Yasuko Yamanouchi,† and Takaaki Satou*

**Institute of Materials Science, University of Tsukuba, Tsukuba, Japan; and †Department of Hygiene and Public Health, Teikyo University School of Medicine, Tokyo, Japan*

The viability of human lymphoblasts was investigated after compression at 37°C for 30 min. Immediately after decompression, necrotic cells were observed and the viability decreased sigmoidally to 0 with increasing pressure from 85 to 200 MPa. Apoptotic cells began to be observed from 8 h after decompression in the case of compression at 100 MPa for 30 min at 37°C. The apoptosis was confirmed to be pressure-induced by the Tunel method and by optical and electron microscopy. Cell death by both necrosis and apoptosis due to compression was accelerated in the S phase of the cell cycle. © 1997 Academic Press

INTRODUCTION

Pressure is the fundamental physical quantity controlling the mean distance between molecules. The role of pressure cannot be replaced by that of temperature. Hence, the knowledge of the role of pressure aids to understand the whole scheme of cell biology.

Chemical reaction, denaturation of molecules, and phase transition, which can give obvious influences to living bodies, depend not only on temperature but also on pressure. The pressure-induced phase transition in membranes causes sudden cell death. Denaturation of enzymes by compression may suppress the normally catalyzed reaction. It is probable that enzyme activities can be affected by high pressures. Cells that have experienced higher pressures than the atmospheric pressure in the remote past may retain some memories programmed in their DNA, and this genetic program may be executed upon the cells being subject to high pressures. Hence it is interesting to study the physiology of cells subject to high pressures. To date, there have been several biological studies at high pressures including studies using bacteria [1, 2], yeast [3], protozoa [4], and echinoids [5]. In particular, there have only been a few reports of studies involving human cells [6, 7].

Recently, cell death has been explained by two modes, necrosis and apoptosis. Necrosis can result from the swelling of the cells, irreversible damage to mitochondria, altered ionic concentrations within cells, and falling energy supplies [8], while in apoptosis there are different morphological changes such as cell shrinkage, chromatin condensation, nuclear fragmentation, and the appearance of apoptotic bodies. Apoptosis is regulated by genes and is triggered by external stimuli such as radiation, heat, toxins, virus, antitumor drugs, and so on. It is not known, however, whether pressure induces apoptosis. In this study, human cell death is investigated at high pressures using Epstein–Barr virus-transformed human lymphoblasts.

MATERIALS AND METHODS

Cell line and culture conditions. Lymphocytes derived from the peripheral blood of a healthy male donor were transformed by the Epstein–Barr virus [9]. These lymphoblasts (EB3 cells) were cultured in RPMI 1640 medium (Gibco BRL, NY) supplemented with 10% (v/v) heat-inactivated fetal bovine serum (JRH Biosciences, KS) in a chamber (5% CO_2 and 95% air) at 37°C and were used for experiments during the exponential phase of growth. In the case of compression during the S phase of the cell cycle, the cells were synchronized twice in the G_1/S boundary using an excess thymidine block (2.5 m*M*) [10].

Compression. Cells in culture medium were transferred to the pressure chamber and were kept under constant pressure for 30 min at 37°C using an optical liquid high-pressure apparatus [11] or a high-pressure apparatus of the piston–cylinder type. The variations in pressure and temperature control during the 30 min were only ±0.3 MPa and ±0.05°C, respectively. The desired pressure was obtained in less than 1 min, while decompression required about 30 s. Cells after decompression and the experimental controls (i.e., uncompressed) were maintained in the CO_2 chamber.

Cell viability and morphological observation. Cell counts and viability (the fraction of viable cells) were assessed using a 0.1% trypan blue dye exclusion test [12]. Cells were observed by phase-contrast microscopy (×150) and were monitored by incubating the cells in the CO_2 chamber for 48 h after decompression. The cells were fixed in 1% glutaraldehyde for 1 h and stained with 0.2 m*M* Hoechst 33258 (bis-benzimide) for 10 min. The nuclei were then observed with an epifluorescence microscope with excitation at 320–380 nm and emission above 420 nm (×100) [13].

DNA synthesis. To detect DNA synthesis immunologically by BrdU (5-bromo-2′-deoxyuridine; a thymidine analog) incorporation into DNA in the S phase [14, 15], the cells were synchronized in the G_1/S boundary using a thymidine block (1.2 m*M*, 15 h) [16] and

---

[1] To whom correspondence should be addressed at Institute of Materials Science, University of Tsukuba, Tsukuba, Ibaraki 305, Japan. Fax: (81)-298-55-7440. E-mail: takano@mat.ims.tsukuba.ac.jp.

0014-4827/97 $25.00
Copyright © 1997 by Academic Press
All rights of reproduction in any form reserved.

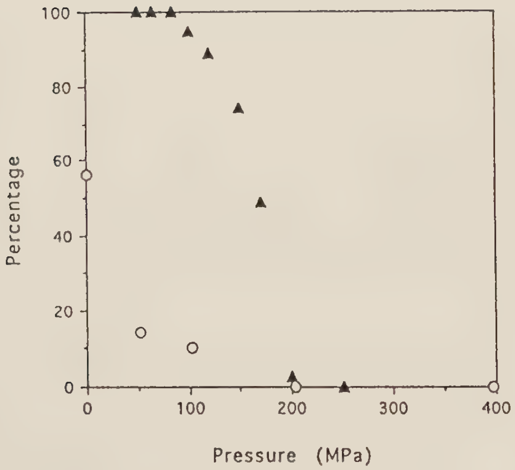

FIG. 1. Effect of pressure on cell viability and the DNA synthesis just after 30 min of pressure treatment. (▲) Cell viability; (○) DNA synthesis (percentage of BrdU uptake).

then washed. The cells were subsequently labeled with 16 μM BrdU during compression for 30 min. Just after decompression, slides of adherent cells were prepared by the standard methods of chromosome analysis and treated with anti-bromodeoxyuridine (Boehringer Mannheim, Mannheim) and FITC (fluorescein isotiocyanate)-conjugated antibody (Jackson Immuno Research Lab., Inc., Baltimore). FITC-positive cells that had incorporated BrdU into their DNA were quantitated by epifluorescence microscopy with excitation at 450–490 nm and emission above 530 nm. Because the DNA synthesis for the controls without compression changed slightly over the course of the experiments, the percentage of DNA synthesis was adjusted by using the first control data after releasing synchronization.

Apoptosis detected by the TUNEL technique. Cells were fixed in 1% glutaraldehyde for 1 h. Apoptosis was detected by the TUNEL (TdT-mediated dUTP nick-end labeling) technique (Boehringer Mannheim) [17] quantitatively and morphologically. The fragmented DNA strands within apoptotic cells were end-labeled with fluorescein dUTP by terminal deoxynucleotidyl transferase (TdT) and were observed by epifluorescence microscopy with excitation at 490–520 nm and emission above 520 nm.

Electron microscopy. Eighteen hours after 30 min of pressure treatment at 100 MPa, the cells were harvested and fixed with 2% glutaraldehyde in 0.1 M phosphate buffer (pH 7.4) for 2 h at 4°C. The cells were postfixed with 1% OsO_4 in 0.1 M phosphate buffer for 1 h at 4°C, dehydrated, and then embedded in Epon 812. Serial sections were cut using Ultracut-S (Reichert-Nissei, Hitachi), stained with uranyl acetate and lead citrate, and observed with a JEOL JEM-100CX electron microscope.

RESULTS

Cell viability ϕ, which is a percentage of cells surviving after pressure treatment, is deduced by the equation, $\phi = 100 \times \phi_s/\phi_c$, where ϕ_s and ϕ_c are the percentages of living cells in sample and control (i.e., uncompressed), respectively. Immediately after decompression, the viability decreased sigmoidally with increasing pressure (Fig. 1). One hundred percent viability was retained under pressures up to 85 MPa. All the cells died at pressures of 250 MPa. A 50% cell viability was attained at a pressure of 160–170 MPa. Morphologically, cell rounding was obvious because the surface protuberances of the cell membranes disappeared just after compression to 170 MPa (Fig. 3C). In the case of compression at 250 MPa, the membrane ruffling was extensive and all cellular components disintegrated (Fig. 3D). The BrdU uptake rapidly decreased with increasing pressure without bound, which means that DNA synthesis is suppressed by the pressure, prior to cell death (Fig. 1).

Cell viability was monitored by incubating the cells in the chamber for 48 h after decompression (Figs. 2A and 2B). In the case of 50 MPa, viability was unchanged during that time and the cell counts increased gradually, which means that the cells divided. In the case of 100 MPa, the cell counts did not increase appreciably and the viability decreased gradually. The rate of decrease reduced remarkably after 12 h.

The occurrence of apoptosis was confirmed by morphological observation (Figs. 3E–3L). Most apoptotic cells were round in shape and shrank. The characteristic segregation of condensed chromatin was seen in apoptotic nuclear fragments. These were confirmed by electron microscopy (Fig. 4). The sharply circumscribed masses of uniformly condensed chromatin (apoptotic body) abutted on the nuclear envelope in the cells 18 h after 30 min of pressure treatment at 100 MPa. Apoptosis was quantitatively detected by the TUNEL technique. In the case of 50 MPa (Fig. 2C), the rate of apoptosis was not obvious. However, in the case of 100 MPa (Fig. 2C), apoptotic cells began to increase from 8 h after decompression. By 24 h, there was an increase in the rate of apoptosis. Necrosis progressed for about 12 h after decompression, and after that apoptosis becomes predominant. The viability after 12 h didn't decrease in spite of the progress of apoptosis, because the trypan blue dye exclusion test doesn't detect the early stage of apoptosis.

To investigate the relationship between pressure-induced cell death and the cell cycle, the cells were synchronized. The cells were compressed at the S phase in the cell cycle. Both necrosis and apoptosis were accelerated in the case of synchronization (Figs. 2D and 2E) compared with nonsynchronization (Figs. 2B and 2C). Cell death by pressure is accelerated in the S phase.

DISCUSSION

The pressure dependence on cell death in human lymphoblasts was revealed. Both necrosis and apoptosis were observed to be induced by compression. Pressure-induced apoptosis is confirmed for the first time. Apoptotic cells were detected by the following three

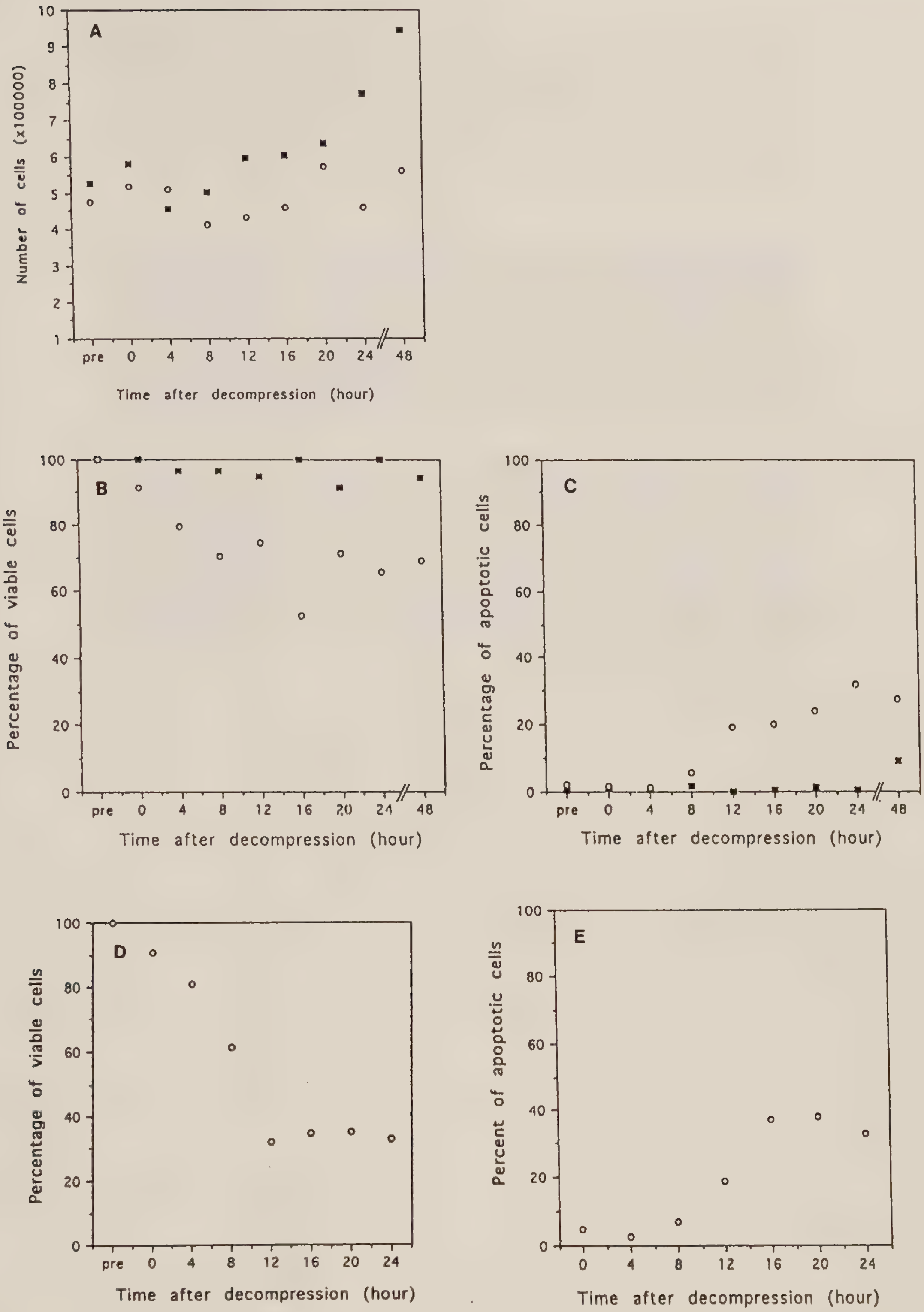

FIG. 2. Cell death after decompression. (A) The number of cells that survived after pressure treatment for 30 min of 50 MPa (■) and 100 MPa (○). (B) The viability during the 48 h after decompression from 50 MPa (■) and 100 MPa (○). (C) Percentage of apoptosis during the 48 h after decompression from 50 MPa (■) and 100 MPa (○) detected by the TUNEL technique. (D) Effect of synchronization on the viability of cells subject to 100 MPa (○). (E) Effect of synchronization on apoptosis of cells subject to 100 MPa (○).

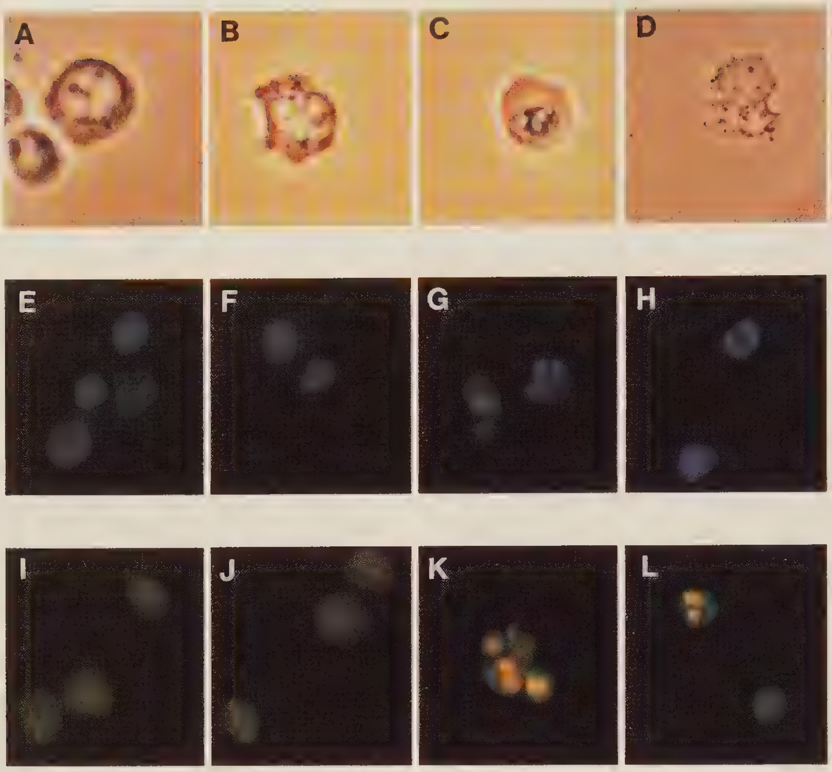

FIG. 3. Pressure-induced morphological changes in human lymphoblasts. EB3 cells were compressed for 30 min at 37°C. Just after decompression, the cells were observed using a phase-contrast microscope (×150). (A) control; (B) 65 MPa; (C) 170 MPa; (D) 250 MPa. Induction of chromatin condensation and apoptotic nuclear fragmentation by pressure (100 MPa). (E to H); Hoechst 33258 (bis-benzimide) nuclear stain. (E) Control, (F) 4 h after decompression; (G) 12 h, (H) 24 h. (I to L) Positive fluorescence indicated apoptotic cells detected by the TUNEL technique. (I) Control; (J) 4 h after decompression; (K) 8 h; (L) 24 h.

methods: the TUNEL method, optical microscopy, and electron microscopy.

Necrotic cells were observed immediately after decompression, and the viability decreased sigmoidally to 0 with increasing pressure. In cases of both synchronization and nonsynchronization, necrosis ceased to progress at about 12 h after decompression, because there was no appreciable decrease in viability (Figs. 2B and 2D). On the other hand, apoptosis detected at about 8 h after decompression and became predominant at about 12 h after decompression (Figs. 2C and 2E). The time course of the appearance of the apoptotic cells seems to be similar in both cases, which means that the execution of apoptosis is independent of the cell cycle.

In the case of nonsynchronization, about 30% of the cells showed necrosis at 12 h after decompression (Fig. 2B). About 30% of the cells showed apoptosis. Hence, 40% of the cells survived for 24 hours after decompression. In the case of synchronization, about 60% of the cells showed necrosis at 12 h after decompression (Fig. 2D). About 40% of the cells showed apoptosis. This means that few of the cells survived 24 h (one cell cycle) after decompression. Both necrosis and apoptosis were accelerated comparatively in the S phase.

The present results show that apoptosis was triggered at pressure of 100 MPa. Protein synthesis and signal transduction are active at those high pressures because DNA synthesis continues even at 100 MPa (Fig. 1). Necrosis seems to progress in connection with apoptosis, which suggests that pressure-induced necrosis is controlled by genes like pressure-induced apoptosis. Recently, Shimizu *et al.* [18] suggested that Bcl-2 and Bcl-2-related proteins prevented hypoxia-induced necrosis and apoptosis. In the present case, Bcl-2 may operate as a suppressor for both pressure-induced apoptosis and necrosis because Epstein–Barr virus-transformed human lymphoblasts express Bcl-2 gene product (data not shown).

Study of pressure-induced cell death will reveal the complete scheme of apoptosis and necrosis. Pressure has such an important merit in that it can be controlled much more rapidly and homogeneously than temperature. This aids not only the analysis of the mechanism of apoptosis, but also the study of cell biology and the medical application of pressure. The de-

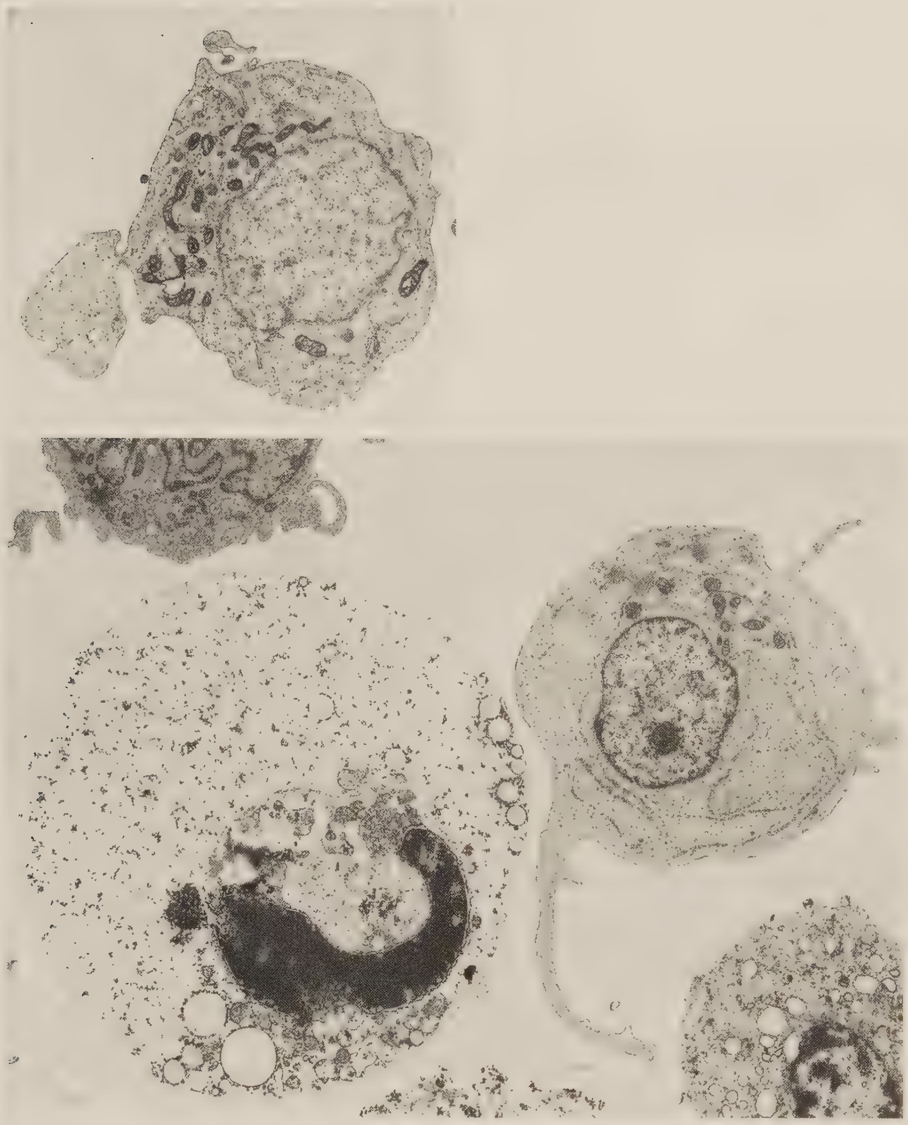

FIG. 4. Electron micrograph of EB3 cells. (Top) Control (without compression) (Bottom) 18 h after 30 min of compression at 100 MPa. Note the uniformly condensed chromatin abutting on the nuclear envelope in the apoptotic cell.

tection of a pressure-induced apoptosis is important in these fields.

This work was supported in part by a Grant-in-Aid for Scientific Research on Priority Areas, Ministry of Education, Science, Sports and Culture, Japan.

REFERENCES

1. ZoBell, C. E. (1970) *in* High Pressure Effects on Cellular Processes (Zimmerman, A. M., Ed.), pp. 85–130, Academic Press, New York.
2. Bartlett, D., Wright, M., Yayanos, A. A., and Silverman, M. (1989) *Nature* **342,** 572–574.
3. Lorenz, R., and Molitoris, H. P. (1992) *Colloq. Iserm.* **224,** 537–539.
4. Murakami, T. H., and Zimmerman, A. M. (1973) *Cytobios* **7,** 171–181.
5. Zimmerman, A. M. (1963) *Exp. Cell Res.* **31,** 39–51.
6. Landau, J. V. (1970) *in* High Pressure Effects on Cellular Processes (Zimmerman, A. M., Ed.), pp. 45–70, Academic Press, New York.
7. Haskin, C. L., Athanasiou, K. A., Klebe, R., and Cameron, I. L. (1993) *Biochem. Cell Biol.* **71,** 361–371.
8. Wyllie, A. H., Kerr, J. F. R., and Currie, A. R. (1980) *Int. Rev. Cytol.* **68,** 251–306.
9. Anderson, M. A., and Gusella, J. F. (1984) *In Vitro* **20,** 856–858.

10. Bootsma, D., Budke, L., and Vos, O. (1964) *Exp. Cell Res.* **33,** 301–309.

11. Takano, K. J., and Wakatsuki, M. (1997) *J. Cryst. Growth* **171,** 591–600.

12. Mishell, B. B., and Shiigi, S. M. (1980) *in* Selected Methods in Cellular Immunology, pp. 1–27, Freeman, San Francisco.

13. Dive, C., Gregory, C. D., Phipps, D. J., Evans, D. L., Milner, A. N., and Wyllie, A. H. (1992) *Biochim. Biophys. Acta* **1133,** 275–285.

14. Gratzner, H. G. (1982) *Science* **218,** 474–475.

15. Greipp, P. R., Witzig, T. E., and Gonchoroff, N. J. (1985) *Am. J. Hematol.* **20,** 289–292.

16. Takahashi, E., Hori, T., O'Connell, P., Leppert, M., and White, R. (1990) *Hum. Genet.* **86,** 14–16.

17. Gavrieli, Y., Sherman, Y., and Ben-Sasson, S. A. (1992) *J. Cell Biol.* **119,** 493–501.

18. Shimizu, S., Eguchi, Y., Kamiike, W., Waguri, S., Uchiyama, Y., Matsuda, H., and Tsujimoto, Y. (1996) *Oncogene* **12,** 2045–2050.

Received February 3, 1997
Revised version received April 24, 1997

EXPERIMENTAL CELL RESEARCH **235,** 161–169 (1997)
ARTICLE NO. EX973673

A Longitudinal Study of Human Age-Related Chromosomal Analysis in Skin Fibroblasts

Asit B. Mukherjee[1] and Samuel Thomas

Department of Biological Sciences, Fordham University, Bronx, New York 10458

Previous chromosomal analyses related to human aging used mainly cross-sectional data on metaphase chromosomes. However, it is difficult to directly relate the cross-sectional results to the specific type(s) of chromosomal mutations possibly occurring within a specific individual with advancing age, because the unique genetic endowment of each individual for longevity might be a modulating factor. We therefore have performed, for the first time, a longitudinal study of both numerical and structural chromosome analyses of skin fibroblasts at interphase and at metaphase derived from eight donors participating in the Baltimore Longitudinal Study. We have used the FISH method with chromosome-specific DNA probes and the data on total aneuploidy of 17 different chromosomes in each of the 16 cell cultures (2 from each of eight individuals) indicate that significantly higher percentages of aneuploid cells are detected at interphase than at metaphase. Mostly, the levels of chromosome-specific aneuploidy increase with the donor's advancing age and, in most individuals, chromosomes 1, 4, 6, 8, 10, and 15 show significantly higher frequencies of aneuploidy at interphase than those of the 11 other chromosomes studied. Although the significance of relatively higher levels of aneuploidy of certain chromosomes with aging remains unclear, it is intriguing to note that some of these chromosomes, such as 1, 4, and 6, have already been assigned to harbor senescence genes and chromosome 8 is known to house the gene for Werner Syndrome (progeroid syndrome), which shows very limited proliferative capacity of fibroblasts. It is conceivable that the degree and/or type of chromosome-specific aneuploidy might have some gene dosage effects in the control of cellular proliferation and selection during aging. We also show that a combination of both interphase and metaphase aneuploidy analyses provides more comprehensive and insightful information on intraindividual cellular dynamics and chromosomal aneuploidy as a function of age. Occasionally, very small proportions of cells in two individuals showed age-related structural chromosome aberrations, such as an acentric fragment derived from an X chromosome and an achromatic gap in chromosome 7. Thus, a comparative analysis of both intra- and interindividual longitudinal studies is very useful in detecting the pattern(s) of chromosome-specific alterations with increasing age. © 1997 Academic Press

INTRODUCTION

The genome-based theories of aging propose that genetic instability is presumably the primary cause of aging in human and other mammalian species [1, 2]. The occurrence of chromosomal abnormalities in cells can be regarded as a classical indicator of genomic instability and, therefore, might be related to aging. An association between advanced chronological aging and increased chromosomal aneuploidy in man was first reported by Jacobs *et al.* [3–5], and a number of subsequent investigations have supported this observation [6–12]. However, a consistent correlation between chromosomal aberrations and human aging still remains to be fully examined, particularly after the development of more sophisticated methods of molecular cytogenetics. For example, some previous studies did not find any significant relationship between the frequencies of various chromosomal aberrations and human age as detected by conventional cytogenetics [13, 14]. Moreover, almost all prior studies of age-related chromosomal aberrations were done utilizing only metaphase chromosomes of lymphocyte cultures. Some reports are also available on chromosomal aberrations at metaphase as a function of *in vitro* aging of human fibroblasts [15–18]. However, the exclusive use of metaphase chromosomes in age-related chromosomal analysis might provide only partial information, since the aneuploidy presumably hidden in nondividing cells would not be detected by this method. We, therefore, have previously analyzed chromosomal aneuploidy at interphase as well as at metaphase as a function of human cellular aging [19–21].

Almost all human age-related chromosomal analyses reported previously utilized only cross-sectional data. However, each individual has a unique genetic endowment for longevity. It is, therefore, difficult to relate

---

[1] To whom correspondence and reprint requests should be addressed. Fax: (718) 817-3645.

0014-4827/97 $25.00
Copyright © 1997 by Academic Press
All rights of reproduction in any form reserved.

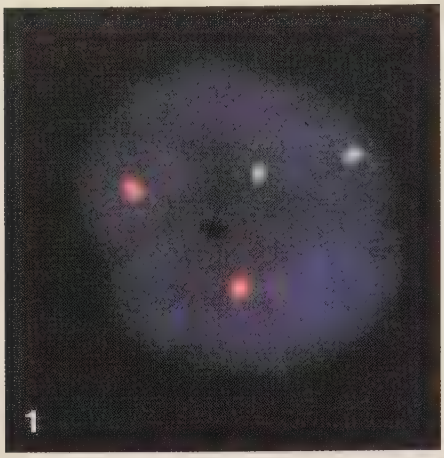

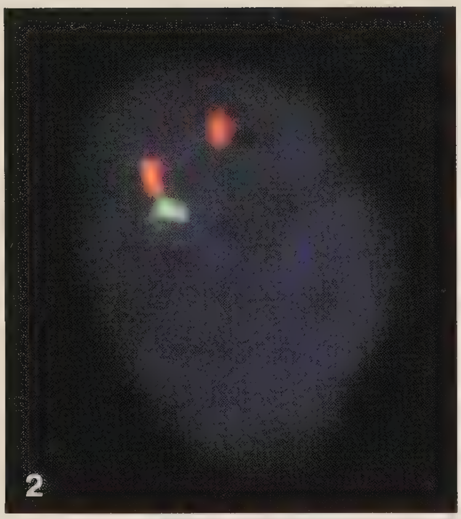

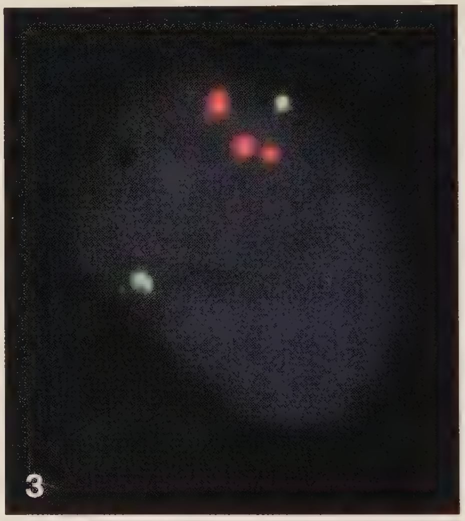

FIG. 1. A diploid fibroblast nucleus from individual 4 showing two red signals for chromosome 8 and two green signals for chromosome 10 by the FISH method.

FIG. 2. An aneuploid fibroblast nucleus from individual 4 showing monosomy for chromosome 15 (one green signal) and disomy for chromosome 6 (two red signals) by the FISH method.

FIG. 3. An aneuploid fibroblast nucleus from individual 4 showing disomy for chromosome 10 (two green signals) and trisomy for chromosome 8 (three red signals) by the FISH method.

directly the cross-sectional data on age-related chromosomal abnormalities to the specific types of chromosomal aberrations that can occur within a specific individual with advancing age. An ideal situation would be to perform an *in vivo* longitudinal study. However, there are many obvious difficulties in performing *in vivo* human experimentations. For this reason, an *in vitro* model system has been developed [22, 23]. Although human fetal fibroblasts have been widely used for studies of *in vitro* cellular aging and senescence, virtually no work has been done on age-related chromosomal studies utilizing the skin fibroblasts derived from adult individuals participating in the Baltimore Longitudinal Study of the Gerontology Research Center (GRC) (Baltimore, MD) [24]. To our knowledge, this is the first attempt to utilize the GRC cultures for a longitudinal study on possible chromosome-specific aberrations in specific individuals. In this study, we have used a powerful molecular-cytogenetic technique, called fluorescence *in situ* hybridization (FISH) [25], along with GTG chromosome banding. We have used 17 chromosome-specific α-satellite and classical satellite DNA probes for accurate detection of chromosomal aneuploidy [26]. Alphoid DNA is a family of primate satellite DNAs localized in the centromeric regions of various chromosomes [27–29].

MATERIALS AND METHODS

Cells. The cells (GRC cultures) were obtained from the NIA Cell Repository at Camden, New Jersey. The biopsy site was the mesial aspect of the mid–upper left arm, taken antemortem. A total of 16

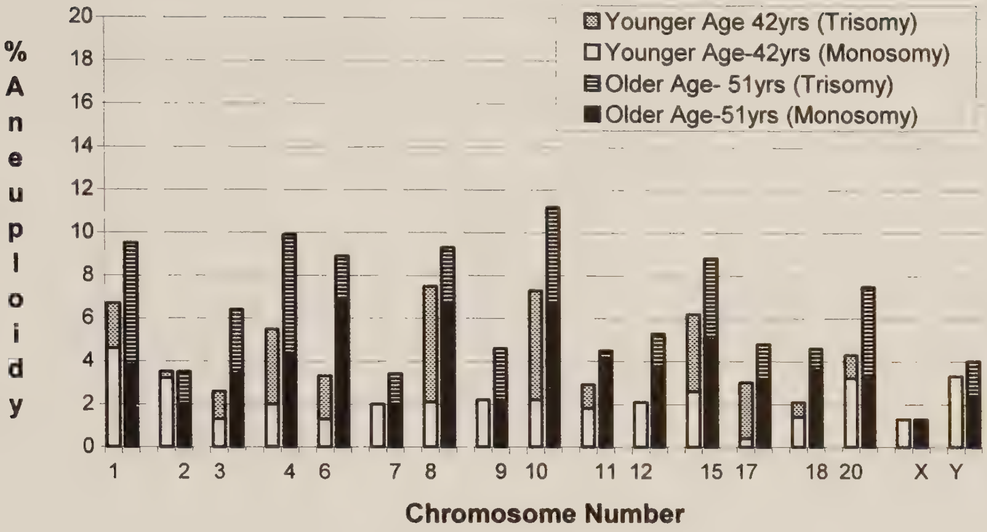

FIGS. 4–11. Interphase aneuploidy analysis by FISH in skin fibroblasts from eight adult individuals, each at younger and at older ages.

cell strains derived from eight individuals (five males and three females), each at younger and at older ages, was used for chromosomal analysis. The skin fibroblast cultures were obtained at the earliest PDLs (population doubling levels) available and the passage numbers of various cell cultures ranged from 3 to 4 when they were received. The specific cell strains utilized and their corresponding Repository Nos. are listed in Table 1. The cells were cultured in T-75 flasks at 37°C using MEM α medium (GIBCO) supplemented with 20% heat-inactivated (56°C for $\frac{1}{2}$ h) fetal bovine serum, 1% L-glutamine, and antibiotics (100 IU/ml penicillin, 100 μg/ml streptomycin (GIBCO). All culture conditions including the serum batch and seeding density were kept constant for the entire experiment and each cell strain was grown only for a short period (1 passage), just to obtain enough cells for chromosome preparation.

Chromosome preparations. For each cell strain, preparations were made for both interphase and metaphase chromosome analysis from the same slide. The cell cultures were treated with colcemid (0.05 μg/ml) for 2–3 h before being trypsinized. The cells were then centrifuged for 10 min at 1000 rpm, exposed to hypotonic solution (complete medium: distilled water, ratio 1:3) for 15 min, and prefixed at the end of hypotonic treatment. The cells were centrifuged again for 10 min at 1000 rpm and fixed in 1:3 fixative (glacial acetic acid:absolute methanol) for 1 h. The cells were fixed at least three more times for 30 min each, before being dropped onto cold, wet slides and air-dried. The slides were stored for at least 1 week before being used.

TABLE 1

Sixteen Skin Fibroblast Cultures Derived from Five Males and Three Females (Each at Two Different Ages) Utilized in the Longitudinal Study

		Skin fibroblasts obtained at	
Individual	Sex	Younger age (years)	Older age (years)
1	M	42 (AG05416)	51 (AG11364)
2	M	55 (AG05192)	63 (AG09844)
3	M	59 (AG04353)	63 (AG05804B)
4	M	63 (AG06881)	69 (AG11247)
5	M	76 (AG04144)	85 (AG09558A)
6	F	47 (AG05837B)	53 (AG11248A)
7	F	73 (AG06952)	79 (AG11020)
8	F	87 (AG05247E)	92 (AG09602)

Note. The numbers in parentheses for each individual indicate the Cell Repository (Rep) numbers for specific cell cultures (GRC cultures). M, male; F, female.

GTG banding. For metaphase chromosome analysis, the GTG banding was used. The slides were aged overnight at 55–60°C. They were treated with 0.05% trypsin solution for 30 s to 1 min, rinsed in Gurr's buffer, pH 6.8, and then stained in Giemsa solution (5%) for 2 min. The Giemsa solution was prepared fresh each time. The slides were then air-dried and dried further in an oven at 60°C for about 10 min. The slides were mounted with mounting medium and were examined under a 100X oil immersion objective. A minimum of 25 metaphases were examined per sample and photographs were taken for detailed banding analysis.

Fluorescence in situ hybridization (FISH). Aneuploidy analyses in all 16 cell strains were done by double-color FISH. Fifteen chromosome-specific α-satellite DNA probes labeled with biotin and/or digoxigenin (chromosomes 1, 2, 3, 4, 6, 7, 8, 10, 11, 12, 17, 18, 20, X, and Y) and 2 classical satellite DNA probes (chromosomes 9 and 15) (ONCOR) were used and the FISH method was performed according to the manufacturer's protocol using the Chromosome In Situ Kit (ONCOR).

Our method for interphase aneuploidy analysis was identical to the previously published methods [21, 30]. For FISH analysis of each chromosome, a separate slide was used. For interphase and metaphase chromosome analyses, an average of 5341 cell nuclei per sample and 556 metaphase spreads per sample were examined, respectively. For viewing the double-color chromosome-specific FISH signals within a single cell, a triple-bandpass filter (ONCOR) was used. All samples were screened blindly with a Leitz photomicroscope and appropriate photographs were taken according to our previously published methods [31, 32].

Statistical analysis. Using Wilcoxon's signed-ranks test, statistical analysis was performed to compare the mean of total aneuploidy values of various chromosomes at both younger and older ages of all

TABLE 2

Mean Percentages of Total Aneuploidy Involving 15 Autosomes and 2 Sex Chromosomes (X and/or Y) at Interphase vs Metaphase in Skin Fibroblasts Derived from 8 Donors, Each at Younger and at Older Ages

Individual	Mean % total aneuploidy at younger age (years)		Mean % total aneuploidy at older age (years)	
	Interphase	Metaphase	Interphase	Metaphase
1	4.0 (42)	0.0 (42)	6.3 (51)	1.0 (51)
2	6.8 (55)	1.9 (55)	10.9 (63)	3.3 (63)
3	8.0 (59)	1.3 (59)	9.9 (63)	1.6 (63)
4	7.5 (63)	1.6 (63)	9.9 (63)	2.0 (69)
5	8.6 (76)	1.3 (76)	10.6 (85)	2.7 (85)
6	7.8 (47)	1.7 (47)	9.1 (53)	2.0 (53)
7	9.5 (73)	2.0 (73)	11.6 (79)	2.7 (79)
8	11.1 (87)	2.7 (87)	12.3 (92)	3.0 (92)

Note. The numbers in parenthesis for each individual indicate ages.

eight individuals ($P < 0.005$). For one-tailed test, $\alpha = 0.005$ and the observed difference is significant at the 1% level. Wilcoxon's signed-ranks test was also used to determine the significance of the age-related aneuploidy values of specific chromosomes of each individual at both interphase and metaphase. Additionally, by using the same statistical test, it was found that the mean frequency of monosomy for each individual is significantly ($P < 0.005$) higher than that of trisomy at both younger and older ages.

RESULTS

In the FISH method, each chromosome-specific fluorescent signal in a particular cell represented the presence of a specific chromosome. Figures 1 to 3 represent both diploid and aneuploid cell nuclei at interphase. Numerical analysis of specific chromosomes at metaphase was also done by double-color FISH. In this study, only monosomy and trisomy for a particular autosome and an X chromosome in female at both interphase and metaphase were taken into account to determine the total yield of aneuploidy, since other categories of aneuploidy were extremely small. In males, both nullisomy and disomy for the X and/or Y chromosome constituted the total aneuploidy levels. A total of 85,454 interphase cells (average 5341/sample) and a total of 8896 metaphase cells (average 556/sample) representing 15 autosomes and 2 sex chromosomes (X and/or Y) were screened for aneuploidy analysis.

Figures 4 to 11 presented 17 chromosome-specific aneuploidy data sets (monosomy and trisomy) of skin fibroblasts at interphase derived from five males and three females, each at younger and at older ages. The ages of various individuals ranged from 42 to 85 years for the males and from 47 to 92 years for the females (Table 1). The means of the younger and older ages of the five males were 59 and 66.2 years, respectively, whereas those of the three females were 69 and 74.7 years, respectively. A comparative analysis of the interphase aneuploidy values of 17 different chromosomes indicated the following: (a) the mean percentage of cells with total chromosome-specific aneuploidy increased significantly with the advancing age of each individual ($P < 0.005$) (Table 2) and the pattern of age-related, chromosome-specific aneuploidy was individual-specific. The lowest mean percentage of cells with total aneuploidy (4%) was recorded for individual 1 at age 42, whereas the highest mean frequency of cells with total aneuploidy (12.3%) was noted for individual 8 at age 92 (Table 2); (b) the aneuploidy values of 15 separate autosomes varied from chromosome to chromosome in each of eight individuals at different ages, ranging from 2% for chromosome 7 in individual 1 at age 42 (Fig. 4) to 36.5% for chromosome 8 in individual 2 at age 63 (Fig. 5). For certain autosomes, such as chromosome 2 in individuals 1, 2, and 8, chromosome 3 in individuals 3, 7, and 8, chromosome 7 in individuals 6, 7, and 8, chromosome 9 in individuals 4, 5, and 6, chromosome 11 in individuals 3, 4, 6, and 8, chromosome 12 in individuals 3, 6, and 8, chromosome 17 in individual 2, 6, and 8, chromosome 18 in individuals 6 and 8, and chromosome 20 in individuals 3 and 5, the relative aneuploidy values remained similar at both younger and older ages. In all other cases, the relative frequencies of autosomal aneuploidy increased significantly with increasing age of each individual ($P < 0.005$); (c) in the five males (individuals 1–5), the lowest percentage of aneuploidy among all chromosomes was obtained for the X chromosome (1.3% in individual 2 at age 63) and the relative frequencies of cells with the Y-chromosomal aneuploidy were higher than that of the X chromosome (3.3% in individual 1 at age 42 to 5.8% in individual 5 at age 76); (d) in the three females (individuals 6–8), the relative frequencies of cells with X-chromosomal aneuploidy were higher than that of Y-chromosomal aneuploidy in the five males, ranging from 4.2% in individual 6 at age 47 (Fig. 9) to 6.9% in

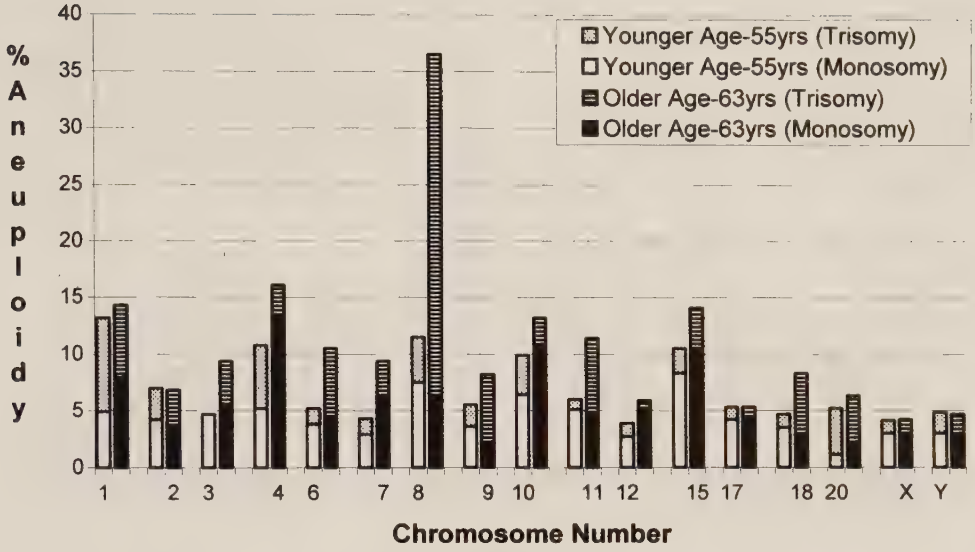

FIGURE 5

individual 7 at age 73 (Fig. 10); (e) of all the 15 autosomes studied, chromosomes 1, 4, 6, 8, 10 and 15 showed significantly higher proportions of aneuploidy in most individuals usually at both younger and older ages ($P < 0.005$).

The mean values of total aneuploidy involving 17 different chromosomes at interphase vs metaphase indicated that, in all cases, significantly higher proportions of aneuploid cells were detected at interphase than at metaphase ($P < 0.005$) (Table 2).

Age-related numerical and structural chromosome aberrations were also examined by the GTG banding of metaphase chromosomes. The vast majority of metaphase figures (98–100%) from various individuals at different ages showed a structurally normal chromosome complement. Rarely, a very small proportion (approx. 2%) of metaphase figures showed an X-chromosomal fragment in individual 7 at age 79 and an achromatic gap of chromosome 7 in individual 8 at age 92. Only cells derived from individual 2 at age 63 showed

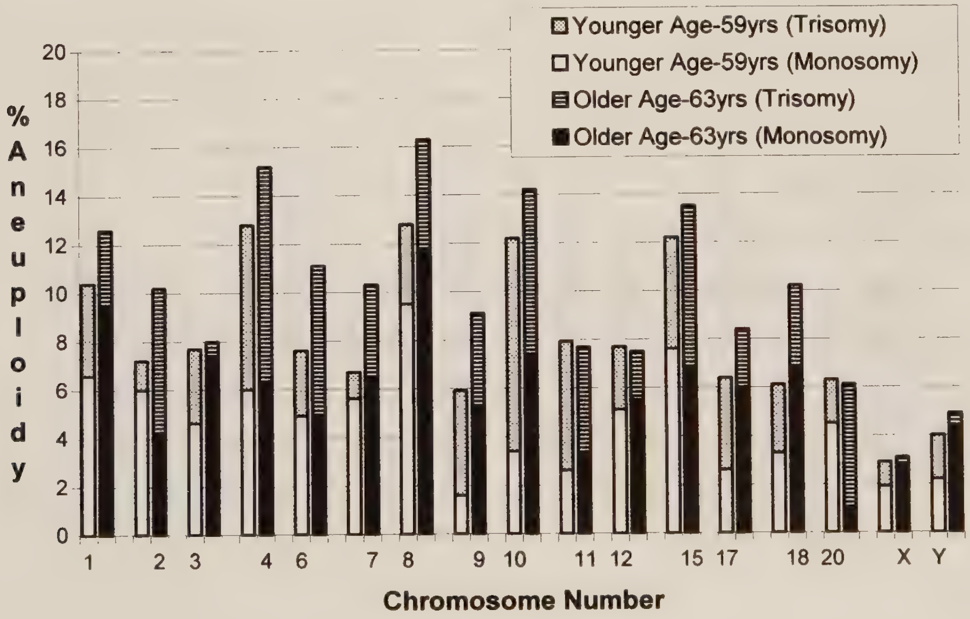

FIGURE 6

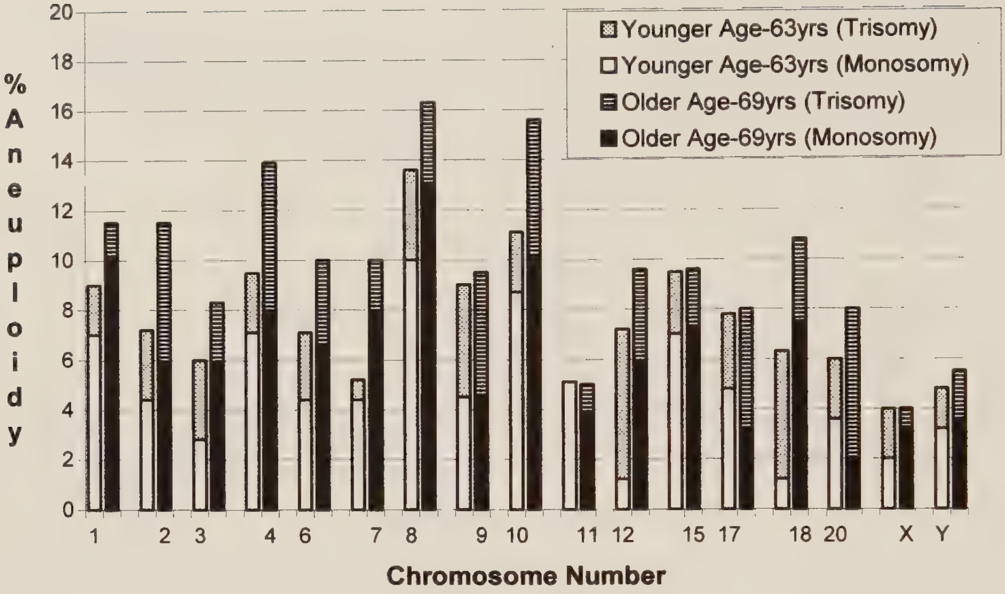

FIGURE 7

mosaicism for trisomy-8, 46,XY[65%]/47,XY+8[35%], and the patterns of aneuploidy values by GTG banding were consistent with that of the FISH method.

DISCUSSION

To date, only one paper previous to this report presented results of a longitudinal study on human age-related chromosomal aneuploidy at metaphase [33]. However, this study did not make any attempt to detect any age-related chromosome-specific aneuploidy and/or structural aberrations. We have now carried out a chromosome-specific longitudinal study by modern cytogenetic techniques. Every effort was made to avoid *in vitro* chromosomal alterations due to variations in culture conditions.

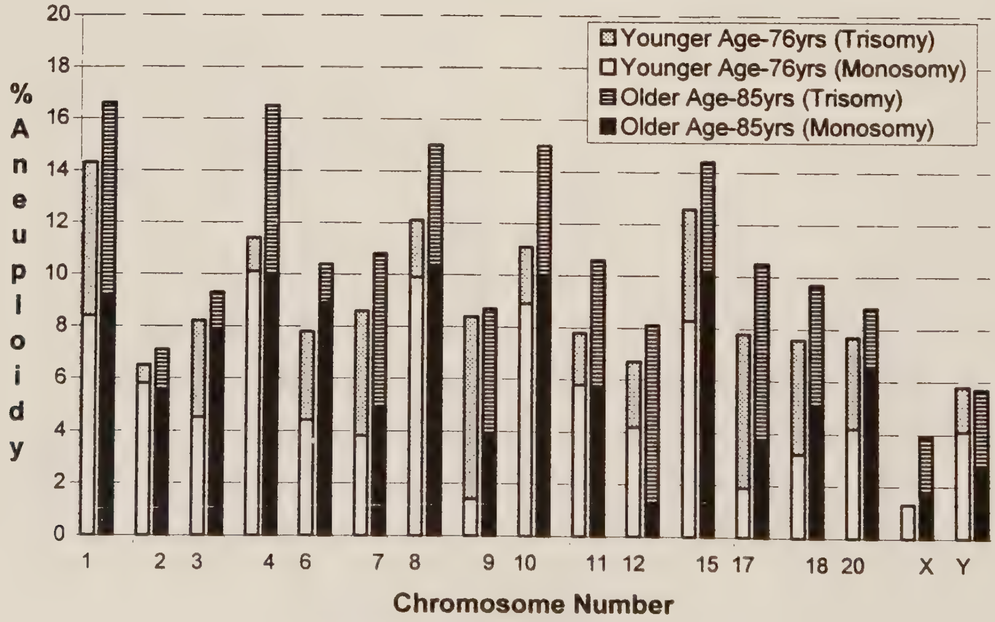

FIGURE 8

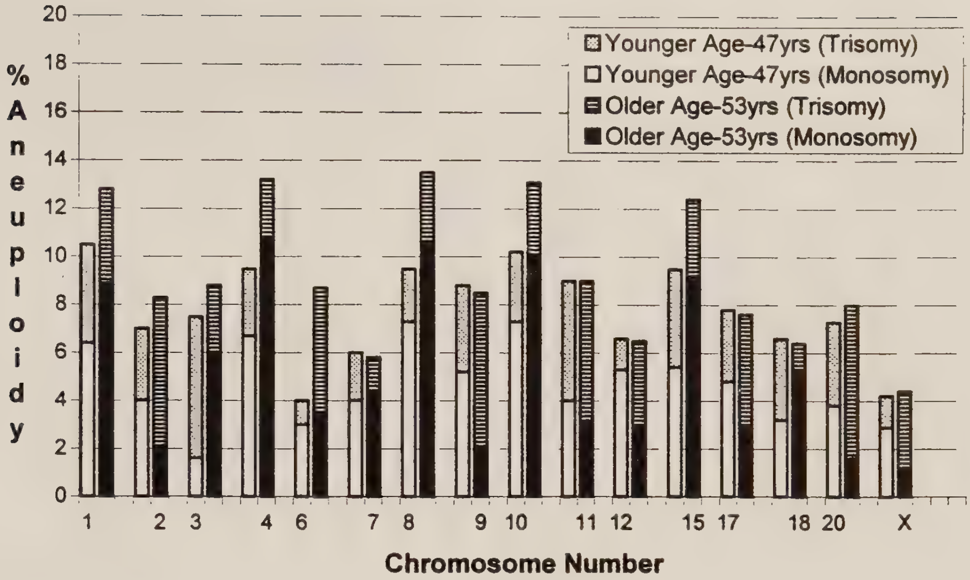

FIGURE 9

The FISH technique has been a powerful tool for cytogenetic analysis at both interphase and metaphase stages [25]. However, with the exception of our reports [19–21], all previous studies on human age-related chromosomal analysis were done by conventional cytogenetics of a small number of metaphases per sample. However, this method might provide only partial information since many chromosome-specific aberrations might remain hidden in nondividing interphase cells. We, therefore, have analyzed the age-related aneuploidy values at both interphase and metaphase.

Our study clearly showed that cell populations at interphase consistently showed significantly higher mean frequencies of total aneuploidy ($P < 0.005$) compared to that at metaphase (Table 2). This finding from the adult cell strains (GRC cultures) was completely consistent with that of fetal cell strains (IMR-90 and IMR-91) previously reported by us [20]. This intriguing finding presumably indicated that, during active division of fibroblasts, a relatively greater proportion of cells with aneuploidy than with diploidy was selected against entry to and continuation of mitosis (Selection

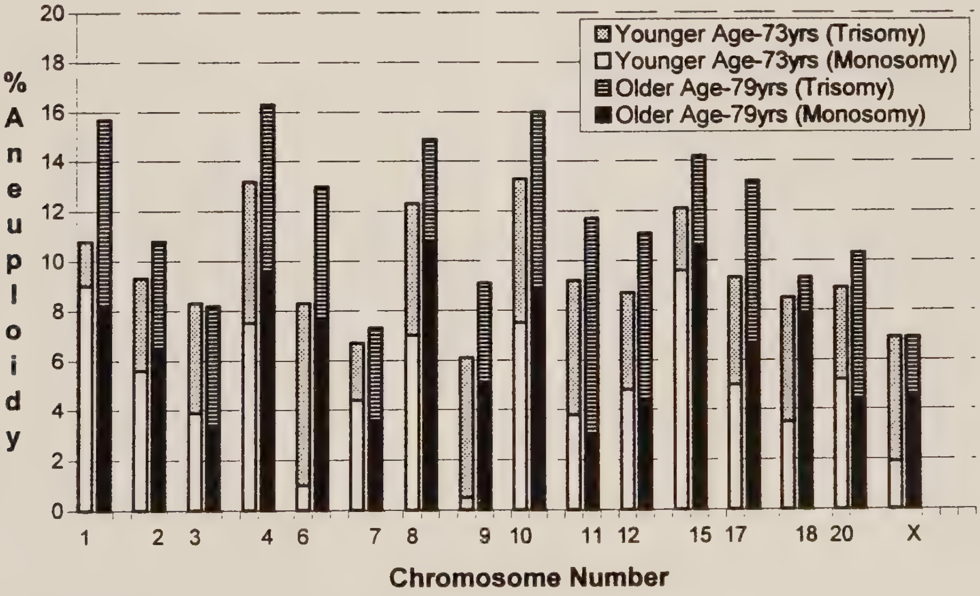

FIGURE 10

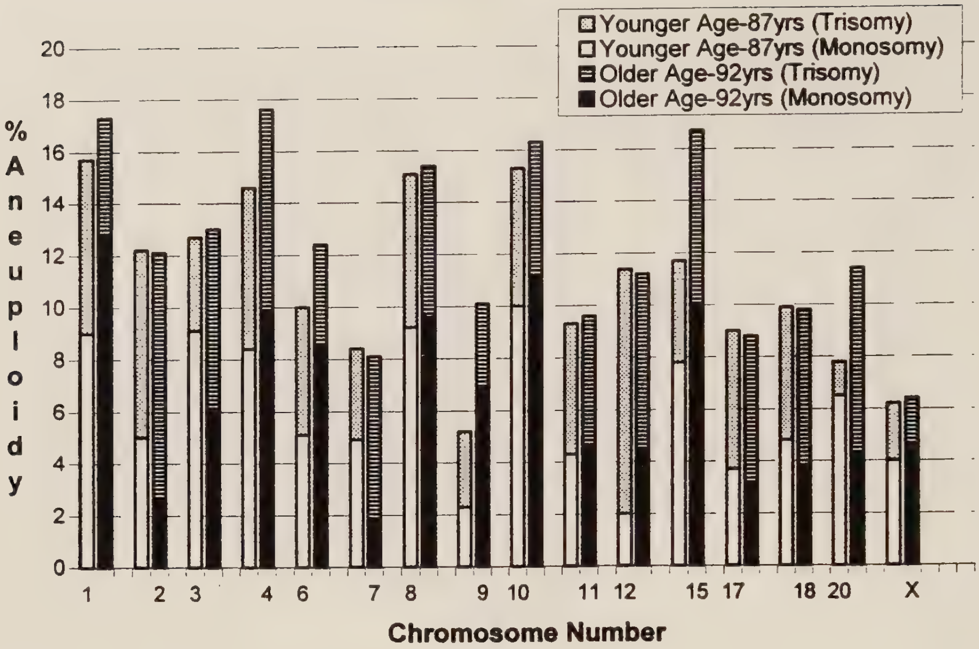

FIGURE 11

Hypothesis). Our study, therefore, showed that cellular dynamics with regard to aneuploidy involving various chromosomes differed markedly between interphase and metaphase stages, as observed during cellular proliferation in various individuals at different ages. It was interesting to note that, of all eight individuals studied, only one person (individual 2 at age 63), exhibited very similar frequencies of aneuploidy for chromosome 8 at both interphase (36.5%) and at metaphase (35%). At a younger age (55 years), the same person showed a normal diploid chromosome complement at metaphase in the vast majority of cases (96.1%) when the interphase aneuploidy value for chromosome 8 (11.4%) was significantly higher than that of metaphase (3.9%). Our chromosomal analyses by FISH as well as by GTG banding indicated that the unusually higher levels of aneuploidy for chromosome 8 in individual 2 at age 63 was due to the development of a trisomy-8 mosaicism and not due to monosomy for chromosome 8. It therefore appeared that, in this case, cell populations with trisomy-8 might have developed a selective advantage over other types of aneuploidy, such as monosomy for chromosome 8, for entry to and continuation of mitosis. However, this could also happen due to stochastic clonal amplification in a particular system of clonal successions.

It was noteworthy that, of all the 17 chromosomes studies, chromosomes 1, 4, 6, 8, 10, and 15 showed significantly higher frequencies of aneuploidy at interphase (nonrandom), usually at both younger and older ages of most individuals. There appeared to be no sex difference with respect to this aneuploidy pattern. Recently, we have also reported significantly higher frequencies of aneuploidy at interphase for chromosomes 4 and 6 in differentiated myeloid blood cells *in vivo* as a function of human aging [21]. To date, a number of human chromosomes had been identified which were involved in senescence-inducing activity for various immortal cell lines [34]. Chromosomes 1 [35, 36], 4 [37], and 6 [38], which house senescence genes, also showed significantly higher levels of aneuploidy at interphase (in most cases) in the present study. Additionally, we have noted 3 other chromosomes (Nos. 8, 10, and 15) exhibiting significantly higher levels of aneuploidy at interphase. Of these chromosomes, chromosome 8 has already been assigned to house the gene for Werner Syndrome (WS) [39], which displays very limited cellular replicative capacity and earlier senescence [40]. The possible relationship between the degree and/or type of chromosome-specific aberrations, cellular selection during active proliferation, and the control of senescence in normal cells is not known at this time. It is conceivable that greater levels of aneuploidy of specific chromosomes, such as chromosomes 1, 4, 6 and 8, 10, and 15 might have some gene dosage effect in the control of cellular proliferation/selection during aging. The mapping of over 10 senescence genes has already been achieved [34], and evidence has also been provided for multiple pathways to cellular senescence [41].

Although the degree of aneuploidy of specific chromosomes exhibited interchromosomal and interindividual variations at both younger and older ages, there was a general trend in the increase of the mean percentages of total aneuploidy with advancing age. These higher frequencies of cells with aneuploidy were more readily detectable at interphase than at metaphase. A comparative analysis of both intra- and interindividual studies was also very useful in detecting the pattern(s) and degrees of chromosome-specific aberrations with advancing age.

In this study, no consistent chromosome structural aberrations as a function of age were detected by the GTG-banding method.

We thank Dr. John Wehr for his valuable assistance and advice in the statistical analysis.

REFERENCES

1. Strehler, B. L. (1986) *Exp. Gerontol.* **21,** 283–319.
2. Gaubatz, J. W. (1995) *in* Molecular Basis of Aging (Macieira-Coelho, A., Ed.), pp. 71–135, CRC Press, New York.
3. Jacobs, P. A., Court-Brown, W. M., and Doll, R. (1961) *Nature* **191,** 1178–1180.
4. Jacobs, P. A., Brunton, M., Court-Brown, W. M., Doll, R., and Goldstein, H. (1963) *Nature* **197,** 1080–1081.
5. Jacobs, P. A., Brunton, M., and Court-Brown, W. M. (1964) *Ann. Hum. Genet.* **27,** 353–365.
6. Hamerton, J. L., Taylor, A. I., Angell, R., and McGuire, V. M. (1965) *Nature* **206,** 1232–1234.
7. Sandberg, A. A., Cohen, M. M., Rimm, A. A., and Levin, M. L. (1967) *Am. J. Hum. Genet.* **19,** 633–343.
8. Goodman, R., Fechheimer, N., Miller, F., Miller, R., and Zartman, O. (1969) *Am. J. Med. Sci.* **258,** 26–33.
9. Jarvik, L. F., and Kato, T. (1970) *Am. J. Hum. Genet.* **22,** 562–573.
10. Jarvik, L. F., Yen, F. S., and Moralishvili, E. (1974) *J. Gerontol.* **29,** 269–276.
11. Mattevi, M. S., and Salzano, F. M. (1975) *Humangenetik* **27,** 1–8.
12. Galloway, S. M., and Buckton, K. E. (1978) *Cytogenet. Cell Genet.* **20,** 78–95.
13. Bloom, A. D., Archer, P. G., and Awa, A. A. (1967) *Nature* **216,** 487–489.
14. Bender, M. A., Preston, R. J., Leonard, R. C., Pyatt, B. E., and Gooch, P. C. (1989) *Mutat. Res.* **212,** 149–154.
15. Saksela, E., and Moorhead, P. S. (1963) *Proc. Natl. Acad. Sci. USA* **50,** 390–395.
16. Littlefield, L. G., and Mailhes, J. B. (1975) *Am. J. Hum. Genet.* **27,** 190–197.
17. Thomson, K. V. A., and Holliday, R. (1975) *Exp. Cell Res.* **96,** 1–6.
18. Benn, P. A. (1976) *Am. J. Hum. Genet.* **28,** 465–473.
19. Mukherjee, A. B., and Wallace, K. C. (1990) *Mech. Age. Dev.* **52,** 61–71.
20. Mukherjee, A. B., Thomas, S., and Schmitt, E. (1995) *Mech. Age. Dev.* **80,** 11–23.
21. Mukherjee, A. B., Alejandro, J., Payne, S., and Thomas, S. (1996) *Mech. Age. Dev.* **90,** 145–156.
22. Hayflick, L., and Moorhead, P. S. (1961) *Exp. Cell Res.* **25,** 586–620.
23. Hayflick, L. (1965) *Exp. Cell Res.* **37,** 614–636.
24. Schneider, E. E., Monticone, R., Smith, J., Braunschweiger, K., and Roberts, T. (1981) *Cytogenet. Cell Genet.* **31,** 40–46.
25. Pinkel, D., Straume, T., and Gray, J. W. (1986) *Proc. Natl. Acad. Sci. USA* **83,** 2934–2938.
26. Willard, H. F., and Waye, J. S. (1987) *Trends Genet.* **3,** 192–198.
27. Maio, J. J. (1971) *J. Mol. Biol.* **56,** 579–595.
28. Kurnit, D. M., and Maio, D. M. (1973) *Chromosoma* **42,** 23–36.
29. Manuelidids, L. (1978) *Chromosoma* **6,** 23–32.
30. Eastmond, D. A., and Pinkel, D. (1990) *Mutat. Res.* **234,** 303–318.
31. Mukherjee, A. B., and Parsa, N. Z. (1990) *Chromosoma* **99,** 432–435.
32. Mukherjee, A. B., Murty, V. V. V. S., Rodriguez, E., Reuter, V. E., Bosl, C. J., and Chaganti, R. S. K. (1991) *Genes Chrom. Cancer* **3,** 300–307.
33. Jarvik, L. F., Yen, F. S., Fu, T. K., and Matsuyama, S. S. (1976) *Hum. Genet.* **33,** 17–22.
34. Vojta, P. J., and Barrett, J. C. (1995) *Biochim. Biophysica Acta* **1242,** 29–41.
35. Sugawara, O., Oshimura, M., Koi, M., Annab, L. A., and Barrett, J. C. (1990) *Science* **247,** 707–710.
36. Hensler, P. J., Anna, L. A., Barrett, J. C., and Pereira-Smith, O. M. (1994) *Mol. Cell Biol.* **14,** 2291–2297.
37. Ning, Y., Weber, J. L., Killary, A. M., Ledbetter, D. H., and Smith, J. R. (1991) *Proc. Natl. Acad. Sci. USA* **88,** 5635–5639.
38. Sandhu, A. K., Hubbard, K., Kaur, G. P., Jha, K. K., Ozer, H. L., and Athwal, R. S. (1994) *Proc. Natl. Acad. Sci. USA* **91,** 5698–5702.
39. Goto, M., Rubenstein, M., Weber, J., Woods, K., and Drayna, D. (1992) *Nature* **355,** 735–738.
40. Martin, G. M., Sprague, C. A., and Epstein, C. J. (1970) *Lab Invest.* **23,** 86–92.
41. Sasaki, M., Honda, T., Yamada, H., Wake, N., Barrett, J. C., and Oshimura, M. (1994) *Cancer Res.* **54,** 6090–6093.

Received December 5, 1996
Revised version received June 10, 1997

EXPERIMENTAL CELL RESEARCH **235**, 170–179 (1997)
ARTICLE NO. EX973698

Growth and Differentiation Factors Inhibit the Migratory Phenotype of Cultured Neonatal Rat Hepatocytes Induced by HGF/SF

Roser Pagan,* Isabel Martín,* Miquel Llobera,† and Senén Vilaró*,[1]

**Departament de Biologia Cellular i †Departament de Bioquímica i Biologia Molecular; Universitat de Barcelona; Avgda. Diagonal, 645, 08028 Barcelona, Catalonia, Spain*

Previous studies have demonstrated that neonatal rat hepatocytes cultured in a serum-free medium adopt a fibroblast-like morphology and form a well-developed vimentin network. By immunoblotting, phase-contrast microscopy, and immunolocalization studies we report here that hepatocyte growth factor (HGF) induces a pronounced migratory/scatter phenotype in neonatal hepatocytes in primary culture. These fibroblast-like cells are highly elongated and adopt a pronounced spindle shape in the presence of this growth factor. Most of them coexpress vimentin and cytokeratin intermediate filaments. Both EGF and TGF-β_1 also induced vimentin expression in cytokeratin-positive cells but this effect was not correlated with a change of epithelial phenotype. Only in DMSO-supplemented cultures was vimentin expression of hepatocytes inhibited and no coexpression was observed in the presence of this factor. Remarkably, the effect induced by HGF was totally inhibited when DMSO, TGF-β_1, or EGF was added to HGF-supplemented cultures. Epithelial sheets of well-defined hepatocytes were observed with these combinations although the complete epithelial morphology was achieved by combining DMSO with a growth factor. Taken together these results suggest that growth and differentiation factors modulate the migratory effect of HGF/SF in hepatocytes. © 1997 Academic Press

INTRODUCTION

Adult hepatocytes are highly differentiated but retain a replicative potential and they proliferate in response to the loss of liver mass or cell death caused by hepatic injuries. The identification of the cellular and molecular mechanisms that control the differentiation of hepatocytes is essential to understanding growth regulation during development, hepatic injury, and carcinogenesis. Progress has been made in identifying signals involved in the regulation of growth and differentiation of hepatocytes [1–4]. Most known growth factors, such as epidermal growth factor (EGF),[2] transforming growth factor-alpha (TGF-α), or transforming growth factor-beta (TGF-β) have been implicated in liver development [5–7]. Furthermore, most of them induce the epithelial–mesenchymal transition (EMT) in certain epithelial cells [8–10], a crucial process in the morphogenesis of many organs [11, 12]. In the past few years, hepatocyte growth factor/scatter factor (HGF/SF) has become the key factor in the study of liver organogenesis and the differentiation of hepatic cells [7, 13, 14].

HGF/SF was identified as a mesenchymal cell-derived cytokine that dissociates ("scatters") epithelial sheets into individual cells [15, 16]. HGF/SF is a mitogen for hepatocytes [17], renal tubule cells and keratinocytes [18], melanocytes [19], endothelial cells [20], and several epithelial cell lines in culture [21], whereas in other epithelial cell lines HGF/SF induces cell dispersion and motility [22, 23]. A scatter effect of HGF has also been described in adult rat hepatocytes in culture but the concentrations used in these studies are five times higher than that which produces mitogenic activity in this cell type [7, 24]. The formation of acinar–ductular structures similar to those produced in embryonic liver when HGF/SF is expressed at high levels [7, 13] characterizes this morphogenic effect. Scatter factor often promotes the acquisition of a mesenchymal phenotype by epithelial cells [25, 26]. This transformation involves the redistribution of desmosomal plaque proteins and the reorganization of the cytokeratin and the actin–fodrin systems [27, 28]. Moreover, intermediate-sized filaments of the vimentin type are formed in fibroblast-like cells [11, 29, 30].

A profound morphological change and a progressive replacement of the cytokeratin network by vimentin intermediate filaments (IFs) is also produced in the

---

[1] To whom correspondence and reprint requests should be addressed. Fax: 34-3-4112967. E-mail: senen@porthos.bio.ub.es.

[2] Abbreviations used: IFs, intermediate filaments; EGF, epidermal growth factor; HGF/SF, hepatocyte growth factor/scatter factor; TGF-β_1, transforming growth factor-beta1; CK, cytokeratin; DMSO, dimethyl sulfoxide; EMT, epithelial–mesenchymal transition; FITC, fluorescein isothiocyanate; TRITC, tetramethylrhodamine isothiocyanate.

0014-4827/97 $25.00

Copyright © 1997 by Academic Press
All rights of reproduction in any form reserved.

EMT in neonatal rat hepatocytes cultured in standard serum-free medium [31, 32]. Growth and differentiation factors such as EGF and dimethyl sulfoxide (DMSO) modulate the EMT in cultured neonatal hepatocytes [33]. Here we present evidence that, in addition to their effects on cytoskeletal protein levels, growth and differentiation factors modify the morphology of neonatal rat hepatocytes in primary cultures. By phase-contrast microscopy, immunofluorescence, and Western blotting we show that HGF induces cell dispersion and motility in neonatal hepatocytes which exhibit a fibroblast-like morphology and coexpressed cytokeratin and vimentin IFs. In contrast, EGF and TGF-β_1 did not produce this effect regardless of their induction of vimentin expression. Only in DMSO-supplemented (DMSO, EGF + DMSO, and HGF + DMSO) cultures was vimentin expression of hepatocytes inhibited. Surprisingly, the effect of HGF on epithelial morphology of neonatal hepatocytes was totally inhibited when EGF, TGF-β, or DMSO was added to HGF-supplemented cultures.

MATERIALS AND METHODS

Reagents. Bovine serum albumin (BSA), penicillin, streptomycin sulfate, Hoechst 33342, DMSO, and EGF were obtained from Sigma Chemical Co. (St. Louis, MO). HGF was obtained from Becton–Dickinson (Bedford, MA). TGF-β_1 was from Austral Biologicals (San Ramon, CA). Collagenase, fluorescein isothiocyanate (FITC)-conjugated sheep anti-mouse immunoglobulins and monoclonal anti-vimentin (clone V9) were obtained from Boehringer Mannheim (Mannheim, Germany). Newborn calf serum and culture media were from Ingelheim Diagnostica (Boehringer Ingelheim, Ingelheim, Germany). Culture dishes were from Nunc Inc. (Napperville, IL). Polyclonal anti-cytokeratin (CK18) was kindly provided by Professor O. Bachs and Dr. R. Bastos. Tetramethylrhodamine isothiocyanate (TRITC)-conjugated goat anti-rabbit immunoglobulin was from Dako Corp. (Santa Barbara, CA). The immunofluorescent mounting medium was Mowiol obtained from Calbiochem (La Jolla, CA).

Cell isolation and culture. Neonatal hepatocytes were isolated from 3-day-old rats by retrograde perfusion of the liver with collagenase (0.17 mU/mg sp act) as previously described [31–33]. The cell suspension was filtered through a double-layered nylon 100-mesh gauze and centrifuged twice for 3 min at 50*g*. The resulting pellet was a mixture of hepatocytes and hematopoietic cells. To separate these cell types, the pellet was resuspended and centrifuged twice at 30*g* (1 min) and twice at 15*g* (1 min). Viability of isolated hepatocytes was always more than 85% as determined by trypan blue exclusion.

The hepatocyte-enriched fraction was plated on tissue culture dishes (35 mm in diameter) at 50,000 cells/cm^2 in E-199 medium supplemented with newborn calf serum (10%), glutamine (2 m*M*), penicillin (100 U/ml), and streptomycin sulfate (100 μg/ml) at 37°C in a humidified 5% CO_2/95% air atmosphere. After 4 h, the medium was replaced by a serum-free medium supplemented with BSA (0.2%). At 1 day of culture growth factors were added to the culture medium: EGF and HGF were used at 10 ng/ml; TGF-β_1 was used at 0.5 ng/ml; and DMSO was used at 2% v/v (280 m*M*). Thereafter, the medium was changed every 24 h.

Light and immunofluorescence microscopy. Phase-contrast micrographs were obtained at day 3 posttreatment with a Zeiss inverted research microscope using Kodak TMAX 400 films. For immunofluorescence, the hepatocyte-enriched fraction was plated on tissue culture dishes containing sterile glass coverslips. Fibronectin (15 μg/ml) was added to the culture medium to facilitate the attachment of the cells to the glass coverslips. At day 3 posttreatment, cells were rinsed briefly in PBS, fixed in methanol (−20°C) for 2 min, rinsed in PBS, and processed for indirect double immunofluorescence [34]. As primary antibodies we used monoclonal anti-vimentin and polyclonal anti-cytokeratin. To visualize the primary antibody, we used the following labeled secondary antibodies: FITC-conjugated sheep anti-mouse immunoglobulins and TRITC-conjugated goat anti-rabbit immunoglobulins. All antibodies were diluted in PBS containing 1% RSA. Double immunofluorescence assays were performed by applying a mixture of mouse and rabbit primary antibodies, followed by extensive washing and incubation with a mixture of FITC-conjugated anti-mouse and TRITC-conjugated anti-rabbit. Primary antibodies were applied for 1 h at 37°C, followed by four 5-min washes in PBS, a 45-min incubation with fluorescent-conjugated antibodies, and four final washes of 5 min in PBS. Finally, cells were stained with Hoechst 33342 diluted in PBS.

The coverslips were mounted in immunofluorescent medium and viewed with a 40 or 100X objective using a Reichert Jung Polyvar II microscope equipped with epifluorescence illumination. Photographic exposures were made on Kodak Ektachrome 160 film. For immunofluorescence figures, the photographs represent triple exposures of the same field. Specificity of the double immunofluorescence staining was corroborated by using the different antibodies separately and incubating the cells with the different secondary antibodies used. Representativity of the results is stated in the figure legends.

Cell fractionation, electrophoresis, and Western blots. Cultured hepatocytes were extracted in cytoskeleton buffer containing Triton X-100 following the method of Franke *et al.* [35] to detect vimentin and cytokeratin proteins. Briefly, the cells were washed in 100 m*M* PBS at room temperature. Then they were incubated with detergent buffer (10 m*M* Tris–HCl, 140 m*M* NaCl, 1.5 *M* KCl, 5 m*M* EDTA, 0.5% Triton X-100, pH 7.6) for 30 min at 4°C. The buffer extract was then decanted and the remaining insoluble cytoskeletal residues were scraped off and resuspended in the same buffer. The high-salt buffer-insoluble material obtained as a pellet after centrifugation (2500*g*, 30 min, 4°C) was washed briefly in PBS, pelleted once more (3000*g*, 10 min, 4°C), and stored at −80°C until use.

One-dimensional SDS–polyacrylamide gels (10%) were run and proteins were electrophoretically transferred to nitrocellulose paper in a Bio-Rad Trans-Blot cell (20 V, 2 h). Membranes were blocked for 1 h in PBS containing 5% dried milk and then incubated overnight with PBS containing primary antibodies diluted in 3% dried milk. Secondary antibodies were conjugated with peroxidase. The blot was developed with the ECL system (Amersham).

RESULTS

Morphologic Effects of Growth and Differentiation Factors on Neonatal Hepatocytes Maintained in Primary Culture for 3 Days

Distinct morphologic changes were induced in hepatocytes in cultures supplemented with different factors. Liver cells were cultured in the presence of growth and differentiation factors and were photographed 3 days after treatment (Fig. 1). At that time in the control cultures we observed two cell types, as described in previous papers [31, 32]: polygonal cells organized in islands with typical epithelial morphology (arrows) and cells with a fibroblast-like appearance (arrowheads) that colonized the empty spaces between islands. We had shown previously that some of these fibroblast-like cells originated from hepatocytes [31].

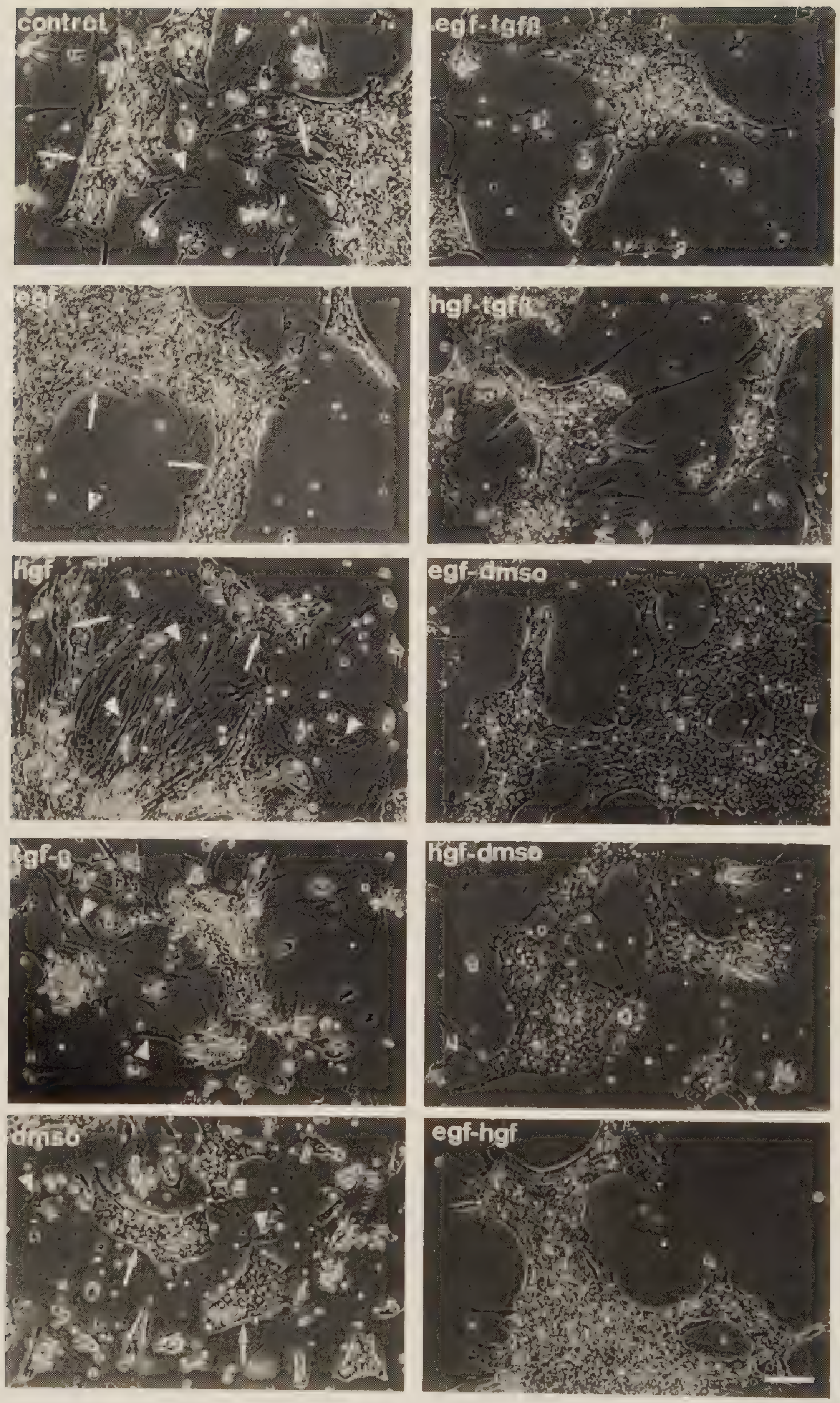
control
egf-tgfß
egf
hgf-tgfß
hgf
egf-dmso
egf-ß
hgf-dmso
dmso
egf-hgf

In EGF-supplemented cultures the epithelial islands (arrows) were larger and more extended than in serum-free medium and we observed fewer fibroblast-like cells (arrowheads) in the presence of this growth factor. In contrast, a large number of fibroblast-like cells (arrowheads) appeared when HGF was added to the culture medium. The fibroblast-like cells emerging from epithelial islands were flatter and more elongated than those under control conditions. They showed a pronounced spindle-like morphology and overlapped. Not all hepatocytes responded to HGF by changing their morphology (arrows). TGF-β_1 also induced changes in the morphology of cultured neonatal hepatocytes. This factor had a cytotoxic effect on these cultures, since a large number of dead cells were observed when the medium was refreshed. Fibroblast-like cells (arrowheads) were also present in the cultures supplemented with TGF-β_1 and they appear healthier than cells with epithelial morphology. Some of these cells presented pyknotic nuclei. DMSO maintained the epithelial morphology of neonatal hepatocytes. In DMSO-supplemented cultures, hepatocytes (arrows) were arranged in small, well-defined patches. The number of fibroblast-like cells (arrowheads) was low in the presence of DMSO.

The effect induced by HGF was not observed when TGF-β_1, DMSO, or EGF was added to the cultures supplemented with this growth factor. In cultures supplemented with EGF + TGF-β_1 and with EGF + HGF well-organized islands of hepatocytes and fewer cells with fibroblast morphology were observed. Neonatal liver cells cultured in the presence of HGF and TGF-β_1 had a similar appearance. However, a higher number of fibroblast-like cells were observed although the migrating phenotype was not so pronounced as in HGF-supplemented cultures. In cultures supplemented with growth factors and DMSO, cells with epithelial morphology predominated over cells with fibroblast morphology and they were distributed in large sheets resembling liver parenchyma.

Expression of Cytokeratin and Vimentin Intermediate-Type Filaments

In order to determine whether the growth and differentiation factors could affect levels of vimentin and cytokeratin (intermediate filament proteins which are regulated during EMT of cultured neonatal rat hepatocytes [31, 32]) we performed Western blotting analysis of cytoskeletal fraction to detect these markers at day 3 of treatment (Fig. 2). At that time, both EGF and HGF, alone or in combination, increased cytokeratin levels. EGF also increased vimentin levels but in HGF-supplemented cultures vimentin was slightly reduced. TGF-β maintained cytokeratin but decreased vimentin. When TGF-β was added to the cultures supplemented with EGF, vimentin levels remained similar but cytokeratin was found slightly reduced compared to EGF-supplemented cultures. In TGF-β plus HGF-treated cultures vimentin levels were higher than in the cultures treated with TGF-β or HGF alone. When DMSO was added to the cultures supplemented with these growth factors, the increase in cytokeratin induced by EGF and HGF was slightly reduced, but a dramatic decrease in vimentin was observed.

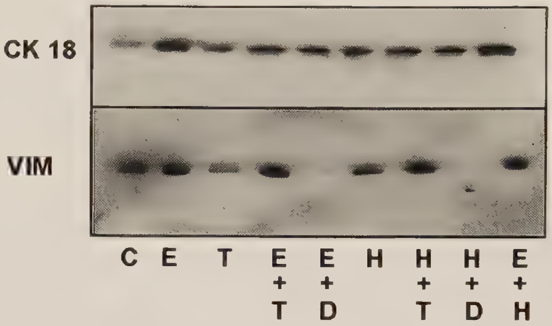

FIG. 2. Western blot analysis for cytokeratin and vimentin of neonatal rat hepatocytes cultured in the presence of different growth factors. Liver cells from 3-day-old rats were cultured for 3 days in the presence of different growth factors as described in Fig. 1. Cells were processed as indicated under Materials and Methods and samples of each condition were processed for SDS–PAGE and Western blotting using a polyclonal antibody against cytokeratin 18 and a monoclonal antibody against vimentin as primary antibodies. Second antibodies were conjugated with peroxidase. Figure shows cytokeratin and vimentin levels in the presence of growth factors after 3 days of treatment. A representative experiment of four is shown.

To identify the cell types that express vimentin and cytokeratin or both proteins in the cultures supplemented with these factors, indirect immunofluorescence experiments were performed using specific antibodies against either cytokeratin or vimentin (Figs. 3 and 4). Under control conditions, cells with epithelial morphology were cytokeratin-positive (arrows) and most fibroblast-like cells were vimentin-positive (arrowheads). Cells coexpressing cytokeratin and vimentin filaments were detected. A high-magnification (Fig.

FIG. 1. Morphological appearance of neonatal hepatocytes cultured in the presence of different growth and differentiation factors. Neonatal hepatocytes were isolated as described under Materials and Methods and seeded at a density of 50,000 cells/cm^2 in E-199 medium supplemented with 10% fetal calf serum during the first 4 h of culture. Then the medium was replaced by a serum-free medium. After 1 day of culture, 10 ng/ml EGF, 10 ng/ml HGF, 0.5 ng/ml TGF-β_1, or 2% DMSO was added to the culture medium. Phase-contrast micrographs were obtained 3 days posttreatment. Results are representative of more that 10 different cultures. Arrows point to epithelial islands, arrowheads to fibroblast-like cells. Bar, 50 μm.

3) image shows an epithelial cell located at the edge of an epithelial cluster coexpressing both types of IF. Vimentin fibrils (yellow color indicates colocalization) appeared around the nuclear area and they extended, colocalizing with cytokeratin filaments (red), from the perinuclear zone to the periphery of the cell.

In EGF-supplemented cultures, a high percentage of cytokeratin-positive cells were also vimentin-positive (arrows). It was remarkable that, regardless of their vimentin expression, these cells remained epitheloid. A high-magnification image shows an epithelial cluster with cells presenting a well-developed vimentin network, which in part also colocalizes with cytokeratin filaments. Cells that maintained an epithelial morphology in HGF-supplemented cultures stained with anti-cytokeratin antibodies (arrows) and cells with a migrating phenotype presented vimentin filaments (arrowheads). However, most of these fibroblast-like cells were also cytokeratin-positive (short arrows) although colocalization of both networks was not so pronounced as under the other conditions. Most mesenchymal cells (arrowheads) in TGF-β_1-supplemented cultures were only vimentin-positive but most epitheloid cells (arrows) coexpressed both IFs. A high-magnification image shows that colocalization of both networks was also pronounced in the presence of this growth factor. Few cells expressed only cytokeratin filaments. In contrast, in DMSO-supplemented cultures cytokeratin-positive cells (arrows) never presented vimentin intermediate filaments. Thus, in cultures supplemented with DMSO we did not find cells coexpressing both intermediate filament proteins. Vimentin-positive cells in DMSO-supplemented cultures did not overlap hepatocytes, as observed in most other conditions. These cells did not show a fibroblastic morphology but adopted a more polygonal shape.

In Fig. 4, vimentin and cytokeratin expression in cultures supplemented with combinations of different factors is shown in comparison with the expression of these proteins in cultures supplemented with HGF. As observed in phase-contrast micrographs the cell dispersion and motility induced by HGF was totally inhibited when EGF, TGF-β_1, or DMSO was added to the cultures supplemented with HGF. Epithelial sheets of well-defined hepatocytes expressing cytokeratin filaments (short arrows) were observed with all the combinations used in this study, although complete epithelial morphology was achieved by combining DMSO with a growth factor. Moreover, when DMSO was added to the cultures supplemented with growth factors, expression of vimentin in cytokeratin-positive cells was not observed. In contrast, when TGF-β_1 was added to the cultures supplemented with HGF or EGF, and when both factors were added together, coexpression of cytokeratin and vimentin IFs by hepatocytes was not inhibited (long arrows). Few vimentin-positive cells with fibroblastic morphology were observed in all conditions (arrowheads).

DISCUSSION

Profound transformation of cell morphology and replacement of the cytokeratin network by vimentin IFs are early events associated with the EMT in neonatal rat hepatocytes cultured in standard serum-free medium [31–33]. The physiological significance of the EMT in neonatal hepatocytes is not understood. However, previous studies have suggested that the morphological changes and the expression of vimentin intermediate filaments reflect the state of their differentiation program (31). Here we report that agents that affect liver differentiation, such as EGF, HGF, TGF-β_1, or DMSO, differentially modulate cytokeratin and vimentin expression in cultures of neonatal rat hepatocytes. Only HGF induced a pronounced migratory/scatter phenotype on cultured neonatal hepatocytes. In contrast, in cultures supplemented with EGF or with TGF-β_1 the induction of vimentin expression was not correlated with a transformation of the epithelial phenotype and cytokeratin-positive cells maintained an epitheloid morphology. Moreover, the epithelial morphology was well-maintained in DMSO-supplemented cultures (either alone or in combination with other growth factors) and in this system cytokeratin-positive cells never expressed vimentin IFs. It is noteworthy that the effect induced by HGF was inhibited by the addition of EGF, TGF-β_1, or DMSO to the cultures supplemented with this growth factor. Taken together, the results suggest that the EMT of neonatal rat hepatocytes *in vitro* could be modulated by growth factors that contribute to liver organogenesis during development.

Liver cells respond to HGF/SF. Indeed, it has been described as the most powerful mitogenic agent for adult hepatocytes [36, 37]. Moreover, HGF/SF is not only a mitogenic agent but also motogenic and morphogenic for epithelial cells [38–40]: formation of branching tubules, scattering, induction of motility and invasion are other effects produced by this growth factor. Some morphogenic effects such as formation of long processes and induction of cell migration are also observed in cultures of adult rat hepatocytes supplemented with 50 ng/ml of HGF [7, 13], which is 2.5-fold higher than which produced the mitogenic effect. This migratory effect was very different from morphogenic changes observed in adult hepatocytes and at a 5-fold lower concentration: neonatal hepatocytes in HGF-supplemented cultures were transformed into highly elongated, flattened mesenchymal cells with a more pronounced spindle shape than found in serum-free medium. Some hepatocytes did not change their morphology in the presence of HGF. It has been described that the scatter effect of HGF in certain carcinoma cells depends on their degree of differentiation, and cell lines that had lost their epithelial characteristics [25] were more susceptible to the factor. It is likely that the differentiation state of neonatal hepatocytes varies from one to another and cells expressing a less differentiated phenotype could show a more pronounced response to the factor. The scatter effect induced by HGF was also accompanied by an induction of vimentin in fibroblast-like cells. It has been reported that a vimentin cytoskeleton may be required for cell invasion and migration [41]. Although keratin IFs seem to be dependent on the maintenance of intercellular interactions [42], most of these vimentin-positive cells continued to react intensely for cytokeratin. It is remarkable that mesenchyme-like cells were able to migrate carrying keratin IFs. Indeed, it has been shown that the presence of cytokeratin IFs did not inhibit cell motility *in vitro,* as indicated by the presence of CK IFs in certain cultured fibroblastoid cells or even smooth muscle-like cells [43].

In contrast, EGF and TGF-β_1, inductors of fibroblast-like cells in other cell systems [8, 9, 44, 45], did not produce this effect in neonatal hepatocytes. Michalopoulos *et al.* [13] reported that EGF could induce a similar morphogenic effect on adult rat hepatocytes in culture to that produced by HGF, but less pronounced. EGF did not produce the migratory effect in neonatal hepatocytes since epithelial morphology was well maintained. The appearance of neonatal rat hepatocytes was different in the presence of TGF-β_1: cells were dispersed and dead cells were detected when the medium was changed. Reduction of total cell number and presence of pyknotic nuclei in some epitheloid cells of these cultures suggest a possible cytotoxic effect of this factor, as described in adult and fetal hepatocytes [46, 47]. Both EGF and TGF-β_1 also induced vimentin expression in neonatal rat hepatocytes in culture and these cells maintained cytokeratin staining. Thus, the presence of vimentin IFs is not enough to induce a fibroblast-like morphology, and epithelial shape can persist regardless of vimentin expression.

In 2% DMSO-supplemented cultures epithelial morphology was also well maintained, as described previously [33], although there were fewer epithelial sheets than in control conditions. Indeed, Isom *et al.* [48] reported that adult rat hepatocytes cultured in medium supplemented with 2% DMSO retained all the morphological and biochemical characteristics typical of the differentiated state. DMSO inhibited vimentin expression in neonatal hepatocytes [33 and present results]. Thus, no coexpressing cells were found in these cultures, suggesting that this factor also maintains the differentiation state of neonatal hepatocytes.

Interestingly, EGF, TGF-β_1, and DMSO inhibited the effect on hepatocyte morphology induced by HGF and maintained the epithelial shape of neonatal rat hepatocytes in primary culture. HGF causes scattering of certain epithelial cell lines by inhibiting junctional communication and reducing desmoplakin, a component of desmosomes [49]. Recently, Ikejima *et al.* [50] demonstrated that HGF also blocks junctional communications and increases cell spreading in cultures of adult rat hepatocytes, and they reported that TGF-β_1 is able to inhibit HGF-induced reduction of junctions. On the other hand, TGF-β_1 also inhibits HGF/SF-induced epithelial branching in MDCK cells in culture [51]. Moreover, when 2% DMSO was added to cultures of proliferating adult hepatocytes expression of gap junctions proteins was induced [52]. Thus, HGF may induce cell dispersion and motility in neonatal hepatocytes by reducing intercellular communication, and EGF, TGF-β_1, and DMSO could block this effect. Moreover, inhibition of this effect in cultures supplemented with DMSO and HGF was accompanied by an inhibition of vimentin expression in epithelial cells. This inhibition was also produced in EGF + DMSO-supplemented cultures. In fact, DMSO was the only factor able to inhibit vimentin expression induced by growth factors.

In summary, factors that affect liver growth and differentiation produced morphological changes in neonatal hepatocytes in primary culture which were accompanied by alterations in levels and in the expression of IF proteins. The most important effect is produced by HGF, which induced cell dispersion and motility in this cell type. It has been suggested that cell scattering in monolayer cultures is the equivalent of branching tubulogenesis in 3-D culture [40, 53, 54]. Experiments with neonatal rat hepatocytes cultured in 3D-collagen gels should be performed in order to demonstrate a morphogenic effect of HGF on neonatal liver cells. Remarkably, EGF, TGF-β_1, and DMSO inhibited the mor-

FIG. 3. Immunofluorescence detection of vimentin and cytokeratin filaments of neonatal rat liver cells cultured in the presence of different growth and differentiation factors. Cells were cultured as described in Fig. 1. Three days later, cells were fixed and processed for double immunofluorescence and nuclear staining (blue). Cytokeratin was detected by a rabbit anti-CK18 immunoglobulin and a TRITC-conjugated goat anti-rabbit immunoglobulin (red). We used a mouse anti-vimentin immunoglobulin and an FITC-conjugated goat anti-mouse immunoglobulin (green) to detect this IF protein. Pictures are triple-exposure micrographs of all fluorescent markers used. Yellow indicates colocalization of the fluorochromes used. Large arrows point to cytokeratin-positive cells in epithelial islands, arrowheads to fibroblast-like vimentin-positive cells, and short arrows to fibroblast-like, cytokeratin- and vimentin-positive cells in HGF-supplemented cultures. Results are representative of five different cultures. Bars: 40 μm in low-magnification images (control, egf, hgf, tgf-β_1 on the right of the figure and the two images of DMSO-supplemented cultures) and 20 μm in high-magnification images (control, egf, hgf, tgf-β_1 on the left of the figure).

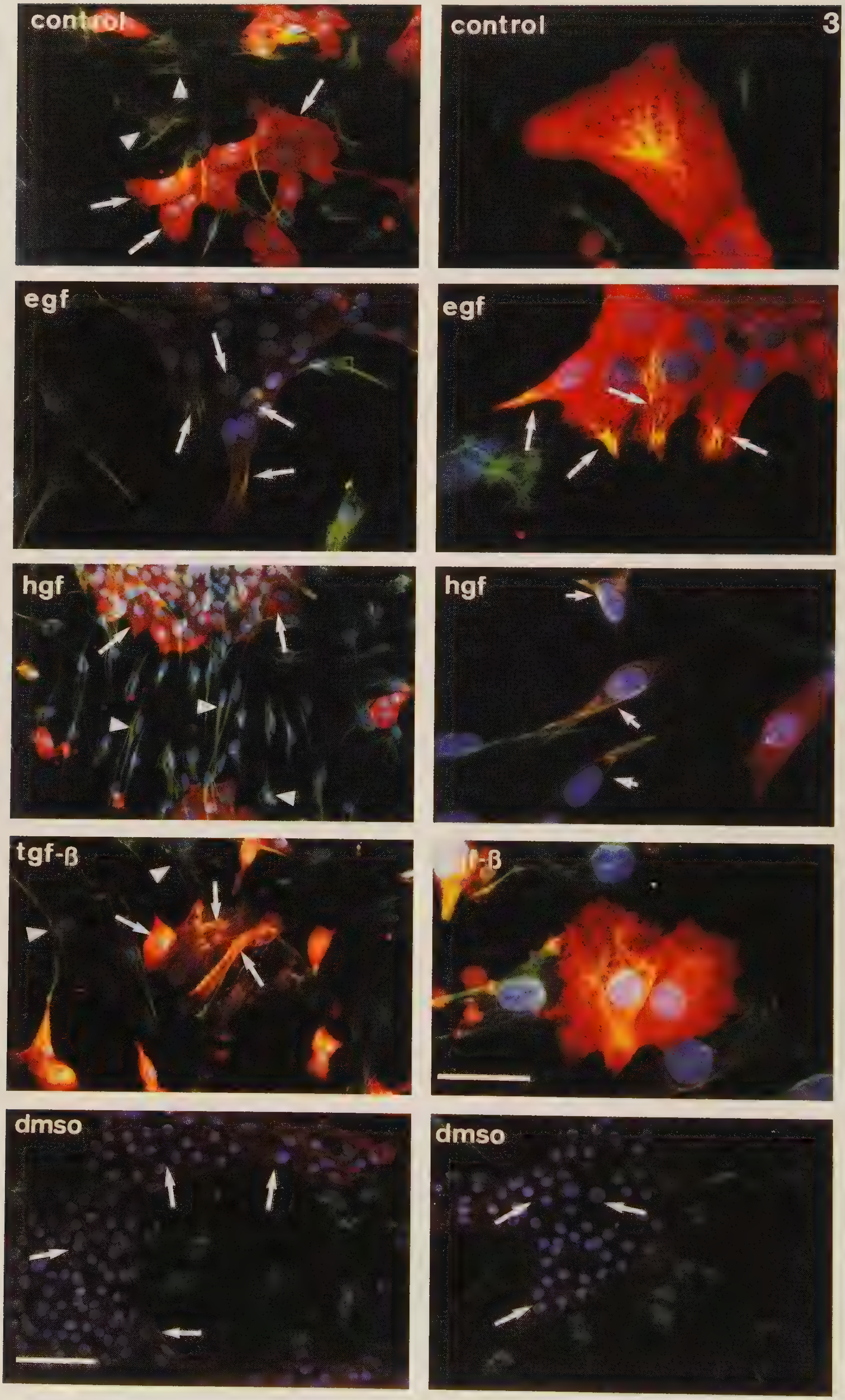
control
control
3
egf
egf
hgf
hgf
tgf-β
tgf-β
dmso
dmso

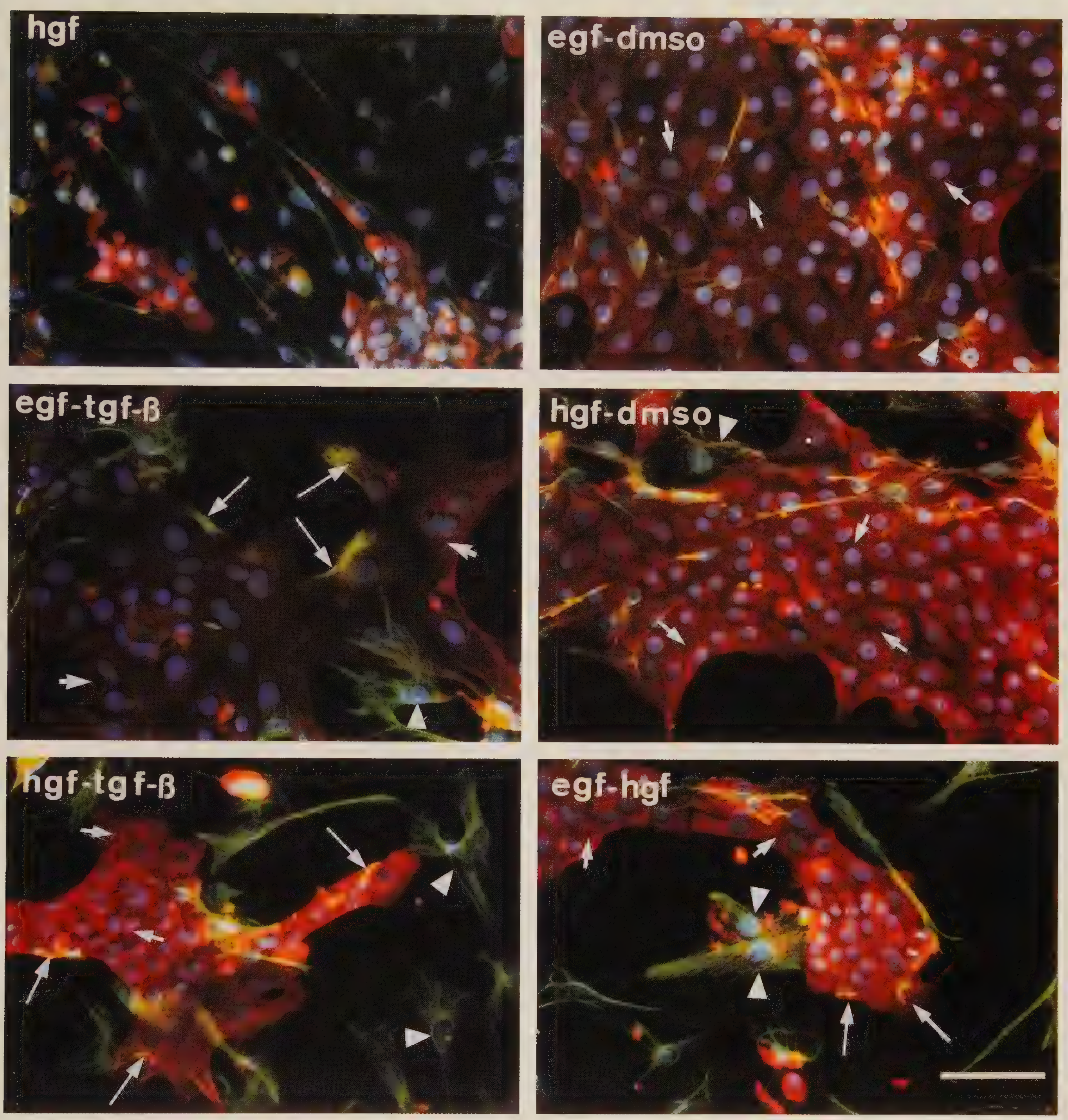

FIG. 4. Double immunofluorescence detection of vimentin and cytokeratin in cultures of neonatal rat liver cells supplemented with different combinations of factors. Cells were cultured as described in the legend to Fig. 1. Immunofluorescence analysis was performed as indicated in Fig. 2. Large arrows point to cytokeratin and vimentin coexpressing cells, arrowheads to fibroblast-like, vimentin-positive cells, and short arrows to cytokeratin-positive cells. Results are representative of five different cultures. Bar, 40 m.

phological change induced by HGF, and DMSO was also able to inhibit vimentin expression induced by HGF and EGF. Because most of these factors can affect growth, differentiation and EMT in neonatal liver cells, our present results suggest that together they may modulate liver differentiation.

We thank Drs. Oriol Bachs and Ricard Bastos for their kind gift of polyclonal anti-CK45 and Dr. Isabel Fabregat and Dr. Arantxa Sanxhez for their stimulating comments. We also thank David García for his expert technical assistance and Robin Rycroft for his expert editorial help. This work was supported by the Comision Interministerial de Ciencia y Tecnologia (PB94-1548), the Fondo de Investigaciones Sanitarias from Ministerio de Sanidad (Grant 96/2099), and the Generalitat de Catalunya.

REFERENCES

1. Michalopoulos, G. K. (1990) Liver regeneration: Molecular mechanisms of growth control. *FASEB J.* **4,** 240–249.
2. de Juan, C., Benito, M., and Fabregat, I. (1992) Regulation of albumin expression in fetal rat hepatocytes cultured under proliferative conditions: Role of Epidermal growth factor and hormones. *J. Cell. Physiol.* **152,** 95–101.
3. Baribault, H., and Marceau, N. (1986) Dexamethasone and dimethyl sulfoxide as distinct regulators of growth and differentiation of cultured suckling rat hepatocytes. *J. Cell. Physiol.* **129,** 77–84.
4. Baffet, G., Loyer, P., Glaise, D., Corlu, A., Etienne, P. L., and Guguen-Guillouzo, C. (1991) Distinct effects of cell-cell communication and corticosteroids on the synthesis of cytokeratins in cultured rat hepatocytes. *J. Cell. Sci.* **99,** 609–661.
5. Kost, D. P. (1991) Michalopoulos GK. Effect of 2% dimethyl sulfoxide on the mitogenic properties of epidermal growth factor in primary hepatocyte culture. *J. Cell. Physiol.* **147,** 274–280.
6. Sánchez, A., Alvarez, A. M., Benito, M., and Fabregat, I. (1995) Transforming growth factor-β modulates growth and differentiation of fetal hepatocytes in primary culture. *J. Cell. Physiol.* **165,** 398–405.
7. Block, G. D., Locker, J., Bowen, W. C., Petersen, B. E., Katyal, S., Strom, S. C., Riley, T., Howard, T. A., and Michalopoulos, G. K. (1996) Population expansion, clonal growth, and specific differentiation patterns in primary cultures of hepatocytes induced by HGF/SF, EGF and TGFα in a chemically defined (HGM) medium. *J. Cell Biol.* **132,** 1133–1149.
8. Connell, N. D., and Rheinwald, J. G. (1983) Regulation of the cytoskeleton in mesothelial cells: reversible loss of cytokeratin and increase in vimentin during rapid growth in culture. *Cell* **34,** 245–253.
9. Caulin, C., Scholl, F. G., Frontelo, P., Gamallo, C., and Quintanilla, M. (1996) Chronic exposure of cultured transformed mouse epidermal cells to transforming growth factor beta 1 induces an epithelial-mesenchymal transdifferentiation and a spindle tumoral phenotype. *Cell. Growth. Differ.* **6,** 1027–1035.
10. Savagner, P., Vallès, A. M., Jounneau, J., Yamada, K. M., and Thiery, J. P. (1994) Alternative splicing in fibroblast growth factor receptor 2 is associated with induced epithelial-mesenchymal transition in rat bladder carcinoma cells. *Mol. Biol. Cell.* **5,** 851–862.
11. Hay, E. D. (1993) Epithelial-mesenchymal transitions. *Semin. Dev. Biol.* **1,** 347–356.
12. Guarino, M. (1995) Epithelial-to-mesenchymal change of differentiation: From embryogenetic mechanism to pathological patterns. *Histol. Histopathol.* **10,** 171–184.
13. Michalopoulos, G. K., Bowen, W., Nussler, A. K., Becich, M. J., and Howard, T. A. (1993) Comparative analysis of mitogenic and morphogenic effects of HGF and EGF on rat and human hepatocytes maintained in collagen gels. *J. Cell. Physiol.* **156,** 443–452.
14. Streit, A., Stren, C. D., Thery, C., Ireland, G. W., Aparicio, S., Sharpe, M. J., and Gherardi, E. (1995) A role for HGF/SF in neural induction and its expression in Hensen's node during gastrulation. *Development* **121,** 813–824.
15. Rosen, E. M., Nigam, S. K., and Goldberg, I. D. (1994) Scatter factor and the *c*-Met receptor: A paradigm for mesenchymal/epithelial interaction. *J. Cell Biol.* **127,** 1783–1787.
16. Stoker, M., Gherardi, E., Perryman, M., and Gray, J. (1987) Scatter factor is a fibroblast-derived modulator of epithelial motility. *Nature* **327,** 239–242.
17. Nakamura, T. (1991) Structure and function of hepatocyte growth factor. *Prog. Growth. Factor. Res.* **3,** 67–85.
18. Kan, M., Zhang, G. H., Zarnegar, R., Michalopoulos, G., Myoken, Y., Mckeehan, W. L., and Stevens, J. L. (1991) Hepatocyte growth factor/hepatopoietin A stimulates the growth of rat kidney proximal tubule epithelial cells (RPTE), rat non-parenchymal liver cells, human melanoma cells, mouse keratinocytes and stimulates anchorage-independent growth of SV40-transformed RPTE. *Biochem. Biophys. Res. Commun.* **174,** 331–337.
19. Rubin, J. S., Chan, A. M. L., Bottaro, D. P., Burgess, W. H., Taylor, W. G., Cech, A. C., Hirschfield, D. W., Wong, J., Miki, T., Finch, P. W., and Aaronson, S. A. (1991) A broad-spectrum human lung fibroblst.derived mitogen is a variant of hepatocyte growth factor. *Proc. Natl. Acad. Sci. USA* **88,** 415–419.
20. Grant, D. S., Kleinman, H. K., Goldberg, I. D., Bhargava, M. M., Nickoloff, B. J., Kinsella, J. L., Polverini, P., and Rosen, E. M. (1993) Scatter factor induces blood vessel formation in vivo. *Proc. Natl. Acad. Sci. USA* **90,** 1937–1941.
21. Yang, X. M., and Park, M. (1993) Expression of the met/Hepatocyte grosth factor/Scatter factor receptor and its ligand during differentiations of murine P19 embryonal carcinoma cells. *Dev. Biol.* **157,** 308–320.
22. Stoker, M., and Perryman, M. (1985) A epithelial scatter factor released by embryo fibroblasts. *J. Cell. Sci.* **77,** 209–223.
23. Gherardi, E., Gray, J., Stoker, M., Perryman, M., and Furlong, R. (1989) Purification of scatter factor, a fibroblast-derived basic protein which modulates epithelia interactions and movement. *Proc. Natl. Acad. Sci. USA* **86,** 5844–5848.
24. Hernández, J., Zarnegar, R., and Michalopoulos, G. K. (1992) Characterization of the effects of human placental HGF on hepatocytes. *J. Cell. Physiol.* **150,** 116–121.
25. Weidner, K. M., Beherens, J., Vandekerckhove, J., and Birchmeier, W. (1990) Scatter factor: Molecular characteristics and effect of the invasiveness of epithelial cells. *J. Cell Biol.* **111,** 2097–2108.
26. Bellusci, S., Moens, G., Gaudino, G., Comoglio, P., Nakamura, T., Thiery, J. P., and Jouanneau, J. (1994) Creation of an hepatocyte growth factor/scatter factor autocrine loop in carcinoma cells induces invasive properties associated with increased tumorigenicity. *Oncogene* **9,** 1091–1099.
27. Boyer, B., Tucker, G., Vallès, A. M., Franke, W. W., and Thiery, J. P. (1989) Rearrangements of desmosomal and cytoskeletal proteins during the transition from epithelial to fibroblastoid organization in cultured bladder carcinoma cells. *J. Cell Biol.* **109,** 1495–1509.
28. Thiery, J. P., Boyer, B., Tucker, G., Gavrilovic, J., and Vallès, A. M. (1988) Adhesion mechanisms in embryogenesis and in cancer invasion and metastasis. *Ciba Found. Symp.* **141,** 48–74.
29. Birchmeier, W., and Birchmeier, C. (1995) Epithelial-mesenchymal transitions in development and tumor progression, *in* Epithelial-Mesenchymal Interactions in Cancer (Goldberg, I. D., and Rosen, E. M., Eds.), Birkhäuser Verlag, Basel, Switzerland.
30. Birchmeier, C., and Birchmeier, W. (1993) Molecular aspects of mesenchymal-epithelial interactions. *Annu. Rev. Cell. Biol.* **9,** 511–540.

31. Pagan, R., Llobera, M., and Vilaró, S. (1995) Epithelial-mesenchymal transition in cultured neonatal hepatocytes. *Hepatology* **21,** 820–831.
32. Pagan, R., Martin, I., Alonso, A., Llobera, M., and Vilaró, S. (1996) Vimentin filaments follow the preexisting cytokeratin network during epithelial-mesenchymal transition of cultured neonatal rat hepatocytes. *Exp. Cell. Res.* **222,** 333–344.
33. Pagan, R., Martin, I., Llobera, M., and Vilaró, S. (1997) Epithelial-mesenchymal transition of cultured rat neonatal hepatocytes is differentially regulated in response to epidermal growth factor (EGF) and dimethyl sulfoxide (DMSO). *Hepatology* **25,** 598–606.
34. Alcalde, J., Bonay, P., Roa, A., Vilaró, S., and Sandoval, I. (1992) Assembly and disassembly of the Golgi complex: Two processes arranged in a cis to trans direction. *J. Cell Biol.* **16,** 69–83.
35. Franke, W. W. (1986) Separation of cytokeratin polipeptides by gel electrophoretic and chromatographic techniques and their identification by immunoblotting. *Methods Enzymol.* **134,** 355–371.
36. Nakamura, T., Nishizawa, T., Hagiya, M., Seki, T., Shimonishi, M., Sugimura, A., Tashiro, K., and Shimizu, S. (1989) Molecular cloning and expression of human hepatocyte growth factor. *Nature* **342,** 440–443.
37. Michalopoulos, G., and Zarnegar, R. (1992) Hepatocyte growth factor. *Hepatology* **15,** 149–155.
38. Weidner, K. M., Arakaki, N., Vandekerchove, J., Weingart, S., Hartmann, G., Rieder, H., Fonatsch, C., Tsubouchi, H., Hishida, T., Daikuhara, Y., and Birchmeier, W. (1991) Evidence for the identity of human scatter factor and hepatocyte growth factor. *Proc. Natl. Acad. Sci. USA* **88,** 7001–7005.
39. Naldini, L., Weidner, M., Vigna, E., Gaudino, G., Bardelli, A., Ponzetto, C., Narsimhan, R. P., Hartman, G., Zarnegar, R., Michalopoulos, G., Birchmeier, W., and Comoglio, P. M. (1991) Scatter factor and hepatocyte growth factor are indistinguishable ligands for the *Met* receptor. *EMBO J.* **10,** 2867–2878.
40. Montesano, R., Schaller, G., and Orci, L. (1991) Induction of epithelial tubular morphogenesis in vitro by fibroblast-derived soluble factors. *Cell* **66,** 697–711.
41. Jackson, B. W., Grund, C., Winter, S., Franke, W. W., and Illmensee, K. (1981) Formation of cytolskeletal elements during mouse embryogenesis II. Epithelial-differentiation of intermediate-sized filaments in early postimplantation embryos. *Differentiation* **20,** 203–216.
42. Ben-Ze'ev, A. (1984) Differential control of cytokeratins and vimentin synthesis by cell-cell contact and cell spreading in cultured epithelial cells. *J. Cell Biol.* **99,** 1424–1433.
43. Bader, B. L., Jahn, L., and Franke, W. W. (1988) Low level expression of cytokeratins 8, 18 and 19 in vascular smooth muscle cells of human umbilical cord and in cultured cells derived therefrom, with an analysis of the chromosomal locus containing the cytokeratin 19 gene. *Eur. J. Cell. Biol.* **47,** 300–319.
44. Kim, K. H., Stellmach, V., Javors, J., and Fuchs, E. (1987) Regulation of human mesothelial cell differentiation: Opposing roles of retinoids and epidermal growth factor in the expression of intermediate filament proteins. *J. Cell Biol.* **105,** 3039–3051.
45. Miettinen, P. J., Ebner, R., Lopez, A. F., and Derynck, R. (1994) TGF-beta induced transdifferentiation of mammary epithelial cells to mesenchymal cells: Involvement of type I receptors. *J. Cell Biol.* **127,** 2021–2036.
46. Fabregat, I., Sánchez, A., Alvarez, A., Nakamura, T., and Benito, M. (1996) Epidermal growth factor, but not hepatocyte growth factor, suppresses the apoptosis induced by transforming growth factor-beta in fetal hepatocytes in primary culture. *FEBS Lett.* **384,** 14–18.
47. Sánchez, A., Alvarez, A., Benito, M., and Fabregat, I. (1996) Apoptosis induced by transforming growth factor-beta in fetal hepatocytes in primary culture. *J. Biol. Chem.* **271,** 7416–7422.
48. Isom, H. C., Seccot, T., Georgoff, I., Woodworth, C., and Mummaw, J. (1985) Maintenance of differentiated rat hepatocytes in primary culture. *Proc. Natl. Acad. Sci. USA* **82,** 3252–3256.
49. Moorby, D. C., Stoker, M., and Gherardi, E. (1995) HGF/SF inhibits junctional communication. *Exp. Cell. Res.* **219,** 657–663.
50. Ikejima, K., Watanabe, S., Kitamura, T., Hirose, M., Miyazaki, A., and Sato, N. (1995) Hepatocyte growth factor inhibits intercellular communication via gap junctions in rat hepatocytes. *Biochem. Biophys. Res. Commun.* **214,** 440–446.
51. Santos, O. F. P., and Nigam, S. K. (1993) HGF-induced tubulogenesis and branching of epithelial cells is modulated by extracellular matrix and TGF-β. *Dev. Biol.* **160,** 293–302.
52. Kojima, T., Mitaka, T., Paul, D. L., Mori, M., and Mochizuki, Y. (1995) Reappearance and long-term maintenance of connexin32 in proliferated adult rat hepatocytes: Use of serum-free L-15 medium supplemented with EGF and DMSO. *J. Cell. Sci.* **108,** 1347–1357.
53. Gumbiner, B. M. (1992) Epithelial morphogenesis. *Cell* **69,** 385–387.
54. Clark, P. (1994) Modulation of scatter factor/hepatocyte growth factor activity by cell-substratum adhesion. *J. Cell. Sci.* **107,** 1265–1275.

Received April 9, 1997
Revised version received June 19, 1997

EXPERIMENTAL CELL RESEARCH **235**, 180–187 (1997)
ARTICLE NO. EX973676

Fibroblasts Can Modulate the Phenotype of Malignant Epithelial Cells *in Vitro*

Sari Atula,*[,1] Reidar Grenman,† and Stina Syrjänen*‡

**Medicity Research Laboratory, University of Turku, Turku, Finland; †Department of Otorhinolaryngology, Turku University Central Hospital, and Department of Medical Biochemistry, University of Turku, Turku, Finland; and ‡Department of Oral Pathology, Institute of Dentistry, University of Turku, Turku, Finland*

An organotypic, tridimensional cell culture, also called a raft system, was used to study the influence of fibroblasts on epithelial carcinogenesis in a cell line derived from laryngeal squamous cell carcinoma and harboring a mutated *p53*. Differences between the effects of normal fibroblasts and those of tumor-derived fibroblasts were compared by means of fibroblasts taken from the normal skin and from the tumor of a cancer patient and cultivated with epithelial carcinoma cells in an organotypic culture. To study cell contact-mediated changes, the fibroblasts were either simply embedded in collagen matrix or additionally brought into direct contact with epithelial cells. Control epithelial cells were cultivated without any fibroblasts in an organotypic model. A protein panel [p53, p21, PCNA, bcl-2, Ki67, total cytokeratin (CK), CK 8, CK 10, CK 17, CK 18, CK 19, vimentin] involved in cell cycling and epithelial differentiation was assessed immunocytochemically in all organotypic cultures with fibroblasts, in tumor cells cultivated as a monolayer, and in the original tumor sample. The most dysplastic phenotype was obtained when tumor-derived fibroblasts were used in direct contact with epithelial cells, whereas the most benign phenotype was seen when skin fibroblasts had no contact with them. The intensive staining seen for p53 can be explained by *p53* mutations also reflecting the weak expression of p21 and abundant expression of PCNA. The intensive Ki67 staining seen in all sections paralleled that of PCNA and marked active cellular proliferation. The CK staining pattern seen in cultured epithelia toward embryonic CKs, CK 8 and CK 18, suggested a simple epithelial phenotype. CK 19 was found only in the epithelium where no direct contacts had occurred. Vimentin expression increased when the raft epithelium was shifting toward a more benign phenotype. The results stress the importance of the origin of fibroblasts as well as the role of direct cellular contacts in modifying the epithelial phenotype even when the epithelial cells are malignant. © 1997 Academic Press

---

INTRODUCTION

Epithelial–mesenchymal interactions are known to be crucial for regular epithelial growth and differentiation during embryogenesis and in the adult organism. Epidermal homeostasis is controlled by multifactorial signaling between the epithelium and the underlying mesenchymal fibroblasts. Direct contact of fibroblasts and keratinocytes has been found to induce cytokine interleukin-1 (IL-1) secretion in epidermal cells. IL-1 stimulates the expression of keratinocyte growth factor (KGF) [1] and IL-6 [2] in mesenchymal cells, whereas KGF [3] and IL-6 [4] excite epithelial proliferation in a paracrine fashion. Mesenchymal stroma is also involved in epithelial carcinogenesis. Fibroblasts have been shown to be capable of promoting [5, 6] or suppressing [7, 8] the development of cancer. This dual role is probably mediated through modified cross-talking between the epithelium and fibroblasts.

In conventional epithelial cell cultures, differentiation is rudimental owing to a lack of proper epithelial–mesenchymal interactions. Subsequently, deficiencies both in the structural arrangement of tissue and in the expression of differentiation markers are obvious. Bell and his colleagues [9] established the method of recombining keratinocytes and fibroblasts *in vitro* on collagen gel. Asselineau and Prunieras [10] developed the method further by lifting the epithelial layer onto an air–liquid interface. At present, this organotypic culture system best imitates the *in vivo* situation. The pattern of epithelial growth and differentiation in reformed tissue in this type of raft culture is usually visible in stained cross-section preparations. The mechanisms of cellular interactions can be further assessed using immunocytochemical methods.

The cell cycle is coordinated by multiple genetic pathways acting in concert to maintain cellular homeostasis. *p53* arrests the cell cycle after DNA damage and is thereafter involved in selection between cell cycle halt and apoptosis. The p53 protein regulates the cell cycle partly via its downstream target p21 (also called WAF1 or CIP1), which inhibits cyclin-dependent ki-

[1] To whom correspondence and reprint requests should be addressed at Medicity Research Laboratory, Tykistökatu 6A, 20520 Turku, Finland. Fax: 358-2-3337000.

0014-4827/97 $25.00

Copyright © 1997 by Academic Press
All rights of reproduction in any form reserved.

nases, resulting in G1 phase arrest and possibly also in S phase arrest [11]. Proliferating cell nuclear antigen (PCNA), earlier known to be essential for DNA replication, has been found to form a complex with p21. This interaction, also induced by *p53,* blocks the function of PCNA and inhibits DNA synthesis [12]. Yet, p21 does not block the nucleotide excision repair functions of PCNA [13]. In the presence of excessive genomic damage, the apoptotic pathway is partly regulated by mutual interactions between *p53* and the apoptosis inhibiting gene *bcl-2* [11]. Ki67 antigen, like PCNA, provides information about the proportion of actively cycling cells [14].

The cytoskeleton of epithelial cells mainly comprises cytokeratin (CK) filaments, divided into basic CKs, CK 1–CK 8, and acidic CKs, CK 9–CK 20, according to their molecular weights and isoelectric pH values. CKs are coexpressed as acidic–basic pairs during epithelial differentiation in tissue-specific manner [15, 16]. Aberrant CK expression patterns have been observed in epithelial malignancies of the skin [17], head and neck [18], and genital regions [19]. Vimentin is another group of intermediate filaments mainly expressed by cells of mesenchymal origin. Vimentin expression has been detected in wound repair process [20] and in cervical carcinogenesis [21].

The ability of fibroblasts of different origins to modify a transformed epithelium in an organotypic culture is not known. In this study, contact-mediated changes were compared with the potential paracrine effects of two kinds of fibroblasts on the phenotype of malignant epithelial cells in an organotypic raft culture system. Laryngeal carcinoma cells were cultivated with fibroblasts derived either from a normal skin or from the laryngeal cancer of the same patient. For the analysis of direct cellular contacts in interactions, epithelial cells were grown either on a collagen gel containing fibroblasts without any contacts with them or fibroblasts were also seeded on a gel bringing them into direct contact with epithelial cells. Control carcinoma cells were cultivated in the raft system without any fibroblasts. Furthermore, proteins associated with cell cycle regulation, p53, p21, PCNA, and bcl-2, proliferation marker Ki67 as well as cytoskeletal markers, CKs, and vimentin, were assessed immunocytochemically in organotypic tissue cultures with fibroblasts, in laryngeal carcinoma cells cultured conventionally as a monolayer, and in the original tumor biopsy sample.

MATERIALS AND METHODS

Epithelial cells. The UT-SCC-19A cell line was established from a moderately well differentiated squamous cell carcinoma of the right vocal cord (T4N0M0) of a 44-year-old man prior to any treatment. The patient, who had a history of heavy smoking and alcohol abuse, received preoperative radiotherapy (62 gy), and total laryngectomy was performed.

To establish the cell line, cancer tissue was transported to the laboratory immediately after removal and cooled to +4°C in a balanced salt solution (Puck's saline A) containing 100 IU/ml penicillin and 100 μg/ml streptomycin. Carcinoma cells were grown in Dulbecco's minimal essential medium (D-MEM) supplemented with 1% nonessential amino acids, 2 m*M* L-glutamine, 50 μl/ml streptomycin, 100 u/ml penicillin, and 15% fetal calf serum (Gibco Laboratories, Grand Island, NY). The culture was incubated at 37°C in a humidified atmosphere containing 5% CO_2 and 95% air for 7 days, after which the cultures were observed and fed weekly. The cancer cell line, when established, was passaged once a week at a ratio of one to five.

The established carcinoma cell line was morphologically similar to epithelial malignant cells with a DNA index of 1.9 flow cytometrically measured. When heterotransplanted to nude mice, carcinoma cells produced tumors, which recapitulated the histology of the original carcinoma. There is a *p53* transition mutation GAG-AAG in exon 8, codon 285, in one allele of these carcinoma cells changing glutamine to lysine and the other allele is deleted. Thus, there is no wild-type p53 protein in this cell line [22].

Fibroblasts derived from normal skin and carcinomatous tissue. Fibroblasts were grown both from the same tumor sample and from the skin biopsy sample from the neck region of the same patient. The fibroblasts were separated from the epithelial cell culture by trypsinization and grown in D-MEM supplemented with 1% nonessential amino acids, 2 m*M* L-glutamine, 50 μl/ml streptomycin, 100 u/ml penicillin, and 10% fetal calf serum.

Preparation of collagen gel. Vitrogen 100 collagen (Celtrix Pharmaceuticals, Inc., Santa Clara, CA) was mixed with 10× D-MEM and neutralized with 0.1 *M* NaOH to pH 7.4 ± 0.2. Fibroblasts were suspended in a collagen solution at a cell density of 280,000 cells/0.7 ml. This suspension was plated in 16-mm tissue culture dishes (Costar, Cambridge, MA). Fibroblasts from a normal skin were used in two experiments, while in the other two fibroblasts from carcinoma tissue were used. The collagen–fibroblast suspension was allowed to gel at 37°C for 1 h. Then, the dishes were filled with Green's medium. The medium consisted of D-MEM–Ham F12 3:1, 10% fetal calf serum, 4 m*M* glutamine, 5 μg/ml insulin (Sigma, St. Louis, MO), 0.18 m*M* adenine (Sigma), 0.4 μg/ml hydrocortisone (Sigma), 0.1 n*M* cholera toxin (Sigma), and 5 ng/ml epidermal growth factor (Boehringer Mannheim, Germany). The collagen gel was maintained at 37°C in an atmosphere of 5% CO_2 with 90% relative humidity. The medium was changed three times a week.

Organotypic cell culture. Two methods with two different fibroblast cell lines were used to produce raft cultures; the epithelial carcinoma cells either had no direct contact with fibroblasts or they were in direct contact with them. Furthermore, no fibroblasts were used as controls. The design of the experiments was as follows: 1. Fibroblasts from a normal skin were mixed in collagen gel with epithelial cells added to the gel. 2. Fibroblasts from carcinoma tissue were mixed in collagen gel with epithelial cells added to the gel. 3. Fibroblasts from a normal skin were mixed in collagen gel. A monolayer of fibroblasts was grown on the gel. Then, epithelial cells were seeded. 4. Fibroblasts from carcinoma tissue were mixed in collagen gel. A monolayer of fibroblasts was grown on the gel. Then, epithelial cells were seeded. 5. Epithelial cells were seeded on collagen gel without any fibroblasts. Fibroblasts from their fifth passage were used for all experiments.

UT-SCC-19A cells, passage 15 (200,000 cells/well), were gently added onto the surface of fibroblast–collagen gels. Epithelial cells from passage 23 were used in the control experiment without fibroblasts. Green's medium was changed every second day. After 3 days, when the cells had reached confluence, the cultures were lifted on a stainless steel grid at the air–liquid interface. Epithelial cells with fibroblasts were allowed to stratify for 18 days and the raft culture without fibroblasts for 10 days. The medium was changed every second or third day.

To confirm the results, experiment 1 was repeated once and experi-

TABLE 1

Antibodies Used for Immunocytochemistry

Antibody	Company	No.	Dilution	Pretreatment	Positive controls
p53	Nova Castra	NLC-p53-DO7	1:100	Microwave, 10 mM citric acid, pH 6.0, 5 min	Breast cancer
p21	Nova Castra	NCL-WAH1	1:2	Microwave, 10 mM citric acid, pH 6.0, 5 min	Verruca
PCNA	Dako	M 879	1:1000	No pretreatment	Oral mucosa
bcl-2	Dako	M 887	1:100	Microwave, 10 mM citric acid, pH 6.0, 5 min	Oral mucosa
Ki67	Immunotech	0505	1:200	Microwave, 10 mM citric acid, pH 6.0, 2 × 5 min	Verruca
Cytokeratin (5, 6, 8, 17, 19)	Dako	M821	1:200	Trypsin, 10 min, 37°C	Skin
Cytokeratin 8	Dako	M 631	1:150	Pepsin, 30 min, 37°C	Fibrous hyperplasia
Cytokeratin 10	Dako	M7002	1:10	No pretreatment	Fibrous hyperplasia
Cytokeratin 17	Dako	M7046	1:75	Microwave, 10 mM citric acid, pH 6.0, 5 min	Oral cancer
Cytokeratin 18	Dako	M 7010	1:75	Trypsin, 10 min, 37°C; microwave, 10 mM citric acid, pH 6.0, 5 min	Prostate
Cytokeratin 19	Dako	M 888	1:500	Trypsin, 10 min, 37°C	Breast tissue
Vimentin	Dako	M 7020	1:500	Trypsin, 10 min, 37°C	Cervix

ments 2, 3, and 4 twice. Four to seven parallel wells were used in each experiment.

Fixation and preparation of tissue cultures. Organotypic cultures with fibroblasts were collected at Day 18 and the culture without fibroblasts at Day 10. The cultures were divided into two parts. One part was fixed in buffered 10% Formalin for 24 h and the other was snap frozen and kept at −70°C for further analysis. The Formalin-fixed material was embedded in paraffin and cut into 5-μm sections to be placed onto organosilan-coated slides for hematoxylin–eosin staining and immunocytochemistry. The epithelial cells cultivated as a monolayer were trypsinized, centrifuged, and transferred onto organosilan-coated glasses. The cell samples were fixed with Carnoy's fixative (60% ethanol, 30% chloroform, and 10% acetic acid) for immunocytochemistry.

The histomorphology of samples was analyzed according to standard criteria for epithelial malignancy in head and neck region [23]: derangement of cellular organization, the variable size and shape of cells, an increased nucleocytoplasmic ratio, and increased rate and exceptional sites of mitoses.

Immunocytochemistry. The expression of p53, p21, PCNA, bcl-2, and Ki67 proteins as well as a panel of CKs and vimentin was analyzed in sections from raft cultures with fibroblasts and from cell samples cultured as a monolayer. The original tumor sample taken at operation after preoperative radiation treatment was also included in the immunocytochemical analysis.

Formalin-fixed, paraffin-embedded sections placed on organosilan-coated slides were deparaffinized in xylene and rehydrated with graded alcohol. To enhance the staining reaction, the sections was pretreated according to the manufacturer's recommendations. Monolayer cells were not pretreated, since no paraffin embedding was used and the sample cells were fresh. Table 1 shows the pretreatment protocols and dilutions of monoclonal antibodies. Endogenous peroxidase activity was blocked using 5% H_2O_2 for 5 min. The sections were first incubated in 1.5% normal goat serum (Vector Laboratories Inc., Burlingame, CA) for 5 min, followed by incubation of primary antibody at +4°C overnight. Then, the sections were incubated with secondary biotinylated anti-mouse IgG antibody (Vector Laboratories Inc.) for 30 min, followed by incubation with an avidin–biotin peroxidase complex (Vectastain ABC kits, Vector Laboratories Inc.) for 30 min. Immunoperoxidase reaction was developed using 3,3′-diaminobenzidine (Sigma) for 5 min. Finally, the sections were counterstained with Meyer's hematoxylin, dehydrated, and mounted with Permount.

Positive and negative controls were included in all stainings. Sections treated with blocking serum without any primary antibody were used as negative controls. Table 1 shows the positive controls used for each antibody.

The intensity of immunocytochemical reactions was classified as negative (−), weak (+), moderate (++), strong (+++), or intense (++++). The sites of positive cells were also recorded.

RESULTS

Morphology

The carcinoma cells were initially able to redifferentiate and attained a more benign phenotype when detached from their original mesenchymal environment and induced to grow in an organotypic model. The alterations found in epithelial tissue in the different experimental settings correlated both with the origin of fibroblasts and with their direct cellular contacts. The most dysplastic epithelial tissue resembling carcinomatous tissue was obtained when fibroblasts from tumor tissue were cultured both in collagen gel and in direct contact with epithelial cells. Epithelial cells showed a complete lack of maturation; they were pleomorphic, had an increased nucleocytoplasmic ratio, and showed aberrant mitoses. A full invasion of epithelial cells into the underlying collagen matrix was seen (Fig. 1A). If a direct contact occurred between the epithelium and cutaneous fibroblasts, prominent hyperproliferation was seen in addition to epithelial invasion and a lack of cellular polarity (Fig. 1B). However, epithelial cell size did not vary much and there were fewer aberrant mitoses than with the model using tumor-derived fibroblasts. The differentiation of epithelial cells was greater when tumor fibroblasts were embedded in collagen matrix. Only a few cells invaded into the underlying mesenchymal matrix, and epithelial thickness was

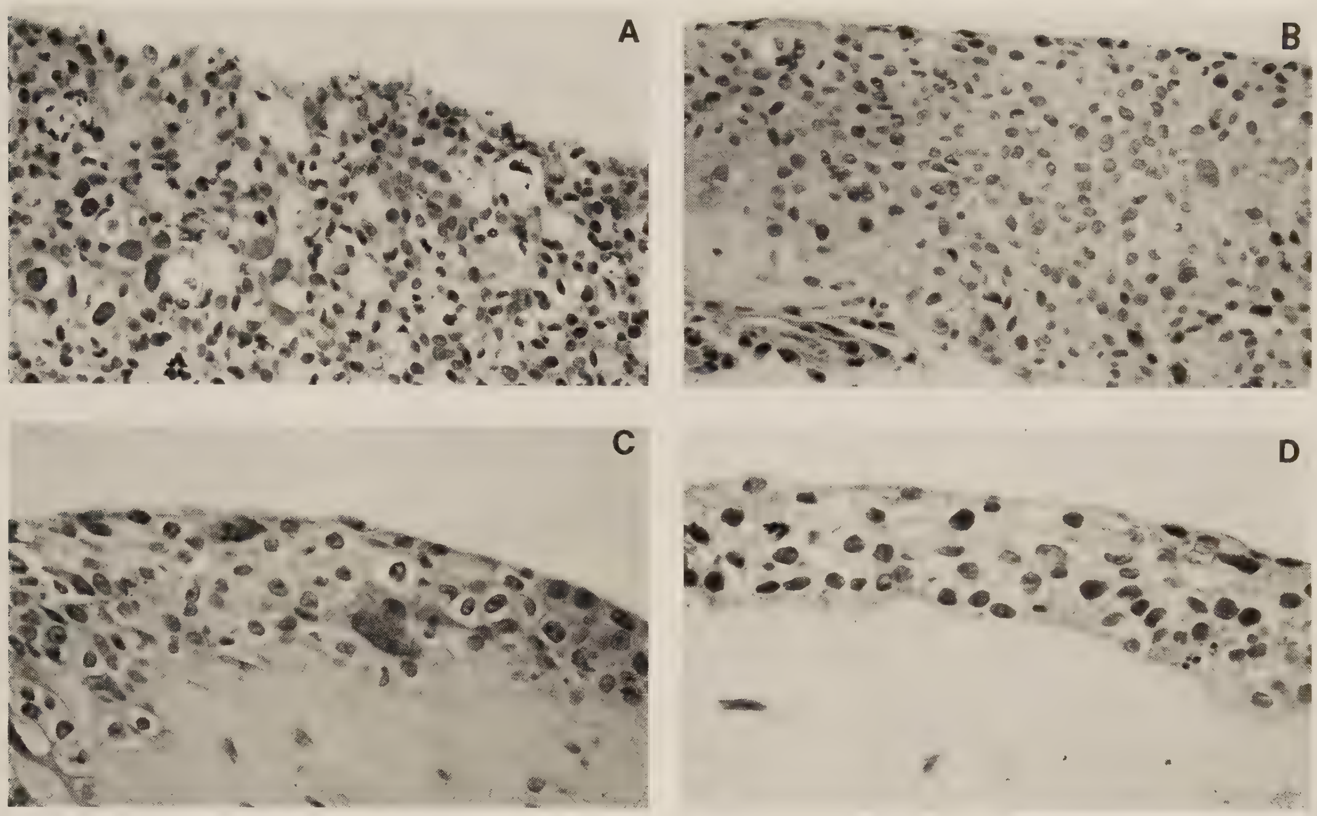

FIG. 1. (A) A raft culture with tumor fibroblasts mixed in collagen matrix and seeded as a monolayer onto the matrix to form a direct contact with epithelial cells. The most malignant phenotype was produced. The border between the epithelium and collagen matrix is diffuse (original magnification, 250×). (B) The same construction of the raft culture as in A, but now skin fibroblasts were used. A hyperplastic epithelium was produced (original magnification, 100×). (C) Tumor derived fibroblasts mixed in collagen matrix. The epithelium had a more benign appearance (original magnification, 100×). (D) Skin fibroblasts embedded in collagen matrix. The most benign phenotype was produced (original magnification, 100×).

almost normal (Fig. 1C). If the organotypic culture contained skin fibroblasts embedded in collagen without any direct epithelial contacts, the phenotype of the epithelium was nearly normal with respect to cellular polarity, tendency to form parabasal layers, and to regular nuclei (Fig. 1D). The culture without any fibroblasts had the most benign phenotype in this study, with normal cell organization, epithelial thickness, and regular nuclei. However, degerative vacuolization was seen in the epithelium. A basement membrane was seen in none of the raft cultures described above.

Immunocytochemistry

Cell cycle regulators: Organotypic culture. Nuclear expression of p53 protein was intensive throughout epithelial cell layers in all tissue culture designs (Fig. 2, Column I, A–D). The nuclear expression of p21 was weak, with only a few positive cells in all organotypic culture samples. PCNA protein showed intense nuclear staining throughout the epithelium in three organotypic samples. In the raft culture with the most dedifferentiated phenotype it was strong. The PCNA staining pattern was similar to that found with p53. Bcl-2 protein expression was not seen in any raft culture sections. Ki67 showed intensive staining in all sections.

Cell cycle regulators: Cell monolayers, the original biopsy sample. Similar to the raft samples, cells cultured as a monolayer and also the original carcinomatous tissue showed intense p53 immunopositivity (Fig. 2, Column I, E–F). No p21 expression occurred in monolayer cells, and staining was weak in the original tumor sample. PCNA was strongly expressed in monolayer culture cells but only weakly in the original tumor section. Bcl-2 expression was weak in monolayers and absent in the original tumor section. Ki67 staining was intensive in monolayers and in the original tumor sample.

Differentiation markers: Organotypic culture. All cytoplasmic CK stainings were epithelial. Total CK staining was intensive or strong throughout all epithelial layers in three raft culture models with a dysplastic phenotype. Expression was weak when skin fibroblasts were mixed in collagen matrix. CK 8 staining, typical of embryonic or simple epithelial cells [17],

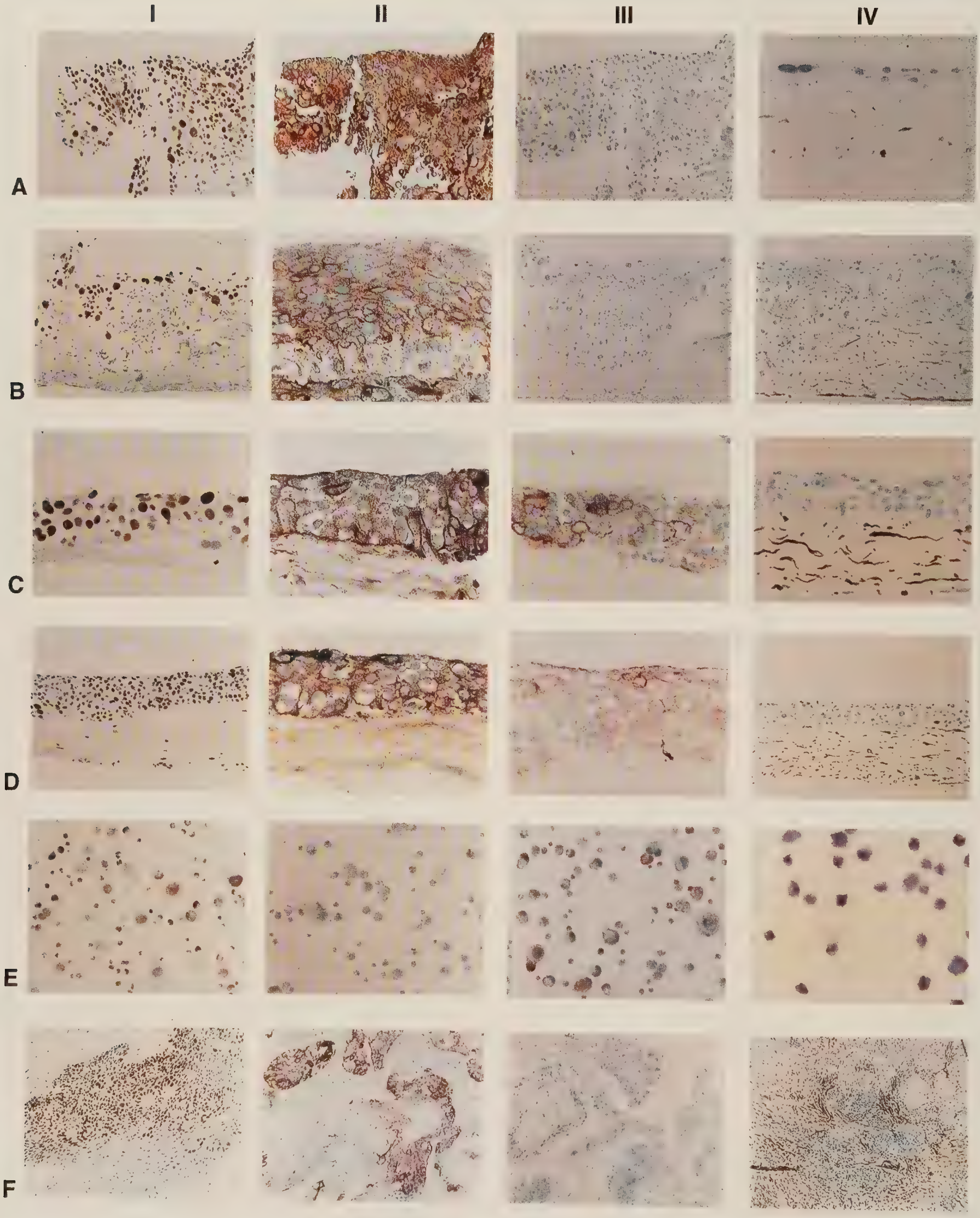

FIG. 2. Immunocytochemical staining of raft cultures. Each line characterizes an individual experimental tissue or cell culture setting. Line A: Tumor fibroblasts embedded in collagen matrix and in direct contact with epithelial cells. Line B: Skin fibroblasts embedded in collagen matrix and in direct contact with epithelial cells. Line C: Tumor fibroblasts embedded in collagen matrix. Line D: Skin fibroblasts embedded in collagen matrix. Row E: Cells cultivated as a monolayer. Line F: Sections from the original tumor sample. Column I: Intensive

showed intensive or strong staining throughout all epithelial layers in all settings (Fig. 2, Column II, A–D). CK 10, normally seen in differentiated skin epithelium [15], was not seen in any samples. The expression of CK 17, typical of hyperproliferation and neoplasms [15], was very weak in all samples. Parallel to CK 8, CK 18, also typical of embryonic epithelium [17], was intensively or strongly expressed in all raft sections. CK 19, normally be found in both simple and stratified epithelia [24], was moderately or strongly expressed in sections without a direct epithelial–mesenchymal contact and undetectable elsewhere (Fig. 2, Column III, A–D). Vimentin staining was restricted to the cytoplasm of fibroblasts in all experimental models. The expression of vimentin tended to increase toward the experimental settings of a more benign phenotype. It was intense when fibroblasts were not in contact with the epithelium, regardless of their origin (Fig. 2, Column IV, A–D).

Differentiation markers: Cells cultured as a monolayer and the original biopsy sample. Total CK expression was weak in monolayer culture but strong in the basal and parabasal layers of the original biopsy sample. CK 8 staining was weak in monolayers but intensive in the tumor sample (Fig. 2, Column II, E–F). In contrast to all other samples, CK 10 was moderately expressed in monolayer cells. Similar to raft cultures, CK 10 was not seen in the tumor section. CK 17, which was not found in organotypic culture samples, showed strong staining both in monolayer cells and in the tumor section. Also in contrast to the rafts, CK 18 was only weakly seen in monolayers but intensively positive in the original sample. Strong CK 19 expression was found in monolayer cells but no staining was found in the tumor biopsy sample (Fig. 2, Column III, E–F). As expected, no vimentin staining was seen in epithelial monolayers, whereas it was intensive in the tumor stroma (Fig. 2, Column IV, F).

Table 2 summarizes the immunocytochemical results.

DISCUSSION

The organotypic cell culture system has been shown to be an effective tool for the study of *in vivo* mechanisms in head and neck carcinomas [25]. In the present study, this raft system was used to analyze the effects of fibroblasts on epithelial cancer cells by characterization of the morphology and expression of proteins involved in cell cycle regulation and differentiation.

The behavior of carcinoma is determined by genetic alterations of epithelial cells together with their cellular microenvironment [7]. In this study, fibroblasts, as elements of this mesenchymal environment, modulated the epithelium in accordance with their origin: the most malignant epithelial phenotype was obtained using tumor fibroblasts. Normal fibroblasts also retained their ability to modify carcinoma cells toward a benign phenotype in certain respects. Breast fibroblasts from benign and malignant lesions have been shown to express different growth factors [26]. This aberrant fibroblast signaling may have contributed to their malignant effects in this study. The importance of fibroblasts in cellular cross-talking was further stressed by the fact that epithelial carcinoma cells achieved almost normal phenotype but showed degenerative vacualization when cultivated in the absence of fibroblasts.

Early melanoma has been found to become depressed by normal dermal fibroblasts, whereas advanced melanoma is stimulated by them [27]. Similarly, normal urothelium and papillary bladder carcinoma have been found to be unresponsive to the signals of normal fibroblasts, whereas invasive bladder carcinoma is induced to active growth by them [28]. It is conceivable that these dual intrinsic properties of fibroblasts originate from the signaling of carcinoma cells. Normal cutaneous environment has been reported to be able to suppress initial cancer lesions [29], possibly because of retained orderly cross-talking between the cells. Respectively, advanced carcinomas, such as the laryngeal carcinoma studied, may produce excessively aberrant growth factors, resulting in defective epithelial overstimulation by fibroblasts, promoting oncogenesis.

We found that direct contact between fibroblasts and epithelium is another determinative factor in cellular communication, since our experiments with direct cell-to-cell contacts resulted in the most dysplastic phenotype. Yaeger *et al.* [30] found a direct cellular contact a prerequisite for the growth signaling effects of the mesenchymal layer. They found that this conditionality is dependent on keratin growth-promoting factor bound to the plasma membrane of fibroblasts, thus requiring a direct epithelial contact for their effects. Waelti *et al.* [31] found that direct cellular con-

---

nuclear p53 staining in the entire epithelium is seen in all raft cultures, as well as in monolayer cells and in the original biopsy sample (original magnifications: A–B, 100×; C, 250×; D, 100×; E–F, 100×). Column II: Intensive cytoplasmic CK 8 expression was found in all raft cultures and in the original tumor section, but CK 8 was only weakly stained in monolayers (original magnifications: A, 100×; B–D, 250×; E–F, 100×). Column III: CK 19 was not detected in the epithelium in direct contact with fibroblasts or in the tumor biopsy sample, while it was moderately or strongly expressed in the epithelium without direct contact with fibroblasts and also in monolayer cells (original magnifications: A–B, 100×; C–D, 250×; E, 100×; F, 40×). Column IV: Vimentin staining in collagen matrix was intensive in more benign phenotypes. No expression was seen in monolayers but it was strong in the original tumor sample (original magnifications: A–B, 250×; C, 250×; D, 100×; E, 100×; F, 100×).

TABLE 2

Expression of Markers Involved in Cell Cycling and Epithelial Differentiation

Model	p53	p21	PCNA	Bcl-2	Ki67	Total CK (5, 6, 8, 17, 19)	CK 8	CK 10	CK 17	CK 18	CK 19	Vimentin
Tumor fibroblasts—direct contact and in collagen matrix	++++	+	+++	–	++++	+++	++++	–	+	++++	–	+
Skin fibroblasts—direct contact and in collagen matrix	++++	+	++++	–	++++	++++	++++	–	+	+++	–	++
Tumor fibroblasts—in collagen matrix	++++	+	++++	–	++++	+++	++++	–	+	++++	+++	++++
Skin fibroblasts—in collagen matrix	++++	+	++++	–	++++	+	++++	–	+	++++	++	++++
Cells from monolayer culture	++++	–	+++	+	++++	+	+	++	+++	+	+++	–
Original tumor sample	++++	+	+	–	++++	+++	++++	–	+++	++++	–	++++

tact between keratinocytes and fibroblasts is responsible for an abnormal increase in IL-6 production. However, all workers have not considered cell-to-cell contacts necessary [2, 27, 28]. In the light of these studies, the fibroblastic signals on an overlying epithelium are probably mediated by close cellular contacts together with diffusible growth factors [32].

The invasion of carcinoma cells into the underlying collagen matrix was especially extensive when the epithelial cells were in direct contact with fibroblasts, regardless of the origin of the fibroblasts. During *in vivo* tumor invasion, epithelial cells, which are normally separated from mesenchyme by a basement membrane, come into direct contact with fibroblasts. This probably stimulates inappropriate growth factor production, further promoting cancer cell invasion. No basement membrane was found in our organotypic cultures. This lack of a natural barrier combined with the close contact of cells could have promoted the invasion. Yet, carcinomatous cells spread in collagen matrix even without cellular contact, although to a low extent.

Despite a good resemblance to the *in vivo* situation, the raft system has some defects compared with the normal skin. The basement membrane, which could not be obtained in this study, has been found to be of utmost importance for the normal function of the three-dimensional organotypic structure [33]. However, Bohnert *et al.* [34] regarded the basement membrane as a mere cofactor in maintaining epidermal homeostasis. The barrier function of the epidermis is not complete in the raft culture, either. With these properties, an organotypic culture has been shown to resemble the skin under wound repair [35]. Thus, the differences between a normal living skin and a raft culture may derive from the intrinsic properties of epithelial tissue rather than from the artificial setting.

No differences were found in the present study between tumor derived and normal fibroblasts in cell cycle regulation. p53 was mutated in the laryngeal carcinoma cell line, which was presumably reflected in the abnormal accumulation of aberrant p53 protein in all studied sections. Defective p53 can not activate p21 expression [36], which probably resulted in absent or weak p21 expression in all cell culture samples of our study. p21 has been shown to be a central factor in cell shift from a proliferative to a differentiated state [37]. Thus, without normal p21 function, carcinomatous cells could have remained in a continuous proliferative state. The overexpression of PCNA speaks for the activation of its nucleotide-repairing functions, upregulated by p53-independent pathways. Alternatively, the detection of PCNA could have been a mere sign of active cellular replication due to weak p21 expression. This concept was supported by the intensive Ki67 expression detected throughout the sections. It is doubtful if p53 could have downregulated bcl-2 expression, since wild-type p53 is required for these mechanisms [38]. Other genetic factors are probably involved in the regulation of *bcl-2*.

Immature types of CKs, CK 8 and CK 18, were inappropriately expressed in the organotypic culture sections of this study, in agreement with the results of a recent study on laryngeal cancer [18]. In the monolayer culture, CK 8 and CK 18 were only faintly expressed, suggesting that those cells were more differentiated. However, the Ca^{2+} content (2 m*M*) in monolayer cultures may also have provocated the differentiation. CK 10 as a keratinocyte differentiation marker was not seen in the raft cultures. CK 19 was seen in the raft models without direct cellular contacts. It might suggest a restored differentiation capacity in those epithelial cells, considering the possible function of CK 19 as an indicator of a labile differentiation state [39]. Overall, CK expression was suggestive of the immature phenotype of epithelial cells cultured in the raft system, even though they partially took a more benign appearance. Vimentin expression has been observed in the absence of cellular contacts [40], in agreement with our results, which showed intense vimentin expression in the absence of direct contacts. However, vimentin expression has also been associated with a high capacity for invasion [21], which is in contrast to our findings.

In conclusion, our results emphasize the deteriorating effects of tumor fibroblasts on cancer cell epithelium. The most malignant phenotype was produced when tumor fibroblasts were in direct contact with epithelial cells.

We express our gratitude to Marja Nykänen, Sari Mäki, and Marita Potila for skillful technical assistance. This study was supported by the Medical Council of the Academy of Finland.

REFERENCES

1. Chedid, M., Rubin, J., Csaky, K. G., and Aaronson, S. A. (1994) *J. Biol. Chem.* **269,** 10753–10757.
2. Boxman, I., Löwik, C., Aarden, L., and Ponec, M. (1993) *J. Invest. Dermatol.* **101,** 316–324.
3. Rubin, J. S., Bottaro, D. P., Chedid, M., Miki, T., Ron, D., Cheon, H-G., Taylor, W. G., Fortney, E., Sakata, H., Finch, P. W., and LaRochelle, W. J. (1995) *Cell. Biol. Int.* **19,** 399–411.
4. Grossman, R. M., Kruger, J., Granelli-Piperno, A., Murphy, D. P., May, L. T., Kupper, T. S., Seghal, P. B., and Gottlieb, A. (1989) *Proc. Natl. Acad. Sci. USA* **86,** 6367–6371.
5. Camps, J. L., Chang, S-M., Hsu, T. C., Freeman, M. R., Hong, S-J., Zhau, H. E., von Eschenbach, A. C., and Chung, L. W. K. (1990) *Proc. Natl. Acad. Sci. USA* **87,** 75–79.
6. Zheng, J., and Vaheri, A. (1995) *Int. J. Cancer* **61,** 658–665.
7. Dotto, G. P., Weinberg, R. A., and Ariza, A. (1988) *Proc. Natl. Acad. Sci. USA* **85,** 6389–6393.
8. Cunha, G. R. (1994) *Cancer* **74,** 1030–1044.
9. Bell, E., Sher, S., Hull, B., Merrill, C., Rosen, S., Chamson, A., Asselineau, A., Dubertret, L., Coulomb, B., Lapiere, C., Nusgens, B., and Neveux, Y. J. (1983) *Invest. Dermatol.* **81**(Suppl), 2s–10s.
10. Asselineau, D., and Prunieras, M. (1984) *Br. J. Dermatol.* **111**(Suppl.), 27, 219–222.
11. Cox, L. S., and Lane, D. P. (1995) *Bioessays* **17,** 501–508.
12. Waga, S., Hannon, G. J., Beach, D., and Stillman, B. (1994) *Nature* **369,** 574–578.
13. Shivji, M. K. K., Grey, S. J., Strausfeld, U. P., Wood, R. D., and Blow, J. J. (1994) *Curr. Biol.* **4,** 1062–1068.
14. Brown, D. C., and Gatter, K. C. (1990) *Histopathology* **17,** 489–503.
15. Moll, R., Franke, W. W., Schiller, D. L., Geiger, B., and Krepler, R. (1982) *Cell* **31,** 11–24.
16. Cooper, D., Schermer, A., and Sun, T-T. (1985) *Lab. Invest.* **52,** 243–256.
17. Markey, A. C., Lane, E. B., Churchill, L. J., MacDonald, D. M., and Leigh, I. M. (1991) *J. Invest. Dermatol.* **97,** 763–770.
18. Mallofre, C., Cardesa, A., Campo, E., Condom, E., Palacin, A., Garin-Chesa, P., and Traserra, J. (1993) *Pathol. Res. Pract.* **189,** 275–282.
19. Smedts, F., Ramaekers, F., Robben, H., Pruszczynski, M., van Muijen, G., Lane, B., Leigh, I., and Vooijs, P. (1990) *Am. J. Pathol.* **136,** 657–668.
20. Buisson, A-C., Gilles, C., Polette, M., Zahm, J-M., Birembaut, P., and Tournier, J-M. (1996) *Lab. Invest.* **74,** 658–669.
21. Gilles, C., Polette, M., Piette, J., Birembaut, P., and Foidart, J-M. (1994) *Int. J. Cancer* **59,** 661–666.
22. Servomaa, K., Kiuru, A., Grenman, R., Pekkola-Heino, K., Pulkkinen, J. O., and Rytömaa, T. (1996) *Cell. Proliferation* **29,** 219–230.
23. Anneroth, G., Batsakis, J., and Luna, M. (1986) *Scand. J. Dent. Res.* **95,** 229–249.
24. Bartek, J., Bartkova, J., Taylor-Papadimitriou, J., Rejthar, A., Kovarik, J., Lukas, Z., and Vojtesek, B. (1986) *Histochem. J.* **18,** 565–575.
25. Eicher, S. A., Clayman, G. L., Liu, T-J., Shillitoe, E. J., Storthz, K. A., Roth, J. A., and Lotan, R. (1996) *Clin. Cancer Res.* **2,** 1659–1664.
26. Cullen, K. J., Smith, H. S., Hill, S., Rosen, N., and Lippman, M. E. (1991) *Cancer Res.* **51,** 4978–4985.
27. Cornil, I., Theodorescu, D., Man, S., Herlyn, M., Jambrosic, J., and Kerbel, R. S. (1991) *Proc. Natl. Acad. Sci. USA* **88,** 6028–6032.
28. Pritchett, T. R., Wang, J. K. M., and Jones, P. A. (1989) *Cancer Res.* **49,** 2750–2754.
29. Dotto, G. P., Moellmann, G., Ghosh, S., Edwards, M., and Halaban, R. (1989) *J. Cell. Biol.* **109,** 3115–3128.
30. Yaeger, P. C., Stiles, C. D., and Rollins, B. J. J. (1991) *Cell. Physiol.* **149,** 110–116.
31. Waelti, E. R., Inaebnit, S. P., Rast, H. P., Hunziker, T., Limat, A., Braathen, L. R., and Wiesmann, U. J. (1992) *Invest. Dermatol.* **98,** 805–808.
32. Smola, H., Thiekötter, G., and Fusenig, N. E. J. (1993) *Cell. Biol.* **122,** 417–429.
33. Boudreau, N., Werb, Z., and Bissell, M. J. (1996) *Proc. Natl. Acad. Sci. USA* **93,** 3509–3513.
34. Bohnert, A., Hornung, J., Mackenzie, I. C., and Fusenig, N. E. (1986) *Cell Tissue Res.* **244,** 413–429.
35. Bilbo, P. R., Nolte, C. J. M., Oleson, M. A., Mason, V. S., and Parenteau, N. L. (1993) *J. Toxicol.—Cut. Ocular Toxicol.* **12,** 183–196.
36. Harper, J. W., Adami, G. R., Wei, N., Keyomarsi, K., and Elledge, S. J. (1993) *Cell* **75,** 805–816.
37. Halevy, O., Novitch, B. G., Spicer, D. B., Skapek, S. X., Rhee, J., Hannon, G. J., Beach, D., and Lassar, A. B. (1995) *Science* **267,** 1018–1021.
38. Selvakumaran, M., Lin, H-K., Miyashita, T., Wang, H. G., Krajewski, S., Reed, J. C., Hoffman, B., and Liebermann, D. (1994) *Oncogene* **9,** 1791–1798.
39. Stasiak, P. C., Purkis, P. E., Leigh, I. M., and Lane, E. B. (1989) *J. Invest. Dermatol.* **92,** 707–716.
40. Pagan, R., Martin, I., Alonso, A., Llobera, M., and Vilaro, S. (1996) *Exp. Cell Res.* **222,** 333–344.

Received February 5, 1997
Revised version received May 15, 1997

EXPERIMENTAL CELL RESEARCH **235**, 188–197 (1997)
ARTICLE NO. EX973646

v-Ras and v-Raf Block Differentiation of Transformable C3H10T1/2-Derived Preadipocytes at Lower Levels Than Required for Neoplastic Transformation

Leda Raptis,*[,1] Heather L. Brownell,* Ying Lu,† Thomas Preston,* Radha P. Narsimhan,‡
Stephen Anderson,§ Erik Schaefer,¶ and Tina Haliotis†[,2]

**Department of Microbiology and Immunology and †Department of Pathology, Queen's University, Kingston, Ontario, Canada; ‡Dana-Farber Cancer Institute, Harvard Medical School, Cambridge, Massachusetts 02138; §National Cancer Institute, Frederick, Maryland 21702; and ¶Promega Corporation, Madison, Wisconsin 53711–5399*

To investigate the functional relationship between the transforming ability of Ras and its role as an integral component of the differentiative insulin signaling pathway, we introduced a leu61-activated *ras* gene into a Ras-transformable, C3H10T1/2-derived preadipocytic cell line. The results demonstrate that *ras*$^{\text{leu61}}$ expression in this line blocks differentiation and that this block appears at lower levels than required for full neoplastic transformation. In addition, to examine whether the inability of Ras$^{\text{leu61}}$ to induce differentiation by replacing the insulin signal could be attributed to its transforming effect in this system, we examined the effect of Ras$^{\text{leu61}}$ at levels below the baseline, by expressing *ras*$^{\text{leu61}}$ in a series of preadipocytes which were rendered deficient in endogenous c-Ras activity. The results show that even very low Ras$^{\text{leu61}}$ levels, insufficient to restore the growth rate of these cells to normal, blocked rather than enhanced differentiation, indicating that *ras*$^{\text{leu61}}$ expression alone is not sufficient to promote adipocytic differentiation in this system, even in the absence of neoplastic transformation. Consistent with its established role as a downstream effector of Ras, v-Raf expression mirrored the v-Ras effects upon adipocytic differentiation and transformation. © 1997 Academic Press

INTRODUCTION

An accruing body of evidence suggests that many types of cells regulate their growth rate in the animal by expressing a differentiated phenotype [1–3]. It follows that to obtain physiologically significant data on the effect of oncogenes *in vivo,* it is imperative to study the functional relationship between cellular transformation and differentiation.

The *ras* genes are members of a ubiquitous eukaryotic multigene family encoding small guanine nucleotide-binding proteins which are involved in a number of signaling pathways [4]. Extensive genetic and biochemical evidence indicates that the Ras proteins function downstream of growth-factor-activated receptor tyrosine kinases and upstream of cytosolic serine/threonine kinases in proliferative pathways [5–8]. Aside from its role in mitogenesis, Ras has also been shown to play a key role in a number of differentiation systems, including insulin-induced adipocytic differentiation [9–11].

The peptide hormone insulin exerts a mitogenic effect on fibroblasts and cycling preadipocytes, whereas treatment of quiescent preadipocytes with insulin leads to a potent acceleration of adipocytic differentiation [12]. A compelling body of evidence suggests that c-Ras is an integral and essential component of both proliferative and differentiation-promoting insulin signaling pathways. In fibroblasts, insulin treatment activates c-Ras [5, 13, 14], while introduction of the *ras*$^{\text{asn17}}$ or *ras*$^{\text{lys12,ser186}}$ dominant-negative mutants abrogates the insulin mitogenic signal [15, 16]. On the other hand, c-Ras downregulation through expression of dominant-negative mutants [15] blocked insulin-induced adipocytic differentiation.

The mechanism whereby the insulin–Ras signal is interpreted biochemically, sometimes as differentiative and other times as proliferative, is not clear. Previous reports investigated the effect of v-*ras* in adipogenesis [9, 17]. In those studies, v-*ras* expression led to the induction of adipocytic differentiation, obviating the insulin requirement. Those experiments were carried out using lines (REF52 fibroblasts or a subclone of 3T3 L1) which are notable for the fact that they cannot be transformed by v-Ras. Consequently, while invaluable for the study of the differentiative function of v-Ras in isolation, such systems are inherently limited in their

---

[1] To whom correspondence and reprint requests should be addressed. Fax: (613) 545-6796. E-mail: RaptisL@Post.QueensU.ca.

[2] Present address: Department of Pathology, Beth Israel Hospital, Harvard Medical School, Cambridge, Massachusetts 02138.

0014-4827/97 $25.00

Copyright © 1997 by Academic Press
All rights of reproduction in any form reserved.

capacity to establish the relationship between the proliferative/transforming function of Ras and its role as an integral component of the differentiative insulin-signaling pathway. A cellular system, however, in which the insulin stimulus can be variably interpreted as either differentiative or proliferative has the potential (i.e., possesses the molecular machinery) to respond to both types of signals, thus offering the opportunity to study the interrelatedness of these two processes. Since Ras participates in both types of responses [9, 15, 16], it may provide a molecular handle for the specificity of that signal. To address this question, we investigated the effect of activated *ras*$^{\text{leu61}}$ expression in the C3H10T1/2 (10T1/2)-derived preadipocytic clone 1C3 [18], which is transformable by v-Ras. Our results demonstrate a quantitative reciprocal regulation of differentiation and several transformation-associated properties, in response to graded levels of *ras* gene expression, indicating that activated Ras expression in transformable preadipocytes inhibits differentiation while inducing transformation. In addition, to examine whether the inability of Ras$^{\text{leu61}}$ to induce differentiation could be attributed to its transforming effect [9], we examined the effect of Ras$^{\text{leu61}}$ at levels below the baseline, by expressing *ras*$^{\text{leu61}}$ in a series of preadipocytes which were rendered deficient in endogenous c-Ras activity [18]. The results show that even very low Ras$^{\text{leu61}}$ levels, insufficient to restore the growth rate of these cells to normal, blocked rather than enhanced differentiation, indicating that *ras*$^{\text{leu61}}$ expression alone is not sufficient to promote adipocytic differentiation in this system, even in the absence of full neoplastic transformation.

MATERIALS AND METHODS

Materials. Tissue culture media and sera were from Flow Labs, Inc. Geneticin (G418 sulfate) was from Gibco Laboratories (Grand Island, NY). Dexamethasone, insulin, oil red-O, and hematoxylin were from Sigma. [α-^{32}P]dATP was purchased from DuPont-New England Nuclear (NEG-012) and cold nucleotides were from Pharmacia.

Cell lines and culture techniques. 10T1/2 is a murine embryonic mesenchymal cell line [19]. 1C3 is a 10T1/2 derivative which exhibits insulin-dependent adipocytic differentiation [18]. The 2H1 line is a 10T1/2 derivative expressing the activated EJ-*ras* gene under control of the mouse metallothionein promoter. Induction of this promoter was achieved through the addition of 50 μM $ZnSO_4$ to the culture medium [18]. The Rev3 cell line is a conditional antisense-*ras* derivative produced by transfection of 10T1/2 with a plasmid containing the coding sequence of the EJ-*ras* gene inserted downstream and in the opposite orientation from the mouse metallothionein promoter [18, 42]. The 24D4 is a Rev3-derived preadipocytic clone, isolated from areas with a high proportion of morphologically differentiated cells [18] and further subcloned by limiting dilution. For all lines, a large number of vials were frozen in liquid nitrogen as soon as possible after isolation and cells were used for a maximum of six passages after thawing.

Cell cultures were maintained at 37°C in a humidified, 5% CO_2 incubator. Standard tissue culture medium consisted of 10% heat-inactivated fetal calf serum (FCS, Gibco) in Dulbecco's modified Eagle's medium (DMEM). The medium was changed every 2–3 days unless otherwise specified.

Anchorage-independent growth was assessed by suspending the cells in semisolid agar medium. Quantitation was achieved by suspending the cells in 2 ml of methocel containing 10 μCi [^{3}H]thymidine per milliliter. Twenty days later, cells were washed from the water-soluble methocel and trichloroacetic acid-precipitable counts were determined [20].

Constitutive expression of ras$^{\text{leu61}}$ *and p42*^{raf}*.* For the expression of a transforming *ras* gene, the Nψ6 line, which produces recombinant retrovirus carrying a leucine-61-activated c-H-*ras*-1 cDNA in the pDOL retroviral vector, was used [21]. 1C3 preadipocytes were infected with the culture supernatant from Nψ6 cells when they were approximately 50% confluent in 3-cm plates. Twenty-four hours later, cells were passed into 10-cm plates and selected for G418 resistance. For the expression of *ras*$^{\text{leu61}}$ in the G418-resistant lines (e.g., 24D4), very sparse cultures (approximately 2×10^4 cells per 10-cm petri dish) were infected with the culture supernatant from the Nψ6 packaging line. Ten days later, individual colonies were picked, expanded into lines, and tested for Ras levels as described below.

A similar approach was used for the expression of activated Raf using the culture supernatant from line ψ2LN42K, which secretes a retroviral vector able to express the transforming p42^{raf} gene product in target lines [22].

Quantitation of ras and raf gene expression levels. *ras*-specific RNA levels were quantitated by Northern blotting of total cellular RNA by probing with *ras*-specific DNA labeled by random priming [23]. As a control, the probe was stripped and the same membrane was reprobed for β_2-microglobulin.

Ras protein was quantitated by immunoblotting, utilizing the monoclonal anti-Ras antibody pan-Ras Ab2 (Oncogene Science). Proteins were extracted with 1% NP-40 essentially as described [24] and protein concentration was carefully determined using a protein determination kit (Bio-Rad). Lysate (300 μg) was resolved by SDS–PAGE and electrophoretically transferred to a Hybond enhanced chemiluminescence (ECL) nitrocellulose membrane (Amersham, Arlington Heights, IL). The membrane was probed with the monoclonal antibody pan-Ras Ab2 at 5–10 μg/ml, followed by an alkaline phosphatase-conjugated goat anti-mouse antibody. The 21-kDa band representing Ras was visualized through the use of an alkaline phosphatase-based, ECL detection system followed by exposure to XAR-5 film, according to the manufacturer's instructions (Oncogene Science). To more precisely quantitate Ras levels, a duplicate membrane was probed with the same anti-Ras antibody, followed by premium quality, phosphatase-labeled goat anti-mouse IgG (H + L) (Gibco), and washed once in attophos buffer (50 mM Tris, pH 9.5, 100 mM NaCl, 0.1 mM $MgCl_2$). The filter was then developed for 10 min in attophos buffer containing attophos, alkaline phosphatase substrate, according to the manufacturer's instructions (JBL Co., San Luis Obispo, CA) at a 1:20 dilution and subjected to analysis by a Molecular Dynamics Model 575 Fluorimager (Molecular Dynamics, Inc., Sunnyvale, CA). Relative band intensities were computed using the ImageQuaNT program. To improve quantitation, the experiments were conducted in triplicate and mean values obtained. To control for transfer efficiency, the gel was stained with Coomassie blue after the electrophoretic transfer. As a further control for total protein concentration, the same protein samples were run on a parallel gel which was similarly stained. The values obtained closely correlated with those obtained through *in vivo* [^{35}S]methionine labeling [20] and immunoprecipitation of the same number of counts for each treatment (10^7) with the same anti-Ras antibody and with values obtained by Northern blotting for *ras*-specific RNA as above.

A similar technique was employed for the detection of p42^{raf}, using an anti-Raf polyclonal serum raised in rabbits against a peptide corresponding to the 12 carboxy-terminal amino acids of Raf-1.

Assessment of Ras activity levels. A recently described technique [25] was employed. Briefly, ~2 million cells were grown on a glass slide coated with indium–tin oxide, a transparent and electrically conductive material. An electrical pulse of precisely controlled intensity (145 V) was applied in the presence of 100 μCi [α-^{32}P]GTP in 10 m*M* Hepes, 140 m*M* NaCl, pH 7.2. Previous results demonstrated that under these conditions, pores open in the cell membrane which rapidly reseal with minimal effect upon the cell. After a 30-min incubation in phosphate-free DMEM at 37°C, the cells were stimulated with insulin. Cells were harvested at the indicated time points after stimulation, detergent extracts containing 10^7 cpm on protein (determined by binding to nitrocellulose filters [26]) were precipitated with the pan-Ras Ab2 antibody as above, and the Ras-bound GTP and GDP were eluted and resolved by thin-layer chromatography (TLC) as described [25]. The TLC plates were exposed to Kodak XAR-5 film or scanned directly for beta emission of the spots corresponding to GTP or GDP cold standards in a Molecular Dynamics PhosphorImager. Quantitation was achieved by scintillation counting of the spots.

Assessment of mitogen-activated protein kinase (MAPK) activation. Cells were stimulated with insulin and at the indicated time points extracted with lysis buffer (50 m*M* Hepes, 150 m*M* NaCl, 10 m*M* EDTA, 10 m*M* $Na_4P_2O_7$, 100 m*M* NaF, 2 m*M* sodium vanadate, 0.5 m*M* phenylmethylsulfonyl fluoride, 10 μg aprotinin per milliliter, 10 μg leupeptin per milliliter, 1.0% Triton X-100, pH 7.4). Then 300 μg of total protein was loaded on a polyacrylamide gel and transfered to a nitrocellulose membrane, which was probed with an antibody raised against the phosphorylated (i.e., activated) form of mitogen-activated protein kinase of (MAPK) (Promega Corp.). The bands were visualized using an alkaline phosphatase-conjugated secondary antibody followed by chemiluminescent substrates (Western-Light Chemiluminescent Detection System), according to the manufacturer's instructions (Tropix).

Induction and quantitation of cell differentiation. Approximately 1000 cells were seeded into each well of a 24-well Linbro plate (Corning) in 10% FCS. A number of sera were tested for their ability to sustain differentiation in the presence of insulin and low backgrounds in its absence. At confluence, defined as high cell density with extensive cell to cell contact, cultures were treated with differentiation medium containing 10 μg/ml insulin. Lipid droplets appeared approximately 10 days later.

To increase the attachment of transformed cells to the culture plates, cells were plated onto Cell-Tak, a polyphenolic protein extracted from a marine mussel, according to the manufacturer's instructions (Collaborative Research).

Oil red-O staining for the assessment of adipose conversion frequency was performed as described [18, 32]. To assess the degree of differentiation, Northern blotting of total cellular RNA was conducted using the acid phenol method and was probed with DNA coding for adipocyte-specific genes labeled by random priming [23]. The cloned aP_2, glycerophosphate dehydrogenase (GPD), and adipsin DNA probes were gifts from Dr. B. Spiegelman, Harvard University [27]. As a control, the probe was stripped and the same membrane was reprobed for β_2-microglobulin, a gift from Dr. J. Seidman, Harvard Medical School [28].

RESULTS

Ras Transduces the Insulin Signal in 1C3 Cells

Results from a number of laboratories indicated that c-Ras is an integral component of the insulin signaling pathway [5, 13–16]. This was verified in the present system using a novel technique of *in situ* electroporation of [α-^{32}P]GTP [25]. After [α-^{32}P]GTP loading and insulin stimulation, Ras-bound ^{32}P-labeled GTP and GDP were separated by thin layer chromatography followed by exposure to X-ray film and scintillation counting, as described under Materials and Methods. As shown in Fig. 1A, insulin addition increased the Ras-bound, guanine-nucleotide exchange rate in 1C3 cells by approximately threefold and the GTP/GTP + GDP ratio by twofold. This increase translated into a potent activation of the Ras downstream effector, MAPK (Fig. 1B), indicating that the Ras/MAPK pathway is mediating the insulin signal in this system. This conclusion is further strengthened by the recent demonstration that c-Ras downregulation blocks insulin-induced adipocytic differentiation in 1C3 cells [29].

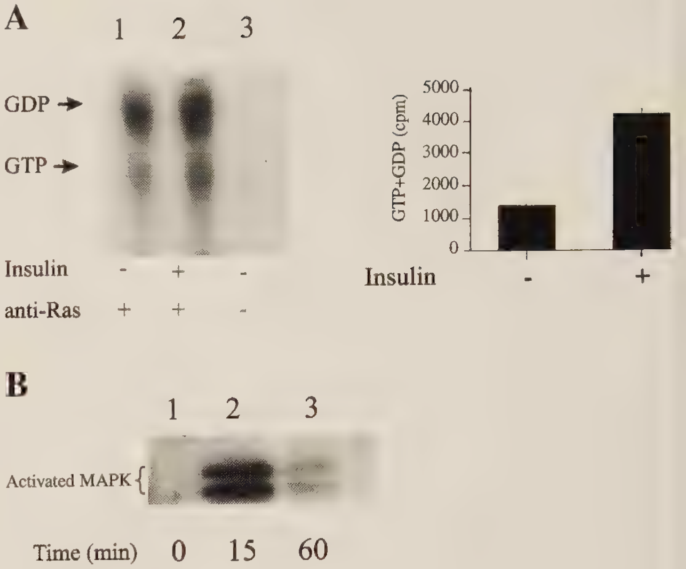

FIG. 1. Insulin activates the Ras pathway in 1C3 preadipocytes. (A) c-Ras activation. (Left) 1C3 cells were serum-starved for 48 h and electroporated with [α-^{32}P]GTP (see Materials and Methods). Cells were subsequently detergent-extracted, before (lane 1) or after a 5-min incubation with 10 μg/ml insulin (lane 2). After immunoprecipitation of extracts containing 10^7 cpm of protein-bound [α-^{32}P]-GTP, the Ras-bound GTP and GDP were eluted and resolved by thin-layer chromatography [25]. The plate was exposed to Kodak XAR-5 film for 2 h. Lane 3 shows a control immunoprecipitation with non-specific mouse IgG. Arrows point to the positions of cold GTP and GDP standards. (Right) Values obtained by scintillation counting of the spots. Numbers represent averages of three separate experiments. (B) Activation of MAPK. 300 μg of detergent extracts from serum-starved 1C3 cells, stimulated for 0 (lane 1), 15 (lane 2), or 60 (lane 3) min were resolved by acrylamide gel electrophoresis and transferred to a nitrocellulose membrane, which was probed with an antibody specific for the activated form of MAPK (see Materials and Methods). The bracket points to the positions of the 42- and 44-kDa activated MAPK.

Production of 10T1/2-Derived Preadipocytic Lines Expressing Varying Ras^{leu61} Levels

To examine the role of Ras in transformation and adipocytic differentiation we expressed ras^{leu61} in 1C3 preadipocytes [18], which are transformable by acti-

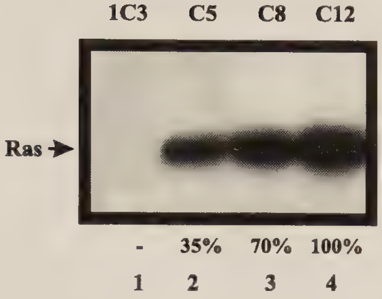

FIG. 2. Quantitation of Ras levels in Ras^{leu61}-expressing 1C3 cells. 300 μg of total cellular protein from 1C3 preadipocytes (lane 1) and a panel of derivatives, constitutively expressing *ras*^{leu61} through infection with a retroviral vector (lanes 2–4), were resolved by polyacrylamide gel electrophoresis and transferred to a nitrocellulose membrane, which was probed with an anti-Ras monoclonal antibody, followed by Fluorimager scanning (see Materials and Methods). Numbers represent units obtained, with the values of the Ras-transformed line 2H1 (after induction with 50 μM $ZnSO_4$) defined as 100%. Arrow points to the position of the 21-kDa Ras protein.

vated Ras. To avoid potential problems associated with inducers of commonly used regulatable promoters which might affect differentiation [12], the leucine-61-activated *ras* gene was introduced under control of the strong constitutive MoMLV promoter, through infection with the culture supernatant from the Nψ6 packaging line, which secretes virus carrying the *ras*^{leu61} gene (see Materials and Methods). A number of resistant colonies were isolated, expanded into clones, and tested for *ras* gene expression levels by Western blotting. As shown previously [6], individual clones expressed different levels of Ras^{leu61}. Twelve clones were selected for further experiments and named C1 to C12 in order of increasing Ras^{leu61} level (Fig. 2 and Table 1, lines 3–12).

Reciprocal Regulation of Transformation and Differentiation by Ras

Previous results demonstrated a quantitative regulation of the manifestation of transformation-related properties in response to graded levels of expression of the middle tumor antigen of polyoma virus or v-*src* in murine fibroblasts [20, 30]. Therefore, we examined the dependence of various parameters of transformation upon the levels of *ras* gene expression in the series of Ras^{leu61}-expressing 1C3 preadipocytes described above.

Anchorage-independent proliferation requires maximal levels of ras gene expression. Ras^{leu61}-expressing, 1C3 preadipocytes were plated in soft agar (see Materials and Methods). As shown in Fig. 3, Ras levels comparable to those present in the 2H1, *ras*-transformed line described previously [31] rendered the cells anchorage-independent to the same extent as the 2H1 cells themselves, while no growth was observed upon infection with the vector alone, lacking *ras*^{leu61} (e.g., Table 1, line 1C3-neo). Lines with intermediate Ras^{leu61} levels were used to examine this dependence further. As shown in Fig. 3, some agar growth was observed when Ras levels were approximately 35% of the levels in the 2H1 line, and the growth response increased roughly proportionally to the amount of Ras present in the cell, up to 100% (Table 1, lines 1–12).

Loss of differentiative capacity and morphological transformation have lower requirements for ras gene expression than anchorage-independent proliferation. A change in cell morphology is a characteristic feature of neoplastically transformed or differentiating cells. The degree of adipocytic differentiation was quantitated using two criteria: (i) morphological changes such as cell rounding and accumulation of intracellular lipid, visible by phase-contrast microscopy of live cultures or after staining for lipid with oil red-O following fixation [32] (Figs. 3 and 5); and (ii), Northern blotting analysis of several mRNAs known to be adipocytic differentiation-specific markers, including those encoding GPD, the fatty acid-binding protein aP2, and adipsin [9] (Table 1, see Materials and Methods).

The results using either of the above criteria showed that, in contrast to anchorage-independent proliferation, the block of differentiation and acquisition of a transformed morphology are remarkably sensitive to *ras*^{leu61} expression; Ras^{leu61} levels as low as 5% of the levels of the 2H1 (e.g., C1, Fig. 3 and Table 1) caused a visually detectable reduction in differentiation efficiency, while levels higher than 28% resulted in a total loss of the ability to differentiate (e.g., C4, Table 1).

The Inability of Ras^{leu61} to Induce Differentiation Can Be Uncoupled from Its Transforming Effect

The above results indicate that in the 1C3, Ras-transformable preadipocytic line, even low Ras^{leu61} levels, which are unable to cause full neoplastic transformation, can very effectively block differentiation. Given the ability of v-Ras to induce, rather than block, differentiation of the nontransformable 3T3 L1 preadipocytes, it was important to determine whether the reason for the differentiation block upon the 1C3 might be the Ras^{leu61}-transforming effect upon this line. If that were the case, expression of Ras^{leu61} in 1C3 cells under conditions precluding transformation might enhance or accelerate differentiation in this system. In an attempt to answer this question, the effect of *ras* expression across a broader range of levels, very close to or below the baseline (i.e., unable to induce transformation), may be examined. Since, however, the differentiation of 1C3 preadipocytes is insulin- (hence c-Ras-) dependent, blocking c-Ras function precludes differentiation (e.g., 1C3α*ras*13d, Table 1, lines 13 and 14) [15]. To circumvent this problem, we examined the effect of

TABLE 1

Effect of Oncogenes upon the Differentiation of Transformable Preadipocytes

						Differentiation[e]		
Line	Ras$^{\text{leu61}}$[a]	c-Ras[b]	mT	Methocel[c]	Growth[d]	aP2	GPD	Adipsin
1C3 preadipocytes								
1. 1C3	—	100%	–	0%	23	100 ± 2%	100 ± 3%	100 ± 4%
2. 1C3[f]	—	100%	–	0%	23	100 ± 1%	100 ± 4%	100 ± 5%
ras$^{\text{leu61}}$-expressing 1C3 lines								
3. C1	5%	100%	–	0%	22	20 ± 3%	22 ± 1%	19 ± 2%
4. C2	7%	100%	–	0%	22	10%	9 ± 1%	11 ± 1%
5. C4	28%	100%	–	0%	21	0%	0%	0%
6. C5	35%	100%	–	5%	21	0%	0%	0%
7. C6	42%	100%	–	15%	21	0%	0%	0%
8. C7	58%	100%	–	20%	20	0%	0%	0%
9. C8	70%	100%	–	30%	21	0%	0%	0%
10. C9	79%	100%	–	60%	20	0%	0%	0%
11. C11	88%	100%	–	65%	20	0%	0%	0%
12. C12	100%	100%	–	100%	20	0%	0%	0%
13. 1C3*αras*13d[g]	—	95%	–	0%	25	95 ± 2%	92 ± 4%	96 ± 3%
14. 1C3*αras*13d[f]	—	30%	–	0%	60	0%	0%	0%
15. 1C3-mT[h]	—	100%	+	100%	19	0%	0%	0%
c-Ras-deficient preadipocytes								
16. 24D4	—	18%	–	0%	80	100 ± 3%	98 ± 3%	101 ± 2%
17. Rev3	—	28%	–	0%	60	100 ± 4%	101 ± 4%	100 ± 1%
18. 25B8	—	18%	–	0%	80	100 ± 2%	100 ± 3%	99 ± 2%
c-Ras-deficient preadipocytes expressing *ras*$^{\text{leu61}}$								
19. 24V2	30%	18%	–	5%	80	0%	0%	0%
20. 24T2	88%	18%	–	60%	20	0%	0%	0%
21. Rev3*ras*	80%	18%	–	50%	20	0%	0%	0%
22. 25B8*ras*	80%	18%	–	45%	20	0%	0%	0%
24D4, c-Ras-deficient preadipocytes expressing mT								
23. 24D4-mT[h]	—	18%	+	0%	80	100 ± 3%	98 ± 2%	101 ± 4%

Note. ras$^{\text{leu61}}$, v-*raf,* or the membrane-bound, polyoma virus middle tumor antigen (mT) was expressed in the Ras-transformable 1C3 and the c-Ras-deficient preadipocytes using a retroviral vector and the cells' ability to differentiate was examined (see Materials and Methods).

[a] Ras$^{\text{leu61}}$ expression levels were quantitated by Western blotting using the pan-Ras Ab2 antibody and Fluorimager scanning, as described under Materials and Methods. The numbers represent percentages, with the levels of the *ras*-transformed line 2H1 after induction with 50 μM $ZnSO_4$ defined as 100%.

[b] c-Ras expression was quantitated as above, with the levels of the parental 1C3 line defined as 100%.

[c] Anchorage-independent growth was quantitated by suspending 50,000 cells in methocel containing 10 μCi/ml [^{3}H]thymidine and measuring incorporation 20 days later (see Materials and Methods). The numbers represent percentages, with the levels of the *ras*-transformed line, 2H1 after induction with 50 μM $ZnSO_4$ defined as 100%.

[d] 30,000 cells were seeded in 60-mm dishes and counted at several time points over 7 days. Doubling times are shown in hours.

[e] 10 μg/ml insulin was added to all lines at confluence. Differentiation is expressed as RNA levels of the adipocyte-specific genes (aP2, adipsin, and GPD) assessed by densitometric scanning of Northern blots, after normalization for β2-microglobulin expression with the levels of the parental lines 1C3 or 24D4 taken as 100% (see Materials and Methods). The numbers represent averages of three experiments ± SEM.

[f] Cells were treated with the inducers of the hMT-IIA(lacO) promoter [47], 0.25 μM dexamethasone, 20 m*M* IPTG, and 50 μM $ZnSO_4$.

[g] 1C3 preadipocytes expressing a *ras*-antisense RNA under control of the hMT-IIA(lacO) promoter [42].

[h] Polyoma virus middle tumor antigen-expressing preadipocytes.

leu61-activated Ras in the 10T1/2-derived preadipocyte 24D4, where the endogenous, cellular Ras gene is downregulated through expression of an antisense *ras* RNA [18]. This line, being largely insulin-independent for differentiation, offers the advantage of differentiating in spite of the c-Ras deficiency.

ras$^{\text{leu61}}$ was expressed in 24D4 cells using the same retroviral vector described above. Individual colonies were picked, expanded into clones, and tested for Ras expression by Western blotting. Twelve lines with varying Ras$^{\text{leu61}}$ levels were chosen for further experiments (Fig. 4A). As shown previously [6, 18], due to the downregulation of expression of this essential cellular gene, the growth rate of the 24D4 clone was substantially lower than that of the parental 10T1/2 line (doubling times 80 h vs 22.3 h, Fig. 5), and Ras$^{\text{leu61}}$ levels up to

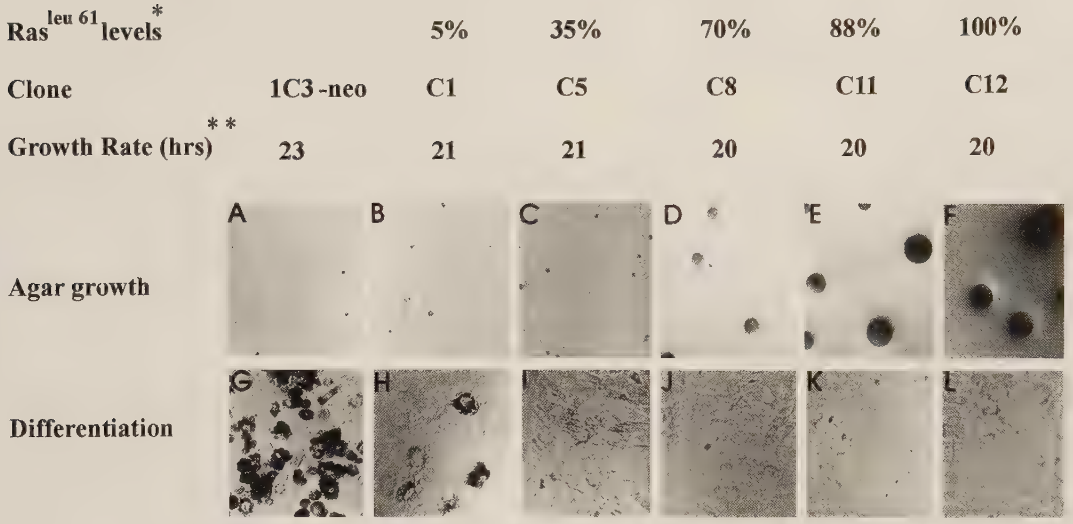

FIG. 3. Dependence of phenotypic expression upon Ras levels in 1C3 preadipocytes. 1C3 preadipocytes or their derivatives expressing different levels of Ras^{leu61} were suspended in agar or placed under differentiation-inducing conditions. *Numbers represent Ras levels quantitated by Fluorimager scanning of a Western blot as in Fig. 1. The Ras levels of line 2H1 were defined as 100%. **30,000 cells were seeded in 60-mm dishes and counted at several time points over 7 days. Doubling times are shown in hours. (A–F) Anchorage independent growth assays. Cells were trypsinized and placed in agar [20]. Pictures were taken 3 weeks later. (G–L) Cellular morphology under differentiation-inducing conditions. At confluence cells were treated with 10 μg/ml insulin. Photographs were taken 10 days later after cell staining with oil red-O and hematoxylin (see Materials and Methods).

30% of the Ras levels present in the 2H1 line (e.g., clone 24V2) were insufficient to correct this growth defect (Fig. 5). Despite this, Ras levels as low as 20% of the level present in the 2H1 line (e.g., clone 24V7) totally abolished differentiation (Figs. 4B and 5). A further increase in Ras^{leu61} resulted in a dramatic stimulation of growth rate on plastic, from doubling times of 80 to 20 h, as well as acquisition of the ability for anchorage-independent proliferation (Fig. 5). Similar results were obtained with three additional independently derived, *ras*-antisense expressing, 10T1/2 preadipocytic cell lines (Rev3, 25B8, and 21F1 [18]; see Table 1, lines 16–22). These results indicate that even very low Ras^{leu61} levels, insufficient to restore the

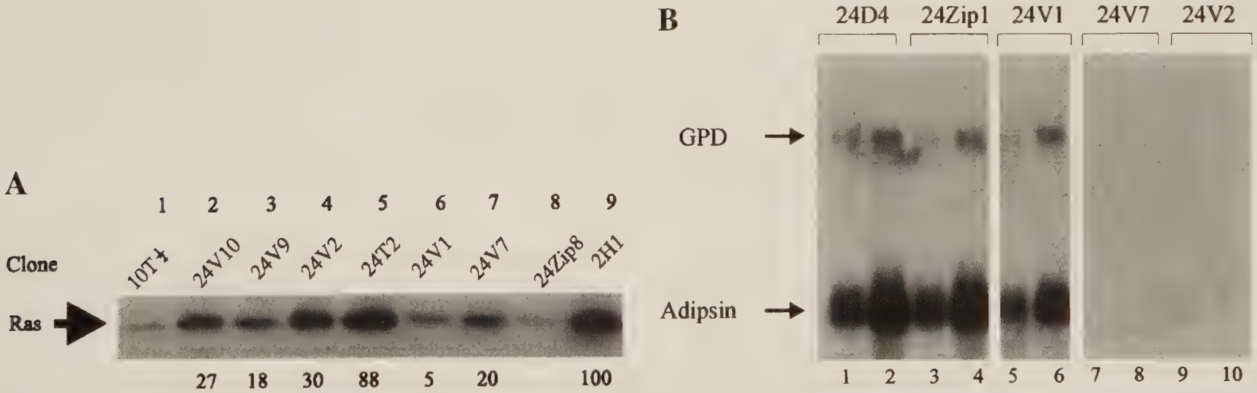

FIG. 4. *ras*^{leu61} blocks adipocytic differentiation of the Ras-deficient line 24D4. (A) Quantitation of Ras levels in a panel of 24D4 lines, constitutively expressing *ras*^{leu61}, by Western blotting analysis (see Materials and Methods). Arrow points to the position of the 21-kDa Ras protein. (24Zip8) 24D4 line, infected with the control pZipNEO retroviral vector lacking an insert. (2H1) *ras*-transformed 10T1/2 line, induced with 50 μM $ZnSO_4$. Numbers under the lanes refer to relative values obtained by Fluorimager scanning, with the value of the induced 2H1 line taken as 100%. (B) Examination of expression of the adipocyte-specific genes GPD and adipsin by Northern blotting analysis in a panel of representative *ras*^{leu61}-expressing 24D4 lines placed under differentiation-inducing conditions. Cells were grown in 10% FCS and RNA was extracted 10 days after confluence (see Materials and Methods). (Lanes 1, 3, 5, 7, and 9) No insulin added. (Lanes 2, 4, 6, 8, and 10) 10 μg/ml insulin added to the cultures at confluence. To ensure equal loading of all lanes, the blot was stripped and reprobed for β_2-microglobulin (not shown).

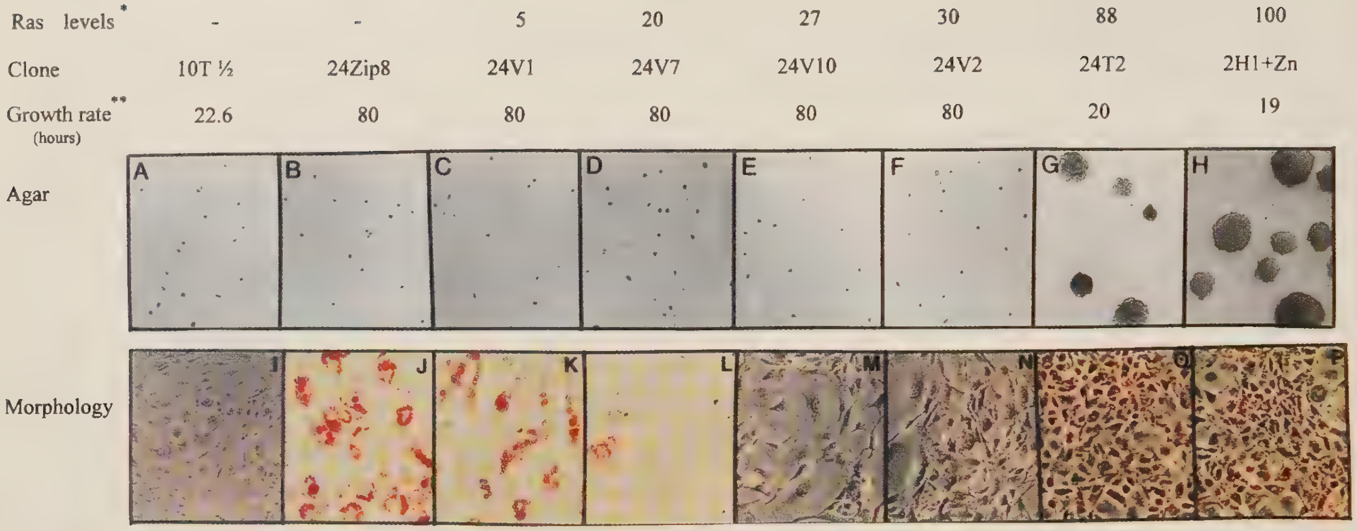

FIG. 5. Dependence of phenotypic expression upon *ras* levels in Ras-deficient preadipocytes. c-Ras-deficient 24D4 cells or their derivatives expressing different levels of ras^{leu61} were suspended in agar or placed under differentiation-inducing conditions. *Numbers represent Ras levels quantitated by Fluorimager scanning of a Western blot as in Fig. 3. The Ras levels of line 2H1 after induction with 50 μM $ZnSO_4$ were defined as 100%. **30,000 cells were seeded in 60-mm dishes and counted at several time points over 7 days. Doubling times are shown in hours. (A–H) Anchorage-independent growth assays. Cells were trypsinized and placed in agar [20]. Pictures were taken 3 weeks later. (I–P) Cellular morphology under differentiation-inducing conditions. At confluence cells were treated with 10 μg/ml insulin. Photographs were taken 10 days later after cell staining with oil red-O and hematoxylin (see Materials and Methods).

growth rate of the c-Ras-deficient cells to normal, blocked, rather than enhanced or accelerated, adipocytic differentiation, pointing to the possibility that the inability of Ras^{leu61} to induce differentiation can be uncoupled from its transforming effect.

v-raf Expression Mirrors the Ras Effects

The Raf oncogene product has been shown to be physically and functionally associated with v-*ras* [33–37]. Therefore, we investigated the possibility that Raf might have an effect upon transformation and differentiation similar to that produced by Ras. To that end, 1C3 and the Ras-deficient 24D4 cells were infected with the culture supernatant from the ψ2LN42k packaging line, which secretes a v-*raf*-expressing retroviral vector [22] in the same way as described with respect to ras^{leu61} above (see Materials and Methods). Individual colonies were picked, expanded into clones, and tested for levels of the 42-kDa *raf* gene product by Western blotting (see Materials and Methods). Consistent with the notion that Raf lies downstream of Ras, v-*raf* expression had an effect similar to that of ras^{leu61} in both 1C3 and 24D4 cells (Figs. 6A and 6B, respectively). Loss of differentiative capacity was the most sensitive indicator of the v-Raf effect, observed in infected cells in the absence of an overtly transformed morphology, increased growth rate, or ability to grow in soft agar (Figs. 6A and 6B). These data indicate that, in parallel with the Ras effect, $p42^{raf}$ blocks adipocytic differentiation at lower levels than required for full neoplastic transformation. As a control, the membrane-bound middle tumor antigen of polyoma virus (mT) was expressed in 1C3 and 24D4 cells [18]. As shown in Table 1, although mT could block the differentiation of 1C3 (Table 1, line 15), it could not block differentiation in the Ras-deficient 24D4 (Table 1, line 23), 25B8, or Rev3 cells (not shown). Therefore, it appears that in the pathway controlling the block of differentiation, Raf is downstream of Ras, while the membrane-bound mT is upstream thereof.

DISCUSSION

Previous results demonstrated a quantitative hierarchy in the manifestation of a number of transformation-related properties. Graded levels of expression of the middle tumor antigen of polyoma virus or v-*src* in murine fibroblasts revealed that morphological transformation, focus formation, and anchorage-independent proliferation require increasing amounts of oncogene product [20, 30]. The present study adds *ras* to that list of oncogenes. In addition, it incorporates differentiative capacity into the gamut of transformation-related parameters which can be regulated by graded levels of oncogene expression. The decrease in differentiative capacity was inversely related to the level of

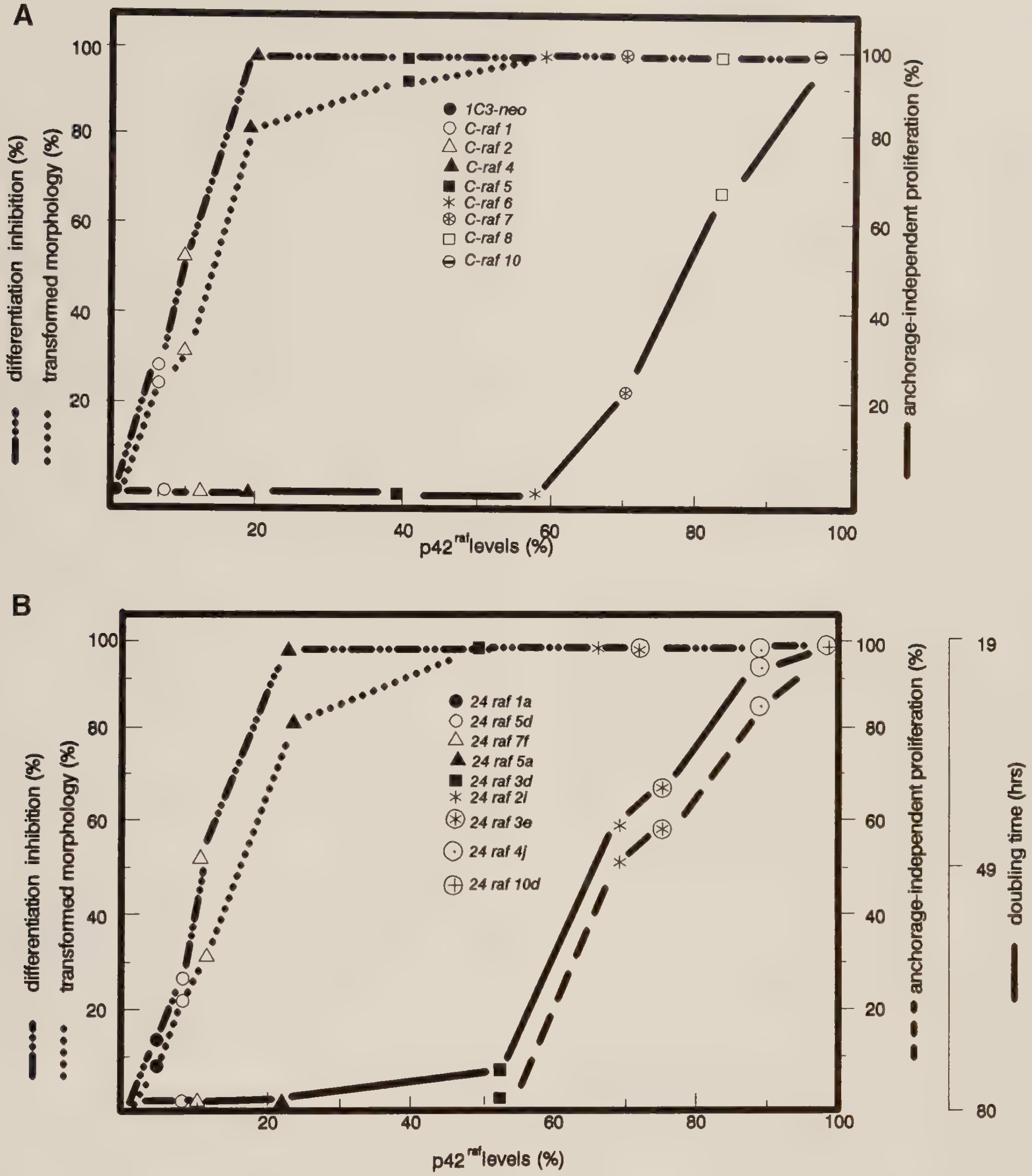

FIG. 6. Dependence of phenotypic expression upon activated p42^{raf} levels in a panel of v-*raf*-expressing (A) 1C3 or (B) 24D4 preadipocytes. p42^{raf} was expressed in 1C3 or 24D4 preadipocytes using a retroviral vector (see Materials and Methods). Individual colonies were picked and tested for p42^{raf} levels, and the phenotype of representative clones expressing different activated Raf levels was examined as indicated. p42^{raf} expression levels were quantitated by Western blotting using an anti-Raf polyclonal serum and Fluorimager scanning, as described under Materials and Methods. Numbers represent percentages of averages of three experiments, with the levels of the highest expressors (C-*raf*10 and 24*raf*10d) defined as 100%. To measure the ability to differentiate, 10 μg/ml insulin was added at confluence. Adipocytic differentiation was quantitated by densitometric scanning of Northern blots probed for the adipocyte-specific genes, aP2 and GPD (see Materials and Methods), with the values obtained for the parental 1C3 or 24D4 lines, respectively, designated as 100%. (The results are plotted as percentage of inhibition of differentiation, which is 0% for the parental lines). The points represent averages of three independent experiments. Transformed morphology was estimated by microscopic observation. Anchorage-independent proliferation was quantitated by suspending 50,000 cells in 2 ml of methocel containing 10 μCi/ml [^{3}H]thymidine as described under Materials and Methods. The incorporation of the highest expressors was designated as 100%. Growth rate on plastic was measured as in Fig. 4. Note that for both lines loss of differentiative capacity is the most sensitive indicator of the v-Raf-transforming effect, observed in infected cells in the absence of an overtly transformed morphology, increased growth rate, or ability to grow in soft agar. The symbols indicate individual clones with different p42^{raf} levels.

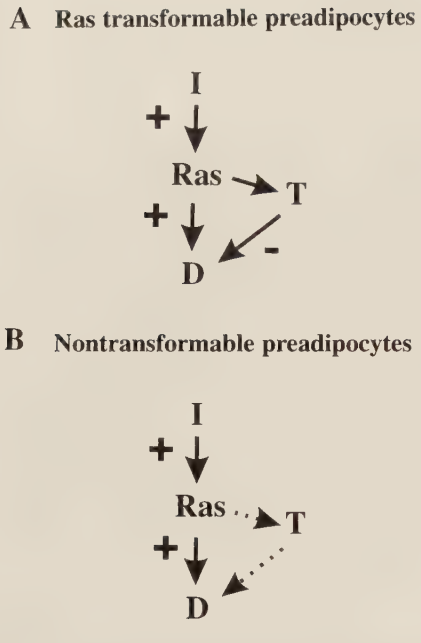
A Ras transformable preadipocytes
I
+
Ras
T
+
-
D
B Nontransformable preadipocytes
I
+
Ras
T
+
D

FIG. 7. Model depicting the functional integration of the insulin and Ras signals. v-Ras shares a common signaling pathway with c-Ras and insulin. In Ras-transformable preadipocytes (A), the pathway diverges at the c-Ras/v-Ras point, leading (directly or indirectly) to the activation of an additional set of genes (T), whose products promote cell proliferation and antagonize (−) the transcriptional upregulation of growth-arresting, differentiation-promoting genes (D). When expressed in nontransformable preadipocytes (B), the v-Ras signal is ineffective due to the lack of the appropriate substrates (dotted line). For simplicity, the model depicts both targets of the insulin and Ras pathways at the level of the promoter. However, it is equally possible that they could be cytoplasmic components of signal transduction pathways.

Ras, indicating that the amount of Ras is critical in determining its effect upon the differentiation process. Progressively higher Ras levels induced the morphological features of cellular transformation, increased the rate of cell proliferation, and conferred anchorage-independent proliferation. Furthermore, at below-baseline Ras levels, achieved in cells in which endogenous Ras was reduced through constitutive expression of an antisense *ras* message, low $\text{Ras}^{\text{leu61}}$ expression blocked adipocytic differentiation without restoring the growth rate of these cells to normal or inducing morphological transformation. These results demonstrate that, in Ras-transformable preadipocytes, the differentiative process is exquisitely sensitive to the activated *ras* gene, whose expression leads to a block of cell differentiation and acquisition of neoplastic transformation properties, in a dose-dependent manner.

Why activated Ras could not enhance differentiation by mimicking the insulin signal is unclear. One possibility is that v-Ras shares a common signaling pathway with c-Ras and insulin (Fig. 7). In cells which can be transformed by v-Ras, the pathway diverges at the c-Ras/v-Ras point, leading to the activation of an additional set of genes (T), whose products promote cell proliferation and antagonize the transcriptional upregulation of growth-arresting, differentiation-promoting genes (Fig. 7A). When expressed in nontransformable preadipocytes, on the other hand, the $\text{Ras}^{\text{leu61}}$ signal is unable to cause transformation due to lack of the appropriate substrates (Fig. 7B).

The identity of the nuclear targets of the differentiation-inhibiting v-Ras signals is not known. Previous reports showed that insulin stimulation of cycling fibroblasts is c-Ras dependent and triggers a proliferative signal which includes *myc* induction [38]. We postulate that v-Ras overexpression in preadipocytes forces the cells to continue cycling, precluding cell entry into the differentiation-permissive state of growth arrest. Furthermore, it was shown that myc expression in 3T3 L1 cells prohibits transcriptional upregulation of the transcription factor gene C/EBPα, known to play a key regulatory role in the induction of adipocytic differentiation and to deliver a potent growth-arresting signal in cycling preadipocytes [39, 40]. c-*myc* is postulated to contribute to the suppression of C/EBPα transcriptional upregulation by binding to its cognate site in the C/EBPα gene promoter [40, 41]. Given that c-*myc* is a downstream target of the Ras signal pathway, it is conceivable that v-Ras may, in part, block adipocytic differentiation through induction of negative control factors such as c-*myc,* thereby precluding expression of transcriptional activators of differentiation, such as C/EBPα.

The system of v-*ras* expression in the transformable 10T1/2-derived preadipocytic line on which the present study was based permits the investigation of the functional integration of a differentiative signal (provided by insulin) and a transforming signal (provided by $\text{Ras}^{\text{leu61}}$). Our data suggest that, in Ras-transformable preadipocytes, Ras blocks differentiation while inducing transformation.

The authors thank Dr. Van Cherington (ALG Co., Marlboro, MA) for many helpful discussions and Dr. Ken Wood and Dr. M. J. Corbley for generous gifts of the *raf* and *ras* retroviral vectors, respectively. The financial assistance of the Cancer Research Society, Inc., and the Natural Sciences and Engineering Research Council of Canada through grants to L.R. and T.H. is gratefully acknowledged.

REFERENCES

1. Filipak, M., Estervig, D. N., Tzen, C. Y., Minoo, P., Hoerl, B. J., Maerklein, P. B., Zschunke, M. A., Edens, M., and Scott, R. E. (1989) *Environ. Health Perspect.* **80,** 117.
2. Weir, M. L., and Scott, R. E. (1985) *Cancer Res.* **45,** 3339.
3. Sparks, R. L., Seibel-Ross, E. I., Weir, M. L., and Scott, R. E. (1986) *Cancer Res.* **46,** 5312.
4. Lowy, D. R., and Willumsen, B. M. (1993) *Annu. Rev. Biochem.* **62,** 851.

5. Burgering, B. M. T., Medema, R. H., Maassen, J. A., Van de Wetering, M. L., van der Eb, A. J., McCormick, F., and Bos, J. L. (1991) *EMBO J.* **10,** 1103.
6. Raptis, L., Marcellus, R., Corbley, M. J., Krook, A., Whitfield, J., Anderson, S. K., and Haliotis, T. (1991) *J. Virol.* **65,** 5203.
7. Mulcahy, L. S., Smith, M. R., and Stacey, D. W. (1985) *Nature* **313,** 241.
8. Smith, M. R., DeGudicibus, S. J., and Stacey, D. W. (1986) *Nature* **320,** 540.
9. Benito, M., Porras, A., Nebreda, A. R., and Santos, E. (1991) *Science* **253,** 565.
10. Noda, M., Ko, M., Ogura, A., Liu, D. G., Amano, T., Takano, T., and Ikawa, Y. (1985) *Nature* **318,** 73.
11. Shirouzu, M., Fujita-Yoshigaki, J., Ito, Y., Koide, H., Nishimura, S., and Yokoyama, S. (1992) *Oncogene* **7,** 475.
12. Ringold, G. M., Chapman, A. B., Knight, D. M., Navre, M., and Torti, F. M. (1988) *Recent. Prog. Horm. Res.* **44,** 115.
13. Medema, R. H., de Vries-Smits, A. M., van der Zon, G. C., Maassen, J. A., and Bos, J. L. (1993) *Mol. Cell. Biol.* **13,** 155.
14. Yonezawa, K., Ando, A., Kaburagi, Y., Yamamoto-Honda, R., Kitamura, T., Hara, K., Nakafuku, M., Okabayashi, Y., Kadowaki, T., and Kaziro, Y., *et al.* (1994) *J. Biol. Chem.* **269,** 4634.
15. Porras, A., Nebreda, A. R., Benito, M., and Santos, E. (1992) *J. Biol. Chem.* **267,** 21124.
16. Jhun, B. H., Meinkoth, J. L., Leitner, J. W., Draznin, B., and Olefsky, J. M. (1994) *J. Biol. Chem.* **269,** 5699.
17. Hirakawa, T., Maruyama, K., Kohl, N. E., Kodama, T., and Ruley, H. E. (1991) *Oncogene* **6,** 289.
18. Lu, Y., Raptis, L., Anderson, S., Corbley, M. J., Zhou, Y. C., Pross, H., and Haliotis, T. (1992) *Biochem. Cell Biol.* **70,** 1249.
19. Reznikoff, C. A., Brankow, D. W., and Heidelberger, C. (1973) *Cancer Res.* **33,** 3231.
20. Raptis, L., Lamfrom, H., and Benjamin, T. L. (1985) *Mol. Cell. Biol.* **5,** 2476.
21. Corbley, M. J., Feig, L. A., Cherington, V., Cooper, G. M., Lydon, N. B., and Roberts, T. M. (1994) *Biotechniques* **17,** 1102.
22. Wood, K. W., Qi, H., D'Arcangelo, G., Armstrong, R. C., Roberts, T. M., and Halegoua, S. (1993) *Proc. Natl. Acad. Sci. USA* **90,** 5016.
23. Chomczynski, P., and Sacchi, N. (1987) *Anal. Biochem.* **162,** 156.
24. Anderson, S. K., Stankova, J., and Roder, J. C. (1989) *Mol. Immunol.* **26,** 985.
25. Brownell, H. L., Firth, K. L., Kawauchi, K., Delovitch, T. L., and Raptis, L. (1997) *DNA Cell Biol.* **16,** 103.
26. Buday, L., and Downward, J. (1993) *Mol. Cell. Biol.* **13,** 1903.
27. Spiegelman, B. M., Frank, M., and Green, H. (1983) *J. Biol. Chem.* **258,** 10083.
28. Parnes, J. R., and Seidman, J. G. (1982) *Cell* **29,** 661.
29. Preston, T., Brownell, H. L., and Raptis, L. (1997) *Cancer Lett.* **115,** 165–171.
30. Jakobovits, E. B., Majors, J. E., and Varmus, H. E. (1984) *Cell* **38,** 757.
31. Trimble, W. S., Johnson, P. W., Hozumi, N., and Roder, J. C. (1986) *Nature* **321,** 782.
32. Pearse, A. G. E., (1968) Histochemistry, 3rd ed., p. 697, Little Brown, Boston.
33. Moodie, S. A., Willumsen, B. M., Weber, M. J., and Wolfman, A. (1993) *Science* **260,** 1658.
34. Vojtek, A. B., Hollenberg, S. M., and Cooper, J. A. (1993) *Cell* **74,** 205.
35. Zhang, X. F., Settleman, J., Kyriakis, J. M., Takeuchi-Suzuki, E., Elledge, S. J., Marshall, M. S., Bruder, J. T., Rapp, U. R., and Avruch, J. (1993) *Nature* **364,** 308.
36. Warne, P. H., Viciana, P. R., and Downward, J. (1993) *Nature* **364,** 352.
37. van Aelst, L., Barr, M., Marcus, S., Polverino, A., and Wigler, M. (1993) *Proc. Natl. Acad. Sci. USA* **90,** 6213.
38. Burgering, B. M., Snijders, A. J., Maassen, J. A., van der Eb, A. J., and Bos, J. L. (1989) *Mol. Cell. Biol.* **9,** 4312.
39. Cornelius, P., MacDougald, O. A., and Lane, M. D. (1994) *Annu. Rev. Nutr.* **14,** 99.
40. Christy, R. J., Yang, V. W., Ntambi, J. M., Geiman, D. E., Landschulz, W. H., Friedman, A. D., Nakabeppu, Y., Kelly, T. J., and Lane, M. D. (1989) *Genes Dev.* **3,** 1323.
41. Freytag, S. O. (1988) *Mol. Cell. Biol.* **8,** 1614.
42. Hu, M. C. T., and Davidson, N. (1990) *Mol. Cell. Biol.* **10,** 6141.

Received September 5, 1996
Revised version received March 20, 1997

EXPERIMENTAL CELL RESEARCH 235, 198–209 (1997)
ARTICLE NO. EX973669

Insulin-like Growth Factor-1 Receptor and Its Ligand Regulate the Reentry of Adult Ventricular Myocytes into the Cell Cycle

Krzysztof Reiss, Wei Cheng, Piotr Pierzchalski, Satish Kodali, Baosheng Li,
Shenglun Wang, Yu Liu, and Piero Anversa[1]

Department of Medicine and Division of Cardiology, New York Medical College, Valhalla, New York 10595

To determine whether insulin-like growth factor-1 (IGF-1) stimulation *in vitro* of ventricular myocytes isolated from infarcted hearts is characterized by the reentry of cells into the cell cycle, the expression and kinase activity of cyclins E, A, and B and DNA synthesis were evaluated 5 days after coronary artery occlusion and 24 and 48 h following the addition of IGF-1. Myocytes surviving an acute myocardial infarction were employed because of their increase in surface insulin-like growth factor-1 receptors (IGF-1R). Western blot analysis documented that IGF-1 resulted in an upregulation of cyclins D_1, E, A, and B in viable postinfarcted myocytes. Cyclin E- and A-associated histone H_1 kinase activity and cyclin D_1-associated retinoblastoma protein-associated kinase activity also increased, but cyclin B kinase activity was not enhanced by IGF-1. These changes in cyclins and kinase activities were characterized by a significant increase in the number of cells labeled by bromodeoxyuridine, from approximately $630/10^6$ to nearly $9{,}000/10^6$ myocytes. This latter value was reduced by more than 50% by antisense oligodeoxynucleotide to IGF-1R mRNA. However, IGF-1 stimulation did not induce nuclear mitotic division and cytokinesis. In conclusion, the growth-promoting effect of IGF-1 on adult myocytes is regulated by the density of IGF-1R, which conditions the activation of the replicatory machinery of the cells. The failure of IGF-1 to enhance cyclin B kinase activity may be responsible for a block in the cell cycle and the inability of myocytes to progress through the M phase and subsequently divide. © 1997 Academic Press

INTRODUCTION

During postnatal maturation, ventricular myocytes withdraw progressively from the cell cycle [1] and this phenomenon is characterized by a marked decrease in the expression of insulin-like growth factor-1 (IGF-1) and its receptor (IGF-1R) in the hypertrophying cells [2]. Conversely, conditions of overload in the adult heart are accompanied by myocardial hypertrophy and upregulation of the IGF-1–IGF-1R autocrine system [3]. Additionally, therapeutic interventions with IGF-1 and growth hormone enhance cardiac hypertrophy and ameliorate the mechanical performance of the failing heart [4–6]. Findings in the developing myocardium suggest that this effector pathway is implicated in myocyte proliferation [2], which is consistent with observations in transgenic animals overexpressing IGF-1 in myocytes [7]. However, the cellular growth adaptations associated with induced cardiac hypertrophy and the administration of IGF-1 in the adult pathologic heart remain to be defined. Overt cardiac failure following myocardial infarction results in the induction of late growth related genes, activation of cyclins and cyclin-dependent kinases (cdks), DNA replication, nuclear mitotic division, and possibly myocyte proliferation [8–10]. Importantly, these cellular responses are characterized by upregulation of IGF-1 and IGF-1R in the cells [8, 9], emphasizing the potential implication of IGF-1 in myocyte regeneration. However, difficulties exist in the interpretation of these *in vivo* results. In the failing postinfarcted heart, the enhanced expression of IGF-1 and IGF-1R and the reentry of cells into the cell cycle may not be causally related [9]. Moreover, increases in IGF-1 and/or IGF-1R in the cells after infarction may not be responsible for the expression of cyclins E, A, and B and their associated kinase activities [10]. In an attempt to address these issues, short-term primary cultures of adult ventricular myocytes isolated from sham-operated and infarcted rats were employed. This approach was utilized to test the effects of IGF-1 stimulation on the expression and associated kinase activity of cyclins D_1, E, A, and B, DNA synthesis, and mitotic division of myocytes. A 5-day time interval after infarction was selected because it is characterized *in vivo* by an increase in IGF-1R receptor protein on the cells, DNA synthesis, and mitosis [9]. The upregulation of IGF-1R was postulated to constitute the critical factor for IGF-1-induced myocyte growth.

MATERIALS AND METHODS

Animals. Experiments were carried out in male Sprague–Dawley rats at approximately 3 months of age (Charles River Breeding

---

[1] To whom correspondence and reprint requests should be addressed at New York Medical College, Department of Medicine, Vosburgh Pavilion-302, Valhalla, New York 10595. Fax: (914) 993-4406.

0014-4827/97 $25.00

Copyright © 1997 by Academic Press
All rights of reproduction in any form reserved.

Laboratories, North Wilmington, MA). Coronary artery occlusion was performed in 65 rats. Thirty-one animals in this group died during the period of experimentation. The remaining 34 rats were included in the study. Nine sham-operated animals served as controls. Sham operation carried no mortality. Animals were killed 5 days after surgery.

Myocardial infarction. Under ether anesthesia, by means of a procedure previously described (8–10), the thorax was opened, the heart was exteriorized, and the left main coronary artery was ligated 2 mm from its origin. The chest was closed, pneumothorax was reduced by negative pressure, and the animals were allowed to recover. Sham-operated animals were treated similarly except that the ligation was not tied.

Cardiac function. Just before killing, animals were anesthetized with chloral hydrate (300 mg/kg ip) and the right carotid artery was cannulated with a microtip pressure transducer catheter (Millar SPR-249, Houston, TX) connected to an electrostatic chart recorder (Gould ES 2000, Cleveland, OH). After monitoring arterial blood pressure, the catheter was advanced into the left ventricle for the evaluation of left ventricular pressures and + and − dP/d*t*. Subsequently, a second catheter (Millar SPR-595), with a 120° curved tip, was inserted in the right jugular vein and advanced through the superior vena cava and the right atrium into the right ventricular chamber for the measurements of central venous pressure, right ventricular pressures, and dP/d*t* [8–10].

Cell culture. At the end of the hemodynamic determinations, hearts were rapidly excised and myocytes from the left ventricle were enzymatically dissociated [8–10]. Rectangular, trypan blue-excluding cells constituted nearly 80% of all myocytes. The average numbers of myocytes obtained from the left ventricles of sham-operated controls and infarcted rats were 5.5 and 3×10^6, respectively. The contribution of interstitial cells was assessed by counting 1000 cells in each left ventricle and then computing from these counts the respective fractions of myocytes and nonmyocytes encountered. Consistent with previous results [8–10], nonmyocytes accounted for 1% of the cell population.

Myocytes were plated in petri dishes (Corning, Corning, NY) coated with 0.5 μg/cm^2 of laminin (Sigma Chemical Co., St. Louis, MO), at a density of 2×10^4 cells/cm^2. Cells were incubated in serum-free medium (SFM), consisting of Eagle's minimal essential medium (EMEM) with nonessential amino acids (Sigma), supplemented with penicillin (100 U/ml), streptomycin (50 μg/ml), transferrin (10 μg/ml), and bovine serum albumin (0.1%). Cultures were incubated at 37°C in an atmosphere containing 5% CO_2. SFM was changed 30 min after plating to remove myocytes that did not attach to the dish (Fig. 1).

Cross-linking assay. Myocytes from sham-operated and infarcted rats were cultured in SFM for 48 and 96 h before a cross-linking assay was performed. The assay was done according to the methodology previously described [12, 13]. Cells were washed twice with 5 ml of phosphate-buffered saline (PBS) and incubated in 5 ml of SFM for 1 h at 37°C. After a change of medium, one sample was pretreated with 100 ng/ml of cold (nonradioactive) IGF-1 for 5 min at 37°C and then all samples were incubated with ^{125}I-labeled IGF-1 (2×10^6 cpm/ml) for 3 h at 4°C. Subsequently, samples were washed once with 5 ml of PBS and incubated with 0.2 *M* disuccinimidyl subarate (DSS) for 15 min at room temperature. DSS solution was aspirated and 9 ml of 0.005 *M* tris(hydroxymethyl)aminomethane (Tris)–HCl, pH 7.4, was added to stop the cross-linking reaction. After 5 min of incubation, myocytes were lysed with 190 μl of lysis buffer (0.1 *M* Tris–HCl, 15% glycerol, 2 m*M* EDTA, 2% sodium dodecyl sulfate (SDS), 2% mercaptoethanol, and 0.075% bromphenol blue), and boiled for 2 min, and proteins were separated on 10% acrylamide gels. The gels were dried after electrophoresis and exposed to X-ray film to visualize radioactive bands. The 135-kDa band corresponding to the IGF-1R α subunit was quantitated with an image analysis system (Jandel Scientific, Corte Madera, CA).

Bromodeoxyuridine (BrdU) labeling. To evaluate the effects of IGF-1 on DNA replication, cells were stimulated with various concentrations of IGF-1 varying from 10 to 200 ng/ml (Genzyme Corp., Cambridge, MA) for 48 h in the presence of 10 μ*M* BrdU (Boehringer Mannheim Biochemicals, Indianapolis, IN). Cells were fixed in 94.5% ethanol, 5% acetic acid, and 0.5% NP-40 (Sigma). The incorporation of BrdU was detected by immunofluorescence [9], using a BrdU Detection Kit (Boehringer Mannheim). Primary (mouse monoclonal BMC 9318) and secondary (sheep anti-mouse IgG, FITC labeled) antibodies were applied at a dilution of 1:10. Myocytes were also stained with monoclonal antibody for α-sarcomeric actin (Sigma, clone 5C5) to label the cell cytoplasm. Cultures were incubated at 37°C with the primary antibody diluted 1:10 in PBS and subsequently with the anti-mouse IgG tetramethylrhodamine isothiocynate (TRITC)-labeled antibody diluted 1:20 in PBS. The concentrations of the antibodies used have minimized cross-reactivity between TRITC-labeled anti-mouse IgG in the second reaction and anti-BrdU antibody. Finally, Vectashield (Vector Laboratories, Burlingame, CA) mounting medium was applied and the BrdU labeling index determined using an Olympus microscope working in epifluoresence mode (×500). This microscope was equipped with a set of excitation–emission filters for fluorescein (excitation blue, emission green) and rhodamine (excitation green, emission red). In randomly selected fields, myocytes were identified first by the red staining of α-sarcomeric actin, and then excitation–emission filters were changed to visualize BrdU-labeled nuclei (green staining). Ten thousand myocytes were counted in each preparation to determine the BrdU labeling index.

Antisense oligonucleotides. To analyze the effects of inhibition of IGF-1R translation on DNA synthesis, cultures of myocytes grown in the presence of 100 ng/ml IGF-1 were treated with antisense oligonucleotides (5 μ*M*) to IGF-1R mRNA, and this treatment was repeated 24 h later. Control cultures were left intact or were treated with mismatched oligonucleotides. In addition, a cross-linking assay was performed to document whether antisense affected the level of IGF-1R protein on myocytes. These studies were done following the methodology described above.

The sequences of phosphorothioate antisense (antisense 1) and mismatched (mismatched 1) oligonucleotides to IGF-1R mRNA (GenBank: M27293) were as follows: IGF-1R antisense, position 156–175 bp, 5′GATAGTCGTTGCGGATGTCA3′; IGF-1R mismatched, $5'\mathrm{GA\overset{*}{C}AG\overset{*}{A}CTT\overset{*}{C}\overset{*}{A}\overset{*}{G}G\overset{*}{A}\overset{*}{T}TGTC\overset{*}{T}3'}$, with asterisks indicating the positions of mismatched nucleotides.

A second phosphorothioate antisense (antisense 2) and mismatched (mismatched 2) oligonucleotides to IGF-1R mRNA were employed. The sequences were as follows: IGF-1R antisense, position 169–188 bp, 5′CGCTTCAGCTGCTGATAGTC3′; IGF-1R mismatched, $5'\mathrm{C\overset{*}{T}CT\overset{*}{A}CA\overset{*}{T}\overset{*}{G}\overset{*}{A}\overset{*}{T}\overset{*}{A}T\overset{*}{A}ATA\overset{*}{T}\overset{*}{C}\overset{*}{G}3'}$, with asterisks indicating the positions of mismatched nucleotides.

BrdU (10 μ*M*) was added to the medium at the time of treatment of cultures with antisense oligonucleotides to IGF-1R mRNA and mismatched oligonucleotides. Twenty-four hours later, cells were fixed and stained. BrdU labeling and α-sarcomeric actin staining were performed following the protocol described in the preceding section. The percentage of BrdU-positive myocytes was obtained by counting 10,000 cells per preparation. An equal number of cultures left intact or treated with the same concentration of mismatched oligonucleotides were counted as well.

Western blot. Total proteins were extracted from actively proliferating human B lymphoid cell line LG_2 cells [14] and from myocytes isolated from infarcted rats. Myocytes were suspended on ice in 200 μl of lysis buffer [50 m*M* Tris–HCl, pH 7.4; 5 m*M* ethylenediaminetetraacetic acid (EDTA), pH 8.0; 250 m*M* NaCl; 50 m*M* NaF; 0.1 m*M* Na_3VO_4; 0.1% Triton X-100; 1 m*M* phenylmethylsulfonyl fluoride (PMSF); 10 μg/ml leupeptin], incubated on ice for 30 min, and spun down at 16,000 rpm for 15 min. Protein concentration was measured by the method of Lowry *et al.* [15], and samples containing 50 μg of

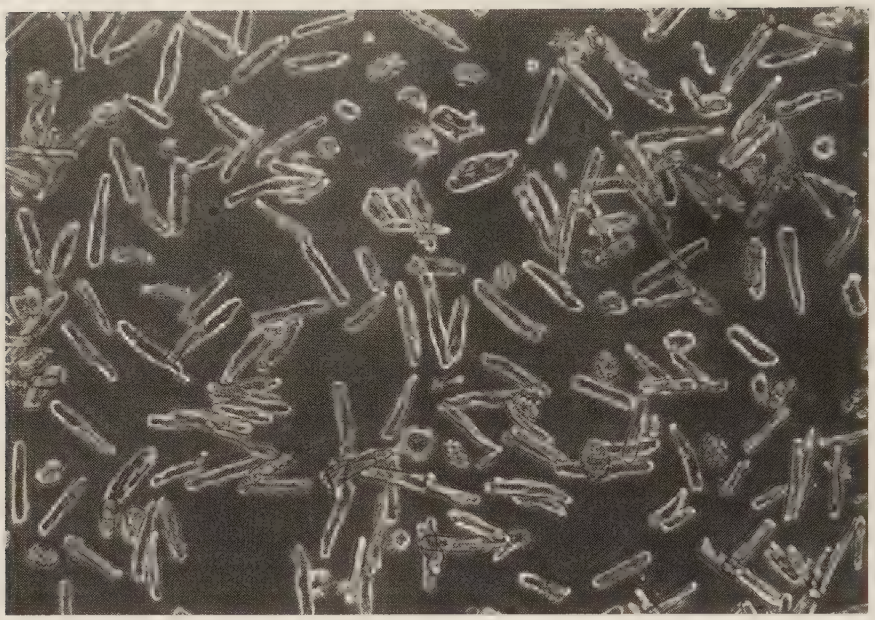

FIG. 1. Cultures of adult left ventricular myocytes isolated from an infarcted heart 5 days after coronary artery occlusion. Cells were kept for 24 h in SFM. Phase-contrast microscopy ×120.

total proteins were mixed with loading buffer [20% glycerol; 3% sodium dodecyl sulfate (SDS); 3% dithiothreitol (DTT); 10 m*M* EDTA; 0.05% bromophenol blue], boiled for 5 min, and loaded on 10% SDS–polyacrylamide gels. Proteins were electroblotted onto Trans-Blot nitrocellulose membranes (Bio-Rad, Hercules, CA), blocked with 5% powered milk in TBST (0.01 *M* Tris–HCl; 0.15 *M* NaCl; 0.5% Tween 20) for 1 h at room temperature, and incubated with the primary antibodies: rabbit anti-human cyclin A and rabbit anti-human cyclin B [16, 17] diluted 1:500 in TBST and also with rabbit anti-human cyclin D_1 and rabbit anti-rat cyclin E antibody (Santa Cruz Biotechnology, Santa Cruz, CA) diluted 1:1000 in TBST. Blots were subsequently washed in TBST and incubated with goat anti-rabbit horseradish peroxidase-conjugated antibody (Amersham, Arlington Heights, IL) diluted 1:15,000 in TBST. Bound antibodies were detected with ECL detection reagents (Amersham) and quantitated with an image analysis system. In control reactions, nonimmune rabbit serum was used instead of primary antibody. In all experiments control reactions were negative.

Kinase activity assay. Prior to immunoprecipitation of cyclin–cdk complexes, 300 μg of myocyte proteins was precleaned with 1 μg of rabbit IgG and 20 μl of protein G–Sepharose (Pierce, Rockford, IL) for 1 h at 4°C. Samples were spun down and cyclin–cdk complexes immunoprecipitated with primary antibodies and 50 μl of protein G–Sepharose for 2 h at 4°C. The same primary antibodies used for Western blot (see above) were employed here. Following several washings with lysis buffer, protein G–Sepharose beads containing the immunocomplexes were incubated with 20 μl of kinase buffer (20 m*M* Hepes; 10 m*M* magnesium acetate; 20 μ*M* ATP; 1 m*M* DTT), 2 μg of histone H1 for cyclins A, B, and E or 1 μg of p56 substrate domain of retinoblastoma protein (pRb) for cyclin D_1, and 2 μl of (3000 Ci/m*M*) [γ-^{32}P]ATP (DuPont NEN, Boston, MA), for 30 min at 30°C. The reaction was terminated by adding 5 μl of loading buffer. Samples were boiled, spun down, and immediately loaded on 10% SDS–PAGE gels. To assess background kinase activity, the immunoprecipitation was performed in the presence of nonimmune rabbit serum and the background kinase activity was subtracted from all samples. This procedure was described previously [10, 18].

Data collection and analysis. Autoradiograms were analyzed densitometrically by an image analyzer (Jandel Scientific). All results are presented as means ± standard deviation. An identical approach was employed for functional data. Statistical significance for comparison among groups was determined using analysis of variance and the Bonferroni method [19]. Values of P less than 0.05 were considered significant. Because measurements presented were not obtained in all animals and, at times, animals were employed for more than one determination, n values for each parameter are listed in the text or in the legend to each figure. In all cases, n values correspond to number of animals or preparations.

RESULTS

Ventricular Hemodynamics

Measurements of heart weight, body weight, and left ventricular performance were found to be comparable to those previously reported in this animal model in recent publications from our laboratory [8–11, 13]. Briefly, myocardial infarction did not alter body weight, from 358 ± 35 g in controls to 346 ± 42 g in infarcted rats. Similarly, total heart weight remained essentially constant, 1480 ± 139 mg in sham-operated and 1549 ± 215 mg in coronary artery-occluded rats. Evaluations of ventricular function showed that myocardial infarction at 5 days was characterized by an increase in left ventricular end-diastolic pressure from 7.2 ± 4.5 to 26 ± 7.3 mm Hg ($P < 0.001$). In contrast, left ventricular peak systolic pressure decreased from 115 ± 12 to 87 ± 9 mm Hg ($P < 0.001$) and +dP/d*t* from 10,980 ± 1013 to 6980 ± 975 mm Hg/s ($P < 0.001$); −dP/d*t* also decreased from 8850 ± 945 to 6235 ± 735 mm Hg/s ($P < 0.001$). In addition, right ventricular peak systolic pressure increased from 25 ± 2 to 29 ± 3 mm Hg ($P < 0.001$) and central venous pressure from 1.5 ± 1.8 to 7.1

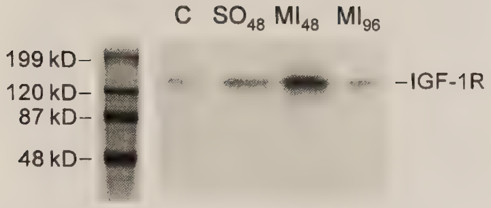

FIG. 2. ^{125}I-labeled IGF-1 cross-linked to left ventricular myocytes obtained from sham-operated (SO) and infarcted rats (MI) maintained in SFM for 48 h (SO_{48}; MI_{48}) and 96 (MI_{96}) h. Ligand binding was higher in myocytes from infarcted rats at 48 h (MI_{48}). C corresponds to myocytes pretreated with cold IGF-1. Molecular weight markers are shown on the left.

± 2.4 mm Hg ($P < 0.001$). To minimize the variability of infarct size in these experiments, only animals with marked increases in left ventricular end-diastolic pressure were utilized [8–11, 13]. In summary, myocardial infarction was characterized by left ventricular failure and right ventricular dysfunction.

IGF-1R and Ventricular Myocytes

To document whether myocardial infarction was associated with an increase in IGF-1R protein on myocytes which persisted in culture, a cross-linking assay was performed in cells isolated from sham-operated and infarcted rats kept in SFM for 48 h. An additional time point, 96 h, was examined in myocytes from infarcted ventricles. These time periods were preceded by a 30-min interval required for the cells to attach to the dish. Cross-linking of ^{125}I-labeled IGF-1 to myocytes showed that at 48 h more ligand was cross-linked to the 135-kDa α-subunit of the receptor following infarction (Fig. 2). In comparison with control myocytes (OD: 42 ± 6, $n = 3$), the relative quantity of IGF-1R protein increased 2.3-fold in cells from infarcted ventricles (OD: 98 ± 7, $n = 3$) and this difference was statistically significant ($P < 0.001$). In contrast, from 48 to 96 h, myocytes from infarcted hearts exhibited a 67% ($P < 0.001$) reduction in receptor protein, reaching a value lower (OD: 32 ± 8, $n = 3$) than that detected in cells from control animals. However, this latter difference was not statistically significant. In summary, the upregulation of IGF-1R on myocytes *in vivo* after infarction [9, 13] was maintained *in vitro* for 48 h, which constituted the endpoint of the experiments described below.

IGF-1 and BrdU Labeling of Ventricular Myocytes

Freshly isolated ventricular myocytes from noninfarcted and infarcted hearts were plated in SFM for 30 min to allow their attachment and were subsequently kept under these conditions or exposed to IGF-1 (100 ng/ml) for an additional 48 h. IGF-1 stimulation was associated with BrdU labeling of myocytes from both groups of rats. However, the number of positive cells was higher in the samples corresponding to infarcted animals (Fig. 3). Myocytes tended to change their rod-shaped configuration in culture with time. This is apparent in Figs. 3A and 3C, in which both cultures were treated with IGF-1. However, this phenomenon did not affect BrdU labeling. The more intense staining at the periphery of nuclei most likely reflected the distribution of chromatin within the nuclei. Quantitatively, the administration of IGF-1 to myocytes from infarcted hearts increased by 13-fold ($P < 0.001$) the number of cells stained by BrdU, from a baseline value of 635 ± 356/10^6 ($n = 4$) to 8586 ± 2871/10^6 ($n = 7$). A similar phenomenon was observed in myocytes from control ventricles, although in these cells IGF-1 increased BrdU labeling by only 3.8-fold ($P < 0.002$), from 223 ± 111/10^6 ($n = 3$) to 843 ± 76/10^6 ($n = 3$). As a consequence, a 10-fold ($P < 0.003$) difference in the magnitude of BrdU staining was measured between control and postinfarcted myocytes exposed to IGF-1. However, nuclear mitotic divisions and cytokinesis in myocytes were not detected following IGF-1 stimulation.

To document whether IGF-1 stimulation influenced BrdU labeling of myocytes after infarction in a dose-dependent manner, cells were treated with 0, 10, 50, 100, and 200 ng/ml for 48 h in SFM and the number of cells synthesizing DNA was measured (Fig. 4). BrdU labeling increased as a function of IGF-1 concentration up to 100 ng/ml. IGF-1 at 200 ng/ml did not increase further this parameter. In summary, IGF-1 stimulated the reentry of myocytes into the cell cycle in a dose-dependent manner and this response was greater after infarction.

Antisense to IGF-1R and DNA Replication

To determine whether the upregulation of IGF-1R on myocytes after infarction was the determining factor in IGF-1-induced DNA synthesis, myocytes from infarcted hearts were cultured in SFM for 30 min and subsequently were exposed to two different antisense oligodeoxynucleotides, AS1 and AS2, to rat IGF-1R mRNA for 48 h. Two distinct mismatched oligodeoxynucleotides, MM1 and MM2, were used as controls. At 1 day of treatment, 100 ng/ml IGF-1 was added in combination with BrdU. A reduction in IGF-1R protein was anticipated under these conditions, because new receptors were expected to be formed at early time points in culture. Moreover, the half-life of IGF-1R is approximately 16–20 h (personal communication, Dr. Renato Baserga) and new receptors could have been generated from the translation of previously transcribed mRNA.

In comparison with cells exposed to MM1, the level of BrdU labeling in myocytes treated with AS1 was

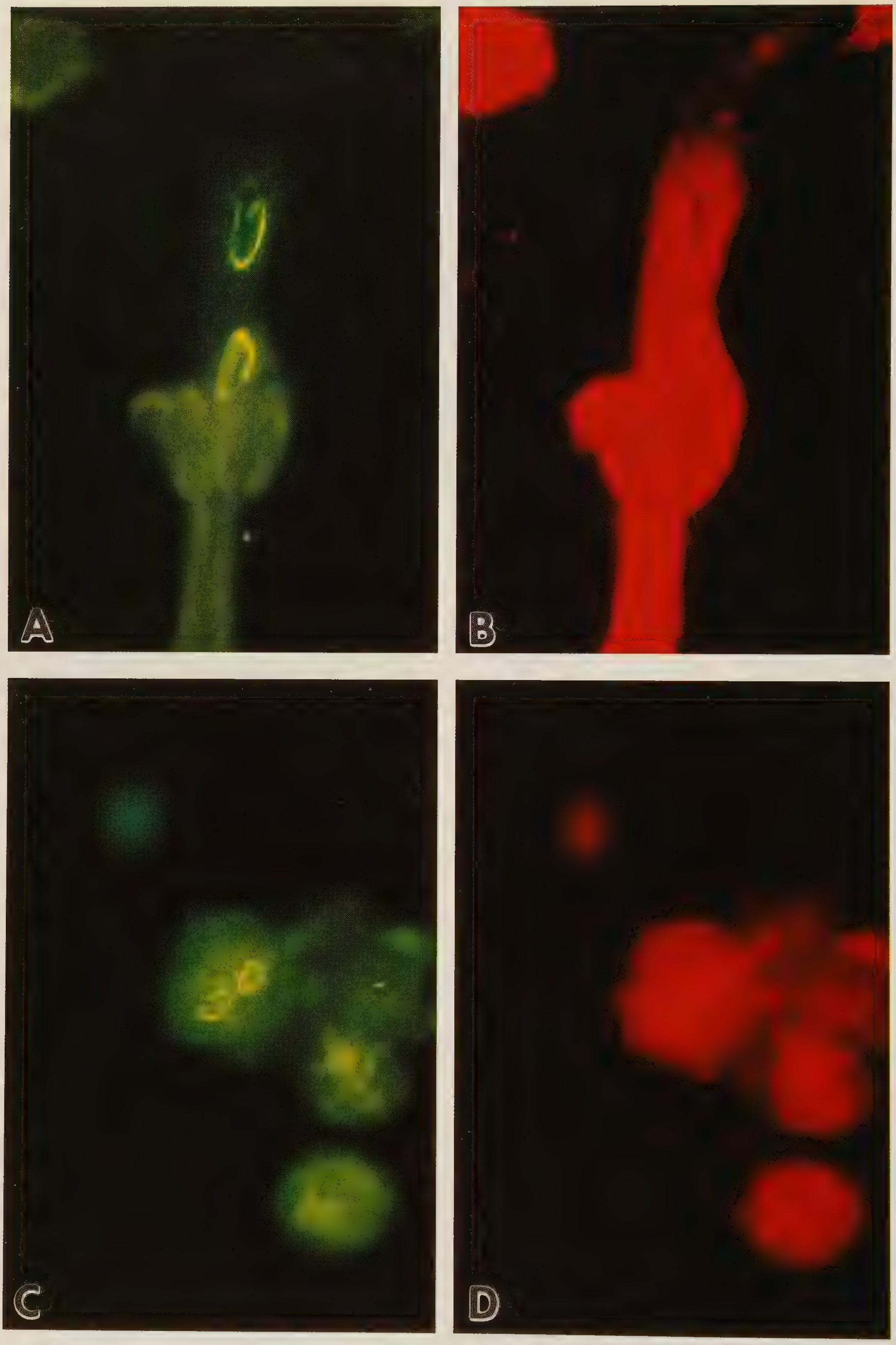

FIG. 3. BrdU labeling of left ventricular myocytes isolated for infarcted rats and stimulated *in vitro* with IGF-1 for 48 h (A and C). Myocytes were identified by α-sarcomeric actin antibody staining (B and D) ×450. The lack of cross-reactivity between anti-BrdU antibody and TRITC-labeled anti-mouse IgG is documented by the inability to detect profiles of BrdU-positive nuclei in B and D. Note the variability in myocyte shape which is commonly found in cultures of adult ventricular myocytes.

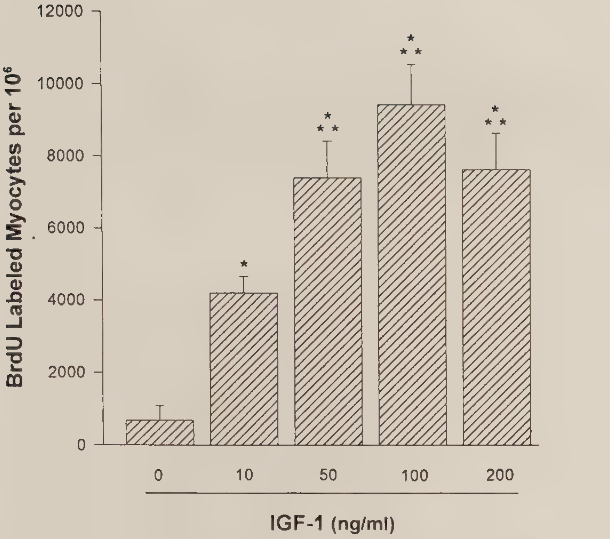

FIG. 4. Effects of various concentrations of IGF-1 on the number of BrdU-labeled myocytes obtained from infarcted rats and cultured for 48 h. Results are presented as means ± SD. *Significantly different from cells kept in SFM (0 ng/ml IGF-1), $P < 0.05$. **Significantly different from cells kept in 10 ng/ml IGF-1, $P < 0.05$. $n = 3$ at each IGF-1 concentration.

reduced by 69% ($P < 0.01$). The corresponding value for AS2 was 48% ($P < 0.03$). A 20% (NS) and 12% (NS) reduction in the BrdU labeling index was observed in the presence of MM1 and MM2, respectively (Fig. 5). The ability of the antisense procedure to reduce IGF-1R on myocytes after infarction was confirmed by cross-linking (Fig. 5, inset): AS1 (OD: AS1 = 47 ± 5, $n = 3$; MM1 = 76 ± 8, $n = 3$) and AS2 (OD: AS2 = 51 ± 5, $n = 3$; MM2 = 80 ± 10, $n = 3$) resulted in 38% ($P < 0.01$) and 36% ($P < 0.01$) reductions in binding of ^{125}I-labeled IGF-1 to the α-subunit of IGF-1R. Since control cells had an optical density value of 86 ± 6 ($n = 3$), minimal effects on this parameter were observed with MM1, −12% (NS), and MM2, −7% (NS). In summary, antisense oligodeoxynucleotides to IGF-1R mRNA decreased receptor protein, attenuating IGF-1-mediated DNA replication in myocytes.

IGF-1 and Expression of Cyclins D_1, E, A, and B

As indicated above, mitotic figures in myocytes collected from infarcted hearts were not detected in *in vitro* preparations. This observation was in contrast with results *in vivo* in which mitotic images were present in viable myocytes in the region adjacent to and remote from the infarcted myocardium [9]. Such apparent inconsistency raised the possibility that IGF-1 stimulation *in vitro* was not capable of upregulating cyclins and their histone H_1-associated kinase activity in a manner comparable to that demonstrated *in vivo* after myocardial infarction [10]. Thus, the effects of IGF-1 on cyclins involved in the G_1–S boundary, early and late S phases, and the G_2–M transition were determined in postinfarcted myocytes.

Figure 6A illustrates that cyclin D_1 levels, represented by two adjacent bands, were apparent in myocytes kept in SFM (OD: 25 ± 4, $n = 5$). IGF-1 administration did not change the expression of this cyclin at 12 h (OD: 23 ± 2, $n = 3$). However, 1.9-fold ($P < 0.02$) and 3.7-fold ($P < 0.001$) increases was found at 24 (OD: 47 ± 5, $n = 5$) and 48 (OD: 92 ± 27, $n = 5$) h following IGF-1 stimulation. At the later interval, the quantity of this protein was similar to that measured in freshly isolated myocytes from infarcted ventricles (OD: 71 ± 13, $n = 5$). Cyclin D_1-associated pRb kinase activity (Fig. 6B) increased 1.8-fold ($P < 0.001$) at 12 and 2.3-fold ($P < 0.001$) at 24 h after IGF-1 stimulation, returning to baseline value at 48 h. No difference in kinase activity was found between myocytes isolated from infarcted heart and cells maintained in SFM.

Figure 7A illustrates that low levels of cyclin E were detectable in myocytes cultured in SFM for 48 h (OD:

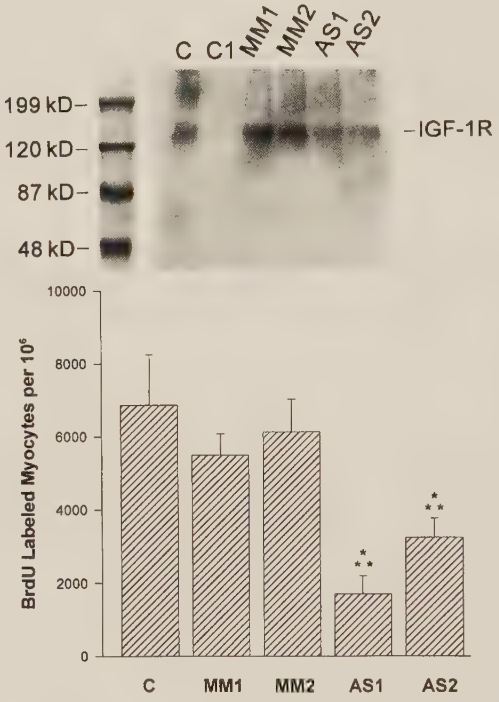

FIG. 5. Effects of antisense to IGF-1R mRNA on BrdU labeling of left ventricular myocytes obtained from infarcted heart and stimulated with IGF-1 in culture. Results are presented as means ± SD ($n = 3$). *Significantly different from untreated cells, $P < 0.05$. **Significantly different from the corresponding mismatched oligodeoxynucleotide, $P < 0.05$. C, untreated; MM1 and MM2, mismatched 1 and 2, respectively; AS1 and AS2, antisense 1 and 2, respectively. Inset: effects of antisense to IGF-1 mRNA on ^{125}I-labeled IGF-1 ligand binding (cross-linking assay). C, untreated cells, C1, mismatched-treated cells exposed to cold IGF-1. Antisense treatment markedly attenuated ^{125}I-labeled IGF-1 ligand binding.

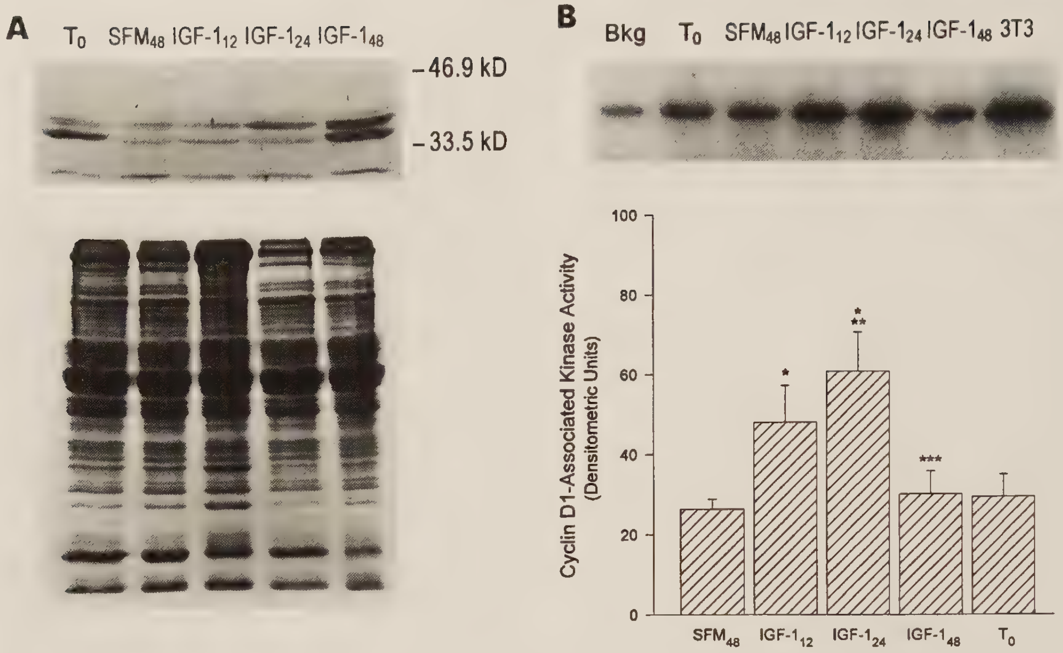

FIG. 6. (A) (Top) Detection of cyclin D_1 protein by Western blotting in left ventricular myocytes obtained from infarcted hearts and stimulated with IGF-1. T_0, freshly isolated myocytes; SFM_{48}, myocytes maintained in SFM for 48 h; IGF-1_{12}, myocytes stimulated with IGF-1 for 12 h; IGF-1_{24}, myocytes stimulated with IGF-1 for 24 h; IGF-1_{48}, myocytes stimulated with IGF-1 for 48 h. (Bottom) Loading of proteins is illustrated by Coomassie blue staining. (B) (Top) Detection of cyclin D-associated kinase activity measured by its ability to phosphorylate pRb. Background kinase activity (Bkg) was obtained following immunoprecipitation with nonimmune rabbit serum. (Bottom) Densitometric analysis of cyclin D_1-associated pRb kinase activity. Values were calculated by subtracting background kinase activity. Data are presented as means ± SD; $n = 3$ for all determinations. *Significantly different from SFM_{48}, $P < 0.05$. **Significantly different from IGF-1_{12}, $P < 0.05$. ***Significantly different from IGF-1_{24}, $P < 0.05$. For symbols see description of A.

$5 \pm 1, n = 3$). The addition of IGF-1 to myocytes, shortly after plating and for a period of 48 h, resulted in a 16-fold ($P < 0.001$) increase in this nuclear protein (OD: $80 \pm 10, n = 3$). Moreover, IGF-1 increased the quantity of cyclin E in myocytes by 45% ($P < 0.02$), from 24 (OD: $55 \pm 6, n = 3$) to 48 h. When myocytes treated with IGF-1 were compared with cells immediately after isolation (OD: 40 ± 4, $n = 3$), 38% (NS) and 100% ($P < 0.001$) increases in cyclin E were observed at 24 and 48 h, respectively. In contrast, myocytes in SFM had an 87% ($P < 0.002$) lower amount of this protein than freshly isolated cells from infarcted heart.

Cyclin E associated histone H_1 kinase activity was barely detectable in myocytes kept in SFM (Fig. 7B). IGF-1 increased this parameter 7-fold ($P < 0.02$) at 48 h. However, the value at 24 h was 2.5-fold ($P < 0.002$) higher than that at 48 h. This reflected a 60% reduction in cyclin E kinase activity from the earlier to the later time point after IGF-1 stimulation. In addition, IGF-1-induced cyclin E-associated histone H_1 kinase activity of myocytes *in vitro* at 24 and 48 h was 53% ($P < 0.001$) and 81% ($P < 0.001$) lower than that in freshly isolated myocytes. Cells maintained in SFM for 48 h had an enzyme activity which was only 2% ($P < 0.001$) of that found in myocytes shortly after collagenase digestion.

The effects of IGF-1 stimulation on the protein level of cyclin A in myocytes collected from infarcted ventricles are illustrated in Fig. 8A. In comparison with myocytes in SFM for 48 h (OD: 37 ± 6, $n = 3$), an identical period of IGF-1 exposure produced a 2-fold ($P < 0.006$) increase in this protein (OD: 74 ± 8, $n = 3$). A similar optical density value was observed following IGF-1 at 24 h (OD: 79 ± 10, $n = 3$), indicating that the longer time of stimulation did not further increase the amount of cyclin A in the cells. Although the quantity of cyclin A in postinfarcted myocytes immediately after isolation (OD: 96 ± 14, $n = 3$) was approximately 25% higher than that in myocytes cultured in the presence of IGF-1, such a difference was not statistically significant. In contrast, this nuclear protein decreased 61% ($P < 0.002$) in myocytes kept in SFM for 48 h.

Cyclin A-associated histone H_1 kinase activity in myocytes increased markedly with IGF-1 stimulation (Fig. 8B). In comparison with cells in SFM, 48 h of IGF-1 treatment resulted in an 11-fold ($P < 0.001$) increase in this parameter. From 24 to 48 h of IGF-1 administration, cyclin A kinase activity increased 5.6-fold and this time-dependent change was statistically significant ($P < 0.001$). Moreover, enzyme activity 48 h following IGF-1 exceeded by 3.5-fold ($P < 0.001$) that measured

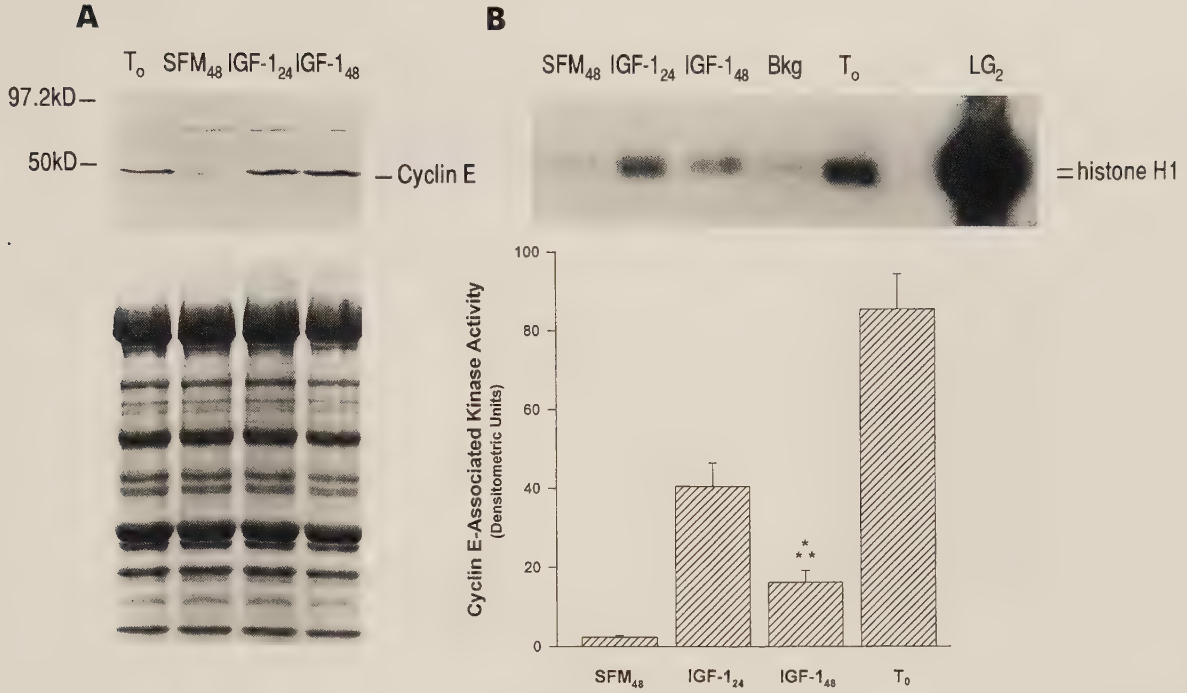

FIG. 7. (A) (Top) Detection of cyclin E protein by Western blotting in left ventricular myocytes obtained from infarcted hearts and stimulated with IGF-1. T$_0$, freshly isolated myocytes; SFM$_{48}$, myocytes maintained in SFM for 48 h; IGF-1$_{24}$, myocytes stimulated with IGF-1 for 24 h; IGF-1$_{48}$, myocytes stimulated with IGF-1 for 48 h. (Bottom) Loading of proteins is illustrated by Coomassie blue staining. (B) (Top) Detection of cyclin E-associated kinase activity measured by its ability to phosphorylate histone H1 protein. Background kinase activity (Bkg) was obtained following immunoprecipitation with nonimmune rabbit serum. (Bottom) Densitometric analysis of cyclin E-associated histone H1 kinase activity. Values were calculated by subtracting background kinase activity. Data are presented as means ± SD; $n = 3$ for all determinations. *Significantly different from SFM$_{48}$, $P < 0.05$. **Significantly different from IGF-1$_{24}$, $P < 0.05$. For symbols see description of A.

in freshly isolated myocytes. However, this latter cell population had an activity which was 3.2-fold ($P < 0.05$) higher than that in myocytes cultured in SFM.

Figure 9A illustrates that the low level of cyclin B in myocytes maintained in SFM (OD: 11 ± 2, $n = 3$) increased 7-fold ($P < 0.001$) 48 h after IGF-1 administration (OD: 81 ± 9, $n = 3$). The value at 24 h following IGF-1 (OD: 101 ± 12, $n = 3$) was not different from that measured at the later time point. With respect to freshly isolated myocytes (OD: 60 ± 7, $n = 3$), 24 h of IGF-1 stimulation resulted in a 68% ($P < 0.01$) higher amount of cyclin B, whereas cells in SFM showed a 72% ($P < 0.002$) reduction in this nuclear protein. In spite of the ability of IGF-1 to upregulate cyclin B content in myocytes, this growth factor had no impact on cyclin B-associated histone H$_1$ kinase activity (Fig. 9B). Values essentially comparable to those detected in cells in SFM were observed with IGF-1 stimulation. As a consequence, the three *in vitro* conditions showed marked reductions in this enzyme when compared with myocytes shortly after collagenase digestion. In summary, IGF-1 induced an upregulation in the quantity of cyclins E, A, and B and cyclin E- and A-associated kinase activities, but did not enhance cyclin B kinase activity in myocytes.

DISCUSSION

Findings in the present study indicate that IGF-1 stimulation *in vitro* of left ventricular myocytes surviving an acute myocardial infarct resulted in an upregulation of the quantity of cyclins D$_1$, E, A, and B in the cells. Cyclin D$_1$-, E-, and A-associated kinase activities were enhanced, but cyclin B kinase activity was not affected by IGF-1. These molecular reactions were accompanied by the reentry of cells into the cell cycle and DNA synthesis. Such adaptation was modulated by the number of IGF-1R on myocytes, which influenced the magnitude of this response. However, nuclear mitotic division and cytokinesis were not detected. Thus, the growth-promoting effect of IGF-1 on adult myocytes involves the activation of the replicatory machinery of these cells, which is conditioned by the density of surface IGF-1R. The inability of IGF-1 to induce mitosis may be related to the lack of diastolic and systolic loads on myocytes *in vitro* or to the possibility that G$_2$-M

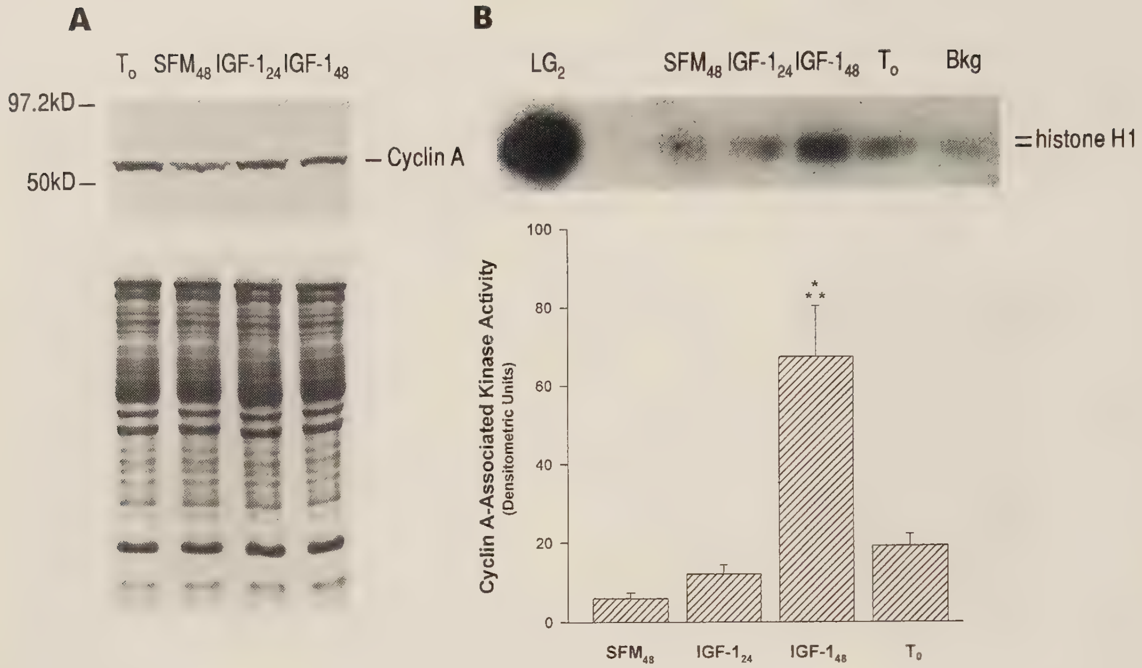

FIG. 8. (A) (Top) Detection of cyclin A protein by Western blotting in left ventricular myocytes obtained from infarcted hearts and stimulated with IGF-1. T_0, freshly isolated myocytes; SFM_{48}, myocytes maintained in SFM for 48 h; IGF-1_{24}, myocytes stimulated with IGF-1 for 24 h; IGF-1_{48}, myocytes stimulated with IGF-1 for 48 h. (Bottom) Loading of proteins is illustrated by Coomassie blue staining. (B) (Top) Detection of cyclin A-associated kinase activity measured by its ability to phosphorylate histone H1 protein. Background kinase activity (Bkg) was obtained following immunoprecipitation with nonimmune rabbit serum. (Bottom) Densitometric analysis of cyclin E-associated histone H1 kinase activity. Values were calculated by subtracting background kinase activity. Data are presented as means ± SD; $n = 3$ for all determinations. *Significantly different from SFM_{48}, $P < 0.05$. **Significantly different from IGF-1_{24}, $P < 0.05$. For symbols see description of A.

transition in this cell population is under the control of other growth factors.

IGF-1, IGF-1R, and DNA Synthesis in Myocytes

In vitro studies of neonatal rat myocytes have documented that IGF-1 stimulation results in DNA synthesis [20] and in the expression of myosin light chain 2, troponin, and skeletal α-actin [21, 22]. The ability of IGF-1 to induce DNA replication has not been shown in long-term cultures of adult rat cardiac myocytes [23], suggesting that this growth factor may be implicated in the activation of cellular hypertrophy. On the other hand, the addition of IGF-1 nearly doubles the percentage of BrdU-labeled adult rabbit ventricular myocytes in culture and this adaptation is associated with enhanced rates of protein accumulation [24]. Our observations in rat adult myocytes indicate that an upregulation of IGF-1R on these cells was required to achieve levels of BrdU labeling similar to those measured *in vivo* in the postinfarcted failing heart [9]. Control myocytes showed a minimal degree of DNA synthesis following IGF-1 administration, but this phenomenon was 10-fold greater in myocytes from infarcted ventricles, with a much higher density of IGF-1R. Since values in normal rabbit myocytes [24] are 26-fold and 3-fold higher than those in control and postinfarcted rat myocytes, respectively, the possibility may be advanced that IGF-1R number on myocytes varies in different species, influencing the impact of IGF-1 stimulation. The critical role of IGF-1R in cell proliferation has also been shown in various cell systems in *in vitro* preparations [25, 26].

Results in this and previous studies of adult cardiac myocytes in culture [23, 24] have not been able to document that IGF-1 or other growth factors can induce karyokinesis and cytokinesis. In contrast, overexpression of IGF-1 in the heart of transgenic mice postnatally is characterized by myocyte hyperplasia and cardiac hypertrophy in adult life [7]. Additionally, myocyte nuclear mitotic division and proliferation occur in the failing heart in humans [27] and in animal models [28]. These opposite observations suggest that significant differences exist between *in vitro* and *in vivo* experimentations that may account for the controversy on the potential ability of ventricular myocytes to reenter the cell cycle and regenerate in the overloaded pathologic heart. Importantly, DNA replication in myocytes and mitosis have been

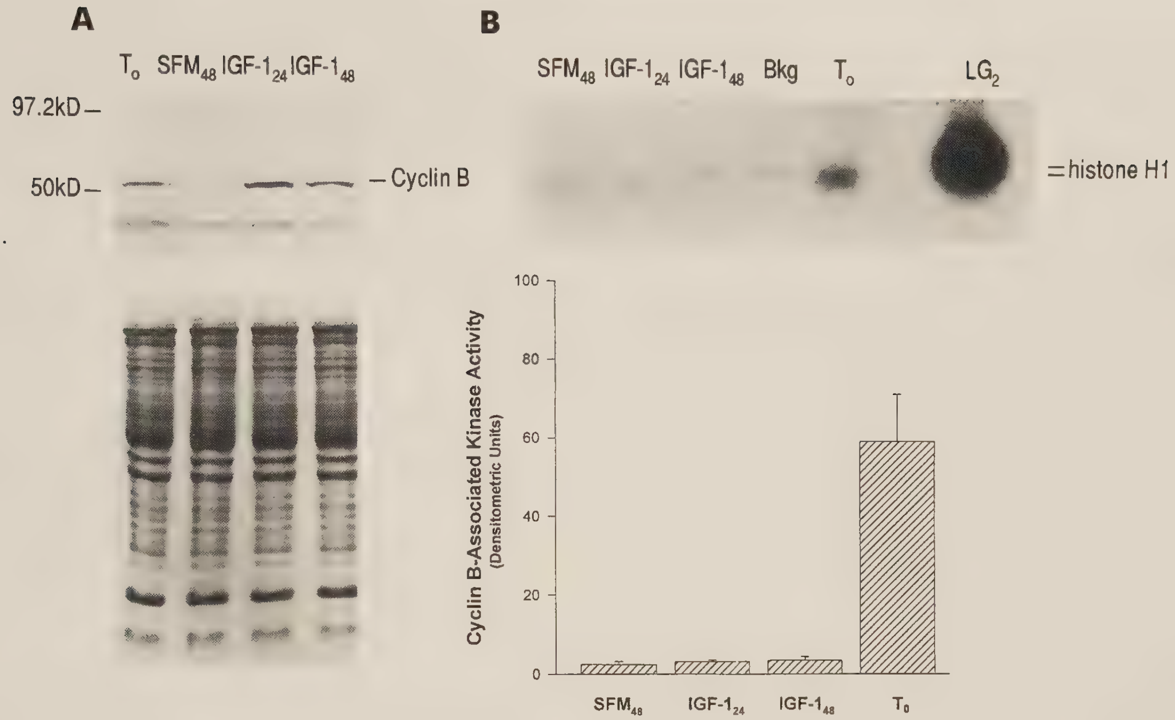

FIG. 9. (A) (Top) Detection of cyclin B protein by Western blotting in left ventricular myocytes obtained from infarcted hearts and stimulated with IGF-1. T_0, freshly isolated myocytes; SFM_{48}, myocytes maintained in SFM for 48 h; IGF-1_{24}, myocytes stimulated with IGF-1 for 24 h; IGF-1_{48}, myocytes stimulated with IGF-1 for 48 h. (Bottom) Loading of proteins is illustrated by Coomassie blue staining. (B) (Top) Detection of cyclin B-associated kinase activity measured by its ability to phosphorylate histone H1 protein. Background kinase activity (Bkg) was obtained following immunoprecipitation with nonimmune rabbit serum. (Bottom) Densitometric analysis of cyclin E-associated histone H1 kinase activity. Values were calculated by subtracting background kinase activity. Data are presented as means ± SD; $n = 3$ for all determinations. For symbols see description of A.

detected *in vivo* only in the presence of ventricular decompensation and failure [3]. Conversely, myocardial hypertrophy of various etiology in its compensated stage typically results in cellular enlargement, in the absence of the activation of the replicatory machinery of the stressed myocytes [3]. Although physical forces coupled with abnormal diastolic wall stress predominate in the failing heart [3], it is problematic to link this mechanical event to a molecular response capable of inducing nuclear and cellular division. However, passive stretch of the myocardium activates an early growth-related gene [29], the release of humoral factors [30], and myocyte hypertrophy [30] and triggers programmed myocyte cell death [31].

IGF-1 and Cyclins D_1, E, A, and B in Myocytes after Infarction

The cell cycle is regulated by the coordinated expression and activation of cyclins and cdks at the G_1–S transition, S phase, and the G_2–M progression [32–35]. In the current study, the detection of DNA replication following IGF-1 stimulation of myocytes surviving an acute myocardial infarct was consistent with the upregulation of cyclins D_1, E, and A in terms of protein quantity and associated kinase activity. Cyclin E, in combination with various forms of cyclin D, is involved at the G_1–S boundary, promoting the entry of cells into the S phase [32–35]. Cyclin A activates cdk2 concurrently with the onset of measurable DNA synthesis, playing a crucial role in the progression of cells through the S phase [32–35]. Although the duration of the cell cycle in myocytes remains to be determined, a time-dependent activation of these two cyclins was noted after the administration of IGF-1: cyclin E kinase activity peaked at 24 h, whereas cyclin A kinase activity was higher at 48 h, possibly reflecting their different functions in the cell cycle. However, the magnitude of DNA synthesis in myocyte nuclei was evaluated only at 48 h. Whether the onset of DNA replication occurred at 24 h following IGF-1 stimulation was not established.

Cyclins D_1, D_2, and D_3, as well as cyclin E, have been documented in myocardial samples of human and rat hearts [36]. However, the question remained whether these nuclear proteins were located in myocytes and/

or interstitial cells. Myocyte preparations from control and infarcted ventricles have demonstrated that cyclin E is detectable in normal cells and this protein is upregulated, shortly after coronary artery occlusion [10]. The observations here in freshly isolated myocytes, 5 days after infarction, confirmed these earlier results, indicating that key regulatory elements of G_1–S transition, cyclins D_1 and E, are present in adult myocytes. On the other hand, cyclin A was not identified by Northern and Western blot analyses of tissue specimens of rat myocardium at 14 days after birth [36]. These findings were considered to constitute the molecular basis for the terminally differentiated state of adult ventricular myocytes. Such a conclusion is not supported by the current *in vitro* data and by previous work *in vivo* following myocardial infarction [10]. Moreover, the disappearance of cyclin A was claimed in myocardial tissue in which fibroblasts and endothelial cells represent nearly 70% of the entire cell population and actively proliferate in the early postnatal period and throughout life [1].

The combination of cyclin B and cdc2 constitutes a mitosis-promoting factor (MPF) modulating G_2–M progression [37]. cdc2 is constitutively present in the cell, whereas cyclin B levels vary between mitosis and interphase [34, 37]. Although cyclin B and its associated histone H_1 kinase activity were high in myocytes isolated from infarcted hearts before plating, IGF-1 stimulation *in vitro* increased the amount of this nuclear protein in the cells, but had no effect on its kinase activity. Cyclin B has to accumulate above threshold for cells to enter the M phase [38], a condition most likely attained here in our *in vitro* preparations, since the quantity of this protein was comparable in myocytes immediately after collagenase digestion and *in vitro* at 24 and 48 h following IGF-1 stimulation. On this basis, the possibility may be raised that MPF has been formed and the lack of mitosis may be the consequence of a defect at the level of cdc25 which is responsible for dephosphorylation and activation of cyclin B-cdc2 kinase activity [37]. Since these events are part of the transition of cells through mitosis [37], IGF-1 appears to be capable only of initiating this process in adult cardiac myocytes in culture. This alteration may also be the consequence of the lack of activation by IGF-1 of Wee 1 kinase, which phosphorylates cdc2 kinase [37].

In summary, the current *in vitro* observations favor the possibility that the interaction of IGF-1 with its receptor leads to the reentry of myocytes into the cell cycle resulting in *de novo* DNA synthesis. However, mitosis is not reached. Several phenomena may be involved in this block of the cell cycle *in vitro*. Myocardial loading may be critical for the progression of myocytes through the M phase of the cell cycle. Mechanical forces are essentially abolished in cell culture and these physical parameters may be crucial in transmitting signals to the nucleus which may activate MPF promoting cell division. Alternatively, IGF-1 alone cannot reverse completely the condition of differentiation of myocytes and another growth factor may be implicated in the activation of regulatory complexes controlling the late stages of the cell cycle.

This work was supported by Grants HL-38132, HL-39902, HL-40561, and PO-1-43023 from the National Heart, Lung, and Blood Institute and by Grant-in-Aid 950321 from the American Heart Association. The expert technical assistance of Maria Feliciano is greatly appreciated.

REFERENCES

1. Rakusan, K. (1984) *in* Growth of the Heart in Health and Disease (R. Zak, Ed.), pp. 131–164, Raven Press, New York.
2. Cheng, W., Reiss, K., Kajstura, J., Kowal, K., Quaini, F., and Anversa, P. (1995) *Lab. Invest.* **72,** 646–655.
3. Anversa, P., Kajstura, J., Cheng, W., Reiss, K., Cigola, E., and Olivetti, G. (1996) *Cardiovasc. Res.* **32,** 484–495.
4. Duerr, R. L., Huang, S., Miraliakbar, H. R., Clark, R., Chien, K. R., and Joss, J., Jr. (1995) *J. Clin. Invest.* **95,** 619–627.
5. Fazio, S., Sabatini, D., Capaldo, B., Vigorito, C., Giordano, A., Guida, R., Pardo, F., Biondi, B., and Sacca, L. (1996) *N. Engl. J. Med.* **334,** 809–814.
6. Stromer, H., Cittadini, A., Douglas, P. A., and Morgan, J. P. (1996) *Circ. Res.* **79,** 227–236.
7. Reiss, K., Cheng, W., Ferber, A., Kajstura, J., Li, P., Li, B., Olivetti, G., Homcy, C. J., Baserga, R., and Anversa, P. (1996) *Proc. Natl. Acad. Sci. USA* **93,** 8630–8635.
8. Reiss, K., Meggs, L. G., Li, P., Olivetti, G., Capasso, J. M., and Anversa, P. (1993) *J. Cell Physiol.* **158,** 160–168.
9. Reiss, K., Kajstura, J., Zhang, X., Li, P., Szoke, E., Olivetti, G., and Anversa, P. (1994) *Exp. Cell Res.* **213,** 463–472.
10. Reiss, K., Cheng, W., Giordano, A., De Luca, A., Li, B., Kajstura, J., and Anversa, P. (1996) *Exp. Cell Res.* **225,** 44–54.
11. Li, P., Park, C., Micheletti, R., Li, B., Cheng, W., Sonnenblick, E. H., Anversa, P., and Bianchi, G. (1995) *Am. J. Physiol.* **268,** H1702–H1713.
12. Phillips, P. D., Pignolo, R. J., and Cristofalo, V. J. (1987) *J. Cell Physiol.* **133,** 135–143.
13. Cheng, W., Reiss, K., Li, P., Chun, M. J., Kajstura, J., Olivetti, G., and Anversa, P. (1996) *Circ. Res.* **78,** 536–546.
14. Gorga, J. C., Horejsi, V., Johnson, D. R., Raghupathy, R., and Strominger, J. L. (1987) *J. Biol. Chem.* **262,** 16087–16094.
15. Lowry, O. H., Rosenburgh, N. J., Farr, A. L., and Randall, R. J. (1951) *J. Biol. Chem.* **193,** 265–275.
16. Jaumot, M., Grana, X., Giordano, A., Reddy, P. V., Agell, N., and Bachs, O. (1994) *Biochem. Biophys. Res. Commun.* **203,** 1527–1534.
17. Wen, S. C., Ku, D. H., De Luca, A., Claudio, P. P., Giordano, A., and Calabretta, B. (1995) *Exp. Cell Res.* **217,** 8–14.
18. Giordano, A., Whyte, P., Harlow, E., Franza, B. R., Jr., Beach, D., and Draetta, G. (1989) *Cell* **58,** 981–990.
19. Wallenstein, S., Zucker, C. L., and Fleiss, J. L. (1980) *Circ. Res.* **47,** 1–9.
20. Kajstura, J., Cheng, W., Reiss, K., and Anversa, P. (1994) *Exp. Cell Res.* **215,** 273–283.
21. Simpson, P. C. (1989) *Annu. Rev. Physiol.* **51,** 189–202.

22. Parker, T. G., and Schneider, M. D. (1991) *Annu. Rev. Physiol.* **53,** 179–200.
23. Donath, M. Y., Zapf, J., Eppenberger-Eberhardt, M., Froesch, R., and Eppenberger, H. M. (1994) *Proc. Natl. Acad. Sci. USA* **91,** 1686–1690.
24. Decker, R. S., Cook, M. G., Behnke-Barclay, M., and Decker, M. L. (1995) *Circ. Res.* **77,** 544–555.
25. Baserga, R. (1995) *Cancer Res.* **55,** 249–252.
26. Baserga, R., and Rubin, R. (1993) *Crit. Rev. Eukar. Gene Express.* **3,** 47–61.
27. Quaini, F., Cigola, E., Lagrasta, C., Saccani, G., Quaini, E., Ross, C., Olivetti, G., and Anversa, P. (1994) *Circ. Res.* **75,** 1050–1063.
28. Kajstura, J., Zhang, X., Reiss, K., Szoke, E., Li, P., Lagrasta, C., Cheng, W., Darzynkiewicz, Z., Olivetti, G., and Anversa, P. (1994) *Circ. Res.* **74,** 383–400.
29. Sadoshima, J., Takahashi, T., Jahn, L., and Izumo, S. (1992) *Proc. Natl. Acad. Sci. USA* **89,** 9905–9909.
30. Sadoshima, J., Xu, Y., Slayter, H. S., and Izumo, S. (1983) *Cell* **75,** 977–984.
31. Cheng, W., Li, B., Kajstura, J., Li, P., Wolin, M. S., Sonnenblick, E. H., Hintze, T. H., Olivetti, G., and Anversa, P. (1995) *J. Clin. Invest.* **96,** 2247–2259.
32. Prem Veer Reddy, G. (1994) *J. Cell. Biochem.* **54,** 379–386.
33. Sherr, C. J. (1994) *Cell* **79,** 551–555.
34. Weinberg, R. A. (1995) *Cell* **81,** 323–330.
35. Koff, A., Giordano, A., Desai, D., Yamashita, K., Harper, J. W., Elledge, S., Nishimoto, T., Morgan, D. O., Franze, B. R., and Roberts, J. M. (1992) *Science* **257,** 1689–1694.
36. Yoshizumi, M., Lee, W-S., Hsieh, C-M., Tsai, J-C., Li, J., Perrella, M. A., Patterson, C., Endege, W. O., Schlegel, R., Lee, M-E. (1995) *J. Clin. Invest.* **95,** 2275–2280.
37. King, R. W., Jackson, P. K., and Kirschner, M. W. (1994) *Cell* **79,** 563–571.
38. Solomon, M. J., Glotzer, M., Lee, T. H., Philippe, M., and Kirschner, M. W. (1990) *Cell* **63,** 1013–1024.

Received December 30, 1996
Revised version received May 5, 1997

EXPERIMENTAL CELL RESEARCH **235**, 210–217 (1997)
ARTICLE NO. EX973667

Antiapoptotic Action of 1,25-Dihydroxyvitamin D_3 Is Associated with Increased Mitochondrial MCL-1 and RAF-1 Proteins and Reduced Release of Cytochrome c

Xuening Wang and George P. Studzinski[1]

Department of Pathology and Laboratory Medicine, UMDNJ–New Jersey Medical School,
185 South Orange Avenue, Newark, New Jersey 07103

Release of mitochondrial cytochrome c has been recently linked to the activation of the "executioner" phase of the cellular programs for death by apoptosis. This release is known to be negatively regulated by Bcl-2 and Bcl-X_L proteins. We show here that treatment of human leukemia cells HL60 with 1,25-dihydroxyvitamin D_3 (1,25D_3) results in progressive increases in the levels of cellular antiapoptotic protein Mcl-1, a transient increase in Al protein level, but no increases in Bcl-2 or Bcl-X_L proteins. The increase in Mcl-1 protein levels correlates with a reduced extent of apoptotic cell death induced by etoposide or the calcium ionophore A23187. The Mcl-1 protein is primarily localized in the mitochondria, and etoposide- or A23187-induced cytochrome c release is reduced in cells in which the mitochondria contain the Mcl-1 protein demonstrable by immunoblots. Raf-1 protein can also be detected in the mitochondrial fractions that contain Mcl-1 protein but not in the Mcl-1-negative fractions. These findings suggest that in these promyelocytic leukemia cells Mcl-1 has a function analogous to that of Bcl-2 in other cells, i.e., to target Raf-1 to mitochondria and to reduce cell damage-induced release of mitochondrial cytochrome c. Our findings provide a potential mechanism for the antiapoptotic action of 1,25D_3 and show that differentiation and apoptosis signaling pathways not only interact but involve a proliferation-associated gene, Raf-1. © 1997 Academic Press

INTRODUCTION

Programs for cell death, morphologically and biochemically recognizable as apoptosis, can be induced by drugs effective in the treatment of many types of neoplastic diseases [1, 2]. Improvements in cancer chemotherapy are therefore contingent on a better understanding of the cellular signaling pathways that result in apoptosis.

The Bcl-2 family of proteins consists of members with both survival-enhancing and proapoptotic activities. Bcl-2, the founding member of the group, is overexpressed in many human tumors and is considered to be an oncogene since by increasing the probability of cell survival it contributes to the uncontrolled cell proliferation which results in the formation of tumors and lymphomas [3–7]. The Bcl-2 gene encodes a 26-kDa protein which localizes to cellular membranes, most notably to the outer layer of the mitochondrial membrane [8–11]. The more recently described homologs of Bcl-2, Bcl-X_L, A1, and Mcl-1 are also known to have cell survival-enhancing actions [12–14], but their characteristics and subcellular distribution have been less well studied. In contrast, other members of the Bcl-2 family, such as Bax, Bad, and Bak, have apoptosis-enhancing effects by mechanisms that are still not fully understood [15–17]. One possibility is that the known protein–protein interactions, exemplified by the Bcl-2 and Bax heterodimer formation, provide a network of signals, the balance of which decides the cell fate—its survival or its death [18].

Recently, impressive evidence has been provided that at least one Bcl-2 function is to reduce the release of cytochrome c from the mitochondria [19–21]. The released cytochrome c, an oxidant, then appears to activate caspase-3 (CPP32), which in turn cleaves the 45-kDa subunit of the DNA fragmentation factor (DFF) to produce an active factor which triggers apoptotic DNA fragmentation [22]. The antiapoptotic action of Bcl-2 is aided by Raf-1 kinase, which is targeted to mitochondria by Bcl-2 and phosphorylates the proapoptotic Bad protein, thereby enhancing cell survival [23, 24]. It has not been established if other antiapoptotic proteins can function in a manner analogous to Bcl-2 and associate with Raf-1 to control the release of cytochrome c from the mitochondria.

This laboratory [25, 26] and others [e.g., 27, 28] demonstrated that exposure of leukemia cells to differentiating agents protects these cells from apoptosis induced by cancer chemotherapeutic drugs. Since tumors and hematopoietic malignancies often contain a proportion

---

[1] To whom correspondence and reprint requests should be addressed. Fax: (973) 972-7293.

0014-4827/97 $25.00

Copyright © 1997 by Academic Press
All rights of reproduction in any form reserved.

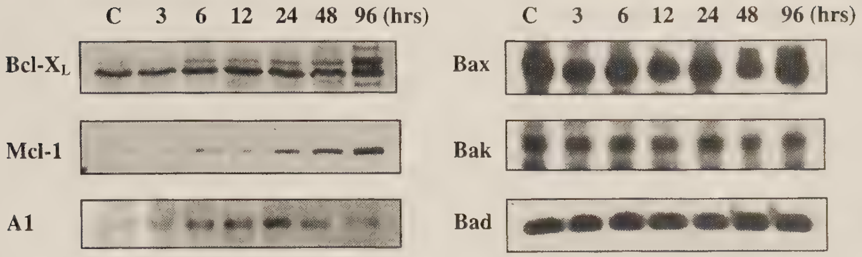

FIG. 1. Immunoblot analysis of the time course of 1,25D$_3$ effects on the expression of Bcl-2 gene family in HL60-G cells. The HL60-G cells were treated with 10^{-7} *M* 1,25D$_3$ for the indicated times.

of cells in varying stages of differentiation, and these cells may be more difficult to eradicate during chemotherapy and subsequently cause tumor recurrence, it is important to elucidate the basis for the differentiation-related resistance to apoptosis. In this study we utilized the well-characterized differentiation system of 1,25D$_3$-induced monocytic differentiation of HL60 cells [e.g., 29, 30] to determine if the protection from two apoptosis-inducing agents, etoposide and calcium ionophore A23187, elicited by pretreatment with 1,25D$_3$, involves the cytochrome c release–caspase 3 pathway to the execution of apoptosis. We found that as previously reported [26], Bcl-2 does not appear to participate in the 1,25D$_3$-mediated protection from apoptosis, but that Mcl-1 and Raf-1 proteins associate with mitochondria in parallel with the reduced cytochrome c release, caspase 3 activity, and the decreased DNA ladder formation.

MATERIALS AND METHODS

Reagents and antibodies. The 1,25D$_3$ was a kind gift from Dr. Uskokovic (Hoffmann–LaRoche, Nutley, NJ). Calcium ionophore A23187 and etoposide (VP16) were from Sigma (St. Louis, MO). Bcl-2 monoclonal antibody was obtained from Upstate Biotechnology, Inc. (Lake Placid, NY). Anti-Mcl-1, anti-Bad, and anti-CPP32 antibodies were obtained from Transduction Laboratories (Lexington, KY). Anti-Bcl-X$_L$, anti-A1, and anti-Bak antibodies were obtained from Santa Cruz Biotechnology, Inc. (Santa Cruz, CA). Anti-cytochrome c monoclonal antibody was obtained from PharMingen (San Diego, CA).

Tissue culture. HL60-G cells [31] were grown suspended at 37°C in a closed atmosphere in RPMI 1640 medium (Mediatech, Washington, DC) containing 10% heat-inactivated, defined, iron-supplemented bovine calf serum (Hyclone, Logan, UT) and 1% L-glutamine. Cell viability was determined by trypan blue exclusion. For experiments, the cells were suspended in fresh medium at 3×10^5 cells/ml and fed with fresh medium every 72 h.

Flow cytometry. The appearance of the differentiation surface markers CD14 and CD11b [32] was monitored by flow cytometry using mouse anti-human antibodies MY4-RD1 and Mol-FITC (Coulter Corporation, Miami, FL). Briefly, aliquots of 10^6 cells were washed with PBS and then incubated with MY4-RD1 and Mol-FITC antibodies at RT for 45 min according to the procedures recommended by the manufacturer. The cells were analyzed by two-param-

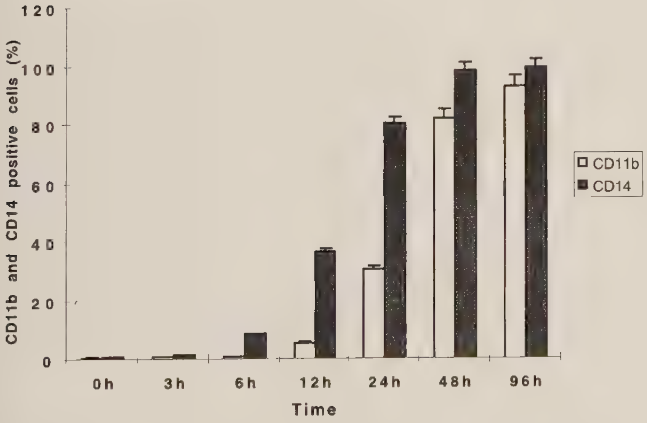

FIG. 2. The expression of two differentiation markers, CD11b and CD14, in HL60-G cells after treatment with 10^{-7} *M* 1,25D$_3$ for the indicated times. Mean values ± SD of three experiments are shown in the chart.

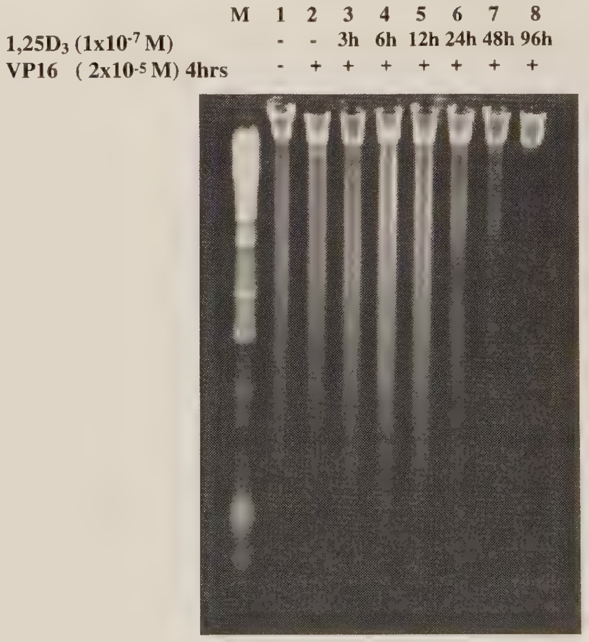
M 1 2 3 4 5 6 7 8
1,25D$_3$ (1x10^{-7} M) - - 3h 6h 12h 24h 48h 96h
VP16 (2x10^{-5} M) 4hrs - + + + + + + +

FIG. 3. The DNA fragmentation assay of apoptosis in HL60-G cells. The HL60-G cells were pretreated with 10^{-7} *M* 1,25D$_3$ for the indicated times and then treated with 20 μM etoposide (VP16) for 4 h, and the DNA ladders were demonstrated by gel electrophoresis.

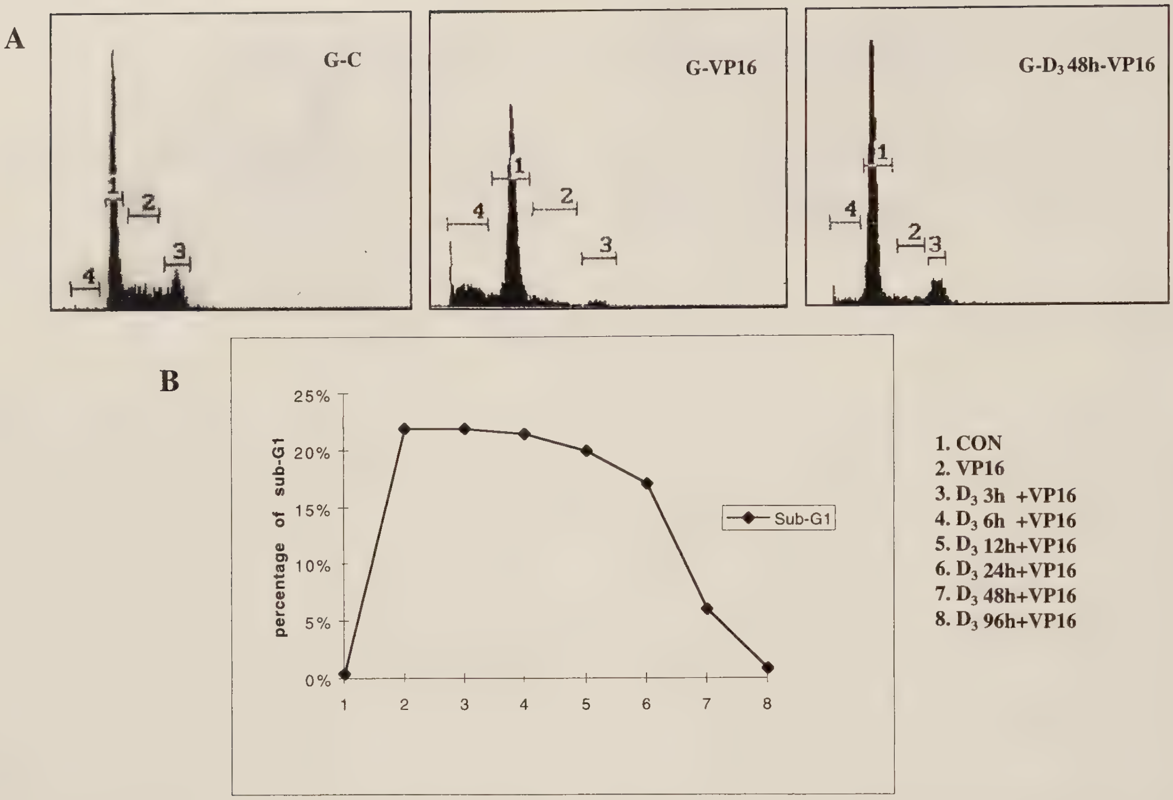

FIG. 4. Cell cycle distribution of HL60-G cells after exposure to 10^{-7} *M* $1{,}25D_3$ ± 2×10^{-6} *M* VP16 at the indicated times (A). The three frames are examples of cell cycle distribution of DNA content. The marker "1" in each frame shows the G1 phase DNA content, "2" shows S phase DNA content, "3" shows G2/M phase DNA content, and "4" shows sub-G1 phase DNA content. (B) The percentage of cells with sub-G1 DNA content after treatment with $1{,}25D_3$ ± VP16 for the indicated times.

eter flow cytometry using an Epic Profile II Cytometer (Coulter). Threshold settings for nonspecific fluorescence were obtained by using isotypic IgG2b. To determine the proportion of apoptotic cells the cells were stained with propidium iodide as previously described in detail [33], and cells with DNA content lower than G1 values were taken as the estimate of the apoptotic fraction. In these and subsequent studies, each experiment was repeated at least two times.

Cell fractionation. HL60-G cells were harvested by centrifugation at 1000*g* for 10 min at 4°C. The cell pellets were washed once with ice-cold PBS. Whole cell extracts were prepared by homogenizing frozen cell pellets with a hypotonic buffer (20 m*M* Tris–HCl, 0.2 *M* sucrose, 1 m*M* phenylmethylsulfonyl fluoride, 2 m*M* EDTA, 10 m*M* EGTA, 10 μg/ml leupeptin, and 2 μg/ml aprotinin). The protein concentrations were determined using a Bio-Rad (Hercules, CA) protein assay kit according to the instructions of the manufacturer. The mitochondrial and cytosol extracts were isolated by differential centrifugation [34]. To this end, cell pellets were resuspended with lysis buffer (20 m*M* Hepes–KCl, pH 7.5, 20 m*M* KCl, 1.5 m*M* $MgCl_2$, 1 m*M* EDTA, 1 m*M* EGTA, 1 m*M* DTT, 0.1 m*M* PMSF, and 0.25 *M* sucrose). The lysed pellets were centrifuged at 10,000*g* for 15 min at 4°C, and the resulting mitochondria-containing pellets were resuspended in lysis buffer and stored at −80°C. The supernatants of the 10,000*g* centrifugation were further centrifuged at 100,000*g* for 1 h at 4°C. The resulting supernatants were considered "cytosol" and were frozen at −80°C for further experiments.

Western blotting. Forty micrograms of protein samples was separated on 10% SDS–PAGE gel and transferred to nitrocellulose membranes (Amersham, Arlington Heights, IL). Ponceau S staining was applied to verify that an equal amount of protein was present in each lane. The membranes were blocked with 5% milk in TBS/0.01% Tween 20 for 1 h and subsequently blotted with primary antibodies and then the membranes were blotted with horseradish-linked secondary antibody for 1 h. The protein bands were visualized with a chemiluminescence assay system (Amersham). The optical density (OD) of each band was quantitated using an image quantitator (Molecular Dynamics, Sunnyvale, CA).

DNA fragmentation assay. Cells were analyzed by the gel electrophoresis method adapted from Eckhardt [35]. Agarose (2%) in TBE (Tris–boric acid–EDTA) buffer was poured into a minigel apparatus. After the gel solidified, the portion of the gel above the comb was removed and then this space was filled with 16 ml of 0.8% agarose–2% SDS in TBE to which 1.25 mg/ml proteinase K was added. Each pellet of 10^6 cells was suspended in 15 μl sample buffer (10 mg/ml RNase A, 15% Ficoll, 0.01% bromophenol blue) and the suspended pellets were loaded into the wells. DNA fragments were then separated at 20 V for 16 h. Following electrophoresis, the gel was rinsed with distilled water and incubated for 4 h at RT with gentle shaking in 100 ml of TE buffer (Tris–EDTA) with 2 mg of ribonuclease A. The gel was then stained for 30 min in 100 ml of water containing 50 μg ethidium bromide, destained in water for 3 h, and photographed in ultraviolet light.

RESULTS

Up-regulation of cellular Mcl-1 by $1{,}25D_3$. HL60 cells are protected from apoptosis by exposure to $1{,}25D_3$, but protein levels of bcl-2 are reduced, rather than increased, by $1{,}25D_3$ treatment [26]. We therefore explored the possibility that an up-regulation of another antiapoptotic member of the Bcl-2 family, or perhaps down-regulation of a proapoptotic protein, is responsible for this effect. Figure 1 shows that the only antiapoptotic protein studied here that exhibited a sustained increase in its abundance was Mcl-1, and the proapoptotic proteins examined showed no decreases. The protein levels of A1 also increased, but this increase was transient with a peak at about 24 h. An increase in Bcl-X_L levels was noted in some experiments but only after exposure to $1{,}25D_3$ for at least 96 h. In addition, a Bcl-X_L band with lower electrophoretic mobility increased in intensity at 6 h of $1{,}25D_3$ exposure, suggesting a higher phosphorylation state of this protein. When these changes were compared with the appearance of simultaneously determined markers of monocytic differentiation, CD11b and CD14 [32], only the increased levels of Mcl-1 protein were found to correspond to the expression of these markers (Fig. 2). Further, testing of the apoptosis-inducing effect of VP16, a topoisomerase II inhibitor that induces apoptosis in a variety of neoplastic cells [36, 37], showed that the appearance of $1{,}25D_3$-induced Mcl-1 protein occurred at the time that the VP16-induced DNA ladder formation (Fig. 3), and the presence of cells with sub-G1/G0 DNA content, was reduced (Fig. 4). There was no correlation between changes in the abundance of other members of the Bcl-2 family studied here and these indicators of apoptosis or with the appearance of differentiation markers.

$1{,}25D_3$ reduces the VP16-induced release of mitochondrial cytochrome c. Recent reports link the release of mitochondrial cytochrome c to drug-induced apoptosis [19–21]. We initiated the investigation of the effects of $1{,}25D_3$ on this phenomenon by subjecting HL60 cells to increasing concentrations of VP16; 4 h after addition of 5 μM VP16 a slight increase in cytoplasmic cytochrome c was noted, which became marked when 20 or 50 μM VP16 was added (Fig. 5). Pretreatment of the cells for 24 h with 10^{-7} M $1{,}25D_3$ reduced the cytoplasmic cytochrome c signal in cells treated with VP16 (Fig. 5). This paralleled the amount of activated form of 20-kDa CPP32 protein (caspase 3) in these cytoplasmic fractions, shown by the appearance of approximately 20-kDa bands with a concurrent reduction in the intensity of the 32-kDa band (Fig. 5). We concluded that pretreatment of the cells with $1{,}25D_3$ reduces the release from mitochondria of cytochrome c and the activation of caspase 3 by VP16.

When the effect of $1{,}25D_3$ pretreatment on the time course of cytochrome c release from the mitochondria was studied, the VP16-induced loss of cytochrome c from mitochondria was reduced by $1{,}25D_3$ (Fig. 6, top panel) as well as the extent of its appearance in the cytosol (Fig. 6, second panel). At the same time the Bcl-2 protein showed little change in the mitochondria, while Mcl-1 protein markedly increased in these organelles (Fig. 6, bottom two panels).

Prolongation of the exposure to $1{,}25D_3$ increases protection from apoptosis and the mitochondrial Mcl-1 protein levels. We compared the effects of longer exposure to $1{,}25D_3$ on the parameters of apoptosis and mitochondrial accumulation of the Bcl-2 family proteins. In these experiments apoptosis was induced also by the calcium ionophore A23187, to which HL60 cells are highly sensitive [26]. DNA ladder formation (Fig. 7, top panel) and the activation of CPP32 protease, shown again by its cleavage (Fig. 7, bottom panel), were markedly reduced by pretreatment of the cells with $1{,}25D_3$, though the protection from the calcium ionophore was more rapidly achieved than from the topoisomerase II inhibitor. Loss of cytochrome c from the mitochondria and its appearance in the cytoplasm again paralleled the extent of apoptosis (Fig. 8). Although there were no $1{,}25D_3$-induced changes in the levels of mitochondria-associated Bcl-2, or Bcl-X_L (data not shown), the levels of Mcl-1 protein were markedly increased by $1{,}25D_3$-pretreatment, but not by the toxic agents (Fig. 8). The Bad protein, which was approxi-

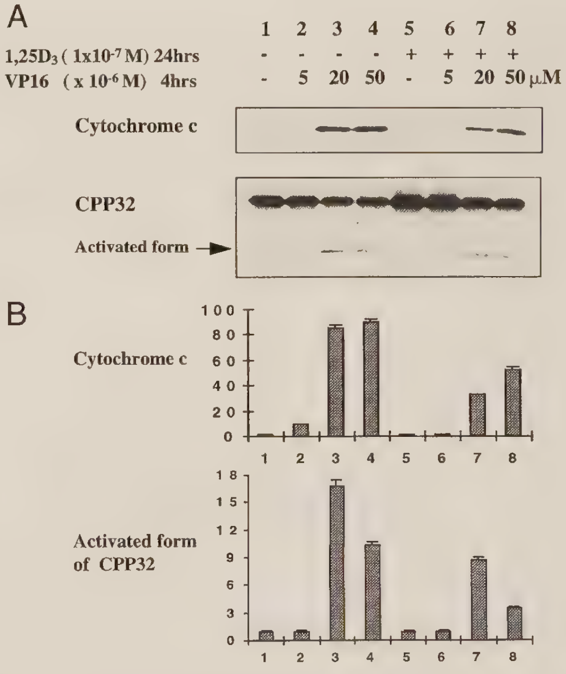

FIG. 5. The effect of $1{,}25D_3$ on the release of mitochondrial cytochrome c into the cytosol induced by VP16. (A) The top panel is an immunoblot analysis of the levels of cytochrome c protein in the cytosol; the bottom panel shows the levels of the CPP32 protein in the cytosol after membrane was stripped using stripping solution (62.5 μM Tris, pH 6.7, 100 mM β-mercaptoethanol, 2% SDS) and then reprobed with the CPP32 antibody. HL60-G cells were pretreated with 10^{-7} M $1{,}25D_3$ for 24 h and then treated with VP16 for 4 h at the indicated concentrations. (B) Quantitation of the optical density of experiments shown above. Means ± SD of two determinations are shown.

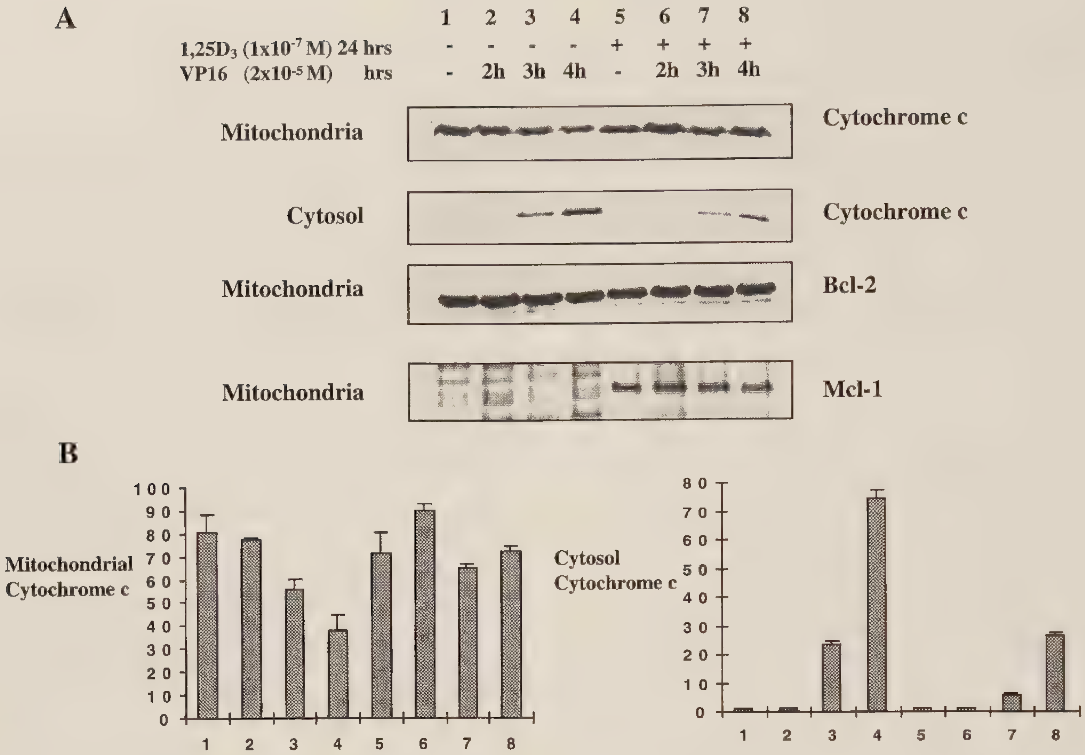

FIG. 6. Immunoblot analysis of the effect of 1,25D$_3$ pretreatment on the time course of cytochrome c release from the mitochondria to cytosol and on the levels of Bcl-2 and Mcl-1 in the mitochondria. The original membrane was stripped and successively reprobed with Bcl-2 and Mcl-1 antibodies. HL60-G cells were pretreated with 10^{-7} *M* 1,25D$_3$ for 24 h and then treated with 20 *μM* VP16 at the indicated times. Quantitation was performed as described under Materials and Methods and in the legend to Fig. 5.

mately equally distributed between the mitochondria and the cytosol, showed little change following treatment of the cells with these combinations of the compounds (Fig. 8, bottom panels). Consistent with their proposed mitochondrial membrane function, the Bcl-2, Mcl-1, and Bcl-X$_L$ proteins were found in only trace amounts in the cytoplasm (Fig. 8 and data not shown).

Exposure of HL60 cells to 1,25D$_3$ targets Raf-1 protein to the mitochondria. Raf-1 has been recently shown to enhance the antiapoptotic effect of Bcl-2 by phosphorylating the Bad protein at the mitochondrial membrane and thereby preventing Bad from neutralizing Bcl-2 activity [24]. We therefore determined the effect of the exposure of HL60 cells to 1,25D$_3$ on the cellular Raf-1 levels. In a preliminary experiment total cellular levels of Raf-1 were found to increase following treatment with 1,25D$_3$ (Fig. 9A). When the mitochondrial and cytosol fractions were examined, no Raf-1 protein was detected in the mitochondria from cells not treated with 1,25D$_3$, but became detectable following 1,25D$_3$ exposure (Fig. 9B). The cytosol also showed an increase in Raf-1 protein following treatment of the cells with 1,25D$_3$.

DISCUSSION

The relationship between differentiation and cell death is an intriguing one. Physiologically, differentiation is usually followed by apoptosis, and DNA strand breaks have even been detected during the early stages of differentiation [38, 39]. In culture, addition of differentiation inducers to cells damaged by cytotoxic drugs increases cell death [25, 28], and this has been suggested as a novel strategy to improve the effectiveness of cancer chemotherapy [2]. However, when cultured leukemia cells are induced to differentiate before the addition of an apoptosis-promoting agent, cell death is markedly reduced [25–28]. It is therefore necessary to elucidate the mechanisms responsible for these effects in order to better manipulate the cell fate by pharmacological agents.

Mcl-1 protein has both structural [14] and functional [40, 41] homology to the survival-enhancing Bcl-2 protein, but the presence of these proteins has in general a reciprocal distribution in different tissues: Mcl-1 is more common in differentiating tissues, while Bcl-2 is more abundant in proliferating tissues [42]. Mcl-1 is also transiently expressed in primitive myeloid leukemia cells ML-1 induced to differentiate with TPA [14] and delays apoptosis in c-*myc*-overexpressing Chinese hamster ovary cells [40]. Thus, Mcl-1 has credentials as a survival-enhancing agent and a differentiation-related protein, and this fits well with the finding reported here that its abundance increases in primitive, myeloid stem cell-like HL60 cells induced to monocytic differen-

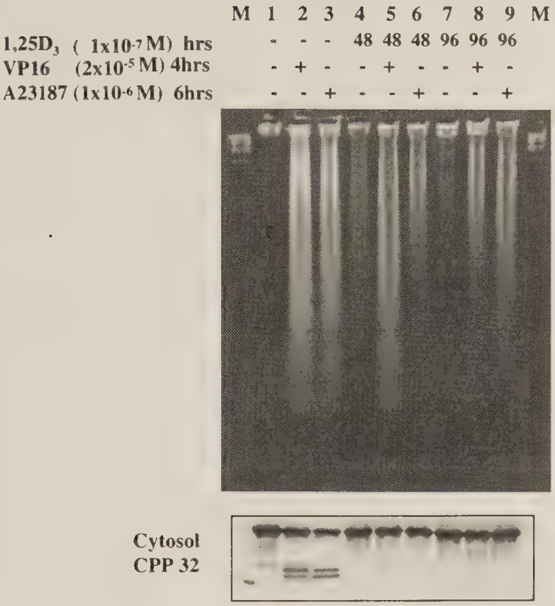
M 1 2 3 4 5 6 7 8 9 M
$1,25D_3$ ($1x10^{-7}$M) hrs - - - 48 48 48 96 96 96
VP16 ($2x10^{-5}$M) 4hrs - + - - + - - + -
A23187 ($1x10^{-6}$M) 6hrs - - + - - + - - +
Cytosol
CPP 32

FIG. 7. The protective effect of $1,25D_3$ on apoptosis of HL60-G cells induced by VP16 or A23187. The top panel shows the DNA ladders of HL60-G cells, after the cells were pretreated with $1,25D_3$ for 48 or 96 h and then exposed to either 20 μM VP16 for 4 h or 10 μM A23187 for 6 h. The DNA ladders were demonstrated by gel electrophoresis. The bottom panel is an immunoblot which shows the cytosol CPP32 protease in its inactive 32-kDa form and the active lower molecular weight forms. M, molecular weight protein markers.

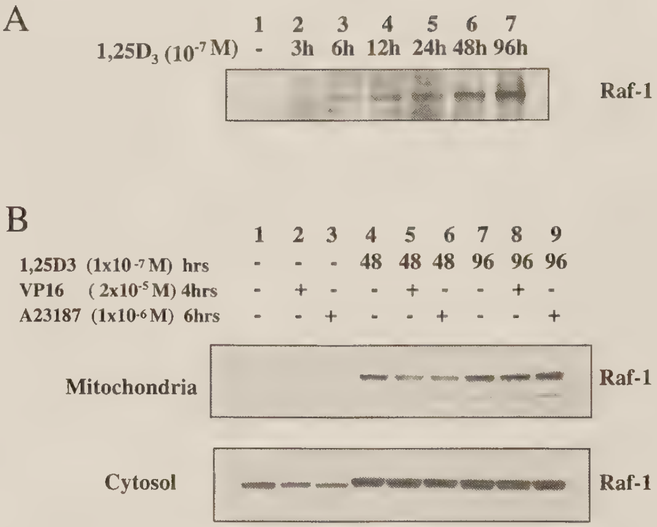
A
1 2 3 4 5 6 7
$1,25D_3$ (10^{-7}M) - 3h 6h 12h 24h 48h 96h
Raf-1
B
1 2 3 4 5 6 7 8 9
1,25D3 ($1x10^{-7}$M) hrs - - - 48 48 48 96 96 96
VP16 ($2x10^{-5}$M) 4hrs - + - - + - - + -
A23187 ($1x10^{-6}$M) 6hrs - - + - - + - - +
Mitochondria
Raf-1
Cytosol
Raf-1

FIG. 9. The effect of $1,25D_3$ on the levels of Raf-1 protein. (A) Immunoblot analysis of the time course of the increase of Raf-1 protein in whole cell extracts after treatment of the cells with 10^{-7} M $1,25D_3$ for the indicated times. (B) The Raf-1 protein level in the mitochondrial and cytosol fractions. HL60-G cells were either untreated or pretreated with 10^{-7} M $1,25D_3$ for 48 or 96 h, as indicated, and then treated with either 20 μM VP16 for 4 h or 10 μM A23187 for 6 h.

tiation by the secosteroid hormone $1,25D_3$. As in other cell types, the increase in Mcl-1 was not accompanied by increased levels of Bcl-2 protein. The steady-state cellular levels of several other members of the Bcl-2 family that were studied here showed no correlation with differentiation or with protection from apoptosis.

The subcellular localization of Mcl-1 protein has, to our knowledge, not been previously studied biochemically. Our finding of Mcl-1 in the mitochondrial fractions is consistent with its granular cytoplasmic immu-

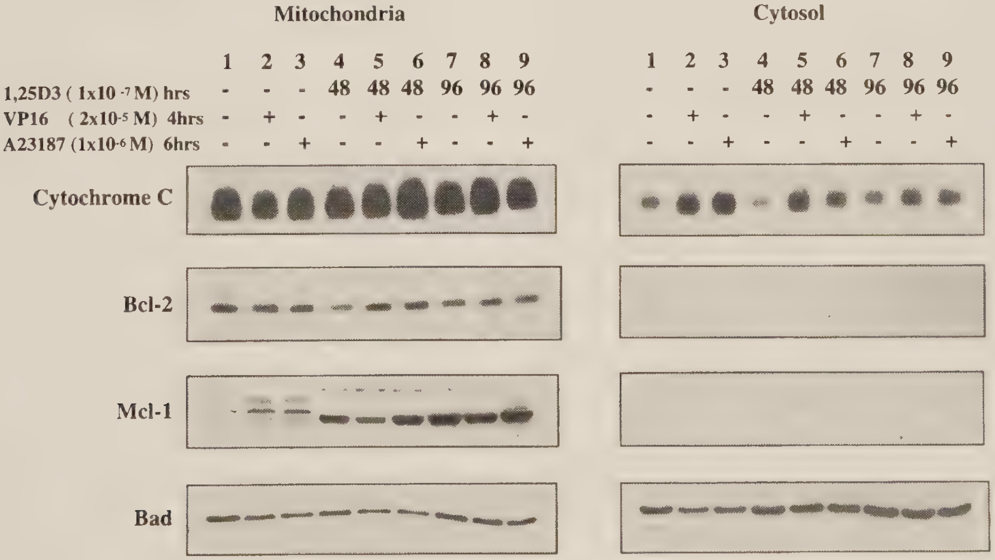
Mitochondria
1 2 3 4 5 6 7 8 9
1,25D3 ($1x10^{-7}$M) hrs - - - 48 48 48 96 96 96
VP16 ($2x10^{-5}$M) 4hrs - + - - + - - + -
A23187 ($1x10^{-6}$M) 6hrs - - + - - + - - +
Cytosol
1 2 3 4 5 6 7 8 9
- - - 48 48 48 96 96 96
- + - - + - - + -
- - + - - + - - +
Cytochrome C
Bcl-2
Mcl-1
Bad

FIG. 8. Immunoblot analysis of the levels of cytochrome c, Bcl-2, Mcl-1, and Bad proteins in the mitochondria and the cytosol. The original membranes were stripped and reprobed successively with Bcl-2, Mcl-1, and Bad antibody. The HL60-G cells were either untreated or pretreated with 10^{-7} M $1,25D_3$ for 48 or 96 h and then treated with either 20 μM VP16 for 4 h or with 10^{-7} M A23187 for 6 h, as indicated in the figure.

nostaining pattern in diverse human cell types [42] and with the notion that it functions as an alternate for Bcl-2 in mitochondrial permeability transitions. A further parallel between Bcl-2 and Mcl-1 is provided by finding Raf-1 in the mitochondrial fractions of $1,25D_3$-treated cells, which also show enhanced Mcl-1 levels but a reduced cytochrome c content. Since Raf-1 has recently been shown to be targeted to mitochondria by Bcl-2 [24], this suggests that in differentiating HL60 cells recruitment of Raf-1 to the mitochondrial membrane may increase Mcl-1-mediated resistance to apoptosis. This could occur by phosphorylation by Raf-1 of a protein which participates in the complexes that limit the release of cytochrome c from the mitochondria to the cytoplasm.

Indeed, phosphorylation of the Bad protein by Raf-1 has been demonstrated *in vitro,* though other substrates resident or recruited to the mitochondrial membrane have also been considered as targets for Raf-1 [24]. Since Raf-1 plays a major role in the activation of MAP kinase pathways initiated by growth factor receptors [43], there is an interesting connection in the HL60-$1,25D_3$ system between the pathways that ordinarily signal proliferation [43; this report] and those that signal a reversible G1 block [44] as well as survival [26; this report].

In our experiments the extent of protection from apoptosis by $1,25D_3$ pretreatment was slightly different when VP16 or A23187 was used to trigger apoptosis. This suggests that factors other than Mcl-1 and Raf-1 are involved in the increased survival of cell pretreated with $1,25D_3$. In addition to cytochrome c release from mitochondria, an apoptosis-inducing factor (AIF) derived from mitochondria [45] and a DNA fragmentation factor (DFF) that functions downstream from caspase 3/CPP32 [22] have also been described, and these may also be regulated by $1,25D_3$. The subcellular localization of DFF is not known, but it does not appear to be predominantly a mitochondrial protein [22], so mitochondrial involvement in apoptosis may be only a part of the story. It is likely that survival or death of HL60 leukemia cells is decided by the interplay of a complex network of cellular signals.

Enhancement of cellular antiapoptosis mechanisms during monocytic differentiation may have a special physiological significance. Phagocytosis, a process which involves generation of reactive oxygen species, is an important function of the monocyte, so protection of the cell from accidental damage by these oxidants may be necessary in this phenotype. Together with previous studies, our data serve to establish Mcl-1 as a differentiation-related mitochondrial antiapoptosis factor.

We are grateful to Dr. Milan Uskokovic, Hoffmann–LaRoche, Nutley, New Jersey, for the gift of $1,25D_3$. This work was supported by the NIH Grant RO1 CA 44722 from the National Cancer Institute and a Fellowship from the New Jersey Commission on Cancer Research to X. Wang.

REFERENCES

1. Barry, M. A., Behnke, C. A., and Eastman, A. (1990) *Biochem. Pharmacol.* **40,** 2353–2353.
2. Darzynkiewicz, Z. J. (1995) *Cell. Biochem.* **58,** 151–159.
3. Tsujimoto, Y., Gorham, J., Cossman, J., Jaffee, E., and Croce, C. M. (1985) *Science* **229,** 1390–1393.
4. Bakhshi, A., Jensen, J. P., Goldman, P., Wright, J. J., McBride, O. W., Epstein, A. L., and Korsmeyer, S. J. (1985) *Cell* **41,** 899–906.
5. Cleary, M. L., and Sklar, J. (1985) *Proc. Natl. Acad. Sci. USA* **82,** 7439–7443.
6. Vaux, D. L., Cory, S., and Adams, J. M. (1988) *Nature* **335,** 440–442.
7. Hockenbery, D., Nunez, G., Milliman, C., Schreiber, R. D., and Korsmeyer, J. (1990) *Nature* **348,** 334–336.
8. Monaghan, P., Robertson, D., Amos, S., Dyer, M. J. S., Mason, D. Y., and Greaves, M. F. (1992) *J. Histochem. Cytochem.* **40,** 1819–1825.
9. Krajewski, S., Tanaka, S., Takayama, S., Schibler, M. J., Fenton, W., and Reed, J. C. (1993) *Cancer Res.* **53,** 4701–4714.
10. Jacobson, M. D., Burne, J. F., King, M. P., Miyashita, T., Reed, J. C., and Raff, M. C. (1993) *Nature* **361,** 365–386.
11. de Jong, D., Prins, F. A., Mason, D. Y., Reed, J. S. D., van Ommen, G. B., and Kluin, P. M. (1994) *Cancer Res.* **54,** 256–260.
12. Boise, L. H., Gonaalez-Garcia, M., Postema, C. E., Ding, L., Lindsten, T., Turka, L. A., Mao, Z., Nunez, G., and Thompson, G. B. (1993) *Cell* **74,** 609–619.
13. Lin, E. Y., Orlofsky, A., Bergar, M., and Prystowsky, M. B. (1993) *J. Immunol.* **151,** 1979–1988.
14. Kozopas, K. M., Yang, T., Buchanm, H. L., Zhou, P., and Craig, R. W. (1992) *Proc. Natl. Acad. Sci. USA* **90,** 3516–3520.
15. Oltvai, Z. N., Millman, C. L., and Korsmeyer, S. J. (1993) *Cell* **74,** 609–619.
16. Yang, E., Zha, J., Jockel, J., Boise, L. H., Thompson, C. B., and Korsmeyer, S. J. (1995) *Cell* **80,** 285–291.
17. Chittenden, T., and Harrington, E. A. (1995) *Nature* **374,** 733–736.
18. Sedlak, T. W., Oltvai, Z. N., Yang, E., Wang, K., Boise, L. H., Thompson, C. B., and Korsmeyer, S. J. (1995) *Proc. Natl. Acad. Sci. USA* **92,** 7834–7838.
19. Liu, X., Kim, C. N., Yang, J., Jemmerson, R., and Wang, X. (1996) *Cell* **86,** 147–157.
20. Yang, J., Liu, X., Bhalla, K., Kim, C., Ibrado, A. M., Cai, J., Peng, T. I., Jones, D. P., and Wang, X. (1997) *Science* **275,** 1129–1132.
21. Kluck, R. M., Bossy-Wetzel, E. N., Green, D. R., and Newmeyer, D. D. (1997) *Science* **275,** 1132–1136.
22. Liu, X., Zou, H., Slaughter, C., and Wang, X. (1997) *Cell* **89,** 175–181.
23. Wang, H. G., Miyashita, T., Takayama, S., Sato, T., Torigoe, T., Krajewski, S., Tranaka, S., Hovey, L., Troppmair, J., Rapp, U. R., and Reed, J. C. (1994) *Oncogene* **9,** 2751–2756.
24. Wang, H. G., Rapp, U. R., and Reed, J. C. (1996) *Cell* **87,** 629–638.
25. Studzinski, G. P., Bhandal, A. K., and Brelvi, Z. S. (1986) *J. Natl. Cancer Inst.* **76,** 641–648.
26. Xu, H-M., Tepper, G. C., Jones, J. B., Fernandez, C. E., and Studzinski, G. P. (1993) *Exp. Cell Res.* **209,** 367–374.

27. Solary, E., Bertrand, R., Kohn, K. W., and Pommier, Y. (1993) *Blood* **81,** 1359–1368.
28. DelBino, G., X, Li, Traganos, F., and Darzynkiewics, Z. (1994) *Leukemia* **8,** 281–288.
29. Wajchman, H. J., Rathod, B., Song, S., Xu, H., Wang, X., Uskokovic, M. R., and Studzinski, G. P. (1996) *Exp. Cell Res.* **224,** 312–322.
30. Zhang, F., Rathod, B., Jones, J. B., Wang, Q. M., Bernhard, E., Godyn, J. J., and Studzinski, G. P. (1996) *J. Cell. Physiol.* **168,** 18–25.
31. Studzinski, G. P., Reddy, R. B., Hill, H. Z., and Bhandal, A. R. (1991) *Cancer Res.* **51,** 3451.
32. Griffin, J. D., Ritz, J., Nadler, L. M., and Schlossman, S. F. (1981) *J. Clin. Invest.* **68,** 932–941.
33. Godyn, J. J., Xu, H. M., Zhang, F., Kolla, S. S., and Studzinski, G. P. (1994) *Cell Prolif.* **27,** 37–46.
34. Yang, J., Liu, X., Bhalla, K., Kim, C., and Wang, X. (1997) *Science* **275,** 1129–1132.
35. Eckhardt, T. (1978) *Plasmid* **1,** 584–588.
36. Walker, P. R., Smith, C., Youdale, T., Leblanc, J., Whitfield, J. F., and Sikorska, M. (1991) *Cancer Res.* **51,** 1078–1085.
37. Bertrand, R., Sarang, M., Jenkin, J., Kerrigan, D., and Pommier, Y. (1991) *Cancer Res.* **51,** 6280–6285.
38. Farzaneh, F., Zalin, R., Brill, D., and Shall, S. (1982) *Nature* **300,** 363–366.
39. Gunji, H., Hass, R., and Kufe, D. (1992) *J. Clin. Invest.* **89,** 954–960.
40. Reynolds, J. E., Yang, T., Qian, L., Jenkinson, J. D., Zhou, P., Eastman, A., and Craig, R. W. (1994) *Cancer Res.* **54,** 6348–6352.
41. Wang, S., Rowe, M., and Lundgren, E. (1996) *Cancer Res.* **56,** 4610–4613.
42. Krajewski, S., Bodrug, S., Krajewska, M., Shabaik, A., Gascoyne, R., Berean, K., and Reed, J. C. (1995) *Am. J. Pathol.* **146,** 1309–1319.
43. Daum, G., Eisenmann-Tappe, I., Fries, H., Troppmair, J., and Rapp, U. (1994) *Trends Biochem. Sci.* **19,** 474–480.
44. Studzinski, G. P., and Brelvi, Z. S. (1987) *J. Natl. Cancer Inst.* **79,** 67–76.
45. Susin, S. A., Zamzami, N., Castedo, M., Hrisch, T., Marchetti, P., Macho, A., Daugas, E., Geuskens, M., and Kroemer, G. (1996) *J. Exp. Med.* **184,** 1331–1341.

Received May 8, 1997
Revised version received May 15, 1997

EXPERIMENTAL CELL RESEARCH **235,** 218–226 (1997)
ARTICLE NO. EX973664

Growth/Differentiation Factor-5 Induces Angiogenesis *in Vivo*

Hidetoshi Yamashita,*,†,[1] Akira Shimizu,* Mitsuyasu Kato,* Hideki Nishitoh,* Hidenori Ichijo,* Aki Hanyu,*
Ikuo Morita,‡ Michio Kimura,§ Fusao Makishima,§ and Kohei Miyazono*

**Department of Biochemistry, the Cancer Institute, Tokyo, Japanese Foundation for Cancer Research, Kami-ikebukuro, Toshima-ku, Tokyo 170, Japan; †Department of Ophthalmology, Faculty of Medicine, University of Tokyo, Hongo, Bunkyo-ku, Tokyo 113, Japan; ‡Department of Physiological Chemistry, Graduate School, Tokyo Medical and Dental University, Yushima, Bunkyo-ku, Tokyo 113, Japan; §Discovery Research Laboratories, Research and Development Division, Nippon Hoechst Marion Roussel Limited, Minamidai, Kawagoe 350-11, Japan*

Bone morphogenetic proteins (BMPs) are multifunctional cytokines, which induce bone and cartilage formation and exert various other effects on many tissues. Since angiogenesis is involved in the bone formation process, certain members in the BMP family may induce angiogenesis. We examined the *in vivo* angiogenic activity of BMP family members, i.e., growth/differentiation factor (GDF)-5 and BMP-2. GDF-5 induced angiogenesis in both chick chorioallantoic membrane and rabbit cornea assays. In contrast, BMP-2 did not induce angiogenesis. In order to elucidate the mechanism of angiogenesis, we examined the effects of GDF-5 on cultured bovine aortic endothelial cells (BECs). GDF-5 induced plasminogen activator activity and accelerated the migration of BECs in a chemotactic fashion, which may contribute to the process of angiogenesis *in vivo*. These results suggest that GDF-5 is one of the molecules which induce angiogenesis in the bone formation process. © 1997 Academic Press

INTRODUCTION

Bone morphogenetic proteins (BMPs)[2] are dimeric proteins that were originally identified as proteins inducing bone and cartilage in nonskeletal tissues [1, 2]. The BMP family includes various proteins, which are divided into several subgroups, i.e., a group containing BMP-2, BMP-4, and the *Drosophila decapentaplegic* gene product, a group containing osteogenic protein-1 (OP-1, also termed BMP-7), OP-2 (BMP-8), BMP-5, BMP-6 (also termed Vgr1), and *Drosophila 60A* gene product, a group containing growth/differentiation factor (GDF)-5, GDF-6, and GDF-7, and others [3]. In addition to bone and cartilage formation, BMPs regulate proliferation, differentiation, migration, and apoptosis of many types of cells [2, 3]. BMPs are expressed in nonskeletal tissues including the nervous system, lung, kidney, skin, and gonads [3]. These observations suggest that BMPs are multipotent cytokines not only in mesenchymal tissues, but also in other tissues, and raise the possibility that members of the BMP family may have disparate functions in various tissues. Since angiogenesis and vascular invasion into bone are important steps in the sequential cascade of the bone formation processes [2], it may be important to elucidate whether the BMP family members have angiogenic activity *in vivo*.

The BMP family belongs to transforming growth factor (TGF)-β superfamily, which includes TGF-βs, activins, and Müllerian inhibiting substance [4, 5]. The significant amino acid sequence similarities are observed among the members of TGF-β superfamily, and they transduce signals via serine/threonine kinase receptors [4, 5]. Members of the TGF-β superfamily exert various effects on the cellular constituents of vascular wall directly and indirectly [6]. TGF-β and activin A inhibit the proliferation of endothelial cells [7–9], whereas TGF-β stimulates the proliferation of smooth muscle cells under certain conditions [10]. TGF-β inhibits the migration of endothelial cells [11] and stimulates capillary-like structure formation *in vitro* [12]. In addition to those *in vitro* effects, TGF-β1 was shown to induce angiogenesis *in vivo* using various angiogenesis assays [13, 14]. Moreover, a certain number of the TGF-β1 knockout mice die due to defective vasculogenesis [15]. Angiogenic activity of TGF-β has also been shown by the phenotypes of null mutations of TGF-β type II receptor and endoglin, which is a cell surface binding

---

[1] To whom correspondence and reprint requests should be addressed at Department of Biochemistry, the Cancer Institute, Tokyo, Japanese Foundation for Cancer Research, 1-37-1 Kami-ikebukuro, Toshima-ku, Tokyo 170, Japan. Fax and phone: +81-3-3918-0342. E-mail: hyama-tky@umin.u-tokyo.ac.jp.

[2] Abbreviations used: BMP, bone morphogenetic protein; OP, osteogenic protein; GDF-5, growth/differentiation factor 5; TGF-β, transforming growth factor-β; ALK, activin receptor-like kinase; VEGF, vascular endothelial growth factor; FGF, fibroblast growth factor; BSA, bovine serum albumin; PBS, phosphate-buffered saline; CAM, chorioallantoic membrane; BMPR, BMP receptor; ActR, activin receptor; BECs, bovine aortic endothelial cells; MEM, minimum essential medium; FCS, fetal calf serum; PA, plasminogen activator; uPA, urokinase-type plasminogen activator.

0014-4827/97 $25.00

Copyright © 1997 by Academic Press
All rights of reproduction in any form reserved.

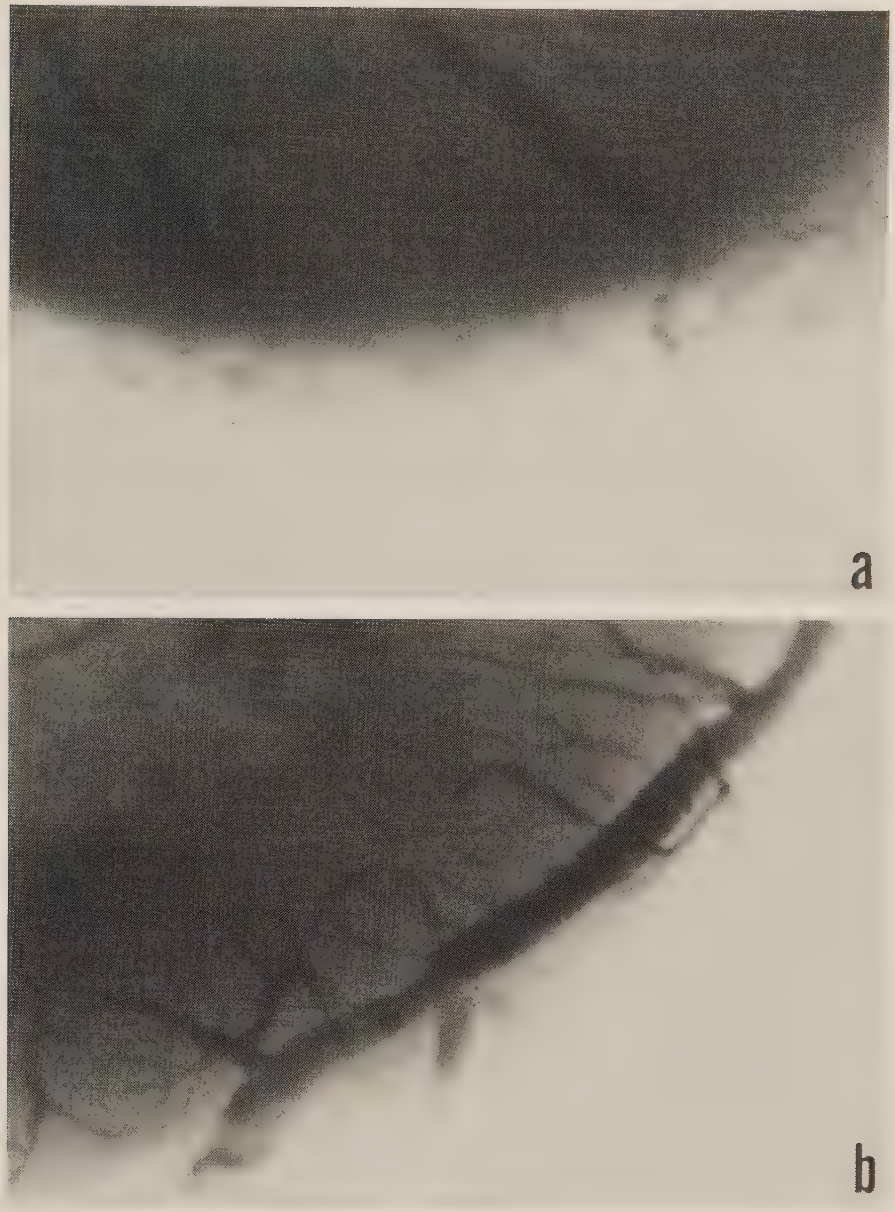

FIG. 1. Angiogenesis induced by GDF-5 in the CAM assay. Disks containing only solvent (control disk) or GDF-5 were plated on the CAMs of 10- to 11-day-old chicken eggs. After 3–4 days, the formation of new vessels around the disk was examined. (a) Control disk containing solvent composed of 0.05% trifluoroacetic acid and 35% acetonitrile. (b) Disk containing GDF-5 (13 p*M*).

protein for TGF-β. Null mutation in the TGF-β type II receptor gene results in defects of yolk sac hematopoiesis and vasculogenesis during development stages [16]. Mutations in the human endoglin gene cause hereditary haemorrhagic telangiectasia type 1, in which vascular dysplasia occurs in various organs [17]. Mutations in activin receptor-like kinase-1 (ALK-1) also cause hereditary hemorrhagic telangiectasia type 2 [18]. ALK-1 is an orphan receptor; however, based on the structural similarity it was shown to belong to the type I receptor family of the TGF-β superfamily members. This evidence clearly shows that TGF-β and possibly other members of the TGF-β superfamily may play important roles in vasculogenesis, angiogenesis, and maintenance of the vascular system.

To investigate the angiogenic activity of the members in BMP family, we examined the effects of BMP-2 and GDF-5. Some angiogenic molecules, including TGF-β [13, 14] and tumor necrosis factor-α [19, 20], show paradoxical effects; they inhibit the proliferation of vascular endothelial cells *in vitro,* but they induce angiogenesis in *in vivo* experimental systems. Therefore, both *in vivo* and *in vitro* experimental systems were used to understand the mechanisms of angiogenesis.

TABLE 1

Angiogenesis Induced in CAM

Sample	Dose (p*M*) 1	3–5	10–13	17–20
GDF-5	0/2	4/8	4/5	6/8
TGF-β1	1/1	2/2	1/1	1/2
Activin A	—	—	—	0/5
BMP-2	0/1	—	0/3	0/1

Note. The rate of positive responses (number of positive disks/number of all tested disks) in each dose is listed. The responses are scored as positive when the vasculature is more around the tested disks than around the control disks. (—) Not tested.

MATERIALS AND METHODS

Reagents. Recombinant human GDF-5 and recombinant human BMP-2 were obtained as described previously [21]. Recombinant human TGF-β1 and recombinant human activin A were obtained from Kirin Brewery Co. Ltd. and Ajinomoto Co. Ltd., respectively. Recombinant human vascular endothelial growth factor (VEGF) and bovine brain fibroblast growth factor-1 (FGF-1) were purchased from Pepro Tech Co. (Rocky Hill, NJ) and WAKO Co. (Tokyo, Japan), respectively.

GDF-5 was dissolved in solution containing 0.05% trifluoroacetic acid and 35% acetonitrile. BMP-2 and TGF-β1 were dissolved in a solution containing 4 m*M* HCl and 0.1% bovine serum albumin (BSA). Activin A, FGF-1, and VEGF were dissolved in the phosphate-buffered saline (PBS) with 0.1% BSA.

Angiogenesis assay using chick chorioallantoic membranes (CAMs). CAMs of 10- to 11-day-old fertilized white Leghorn chicken eggs were used for the assay according to a method reported previously [14], with certain modifications. The fertilized eggs were set upright and incubated at 37°C. After 10 to 11 days incubation, a window was made in the eggshell overlying the air sac and the CAM was exposed in each egg. Implant disks of 3 mm in diameter were made of filter paper (Showa Yakuhinkagaku, Tokyo, Japan). Twenty microliters of solution containing 0.5% (w/v) methyl cellulose (Sigma, St. Louis, MO) and growth factors in appropriate solvents was added into the disks and air-dried completely. The doses for each growth factor in the disks ranged from 1 p*M* to 20 p*M*/disk (Table 1). The disks were plated on the CAMs and the zones around the disks were observed 3–4 days after placement of the disks. As controls, disks containing only the solvents were plated.

Angiogenesis assay using rabbit corneas. To confirm the results of CAM assay, rabbit corneas were used for angiogenesis assay according to a method reported previously [20], with certain modifications. The experimental procedures were undertaken in compliance with the guiding principles in the Care and Use of Animals described in the *American Journal of Physiology.* Rabbits of 2–2.5 kg were anesthetized with intravenous injections of pentobarbital sodium and used for the experiments. One microliter of solution containing GDF-5 was mixed in 10 μl of a solution of ethylene vinyl acetate copolymer (Mitsui Dupon Chemical, Tokyo, Japan) in dichloromethane (WAKO) and frozen on dry ice. Pellets were dried overnight at −20°C and became 1 mm in diameter. Pellets were inserted surgically into pockets created in the rabbit corneal stroma and set 1–2 mm from the corneoscleral limbus. As control, 1 μl of solvent for GDF-5 (0.05% trifluoroacetic acid and 35% acetonitrile) was used (Table 2). Rabbits were sacrificed 7 days after pellet implantation and new vessel formation in clear cornea was analyzed.

Histological and immunohistochemical observation. The expression of receptors for BMPs and activins was studied immunohistochemically in the rabbit corneas used in the angiogenesis assay. Fixed rabbit corneas were embedded in paraffin and 4-μm-thick sections were prepared. The vessels in the corneal stroma were stained for BMP receptor type IA (BMPR-IA), BMPR-IB, activin receptor type I (ActR-I), BMPR-II, and ActR-II by using biotinylated antibodies. Antisera to ActR-I, BMPR-IA, and BMPR-IB were raised in rabbits against the synthetic peptides corresponding to the intracellular juxtamembrane parts of the type I receptors, as previously reported [22]. Antiserum to ActR-II was made against a peptide to the COOH-terminal tail of ActR-II [23]. Antiserum to BMPR-II was raised against a fragment from the human receptor, i.e., amino acids 185–202 [24]. These antisera were affinity-purified in CNBr-activated Sepharose CL-4B (Pharmacia Biotech AB, Uppsala, Sweden) columns conjugated with immobilized peptides according to the manufacturer's instructions for histochemical use and thereafter biotinylated with long arm biotin *N*-hydroxysuccinimide ester (Vector Labs, Burlingame, CA) according to the manufacturer's protocol. As negative controls, nonimmune rabbit IgG or PBS was replaced for the primary antibodies. Binding sites of biotinylated primary antibodies in the tissues were visualized with 3,3′-diaminobenzidine (Sigma), after which the sections were counterstained with methyl green.

Cell culture. Bovine aortic endothelial cells (BECs) were obtained from bovine aorta [25], grown in Eagle's minimum essential medium (MEM) with 10% fetal calf serum (FCS), and used for the experiments at the 24th through 47th passage.

PA activity. BECs were seeded into 12-well plates at a density of 1–3 × 10^5 cells/well and grown at 37°C overnight. The cells were starved overnight in MEM with 1% FCS and the medium was changed into MEM with 0.1% FCS with or without BMP-2 and GDF-5. The cells were incubated for 24 h; thereafter, the medium was collected and the supernatant after centrifugation was stored at −20°C until zymography. Zymographic assay of PA activity was performed according to the modified method of Vassalli *et al.* [26, 27]. Aliquots of the stored conditioned medium were electrophoresed on SDS–polyacrylamide gels (7% polyacrylamide) under nonreducing conditions. Thereafter, the gel was washed extensively in PBS containing 2.5% Triton X-100 to remove SDS. The gel was put on 1.1% agarose gel containing 1.2% fat-free milk as a source of casein and 0.12 U/ml plasminogen (Sigma) and incubated at 37°C for 2–3 days. PA activity was detected as a lucent area in the white agarose gel. The gel was photographed, and quantification was performed using the software program NIH Image version 1.60 manual by Dr. Wayne Rasband (National Institute of Health, Bethesda, MD).

Regulation of migration. Migration was assayed by the Boyden chamber method, using a Chemotaxis Chamber (MBB98) and an 8-μm-pore filter (PFD8/A) (Neuro Probe, Inc., Cabin John, MD) according to the manufacturer's protocol. The lower chambers were filled with MEM with 1% FCS with or without GDF-5 and covered with the filter membrane. One hundred and fifty microliters of the BEC suspension at a final density of 2 × 10^5 cells/ml in MEM with 1% FCS with or without GDF-5 was added into the upper chambers. The chamber was incubated at 37°C overnight, and thereafter the filter was removed, fixed in methanol, and stained with Diff-Quik (Green Cross Co., Kobe, Japan). Data are presented as the numbers of the cells that migrated through the filter pores in the fields magnified 200 times with a light microscope. A checkerboard analysis [20, 28] was carried out to determine whether the migration activation was in chemotactic or chemokinetic fashion.

Regulation of proliferation. BECs were seeded in 24-well plates at a density of 2–5 × 10^5 cells per well in MEM with 10% FCS. After 24 h, the medium was changed into MEM with 0.1% FCS containing various concentrations of TGF-β1 and GDF-5. After 16–18 h incubation, 0.25 μCi of [^{3}H]thymidine was added and the cells were incubated for 1–4 h. After incubation, the cells were fixed in 10% ice-cold trichloroacetic acid for 15 min and solubilized in 1 *M* NaOH for 20 min, followed by neutralization with 1 *M* HCl. ^{3}H-radioactivity was determined in a liquid scintillation counter using an Aqueous counting scintillant (ACS II) (Amersham, Arlington Heights, IL).

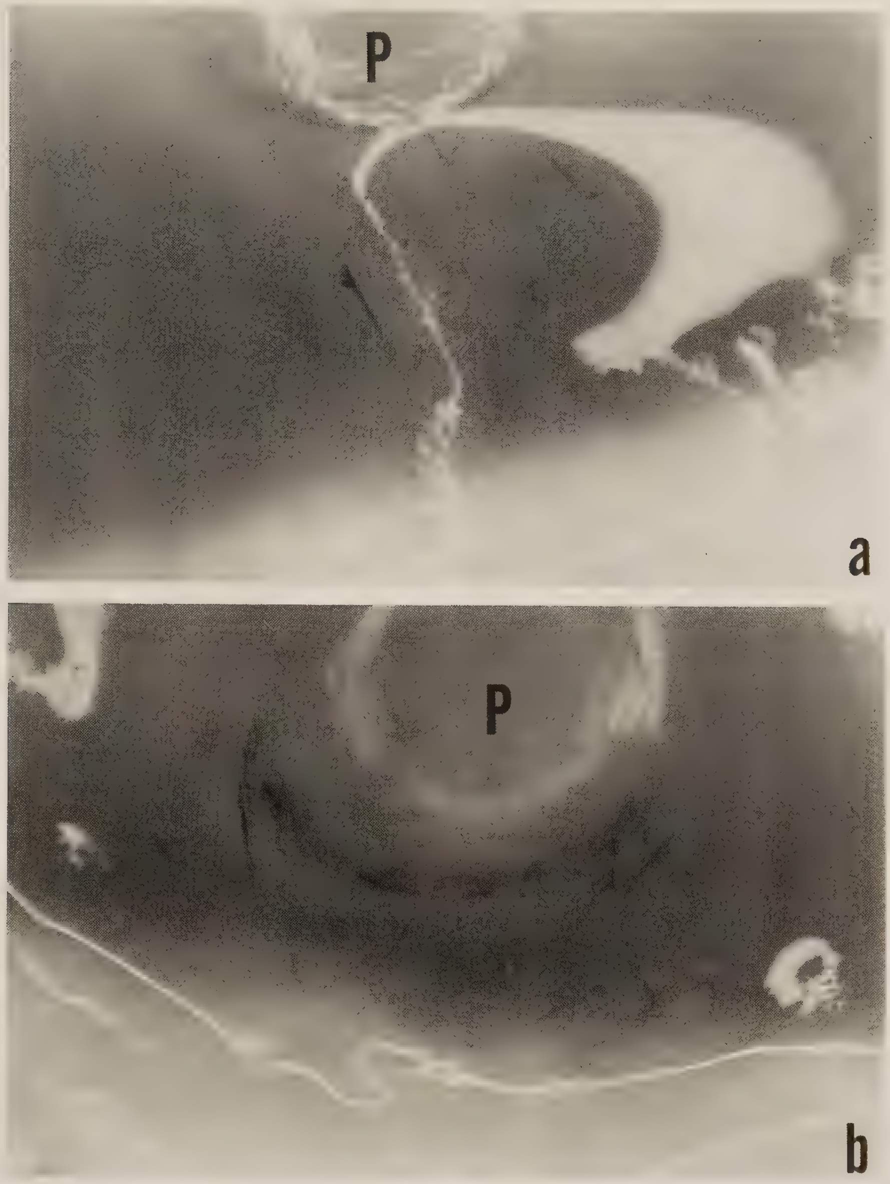

FIG. 2. Angiogenesis induced by GDF-5 in the rabbit cornea assay. Ethylene vinyl acetate copolymer pellets containing only solvent (control pellet) or GDF-5 were inserted into pockets in the rabbit clear cornea. After 7 days, the new vessel formation in clear cornea was examined. (a) Control pellet containing solvent composed of 0.05% trifluoroacetic acid and 35% acetonitrile. (b) Pellet containing GDF-5 (17 p*M*). P, pellet.

Formation of capillary-like structure in vitro. Capillary formation of BECs *in vitro* was performed on type I collagen gel [25, 29]. Type I collagen gel (Nitta Gelatin Co., Osaka, Japan) was put into the wells of 12-well plates. After gelation, the cell suspension of BECs at a density of $1-2 \times 10^5$ cells/ml in MEM containing 10% FCS was seeded with or without GDF-5 or VEGF and incubated at 37°C. After attachment of the cells on the collagen gel, the medium was removed and type I collagen solution was added on the cell layer. MEM with 1% FCS with or without GDF-5 was added after the gelation of the upper layer and incubated up to 6 days at 37°C. The capillary-like structure formation was observed with a phase-contrast microscope.

Statistical analysis. Comparisons of the incidence rates of angiogenesis in the CAM assay and the rabbit cornea assay were performed by χ^2 test. Comparisons of means of the numbers of migrated cells in the checkerboard analysis *in vitro* were performed by Student's *t* test.

RESULTS

Angiogenesis in Vivo

CAM assay [14, 20] was used to investigate the induction of angiogenesis by GDF-5 and other factors. More than 3 p*M* (100 ng)/disk of GDF-5 induced angiogenesis (Fig. 1 and Table 1). A significant induction of microvessels was observed by GDF-5 on the edges around disks. Microvessels were also seen at the areas

TABLE 2

Angiogenesis Induced by GDF-5 in the Rabbit Cornea Assay

Sample	Positive responses (%)[a]
Control[b]	6/14 (43%)
GDF-5	
17 p*M*	2/2 (100%)
33 p*M*	8/10 (80%)
67 p*M*	2/2 (100%)

[a] The rate of positive responses (the vasculature in the clear cornea) is listed.

[b] The control disk contains 0.05% trifluoroacetic acid and 35% acetonitrile, which is used as a solvent for GDF-5.

attaching disks. The angiogenesis induction by GDF-5 at the dose of 10 or 20 p*M* was statistically significant in comparison with the control without any factors ($P < 0.025$, χ^2 test, respectively). TGF-β1 induced angiogenesis with doses of more than 1 p*M* (25 ng)/disk. As positive controls, VEGF and FGF-1 also induced angiogenesis at a dose of 10–13 p*M*/disk (Table 1), but activin A or BMP-2 did not induce the angiogenesis in the CAM assay even at a dose of 17–20 p*M*/disk (Table 1). Higher doses of GDF-5 were required to induce angiogenesis than with TGF-β1, which is consistent with the previous *in vitro* studies that about 10 n*M* GDF-5 (300 ng/ml) was required to induce alkaline phosphatase in a rat osteoprogenitor-like cell line (ROB-C26 cells) [21], but that TGF-β1 was effective at a lower dose (0.2 n*M*) on osteoblast-like osteosarcoma cell lines, e.g., MG-63 and TE-85 [30, 31].

The rabbit cornea assay was used to confirm the angiogenesis induced by GDF-5. In the normal state, no vessels were observed in rabbit corneas. Ethylene vinyl acetate copolymer pellets containing GDF-5 or control medium were implanted into the clear part of the cornea, and rabbit eyes were examined after 7 days. Formation of only the stromal tunnel did not induce corneal angiogenesis (data not shown). The control pellets containing only the solvent for GDF-5 induced angiogenesis in 43% of eyes (6 eyes/14 eyes). Pellets containing GDF-5 of 17–67 p*M*/pellet (0.5–2 μg/pellet) induced angiogenesis in 80–100% of eyes (Fig. 2 and Table 2). The angiogenesis induction by GDF-5 at 33 p*M* tended to be more significant than that of the control (80% of incidence vs 43%, respectively; χ^2 test, $0.05 < P < 0.07$). The density of newly formed microvessels was not affected by the different doses of GDF-5. In total, the incidence of angiogenesis induced by GDF-5 was 86% (12 eyes/14 eyes), which was significantly higher than that by the control pellets (χ^2 test, $P < 0.025$). The angiogenesis induction in the rabbit cornea assay by GDF-5 was similar to those of TGF-β1 (2/3) and VEGF (2/3).

Expression of BMP Receptors in Endothelial Cells of New Vessels

Histological examination of the cornea 7 days after the implantation of growth factor pellets revealed that new vessels were observed in the surface half-layer of cornea, and fibroblast-like cells were observed around new vessels. Infiltration of inflammatory cells was not detected after 7 days. Expression of the receptors for GDF-5 in the rabbit cornea was investigated immunohistochemically using specific antibodies to BMP receptors [32]. We have previously shown that GDF-5 binds to BMPR-IB and BMPR-II, which are shared with BMP-2 and OP-1 [21]. Binding of GDF-5 to BMPR-IA was very weak and was observed only in cotransfection with ActR-II or ActR-IIB [21]. The endothelial cells of the new vessels and the surrounding fibroblast-like cells in the corneal stroma expressed BMPR-IA, BMPR-IB, and BMPR-II (Fig. 3). However, the expression of ActR-I or ActR-II was not observed immunohistochemically (data not shown).

Effects of GDF-5 on Cultured Endothelial Cells

In the process of angiogenesis, four steps, i.e., activation of PA, migration, proliferation, and differentiation into a capillary-like structure of endothelial cells, have been shown to be involved [6, 33, 34] and they can be investigated by *in vitro* experimental systems using cultured endothelial cells. In this study, in order to investigate the direct effects of GDF-5 on endothelial cells *in vitro,* PA activity induction, migration by the Boyden chamber method, regulation of proliferation by [^{3}H]thymidine incorporation, and capillary-like structure formation in the collagen gel were investigated using cultured BECs.

Effects on PA activity induction. PA activity in conditioned media of BECs was assayed using zymography. GDF-5 stimulated PA activity at concentrations of 10 and 33 n*M* in BECs (Fig. 4). The apparent molecular weight of PA induced in our experimental system was about 55–60 kDa, corresponding to urokinase-type PA (uPA) [35, 36], which was confirmed by Western blot analysis using anti-uPA antibody (ADI, Greenwich, CT) (data not shown). A 49-kDa molecule had also PA activity, of which the origin is not clear. The stimulation of PA activity *in vitro* by GDF-5 is consistent with angiogenesis induction *in vivo.* This is in clear contrast with BMP-2, which inhibited PA activity (Fig. 4) and lacked angiogenic activity *in vivo.*

Effect on cell migration. The effect of a concentration gradient of GDF-5 on the migration of BECs was investigated using the Boyden chamber technique [20, 28]. GDF-5 stimulated migration in comparison with the control (data not shown). When the effect of GDF-5 on cell migration was analyzed by checkerboard analysis [20, 28], GDF-5 stimulated migration in a chemotactic fashion (Fig. 5).

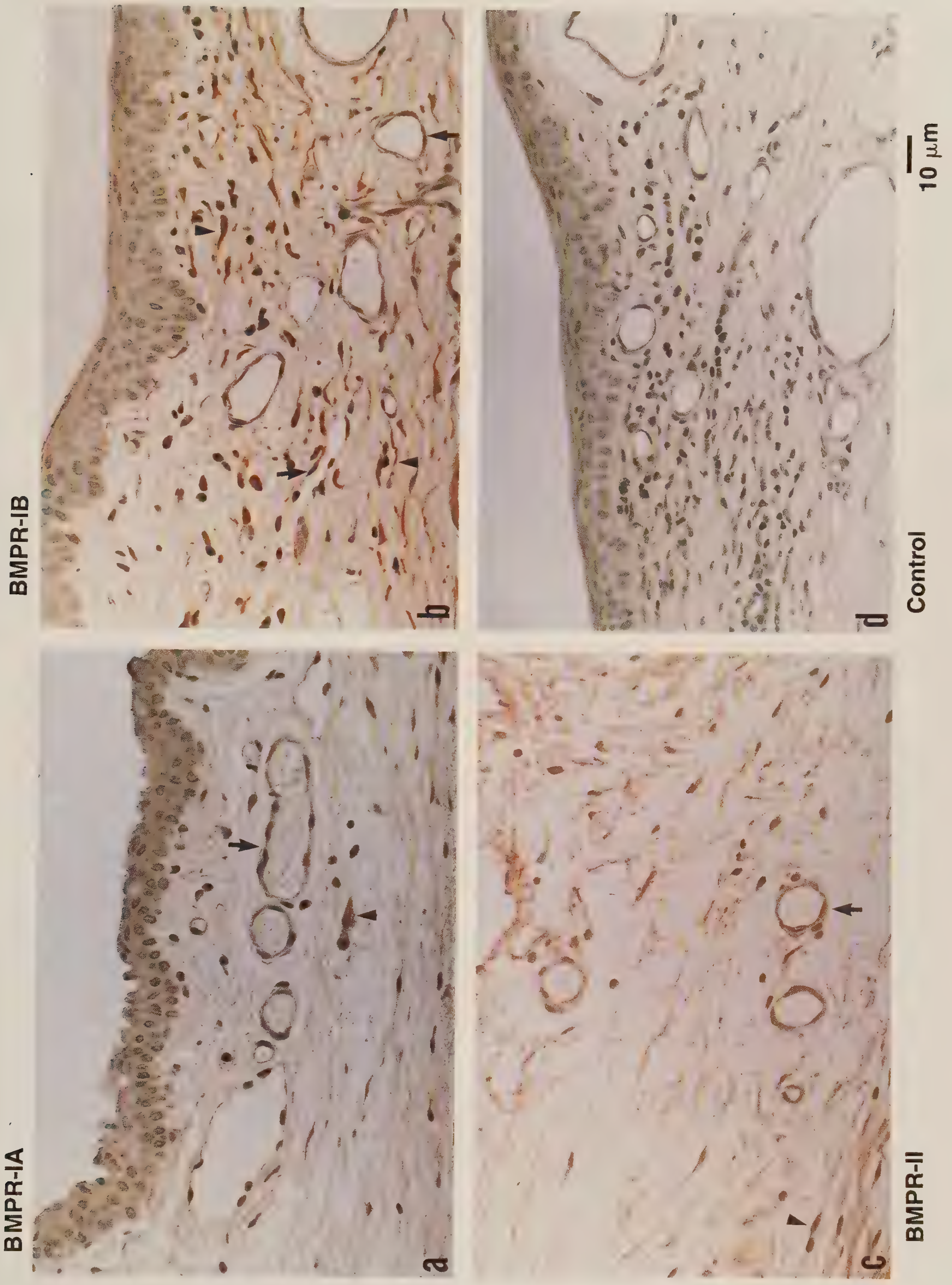
BMPR-IA
a
BMPR-IB
b
BMPR-II
c
Control
d
10 μm

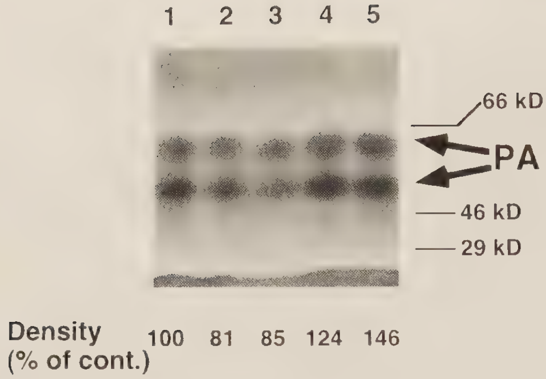

FIG. 4. Effects of growth factors on PA activity in the cultured BECs. BECs were cultured for 24 h in the presence or the absence of various growth factors after 24-h serum starvation. The conditioned media were collected and separated by SDS–PAGE under nonreducing conditions. The polyacrylamide gel was washed, put on top of an agarose gel containing fat-free milk and plasminogen, and incubated for 2 days at 37°C. The bands corresponding to uPA activity were visualized as lucent bands of 55–60 kDa in the agarose gel. The densities of bands were quantified using a software program (NIH Image, version 1.60 manual). The densities are presented as percentages of that of the control culture (BECs treated with 1% FCS). Lanes: 1, control; 2, BMP-2 (3.2 n*M*); 3, BMP-2 (9.7 n*M*); 4, GDF-5 (10 n*M*); 5, GDF-5 (33 n*M*). The experiments were repeated four times and similar results were obtained. A result of representative experiment is shown.

Regulation of proliferation. The growth regulatory effect of GDF-5 was compared with that of TGF-β1. TGF-β1 inhibited [^{3}H]thymidine incorporation into BECs. In contrast, GDF-5 did not significantly affect [^{3}H]thymidine incorporation (Fig. 6).

Capillary-like structure formation in collagen gel. Capillary-like structure formation by BECs [26, 29] was studied *in vitro.* Cells were seeded in the middle of two layers of type I collagen and incubated up to 6 days in the presence or the absence of GDF-5 (3.3 n*M*) or VEGF (2.6 n*M*). GDF-5 and VEGF did not induce differentiation into a capillary-like structure in BECs (data not shown).

DISCUSSION

GDF-5 (nM) in lower chamber	GDF-5 (nM) in upper chamber		
	0	3.3	10
0	29±22	48±8	47±21
3.3	65±15	15±12	26±14
10	142±16	99±17	38±20

FIG. 5. Effect of GDF-5 on cell migration of BECs using checkerboard analysis. Migration of cells was assayed by the Boyden chamber method. The lower and upper chambers were filled with medium with or without various concentrations of GDF-5. BECs were added to the upper chambers. The Boyden chamber was incubated at 37°C overnight. The numbers of cells that migrated through the filter pores were counted with a light microscope. Data are presented as the numbers of cells which migrated through the filter in a field magnified 200 times. Each point shows mean ± standard deviation of three independent wells. The experiments were repeated three times and similar results were obtained. Results of a representative experiment are shown. Difference of means was analyzed by Student's *t* test. $^*P < 0.05$, $^{**}P < 0.01$.

In the present study, CAM assay revealed that GDF-5 induced angiogenesis *in vivo.* In contrast, BMP-2 or activin A did not induce angiogenesis *in vivo.* VEGF, FGF-1, and TGF-β1 have been identified as mediators of angiogenesis by others [6, 13, 14, 37], and their angiogenic activities were confirmed in the CAM assay in the present study. Angiogenic activity of GDF-5 was further confirmed using the rabbit cornea assay. The effects of GDF-5 evaluated by the cornea assay were similar to those by TGF-β1 and VEGF. Thus, among BMP family members GDF-5 is an angiogenic mediator *in vivo,* but BMP-2 is not angiogenic.

The present study suggests two possibilities to account for the mechanisms of the angiogenic effect of GDF-5. The first possibility is that the direct effects of GDF-5 on endothelial cells are important to induce angiogenesis. GDF-5 induced PA activity and chemotactic migration of BEC, which may be related to *in vivo* angiogenesis. GDF-5 did not induce capillary-like structure formation of BECs. VEGF did not induce capillary-like structure formation either, which may be due to the characteristics of BECs. The effect of GDF-5 on capillary-like structure formation was further confirmed using endothelial cells from dermal capillaries; in this cell type, only VEGF, but not GDF-5, induced capillary-like structure formation (H.Y., unpublished data). Most of the angiogenic factors do not necessarily contribute to all the steps in angiogenesis [6], so the above effects of GDF-5 suggest that the induction of angiogenesis *in vivo* may depend on the direct effects of GDF-5 on endothelial cells.

Endothelial cells of the new vessels in rabbit corneas

FIG. 3. Histology of rabbit cornea treated with GDF-5 and immunohistochemical observation of BMP receptors. New vessel formation was observed in the rabbit cornea 7 days after pellet implantation. Thereafter, the rabbits were sacrificed and the eyes were enucleated, fixed, and embedded in paraffin. Biotinylated antibodies were used to detect BMP receptor expression in the cornea sections. Immunohistochemistry was performed using BMPR-IA antibody (a), BMPR-IB antibody (b), and BMPR-II antibody (c). Staining was also done with PBS (d) and nonimmune IgG (not shown) in place of specific primary antibodies as negative controls. Arrowheads, fibroblast-like cells; arrows, endothelial cells (magnification: ×680; bar, 10 μm).

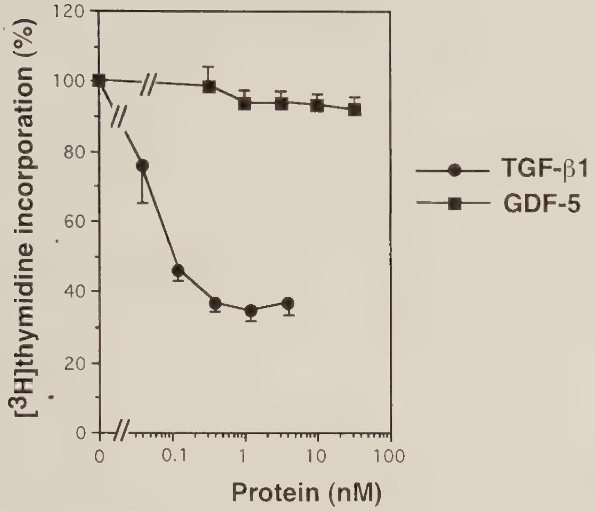

FIG. 6. Effects of various growth factors on [^{3}H]thymidine incorporation into BECs. BECs were seeded in 24-well plates at a density of 2–5 × 10^5 cells/well. After 24 h, the cells were incubated with various concentrations of GDF-5 or TGF-β. After 16–18 h, 0.25 μCi of [^{3}H]thymidine was added and incubated for 1–4 h. The cells were fixed in 10% trichloroacetic acid, solubilized in NaOH, and neutralized with HCl and ^{3}H-radioactivity was determined in a liquid scintillation counter. Data are presented as percentage of the baseline level. The experiments were repeated three times and similar results were obtained. Results of a representative experiment are shown.

expressed the receptors for BMPs (BMPR-IA, BMPR-IB, and BMPR-II), which suggests that endothelial cells *in situ* can respond to BMPs. We have recently found that GDF-5 binds to BMPR-IB and BMPR-II, which are shared at least in part with BMP-2 as well as with OP-1 [21]. However, in contrast to GDF-5, BMP-2 did not induce angiogenesis. Whether GDF-5 induces angiogenic activity through yet unidentified receptors, or whether binding of GDF-5 to these receptors with different affinities may transduce signals different from BMP-2, remains to be determined.

The second possibility is that GDF-5 induces angiogenesis *in vivo* through indirect effects of GDF-5. TGF-β1 is widely known as an angiogenic factor. TGF-β1 inhibits the induction of PA activity, migration, and proliferation of cultured endothelial cells *in vitro* [6, 7, 11, 26], but it induces angiogenesis *in vivo*. The mechanisms of angiogenesis by TGF-β have not been clarified, and several indirect effects from the surrounding cells on endothelial cells are speculated, i.e., cytokines secreted from macrophages, which accumulate by the effect of TGF-β1 [6, 14, 38], VEGF secreted from fibroblasts upon the stimulation by TGF-β1 [39], and extracellular matrix which becomes the scaffold for endothelial cell migration [40]. Since fibroblast-like cells in the rabbit corneal stroma around new vessels expressed BMP receptors, GDF-5 may exert indirect effects on endothelial cells through fibroblast-like cells in a mechanism similar to that of TGF-β.

GDF-5 has been identified as the product of the *Gdf5* gene, which is responsible for skeletal alterations in *brachypodism* mice [41]. *Brachypodism* mutant mice have short limbs, tiny paws, and reduced numbers of digit bones. A similar skeletal abnormality, known as Hunter–Thompson-type chondrodysplasia, has been shown to be due to mutations in the human cartilage-derived morphogenetic protein-1 gene, the human homologue of GDF-5 [42]. Hunter–Thompson-type chondrodysplasia exhibits abnormalities restricted to the limbs. In addition, GDF-5 has been shown to induce bone and cartilage formation *in vivo* as BMP-2 [43]. The present study revealed that GDF-5 induced angiogenesis *in vivo*. This suggests that the *in vivo* roles of members in the BMP family may be different [3] and that GDF-5 may work as one of the angiogenic mediators in the bone formation process, which may be consistent with the multiple roles of BMPs in skeletal formation.

We appreciate the Kirin Brewery Co. for recombinant human TGF-β1 and the Ajinomoto Co. for recombinant human activin A. H.Y. and K.M. are supported by grants-in-aid for scientific research from the Ministry of Education, Science, Sports, and Culture of Japan. H.Y. is supported by grants from the Japan Cardiovascular Research Foundation, the Foundation for Total Health Promotion, and the Sankyo Foundation of Life Science. K.M. is supported by the Research for the Future Program of the Japan Society for the Promotion of Science, the Japan Heart Foundation, and an IBM Japan Research Grant for 1995.

REFERENCES

1. Wozney, J. M., Rosen, V., Celeste, A. J., Mitsock, L. M., Whitters, M. J., Kriz, R. W., Hewick, R. M., and Wang, E. A. (1988) *Science* **242,** 1528–1534.
2. Reddi, A. H. (1992) *Curr. Opin. Cell Biol.* **4,** 850–855.
3. Hogan, B. L. M. (1996) *Genes Dev.* **10,** 1580–1594.
4. Massagué, J., Attisano, L., and Wrana, J. L. (1994) *Trends Cell Biol.* **4,** 172–178.
5. Yamashita, H., ten Dijke, P., Heldin, C.-H., and Miyazono, K. (1996) *Bone* **19,** 569–574.
6. Risau, W. (1990) *Prog. Growth Factor Res.* **2,** 71–79.
7. Jennings, J. C., Mohan, S., Linkhart, T. A., Widstrom, R., and Baylink, D. J. (1988) *J. Cell. Physiol.* **137,** 167–172.
8. D'Amore, P. A., and Smith, S. R. (1993) *Growth Factors* **8,** 61–75.
9. McCarthy, S. A., and Bicknell, R. (1993) *J. Biol. Chem.* **268,** 23066–23071.
10. Battegay, E. J., Raines, E. W., Seifert, R. A., Bowen-Pope, D. F., and Ross, R. (1990) *Cell* **63,** 515–524.
11. Sato, Y., and Rifkin, D. B. (1989) *J. Cell Biol.* **109,** 309–315.
12. Choi, M. E., and Ballermann, B. J. (1995) *J. Biol. Chem.* **270,** 21144–21150.
13. Roberts, A. B., Sporn, M. B., Assoian, R. K., Smith, D. M., Rocke, N. S., Wakefield, L. M., Heine, U. I., Liotta, L. A., Falanga, V., Kehrl, J. H., and Fauci, A. S. (1986) *Proc. Natl. Acad. Sci. USA* **83,** 4167–4171.
14. Yang, E. Y., and Moses, H. L. (1990) *J. Cell Biol.* **111,** 731–741.
15. Dickson, M. C., Martin, J. S., Cousins, F. M., Kulkarni, A. B.,

Karlsson, S., and Akhurst, R. J. (1995) *Development* **121,** 1845–1854.

16. Oshima, M., Oshima, H., and Taketo, M. M. (1996) *Dev. Biol.* **179,** 297–302.
17. McAllister, K. A., Grogg, K. M., Johnson, D. W., Gallione, C. J., Baldwin, M. A., Jackson, C. E., Helmbold, E. A., Markel, D. S., McKinnon, W. C., Murrell, P., McCormick, M. K., Pericak-Vance, M. A., Heutink, P., Oostra, B. A., Haitjema, T., Westerman, C. J. J., Porteous, M. E., Guttmacher, A. E., Letarte, M., and Marchuk, D. A. (1994) *Nature Genet.* **8,** 345–351.
18. Johnson, D. W., Berg, J. N., Baldwin, M. A., Gallione, C. J., Marondel, I., Yoon, S.-J., Stenzel, T. T., Speer, M., Pericak-Vance, M. A., Diamond, A., Guttmacher, A. E., Jackson, C. E., Attisano, L., Kucherlapati, R., and Porteous, M. E. M. (1996) *Nature Genet.* **13,** 189–195.
19. Fràter-Schröder, M., Risau, W., Hallmann, R., Gautschi, P., and Böhlen, P. (1987) *Proc. Natl. Acad. Sci. USA* **84,** 5277–5281.
20. Pandey, A., Shao, H., Marks, R. M., Polverini, P. J., and Dixit, V. M. (1995) *Science* **268,** 567–569.
21. Nishitoh, H., Ichijo, H., Kimura, M., Matsumoto, T., Makishima, F., Yamaguchi, A., Yamashita, H., Enomoto, S., and Miyazono, K. (1996) *J. Biol. Chem.* **271,** 21345–21353.
22. ten Dijke, P., Yamashita, H., Sampath, T. K., Reddi, A. H., Estevez, M., Riddle, D. L., Ichijo, H., Heldin, C.-H., and Miyazono, K. (1994) *J. Biol. Chem.* **269,** 16985–16988.
23. Ichijo, H., Yamashita, H., ten Dijke, P., Eto, Y., Heldin, C.-H., and Miyazono, K. (1993) *Biochem. Biophys. Res. Commun.* **194,** 1508–1514.
24. Rosenzweig, B. L., Imamura, T., Okadome, T., Cox, G. N., Yamashita, H., ten Dijke, P., Heldin, C.-H., and Miyazono, K. (1995) *Proc. Natl. Acad. Sci. USA* **92,** 7632–7636.
25. Morita, I., Kanayasu, T., and Murota, S. (1984) *Biochim. Biophys. Acta* **792,** 304–309.
26. Kanda, S., Landgren, E., Ljungström, M., and Claesson-Welsh, L. (1996) *Cell Growth Differ.* **7,** 383–395.
27. Vassalli, J. D., Dayer, J. M., Wohlwend, A., and Belin, D. (1994) *J. Exp. Med.* **159,** 1653–1668.
28. Zigmond, S. H., and Hirsch, J. G. (1973) *J. Exp. Med.* **137,** 387–410.
29. Sato, Y., Shimada, T., and Takaki, R. (1991) *Biochem. Biophys. Res. Commun.* **180,** 1098–1102.
30. Bonewald, L. F., Kester, M. B., Schwartz, Z., Swain, L. D., Khare, A., Johnson, T. L., Leach, R. J., and Boyan, B. D. (1992) *J. Biol. Chem.* **267,** 8943–8949.
31. Johnson-Pais, T. L., and Leach, R. J. (1996) *Exp. Cell Res.* **226,** 67–74.
32. Ishidou, Y., Kitajima, I., Obama, H., Maruyama, I., Murata, F., Imamura, T., Yamada, N., ten Dijke, P., Miyazono, K., and Sakou, T. (1995) *J. Bone Miner. Res.* **10,** 1651–1659.
33. Folkman, J. (1986) *Cancer Res.* **46,** 467–473.
34. D'Amore, P. A., and Thompson, R. W. (1987) *Annu. Rev. Physiol.* **49,** 453–464.
35. Pepper, M. S., Ferrara, N., and Orci, L. (1991) *Biochem. Biophys. Res. Commun.* **181,** 902–906.
36. Mandriota, S. J., Seghezzi, G., Vassalli, J.-D., Ferrara, N., Wasi, S., Mazzieri, R., and Mignatti, P. (1995) *J. Biol. Chem.* **270,** 9709–9716.
37. Fidler, I. J., and Ellis, L. M. (1994) *Cell* **79,** 185–188.
38. Wiseman, D. M., Poverini, P. J., Kamp, D. W., and Leibovich, S. J. (1988) *Biochem. Biophys. Res. Commun.* **157,** 793–800.
39. Pertovaara, L., Kaipainen, A., Mustonen, T., Orpana, A., Ferrara, N., Saksela, O., and Alitalo, K. (1994) *J. Biol. Chem.* **269,** 6271–6274.
40. Schor, S. L. (1994) *Prog. Growth Factor Res.* **5,** 223–248.
41. Storm, E. E., Huynh, T. V., Copeland, N. G., Jenkins, N. A., Kingsley, D. M., and Lee, S.-J. (1994) *Nature* **368,** 639–643.
42. Thomas, J. T., Lin, K., Nandedkar, M., Camargo, M., Cervenka, J., and Luyten, F. P. (1996) *Nature Genet.* **12,** 315–317.
43. Hötten, G. C., Matsumoto, T., Kimura, M., Bechtold, R. F., Kron, R., Ohara, T., Tanaka, H., Satoh, Y., Okazaki, M., Shirai, T., Pan, H., Kawai, S., Pohl, J. S., and Kudo, A. (1996) *Growth Factors* **13,** 65–74.

Received April 3, 1997
Revised version received May 26, 1997

EXPERIMENTAL CELL RESEARCH **235,** 227–237 (1997)
ARTICLE NO. EX973672

Antibody Cross-Linking of the Thymocyte-Specific Cell Surface Molecule CTX Causes Abnormal Mitosis and Multinucleation of Tumor Cells[1]

Jacques Robert,*[,2] Deborah M. Brown,* Louis Du Pasquier,† and Nicholas Cohen*

**University of Rochester Medical Center, Rochester, New York 14642; and †Basel Institute for Immunology, CH-4005 Basel, Switzerland*

The thymocyte-specific cell surface molecule CTX is a developmentally regulated type I transmembrane protein of the immunoglobulin superfamily which, in the amphibian *Xenopus,* is exclusively expressed by a large fraction of cortical thymocytes and by different cell lines derived from independent spontaneous thymic tumors. Antibody cross-linking of CTX *in vitro* inhibits the growth of tumor cells and causes morphological alterations. Cells divide abnormally, accumulate in the G2/M phase of the cell cycle, and become multinucleated. This demonstrates, for the first time, that multinucleation can be induced by specifically cross-linking a cell surface molecule. © 1997 Academic Press

INTRODUCTION

The multiple genetic changes that occur during the transformation of normal cells into cancer cells are thought to be facilitated by a loss of fidelity in the processes that replicate, repair, and segregate the genome [1]. States such as polyploidy or multinucleation, for example, may change the "genetic balance" and result in gene disregulation. Multinucleated cells have been observed in biopsies of a variety of human tumors [2, 3], and it has been proposed that multinucleation contributes to abnormal mitosis and aneuploidy [3, 4].

During the initial steps of neoplastic transformation *in vivo,* multinucleation, abnormal mitosis, and aneuploidy are relatively rare events. Therefore, investigators interested in studying the aberrant cellular mechanisms responsible for such genomic instabilities have resorted to inducing multinucleation and polyploidy of transformed mammalian cell lines *in vitro* with deacetylases, topoisomerases, kinases, and other inhibitors of the spindle apparatus [4, 6]. These drugs generally induce cell cycle arrest during the G2 or M phase. During prolonged drug treatment, however, a fraction of arrested cells enter G1 again without having completed mitosis; this suggests some deregulation or dysfunction of the checkpoint complex at the G2/M transition [7]. Another possible (not mutually exclusive) mechanism responsible for multinucleation involves the failure of cytokinesis [1, 8]. In some instances, multinucleated tumor cells have been shown to retain their capacity to proliferate *in vitro* [9] as well as *in vivo* [4]. Thus, such multinucleated cells could function as precursors of newly arising tumor variants.

Although studies of the effects of chemical inducers on tumor cell lines can provide information about mechanisms responsible for multinucleation *in vitro,* little is known about those signals or factors that can induce or favor multinucleation *in vivo.* Indeed, the possibility that aberrant modulation signals from cross-linking cell surface receptors may contribute to deregulation of the cell cycle and the genetic instabilities that follow has not been considered. Receptor–ligand interactions characterize the intrathymic development of mammalian T-cells, where a complex series of differentiation and selection events are, at least in part, regulated by interactions of the T-cell receptor (TCR) of immature thymocytes with products of the major histocompatibility complex (MHC) expressed by the thymic stroma (reviewed in [10]). These programmed intrathymic interactions also involve receptors or coreceptors other than the TCR [11–14]. In this regard, CTX, a new surface receptor that has been recently identified in the amphibian *Xenopus* and implicated in thymocyte selection and/or differentiation [15] may be of interest. This receptor is a developmentally regulated type I transmembrane glycoprotein with a long cytoplasmic tail. It is a member of the immunoglobulin (Ig) superfamily and is expressed exclusively by a major subpopulation of *Xenopus* cortical thymocytes that corresponds to the $CD4^+/CD8^+$ double-positive immature thymocyte of mammals [15]. Given the structural and functional similarities between the

---

[1] To view time-lapse video of cultured cells go to www.bii.ch/movies/louisplus.html.

[2] To whom correspondence and reprint requests should be addressed at Department of Microbiology and Immunology—Box 672, University of Rochester Medical Center, 601 Elmwood Ave., Rochester, NY 14642. Fax: (716) 473-9573. E-mail: robert@uhura.cc.rochester.edu.

0014-4827/97 $25.00
Copyright © 1997 by Academic Press
All rights of reproduction in any form reserved.

mammalian and *Xenopus* thymus (reviewed in [16]), the mechanisms underlying thymocyte differentiation are also likely to be similar in the two species.

Although *in vivo,* CTX is only expressed by a cell subset that is likely to be noncycling (the majority of double-positive mammalian thymocytes are resting cells [17]), CTX is also strongly expressed by several stable lymphoid tumor cell lines derived from spontaneous thymic tumors in *Xenopus.* These cell lines resemble rare mammalian leukemias with a dual T/B-cell phenotype since they have undergone complete Ig in-frame heavy and light chain gene rearrangement [18], and they express several T-cell markers (e.g., ß-chain TCR message, CD8, CD5). These unusual spontaneous thymic tumors have been observed five times in genetically different adults of our animal colony. Similar thymic tumors have also been reported by other laboratories [19]. When CTX-expressing lymphoid tumor cells of the *Xenopus* cell line B3B7 are incubated in culture wells coated with the anti-CTX monoclonal antibody (mAb) X71, 30–50% of them rapidly undergo a morphological change (elongation and flattening) that is followed by an inhibition of growth [20]. Growth inhibition does not occur with antibody in solution, is not due to apoptosis, and is not accompanied by intracellular calcium influx [20].

In this paper, we report that after CTX cross-linking at the cell surface with the anti-CTX mAb X71, cells accumulate in the G2/M phase of the cell cycle and then undergo defective mitosis and multinucleation.

MATERIALS AND METHODS

Reagents and cell lines. The lymphoid tumor cell lines B3B7 and ff-2 were derived from spontaneously arising thymic tumors [21, 22]. Culture media and conditions for perpetuating these lines *in vitro* have been described elsewhere [21, 23]. The following *Xenopus*-specific mAbs were used in this study: X71 (IgG1), which detects CTX [15]; X46 (IgG1), which recognizes an unnamed 80-kDa lymphoid tumor-specific cell surface antigen (Robert, unpublished); AM22, which detects the *Xenopus* homologue of CD8 [24] and 2B1, which reacts with a CD5-equivalent of *Xenopus* [25].

In vitro stimulation. Ninety-six- and 24-well culture plates were aseptically coated overnight at 4°C with 100 and 500 μl (100 μg/ml), respectively, of a goat anti-mouse Ig antibody (Sigma, St. Louis, MO), washed, and blocked 20 min at room temperature with 1% BSA in amphibian PBS (APBS). Supernatants containing the mAb X46 or X71 were then absorbed twice to the plates for 2–4 h at room temperature (2× 100 μl or 2× 500 μl, respectively). After an additional wash with APBS, B3B7 or ff-2 cells were added to the coated plates at a concentration of 8×10^3 cells/well in a total volume of 200 μl for 96-well plates, or 2×10^5 cells/well in a total volume of 1 ml for 24-well plates, and incubated for 24 to 72 h at 26°C.

Cells were recovered by replacing the culture medium with 0.1% EDTA in APBS. After 5 min incubation at room temperature, cells were collected by gentle agitation and aspiration with a sterile pipette. This treatment does not damage the cells, at least as judged by the unchanged surface expression of different surface markers (CD8, CD5, CTX) and by the absence of significant cell death (determined by trypan blue dye exclusion).

Alternatively, cells were cultured (2×10^4 cells in a total volume of 400 μl) on microscope slides with independent sterile chambers (Nunc No. 177402, NY) that had been precoated with X71 or X46 mAbs as described for the 24-well culture plates. At several time points, cells were fixed in 100% methanol for 5 min at room temperature and blocked in APBS containing 1% BSA, 1% goat serum, and 1% normal *Xenopus* serum. Anti-tubulin antibody (Boehringer Mannheim, Indianapolis, IN) was added at a 1:25 dilution and incubated for 1 h at room temperature. FITC-conjugated goat anti-mouse IgG was added at a dilution of 1:100 and incubated at room temperature for 1 h. Finally, the DNA was stained with 0.1 μg/ml 4′,6′-diamidine-2′-phenylindole dihydrochloride (DAPI) (Boehringer Mannheim) in methanol for 1 min at room temperature. Slides were coverslipped with DABCO (9 parts 2.5 mg/ml 1,4-diazybicyclo(2,2,2)octane in glycerol and 1 part APBS) and photographed using a BX-40 microscope (Olympus, Lake Success, NY) under UV excitation. For plasma membrane staining, cells were fixed 1 h in 2% paraformaldehyde and permeabilized with 0.2% TX-100. Plasma membranes were stained with PKH26-GL (Sigma, St. Louis, MO) and DNA with 0.1 μg/ml Hoechst 33258 (Molecular Probes, Inc., OR) in water.

Time-lapse direct videorecording of cells in 96-well culture plates (maintained at 26°C) was performed for 3 days with an inverted Zeiss Axiovert microscope equipped with Nomarsky optics and a CO_2 chamber.

Cell cycle analysis and BrdU staining of B3B7 cells. B3B7 and ff-2 cells were cultured at a density of 1×10^6 cells/well in a total volume of 4 ml in 6-well culture plates that had been coated with anti-X46 or anti-X71 mAb as described above. Plates were incubated for 24, 48, or 72 h at 26°C. Cells were then counted and fixed at a concentration of 1×10^6 cells/3 ml of 75% ethanol for 18–20 h at 4°C. One $\times 10^6$ cells per group were treated with 0.5 ml of RNase A (Sigma) at 1 mg/ml for 30 min at room temperature. The cells were washed three times and resuspended in 1 ml of a 10 μg/ml solution of propidium iodide (PI). The cells were then incubated for 30 min at 4°C and 10,000 cellular events were analyzed on an EPICS profile flow cytometer (Coulter Corp.). Histograms were analyzed using Multicycle software (Coulter Corp.).

Double staining of B3B7 cells for BrdU incorporation and DNA content was performed as previously described [26], with minor modifications for *Xenopus* cells. The cells were labeled with 5-bromo-2′-deoxyuridine-5′-monophosphate (BrdU) (Boehringer Mannheim) at a final concentration of 30 μM for the last 6 h of culture. The cells were then fixed at a concentration of 1×10^6 cells/3 ml of 75% ethanol for 18–20 h at 4°C. After fixation, B3B7 cells were incubated with a 0.2 mg/ml pepsin solution in 2 N HCl for 20 min at 37°C to disrupt cells and isolate nuclei. The nuclei were washed and blocked with a 2% solution of FBS in 1× PBS for 20 min at room temperature. After washing, the nuclei were incubated with a FITC-conjugated mouse IgG1 anti-BrdU antibody (Boehringer Mannheim) for 45 min at room temperature. Nuclei were then washed and treated with RNase A and PI as described above, and 10,000 events were analyzed on an ELITE flow cytometer (Coulter Corp.). Centrifugal elutriation has been described elsewhere [26].

RESULTS

Cross-Linking CTX with X71 mAb Increases the Incidence of Multinucleated Tumor Cells

Figure 1 shows the results of a representative experiment in which B3B7 and ff-2 cells were incubated 48 h on microscope chamber slides coated with either anti-CTX mAb X71 or isotype-matched mAb control and stained directly in the chamber slides with an

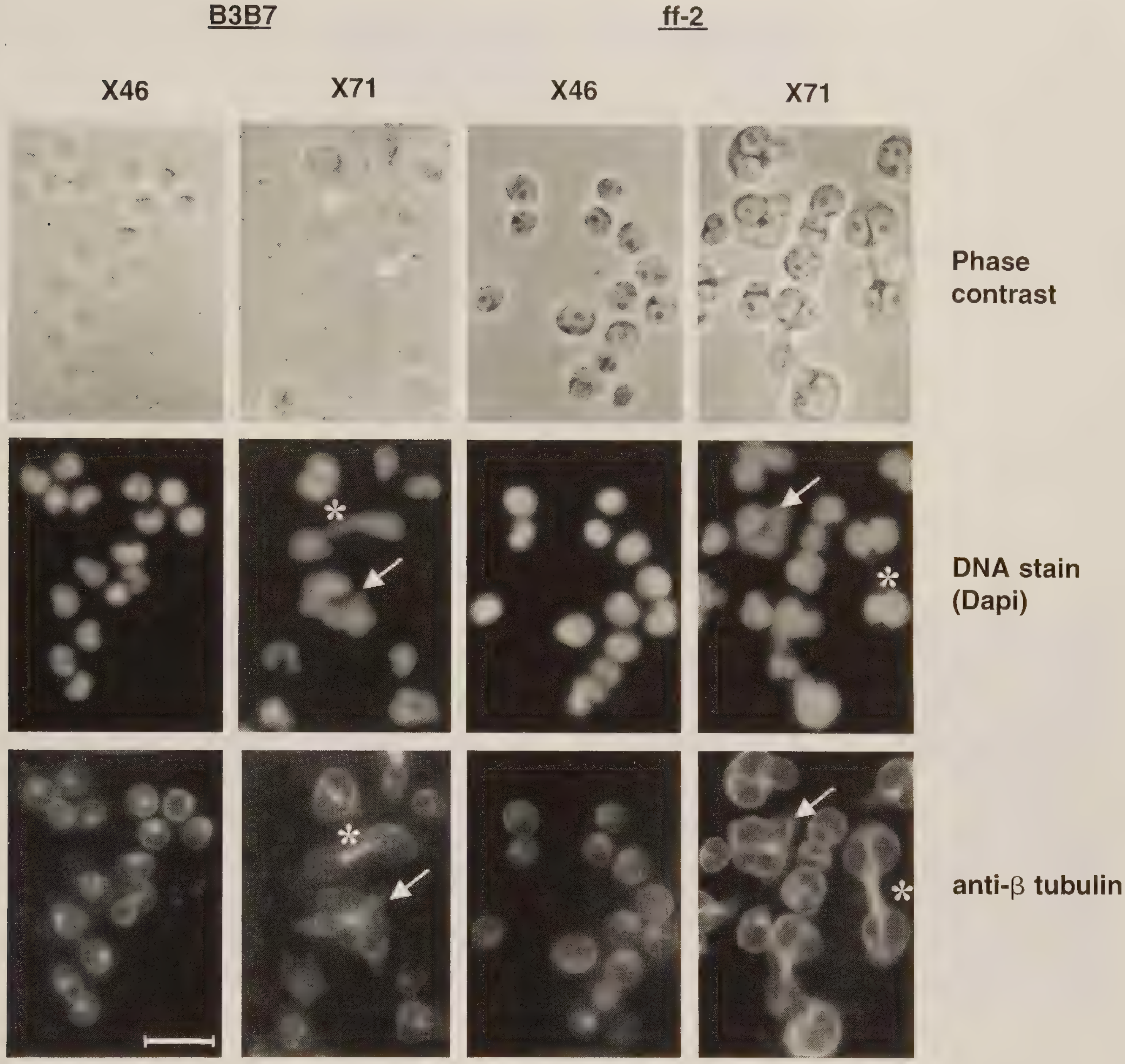

FIG. 1. Anti-CTX mAb X71 induces morphological changes, alteration of the microtubule network, an abnormal cellular "bridge"(asterisks), and multinucleation (arrows) of cells from two different thymic tumor- derived cell lines, B3B7 and ff-2. Chamber slides were precoated with goat anti-mouse Ig followed by X71 (anti-CTX) mAb or X46 (isotype-matched control). Tumor cells (2×10^4 per well) were incubated for 48 h at 26°C. The cells were then stained with anti-β-tubulin mAb and DAPI. Cells were photographed using an Olympus BX-40 microscope. Bar, 25 μm.

anti-β-tubulin antibody and a DNA dye to reveal both cytoplasmic and nuclear details. In X71-coated chambers, both B3B7 and ff-2 cells that are derived from independent spontaneous thymic tumors undergo morphological transformations. They become flattened and tightly adherent to the plate, and their phase-dense nucleoli become apparent. The first morphological alteration was detected 30 min after incubation in X71-coated chambers. Longer incubation for 2–3 days resulted in the appearance of larger cells with 3–5 phase-dense nucleoli, suggesting that they had become multinucleated. In certain instances, a cellular "bridge" was formed between two cells that appeared to be undergoing cytokinesis, but had been arrested in that position at the time of fixation (Figs. 1 and 2C asterisks).

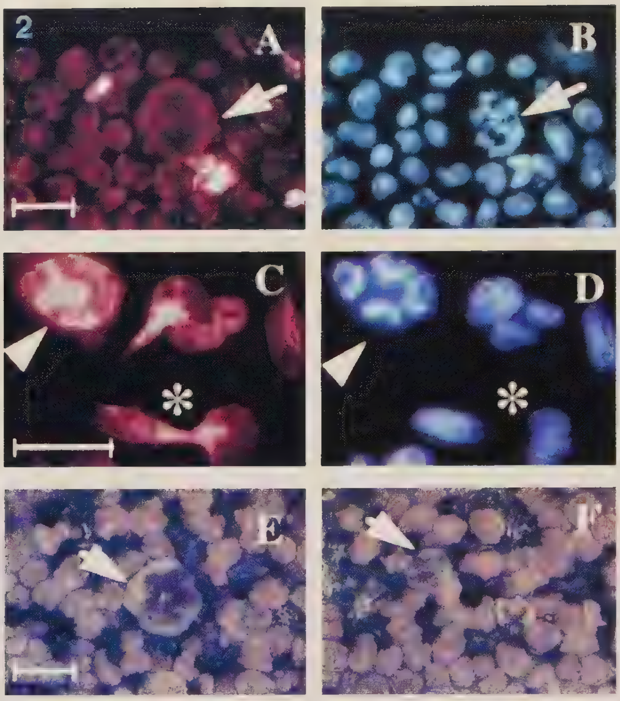

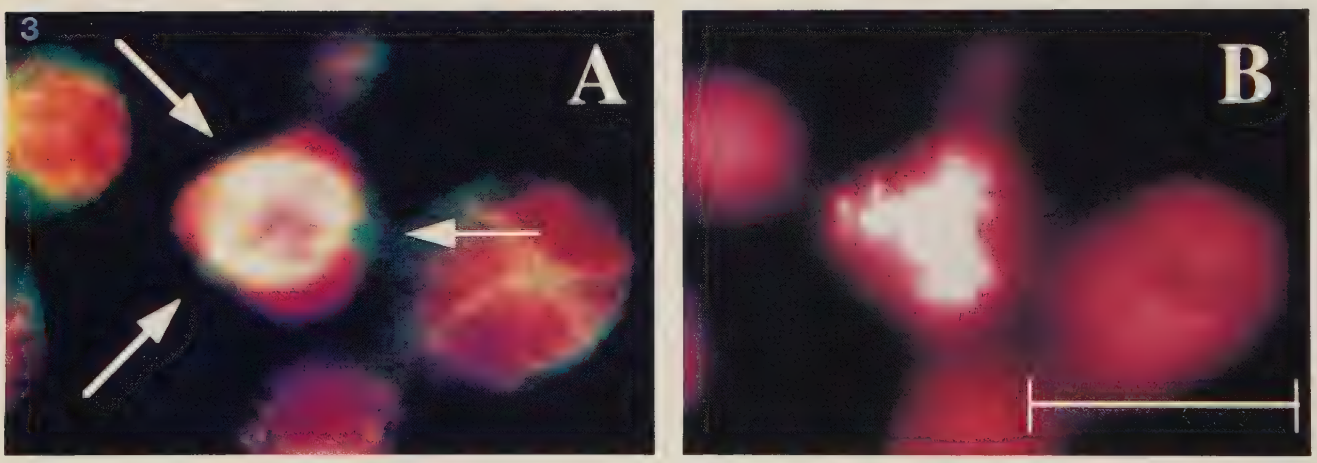

FIG. 2. Anti-CTX mAb X71 induces abnormal mitosis (arrows) and an abnormal cellular "bridge"(asterisks) of the thymic tumor-derived cell line B3B7. Chamber slides were precoated with goat anti-mouse Ig followed by X71 (anti-CTX) mAb. (A to D) Tumor cells (2×10^4 per well) were incubated 48 h at 26°C, directly fixed with 2% paraformaldehyde, and permeabilized with 0.2% TX-100. Plasma membranes (A, C) were stained with PKH26-GL (Sigma) and DNA (B, D) with Hoechst 33258. Cells were photographed using an Olympus BX-40 microscope. (E, F) Giemsa-stained cytospin from B3B7 cells cultured for 48 h in X71-coated wells. Only normal mitosis were observed in control experiments with immobilized isotype-matched X46 mAb (data not shown). Bar, 25 μm.

FIG. 3. Some B3B7 cells treated for 48 h in X71-coated chamber slides displayed aberrant mitosis. Anti-tubulin staining and PI show a spindle located between three centrioles (arrows). Bar, 25 μm.

In addition to cellular alterations, multinucleation occurred in some B3B7 or ff-2 cells after a 24-h incubation with the anti-CTX mAb X71 and become more frequent after 48 h. (Fig. 1). Many large cells containing more than one nucleus (some displaying five nuclei) were seen, as was aberrant mitosis in X71-coated chambers (Fig. 2). Some of these dividing cells contained a higher number of chromosomes than normal (Fig. 2B) and presented abnormal segregation patterns, involving multiple anaphases (Fig. 2D). Similar observations (large multinucleated cell, Fig. 2E, and abnormal mitosis, Fig. 2F) were made on a cytospin preparation of B3B7 and ff-2 cells recovered from culture plates after treatment with EDTA and stained with Giemsa. The use of a dye specific for the plasma membrane (PKH26-GL) further substantiates the occurrence of abnormal mitosis involving a high number of chromosomes inside single cells (Fig. 2A). In a few cases, cells undergoing aberrant mitosis with the spindle located between three centrioles was observed using anti-tubulin staining and PI (Fig. 3).

Although B3B7 cells cultured in the presence of the isotype-matched X46 mAb also adhered tightly to these wells (B3B7 incubated in wells coated with either X71 or X46 mAb cannot be removed by simple washing), they did not become multinucleate, increase in size, or stain abnormally with anti-tubulin antibody (Fig. 1). No morphological alteration of ff-2 cells was induced by X46 mAb either. Although in this situation, ff-2 cells adhered less strongly because of their lower surface expression of X46 antigens, cross-linking ff-2 (or B3B7) tumor cells with the *Xenopus* CD5-equivalent 2B1 mAb, with an anti-*Xenopus* CD8 mAb (AM22), or with the XT-1 mAb (which recognizes surface molecules expressed by thymocytes and a T-cell subset) did cause the tumor cells to tightly adhere to the plastic substrate, and it did not result in the dramatic morphological alterations or multinucleation observed with X71. (These surface antigens are all highly expressed on the two tumor cell lines [22].) Finally, changes induced by X71 were not simply the result of adhesion to the plastic surface of the culture wells since "artificial adhesion" of the tumor cells with poly-L-lysine killed the cells within a few hours without inducing any nuclear alteration (data not shown).

Kinetics and Quantification of Multinucleation

Multinucleated cells were seen as early as 6 h after incubation on X71-coated slides (Fig. 4A, first histogram). The fraction of multinucleated cells increased during the following 2 days and reached a plateau in which about 30% of the total number of activated cells were multinucleated (Fig. 4A, second histogram). The kinetics of the increase in the number of nuclei per cell paralleled the increase in the number of multinucleated cells (Fig. 4B). Although apoptotic large multinucleated cells were seen, their number did not exceed 5% of the total cell number during the 8 days cells were cultured in X71-coated wells [20]. Control B3B7 cells treated with the isotype-matched X46 mAb did not show a significantly increased number of multinucleated cells during this time (Fig. 4A).

To obtain more detailed information on the fate of cells during mitosis following X71 stimulation, a videocamera was attached to an inverted microscope and the behavior of cells cultured in antibody-coated wells was recorded continuously. When compared with controls, cells incubated in X71-coated wells underwent fewer mitotic divisions, most of which were abnormal. At the moment of cytokinesis, the cells did not separate completely, and eventually they formed a single binucleated cell (Fig. 5A). Several of these cells with mitotic defects were observed for 2 to 3 days. After the first abortive mitosis, the two nuclei in the cell seemed to behave asynchronously, giving rise at the time of cytokinesis to three cells that fused back into a multinucleated cell. Some other large cells gave rise to four or even five well-separated cells that fused again into a giant multinucleated cell (Fig. 5B).

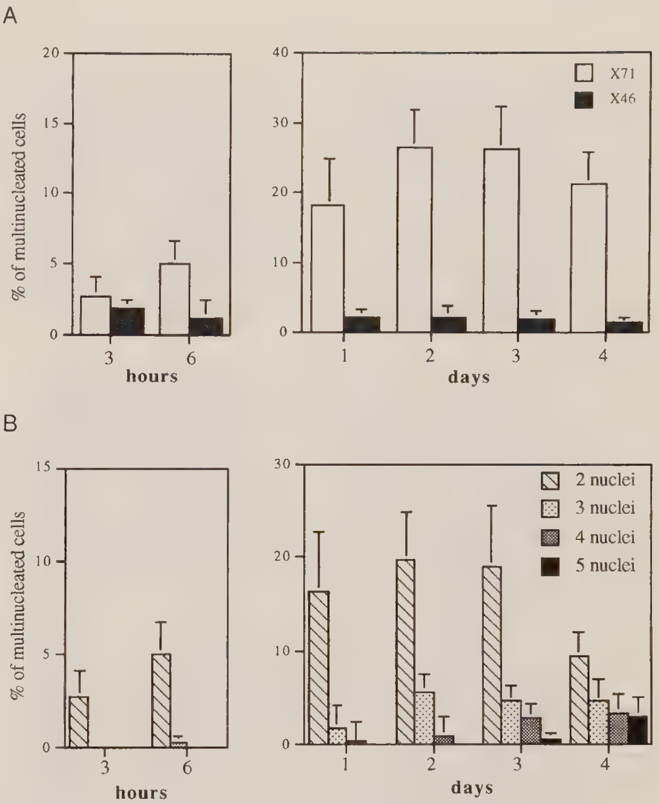

FIG. 4. Immobilized anti-CTX mAb X71 produces an increase in the number of multinucleated cells. (A) Percentage of total multinucleated B3B7 cells cultured for from 3 h (left panel) to 4 days (right panel) directly on microscope chambers coated with either X71 or X46 mAb (X46 is an isotype-matched control). (B) Detailed percentage of nuclei number per multinucleated cells in X71-coated chambers of the same experiment as in A. Cells in microscope slide chambers were directly fixed in paraformaldehyde and permeabilized with TX-100. Plasma membranes were stained with PKH26-GL (Sigma) and DNA with Hoechst 33258. The different cell fractions were counted in 10 different quadrants (200 cell/quadrants).

Cross-Linking CTX with X71 mAb Increases the Percentage of Cells in the G2/M Phase of the Cell Cycle

To further investigate the basis for the observed heterogeneity in morphological alterations induced by immobilized X71 mAb, we examined the relationships be-

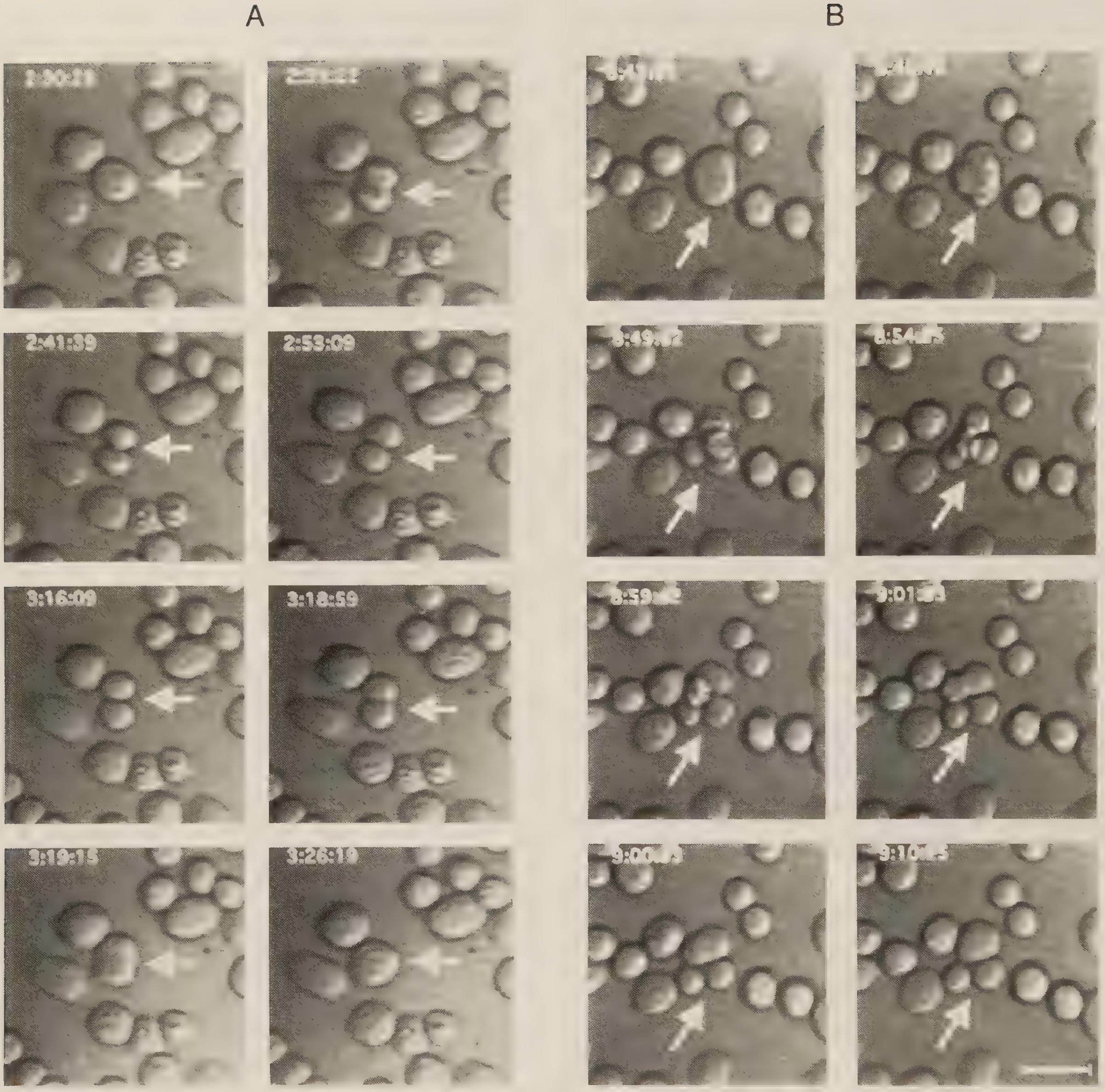

FIG. 5. Direct videorecording of two different cultures of cells in X71-coated 96-well culture plates performed for 48 h with a Nomarsky optics inverted Zeiss Axiovert microscope equipped with a CO_2 chamber maintained at 26°C. Time points are in the corner of each picture.

tween these changes and the cell cycle by flow cytometry of PI-stained cells. B3B7 and ff-2 cells were incubated in 6-well plates coated with anti-CTX antibody for 24 h. Table 1 shows the percentage of B3B7 cells in each phase of the cell cycle as determined by Multicycle software analysis (Coulter Corp.). Anti-CTX mAb induced an increase in the percentage of cells in the G2/M phase of the cell cycle, with a concomitant decrease in the percentage of cells in S phase. An increase of tumor cells in G2/M was already detectable after 6 h incubation in X71-coated wells, and the number of cells in the blocked cell fraction increased further during the following 14 h (approximately a threefold increase in this fraction compared with controls incubated with goat anti-mouse antibody or with X46 mAb).

Published data [20] as well as data from experiments repeated in the present study (data not shown) from [^{3}H]thymidine assays suggest that the proliferation of B3B7 cells is inhibited by 50% 24 h after cross-linking CTX. In contrast, PI staining of DNA (Table 1) indicates only a slight decrease in the percentage of cells in S phase and an increase of cells in the G2/M phase of the cell cycle.

To dissect this phenomenon further, two-color flow cytometric analysis was performed by staining DNA with PI and staining tumor cells incorporating BrdU (i.e., synthesizing DNA) with a fluorescein-conjugated antibody to BrdU. Figure 6 depicts a representative experiment in which profiles were obtained after a 24- or 48-h treatment of B3B7 cells with anti-CTX mAb and a 6-h pulse with BrdU. Control B3B7 cells incubated in plates coated with X46 showed a typical cell cycle pattern, with approximately 40% of cells incorporating BrdU and being in S phase. When CTX was cross-linked, this percentage decreased to 29%, but there was an increase in the percentage of cells in the G2/M phase that were not incorporating BrdU (Fig. 6, box 2). At 24 h, the percentage of G2/M cells was 3.5% in X46-coated control wells and 13% in X71-coated wells. By 48 h, the difference between X46- and X71-treated cells was less pronounced (4.4 and 9%, respectively), probably because of a dilution by normal cells. Once again, the percentage of cells in S phase was lower for X71-cross-linked cells than it was for X46-treated control cells (34% vs 42%, respectively). In addition, the mean fluorescence intensity (MFI) of BrdU staining of X71-treated (5.6) versus X46-treated (7.6) cells was reproducibly lower, suggesting that whereas the percentage of cells in S phase did not change markedly, the amount of DNA synthesis was decreased by CTX cross-linking. The number of cells recovered from wells coated with X46 relative to X71 mAbs supports this hypothesis. Specifically, the number of B3B7 cells retrieved from X46-coated wells doubled within 24 h, whereas the number of cells recovered from X71-coated wells was only slightly increased over the input cell number. We have previously reported [20] that the overall number of B3B7 cells cultured in wells coated with X71 did not markedly increase or drop and that the number of dead cells increased at a similar rate both in wells coated with X71 and X46 control mAb. This suggests that a fraction of cells are unresponsive to CTX cross-linking, and indeed a few normal divisions have been observed by videorecording and fluorescence microscopy. The growth inhibition effect determined on the whole cell population, therefore, is an underestimate when it is measured late. The reason a fraction of cells is not affected by X71 cross-linking is still unknown and we have been unsuccessful in our attempts to separate responsive from unresponsive cell populations.

Finally it should be noted that the increase of cells in the G2/M fraction seen by flow cytometry corresponds to the increase in the number of multinucleated cells observed by microscopy. Indeed, a microscopic analysis of the G2/M fraction obtained by cell sorting revealed the presence of binucleated cells (data not shown).

Effect of CTX Cross-Linking on Purified Cell Fractions According to Their Cell Cycle Phase

Cross-linking CTX on B3B7 cells appears to affect only a subset of the total treated population since only 50% are growth inhibited and ~20% are multinucleated (Figs 1, 2, and 4). To determine if the heterogeneity of the cells' response to CTX cross-linking depends on the stage of the cell cycle when the cells are exposed to the X71 mAb, we have isolated pure fractions of B3B7 and ff-2 cells (> 96% pure as determined by DNA analysis with flow cytometry) at three different phases of the cell cycle (G1, S, and G2/M) by centrifugal elutriation. The three different cell subpopulations had normal growth capacity (determined by tritiated thymidine incorporation) as well as a comparable level of surface expression of CTX, CD8, and CD5 molecules as determined by flow cytometry (data not shown). These cells were incubated on plates coated with X46 or X71 mAb and examined in proliferation assays and cell cycle analyses by one-color flow cytometry (only data with B3B7 cells are presented). Figure 7A demonstrates that regardless of their initial phase of the cell cycle (G1, S, or G2/M), CTX cross-linking of B3B7 cells induces a growth inhibition of 40–50% after 48 h as determined by thymidine incorporation. Furthermore, CTX cross-linking results in a similar higher percentage of cells in S phase for each of the three cell fractions (Fig. 7B). For example, 25–30% of cells initially in G1 phase (99% pure) were in S phase after 48 h culture in X71-coated, in contrast to 15% in control wells.

These data suggest that cross-linking CTX slows down normal progression through the cell cycle and results in an increase of cells in G2/M that later become multinucleated.

TABLE 1

Percentage of B3B7 Cells in Each Phase of the Cell Cycle after 20 h of Antibody Cross-Linking, as Determined by Flow Cytometry on Fixed Cells Stained with Propidium Iodide Using a Multicycle Software Analysis (Coulter Corp.)

	Goat anti-mouse Ig	X46	X71
G1	44.8 ± 3.1	46.7 ± 5.9	41.0 ± 5.4
S	41.5 ± 2.5	41.75 ± 4.3	31.9 ± 2.4
G2/M	13.6 ± 1.0	11.5 ± 3.0	27.1 ± 5.5

Note. Data represent the mean ± SD of four different experiments.

DISCUSSION

In vitro, multinucleation can be induced by a variety of drugs including inhibitors of the spindle apparatus, deacetylases, topoisomerases, and kinases. All these drugs act at the cytoplasmic or the nuclear level and induce a cell cycle arrest during the G2 or M [5]. The induction of a similar phenomenon by cross-linking a cell surface protein is new and suggests that genetic instability can be generated by stimuli coming from the microenvironment. Multinucleation and aberrant

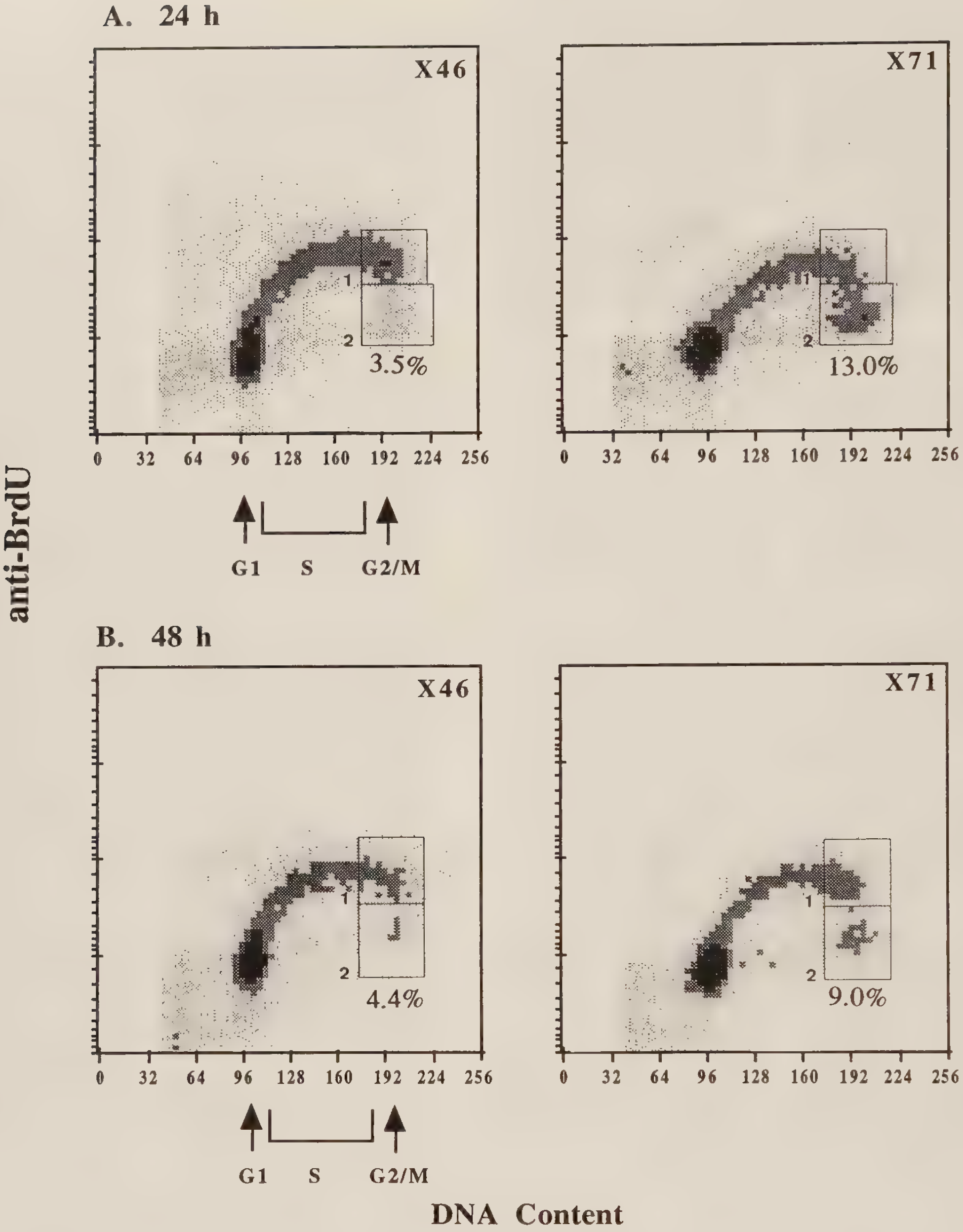

FIG. 6. Cell cycle analysis by two-color flow cytometry of B3B7 cells cultured for 24 h (A) or 48 h (B) in wells coated with either X71 or an isotype-matched control, X46. Cells were pulsed for 6 h with 30 m*M* bromodeoxyuridine (BrdU) at 26°C. Adherent cells were collected using 0.1% EDTA, fixed, and stained as described under Materials and Methods. 10,000 events were analyzed on an ELITE flow cytometer (Coulter Corp.).

mitosis have been reproducibly and significantly generated by treatment with immobilized anti-CTX mAb with two different tumor cell lines derived from distinct, genetically independent thymic tumors. The biological relevance of this phenomenon is supported by the facts that other immobilized antibodies that cause adherence of tumor cells (X46, anti-CD8, CD5, XT1) do not induce any change of ploidy and that mechanical adherence by poly-L-lysine kills the cells within a few hours without any nuclear alteration.

Karyotypic alterations like chromosome or whole genome changes are common in cancer cells [1]. The presence of cells with higher ploidy than the modal cell population is well documented in various mammalian tumor types and tumor cell lines [1, 9]. For example, the large multinucleated Reed–Sternberg cells charac-

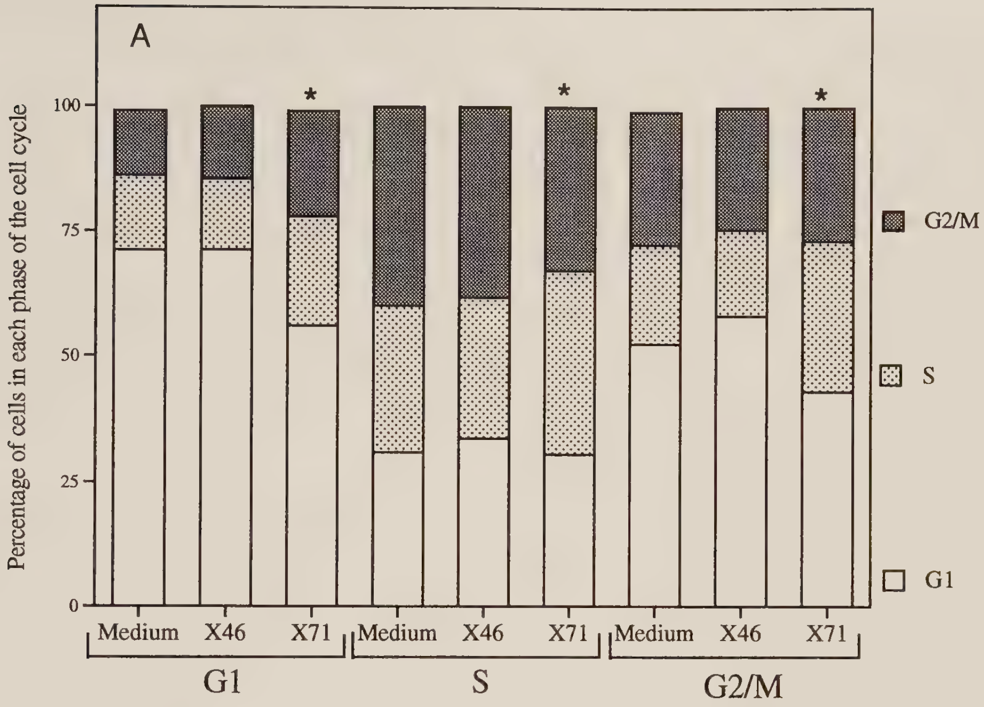

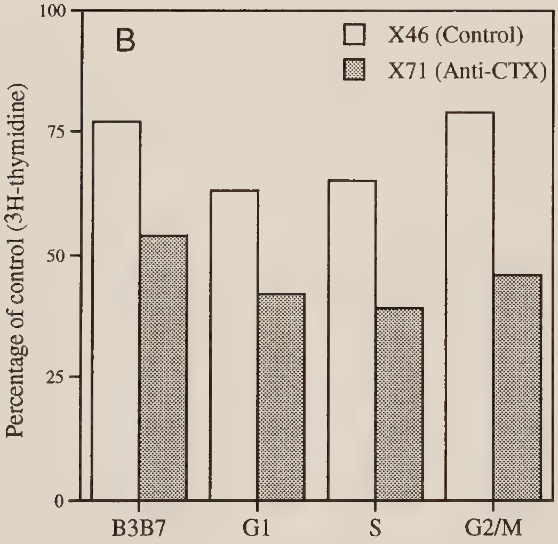

FIG. 7. Anti-CTX mAb X71 inhibits the growth of B3B7 tumor cells at all phases of the cell cycle. (A) B3B7 cells were subjected to centrifugal elutriation at a flow rate of 28 ml/min and an initial rotor speed of 3250 rpm [26]. Each fraction was assayed for cell size and purity using a Coulter Channelyzer. Confirmation of the cell cycle stage for each fraction was performed by propidium iodide staining, as described in the text. Cells were then incubated with medium, isotype-matched control X46, or anti-CTX X71 mAb for 48 h. Recovered cells were stained with PI and analyzed by flow cytometry. Percentage for each phase of the cell cycle was determined using Multicycle software (Coulter) with 10,000 events. (B) Proliferation assays of synchronized B3B7 cells cross-linked for 48 h. B3B7 cells obtained by elutriation were added (8,000/wells) in wells of a 96-well culture plate coated with goat anti-mouse alone, or goat anti-mouse and anti-CTX X71, or isotype-matched X46 mAbs. [^{3}H]thymidine was added to each well after 48 h for an additional 8 h, and cells were harvested using a Matrix 96 direct beta counter (Packard). The [^{3}H]thymidine incorporation (cpm) of controls for each corresponding to 100% is : G1 = 22,306 ± 599; S = 28,456 ± 903; G2 = 26,185 ± 747; and total population, 24,208 ± 992.

teristic of Hodgkin's lymphoma [27] overexpress p53 proteins, supporting their involvement as a malignant progenitor [2]. Cells morphologically similar to Reed–Sternberg cells have been described in *Xenopus* [28]. Multinucleation can be the source of genetic instability and of aneuploidy because of abnormal mitosis [4]. The process by which such transformations occur *in vivo* during neoplasia is largely unknown.

Spontaneous thymic tumors have been found in genetically distinct *Xenopus* on five different occasions in our frog colony, as well as in two additional occasions in another unrelated colony [19]. Although tumor cell lines derived from these different tumors vary in some features (e.g., expression of MHC antigens), they also exhibit striking common characteristics [22], one of which is their high level of CTX surface expression [20]. Therefore, the dramatic effects obtained by incubating these tumor cells with immobilized anti-CTX mAb X71 may provide some insight into both normal thymocyte differentiation and tumorigenesis. Of particular interest for oncogenic transformation is the observation that cross-linking a surface receptor can result in multinucleation. It is tempting to speculate, for example, that some defect at the level of CTX stimulation in the thymus may favor genetic imbalance and contribute to the generation of more tumorigenic cell variants.

In mammals, the G2/M transition of the cell cycle is controlled by a complex of cyclins and cyclin kinases, among which the $p34^{cdc2}$ kinase plays a key role (reviewed in [29, 30]). The coordination and control of the different events in mitosis by this checkpoint involves multiple tyrosine phosphorylation cascades. For example, the kinase activity of $p34^{cdc2}$, which is essential for entry in mitosis, requires the dephosphorylation of tyrosine 14 and 15 in the ATP-binding site. Although no obvious motifs known to be involved in signal transduction have been found in the long cytoplasmic tail of CTX (64 amino acids; [15]), perhaps it can associate with other cytoplasmic protein having kinase or phosphatase activity. It is conceivable, therefore, that CTX cross-linking induces a signal cascade of factors involved in the control of the G2/M transition and as such, CTX functions as a receptor involved in the modulation of cell cycle by external stimuli. Of particular interest is the report that overexpression of a cytoplasmic truncated T-cell protein, tyrosine phosphatase, induces multinucleation and asynchronous nuclear division as a result of a failure in cytokinesis [8]; all these effects very similar to those induced by CTX cross-linking.

The reason only a fraction of treated cells undergoes a detectable effect (50% with morphological alteration and 20% with multinucleation) is as yet unresolved. The whole tumor cell population at all stages of the cell cycle expresses CTX homogeneously at the cell surface as determined by flow cytometry, and cells synchronized into discrete cell cycle phases by centrifugal elutriation did not show a marked difference in their response to CTX stimulation. We have shown by using chemical cross-linker that a fraction of CTX (50% to 60%) is present at the cell surface as a noncovalent homodimer [20]. Whether X71, which preferentially recognizes the monomeric form, will induce the aforementioned morphological alteration and multinucleation may depend on the ratio between free monomers and dimers of CTX.

In conclusion, our results suggest that CTX may be a new type of surface receptor implicated in the control of the cell cycle. Furthermore, abnormal mitosis and multinucleation induced *in vitro* upon CTX cross-linking may provide a new model with which to study the regulation of the G2/M transition and cytokinesis.

We gratefully acknowledge Chantal Guiet and Janice Miller for their technical participation in this work, André Traunecker for his image analysis of video recording, and Dr. Max Cooper for kindly providing us with *Xenopus*-specific anti-CD5 mAb 2B1. We also thank Edith Lord for her criticisms and helpful discussions. Research at the University of Rochester was supported by Grant USPHS R37 HD-07901. The Basel Institute for Immunology was founded and is supported by F. Hoffman La Roche, Basel, Switzerland.

REFERENCES

1. Hartwell, H., and Kastan, M. B. (1994) *Science* **266,** 1821–1828.
2. Gupta, R. K., Patel, K., Bodmer, W. F., and Bodmer, J. G. (1993) *Proc. Natl. Acad.Sci. USA* **90,** 2817–2821.
3. Shackney, S. E., Smith, C. A., Miller, B. W., Burholt, D. R., Murtha, K., Giles, H. R., Ketterer, D. M., and Pollice, A. A. (1989) *Cancer Res.* **49,** 3344–3354.
4. Levine, D. S., Sanchez, C. A., Rabinovitch, P. S., and Reid, B. J. (1991) *Proc. Natl. Acad. Sci. USA* **88,** 6427–6431.
5. Hall, L. L., Th'ng, P. H., Guo, X. W., Teplitz, R. L., and Bradbury, E. M. (1996) *Cancer Res.* **56,** 3551–3559.
6. Bruno, S., Ardelt, B., Skierski, J. S., Traganos, F., and Darzynkiewicz, Z. (1992) *Cancer Res.* **52,** 470–473.
7. Usui, T., Yoshida, M., Abe, K., Osada, H., Isono, K., and Beppu, T. (1991) *J. Cell Biol.* **115,** 1274–1282.
8. Cool, D. E., Andreassen, P. R., Tonks, N. K., Krebs, E. G., Fischer, E. H., and Margolis, R. L. (1992) *Proc. Natl. Acad. Sci. USA* **89,** 5422–5426.
9. Hoz, C., and Baroja, A. (1993) *J. Cell Sci.* **104,** 31–36.
10. Kisielow, P., and von Boehmer, H. (1995) *Adv. Immunol.* **58,** 87–209.
11. Ritter, M. A., and Boyd, R. L. (1993) *Immunol. Today* **14,** 462–468.
12. Anderson, G., Jenkinson, E. J., Moore, N. C., and Owen, J. T. (1993) *Nature* **362,** 70–73.
13. Giunta, M., Favre, A., Ramarli, D., Grossi, C. E., and Corte, G. (1991) *J. Exp. Med.* **137,** 1537–1542.
14. Takeuchi, T., Tamamoto, T., Tamura, H., and Yamamoto, H. (1995) *Int. Immunol.* **7,** 583–590.
15. Chrétien, I., Robert, J., Marcuz, A., Garcia-Sanch, J., Courtet, M., and Du Pasquier, L. (1996) *Eur. J. Immunol.* **26,** 780–791.
16. Du Pasquier, L., Schwager, J., and Flajnik, M. F. (1989) *Annu. Rev. Immunol.* **7,** 251–275.

17. Pénit, C., Lucas, B., and Vasseur, F. (1995) *J. Immunol.* **154,** 5103–5113.
18. Du Pasquier, L., Courtet, M., and Robert, J. (1995) *Mol. Immunol.* **32,** 583–593.
19. Earley, E. M., Reinschmidt, D. C., Tompkins, R., and Gebhardt, B. M. (1995) *In Vitro Cell. Dev. Biol. Anim.* **31,** 255–257. [Letter].
20. Robert, J., Chrétien, I., Guiet, C., and Du Pasquier, L. (1997) *Mol. Immunol.* **34,** 133–143.
21. Du Pasquier, L. and Robert, J. (1992) *Dev. Immunol.* **2,** 295–307.
22. Robert, J., Guiet, C., and Du Pasquier, L. (1994) *Dev. Immunol.* **3,** 297–307.
23. Robert, J., and Du Pasquier, L. (1996) *in* Immunological Methods (Lefkovitz, I., Ed.), p. 2367, Academic Press, New York.
24. Du Pasquier, L., and Flajnik, M. F. (1990) *Dev. Immunol.* **1,** 85–95.
25. Jürgens, J. B., Gartland, L. A., Kishimoto, T., Du Pasquier, L., Horton, J. D., and Cooper, M. D. (1995) *J. Immunol.* **155,** 4218–4223.
26. Brown, M., and Phipps, P. (1996) *J. Immunol.* **157,** 1359–1370.
27. Stein, H., Herbst, H., Anagnostopoulos, I., Niedobitek, G., Dallenbach, F., and Kratzsch, C. (1991) *Ann. Oncol.* **2,** 33–38.
28. Baldwin, W. M., and Cohen, N. (1980) *in* Aspects of Developmental and Comparative Immunology (Solomon, I. J. B., Ed.), pp. 179–182, Pergamon Press, Oxford.
29. Nasmyth, K., and Hunt, T. (1993) *Nature* **366,** 634–635.
30. Norbury, C., and Nurse, P. (1992) *Annu. Rev. Biochem.* **61,** 441–470.

Received April 10, 1997
Revised version received June 2, 1997

EXPERIMENTAL CELL RESEARCH **235**, 238–244 (1997)
ARTICLE NO. EX973675

Nitric Oxide and cGMP Regulate Endothelial Permeability and F-Actin Distribution in Hydrogen Peroxide-Treated Endothelial Cells

Shu Ming Liu[1] and Tommy Sundqvist

Department of Medical Microbiology, Linköping University, Faculty of Health Sciences, Linköping, S-581 85, Sweden

We have previously reported that hydrogen peroxide (H_2O_2) has a concentration-dependent effect on endothelial permeability and F-actin distribution. In the present study, we considered the involvement of endogenous production of nitric oxide (NO) in the indicated effect of H_2O_2. This was done by measuring endothelial permeability to sodium fluorescein (MW 376 Da, Na-F) and to different-sized fluorescein-isothiocyanate-labeled dextrans (FITC-dextrans) and by staining F-actin with rhodamine-labeled phalloidin in cultured bovine aortic endothelial cells growing on filters. A low concentration of H_2O_2 (10^{-5} *M*) had no effect on either dense peripheral bands of F-actin (DPBs) or permeability. When *N*-nitro-L-arginine methylester (L-NAME), an inhibitor of NO production, was coadministrated with 10^{-5} *M* H_2O_2, DPBs were disrupted and the permeability to FITC-dextran 40 and FITC-dextran 70, but not to Na-F and FITC-dextran 20, was increased. Combining of 10^{-5} *M* H_2O_2 with L-arginine, a substrate for nitric oxide synthase, caused an increase in DPBs and a decrease in permeability to FITC-dextran 40 and FITC-dextran 70. L-arginine or L-NAME alone had no effect on either F-actin structure or endothelial permeability. A 10-fold higher concentration of H_2O_2 caused a disruption of DPBs and an increase in permeability; this could be prevented by adding L-arginine. An analogue of cGMP, i.e., 8-Br-cGMP, maintained DPBs and abolished the increase in permeability induced by the treatment with either 10^{-4} *M* H_2O_2 or a combination of H_2O_2 and L-NAME. These results suggest that the endogenous production of NO is involved in maintaining endothelial junctions in H_2O_2-treated cells and that this involvement occurs via a cGMP-dependent mechanism. © 1997 Academic Press

INTRODUCTION

The vascular endothelium is sensitive to oxidative injury mediated by oxygen metabolites that are either released from inflammatory cells [1, 2] or produced by the endothelial cells themselves [3–5]. Extracellularly added hydrogen peroxide (H_2O_2) provokes a variety of adverse biological effects in the endothelial cells, e.g., it impairs endocytic activity [6], alters cell morphology [7], and interferes with neutrophil adhesion [8]; all of these effects may be part of an acute inflammatory process. Nitric oxide (NO), a compound synthesized from L-arginine in a reaction catalyzed by nitric oxide synthase (NOS; for review, see 9) has previously been shown to have a direct anti-inflammatory effect on the vasculature *in vivo,* either by reducing microvascular permeability or by decreasing neutrophil adhesion (for review, see 10). On the other hand, NO can also increase endothelial permeability [11, 12] and it is known that NO can induce the generation of cGMP by activating soluble guanylate cyclase, not only in smooth muscle cells and platelets [13, 14] but in endothelial cells as well [15–17]. In cultured bovine thoracic aorta endothelial cells, H_2O_2 increases in the formation of L-citrulline from L-arginine in a concentration-dependent manner, and this effect can be prevented by adding inhibitors of NOS, NG-nitro-L-arginine, or NG-methyl-L-arginine [18]. The cited finding indicates that NO production is increased in H_2O_2-treated cells. Westendorp and coauthors found that cGMP is a mediator of endothelial permeability in human umbilical and pulmonary artery [19], but how this is associated with the structural change of endothelial cytoskeleton still remains unclear.

In an earlier study, we observed that H_2O_2 has a concentration-dependent effect on endothelial permeability and F-actin structure [6, 20]. The objective of the present study was to determine whether endogenous NO production and cGMP are involved in maintaining endothelial junctions in cultured bovine aortic endothelial cells treated with H_2O_2.

MATERIAL AND METHODS

Endothelial cell culture. Bovine aortic endothelial cells were isolated, cultured, and identified according to a method we described in a previous publication [20]. Cells were used from passage 8 up to

---

[1] To whom correspondence and reprint requests should be addressed at Department of Psychiatry and Langley Porter Psychiatric Institute, University of California, San Francisco, 401 Parnassus Avenue, Box 0984, San Francisco, CA 94143-0984. Fax: (415) 476-7320.

0014-4827/97 $25.00

Copyright © 1997 by Academic Press
All rights of reproduction in any form reserved.

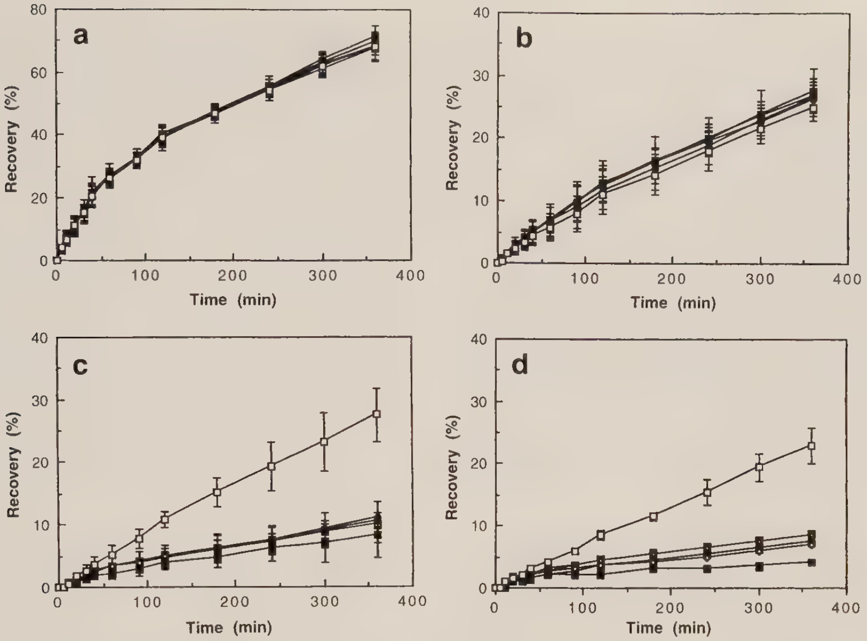

FIG. 1. Time course of endothelial permeability to four tracers of different size. Exposure to 10^{-5} M H_2O_2 (— ◇ —) had no effect on permeability to any of the tracers used. The addition of L-arginine together with 10 ^{5} M H_2O_2 (—■—) caused a slight decrease in permeability to FITC-dextran 40 (c) and FITC-dextran 70 (d), but had no effect on permeability to Na-F (a) or FITC-dextran 20 (b). Coadministration of L-NAME and 10^{-5} M H_2O_2 (—□—) resulted in an increase in permeability to FITC-dextran 40 (c) and FITC-dextran 70 (d) but not to FITC-dextran 20 (b) or Na-F (a). L-arginine (— ♦ —) or L-NAME (—◘—) alone had no effect on permeability, as compared to that seen in untreated endothelial cells (—⊡—). The values are means ± SD, $n = 4–8$.

passage 10. Culture-plate inserts equipped with filters with a pore size of 0.4 μm and a surface area of 0.6 cm^2 were purchased from the Millipore Corp. (Bedford, MA). The insert filters were coated with type-I collagen solubilized in 0.1 N HCl and placed in petri dishes (outer chamber) containing 5 ml of culture medium. A cell suspension (10 ml) with a density of 5×10^5 cells/ml was then prepared in a large bottle, and a 0.3-ml portion was placed in each insert (inner chamber). This was done to decrease variation in endothelial cell density on the filters.

Permeability test. All experiments were performed at 37°C on the fifth day after plating. The permeability of the endothelial monolayer was assessed by measuring the rate at which various fluorescent markers moved from the inner chamber (i.e., within the filter inserts) to the outer chamber of the insert in the petri dishes. Sodium fluorescein (Na-F, MW 376 Da) and fluorescein-isothiocynate-labeled dextran (FITC-dextran, with molecular weights of 20, 40, and 70 kDa) were used as markers. A fluorescent marker (0.3 ml) was dissolved in Krebs-Ringer glucose solution (KRG, 10 mM glucose phosphate buffer with 1 mM Ca^{2+} and Mg^{2+}, pH 7.3) and then added in the inner chamber of the culture-plate insert which was placed in a petri dish with 5 ml KRG as outer chamber. Fifty-microliter samples of the KRG medium in the outer chamber were withdrawn at various times for permeability assessments. One hundred percent of the recovery represents the concentration of adding 0.3 ml tracer directly into 5 ml KRG. The measurements were performed on a fluorescence spectrometer (Perkin–Elmer Ltd., Beaconsfield, Buckinghamshire, England) using an excitation wave length of 483 nm and an emission wave length of 517 nm. H_2O_2 (10^{-5} M), H_2O_2 (10^{-4} M), L-arginine (3×10^{-4} M), L-NAME (3×10^{-4} M), 8-Br-cGMP (10^{-3} M), or different combination of these compounds, were added to both the inner and the outer chamber. All reagents were purchased from Sigma Chemical Co. (St. Louis, MO).

Microfilament staining. The endothelial F-actin was stained according to a previously described method [18], with slight modifications. Cells growing on filters, which had been fixed in 3% paraformaldehyde for 30 min were washed with PBS and permeabilized with 0.1% Triton X-100 in PBS for 5 min. The cells were then washed again and incubated for 45 min at 37°C with rhodamine-labeled phalloidin (Molecular Probes, Eugene, OR) at a final dilution of 1:10. There after, the cells were gently rinsed several times with PBS, and the filters with cells were mounted on glass microscope slides in "ultimate mounting medium" [8 g H_2O, 2 g AIRVOL-203 (AIR PRODUCTS, Utrecht, Netherlands) mixed with 0.2 M Tris buffer, pH 8.5, and 4 ml Citifluor/Glycerol solution (CITIFLUOR Ltd, London, UK)]. The slides were examined in an axiophoto microscope equipped with a 100× oil-immersion objective (Karl-Zeiss, Oberkochen, Germany).

RESULTS

Effect of H_2O_2 on Endothelial Permeability

Exposure of the endothelial cells to 10^{-5} M H_2O_2 had no effect on the permeability to tracers of different sizes (Fig. 1). When L-NAME, an inhibitor of nitric oxide synthase, was coadministrated with this concentration of H_2O_2, there was an increase in permeability to FITC-dextran 40 and 70 (Figs. 1c and 1d), but not to Na-F or FITC-dextran 20 (Figs. 1a and 1b). Adding L-arginine, a substrate for nitric oxide synthase, together with 10^{-5} M H_2O_2 caused a slightly significant decrease ($P < 0.001$, Student's t test, $n = 8$) in permeability to

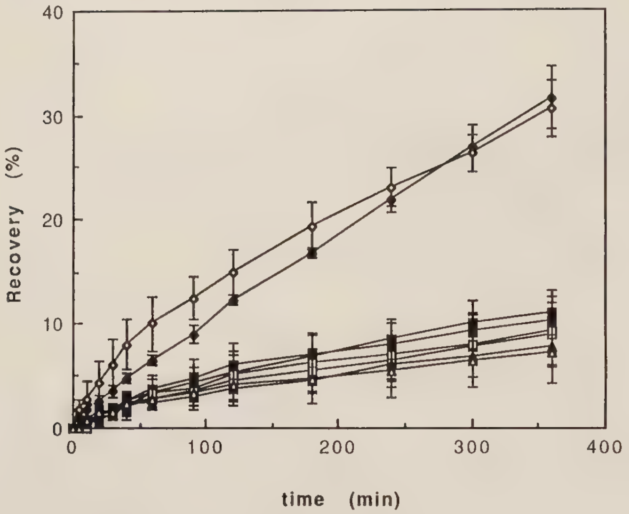

FIG. 2. Time course of endothelial permeability to FITC-dextran 40. Exposure to 10^{-4} M H_2O_2 increased the permeability (—♦—), and this increase was prevented when L-arginine was added together with 10^{-4} M H_2O_2 (—◘—). Coadministration of L-NAME and 10^{-4} M H_2O_2 (—◇—) resulted in a slightly larger increase in permeability at the beginning of the experiments, but the final level was the same as that reached when treating with 10^{-4} M H_2O_2 alone. Exposure to 8-Br-cGMP prevented the increase induced by either 10^{-4} M H_2O_2 (—□—) alone or 10^{-4} M H_2O_2 and L-NAME together (—△—). Permeability upon coadministration of 8-Br-cGMP, 10^{-4} M H_2O_2, and L-arginine (—▲—) or upon 8-Br-cGMP alone (—■—) did not differ from that observed in untreated cells (—⊡—). The values are means ± SD, $n = 4$.

FITC-dextran 40 and 70 (Figs. 1c and 1d). A 10-fold higher concentration of H_2O_2 (i.e., 10^{-4} M) increased the permeability to FITC-dextran 40 (Fig. 2), and this increase could be prevented by adding extracellular L-arginine. When cells were exposed to L-NAME and 10^{-4} M H_2O_2 simultaneously, the increase in permeability was initially more rapid than during the treatment with H_2O_2 alone; however, in both cases, permeability levels were the same after 6 h (Fig. 2). Trypan blue staining showed that none of the observed increases in endothelial permeability were due to a loss of cell viability (data not shown). L-arginine or L-NAME alone had no effect on endothelial permeability, as compared to untreated cells (Fig. 2).

The involvement of cGMP was further investigated by introducing an analogue of cGMP, i.e., 8-Br-cGMP, to the endothelial cells. The increase in endothelial permeability induced by either 10^{-4} M H_2O_2 or 10^{-4} M H_2O_2 and L-NAME combined was abolished by administration of 8-Br-cGMP (Fig. 2). However, when added alone, 8-Br-cGMP had no effect on the permeability of the endothelial cells.

Effect of H_2O_2 on endothelial F-actin distribution. All treatments that included 10^{-5} or 10^{-4} M H_2O_2 increased the density of the endothelial F-actin stress fibers spanning the cells (Fig. 4), as compared to such fibers in untreated cells (Figs. 3d and 3e). The lower concentration of H_2O_2 (10^{-5} M) had no effect on F-actin dense peripheral bands (DPBs; Fig. 4a), whereas the higher concentration (10^{-4} M) did (Fig. 4d). Coadministration of L-NAME and 10^{-5} M H_2O_2, but not L-arginine and 10^{-4} M H_2O_2, disrupted DPBs (Figs. 4c and 4e). L-arginine or L-NAME alone had no effect on F-actin structure (Figs. 3a and 3b), as compared to that seen in untreated cells (Figs. 3d and 3e).

The combination of 8-Br-cGMP and 10^{-4} M H_2O_2 or the combination of 8-Br-cGMP, 10^{-4} M H_2O_2, and L-NAME (Figs. 4g and 4i) prevented the disruption of DPBs and maintained the same actin filament pattern as seen in 10^{-5} M H_2O_2. On the other hand, exposure to 8-Br-cGMP alone induced the same filament pattern (Fig. 3c) as observed in untreated cells (Figs. 3d and 3e).

DISCUSSION

In the present study, we demonstrated that endogenous production of NO was involved in both the alteration of endothelial permeability and the redistribution of F-actin, induced by hydrogen peroxide via a cGMP-dependent mechanism.

Kuo *et al.* [21] examined artherosclerotic vessels and found that damaged endothelial cells appear to release very little nitric oxide and that nitric oxide production by the endothelium can be reestablished by administration of L-arginine. Weyrich *et al.* [22] obtained similar results in an investigation of postischemic coronary arteries exposed to high levels of L-arginine. Kubes and coworkers [23, 24] demonstrated that oedema in cats was increased by inhibitors of NO and they suggested that inhibition of NO production, resulting in loss of the protective effect of NO, could have caused an increase in permeability in the mesenteric circulation. On the other hand, the inhibition of NO has been found to decrease endothelial permeability and oedema formation in rat skin and paw [11] and also to lessen oedema in guinea-pig skin [12]. H_2O_2, which plays an important role in inflammation [7, 8], has been shown to increase intracellular Ca^{2+}, which is required for constitutive NOS and stimulates the formation of L-citrulline from L-arginine [18, 25, 26]. In our experiments, when 10^{-5} M H_2O_2, which had no effect on endothelial permeability, was coadministrated with L-NAME, the permeability was increased (Figs. 1c and 1d), suggesting that this low concentration of H_2O_2 may stimulate endogenous production of NO, which then plays a role in maintaining endothelial junctions. If NO production was inhibited by L-NAME, the junction could not have been kept as tight as in untreated cells,

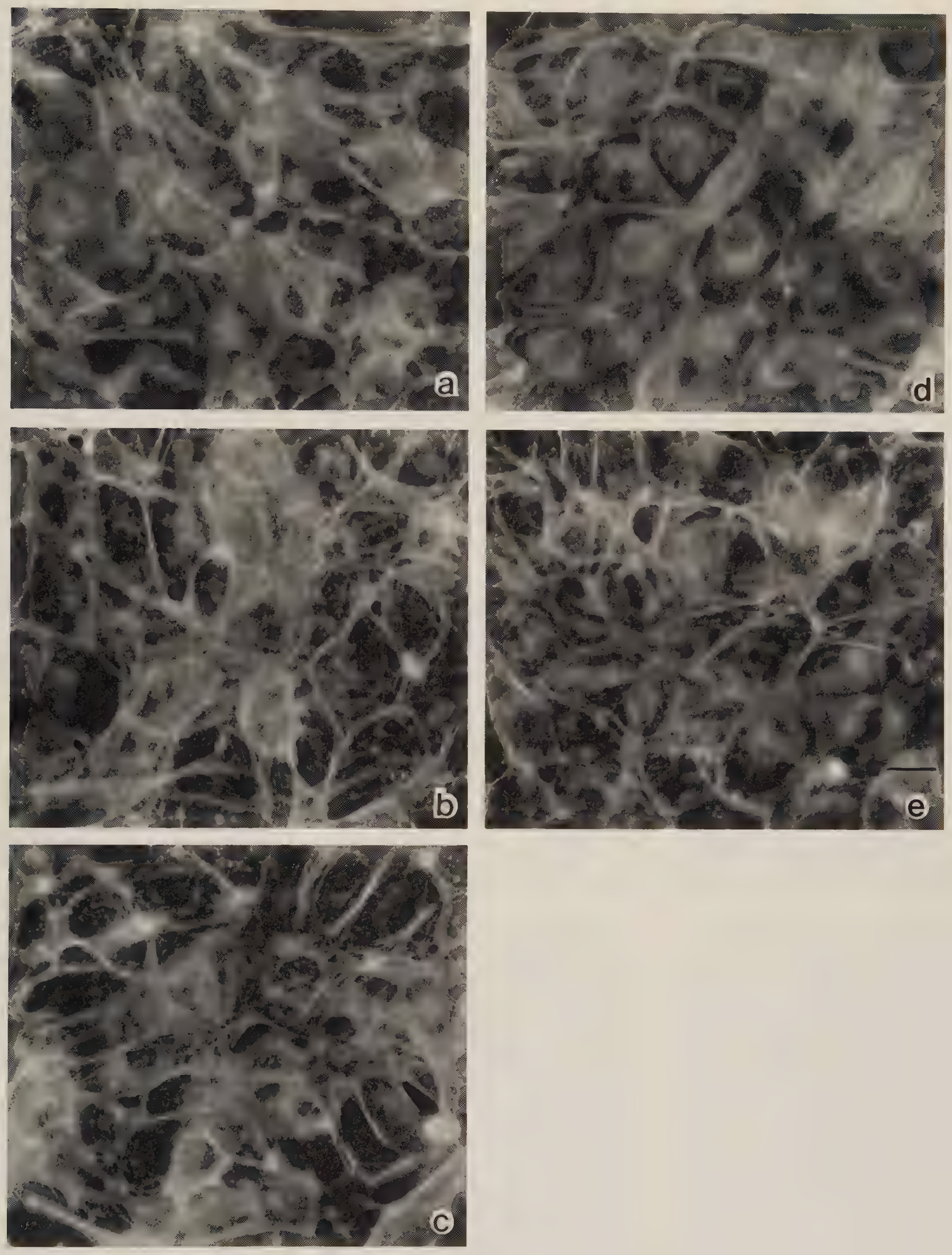

FIG. 3. Rhodamine-phalloidin staining of actin filament structures in endothelial monolayers that were grown on filters and then treated in different ways. The micrographs show cells incubated for 6 h in L-arginine (a), L-NAME (b), 8-Br-cGMP (c), and KRG-buffer (d), and also cells before such incubation (e). Bar, 10 μm.

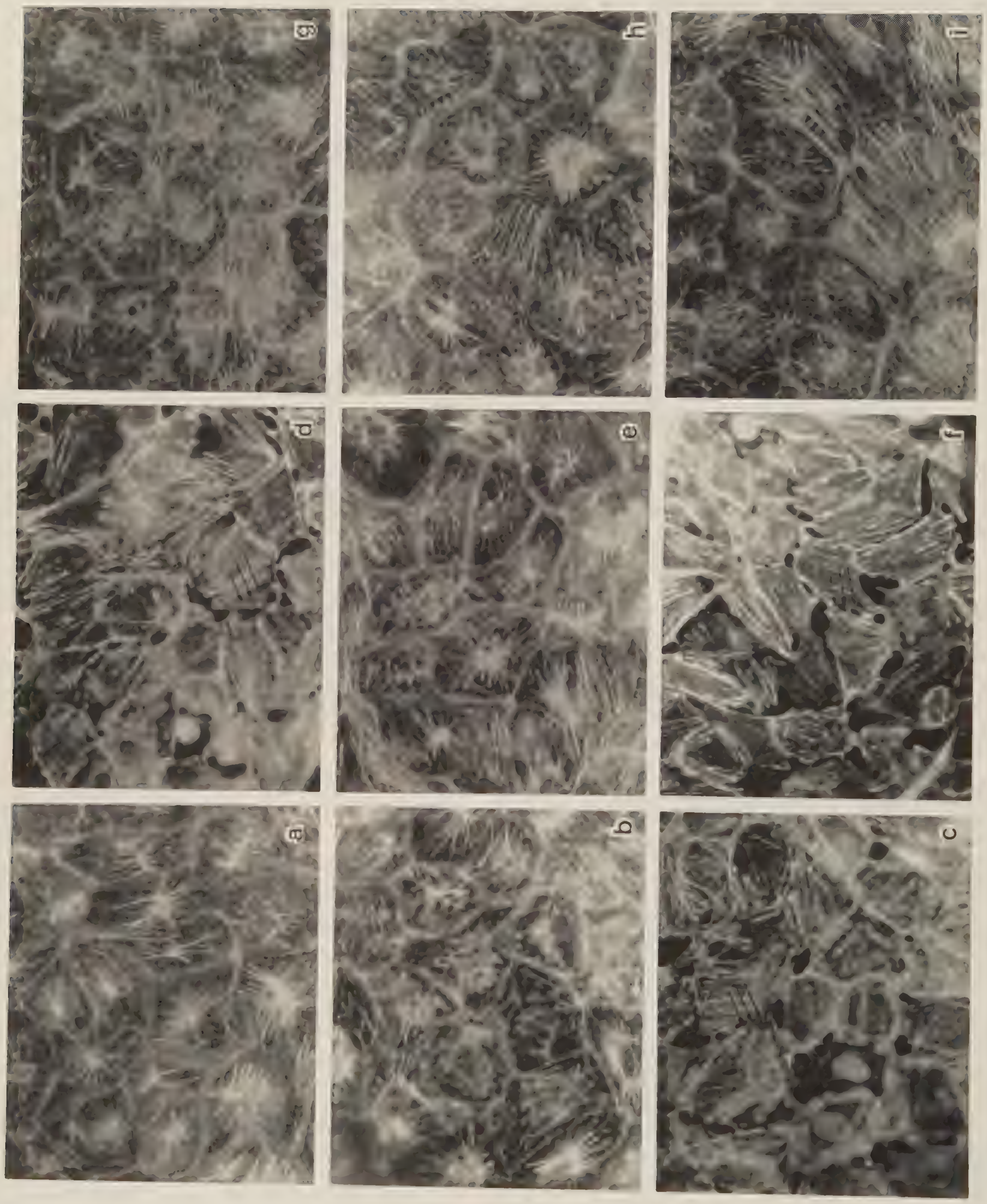
a
b
c
d
e
f
g
h
i

hence the permeability would have increased. A possible explanation for the lesser effect of NAME on the permeability of H_2O_2-treated cells to smaller molecules (e.g., Na-F and FITC-dextran 20; Figs. 1a and 1b) is that these molecules were already (i.e., normally) easily transported through a substantial number of the small pores, and only very few pores were enlarged enough by treatment with H_2O_2 and NAME to allow the entrance of FITC-dextran 40 and 70, two compounds which were only slightly permeable in untreated cells. The fact that the addition of L-arginine together with 10^{-5} *M* H_2O_2 caused a slight decrease in permeability (Figs. 1c and 1d) implies that if NO production is responsible for preserving junctions, the extracellular L-arginine may cause additional production of NO, which may in turn tighten junctions and decrease permeability. Furthermore, the observation that L-arginine could prevent the increase induced by 10^{-4} *M* H_2O_2 (Fig. 2) indicated that this higher concentration of H_2O_2 may have increased the endogenous production of NO which led to a shortage of L-arginine. When this shortage was compensated for by extracellular addition of L-arginine, the production of NO may have been sufficient to maintain the tight contact between cells and the same low permeability as in untreated cells. L-arginine and NAME, respectively, were only able to alter the permeability in H_2O_2-treated cells (Fig. 1), which probably means that H_2O_2 can stimulate endogenous production of NO.

It is not known what mechanisms are responsible for the increase in the endothelial permeability associated with the inhibition of nitric oxide synthesis. In our experiments, permeability increased by H_2O_2, or a combination of H_2O_2 and L-NAME could be abolished by adding agents that increase cellular production of cGMP (Fig. 2). These findings indicate that the cellular level of cGMP is important for preservation of a low permeability after stimulation with H_2O_2. In smooth muscle cells and platelets [13, 14] as well as in endothelial cells [15–17], nitric oxide can induce cGMP generation by activation of soluble guanylate cyclase and leads to increased conversion of GTP to cGMP [27]. Subsequently, cGMP reacts with cGMP-dependent protein kinase and causes a cascade of changes in protein phosphorylation [28–30], including, for example, cytoskeletal protein phosphorylation [31]. The results of our study show a close association between endothelial permeability and F-actin peripheral bands. Moreover, in agreement with other reports [32–34], H_2O_2-induced increases in endothelial permeability were associated with a characteristic loss of peripheral actin bands and an increased density of the F-actin stress fibers spanning the cell (Fig. 4). This finding implies that H_2O_2 may stimulate the production of NO, which then causes a rise in F-actin content by increasing cGMP. On the other hand, it has been demonstrated that NO can stimulate ADP-ribosylation of actin [8] and also that the polymerization of F-actin can be decreased by adding a NO-producing compound, *S*-nitroso-*N*-acetylpenicillamine [35]. These findings, together with the present results, imply that stimulating NO production by exposure to H_2O_2, as was done in our study, may induce a shift in the decrease and increase in F-actin via regulation of the cGMP level in the cells. In conclusion, it seems apparent that NO regulates endothelial permeability and F-actin distribution in hydrogen peroxide-treated cells via a cGMP-dependent mechanism.

This research was supported by grants from the Swedish Medical Research Council, the Swedish Society of Medicine, the Swedish Association against Rheumatism, King Gustaf the Vth 80-Year Fund, Östergötlands Läns Landstings Research Fund, and the Lions Research Fund for Heart and Vascular Diseases.

REFERENCES

1. Varani, J., Fligiel, S. E., Till, G. O., Kunkel, R. G., Ryan, U. S., and Ward, P. A. (1985) *J. Lab. Invest.* **53,** 656–663.
2. Weiss, S. J., Young, J., LoBuglio, A. F., Slivka, A., and Nimeh, N. F. (1981) *J. Clin. Invest.* **68,** 714–721.
3. Block, E. R. (1991) *J. Cell. Physiol.* **64,** 308–322.
4. Sundqvist, T. (1992) *J. Cell. Physiol.* **148,** 152–156.
5. Zweier, J. L., Kuppusamy, P., and Lutty, G. (1988) *Proc. Natl. Acad. Sci. USA* **85,** 4046–4050.
6. Sundqvist, T., and Liu, S. M. (1993) *Acta Physiol. Scand.* **149,** 127–131.
7. Hinshaw, D. B., Burger, J. M., Delius, R. E., and Hyslop, P. A. (1990) *Surgery* **108,** 298–305.
8. Lewis, M. S., Whatley, R. E., Cain, P., McIntyre, T. M., Prescott, S. M., and Zimmerman, G. A. (1988) *J. Clin. Invest.* **82,** 2045–2055.
9. Stuehr, D. J., and Griffith, O. W. (1992) *Adv. Enzymol. Rel. Areas Mol. Biol.* **65,** 287–346.
10. Kubes, P. (1993) *Can. J. Physiol. Pharmacol.* **71,** 88–97.

FIG. 4. Rhodamine-phalloidin staining of actin filament structures in endothelial monolayers that were grown on filters and then incubated for 6 h with the following: 10^{-5} *M* H_2O_2 (a); 10^{-5} *M* H_2O_2 and L-arginine (b); 10^{-5} *M* H_2O_2 and L-NAME (c); 10^{-4} *M* H_2O_2 (d); 10^{-4} *M* H_2O_2 and L-arginine (e); 10^{-4} *M* H_2O_2 and L-NAME (f); 8-Br-cGMP and 10^{-4} *M* H_2O_2 (g); 8-Br-cGMP, 10^{-4} *M* H_2O_2, and L-arginine (h); 8-Br-cGMP, 10^{-4} *M* H_2O_2, and L-NAME (i). In all cells treated with hydrogen peroxide (10^{-5} or 10^{-4} *M*), there was an increase in the density of the F-actin stress fibers spanning the cells, as compared to the fiber density in untreated cells (see Figs. 3d and 3e). The peripheral bands were disrupted (arrows) by treatment with 10^{-5} *M* H_2O_2 and L-NAME (c), 10^{-4} *M* H_2O_2 (d), and 10^{-4} *M* H_2O_2 and L-NAME (f), and were slightly increased by treatment with 10^{-5} *M* H_2O_2 and L-arginine (b); 10^{-5} *M* H_2O_2 had no effect on these bands (a). Treatments comprising 8-Br-cGMP maintained the F-actin peripheral bands (arrowheads in g, h, and i). Bar, 10 μm.

11. Ialenti, A., Ianaro, A., Moncada, S., and Rosa, M. D. (1992) *Eur. J. Pharmacol.* **211,** 177–182.
12. Teixeira, M. M., Williams, T. J., and Hellewell, P. G. (1993) *Br. J. Pharmacol.* **110,** 1515–1521.
13. Ignarro, L. J. (1992) *Biochem. Soc. Trans.* **20,** 465–469.
14. Geiger, J., Nolte, C., Butt, E., Sage, S. O., and Walter, U. (1992) *Proc. Natl. Acad. Sci. USA* **89,** 1031–1035.
15. Shin, W. S., Sasaki, T., Kato, M., Hara, K., Seko, A., Yang, W-D, Shimamoto, N., Sugimoto, T., and Toyo-oka, T. (1992) *J. Biol. Chem.* **267,** 20377–20382.
16. Boulanger, C., Schini, V. B., Moncada, S., and Vanhoutte, P. M. (1990) *Br. J. Pharmacol.* **101,** 152–156.
17. Moncada, S. (1992) *Acta Physiol. Scand.* **145,** 201–227.
18. Shimizu, S., Saitoh, Y., Yamamoto, T., and Momose, K. (1994) *Res. Commun. Chem. Pathol. Pharmacol.* **64**(3), 315–329.
19. Westendorp, R. G. J., Draijer, R., Meinders, A. E., and van Hinsbergh, V. W. M. (1994) *J. Vasc. Res.* **31,** 42–51.
20. Liu, S. M., and Sundqvist, T. (1995) *Exp. Cell Res.* **217,** 1–7.
21. Kuo, L., Davis, M. J., Cannon, M. S., and Chilian, W. M. (1992) *Circ. Res.* **70,** 465–476.
22. Weyrich, A. S., Xin-Liang, M., and Lefer, A. M. (1992) *Circulation* **86,** 279–288.
23. Kubes, P., Suzuki, M., and Granger, D. N. (1991) *Proc. Natl. Acad. Sci. USA* **88,** 4651–4655.
24. Kubes, P., and Granger, D. N. (1992) *Am. J. Physiol.* **262,** H611–H615.
25. Pollock, J. S., Forstermann, U., Mitchell, J. A., Warner, T. D., Schmidt, H. H. H. W., Nakane, M., and Murad, F. (1991) *Proc. Natl. Acad. Sci. USA* **88,** 10480–10484.
26. Schmidt, H. H. H. W., Pollock, J. S., Nakane, M., Forstermann, U., and Murad, F. (1992) *Cell Calcium* **13,** 42–434.
27. Ignarro, L. J. (1989) *Circ. Res.* **65,** 1–21.
28. Ignarro, L. J., Harbison, R. G., Wood, K. S., and Kadowitz, P. J. (1986) *J. Pharmacol. Exp. Ther.* **237,** 893–237.
29. Madara, J. L., Moore, R., and Carlson, S. (1990) *Am. J. Physiol.* **253**(Cell Physiol. **22**), C854–C861.
30. Wysolmerki, R. B., and Lagunoff, D. (1990) *Proc. Natl. Acad. Sci. USA* **87,** 16–20.
31. Lincoln, T. M., Komalavilas, P., and Cornwell, T. L. (1994) *Hypertension* **23,** 1141–1147.
32. Johnson, A., Phillips, P., Hocking, D., Tsan, M.-F., and Ferro, T. (1989) *Am. J. Physiol.* **256** (Heart Circ. Physiol. **25**), H1012–H1022.
33. Siflinger-Birnboim, A., Goligorsky, M. S., Del Vecchio, P. J., and Malik, A. B. (1992) *Lab. Invest.* **67,** 24–30.
34. Wong, M. K., and Gotlieb, A. I. (1986) *Arteriosclerosis* **6,** 212–219.
35. Sundqvist, T., Forslund, T., Bengtsson, T., and Axelsson, K. L. (1994) *Inflammation* **18,** 625–631.

Received December 16, 1996
Revised version received May 5, 1997

EXPERIMENTAL CELL RESEARCH **235,** 245–253 (1997)
ARTICLE NO. EX973670

Genomic Instability and Telomerase Activity in Human Bronchial Epithelial Cells during Immortalization by Human Papillomavirus-16 E6 and E7 Genes

Jill D. Coursen,*[1] William P. Bennett, *[1] Lauren Gollahon,† Jerry W. Shay,† and Curtis C. Harris*[2]

**Laboratory of Human Carcinogenesis, National Cancer Institute, National Institutes of Health, Bethesda, Maryland 20892-4255; and*
†Department of Cell Biology and Neuroscience, UT Southwestern Medical Center, Dallas, Texas 75235-9039

Human papilloma virus types 16 and 18 contribute to the development of cervical carcinomas in which the E6 and E7 genes are frequently retained and expressed in the tumors. Our study explored the ability of the E6 and/or E7 genes to immortalize normal human bronchial epithelial (NHBE) cells and to reactivate telomerase expression in these cells. We have introduced the human papillomavirus type 16 E6 or E7 genes alone or in combination (E6/E7) into NHBE cells using the retroviral construct pLXSN. Cells expressing either the E6 or the E7 oncoproteins alone displayed an increased colony-forming efficiency and a slightly extended *in vitro* life span before entering a crisis, from which immortalized cell lines were not obtained. Telomerase activity was not detected in cells expressing either E6 or E7 individually. Cells expressing the E6/E7 oncoproteins in combination had a substantially increased life span before entering crisis. A subpopulation of these cells escaped from crisis and achieved 130 population doublings, suggesting immortalization. Telomerase activity was detected in these postcrisis cells, but was not detected prior to crisis. In addition, karyotypic analysis showed evidence of genomic instability in mass cultures as well as clones expressing E6, E7, or E6/E7. Abnormalities included numerous monosomies and trisomies, chromatid gaps and breaks, double minutes, and aberrant chromosomes. These results demonstrate that expression of E6 and/or E7 is sufficient to induce genomic instability and an extended life span to NHBE cells, but the presence of both E6 and E7, along with at least one additional genetic or epigenetic event achieved during crisis, was required for reactivation of telomerase and the immortalization in this human cell type. © 1997 Academic Press

INTRODUCTION

The papillomaviruses are small, nonenveloped DNA viruses. The human papilloma viruses (HPV) are divided into low-risk and high-risk types based on their association with human cancers. Low-risk HPV types, including types 6 and 11, result in benign lesions such as genital warts. HPV types 16 and 18 are considered high risk because they are associated with the majority of invasive cervical carcinomas (reviewed in [1]). The human papilloma viruses specifically infect epithelial cells. This tissue trophism may be determined by an epithelial-specific transcription enhancer, which was first identified in HPV-16 and -18 (reviewed in [2]). HPV DNA sequences have been detected in 84% of human cervical cancers [3–5] and less frequently in respiratory tract cancers [6–9]. This transforming ability of HPV-16 and -18 has been attributed to the E6 and E7 proteins, which are frequently retained and expressed in tumors.

HPV-16 E6 and E7 act by binding to cellular proteins. The E6 protein binds to the p53 tumor-suppressor protein, resulting in enhanced ubiquitin degradation of p53 [10, 11]. This interaction between E6 and p53 is mediated by the cellular protein E6-AP, which is a component of the ubiquitin pathway [12–14]. It has been demonstrated in human mammary epithelial cells that degradation of p53 is required for their immortalization by E6 [15]. p53 is frequently mutated in a variety of human cancers [16] and it is currently thought that its main function is to induce cellular growth arrest and/or apoptosis in response to DNA damage [17]. In addition, p53 is important for maintaining the fidelity of centrosomal duplication and lack of wild-type p53 leads to aneuploidy [18]. Therefore, inactivation of p53 by E6 could permit aneuploidy and the accumulation of genetic damage which could lead to neoplastic transformation. In fact, it has been demonstrated that E6, as well as E7, can inhibit DNA damage-induced growth arrest [19, 20] and produce aneuploidy [21, 22]. E6 also can abrogate p53-mediated DNA binding [23, 24], transcriptional transactivation

---

[1] These authors have contributed equally to this study.

[2] To whom correspondence and reprint requests should be addressed at Laboratory of Human Carcinogenesis, National Cancer Institute, Building 37, Room 2C05, 37 Convent Drive MSC 4255, Bethesda, MD 20892-4255. Fax: (301) 496-0497. E-mail: Curtis_Harris@nih.gov.

0014-4827/97 $25.00
Copyright © 1997 by Academic Press
All rights of reproduction in any form reserved.

[25–28], and apoptosis [29]. The E7 protein binds to and causes the ubiquitin degradation of the retinoblastoma (Rb) tumor suppressor protein [30, 31], thereby preventing Rb from binding to the cellular transcription factor E2F [32]. Disruption of the Rb–E2F complex by E7 allows for uncontrolled proliferation. Although E7 does not directly interact with p53, overexpression of HPV-16 E7 can abrogate p53-induced G1 arrest [19, 20, 33, 34]. However, E7 does not inhibit p53-induced apoptosis [33] and actually enhances the apoptotic response following exposure to γ-radiation [35].

E6 and E7 are sufficient for immortalization of normal human epithelial cells by HPV *in vitro*. Primary human foreskin epithelial cells [20] and normal human keratinocytes [22, 36–39] can be immortalized by expression of HPV-16 E7 alone, while coexpression with E6 increases the frequency of immortalization. In contrast, transfection of the HPV-16 E6 gene alone, but not E7, is sufficient for immortalization of normal human mammary epithelial cells [40, 41]. In human cervical keratinocytes, both E6 and E7 are required for immortalization [42]. Normal human bronchial epithelial cells (NHBE) have previously been immortalized by full-length HPV-16 or HPV-18 [8] or by transfection with a plasmid expressing the HPV-16 E6 and E7 genes [43]. We have investigated whether HPV-16 E6 or E7 individually would be sufficient for immortalization of NHBE cells. In addition, we examined the ability of E6 and/or E7 to induce genomic instability and reactivate telomerase expression in NHBE cells.

MATERIALS AND METHODS

Retroviral vectors. Retroviral constructs consisted of the pLXSN defective retroviral vector containing the HPV-16 E6 and E7 genes, either alone or in combination (E6/E7) [41]. The pLXSN vector confers resistance to neomycin (G418) and transcription of the HPV-16 sequences is under control of the Moloney murine leukemia virus promoter. Viral supernatants were generated in the amphotrophic packaging cell line PA317 using previously described procedures [44].

Cell culture. Primary NHBE cells were cultured from explants of autopsy tissues and grown in LHC-9 medium according to the methods of Lechner and LaVeck [45]. Cells from primary outgrowths, at approximately 5 to 10 population doublings, were subcultured by trypsinization, counted, and transferred into 100-mm^2 dishes. Cells were infected 24 h after plating. For infections, 1×10^6 cells were exposed to approximately 10^6 colony-forming units of retrovirus at 37°C for 2 h in serum-free medium containing 8 μg/ml polybrene. The medium was then changed to fresh LHC-9. Forty-eight hours after infection, the cells were exposed to 125 μg/ml G418 in LHC-9 medium with 3% chemically denatured serum to select for neomycin resistance. Clones were obtained by isolating neomycin-resistant colonies using glass cloning cylinders. Mass cultures were generated by pooling together neomycin-resistant colonies from three 100-mm^2 dishes. Following selection, cultures were maintained in LHC-9 with G418. Estimated population doublings were calculated at each passage using the equation log (final cell number/initial cell number)/log (2).

Colony-forming efficiency. Colony-forming efficiency assays were performed by infecting NHBE cells as described above. Forty-eight hours after infection, the cells were trypsinized and reseeded into 60-mm^2 dishes at a density of 1×10^3 cells/dish in LHC-9 medium with or without G418 selection. After 10 days of incubation, dishes were fixed with 10% formaldehyde and stained with crystal violet.

RT-PCR. RT-PCR was performed to confirm expression of the HPV16 E6 and/or E7 mRNA. Total cellular RNA was isolated using the guanidium thiocyanate–phenol–chloroform method [46]. Following treatment with DNase I, cDNA was synthesized from 0.75 μg RNA using random hexamers for reverse transcription. The reverse transcription and PCR were performed using the Gene-Amp RNA PCR kit (Perkin–Elmer). Amplification of the E6 sequence was accomplished using the following primer set [47], which amplified 454- and 272-bp fragments of the E6 gene: E6 sense 5′-GAGAACTGCAATGTTTCAAGG-3′ and E6 antisense 5′-TTTCTCTACGTGTTCTTGATG-3′. The E7 sequence was amplified using primers which amplified a 200-bp fragment: E7 sense 5′-GATTTGCAACCAGAGACAAC-3′ and E7 antisense 5′-TCCAAAGTACGAATGTCTAC-3′.

Cytogenetic analysis. Isozyme and cytogenetic analyses were performed by Dr. Joseph Kaplan and Dr. Bharati Hukku at Children's Hospital of Michigan (Detroit, MI). Chromosome counts were determined on 100 metaphases and 5 to 8 karyotypes were prepared for each cell culture examined.

Telomerase assay. A one-tube PCR-based telomerase assay was performed as originally described [48] with some modifications [49]. The assay was performed in two steps: (i) telomerase-mediated extension of an oligonucleotide primer (TS), which serves as a substrate for telomerase; and (ii) PCR amplification of telomerase activity product (an incremental 6-nt ssDNA ladder) with the oligonucleotide primer CX in a competitive amplification reaction with a 150-bp fragment encoding aa 97–132 of rat myogenin as an internal telomerase amplification standard. H1299 cells, a non-small-cell lung carcinoma-derived cell line (gift of J. Minna to J. Shay), were used as a positive control. The PCR products were electrophoresed on a 10% acrylamide gel as previously described [48].

RESULTS

Effect of E6 and/or E7 on Growth of NHBE Cells

The HPV-16 E6 or E7 genes alone or in combination were introduced into primary NHBE cells using the retroviral construct pLXSN. The cells were then exposed to G418 selection. Approximately 20–25 clones were isolated from each culture. Twelve to 13 clones each of E6, E7, and E6/E7 could be expanded for further evaluation. However, only 3 clones of cells carrying the pLXSN vector control could be expanded. Expression of the E6 and E7 mRNA transcripts in G418-resistant mass cultures and clones was confirmed by RT-PCR (Fig. 1).

HPV-16 E6, E7, and E6/E7 each produced an increased colony-forming efficiency in NHBE cells when compared to the pLXSN vector control. E6 or E7 alone each produced an approximately threefold increase in the number of colonies. The combination of both genes, E6/E7, provided a fourfold increase in the colony-forming efficiency of NHBE cells (Fig. 2).

To assess the effect of E6 and/or E7 on the life span of NHBE cells, mass cultures and clones were maintained until senescence. Cells transfected with E7 alone displayed a different morphology by phase-contrast microscopy than cells transfected with E6 or E6/E7 (Fig.

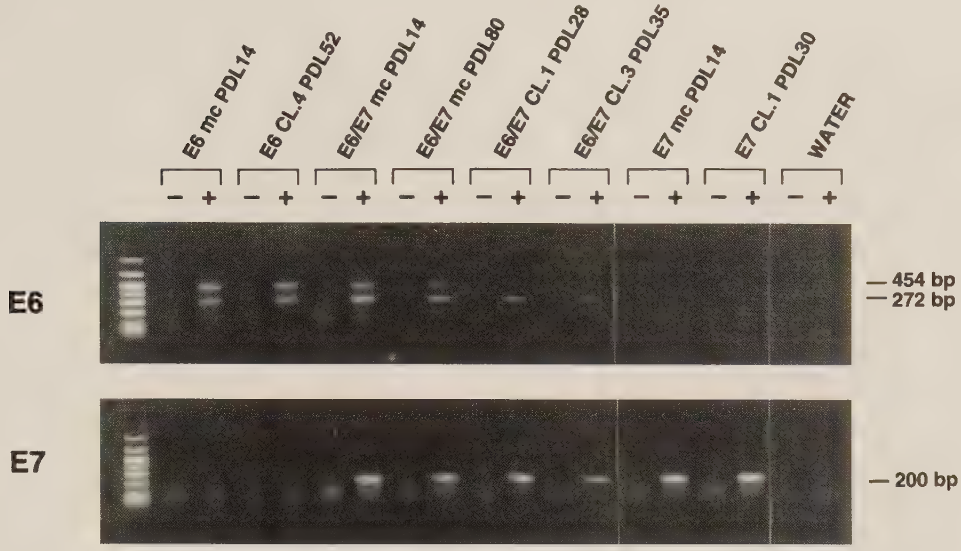

FIG. 1. Expression of the HPV-16 E6 and E7 transcripts in mass cultures and clones of NHBE cells was confirmed by RT-PCR. The primers used for the E6 gene amplified a 454-bp fragment, representing the full-length E6 transcript, and a 272-bp fragment, representing the alternatively spliced E6* transcript. Primers for the E7 gene amplified a single 200-bp fragment. Reactions with (+) and without (−) reverse transcriptase are shown for each sample.

3). E6 and E6/E7 cultures maintained an epithelial morphology, while E7 cells were smaller, more rounded, and did not attach well to the surface. Cultures were passaged when they achieved approximately 90% confluence and were considered senescent when they stopped proliferating and developed the characteristic flattened morphology with increased cell surface area. Population doubling levels (PDL) were calculated at each passage. E6 and E7 each provided a slightly increased life span. The pLXSN control mass culture grew for approximately 24 PDL after the retroviral infection (Fig. 4A), while the pLXSN clones se-

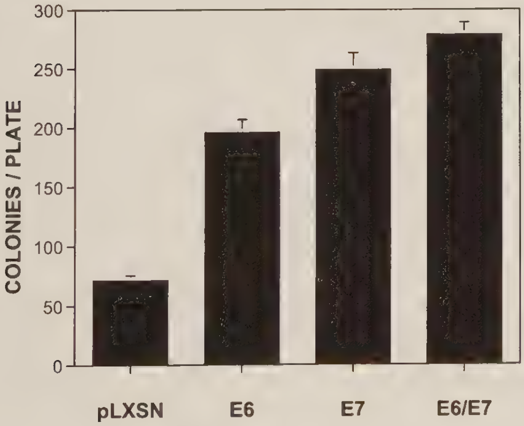

FIG. 2. HPV-16 E6, E7, and E6/E7 each produced an increased colony-forming efficiency in NHBE cells when compared to the pLXSN vector control. Cells were infected as described under Materials and Methods. Two days after infection, 1×10^3 cells were seeded into 60-mm^2 dishes in LHC-9 medium. After 10 days of incubation, dishes were fixed with 10% formaldehyde and stained with crystal violet. Colonies were counted using a Dynatech Autocount (Dynatech Laboratories, Inc.).

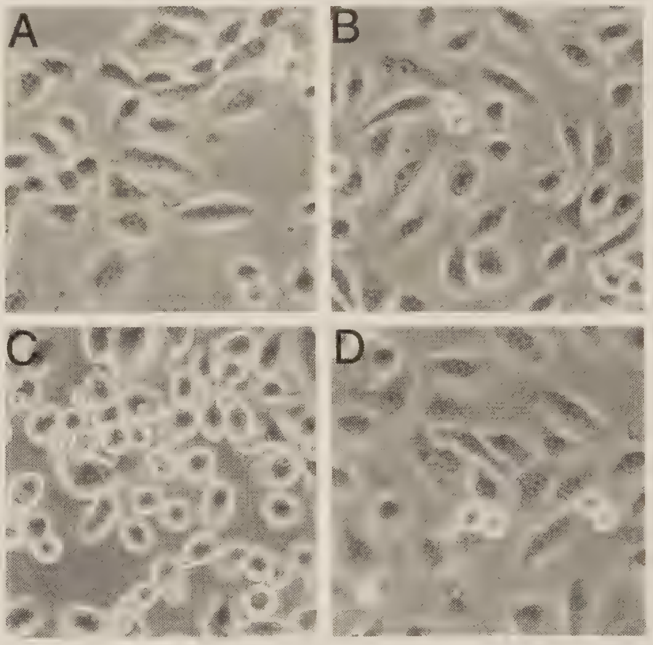

FIG. 3. Phase-contrast photomicrographs of NHBE cells expressing (A) pLXSN vector, (B) HPV-16 E6/E7, (C) E6, or (D) E7. Cultures of NHBE cells expressing E7 contained a large number of small, rounded cells. PLXSN, E6, and E6/E7 cultures maintained an epithelial morphology until senescence.

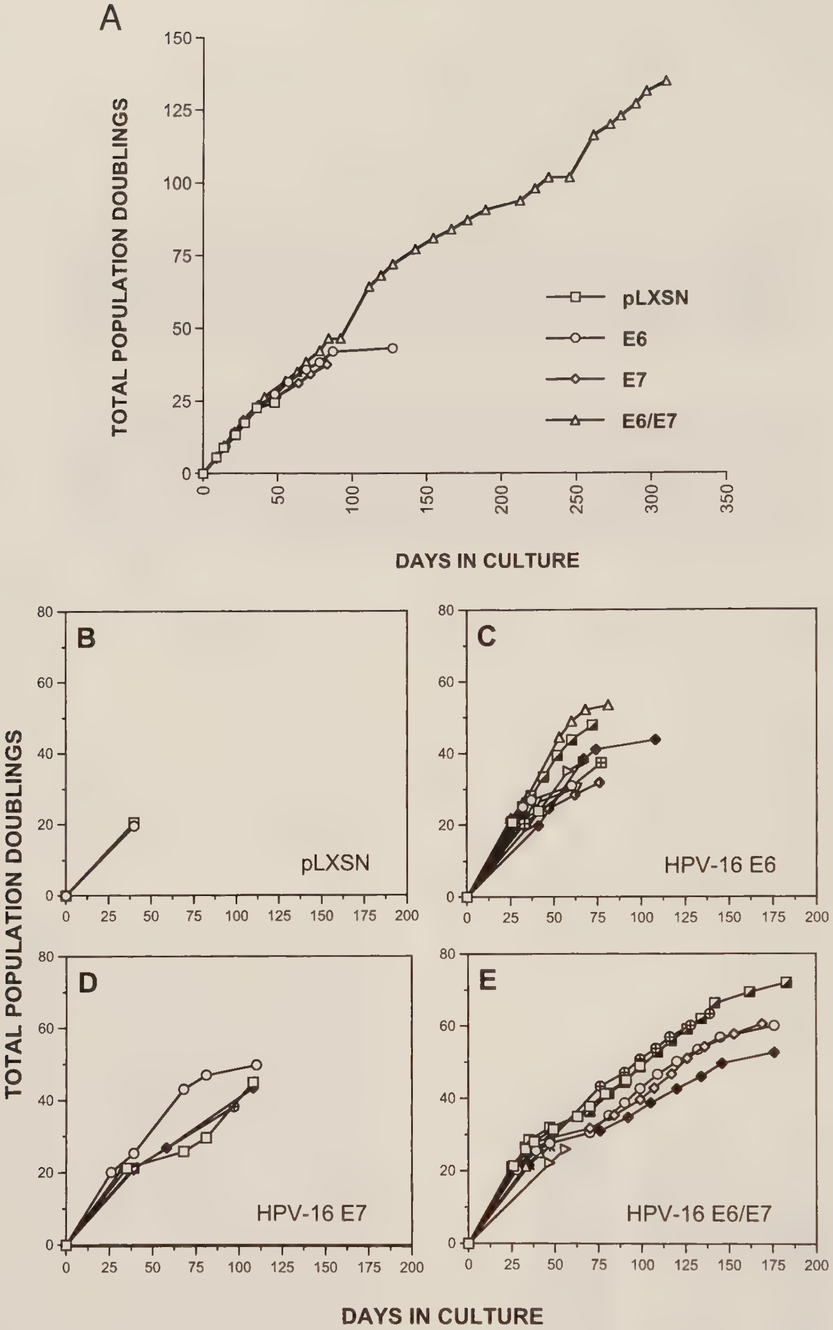

FIG. 4. (A) In a mass culture, HPV-16 E6/E7 increased the *in vitro* life span of NHBE cells to at least 130 population doublings. Cells with the pLXSN vector control senesced at approximately 24 population doublings. Mass cultures expressing the E6 or E7 genes alone went through roughly 43 or 38 population doublings, respectively. G418-resistant clones were selected from cells infected with (B) pLXSN, (C) E6, (D) E7, and (E) E6/E7, and population doublings were calculated at each passage.

nesced after only 20 PDL (Fig. 4B). Thirteen clones each of E6 alone (Fig. 4C) and E7 alone (Fig. 4D) were expanded and showed extensive variability in life span, ranging from 20 to 50 PDL. The E6 or E7 mass cultures grew for approximately 43 or 38 PDL, respectively (Fig. 4A). Mass cultures and clones of NHBE cells expressing either E6 or E7 alone entered crisis from which immortalized cell lines could not be obtained (Fig. 4A). The E6 and E7 genes combined produced a greater increase in life span than either gene alone. The life spans of 12 E6/E7 clones analyzed ranged from 25 to 72 PDL (Fig. 4E). All of these clones eventually entered crisis

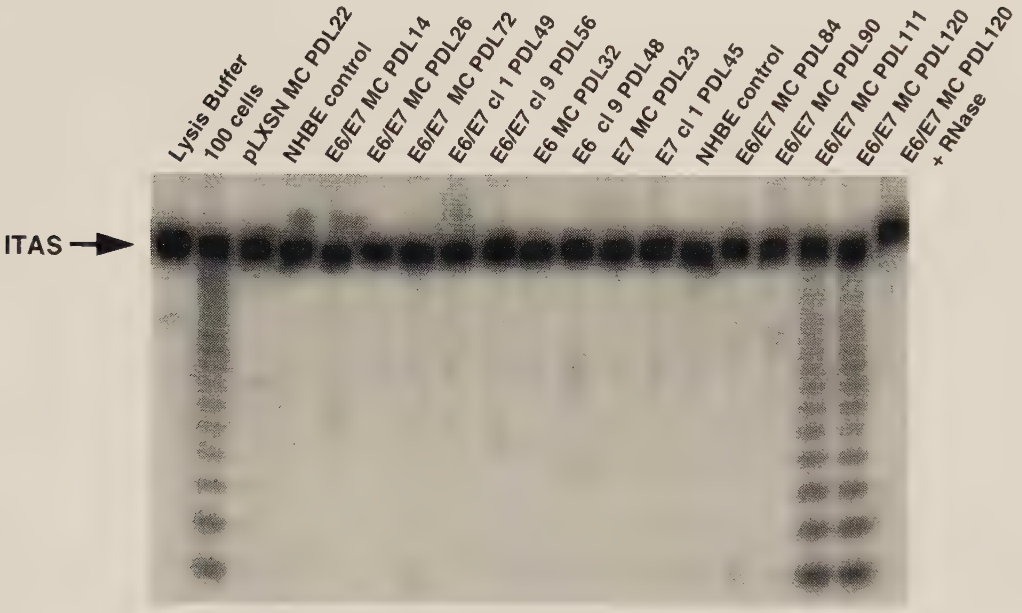

FIG. 5. Telomerase activity in NHBE cells expressing either pLXSN, E6, E7, or E6/E7. A PCR-based telomerase assay was performed as described under Materials and Methods. E6/E7 mass cultures were examined both precrisis (PDL ≤ 90) and postcrisis (PDL111 and 120). The 150-bp band seen in each lane is an internal telomerase amplification standard (ITAS). H1299 cells were used as the 100 cells control.

and did not become immortalized. The E6/E7 mass culture (Fig. 4A) entered an initial period of crisis at approximately 46 PDL, at which time most of the cells stopped proliferating. After approximately 4 weeks, 35 colonies of proliferating cells emerged and were pooled together into a mass culture. This culture then entered a second crisis at approximately 100 PDL. After this second crisis period, more than 200 proliferating colonies were pooled into a mass culture. This culture has continued to proliferate for more than 130 PDL, suggesting that it may be immortalized.

Activation of Telomerase by E6/E7

It has been proposed that progressive telomere shortening leads to normal cellular senescence. Telomerase, an RNA-dependent DNA polymerase that lengthens telomeric DNA, is the primary mechanism for maintaining telomere length in eukaryotic cells (reviewed in [50, 51]). Reactivation of telomerase occurs in 85% of human tumors and most immortal human cell lines, suggesting that genetic or epigenetic inactivation of the telomerase repression pathway may be important for immortalization [50].

Telomerase activity was examined in the cells at multiple passages (Fig. 5). The NHBE parental cells and pLXSN vector control cells were each negative for telomerase activity. The E6 mass culture at PDL 32 and an E6 clone at PDL 48 were each telomerase negative. The E7 mass culture at PDL 23 and an E7 clone at PDL 45 also were telomerase negative. These cell cultures senesced at nearly the same time as or shortly after these same PDLs. Therefore, expression of either E6 or E7 alone was not sufficient to activate telomerase in NHBE cells.

E6/E7 clones 1 (PDL 49) and 9 (PDL 56) were negative for telomerase. In addition, the E6/E7 mass culture was telomerase negative at PDL 14 through 84. The culture showed very weak telomerase activity at PDL 90, shortly before entering the second crisis. The cell line which emerged from the crisis was much more strongly telomerase positive at PDL 111 and 120. It is likely that a small population of telomerase-positive cells began proliferating shortly before the entire population of cells entered crisis. As the normal cells senesced, these telomerase-positive cells became more abundant and eventually dominated the population, thus giving rise to an immortal cell line.

Genomic Instability in NHBE Cells Expressing E6 or E6/E7

Cytogenetic analysis showed evidence of genomic instability in mass cultures and colonies expressing E6, E6/E7, and, to a lesser extent, E7. In the pLXSN vector control mass culture, the majority of the cell population was normal diploid. In the mass culture of cells transfected with E7, most of the cells were also primarily diploid with a small population being monosomic for chromosome 6. The E7 cultures were difficult to ana-

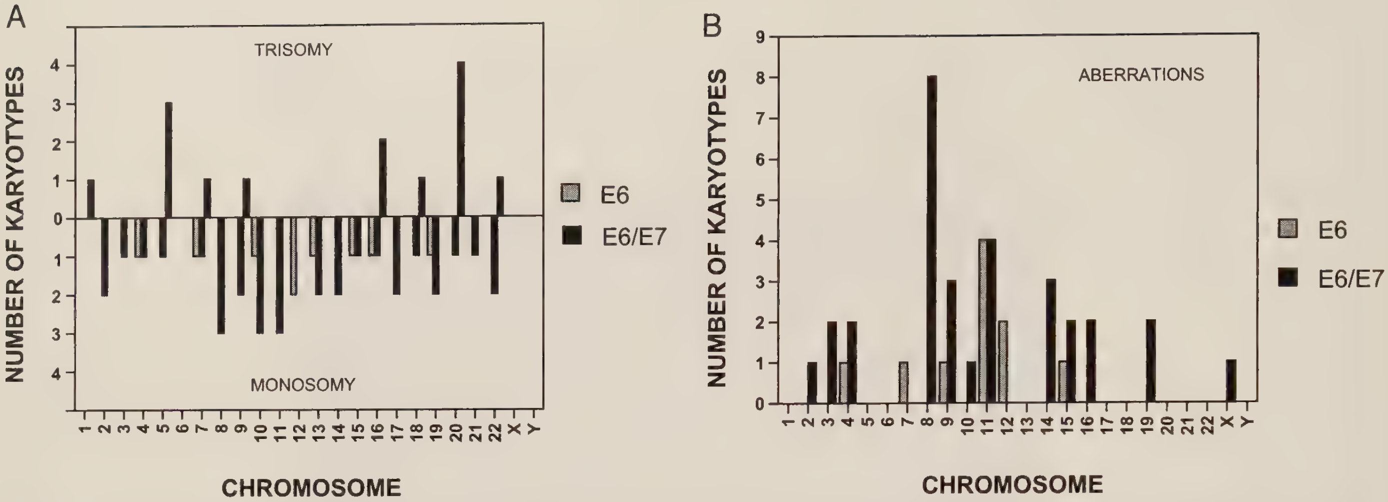

FIG. 6. Cytogenetic analysis was performed on precrisis cultures of NHBE cells expressing pLXSN, E6, E7, or E6/E7. The pLXSN control was normal diploid. E7-expressing cultures were also mostly normal diploid with a small population monosomic for chromosome 6 (results not included in figure). (A) The distribution of chromosome gains (monosomy) and losses (trisomy); and (B) the distribution of chromosome aberrations detected in E6 and E6/E7 cultures. The results of the mass culture and clones were combined to obtain the overall distribution of chromosome abnormalities. A total of 14 karyotypes of E6 cultures and 41 karyotypes of E6/E7 cultures were examined.

lyze because of the growth properties of the cells. Therefore, only one E7 clone was analyzed. In these clonal cells, approximately 10% of the population was tetraploid and 2% of the cells showed chromosome or chromatid gaps. In the E6 mass culture, the cells were also primarily diploid with minor populations that were monosomic for chromosomes 4, 7, 10, 12, 13, 15, or 16 (Fig. 6A). Later passages of E6 clones, however, showed numerous abnormalities involving chromosome 11 in particular (Fig. 6B). Each of the four E6 clones examined also showed evidence of gene amplification by the presence of double minutes. The precrisis E6/E7 mass culture had an increased aneuploid population with random monosomies and trisomies (Fig. 6A). Karyotypes of seven different E6/E7 clones showed aberrations in many chromosomes, but particularly chromosome 8 (Fig. 6B). There were also numerous monosomies and trisomies (Fig. 6A). Monosomy of chromosomes 8, 10, and 11 and particularly trisomy of chromosome 20 were especially prevalent. The majority of E6/E7 clones examined also contained double minutes and acentric fragments, as well as numerous additional aberrations. In addition, all E6, E7, and E6/E7 clones displayed tetraploidy in 7 to 25% of the metaphases examined.

Nine karyotypes were prepared from the postcrisis culture of E6/E7 cells. Eleven marker chromosomes were observed, mainly involving chromosomes 11, 14, 19, 20, and 21 (Table 1). Five of these marker chromosomes were present in the majority of karyotypes examined. M2 and M4 were present in all nine karyotypes, suggesting that this immortalized cell line was derived from a single cell. In addition, loss of both normal copies of chromosome 14 was observed in all karyotypes and trisomy of chromosome 5 was seen in eight of nine karyotypes.

DISCUSSION

We have investigated the ability of HPV-16 E6 and/or E7 to immortalize NHBE cells. Expression of either E6 or E7 alone was sufficient to increase the proliferative potential of NHBE cells, as demonstrated by increased colony formation and increased life span. However, only cells expressing both E6 and E7 together became immortalized and had detectable telomerase expression. Immortalization by E6/E7 was an infrequent occurrence since this immortalized population

TABLE 1

Frequency of Marker Chromosomes Detected in NHBE Cells Immortalized with HPV-16 E6 and E7

Marker chromosomes	Frequency
M1 = der(11) t(11;?)(p14;?)	8/9
M1A = del(11)(q10)	1/9
M1B = der(M1) dic(M1;8)	1/9
M2 = del(14)(q21)	9/9
M2A = der(14) t(14;?)	3/9
M2B = der(14) t(14q;17q)	1/9
M3 = der(20) t(14,20)(q12;q13)	5/9
M3A = der(20) t(14,20)(q30;q13)	1/9
M3B = der(20) t(20;?)(q13;?)	1/9
M4 = der?(19) t(19;?)(p12>q13::?)	9/9
M5 = der(21) t(16?;21)(p11;q10)	8/9

appears to have been derived from a single cell out of a mass culture in which approximately 10^6 cells were exposed to the E6/E7 retrovirus. This conclusion is also supported by the fact that all of the E6/E7 clones (12/12) analyzed senesced without immortalization.

A two-stage model of *in vitro* immortalization consisting of a mortality stage 1 (M1) and a mortality stage 2 (M2) has been previously described [52–55]. Human cells in culture undergo a limited number of population doublings before they senesce. M1 leads to normal cellular senescence, when normal cells have reached the end of their proliferative capacity. M1 senescence may be controlled by the p53 and Rb tumor suppressor proteins since the inactivation of p53 and Rb by viral proteins, such as E6 and E7, allows cells to overcome M1. Escape from M1 results in an extended *in vitro* life span during which cells continue to proliferate until reaching M2. At this point most cells enter crisis. Those cells that survive M2 have the ability to proliferate indefinitely (e.g., immortalization). The immortalization of NHBE cells by the combination of E6 and E7 in this study followed this two-stage model of *in vitro* immortalization. The E6/E7 mass culture exhibited an extended *in vitro* life span. While a subpopulation of clones within the culture reached M2 crisis at approximately 46 PDL, the remaining cells in the culture continued to proliferate at a constant growth rate until reaching M2 at approximately 100 PDL. More than 200 colonies of proliferating cells survived crisis and were pooled together to produce the immortalized cell line. Our results indicate that inactivation of either p53 or Rb individually was sufficient for NHBE cells to overcome the M1 stage of senescence. However, inactivation of both p53 and Rb, through expression of E6 and E7 together, was required to overcome crisis in M2.

It is thought that a critical step in overcoming the M2 senescence stage may be the reactivation of telomerase expression [50]. Telomerase reactivation has been reported in cells immortalized by SV40, adenovirus [51], HPV [42, 56], Epstein–Barr virus [57], and mutant p53 [55]. However, not all human immortalized and tumor cells express telomerase. Several investigators have reported immortal human cell lines with no detectable telomerase activity [48, 58, 59]. It is evident that, while telomere maintenance is critical for immortalization of human cells, it can occur more frequently by telomerase reactivation or less frequently by telomerase-independent mechanisms [48, 60–62]. We examined telomerase activity in precrisis and postcrisis cells. NHBE cells expressing either E6 or E7 alone were telomerase negative at all passages analyzed, including later passages shortly before crisis. Only cells expressing both E6 and E7 together expressed telomerase activity, and this telomerase was not detectable until approximately 90 population doublings after the E6/E7 retroviral infection. This suggests that telomerase activation was a late step in the immortalization of NHBE cells by HPV-16 E6/E7. Our results are in contrast to a recent study in which it was reported that telomerase can be activated soon after the introduction of E6 [42]. In human foreskin keratinocytes and human mammary epithelial cells, low-level telomerase activity was detected within one passage after introduction of E6. However, this early E6-associated activation of telomerase was found to be cell-type specific since telomerase was not detected in early passage human fibroblasts expressing E6. It is apparent that this early activation of telomerase by E6 also does not occur in primary NHBE cells.

HPV is thought to be associated with genomic instability, which may be the result of loss of functional p53 protein through degradation by E6. HPV-immortalized oral keratinocytes have a reduced DNA repair capacity when exposed to MNNG [63], indicating that the p53-mediated DNA damage response is impaired in these cells. HPV-immortalized cells also show evidence of increased gene amplification [64] and there are numerous reports of HPV-associated cytogenetic alterations (reviewed in [65]). Alterations of chromosome 3 [21] and chromosomes 4 and 5 [21, 66] and loss of chromosomes 11 and 19 are common in HPV-immortalized cells. A study which analyzed cytogenetic alterations in 148 cervical carcinomas found that chromosome 1 alterations occurred most frequently [67]. Several other studies have also detected frequent alterations of chromosome 1 [64, 66]. In addition, it was recently shown that HPV immortalization of human foreskin keratinocytes involves genes on chromosomes 3, 10, 11, and 18 and that allelic losses at 3p and 10p may be associated with telomerase reactivation [68].

Cytogenetic analysis of precrisis human bronchial epithelial cells expressing E6 or E6/E7 showed evidence of genomic instability in all of the cultures examined, whereas the pLXSN control cells were normal diploid. NHBE cells expressing E7 showed slight evidence of instability; however, analysis of E7 cultures was limited to the mass culture and one clone. Precrisis cultures of E6 and E6/E7 displayed numerous monosomies and trisomies, double minutes, and chromosomal aberrations most frequently involving chromosomes 8 and 11. We did not detect chromosome 1 alterations in precrisis cells or in the E6/E7 immortalized bronchial epithelial cell line generated in this study. In addition, alterations of chromosomes 3 or 10, which are thought to contain genes involved in telomerase regulation, were infrequent in the precrisis cells and not detected in the immortal cell line. However, 11 marker chromosomes were detected, 5 of which were present in the majority of karyotypes examined. Two aberrant chromosomes, (del(14)(q21) and der?(19) t(19;?) (p12 >13::?) were present in all of the karyotypes examined, indicating that these alterations were present in the cell that initially gave rise to the immortalized population. Also, trisomy 5 was present in eight of nine karyotypes.

In conclusion, our results show that expression of both E6 and E7 is required for the immortalization of normal human bronchial epithelial cells by HPV-16. Expression of E6 and/or E7 was able to disrupt the genetic stability of these cells, possibly by inactivating p53-mediated growth arrest, p53 modulation of centrosomal function, or gene amplification. This genomic instability is likely to lead to the immortalization of NHBE cells by E6/E7, which was associated with reactivation of telomerase.

We thank Dr. Denise Galloway, for providing the HPV-16 E6 and E7 retrovirus, and Dr. Joseph Kaplan and Dr. Bharati Hukku of Children's Hospital of Michigan, for performing cytogenetic analyses. The editorial assistance of Dorothea Dudek also is appreciated.

REFERENCES

1. Laimins, L. A. (1993) *Infect. Agents. Dis.* **2,** 74–86.
2. Bernard, H. U., and Apt, D. (1994) *Arch. Dermatol.* **130,** 210–215.
3. Pfister, H. (1987) *Obstet. Gynecol. Clin. North Am.* **14,** 349–361.
4. Riou, G., Favre, M., Jeannel, D., Bourhis, J., Le Doussal, V., and Orth, G. (1990) *Lancet* **335,** 1171–1174.
5. Macnab, J. C., Walkinshaw, S. A., Cordiner, J. W., and Clements, J. B. (1986) *N. Engl. J. Med* **315,** 1052–1058.
6. zur Hausen, H., and Schneider, A. (1987) *in* The Papovaviridae 2: The Papillomaviruses (Salzman, N. P., and Howley, P. M., Eds.), pp. 245–263, Plenum, New York.
7. zur Hausen, H. (1989) *Cancer Res.* **49,** 4677–4681.
8. Willey, J. C., Broussoud, A., Sleemi, A., Bennett, W. P., Cerutti, P., and Harris, C. C. (1991) *Cancer Res.* **51,** 5370–5377.
9. Thomas, P., De Lamballerie, X., Garbe, L., Douagui, H., and Kleisbauer, J. P. (1995) *Cell Mol. Biol. (Noisy-le-grand)* **41,** 1093–1097.
10. Werness, B. A., Levine, A. J., and Howley, P. M. (1990) *Science* **248,** 76–79.
11. Scheffner, M., Werness, B. A., Huibregtse, J. M., Levine, A. J., and Howley, P. M. (1990) *Cell* **63,** 1129–1136.
12. Huibregtse, J. M., Scheffner, M., and Howley, P. M. (1991) *EMBO J.* **10,** 4129–4135.
13. Huibregtse, J. M., Scheffner, M., and Howley, P. M. (1993) *Mol. Cell Biol.* **13,** 775–784.
14. Scheffner, M., Huibregtse, J. M., Vierstra, R. D., and Howley, P. M. (1993) *Cell* **75,** 495–505.
15. Band, V., Dalal, S., Delmolino, L., and Andophy, E. J. (1993) *EMBO J.* **12,** 1847–1852.
16. Hollstein, M., Sidransky, D., Vogelstein, B., and Harris, C. C. (1991) *Science* **253,** 49–53.
17. Ko, L. J., and Prives, C. (1996) *Genes Dev.* **10,** 1054–1072.
18. Fukasawa, K., Choi, T., Kuriyama, R., Rulong, S., and Vande Woude, G. F. (1996) *Science* **271,** 1744–1747.
19. Hickman, E. S., Picksley, S. M., and Vousden, K. H. (1994) *Oncogene* **9,** 2177–2181.
20. Demers, G. W., Foster, S. A., Halbert, C. L., and Galloway, D. A. (1994) *Proc. Natl. Acad. Sci. USA* **91,** 4382–4386.
21. Smith, P. P., Bryant, E. M., Kaur, P., and McDougall, J. K. (1989) *Int. J. Cancer* **44,** 1124–1131.
22. Hawley-Nelson, P., Vousden, K. H., Hubbert, N. L., Lowy, D. R., and Schiller, J. T. (1989) *EMBO J.* **8,** 3905–3910.
23. Thomas, M., Massimi, P., Jenkins, J., and Banks, L. (1995) *Oncogene* **10,** 261–268.
24. Lechner, M. S., and Laimins, L. A. (1994) *J. Virol.* **68,** 4262–4273.
25. Lechner, M. S., Mack, D. H., Finicle, A. B., Crook, T., Vousden, K. H., and Laimins, L. A. (1992) *EMBO J.* **11,** 3045–3052.
26. Mietz, J. A., Unger, T., Huibregtse, J. M., and Howley, P. M. (1992) *EMBO J.* **11,** 5013–5020.
27. Crook, T., Fisher, C., Masterson, P. J., and Vousden, K. H. (1994) *Oncogene* **9,** 1225–1230.
28. Gu, Z., Pim, D., Labrecque, S., Banks, L., and Matlashewski, G. (1994) *Oncogene* **9,** 629–633.
29. Thomas, M., Matlashewski, G., Pim, D., and Banks, L. (1996) *Oncogene* **13,** 265–273.
30. Munger, K., Werness, B. A., Dyson, N., Phelps, W. C., Harlow, E., and Howley, P. M. (1989) *EMBO J.* **8,** 4099–4105.
31. Boyer, S. N., Wazer, D. E., and Band, V. (1996) *Cancer Res.* **56,** 4620–4624.
32. Helin, K., Lees, J. A., Vidal, M., Dyson, N., Harlow, E., and Fattaey, A. (1992) *Cell* **70,** 337–350.
33. Wang, Y., Okan, I., Pokrovskaja, K., and Wiman, K. G. (1996) *Oncogene* **12,** 2731–2735.
34. Demers, G. W., Halbert, C. L., and Galloway, D. A. (1994) *Virology* **198,** 169–174.
35. Puthenveettil, J. A., Frederickson, S. M., and Reznikoff, C. A. (1996) *Oncogene* **13,** 1123–1131.
36. Barbosa, M. S., and Schlegel, R. (1989) *Oncogene* **4,** 1529–1532.
37. Munger, K., Phelps, W. C., Bubb, V., Howley, P. M., and Schlegel, R. (1989) *J. Virol.* **63,** 4417–4421.
38. Halbert, C. L., Demers, G. W., and Galloway, D. A. (1991) *J. Virol.* **65,** 473–478.
39. Woodworth, C. D., Cheng, S., Simpson, S., Hamacher, L., Chow, L. T., Broker, T. R., and DiPaolo, J. A. (1992) *Oncogene* **7,** 619–626.
40. Band, V., De Caprio, J. A., Delmolino, L., Kulesa, V., and Sager, R. (1991) *J. Virol.* **65,** 6671–6676.
41. Shay, J. W., Wright, W. E., Brasiskyte, D., and Van Der Haegen, B. A. (1993) *Oncogene* **8,** 1407–1413.
42. Klingelhutz, A. J., Foster, S. A., and McDougall, J. K. (1996) *Nature* **380,** 79–82.
43. De Silva, R., Whitaker, N. J., Rogan, E. M., and Reddel, R. R. (1994) *Exp. Cell Res.* **213,** 418–427.
44. Miller, A. D., and Rosman, G. J. (1989) *BioTechniques* **7,** 980–982, 984–986, 989–990.
45. Lechner, J. F., and La Veck, M. A. (1985) *J. Tissue Culture Methods* **9,** 43–48.
46. Chomczynski, P., and Sacchi, N. (1987) *Anal. Biochem.* **162,** 156–159.
47. Chen, L., Ashe, S., Singhal, M. C., Galloway, D. A., Hellstrom, I., and Hellstrom, K. E. (1993) *Proc. Natl. Acad. Sci. USA* **90,** 6523–6527.
48. Kim, N. W., Piatyszek, M. A., Prowse, K. R., Harley, C. B., West, M. D., Ho, P. L., Coviello, G. M., Wright, W. E., Weinrich, S. L., and Shay, J. W. (1994) *Science* **266,** 2011–2015.
49. Wright, W. E., Shay, J. W., and Piatyszek, M. A. (1995) *Nucleic Acids Res.* **23,** 3794–3795.

50. Shay, J. W., and Woodring, E. W. (1996) *Curr. Opin. Oncol.* **8,** 66–71.
51. Counter, C. M., Avilion, A. A., LeFeuvre, C. E., Stewart, N. G., Greider, C. W., Harley, C. B., and Bacchetti, S. (1992) *EMBO J.* **11,** 1921–1929.
52. Wright, W. E., Pereira-Smith, O. M., and Shay, J. W. (1989) *Mol. Cell Biol.* **9,** 3088–3092.
53. Shay, J. W., and Wright, W. E. (1989) *Exp. Cell Res.* **184,** 109–118.
54. Wright, W. E., and Shay, J. W. (1992) *Trends Genet.* **8,** 193–197.
55. Gollahon, L. S., and Shay, J. W. (1996) *Oncogene* **12,** 715–725.
56. Klingelhutz, A. J., Barber, S. A., Smith, P. P., Dyer, K., and McDougall, J. K. (1994) *Mol. Cell Biol.* **14,** 961–969.
57. Counter, C. M., Botelho, F. M., Wang, P., Harley, C. B., and Bacchetti, S. (1994) *J. Virol.* **68,** 3410–3414.
58. Bryan, T. M., Englezou, A., Gupta, J., Bacchetti, S., and Reddel, R. R. (1995) *EMBO J.* **14,** 4240–4248.
59. Whitaker, N. J., Bryan, T. M., Bonnefin, P., Chang, A. C., Musgrove, E. A., Braithwaite, A. W., and Reddel, R. R. (1995) *Oncogene* **11,** 971–976.
60. Murnane, J. P., Sabatier, L., Marder, B. A., and Morgan, W. F. (1994) *EMBO J.* **13,** 4953–4962.
61. Rogan, E. M., Bryan, T. M., Hukku, B., Maclean, K., Chang, K., Moy, A. C.-M., Englezou, E. L., Warneford, S. G., Dalla-Pozza, L., and Reddel, R. R. (1995) *Mol. Cell. Biol.* **15,** 4745–4753.
62. Strahl, C., and Blackburn, E. H. (1996) *Mol. Cell Biol.* **16,** 53–65.
63. Shin, K. H., Tannyhill, R. J., Liu, X., and Park, N. H. (1996) *Oncogene* **12,** 1089–1096.
64. Popescu, N. C., and DiPaolo, J. A. (1990) *Cancer Res.* **50,** 1316–1323.
65. DiPaolo, J. A., Popescu, N. C., Alvarez, L., and Woodworth, C. D. (1993) *Crit. Rev. Oncogenesis* **4,** 337–360.
66. Atkin, N. B. (1986) *Cancer Genet. Cytogenet.* **21,** 279–285.
67. Sreekantaiah, C., De Braekeleer, M., and Haas, O. (1991) *Cancer Genet. Cytogenet.* **53,** 75–81.
68. Steenbergen, R. D., Walboomers, J. M., Meijer, C. J., van der Raaij-Helmer, E. M., Parker, J. N., Chow, L. T., Broker, T. R., and Snijders, P. J. (1996) *Oncogene* **13,** 1249–1257.

Received January 16, 1997
Revised version received June 4, 1997

EXPERIMENTAL CELL RESEARCH **235,** 254–264 (1997)
ARTICLE NO. EX973674

A Central Segment of the NG2 Proteoglycan Is Critical for the Ability of Glioma Cells to Bind and Migrate toward Type VI Collagen

Michael A. Burg,*,[1] Akiko Nishiyama,† and William B. Stallcup*

*The Burnham Institute, La Jolla Cancer Research Center, 10901 North Torrey Pines Road, La Jolla, California 92037;
and †Department of Neurosciences, The Cleveland Clinic Foundation, Cleveland, Ohio 44101

Previous studies have established that the NG2 proteoglycan binds directly to type VI collagen. To further our understanding of the biochemical and functional significance of this interaction we have used NG2 cDNA to construct a series of NG2 mutants with deletions spaced throughout the entire length of the 260-kDa NG2 core protein. Following transfection of these mutant cDNAs into B28 glioma cells, we determined the ability of mutant NG2 molecules to anchor type VI collagen on the cell surface. Eight of 11 transfectant populations were able to anchor type VI collagen. The three NG2 variants incapable of anchoring type VI collagen have deletions clustered within the central one-third of the NG2 ectodomain. These deletions identify a 469-amino-acid domain of NG2 responsible for binding of type VI collagen. Functional consequences of the NG2–type VI collagen interaction were explored by testing the relative ability of NG2-transfected and untransfected glioma cells to migrate toward type VI collagen. NG2-expressing cells exhibited a greater migratory response toward type VI collagen than their NG2-negative counterparts. This enhanced migration could be specifically inhibited with NG2 antibodies. Furthermore, glioma cells expressing NG2 in which the collagen-binding domain was deleted failed to exhibit this enhanced migration, whereas NG2 mutants in which non-collagen-binding regions were deleted continued to exhibit increased chemotaxis toward the type VI collagen. These comparisons confirm the importance of the central collagen-binding domain in mediating functionally important interactions between NG2 and type VI collagen. © 1997 Academic Press

INTRODUCTION

The ability of cells to interact with components of the surrounding extracellular matrix (ECM) has been shown to affect numerous cellular processes, including proliferation, migration, and differentiation [1–3]. Moreover, improper expression of matrix components and their receptors has been linked to tumor growth, tumor-associated angiogenesis, and metastasis [4–8]. The best characterized cell-surface receptors for matrix components belong to the integrin family of proteins [9]. This family of heterodimeric proteins has been shown to bind a wide variety of matrix molecules including fibronectin, laminin, thrombospondin, tenascin, and collagens [10]. Integrin-mediated cell attachment to these matrix components is known to activate cellular second messenger systems, leading to changes in cell shape, motility, and proliferation [3]. Alterations in integrin function and expression levels have been linked to the transformation and spread of carcinomas [6, 11]. Matrix components themselves have been shown to modulate integrin expression, further demonstrating the importance of matrix in regulating cellular function [12].

Another group of cell-surface molecules capable of binding extracellular matrix components are cell-surface proteoglycans [13]. The best characterized of these are the syndecans [14], which are capable of binding fibronectin [15], interstitial collagens [16], thrombospondin [17], and tenascin [18]. Binding of these molecules is mediated by the glycosaminoglycan moieties of the syndecans. Syndecan-mediated cell attachment to these matrix components leads to cytoskeletal reorganization and in general appears to augment the function of the other matrix receptors present on the cell surface [19]. Other cell-surface proteoglycans such as betaglycan, glypican, and CD44 have also been shown to interact with matrix molecules [20–22] and to modulate the interaction of integrins with their ECM ligands [13]. Importantly, altered expression of these cell-surface proteoglycans has been implicated in affecting the proliferative and metastatic properties of various neoplastic cells [23–25], thereby underscoring the importance of cell-surface proteoglycans in maintaining proper cellular contacts with the surrounding matrix.

We have been studying a unique integral-membrane chondroitin sulfate proteoglycan, NG2 [see 26 for review]. Both the rat and the human homologs of NG2 have been cloned, and sequence analysis reveals little

---

[1] To whom correspondence and reprint requests should be addressed. Fax: (619) 646-3197. E-mail: mburg@ljcrf.edu.

0014-4827/97 $25.00

Copyright © 1997 by Academic Press
All rights of reproduction in any form reserved.

homology to any other protein or proteoglycan [27, 28]. In the rat, NG2 is found on O2A progenitor cells of the central nervous system [29, 30], chondroblasts of the limbs and spinal column [31, 32], vascular smooth muscle cells, and brain capillary endothelial cells [33]. NG2 expression in these tissues is down-regulated upon terminal differentiation of immature precursor cells, suggesting that NG2 may play a role in the proliferation and/or differentiation of these cells. In support of this idea several studies have suggested that NG2 is capable of modulating cellular responses to PDGF. NG2 and the PDGF-α receptor are colocalized on O2A glial progenitor cells *in vivo* [34]. *In vitro* studies have demonstrated that antibodies against NG2 can diminish PDGF-stimulated proliferation of O2A cells [35]. NG2 antibodies were also found to inhibit PDGF-stimulated proliferation and migration of aortic smooth muscle cells [33], strongly suggesting that NG2 may modulate PDGF function. Significantly, NG2 is reexpressed in several types of cancerous cells, including chondrosarcomas [36], gliomas [37], and melanomas [38], suggesting that NG2 expression may contribute to the neoplastic phenotype of these cells.

In a recent study, we have identified several putative ECM ligands for NG2. These include laminin, tenascin, and types II, V, and VI collagen [39]. The best characterized of these interactions is that of NG2 with type VI collagen. Earlier studies demonstrated that antibodies against NG2 coprecipitate type VI collagen from detergent extracts of glioma cells [32, 40]. In addition, studies have shown that NG2 and type VI collagen display a similar spatiotemporal pattern of expression in several tissues including developing limbs, intervertebral disks, peripheral nerve, and some blood vessels [31, 32]. The strongest evidence linking NG2 and type VI collagen comes from *in vitro* studies. Several different mesenchymal and glioma cell lines which produce both NG2 and type VI collagen have been shown to coexpress both molecules in an identical pattern on cell surfaces [32, 40]. Cells such as B28 glioma cells, which produce type VI collagen but not NG2, are not able to anchor type VI collagen to the cell surface. Transfection of these cells with full-length NG2 cDNA results in colocalization of NG2 and type VI collagen on the cell surface, strongly suggesting that NG2 may represent a cellular receptor for type VI collagen [40]. Solid-phase binding assays demonstrate that purified NG2 is capable of binding directly to pepsin-solubilized type VI collagen. In addition, NG2 binds to the recombinant α2 (VI) collagen chain but not to the α1 (VI) chain or the N-terminal domain of α3 (VI). Binding of NG2 to these type VI collagen substrates appears to depend mainly on the NG2 protein core, since chondroitinase-treated NG2 binds the collagen as well as undigested proteoglycan samples [39].

The NG2 core protein can be divided into a short cytoplasmic region, a transmembrane domain, and a large extracellular domain [27]. This extracellular domain can roughly be subdivided into three regions: an aminoterminal cysteine-rich domain (domain 1), a central domain to which the chondroitin sulfate chains are attached (domain 2), and another cysteine-rich region juxtaposed to the membrane (domain 3). Based on immunoprecipitation data we initially suggested that the central domain of the core protein might be important for type VI collagen binding [27]. Recent binding studies using purified NG2 recombinant fragments have also supported this hypothesis [41]. In the present study our aim has been to verify and extend this observation in a cellular system which more accurately represents the natural environment for cell–matrix interactions. A series of variant cDNAs containing specific deletions in the NG2 coding sequence was transfected into B28 glioma cells, and the ability of the mutant NG2 molecules to anchor endogenously synthesized type VI collagen at the cell surface was tested using double-immunofluorescence staining. Our results from these assays allow us to pinpoint the type VI collagen-binding domain to a 469-amino-acid segment in the N-terminal portion of NG2 domain 2. To further our understanding of the functional role that the NG2–type VI collagen interaction may play in cell behavior, we compared the relative ability of NG2-negative, NG2-positive, and variant NG2-expressing glioma cells to migrate in response to type VI collagen. These results also implicate the central collagen-binding domain of NG2 as the key player in mediating functional cellular responses to type VI collagen.

MATERIALS AND METHODS

Cell lines. The rat B28 glioma cells used in the present study were originally isolated from a central nervous system tumor induced by ethylnitrosurea [42]. The U251MG human astrocytoma cell line was provided to us by Eva Engvall (The Burnham Institute). In some cases NG2-transfected clones of these cell lines were used. Production of these clones has been previously described [40].

Construction and transfection of NG2 deletion cDNAs. A cDNA encoding the entire rat NG2 sequence has been previously cloned into the pcDNAI/amp expression vector (Invitrogen, San Diego, CA). This construct, pcDNAamp/NG2, was used for the generation of NG2 deletion cDNAs. In some cases the deletions were produced by restriction digestion, removal of the fragment, and religation. Other cDNAs were generated by production of PCR fragments in which specific NG2 sequences were removed. These PCR fragments were then reannealed into the appropriate restriction sites of pcDNAamp/NG2.

The positions of these deletions are shown in Fig. 1. The correct in-frame placement of the deletions was verified by restriction mapping and sequencing. These NG2 cDNAs were transfected into the rat B28 glioma cell line as previously described [40]. Briefly 8–16 μg of cDNA was cotransfected with 0.4 μg of the psv2/neo plasmid (Invitrogen) into 60-mm dishes of subconfluent B28 cells using Lipofectin (Gibco BRL). Cells were diluted into 100-mm dishes, and transfected cells were selected in the presence of 250 μg/ml neomycin (G418). Resistant colonies were isolated and screened for the

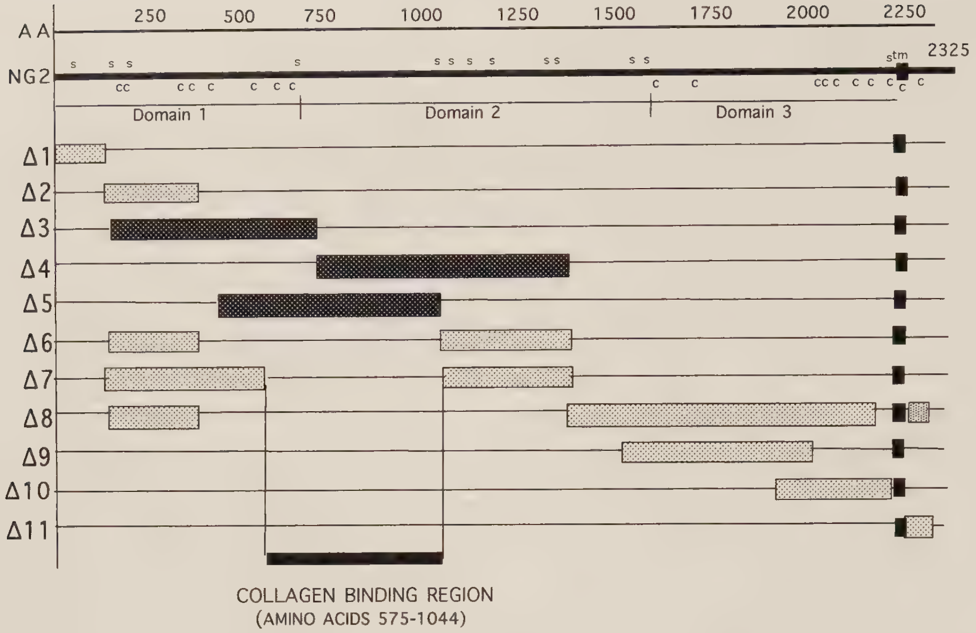

FIG. 1. NG2 deletion map. A schematic representation of the NG2 core protein is shown. A series of 11 NG2 deletion mutants was constructed and transfected into B28 glioma cells. Boxed regions indicate the deleted segments. The ability of the mutant NG2 molecules to anchor type VI collagen to the glioma cell surface was tested using immunofluorescence. Eight of 11 mutants retained the ability to anchor type VI collagen (light stippled boxes). Three deletions abolished NG2's ability to anchor type VI collagen (black boxes). These deletions define a collagen-binding region between amino acids 575 and 1044 of the NG2 core protein. s, Ser–Gly amino acid pair; c, cysteine; tm, transmembrane domain.

expression of NG2 by immunofluorescence using monoclonal and polyclonal anti-NG2 antibodies. Initial studies were carried out using transiently transfected B28 cells. Subsequent analyses of relevant constructs were performed using clones isolated from stably transfected cells.

Immunofluorescence. In order to test for the ability of different NG2 species to anchor type VI collagen on cells, untransfected, mock-transfected, and NG2-transfected B28 cells were grown in 60-mm dishes in DMEM containing 15% FCS for 2–3 days. In order to detect surface expression of NG2 and type VI collagen, live cells were stained using a polyclonal antibody directed against human type VI collagen [43] and a monoclonal antibody mixture against NG2 [27]. These molecules were then visualized using an FITC-conjugated anti-rabbit secondary antibody and RITC-conjugated anti-mouse secondary antibodies.

Migration assays. Migration assays were performed using a Boyden chamber (Neuroprobe, Inc., Cabin John, MD) as previously described [33]. To assess the relative ability of glioma cells to migrate in response to soluble type VI collagen, purified pepsin-solubilized type VI collagen [44] was diluted into DMEM +0.1% BSA at a final concentration of 20 μg/ml and placed in the lower wells of the chamber. DMEM + 0.1% BSA alone was also placed in some wells to monitor the basal migration of the cells. An uncoated micropore filter (pore size 8 μm; Poretics, Livermore, CA) was placed between the top and bottom chambers. Glioma cells were removed from tissue culture dishes using enzyme-free cell dissociation buffer (Gibco BRL) and resuspended in DMEM + 0.1% BSA. Cells were added to the upper wells of the chamber (15,000–20,000 cells/well), and the chamber was incubated at 37°C for 4 h. In some cases cells were preincubated with normal rabbit serum or anti-NG2 antisera for 30 min at 37°C prior to addition to the wells. The anti-NG2 antibodies used in these studies consisted of a cocktail of three different polyclonal antibodies produced against the intact rat NG2 molecule, a cyanogen bromide fragment derived from domain 2, and a cyanogen bromide fragment derived from domain 3 [27]. To determine the number of migrating cells, filters were removed, briefly fixed in methanol, and stained (Dif Quick stain, American Hospital Supply Corp., McGaw Park, IL) to visualize cells. Cells on the top of the filter were scraped off, and migratory cells on the underside of the filters were counted at a magnification of 200× using a Nikon Optiphot microscope. All conditions were tested in triplicate, and five independent 100-mm^2 fields were counted per well. All experiments were repeated a minimum of three times. Data from three separate experiments were used for construction of the figures.

Immunoprecipitations. Type VI collagen was immunoprecipitated from the conditioned media of various transfected B28 cell lines as previously described [40]. Briefly, confluent cultures of untransfected or transfected B28 cells were labeled overnight in the presence of 100 μCi/ml of [^{35}S]methionine (NEN) in methionine-free DMEM supplemented with 1% FCS. Type VI collagen was immunoprecipitated from the [^{35}S]methionine-labeled conditioned media using a rabbit anti-human type VI collagen antiserum and protein A–Sepharose. Samples were boiled in SDS–PAGE sample buffer containing 5% 2-mercaptoethanol and electrophoresed through a 3–20% acrylamide gel. Labeled bands were visualized by fluorography after treatment of the gel with Enhance (NEN).

NG2 and the various truncated NG2 molecules were immunoprecipitated from transfected B28 cells as previously described [27, 40]. Cells were surface labeled with ^{125}I using the lactoperoxidase method [45]. Labeled cells were extracted with 1% NP-40 in PBS in the presence of soybean trypsin inhibitor. Extracts were then incubated with a rabbit antibody against NG2 followed by incubation with protein A–Sepharose. In some cases the precipitates were treated with 0.02 units of chondroitinase ABC (ICN Biomedicals, Costa Mesa, CA) at room temperature for 45 min to remove chondroitin sulfate chains. Samples were then boiled in SDS–PAGE reducing sample buffer, electrophoresed through a 3–20% acrylamide gel, and visualized using autoradiography.

RESULTS

Construction and Expression of NG2 Deletion Mutants

A series of 11 deletion mutants was constructed utilizing the full-length NG2 cDNA (Materials and Methods). Figure 1 shows the location of the various deletions within the NG2 polypeptide sequence, which can be divided into three major extracellular regions, a transmembrane domain, and a short cytoplasmic tail (27). Several of the deleted sequences overlap, while some delete unique segments of NG2. Together, this series of deletions encompasses the entire coding sequence of the NG2 core protein.

In order to test the ability of the various mutant NG2 molecules to bind type VI collagen, the expression pattern of both NG2 and type VI collagen in transfected B28 cells was monitored using double-immunofluorescence with anti-NG2 monoclonal antibodies and a polyclonal antibody against type VI collagen. These studies first were done using transient transfectants and subsequently repeated using stable transfectants. Several different stable clones for each mutant were selected and tested. Representative results are shown in Figs. 2 and 3. As previous studies have demonstrated, untransfected B28 cells or CMV control transfected cells both fail to express NG2 or type VI collagen on the cell surface. In contrast, B28 cells expressing the wild-type NG2 molecule show colocalized expression of both NG2 and type VI collagen on their cell surface [40]. B28 cells expressing mutant NG2 molecules in which portions of the N-terminal domain 1 (Δ1, Δ2) were deleted retained the ability to anchor type VI collagen (Figs. 2a and 2b). Similarly, removal of portions of the membrane proximal domain 3 (Δ9, Δ10) did not diminish the ability of NG2 to retain type VI collagen (Figs. 2g and 2h). Expression of an NG2 variant in which all but six amino acids of the cytoplasmic domain were deleted (Δ11) also resulted in colocalized expression of NG2 and type VI collagen on the cell, suggesting that the cytoplasmic domain of NG2 is not critical for type VI collagen retention on the B28 glioma cell surface (data not shown). In contrast, two nonoverlapping deletions which removed central portions of the NG2 extracellular domain (Δ3, Δ4) appeared to abolish the ability of NG2 to anchor type VI collagen to the B28 cell surface even though expression of these variant NG2 molecules appears to occur normally (Figs. 2c–f). Since these deletions suggest that the central extracellular region of NG2 is responsible for binding to type VI collagen, we examined this region in more detail. First, we demonstrated that an NG2 variant (Δ8) lacking the entire extracellular domain of NG2 except the signal sequence, the N-terminal two-thirds of domain 2, the transmembrane domain, and a small part of the cytoplasmic domain still allowed NG2 to anchor type VI collagen (Figs. 3a and 3b). This result shows that the central domain of NG2 is sufficient for collagen binding. In contrast, deletion of a major portion of this sequence (Δ5) abolished the ability of NG2 to anchor type VI collagen at the cell surface (Figs. 3c and 3d). Together these two mutants (Δ5, Δ8) localize the collagen-bind-

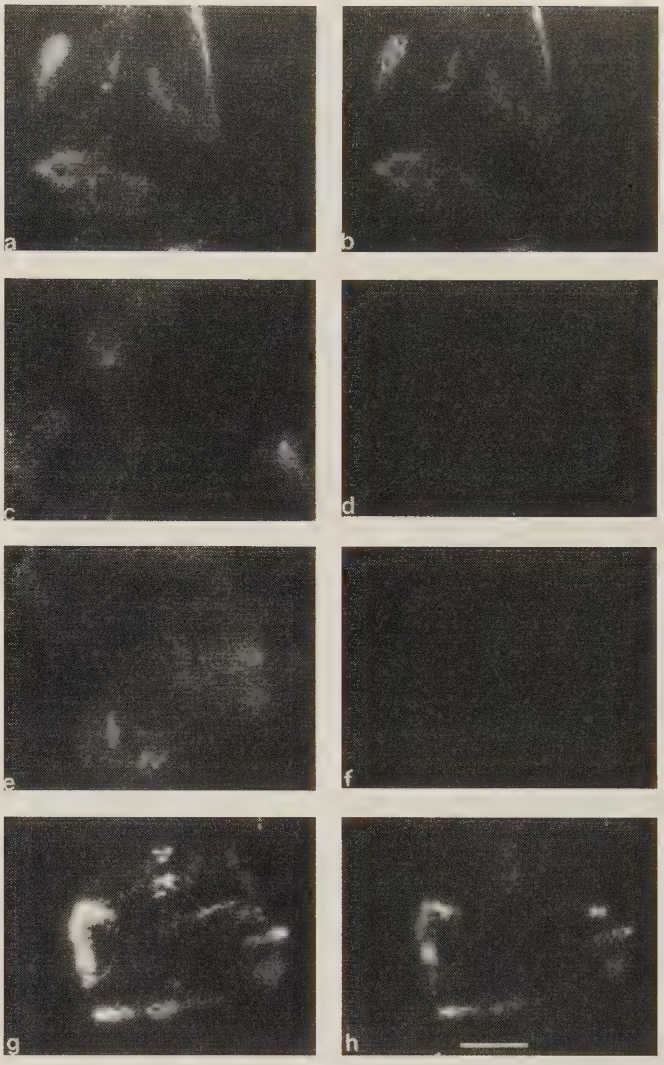

FIG. 2. Immunofluorescent staining for NG2 and type VI collagen on B28 cells transfected with NG2 deletion mutants. Surface expression of NG2 and type VI collagen was visualized by staining B28 cells with an NG2 monoclonal antibody cocktail (a, c, e, g) and a polyclonal antiserum against type VI collagen (b, d, f, h), followed by staining with FITC- and RITC-conjugated secondary antibodies. Deletions which removed an N-terminal segment (Δ2; a, b) or a C-terminal region of the NG2 core (Δ10; g, h) retain the ability to anchor type VI collagen. Two deletions (Δ3; c, d, Δ4; e, f) within the central region of the NG2 ectodomain fail to anchor type VI collagen. Bar in h, 20 μm.

ing region of NG2 to a 700-amino-acid segment contained within the central domain 2. In an attempt to narrow down the collagen-binding region further, we constructed and tested two additional mutants with deleted segments bordering on the N-terminal and C-terminal ends of this central segment. $\Delta6$ deletes sequences on both sides of the 700-amino-acid putative collagen-binding region described by $\Delta8$, but contains most of the sequence deleted in $\Delta5$. Expression of this NG2 variant results in anchoring of type VI collagen (Figs. 3e and 3f), thereby narrowing the putative collagen-binding region of NG2 to a 644-amino-acid segment. Another mutant ($\Delta7$) with a larger N-terminal portion of the central domain of NG2 deleted was also seen to retain the type VI collagen-anchoring ability (Figs. 3g and 3h). Together, these deletions localize the major type VI collagen-binding region of NG2 to a 469-amino-acid segment between residues 575 and 1044, i.e., the amino-terminal half of domain 2 (Fig. 1).

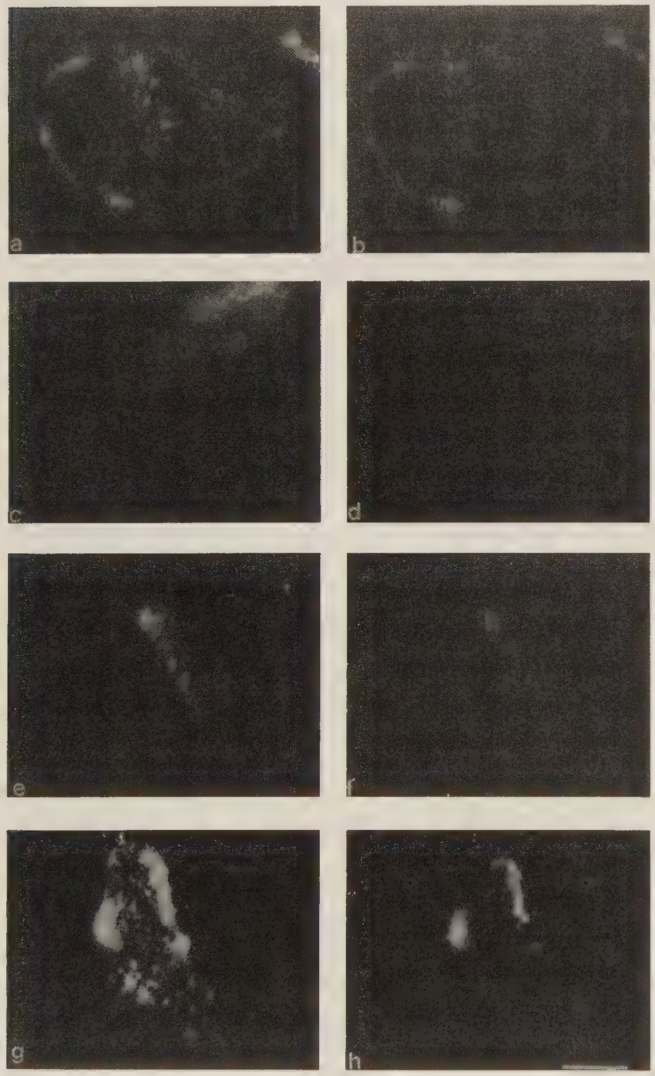

FIG. 3. Further immunofluorescence analysis of NG2 deletion mutants. B28 cells transfected with NG2 deletion mutants were analyzed as in Fig. 2. NG2 staining (a, c, e, g) and type VI collagen staining (b, d, f, h) are shown. $\Delta8$ (a, b), $\Delta6$ (e, f), and $\Delta7$ (g, h) all retain the ability to anchor type VI collagen, while $\Delta5$ (c, d) abolishes type VI collagen binding. Bar in h, 20 μm.

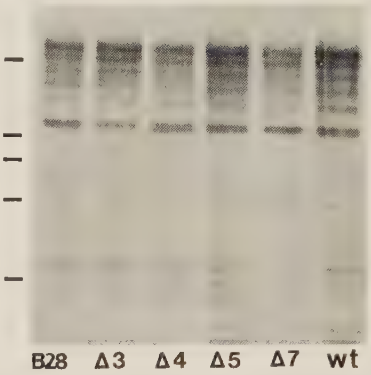

FIG. 4. Type VI collagen immunoprecipitations. Untransfected B28, B28 cells transfected with wild-type NG2 (wt), or B28 cells transfected with the indicated mutants were labeled overnight with $[^{35}S]$methionine. Type VI collagen was immunoprecipitated from the media using an anti-type VI collagen antiserum. The $\alpha1$ (VI) and $\alpha2$ (VI) subunits (130–140 kDa) and the $\alpha3$ (VI) (200–260 kDa) subunit of type VI collagen were detected in the conditioned media from all cell lines tested. The positions of molecular weight standards of 200, 116, 93, 67, and 45 kDa are indicated on the left of the gel.

Biochemical Characterization of NG2 and Type VI Collagen Expressed by Transfected Cells

Since our immunofluorescence studies relied on the relative ability of variant NG2 species to bind type VI collagen at the cell surface, it was important to demonstrate that the panel of transfected B28 clones all produced similar levels of type VI collagen. To test this, secreted type VI collagen was immunoprecipitated from conditioned media of $[^{35}S]$methionine-labeled cells using a rabbit antibody against type VI collagen. As shown in Fig. 4, we found that each of the B28 transfectants exhibited a typical profile for type VI collagen. This consists of two bands of 130 to 140 kDa ($\alpha1$ (VI) and $\alpha2$ (VI)) and a heterodisperse band of approximately 200 kDa ($\alpha3$ (VI)). There appear to be no major differences in size of the $\alpha1$, $\alpha2$, and $\alpha3$ chains or in the quantity of type VI collagen components secreted by the various transfectants. Clones that are able to anchor type VI collagen (wt, $\Delta7$) are indistinguishable from those that are unable to anchor type VI collagen ($\Delta3$, $\Delta4$, $\Delta5$), suggesting that type VI collagen anchorage is due to the presence of a functional NG2 species rather than to differences in type VI collagen production.

In order to confirm that the NG2 variants were correctly expressed in the transfected cells, cell-surface

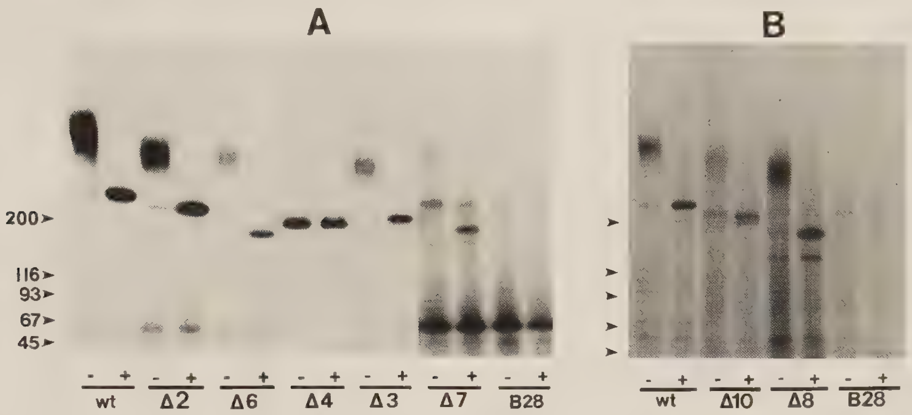

FIG. 5. NG2 immunoprecipitations. NG2 was immunoprecipitated from ^{125}I-labeled detergent extracts prepared from the different NG2 clones using an anti-NG2 polyclonal antiserum. B28 cells transfected with wild-type NG2 (wt; −) display a typical heterodisperse band of 350–600 kDa, which is converted into the 300-kDa protein core upon chondroitinase ABC treatment (wt; +). All the deletion mutants tested exhibited truncated core proteins consistent with the amounts of sequence deleted from the NG2 cDNA. NG2 was not detected in the untransfected B28 cells. Immunoprecipitations shown in A and B were performed on different days and electrophoresed on separate gels. Locations of the molecular weight markers of 200, 116, 93, 67, and 45 kDa are shown at left. (−) Untreated precipitates. (+) Chondroitinase-treated precipitates.

NG2 was immunoprecipitated from detergent extracts prepared from the different ^{125}I-labeled NG2 clones. The results show that B28 cells transfected with wild-type NG2 display a typical heterodisperse band of 350–600 kDa. This band is converted to the 300-kDa NG2 protein core upon digestion with chondroitinase ABC (Fig. 5). These components are absent in the B28 parental cells. All of the deletion mutants tested exhibited core proteins smaller than the wild-type molecule. The sizes of the truncated core proteins were consistent with the amounts of sequence deleted from the variant cDNA species.

This biochemical analysis also allows us to analyze which serines may be serving as sites for chondroitin sulfate chain addition. There are 13 Ser–Gly pairs within the NG2 ectodomain which could serve as GAG acceptor sites (Fig. 1). Our analysis reveals that, with one exception, all of the NG2 variants analyzed contain glycosaminoglycan chains. Δ4 (which lacks amino acids 711–1377) appears to lack glycosaminoglycans, as judged by the identical 200-kDa protein bands present both before and after chondroitinase digestion. Six of the 13 Ser–Gly pairs are found within this segment. These data therefore suggest that the other 7 Ser–Gly pairs found outside of amino acids 711–1377 do not have chondroitin sulfate chains attached to them. These data are consistent with our previous finding that the chondroitin sulfate chains of NG2 are located in domain 2 [27]. In contrast to Δ4, deletions Δ6 and Δ7, which delete only the C-terminal half of the deleted sequence of Δ4 (amino acids 1044–1377), do contain chondroitin sulfate chains, as revealed by the presence of heterodisperse species which are converted to discrete bands upon chondroitinase digestion. Since there is only one Ser–Gly pair in domain 2 which is not common to Δ4, Δ6, and Δ7 (amino acids 999–1000; Ref. [27]), the data suggest that chondroitin sulfate chains are attached at this specific serine residue. The data do not rule out the possibility that one or more of the other 5 Ser–Gly pairs found between amino acids 1044–1377 may also be substituted with GAG chains.

Structural Analysis of the Type VI Collagen-Binding Region of NG2

Searches of the Swiss-Prot and NBRF-PIR protein data bases have not revealed any obvious homologies between NG2 and other collagen-binding proteins. Therefore, we were interested in identifying structural features within the 469-amino-acid collagen-binding domain that might be responsible for NG2–type VI collagen interaction. Since it is thought that secondary structure plays a pivotal role in collagen–protein interactions [46, 47], we used the Chou and Fasman method [48] to generate a secondary structure prediction for the NG2 core protein (Fig. 6). This analysis suggests that the N- and C-terminal domains of NG2 should be highly globular. By comparison, the central region of NG2 is predicted to have a rather extended conformation (Fig. 6A). One segment in particular is seen to have a very extended α helical region. This extended region in the N-terminal segment of NG2 domain 2 falls directly within the collagen-binding region identified by our deletion analysis (Fig. 6B).

Migration Studies

Our transfection studies with NG2 deletion mutants have pinpointed a specific segment of the NG2 core protein which enables the proteoglycan to serve as a cell surface receptor for type VI collagen. An important issue to be resolved concerns the potential role of the NG2/type VI collagen interaction in modulating cell behavior. To determine if NG2 expression affects the ability of glioma cells to migrate in response to type VI collagen, we have used a Boyden chamber assay to compare the relative ability of NG2-negative, NG2-positive, and NG2 variant-expressing B28 cells to migrate toward type VI collagen. For these assays, type VI collagen was placed in the lower chamber of the Boyden apparatus to serve as a soluble chemoattractant. As shown in Fig. 7, we found that all of the B28 variants exhibit similar low rates of migration under basal conditions (DMEM + 0.1% BSA). The presence of type VI collagen in the bottom chamber stimulates migration of the B28 parental cells, but B28 cells which also express wild-type NG2 exhibit an even larger migratory response to the type VI collagen. To further establish the role of NG2 in this process, we tested three NG2 mutants for their relative ability to migrate toward type VI collagen. B28 cells expressing Δ4, an NG2 variant missing the collagen-binding domain, migrate in response to type VI collagen at rates comparable to those of untransfected (Fig. 7) or mock-transfected B28 cells (data not shown). In contrast, deletions Δ2 and Δ10, which delete amino-terminal and carboxy-terminal sequences of NG2 but contain an intact central collagen-binding domain, both display enhanced migration comparable to that seen with cells expressing the wild-type NG2 (Fig. 7). To further substantiate the role of NG2 in type VI collagen-directed migration, we tested the ability of anti-NG2 antibodies to inhibit the enhanced migratory response of NG2-positive glioma cells to type VI collagen. Pretreatment of glioma cells with polyclonal antisera against NG2 inhibited the migration of NG2-positive cells toward type VI collagen in a dose-dependent manner. As a control, pretreatment of glioma cells with normal rabbit serum had no effect on migration (Fig. 8). In addition, anti-NG2 antibodies had no effect on the migration of untransfected (Fig. 8) or mock-transfected B28 cells (data not shown). Similar migratory responses were observed with a human glioma cell line, U251. NG2-transfected U251 cells displayed an enhanced migratory response toward type VI collagen compared to the untransfected parental line. This enhanced response could be overcome with increasing concentrations of anti-NG2 antibodies (Fig. 9).

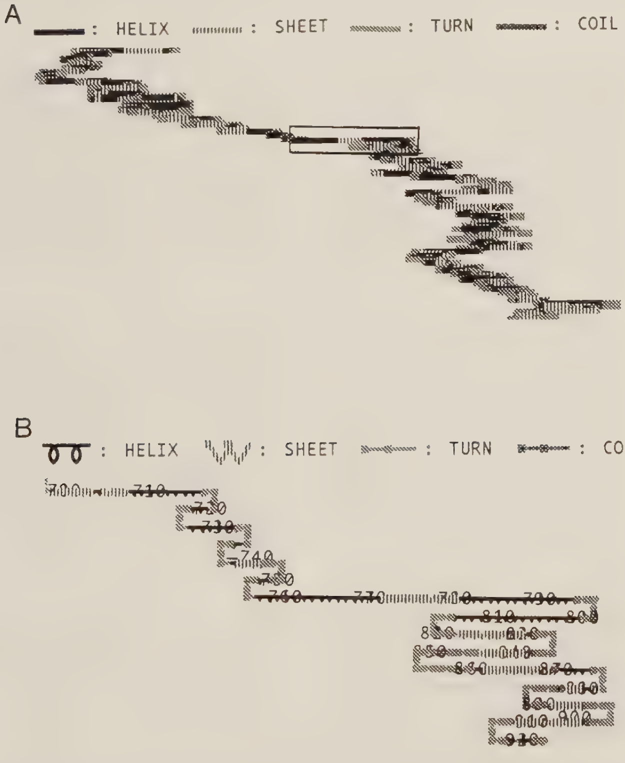

FIG. 6. NG2 secondary structure prediction. A secondary structure map of NG2 was generated using the Chou and Fasman method [48]. The NG2 core protein is predicted to contain rather globular N- and C-termini with a region of extended secondary structure connecting these domains (A). Examining this central extended region in more detail we observe that the extended sequence consists of alternating α-helical and β-sheet regions (B). This region (approximately amino acids 750–850) falls directly within the collagen-binding domain of NG2 (see Fig. 1). B is an enlargement of the boxed area in A.

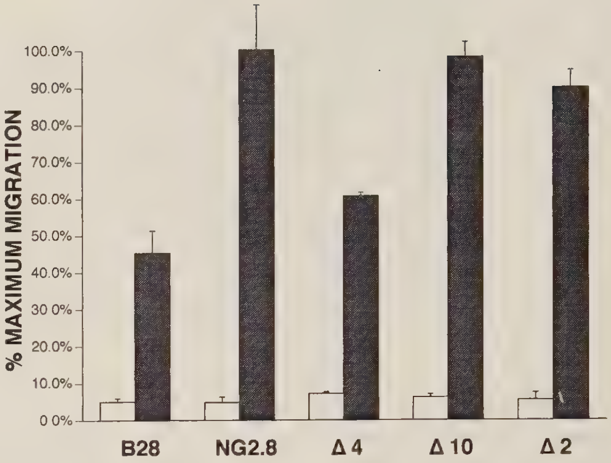

FIG. 7. Type VI collagen-mediated migration of B28 cells. The relative ability of NG2-negative B28 cells, B28 cells transfected with wild-type NG2 (NG2.8), and B28 cells transfected with various NG2 deletion mutants to migrate toward BSA (white columns) or type VI collagen (black columns) was tested using a Boyden chamber. The migration rate of NG2.8 was set at 100% and all other data were normalized to this figure. Values represent means ± SD from three separate experiments.

DISCUSSION

In the present study we have further characterized the interaction of type VI collagen with a cell-surface proteoglycan receptor, NG2. In order to localize the type VI collagen-binding domain of NG2 we have utilized a series of NG2 cDNA variants with deletions placed strategically throughout the entire coding sequence of the NG2 polypeptide. Transfection of these NG2 cDNAs into B28 glioma cells and subsequent testing of the ability of the expressed NG2 variants to anchor type VI collagen to the cell surface reveal that all but three of the deletion mutants are capable of anchoring type VI collagen. These three mutants have deletions clustered within the central extracellular domain of NG2. The panel of mutants enables us to localize the collagen-binding domain of NG2 to a 469-amino-acid segment between amino acids 575 and 1044 of the NG2 protein core. These data support earlier biochemical data which suggested that the central domain of NG2 might be involved in binding to type VI collagen [27]. The data are also in agreement with recent studies which demonstrate that a soluble recombinant fragment of NG2-containing 700 amino acids of the central domain is capable of binding to immobilized type VI collagen [41]. The present study suggests that the first 469 amino acids of this domain are the most critical for mediating the interaction between NG2 and type VI collagen. The use of solid-phase binding assays to test smaller recombinant NG2 fragments representing this N-terminal portion of domain 2 is currently in progress.

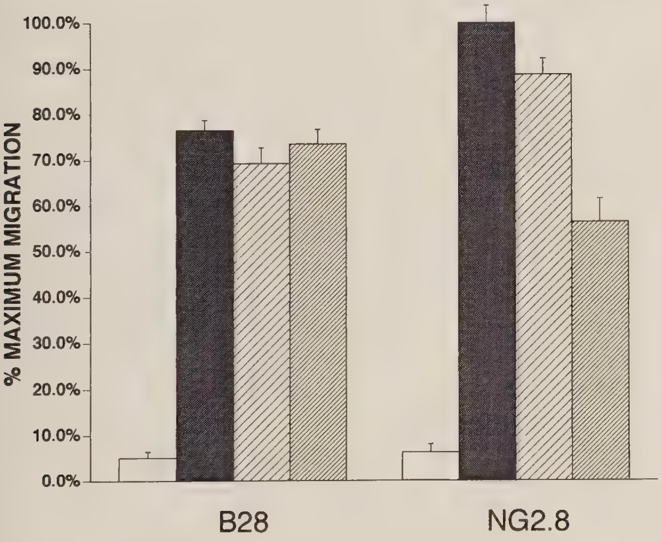

FIG. 8. Inhibition of type VI collagen-mediated migration with anti-NG2 antibodies. The relative ability of NG2-negative B28 cells and B28 cells transfected with wild-type NG2 (NG2.8) to migrate toward BSA or type VI collagen was tested in the presence of increasing concentrations of anti-NG2 polyclonal antibodies or normal rabbit serum. The migration rate of NG2.8 in the presence of normal rabbit serum was set at 100% and all other data were normalized to this figure. Values represent means ± SD from three separate experiments. □, BSA; ■, type VI collagen, NRS; ▨, type VI collagen, anti-NG2 1:300; ▩, type VI collagen, anti-NG2 1:100.

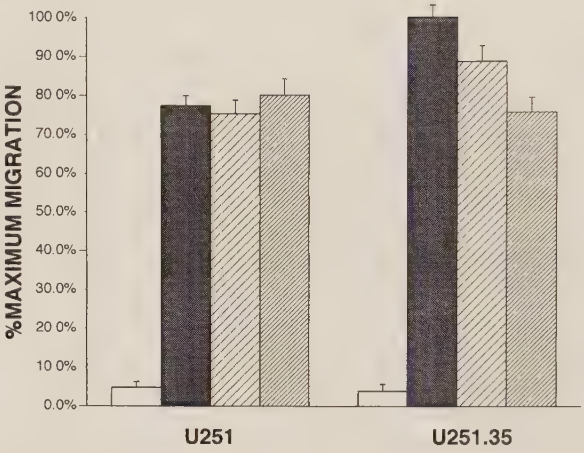

FIG. 9. Type VI collagen-mediated migration of human U251 glioma cells. The relative ability of NG2-negative U251 cells and U251 cells transfected with wild-type NG2 (U251.35) to migrate toward BSA or type VI collagen was tested in the presence of increasing concentrations of anti-NG2 antibodies or normal rabbit serum. The migration rate of U251.35 cells in the presence of normal rabbit serum was set at 100% and all other data were normalized to this figure. Values represent means ± SD from three separate experiments. □, BSA; ■, type VI collagen, NRS; ▨, type VI collagen, anti-NG2 1:300; ▩, type VI collagen, anti-NG2 1:100.

Our previous studies showed that the leucine-rich proteoglycan decorin was capable of inhibiting the binding of NG2 to type VI collagen, suggesting that the two proteoglycans might bind to overlapping regions on the collagen substrate [39]. The possibility that the two proteoglycans themselves might share similar collagen-binding motifs in their protein cores is not supported by sequence comparisons. Although the type VI collagen-binding domain of NG2 contains a high percentage of leucine residues (>15%), there is no sequence similarity between this region and the leucine-rich regions of collagen-binding proteoglycans such as decorin and biglycan [46]. The interaction of the leucine-rich proteoglycans with collagen is thought to occur via a unique feature of the proteoglycan secondary structure. The leucine-rich repeats are thought to form alternating α-helical and β-turn units which serve to form an open horseshoe-like structure in which the collagen helices can bind [46, 47]. A similar type of secondary structure may exist in the NG2 collagen-binding domain. Secondary structure predictions suggest that this region of NG2 assumes a rather extended conformation in comparison to the N-terminal and C-terminal globular regions surrounding it. Recently, electron microscopy of rotary shadowed NG2 has confirmed that NG2 is composed of two globular domains separated by a nonglobular rod-like central region. Rotary shadowing studies also demonstrate that pepsin-digested type VI collagen associates with NG2 along this central rod-like domain when complexes of the two molecules are allowed to form [41].

Functionally, expression of NG2 molecules containing the 469-amino-acid collagen-binding domain enables glioma cells to assemble a type VI collagen matrix on their cell surface. While the exact function of type VI collagen has not been fully elucidated, studies have suggested that this collagen may serve as a bridging molecule anchoring cells to the surrounding matrix [49, 50]. Immunohistochemical analysis has revealed that type VI collagen is concentrated around the basement membranes and cell surfaces surrounding developing nerves, blood vessels, and fat cells [50]. The ability of type VI collagen to bind to a number of extracellular matrix components such as hyaluronic acid [51], tenascin [52], and fibrillar collagens [53] as well as to cell surface receptors such as CD44 [54], integrins [55, 56], and NG2 [32, 39–41] strengthens this idea. Indeed, NG2 and type VI collagen display an overlapping expression pattern in many tissues, most notably in developing blood vessels [32, 33] and cartilage [31, 32]. The *in vitro* data presented in earlier studies [32, 40] along with findings from the present studies suggest that the collagen-binding capability of NG2 may greatly assist in the anchoring function of type VI collagen.

In addition to serving a structural role, type VI collagen interactions with cells have been implicated in affecting processes such as cell proliferation, migration, and differentiation [57]. Type VI collagen is found along migratory pathways for neural crest cells during development [58], and neural crest cells have been shown to bind and migrate along type VI collagen substrates *in vitro* [58, 59]. Several studies have shown that glial cells [60] and uveal melanoma cells [61] which produce type VI collagen are more invasive than those that do not, suggesting that the modified type VI collagen matrix produced by these cells may lead to the increased invasiveness seen with these malignancies. In the present study we demonstrate that both rat and human glioma cells are capable of migrating toward type VI collagen, suggesting that NG2-negative glioma cells have type VI collagen recognition mechanisms. Known type VI collagen receptors include $\alpha1\beta1$ and $\alpha2\beta1$ integrins [55, 56] and the CD44 proteoglycan [54], all of which are present on the glioma cells tested in these studies (unpublished observation). Significantly, NG2 expression on these cells results in enhanced migratory responses to type VI collagen. This NG2-mediated enhancement could be abolished by treatment with anti-NG2 antibodies or by deletion of the collagen-binding region. Several possible mechanisms may account for NG2's ability to potentiate glioma migration toward type VI collagen. First, the binding of type VI collagen to NG2 may change the interaction of NG2 with the actin cytoskeleton, resulting in increased cellular motility. Previous studies have indeed shown that NG2 is localized to specific actin-containing filopodia on spreading and migrating glioma cells, suggesting that NG2 may participate in cell locomotion [62, 63]. Alternatively, binding to NG2 might alter the interaction of type VI collagen with its other receptors in such a way as to potentiate cell motility. Finally, the ability of NG2 to modulate integrin function has been demonstrated in the case of interaction of the $\alpha4\beta1$ integrin with fibronectin. McCarthy *et al.* have shown that NG2 potentiates $\alpha4\beta1$-mediated spreading of melanoma cells on a CS1 fibronectin peptide [64, 65]. The possibility that NG2 may enhance cell migration by directly modulating the activity of the collagen-binding integrins $\alpha1\beta1$ and $\alpha2\beta1$ awaits further study.

It is somewhat paradoxical that NG2-negative glioma cells were able to migrate toward type VI collagen even though they were not able to anchor type VI collagen produced by cells in culture. This paradox may be resolved by the fact that migration was tested on pepsin-digested type VI collagen, whereas cell-surface anchorage in culture involves native type VI collagen. It is well established that integrin-mediated cell adhesion to type VI collagen appears to occur primarily with denatured collagen preparations in which "cryptic" RGD sites are exposed [55]. With native type VI collagen produced in culture these sites may be unavailable for integrin binding. However, cellular NG2 may interact with the native type VI collagen molecules, anchoring them to the cells. It would be instructive to learn if NG2 can mediate glioma cell migration toward native type VI collagen either by direct binding or alternatively by changing the conformation of type VI collagen, thereby exposing cryptic integrin-binding domains.

Several studies have indicated a role for NG2 in glioma progression. NG2 expression occurs in the most malignant glioma phenotypes, glioblastomas, and astrocytomas [37]. In these tumors NG2 expression is found on the glioma cells themselves as well as in the supporting vasculature. Malignant gliomas are characterized by their extensive invasiveness of brain tissue [66]. The composition of brain matrix is unique in that it normally contains very little collagen, laminin, and fibronectin but contains an abundance of hyaluronic acid and matrix proteoglycans of the lectican family [67]. However, during the spread of gliomas, the glioma cells themselves transform the ECM by their increased expression of tenascin, HA, and in some cases, type VI collagen [68–70]. This neoplastic transformation of the matrix by the glioma cells is thought to enhance the growth and spread of these cells through the brain parenchyma. The fact that NG2 binds both tenascin and type VI collagen suggests that NG2 may assist in the spread of glioma cells via interactions with these components of the neoplastic ECM. In addition, since type VI collagen is known to bind both tenascin and HA directly, NG2's interaction with type VI collagen may indirectly augment the cell's ability to spread and migrate on these matrix molecules.

NG2–type VI collagen interactions may also potentiate growth factor-driven proliferative and migratory responses. PDGF and PDGF receptors are up-regulated in many malignant glioma cells [71, 72]. A recent study has shown that several different collagen types, including type VI collagen, are capable of binding PDGF and that the collagen-bound PDGF is still functional [73]. An intriguing possibility is that NG2 may bind the type VI collagen–PDGF complex and enhance the growth factor's interaction with PDGF receptors on the glioma cell surface. The fact that NG2 has been shown to enhance PDGF-driven growth and migratory responses in both O2A glial progenitors [35] and smooth muscle cells [33] suggests that NG2 may function similarly in modulating PDGF effects on glioma cells.

In summary, in the present study we have used a series of NG2 deletion mutants to localize the type VI collagen-binding region of NG2 to a 469-amino-acid segment in the amino-terminal portion of NG2 extracellular domain 2. B28 glioma cells expressing NG2 variants containing this region were capable of anchoring type VI collagen to their cell surfaces. In contrast, NG2-negative B28 parental cells or B28 cells expressing truncated NG2 species lacking large portions of this 469-amino-acid domain failed to anchor the type VI collagen molecules. These studies have also extended our understanding of the functional significance of NG2's role as a type VI collagen receptor by showing that NG2 expression enhances the migratory response of glioma cells to type VI collagen. A mounting body of evidence suggests that increased levels of type VI collagen occur along certain migratory paths during development, in tissue remodeling after injury, and in the tumor stroma of melanomas, gliomas, and chondrosarcomas. The correlation of this localization with increased migration and invasiveness of cells points to the importance of NG2–type VI collagen interactions in these processes.

This work was supported by NIH Grant R01 21990 to W.B.S. and by NIH Fellowship F32 CA72220 to M.A.B. We thank Dr. Rupert Timpl for the gift of purified type VI collagen.

REFERENCES

1. Sage, E. H., and Bornstein, P. (1991) *J. Biol. Chem.* **266,** 14831–14834.
2. Ruoslahti, E., and Reed, J. (1994) *Cell* **77,** 477–478.
3. Lafrenie, R. M., and Yamada, K. M. (1996) *J. Cell. Biochem.* **61,** 543–553.
4. Ruoslahti, E. (1992) *Br. J. Cancer* **66,** 239–242.
5. Liotta, L. A. (1986) *Cancer Res.* **46,** 1–7.
6. Albelda, S. M. (1993) *Lab. Invest.* **68,** 4–17.
7. Lester, B. R., and McCarthy, J. B. (1992) *Cancer Metab. Rev.* **11,** 31–44.
8. Brooks, P. C. (1996) *Cancer Metastasis Rev.* **15,** 187–194.
9. Hynes, R. O. (1992) *Cell* **69,** 11–25.
10. Ruoslahti, E. (1991) *J. Clin. Invest.* **87,** 1–5.
11. Pignatelli, M., and Stamp, G. (1995) *Cancer Surv.* **24,** 113–127.
12. Delcommenne, M., and Streuli, C. H. (1995) *J. Biol. Chem.* **270,** 26794–26801.
13. Jalkanen, M., Jalkanen, S., and Bernfield, M. (1991) *in* "Receptors for Extracellular Matrix" (McDonald, J. A., and Mecham, R. P., Ed.), pp. 1–37, Academic Press, San Diego.
14. Bernfield, M., Kokenyesi, R., Kato, M., Hinkes, M. T., Spring, J., Gallo, R. L., and Lose, E. J. (1992) *Annu. Rev. Cell Biol.* **8,** 365–393.
15. Sauders, S., and Bernfield, M. (1988) *J. Cell Biol.* **106,** 423–430.
16. Koda, J. E., Rapraeger, A., and Bernfield, M. (1985) *J. Biol. Chem.* **260,** 8157–8162.
17. Sun, X., Mosher, D. F., and Rapraeger, A. (1989) *J. Biol. Chem.* **264,** 2885–2889.
18. Salmivirta, M., Elenius, K., Vainio, S., Hofer, U., Chiquet-Ehrismann, R., Thesleff, I., and Jalkanen, M. (1991) *J. Biol. Chem.* **266,** 7733–7739.
19. Woods, A., and Couchman, J. R. (1994) *Mol. Biol. Cell* **5,** 183–192.
20. Lesley, J., Hyman, R., and Kincade, P. W. (1993) *Adv. Immunol.* **54,** 271–335.
21. Lopez-Casillas, F., Wrana, J. L., and Massague, J. (1993) *Cell* **73,** 1435–1444.
22. Vogel, K. G. (1994) *in* "Extracellular Matrix Assembly and Structure," (Yurchenko, P. D., Bird, D. E., and Mecham, R. P., Eds.), pp. 243–279. Academic Press, San Diego.
23. Gunthert, U., Hofmann, M., Rudy, W., Reber, S., Zoller, M., Hausmann, I., Matzku, S., Wenzel, A., Ponta, H., and Herrich, P. (1991) *Cell* **65,** 13–24.
24. Pals, S. T., Koopman, G., Griffioen, A., Ponta, H., Herrlich, P., van denBerg, F., and Horst, E. (1993) *in* "Lymphocyte Adhesion Molecules" (Shimizu, Y., Ed.), Landes.
25. Mali, M., Andtfolk, H., Miettinen, H. M., and Jalkanen, M. (1994) *J. Biol. Chem.* **269,** 27795–27798.
26. Levine, J. M., and Nishiyama, A. (1996) *Perspect. Dev. Neurobiol.* **3,** 245–259.
27. Nishiyama, A., Dahlin, K. J., Prince, J. T., Johnstone, S. R., and Stallcup, W. B. (1991) *J. Cell Biol.* **114,** 359–371.
28. Plushscke, G., Vanek, M., Evans, A., Dittmar, T., Schmid, P., Itin, P., Filardo, E., and Reisfeld, R. (1996) *Proc. Natl. Acad. Sci. USA* **93,** 9710–9715.
29. Stallcup, W. B., and Beasley, L. (1987) *J. Neurosci.* **7,** 2737–2744.
30. Levine, J. M., and Stallcup, W. B. (1987) *J. Neurosci.* **7,** 2721–2731.
31. Nishiyama, A., Dahlin, K. J., and Stallcup, W. B. (1991) *Development* **111,** 933–944.
32. Stallcup, W. B., Dahlin, K., and Healy, P. (1990) *J. Cell Biol.* **111,** 3177–3188.
33. Grako, K. A., and Stallcup, W. B. (1995) *Exp. Cell Res.* **221,** 231–240.
34. Nishiyama, A., Lin, X. H., Giese, N., Heldin, C. H., and Stallcup, W. B. (1996) *J. Neurosci. Res.* **43,** 299–314.
35. Nishiyama, A., Lin, X. H., Giese, N., Heldin, C. H., and Stallcup, W. B. (1996) *J. Neurosci. Res.* **43,** 315–330.

36. Leger, O., Johnson-Leger, P., Jackson, E., Coles, B., and Dean, C. (1994) *Int. J. Cancer* **58,** 700–705.

37. Schrappe, M., Klier, F. G., Spiro, R. C., Waltz, T. A., Reisfeld, R. A., and Gladstone, C. L. (1991) *Cancer Res.* **51,** 4986–4993.

38. Morgan, A. C., Woodhouse, C., Bartholemew, R., and Schroff, R. (1986) *Mol. Immunol.* **23,** 193–200.

39. Burg, M. A., Tillet, E., Timpl, R., and Stallcup, W. B. (1996) *J. Biol. Chem.* **271,** 26110–26116.

40. Nishiyama, A., and Stallcup, W. B. (1993) *Mol. Biol. Cell* **4,** 1097–1108.

41. Tillet, E., Ruggiero, F., Nishiyama, A., and Stallcup, W. B. (1997) *J. Biol. Chem.* **272:** 10769–10776.

42. Schubert, D., Heinemann, S., Carlisle, W., Tarikas, H., Kines, B., Patrick, J., Steinbach, J., Culp, W., and Brandt, B. (1974) *Nature* **249,** 224–227.

43. Hessle, H., and Engvall, E. (1984) *J. Biol. Chem.* **259,** 3955–3961.

44. Odermatt, E., Risteli, J., van Delden, V., and Timpl, R. (1983) *Biochem. J.* **211,** 295–302.

45. Hubbard, A., and Cohn, A. (1972) *J. Cell Biol.* **44,** 390–405.

46. Kobe, B., and Deisenhofer, J. (1994) *Trends Biochem. Sci.* **19,** 415–421.

47. Scott, J. E. (1996) *Biochemistry* **35,** 8795–8799.

48. Chou, P. Y., and Fasman, G. D. (1978) *Adv. Enzym. Relat. Areas Mol. Biol.* **47,** 45–148.

49. Hessle, H., and Engvall, E. (1984) *J. Biol. Chem.* **259,** 3955–3961.

50. Keene, D. R., Engvall, E., and Glanville, R. W. (1988) *J. Cell Biol.* **107,** 1995–2006.

51. McDevitt, C. A., Marcelino, J., and Tucker, L. (1991) *FEBS Lett.* **294,** 167–170.

52. Faissner, A., Kruse, J., Kuhn, K., and Schachner, M. (1990) *J. Neurochem.* **54,** 1004–1015.

53. Hedbom, E., and Heinegard, D. (1993) *J. Biol. Chem.* **268,** 27307–27312.

54. Carter, W. G. (1982) *J. Biol. Chem.* **257,** 3249–3257.

Received March 25, 1997

55. Pfaff, M., Aumailley, M., Specks, U., Knolle, J., Zerwes, H. G., and Timpl, R. (1993) *Exp. Cell Res.* **206,** 167–176.

56. Doane, K. J., Yang, G., and Birk, D. E. (1992) *Exp. Cell Res.* **200,** 490–499.

57. Timpl, R., and Chu, M.-L. (1994) *in* "Extracellular Matrix Assembly and Structure" (Yurcheno, P. D., Bird, D. E., and Mecham, R. P., Eds.), pp. 207–242. Academic Press, San Diego.

58. Perris, R., Kuo, H.-J., Glanville, R. G., Leibold, S., and Bronner-Fraser, M. (1993) *Exp. Cell Res.* **209,** 103–117.

59. Perris, R., Kuo, H.-J., Glanville, R. G., Leibold, S., and Bronner-Fraser, M. (1993) *Dev. Dyn.* **198,** 135–149.

60. Han, J., Daniel, J. C., and Pappas, G. D. (1995) *Cancer Lett.* **88,** 127–132.

61. Daniels, K. J., Boldt, H. C., Martin, J. A., Gardner, L. M., Meyer, M., and Folberg, R. (1996) *Lab. Invest.* **75,** 55–66.

62. Lin, X-H., Dahlin, K., and Stallcup, W. B. (1996) *J. Cell. Biochem.* **63,** 463–477.

63. Lin, X-H., Grako, K., Burg, M., and Stallcup, W. B. (1996) *Mol. Biol. Cell* **7,** 1977–1993.

64. Iida, J., Skubitz, A., Furcht, L., Wayner, E., and McCarthy, J. (1992) *J. Cell Biol.* **118,** 431–444.

65. Iida, J., Meijne, A., Spiro, R., Roos, E., Furcht, L., and McCarthy, J. (1995) *Cancer Res.* **55,** 2177–2185.

66. Russel, D. S., and Rubinstein, L. J. (1989) *in* "Pathology of Tumors of the Nervous System," pp. 219–231, Arnold, Sevenoaks.

67. Ruoslahti, E. (1996) *Annu. Rev. Cell Dev. Biol.* **12,** 697–715.

68. McKeever, P. E., Fligiel, S. E., Vami, J., Castle, R. I., and Hood, T. W. (1989) *Lab. Invest.* **60,** 286–295.

69. Paulus, W., Roggendorf, W., and Schuppan, D. (1988) *Virchows A Pathol. Anat.* **413,** 325–332.

70. Chintala, S. K., Gokaslan, L., Go, Y., Sawaya, R., Nicolson, G. L., and Rao, J. S. (1996) *Clin. Exp. Metastasis* **14,** 358–366.

71. Nister, M., Claesson-Welsh, L., Eriksson, A., Heldin, C-H., and Westermark, B. (1991) *J. Biol. Chem.* **266,** 16755–16763.

72. Westermark, B., Heldin, C-H., and Nister, M. (1995) *Glia* **15,** 257–263.

73. Somasundaram, R., and Schuppan, D. (1996) *J. Biol. Chem.* **271,** 26884–26891.

EXPERIMENTAL CELL RESEARCH **235,** 265–273 (1997)
ARTICLE NO. EX973663

Nuclear Accumulation of the U1 snRNP-Specific Protein C Is Due to Diffusion and Retention in the Nucleus

Jacqueline M. T. Klein Gunnewiek, Yvonne van Aarssen, Annemiete van der Kemp, Rob Nelissen,[1]
Ger J. M. Pruijn, and Walther J. van Venrooij[2]

Department of Biochemistry, University of Nijmegen, P.O. Box 9101, 6500 HB Nijmegen, The Netherlands

The U1 small nuclear ribonucleoprotein particle (snRNP) has an important function in the early formation of the spliceosome, the multicomponent complex in which pre-mRNA splicing takes place. The nuclear localization signals of two of the three U1 snRNP-specific proteins, U1-70K and U1A, have been mapped. Both proteins are transported actively to the nucleus. Here we show by microinjection of *Xenopus laevis* oocytes that the third U1 snRNP-specific protein, U1C, passively enters the nucleus. Furthermore, we show that in both *X. laevis* oocytes and cultured HeLa cells mutant U1C proteins that are not able to bind to the U1 snRNP do not accumulate in the nucleus, indicating that nuclear accumulation of U1C is due to incorporation of the protein into the U1 snRNP. © 1997 Academic Press

INTRODUCTION

Small nuclear ribonucleoprotein particles (snRNPs) play an essential role in splicing, a process in which sequences are excised from precursor mRNAs. The catalysis of this process occurs in a large complex known as the spliceosome. In the first step of spliceosome formation the U1 snRNP binds to the 5′ splice site [reviewed in 1].

The U1 snRNP consists of an RNA backbone with several proteins associated with it. These proteins can be divided into two groups: (i) the common or Sm proteins B/B′, D1, D2, D3, E, F, and G, which are also present in other snRNPs, and (ii) the particle-specific proteins 70K, A, and C [reviewed in 2]. The U1-70K and U1A proteins bind directly to the first and second stem–loop structures, respectively, of the U1 snRNA [3, 4]. The U1C protein binds to the U1 snRNP via protein–protein interactions [5] and needs the presence of the U1-70K and some of the Sm proteins [6]. The U1C protein contains a zinc finger-like region which encompasses the first 30 amino acid residues of the protein. This region is necessary and sufficient for binding to the U1 snRNP [5]. Recently, it also has been shown that the U1C protein is able to dimerize. The region between amino acids 23 and 30, encompassing part of the zinc finger-like region, is involved in dimer formation [7].

The function of the U1 snRNP-specific proteins in splicing is not precisely known. It has been suggested that the state of phosphorylation is critical for the participation of U1-70K in splicing [8–10]. The U1A protein has been suggested to be necessary for 5′ splice site switching [11], although U1A is dispensable for binding of the U1 snRNP to the 5′ splice site. The U1C protein can augment the interaction of the U1 snRNP with the 5′ splice site [12, 13]. Possibly related to this, it has been shown that the U1C protein is involved in the formation of the E (early) spliceosomal complex [14]. Moreover, when present in the U1 snRNP, the U1C protein can be cross-linked to an RNA oligonucleotide comprising the 5′ splice site [15].

The U1 snRNA, an RNA polymerase II product characterized by a monomethyl cap structure (m^7GpppN) at the 5′ end of the newly synthesized RNA, is exported from the nucleus to the cytoplasm. Both the monomethyl cap and a nuclear cap binding complex (CBC), composed of two proteins, CBP80 and CBP20, are involved in this process [16, 17]. In the cytoplasm the Sm proteins assemble onto the conserved Sm site of the RNA. The assembly of the Sm proteins is a multistep process in which, prior to RNA binding, D1–D2, E–F–G, D1–D2–E–F–G, and B/B′–D3 protein complexes are formed. Subsequently, the D1–D2–E–F–G complex binds to the conserved Sm site of the U1 snRNA. Finally, the binding of B/B′–D3 generates a so-called core U1 snRNP [18, 19]. After binding of the Sm proteins, which is essential for subsequent trimethylation of the cap structure [20], the core U1 snRNP returns to the nucleus. In *Xenopus laevis* the remigration to the nucleus depends on the presence of the Sm proteins and the trimethyl cap structure [21] but in somatic cells the presence of the Sm proteins alone is both necessary and sufficient [22, 23]. It has been suggested

---

[1] Present address: Department of Immunology, N.V. Organon, P.O. Box 20, 5340 BH Oss, The Netherlands.

[2] To whom correspondence and reprint requests should be addressed. Fax: +31-243540525. E-mail: W.vanVenrooij@BIOCH.KUN.NL.

0014-4827/97 $25.00
Copyright © 1997 by Academic Press
All rights of reproduction in any form reserved.

that the association of the U1 snRNP-specific proteins takes place in the nucleus since it has been shown that all three specific proteins are able to enter the nucleus independent of the U1 snRNA [24–26].

Nuclear import of proteins, which is usually mediated by nuclear localization signals (NLS), is a well-studied process [reviewed in 27, 28]. Active protein import encompasses the binding in the cytoplasm of the NLS-containing protein by the importin α-β heterodimer where the α subunit provides the NLS binding site. Subsequently this complex is docked at the nuclear pore complex where translocation of the NLS-bearing protein and importin α takes place. This final step needs the presence of Ran, a small GTP binding protein [reviewed in 27, 28]. Recently the requirement of Ran in U1 snRNP nuclear import has been studied by two groups [29, 30]. Different results were obtained in both studies, which might be explained by the fact that different assays were used.

The NLSs of both U1-70K and U1A have been mapped [24, 26]. Two NLSs, one ranging from amino acids 92 to 199 and another one ranging from amino acids 183 to 437, have been shown to be present in the U1-70K protein. Both are independently capable of directing the protein to the nucleus [26]. The NLS of the U1A protein includes amino acid residues 94–204 [24]. Since little is known about the nuclear import of the U1C protein we studied this phenomenon in both *X. laevis* oocytes and HeLa cells. Here we show that the nuclear import of the U1C protein is not an energy requiring process and that nuclear accumulation of this protein is primarily controlled by its association with U1 snRNPs.

MATERIALS AND METHODS

Plasmids and cDNA constructs. To produce templates for the *in vitro* translation of U1C protein [31] and mutants thereof, we used cDNA fragments which have been described before [5–7].

To produce the truncated U1C protein containing amino acids 1–60 (hC_{1-60}), and point mutants thereof, the corresponding cDNA fragments [5] were amplified by PCR using a DNA oligonucleotide encompassing the *Eco*RI site at the 5′ end of the cDNA and an oligonucleotide complementary to bases encoding amino acid residues 54–60, which additionally contained three ATG codons and a *Bam*HI site. A fusion protein of mutant hC_{1-60} with mDHFR was subsequently constructed by cloning the *Eco*RI/*Bam*HI fragment of the truncated U1C into the *Eco*RI/*Bam*HI sites of mDHFR in pBS(−), which has been described before by Kambach and Mattaj [24]. To produce hC_{1-60}(DHFR)$_3$ the *Bam*HI/*Hin*dIII fragment of DHFR was cloned into the *Bgl*II/*Hin*dIII sites of hC_{1-60}DHFR, which resulted in the formation of hC_{1-60}(DHFR)$_2$. Finally, a second *Bam*HI/*Hin*dIII fragment of DHFR was cloned into the *Bgl*II/*Hin*dIII sites of hC_{1-60}(DHFR)$_2$.

To produce triple hC we first introduced an *Nde*I site at the start position via site-directed mutagenesis. This construct was partially digested with *Nde*I at amino acid positions 1 and 129. The resulting fragment was fused at its 5′ end to the cDNA encoding U1C digested with *Nde*I at amino acid position 129 and at its 3′ end to a U1C cDNA digested with *Nde*I at amino acid position 1.

The fusion proteins, hC_{1-60} and mutants thereof with the green fluorescent protein (GFP), were obtained by subcloning an *Eco*RI/*Bam*HI fragment of the corresponding truncated U1C mutants into the *Eco*RI/*Bam*HI sites of pEGFP-N3 (Clontech). The integrity of all constructs was subsequently checked by sequence analysis.

To produce hA(his)$_6$, the translational stop codon of the U1A cDNA [32] was replaced by the codons for six histidine residues followed by a stop codon and a *Bam*HI site by PCR. The hA(his)$_6$ cDNA was subsequently cloned into the *Nco*I/*Bam*HI site of the expression vector pET-8c.

Expression and purification of recombinant proteins. The proteins hC(his)$_6$, hC(s25)(his)$_6$, hC_{30-159}(his)$_6$, and hA(his)$_6$ were induced and purified as described before [7]. The proteins were eluted in buffer D^- (10 m*M* Hepes-KOH, pH 7.9; 5 m*M* $MgCl_2$, 0.1 m*M* EDTA; 50 m*M* NaCl; 17% glycerol (v/v); 1 m*M* PMSF; 10 m*M* NaF) with 200 m*M* imidazole except for hA(his)$_6$, which was eluted in PBS with 250 m*M* imidazole.

In vitro transcription and translation. To produce hC or hC_{1-60}DHFR T7 mRNAs or mutants of both for translation, 1 μg of linearized template was transcribed in essentially the same manner as described in [4]. To produce ^{35}S-labeled proteins, 200 ng (2 μl) of the mRNA was incubated with wheat germ extract and [^{35}S]methionine (ICN) in essentially the same manner as described in [4].

Oocyte injection. Oocytes were released from the ovary by treatment with collagenase B (2.5 mg/ml) in Barth's medium [33] without Ca^{2+}. *In vitro* translated proteins were injected into the cytoplasm (30 nl per oocyte). Oocytes were incubated in Barth's medium containing cycloheximide (100 μg/ml) to inhibit incorporation of [^{35}S]methionine into endogenous proteins. After 18 h of incubation (or other time periods as indicated in the text) at 18°C or 0°C, the oocytes were manually dissected in J-buffer (20 m*M* Tris–HCl, pH 7.5; 70 m*M* NH_4Cl; 7 m*M* $MgCl_2$; 0.1 m*M* EDTA, 2.5 m*M* dithiothreitol; 10% glycerol). Isolated nuclei (N) were immediately precipitated in ethanol, whereas the "total" oocyte (T) and cytoplasmic (C) fractions were transferred to 300 μl $TN_{50}E$ (10 m*M* Tris–HCl, pH 8.0; 50 m*M* NaCl; 1 m*M* EDTA). For the protein injection experiments six oocytes per sample were used. The total and cytoplasmic fractions were homogenized and spun for 15 min at 12,000*g* to remove yolk and insoluble components. Two hundred microliters of the supernatant was precipitated with 5 vol acetone for 1 h at −70°C. After spinning for 15 min, the samples were dried, dissolved in SDS–PAGE sample buffer, incubated for 5 min at 95°C, and loaded on a 10% SDS–polyacrylamide gel.

Immunodepletion. After an overnight incubation at 18°C, 18 oocytes injected with ^{35}S-labeled U1C were dissected and both cytoplasmic and nuclear fractions were homogenized in 600 μl $TN_{150}E$ (10 m*M* Tris–HCl, pH 8.0; 150 m*M* NaCl; 1 m*M* EDTA) and spun for 15 min at 12,000*g*. Subsequently 400 μl of the supernatant was incubated with monoclonal anti-Sm antibodies (Y12 [34]) coupled to protein-A–agarose beads (20 μl of 50% slurry, Biozym). Nonidet-P40 was added to a final concentration of 0.05%. After 2 h rotation at 4°C the supernatants were transferred to fresh tubes with monoclonal anti-Sm antibodies (Y12) coupled to protein-A–agarose beads (20 μl of 50% slurry). Similar immunoprecipitations were subsequently performed twice with anti-m_3G antibodies (H20; Euro-Diagnostica BV, Arnhem, the Netherlands) coupled to protein-G–agarose beads (20 μl 50% slurry, Pharmacia). After the final immunoprecipitation the supernatant was precipitated with 5 vol acetone for 1 h at −70°C and subsequently loaded on a 10% SDS–polyacrylamide gel as described above.

Electroporation of HeLa cells. A total of 2×10^6 HeLa cells were transfected with 5 μg of the corresponding DNAs in a total volume of 400 μl Dulbecco's modified Eagles medium (DMEM). Electroporation was performed at 296 V with a capacitance of 950 μFa. After electroporation, cells were resuspended in 10 ml DMEM, divided in two portions, and allowed to grow on a coverslip. Two days later, the cells were washed twice with PBS and subsequently examined using a fluorescence microscope (with FITC adjustment).

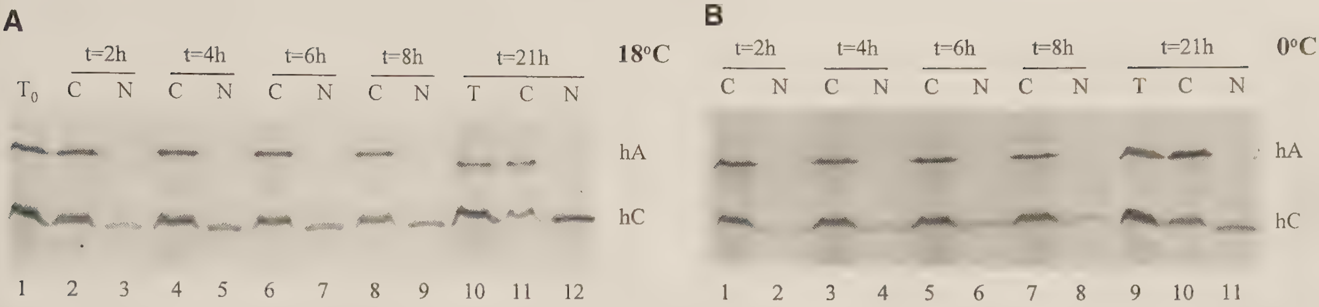

FIG. 1. Nuclear accumulation of the U1 snRNP-specific protein C. A mixture of *in vitro* translated ^{35}S-labeled U1C and U1A (indicated as hC and hA, respectively) was injected into the cytoplasm of *X. laevis* oocytes and after incubation at 18°C (A) or 0°C (B) oocytes were dissected in cytoplasmic (C) and nuclear (N) fractions and subsequently analyzed by 10% SDS–PAGE. (A) Cytoplasmic and nuclear fractions after incubation of 2 (lanes 2–3), 4 (lanes 4–5), 6 (lanes 6–7), 8 (lanes 8–9), and 21 (lanes 10–12) h. The amount of injected ^{35}S-labeled proteins is shown in lane 1 (T_0). (B) Cytoplasmic and nuclear fractions after incubation of 2 (lanes 1–2), 4 (lanes 3–4), 6 (lanes 5–6), 8 (lanes 7–8), and 21 (lanes 9–11) h. T, total oocyte fraction.

In vitro reconstitution in HeLa S100. *In vitro* translated ^{35}S-labeled proteins (2 or 3 μl of an *in vitro* translation mixture of 15 μl) were incubated in a final volume of 20 μl with 5 μl HeLa S100 extract (extract of 5×10^5 cells in 25 m*M* Tris–HCl, pH 7.4; 0.1 m*M* EDTA; 0.25 m*M* DTE; 0.5 m*M* PMSC; 0.1 *M* KCl; 0.01% Nonidet-P40; 20% (v/v) glycerol as described previously [5]), 2 μl buffer B (200 m*M* Hepes-KOH, pH 7.9; 1 *M* KCl; 10 m*M* $MgCl_2$; 0.5% Nonidet-P40), and 5 μl BSA (10 mg/ml). After 90 min of incubation at 20°C monoclonal anti-U1A antibodies (9A9; Euro-Diagnostica BV) coupled to protein-A–agarose beads (20 μl 50% slurry) were added together with 300 μl IPP_{150} (10 m*M* Tris–HCl, pH 8.0; 150 m*M* NaCl; 0.05% Nonidet-P40). The beads were rotated during 90 min at 20°C and subsequently washed three times with IPP_{150}. The beads were finally resuspended in SDS–PAGE sample buffer, heated for 5 min at 95°C, and separated on a 10% SDS–polyacrylamide gel.

RESULTS

Nuclear Import of the U1C Protein

Not much is known about the nuclear import of the U1C protein. The U1C protein does not contain an NLS similar to the prototype SV40 T antigen NLS, which consists of a short stretch of basic amino acid residues [35], nor does it contain a so-called bipartite NLS consisting of two stretches of basic amino acids separated by a spacer of approximately 10 random amino acids [36]. In order to investigate the mechanism of nuclear accumulation of U1C we first injected ^{35}S-labeled U1C protein (*in vitro* translated in a cell-free system) into the cytoplasm of *X. laevis* oocytes. After various incubation times (2, 4, 6, 8, and 21 h) at 18°C the oocytes were dissected and the presence of ^{35}S-labeled protein in both the nuclear and the cytoplasmic fraction was analyzed by SDS–PAGE. The U1C protein gradually migrated into the nucleus (see Fig. 1A). After 4 h a substantial part of the labeled protein (Fig. 1A, lane 5) and after 21 h. more than 50% of the injected protein had entered the nucleus (see Fig. 1A, lanes 11–12). The U1A protein which was included as an internal control was also transported to the nucleus (lanes 11–12 of Fig. 1A). The fraction of the U1A protein found in the nucleus was relatively small, which is consistent with the results obtained by Kambach and Mattaj [24].

Parallel incubations of oocytes injected with ^{35}S-labeled U1C were performed at 0°C. At this temperature energy-dependent transport is severely hampered, in contrast to passive diffusion [37, 38]. At 0°C nuclear accumulation of the U1C protein is still observed although the rate of nuclear entry appeared to be somewhat lower than that observed at 18°C (compare lanes 2–12 of Fig. 1A with lanes 1–11 of Fig. 1B). At 0°C no transport of the U1A protein from cytoplasm to nucleus was observed, which is consistent with the idea that U1A transport is energy-dependent [24]. The results presented in Fig. 1 suggest that nuclear accumulation of the U1C protein is not an energy-dependent process.

The U1C Protein Diffuses into the Nucleus

In order to find out if the U1C protein accumulates in the nucleus via diffusion, we fused the first 60 amino acid residues which encompass the zinc finger-like region of the U1C protein to mouse DHFR (dihydrofolate reductase). Oocytes were injected with ^{35}S-labeled hC_{1-60}DHFR and after an overnight incubation at 18°C the nuclear and cytoplasmic fractions were analyzed on a 10% SDS–polyacrylamide gel. About 50% of the injected hC_{1-60}DHFR had accumulated in the nucleus (see Fig. 2, lanes 5–6). In contrast, the injected ^{35}S-labeled DHFR was still localized in the cytoplasm (see lanes 8–9 of Fig. 2). When oocytes injected with hC_{1-60}DHFR were incubated at 0°C for 18 h, the transport of the fusion protein to the nucleus was hampered but not completely inhibited (lanes 14–15 of Fig. 2). The transport of the wild-type U1C protein was also slowed down under these conditions (Fig. 2, lanes 11–12), as was observed before.

The nuclear accumulation of hC_{1-60}DHFR at both 18 and 0°C was less efficient compared to that of the wild-type U1C protein (compare lanes 2–3 with lanes 5–6

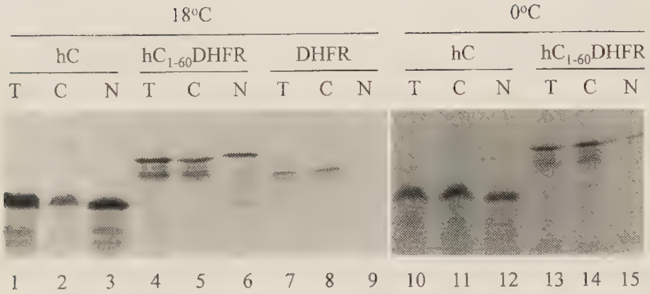

FIG. 2. Nuclear accumulation of hC$_{1-60}$DHFR. *In vitro* translated ^{35}S-labeled hC (lanes 1–3 and 10–12), hC$_{1-60}$DHFR (lanes 4–6 and 13–15) and DHFR (lanes 7–9) were injected into the cytoplasm of *X. laevis* oocytes and incubated for 18 h at 18°C (lanes 1–9) or 0°C (lanes 10–15). After incubation oocytes were dissected in cytoplasmic (C) and nuclear (N) fractions and analyzed by 10% SDS–PAGE. T, total oocyte fraction.

in Fig. 2). To investigate whether this was due to the larger size of hC$_{1-60}$DHFR (±33 kDa), we fused three copies of DHFR to the first 60 amino acid residues of U1C (hC$_{1-60}$DHFR$_3$: molecular weight of this polypeptide is 80–85 kDa) as described under Materials and Methods. After an overnight incubation at 18°C no nuclear accumulation for hC$_{1-60}$DHFR$_3$ could be observed (data not shown). We also made a construct in which almost the complete coding sequence of the U1C protein was repeated three times (triple hC; molecular weight of the polypeptide is 55–60 kDa. See Materials and Methods). Also, with this fusion protein no nuclear accumulation was observed after 18 h incubation at 18°C (data not shown). The observations that (i) nuclear entry of U1C is hardly temperature dependent and (ii) the rate of nuclear entry is dependent on the size of the fusion protein indicate that nuclear entry of the U1C protein is due to diffusion of the protein.

The nuclear accumulation of U1C and hC$_{1-60}$DHFR can only be explained by assuming that both proteins are able to bind to some nuclear components, most likely the U1 snRNP. To investigate this possibility we performed an *in vitro* reconstitution assay in HeLa S100 extract. ^{35}S-labeled U1C, hC$_{1-60}$DHFR, and DHFR were added to HeLa S100 cell extract and subsequently immunoprecipitated with monoclonal antibodies directed to the U1A protein. The immunoprecipitated proteins, most probably contained in U1 snRNP, were analyzed by SDS–PAGE. Indeed, U1C and hC$_{1-60}$DHFR were precipitated by the antibodies (lanes 4 and 6 of Fig. 3) although some background binding of both proteins to the antibodies coupled to protein-A–agarose beads was observed (lanes 5 and 7, Fig. 3). DHFR was not precipitated by the anti-U1A antibodies (lanes 8–9, Fig. 3). Similar results were obtained when monoclonal anti-Sm antibodies (Y12) were used. These results strongly suggest that both U1C and hC$_{1-60}$DHFR accumulate in the nucleus due to diffusion and subsequent incorporation into the U1 snRNPs.

The Zinc Finger-like Region of U1C Is Involved in Nuclear Accumulation

If nuclear accumulation of U1C is dependent on its binding to U1 snRNPs, as has been suggested above, it would be expected that mutant U1C proteins that are not able to bind to the U1 snRNP do not accumulate in the nucleus. To investigate this in more detail we constructed several ^{35}S-labeled mutants of the U1C protein: a deletion mutant lacking the C-terminal end (hC$_{1-60}$); deletion mutants lacking the N-terminal 22, 29, or 46 amino acids (hC$_{23-159}$, hC$_{30-159}$ and hC$_{47-159}$, respectively), in which the zinc finger-like region is partially or completely deleted; and amino acid substitution mutants in which the conserved cysteines at positions 6 and 9 and the cysteine at position 25 were changed into serines (mutants s6, s9, and s25), the conserved histidines at positions 24 and 30 were changed into glutamines (mutants s24 and s30), or the arginines and lysines at positions 21/22 and 28/29 were changed into glycine-serine (mutants s21/22 and s28/29). Mutants hC$_{23-159}$, hC$_{30-159}$, hC$_{47-159}$, s6, s9, s21/22, s24, and s30 are not able to bind to the U1 snRNP [5, 7]. The ^{35}S-labeled mutant U1C proteins were injected into the cytoplasm of *X. laevis* oocytes and after an overnight incubation at 18°C the cytoplasmic and nuclear fractions were analyzed by SDS–PAGE. U1C mutants that are able to bind to the U1 snRNP accumulated in the nucleus to an extent similar to that observed for the wild-type protein (data not shown). In contrast, mutant proteins that were not able to bind to the U1 snRNP appeared to be quite unstable after an overnight incubation at 18°C (data not shown).

If indeed energy is not required for nuclear uptake of U1C, as suggested by the data described above, this would allow analysis of the U1C mutants at 0°C, i.e.

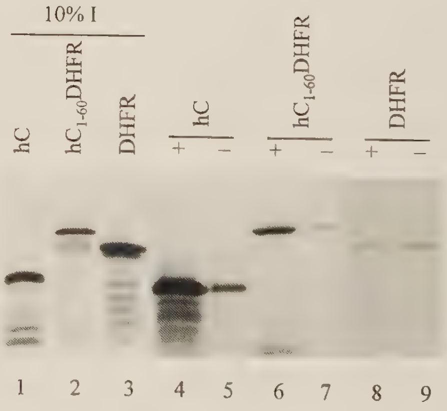

FIG. 3. Reconstitution of U1 snRNP in HeLa S100. *In vitro* translated ^{35}S-labeled hC (lanes 4–5), hC$_{1-60}$DHFR (lanes 6–7) and DHFR (lanes 8–9) were incubated with (+) or without (−) HeLa S100 and precipitated via monoclonal anti-U1A antibodies. The bound proteins were analyzed on a 10% SDS–polyacrylamide gel. 10% of the inputs was analyzed in parallel (lanes 1–3).

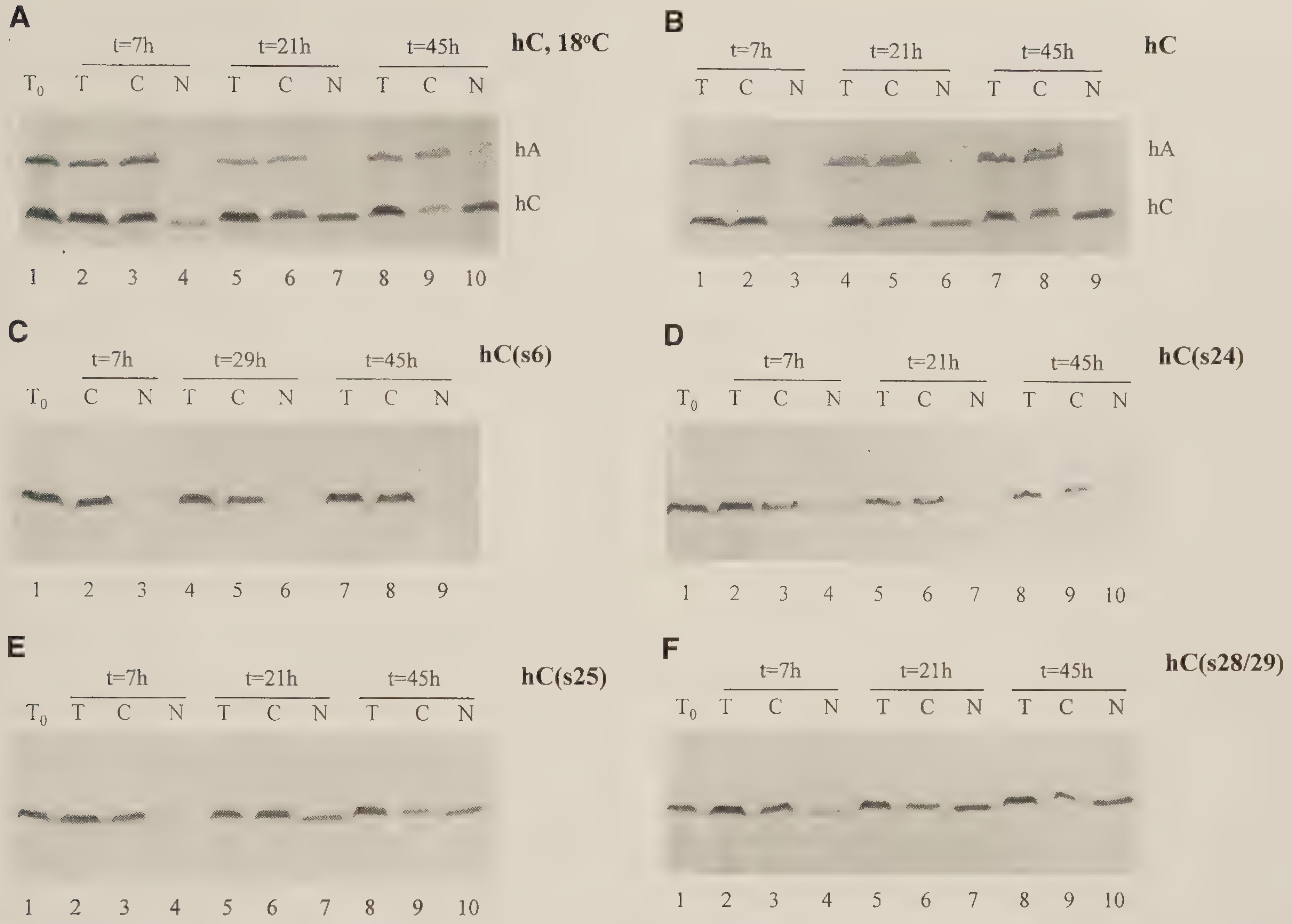

FIG. 4. Nuclear accumulation of mutant U1C proteins. *In vitro* translated ^{35}S-labeled hC (A and B), hC(s6) (C), hC(s24) (D), hC(s25) (E), and hC(s28/29) (F) were injected into the cytoplasm of *X. laevis* oocytes. ^{35}S-labeled U1A was co-injected as an internal control (indicated hA in A and B). After incubation at 18°C (A) or 0°C (B–F) oocytes were dissected in cytoplasmic (C) and nuclear (N) fractions, which were subsequently analyzed by 10% SDS–PAGE. (A, D–F) Total oocyte (T), cytoplasmic and nuclear fractions after 7 (lanes 2–4), 21 (lanes 5–7) and 45 (lanes 8–10) h of incubation. The amount of ^{35}S-labeled protein injected is indicated in lane 1 (T_0). (B) Total, cytoplasmic, and nuclear fractions after incubations of 7 (lanes 1–3), 21 (lanes 4–6), and 45 (lanes 7–9) h. (C) Total, cytoplasmic, and nuclear fractions after incubation of 7 (lanes 2–3), 29 (lanes 4–6), and 45 (lanes 7–9) h.

under conditions where protein degradation will be limited. Therefore, we studied the nuclear accumulation of the ^{35}S-labeled wild-type U1C and U1C mutants at 0°C and incubated the injected oocytes also for a longer period of time (up to 45 h of incubation) to reach higher levels of nuclear accumulation. After 45 h of incubation at 0°C more than 50% of the injected wild-type protein was present in the nucleus (see Fig. 4B, lanes 8–9). As expected, the control protein U1A did not enter the nucleus at all under these conditions (Fig. 4B). Injection of *X. laevis* oocytes with ^{35}S-labeled U1C mutants and subsequent incubation at 0°C indicated that U1C mutants unable to bind to the U1 snRNP did not accumulate in the nucleus (see Figs. 4C and 4D for the mutant proteins hC(s6) and hC(s24)). No or only slight degradation of these proteins was observed under these conditions. In contrast, U1C mutants that are able to bind to the U1 snRNP accumulated in the nucleus to the same extent as the wild-type protein (see Figs. 4E and 4F for the mutant proteins hC(s25) and hC(s28/29)). In Fig. 5 the results obtained with all U1C mutant proteins are summarized and correlated with their ability to bind to the U1 snRNP.

Taken together, our results indicate that the U1C protein passively enters the nucleus and is retained in this compartment via binding to the U1 snRNP.

Nuclear Accumulation of the U1C Protein Is Dependent on Nuclear Binding Sites

Since the number of U1 snRNPs in the nucleus that do not contain the (*X. laevis*) U1C protein is limiting, one would expect that nuclear retention of U1C as described above is a saturable process. Therefore, we injected 1 ng hC(his)$_6$, hC(s25)(his)$_6$, hC$_{30-159}$(his)$_6$, or hA(his)$_6$ in the nucleus prior to cytoplasmic injection

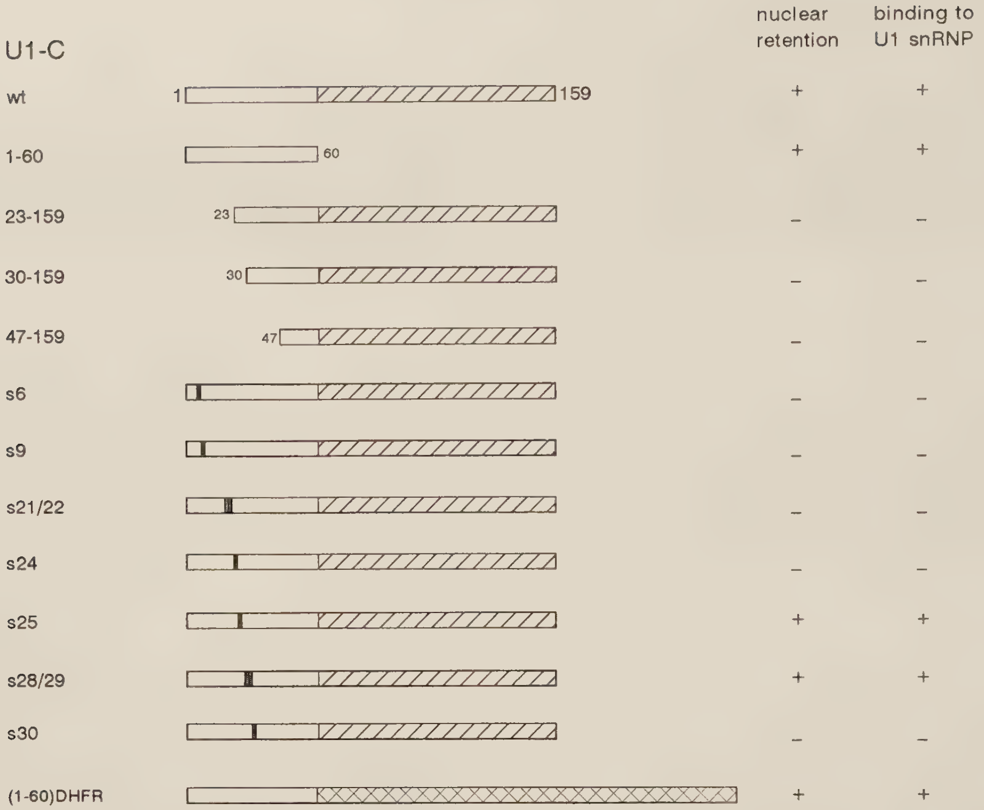

FIG. 5. Nuclear accumulation and binding to the U1 snRNP of U1C and its mutants. Summary of the different mutants of the U1C protein used in *X. laevis* oocyte injection experiments and their ability to accumulate in the nucleus and to bind to the U1 snRNP. The amino acid numbers are indicated. The shaded box represents the proline and methionine rich C-terminal domain, starting at residue 61. Dark gray boxes indicate the position at which an amino acid is substituted by another residue (U1C mutants s6, s9, and s25: substitution of cysteine by serine; s24 and s30: substitution of histidine by glutamine; s21/22 and s28/29: substitution of arginine-lysine by glycine-serine). Mutant (1–60)DHFR represents the first 60 amino acids of U1C (open box) fused to DHFR (cross-hatched box).

of ^{35}S-labeled U1C. ^{35}S-labeled U1A protein was co-injected as an internal control. hC(his)$_6$, hC(s25)(his)$_6$, hC$_{30-159}$(his)$_6$, and hA(his)$_6$ were expressed and purified as described under Materials and Methods. After an overnight incubation at 18°C the oocytes were dissected and cytoplasmic and nuclear fractions were analyzed by SDS–PAGE. Injection of hA(his)$_6$ prior to injection of the ^{35}S-labeled U1C protein did not markedly affect nuclear accumulation of the U1C protein since more than 50% was found in the nucleus (see Fig. 6, lanes 2–3). Unfortunately, U1A signals are too weak to observe a decrease in nuclear accumulation of ^{35}S-labeled U1A as would be expected based on results obtained by Kambach and Mattaj [24]. When hC$_{30-159}$(his)$_6$, which is unable to bind to the U1 snRNP, was injected in the nucleus again more than 50% of the ^{35}S-labeled U1C accumulated in the nucleus (see Fig. 6, lanes 11–12). However, when hC(his)$_6$ or hC(s25)(his)$_6$, which both are able to bind to the U1 snRNP, were injected in the nucleus the nuclear accumulation of the ^{35}S-labeled U1C protein was severely reduced (compare lanes 2–3 with lanes 5–6 and lanes 8–9 of Fig. 6). These results support the previous conclusion that nuclear accumulation of the U1C protein is dependent on the presence of U1C binding sites in the nucleus.

To confirm that indeed the microinjected human U1C

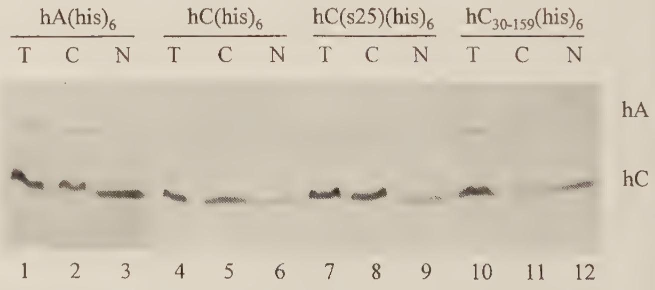

FIG. 6. Nuclear accumulation of U1C is saturable. Prior to cytoplasmic injection of a mixture of *in vitro* translated ^{35}S-labeled U1C and U1A (indicated as hC and hA, respectively), the nuclei of *X. laevis* oocytes were microinjected with 1 ng hA(his)$_6$ (lanes 1–3), hC(his)$_6$ (lanes 4–6), hC(s25)(his)$_6$ (lanes 7–9), or hC$_{30-159}$(his)$_6$ (lanes 10–12). After 18 h of incubation at 18°C oocytes were dissected in cytoplasmic (C) and nuclear (N) fractions and analyzed by 10% SDS–PAGE. T, total oocyte fraction.

protein associates with *Xenopus* U1 snRNP, the nuclear snRNPs were immunoprecipitated from extracts prepared from oocytes microinjected with the radiolabeled U1C protein. To warrant quantitative immunoprecipitation of snRNPs, a number of subsequent immunoprecipitations were performed using monoclonal anti-Sm and anti-m_3G antibodies as described under Materials and Methods. These experiments showed that the majority (85–95%) of the detectable ^{35}S-labeled U1C protein molecules present in the nucleus were associated with U1 snRNP (data not shown).

Nuclear Accumulation of U1C in Cultured HeLa Cells

Studies of nuclear import of U1 snRNA have shown that the requirements in cultured human cells may be (partially) different from those in *X. laevis* oocytes. To study nuclear accumulation of U1C in HeLa cells we fused the N-terminal 60 amino acid residues of the U1C protein or mutants thereof (i.e., mutants s6, s24, s25, s28/29) to the N-terminal end of a variant of the green fluorescent protein (GFPmut1) [39]. The fusion proteins were expressed by transfection of HeLa cells with the corresponding constructs. Two days after electroporation expression of GFP and GFP fusion proteins was examined by fluorescence microscopy. GFP alone showed an intense staining of both cytoplasm and nucleus (Fig. 7A). However, when the N-terminal 60 amino acids of the U1C protein were fused to GFP, the nucleus showed a speckled pattern, characteristic for snRNP staining (see Fig. 7B), while no fluorescence was detected in the cytoplasm. When we transfected hC_{1-60}(s25)GFP and hC_{1-60}(s28/29)GFP, which are still able to bind to the U1 snRNP, a similar pattern was obtained (see Figs. 7E and 7F). However, hC_{1-60}(s28/29)GFP showed a weak cytoplasmic staining in addition to the nuclear staining (Fig. 7F). This might be due to the fact that two charged amino acid residues (i.e., arginine and lysine) are substituted in this mutant. Alternatively, the faint cytoplasmic staining might be due to the expression level of hC_{1-60}(s28/29)GFP. When hC_{1-60}(s6)GFP or hC_{1-60}(s24)GFP, in which a conserved cysteine and histidine, respectively, were substituted, were expressed no nuclear accumulation was observed (see Figs. 7C and 7D). Note that the intensity of fluorescence obtained with the hC_{1-60}GFP fusion protein or mutants thereof is markedly reduced in comparison with the GFP control.

Taken together, these experiments suggest that also in cultured HeLa cells nuclear accumulation of the U1C protein is dependent on its incorporation into U1 snRNP complexes.

DISCUSSION

Jantsch and Gall [25] have shown that the *X. laevis* U1C protein, which has no amino acid differences in the zinc finger-like region compared to the human U1C, is localized within structures known to contain U1 snRNPs after injection of transcripts encoding a *myc*-tagged C protein into oocytes. They suggested that the U1C protein might be able to enter the nucleus via diffusion and might be retained in the nucleus via binding to the U1 snRNP.

In this study we present evidence that the U1C protein indeed enters the nucleus by diffusion. Nuclear accumulation of U1C is reduced but not drastically inhibited by cooling to 0°C (Fig. 1), excluding an energy-dependent transport mechanism. Furthermore, the nucleocytoplasmic distribution of ^{35}S-labeled U1C microinjected into the cytoplasm of *X. laevis* oocytes and incubated for 45 h at 0°C is comparable to that observed when oocytes injected with ^{35}S-labeled U1C were incubated at 18°C for 21 h (compare Figs. 4A and 4B). The diffusion rate depends on the size of the U1C proteins used. When larger constructs like triple hC (55–60 kDa) and $hC_{1-60}(DHFR)_3$ (80–85 kDa) were used virtually no import into the nucleus was observed.

We also show in this study that the nuclear accumulation of the U1C protein is controlled by the binding of the protein to the nuclear U1 snRNP since mutants of the U1C proteins that are able to bind to the U1 snRNP accumulate in the nucleus while mutants that are unable to bind to the U1 snRNP do not (results summarized in Fig. 5). This mechanism is substantiated by the nuclear accumulation of hC_{1-60}DHFR which, due to its relatively small size (±33 kDa) and its ability to bind to the U1 snRNP (Fig. 3), showed the same behavior as U1C. In addition, we showed that most of the nuclear ^{35}S-labeled U1C protein was bound to the U1 snRNP, consistent with results obtained by Jantsch and Gall [25].

The presence of an excess of U1C protein in the nucleus resulted in a reduced nuclear accumulation of ^{35}S-labeled U1C protein (Fig. 6). Similar results have been obtained previously with the U1A protein. Kambach and Mattaj [24] showed that the nucleocytoplasmic distribution of the U1A protein at equilibrium is not determined by its transport rate but rather by the number of free binding sites in the two compartments. The U1-70K protein has been reported to contain two independent NLSs: one encompasses the RNA binding domain and the other one is located in the C-terminal region of the protein [26]. The C-terminal region of the protein might represent a true NLS. When this part of the protein is deleted the mutant protein still contains a functional RNA binding domain and might be able, in view of its size (20–25 kDa), to diffuse through the nuclear pore and bind to the U1 snRNP in a way similar to what we observed for the U1C protein.

We also showed that expression of wild-type hC_{1-60}GFP in HeLa cells results in a speckled nuclear pattern, characteristic for snRNP staining (Fig. 7B). Jantsch and Gall [25] also showed that transfection of

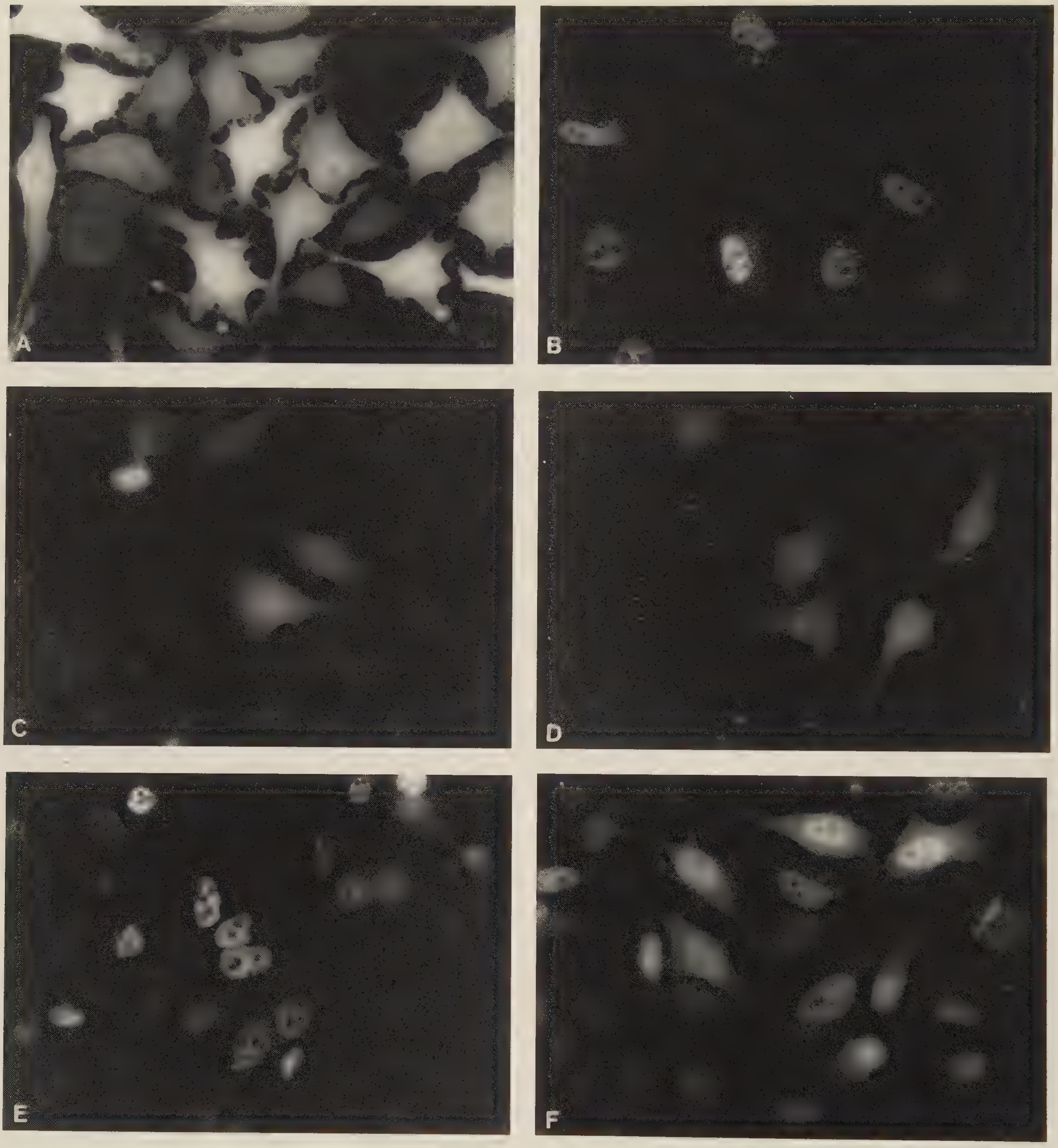

FIG. 7. Nuclear accumulation of hC_{1-60}GFP and hC_{1-60}GFP mutants in cultured HeLa cells. GFP (A), hC_{1-60}GFP (B), hC_{1-60}(s6)GFP (C), hC_{1-60}(s24)GFP (D), hC_{1-60}(s25)GFP (E), and hC_{1-60}(s28/29)GFP (F) were transiently expressed in cultured HeLa cells. Two days after transfection, GFP and GFP fusion protein expression were examined by fluorescence microscopy.

HeLa cells with a plasmid encoding *myc*-tagged U1C resulted in a nuclear distribution similar to the distribution of U1 snRNPs. It is very likely that hC_{1-60}GFP is also able to bind to the U1 snRNP like hC_{1-60}DHFR since hC_{1-60}GFP mutant proteins that are assumed not to bind to the U1 snRNP do not accumulate in the nucleus of cultured HeLa cells, thereby confirming the results we obtained in the *X. laevis* oocytes. However,

hC_{1-60}(s28/29)GFP showed a weak cytoplasmic staining in addition to the nuclear staining (Fig. 7F). This might be due to the fact that the expression of hC_{1-60}(s28/29)GFP is higher compared to that of the other hC_{1-60}GFP constructs, resulting in saturation of the available U1C binding sites in the nucleus. Another explanation would be that substitution of the arginine and lysine in this mutant has a minor effect on the binding to the U1 snRNP, resulting in less efficient nuclear retention. Such a reduced binding affinity would be in accordance with the observation that mutant hC(s28/29) is also less efficient in supporting formation of the E (early) complex of the spliceosome [14].

In conclusion, we showed that the U1C protein enters the nuclear compartment via diffusion and is retained in the nucleus by binding to the U1 snRNP.

We thank M. Lambermon for excellent technical assistance and C. Kambach for providing the mDHFR cDNA. This work was supported in part by the Netherlands Foundation for Chemical Research (SON) with financial aid from the Netherlands Organization for Scientific Research (NWO). Dr. G. Pruijn was supported by a fellowship of the Royal Netherlands Academy of Arts and Sciences.

REFERENCES

1. Sharp, P. A. (1994) *Cell* **77,** 805–815.
2. Will, C., Behrens, S. E., and Lührmann, R. (1993) *Mol. Biol. Rep.* **18,** 121–126.
3. Surowy, C. S., van Santen, V. L., Scheib-Wixted, S. M., and Spritz, R. A. (1989) *Mol. Cell. Biol.* **9,** 4179–4186.
4. Scherly, D., Boelens, W., van Venrooij, W. J., Dathan, N. A., Hamm, J., and Mattaj, I. W. (1989) *EMBO J.* **8,** 4163–4170.
5. Nelissen, R. L. H., Heinrichs, V., Habets, W. J., Simons, F., Lührmann, R., and van Venrooij, W. J. (1991) *Nucleic Acids Res.* **19,** 449–454.
6. Nelissen, R. L. H., Will, C. L., van Venrooij, W. J., and Lührmann, R. (1994) *EMBO J.* **13,** 4113–4125.
7. Klein Gunnewiek, J. M. T., van Aarssen, Y., Wassenaar, R., van Venrooij, W. J., and Nelissen, R. L. H. (1995) *Nucleic Acids Res.* **23,** 4864–4871.
8. Woppmann, A., Patschinsky, T., Bringmann, P., Godt, F., and Lührmann, R. (1990) *Nucleic Acids Res.* **18,** 4427–4438.
9. Mermoud, J. E., Cohen, P., and Lamond, A. I. (1992) *Nucleic Acids Res.* **20,** 5263–5269.
10. Tazi, J., Kornstädt, U., Rossi, F., Jeanteur, P., Cathala, G., Brunel, C., and Lührmann, R. (1993) *Nature* **363,** 283–286.
11. Tarn, W. Y., and Steitz, J. A. (1995) *Proc. Natl. Acad. Sci. USA* **92,** 2504–2508.
12. Heinrichs, V., Bach, M., Winkelmann, G., and Lührmann, R. (1990) *Science* **247,** 69–72.
13. Jamison, S. F., Pasman, Z., Wang, J., Will, C., Lührmann, R., Manley, J. L., and Garcia-Blanco, M. A. (1995) *Nucleic Acids Res.* **23,** 3260–3267.
14. Will, C. L., Rümpler, S., Klein Gunnewiek, J., van Venrooij, W. J., and Lührmann, R. (1996) *Nucleic Acids Res.* **24,** 4614–4623.
15. Rossi, F., Forné, T., Antoine, E., Tazi, J., Brunel, C., and Cathala, G. (1996) *J. Biol. Chem.* **271,** 23985–23991.
16. Hamm, J., and Mattaj, I. W. (1990) *Cell* **63,** 109–118.
17. Izaurralde, E., Lewis, J., Gamberi, C., Jarmolowski, A., McGuigan, C., and Mattaj, I. W. (1995) *Nature* **376,** 709–712.
18. Lehmeier, T., Raker, V., Hermann, H., and Lührmann, R. (1994) *Proc. Natl. Acad. Sci. USA* **91,** 12317–12321.
19. Raker, V. A., Plessel, G., and Lührmann, R. (1996) *EMBO J.* **15,** 2256–2269.
20. Mattaj, I. W. (1986) *Cell* **46,** 905–911.
21. Hamm, J., Darzynkiewics, E., Tahara, S. M., and Mattaj, I. W. (1990) *Cell* **62,** 569–577.
22. Marshallsay, C., and Lührmann, R. (1994) *EMBO J.* **13,** 222–231.
23. Fischer, U., Heinrich, J., van Zee, K., Fanning, E., and Lührmann, R. (1994) *J. Cell Biol.* **125,** 971–980.
24. Kambach, C., and Mattaj, I. W. (1992) *J. Cell Biol.* **118,** 11–21.
25. Jantsch, M. F., and Gall, J. G. (1992) *J. Cell Biol.* **119,** 1037–1046.
26. Romac, J. M. J., Graff, D. H., and Keene, J. D. (1994) *Mol. Cell. Biol.* **14,** 4662–4670.
27. Görlich, D., and Mattaj, I. W. (1996) *Science* **271,** 1513–1518.
28. Koepp, D. M., and Silver, P. A. (1996) *Cell* **87,** 1–4.
29. Marshallsay, C., Dickmanns, A., Bischoff, F. R., Ponstingl, H., Fanning, E., and Lührmann, R. (1996) *Nucleic Acids Res.* **24,** 1829–1836.
30. Palacios, I., Weis, K., Klebe, C., Mattaj, I. W., and Dingwall, C. (1996) *J. Cell Biol.* **133,** 485–494.
31. Sillekens, P. T. G., Beijer, R. P., Habets, W. J., and van Venrooij, W. J. (1988) *Nucleic Acids Res.* **16,** 8307–8321.
32. Sillekens, P. T. G., Beijer, R. P., Habets, W. J., and van Venrooij, W. J. (1987) *EMBO J.* **6,** 3841–3848.
33. Gurdon, J. B. (1976) *J. Embryol. Exp. Morphol.* **36,** 523–540.
34. Lerner, E. A., Lerner, M. R., Janeway, C. A. J., and Steitz, J. A. (1981) *Proc. Natl. Acad. Sci. USA* **78,** 2737–2741.
35. Kalderon, D., Roberts, B. L., Richardson, W. D., and Smith, A. E. (1984) *Cell* **39,** 499–509.
36. Dingwall, C., and Laskey, R. A. (1991) *Trends Biochem. Sci.* **16,** 478–481.
37. Newmeyer, D. D., Finlay, D. R., and Forbes, D. J. (1986) *J. Cell Biol.* **103,** 2091–2102.
38. Breeuwer, M., and Goldfarb, D. S. (1990) *Cell* **60,** 999–1008.
39. Cormack, B. P., Valdivia, R. H., and Falkow, S. (1996) *Gene* **173,** 33–38.

Received February 3, 1997
Revised version received May 26, 1997

EXPERIMENTAL CELL RESEARCH **235,** 274–286 (1997)
ARTICLE NO. EX973671

The $\alpha7\beta1$ Integrin Mediates Adhesion and Migration of Skeletal Myoblasts on Laminin[1]

Suzanne Crawley,* Eleanor M. Farrell,* Weigwang Wang,† Maojian Gu,† Hui-Yu Huang,† Vu Huynh,† Bradley L. Hodges,† Douglas N. W. Cooper,*,[2] and Stephen J. Kaufman†

**Departments of Psychiatry and Anatomy, Center for Neurobiology and Psychiatry, University of California at San Francisco, San Francisco, California 94143-0984; and †Department of Cell and Structural Biology, University of Illinois, Urbana, Illinois 61801*

Many aspects of myogenesis are believed to be regulated by myoblast interactions with specific components of the extracellular matrix. For example, laminin has been found to promote adhesion, migration, and proliferation of mammalian myoblasts. Based on affinity chromatography, the $\alpha7\beta1$ integrin has been presumed to be the major receptor mediating myoblast interactions with laminin. We have prepared a monoclonal antibody, O26, that specifically reacts with both the X1 and the X2 extracellular splice variants of the $\alpha7$ integrin chain. This antibody completely and selectively blocks adhesion and migration of rat L8E63 myoblasts on laminin-1, but not on fibronectin. In contrast, a polyclonal antibody to the fibronectin receptor, $\alpha5\beta1$ integrin, blocks myoblast adhesion on fibronectin, but not on laminin-1. The $\alpha7\beta1$ integrin also binds to a mixture of laminin-2 and laminin-4, the major laminin isoforms in developing and adult skeletal muscle, but O26 is a much less potent inhibitor of myoblast adhesion on the laminin-2/4 mixture than on laminin-1. Based on affinity chromatography, we suggest that this may be due to higher affinity binding of $\alpha7$X1 to laminin-2/4 than to laminin-1. © 1997 Academic Press

---

INTRODUCTION

During skeletal muscle development, proliferating myogenic cells migrate from somite myotomes to peripheral sites where they differentiate to form contractile multinuclear myofibers. Regulation of this process has been shown to depend on cytokines, cell adhesion molecules, and extracellular matrix (ECM) components. Prominent among the cell adhesion molecules are several members of the integrin receptor family [1] which recognize specific ECM components such as laminin or fibronectin, resulting in pronounced effects on myoblast behavior. For instance, laminin promotes adhesion, proliferation, motility, and differentiation [2–7], whereas fibronectin promotes adhesion, but only weakly promotes motility [2, 3]. The studies reported here were aimed at further elucidating the role of specific receptors in regulating myoblast responses to laminin.

Myoblasts express multiple potential laminin-binding integrins, including the $\alpha1\beta1$, $\alpha3\beta1$, $\alpha6\beta1$, and $\alpha7\beta1$ integrins [1, 8–19], but it is clear that the major, if not sole, myoblast integrin that binds to a laminin-1 column is $\alpha7\beta1$ [8, 18, 19]. Several isoforms of this integrin are expressed during muscle development. Alternative splicing generates two variants in the extracellular ligand-binding domain ($\alpha7$X1 and $\alpha7$X2) and three possible variants in the cytoplasmic domain ($\alpha7$A, $\alpha7$B, and $\alpha7$C) [20–23]. In addition, these $\alpha7$ subunit variants combine with two major $\beta1$ cytoplasmic domain splice variants [24–26]. Although differences have been noted in their developmental expression and subcellular distribution [26, 27], functional differences between these splice variants have not yet been identified.

Laminin, too, is expressed as a family of proteins, each a trimer composed of α, β, and γ chains [28]. Tissue-specific, developmentally regulated expression of multiple laminin isoforms has been presumed to reflect important functional differences between isoforms, and some functional differences have been demonstrated depending on cell type [e.g., 7, 29–32]. During skeletal muscle development at least four major laminin isoforms are expressed, laminin-1 ($\alpha1\beta1\gamma1$), laminin-2 ($\alpha2\beta1\gamma1$), laminin-3 ($\alpha1\beta2\gamma1$), and laminin-4 ($\alpha2\beta2\gamma1$) [33–36], with laminin-2 predominating [34]. Most *in vitro* studies of myoblast responses to laminin have been limited to the most easily purified laminin isoform, laminin-1, secreted from mouse EHS tumors. However, myoblast $\alpha7\beta1$ integrin has been

---

[1] This research project was supported by research grants to D.N.W.C. from the Muscular Dystrophy Association and the National Institutes of Health (AR41459) and to S.J.K. from the National Institutes of Health (GM28842, AG14632), Muscular Dystrophy Association, and the University of Illinois Research Board.

[2] To whom correspondence and reprint requests should be addressed at LPPI-Box F-0984, 401 Parnassus Ave., San Francisco, CA 94143. Fax: (415) 476-7320. E-mail: cooper@cgl.ucsf.edu.

0014-4827/97 $25.00

Copyright © 1997 by Academic Press
All rights of reproduction in any form reserved.

shown to bind either to laminin-1 or to a mixture of laminin-2 and laminin-4 purified from human placenta (laminin-2/4) [12, 37]. Like adult muscle laminin, this placental laminin mixture is composed predominantly of laminin-2 [38].

To further define the biological activities of $\alpha7$ integrin we identified a function-blocking mouse monoclonal antibody, O26, that reacts with the extracellular domain of all variants of the rat $\alpha7$ integrin subunit, and we tested the effects of this antibody on migration and adhesion of rat myoblasts on laminin-1 or laminin-2/4. Although O26 completely blocks adhesion and migration on laminin-1, a much higher antibody concentration is required to inhibit adhesion on laminin-2/4. This suggests that $\alpha7\beta1$ integrin binds with higher affinity to laminin-2/4 than to laminin-1. Comparison of the relative binding of $\alpha7\beta1$ integrin to affinity columns conjugated with either laminin-1 or laminin-2/4 supports this hypothesis. Although the α7X2 isoform bound well to both columns, the α7X1 isoform only bound well to the laminin-2/4 column.

EXPERIMENTAL PROCEDURES

Cell culture. Rat L8E63 and mouse C2C12 myoblasts were grown and passaged as described [39, 40]. To assay adhesion or mobility, cells in these cultures were suspended with 0.05% trypsin + 0.02% EDTA and added to an equal volume of cold PBS with 1 mM each $CaCl_2$ and $MgCl_2$ (PBS-CM) and 0.5 mg/ml soybean trypsin inhibitor (Gibco BRL, Gaithersburg, MD).

Cell surface biotinylation. L8E63 cultures were scraped into cold PBS with 2 mM EDTA, washed twice with cold PBS-CM, counted, and adjusted to a cell density of $0.5-1.0 \times 10^7$ cells/ml. Biotin labeling of cell surface proteins was initiated by addition of NHS-LC-Biotin (Pierce) in DMSO (10 mg/ml stock) to a final concentration of 0.1 mg/ml. After incubation for 1 h at 4°C with gentle rocking to keep the cells suspended, the cells were washed three times with cold PBS-CM and snap frozen as cell pellets in liquid nitrogen. For later analysis, aliquots were thawed, triturated, and extracted for 30 min at 4°C in 50 mM Tris–HCl, pH 7.4, 1 mM $MnCl_2$, 1 mM phenylmethylsulfonylfluoride (Sigma), 100 mM n-octyl-β-D-glucoside (ICN Biomedicals, Inc, Aurora, OH), 20 μg/ml aprotinin (Sigma). This solution was centrifuged for 5 min at 14,000g at 4°C, and the supernatant was used for affinity chromatography or immunoprecipitation.

Extracellular matrix proteins. Mouse laminin-1 was purified from mouse EHS tumors by standard techniques involving solubilization with EDTA, ion-exchange chromatography, and molecular sieve chromatography [41]. Human laminin-2/4, prepared by similar techniques, was purchased from Gibco BRL (human merosin, No. 12162). Human plasma fibronectin was either purified by standard techniques [42] or purchased from Gibco BRL (No. 33016). All other extracellular matrix proteins and peptides were obtained commercially, including mouse vitronectin (Gibco BRL), rat collagen-I (Collaborative Biomedical Products, Bedford, MA), mouse collagen-IV (Gibco BRL), and GRGRDNP competitive peptide (Gibco BRL). All protein concentrations were determined using a bicinchoninic acid protein assay (BCA protein assay, Pierce, Rockford, IL).

Laminin affinity purification of $\alpha7\beta1$ integrin. Biotin-labeled cell extracts prepared as described above were circulated 20 times through 2-ml columns of either laminin-1 or laminin-2/4 conjugated to cyanogen bromide-activated Sepharose 4B (1 mg protein coupled per milliliter of gel) (Pharmacia Biotech). Unbound material was washed off with 5 column vol of 50 mM Tris–HCl, pH 7.4, 150 mM NaCl, 1 mM $MnCl_2$, 40 mM n-octyl-β-D-glucoside, and integrins were eluted with 5 column vol of 10 mM EDTA in the same buffer without $MnCl_2$. $CaCl_2$ was immediately added to eluted fractions to a final concentration of 20 mM. Presence of biotin-labeled $\alpha7\beta1$ integrin in column fractions was assessed by immunoprecipitation (see below).

Antibodies. The O5 and O26 monoclonal antibodies were prepared from BALB/c mice immunized with purified $\alpha7\beta1$ integrin [19]. In brief, hybridomas were prepared by fusion of immune spleen cells with SP2/0 cells and were screened, subcloned, and grown as ascites. Antibodies were purified from ascites fluids by ion-exchange chromatography on DEAE–Sephacel (Bio-Rad) followed by precipitation with ammonium sulfate [43] or by polymer partition using E-Z-Sep (Pharmacia Biotech) according to the manufacturer's instructions. Prior to use the antibodies were dialyzed against DME. These antibodies are IgG1, κ-chain immunoglobulins, as determined by radial immunodiffusion and immunofluorescence using light-chain- and subclass-specific antibodies.

A rabbit antibody specific for the α7X2 extracellular splice variant was prepared by immunization with an X2-specific peptide (NH2-QLVYKTLDPADRLTGPAGD) synthesized with an amino terminal cysteine, purified by HPLC, and coupled to maleimide-activated keyhole limpet hemocynanin by Quality Controlled Biochemicals, Inc. (Hopkinton, MA). The serum was delipidated with 0.25% sodium dextran sulfate, 1% $CaCl_2$, and centrifuged at 10,000g for 10 min. Antibody was precipitated from the supernatant with 50% ammonium sulfate and then dialyzed extensively against PBS. Immunoblot analyses using the peptide coupled to bovine serum albumin demonstrated the specificity of the respective sera for the immunizing peptide. All immunoreactivity could be blocked with the immunizing peptide.

Other antibodies used in this study included the 3A3 mouse monoclonal anti-$\alpha1\beta1$ integrin [44] and Ralph 3-1 mouse monoclonal anti-$\alpha3\beta1$ integrin [45], both kindly provided by Lou Reichardt (University of California, San Francisco), a polyclonal anti-$\alpha3\beta1$ integrin (purified, AB1920P, Chemicon, Temecula, CA), the HP2.1 mouse monoclonal anti-$\alpha4$ integrin (purified, Immunotech, Inc., Westbrook, ME), a polyclonal rabbit antibody raised to mouse $\alpha5\beta1$ integrin [46] kindly provided by Vikram Patel (Human Genome Sciences, Rockville, MD), the GoH3 rat monoclonal anti-$\alpha6$ integrin [47] kindly provided by Arnoud Sonnenberg (University of Amsterdam, the Netherlands) and purified from hybridoma culture supernatant, a mouse monoclonal anti-rat $\alpha6\beta1$ integrin (ascites, MAB-5A, MCA2034, Serotec, Washington, DC), a hamster monoclonal anti-αV (purified, H9.2B8, PharMingen, San Diego, CA), a rabbit polyclonal antibody to fibronectin (55038, Cappel, Organon-Teknika, Durham, NC), and a mouse monoclonal antibody to vitronectin (MAB1945, Chemicon).

Analysis of antibody specificity. To initially test reaction of O5 and O26 monoclonal antibodies with $\alpha7\beta1$, this integrin was purified from the hindlimbs of 5-day-old rat pups by immunoaffinity chromatography using H36-$\alpha7$ monoclonal antibody as described [19], resolved by 8% SDS–PAGE under nonreducing conditions, and transferred to nitrocellulose. The blots were then reacted with the monoclonal antibodies purified from their respective ascites fluids [19]. Bound antibody was detected using alkaline phosphatase-conjugated goat anti-mouse immunoglobulin (Jackson Immunoresearch Laboratories, Inc., Westgrove, PA), followed by reaction with nitroblue tetrazolium and 5-bromo-4-chloro-3-indolyl phosphate. Approximate molecular masses were determined by comparison with prestained protein standards (Sigma).

Specificity of these and other antibodies was further tested by immunoprecipitation of biotinylated cell surface proteins from L8E63 myoblasts. Extract equivalent to 6×10^5 cells was brought to 40 mM octylglucoside, 0.1% Tween-20, 65 mM Tris-HCl, pH 7.4, 0.2 M NaCl, 0.5% bovine serum albumin (BSA) (RIA grade, Sigma), 30 μg/ml aprotinin (165 μl final volume). For immunoprecipitation with O26 or antibody to α7X2 peptide, these antibodies were first covalently coupled to Protein G–Sepharose (Zymed Laboratories Inc., South San Francisco, CA) using dimethylpimelimidate [48]. For rabbit antibodies, 2 μl of rabbit serum plus 20 μl of Protein A–Sepharose gel (Pharmacia Biotech) was used to preclear the sample. For mouse antibodies, 20 μl of Protein G–Sepharose alone was used to preclear the sample. After incubating for 1 h, the Sepharose beads were pelleted in a microfuge and the supernatants were transferred to a new tube. Twenty-five microliters of O26 coupled to Protein G–Sepharose or 2–10 μl of other soluble test antibodies was added and the samples were mixed overnight at 4°C. Then 20 μl of Protein A– or Protein G–Sepharose was added and the samples were mixed for an additional 2 h. Sepharose beads with bound proteins were pelleted in a microfuge; washed with 1.0 ml of 25 m*M* Tris–HCl, pH 7.4, 0.140 m*M* NaCl, 3 m*M* KCl (TBS) plus 0.1% Tween 20; washed three times with TBS; and boiled in SDS–PAGE sample buffer. Eluted proteins were separated on a 7% SDS–PAGE gel and electroblotted onto nitrocellulose. Blots were blocked with 2% BSA in TBS with 0.1% Tween 20 and then incubated with streptavidin–biotinylated horseradish peroxidase complex (1:1000, RPN 1051, Amersham Life Science Inc.). After thorough washing, bound peroxidase was detected using a chemiluminescent reaction (ECL, Amersham) to expose X-ray film. Approximate molecular masses were determined by comparison with biotinylated protein standards (High Range, Bio-Rad Laboratories, Hercules, CA).

Transfection and detection of α7 isoforms in CHO cells. α7X1 and α7X2 cDNAs were ligated into the polylinker of the pCMV5 eukaryotic expression vector (David W. Russell, University of Texas Southwestern Medical Center) and the resulting pCMV5-α7X1 and pCMV5-α7X2 plasmids were used to transfect Chinese hamster ovary (CHO) cells. CHO cells were grown on 12-mm-diameter, No. 1 glass coverslips, coated with 0.1% gelatin, in Ham's F-12 medium (Sigma) containing 10% fetal bovine serum (Sigma), 100 units/ml penicillin, 100 μg/ml streptomycin, 10 μg/ml kanamycin, and 0.5 m*M* glutamine. When the cells were approximately 60% confluent they were transfected using Lipofectin according to the method provided by Gibco BRL. Cells were incubated with 2 μg of DNA and 10 μl Lipofectin reagent in serum-free Ham's F-12 medium for 6 h. The medium was then replaced with complete Ham's F-12 medium, and incubation was continued for an additional 48 h at 37°C.

Expression of the α7 integrin chain was detected by immunofluorescence analysis of live cells using O26 monoclonal antibody (25 μl per coverslip at 10 μg/ml). Fluorescein-conjugated donkey anti-mouse IgG (Jackson Immunoresearch) diluted 1:100 (25 μl per coverslip) was used to localize the bound O26 antibody. Washes were done in serum-free Ham's F-12 medium as described [19]. The cells were then fixed for 10 min with fresh 4% *p*-formaldehyde and mounted in glycerol:PBS (9:1), pH 8.5, with 0.01 m*M* *p*-phenylenediamine (Eastman). The slides were sealed with Flo-Texx (Lerner Laboratories) and viewed with epi-illumination optics using a Zeiss photomicroscope II equipped with a 100-W mercury lamp.

Cell adhesion assay. ECM proteins (50 μl at 0–80 μg/ml) were adsorbed to polystyrene ELISA plates (96 wells, Costar) in the presence of 0.1% BSA (RIA grade, Sigma) in PBS for 2 h at room temperature. The wells were then washed three times with PBS and blocked for 2 h with 1% BSA in PBS. Under these conditions binding of ^{125}I-labeled (Bolton-Hunter) fibronectin, laminin-1, or laminin-2/4 is linearly dependent on their concentrations (D. N. W. Cooper, P. Marschal, and A. Sucher, unpublished results). DME with 0.1% BSA (RIA grade, sterile filtered) and with or without tested inhibitors was added to the wells (50 μl per well) and preincubated for 1 h at 37°C. Cells were washed once, resuspended in DME containing 1% BSA, and counted by hemocytometer. Cells (10^4) in 50 μl were added to each well and incubated at 37°C for 30 min. After nonadherent cells had been removed by gentle washing with PBS, the remaining cells were fixed and stained in PBS with 4% *p*-formaldehyde, 1% glutaraldehyde, and 1% toluidine blue. After destaining by several rinses in distilled water, stained cells were counted in a 0.156-mm^2 microscopic field using a Leitz inverted microscope equipped with an ocular micrometer grid.

Transfilter mobility assay. Two different assays were developed to measure cell mobility. In the first, a transfilter migration assay, polycarbonate filters separating the two chambers of Transwells (8-μm pores, 24-well plates, Costar) were coated with given ECM proteins and blocked with BSA as above. DME with 0.1% BSA (RIA grade, sterile filtered) with or without tested inhibitors was added to each chamber (400 μl in the bottom chamber and 80 μl in the top chamber) and preincubated for 1 h at 37°C. Cells (10^4) in 20 μl were then added to each upper chamber and incubated at 37°C for 4 h. After gently washing with PBS, cells were fixed, stained, destained, and counted. Cells on the upper Transwell filter surface were then gently removed with a cotton swab and those on the lower surface were recounted to determine the number of cells that had migrated through the membrane.

Radial mobility assay. A radial mobility assay was also developed to measure over time the outward migration of cells initially confined to small areas on plates coated with ECM proteins. These assays were carried out in 35-mm tissue culture dishes (Costar) to which laminin-1 or fibronectin (purified from human plasma) was adsorbed by incubation overnight at 4°C. Remaining protein-binding sites were then blocked with 1% BSA for 1 h at 25°C. Actively growing cells were trypsinized (PBS with 0.05% trypsin, 0.5 m*M* EDTA), washed once in DME + 10% horse serum, and suspended in DME at 3 × 10^5 cells/ml. Fifty microliters of cells was then added to cloning rings (Bellco, Cat. No. 2090-00608) placed upright on the culture plates. The cells were allowed to attach at 37°C for 30 min. The cloning rings were then removed, and the dishes were gently washed with DME to remove unattached cells. The attached cells were then incubated for 4 to 24 h in DME with or without antibody at 37°C. After fixing and staining with 0.2% crystal violet in 95% ethanol, the diameter of the region occupied by the cells was measured using a Zeiss inverted microscope equipped with an ocular micrometer. The differences in diameters at the beginning and end of incubation were recorded as an index of cell mobility. Mean values were determined for fivefold replicates.

RESULTS

O26 specificity. Three monoclonal antibodies (H36, O5, and O26) reacting with the α7 integrin subunit were previously identified and shown to react with the extracellular domain of the α7 chain by immunofluorescence, immunoblotting, and immunoprecipitation [19]. The O26 and O5 antibodies each detected a band with an apparent mobility of 120 kDa. This band represents the intact α7 chain (Fig. 1A) on immunoblots of $\alpha7\beta1$ integrin that had been purified from rat muscle tissue by immunoaffinity chromatography using the H36 antibody and resolved by nonreducing SDS–PAGE. The band identified at approximately 54 kDa represents H36 immunoglobulin heavy chain released from the column during affinity purification of the integrin and recognized by the secondary antibody to mouse IgG used in the immunoblotting procedure. The 35-kDa band is a proteolytic fragment of the α7 chain [19].

Specificity of the O26 antibody was also demonstrated by immunoprecipitation of cell surface biotin-labeled proteins extracted with octylglucoside from L8E63 myoblasts (Fig. 1B). Immunoprecipitation with

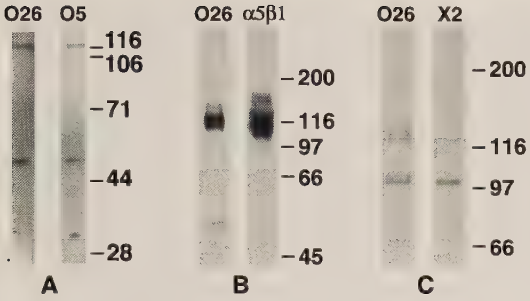

FIG. 1. Analysis of antibody specificity by immunoblotting and immunoprecipitation. (A) Immunoblot analysis of the $\alpha7$ integrin chain using O26 (left lane) and O5 (right lane) monoclonal antibodies. Purified $\alpha7\beta1$ integrin was separated by 8% SDS–PAGE under nonreducing conditions and electroblotted onto nitrocellulose. The O5 and O26 antibodies both react with a band having apparent mobility of 120 kDa, representing the intact $\alpha7$ chain. The band at approximately 54 kDa represents immunoglobulin heavy chain derived from immunoaffinity purification of the integrin. The 35-kDa band detected by O5 antibody is a proteolytic fragment of the $\alpha7$ chain [27]. The mobilities of prestained molecular mass markers (β-galactosidase, phosphorylase b, bovine albumin, ovalbumin, and carbonic anhydrase) are indicated. (B) Immunoprecipitation of cell surface biotinylated proteins from L8E63 myoblasts with O26 antibody to integrin $\alpha7$ (left lane) or polyclonal antibody to integrin $\alpha5\beta1$ (right lane). Extract equivalent to 6×10^5 cells was immunoprecipitated, separated by 7% SDS–PAGE under nonreducing conditions, and electroblotted onto nitrocellulose. Blots were incubated with streptavidin-biotinylated horseradish peroxidase complex and bound peroxidase was detected by chemiluminescence. Immunoprecipitation with O26 antibody results in one predominant band with an apparent mobility of 120 kDa, as expected for the overlapping $\alpha7$ and coprecipitated $\beta1$ integrin subunits. Immunoprecipitation with a polyclonal antiserum to integrin $\alpha5\beta1$ results in bands with apparent mobilities of 155 and 130 kDa, as expected for the $\alpha5$ subunit, and 110–120 kDa, as expected for the $\beta1$ subunit. The mobilities of biotinylated molecular mass markers are indicated (myosin, β-galactosidase, phosphorylase b, bovine serum albumin, and ovalbumin). (C) Immunoprecipitation of $\alpha7$ integrin from cell surface-biotinylated L8E63 myoblasts with O26 antibody which recognizes both the X1 and X2 splice variants (left lane) or with a polyclonal antibody specific for the X2 splice variant (right lane). Proteins were electrophoresed under reducing conditions. Immunoprecipitation with O26 antibody results in bands with apparent mobility of 130 kDa, as expected for the $\beta1$ integrin subunit, and 102 and 98 kDa, apparently representing the X1 and X2 splice variants of the $\alpha7$ integrin subunit. Antibody specific for the X2 splice variant precipitates only the band with apparent mobility of 98 kDa.

O26 antibody resulted in one predominant band (Fig. 1B, left lane) with apparent mobility of 115–120 kDa on nonreducing SDS–PAGE gels, as expected for the overlapping $\alpha7$ subunit and coprecipitated $\beta1$ subunit [19]. In contrast, immunoprecipitation with a polyclonal antiserum to integrin $\alpha5\beta1$ [46] produced a broad band with apparent mobility of 110–120 kDa, another band with apparent mobility of 130 kDa, and a weaker band with apparent mobility of 155 kDa on nonreducing SDS–PAGE gels (Fig. 1B, right lane). These presumably represent the $\alpha5$ (155 and 130 kDa) and $\beta1$ (110–120 kDa) subunits, but some cross-reaction with other $\beta1$ containing integrins is likely given the polyclonal nature of this antibody.

To test whether the O26 antibody recognizes both splice variants in the $\alpha7$ extracellular domain, $\alpha7$X1 and $\alpha7$X2, CHO cells were transfected to express either $\alpha7$X1 or $\alpha7$X2. Specific recognition of both isoforms by O26 was demonstrated by immunofluorescence staining of transfected cells, but not untransfected cells (Fig. 2) or cells transfected with vector alone (not shown).

O26 recognition of both extracellular splice variants of $\alpha7$ integrin was further demonstrated by immunoprecipitation of myoblast proteins. $\alpha7$X1 and $\alpha7$X2 are expressed in approximately equal amounts in replicating myoblasts in combination primarily with the $\alpha7$B cytoplasmic domain [20, 21]. When biotin-labeled myoblast surface proteins were immunoprecipitated with O26 and resolved by SDS–PAGE under reducing conditions, two $\alpha7$ integrin bands were detected with apparent mobilities of 98 and 102 kDa (Fig. 1C, left lane). We presume that these represent the $\alpha7$X1 and $\alpha7$X2 splice variants, respectively, because immunoblotting or immunoprecipitation with X2-specific anti-peptide antibody only detects the 98-kDa band (Fig. 1C, right lane). The alternative X1 and X2 exons encode 43 and 39 amino acid residues, respectively, and this sequence difference would theoretically account for a size difference of only 846 Da [20]. The greater difference in electrophoretic mobility remains unexplained, but might reflect a difference in posttranslational modification.

O26 inhibits myoblast adhesion and mobility on laminin-1. Conditions were optimized to assay myoblast adhesion and mobility as described under Materials and Methods. Dependence of L8E63 adhesion on substrate concentration was similar for fibronectin, laminin-1, and laminin-2/4 substrates (Fig. 3A). Cell adhesion on each substrate was close to maximal for plates coated with 3 μg/ml of protein and approximately 50% of maximal for plates coated with half that concentration. Mouse C2C12 cells gave similar results (not shown). Subsequent assays to test for antibody inhibition of adhesion were conducted using substrate coating concentrations of 5 μg/ml.

The dependence of L8E63 mobility on substrate concentration was similar for laminin-1 or laminin-2/4 (Fig. 3B). In contrast, these cells showed only minimal migration on fibronectin (Figs. 3B and 3C). Subsequent mobility assays were conducted using coating concentrations of 5 μg/ml for laminin-1 or laminin-2/4. This concentration supported about 50% of maximal migration. Under these conditions, essentially all cells adhered and approximately 20% migrated across filters coated with either laminin-1 or laminin-2/4 after 4 h incubation. In contrast, less than 2% adhered and migrated across filters coated with BSA.

Inhibition of adhesion by O26 antibody was depen-

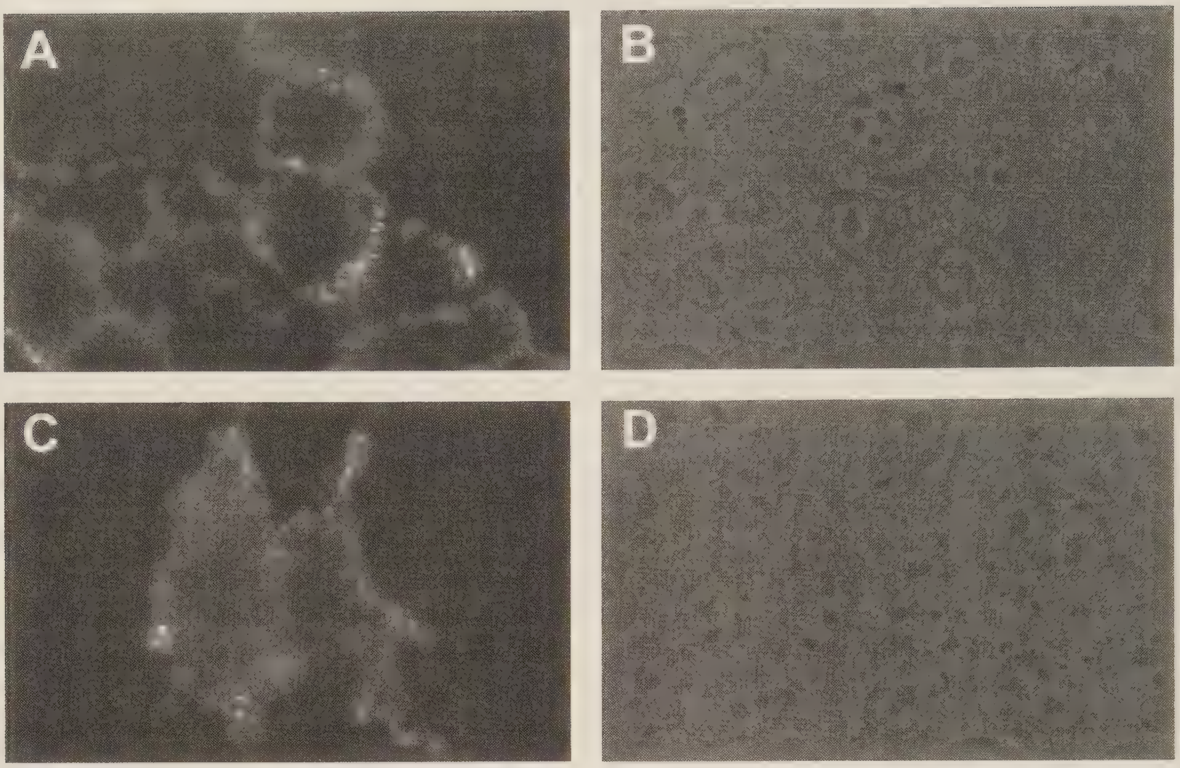

FIG. 2. Immunofluorescence detection of $\alpha7$ integrin chain on Chinese hamster ovary (CHO) cells transfected to express $\alpha7$X1 or $\alpha7$X2. CHO cells were transfected with $\alpha7$ integrin cDNA encoding the X1 (A and B) or X2 (C and D) alternative extracellular domains. Forty-eight hours later the cells were stained with O26 anti-$\alpha7$ monoclonal antibody, followed by FITC-conjugated donkey anti-mouse immunoglobulin, and observed using fluorescence (A and C) or phase contrast optics (B and D).

dent on both antibody and substrate concentrations (Fig. 4). When assayed after 30 min incubation, adhesion and spreading of L8E63 cells were almost completely inhibited by 10 μg/ml O26 in wells coated with 5 μg/ml laminin-1 (Fig. 4A) and about 50% inhibited in wells coated with 50 μg/ml laminin-1 (Fig. 4B). Less inhibition was observed with lower O26 concentrations. Inhibition by O26 was transient, such that adhesion in the presence of antibody returned to control levels after the first hour of incubation (Fig. 4C). Inhibition by O26 was specific, because the antibody did not inhibit adhesion to fibronectin.

Myoblasts express multiple fibronectin-binding integrins [8–12, 49, 50], but myoblast responses to fibronectin are believed to be primarily mediated by integrin $\alpha5\beta1$ [49]. Indeed, we found that adhesion to fibronectin was almost completely inhibited by an antiserum to $\alpha5\beta1$ integrin (1:200 dilution) which had little effect (maximum 10–15% inhibition) on adhesion to laminin-1.

The O26 antibody also strongly inhibited myoblast mobility on laminin-1 in transfilter or radial migration assays. Inhibition of migration by O26 antibody was dependent on both antibody and laminin-1 concentrations. At 10 μg/ml, O26 antibody almost completely inhibited L8E63 migration across filters coated with 5 μg/ml laminin-1 (Fig. 5A). Inhibition of radial migration by O26 was biphasic with maximal inhibition of about 80% at 1 to 5 μg/ml of antibody (Fig. 5B). Inhibition of cell mobility in these assays cannot be simply attributed to inhibition of cell adhesion, which was transient and no longer detectable when the assay duration was extended from 30 to 60 min, whereas O26 continued to inhibit migration for at least 24 h in radial mobility assays (Fig. 5B) and for at least 6 h in transwell mobility assays (Fig. 5C).

O26 antibody only weakly inhibits myoblast adhesion and mobility on laminin-2/4. Although $\alpha7\beta1$ integrin recognizes both laminin-1 and laminin-2/4, the inhibitory activity of the O26 antibody is dependent on the laminin isoform. O26 at 10 μg/ml did not inhibit L8E63 adhesion or migration on laminin-2/4, although in the same experiments this antibody concentration produced at least 70% inhibition on laminin-1 (Figs. 4 and 5). Increasing the antibody concentration to 30 μg/ml did result in almost 70% inhibition of L8E63 adhesion on laminin-2/4, but this was still less than the almost complete inhibition on laminin-1 (Fig. 6A). Furthermore, even at 30 μg/ml the O26 antibody still failed to inhibit L8E63 mobility on laminin-2/4 (Fig. 6B).

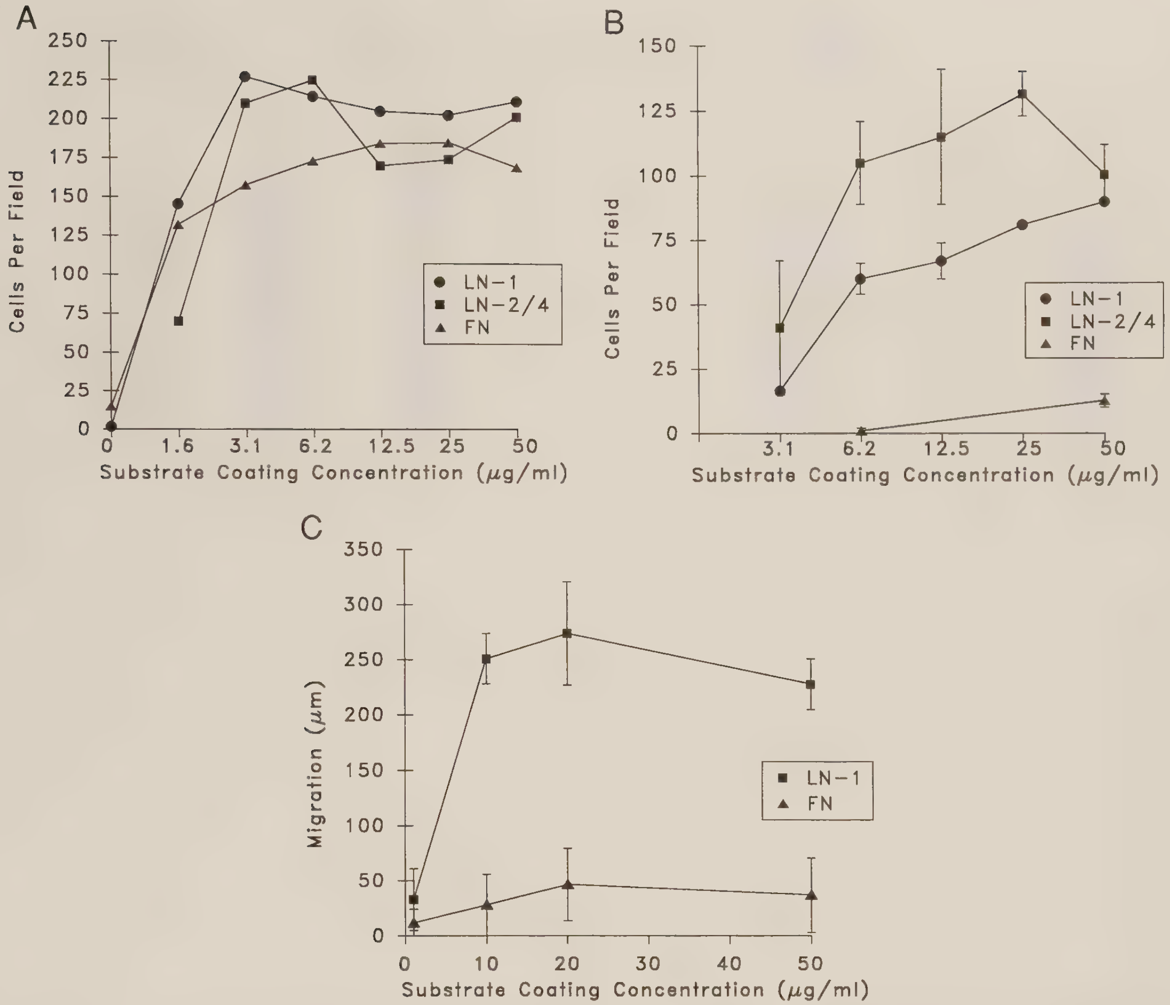

FIG. 3. Dependence on laminin-1 (●), laminin-2/4 (■), or fibronectin (▲) substrate concentration for L8E63 myoblast adhesion and motility. (A) Dependence of L8E63 adhesion on substrate concentration was very similar for fibronectin, laminin-1, or laminin-2/4 substrates in a standard adhesion assay (each point is the mean of two experiments). (B and C) Both laminin-1 and laminin-2/4 promoted L8E63 migration with similar dependence on substrate concentration, but these cells showed only minimal migration on fibronectin in either 4-h duration transwell motility assays (B, each point is the mean ± standard error of three or four experiments) or 12-h duration radial motility assays (C, each point is the mean ± standard deviation of five experiments).

Since possible differences in purity of the two laminin preparations might contribute to differences in efficacy of O26 antibody inhibition of adhesion, we tested and were able to rule out significant differences in contamination with fibronectin, vitronectin, collagen I, collagen IV, or entactin. Myoblast adhesion to fibronectin, but not to laminin-1 or laminin-2/4, could be completely blocked by antibody to $\alpha5\beta1$ integrin (Fig. 4), by antibody to fibronectin, or by the competitive peptide GRGDNP (data not shown). Similarly, adhesion to vitronectin, but not to laminin-1 or laminin-2/4, could be completely blocked by antibody to vitronectin (data not shown). Neither collagen I nor collagen IV supported adhesion or migration of L8E63 or C2C12 myoblasts in these assays. Entactin, a protein tightly and stoichiometrically associated with laminin [28], can affect the adhesive properties of the laminin complex [51]. However, the standard procedures for laminin-1 and laminin-2/4 purification used here would not be expected to cause entactin dissociation, and silver staining after SDS–PAGE revealed bands presumed to represent entactin at 150 kDa with about the same intensity in the two laminin preparations (not shown). Furthermore, two sites mediating cell adhesion have been identified in entactin, one including an RGD sequence recognized by $\alpha V\beta3$ integrin [52–54] and another RGD-independent site recognized by $\alpha3\beta1$ integrin [54, 55], but neither the competitive peptide GRGDNP (at 100 μg/ml), which totally inhibits adhesion to fibronectin, nor a function-blocking antibody to $\alpha3$ integrin (Ralph 3-1, 30 μg/ml) inhibited myoblast adhesion or mobility on laminin-1 or laminin-2/4, even in

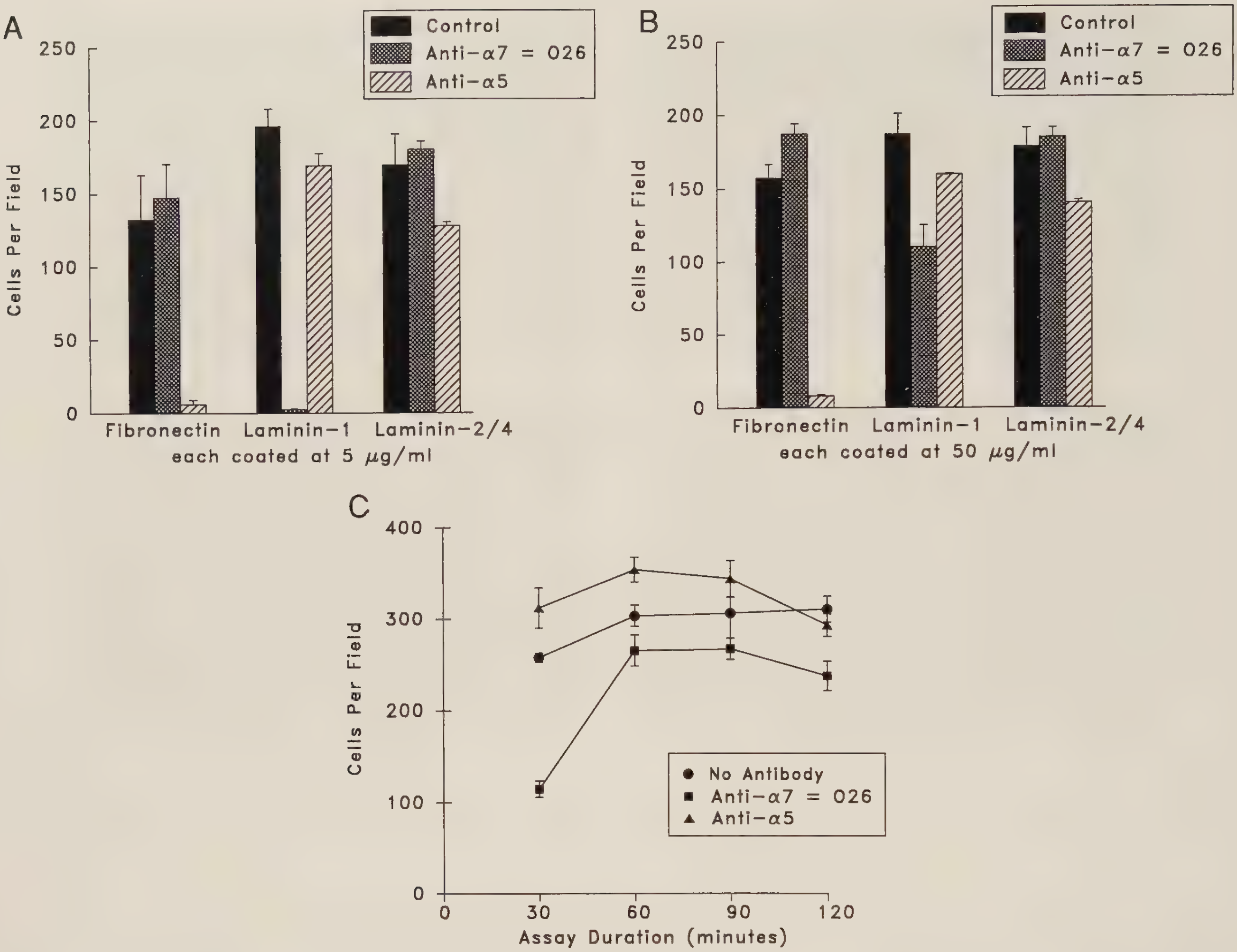

FIG. 4. Inhibition by O26 antibody of L8E63 myoblast adhesion on laminin-1 or laminin-2/4, but not on fibronectin. (A and B) In a standard 30-min adhesion assay L8E63 cells adhere about equally on laminin-1, laminin-2/4, or fibronectin in the absence of antibody (solid bars). O26 antibody (10 μg/ml, cross-hatched bars) inhibits adhesion on laminin-1 or laminin-2/4 but not on fibronectin, whereas antiserum to integrin $\alpha5\beta1$ (1:200, hatched bars) inhibits adhesion only on fibronectin but not on laminin-1 or laminin-2/4. Inhibition by O26 is dependent on substrate concentration (A, 5 μg/ml; B, 50 μg/ml). Each bar represents the number of adherent cells counted per high power field (mean ± standard error of three to five experiments). (C) Varying the assay duration from 30 to 120 min reveals that O26 (■, 10 μg/ml) inhibition of L8E63 cell adhesion on laminin-1 lasts less than 1 h. Adhesion in the absence of antibody (●) is already almost maximal after 30 min and remains level over the succeeding 90 min. Antiserum to integrin $\alpha5\beta1$ (▲) fails to significantly inhibit adhesion at any of these times. Each data point represents the number of adherent cells counted per high power field (mean ± standard error of three to five experiments).

combination with O26 antibody. Therefore, it seems unlikely that differences between the laminin-1 and laminin-2/4 preparations in the content of these other ECM proteins could account for the difference in sensitivity to O26 antibody inhibition of myoblast adhesion and migration.

We also considered the possibility that the difference in myoblast sensitivity to inhibition by O26 on laminin-1 versus laminin-2/4 might arise if myoblasts primarily depend on $\alpha7\beta1$ to interact with laminin-1, but on another receptor to interact with laminin-2/4. Adhesion of L8E63 myoblasts to either laminin-1 or laminin-2/4 was completely inhibited by 2 m*M* EDTA, as expected for integrin-mediated association. The $\alpha1\beta1$, $\alpha3\beta1$, and $\alpha6\beta1$ integrins are other potential laminin-binding integrins that have been reported to be expressed on myoblasts, although perhaps not in an active laminin-binding conformation [13, 18]. We confirmed the presence of these integrins on L8E63 cells by immunoprecipitation (data not shown) and used function-blocking antibodies to test their role in myoblast adhesion on laminin-2/4. However, no detectable inhibition of adhesion of L8E63 myoblasts on laminin-1 or laminin-2/4 was obtained with anti-rat-$\alpha1$ (3A3 at 6 μg/ml) or anti-rat-$\alpha3$ (Ralph

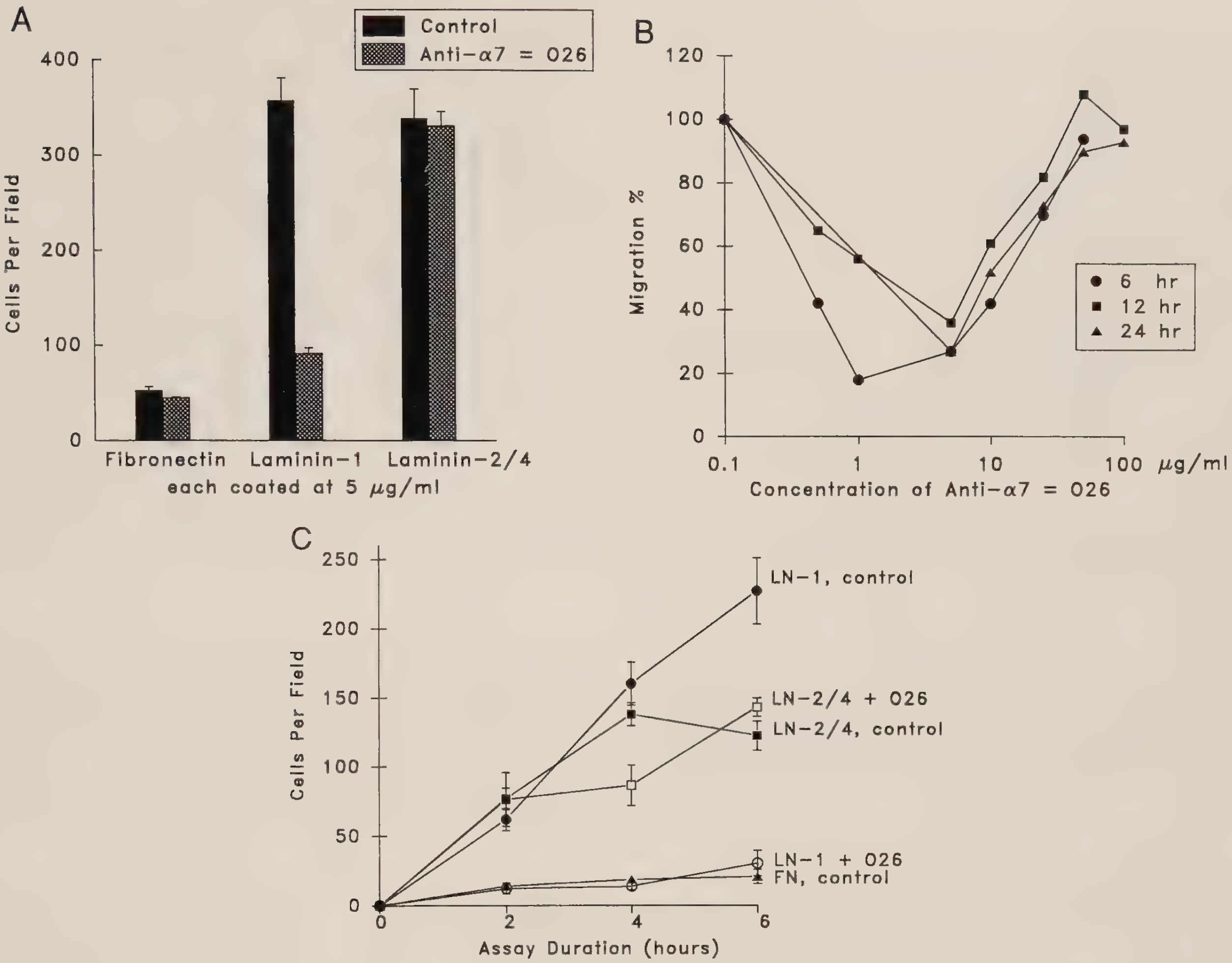

FIG. 5. Inhibition by O26 antibody of L8E63 myoblast migration on laminin-1. (A) L8E63 cells migrate about equally on laminin-1 or laminin-2/4, but negligibly on fibronectin (each coated at 5 μg/ml) in transwell mobility assays of 4-h duration in the absence of antibody (solid bars). O26 antibody at 10 μg/ml (cross-hatched bars) almost completely inhibits migration on laminin-1, but has no significant effect on migration on laminin-2/4. Each bar represents the number of adherent cells counted per high power field (mean ± standard error of three to five experiments). (B) O26 antibody inhibition of L8E63 cell migration on laminin-1 (20 μg/ml) is dependent on antibody concentration, but stable over time, as demonstrated for radial motility assays of 6- (●), 12- (■), or 24-h (▲) duration. Myoblast migration in the presence of increasing amounts of O26 antibody is calculated as a percentage of migration in the absence of added antibody. Inhibition exhibits similar biphasic concentration dependence regardless of assay duration, with maximal inhibition at 1 to 5 μg/ml of O26 antibody. (C) Inhibition of L8E63 myoblast migration on laminin-1 by O26 antibody is also stable in transwell migration assays of 30 to 120 min duration. In the absence of antibody, myoblasts appear to migrate at a constant rate for at least 120 min across filters coated with 50 μg/ml laminin-1 (●), but in the presence of O26 antibody at 10 μg/ml (○) the number of cells that have migrated across the filter is negligible even after 120 min. In this experiment, the rate of L8E63 cell migration across filters coated with 50 μg/ml laminin-2/4, even in the absence of antibody (■), appears somewhat slower than on laminin-1, but is not significantly affected by O26 antibody at 10 μg/ml (□). The number of cells migrating across filters coated with 50 μg/ml of fibronectin (▲) is negligible even after 120 min. Each data point represents the number of cells counted per high power field (mean ± standard error of three to five experiments) on the bottom of the filter.

3-1 at 30 μg/ml). Lacking an equivalent function-blocking antibody to rat α6β1, the effect of GoH3 anti-mouse-α6β1 was tested on adhesion of mouse C2C12 myoblasts. Although this antibody did somewhat inhibit adhesion on laminin-1 (maximum inhibition of about 20%), it did not detectably inhibit adhesion on laminin-2/4.

We therefore tested the possibility that one or both α7 extracellular splice variants might bind with higher affinity to laminin-2/4 than to laminin-1. Extracts of cell surface biotinylated L8E63 myoblasts were chromatographed over columns of laminin-2/4 or laminin-1 conjugated to Sepharose. Unbound proteins were washed free, and bound proteins were eluted with EDTA. α7 integrin in the initial extract (Fig. 7A, lane 1) and in collected column fractions was detected by immunoprecipitation of matching aliquots using O26 antibody (Figs. 7A, lanes 1–7, and 7B, lanes 8 and 9)

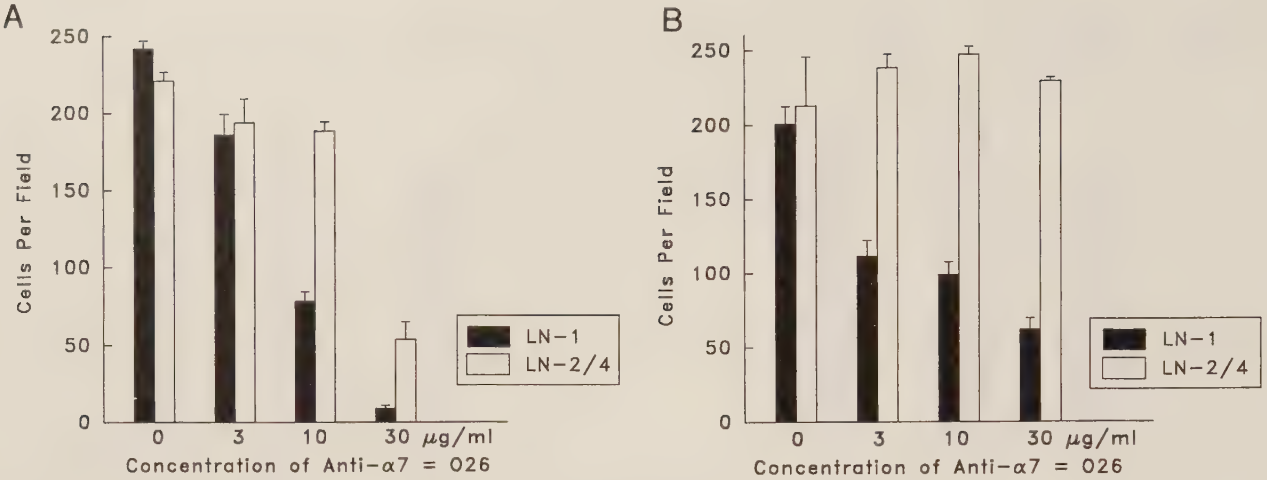

FIG. 6. O26 is a more potent inhibitor of L8E63 myoblast adhesion and migration on laminin-1 than on laminin-2/4. (A) Concentration dependence of O26 antibody inhibition of adhesion on wells coated with 5 μg/ml laminin-1 (closed bars) or laminin-2/4 (open bars). (B) Concentration dependence of O26 antibody inhibition of migration across filters coated with 5 μg/ml laminin-1 (closed bars) or laminin-2/4 (open bars).

or antibody specific to the α7X2 splice variant (Fig. 7B, lanes 10 and 11). As described above, when separated by SDS–PAGE under reducing conditions, α7 integrin can be resolved as two closely spaced bands with apparent mobilities of 98 and 102 kDa (separation is emphasized in Fig. 7B by longer electrophoresis). Whereas

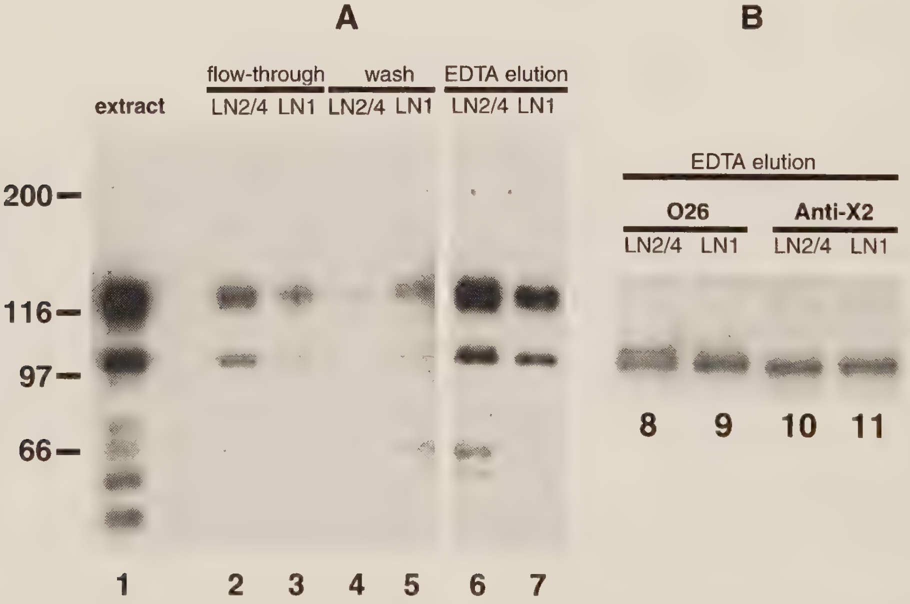

FIG. 7. The α7β1 integrin binds to both laminin-2/4 and laminin-1. Extract from 5 × 10^6 surface biotinylated L8E63 myoblasts was circulated over columns of either laminin-2/4 (lanes 2, 4, 6, 8, and 10) or laminin-1 (lanes 3, 5, 7. 9, and 11) conjugated to Sepharose. After thorough washing, specifically bound proteins were eluted with 15 m*M* EDTA. Immunoprecipitation with O26 antibody (lanes 1–9) or antibody specific for the X2 splice variant (lanes 10 and 11) was used to detect α7β1 integrin in the initial extract (lane 1) and column fractions pooled for the flow-through (lanes 2 and 3), wash (lanes 4 and 5), and EDTA eluate (lanes 6–11). One-eight of each pool was immunoprecipitated and the α7 subunit (100-kDa band) and coprecipitated β1 subunit (130-kDa band) were separated by SDS–PAGE on 7% gels under reducing conditions, electroblotted onto nitrocellulose, and incubated with streptavidin–biotinylated horseradish peroxidase complex. Bound peroxidase was detected by chemiluminescence. The mobilities of biotinylated molecular mass markers are indicated (myosin, β-galactosidase, phosphorylase b, and bovine serum albumin). The gel in B was electrophoresed longer and is shown in higher magnification than the gel in A to better demonstrate separation of the X1 and X2 splice variants.

these two isoforms appear to be approximately equally abundant in the initial cell extract, immunoprecipitation with O26 revealed marked enrichment for the 98-kDa (X2) isoform in material flowing through the laminin-2/4 column (Fig. 7A, lane 2). In contrast, the 102-kDa (X1) isoform was enriched in the material flowing through the laminin-1 column (Fig. 7A, lanes 3 and 5). Both isoforms were detected in approximately equal amounts in the material eluted with EDTA from the laminin-2/4 column (Figs. 7A, lane 6, and Fig. 7B, lane 8), but the 98-kDa isoform predominates in the eluate from the laminin-1 column (Figs. 7A, lane 7, and Fig. 7B, lane 9). Identification of the 98-kDa isoform as α7X2 was confirmed by immunoprecipitation of the column eluates with antibody specific for the X2 splice variant (Fig. 7B, lanes 10 and 11). We therefore conclude that $\alpha7X1\beta1$ preferentially binds to laminin-2/4 compared to laminin-1.

DISCUSSION

Inhibition of rat L8E63 myoblast adhesion and migration on laminin-1 by the O26 antibody specific for α7 integrin strongly supports the conclusion that $\alpha7\beta1$ integrin is the major myoblast receptor mediating interactions with laminin-1. While this paper was in preparation, similar results were reported using mouse C2C12 myoblasts and a different function-blocking antibody to α7 integrin [12]. Furthermore, expression of transfected α7 subunit in cells normally lacking it has been shown to induce mobility on laminin-1 or laminin-2/4 [37, 56; H. Y. Huang and S. J. Kaufman, unpublished results]. Although $\alpha7\beta1$ integrin can also bind to fibronectin *in vitro* [8], O26 had no effect on myoblast adhesion or migration on fibronectin. Instead, myoblast interactions with fibronectin seem to primarily rely on $\alpha5\beta1$ integrin, because both adhesion and migration on fibronectin were almost completely blocked by polyclonal anti-$\alpha5\beta1$ function-blocking antibodies. This antiserum has been reported to also inhibit the activity of $\alpha4\beta1$ integrin [57], but the α4 subunit is not expressed until after myoblast differentiation [58], and we could not detect it in L8E63 myoblast extracts with a specific anti-α4 antibody.

The mechanism of O26 antibody inhibition of $\alpha7\beta1$ integrin function is unclear. In particular, it is unclear why O26 causes only a brief inhibition of myoblast adhesion, but a long-lasting inhibition of migration. The biphasic concentration dependence of O26 inhibition of migration (Fig. 5B) suggests that this antibody inhibits $\alpha7\beta1$ integrin function by cross-linking, perhaps aggregating, receptor molecules in the cell membrane as opposed to directly blocking receptor function. Aggregation might interfere with receptor function, for instance, due to steric constraints or by causing internalization. Also, cross-linking of $\alpha7\beta1$ integrin induced by antibody or by soluble laminin-1 has been found to promote association with the cell cytoskeleton [22] and stable association might be antithetical to migration. If aggregation of $\alpha7\beta1$ integrin is important for O26 antibody inhibition of migration, this might also explain why O26 inhibition of migration depends on laminin substrate concentration. Perhaps higher substrate ligand concentrations or higher affinity binding of $\alpha7\beta1$ integrin to the substrate effectively compete with the receptor crosslinking effect of the O26 antibody.

An unexpected result is that the inhibitory effect of the O26 antibody depends on laminin composition such that O26 is much less effective at inhibiting myoblast adhesion and migration on human laminin-2/4 than on mouse laminin-1. A similar result was recently reported using a different function-blocking antibody to $\alpha7\beta1$ [12]. In that case, higher antibody concentrations were required to inhibit adhesion and migration of MM14 mouse myoblasts on laminin-2/4 than on laminin-1. C2C12 myoblasts spread more rapidly on laminin-2/4 than on laminin-1 [34] and this, too, might correlate with stronger adhesion.

We considered several possible explanations for the observed difference in O26 inhibition of myoblast interaction with laminin-1 compared with laminin-2/4. A simple explanation would be that $\alpha7\beta1$ integrin binds with higher affinity to at least one of the two laminin isoforms in the laminin-2/4 mixture than to laminin-1. It is also possible that, although the O26 antibody binds to both the α7X1 and α7X2 variants, it could be more effective at inhibiting the activity of one or the other. Similar arguments could be made for variant forms of integrin $\alpha7\beta1$ generated by differences in posttranslational modification [59].

Structural differences between laminin isoforms could result in different binding affinities for the α7 isoforms. The binding site for $\alpha7\beta1$ integrin residues in the E8 proteolytic fragment of laminin-1 [18], and it is this fragment that supports myoblast migration [3, 60]. Laminin-1 (a trimer of laminin subunits $\alpha1$, $\beta1$, and $\gamma1$) and laminin-2 (a trimer of $\alpha2$, $\beta1$, and $\gamma1$) differ only in their α subunits. There is less than 42% amino acid sequence identity between the E8 portions of the $\alpha1$ and $\alpha2$ laminin subunits [61–63]. This difference might account for the apparent difference in binding affinities for the α7X1 versus α7X2 isoforms. We found that α7X1 in contrast to α7X2 washed off of a laminin-1 column, but was well retained on a laminin-2/4 column. Although direct measurements of these ligand–integrin-binding affinities have not been made, our data are consistent with the possibility that the association of $\alpha7X1\beta1$ with laminin-2/4 is more tenacious than with laminin-1. This would explain why higher concentrations of O26 antibody are required to inhibit myoblast interaction with laminin-2/4 compared with laminin-1.

This suggestion is also consistent with different roles postulated for $\alpha7\beta1$ integrin during muscle development. Laminin-2 is the major laminin isoform produced in developing myoblasts and deposited in basement membranes surrounding adult skeletal muscle [33, 34]. Thus, although myoblasts might encounter laminin-1 in adjacent tissues or early in development, laminin-2 is the major isoform that would be encountered by fetal myoblasts, by adult myofibers, and by muscle satellite cells during wound healing and regeneration. Whereas $\alpha7\beta1$ integrin might primarily mediate migration in a laminin-1-rich environment (where readily reversible interactions are required), it might provide structural integrity along junction and lateral contacts of muscle fibers in a laminin-2/4-rich environment (where more permanent interactions are established) [27]. Selective localization of different $\alpha7$ integrin variants at junctional and nonjunctional sites of adult muscle where different laminin isoforms also reside is consistent with this idea [27].

Although we have not completely ruled it out, our results do not support the possibility that a receptor other than $\alpha7\beta1$ integrin preferentially recognizes laminin-2/4 and plays a major role in mediating myoblast migration on this laminin isoform. Cultured myoblasts express small amounts of $\alpha1\beta1$, $\alpha3\beta1$, and $\alpha6\beta1$ integrins, but these seem to have little activity as laminin receptors in myoblasts [12, 13, 18]. Furthermore, function-blocking antibodies to these integrins, even in combination with O26 antibody, had little or no effect on myoblast adhesion or migration on laminin-2/4. A novel α integrin, distinct from the above, with apparent mobility of 145 kDa has been reported to be induced upon differentiation of cultured human fetal myoblasts, but no ligand for this integrin has yet been identified [11]. Several nonintegrin laminin receptors have also been described [64], but in contrast to the integrins, with the exception of α-dystroglycan [65], the binding of these nonintegrin receptors is insensitive to EDTA, yet EDTA completely blocked myoblast adhesion on laminin-1 or laminin-2/4, and dystroglycan is not expressed on undifferentiated myoblasts [66, 67].

In summary, the O26 monoclonal antibody is specific for the $\alpha7\beta1$ integrin and inhibits myoblast adhesion and migration on laminin-1. This demonstrates the functional importance of $\alpha7\beta1$ integrin in myoblast adhesion and migration. The $\alpha7\beta1$ integrin also binds to a laminin-2/4 preparation, but O26 is much less effective in inhibiting myoblast interactions with laminin-2/4 compared to laminin-1. Our evidence suggests that this selective inhibition results from stronger binding of myoblasts to laminin-2/4 than laminin-1 through the $\alpha7X1\beta1$ integrin.

We thank Dr. Vikram Patel (Human Genome Sciences, Rockville, MD), Dr. Louis Reichardt (University of California, San Francisco), and Dr. Arnoud Sonnenberg (University of Amsterdam, the Netherlands) for generously providing antibodies and advice.

REFERENCES

1. McDonald, K., Horwitz, A., and Knudsen, K. (1995). Adhesion molecules and skeletal myogenesis. *Semin. Dev. Biol.* **6,** 105–116.
2. Ocalan, M., Goodman, S. L., Kuhl, U., Haushka, S. D., and von der Mark, K. (1988). Laminin alters cell shape and stimulates mobility and proliferation of murine skeletal myoblasts. *Dev. Biol.* **125,** 158–167.
3. Goodman, S. L., Risse, G., and von der Mark, K. (1989). The E8 subfragment of laminin promotes locomotion of myoblasts over extracellular matrix. *J. Cell Biol.* **109,** 799–809.
4. Kuhl, U., Ocalan, M., Timpl, R., and von der Mark, K. (1986). Role of laminin and fibronectin in selecting myogenic versus fibrogenic cells from skeletal muscle in vitro. *Dev. Biol.* **117,** 628–635.
5. Foster, R. F., Thompson, J. M., and Kaufman, S. J. (1987). A laminin substrate promotes myogenesis on rat skeletal muscle cultures: Analysis of replication and development using anti-desmin and anti-BrdU monoclonal antibodies. *Dev. Biol.* **122,** 11–20.
6. Goodman, S. L., Deutzman, R., and Nurcombe, V. (1989). Locomotory competence and laminin-specific cell surface binding sites are lost during myoblast differentiation. *Development* **106,** 795–802.
7. Vachon, P. H., Loechel, F., Xu, H., Wewer, U. M., and Engvall, E. (1996). Merosin and laminin in myogenesis: Specific requirement for merosin in myotube stability and survival. *J. Cell Biol.* **134,** 1483–1497.
8. Gu, M., Wang, W., Song, W. K., Cooper, D. N. W., and Kaufman, S. J. (1994). Selective modulation of the interaction of $\alpha7\beta1$ integrin with fibronectin and laminin by L-14 lectin during skeletal muscle differentiation. *J. Cell Sci.* **107,** 175–181.
9. Mechtersheimer, G., Barth, T., Quentmeier, A., and Moller, P. (1994). Differential expression of $\beta1$ integrins in nonneoplastic smooth and striated muscle cells and in tumors derived from these cells. *Am. J. Pathol.* **144,** 1172–1182.
10. Gullberg, D., Sjoberg, G., Velling, T., and Sejersen, T. (1995). Analysis of fibronectin and vitronectin receptors on human fetal skeletal muscle cells upon differentiation. *Exp. Cell Res.* **220,** 112–123.
11. Gullberg, D., Velling, T., Sjoberg, G., and Sejersen, T. (1995). Up-regulation of a novel integrin α-chain (α_{mt}) on human fetal myotubes. *Dev. Dynam.* **204,** 57–65.
12. Yao, C.-C., Ziober, B. L., Sutherland, A. E., Mendrick, D. L., and Kramer, R. H. (1996). Laminins promote the locomotion of skeletal myoblasts via the alpha7 integrin receptor. *J. Cell Sci.* **109,** 3139–3150.
13. Goodman, S. L., Aumailley, M., and von der Mark, H. (1991). Multiple cell surface receptors for the short arms of laminin. *J. Cell Biol.* **113,** 931–941.
14. Duband, J., Belkin, A., Syfrig, J., Thierry, J., and Koteliansky, V. (1992). Expression of $\alpha1$ integrin, a laminin-collagen receptor, during myogenesis and neurogenesis in the avian embryo. *Development* **116,** 585–600.
15. Bronner-Fraser, M., Artinger, M., Muschler, J., and Horwitz, A. (1992). Developmentally regulated expression of the $\alpha6$ integrin in avian embryos. *Development* **115,** 197–211.
16. Pow, C. S., and Hendrickx, A. G. (1995). Localization of the inte-

grin subunits $\alpha6$ and $\beta1$ during somitogenesis in the long-tailed macaque (M. fascicularis). *Cell Tissue Res.* **281,** 101–108.

17. George-Weinstein, M., Foster, R. F., Gerhart, J. V., and Kaufman, S. J. (1993). In vitro and in vivo expression of $\alpha7$ integrin and desmin define the primary and secondary myogenic lineages. *Dev. Biol.* **156,** 209–229.
18. von der Mark, H., Durr, J., Sonnenberg, A., von der Mark, K., Deutzmann, R., and Goodman, S. L. (1991). Skeletal myoblasts use a novel $\beta1$-series integrin and not $\alpha6\beta1$ for binding to E8 and T8 fragments of laminin. *J. Biol. Chem.* **266,** 23593–23601.
19. Song, W. K., Wang, W., Foster, R. F., Bielser, D. A., and Kaufman, S. J. (1992). H36-$\alpha7$ is a novel integrin alpha chain that is developmentally regulated during skeletal myogenesis. *J. Cell Biol.* **117,** 643–657.
20. Ziober, B. L., Vu, M. P., Waleh, N., Crawford, J., Lin, C.-S., and Kramer, R. H. (1993). Alternative extracellular and cytoplasmic domains of the integrin $\alpha7$ subunit are differentially expressed during development. *J. Biol. Chem.* **268,** 26773–26783.
21. Hodges, B. L., and Kaufman, S. J. (1996). Developmental regulation and functional significance of alternative splicing of NCAM and $\alpha7\beta1$ integrin in skeletal muscle. *Basic Appl. Myol.* **6,** 437–447.
22. Song, W. K., Wang, W., Sato, H., Bielser, D. A., and Kaufman, S. J. (1993). Expression of $\alpha7$ integrin cytoplasmic domains during skeletal muscle development: Alternate forms, conformational change, and homologies with serine/threonine kinases and tyrosine phosphatases. *J. Cell Sci.* **106,** 1139–1152.
23. Collo, G., Starr, L., and Quaranta, V. (1993). A new isoform of the laminin receptor integrin $\alpha7\beta1$ is developmentally regulated in skeletal muscle. *J. Biol. Chem.* **268,** 19019–19024.
24. van der Flier, A., Kuikman, I., Baudoin, C., van der Neut, R., and Sonnenberg, A. (1995). A novel $\beta1$ integrin isoform produced by alternative splicing: Unique expression in cardiac and skeletal muscle. *FEBS Lett.* **369,** 340–344.
25. Zhidkova, N. I., Belkin, A. M., and Mayne, R. (1995). Novel isoform of $\beta1$ integrin expressed in skeletal and cardiac muscle. *Biochem. Biophys. Res. Commun.* **214,** 279–285.
26. Belkin, A. M., Zhidkova, N. I., Balzac, F., Altruda, F., Tomatis, D., Maier, A., Tarone, G., Koteliansky, V. E., and Burridge, K. (1996). $\beta1$D integrin replaces the $\beta1$A isoform in striated muscles: Localization at junctional structures and signaling potential in nonmuscle cells. *J. Cell Biol.* **132,** 211–226.
27. Martin, P. T., Kaufman, S. J., Kramer, R. H., and Sanes, J. R. (1996). Synaptic integrins in developing, adult, and mutant muscle: Selective association of $\alpha1$, $\alpha7$A, and $\alpha7$B integrins with the neuromuscular junction. *Dev. Biol.* **174,** 125–139.
28. Timpl, R., and Brown, J. C. (1994). The laminins. *Matrix Biol.* **14,** 275–281.
29. Rouselle, P., and Aumailley, M. (1994). Kalinin is more efficient than laminin in promoting adhesion of primary keratinocytes and some other epithelial cells and has a different requirement for integrin receptors. *J. Cell Biol.* **125,** 205–214.
30. Brandenberger, R., and Chiquet, M. (1995). Distinct heparin-binding and neurite promoting properties of laminin isoforms isolated from chick heart.*J. Cell Sci.* **108,** 3099–3108.
31. Delwel, G. O., de Melker, A. A., Hogervorst, F., Jaspars, L. H., Fles, D. L., Kuikman, I., Lindblom, A., Paulsson, M., Timpl, R., and Sonnenberg, A. (1994). Distinct and overlapping ligand specificities of the $\alpha3$A$\beta1$ and $\alpha6$A$\beta1$ integrins: Recognition of laminin isoforms. *Mol. Biol. Cell* **5,** 203–215.
32. Brandenberger, R., Kammerere, R. A., Engel, J., and Chiquet, M. (1996). Native chick laminin 4 containing the $\beta2$ chain (s-laminin) promotes motor axon growth. *J. Cell Biol.* **135,** 1583–1592.
33. Sanes, J. R., Engvall, E., Butkowski, R., and Hunter, D. D. (1990). Molecular heterogeneity of basal laminae: Isoforms of laminin and collagen IV at the neuromuscular junction and elsewhere. *J. Cell Biol.* **111,** 1685–1699.
34. Schuler, F., and Sorokin, L. M. (1995). Expression of laminin isoforms in mouse myogenic cells in vitro and in vivo. *J. Cell Sci.* **108,** 3795–3805.
35. Sewry, C. A., Chevallay, M., and Tome, F. M. (1995). Expression of laminin subunits in human fetal skeletal muscle. *Histochem. J.* **27,** 497–504.
36. Miner, J. H., Lewis, R. M., and Sanes, J. R. (1995). Molecular cloning of a novel laminin chain, $\alpha5$, and widespread expression in adult mouse tissues. *J. Biol. Chem.* **270,** 28523–28526.
37. Yao, C.-C., Ziober, B. L., Sqillace, R. M., and Kramer, R. H. (1996). $\alpha7$ integrin mediates cell adhesion and migration on specific laminin isoforms. *J. Biol. Chem.* **271,** 25598–25603.
38. Engvall, E., Earwicker, D., Haaparanta, T., Ruoslahti, E., and Sanes, J. R. (1990). Distribution and isolation of four laminin variants: Tissue restricted distribution of heterotrimers assembled from five different subunits. *Cell Regul.* **1,** 731–740.
39. Kaufman, S. J., and Parks, C. M. (1977). Loss of growth control and differentiation in the fu-1 variant of the L8 line of rat myoblasts. *Proc. Natl. Acad. Sci. USA* **74,** 3888–3892.
40. Olwin, B. B., and Hall, Z. W. (1985). Developmental regulation of laminin accumulation in the extracellular matrix of a mouse muscle cell line. *Dev. Biol.* **112,** 359–367.
41. Wewer, U. M., and Engvall, E. (1994). Laminins. *Methods Enzymol.* **245,** 85–104.
42. Ruoslahti, E., Hayman, E. G., Pierschbacher, M., and Engvall, E. (1982). Fibronectin: Purification, immunochemical properties, and biological activities. *Methods Enzymol.* **82,** 803–816.
43. Kaufman, S. J., Foster, R. F., Haye, K. R., and Faiman, L. E. (1985). Expression of a developmentally regulated antigen on the surface of skeletal and cardiac muscle cells. *J. Cell Biol.* **100,** 1977–1987.
44. Tomaselli, K. J., Hall, D. E., Flier, L. A., Gehlsen, K. R., Turner, D. C., Carbonetto, S., and Reichardt, L. F. (1990). A neuronal cell line (PC12) expresses two $\beta1$-class integrins—$\alpha1\beta1$ and $\alpha3\beta1$—that recognize different neurite outgrowth promoting domains in laminin. *Neuron* **5,** 651–662.
45. DeFreitas, M. F., Yoshida, C. K., Frazier, W. A., Mendrick, D. L., Kypta, R. M., and Reichardt, L. F. (1995). Identification of integrin $\alpha3\beta1$ as a neuronal thrombospondin receptor mediating neurite outgrowth. *Neuron* **15,** 333–343.
46. Bernardi, P., Patel, V. P., and Lodish, H. F. (1987). Lymphoid precursor cells adhere to two different sites on fibronectin. *J. Cell Biol.* **105,** 489–498.
47. Sonnenberg, A., Linders, C. J. T., Daams, J. H., and Kennel, S. J. (1990). The $\alpha6\beta1$ (VLA-6) and $\alpha6\beta4$ protein complexes: tissue distribution and biochemical properties. *J. Cell Sci.* **96,** 207–217.
48. Harlow, E., and Lane, D. (Eds.) (1988). *"Antibodies: A Laboratory Manual,"* Cold Spring Harbor Laboratory Press, Cold Spring Harbor, NY.
49. Enomoto, M., Boettiger, D., and Menko, A. (1993). Alpha 5 integrin is a critical component of adhesion plaques in myogenesis. *Dev. Biol.* **155,** 180–197.
50. Hirsch, E., Gullberg, D., Balzac, F., Altruda, F., Silengo, L., and Tarone, G. (1994). α_v integrin subunit is predominantly located in nervous tissue and skeletal muscle during mouse development. *Dev. Dynam.* **201,** 108–120.
51. Levavasseur, F., Mayer, U., Guillouzo, A., and Clement, B. (1994). Influence of nidogen complexed or not with laminin on

attachment, spreading, and albumin and laminin B2 mRNA levels of rat hepatocytes. *J. Cell. Physiol.* **161,** 257–266.

52. Senior, R. M., Gresham, H. D., Griffin, G. L., Brown, E. J., and Chung, A. E. (1992). Entactin stimulates neutrophil adhesion and chemotaxis through interactions between its Arg–Gly–Asp (RGD) domain and the leukocyte response integrin. *J. Clin. Invest.* **90,** 2251–2257.
53. Yelian, F. D., Edgeworth, N. A., Dong, L. J., Chung, A. E., and Armwnt, D. R. (1993). Recombinant entactin promotes mouse primary trophoblast cell adhesion and migration through the Arg–Gly–Asp (RGD) recognition sequence. *J. Cell Biol.* **121,** 923–929.
54. Dong, L. J., Hsieh, J. C., and Chung, A. E. (1995). Two distinct cell attachment sites in entactin are revealed by amino acid substitutions and deletion of the RGD sequence in the cysteine-rich epidermal growth factor repeat 2. *J. Biol. Chem.* **270,** 15838–15843.
55. Dedhar, S., Jewell, K., Rojiani, M., and Gray, V. (1992). The receptor for the basement membrane glycoprotein entactin is the integrin $\alpha3/\beta1$. *J. Biol. Chem.* **267,** 18908–18914.
56. Echtermeyer, F., Schober, S., Poschl, E., von der Mark, H., and von der Mark, K. (1996). Specific induction of cell mobility on laminin by $\alpha7$ integrin. *J. Biol. Chem.* **271,** 2071–2075.
57. Williams, D. A., Rios, M., Stephens, C., and Patel, V. P. (1991). Fibronectin and VLA-4 in haematopoietic stem cell-microenvironment interactions. *Nature* **352,** 438–441.
58. Rosen, G. D., Sanes, J. R., LaChance, R., Cunningham, J. M., Roman, J., and Dean, D. C. (1992). Roles for the integrin VLA-4 and its counter receptor VCAM-I in myogenesis. *Cell* **69,** 1107–1119.
59. Zolkiewska, A., and Moss, J. (1995).Processing of ADP-ribosylated integrin $\alpha7$ in skeletal muscle myotubes. *J. Biol. Chem.* **270,** 9227–9233.
60. Goodman, S. L., Deutzman, R., and von der Mark, H. (1987). Two distinct cell binding domains in laminin can independently promote nonneuronal cell adhesion and spreading. *J. Cell Biol.* **105,** 595–610.
61. Nissinen, M., Vuolteenaho, R., Boot-Handford, R., Kallunki, P., and Tryggvason, K. (1991). Primary structure of the human laminin A chain: Limited expression in human tissues. *Biochem. J.* **276,** 369–379.
62. Vuolteenaho, R., Nissinen, M., Sainio, K., Byers, M., Eddy, R., Hirvonen, H., Shows, T. B., Sariola, H., Engvall, E., and Trygvason, K. (1994). Human laminin M chain (merosin): Complete primary structure, chromosomal assignment, and expression of the M and A chain in human fetal tissues. *J. Cell Biol.* **124,** 381–394.
63. Bernier, S. M., Utani, A., Sugiyama, S., Doi, T., Polistina, C., and Yamada, Y. (1995). Cloning and expression of laminin alpha 2 chain (M-chain) in the mouse. *Matrix Biol.* **14,** 447–455.
64. Mecham, R. P. (1991). Receptors for laminin on mammalian cells. *FASEB J.* **5,** 2538–2546.
65. Ervasti, J. M., and Campbell, K. P. (1993). A role for the dystrophin-glcyoprotein complex as a transmembrane linker between laminin and actin. *J. Cell Biol.* **122,** 809–823.
66. Dickson, G., Azad, A., Morris, G. E., Simon, H., Noursadeghi, M., and Walsh, F. S. (1992). Co-localization and molecular association of dystrophin with laminin at the surface of mouse and human myotubes. *J. Cell Sci.* **103,** 1223–1233.
67. Kostrominova, T. Y., and Tanzer, M. L. (1995). Temporal and spatial appearance of α-dystroglycan in differentiated mouse myoblasts in culture. *J. Cell. Biochem.* **58,** 527–534.

Received March 20, 1997
Revised version received June 3, 1997

EXPERIMENTAL CELL RESEARCH **235,** 287–294 (1997)
ARTICLE NO. EX973683

Effect of the Insulin-like Growth Factor I Receptor on Ionizing Radiation-Induced Cell Death in Mouse Embryo Fibroblasts

Shin Nakamura, Hiroshi Watanabe, Masahiko Miura,[1] and Takehito Sasaki

*Department of Dental Radiology and Radiation Research, Faculty of Dentistry, Tokyo Medical and Dental University,
Yushima 1-5-45, Bunkyo-ku, Tokyo 113, Japan*

We have investigated the effect of the insulin-like growth factor I receptor (IGF-IR) on ionizing radiation (IR)-induced cell death using the following two mouse embryo fibroblast cell lines: (i) R^- cells with a null mutation of the IGF-IR gene, therefore expressing no endogenous IGF-IR; (ii) R^+ cells derived from R^- cells, a stable transfectant overexpressing the human IGF-IR. Numbers of R^- cells began to detach from dishes and float into the medium about 48 h after 10 Gy of X-irradiation. Internucleosomal DNA fragmentation detected by agarose gel electrophoresis, which is characteristic of apoptosis, was observed in the floating R^- cells, but not in the attached cells. Unexpectedly, morphological analysis of the floating cells 72 h after irradiation revealed that only about half of them showed apoptotic death and the rest showed a nonapoptotic, presumably necrotic, one. On the other hand, R^+ cells retained more than 90% viability even 4 days after irradiation, and very few floating cells were observed. The G_2 arrest was induced in both cell lines following irradiation and G_2/M fractions similarly returned to normal levels by around 20 h after irradiation, indicating that the cell death which appeared thereafter in R^- cells is mediated through mitosis. Significant induction of p53 following irradiation was not detected by Western blot analysis in either R or R^+ cells. Collectively, these results demonstrate that signal transduction pathways originating from the IGF-IR may be involved in preventing IR-induced apoptosis and necrosis without affecting cell cycle arrest or p53 pathways. © 1997 Academic Press

INTRODUCTION

Ionizing radiation (IR) induces two modes of cell death depending on cell type: (i) interphase death; cells such as thymocytes die in the quiescent stage or before entry into next divisions [1–4]; (ii) mitotic death; cells such as fibroblasts die after one or even several divisions following irradiation [5]. The former has been referred to an example of programmed cell death, often termed as apoptosis, characterized by cell shrinking, chromatin condensation, and, in some instances, internucleosomal DNA fragmentation by endonuclease activation [3, 6, 7]. The latter, on the other hand, is considered necrosis characterized by swelling and disrupted cytoplasmic and nuclear structures [8–10]. However, it was recently reported that cells undergoing mitotic death also show characters of apoptosis in some tumor cell lines [11–16].

It is well known that IR stimulates transduction pathways leading to cell cycle arrest at the G_1/S or G_2/M boundary in proliferating cells [17–19]. While functional wild-type p53 is required for the G_1 arrest through induction of p21/Waf1/Cip1, the G_2 arrest appears to occur in a manner which is independent of normal p53 functions [17–20]. Although irradiated cells eventually undergo apoptosis or necrosis as described above, the link between cell cycle arrest and IR-induced cell death is not fully understood. A model has been invoked to explain the induction of apoptosis that apoptosis is a consequence of imbalance or conflict in proliferative transduction pathways [21, 22]. Since IR inhibits cell cycle progression, the "conflict model" seems to be a plausible explanation for IR-induced apoptosis in proliferating cells.

Activation of the insulin-like growth factor I receptor (IGF-IR) by its ligands IGF-I and IGF-II plays a crucial role in cell growth and transformation [23–25]. A null mutation of the IGF-IR genes in mice causes significant growth deficiency of embryos and death at birth by respiratory failure [26]. Both pre- and postcrisis fibroblast-like cells derived from the embryos show a reduced growth rate in 10% serum medium and complete growth deficiency in serum-free medium supplemented with IGF-I, EGF, and PDGF [27, 28]. Furthermore, the postcrisis cells are refractory to transformation in soft agar even when an activated Ras and SV40 T-antigen are expressed [28]. However, overexpression of the wild-type IGF-IR in the cells restores the mitogenicity and transforming abilities [28]. It is thus reasonable

---

[1] To whom correspondence and reprint requests should be addressed. Fax: 03-5803-0205. E-mail: masa.drad@dent.tmd.ac.jp.

0014-4827/97 $25.00
Copyright © 1997 by Academic Press
All rights of reproduction in any form reserved.

to say that the IGF-I, through activation of the IGF-IR, acts as a strong cell cycle progression factor. In addition to these functions of the IGF-I, recent evidence has shown that the IGF-I has the function of preventing apoptosis. This was shown by the fact that IGF-I completely prevents apoptosis in rat fibroblasts expressing high levels of c-Myc under serum-free conditions [29].

In this paper, we have addressed the question as to whether the IGF-I contributes to the prevention of IR-induced cell death in the exponentially growing phase. For this purpose, we utilized R^- cells derived from a mouse littermate with a targeted disruption of the IGF-IR gene, therefore expressing no endogenous IGF-IR [28], and, as a control, R^+ cells derived from R^- cells stably transfected with a plasmid containing a human IGF-IR cDNA [29]. We show here that mouse fibroblast-like cells with a null mutation of the IGF-IR gene die of apoptosis and necrosis in a mode of mitotic death following IR irradiation, but overexpression of the IGF-IR significantly prevents both types of cell death.

MATERIALS AND METHODS

Cell lines and cultures. Well-established postcrisis cell lines, R^- and R^+ cells were utilized in the present study [27, 28, 30–33]. R^- cells were obtained from a mouse embryo with a targeted disruption of the IGF-IR gene [27, 28]. R^+ cells were obtained from R^- cells stably transfected with a plasmid containing a human IGF-IR cDNA, expressing about 10^6 receptors per cell [28, 32]. Both cell lines were generous gifts of Dr. R. Baserga (Kimmel Cancer Institute, Thomas Jefferson University). Cells were passaged in Eagle's minimum essential medium containing 1 m*M* sodium pyruvate, 100 units/ml penicillin, and 100 μg/ml streptomycin supplemented with 10% fetal bovine serum.

Determination of IGF-IR levels. Expression levels of the IGF-IR were determined by FACS analysis as previously described [32]. Briefly, R^- and R^+ cells were incubated with an anti-IGF-IR antibody (Calbiochem, Cambridge, MA) at 4°C for 30 min and then incubated with an anti-mouse IgG conjugated with FITC (Southern Biotechnology Associates, Birmingham, AL) at 4°C for 30 min. Stained cells were analyzed with FACScan (Becton–Dickinson, Sunnyvale, CA).

Soft agar assay. Exponentially growing R^- and R^+ cells (2×10^4) containing 0.3% agarose were plated in 60-mm dishes underlaid with 0.5% agarose-containing growth medium. Microphotographs of colonies were taken 14 days after plating.

Detection of internucleosomal DNA fragmentation. DNA fragmentation of X-irradiated cells was visualized according to the methods of Liu *et al.* [34] with modifications. Exponentially growing R^- and R^+ cells (2×10^5) were X-irradiated at a dose of 10 Gy and floating cells were collected from eight dishes at the times indicated by mixing overlying medium and that from washes of remaining attached cell layers. About 10^6 R^- cells could usually be collected 72 h after irradiation under these conditions. On the other hand, the number of floating R^+ cells was less than $\frac{1}{10}$ that of R^- cells. Cells remaining attached to the dishes were also collected following trypsinization and adjusted to 10^6. The collected cells were washed with PBS and resuspended in 20 μl of solution containing 10 m*M* EDTA, 50 m*M* Tris–HCl (pH 8.0), 0.5% sodium lauryl sarkosinate, and 0.5 mg/ml proteinase K. After incubation at 50°C for 1 h, 10 μl of 0.5 mg/ml RNase A was added and the mixture was further incubated at 50°C for 1 h. After heating up to 70°C for 5 min, 10 μl of preheated solution (10 m*M* EDTA, 50 m*M* Tris–HCl (pH 8.0), 1% low-melting-temperature agarose, 0.25% BPB, and 40% sucrose) was added. Mixed samples kept at 70°C were loaded into wells of 2% agarose gel containing 0.5 μg/ml ethidium bromide and then electrophoresed at 50 V. Photographs were taken under UV illumination.

Cell viability and growth assay. R^- and R^+ cells (1×10^5) were plated in 60-mm dishes and were given 5 to 20 Gy of X-irradiation 24 h after plating. At the times indicated, the cells were trypsinized and collected together with floating cells by centrifugation. Cells were resuspended with an erythrosine-B solution and counted using a hemocytometer. Unstained cells were considered viable.

Morphological analysis of dead cells. Floating R^- and R^+ cells 72 h after 10 Gy of X-irradiation were collected and fixed in 4% neutral buffered Formalin. Cells were dried on a microscope slide, washed with PBS, and stained with a propidium iodide (PI) staining solution (5 μg/ml PI, 50 μg/ml RNase A in pH 7.4 PBS). Thereafter, the stained cells were washed with PBS, added with glycerin, and mounted with a cover glass. The percentages of apoptotic and nonapoptotic cells were determined with a fluorescent microscope BH2 (Olympus, Tokyo, Japan) by counting at least 1000 cells. A terminal deoxynucleotidyltransferase labeling assay was also applied to R^- cells using an ApopTag Plus kit according to the manufacturer's instructions (Oncor, Bethesda, MD).

Determination of tyrosine phosphorylation of IGF-IR and insulin receptor substrate-1 (IRS-1) and p53 protein levels. For determination of tyrosine phosphorylation of IGF-IR and IRS-1, cells grown on 100-mm plates were incubated in serum-free medium for 24 h and were untreated or treated with 50 ng/ml of IGF-I (GibcoBRL, Gaithersburg, MD) for 5 min. The cells were lysed with a solution containing 50 m*M* Hepes, pH 7.5, 150 m*M* NaCl, 1.5 m*M* $MgCl_2$, 1 m*M* EGTA, 10% glycerol, 1% Triton X-100, 100 m*M* NaF, 0.2 m*M* sodium vanadate, 10 m*M* sodium pyrophosphate, 1 m*M* PMSF, and 1 μg/ml aprotinin. Equal amounts of whole cell lysates were separated by SDS–polyacrylamide gel electrophoresis and electroblotted onto nitrocellulose filters. Phosphorylated tyrosines were visualized using a monoclonal anti-phosphotyrosine antibody conjugated with a horseradish peroxidase (PY20H) (Transduction Laboratory, Lexington, KY) and ECL system (Amersham, Arlington Heights, IL). For determination of p53 protein levels, cells irradiated at a dose of 10 Gy were lysed at the indicated times with a solution containing 50 m*M* Tris–HCl, pH 8.0, 150 m*M* NaCl, 0.02% sodium azide, 0.1% SDS, 100 μg/ml PMSF, 1 μg/ml aprotinin, 1% NP-40, and 0.5% sodium deoxycholate. Equal amounts of whole cell lysates were separated as described above and visualized using a monoclonal anti-p53 antibody (Pab240) (Calbiochem), an anti-mouse IgG conjugated with a horseradish peroxidase (Southern Biotechnology Associates) and ECL system. Pab240 recognizes epitopes of both mutant and wild-type p53.

Analysis of cell cycle distribution. Exponentially growing cells were X-irradiated at a dose of 10 Gy and trypsinized at the times indicated. Only the attached cells were washed with PBS and fixed in 70% ethanol at −20°C until cells were analyzed. After centrifugation, 70% ethanol was aspirated and resuspended with 1 ml of PBS containing 50 μg/ml propidium iodide (PI) and 100 μg/ml RNase A. One hour after incubation at room temperature, cells were analyzed with FACScan and percentages of each cell cycle phase were determined by sum of broadened rectangles model (Becton–Dickinson). Ten thousand events were collected for each sample.

X-Irradiation. Cells were X-irradiated with a Siemens X-ray therapeutic machine (Siemens, Erlangen, Germany) operated at 250 kV, 15 mA, filtered with 1.0 mm Cu at a dose rate of 0.85 or 0.71 Gy/min, or a Pantak X-ray machine (Pantak, Berkshir, UK) operated at 100 kV, 30 mA, filtered with 0.115 mm Cu and 0.502 mm Al at a dose rate of 0.60 Gy/min.

RESULTS

Characterization of Cell Lines

To confirm the characters of postcrisis R^- and R^+ cells [27, 28, 30–33], the following properties on the IGF-IR were examined. FACS analysis of the IGF-IR levels using an anti-IGF-IR antibody revealed that R^+ cells express high levels of IGF-IR in contrast to R^- cells showing signals of nonspecific binding levels (Fig. 1A). IGF-I clearly stimulated tyrosine phosphorylation of IGF-IR-β subunit, IRS-1, and some other high-molecular-weight proteins, including p220 in R^+ cells (Fig. 1B) [35]. On the other hand, in R^- cells, IGF-I did not stimulate any of the tyrosine phosphorylation observed in R^+ cells (Fig. 1B). As one of the most biologically characterized properties on the IGF-IR, transforming abilities of the cell lines were also tested [30–33]. R^- cells could not grow in soft agar and cells were observed as a single cell (Fig. 1C), whereas R^+ cells could grow vigorously and were identified as large colonies (Fig. 1C). The mean values ± SD of doubling time in monolayer cultures for R^- and R^+ cells were 18.0 ± 0.7 h (n = 3) and 11.8 ± 1.2 h (n = 3), respectively ($P < 0.001$, Student's t test). The cell cycle distribution for exponentially growing R^- and R^+ cells was shown in Table 1. At variance with precrisis R^- cells (doubling time = 109 h, S-phase = 15%) [28], postcrisis R^- cells somehow acquired a much higher growth rate and higher percentage of S-phase in the spontaneously immortalizing process. However, overexpression of the IGF-IR in the postcrisis R^- cells significantly reduced the doubling time and increased the percentage of S-phase shown in R^+ cells. Thus, it was confirmed that typical functional characters of the IGF-IR are expressed in R^+ cells, but not in R^- cells used in the present study.

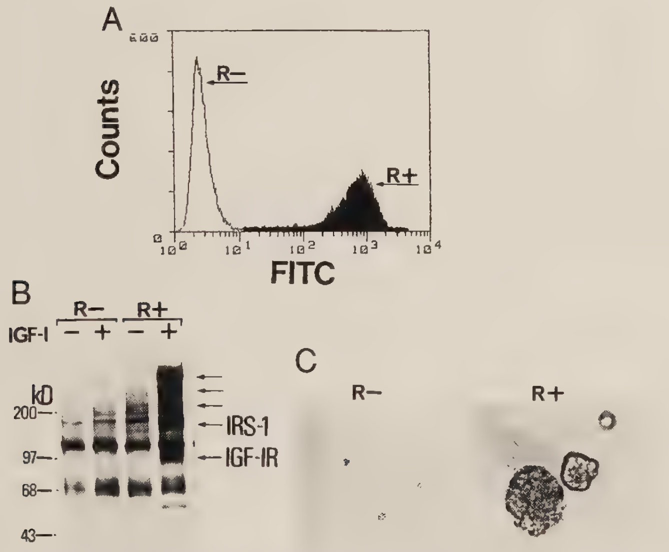

FIG. 1. Characterization of IGF-IR functions in R^- and R^+ cells. (A) FACS analysis of IGF-IR expression in R^- and R^+ cells. The abscissa represents the relative level of FITC intensity bound to cell surface as described under Materials and Methods. The ordinate represents cell number. Mean and mode values of FITC intensity were 3.9 and 2.4 for R^- cells and 668.6 and 769.6 for R^+ cells, respectively. (B) Phosphorylation of IGF-IR and IRS-1. Equal amounts of proteins from unstimulated or stimulated cells with 50 ng/ml IGF-I for 5 min were separated by SDS–PAGE and phosphotyrosines of transferred proteins were visualized as described under Materials and Methods. The arrows indicate IGF-IR-β subunit, IRS-1, p220, and other high-molecular-weight proteins. (C) Transforming abilities in soft agar. R^- and R^+ cells were plated in growth medium containing 0.3% agarose underlaid with growth medium containing 0.5% agarose and microphotographs of colonies were taken at 50× magnification 14 days after incubation.

TABLE 1

Cell Cycle Analysis of R^- and R^+ Cells

	Percentage of cells in		
Cell lines	G_1	S	G_2/M
R^-			
Expt. 1	28	50	22
Expt. 2	28	51	21
R^+			
Expt. 1	27	64	10
Expt. 2	29	64	7

Note. Data were obtained from two independent experiments.

Floating R^- Cells Following IR-Irradiation Show Internucleosomal DNA Fragmentation

To examine the effect of IR-irradiation on cell death, exponentially growing R^- and R^+ cells were X-irradiated. Both cell lines are fibroblast-like cells and grow under conditions where cells adhere to the dish surface. We noticed that when both cells were X-irradiated at a dose of 10 Gy, R^- cells began to detach from the surface of dishes and float into the medium about 48 h after irradiation; on the other hand, most R^+ cells remained attached to the surface. Viability of the floating R^- cells, as collected by mixing overlying medium and that from washes of remaining attached cell layers, was only 8% at 72 h after irradiation.

It is reported that most of the floating cells in monolayer cultures show apoptotic death in colorectal adenoma and carcinoma cells [36], while fibroblasts usually show necrotic death following IR-irradiation [16]. To determine the cell death mode, we attempted to see internucleosomal DNA fragmentation. For this purpose, floating cells were collected 72 h after 10 Gy of irradiation and DNA was separated by agarose gel elec-

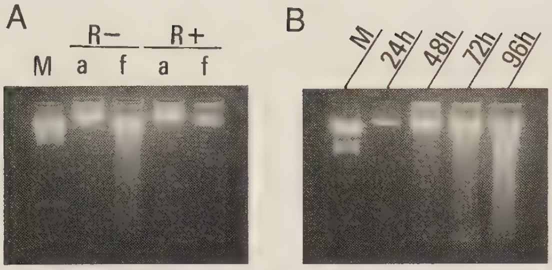

FIG. 2. Internucleosomal DNA fragmentation by agarose gel electrophoresis. (A) DNA fragmentation patterns of DNA from attached and floating cells 72 h after 10 Gy of X-irradiation; M, λ*Hin*dIII marker; a, attached cells; f, floating cells. Attached and floating cells were collected and DNA was prepared as described under Materials and Methods. (B) Time course of DNA fragmentation in R^- cells following X-irradiation. M, λ*Hin*dIII marker; DNA was prepared from floating R^- cells at the indicated times following 10 Gy of X-irradiation.

trophoresis as described under Materials and Methods. A clear laddering pattern characteristic of apoptosis was detected in R^- cells, but not in R^+ cells (Fig. 2A). Cells remaining attached to the dish surface were also examined and showed no laddering patterns (Fig. 2A). Moreover, the time course of the laddering patterns revealed that DNA internucleosomal fragmentation in R^- cells began to appear 48 h after irradiation and the signal intensity increased as cells were further incubated (Fig. 2B).

R^- Cells Show Two Types of Cell Death Following IR-Irradiation

To confirm the apoptotic cell death in R^- cells, morphological analysis of the floating cells was performed. As expected, fragmented nuclei and chromatin condensation characteristic of apoptosis were observed in floating R^- cells by PI staining. However, unexpectedly, cells showing swelling and disrupted structures characteristic of necrosis were also detected (Fig. 3A). Most cells showing fragmented nuclei were positive by terminal deoxynucleotidyltransferase labeling (Fig. 3C). A small number of floating R^+ cells were prepared from many more plates than R^- cells and they also showed mixed types of cell death by PI staining (Fig. 3B). The percentages of apoptotic and nonapoptotic dead cells in R^- cells were 42 and 50%, respectively. The remaining 8% was viable cells as described above. Apoptotic cell death took place at a reduced rate (18%) in R^+ cells.

Cell Viability and Growth Assay Confirms Cell Death Kinetics of Floating R^- Cells Following IR-Irradiation

Cell viability assay by dye-exclusion tests was done using mixed populations of floating and attached cells following X-irradiation. More than 95% of viability under normal conditions was constantly observed in exponentially growing R^- and R^+ cells. The time course following 10 Gy of X-irradiation (Fig. 4A) showed that the viability of R^- cells significantly decreased beginning from 48 h after irradiation and reached about 50% at 4 days after irradiation. In contrast, there was no significant decrease even 4 days after irradiation and viability was about 90% in R^+ cells at that time (Fig. 4A). At 3 days after irradiation, the viability of R^- cells decreased in a dose-dependent manner and reached about 40% at 20 Gy (Fig. 4B). The reduction rate of the viability per dose was significantly small in R^+ cells and the viability at 20 Gy was about 85% (Fig. 4B). R^- and R^+ cells grew at doubling times of 18.0 ± 0.7 ($n = 3$) and 11.8 ± 1.2 h ($n = 3$), respectively, under untreated conditions (Figs. 4C and 4D). When R^- cells were X-irradiated, R^- cells proliferated at a reduced rate until about 24 h after irradiation, and thereafter the viable cell number tended to decrease (Fig. 4C). On the other hand, R^+ cells grew until about 48 h after irradiation at a reduced rate and the cell number reached a plateau (Fig. 4D). This quantitative analysis is consistant with

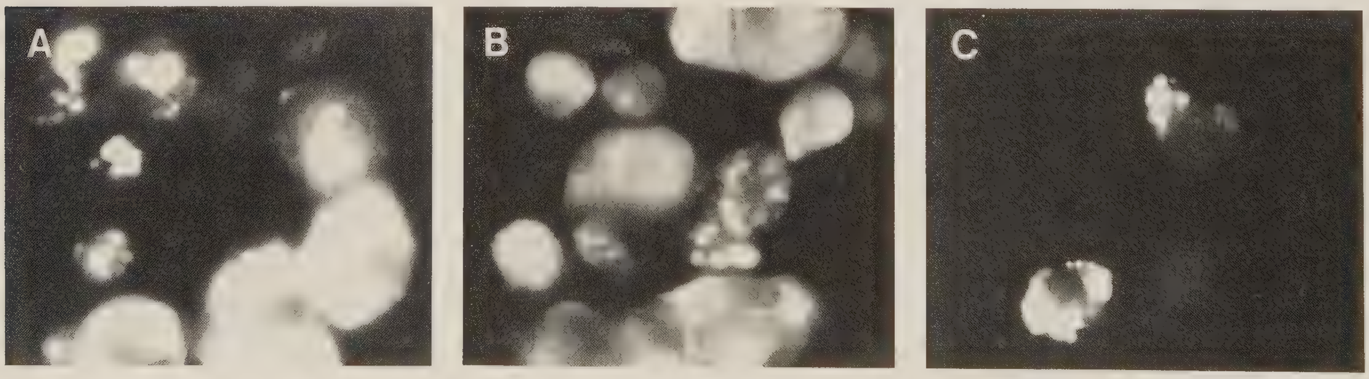

FIG. 3. Morphological analysis of floating cells 72 h after 10 Gy of X-irradiation. Photographs of floating R^- (A) and R^+ (B) cells by PI staining and R^- cells (C) by terminal deoxynucleotidyltransferase labeling. Photographs were taken at 250× magnification.

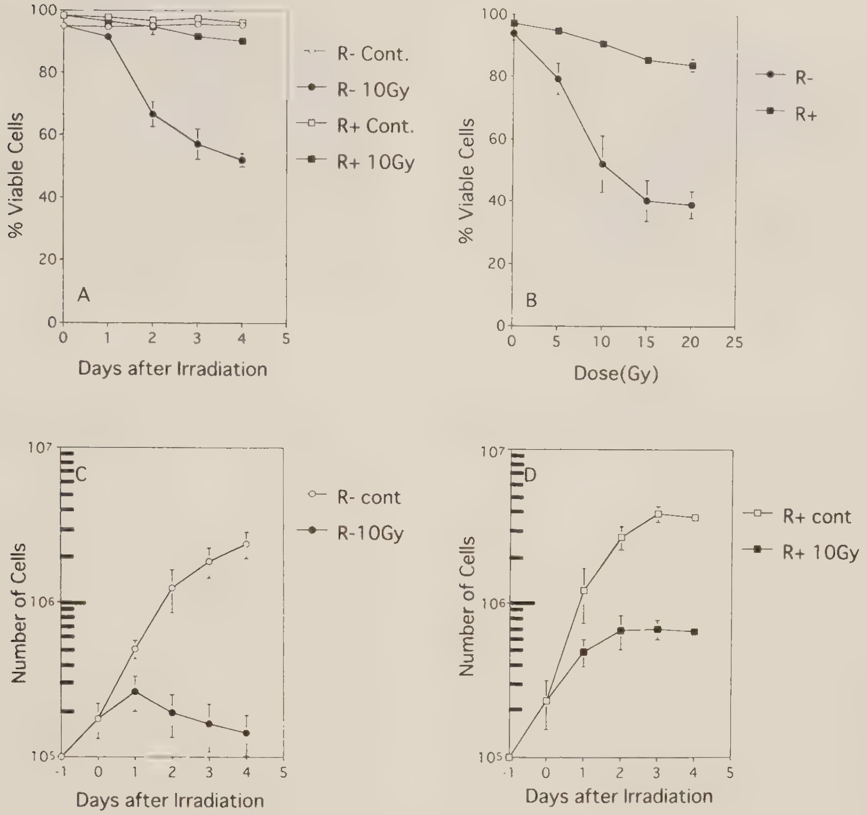

FIG. 4. Cell viability and growth assay in R^- and R^+ cells following X-irradiation. (A) Time course of cell viability in cells unirradiated or irradiated at a dose of 10 Gy; (B) Dose–response curves for cell viability 3 days after irradiation; Growth curves for R^- (C) and R^+ (D) cells following 10 Gy of X-irradiation. Points with bars represent means and standard deviations of three independent experiments.

the fact that about one million floating dead R^- cells could be collected from eight dishes 72 h after 10 Gy of irradiation in the above-described experiments. It was thus confirmed that R^- cells begin to die about 48 h after irradiation, detach from dishes, and float into the medium, while very few R^+ cells die.

R^- and R^+ Cells Show Similar G_2 Arrest Kinetics Following IR-Irradiation

Cell cycle distribution in R^- and R^+ cells following X-irradiation was analyzed by a flow cytometer. Percentages of G_1, S, and G_2/M phase in the exponentially growing phase were 28, 51, and 21% for R^- cells and 29, 64, and 7% for R^+ cells, respectively, under untreated conditions. After 10 Gy of X-irradiation, neither cell type showed G_1 arrest, but did arrest in G_2, as shown in Fig. 5. The fraction of G_2/M rapidly increased and reached a peak of 52% about 9 h after irradiation in R^+ cells; on the other hand, the fraction in R^- cells reached 50% a few hours later than in R^+ cells. Thereafter, the G_2/M fractions of both cells rapidly decreased and returned almost to normal levels up to around 20

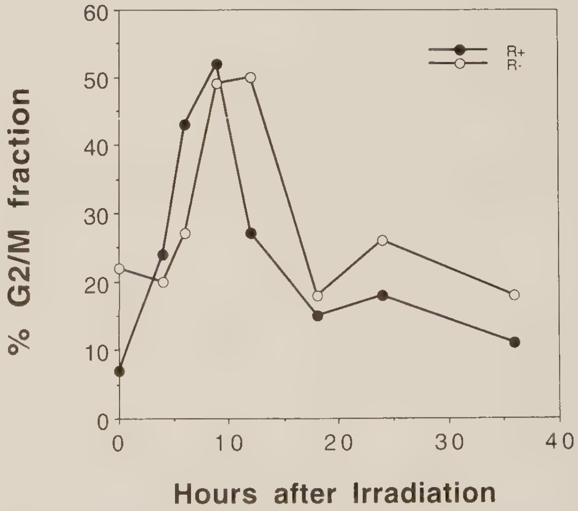

FIG. 5. A typical example for time course of G_2/M fractions in R^- and R^+ cells following 10 Gy of X-irradiation as determined by FACS analysis.

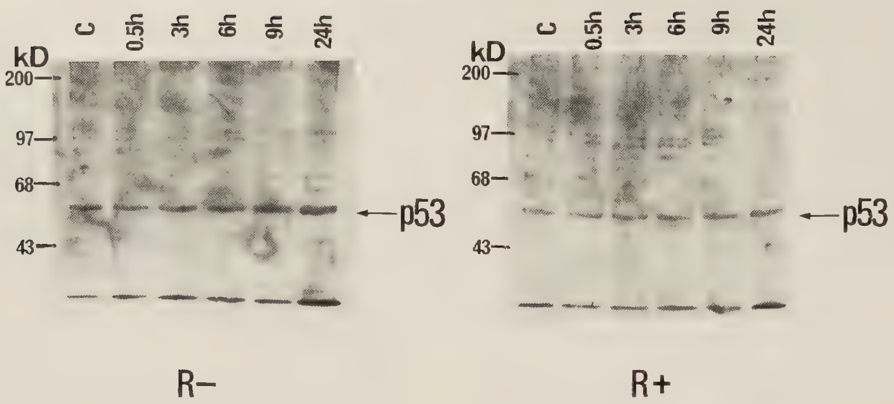

FIG. 6. p53 levels of R^- and R^+ cells following X-irradiation. Proteins were prepared from cells at indicated times after 10 Gy of irradiation and separated by SDS–PAGE. p53 was visualized as described under Materials and Methods.

h after irradiation. The time difference of the peaks between R^- and R^+ cells may be due to the difference of doubling times (18.0 h for R^- cells and 11.8 h for R^+ cells). Thus, remarkable differences of G_2 arrest kinetics following irradiation were not detected between R^- and R^+ cells. These results further provide evidence that the cell death mode in R cells following irradiation is mitotic death.

IR-Induced Cell Death in R^- Cells Is Independent of p53 Induction

To see the possible involvement of p53 in IR-induced cell death in R^- cells, p53 levels following X-irradiation were monitored by Western blot analysis (Fig. 6) and densitmetric analysis was performed (Table 2). Although p53 levels under untreated conditions were somewhat higher in R^- cells than those in R^+ cells, neither cells showed significant induction of p53 up to 24 h after 10 Gy of irradiation (Table 2). These results imply that the cell death following IR-irradiation observed in R^- cells may be independent of p53 pathways.

DISCUSSION

The IGF-IR has a tyrosine kinase domain, which is highly homologous to that of insulin receptor, juxtamembrane domain, and c-terminal domain in the β subunit [37]. Each domain possesses important tyrosines required for signal transductions leading to activation of Ras-dependent and -independent pathways through intermediate substrates including IRS-1 and Shc, and these signals eventually stimulate cell proliferation or transformation [27, 28, 30–33, 38]. Recent evidence has shown that IGF-IR has another function—to prevent apoptosis induced under serum-free conditions [29, 39]. In order to study the role of IGF-IR in IR-induced cell death in 10% serum medium, we introduced a model system utilizing mouse embryo fibroblasts with a null mutation of the IGF-IR gene (R^-) and a transfectant overexpressing the human IGF-IR (R^+).

TABLE 2

Densitmetric Analysis of X-Ray-Induced p53 in R and R^+ Cells

	p53 levels					
Cell lines	Control	0.5 h	3 h	6 h	9 h	24 h
R^-	1.00	0.89	0.94	1.04	1.07	1.06
R^+	0.79	0.74	0.85	0.83	0.82	0.84

Note. p53 levels were calculated by densitmetry from the results of Fig. 6 with the control value in R^- cells normalized to 1.00.

In this work, we presented the following evidence: (i) mouse embryo fibroblasts died with apoptosis and necrosis following IR-irradiation in the situations in which cells express no IGF-IR; (ii) the cell death significantly began to occur about 48 h after irradiation; (iii) overexpression of the IGF-IR remarkably prevented both apoptosis and necrosis; (iv) both cell lines showed similar G_2 arrest kinetics following irradiation and the G_2/M fractions returned to almost normal levels by around 20 h after irradiation; and (v) p53 was not significantly induced in either of these cell lines following irradiation.

Judging from the cell death kinetics and cell cycle analysis following irradiation, it seems likely that the cell death mode observed in R^- cells is a mitotic one. Therefore, mouse embryo fibroblasts die with apoptosis and necrosis after at least the first division in the absence of IGF-IR. On the other hand, in the presence of overexpressed IGF-IR, such cell death is remarkably inhibited. Apoptosis usually occurs immediately after ionizing irradiation, for instance, thymocytes or peripheral lymphocytes die in the quiescent stage or before entry into the first division [1–4]. However, some cell lines including T-cell leukemia [14, 15], lymphoid, myeloid [11, 12], and gastric epithelial tumor lines [16] show slowly occurring apoptotic cell death after the next divisions. In terms of time course for apoptosis, R^- cells should be classified in the latter group, but other cell lines do not have the necrotic death component. Nakano and Shinohara reported two leukemia cell lines, one of which dies with apoptosis and another dies with necrosis following IR-irradiation [10]. The latter shows a very similar time course of cell death to that for R^- cells, but it does not seem to have the apoptotic death component. Thus, R^- cells appear to die in a very unique cell death mode following IR-irradiation. Our experiments are still insufficient to resolve the question of why two different types of cell death occur within the single cell population.

Questions would be also raised as to how IGF-IR prevents IR-induced cell death. In our study, R^- and R^+ cells showed similar G_2 arrest kinetics following irradiation. In this regard, our results cannot be simply explained by the conflict model, as described in the Introduction [21, 22]. This is because apoptosis takes place only in R^- cells but not in R^+ cells despite the fact that stop signals for cell cycle progression, G_2 arrest in this case, occur equally in both cell lines. The G_1 or G_2 arrest is considered to allow cells to repair DNA damage to reduce cell death or genetic abnormalities [17, 18, 40, 41]. In fact, rat embryo fibroblasts transfected with the ras and myc oncogenes are more radioresistant and have a longer G_2 arrest than untransfected control cells [42, 43]. Caffeine is known to abrogate the G_2 arrest induced by IR-irradiation, and the override of the G_2 block is accompanied by increased apoptosis [44]. However, again, our results cannot be explained by this scenario. A consensus has been obtained that wild-type p53 is a key protein in controlling apoptosis [17, 45]. Wild-type p53 protein is accumulated through posttranscriptional mechanisms after IR-irradiation [17, 46]. Although the p53 status of R^- and R^+ cells is not determined, neither cells showed G_1 arrest following IR-irradiation, a typical characteristic of wild-type p53, but did G_2 arrest as described above. Further, significant induction of p53 was not detected in either of these cell lines following IR-irradiation by semiquantitative Western blot analysis, using an antibody which recognizes both mutant and wild-type p53. It is thus unlikely that IGF-IR prevents IR-induced apoptosis through modulation of p53 pathways.

Harrington *et al.* proposed a "dual signal model" that apoptosis is implemented whenever apoptosis inducers exist regardless of a conflict of growth signals and execution of apoptosis is regulated by survival factors [29]. Our findings favor this model if IR and IGF-IR are regarded as an apoptosis inducer and a survival factor, respectively. Indeed, c-Myc and IGF-I are examples in their experiments. According to this model, our results can be interpreted as follows: R^- cells die by apoptosis because IGF-I is not available as a survival factor, while R^+ cells survive because abundant IGF-I is available in 10% serum medium through overexpressed IGF-IR, after IR-irradiation, which is a potential apoptosis inducer. The dual signal model was constructed from experiments using serum-deprived cells, but our results suggest that it could be also applied to exponentially growing cells in 10% serum medium. We, in fact, could rule out the possible involvement of modulation of cell cycle arrest in the mechanisms on the IGF-I-related inhibition of apoptosis in proliferating cells. Moreover, the model may be extended not only to apoptosis, but also to necrosis induction.

Evidence is rapidly accumulating on the mechanisms of cell death pathways. Members of the mammalian interleukin-1-β-converting enzyme (ICE) are known to be homologs of programmed cell death gene products Ced-3 in *Caenorhabditis elegans* [42–44]. The ICE plays an important role in regulating mammalian apoptosis and may function at a convergent step in apoptosis induced by various stimuli [47–49]. It was recently reported that IGF-I suppresses ICE-mediated cell death, and indeed, IGF-I has a function to inhibit ICE activity [50]. Interestingly, inhibition of ICE activity reduces necrosis induced by chemical hypoxia [51]. Taken together, these observations raise the possibility that IGF-IR may prevent IR-induced apoptosis and necrosis through suppression of ICE activity. Our future experiments using R^- cells should help to elucidate these issues.

In summary, our data indicate that signal transduction pathways originating from the IGF-IR may be involved in preventing IR-induced apoptosis and necrosis without affecting cell cycle arrest or p53 pathways.

This work was partly supported by Grants-in-Aid (08771637) from the Ministry of Education, Science, Sports and Culture, Japan. We thank Dr. R. Baserga for providing us with R− and R+ cells. We also thank Ms. T. Ojima for her help in FACS analysis. Our thanks are also extended to Drs. K. Takase and H. Teraoka for their help in DNA fragmentation.

REFERENCES

1. Umansky, S. R., Korol, B. A., and Nelipovich, P. A. (1981) *Biochem. Biophys. Acta* **665,** 9–7.
2. Afansyev, V. N., Korol, B. A., Mantsygin, Y. A., Nelipovich, P. A., Pechatnikov, V. A., and Umansky, S. R. (1986) *FEBS Lett.* **194,** 347–350.
3. Yamada, T., and Oyama, H. (1988) *Int. J. Radiat. Biol.* **53,** 65–75.
4. Shinohara, K., and Nakano, H. (1993) *Radiat. Res.* **135,** 197–205.
5. Okada, S. (1970) *in* Radiation Biochemistry (Altman, K. I.,

Gerber, G. B., and Okada, S., Eds.), Vol. 1, pp. 247–307, Academic Press, New York.

6. Kerr, J. F. R., Wyllie, A. H., and Currie, A. R. (1972) *Br. J. Cancer* **26,** 239–257.
7. Yamada, T., Ohyama, H., Kinja, Y., and Watanabe, M. (1981) *Radiat. Res.* **85,** 544–553.
8. Dewey, W. C., Furman, S. C., and Miller, H. H. (1970) *Radiat. Res.* **43,** 561–581.
9. Joshi, G. P., Nelson, W. J., Revell, S. H., and Shaw, C. A. (1982) *Int. J. Radiat. Biol.* **41,** 161–181.
10. Nakano, H., and Shinohara, K. (1994) *Radiat. Res.* **140,** 1–9.
11. Radford, I. R. (1991) *Int. J. Radiat. Biol.* **59,** 1353–1369.
12. Radford, I. R., Murphy, T. K., Radley, J. M., and Ellis, S. L. (1994) *Int. J. Radiat. Biol.* **65,** 217–227.
13. Radford, I. R., and Murphy, T. K. (1994) *Int. J. Radiat. Biol.* **65,** 229–239.
14. Kruman, I. I., Matykevich, N. P., Beletsky, I. P., Afanasyev, V. N., and Umansky, S. R. (1991) *J. Cell. Physiol.* **148,** 267–273.
15. Warters, R. L. (1992) *Cancer Res.* **52,** 883–890.
16. Yanagihara, K., Nii, M., Numoto, M., Kamiya, K., Tauchi, H., and Sawada, S. (1995) *Int. J. Radiat. Biol.* **67,** 677–685.
17. Kastan, M. B., Onyekwere, O., Sidransky, D., Vogelstein, B., and Craig, R. W. (1991) *Cancer Res.* **51,** 6304–6311.
18. Kuerbitz, S. J., Plunkett, B. S., Walsh, W. B., and Kastan, M. B. (1992) *Proc. Natl. Acad. Sci. USA* **89,** 7491–7495.
19. O'Connor, P. M., Jackman, J., Jondle, D., Bhatia, K., Magrath, I., and Kohn, K. W. (1993) *Cancer Res.* **53,** 4776–4780.
20. DiLeonardo, A., Linke, S. P., Clarkin, K., and Wahl, G. M. (1994) *Genes Dev.* **8,** 2540–2551.
21. Touchette, N. (1992) *J. NIH Res.* **4,** 48–52.
22. Cohen, J. (1993) *Immunol. Today* **14,** 126–130.
23. Sara, V. R., and Hall, K. (1990) *Physiol. Rev.* **70,** 591–614.
24. Baserga, R., and Rubin, R. (1993) *Crit. Rev. Eukaryote Gene Exp.* **3,** 47–61.
25. Lowe, W. L., Jr. (1991) *in* Insulin-like Growth Factors: Molecular and Cellular Aspects (LeRoith, D., Ed.), pp. 49–85, CRC Press, Boca Raton.
26. Liu, J. P., Baker, J., Perkins, A. S., Robertoson, E. J., and Efstratiadis, A. (1993) *Cell* **75,** 59–72.
27. Sell, C., Rubini, M., Rubin, R., Liu, J., Efstratiadis, A., and Baserga, R. (1993) *Proc. Natl. Acad. Sci. USA* **90,** 11217–11221.
28. Sell, C., Dumenil, G., Deveaud, C., Miura, M., Coppola, D., DeAngelis, T., Rubin, R., Efstratiadis, A., and Baserga, R. (1994) *Mol. Cell. Biol.* **14,** 3604–3612.
29. Harrington, E. A., Bennett, M. R., Fanidi, A., and Evan, G. I. (1994) *EMBO J.* **13,** 3286–3295.
30. Li, S., Ferber, A., Miura, M., and Baserga, R. (1994) *J. Biol. Chem.* **269,** 32558–32564.
31. Miura, M., Li, S., and Baserga, R. (1995) *Cancer Res.* **55,** 663–667.
32. Miura, M., Surmacz, E., Burgaud, J.-L., and Baserga, R. (1995) *J. Biol. Chem.* **270,** 22639–22644.
33. Hongo, A., D'Ambrosio, C., Miura, M., Morrione, A., and Baserga, R. (1996) *Oncogene* **12,** 1231–1238.
34. Liu, Y.-J., Cairns, J. A., Holder, M. J., Abbot, S. D., Jansen, K. U., Bonnefoy, J.-Y., Gordon, J., and MacLennan, I. C. M. (1991) *Eur. J. Immunol.* **21,** 1107–1114.
35. Kato, H., Faria, T. N., Stannard, B., Roberts, C. T., and LeRoith, D. (1993) *J. Biol. Chem.* **268,** 2655–2661.
36. Bracey, T. S., Miller, J. C., Preece, A., and Paraskeva, C. (1995) *Oncogene* **10,** 2391–2396.
37. Ullrich, A., Gray, A., Tam, A. W., Yang-Feng, T., Tsubokawa, M., Collins, C., Henzel, W., Le Bon, T., Kahuria, S., Chen, E., Jacobs, S., Francke, U., Ramachandran, J., and Fujita-Yamaguchi, Y. (1986) *EMBO J.* **5,** 2503–2512.
38. Myers, M. G., Sun, X. J., Cheatham, B., Jachna, B. R., Glasheen, E. M., Backer, J. M., and White, M. F. (1993) *Endocrinology* **132,** 1421–1430.
39. Sell, C., Baserga, R., and Rubin, R. (1995) *Cancer Res.* **55,** 303–306.
40. Cohen, S. M., and Ellwein, L. B. (1990) *Science* **249,** 1007–1011.
41. Guillouf, C., Rosselli, F., Krishnaraju, K., Moustacchi, E., Hoffman, B., and Liebermann, D. A. (1995) *Oncogene* **10,** 2263–2270.
42. McKenna, W., Weiss, M. C., Endlich, B., Ling, C. C., Bakanauskas, V. J., Kelsten, M. L., and Muschel, R. J. (1990) *Cancer Res.* **50,** 97–102.
43. McKenna, W. G., Iliakis, G., Weiss, M. C., Bernhard, E. J., and Muschel, R. J. (1991) *Radiat. Res.* **125,** 283–287.
44. Bernhard, E. J., Muschel, R. J., Bakanauskas, V. J., and McKenna, W. G. (1996) *Int. J. Radiat. Biol.* **69,** 575–584.
45. Merritt, A. J., Potten, C. S., Kemp, C. J., Hickman, J. A., Balman, A., and Lane, D. P. (1994) *Cancer Res.* **54,** 614–617.
46. Maltzman, W., and Czyzyk, L. (1984) *Mol. Cell. Biol.* **4,** 1689–1694.
47. Ellis, R. E., Yuan, J., and Horvitz, H. R. (1991) *Annu. Rev. Cell Biol.* **7,** 663–698.
48. Miura, M., Zhu, H., Rotello, R., HartWeig, E., and Yuan, J. (1993) *Cell* **75,** 653–660.
49. Yuan, J., Shaham, S., Ledoux, S., Ellis, H. M., and Horvitz, R. (1993) *Cell* **75,** 641–652.
50. Jung, Y-K., Miura, M., and Yuan, J. (1996) *J. Biol. Chem.* **271,** 5112–5117.
51. Shimizu, S., Eguchi, Y., Kamiike, W., Waguri, S., Uchiyama, Y., Matsuda, H., and Tsujimoto, Y. (1996) *Oncogene* **12,** 2045–2050.

Received March 3, 1997
Revised version received June 9, 1997

EXPERIMENTAL CELL RESEARCH **235,** 295–299 (1997)
ARTICLE NO. EX973665

SHORT NOTE

Changes in Actin Filament Organization during Pseudopod Formation

Eunkyung Lee, Eric A. Shelden,[1] and David A. Knecht[2]

Department of Molecular and Cell Biology, University of Connecticut, Storrs, Connecticut 06269

Fluorescent phalloidin has been introduced into *Dictyostelium* amoebae in order to visualize dynamic changes in the localization of F-actin during pseudopod extension. Phalloidin was initially localized to the peripheral cortex of the cell. Newly formed pseudopods were not fluorescent, indicating that phalloidin was tightly bound to existing F-actin filaments and could not rapidly relocalize to newly formed filaments. As pseudopod extension proceeded, the fluorescent signal disappeared from the region directly underlying the expansion zone, leaving a gap in the actin cortex. Similar results were obtained in both wild-type cells and those lacking myosin II heavy chain. The disappearance of the fluorescent signal from the cortical region underlying the new pseudopod is presumed to be due to breakdown of the actin cortex and dispersion of the remnants. These results suggest that new pseudopods are not built upon the existing actin cortex but rather that the cortex is locally solated as part of the construction of the new actin network. © 1997 Academic Press

INTRODUCTION

The pseudopod is the primary locomotory organelle of free-living amoeboid cells as well as in a variety of mammalian cells. Various evidence supports the notion that pseudopod formation is governed by cytoskeletal reorganization, especially that of actin filaments [see 1 for review]. The pseudopod appears in the light microscope as a vesicle-free zone of protrusion, sometimes highly flattened along the substratum (as in lamellipodia) and sometimes more rounded or off the surface (as in lobopodia). Both fluorescence microscopy and electron microscopy demonstrate that this region invariably contains a dense meshwork of F-actin filaments and few if any microtubules [2, 3]. In living and permeabilized cells, actin polymerization has been shown to occur predominantly near the extending edge of the cell, by the addition of new actin monomers between the filament end and the membrane [4, 5]. Inhibition of actin polymerization by cytochalasins blocks cell motility and pseudopod extension, providing direct evidence for the role of actin filaments in movement [1, 6]. Although the involvement of actin filaments in pseudopod formation is more or less accepted, there are still conflicting ideas about the mechanism by which force is generated. Models invoking forces from actin polymerization acting directly on the membrane, actomyosin contraction, or utilizing gel osmotic forces derived from the gelation of F-actin networks have been proposed to account for the outward expansion of the pseudopod [1].

In order to understand the changes in actin filament networks that occur during cell movement, we have visualized the F-actin organization of living cells during pseudopod formation. F-actin localization in living cells has been previously visualized by microinjecting fluorescent actin [7–9], fluorescent phalloidin [10, 11], or phalloidin stabilized actin filaments [5, 10–12] into fibroblasts and developing eggs [13, 14]. However, none of these experiments have attempted to visualize the changes in F-actin localization during cell movement. In *Dictyostelium,* microinjection is very difficult, so we have introduced fluorescent phalloidin into cells by electroporation and monitored its localization by confocal microscopy. This technique has allowed us to visualize dynamic changes in F-actin localization during pseudopod extension.

MATERIALS AND METHODS

Cell culture and electroporation. NC4A2 wild-type amoebae or HK321 myosin II heavy chain mutants were grown in 100-mm petri dishes at 22°C in HL-5 medium containing 100 μg/ml ampicillin and 100 μg/ml dihydrostreptomycin sulfate [15]. Cells were harvested in mid to late log phase and washed twice with cold H-50 buffer (20 mM Hepes, 50 mM KCl, 10 mM NaCl, 1 mM Mg_2SO_4, 5 mM $NaHCO_3$, 1 mM NaH_2PO_4) [16]. The final pellet containing 10^6–10^7 cells was

---

[1] Current address: Department of Anatomy and Cell Biology, 4769 Medical Science II Building, The University of Michigan Medical School, Ann Arbor, MI 48109-0616.

[2] To whom correspondence and reprint requests should be addressed at U-125, Department of Molecular and Cell Biology, University of Connecticut, Storrs, CT 06269. Fax: (860) 486-4331. E-mail: knecht@uconnvm.uconn.edu.

0014-4827/97 $25.00
Copyright © 1997 by Academic Press
All rights of reproduction in any form reserved.

resuspended in 100 μl of ice-cold H-50 buffer containing fluorescent phalloidin. Rhodamine–phalloidin (Sigma) or Bodipy–phallicidin (Molecular Probes, Inc.) was used at 20 and 5 *μM* final concentrations, respectively. Appropriate amounts of each dye were dissolved in H-50 buffer after being dried from a concentrated stock solution in methanol. The concentration of dye was chosen by optimizing the electroporation loading conditions and then determining a minimum concentration of phalloidin allowing detectable labeling using the imaging conditions described below.

Cells were placed in a prechilled 0.1-mm cuvette. Electroporation was accomplished by applying two pulses using a Bio-Rad Genepulser. The first pulse of 0.85 kV at 25 μF with RC-time of 0.6 ms was followed by the second pulse of 0.13 kV at 25 μF with RC-time of 0.1 ms. One milliliter of HL-5 medium was added to the cuvette immediately after electroporation. Cells were then plated in a glass observation dish made by drilling a 2.5-cm hole in a 60-mm glass dish and then gluing a 0.1-mm round coverslip over the hole. After 10 min, the medium was aspirated and replaced with fresh HL-5 and then imaging was initiated.

Image recording and analysis. Cells were imaged using a Bio-Rad MRC-600 confocal laser scanning microscope (CLSM) equipped with a 25 mW krypton–argon laser (Ion Laser Technology). The laser illumination was attenuated using a 3% neutral density filter. At this laser power, cells can be illuminated every 20 s for at least several hours with no effect on their motility or developmental behavior [15 and data not shown]. A 100X (1.30 NA) or 63X (NA 1.25) Neofluar objective (Carl Zeiss Inc.) was used as indicated. Fluorescence and differential interference contrast (DIC) images were collected simultaneously at 1-min intervals. The confocal aperture was completely open during imaging corresponding to an optical section of approximately 5 μm. This captured the entire volume of a pseudopod in a single optical section.

Quantification of fluorescence intensity, image processing, and pseudocoloring were done using the public domain NIH-Image program (written by Wayne Rasband at the National Institutes of Health and available from the Internet by anonymous FTP from zippy.nimh.nih.gov.). Final images were printed on a dye-sublimation transfer printer.

RESULTS AND DISCUSSION

Dictyostelium amoebae were electroporated in the presence of fluorescent phalloidin and then plated in

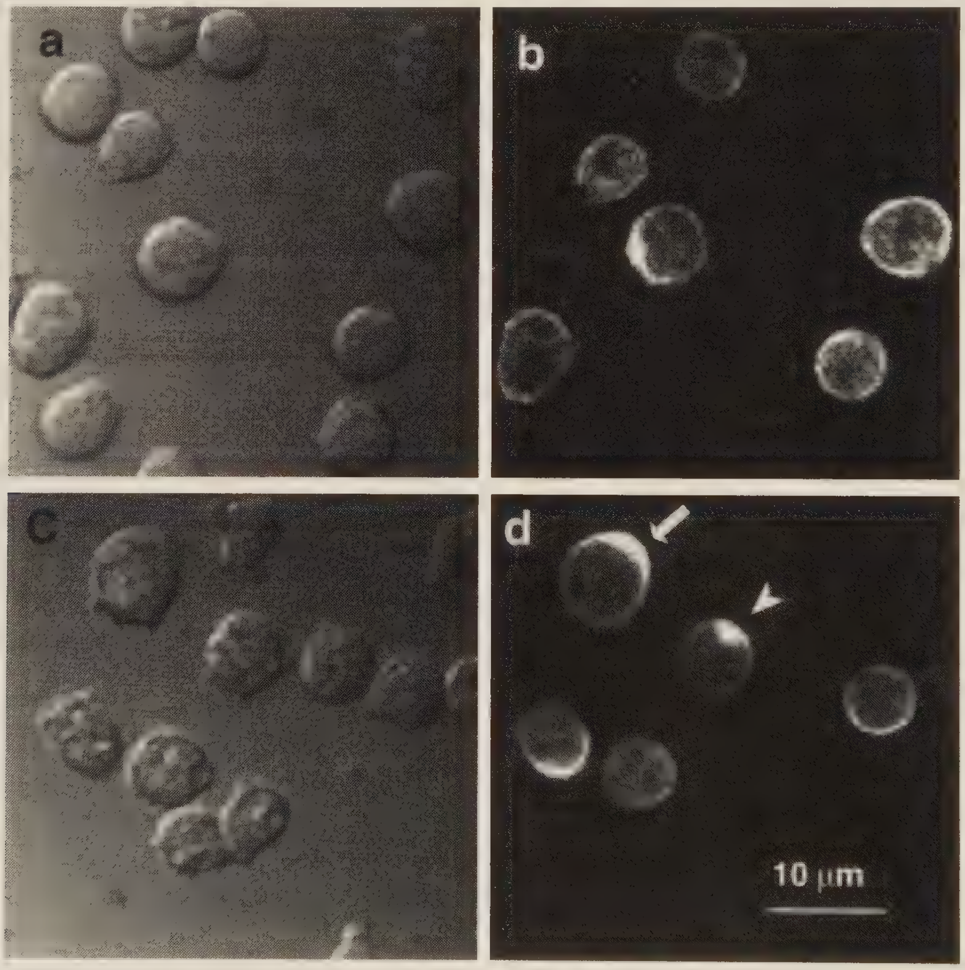

FIG. 1. Electroporation of *Dictyostelium* cells in the presence of phalloidin. NC4A2 wild-type cells were electroporated in the presence of rhodamine–phalloidin and imaged with a CLSM using a 63X objective lens. Fields of cells at 5 (a, b) and 10 min (c, d) after electroporation were shown. Fluorescence staining was initially localized as a distinct ring of the actin cortex (b). Later, most of the phalloidin-labeled actin has been accumulated into a single large aggregate at the rear of the cell (arrowhead in d). DIC images (a, c) and fluorescence images (b, d).

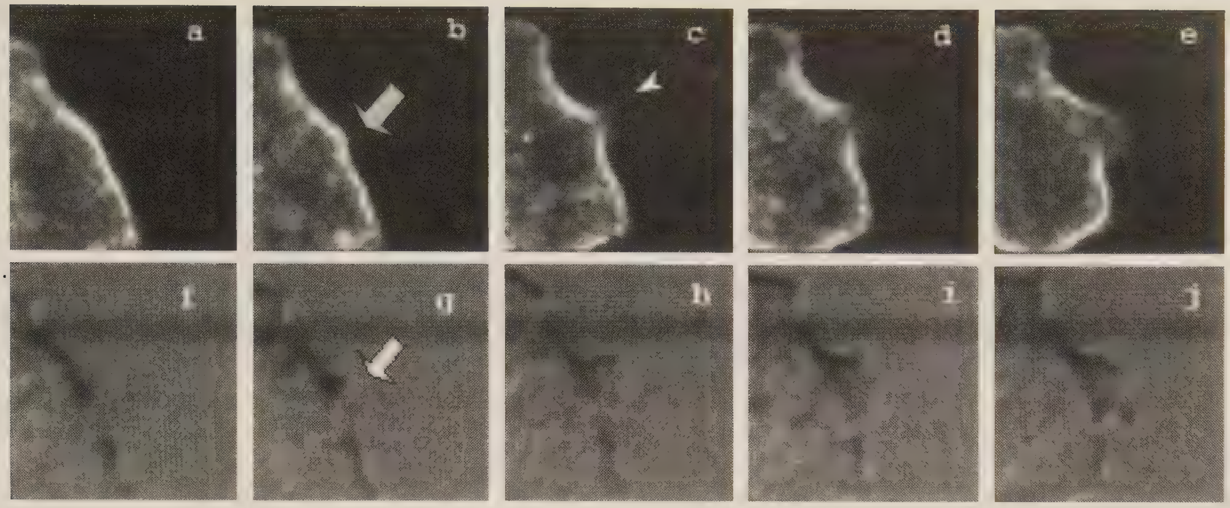

FIG. 2. Pseudopod formation and breakdown of the actin cortex. NC4A2 cells were electroporated with Bodipy–phallicidin and imaged with a CLSM using a 100X objective lens. Fluorescence images (a–e) and computer-enhanced DIC images (f–j) were collected at 1-min intervals. Deformation (b, arrow) and then disruption (c, arrowhead) of actin cortex were observed.

a microscope observation chamber. Immediately after electroporation, all cells were round and unattached (Fig. 1a). Most of the cells were labeled, but there was extensive heterogeneity in the extent of loading of phalloidin into the cells. Cells initially showed a distinct ring of staining underlying the plasma membrane, indicating labeling of the actin cortex (Fig. 1b). Cells recovered slowly from the effects of electroporation, and many took up to 20 min before becoming spread on the coverslip. Within 30 min, most of the phalloidin-labeled actin accumulated in a single large aggregate at the rear of the cell (arrowhead in Fig. 1d; and Lee *et al.*, manuscript in preparation).

In most cells, cortical staining was lost and aggregates started to form even before the cells initiated amoeboid locomotion. However, it was sometimes possible to observe a cell with cortical staining as it first spread and began pseudopod extension. Figures 2 and 3 show the sequence of changes in phalloidin localization in representative cells. Initial extension of the membrane was frequently observed in the DIC image before any change in the fluorescence staining pattern could be visualized (arrow in Fig. 2). An outward deformation of the phalloidin-stained region was evident in some, but not all, cells soon after membrane extension was visualized (arrow in Fig. 2b). As extension proceeded, fluorescence in the cortex became increasingly dim and diffuse, particularly in the center of the protrusion zone (arrowhead in Fig. 2c). In some cases, a complete gap in the fluorescence pattern of the cortical region was observed (Fig. 2d). Since mutants lacking myosin II have altered pseudopod structure and motility (17), we also examined the changes in the actin cortex of these cells by phalloidin electroporation. A similar sequence of events was observed in mutants lacking myosin II (Fig. 3), indicating that myosin II is not required for the mechanism that produces the gap in the cortex. The formation of the gap was observed in more than 15 cells, but not in all cases where a pseudopod was extended. In cases where no gap was observed, it appeared that the pseudopod was extended in a slightly different focal plane than that of the fluorescence image, but it is difficult to exclude the possibility that there are different mechanisms for extending pseudopods and not all involve the formation of a gap.

The absence of fluorescence in the extended region of new pseudopods does not mean that these structures lack actin filaments. As previously reported, pseudopods that were not stained by electroporated or microinjected phalloidin were stained by phalloidin added after fixation [10, 14; E. Lee, data not shown]. It is likely that electroporated phalloidin rapidly binds to existing F-actin so that by the time imaging begins, there is little free phalloidin in the cell. Since phalloidin binds very tightly to F-actin filaments [18], exchange would not occur rapidly enough to visualize newly assembled filaments in the pseudopod. Therefore, changes in the fluorescence pattern of electroporated phalloidin during pseudopod formation are likely to indicate alterations in the existing cortical actin network and not the distribution of new actin filaments.

To our knowledge, this is the first report of phalloidin being used to visualize changes in the F-actin cortex of motile cells during amoeboid locomotion. In fibroblasts, phalloidin was used to visualize stress fibers [10, 11]. In eggs, phalloidin has been used to look for major changes in actin distribution related to cytokinesis [13, 14]. One concern with interpreting these results is the

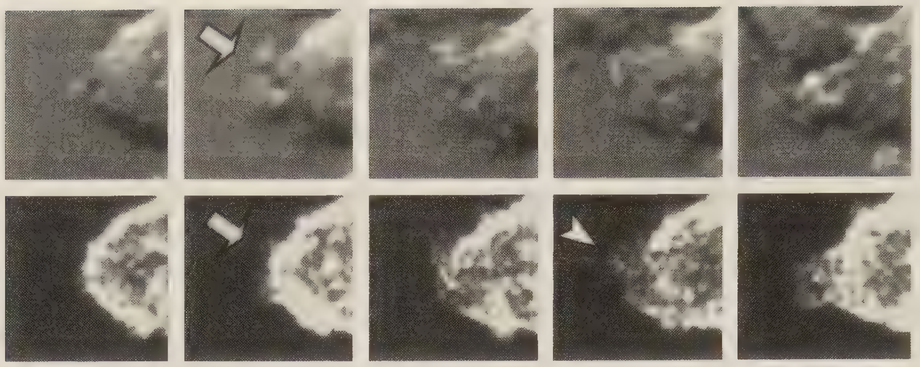

FIG. 3. Pseudopod formation in mutants lacking myosin II heavy chain. HK321 cells (mhcA-) were electroporated with rhodamine–phalloidin and imaged using a 100X objective lens at 1-min intervals as in the legend to Fig. 2. Pseudopod extension occurred before the fluorescence pattern was changed (arrow). Breakdown of the cortex (arrowhead) was also observed.

possibility that phalloidin could be altering F-actin dynamics rather than simply acting as a probe. High doses of microinjected phalloidin can inhibit cell motility, cytokinesis, and cell growth, but at low concentrations where the phalloidin is acting as a tracer, no changes in cell behavior were observed [10, 11, 19, 20]. Because there was a wide range of phalloidin loading by electroporation, it was possible to focus on cells whose fluorescence intensity was at the lower end of the range necessary for visualization. These cells still extend pseudopods and crawl, indicating that if filament stabilization occurs, it does not obviously affect the mechanisms responsible for pseudopod protrusion.

In vitro, binding of phalloidin increases the stability of F-actin filaments by preventing spontaneous disassembly. The formation of actin aggregates at later time points after phalloidin treatment is consistent with this notion. However, the disappearance of the fluorescent phalloidin signal from the pseudopod region during protrusion is the opposite of the effect expected if phalloidin were artifactually stabilizing actin filaments. Phalloidin does not prevent the fragmentation of the cortex by severing proteins since *in vitro,* gelsolin and severin can displace phalloidin from F-actin filaments [21]. Therefore, the apparent remodeling of the actin cortex during pseudopod formation is unlikely to be caused by the introduction of the drug into cells.

We hypothesize that the filaments in the cortex underlying the new pseudopod are severed, depolymerized, or both and dispersed, most likely into the new swelling pseudopod. The fluorescent phalloidin that is either free or bound to small actin fragments would be similarly dispersed to create the "hole" in the cortex. The solation–contraction coupling model [22] proposes that a myosin-driven contraction of the partially solated cortex drives directional flow of cytoplasm. Although this model predicts a dissolution of the existing cortex consistent with our observations, a contractile force other than myosin II must be invoked since the process we have observed appears unaffected by the absence of this molecular motor. The "cortical expansion" model proposed by Condeelis *et al.* [23] predicts that gel swelling occurs after new actin filaments are polymerized and then cross-linked into a loose gel. The model as diagrammed suggested that the underlying cortex would remain intact during expansion. However, the cortex could be broken down prior to expansion as indicated by our data without affecting the other details of the model. The gel swelling model as originally proposed by Oster [24] envisioned a sequence in which the severing of the actin filaments in the cortical network allows osmotic forces to swell the gel. This is entirely consistent with our data. None of the models explains all of our observations, however, as it was clear that extension had already begun before changes in the pattern of actin fluorescence could be observed. Moreover, the outward bending of the cortex (Fig. 2b) implies that it was being subjected to an outward directed force, not a uniform swelling. In conclusion, a substantial reorganization of the underlying cortical actin network appears to occur during pseudopod extension.

This work was supported by grants from the NIH (GM40599) and the Catherine and Weldon Donaghue Medical Research Foundation to D.A.K.

REFERENCES

1. Condeelis, J. (1993) *Annu. Rev. Cell Biol.* **9,** 411–444.
2. Cox, D., Condeelis, J., Wessels, D., Soll, D., Kern, H., and Knecht, D. A. (1992) *J. Cell Biol.* **116,** 943–955.
3. Small, J. V. (1988) *Electron Microsc. Rev.* **1,** 155–174.
4. Redmond, T., and Zigmond, S. H. (1993) *Cell Motil. Cytoskel.* **26,** 7–18.
5. Wang, Y. (1985) *J. Cell Biol.* **101,** 597–602.
6. McRobbie, S. J., and Newell, P. C. (1985) *Exp. Cell. Res.* **160,** 275–286.

7. De Lozanne, A., and Spudich, J. A. (1987) *Science* **236,** 1086–1091.
8. Knecht, D., and Loomis, W. F. (1987) *Science* **236,** 1081–1086.
9. DeBiasio, R. L., Wang, L.-L., Fisher, G. W., and Taylor, D. L. (1988) *J. Cell Biol.* **107,** 2631–2646.
10. Wang, Y. (1987) *J. Cell Biol.* **105,** 2811–2816.
11. Wehland, J., and Weber, K. (1981) *Eur. J. Cell Biol.* **24,** 176–183.
12. Cao, L., and Wang, Y. (1990) *J. Cell Biol.* **110,** 1089–1095.
13. Hamaguchi, Y., and Mabuchi, I. (1982) *Cell Motil. Cytoskel.* **2,** 103–113.
14. Terasaki, M. (1996) *Cell Motil. Cytoskel.* **334,** 49–56.
15. Knecht, D. A., and Shelden, E. (1995) *Dev. Biol.* **170,** 434–444.
16. Shelden, E., and Knecht, D. A. (1995) *J. Cell Sci.* **108,** 1105–1115.
17. Wessels, D., Soll, D. R., Knecht, D., Loomis, W. F., De Lozanne, A., and Spudich, J. (1988) *Dev. Biol.* **128,** 164–177.
18. Cano, M. L., Cassimeris, L., Joyce, M., and Zigmond, S. H. (1992) *Cell Motil. Cytoskel.* **21,** 147–158.
19. Barak, L. S., Yocum, R. R., Nothnagel, E. A., and Webb, W. W. (1980) *Proc. Natl. Acad. Sci. USA* **77,** 980–984.
20. Wehland, J., Osborn, M., and Weber, K. (1977) *Proc. Natl. Acad. Sci. USA* **74,** 5613–5617.
21. Allen, P. G., and Janmey, P. A. (1994) *J. Biol. Chem.* **269,** 32916–32923.
22. Taylor, D. L., and Fechheimer, M. (1982) *Philos. Trans. Soc. London B. Biol. Sci.* **299,** 185–197.
23. Condeelis, J., Brensnick, A., Demma, M., Dharmawardhane, S., Eddy, R., Hall, A. L., Sauterer, R., and Warren, V. (1990) *Dev. Genet.* **11,** 333–340.
24. Oster, G. F. (1984) *J. Embryol. Exp. Morphol.* **83,** 329–364.

Received September 17, 1996
Revised version received May 30, 1997

EXPERIMENTAL CELL RESEARCH **235**, 300–304 (1997)
ARTICLE NO. EX973677

SHORT NOTE

Sequence Determinants for hnRNP I Protein Nuclear Localization

Maria Grazia Romanelli,[1] Florian Weighardt,* Giuseppe Biamonti,* Silvano Riva,* and Carlo Morandi

*Istituto di Biologia e Genetica, Strada Le Grazie, 8, I-37134 Verona, Italy; and *Istituto di Genetica Biochimica ed Evoluzionistica del CNR, Via Abbiategrasso 207, I-27100 Pavia, Italy*

hnRNP I, also referred to as polypyrimidine tract binding protein, is one of the proteins associated with nascent pre-mRNA in the heterogeneous nuclear ribonucleoprotein (hnRNP) complexes. As for all karyophilic proteins, the nuclear import of hnRNP proteins requires specific sequence determinants that in many instances differ from the canonical import signal. In order to identify the sequences responsible for the nuclear localization, various hnRNP I portions were fused to a reporter protein (bacterial chloramphenicol acetyl transferase) and used in transient transfection assay. By this approach we identified a 60-amino-acid sequence located at the amino terminus of hnRNP I (designated NLD-I) that is both necessary and sufficient for nuclear localization. NLD-I represents a novel bipartite type of nuclear localization signal that bears no resemblance to other nuclear localization determinants so far identified in hnRNP proteins. © 1997 Academic Press

INTRODUCTION

In mammalian cells heterogeneous nuclear RNA (hnRNA) is complexed to a set of at least 20 abundant nuclear proteins collectively called hnRNPs (heterogeneous nuclear ribonucleoproteins), many of which have been extensively characterized in recent years [1, 2]. hnRNP proteins bind nascent pre-mRNAs and are directly involved in different steps of pre-mRNA maturation [3–5]. Moreover, it has been recently shown that some hnRNP proteins shuttle between the nucleus and the cytoplasm [6, 7], suggesting an involvement in mature mRNA export [5, 8, 9]. Recent investigations on hnRNP protein localization and transport between the nucleus and the cytoplasm led to the identification of novel types of signals such as the M9 nuclear localization/nuclear export signal in hnRNPs A1 and A2/B1 [6, 8, 10, 11] and the nuclear retention signal in hnRNP C1 [12]. Moreover, a novel transport factor, transportin, mediating the nuclear import of M9-containing proteins [10], has been isolated.

hnRNP I, also known as polypyrimidine tract-binding protein (PTB) [13, 14], is characterized by its preferential binding to a subset of polypyrimidine tracts in certain 3′ splice sites [15]. Recent evidence suggests that hnRNP I may function as a modulator in alternative splicing [16–19] and that the addition of hnRNP I may suppress the ability of rabbit reticulocyte extracts to use internal ribosomal entry sites [20]. In contrast, during viral infection, hnRNP I seems functionally required for internal ribosomal entry in the translation of picornaviruses [21–25] and hepatitis C mRNAs [26].

We previously reported that hnRNP I localizes both in the nucleoplasm of HeLa cells and in a discrete perinucleolar structure [13, 27]. However, contrary to most of the nuclear proteins with a molecular mass greater than 40–50 kDa, hnRNP I lacks a canonical, mono- or bipartite, nuclear localization signal (NLS) [28–31].

To investigate the determinants for nuclear targeting of hnRNP I, we tested a number of hnRNP I protein segments and deletions for their ability to promote nuclear localization of the small chloramphenicol acetyl transferase (CAT) reporter protein, otherwise equally distributed in the whole cell. Here we report that the N-terminal 60-amino-acid sequence of hnRNP I contains an unusual bipartite NLS that is both necessary and sufficient to target the protein to the cell nucleus.

MATERIALS AND METHODS

Plasmid constructs. pHI plasmid [13] contains the full-length cDNA of the human hnRNP I protein (Accession No. X66975). pA1-CAT vector directs the expression, in eukaryotic cells, of proteins C-terminally fused to the bacterial *cat* gene. Different fragments of hnRNP I cDNA, as indicated in Fig. 1, were obtained by polymerase chain reaction (PCR) amplification using primers containing, at their 5′-ends, a *Nsi*I (sense primers) or a *Sal*I (antisense primers) restriction site, linked to sequences complementary to the hnRNP I cDNA.

---

[1] To whom correspondence and reprint requests should be addressed. Fax: 39-045-8098180. E-mail: romane@borgoroma.univr.it.

0014-4827/97 $25.00
Copyright © 1997 by Academic Press
All rights of reproduction in any form reserved.

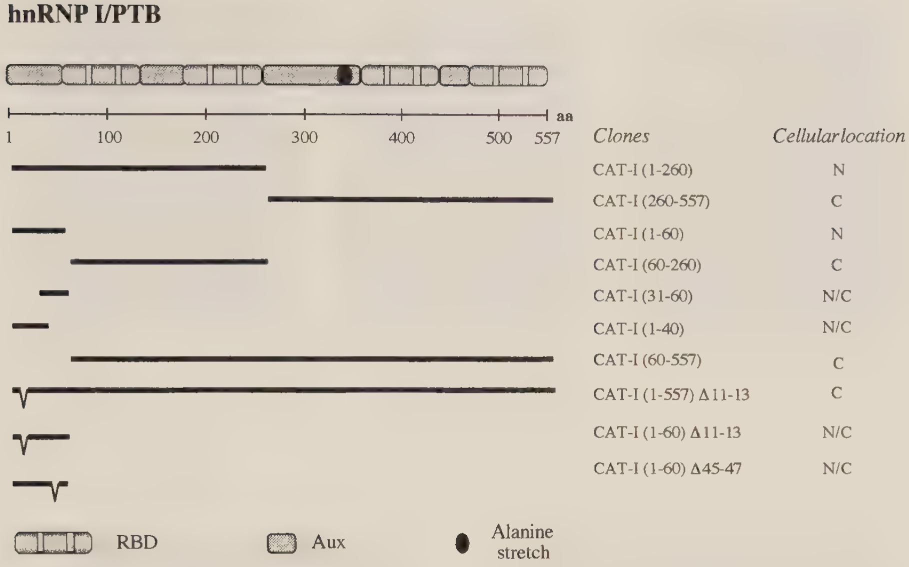

Clones	Cellular location
CAT-I (1-260)	N
CAT-I (260-557)	C
CAT-I (1-60)	N
CAT-I (60-260)	C
CAT-I (31-60)	N/C
CAT-I (1-40)	N/C
CAT-I (60-557)	C
CAT-I (1-557) Δ11-13	C
CAT-I (1-60) Δ11-13	N/C
CAT-I (1-60) Δ45-47	N/C

FIG. 1. Schematic representation of the hnRNP I portions (bold lines) utilized to produce CAT fusion clones. RBD, RNA binding domain; AUX, auxiliary domains.

Primers were synthesized in order to amplify protein regions as indicated in Fig. 1 and to allow carboxy-terminal fusions in frame with the CAT protein. The amplification reactions were carried out with *Taq* polymerase, in a Perkin–Elmer/Cetus thermal cycler. All PCR-amplified fragments were double digested with *Nsi*I and *Sal*I restriction endonucleases and cloned into *Nsi*I–*Sal*I sites of the pA1-CAT vector. Recombinant plasmids containing hnRNP I deleted of amino acids 11–13, i.e., [CAT-I (1–557) Δ11–13] and [CAT-I (1–60) Δ11–13], were produced by using the oligonucleotide ATGGACGGCATTGTCCCAGATATAGCCGTTCGGGGATCTGACGAGCTTTT (positions 88–133 of the hnRNP I cDNA) as sense primer. The recombinant plasmid [CAT-I (1–60) Δ45–47], containing a deletion of amino acids 45–47, was obtained using the oligonucleotide CACTCTAGAGGGGACGCCTGACTTCGGCCTGTCACCTTTGCTGTCATTTCCGTTTGCTG (positions 257–199 of the hnRNP I cDNA) as antisense primer. All PCR products were verified by sequencing with the dideoxy method (Sequenase USB, USA).

DNA transfections. Mouse NIH 3T3 cells were propagated in Dulbecco's modified Eagle's medium (DMEM), supplemented with 10% fetal calf serum, 2 m*M* L-glutamine, and 100 μg/ml streptomycin–penicillin. Cells were plated at 5×10^5 cells per 35-mm tissue culture dish 1 day prior to transfection. DNA transfection was carried out by lipofection using the transfection reagent *N*-[1-(2,3-dioleoyloxy)propyl]-*N,N,N*-trimethylammonium methylsulfate (Boehringer Mannheim) as recommended by the manufacturer. Ten micrograms of recombinant plasmid DNA, purified with the Qiagen Plasmid Kit (Qiagen, Germany), was used for each transfection assay.

Indirect immunofluorescence. At 24 h posttransfection, NIH 3T3 cells were trypsinized and 1×10^4–5×10^4 cells were seeded on slide flasks (18 × 50 mm) (NUNC, USA) in 4 ml DMEM, 10% fetal calf serum, 50 μg/ml gentamicin, and 2 m*M* L-glutamine. After an additional 20 h, cells were washed three times with cold phosphate-buffered saline (PBS), fixed for 10 min in methanol, and immediately rehydrated in PBS prior to the staining reaction. Rabbit polyclonal antibodies to CAT (5 prime → 3 prime Inc., USA) were diluted 1:500 in PBS 1% nonfat milk (DIFCO, USA) and then added to the coverslips. After 30 min of incubation at 37°C in a humid chamber, the coverslips were washed three times with PBS and, subsequently, incubated with FITC-conjugated goat anti-rabbit IgG (1:30) at 37°C for 30 min in a humid chamber. Cells were finally washed three times with PBS buffer, coated with 90% glycerol in PBS, and observed under a Leitz Orthoplan microscope with an epifluorescence attachment.

RESULTS AND DISCUSSION

hnRNP I is a 557-amino-acid long polypeptide containing four RBD-like domains of 80 amino acids, highly similar to those described in hnRNP L [1, 32]. These four RBD-like domains, arranged in tandem and separated by spacers of different length, are preceded at the N-terminus by a 60-amino-acid region that bears no homology with other sequences stored in the data bank. A stretch of eight alanine residues lies in the longest spacer between the second and the third RBD-like domain.

Previous immunofluorescence experiments carried out with monoclonal antibody 7G12 demonstrated that hnRNP I localized in the nucleoplasm and in a specific perinucleolar region of HeLa cells [13]. In order to identify the sequences responsible for nuclear localization, various hnRNP I portions were fused to the *cat* reporter gene and used in transient transfection assays. The subcellular distribution of the fusions was then analyzed by indirect immunofluorescence microscopy. For these experiments we used the pA1-CAT vector, which was developed for the study of the nuclear localization determinants of hnRNP A1 and of human DNA ligase I [11, 33]. This vector allows the expression of C-terminal peptides fused to the CAT reporter protein. As previously demonstrated [11, 33], CAT is a small protein (26 kDa) that can passively diffuse through the nuclear membrane and does not produce a subcellular localiza-

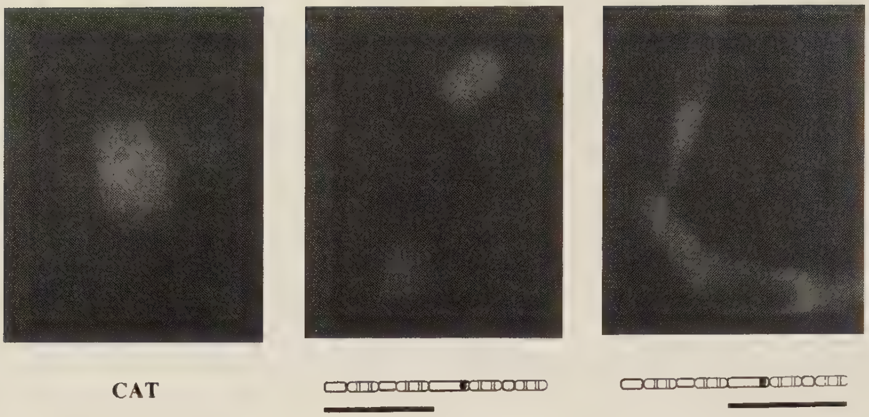

CAT

CAT-I (1-260)

CAT-I (260-557)

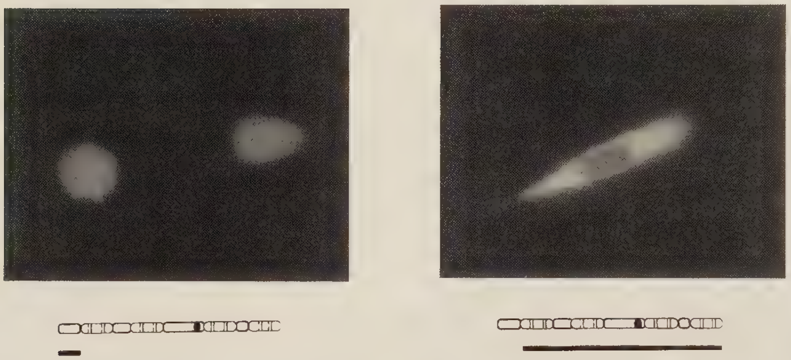

CAT-I (1-60)

CAT-I (60-557)

FIG. 2. Subcellular localization of CAT fused to the amino- or carboxy-terminal portion of hnRNP I protein as determined by indirect immunofluorescence. NIH 3T3 cells were transfected with the indicated constructs: [CAT], [CAT-I (1–260)], [CAT-I (260–557)], [CAT-I (1–60)], or [CAT-I (60–557)]. The distribution of the chimeric proteins was determined approximately 48 h after transfection by indirect immunofluorescence using the rabbit polyclonal antibody to CAT followed by the FITC-labeled goat anti-rabbit antibody, as described under Materials and Methods. For each fusion the cloned hnRNP I fragment is schematically shown in relation to the entire protein.

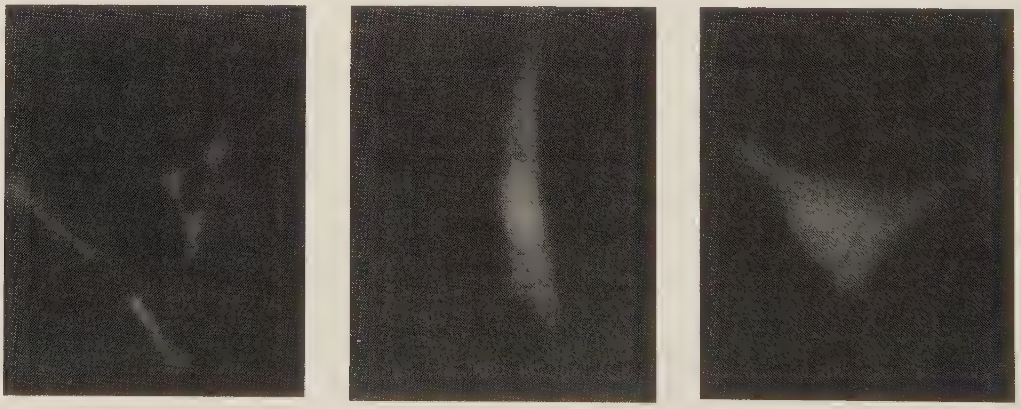

CAT-I (1-557) Δ11-13 CAT-I (1-60) Δ11-13 CAT-I (1-60) Δ45-47

FIG. 3. Definition of the nuclear localization determinants and subcellular localization of the mutated CAT-I fusions. The plasmids encoding [CAT-I (1–557) Δ11–13], [CAT-I (1–60) Δ11–13], or [CAT-I (1–60) Δ45–47] were transfected into NIH 3T3 cells. The distribution of the chimeric proteins was determined as described in Fig. 2.

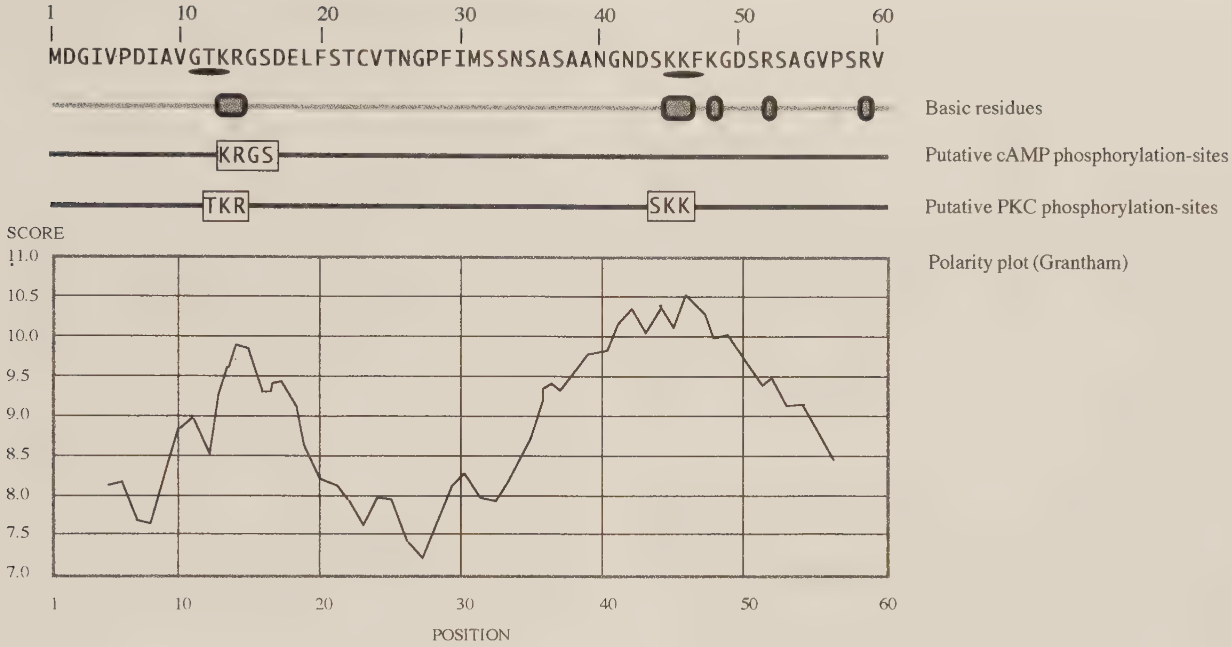

FIG. 4. Amino acid sequence of NLD-I. The two small deletions described in Fig. 3 are underlined. Lines underneath indicate the distribution of the basic residues (filled boxes) in the NLD-I sequence and the locations of the putative cAMP and PKC phosphorylation sites. At the bottom the polarity plot of the NLD-I sequence derived from the Protscale program (ExPASy) is reported.

tion bias, unlike the larger and more commonly used reporter protein β-galactosidase [34]. Therefore the CAT reporter permits the study of subcellular accumulation phenomena promoted not only by active NLSs but also by passive "retention determinants."

The regions of hnRNP I considered in this study are schematically represented in Fig. 1. The first construct expressed only the CAT protein that localized in both the nucleus and the cytoplasm (Fig. 2). We then fused CAT either with the first 260 amino acids of hnRNP I containing the N-terminal region and the first two RBD-like elements [CAT-I (1–260)] or with the last 297 amino acids [CAT-I (260–557)] containing the Ala-rich spacer and the two remaining repeated elements. The fusion between CAT and the first half of hnRNP I [CAT-I (1–260)] was completely nuclear (Fig. 2); in contrast the fusion with the second half [CAT-I (260–557)] was confined to the cell cytoplasm (Fig. 2). To map more precisely the nuclear localization signal of hnRNP I, additional chimeric CAT-I fusions were produced, as shown schematically in Fig. 1 and analyzed by indirect immunofluorescence staining. This analysis showed that the first N-terminal 60 residues are sufficient to produce nuclear localization of the CAT reporter protein [CAT-I (1–60)] (Fig. 2). As expected the complementary construct [CAT-I (60–557)] failed to accumulate in the cell nucleus (Fig. 2).

To further characterize the nuclear localization determinant, we produced mutants of the N-terminal 60-amino-acid region. Deletions of either amino acids 1–30 or 41–60 drastically impaired the functionality and the capacity to direct CAT to the nucleus (data not shown), thus indicating that integrity of the 60-amino-acid region is required for its full activity. This sequence does not show a resemblance to hitherto described NLS. Although there is a considerable sequence variability among the previously characterized NLSs, most of them consist of a short sequence (<20 residues) rich in basic residues [28]. In contrast, only a few basic residues are found in the nuclear localization determinant of hnRNP I. In order to assess their role, we produced fusions in which basic amino aids were deleted, [CAT-I (1–60) Δ11–13] and [CAT-I (1–60) Δ 45–47]. As shown in Fig. 3, when such fusions were expressed in transiently transfected cells, a homogeneous staining of the whole cell was observed. In addition, the fusion of the entire protein lacking the first basic residue [CAT-I (1–557) Δ11–13] was confined in the cell cytoplasm (Fig. 3). Together these results indicate that indeed both clusters of basic residues within the first 60 amino acids are required for the karyophilic activity. Such a novel extended signal was named the hnRNP I nuclear localization determinant or NLD-I.

Extended nuclear localization signals were previously identified, for instance in snRNP U1A protein [35] and in nucleoplasmin [30]. In NLD-I two hydrophilic basic clusters separated by an unusually long (31 residues) hydrophobic region can be envisaged by sequence analysis (Fig. 4). This situation is reminiscent of that described for the estrogen receptor (ER), whose

NLS contains interspersed Lys/Arg-rich motifs that resemble the prototype SV40 T-antigen NLS [36]. Individually none of them is strong enough to translocate wild-type levels of ER mutants into the nucleus, suggesting that multiple NLSs cooperatively generate full nuclear targeting. It has been proposed that this particular arrangement might indicate a regulated mechanism of nuclear import [36]. By analogy, regulated activity of NLD-I can be proposed; this hypothesis is also supported by the fact that the NLD-I region contains serine residues located within putative phosphorylation sites. In effect, one site for cAMP-dependent protein kinase (amino acids 13–16) and two for PKC (residues 12–14 and 44–45) perfectly overlap the two clusters of basic amino acids (Fig. 4).

Concerning the import mechanism of hnRNP I, it should be noticed that no similarity can be seen between NLD-I and the prototype NLS or the M9 sequence of hnRNP A1, raising the possibility that NLD-I may interact in the cytoplasm with "transporters" other than importin α, β, or the recently described transportin [10, 37]. In this context hnRNP proteins seem to exhibit a remarkable repertoire of nuclear localization signals, mostly noncanonical, as in hnRNP A1, A2, C, I, and probably L. Remarkably hnRNP B1 contains both a canonical and a noncanonical signal [5]. Such a differentiation of signal, and probably of nuclear import mechanisms, further points toward a diversified and still largely unexplored role of these proteins in RNA metabolism.

The technical assistance of Ms. Pamela Lorenzi is greatly acknowledged. This work was supported by a grant from Progetto Finalizzato Ingegneria Genetica, MURST 40%, and CNR.

REFERENCES

1. Dreyfuss, G., Matunis, M. J., Pinõl-Roma, S., and Burd, C. G. (1993) *Annu. Rev. Biochem.* **62,** 289–321.
2. Pinõl-Roma, S., Choi, Y. D., Matunis, M. J., and Dreyfuss, G. (1988) *Genes Dev.* **2,** 215–227.
3. Burd, C. G., and Dreyfuss, G. (1994) *Science* **29,** 615–621.
4. Swanson, M. S. (1995) *in* Pre-mRNA Processing, pp. 17–33, Landes, Austin, TX.
5. Weighardt, F., Biamonti, G., and Riva, S. (1996) *BioAssay* **9,** 747–756.
6. Fischer, U., Matthew, W., Luhrmann, R., and Dreyfuss, G. (1996) *Trends Cell Biol.* **6,** 190–293.
7. Pinõl-Roma, S., and Dreyfuss, G. (1993) *Trends Cell Biol.* **3,** 151–155.
8. Michael, W. M., Choi, M., and Dreyfuss, G. (1995) *Cell* **83,** 415–422.
9. Siomi, H., and Dreyfuss, G. (1995) *J. Cell Biol.* **129,** 551–560.
10. Pollard, V. W., Michael, W. M., Nakielny, S., Siomi, M. C., Wang, F., and Dreyfuss, G. (1996) *Cell* **86,** 985–994.
11. Weighardt, F., Biamonti, G., and Riva, S. (1995) *J. Cell Sci.* **108,** 545–555.
12. Nakielny, S., and Dreyfuss, G. (1996) *J. Cell Biol.* **134,** 1365–1373.
13. Ghetti, A., Pinõl-Roma, S., Michael, W. M., Morandi, C., and Dreyfuss, G. (1992) *Nucleic Acids Res.* **20,** 3671–3678.
14. Gil, A., Sharp, P. A., Jamison, S. F., and Garcia-Blanco, M. A. (1991) *Genes Dev.* **5,** 1224–1236.
15. Patton, J. G., Mayer, S. A., Tempst, P., and Nadal-Ginard, B. (1991) *Genes Dev.* **5,** 1237–1251.
16. Guo, W., Mulligan, G. J., Wormsley, S., and Helfman, D. M. (1991) *Genes Dev.* **5,** 2096–2107.
17. Lou, H., Gagel, R. F., and Berget, S. M. (1996) *Genes Dev.* **10,** 208–219.
18. Morris, D. R., Kakegawa, T., Kaspar, R. L., and White, M. W. (1993) *Biochemistry* **32,** 2931–2937.
19. Singh, R., Valcarcel, J., and Green, M. R. (1995) *Science* **268,** 1173–1176.
20. Svitkin, Y. V., Ovchinnikov, L. P., Dreyfuss, G., and Sonenberg, N. (1996) *EMBO J.* **15,** 7147–7155.
21. Borman, A., Howell, M. T., Patton, J. G., and Jackson, R. J. (1993) *J. Gen. Virol.* **74,** 1775–1788.
22. Borovjagin, A., Pestova, T., and Shatsky, I. (1994) *FEBS Lett.* **351,** 299–302.
23. Haller, A. A., and Semler, B. L. (1995) *Virology* **206,** 923–934.
24. Hellen, C. U. T., Pestova, T. V., Litters, M., and Wimmer, E. (1994) *J. Virol.* **68,** 941–950.
25. Vagner, S., Waysbort, A., Marenda, M., Gensac, M. C., Amalric, F., and Prat, A. C. (1995) *J. Biol. Chem.* **270,** 20376–20383.
26. Ali, N., and Siddiqui, A. (1995) *J. Virol.* **69,** 6367–6375.
27. Matera, A. G., Frey, M. R., Margelot, K., and Wolin, S. L. (1995) *J. Cell Biol.* **129,** 1181–1193.
28. Dingwall, D., and Laskey, R. A. (1991) *Trends Biochem. Sci.* **16,** 478–481.
29. Gorkich, D., and Mattaj, I. W. (1996) *Science* **271,** 1513–1518.
30. Robbins, J. Dilworth, S. M., Laskey, R. A., and Dingwall, C. (1991) *Cell* **64,** 615–623.
31. Silver, P. A. (1991) *Cell* **64,** 489–497.
32. Biamonti, G., and Riva, S. (1994) *FEBS Lett.* **28,** 1–8.
33. Montecucco, A., Savini, E., Weighardt, F., Rossi, R., Ciarrocchi, G., and Biamonti, G. (1995) *EMBO J.* **14,** 5379–5386.
34. Reinhard, C., Fernandez, A., Lamb, N. J. C., and Thomas, G. (1994) *EMBO J.* **13,** 1557–1565.
35. Kambach, C., and Mattaj, I. W. (1992) *J. Cell Biol.* **118,** 11–21.
36. Ylikomi, T., Bocquel, M. T., Berry, M., Gronemeyer, H., and Chambon, P. (1992) *EMBO J.* **11,** 3681–3694.
37. Moore, M. S., and Blobel, G. (1993) *Nature* **365,** 661–663.

Received February 24, 1997
Revised version received May 21, 1997

EXPERIMENTAL CELL RESEARCH

http://www.apnet.com/www/journal/ex.htm

Notice to Authors

Experimental Cell Research (*ECR*) is dedicated to publishing manuscripts that significantly advance our understanding of cell and molecular biology. Examples of areas of interest to *ECR* are the cell cycle; gene regulation; chromatin; subcellular organization; cell signaling; signal transduction; nuclear import–export; intracellular trafficking; programmed cell death; the dynamics and function of the cytoskeleton, cell membrane, and extracellular matrix; the biology of meiosis and mitosis; cell motility and migration; mechanisms of cellular growth control and differentiation; and cell–cell interaction between cells in tissues or in culture. Manuscripts in the area of cancer research, particularly those that address fundamental aspects of cell and molecular biology, are also welcomed. Reports describing new experimental techniques and methods or of theoretical work having a direct bearing on experimental approaches are also appropriate for inclusion in the journal. Experimental manuscripts will be given the highest priority and can range from the subcellular to the organism level, including work on transgenic animals. Purely descriptive work, including description of RNA or protein expression patterns, is given lower priority but can be accepted if it provides important new or unexpected information.

Acceptance of manuscripts will be based on scientific excellence and priority as judged by editors and reviewers, on relevance to the central themes of the journal, and on the interest of the results to a broad readership of cell and molecular biology. A manuscript of high intrinsic quality may be returned if it seems better suited to a more specialized journal.

Manuscripts can be published in the format of **regular articles** or **short notes.** There is no strict size limitation on regular articles, although they usually do not exceed 15,000 words, preceded by an Abstract not to exceed 200 words. The length of a short note is 4 printed pages, which is the equivalent of 2000 words, inclusive of tables, figures, and references. *ECR* also publishes **review articles.** As with regular articles, there is no strict size limitation, but review articles in the Minireview format (3–4 pages written text) receive priority. Most review articles are solicited, but authors interested in contributing review articles or suggesting appropriate topics are encouraged to contact the Editor-in-Chief. Review articles will be subject to review before publication.

Original papers only will be considered. Manuscripts are accepted for review on the understanding that the same work has not been published, that it is not under consideration for publication elsewhere, and that its submission for publication has been approved by all of the authors and by the appropriate authority at the institution where the work was carried out. Authors must verify the wording of any cited personal communication with the persons who supplied the information and obtain approval for the use of their names in connection with the quoted information or for the citation of unpublished work; written evidence of such approval should accompany the manuscript. All material published in *ECR* represents the opinions of the authors and should not be construed to reflect the opinions of the Editors or the Publisher.

Authors submitting a manuscript do so on the understanding that if it is accepted for publication, copyright in the article, including the right to reproduce the article in all forms and media, shall be assigned exclusively to the Publisher. The Copyright Transfer Agreement, which may be copied from the pages following the Information for Authors or found on the journal home page listed here, should be signed by the appropriate person(s) and should accompany the original submission of a manuscript to this journal. The transfer of copyright does not take effect until the manuscript is accepted for publication.

It is understood that novel biological reagents described in manuscripts accepted for publication in *ECR,* e.g., DNA and antibodies, will be made available to scientists in academic research. All novel genetic sequence information must be deposited with GenBank or the EMBL database.

Submission of Manuscripts. *Four complete copies* should be sent to one of the Editors or to either journal receiving office:

Editorial Office
Experimental Cell Research
Karolinska Institute
CMB, Doktorsringen 2D
17177 Stockholm
Sweden
E-mail: ecr@cmb.ki.se

Dr. Renato Baserga
Associate Editor for North America
Experimental Cell Research
U.S. Editorial Office
525 B Street
Suite 1900
San Diego, CA 92101-4495

Each copy must include all figures (originals or glossy prints must be supplied with three copies, photocopies may be supplied with the fourth) and tables. *In the case of rejected manuscripts only one copy of the manuscript and the original art will be returned to the author.*

Authors are encouraged to suggest four competent reviewers in their field (include telephone number, fax number, and/or e-mail address for potential reviewers) and may also suggest individuals whom they wish to have excluded from the review process.

Notice to Authors

Form of Manuscript. Manuscripts should be typewritten and double-spaced throughout on one side of 8.5 × 11-in. white paper, with 1-in. margins on all sides. All pages should be numbered consecutively. *Page 1* should contain the article title, author(s), affiliation(s), a short running title (abbreviated form of title) of less than 55 characters including letters and spaces, and the name, complete mailing address, and telephone, fax, and/or email address of the person to whom correspondence should be sent. *Page 2* should contain a short abstract of 50–200 words and 5 or 6 key words.

In the Methods section, authors should draw attention to any particular chemical or biological hazards that may be involved in carrying out the experiments described. Any relevant safety precautions should be described; if an accepted code of practice has been followed, a reference to the relevant standards should be given.

Footnotes should be avoided.

Figures should be numbered consecutively with Arabic numerals in order of mention in the text: each figure should have a descriptive legend. Legends should be typed together on a separate sheet, double-spaced. All illustrations should be in finished form suitable for photoreproduction. They should be planned to fit the proportion of the printed page (7 × 9 in.; column width, $3\frac{1}{2}$ in.). Mark the back of all illustrations (in *soft* pencil) with the author's last name, title of paper, and figure number, and indicate the TOP side of the illustration.

Lettering on drawings should be of professional quality or generated by *high-resolution* computer graphics and should be large enough (10–12 points) to take a reduction of 50–60%. Properly prepared glossy prints are acceptable.

Photographs should be the actual size for reproduction and labeled with letters 2 to 4 mm high. For the best reproduction, provide clear, sharp, glossy prints with adequate contrast. Providing an overlay that indicates the most critical areas of a micrograph will aid in ensuring high-quality reproduction. The best results will be obtained if authors match the contrast and density of all figures appearing on a single plate. Figures that are to appear together as one plate should be mounted on paper. Give magnifications in legends or indicate with a scale marker on photograph.

Suggestions for possible **cover photos** are welcomed.

Color figures. One color plate will be published *free* of charge in each article, provided color is deemed scientifically necessary by the reviewers and the Editorial Board. Additional color figures will be charged to the author. The cost for each additional figure is $800. See the instructions above if mounting is necessary; mounted color figures *must* be submitted on paper or flexible board due to the nature of the reproduction process.

Tables should be typed double-spaced on separate pages, numbered consecutively with Arabic numerals in order of mention in the text. Each table should have a short explanatory title.

References to the literature should be cited in the text by Arabic numerals in square brackets and listed at the end of the paper in consecutive order. Abbreviations of journal titles should follow the style used in the most recent *Chemical Abstracts ServiceSource Index.* Please note the style in the following examples:

1. Goldman, B., Mach, A., and Wurzel, J. (1996). Epidermal growth factor promotes a cardiomyoblastic phenotype in human fetal cardiac myocytes. *Exp. Cell Res.* **228,** 237–245.
2. Yeagle, P. L. (1993). "The Membranes of Cells," 2nd ed., Academic Press, San Diego.
3. Nieto, M. A., Patel, K., and Wilkinson, D. G. (1995). In situ hybridization analysis of chick embryos in whole mount and tissue sections. *In* "Methods in Avian Embryology" (M. Bronner-Fraser, Ed.), Academic Press, San Diego.

Proofs will be sent to the author, with a reprint order form. Authors will be charged for alterations in excess of 10% of the cost of composition.

Reprints. Fifty reprints without covers of each article will be provided free of charge. Additional reprints may be purchased.

Personal Computer Disks. Authors are encouraged to submit floppy disks with their articles once the manuscripts have been accepted and after all revisions have been incorporated onto the disk. Please label the disk with the type of computer used, the type of software and the version number, and the disk format. Clearly indicate the file names and contents of each file.

Manuscripts will be edited according to the style of the journal, and the proofs must be read carefully by the author. Please note that tabular material will be typeset conventionally. Every effort will be made to use the disk for the remainder of the article.

For further information, please contact the publisher (Editorial Supervisor, Journal Division, Academic Press, 525 B Street, Suite 1900, San Diego, California 92101-4495; telephone: (619) 699-6870; fax: (619) 699-6800). Details about the preparation of manuscripts and artwork on disk may be found on the *ECR* home page.

NOTICE

Under the terms of the U.S. copyright law effective January 1, 1978, and the copyright laws of many other countries, journal publishers are required to obtain written confirmation from authors in order to acquire copyright rights for papers published in their journals. We are therefore asking you to sign and return the applicable section of the form printed as follows. If you and your co-authors, if any, own rights in your paper as individuals, please sign Section **A** of the attached form. If you work for a corporation that owns the rights in the paper, please have an authorized officer of the corporation sign Section **B.** If the paper is in the public domain because you created it within the scope of your employment with the U.S. government or another government that does not claim any copyright or the paper is subject to Crown copyright because you are an employee of the British or Canadian government, please sign Section **C.** If any governmental entity other than the U.S., British, or Canadian government owns copyright, please call Academic Press at the number below. No manuscript will be processed until the appropriate form has been returned.

We ask your cooperation because it is of vital importance for the widest possible dissemination of your paper and the continued viability of our journal. We must have your written confirmation in order to authorize libraries and other information centers to use this material and to perform other appropriate publishing functions.

If your manuscript is not published within a reasonable period of time after acceptance, upon written request, AP will promptly return the rights to the manuscript to the author(s).

IMPORTANT: Note that Academic Press may choose to publish an abstract or portions of the paper prior to publishing the paper in the journal. Please contact Academic Press immediately if you would like Academic Press to refrain from such prior publication for any reason, including disclosure of a patentable invention.

If you have any questions about the procedures, please contact Academic Press: U.S.A. telephone (619) 230-1840; fax (619) 699-6305. UK telephone 44-171-482-2893; fax 44-171-267-0362.

Please submit this form with your manuscript to the editorial office listed in the Information for Authors.

Thank you.

Copyright Transfer Agreement

Journal: *Experimental Cell Research*

Tentative Manuscript Title: ____

____

Authors: ____

A. You hereby confirm the assignment to Academic Press (AP) of the entire copyright in and to the manuscript named above (the Work) throughout the world in all forms and media, whether now known or hereafter developed, and in all languages effective if and when it is accepted for publication by AP. You also warrant that the Work has not been published before and contains no materials the publication of which would violate any copyright or other personal or proprietary right of any person or entity, and you acknowledge that AP is relying on this document in publishing this Work. Notwithstanding the assignment of copyright to AP, you:

1. Retain patent rights, if any.
2. May make photocopies of all or part of the Work for use in your classroom teaching.
3. May use your original figures/tables/illustrations/photographs from the Work in future works of your own.
4. May include the Work as part of your dissertation, for noncommercial distribution only.

You agree that all copies and inclusions made under the above conditions will carry a notice of copyright and a citation to the journal article.

To be signed by all the authors (or by an author who has obtained the written assent of the nonsigning authors).

Signed: ____________________________________ Date: ______________

B. The Work was written as part of the duties of the author as an employee of the company signing below or otherwise as a "work made for hire" (as defined in the relevant copyright law) for such company. As the authorized representative of such company, you hereby confirm the assignment to AP of the entire copyright in and to the Work throughout the world in all forms and media, whether now known or hereafter developed, and in all languages effective if and when it is accepted for publication by AP. You also warrant that the Work has not been published before and contains no materials the publication of which would violate any copyright or other personal or proprietary right of any person or entity, and you acknowledge that AP is relying on this document in publishing this Work. Notwithstanding the assignment of copyright to AP, you:

1. Retain patent rights, if any.
2. May prepare derivative works based on the Work, with proper acknowledgment.
3. May reproduce the Work in reasonable quantities for internal use, with proper acknowledgment. However, copies of the Work may not be used for resale or in any way that implies that AP, the journal, or the editorial board endorses any procedures or products of your company.

Signed: ____________________________________ Date: ______________

Title: ____

C. You certify that the Work has been written as part of your official duties either as (a) an employee of the U.S. government or another government whose works are not subject to copyright protection, and as such there is no copyright to transfer; or as (b) an employee of the British, Canadian, or other government whose works are subject to Crown copyright, and via the authorized signature of the relevant government entity below, AP is hereby obtaining a nonexclusive license to publish (and to authorize others to publish) the Work in all forms and media, whether now known or hereafter developed, and in all languages effective if and when it is accepted for publication. If not all of the authors are government employees, the nongovernment employee should sign Section A. You also warrant that the Work has not been published before and contains no materials the publication of which would violate any copyright or other personal or proprietary right of any person or entity, and you acknowledge that AP is relying on this document in publishing this Work.

To be signed by all the authors (or by an author who has obtained the written assent of the nonsigning authors).

Signed: ____________________________________ Date: ______________

Government authorization: ____________________________ Date: ______________

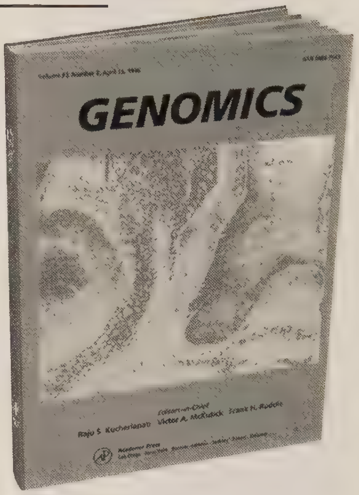

Now Available Online!

GENOMICS

International Journal for Analyses of the Human and Other Genomes

Editors-in-Chief
Victor A. McKusick
The Johns Hopkins University, Baltimore, Maryland
Raju S. Kucherlapati
Albert Einstein College of Medicine, Bronx, New York
Frank H. Ruddle
Yale University, New Haven, Connecticut

CALL for a FREE SAMPLE

Genomics emphasizes the integration of basic and applied research in human and comparative gene mapping, molecular cloning, large-scale restriction mapping, and DNA sequencing and computational analysis. The journal provides a common meeting ground for those involved in molecular biology and genetics. Technologic and methodologic advances in genomic analysis and interpretation are described, and analyses of the human genome in hereditary and neoplastic diseases are reported. Full-length articles, short communications, brief reports, and reviews are included. In addition, ***Genomics*** promotes efficient communication with the major genetic databases.

RESEARCH AREAS INCLUDE

- Chromosomal assignments of genes and DNA fragments by Mendelian and physical mapping approaches
- Reports of nucleic acid sequences of cloned genes and other interesting genomic regions
- Descriptions of distributions of gene families and genes that share nucleic acid or amino acid sequence domains
- Comparative analyses of genomes to yield structural, functional, or evolutionary insights
- Patterns of genome organization that provide insights into gene regulation and development
- Methods for large-scale genomic cloning, restriction mapping, and DNA sequencing
- Computational methods and descriptions of algorithms for the manipulation of DNA and protein sequence data
- Analyses of genetic linkage data in pursuit of information on inherited disorders
- Development of experimental, computational, and database management techniques of broad applicability in genome research

Database coverage includes Biological Abstracts (BIOSIS), CABS, Current Contents/Life Sciences, Genetics Abstracts, Genome Abstracts, Index Medicus (MEDLINE), Research Alert, ISI's Science Citation Index, and SCISEARCH.

Volumes 39–46 (1997), 24 issues

	Institutional Rates	Personal Rates*
In the U.S.A. and Canada:	$1100.00	$295.00
All other countries:	1300.00	333.00

ISSN 0888-7543

Log in to the Academic Press Online Library
URL: http://www.idealibrary.com
URL: http://www.europe.idealibrary.com

IDEAL

Sample are available upon request. For more information, please write or call:

ACADEMIC PRESS
Marketing Department
525 B Street, Suite 1900
San Diego, CA 92101-4495, U.S.A.
800-894-3434 • 619-699-6742
e-mail: apsubs@acad.com

ACADEMIC PRESS, LTD.
Marketing Department
24-28 Oval Road
London NW1 7DX, U.K.
In Europe call: 0181-300-3322

FIND US ON THE WEB!
AP NET
Academic Press
www.apnet.com

All prices are in U.S. dollars and are subject to change without notice. Canadian customers: Please add 7% Goods and Services Tax to your order.
*Personal rates are available only on orders placed directly with the Publisher and paid for with personal funds.

GENOM97A

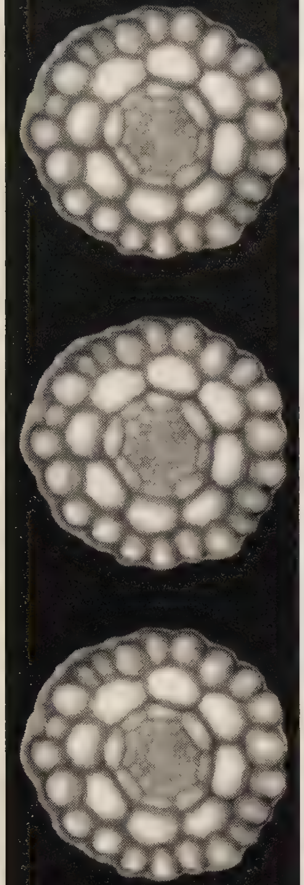

Subscribe at the personal rate and receive a free membership to the Society for Developmental Biology for one year.

All prices are in U.S. dollars and are subject to change without notice. Canadian customers: Please add 7% Goods and Services Tax to your order. Personal rates are available only on orders placed directly with the Publisher and paid for with personal funds. Checks and money orders must be drawn against a U.S. bank.

DB 97A

DEVELOPMENTAL BIOLOGY

An International Journal

INCREASED FREQUENCY

Editor-in-Chief

ERIC N. OLSON

Hamon Center for Basic Cancer Research
The University of Texas, Southwestern Medical Center, Dallas

Developmental Biology publishes original research on mechanisms of development, differentiation, and growth in animals and plants at the molecular, cellular, and genetic levels. Areas of particular emphasis include transcriptional control mechanisms, embryonic patterning, cell–cell interactions, growth factors and signal transduction, and regulatory hierarchies.

Developmental Biology now publishes "Rapid Communications." This new section of brief articles on original research findings makes topics of high current interest available to other researchers as quickly as possible.

Some of the Many Features of this Journal:

- Rapid Communications reviewed within one week
- 50 gratis reprints per article
- No page charges
- Bi-weekly in 1997

Published under the Auspices of the Society for Developmental Biology

Database coverage includes Biological Abstracts (BIOSIS), Chemical Abstracts, Current Contents/Life Sciences, Excerpta Medica (EMBASE), Index Medicus (MEDLINE), and Science Citation Index.

Volumes 181–192 (1997), 24 issues
ISSN 0012-1606

	In the U.S.A. and Canada	All other countries
Institutional:	$2350.00	$2850.00
Personal:	229.00*	229.00*

Log in to the Academic Press Online Library
URL: http://www.idealibrary.com
URL: http://www.europe.idealibrary.com

IDEAL

FIND US ON THE WEB!
AP NET
Academic Press
www.apnet.com

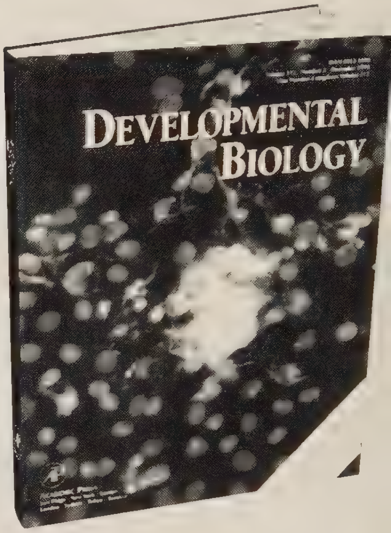

AP

**Free sample copies are available.
For more information, please contact:**

ACADEMIC PRESS
Marketing Department
525 B Street, Suite 1900
San Diego, CA 92101-4495, U.S.A.
1-800-894-3434/1-619-699-6742
E-mail apsubs@acad.com

ACADEMIC PRESS, LTD.
Marketing Department
24–28 Oval Road
London NW1 7DX, U.K.
In Europe call: 0181-300-3322

CALL FOR FREE SAMPLE

NITRIC OXIDE

BIOLOGY AND CHEMISTRY

Part B of *Archives of Biochemistry and Biophysics*

Editor-in-Chief

Louis J. Ignarro

University of California, Los Angeles, School of Medicine, U.S.A.

Associate Editors

Jack R. Lancaster, Jr.

Louisiana State University Medical Center, New Orleans, U.S.A.

Ulrich Forstermann

Johannes Gutenberg University, Mainz, Germany

Although one of the simplest biological molecules in nature, nitric oxide has found its way into nearly every phase of biology and medicine ranging from its role as a critical endogenous regulator of blood flow and thrombosis to a principle neurotransmitter mediating erectile function to a major pathophysiological mediator of inflammation and host defense. These major discoveries have stimulated intense and extensive research into a vase array of fields including chemistry, molecular biology, and gene therapy. *Nitric Oxide: Biology and Chemistry* provides a forum for the rapid publication of scientific investigation of the highest quality across the broad field of nitric oxide research.

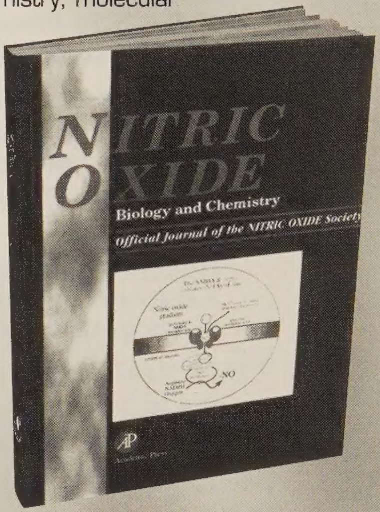

Research areas include basic and clinical topics in

- **Cell biology**
- **Molecular biology**
- **Biochemistry**
- **Immunology**
- **Pathology**
- **Genetics**
- **Physiology**
- **Pharmacology**
- **Disease processes**

Database coverage includes Biological Abstracts (BIOSIS), CABS, Chemical Abstracts, Current Contents/Life Sciences, Excerpta Medica (EMBASE), Genetics Abstracts, Index Medicus (MEDLINE), Research Alert, Science Citation Index, and SCISEARCH.

Volume 1 (1997), 6 issues
ISSN 1089-8603

	Institutional Rates	Personal Rates*
In the U.S.A. and Canada:	$220.00	$110.00
All other countries:	265.00	132.00

AP FREE SAMPLE COPIES AVAILABLE UPON REQUEST.

For more information, please write or call:

ACADEMIC PRESS, INC.
Marketing Department
525 B Street, Suite 1900
San Diego, CA 92101-4495, U.S.A.
1-800-894-3434/1-619-699-6742
e-mail: apsubs@acad.com

ACADEMIC PRESS, LTD.
Marketing Department
24-28 Oval Road
London NW1 7DX, U.K.
In Europe call: 0181-300-3322

Log in to the Academic Press Online Library
URL: http://www.idealibrary.com
URL: http://www.europe.idealibrary.com

IDEAL

FIND US ON THE WEB!
AP NET
Academic Press
www.apnet.com

All prices are in U.S. dollars and are subject to change without notice. Canadian customers: Please add 7% Goods and Services Tax to your order. *Personal rates are available only on orders placed directly with the Publisher and paid for with personal funds.

N097A

Continued from following page

HIDETOSHI YAMASHITA, AKIRA SHIMIZU, MITSUYASU KATO, HIDEKI NISHITOH, HIDENORI ICHIJO, AKI HANYU, IKUO MORITA, MICHIO KIMURA, FUSAO MAKISHIMA, AND KOHEI MIYAZONO. Growth/Differentiation Factor-5 Induces Angiogenesis *in Vivo* 218

JACQUES ROBERT, DEBORAH M. BROWN, LOUIS DU PASQUIER, AND NICHOLAS COHEN. Antibody Cross-Linking of the Thymocyte-Specific Cell Surface Molecule CTX Causes Abnormal Mitosis and Multinucleation of Tumor Cells 227

SHU MING LIU AND TOMMY SUNDQVIST. Nitric Oxide and cGMP Regulate Endothelial Permeability and F-Actin Distribution in Hydrogen Peroxide-Treated Endothelial Cells 238

JILL D. COURSEN, WILLIAM P. BENNETT, LAUREN GOLLAHON, JERRY W. SHAY, AND CURTIS C. HARRIS. Genomic Instability and Telomerase Activity in Human Bronchial Epithelial Cells during Immortalization by Human Papillomavirus-16 E6 and E7 Genes 245

MICHAEL A. BURG, AKIKO NISHIYAMA, AND WILLIAM B. STALLCUP. A Central Segment of the NG2 Proteoglycan Is Critical for the Ability of Glioma Cells to Bind and Migrate toward Type VI Collagen 254

JACQUELINE M. T. KLEIN GUNNEWIEK, YVONNE VAN AARSSEN, ANNEMIETE VAN DER KEMP, ROB NELISSEN, GER J. M. PRUIJN, AND WALTHER J. VAN VENROOIJ. Nuclear Accumulation of the U1 snRNP-Specific Protein C Is Due to Diffusion and Retention in the Nucleus 265

SUZANNE CRAWLEY, ELEANOR M. FARRELL, WEIGWANG WANG, MAOJIAN GU, HUI-YU HUANG, VU HUYNH, BRADLEY L. HODGES, DOUGLAS N. W. COOPER, AND STEPHEN J. KAUFMAN. The $\alpha7\beta1$ Integrin Mediates Adhesion and Migration of Skeletal Myoblasts on Laminin 274

SHIN NAKAMURA, HIROSHI WATANABE, MASAHIKO MIURA, AND TAKEHITO SASAKI. Effect of the Insulin-like Growth Factor I Receptor on Ionizing Radiation-Induced Cell Death in Mouse Embryo Fibroblasts 287

Short Notes

EUNKYUNG LEE, ERIC A. SHELDEN, AND DAVID A. KNECHT. Changes in Actin Filament Organization during Pseudopod Formation 295

MARIA GRAZIA ROMANELLI, FLORIAN WEIGHARDT, GIUSEPPE BIAMONTI, SILVANO RIVA, AND CARLO MORANDI. Sequence Determinants for hnRNP I Protein Nuclear Localization 300

Continued from outside back cover

Kazuto Nakada, Jun-Ichi Miyazaki, Rie Saba, and Tamio Hirabayashi. Natural Occurrence of Fast- and Fast/Slow-Muscle Chimeric Fibers in the Expression of Troponin T Isoforms 93

Sylviane Hennebicq-Reig, Daniel Tetaert, Benoit Soudan, Isabelle Kim, Guillemette Huet, Gilbert Briand, Colette Richet, Dominique Demeyer, and Pierre Degand. O-Glycosylation and Cellular Differentiation in a Subpopulation of Mucin-Secreting HT-29 Cell Line 100

Sonya J. Kamdar, Jane A. Fuller, Shin-Ichi Nishikawa, and Robert Evans. Priming of Mouse Macrophages with the Macrophage Colony-Stimulating Factor (CSF-1) Induces a Variety of Pathways That Regulate Expression of the Interleukin 6 (*Il6*) and Granulocyte–Macrophage Colony-Stimulating Factor (*Csfgm*) Genes 108

Emmapaola Sturani, Adele Abbondio, Paola Branduardi, Cristina Ferrari, Renata Zippel, Enzo Martegani, Marco Vanoni, and Suzanne Denis-Donini. The Ras Guanine Nucleotide Exchange Factor CDC25Mm Is Present at the Synaptic Junction 117

André Lochter and Melitta Schachner. Inhibitors of Protein Kinases Abolish ECM-Mediated Promotion of Neuronal Polarity 124

V. T. Solov'yan, I. O. Andreev, T. Yu. Kolotova, P. V. Pogribniy, D. T. Tarnavsky, and V. A. Kunakh. The Cleavage of Nuclear DNA into High Molecular Weight DNA Fragments Occurs Not Only during Apoptosis but Also Accompanies Changes in Functional Activity of the Nonapoptotic Cells 130

Masaru Kubota, Ikuya Usami, Ken-ichiro Watanabe, Machiko Sawada, Akihiro Kataoka, Seiji Koishi, Ying-Wei Lin, Yuichi Akiyama, and Kenshi Furusho. Apoptosis-Resistant Phenotype Selected by Alternating Exposure to Camptothecin and Etoposide 138

Rajala V. S. Raju, Terence N. Moyana, and Rajendra K. Sharma. *N*-Myristoyltransferase Overexpression in Human Colorectal Adenocarcinomas 145

Kaoru J. Takano, Takako Takano, Yasuko Yamanouchi, and Takaaki Satou. Pressure-Induced Apoptosis in Human Lymphoblasts 155

Asit B. Mukherjee and Samuel Thomas. A Longitudinal Study of Human Age-Related Chromosomal Analysis in Skin Fibroblasts 161

Roser Pagan, Isabel Martín, Miquel Llobera, and Senén Vilaró. Growth and Differentiation Factors Inhibit the Migratory Phenotype of Cultured Neonatal Rat Hepatocytes Induced by HGF/SF 170

Sari Atula, Reidar Grenman, and Stina Syrjänen. Fibroblasts Can Modulate the Phenotype of Malignant Epithelial Cells *in Vitro* 180

Leda Raptis, Heather L. Brownell, Ying Lu, Thomas Preston, Radha P. Narsimhan, Stephen Anderson, Erik Schaefer, and Tina Haliotis. v-Ras and v-Raf Block Differentiation of Transformable C3H10T1/2-Derived Preadipocytes at Lower Levels Than Required for Neoplastic Transformation 188

Krzysztof Reiss, Wei Cheng, Piotr Pierzchalski, Satish Kodali, Baosheng Li, Shenglun Wang, Yu Liu, and Piero Anversa. Insulin-like Growth Factor-1 Receptor and Its Ligand Regulate the Reentry of Adult Ventricular Myocytes into the Cell Cycle 198

Xuening Wang and George P. Studzinski. Antiapoptotic Action of 1,25-Dihydroxyvitamin D_3 Is Associated with Increased Mitochondrial MCL-1 and RAF-1 Proteins and Reduced Release of Cytochrome c 210

Continued on previous page

EXPERIMENTAL CELL RESEARCH
Volume 235, Number 1, August 25, 1997

CONTENTS

Editorial

URBAN LENDAHL 1

Regular Articles

MADELINE LI, BARBARA CHOO, ZEU-MING WONG, JORGE FILMUS, AND RONALD N. BUICK. Expression of OCI-5/Glypican 3 during Intestinal Morphogenesis: Regulation by Cell Shape in Intestinal Epithelial Cells 3

HELEN E. GRUBER, E. CARL FISHER, JR., BHALOO DESAI, AUDREY A. STASKY, GRETCHEN HOELSCHER, AND EDWARD N. HANLEY, JR. Human Intervertebral Disc Cells from the Annulus: Three-Dimensional Culture in Agarose or Alginate and Responsiveness to TGF-β1 13

OLIVER LANGHOLZ, DAGMAR ROECKEL, DIRK PETERSOHN, EVA BROERMANN, BEATE ECKES, AND THOMAS KRIEG. Cell–Matrix Interactions Induce Tyrosine Phosphorylation of MAP Kinases ERK1 and ERK2 and PLCγ-1 in Two-Dimensional and Three-Dimensional Cultures of Human Fibroblasts 22

ALEJANDRO ABALLAY, NORA G. ARENAS, ANDREW F. G. QUEST, AND LUIS S. MAYORGA. A Factor with a Zinc- and Phorbol Ester-Binding Domain Is Necessary for Endosome Fusion 28

SYLVETTE AYALA-TORRES, PETER C. MOLLER, BETTY H. JOHNSON, AND E. BRAD THOMPSON. Characteristics of 25-Hydroxycholesterol-Induced Apoptosis in the Human Leukemic Cell Line CEM 35

M. ISABELLA PÖRN-ARES, SEK C. CHOW, J. PETER SLOTTE, AND STEN ORRENIUS. Induction of Apoptosis and Potentiation of TNF- and Fas-Mediated Apoptosis in U937 Cells by the Xanthogenate Compound D609 48

GERRY MELINO, MURIEL DRAOUI, LORENZA BELLINCAMPI, FRANCESCA BERNASSOLA, SERGIO BERNARDINI, MAURO PIACENTINI, UWE REICHERT, AND PAUL COHEN. Retinoic Acid Receptors α and γ Mediate the Induction of "Tissue" Transglutaminase Activity and Apoptosis in Human Neuroblastoma Cells 55

LI ZHANG, MARIA LUISA MARTELLI, CATERINA BATTAGLIA, FRANCESCO TRAPASSO, DONATELLA TRAMONTANO, GIUSEPPE VIGLIETTO, ANTONIO PORCELLINI, MASSIMO SANTORO, AND ALFREDO FUSCO. Thyroid Cell Transformation Inhibits the Expression of a Novel Rat Protein Tyrosine Phosphatase 62

MICHINORI KITAGAWA, HIDEYUKI MUKAI, AND YOSHITAKA ONO. Molecular Cloning and Characterization of a Novel Mitochondrial Phosphoprotein, MIPP65, from Rat Liver 71

ESPEN STANG AND ODDMUND BAKKE. MHC Class II-Associated Invariant Chain-Induced Enlarged Endosomal Structures: A Morphological Study 79

Continued on inside back cover

0014-4827(19970825)235:1;1-N